

# INDIAN JOURNAL OF PHYSICS

VOL. XXV

AND

## PROCEEDINGS

OF THE

*Indian Association for the Cultivation of Science, Vol. XXXIV*

*(Published in Collaboration with the Indian Physical Society)*

---

( With Thirtythree Plates )

---

PRINTED BY SIBENDRANATH KANJILAL, SUPERINTENDENT (OFFG.), CALCUTTA  
UNIVERSITY PRESS, 48, HAZRA ROAD, BALLYGUNGE, CALCUTTA, AND  
PUBLISHED BY THE REGISTRAR, INDIAN ASSOCIATION FOR  
THE CULTIVATION OF SCIENCE

*Jadavpur, Calcutta*

1951

Price Re. 20 or £2

## BOARD OF EDITORS

K. BANERJEE                      S. K. MITRA  
D. M. BOSE                      P. RAY  
S. N. BOSE                      M. N. SAHA  
D. S. KOTHARI

S. C. SIRKAR, (*Secretary*)

## EDITORIAL COLLABORATORS

DR. R. K. ASUNDI, M.A., PH.D.  
PROF. H. J. BHABHA, PH.D., F.R.S  
DR. P. K. KICHLU, D.Sc.  
PROF. K. S. KRISHNAN, D.Sc., F.R.S  
PROF. K. RANGADHAMA RAO, M.A., D.Sc.  
PROF. G. P. DUBE, M.Sc.  
DR. N. D. SARWATTEY, D.Sc.  
DR. N. N. DASGUPTA, M.Sc., PH.D.  
PROF. N. R. SEN, D.Sc., F.N.I.  
PROF. P. C. MAHANTI, D.Sc., F.N.I.  
PROF. S. R. PALIT, D.Sc.,  
PROF. K. R. DIXIT, PH.D.  
DR. H. RAKSHIT, D.Sc.,  
DR. VIKRAM A. SARABHAI, M.A., PH.D.  
DR. P. S. GILL, PH.D.  
DR. S. R. KHASTGIR, D.Sc., F.N.I.,  
F.R.S.E.  
DR. D. BASU, PH.D.

## ASSISTANT EDITOR

MR. A. N. BANERJEE, M.Sc.

## NOTICE TO INTENDING AUTHORS

Manuscripts for publication should be sent to Mr. A. N. Banerjee, Assistant Editor, 2 & 3, Lady Willingdon Road, Jadavpur, Calcutta-32.

The manuscript of each paper should contain in the beginning a short abstract of the paper.

All references to published papers should be given in the text by quoting the surname of the authors followed by the year of publication within braces, *e.g.*, Sen (1942). The actual references should be given in a list at the end of the paper according to the following specimen :

Sen, B. K., 1942, *Ind. J. Phys.*, 16, 329.

The references should be arranged alphabetically in the list.

All diagrams should be drawn on thick white paper in Indian ink, and letters and numbers in the diagrams should be written neatly in capital type in Indian ink. The size of the diagrams should be at least three times that of the intended size of the actual figure.

Annual Subscription—

Inland Rs. 20

Foreign £ 2



# INDIAN JOURNAL OF PHYSICS

1951

## CONTENTS

### Part 1. January

PAGE

1. Effect of Vertical Transport of Ions caused by Solar Tides in the  $F_2$  Region—By D. C. Choudhury ... 17
2. Reversal of Polarisation of Microwaves from Sunspots—By U.C. Guha ... 21
3. Ultrasonic Studies of Gels—By Arvind Mohan Srivastava ... 25
4. Light Scattering in Gases (A Note) by S. Parthasarathy ... 33
5. On the Absorption of U. H. F. Radio Waves by some Aliphatic Ketones—By S. N. Sen ... 35
6. A New and Quick Method for Detection of the Piezo-electricity and Measurement of Piezo-electric Constants—By Krishna Gopal Srivastava ... 53
7. Gas Turbines. Some Metallurgical Considerations Involved in their Manufacture—By H. Trivedi ... 57
8. On the Raman Spectrum of Diphenyl methane—By S. K. Mukerji and Banarsi Lal ... 61

### Part 2. February

9. On Wave Nature of Matter—By Brahmananda Mishra ... 65
10. A note on the Raman Spectra of  $CH_2Cl_2$  and  $CHCl_3$  in the Vapour state—By M. V. Rao ... 73
11. The Absorption Spectrum of Bismuth sulphide,  $BiS$ —By P. K. Sur ... 79
12. Ultrasonic Velocity in Organic Solutions, II—By K. C. Lal ... 93
13. Low-frequency Raman Lines in Para-dichlorobenzene—By Hari Narain and Bishambhar Dayal Saksena ... 98
14. Aluminium in Steel—By K. C. Mazumder ... 99

#### Reviews :—

- (1). A Text-Book of General Physics—By G. R. Noakes ... 101

### Part 3. March

15. Analysis of Trigger Circuits—By Rais Ahmed ... 103
16. Electrical Properties of Indian Mica. IV. Electric Strength—By S. S. Mandal ... 107
17. Absorption Spectrum of Phenetole—By K. Sreeramamurty ... 123
18. Raman Spectra of Organic Crystals at different Low Temperatures. II. Ethyl benzene and Benzyl chloride—By A. K. Ray ... 131
19. A Note on the effect of Photo-electric Emission from the electrodes on the rectifying action of a discharge—By V. T. Chiplonkar ... 138
20. On a Method of Studying Small-angle Scattering of Monochromatic X-rays—By K. Banerjee and J. C. Maitra ... 141

21.	The Method of Shadow-casting in Photomicrography—By D. L. Bhattacharya ... ..	145
-----	-------------------------------------------------------------------------------	-----

## Part 4. April

22.	Dynamics of the Vibration of a Bar excited by the Longitudinal impact of an Elastic Load—By M. Ghosh and S. K. Ghosh ...	153
23.	Dielectric Properties of Salt Solutions at Ultra-high frequencies—By Ramu Satyanarayana and S. R. Khastgir ... ..	163
24.	An Externally coated Pyrex G-M Counter—By M. Yasin, R. Ahmed and P. S. Gill ... ..	182
25.	On the Absorption of U. H. F. Radio Waves in some Aliphatic Ketones dissolved in Non-polar Solvents—By S. N. Sen ...	187
	On the Poisoning of Oxide-coated Cathode due to Absorption of Particles liberated from the Anode—By S. Deb ... ..	197

## Part 5. May

27.	Studies in Fading of Medium-wave Radio Signals—By B. A. P. Tantry and S. R. Khastgir... ..	217
28.	On the Ultraviolet Absorption Spectra of Anisole in the Liquid and Solid States—By A. R. Deb ... ..	233
29.	On the Absorption of U. H. F. Radio Waves in Fatty Acids—By S. N. Sen ... ..	237
30.	Scattering of Neutrons by Protons at High Energies—By D. Basu... ..	246
31.	Particular Solutions of Einstein's Recent Unified Theories—By G. Bandyopadhyay ... ..	257
32.	On the Absorption Spectra of Toluene in the Liquid and Solid States—By H. N. Swamy ... ..	262

## Reviews :—

(2)	Fundamentals of Optics—By F. A. Jenkins and H. E. White ... ..	265
(3)	Heat and Temperature Measurement—By Robert L. Weber ... ..	266

## Part 6. June

## PAGE

33.	On an Interpretation of the Limits of Predissociation in the Spectrum of Carbon Monoxide and the Latent Heat of Sublimation of Graphite—By P. K. Sen Gupta ... ..	267
34.	Joshi Effect and the H. F. Components—By G. V. Bakore ... ..	274
35.	Pattern Observed in Electrolysis—By Brahmananda Mishra ... ..	277
36.	Standardisation of Wind Pressure and Temperature Variation as regards the Design of Overhead Lines with Particular reference to Condition in West Bengal—By M. Datta ... ..	279
37.	Anomalous Variations in the Angle of Arrival of Down-coming Radio Waves and their Bearing on the Fading of Short Wave Signals—By J. P. Srivastava and V. D. Rajan ... ..	287

38. Ultrasonic Absorption in Normal Air at 456 Kc/s for different Humidities—By Gopalji ... .. 298  
 Proceedings of the Indian Association for the Cultivation of Science  
 1. Lapinone, a New Antimalarial—By L. F. Fieser ... .. 1

**Part 7. July**

39. A Note on Mass Motion of a Gas—By Duleh Singh Kothari and Laxman Singh Kothari ... .. 305  
 40. On the Raman Spectrum of Thianthrene in the Solid State—By S. K. Mukerji and Banarsi Lal ... .. 309  
 41. Energy of Dissociation of Cyanogen—By Prabhat K. Sen Gupta ... 313  
 42. Thermodynamic Behaviour of a Gaseous Assembly of Point-molecules, assuming Association—By M. Dutta ... .. 317  
 43. A study of the Switching Action in a Multivibrator Circuit. Part II. —By B. M. Banerjee ... .. 329  
 44. The Schottky Analogue in the Production of the Positive Joshi Effect in Hydrogen—By H. J. Arnikaar ... .. 353

**Part 8. August**

45. Studies on the Sporadic E-Layer—By R. B. Banerji ... .. 359  
 46. Sodium in the Upper Atmosphere—By Arun Kumar Saha ... .. 375  
 47. On a Dissociation Scheme for the Spectrum of CO<sup>+</sup>—By Prabhat K. Sengupta ... .. 387  
 48. On the Unified Theories of Thermal and Shot Noise—By S. Deb ... 391  
 49. On the Approximate Solutions of Maxwell's Equations in an Infinite Medium with Regions of Finite Conductivity—By K. V. Krishna Prasad ... .. 403

**Part 9. September**

50. The Missing Heavy Elements—By N. K. Saha and Jagdish Verma ... 409  
 51. Rigorous Solution for the case of Electromagnetic Wave Propagation along a Circular Wave guide of Finite Conductivity—By K. V. Krishna Prasad ... .. 417  
 52. Investigation on the Bowed String with an Electrically driven Bow. (Part I)—By K. C. Kar, N. K. Datta and S. K. Ghosh ... 423  
 53. On the Ultraviolet Absorption Spectra of Methyl benzoate and Acetophenone in the Solid state at low Temperatures—By A. R. Deb... 433  
 54. Over-land Refraction of High-frequency Radio Waves in India—By K. R. Saha ... .. 437  
 55. On the Measurement of the Angular Correlation between two Gamma rays of Nickel (60)—By Sudhansu Das and Sunil Kumar Sen ... 451

**Part 10. October**

56. On the Origin of Low-frequency Raman Lines in Para-dichlorobenzene—By A. K. Ray ... .. 459

57.	Influence of the Electrode-surface on the Joshi Effect in Chlorine— By P. G. Deo ... ..	468
58.	Performance of Sessile Drop in Surface Tension Measurements—By N. R. Tawde and K. G. Parvatikar ... ..	473
59.	On an Automatic Wilson Cloud Chamber in a Magnetic Field and some associated Techniques—By Ranjit Kumar Das ... ..	481
60.	Ultrasonic Attenuation in Gels—By Arvind Mohan Srivastava ...	491
61.	Harmonic Distortion in Frequency-modulation Reception, Part I—By K. V. Krishna Prasad ... ..	504
Review :—		
(4)	Static and Dynamic Electricity—By William R. Smythe ...	511

## Part 11. November

62.	Harmonic Distortion in Frequency-modulation Reception. Part II.— By K. V. Krishna Prasad ... ..	513
63.	Electron Microscopic Determination of the Size and Shape of a New Plant Virus (Sann Hemp Mosaic)—By M. L. De ... ..	525
64.	Influence of Joshi Effect on the Emission Spectrum of Chlorine—By P. G. Deo ... ..	530
65.	Electron Diffraction in some Cubical Crystals—By Subodh Kumar Majumdar ... ..	533
66.	On the Existence of Rossi Second and Third Maxima of Cosmic Rays—By P. K. Sen Chaudhury ... ..	539
67.	Soft X-ray L-spectra of Fe, CO, Ni, Cu and their Oxides—By K. Das Gupta and S. B. Bhattacharjee ... ..	555

## Part 12. December

68.	On the East West Asymmetry of the Hard Component of Cosmic Rays—By B. Bhowmik and G. S. Bajwa ... ..	561
69.	Single-phase Operation of Three-phase Motors—By P. Venkata Rao and Chandra Sekhar Ghosh ... ..	565
70.	On the Fluorescence in Diamond Excited by X-rays—By B. M. Bishui	575
71.	Studies on the Sharp Extra Reflections from Phloroglucine Dihydrate Crystal—By M. N. Datta ... ..	581
72.	Poincare's Theorem and its Uses—By R. P. Singh ... ..	585
73.	Electron Diffraction in Sodium and Potassium Chloride Crystals—By Subodh Kumar Majumdar ... ..	594
74.	On the Concentration of Stress in the Neighbourhood of a Circular Hole in a Semi-infinite Plate—By B. Karunes ... ..	599

# AUTHOR INDEX

Author	Subject	Page
Ahmed, Rais ..	... Analysis of Trigger Circuits ...	99
Arnikar, H. J.	... The Schottky Analogue in the Production of the Positive Joshi Effect in Hydrogen ...	353
Bakore, G. V.	... Joshi Effect and the H. F. Components ...	274
Bandyopadhyay, G	... Particular Solutions of Einstein's Recent Unified Theories ...	257
Banerjee, B. M.	... A Study of the Switching Action in a Multi-vibrator Circuit. Part II ...	329
Banerjee, K. and Maitra J. C.	On a Method of Studying Small-angle Scattering of Monochromatic X-rays...	141
Banerjee, R. B.	... Studies on the Sporadic E-Layer ...	359
Basu, D.	... Scattering of Neutrons by Protons at High Energies ...	246
Bhattacharya, D. L	... The Method of Shadow-casting in Photomicrography ...	145
Bhowmik, B. and Bajwa, G. S.	On the East West Asymmetry of the Hard-Component of Cosmic Rays ...	561
Bishui, B. M.	... On the Fluorescence in Diamond Excited by X-rays ...	575
Chiplonkar, V. T.	... A Note on the Photoelectric Emission from the electrodes on the Rectifying action of a Discharge ...	138
Choudhury, D. C.	... Effect of Vertical Transport of Ions caused by Solar Tides in the F <sub>2</sub> Region ...	I
Datta, M.	... Standardisation of Wind Pressure and Temperature Variation as regards the Design of Overhead Lines with particular reference to Condition in West Bengal ...	279
Datta, M. N. ...	... Studies on the Sharp Extra Reflections from Phloroglucine Dihydrate Crystal... ..	581
Das Gupta, K. and Bhattacharjee, S. B.	Soft X-ray L-spectra of Fe, Co, Ni, Cu and their Oxides ...	555
Das, Ranjit Kumar	... On an Automatic Wilson Cloud Chamber in a Magnetic Field and some Associated Techniques ...	481
Das, Sudhansu and Sen, Sunil Kumar	On the Measurement of the Angular Correlation between two Gamma rays of Nickel (60) ...	451

Author	Subject	Page
De, M. L. ...	Electron Microscopic Determination of the size and shape of a New Plant Virus (Sann Hemp Mosaic) ...	525
Deb, A. R. ...	On the Ultraviolet Absorption Spectra of Anisole in the Liquid and Solid States ...	233
„ „ ...	On the Ultraviolet Absorption Spectra of Methyl benzoate and Acetophenone in the Solid State at low Temperatures ...	433
Deb, S. ...	On the Poisoning of Oxide-coated Cathode due to Adsorption of Particles Liberated from the Anode ...	197
„ „ ...	On the Unified Theories of Thermal and Shot Noise ...	391
Deo, P. G. ...	Influence of the Electrode-surface on the Joshi Effect in Chlorine ...	468
„ „ ...	Influence of Joshi Effect on the Emission Spectrum of Chlorine ...	530
Dutta, M. ...	Thermodynamic Behaviour of Gaseous Assembly of Point-molecules, Assuming Association ...	317
Ghosh, M. and Ghosh, S. K.	Dynamics of the Vibration of a Bar Excited by the Longitudinal Impact of an Elastic Load ...	153
Gopalji ...	Ultrasonic Absorption in Normal Air at 456 Kc/s for different Humidities ...	298
Guha, U. C. ...	Reversal of Polarisation of Microwaves from Sunspots ...	8
Kar, K. C., Datta, N. K. and Ghosh, S. K.	Investigation on the Bowed String with an Electrically driven Bow. Part I ...	423
Karunes, B. ...	On the concentration of stress in the Neighbourhood of a Circular Hole in a semi-infinite Plate ...	599
Kothari, Duleh Singh and Kothari, Laxman Singh.	A Note on Mass Motion of a Gas ...	305
Krishna Prasad, K. V....	On the Approximate Solutions of Maxwell's Equations in an Infinite Medium with Regions of Finite Conductivity ...	403
„ „ „ ...	Rigorous Solution for the Case of Electromagnetic Wave Propagation along a Circular Wave Guide of Finite conductivity ...	417
„ „ „ ...	Harmonic Distortion in Frequency-Modulation Reception. Part I ...	504

Author	Subject	Page
Krishna Prasad, K. V....	Harmonic Distortion in Frequency-Modulation Reception. Part II ... ..	513
Lal, K. C. ... ..	Ultrasonic Velocity in Organic Solutions. II	73
Majumdar, S. K. ... ..	Electron Diffraction in some Cubic Crystals ...	533
„ „ ... ..	Electron Diffraction in Sodium and Potassium Chloride Crystals ... ..	594
Mandal, S. S. ... ..	Electrical Properties of Indian Mica. IV. Electric Strength ... ..	111
Mazumder, K. C. ... ..	Aluminium in Steel ... ..	93
Mishra, B. ... ..	On Wave Nature of Matter ... ..	57
„ „ ... ..	Pattern Overserved in Electrolysis ... ..	277
Mukerji, S. K. and Banarsi Lal ... ..	On the Raman Spectrum of Diphenyl methane	53
„ „ „ ... ..	On the Raman Spectrum of Thianthrene in the Solid State ... ..	309
Narain, H. and Saksena, B. D. ... ..	Low-frequency Raman Lines in Para-dichloro-benzene ... ..	79
Parthasarathy, S. ... ..	Light Scattering in Gases (A Note)... ..	21
Rao, M. V. ... ..	A Note on the Raman Spectra of CH <sub>2</sub> Cl <sub>2</sub> and CH Cl <sub>3</sub> in the Vapour State ... ..	61
Rao, P. Venkata and Ghosh, Chandrasekhar	Single-phase Operation of Three-phase Motors	565
Ray, A. K. ... ..	Raman Spectrum of Organic Crystals at different Low Temperatures II. Ethyl benzene and Benzylchloride ... ..	131
„ „ ... ..	On the Origin of Low-frequency Raman Lines in Para-dichlorobenzene ... ..	459
Saha, A. K. ... ..	Sodium in the Upper Atmosphere ... ..	375
Saha, K. R. ... ..	Over-land Refraction of High-frequency Radio Waves in India ... ..	437
Saha, N. K. and Verma, Jagadish	The Missing Heavy Elements ... ..	409
Satyanarayana, Ramu, and Khastgir, S. R.	Dielectric Properties of Salt Solutions at Ultra-high frequencies ... ..	163
Sen, S. N. ... ..	On the Absorption of U. H. F. Radio Waves by some Aliphatic Ketones ... ..	25
„ „ ... ..	On the Absorption of U. H. F. Radio Waves in some Aliphatic Ketones dissolved in Non-polar Solvents ... ..	187
„ „ ... ..	On the Absorption of U. H. F. Radio Waves in Fatty Acids ... ..	237
Sen Chaudhury, P. K.,...	On the Existence of Rossi Second and Third Maxima of Cosmic Rays ... ..	539

Author	Subject	Page
Sen Gupta, Prabhat, K.	On an Interpretation of the Limits of Pre-dissociation in the Spectrum of Carbon monoxide and Latent Heat of Sublimation of Graphite ... ..	267
	Energy of Dissociation of Cyanogen ...	313
	On a Dissociation Scheme for the Spectrum of $\text{CO}^+$ ... ..	387
Singh, R. P. ...	Poincare's Theorem and its Uses ... ..	585
Sreeramamurty, K.	Absorption Spectrum of Phenetole ... ..	123
Srivastava, Arvind Mohan,	Ultrasonic Studies in Gels ... ..	17
„ „ „	Ultrasonic Attenuation in Gels ... ..	491
Srivastava, J. P. and Rajan, V. D.	Anomalous Variations in the Angle of Arrival of Down-coming Radio Waves and their Bearing on the Fading of Short Wave Signals ... ..	287
Srivastava, Krishna Gopal	A New and Quick Method for Detection of Piezo-electricity and Measurement of Piezo-electric Constants ... ..	33
Sur, P. K. .. ..	The Absorption Spectrum of Bismuth sulphide —BiS ... ..	65
Swamy, H. N. ...	On the Absorption Spectra of Toluene in the Liquid and Solid States ... ..	262
Tantry, B. A. P. and Khastgir, S. R.	Studies in Fading of Medium-wave Radio Signals ... ..	217
Tawde, N. R. and Parvatikar, K. G.	Performance of Sessile Drop in Surface Tension Measurements ... ..	473
Trivedi, H. ... ..	Gas Turbines. Some Metallurgical Considerations involved in their Manufacture ...	35
Yasin, M., Ahmed, R. and Gill, P. S.	An Externally Coated Pyrex G-M Counter ...	182



# SUBJECT INDEX

Subject	Author	Page
Absorption Spectra of Toluene in the Liquid and Solid States. On the	H. N. Swamy ...	262
Absorption Spectrum of Bismuth Sulphide, BiS. The	P. K. Sur ...	65
Absorption Spectrum of Phenetole ...	K. Sreeramamurty ...	123
Aluminium in Steel ...	K. C. Mazumder ...	93
Anomalous Variations in the Angle of Arrival of Down-coming Radio Waves and their Bearing on the Fading of Short Wave Signals	J. P. Srivastava and V. D. Rajan	287
Bowed Striag with an Electrically Driven Bow. Investigation on the. Part I	K. C. Kar, N. K. Datta and S. K. Ghosh	423
Cosmic Rays. On the East West Asymmetry of the Hard Component of	B. Bhowmik and G. S. Bajwa	561
Cosmic Rays. On the Existence of Rossi Second and Third Maxima	P. K. Sen Chaudhury ...	539
Design of Overhead Lines with Particular References to Conditions in West Bengal. Standardisation of Wind Pressure and Temperature Variation as regards the	M. Datta ...	279
Dielectric Properties of Salt Solutions at Ultra-high Frequencies	Ramu Satyanarayana and S. R. Khastgir	163
Dissociation of Cyanogen. Energy of ...	Prabhat K. Sen Gupta ...	313
Dissociation Scheme for the Spectrum of CO <sup>+</sup> . On a		387
Einstein's Recent Unified Theories. Particular Solutions of	G. Bandyopadhyay ...	257
Electrolysis. Patterns Observed in ...	Brahmananda Mishra ...	277
Electromagnetic Wave Propagation along a Circular Wave Guide of Finite Conductivity. Rigorous Solution for the case of	K. V. Krishna Prasad ...	417
Electron Diffraction in Some Cubic Crystals.	Subodh Kumar Majumdar	533
Electron Diffraction in Sodium and Potassium Chloride Crystals		594
Electron Microscopic Determination of the Size and Shape of a New Plant Virus (Sann Hemp Mosaic)	M. L. De	525
Fluorescence in Diamond Excited by X-rays. On the	B. M. Bishui	575

Subject	Author	Page
Frequency-modulation Reception. Harmonic Distortion in. Part I	K. V. Krishna Prasad ...	504
Frequency-modulation Reception. Harmonic Distortion in. Part II	„ „ „	513
G. M. Counters. An Externally Coated Pyrex	M. Yasin, R. Ahmed and P. S. Gill	182
Gamma Rays of Nickel (60). On the Angular Correlation between two	Sudhansu Das and Sunil Kumar Sen	451
Gas Turbines. Some Metallurgical Considerations Involved in their Manufacture of	H. Trivedi ...	35
Gaseous Assembly of Point-molecules. Thermodynamic Behaviour of a	M. Dutta ...	317
Indian Mica. Electrical Properties of IV Electric Strength	S. S. Mandal ...	111
Joshi Effect and the H. F. Components ...	G. V. Bakore ...	274
Joshi Effect in Chlorine. Influence of the Electrode-surface on the	P. G. Deo ...	468
Joshi Effect on the Emission Spectrum of Chlorine. Influence of	P. G. Deo ...	530
Light Scattering in Gases A Note on ...	S. Parthasarathy ...	21
Mass Motion of a Gas. A Note on ...	Duleh Singh Kothari and Laxman Singh Kothari	305
Maxwell's Equation is an Infinite Medium with Regions of Finite Conductivity. On the Approximate Solutions of	K. V. Krishna Prasad ...	403
Medium-wave Radio Signals. Studies in Fading of	B. A. P. Tantry and S. R. Khastgir	217
Microwaves from Sunspots. Reversal of Polarisation of	U. C. Guha ...	8
Missing Heavy Elements. The ...	N. K. Saha and Jagdish Verma	409
Multivibrator Circuit. A Study of the Switching Action in a. Part II	B. M. Banerjee ...	329
Photo-electric Emission from the Electrodes on the Rectifying Action of a Discharge, A Note on the Effect of	V. T. Chiplonkar ...	138
Peizo-electricity and Measurement of Peizo-electric Constants. A New and Quick Method for Detection of the	Krishna Gopal Srivastava	33
Poincare's Theorem and its Uses ...	R. P. Singh ...	585
Poisoning of Oxide-coated Cathode due to Adsorption of Particles Liberated from the Anode. On the	S. Deb ...	197

Subject	Author	Page
Predissociation in the Spectrum of Carbon Monoxide and Latent Heat of Sublimation of Graphite. On an Interpretation of the Limits of	Prabhat K. Sen Gupta ...	267
Raman Lines in Para-dichlorobenzene. Low frequency	Hari Narain and Bishambhar Dayal Saksena	79
Raman Lines in Para-dichlorobenzene. On the Origin of Low-frequency	A. K. Ray ...	459
Raman Spectra of $\text{CH}_2\text{Cl}_2$ and $\text{CHCl}_3$ in the Vapour State. A Note on the	M. V. Rao ...	61
Raman Spectra of Organic Crystals at different Low Temperatures. II. Ethyl Benzene and Benzyl Chloride	A. K. Ray ...	131
Raman Spectrum of Diphenylmethane. On the	S. K. Mukerji and Banarsi Lal	53
Raman Spectrum of Thianthrene in the Solid State. On the	„ „ „	309
Refraction of High-frequency Radio Waves in India. Overland	K. R. Saha ...	437
Scattering of Monochromatic X-rays. On a Method of Studying Small-angle	K. Banerjee and J. C. Maitra	141
Scattering of Neutrons by Protons at High Energies	D. Basu ...	246
Schottky Analogue in the Production of the Positive Joshi Effect in Hydrogen. The	H. J. Arnikaar ...	353
Sessile Drops in Surface Tension Measurements. Performance of	N. R. Tawde and K. G. Parvatikar	473
Shadow-casting in Photomicrography. The Method of	D. L. Bhattacharya ...	145
Sharp Extra Reflections from Phloroglucine Dihydrate Crystal. Studies on the	M. N. Datta ...	581
Sodium in the Upper Atmosphere ...	Arun Kumar Saha ...	375
Soft X-ray L-spectra of Fe, Co, Ni and Cu and their Oxides	K. Das Gupta and S. B. Bhattacharjee	555
Sporadic E-Layer. Studies on the	R. B. Banerjee ...	359
Stress in the Neighbourhood of a Circular Hole in a Semi-infinite Plate. On the Concentration of	B. Karunes ...	599
Thermal and Shot Noise. On the Unified Theories of	S. Deb ...	391
Three-phase Motors. Single-phase Operation of	P. Venkata Rao and Chandrasekhar Ghosh	565

Subject	Author	Page
Trigger Circuits. Analysis of ... ..	Rais Ahmed ... ..	99
U. H. F. Radio Waves by some Aliphatic Ketones. On the Absorption of	S. N. Sen ... ..	25
U. H. F. Radio Waves in Fatty Acids. On the Absorption of	„ „ ... ..	237
U. H. F. Radio Waves in some Aliphatic Ketones Dissolved in Non-polar Solvents. On the Absorption of	„ „ ... ..	187
Ultrasonic Absorption in Normal Air at 456 Kc/s for different Humidities	Gopalji ... ..	298
Ultrasonic Attenuation in Gels ... ..	Arvind Mohan Srivastava... ..	491
Ultrasonic Studies of Gels ... ..	„ „ ... ..	17
Ultrasonic Velocity in Organic Solutions. II	K. C. Lal ... ..	73
Ultraviolet Absorption Spectra of Anisole in the Liquid and Solid States. On the	A. R. Deb ... ..	233
Ultraviolet Absorption Spectra of Methyl Benzoate and Acetophenone in the Solid State at Low Temperatures. On the	„ „ ... ..	433
Vertical Transport of Ions caused by Solar Tides in the $F_2$ Region. Effect of	D. C. Choudhury ... ..	1
Vibration of a Bar excited by the Longitudinal Impact of an Elastic Load. Dynamics of the	M. Ghosh and S. K. Ghosh	153
Wave Nature of Matter. On ... ..	Brahmananda Mishra ... ..	57
Wilson Cloud Chamber in a Magnetic Field and some Associated Techniques. On an Automatic	Ranjit Kumar Das ... ..	481

## REVIEWS

Title of book		Author	Page
<b>A Text Book of General Physics ...</b>	...	G. R. Noakes ...	98
<b>Fundamentals of Optics... ..</b>	...	F. A. Jenkins and H. E. White	265
<b>Heat and Temperature Measurement ...</b>	...	Robert L. Weber .	266
<b>Static and Dynamic Electricity ...</b>	...	William R. Smythe .	511

### *Proceedings of the Indian Association for the Cultivation of Science*

Subject		Author	Page
<b>Lapinone, a New Antimalarial ...</b>	...	L. F. Fieser ...	I



# EFFECT OF VERTICAL TRANSPORT OF IONS CAUSED BY SOLAR TIDES IN F<sub>2</sub> REGION\*

By D. C. CHOUHURY

(Received for publication, November, 21, 1950)

**ABSTRACT.** A solution is obtained of the continuity equation of the electro-dynamical theory of tides of Martyn for the night time condition  $\omega$ , neglecting the recombination term. The vertical ionic velocity is assumed to have the general form i.e.,  $v = v_0 e^{-\gamma z} \cos(\omega t + \delta)$  where  $\omega = 30^\circ/\text{hour}$ . Curves depicting the variations of  $N_{\max}$ ,  $h_{\max}$  and  $h_{\min}$  with height, (reduced) are drawn for values of  $\gamma = 0.25, 0.50, 1.00, 1.25$  and  $1.50$ . For each value of  $\gamma$  variation curves for the hours 0.0, 1.0, 3.0, 5.0 and 7.0 (from the time of maximum upward drift) have been drawn. Curves for the value of  $\gamma = 1$  generally agree with the observed results.

## INTRODUCTION

The fundamental equation of the electro-dynamical theory of tides in the ionosphere as developed by Martyn [1947 a] is

$$\frac{\partial N}{\partial t} = I(z, t) - \alpha N^2 + \frac{\partial [Nv]}{\partial z} \quad \dots (1)$$

where  $N$ —electron density in an ionospheric layer at height  $z$

$I$ —rate of ion production per  $\text{cm}^3$ ,

$\alpha$ —effective recombination co-efficient (given by  $\lambda\alpha_1$ , where  $\lambda$  is the ratio of negative ion and electron concentrations  $\alpha_1$ , the co-efficient of mutual neutralization between negative and positive ions),

$v$ —vertical ionic drift velocity (measured positively downwards in units of scale height  $H$  and varying both with height and time),

$z$ —height (reduced height—measured in terms of scale height  $H$ ).

The solution of the complete equation is very difficult. Hence, to establish the salient features [of his theory] Martyn examined the equation for night time condition when  $I = 0$  and also assumed that  $\alpha N^2$  is small compared to  $\frac{\partial [Nv]}{\partial z}$ . The equation thus reduces to the equation of continuity,

$$\frac{\partial N}{\partial t} = \frac{\partial [Nv]}{\partial z} \quad \dots (2)$$

Simple physical considerations show that the vertical drift velocity  $v$  should be periodic in time (with a predominant 12-hourly period), and that in

\* Communicated by Prof. S. K. Mitra, D.Sc., F.N.I.

the region considered ( $F_2$  region) its amplitude will decrease with height owing to increase of viscosity with the same. Martyn considered the effects of the change of  $v$  with height and with time separately and showed that:

(1) If  $v$  varies exponentially with  $z$ , i.e. if  $v = v_0 e^{-\gamma z}$ , the ionized region is distorted so that both  $N_{\max}$  and  $h_{\max}$  depart from those given by Chapman's region; the departure may be in or out of phase [Martyn, 1947a].

(2) If  $v$  varies sinusoidally with time with a 12-hour period and if at the same time its phase varies with  $z$ , i.e. if  $v$  is of the form  $v_0 \sin(\omega t + \sigma z)$ , the variation of  $N_{\max}$  and  $h_{\max}$  leads or lags in phase quadrature according as  $\sigma$  is positive or negative ( $\omega = 30^\circ/\text{hour}$  [Martyn, 1947b]).

In the present paper we shall attempt a general solution of Eqn. (2), assuming

$$v = v_0 e^{-\gamma z} \cos(\omega t + \delta) \quad \dots (3)$$

and determine how the ionization will vary with height, and also with the passage of time for different assumed values of the constant  $\gamma$  in the exponential. In the expression for  $v$  we have assumed that the phase remains constant with height. This is because Martyn has shown [Martyn, 1949, 1950] that there is no phase variation with height in the case of lunar tides. We have therefore, thought it reasonable to assume that for the case of solar tides also the phase remains constant. This assumption naturally considerably simplifies the analysis.

#### SOLUTION OF THE DIFFERENTIAL EQUATION

Putting  $v = \phi(z) \cdot \psi(t)$

where  $\phi(z) = v_0 e^{-\gamma z}$  and  $\psi(t) = \cos(\omega t + \delta)$ ,

$$\text{Eqn. (2) becomes } \frac{1}{\psi(t)} \cdot \frac{\partial N}{\partial t} = \frac{\partial [N\phi(z)]}{\partial z}$$

Substituting in the above Eqn.

$$M = N\phi(z)$$

$$\tau = \int \psi(t) dt$$

and

$$u = \int \frac{dz}{\phi(z)} = g(z)$$

we obtain

$$\frac{\partial M}{\partial \tau} = \frac{\partial M}{\partial u}$$

The most general solution of the equation is given by

$$M = f(u + \tau)$$

Now initially

$$\tau = 0 \text{ and } M = F(z)$$

therefore

$$f(u) = F(z) = F\{g^{-1}(u)\}$$

Hence

$$M = N\phi(z) = F\{g^{-1}(u + \tau)\}$$

or

$$N = \frac{1}{\phi(z)} \cdot F\{g^{-1}(u + \tau)\} \quad (4)$$



## *Effect of Vertical Transport of Ions etc.*

Again since

$$g(z) = \int \frac{dz}{\phi(z)} = \frac{1}{v_0} \int e^{\gamma z} dz = \frac{e^{\gamma z}}{\gamma v_0} = u$$

then

$$z = g^{-1}(u) = \frac{1}{\gamma} \log(\gamma v_0 u)$$

$$\tau = \int \psi(t) dt = \int \cos(\omega t + \delta) dt$$

$$= \frac{\sin(\omega t + \delta)}{\omega} \cdot K$$

$$= \frac{\sin(\omega t + \delta)}{\omega} - \frac{\sin \delta}{\omega}$$

Eqn. (4) becomes

$$\begin{aligned} N &= \frac{1}{\phi(z)} \cdot F \left[ \frac{1}{\gamma} \log \{ \gamma v_0 (u + \tau) \} \right] \\ &= \frac{1}{\phi(z)} \cdot F \left[ \frac{1}{\gamma} \log \left\{ e^{\gamma z} + \frac{\gamma v_0}{\omega} \sin(\omega t + \delta) - \frac{\gamma v_0}{\omega} \sin \delta \right\} \right] \\ &= \frac{1}{\phi(z)} \cdot F \left[ \frac{1}{\gamma} \log \{ e^{\gamma z} + a \sin(\omega t + \delta) - a \sin \delta \} \right] \dots (5) \end{aligned}$$

where

$$a = \gamma v_0 / \omega.$$

Assuming at

$$t = 0,$$

$$n_0 = N_0 e^{\frac{1}{2} [1 - z - e^{-z}]} \dots (6)$$

we have

$$\begin{aligned} M &= F(z) = n_0 \phi(z) \\ &= N_0 v_0 e^{-\gamma z} \cdot e^{\frac{1}{2} [-z - e^{-z}]} \end{aligned}$$

Therefore from Eqn. (5)

$$N = N_0 e^{\gamma z} \cdot e^{-\gamma \left[ \frac{1}{\gamma} \log \{ e^{\gamma z} + a \sin(\omega t + \delta) - a \sin \delta \} \right]}$$

$$\times e^{\frac{1}{2} \left[ 1 - \frac{1}{\gamma} \log \{ e^{\gamma z} + a \sin(\omega t + \delta) - a \sin \delta \} - \exp \{ -\log \{ e^{\gamma z} + a \sin(\omega t + \delta) - a \sin \delta \}^{1/\gamma} \} \right]}$$

$$\begin{aligned} \therefore \frac{N}{N_0} &= \frac{e^{\gamma z}}{e^{\gamma z} + a \sin(\omega t + \delta) - a \sin \delta} \cdot \exp \frac{1}{2} \left[ 1 - \frac{1}{\gamma} \log \{ e^{\gamma z} + a \sin(\omega t + \delta) \right. \\ &\quad \left. - a \sin \delta \} - \{ e^{\gamma z} + a \sin(\omega t + \delta) - a \sin \delta \}^{-1/\gamma} \right] \dots (7) \end{aligned}$$

### VARIATION OF ELECTRON DENSITY WITH (REDUCED) HEIGHT

We can construct with the help of Eqn. (7) illustrative curves to show how, for any assumed value of  $\gamma$ , an initial Chapman distribution of electrons, as given by Eqn. (6) will alter with the passage of time. We

take  $v_0 = 10,000$  cms/sec. and put  $\delta$  equal to  $180^\circ$ , that is, we begin reckoning time ( $t=0$ ) when the drift velocity is maximum negative. Five sets of curves representing variations of  $N/N_0$  with  $z$  are drawn for five assumed values of  $\gamma$ , namely  $\gamma=1.5, 1.25, 1.0, 0.5$  and  $0.25$ . For each value of  $\gamma$

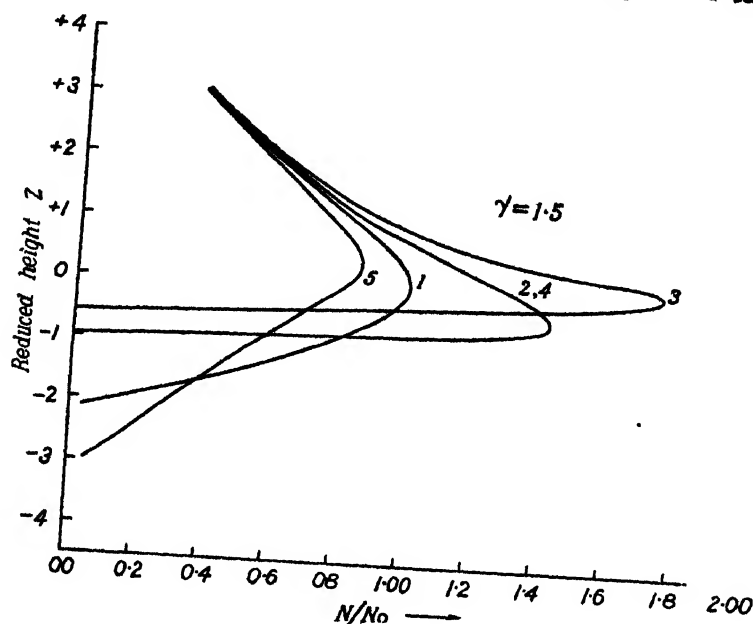


FIG. 1

Variation of  $N/N_0$  with reduced height ( $z$ ) for  $\gamma=1.50$ . Curves 1, 2, 3, 4 and 5 correspond to values of  $t=0, 1, 3, 5$  and  $7$  hours respectively.

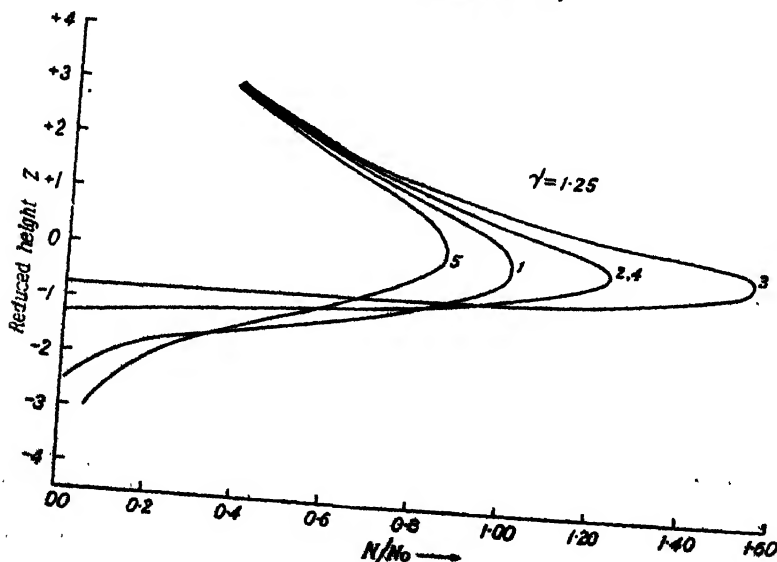


FIG. 2

Variation of  $N/N_0$  with reduced height ( $z$ ) for  $\gamma=1.25$ . Curves 1, 2, 3, 4 and 5 correspond to values of  $t=0, 1, 3, 5$  and  $7$  hours respectively.

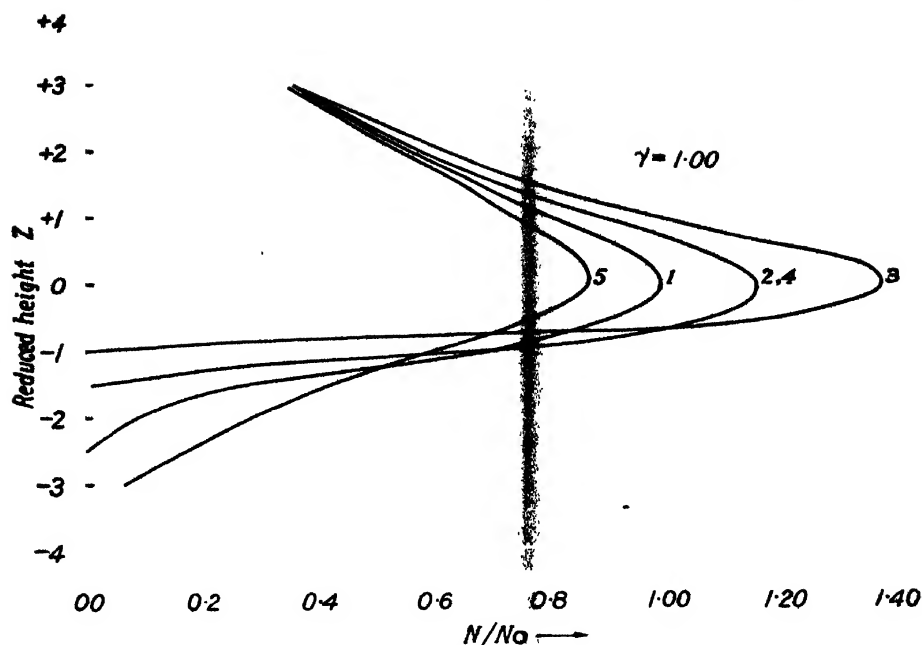


FIG. 3

Variation of  $N/N_0$  with reduced height ( $z$ ) for  $\gamma=1.00$ . Curves 1, 2, 3, 4, and 5 correspond to values of  $t=0, 1, 3, 5$  and 7 hours respectively.

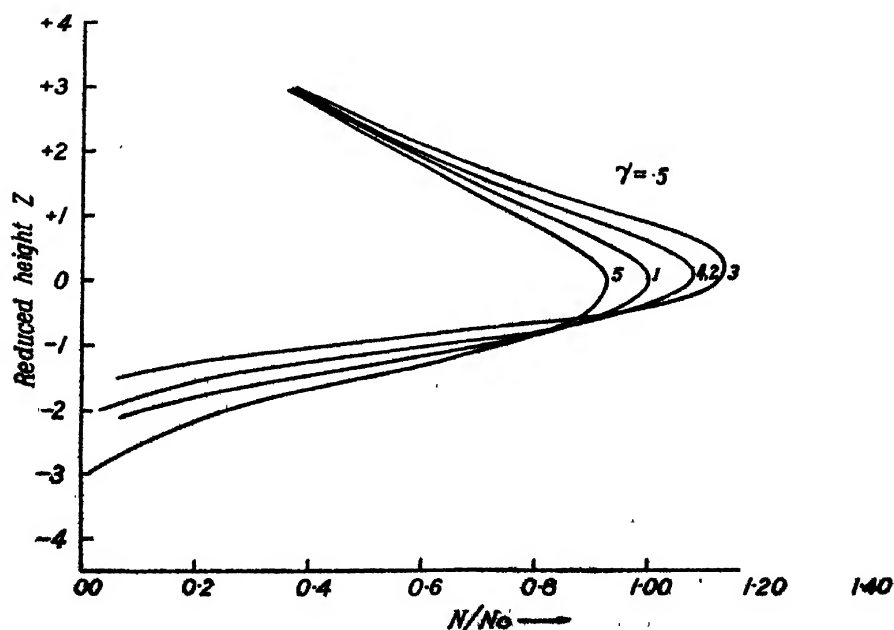


FIG. 4

Variation of  $N/N_0$  with reduced height ( $z$ ) for  $\gamma=0.50$ . Curves 1, 2, 3, 4 and 5 correspond to values of  $t=0, 1, 3, 5$  and 7 hours respectively.

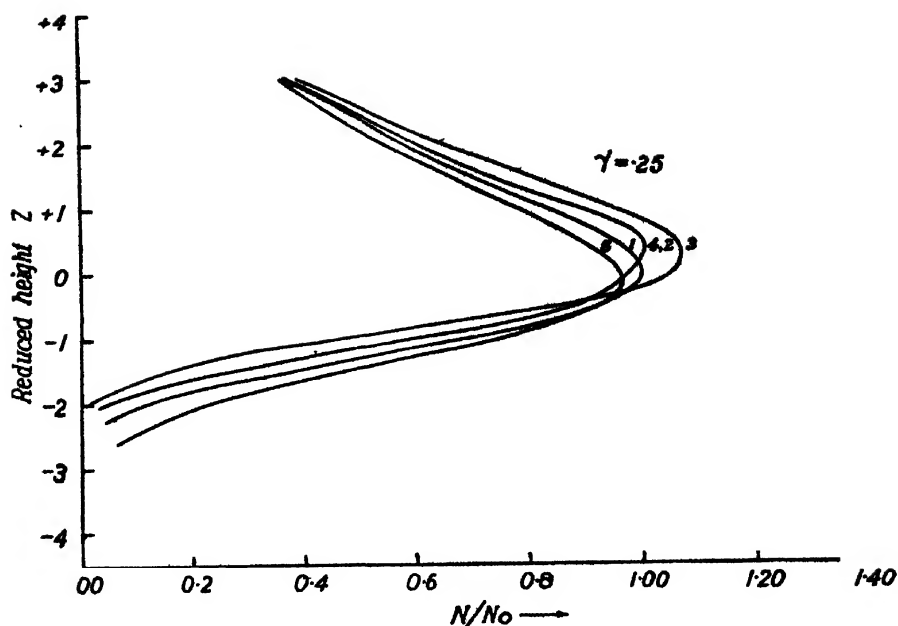


FIG. 5

Variation of  $N/N_0$  with reduced height ( $z$ ) for  $\gamma=0.25$ . Curves 1, 2, 3, 4 and 5 correspond to values of  $t=0, 1, 3, 5$  and 7 hours respectively.

five curves are drawn corresponding to  $t=0, 1, 3, 5$  and 7 hrs. It may be remembered that these curves hold for night-time conditions only.

It will be noticed that the curves change markedly with the change of the value of  $\gamma$ . The notable features of the changes with height and time are summarised below :

(1) The thickness of the region decreases with increasing value of  $\gamma$ . Hence, for very large value of  $\gamma$ , the ionization region is highly compressed (Fig. 1). Further, for any value of  $\gamma$ , the thickness decreases during the first quarter of the period (from  $t=0$  to  $t=3$  hrs.) and then begins to increase. The tendency to increase persists till one hour before the next quarter (up to 7 hrs.).

(2) For all values of  $\gamma$ ,  $N_{\max}$  rises in the first quarter period and then falls. The rise and fall of  $N_{\max}$  are very rapid for large values of  $\gamma$ , but is gradual with small values (Figs. 1, 2, 3, 4, 5). For  $\gamma=0.25$ , variations of  $N_{\max}$  are practically negligible.

(3) The variations in  $h_{\max}$ , unlike those in  $N_{\max}$ , differ in magnitude as well as in sense for different values of  $\gamma$ . For large value of  $\gamma$  (i.e. for  $\gamma=1.5$ ),  $h_{\max}$  falls from 0 to 1 hr., rises from 1 to 3 hrs., falls again from 3 to 5 hrs., and rises again. For low values of  $\gamma$  variations in  $h_{\max}$  are in the reverse order. For intermediate value ( $\gamma=0.5$ ),  $h_{\max}$  remains practically constant throughout the night.

(4) The variations in  $h_{\min}$  differ from those of  $h_{\max}$ . For all values of  $\gamma$ ,  $h_{\min}$  rises from 0 to 3 hrs. and falls steadily afterwards.

It is to be mentioned here that the nature of variation, as obtained for large values of  $\gamma$ , is in agreement with those observed. For example, we may consider the case of a typical low latitude station. Here the drift velocity is maximum negative, i.e.  $\delta = 180^\circ$  at 21 hrs., when  $t = 0$  hr. according to our reckoning.  $N_{\max}$  and  $h_{\min}$  will increase according to our calculation from 21 hrs., become maximum at midnight and will then decrease. This is exactly what is observed of  $N_{\max}$  and  $h_{\min}$  variations. The agreement with the observed  $h_{\max}$  variations is, however, less satisfactory. For this case, the calculated curves give two rises and two falls in course of the night against only one rise and one fall observed.

### CONCLUSION

According to the electrodynamical theory of the tidal effects in the ionosphere, as developed by Martyn, there is marked vertical drift of ions. If the expression for the drift velocity be assumed to be of the form  $v = v_0 e^{-\gamma t} \cos(\omega t + \delta)$ , it is found that the night time Chapman distribution is markedly affected even if electron decay by recombination is taken as negligible. The calculated results generally agree with the observed ones, if the constant in the exponent of the damping term  $\gamma$  is about 1. Better agreement may be obtained if the effect of recombination term, particularly for downward drift velocity, is taken into account.

### ACKNOWLEDGMENTS

The investigations described in the paper were carried out with the help of grants received from the Council of Scientific and Industrial Research, Government of India, and form a part of the programme of the Radio Research Committee. The author feels a pleasure to record his sincere thanks to Dr. S. N. Ghosh for active co-operation in the work. Thanks are also due to Prof. S. K. Mitra for helpful advice in the preparation of the paper.

INSTITUTE OF RADIO PHYSICS AND ELECTRONICS  
UNIVERSITY OF CALCUTTA

### REFERENCES

- Martyn, D. F., 1947a, *Proc. Roy. Soc. A* **189**, 241.
- Martyn, D. F., 1947b, *Proc. Roy. Soc. A* **190**, 273.
- Martyn, D. F., 1949, *Nature*, **163**, 34.
- Report on Tidal Phenomena in the Ionosphere  
(for publication by U.R.S.I., 1950)

# REVERSAL OF POLARISATION OF MICROWAVES FROM SUN-SPOTS

By U. C. GUHA

(Received for publication, November 15, 1950)

**ABSTRACT.** The Zwaan-Kemble method for the calculation of the reflection coefficient of a barrier has been used to obtain the reflection coefficients of the ordinary and the extra-ordinary waves for a parabolic ion barrier. These results have been applied to explain the observed reversal of polarisation of microwaves escaping from sunspots.

## I INTRODUCTION

Different workers at different stations have observed that microwaves received from sun-spots usually consist of a mixture of right-handed and left-handed circularly polarised components. Another characteristic feature observed is that when the sun-spot appears at an edge of the visible solar disc, one of the components is much stronger than the other, that is, the polarisation is almost purely right handed (or left-handed), but as the spot moves near the centre of the solar disc both the components become equally strong and as it disappears at the other edge of the disc the polarisation again becomes roughly pure but of the opposite kind, that is, left-handed (or right-handed). In a paper on the conditions of escape of micro-waves from sun-spots, Saha, Banerjea and Guha (1947) have theoretically shown that the polarisation of the escaping wave should be circular and that the magnetic field of the spot helps in the escape of one of the components. Ryle (1948) has also reached similar conclusions. But the characteristic feature mentioned above, namely, the remarkable change in the relative intensities of the two polarised components, has not been explained. In the present article we shall attempt to explain this feature by calculating the transmission co-efficients of a parabolic ion-barrier in a magnetic field. Since the details of the actually existing conditions in a sun-spot region are likely to be very complicated, the general conclusion reached in sec. VII has only qualitative significance; we have, therefore, based our treatment only on simple assumptions which nevertheless take account of the essential characteristics of the problem.

## II WAVE EQUATIONS

For plane electromagnetic waves travelling in the direction of the concentration gradient of a non-homogeneous friction-free ionosphere, the following differential equations hold (Saha, Banerjea and Guha, 1947).

(A) Transverse case :

$$\frac{d^2 E_x}{dz^2} + \frac{p^2}{c^2} (1 - r) E_x = 0 \quad (\text{ordinary wave}) \quad (2.1)$$

$$\frac{d^2 E_y}{dz^2} + \frac{p^2}{c^2} \left( 1 - \frac{r}{1 - \frac{r}{\omega^2}} \right) E_y = 0 \quad (\text{extraordinary wave}) \quad (2.2)$$

(B). Longitudinal case :  $\frac{d^2}{dZ^2} (E_x \pm iE_y) + \frac{p^2}{c^2} \left( 1 - \frac{r}{1 \pm \omega} \right) (E_x \pm iE_y) = 0 \dots (2.3)$

where  $(E_x, E_y)e^{ipt}$  = components of the electric vector,  $p$  being the pulsance  
 $z$  = distance measured along the direction of propagation

$$r = \frac{4\pi N e^2}{m p^2}$$

$N$  = ion density

$e$  and  $m$  = charge and mass of the electron

$$\omega = \frac{p_h}{p}, \quad p_h = \frac{eH}{mc}$$

$H$  = strength of the external magnetic field.

### III PARABOLIC LAYER

If the ion-barrier is parabolic with half width  $l$ , that is, if

$$N = N_m \left( 1 - \frac{z^2}{l^2} \right), \quad [\text{see Fig. I.}]$$

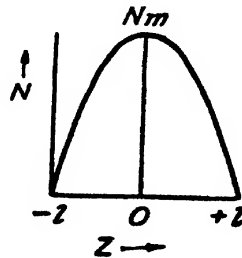


FIG. I

then equations (2.1) and (2.2) respectively reduce to

$$\phi'' + K^2 (z^2 - a^2) \phi = 0 \quad (3.1)$$

and

$$\phi'' + K^2 \frac{(z^2 - b^2)(z^2 - c^2)}{Z^2 - d^2} \phi = 0 \quad \dots (3.2)^*$$

\*. This equation for the extra-ordinary wave was given to the author by Prof. M. N. Saha. It does not appear to have been discussed by any previous worker.

where  $K^2 = \frac{p_0^2}{c^2 l^2}$ ,  $a^2 = \left(1 - \frac{p^2}{p_0^2}\right) l^2$ ,  $b^2 = \left(1 - \frac{p^2}{p_0^2} + \frac{p p_h}{p_0^2}\right) l^2$ ,  
 $c^2 = \left(1 - \frac{p^2}{p_0^2} - \frac{p p_h}{p_0^2}\right) l^2$ ,  $d^2 = \left(1 + \frac{p_h^2}{p^2} - \frac{p^2}{p_0^2}\right) l^2$ ,

$p_0$  = critical pulsance of the ordinary wave.

We shall now calculate the transmission coefficients of the barrier for waves satisfying equations (3.1) & (3.2) respectively. It will be at once noticed that this problem is similar to the quantum-mechanical problem of calculating the transmission coefficient of a potential barrier for matter waves, which, as is well known, has been tackled by different workers in different ways, sometimes yielding different results for the same problem. We shall here adopt a method used by Kemble (1935) but with different approximating functions in place of the B.W.K. approximations used by him. This simplifies the calculations in our case, but to be more sure about the validity of our method, we shall also calculate the transmission coefficient of the ordinary wave in an alternative way. It is assumed that the width of the barrier is sufficiently large for the application of the following methods.

#### IV TRANSVERSE CASE (Ordinary wave)

##### (A) Kemble's method:

Taking equation (3.1) we consider asymptotic representations of  $\phi(z)$  of the form  $z^\sigma e^{P(z)}$  where  $\sigma$  is a constant and  $P(z)$  a polynomial in  $z$ . These are found to be

$$\left. \begin{aligned} f_1(z) &= e^{\frac{1}{2}iKz^2} z^{-\frac{1}{2} - iKa/2} \\ f_2(z) &= e^{-\frac{1}{2}iKz^2} z^{-\frac{1}{2} + iKa/2} \end{aligned} \right\} \dots (4.1)$$

and

The differential equations (in the normal form) satisfied by these functions are

$$\begin{aligned} f_1'' + \left[ K^2(z^2 - a^2) - \frac{\sigma_1(\sigma_1 - 1)}{z^2} \right] f_1 &= 0, \text{ where } \sigma_1 = -\frac{1}{2} - iKa^2 \\ \text{and } f_2'' + \left[ K^2(z^2 - a^2) - \frac{\sigma_2(\sigma_2 - 1)}{z^2} \right] f_2 &= 0, \text{ where } \sigma_2 = -\frac{1}{2} + \frac{iKa^2}{2} \end{aligned} \dots (4.2)$$

Hence  $f_1$  and  $f_2$  will give good approximation for  $\phi$  whenever  $z$  is large. We now propose to fit the linear combination  $a_1(z)f_1(z) + a_2(z)f_2(z)$  to an exact solution  $\phi(z)$  of the equation (3.1), so that we take

$$\left. \begin{aligned} a_1(z)f_1(z) + a_2(z)f_2(z) &= \phi(z) \\ a_1(z)f_1'(z) + a_2(z)f_2'(z) &= \phi'(z) \end{aligned} \right\} \dots (4.3)$$



Solving these equations for  $a_1(z)$  and  $a_2(z)$ , we obtain

$$a_1(z) = \frac{1}{-2iK + \frac{iKa^2}{z}} (\phi f_2' - \phi' f_2)$$

$$\approx \frac{i}{2K} (\phi f_2' - \phi' f_2) \text{ for large } |z|$$

$$\frac{da_1}{dK} \approx \frac{i}{2K} (\phi f_2'' - \phi'' f_2)$$

$$= \frac{i}{2K} \frac{\sigma_2(\sigma_2 - 1)}{z^2} \phi f_2 \text{ from (3.1) and (4.2)}$$

$$= \frac{i\sigma_2(\sigma_2 - 1)}{2Kz^2} \left( \frac{a_1}{z} + \frac{e^{-iKz^2}}{1 - iKa^2} a_2 \right) \text{ from } \phi = a_1 f_1 + a_2 f_2 \text{ and equation (4.1)}$$

Hence 
$$\left| \frac{da_1}{dz} \right| \leq \frac{A_1}{|z|^3} \left[ E_1 |a_1| + |e^{-iKz^2}| |a_2| \right] \quad \dots (4.4)$$

where  $A_1$  and  $B_1$  are positive constants of the problem.

Similarly 
$$\left| \frac{da_2}{dz} \right| \leq \frac{A_2}{|z|^3} \left[ B_2 |a_2| + |e^{iKz^2}| |a_1| \right] \quad \dots (4.5)$$

We notice that on both sides of the barrier  $f_1(z)$  and  $f_2(z)$  respectively represent waves entering and leaving the barrier. Now consider a path  $\Gamma$  in the lower half of the complex  $z$ -plane (Fig. 2), starting at  $+l$ , the right hand end of the barrier and terminating at  $-l$  the left hand end, such that  $|z|$  always remains large on  $\Gamma$ . Now, supposing that waves are incident on the left hand side of the barrier and transmitted through the right hand side, we put  $a_1 = 0$  and  $a_2 = 1$  at  $z = +l$ . From equation (4.4) it follows that



FIG. 2

throughout the first half of the path  $\Gamma$  (i.e. the portion in the 4th quadrant)  $a_1$  remains practically constant (i.e.  $a_1 = 0$ ). Since  $a_1 = 0$  in this portion of the path it follows from equation (4.5) that  $a_2$  also remains constant (i.e.  $a_2 = 1$ ). These equations also show that  $a_2$  remains constant throughout the rest of the path but  $a_1$  may change. Thus, at  $z = -l$  we have  $a_1 = c$ , say, and  $a_2 = 1$ . Hence we have established a connection formula  $f_2 + cf_1 \leftarrow f_2$

where

$$\left. \begin{aligned} f_2(+l) &= e^{-\frac{1}{2}iKl^2} l^{-\frac{1}{2} + \frac{1}{2}iKa^2} \\ f_2(-l) &= i \cdot e^{-\frac{1}{2}iKl^2} l^{-\frac{1}{2} + \frac{1}{2}iKa^2} e^{\frac{1}{2}\pi Ka^2} \\ f_1(-l) &= i \cdot e^{\frac{1}{2}iKl^2} l^{-\frac{1}{2} - \frac{1}{2}iKa^2} e^{-\frac{1}{2}\pi Ka^2} \end{aligned} \right\} \quad \dots (4.6)$$

and

Since damping has been neglected, we have

$$|c|^2 |f_1(-l)|^2 = |f_2(l)|^2 + |f_2(-l)|^2$$

$$\therefore |c|^2 = \frac{1 + e^{\pi K a^2}}{e^{-\pi K a^2}} \quad \text{using (4.6)}$$

If  $T_0$  denotes the transmission coefficient, then

$$T_0^2 = \left| \frac{f_2(+l)}{c f_1(-l)} \right|^2$$

$$= \frac{1}{1 + e^{\pi K a^2}} = \frac{1}{1 + e^{\pi K l^2 (1 - p^2/p_0^2)}} \quad \dots (4.7)$$

(B) *Alternative method :*

We look for a solution  $\phi(z)$  of the differential equation (3.1) behaving asymptotically as follows :

$$\phi(z) \sim \psi_3(z) \text{ in the neighbourhood of } z = +l$$

$$\text{and } \phi(z) \sim \psi_1(z) + \psi_2(z) \quad , , \quad , , \quad z = -l,$$

where  $\psi_2$  and  $\psi_3$  both represent waves leaving the barrier, and  $\psi_1$  represents waves entering the barrier, so that

$$\psi_1(z) \text{ represents the incident wave}$$

$$\psi_2(z) \quad , , \quad , , \quad \text{reflected wave}$$

$$\text{and } \psi_3(z) \quad , , \quad , , \quad \text{transmitted wave}$$

The reflection coefficient  $R_0$  will therefore be given by  $\left| \frac{\psi_2(z)}{\psi_1(z)} \right|$

Change the independent variable in equation (3.1) from  $z$  to  $\xi$  where

$$\xi = \sqrt{2K} e^{i\pi/4} z \text{ and put } n = \frac{iK a^2}{2} - \frac{1}{2}. \quad \text{We get}$$

$$\frac{d^2 \phi}{d\xi^2} + \left( n + \frac{1}{2} - \frac{\xi^2}{4} \right) \phi = 0 \quad \dots (4.8)$$

Moreover,  $\arg \xi = \frac{\pi}{4}$  for  $z$  real and positive

and  $= -\frac{3\pi}{4}$  for  $z$  real and negative.

The differential equation (4.8) is known as Weber's equation. From the properties of its solution  $D_n(\xi)$  discussed in Whittaker and Watson's book on Modern analysis (pp. 347-349) we get

for  $\arg \xi = \frac{\pi}{4}$ ,  $D_n(\xi) \approx e^{-\xi^2/4} \xi^n$  (transmitted wave)

and for  $\arg \xi = -\frac{3\pi}{4}$ ,  $D_n(\xi) \approx e^{-\xi^2/4} \xi^n$  (reflected wave)

$$+ \frac{\sqrt{2\pi}}{\Gamma(-n)} e^{-n\pi i} e^{\xi^2/4} \xi^{-n-1} \text{ (incident wave)}$$

Hence, from the remarks made above, it follows that

$$\begin{aligned} R_0 &= \left| \frac{e^{-\xi^2/4} \xi^n}{\frac{\sqrt{2\pi}}{\Gamma(-n)} e^{-n\pi i} e^{\xi^2/4} \xi^{-n-1}} \right| \\ &= \frac{1}{\sqrt{2\pi}} \left| \Gamma(-n) e^{-\xi^2/4} \xi^{2n+1} e^{n\pi i} \right| \\ &= \frac{e^{\pi K a^2/4}}{\sqrt{2\pi}} \left| \Gamma \left( -\frac{iKa^2}{2} + \frac{1}{2} \right) \right| \\ &= \frac{e^{\pi K a^2/4}}{\sqrt{2 \cosh \pi K a^2/2}} \end{aligned}$$

$\therefore$

$$\begin{aligned} T_0^2 &= 1 - R_0^2 \\ &= \frac{1}{1 + e^{\pi K a^2}} \\ &= \frac{1}{1 + e^{\pi K l^2 (1 - p^2/p_0^2)}} \end{aligned}$$

which is the same as equation (4.7).

#### V. TRANSVERSE CASE (Extra-ordinary wave)

Taking equation (3.2) and adopting method (A) of sec. IV, we find that in this case the asymptotic representations of  $\phi(z)$  are

$$f_1(z) = e^{\frac{iKz^2}{2} z^{-\frac{1}{2}} - iK(b^2 + c^2 - d^2)}$$

and

$$f_2(z) = e^{-\frac{iKz^2}{2} z^{-\frac{1}{2}} + iK(b^2 + c^2 - d^2)}$$

In this case also it can be easily shown that the coefficient function occurring in equation (3.2) differs from the coefficient functions occurring in the differential equations (in the normal form) satisfied by  $f_1(z)$  and  $f_2(z)$  by terms of the order of  $1/z^2$ . Hence, the method applied in (A) of sec IV., can be adopted here without any alteration. Thus, if  $T_e$  denotes the transmission coefficient in this case, then

$$T_e^2 = \frac{1}{1 + e^{\pi K(b^2 + c^2 - d^2)}}$$

$$T_e^2 = \frac{1}{1 + e^{\pi K \left(1 - \frac{p^2}{p_0^2} - \frac{p_h^2}{p_0^2}\right)}} \quad \dots (5.1)$$

$$\approx 1$$

for large  $p_h$ , that is for large magnetic field.

Had we assumed that the magnetic field also varies parabolically, so that  $H = H_m \left(1 - \frac{z^2}{l'^2}\right)$ , say, then in place of equation (3.2) we would have obtained

$$\phi'' + K^2 \frac{(z^2 - a'^2)(z^2 - b'^2)}{(z^2 - c'^2)(z^2 - d'^2)} \phi = 0 \quad \dots (5.2)$$

This gives

$$T_e^2 = 1.$$

Thus when the magnetic field is large and constant, or when it varies as above, the barrier is almost transparent to the extra-ordinary wave.

## VI. LONGITUDINAL CASE

If we consider a parabolic ion-barrier  $N = N_m \left(1 - \frac{z^2}{l^2}\right)$  and a large constant magnetic field so that,  $\omega \gg 1$ , then equation (2.3) gives two circularly polarised waves of opposite senses determined by equations of the type

$$\phi_1'' + K^2(z^2 - a^2)\phi_1 = 0 \quad \dots (6.1)$$

and

$$\phi_2'' - K^2(z^2 - a^2)\phi_2 = 0 \quad \dots (6.2)$$

Since the disturbance satisfying equation (6.2) has no wave character for  $|z| > a$ , it can not leak through the barrier as a wave. Hence, only the component satisfying equation (6.1) leaks through the barrier with a certain transmission coefficient.

But if we assumed a parabolic variation for the magnetic field as well, so that  $H = H_m \left(1 - \frac{z^2}{l'^2}\right)$ , then we would have obtained in place of the equations (6.1) and (6.2) the equations

$$\phi_1'' + K^2 \frac{(z^2 - a^2)}{(z^2 - b^2)} \phi_1 = 0 \quad \dots (6.3)$$

and

$$\phi_2'' + K^2 \frac{(z^2 - a'^2)}{(z^2 - b'^2)} \phi_2 = 0 \quad \dots (6.4)$$

The equations (6.3) and (6.4) are easily seen, by the methods already discussed, to give values of the transmission coefficients

$$\begin{aligned} \text{as} & \quad T_1^2 = 1 \\ \text{and} & \quad T_2^2 = 1 \end{aligned} \quad \dots (6.5)$$

The assumed variation of the magnetic field thus makes the barrier equally transparent to both the circularly polarised components.

## VII. MICROWAVES FROM SUNSPOTS

Now consider a sunspot  $S$  moving along the central equator from one edge of the visible solar disc to the other edge. Consider the plane containing spot  $S$  the direction  $SE$  towards the earth and the normal  $SN$  to the sun's surface at  $S$  (Fig. 3), and suppose that projected on this plane the

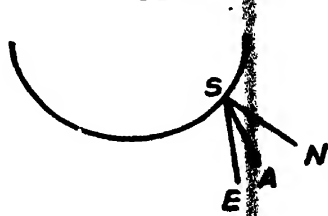


FIG. 3

positive direction of the magnetic lines of force make on the average a mean angle  $\alpha$  ( $\angle NSA$ ) with the positive direction of  $SN$ . Then it follows that the angle  $\theta$  between the direction of propagation of the microwaves towards the earth and the positive direction of the magnetic lines of force

varies in magnitude from  $\left| \frac{\pi}{2} - \alpha \right|$  to  $\frac{\pi}{2} + \alpha$ . The cases  $\theta = 0$ ,  $< \frac{\pi}{2}$ ,  $= \frac{\pi}{2}$ ,  $> \frac{\pi}{2}$ ,  $= \pi$

correspond respectively to south pole, southern hemisphere, equator, northern hemisphere, north pole (in the language of propagation in the earth's ionosphere). Hence, the propagation of the microwaves through the ionosphere of the spot, as the latter moves from one edge of the solar disc to the other edge, has one-to-one correspondence with propagation of radio waves through the earth's ionosphere when the source on the earth traverses an angle  $\pi$  along a meridian from a point  $P$  to a point  $Q$ , say.

From Secs. IV and V it follows that when this propagation becomes transverse,  $T_1^2 \simeq 1$  and is much greater than  $T_2^2$ , so that one of the polarised components is much stronger than the other, whereas when the propagation becomes longitudinal, we have  $T_1^2 = T_2^2 = 1$  from equation (6.5), so that the two polarised components are equally strong. It is natural to expect that similar results will hold for the quasi-transverse and the quasi-longitudinal cases. This gives the reason for the change in the relative intensities of the two polarised components mentioned in sec. I. The reversal of the senses of polarisation of the two components obviously depends upon the angle  $\alpha$ , because the senses of polarisation of the two components are opposite in the two hemispheres.

For example, in the case of a uni-polar spot we may take  $\alpha = 0$  or  $\pi$ , so that the path on the meridian from  $P$  to  $Q$  lies on the same hemisphere and there should therefore be no reversal of the sense of polarisation. On the other hand if the spot is a member of a bi-polar spot group, then  $\alpha$  should be different from 0 and  $\pi$ , so that  $P$  and  $Q$  lie in different

hemispheres. Hence, there will be a reversal of the senses of polarisation, the actual duration through which the stronger component remains left-handed or right-handed depending upon the actual value of  $\alpha$ .

#### ACKNOWLEDGMENTS

The author is greatly indebted to Prof. M. N. Saha F.R.S., for his constant interest and encouragement in the work. This paper forms a part of the work done in the scheme "Theoretical Investigations of the Upper Atmosphere" financed by the Council of Scientific and Industrial Research (India), and the author wishes to thank the Council for providing necessary facilities for research work.

INSTITUTE ON NUCLEAR PHYSICS  
UNIVERSITY OF CALCUTTA

#### REFERENCES

- Kemble, 1935, *Phy. Rev.*, **48**, 549.  
Ryle, 1948, *Proc. Roy. Soc.*, **195**, 82.  
Saha, Banerjee and Guha, 1947, *Ind. J. Phy.*, **21**, 199.  
" " " 1947, " " " **21**, 181.

## ULTRASONIC STUDIES OF GELS

By ARVIND MOHAN SRIVASTAVA

*(Received for publication, August, 18, 1950)*

**ABSTRACT.** Using an ultrasonic pulse technique the elasticities of gels have been obtained at four ultrasonic frequencies. In this paper the effect of temperature and age on the iron silicate gels has been studied. A brief discussion outlines the probable structure and mechanism of gel formation, maintaining that the ultimate units in a gel are groups of atoms producing an interlinked fibrous structure perfectly randomly oriented.

In a series of papers the author has initiated a line of inquiry and study of the gelatinous state of matter quite new to the colloid chemists. The use of an ultrasonic pulse method (Srivastava, 1949) has been made to determine the elastic constants of four gels. In another paper the author (Srivastava, 1950) deals with the effect of temperature and frequency on the elasticities of a certain iron silicate gel. At that time no tentative theory was advanced regarding the mechanism or its structure. Thorium phosphate gel was studied by Prakash, Mehra and Srivastava (1950) in a similar manner.

The importance of this study is great since the information available so far is meagre and this field of inquiry had been almost completely ignored in the past. Furthermore, it is expected that the behaviour of elastic forces on gels will afford a better insight into these problems.

The method consists of a suitable ultrasonic pulse generator which supplies a beam of ultrasonic energy that impinges on a block of gel held vertically supported by a metallic frame immersed in a liquid bath. The slab is capable of rotation in a vertical plane thereby changing the angle of incidence of the beam. Since the velocity in the gel is greater than that in the liquid, the wave-trains are refracted away from the normal. Consequently the rotation of the block results in a vanishing of the emergent rays due to total reflection. The waves in the gel take up two velocities depending upon the two associated deformations of shear and longitudinal extension. The amplitude of the transmitted waves therefore shows two minimum and if  $V_s$  and  $V_l$  are the two velocities then we have

$$V_s = \sqrt{\frac{S}{\rho}}$$

$$V_l = \sqrt{\frac{(1-\sigma)E}{(1+\sigma)(1-2\sigma)\rho}}$$

where  $\rho$  is the density of the gel,  $E$  and  $S$  are the moduli of elongation and shear. If  $V_x$  is the velocity in the tank liquid, which is usually water, then

$$V_l = V_x / \sin \theta_1$$

$$V_s = V_x / \sin \theta_2.$$

from which  $V_l$  and  $V_s$  can be known. Then from the well known relations

$$E = 2(\tau + \sigma)S$$

and,

$$\sigma = \frac{(V_l/V_s)^2 - 2}{2[(V_l/V_s)^2 - 1]}$$

all the elastic constants can be calculated.

In the accompanying figures the variation of Young's modulus with temperature, age and frequency have been shown. A set of values for the velocity have been also shown in Fig. 2. The two dips in the transmitted wave amplitude are seen in Fig. 4. A detailed account of these can be seen in the author's other papers (Srivastava, 1950).

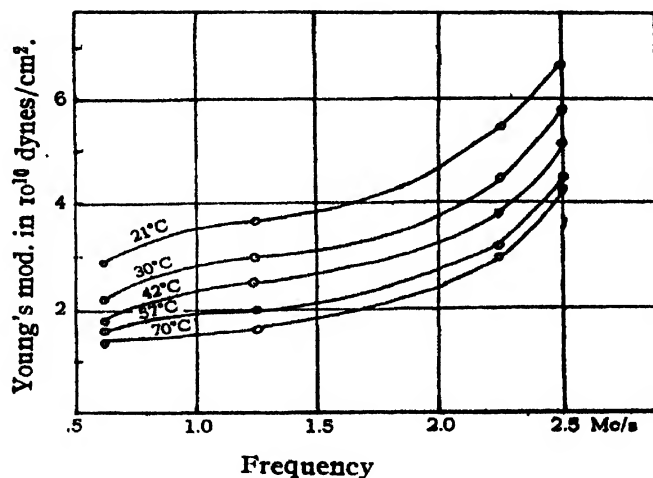


FIG. 1  
Variation of Young's modulus with frequency  
and temperature

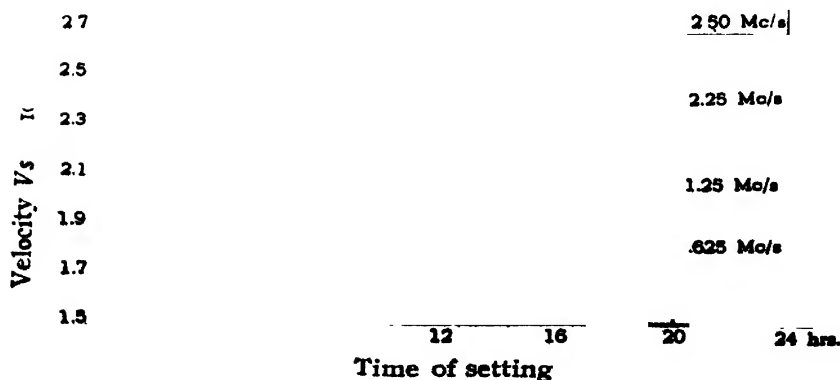


FIG. 2  
The shear wave velocity attaining a constant value after  
twelve hours for the 4 frequencies at 30°C



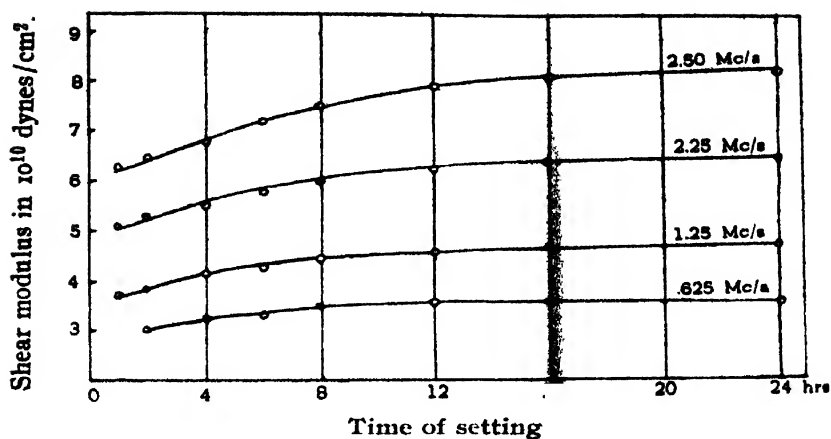


FIG 3

Variation of shear modulus with the time of setting for four frequencies at 30°C

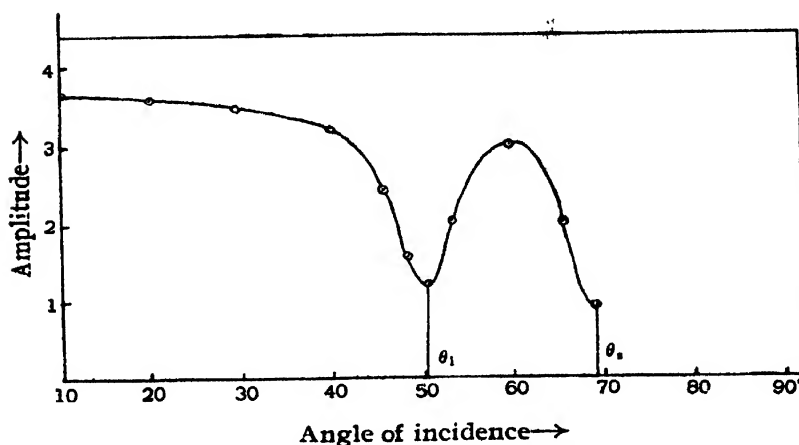


FIG. 4

Variation of amplitude of transmitted waves on altering the angle of incidence for one observation of  $\theta_1$  and  $\theta_2$ .

Though still far from advancing a theory on the exact nature of the mechanism of gel formation and its structure the author, however, has drawn the following conclusions from the data published here and elsewhere (Srivastava, 1950):

The resistance to elastic forces implies that the units in a gel are themselves capable of a similar behaviour. These units, therefore, themselves cannot be atoms; for then larger forces would be required to cause these elongations and shears. The forces required to increase the distance between the adjacent atoms would be comparatively far in excess over that for which the author has accounted in his investigations. It follows, therefore, that the structure should be of the form of groups of atoms to account for the observed elasticities. The elastic processes therefore suggest the following factors.

(a) Groups of atoms producing strong and flexible units:

(b) The forces of cohesion around these fibres must be weak and uniform to account for the changes in state at higher temperatures.

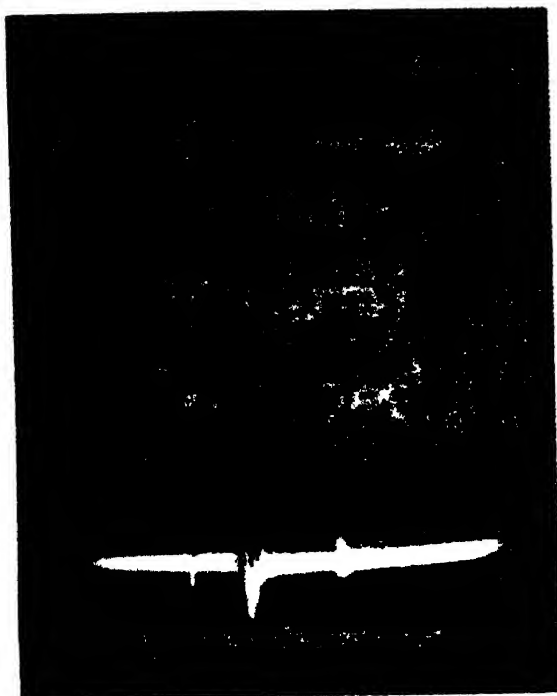


FIG. 5

The oscillogram  
The central vertical displacement being the  
transmitted wave

(c) An interweaving of the fibres in the three dimensional lattices to account for the looseness of the entire structure.

(d) And a perfectly random orientation of the fibres to account for the lack of any anisotropy in the gels studied.

It is clear that the water enmeshed in overwhelmingly large proportions in a gel is chiefly due to the interlacing of the fibres in a three dimensional framework which leaves enough free space for water. Further work is in progress in this laboratory to elucidate these processes more generally.

#### ACKNOWLEDGMENTS

In conclusion the author takes this opportunity to thank Dr. R. N, Ghosh for his help in the development of the technique and to Mr. Ravindra Kumar for his help in calculating the results.

DEPARTMENT OF PHYSICS,  
UNIVERSITY OF ALLAHABAD,  
ALLAHABAD, INDIA.

#### REFERENCES

- Srivastava, A. M. 1949, *Proc Nat. Acad. Sc.*, **18A**, 50.  
 Srivastava A. M. 1950, *Comptes Rendus.*, **22**, 1223.  
 Prakash, S, Mehra, Y and Srivastava, A.M., 1950, *J. Phy. Chem.* (Under publication).  
 Srivastava, A.M., 1950, *J Amer. Chem. Soc.* (Under print).  
 Srivastava, A.M., 1950, *Koll. Zett*, **119**, 3.  
 „ „ 1950, *Zetts. F. Phy.*, **128**, 614.

# LIGHT SCATTERING IN GASES

## (A Note)

By S. PARTHASARATHY

(Received for publication, August 21, 1950)

**ABSTRACT.** The note gives depolarisation factors for a large number of gases after due correction of the earlier values obtained by the author, for the convergence of the lens used.

In a paper on the relation between light scattering and molecular structures, published several years ago, the author (Parthasarathy, 1932) gave factors of depolarisation only as measured, leaving out of account the error due to convergence of the beam, as there were differences of opinion then (Gans, 1927 ; Rao, 1927) on this subject. It is fairly well-established now that corrections have to be made for such convergence of the beam and when the values in the author's earlier paper were corrected for convergence, the data given in the present note would be obtained.

The author (Parthasarathy, 1932) mentioned that the lens used was of focal length 12" and diameter 3". The convergence correction due to this alone would be 0.77 %. But the apertures were placed in all the arms to avoid reflection from the inner portion of the tube. The aperture nearer the glass window of the arm through which light was focused, cut off light still further and the final correction came to nearly 0.5 %. Table I gives the values of depolarisation factors for the gases after due correction for convergence has been made.

TABLE I

Substance	Chemical formula	Corrected values %
<b>Organic</b>		
Methane from cylinder and corrected	CH <sub>4</sub>	0.64
Pure gas ... ..		0.62
Ethane ... ..	C <sub>2</sub> H <sub>6</sub>	0.80
Propane ... ..	C <sub>3</sub> H <sub>8</sub>	1.01
Butane ... ..	C <sub>4</sub> H <sub>10</sub>	1.01
Isobutane ... ..	C <sub>4</sub> H <sub>10</sub>	0.53
Ethylene ... ..	C <sub>2</sub> H <sub>4</sub>	2.42
Acetylene ... ..	C <sub>2</sub> H <sub>2</sub>	4.02
Methyl chloride ... ..	CH <sub>3</sub> Cl	1.54
Methylene chloride ... ..	CH <sub>2</sub> Cl <sub>2</sub>	2.43
Chloroform ... ..	CHCl <sub>3</sub>	1.28
Carbon tetrachloride ... ..	CCl <sub>4</sub>	0.12

TABLE I (contd.)

Substance	Chemical formula	Corrected values %
<b>Organic (continued)</b>		
Methylamine ... ..	$\text{CH}_3\text{NH}_2$	0.27
Ethylamine ... ..	$\text{C}_2\text{H}_5\text{NH}_2$	0.47
Formaldehyde ... ..	$\text{H}\cdot\text{CHO}$	1.38
Acetaldehyde ... ..	$\text{CH}_3\cdot\text{CHO}$	2.18
Methyl ether ... ..	$\text{CH}_3\cdot\text{O}\cdot\text{CH}_3$	1.06
Ethyl ether ... ..	$\text{C}_2\text{H}_5\cdot\text{O}\cdot\text{C}_2\text{H}_5$	2.01
Acetone ... ..	$\text{CH}_3\cdot\text{CO}\cdot\text{CH}_3$	1.12
Allyl alcohol ... ..	$\text{CH}_2\cdot\text{CH}\cdot\text{CH}_2\text{OH}$	1.90
<b>Inorganic gases,</b>		
Air ... ..	...	3.65
Oxygen ... ..	$\text{O}_2$	6.00
Nitrogen ... ..	$\text{N}_2$	3.05
Hydrogen (from cylinder and corrected)	$\text{H}_2$	2.21
Pure gas ... ..	...	2.07
Chlorine ... ..	$\text{Cl}_2$	3.57
Carbon dioxide ... ..	$\text{CO}_2$	9.22
Nitrous oxide ... ..	$\text{N}_2\text{O}$	11.97
Hydrochloric acid gas ... ..	$\text{HCl}$	0.21
Hydrobromic acid gas ... ..	$\text{HBr}$	0.34
Hydriodic acid gas ... ..	$\text{HI}$	0.77
Nitric oxide (gas by both methods)	$\text{NO}$	2.18
Carbon monoxide ... ..	$\text{CO}$	0.80
Ammonia ... ..	$\text{NH}_3$	0.48
Hydrogen sulphide ... ..	$\text{H}_2\text{S}$	0.43
Sulphur dioxide ... ..	$\text{SO}_2$	2.61
Carbonyl sulphide ... ..	$\text{COS}$	8.27
Silicon tetrachloride ... ..	$\text{SiCl}_4$	1.14
Silicon tetrafluoride ... ..	$\text{SiF}_4$	2.61

TABLE I (contd.)

Substance	Chemical formula	Corrected values %
<b>Inorganic gases (Contd.)</b>		
Argon (uncorrected for impurities)	A	0.21
(corrected for impurities)	...	0.06
Helium ... ..	He	2.50

The main conclusions, after correction, may be stated as below :

(1) The anisotropy for argon (and possibly for other rare gases also) vanishes and the structure is therefore in conformity with evidence adduced by other methods.

(2) The optical anisotropy for  $\text{CCl}_4$  vapour is vanishingly small, while

for  $\text{CH}_4$  the depolarisation has a definite, though low, value of 0.62%. This does not mean anything, taken apart from other tetrahedral molecules, as the value is too low to be taken as a factor indicative of the optical anisotropy, but considering that even other molecules of  $\text{RX}_4$  type, e.g.  $\text{SiCl}_4$ ,  $\text{SiF}_4$ , show greater depolarisation ( $\rho$ ), this calls for an explanation. The author's observation, that with relative sizes of R and X atoms, the factor  $\rho$  increases or decreases still holds good and it should be pointed out that, apart from the fact that  $\rho$  arises from mere geometry of form, there must also be some other factor which gives rise to it. To say that it might arise from the bigness of the molecules is out of the question, as the molecule itself is very small compared with the wave-length of light used, but the reason is to be sought elsewhere.

The above observations are further supported by Bhagavantam (1932) who studied the Raman effect in molecules of this type. He finds that the symmetrical vibration in such type of molecules is polarised to different extent in the following series of liquids, in addition to there being rotational wings accompanying the Rayleigh line :

Liquids	Raman frequency $\Delta\nu$	$\rho$
$\text{CCl}_4$	459	4 %
$\text{SiCl}_4$	426	11 %
$\text{TiCl}_4$	382	12 %
$\text{SnCl}_4$	367	16 %

Here the central atom increases in size, keeping X constant, in this series of liquids and such variations in  $\rho$  as between 4 % should certainly be genuine.

(3) Other conclusions arrived at in the paper remain valid, as the correction of 0.77 % is a constant factor throughout. These have been borne out by the later work of Ananthakrishnan (1935).

Regarding the experimental details, the author had always thought it a good plan to avoid errors, as far as practicable, rather than allow them to creep in, later on, making suitable corrections which are always uncertain. On that point, the author's experimental arrangement was superior to that of Ananthakrishnan (1935) who used glass windows fused on to the arms of the cross-tube: there is no meaning in saying that the glass pieces were examined for strain *previous to fusing them* on to the cross-tube, since after fusing they are more likely to develop strains. Further, Ananthakrishnan's cross-tube was definitely of smaller dimensions.

The above considerations show that the author's results were not in the least vitiated by such of the above errors, and still hold good.

NATIONAL PHYSICAL LABORATORY OF INDIA,  
NEW DELHI.

#### REFERENCES

- Ananthakrishnan, R., 1935, *Proc. Ind. Acad. Sci.*, **2**, 153.  
Bhagavantam, S, 1932, *Ind. Jour Phys.*, **7**, 84.  
Gans, R., 1927, *Phys. Zeit.*, **28**, 661  
Parthasarathy, S., 1932, *Ind Jour. Phys.*, **7**, 139.  
Rao, I. R., 1927, *Ind. Jour. Phys.*, **2**, 72.

# ON THE ABSORPTION OF U.H.F. RADIO WAVES BY SOME ALIPHATIC KETONES\*

By S. N. SEN

(Received for publication, December 16, 1950).

**ABSTRACT.** The absorption of U.H.F. radio waves by diethyl ketone, dinormal propyl ketone and ethyl isobutyl ketone at temperatures varying from 0°C to 95°C has been investigated in the region 250–510 Mc/sec. by the optical method. An absorption maximum has been observed in each case and in the first two cases the height of the absorption peak increases with the lowering of temperature. In the case of isobutyl ketone also, the height of the absorption peak increases with lowering of temperature from 90°C to 62°C, and with further lowering of temperature to 30°C the height of the peak increases only slightly, but the width of the band increases enormously.

The centres of the absorption peaks observed in the case of the three liquids mentioned above at 30°C are at 330, 295 and 250 Mc/sec. respectively. The absorption coefficient, calculated at the centre of the band observed at 30°C, is of the same order of magnitude in all the cases as that calculated on Debye's theory. The results have been discussed in the light of the hypothesis put forward earlier by Sirkar and Sen that the permanent electric moment of the molecule is affected by the intermolecular field as the molecule executes rotatory oscillation in the liquid.

## INTRODUCTION

In continuation of the previous work by the author (Sen, 1949, 1950) the study of the absorption of the ultra high frequency radio-waves in higher ketones namely, diethyl ketone, dinormal propyl ketone and ethyl-isobutyl ketone has been made at different temperatures ranging from 0°C to 95°C in all the three cases. The results further verify the hypothesis put forward by Sirkar and Sen (1949) and Sen (1949) regarding the absorption of ultra high frequency electrical oscillations in polar liquids. In that theory, it was assumed that, an extra oscillating part of the dipole moment might be created by the intermolecular field in a liquid having polar molecules, if the molecule would be executing damped oscillations in the liquid due to thermal motion and such oscillations would be excited strongly by radio waves of suitable frequency passing through the liquid. The frequency of such oscillations can be deduced from the frequency of radio waves in the region of absorption peaks. If this hypothesis be true, the effect of intermolecular field would increase at lower temperatures and hence the magnitude of the absorption of electric waves would also increase with the lowering of temperature of the liquid. On the other hand, the molecules would tend to orient themselves at random at higher temperatures making thereby the absorption peak broad.

\* Communicated by Prof. S. C. Sirkar.

In a previous paper (Sen, 1949) it was reported that in the case of acetone the results agreed with the hypothesis mentioned above and in case of methyl-ethyl ketone it was found that the intensity of absorption increases with the lowering of temperature of the liquid upto about 30°C, but the maximum absorption diminishes at still lower temperatures. In order to investigate whether this anomaly is connected with the nature of the alkyl groups in the ketone molecules the present investigation was undertaken.

#### EXPERIMENTAL

The experimental arrangement used in these experiments has been described completely in two previous papers (Sen, 1949, 1950). All the liquids were chemically pure and each was distilled in vacuum three or four times before they were used for taking observations. The experimental arrangement used to study the absorption at different temperatures was as follows: The cell containing the liquid was placed in the water bath which could be kept at different temperatures. When the temperature at which the observation was to be made was attained by the liquid in the cell, as was indicated by the thermometer inserted into the liquid, the cell containing the liquid was taken out quickly and placed between the oscillator and the crystal detector and the diminution in the value of the detected current was noted after tuning the condenser again. The cell was immediately placed in the water bath the temperature of which was kept constant for this particular set of observations. The temperature of the liquid was again taken with the thermometer and it was found that the difference between the two temperatures was always less than 0.5°C. In this way series of observations were taken for the frequency-range 250 Mc/sec to 510 Mc/sec. The attenuation co-efficient was calculated from the formula

$$I = I_0 e^{-\mu x}$$

or

$$\mu = \frac{1}{x} \log \frac{I_0}{I} = \frac{2.34}{x} \log_{10} (I_0/I),$$

where  $\mu$  = attenuation coeff. and  $x$  = thickness of liquid.

In this way, the values of  $\mu$  were calculated for two different thicknesses of the liquid, *e.g.*, 1.95 cm. and 3.95 cm. The same process was repeated in case of all the three liquids for the temperature-range shown. Next, the values of the attenuation co-efficients were plotted in a graph against frequency of the incident radio waves and from the graph thus drawn the value of the maximum frequency of absorption was obtained.

#### RESULTS

The results obtained in the case of three liquids are given in Tables I, II and III and they have been plotted in the form of curves in the figures 1, 2 and 3.



TABLE I

Attenuation coefficient of diethyl ketone. ( $\text{C}_2\text{H}_5\text{CO.C}_2\text{H}_5$ )

Temperature Frequency in Mc/sec.	0°C	30°C	62.5°C	82°C
250	.02806	.02256	.0200	
260	.03014	.02258	.0203	
270	.03323	.02263	.0203	
280	.03856	.02306	.0204	
290	.06723	.02520	.0208	
300	.06923	.02654	.0215	.01873
310	.06602	.04225	.0230	.01975
320	.05303	.04806	.0248	.02003
330	.04522	.05062	.02700	.02004
340	.03630	.04963	.02953	.02018
350	.03258	.04226	.03000	.02009
360	.02732	.03257	.03703	.02093
370	.02506	.02903	.03904	.02163
380	.02255	.02656	.04154	.02256
390	.02156	.02650	.04356	.02496
400	.02100	.02500	.04403	.02763
410	.02100	.02375	.04359	.02954
420	.02000	.02300	.04263	.03175
430	.01889	.02256	.04104	.03258
440	.01878	.02205	.03904	.03389
450	.01003	.02203	.03756	.03306
460	.01003	.02150	.03553	.03854
470	...	.02103	.03433	.03956
480	...	.02100	.03234	.03959
490	...	.02090	.03007	.03958
500	...	.02070	.03005	.03756
510	...	...	.02856	.03504

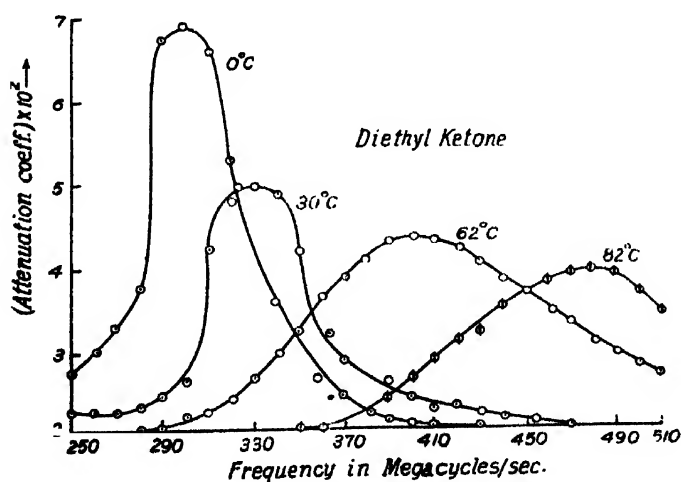


FIG. 1

## DISCUSSIONS

It can be seen from figures 1, 2 and 3 that the frequencies at the absorption peaks due to diethyl- and dinormal propyl ketone at 30°C are 330 and

295 Mc/sec. respectively. In the case of ethyl isobutyl ketone at 30°C the peak occurs at a frequency lower than 250 Mc/sec. It was also observed previously that in the case of acetone and methyl ethyl ketone at the room temperature the positions of the peak are at 400 and 372 Mc/sec. respectively. Thus it is seen that the position of the maximum shifts towards lower frequencies with the increase in the number of CH<sub>2</sub> groups in the molecule. The value of the relaxation time  $\tau$  can be calculated from Debye's theory (Debye, 1929) from the relation

$$\omega\tau = \frac{\epsilon_0 + 2}{\epsilon_1 + 2} \sqrt{\frac{\epsilon_1}{\epsilon_0}}$$

where  $\omega$  is the angular frequency at the absorption peak,  $\epsilon_0$  the square of refractive index for light, and  $\epsilon_1$  the dielectric constant for static field. The value of molecular radius  $a$  can be calculated roughly from the relation

$$a^3 = \frac{\tau k T}{4\pi\eta}$$

where  $k$  is the Boltzmann constant,  $T$  is the absolute temperature and  $\eta$  the coefficient of viscosity. The values obtained in this way are given in the last column of Table IV. It is found that the value of the molecular radius derived from Debye's theory is almost the same for all the ketones studied, although the actual size of the molecules of higher ketones is much larger than that of the lower ketones. The value of  $a$  derived for acetone is too high while those for the higher ketones are almost of the right order of magnitude. The large discrepancy observed in the case of acetone may be due either to the difference between the internal viscosity and the macroscopic viscosity or to association of the molecules in the liquid state.

As regards the values of attenuation co-efficient observed in the present investigation and entered in column 5 of Table IV it is seen that they give the values of  $k_m$ , the extinction coefficient, agreeing approximately with those calculated from the relation

$$k_m = \frac{\sqrt{\epsilon_1} - \sqrt{\epsilon_0}}{\sqrt{\epsilon_1} + \sqrt{\epsilon_0}}$$

In calculating the value of  $k_m$  from that of  $\mu$ , the expression

$$\mu = \frac{2\pi}{\lambda} \tau k_m$$

has been used. Here  $\tau$  has been calculated from the relation

$$\tau^2 = \frac{1}{2} \frac{\sqrt{\epsilon_1 \epsilon_0}}{\epsilon_1 + \epsilon_0} (\sqrt{\epsilon_1} + \sqrt{\epsilon_0})^2$$

TABLE IV

Comparative study of the absorption of U. H. F. electrical oscillations in ketones

Liquid.	Temperature	Max. freq. of oscillation MC/sec.	Viscosity coeff. in centipoises.	Max. value of attenn. coeff: $\mu$	$k_{\max}$ calculated.	$k_{\max}$ observed.	$\tau \times 10^{10}$	$a \times 10^5 \text{ cm}^2$
Acetone $\text{CH}_3\text{CO CH}_3$	5°C	384	.3638	.115				
	31°C	400	.3035	.075	.556	.450	2.227	6.29
	52°C	424	.2405	.067				
Methyl-ethyl ketone $\text{CH}_3\text{CO.C}_2\text{H}_5$	65°C	465	...	.039				
	0°C	320	.5361	.090				
	28°C	378	.3861	.128	.513	.747	2.473	6.00
	50°C	410	.3049	.115				
	65°C	424	.2650	.105				
Diethyl ketone $\text{C}_2\text{H}_5\text{CO C}_2\text{H}_5$	0°C	300	.5014	.069				
	30°C	330	.4228	.051	.501	.413	3.193	6.30
	62°C	407	.3079	.044				
Dinormalpropyl ketone $\text{C}_3\text{H}_7\text{CO.C}_3\text{H}_7$	82°C	473	.2623	.049				
	30°C	295	.5653	.055				
	65°C	338	.4276	.043	.432	.393	3.712	6.30
Ethyl isobutyl ketone $\text{C}_3\text{H}_5\text{CO.C}_4\text{H}_9$	85°C	465	...	.032				
	30°C	250 approx.	...	.036				
	62°C	410	...	.032				
	95°C	495	...	.031				

The height of the absorption peak increases with the lowering of temperatures in all the cases and in the case of diethyl- and dinormal propyl ketone the peak becomes narrower, while in the case of ethyl isobutyl ketone the width of the band increases, with lowering of the temperature. It was previously observed (Sen, 1949) that in the case of methyl ethyl ketone also the height of the peak, instead of increasing, diminishes with lowering of temperature below room temperature, although in the case of acetone the height of the peak increases with the lowering of temperature. Thus it is evident that when the two alkyl groups in the ketone molecule are identical the observed behaviour of the liquids supports the hypothesis put forward by Sirkar and Sen (1949) mentioned earlier that the change in the permanent

electric moment produced by intermolecular field increases with the lowering of temperature. When the two alkyl groups attached to the  $C=O$  group in the ketone molecule are not identical the behaviour of the molecules with the lowering of temperature seems to be a little anomalous, because both methyl ethyl ketone and ethyl isobutyl ketone show such an anomaly. In the case of ethyl isobutyl ketone the integrated absorption increases at low temperatures. The shift of the peak for a change of temperature from  $62^{\circ}.5C$  to  $30^{\circ}C$  is also much larger than that for the same change of temperature from  $95^{\circ}C$  to  $62^{\circ}.5C$ . Hence there is an abrupt change in either the internal viscosity or the size of the molecule with the lowering of temperature below  $62^{\circ}.5C$  in this particular case. Probably both these changes occur simultaneously, and further, the permanent electric moment is affected by the intermolecular field to a larger extent at  $30^{\circ}C$  than at  $62^{\circ}.5C$ . The assymetry of the shape of the molecule may be responsible for heterogeneous distribution of the molecules in the liquid resulting in an intermolecular field varying between wide limits and thus causing the absorption peak to be wide.

In the case of methyl ethyl ketone, on the other hand, the height of the absorption peak as well as the integrated intensity diminish with the lowering of temperature. This may be due to the fact that the molecules abruptly become associated to form groups having a resultant permanent electric moment less than that of the single molecule. No general conclusion can, however, be drawn from the results obtained in the case of a single series of molecules. Investigations with other substances are in progress and the results will be discussed in more detail in a future communication.

#### ACKNOWLEDGMENT

The author is indebted to Prof. S. C. Sirkar for his kind interest and guidance during the progress of the work.

OPTICS DEPARTMENT,  
INDIAN ASSOCIATION FOR THE CULTIVATION OF SCIENCE,  
CALCUTTA.

#### REFERENCES

- Debye, P., 1929, Polar molecules.  
Sen, S. N., 1949, *Ind. J. Phys.*, **23**, 495.  
Sen, S. N., 1950, *Ind. J. Phys.*, **24**, 163.  
Sirkar, S. C. and Sen, S. N., 1949 *Science and Culture*, **18**, 155.

# A NEW AND QUICK METHOD FOR DETECTION OF PIEZO-ELECTRICITY AND MEASUREMENT OF THE PIEZO-ELECTRIC CONSTANTS

By KRISHNA GOPAL SRIVASTAVA

(Received for publication, November, 11, 1950)

**ABSTRACT.** A method using differential transformer has been developed for detection of piezo-electricity. To one of the primaries of the differential transformer the crystal is connected and to the other is connected a variable condenser and resistances in parallel. Balance is obtained at first and frequency of source is then varied. As soon as a crystal-frequency is approached a large current results in the secondary which detects the piezo-electric behaviour of the crystal. The method has been used to measure piezo-electric constant of quartz.

Formerly, two methods had been used for detecting piezo electricity in crystals. The first was due to Giebe and Scheibe, (1925) which is a click-method. The second is a bridge-method by Mason, (1943) in which the crystal is placed in one of the arms of a Wheatstone bridge and sudden changes in the rectified current are observed when the frequency of the source approaches one of the natural frequencies of the crystal. The method developed here uses a differential transformer for the purpose. The circuit arrangement is as given in Fig. 1.

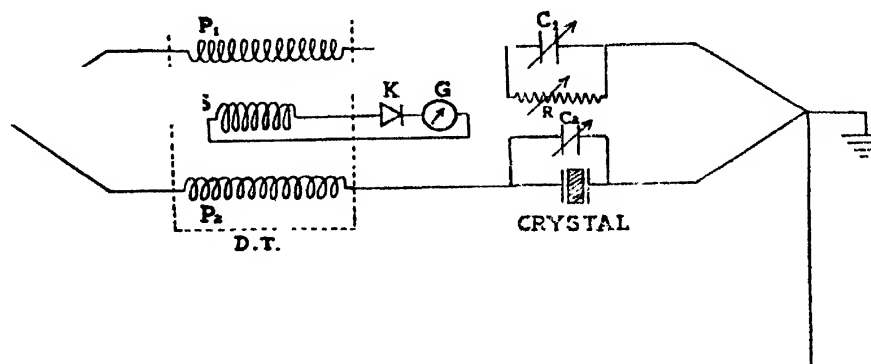


FIG. 1

D.T. is a differential transformer, which, as is well known, consists of two balanced primary coils  $P_1$  and  $P_2$ , and a secondary coil  $S$ .  $K$  is a carborundum crystal rectifier connected to the secondary coil of the differential transformer, and  $G$  is a galvanometer to observe rectified currents.  $T$  is a signal generator which can give a signal of desired radio-frequency. In the present set-up a Ferris signal generator was used. To one of the primary coils of the differential transformer is connected a variable condenser  $C_1$  and a resistance  $R$  in parallel. To the other primary coil is

connected the crystal and a suitable air condenser  $C_2$  of about 100 mmf. in parallel.

At a particular setting of  $C_2$ , which is kept constant throughout the experiment,  $R$  and  $C_1$  are so adjusted that current in the galvanometer is zero. The frequency of the signal generator is then changed. As soon as a natural frequency of the crystal is approached a large current appears in the galvanometer which detects the piezo-electric action of the crystal.

Large current appears in the secondary circuit due to the fact that the

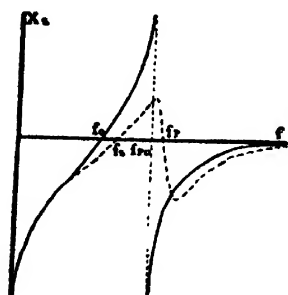


FIG. 2

reactance of the crystal at resonance suddenly drops to zero which unbalances the differential transformer. The reactance curve of the quartz crystal is very well known and is shown in Fig. 2, as given by Cady. It is seen from the curve that reactance passes through the zero value at both series and parallel frequencies  $f_s$  and  $f_p$ . Both of these frequencies are observed and the effective piezo-electric constant  $e$  is calculated by using the bridge method (Mason 1943), from the formula:—

$$e^2 = \frac{\pi k^2 l \rho}{\delta} (f_p^2 - f_s^2)$$

Determination of the piezo-electric constant  $d_{11}$  was carried out using a crystal of frequency 3.9 mc. and the result agrees very well with the standard value. The value obtained is  $5.2 \times 10^{-8}$ . Further work at different temperatures and the determination of  $d_{14}$  is in progress.

The advantage of the present method is that easy detection and measurement of the piezo-electric constants can be made quickly. At the same time the apparatus is simple and easy to set up. It is hoped that this will also lead to the measurement of  $Q$  of the crystal and ultrasonic velocities and absorption in liquids and gases.

#### ACKNOWLEDGMENTS

The author wishes to express thanks to his colleague Shri Krishnaji for lending some of the apparatus used and for discussion and to the Govt. of U.P. for the award of a research scholarship.

DEPARTMENT OF PHYSICS  
UNIVERSITY OF ALLAHABAD

#### REFERENCES

- Cady, W. G. *Piezo-electricity*. McGraw Hill publication, pp. 350.  
Giebe, B., and Scheibe, A. 1925., *Z. f. Ph.*, **83**, 335.  
Mason, W. P. 1943, *Bell, Syst. T.* **22**, 178.

# GAS TURBINES—SOME METALLURGICAL CONSIDERATIONS INVOLVED IN THEIR MANUFACTURE

By H. TRIVEDI

*(Received for publication, September 22, 1950)*

**ABSTRACT.** With the use of jet aircraft, the gas turbine has taken the role of a militarily strategic equipment. This paper deals with the studies of the gas turbine from a metallurgical point of view. The properties of the present day material, used in its manufacture, are reviewed. A new material has been studied for this purpose, which is believed not only to give better service, but will lead, in addition to the design of better gas turbines. That product has been made from raw material abundantly available in India.

It has long been recognised that the internal combustion turbine or gas turbine, as it is more usually called, was the ultimate form into which the internal combustion engine was likely to develop.

In a simple gas turbine air is drawn into the compressor where it is compressed and passed on to the combustion chamber in which fuel is burnt continuously in the excess air. This raises the temperature and pressure of the excess air and products of combustion which are then allowed to expand through the turbine to exhaust. The heat in the exhaust gas from the turbine is used to preheat the compressed air on its way to the combustion chamber.

The compressor, which is directly connected to the turbine and is driven by it, may be of the axial flow, centrifugal, positive displacement lobe type or a combination of these forms.

The efficiency simple gas turbine can be increased by the adoption of any or all of various standard expedients of which the more important ones are :

(1) Increasing the turbine inlet temperature by bringing more fuel per pound of air. This gives an increased output from the same size of plant and markedly improves the fuel consumption.

(2) Improving the efficiencies of any or all of the individual units in the cycle *e.g.*, the compressor, turbine or combustion chamber.

(3) Using one or more interstage coolers to reduce the temperature of the air entering the latter stages of the compressor. The cooled air has lesser volume enabling it to be compressed in a smaller compressor with less expenditure of energy. The heat withdrawn in the intercooler has admittedly to be replaced by the burning of more fuel but this apparent disadvantage is more than outweighed by the saving in the compressor horse power, which appears as additional net horse power output from the plant.

(4) Reheating the gas in the course of its expansion by passing it through one or more combustion chambers, fitted between successive turbine stages. The reason why this gives additional power is obvious.

It is frequently both convenient and advantageous to subdivide one or more of the units in a gas turbine installation. There are many ways in which this can be done, possibly the simplest case being the sub-division of the combustion chambers in air-craft jet engines, which often have as many as ten or more small combustion chambers operating in parallel. The advantage of this lies in the better engine lay-out it provides with reduced overall installation diameter and more uniform distribution of the high temperature gases entering the turbine.

The turbine itself may be sub-divided into two or more separate units *e.g.*, two turbines operating in series. The high pressure turbine drives the compressor and is on a separate shaft from the low pressure turbine developing useful power. Such an arrangement is used for ship propulsion, as it allows the compressor and compressor turbine to be run upto speed before the propeller has got under way.

In general, the efficiency of a gas turbine depends on the basic cycle efficiency of the installation and the efficiency of the individual units. The basic cycle efficiency is inherent in the design, whereas, the individual efficiency depends on the condition of the equipment and the amount of intelligent maintenance given to it.

Of all methods of improving gas turbine efficiencies, the raising of maximum gas temperature is at once the simplest, the most effective and the most reliable.

The heart of the gas turbine is the rotor assembly and it is in the provision of suitable materials for the rotor or disc and the rotor blades that the metallurgists' biggest problem lies. Rotor blades call for a combination of properties not encountered in any other engineering device. In the first place, the temperature at which the blades operate is now generally of the order of 700°C or even more.

Good high temperature properties are required; but something more needed. The material must have certain desired characteristics at room temperature and must have these qualities every time, for uniformity is one of the most important requisites for highly stressed parts.

Oxidation and corrosion resistance are perhaps the most important requirements. If they are oxidised or scaled or fail due to intergranular corrosion, they are no good. Load-carrying ability is the next essential. The property is measured by short time tensile tests at elevated temperatures, by the creep rate and by the stress required to rupture in a given number of hours at the desired temperature. Of these three tests, stress to rupture is the most widely used. Such a data must always be accompanied by stress-elongation curve that shows how much the sample deforms under the load. A metal which will carry the necessary load for 1000 hours without rupturing



may, nevertheless, be useless for gas turbine parts if it were to stretch so much on application of the load that all clearances are destroyed.

The conventional creep test, with both stress and temperature constant, does not offer enough data for design purposes. Creep rate is normally understood as only the minimum value of stretch under continued constant load, but the initial deformation and the onset of third stage creep may be of equal importance. A series of stress-rupture curves for different temperatures with stress plotted against time and another with stress plotted against elongation give a good idea of load carrying ability.

Structural ability is the next requirement. The material must retain its characteristic structure during exposure to heat and stress or else undergo definite predictable changes.

As nearly all parts of gas turbines are subject to vibration, the fatigue strength of metals at elevated temperatures is another requisite. Good damping capacity is preferred for blades, because a blade of high internal damping tends to inhibit the building up of resonant vibration.

In addition to the above qualities, the material for service in gas turbines must be capable of assuming the desired shape, either through machining, forging or casting and of being joined to other parts either mechanically or by welding.

A large number of alloys have been developed during recent years for service at high stresses and high temperatures mostly for use in gas turbines, jet engines and turbo-super-charges. There are some six or seven alloy groups which have been used for this purpose. They are given in the following table showing the more familiar alloy name, and the composition (Research Memorandum, 1947.)

The alloys fall roughly into the following classes :

(1) Stainless steel types with somewhat increased alloy content, such as 19-9 DL, Timken 16-25-6 ; they are essentially Fe-Cr-Ni alloys,

(2) Highly alloyed stainless steel types such as S-495, Refractalloy B ; these are also essentially Fe-Ni-Cr alloys,

(3) Modified stainless steel types wherein cobalt is found in large amounts ; these are essentially Ni-Cr-Co-Fe base alloys such as N-155 or S-590,

(4) Stellite type alloys such as Vitallium which was one of the first of this group ; these are essentially Co-Cr-Mo or Cr-Co-W alloys.

(5) Modified stellite type alloys wherein certain elements are used in increasing amounts notably nickel, tantalum, columbium, tungsten, carbon, etc., such as X-40, 73 J, and others.

(6) Inconel or Chromel or N-chrome types such as Inconel X and Nimonic 80. These are essentially Ni-Cr base alloys which can be made age-hardenable by additions of titanium etc.

An additional group of considerable interest are the chromium base alloys such as CM 469. They are, however, not yet practical alloys because of extreme brittleness, but may eventually be developed into extremely high temperature alloys.

Table II lists, as far as possible, some of the tensile data from 70° to 2000°F for the high temperature alloys of Table I. There are also given some of the representative complete test results for various test temperatures as well as the particular treatment which gave the alloy its properties. These values are neither optimum nor the minimum values and it must be realised that below about 1300°F many other values might be attained, especially among the forged group of alloys. Above about 1300°F the values listed generally are those for the alloy in its optimum condition for maximum rupture life and resistance to creep at the higher temperatures. It can be noted from the table that the forged alloys show superior tensile properties above 1350°F. (ASTM, 1946.)

Creep tests require such a long time for completion of tests that only a small number have been run. Table III gives the stress to obtain various creep rates for temperatures from 1200°F. Practically all of the tests were run for a minimum of 2000 hours. Actually 2000 hours is not sufficient time to establish a minimum creep rate in a test capable of enduring 20,000 or more hours under load, but from practical aspects the value is satisfactory. Some results obtained in 10,000 hours creep tests carried out at the U.S. Naval Eng. Expt. Station are given in Table IV. (Bureau of Ships Research 1947). These tests indicate that the materials will last at least 10,000 hours. The creep rate at 2000 hours is definitely greater than it would be at 10,000 hours, provided third stage creep had not begun.

At 1200°F, K42B is the best of the three alloys tested. At 1350°F alloys S-590 and high carbon N-153 show the best creep resistance. At 1500°F Refractalloy shows the highest value. Alloys S-495, high carbon N-155, S-497, and S-590 show similar creep results. It might be pointed out that the alloys S-495 and S-497 contain only about 15% Cr. Their oxidation and corrosion resistance at 1500°F and above is not so good as that of the 20% or more Cr. alloys. The cast alloys with few exceptions show much higher creep resistance than do the forged alloys at 1500° and 1600°F.

At 1500°F the stress to cause a creep rate of 1% in 100,000 hours varies from about 5000 lb/sq.in. for Vitallium to 15000 lb/sq.in for alloy 108 N-2. Alloys 93 N-2, 100 NT-2 and 108 N-2 show stressess of 13000 to 15000 lb/sq.in. for a creep rate of 1% in 100, 000 hours at 1500°F.

TABLE I

Alloy Name:	Composition of the Alloy:									Remarks.
	C.	Mn.	Si.	Cr.	Ni.	Co.	Mo.	W	Others	
L <sub>1</sub> T <sub>1</sub>	0.3	0.6	0.6	13.9	33.2	10.8	3.5	2.3	Balance Fe	Forged.
H-418	0.4	1.5	0.6	15.4	24.5	25.1	3.3	2	Fe, Bal.	Forged.
H-355	0.3	1.5	0.6	20.6	25.1	25.7	3	—	Fe, Bal.	Forged.
H-439	0.4	1.5	0.6	20.4	29.6	31.3	5	—	Fe, Bal.	Forged.
S-495	0.5	0.7	0.2	15	20	—	4	4	Cb <sub>4</sub> , Fe Bal.	Forged.
Gamma columbium	0.4	0.7	1.8	15	24	—	4	—	Cb <sub>4</sub> , Fe Bal	Forged.
Vitalium	0.2	1	0.6	28	—	64	6	—	—	Cast
422-10	0.4	0.5	0.5	25	16	52	6	—	Fe 0.65	Cast
Timken 16:25:6	0.1	1.5	0.9	16	25	—	6	—	N <sub>2</sub> 0.07, Fe Bal	Forged.
Refractalloy B	0.1	2	—	25	30	—	8	—	Fe Bal	Forged.
N-153	0.4	1.8	0.5	16	15	13	3	2.2	Cb <sub>1</sub> , N <sub>2</sub> 0.07, Fe Bal	Forged.
N-154	0.3	1.6	0.7	16	24	21	3	2.2	Cb <sub>1</sub> , N <sub>2</sub> 0.07, Fe Bal	Forged.
N-155	0.4	1.5	0.7	20	20	20	3	2.2	Cb <sub>1</sub> , N <sub>2</sub> 0.15, Fe Bal	Forged.
N-156	0.3	1.5	0.6	16	33	24	3	2.2	Cb <sub>1</sub> , N <sub>2</sub> 0.04, Fe Bal	Forged.
Nimonic 80	0.04	0.6	0.5	21.2	74.2	—	—	—	Al 0.61, Ti 2.4	Forged.
8685-2	0.4	2.1	1.6	18.7	15.1	19.7	2.7	—	Cb <sub>1</sub> 25, Ta 0.9 Fe Bal	Forged.
8658-1	0.4	2.1	1.7	19.1	15.1	19.9	2.6	—	Cb 0.7, Ti 0.5, Fe Bal	Forged.
S-497	0.4	0.5	0.6	15	20	20	4	4	Cb <sub>4</sub> , Fe Bal	Forged.
19-9DL	0.3	0.5	0.7	19	9	—	1.3	1.2	Cb 0.4, Ti 0.2, Fe Bal	Forged.
X-41	0.5	0.5	0.5	25	8	55	—	7.5	Cr B <sub>2</sub> 1.8	Cast
ATV-3	0.4	1.4	1.2	15	27.4	—	—	4.0	Fe Bal	Forged.
N-153 (no Co)	0.4	1.5	0.7	16	15	—	3	2.2	Cb <sub>1</sub> , N <sub>2</sub> 0.12, Fe Bal	Forged.
N-155 (no Co)	0.4	1.6	0.8	21	21	—	3	2.2	Cb <sub>1</sub> , N <sub>2</sub> 0.14, Bal Fe	Forged.
N-155 (modified)	0.4	1.8	0.7	21	21	—	3	2.2	Cb <sub>1</sub> , Tai 1, N <sub>2</sub> 0.12, Fe Bal	Forged.
TE	0.1	0.7	0.5	20	30	—	4	4	Tai 5, N <sub>2</sub> 0.15, Fe Bal	Forged.
61 (Cast)	0.4	0.3	0.6	24	—	68	—	6	—	Cast
Refratalloy	0.1	2	0.2	20.3	20.1	30.2	8.3	3.8	Fe 15.3	Forged
6059	0.5	0.2	0.8	26	33	34	6	—	—	Cast
X-40	0.5	0.6	0.7	25	10	55	—	7	Fe 0.6	Cast
X-50	0.8	0.6	0.5	23	20	40	—	12	Fe Bal	Cast
S-590	0.5	0.9	0.6	20	20	20	4	4	Cb <sub>4</sub> , Fe Bal	Forged.
S-816	0.4	0.6	0.3	20	20	45	3	4	Cb <sub>4</sub> , Fe Bal	Forged and cast
K42B	0.06	0.7	0.3	18	42	22	—	—	Al 0.5 Fe, 13, Ti 2.6	Forged.

TABLE I (contd.)

Alloy Name:	Composition of the Alloy									Remarks.
	C.	Mn.	Si.	Cr.	Ni.	Co.	Mo.	W.	Others	
Discaloy	0.03	0.5	0.5	13	25	—	3	—	Al 0.6, Fe 56, Ti 2.3	Forged.
Co-Cr-Ni Base (9Mo)	0.5	0.7	0.7	23	19	Balance	9	—	Fe 0.9	Cast
Co-Cr Base (9W)	0.4	0.7	0.7	23	3.2	Balance	—	8.8	Fe 0.8	Cast
Co-Cr Base (9 Mo.	0.4	0.7	0.7	23	2.9	Balance	9.2	—	Fe 0.9	Cast
Co-Cr-Ni Base (5Mo,5W)	0.4	0.8	0.7	22.6	18.2	Balance	5.2	5.1	Fe 0.8	Cast
Refractalloy 26	0.03	0.7	0.7	18	37	20	3	—	Ti 3, Al 0.3 Fe Balance	Forged.
Hastelloy B	0.05	0.6	0.2	—	65.1	—	28.6	—	Fe 4.7	Forged.
Inconel X	0.05	0.5	0.4	14.6	73.4	—	—	—	Cbr, Fe 6.9, Cu 0.04, Ti 2.3, Al 0.7	Forged.
Stellite 6	0.98	1.0	0.7	32	—	60	0.6	4.6	—	Cast
GT-45	0.08	1.25	0.5	17.3	13.8	—	2.9	—	Cb 0.45, Ti 0.3, Cu 3.1, Fe Bal	Forged.
MT-17	0.06	1.5	0.5	21	30	21	3	2.2	Ti 1.6, Fe Bal	Forged.
31 V4	0.31	4	—	23	—	65	6	—	—	Cast
100 NT-2	1	1.5	0.5	20	30	20	3	2.2	Ta 2, Fe Bal	Cast
36 VT 2-3	0.36	2	—	23	—	65	6	—	Ta 2	Cast
110 N-2	1.10	1.5	1	21	30	21	3	2.2	Cbr, N <sub>2</sub> 0.7 Fe Bal	Cast
111 VT 2-2	1.11	—	—	23	—	67	6	—	Ta 2	Cast
73 J	0.73	1	—	23	6	60	6	—	Ta 2	Cast
36 J	0.36	1	—	23	6	60	6	—	Ta 2	Cast
35 H	0.35	1	—	23	2	61	6	3	Ta 2	Cast
CM 469	0.03	—	—	60	—	—	25	—	Fe 14	Vacuum cast

TABLE II

Trade Name:	Temp. °F	Tensile stress lb/Sq. in:	0.2% yield lb/sq. in:	Properties limit lb/Sq. in:	% Elongation:	% R of A	Treatment:
LCN-155	Room	146,750	121,000	70,000	25.5	47	10% CW-1200°F
	1200	116,000	0.1% Yield		13	23	10% CW-1200°F Hot worked
	1350	80,940	65,650		24	37	2300°F-3/4 Hr-WQ
	1500	49,400	29,000		34	35	1500°F-4 Hr-FC
HCN-155	Room	138,000	70,600		16	12.6	2200°F-1 Hr-WQ
	1500	58,000	29,000		34.2	28.8	1500°F-4 Hr-FC
			0.2% Yield.				
S-590	Room	160,500	89,500	30,000	10	10.5	2270°F-1 Hr-WQ, 1100°F-16 Hr
	1200	81,600	49,000		27	31	2300°F-1 Hr-WQ, 1400°F-16 Hr AC
	1300	66,875	58,500	22,000	27	33	2270°F-1 Hr-WQ, 1400°F-16 Hr
			0.1% Yield.				
K 42 B	Room	162,500	97,200		31.0	39.4	2270°F-1 Hr-WQ
	1200	128,000	91,250		10.0	13.3	2270°F-1 Hr-WQ
	1350	101,000	79,700		6.5	10.2	1200°F-72 Hr-FC
	1500	71,000	41,250		2.5	4.2	
	1700	23,900			40.5	66.0	
Hastelloy B	Room	139,200	57,000		49.5	51.1	1950°F-2 Hr-AC
	1500	77,500	42,500		27.0	21.2	1950°F-2 Hr-AC
	1600	52,500	39,700		48.0	41.7	
	1700	39,000	28,400		45.0	51.8	
	1800	31,500	16,100		62.0	53.5	
	1900	18,500	9,800		70.0	53.0	
	2000	13,100	7,600		54.5	46.9	1050°F-2 Hr-AC
			0.2% Yield.			...	
S-816 Forged	Room	175,000			39	45	As rolled
	1200	120,200			17	22	2300°F-1 Hr-WQ,
	1350	98,900			15	22	1400°F-AC

TABLE II (contd.)

Trade Name:	Temp. °F	Tensile Stress lb/sq. in	0.2% Yield lb/sq. in:	Properties limit lb/sq. in:	% Elongation:	% R of A	Treatment
S-816 Forged	Room	175,000	0.2% Yield.		39 17 15 12 18 14	45 22 } 22 } 21 } 20 } 17 }	As rolled. 2300°F—1Hr—WQ, 1400°F—AC
	1200	120,200					
	1850	98,900					
	1500	78,266					
	1600	59,770					
	1700	46,180					
Nimonic 80	Room	153,000		75,000 30,000	36.5 14.5	33.6 } 20.8 }	1950°F—2Hr—WQ, 1300°F—16 Hr.
	1200	97,500					
S-497	Room	154,750		57,500 15,000	10.5 22	20.5 25.9	Finish Forge 1400°F Finish Forge 1400°F
	1200	103,625					
Inconel 'X'	1300	64,400	0.1% Yield.		35 6.5 19.5	32.0 } 8.6 } 18.4 }	2100°F—1Hr—WQ, 1500°F—4Hr—FC.
	1500	63,400					
	1700	28,000					
S-495	Room	192,000	0.2% Yield.	136,000	26 12 3	45 14 } 10 }	Hot rolled—aged Hot rolled—solution treated—aged. Finish forged 1400°F
	1200	118,000					
	1500	70,000					
	Room	147,750					
	1200	87,625					
Gamma Colum- bium. N-156	Room	107,500	0.1% Yield.	35,000 37,500	6.0 24.0	21.7 } 34.3 }	2250°F—3/4 Hr—OQ, 1500°F—50Hr 2200°F—1Hr—WQ—4Hr—1500°F—FC
	1500	43,500					
	1500	55,000					

TABLE II (contd.)

Trade Name :	Temp. °F	Tensile stress lb./sq. in. :	0.2% Yield lb./sq. in. :	Properties limit lb./sq. in. :	% Elongation :	% R of A	Treatment :
ATV-3	Room	121,700	84,000		21.5	36.5	As rolled.
	1200	75,200	46,000		25.0	32.2	
	1350	66,000	30,750		28.0	39.4	
	1500	42,600	15,100		31.0	38.5	
	1700	24,100			38.5	43	
19-9 DL Timken	Room	140,750	115,000	75,000	29	48.1	2100°F—1Hr—AC Finish roll 1200°F, Stress relieve 1200°F—AC
	1200	91,000	81,000	52,500	16	38.8	
16-25-6	Room	162,250	143,500	102,500	15.5	33.6	2100°F—1Hr—AC Finish roll 1200°F—AC Stress relieve 1200°F—AC
	1260	107,500	94,000	60,500	13.0	27.9	
GT-45			0.1% Yield				
	1350	60,100	27,000		40.0	35.5	Preheat 1500—1550°F, 2150°F—WQ 2160°F—2Hr—WQ <del>2160°F—2Hr—WQ</del>
	1500	48,300	31,400		27.5	26.2	
	1800	21,000	12,000		22.0	19.5	
	Room	101,500	61,200	38,700	30	54.4	
	1200	66,500	47,500		27	48.2	
	1350	51,000	35,800	22,000	37	44.1	Hot rolled—1200°F—5Hr
	1500	36,000	24,000	15,500	19	16.7	
Vitalium	Room	110,000	65,000	55,000	10	12	As cast 1350°F—48Hr.
	Room	120,000			5.1	6.6	
	1200	71,000	35,600	25,200	18.4	41.5	As cast
		93,200	71,500	39,300	1.8	5.6	
	1350	76,000	59,300	36,100	3.5	8.2	
		82,700	63,700	33,200	4.0	9.8	
	1500	57,300	47,350	23,300	8.3	19.7	1350°F—50 Hr.
		61,400	50,700	28,100	5.3	4.5	
	1600	49,200	35,000	22,200	9.8	15.8	
		48,600	36,800	19,400	9.5	19.9	
	1700	42,470			27	52.4	As cast
	1800	33,265			35	52.4	As cast
		32,910			49	63.1	1700°F—16Hr, AC

TABLE II (contd)

Trade name:	Temp. °F	Tensile stress lb/sq. in.	0.2% Yield lb/sq. in.	Properties limit lb/sq. in.	% Elongation	% R of A.	Treatment
6059	Room	82,550	46,900		7	10.3	As cast
	1200	76,800	41,100	24,200	3	3.4	1700°F-16Hr-AC
		46,300	34,400	21,500	3.3	7.7	As cast
		51,500	35,600	30,600	4.2	8.2	As cast
	1350		51,900	32,100	—	—	
		66,200	49,800	32,100	3.2	4.6	
	1500	51,400	38,700	26,000	12.0	21.8	1350°F-50Hr.
		51,000	37,700	20,900	8.3	7.0	
	1600	41,500	31,200	13,700	10.0	20.8	
		41,200	30,500	19,500	13.0	19.4	
422-19	1700	42,950			23	26.5	As cast
		45,430			16	34	1700°F-16Hr-AC
	1800	33,400			24	50.3	As cast
		33,690			26	41.7	1700°F-16Hr-AC
	Room	98,100	55,100		5	11.9	As cast
		94,500	56,200		1	0.65	1700°F-16Hr-AC
	1200	58,300	36,900	19,500	7.2	15.7	As cast
		62,100	38,400	24,700	7.0	10.3	As cast
	1350	74,800	59,000	38,300	2.0	2.1	
		80,700	63,800	40,000	1.6	3.3	
	1500	65,000	49,500	29,400	2.7	3.3	
		63,000	45,700	23,700	3.3	3.6	
	1600	49,200	35,000	22,200	9.8	15.8	
		48,600	36,800	19,400	9.5	19.9	
	1700	45,180			17	26	1350°F-50Hr.
		47,135			18	33.3	As cast
	1800	36,290			24	33.7	1700°F-16Hr-AC
		37,800			21	38.7	As cast
61	Room	103,400	58,350		7	11.2	1700°F-16Hr-AC
		108,500	53,900	21,900	6	14.2	As cast
	1200	79,500	39,000	37,300	14.0	18.4	1700°F-16Hr-AC
		103,400	74,000	34,500	2.1	5.8	As cast
	1350	73,600	61,000	34,500	1.2	5.0	
		85,600	65,200	33,900	2.8	7.9	
	1500	59,500	40,000	25,100	7.4	16.1	1350°F-50Hr.
		57,500	41,200	14,500	8.2	9.3	
	1600	46,800	34,200	18,000	9.6	14.8	
		44,800	32,000		10.0	18.8	



TABLE II (contd)

Trade name :	Temp. °F.	Tensile stress lb/sq. in.	0.2% Yield lb/sq. in.	Properties limit lb/sq. in.	% Elongation:	R of A :	Treatment :
61	1700	37,475			7	35.7	As cast.
		43,580			18	35.7	1700°F—16 Hr—AC.
	1800	33,115			32	40.6	As cast.
X-60		33,950			27	30.5	1700°F—16 Hr—AC
	1500	67,000	53,500	22,800	1.0	mil	1500°F—50 Hr.
	1600	54,000	39,200	13,600	1.5	2.1	1600°F—50 Hr.
		50,000	37,000	12,900	1.4	1.1	1500°F—50 Hr.
X-40	Room	101,000	74,100		11	14	As cast.
	1200	76,800	37,400	23,400	18	28.1	As cast.
	1350	77,300	37,800	22,500	20	28.6	As cast.
		82,200	53,400	31,300	7.0	8.1	As cast.
		69,200	53,800	33,100	2.3	7.0	
	1500	57,500	42,000	26,200	14.0	15.4	
		61,400	47,500	32,400	5.0	12.1	1350°F—50 Hr.
	1600	48,500	35,200	22,900	14.3	18.1	
31 V-4		48,500	37,300	24,000			
	Room	136,300	—	—	3.3	6.0	1350°F—48 Hr.
	Room	102,800	—	—	5.9	10.7	As cast.
	Room	120,000	—	—	10.2	—	As cast.
36 J	Room	111,000	—	—	3.0	1.5	As cast.
70 J	Room	120,000	—	—	3.8	1.0	As cast.
111 V12-2	Room	100,000	—	—	1.5	1.0	2260°F—WQ
100 NT-2	Room	112,000	59,000	—	5	13	As cast.
S-816	Room						

TABLE III

*Creep rate data for forged and cast alloys from 1200°F to 1600°F :*

Alloy:	Temp. °F	Stress for minimum creep rates, % per hour of :			Alloy	Temp. °F	Stress for minimum Creep rates, % per hour, of :		
		0.001	0.0001	0.00001			0.001	0.0001	0.00001
Hastelloy B	1200	20,000	7,400	2,650	Vitalium NR-90	1500	11,700	7,600	4,900
Timken	1500	4,800	2,800	1,600		1600	11,200	7,900	5,600
	1200	21,500	14,000	9,000		1500	10,900	12,500	7,900
K 42 B	1500	8,400	5,700	3,800	6059	1500	15,000	11,700	9,000
	1200	29,000	18,800	12,000		1600	11,000	9,000	7,300
19-9 DL	1500	14,000	7,400	3,900	422-19	1500	18,400	13,200	9,500
	1500	10,400	7,100	4,800		1600	14,500	11,600	9,500
Nimonic 80	1500	15,700	9,500	5,700	61	1500	17,000	13,000	10,000
Refractalloy 26	1500	15,700	9,500	5,700	X-50	1500	18,200	13,500	10,100
						1600	13,200	10,500	8,500
N-155 (LC)	1500	9,800	8,300	7,000	73J	1500	20,400	14,300	10,100
N-155 (HC)	1350	25,000	18,400	13,500		1500	18,500	13,700	10,200
	1500	13,800	10,300	7,800	X-40	1600	15,700	11,700	8,700
S-590	1350		19,000	14,300		1500	25,400	15,000	11,000
	1500	12,700	9,600	7,300	III V12-2	1600	15,100	10,300	7,200
TE	1500		9,500	7,500	93N-2	1500	21,100	16,700	13,000
Inconel X	1500	19,600	12,300	7,600	100NT-2	1500	21,800	17,400	13,800
						1600	16,500	11,700	8,500
S-816	1350	26,800	18,000	12,200	110N-2				
	1500	16,400	11,500	8,100		1500	21,900	18,000	14,800
	1600	8,500	5,800	4,000					
S-497	1350	19,700	15,800	12,800					
	1500	12,400	10,000	8,100					
	1600	7,800	6,200	5,000					
S-495	1350	22,400	16,100	11,700					
	1500	12,900	10,400	8,300					
	1600	7,900	5,300	3,500					
Refractalloy	1500	15,200	12,800	11,000					

TABLE IV  
10000 Hour Creep Tests at 1500°F

Alloy	Heat Treatment	Stress lb/sq in	Creep rate % per hour at		Final reading	Length of test, hours
			1000 hours	2000 hours		
92 N-2	2260°F - WQ	10,000	0.000392	0.00040	0.0000015	6,500
N-155	2300°F - WQ	8,500	0.000011	0.000018	0.0000022	10,078
S-816	2350°F - WQ	8,500	0.00003	0.000029	0.000113	10,103

These alloys are all high carbon modifications of N-155, which as a low carbon forged alloy, shows good creep resistance. These alloys are the nickel-chromium-cobalt-iron base compositions as are S-500, S-497, and S-495. Compared to the cobalt-chromium base alloys the former are much superior in creep, but generally poorer in rupture (short time) properties. The best cast cobalt-chromium base alloys at 1500°F show 5000 to 11000 lb/sq.in. for a creep rate of 1% per 100,000 hours. Except for Vitallium, which shows the lowest creep resistance, the stress for a creep rate of 1% per 100,000 hours at 1500°F is fairly constant at  $10,000 \pm 1000$  lb/sq.in. for 111 VT 2-2, X-40, alloy 61, X-50, 73 J, 6059 and 422-19. At 1600°F, X-40 and 100 N-1-2 show the best creep resistance at creep rates of 0.0001% per hour and above, while 422-19 is best in the lower creep rate range.

The above alloys have so far yielded a fair amount of work and have been widely used in turbine blades, jets, venturies and valves at high temperature in air-crafts. There is not, however, very great promise for going further in this direction. The reason lies in the short space between the temperatures at which the alloys are cast or forged into useful shapes and the temperatures at which the finished parts must work in service. For this country there is yet another reason. It is not only economic but strategic as well. All the above mentioned alloys are composed of a very high percentage of metals which are not found in this country, *e.g.*, Ni, Mo, W, Cb, Ta, Co, etc. If gas turbines have to be developed in this country, high temperature materials have to be produced without heavy consumption of these elements which are scarce here.

One has, therefore, to look towards other refractory alloys. Through powder metallurgy combinations of metals may be tried which involve material not very easy to fuse. The hard compounds, which we use for making tools and grinding wheels offer themselves as the most interesting group of promising materials. They could be made into parts by powder metallurgical processes. They are strong in the formed and sintered state and are more erosion and abrasion resistant than pure refractory metals. The borides and carbides of refractory metals (*e.g.*, chromium, molybdenum, tantalum,

columbium, titanium and tungsten) offer a great promise in this field. The author has been experimenting for a fair length of time on titanium carbide and its use for hard cutting tools and for high temperature work. The compound was chosen with a special motive. Titanium is found in fair abundance in this country, in the South as titanium dioxide in ilmenite sand and in the magnetite ore of Mayurbhanj State. The author used the titanium after extracting it from the magnetite ore belonging to Sir Indra Singh, after all the vanadium in it had been extracted in the works of Vanadium Corporation, a sister concern of Tata's. Hundreds of compounds of titanium and carbon were made during the course of experiments and a variety of binding media employed. The properties given below belonged to one particular compound and one particular percentage of the binding medium, which gave the most promising high temperature properties.

Titanium carbide was made in an experimental electric arc furnace and formed into shapes of test rods by the method of powder metallurgy. The carbide was powdered and mixed with finely divided cobalt. It was cold pressed into shape at a pressure of 30 ton./sq.in. and sintered in a graphite furnace at about 1675°C. It was tested at high temperature with the following results:

*Tensile strength at about 1000°C	...	...	8 T/sq.in.
*Transverse strength at about 1000°C	..	...	40 T/sq.in.
Specific gravity	...	...	5.5
Thermal conductivity, calories/sec/°C/cm	...	...	0.09
Hardness [Diamond Pyramid Scale (50 Kg. load)]	...	...	1600

Creep strength could not be determined of this material as no instrument was available.

There was no apparent attack to combustion gases up to 1150°C in 48 hours, nor was there any loss of strength. The material withstands drastic

\* The apparatus in which the material was tested for transverse or tensile strength at 1000°C consisted of 5"×6"×6" platinum-wound furnace which was slipped on the specimen. This permitted the heating of the specimen to 1350°C with less than 5°C difference in temperature over the length of the test section. The load was applied by means of four jawchucks. There were guide rods to prevent misalignment. The entire assembly was mounted on a heavy horizontal bed plate with slots in which the movable head could travel. The heads were hollow cast aluminium and were water cooled. One head was actuated by a hydraulic cylinder operated by hand. The value of the frictional losses was determined by carrying out a blank test with the help of known steel samples with strain gauges attached. The specimens were 10" long and 3/8" in diameter with 1 1/4" long and 1/4" diameter in the centrally thin portion. The tests were carried by applying the load after holding the specimen at the proper temperature for 15 minutes.

For transverse loading, a fused silica edge was placed at the centre of the sample, for which a space was kept in the furnace, and it was loaded hydraulically when the test piece had reached the proper temperature.

thermal shocks. There was no appreciable change in strength when it was heated to about  $1000^{\circ}\text{C}$  and then quenched in water. Air cooling from the same high temperature leaves no effect other than an initial discoloration of the surface. Its thermal conductivity is about  $1/10$  that of copper.

The above data show that titanium carbide, properly bonded, could be used as a high temperature material for use in gas turbines and jet engine parts. The author has just started experimenting with a bond of chromium metal. The work has not advanced sufficiently for any data to be furnished. There are two other methods of converting these refractory compounds into finished parts, and there are reasons to believe that at least one process will yield better results than those given above. Those two methods are : (1) hot pressing and (2) infiltration process.

(1) Hot pressing : By this method the pressing and sintering processes are combined and performed at the same time. The applied heat develops greater plasticity of the powders and permits the use of lower pressures ( $1 \text{ Ton/sq.in.}$ ). Graphite moulds may be used which is an advantage in the case of the carbide type hard compounds, for reasons of obtaining a protective atmosphere. After the part is formed another sintering at higher temperature may be done to complete the alloying and the fusion of components.

(2) The infiltration process : In this case a porous skeleton is formed of the refractory metal or hard compound phase, and thereafter molten materials of adequately high fusion point are drawn by surface tension into every pore and interstice of the sintered skeleton. The advantage of this method lies in the lower forming pressures, it not being necessary or even desirable to reduce the porosity of the original sintered part to a minimum. Only a small percent of the cementing agent may be mixed in with the original hard compounds. The remainder of the cementing material constitutes the impregnant. This technique promises greatest success from the following considerations.

(a) The skeleton manufactured before infiltration is a continuous matrix and so is the pore system which is later filled with the infiltrants with the help of precision casting (e.g., centrifugal casting, vacuum casting or gas pressure casting). With both systems being continuous, there is a lesser opportunity for internal cracks. Both the operations can be performed by using a single investment mould first for forming the original sintered skeleton and then for making the subsequent infiltration.

(b) There is better controllability of grain size and the possibility of developing uniformly large grain sizes by heat-treatment of the parts after infiltration. This may prove to be of great importance from the stand-point of hot strength and creep resistance.

(c) There is an advantage of making complicated shapes by 'keying together' similar sections and heating the assembly so that the infiltrant fuses and welds the simple shapes together.

(d) There is a possibility of using a slight excess of the infiltrant so that it spreads thinly over the entire surface of the part, thereby effectively covering it with corrosion resistant material. This coating will be continuous and entirely merged with the matrix of infiltrant, which previously has permeated the interconnected pore system of the skeleton thereby preventing spalling.

From its inherent properties, chromium boride appears to show signs of interest. There are a number of borides of chromium, all, at least, as resistant to oxidation and chemical attack as pure chromium. Their basic hardnesses are in the region of 1400-1600 on the diamond pyramid scale. The hardness diminishes only very slightly up to about 750°C, *i.e.*, temperatures now employed in turbines and jet engines. They are highly soluble in such metals as nickel, iron, cobalt or chromium so that the latter materials may be used as cementing agents. Moreover, their specific gravity is low.

There appears to be yet another opportunity of the application of power metallurgical techniques for the production of high temperature material with superior service characteristics. It is in the use of oxides and ceramic compounds. It is already known that specific oxides, such as alumina, can be combined effectively with such metals as nickel and cobalt, possibly with the aid of intermediate bridging metals, such as molybdenum or tungsten.

Considerable work is being done at present in America on similar lines. The work carried on there may be divided into two broad divisions: structural bodies and protective coatings for metals. The first classification includes supercharger buckets, turbine bladings, exhausts nozzles, liners for expendable and recoverable rockets and guided missiles. Although it is felt that these dynamic parts are stressed in a manner usually considered outside the realm of ceramics, studies are nevertheless being made of the theoretical mechanics of brittle materials with a view to possible design to eliminate this limitation.

Coatings for metals have, however, received concentrated attention. It is obvious that one way to extend the temperature range and the resistance to chemical attack of an existing alloy is to provide it with a protective coating. This coating must be sufficiently refractory to withstand service conditions; it must have high resistance to chipping and cracking under repeated thermal shocks and it must be resistant to corrosion and erosion by hot gases and fluids. It should further be capable of easy application to complex shapes.

Gas turbine power plant is composed largely of sheet metal parts, *e.g.*, exhaust stack, tail cones, combustion chambers etc. Some ceramic protective coatings have already been developed which have given very good service and the life of engines has been increased by at least 100%.

It is worthwhile to indicate some of the directions in which this work is being carried out in U.S.A. Attempts have been made to coat alloys by spraying refractory materials through a flame directed on the metal similar

to metallizing process. Investigations are also being carried on the alloying of the metallic constituent of metal bonded ceramic bodies with the surface of the metal to which it is applied. Impregnation of the surface of alloys with refractory oxides through pressure is also being explored.

One of the most interesting work in this connection is that pursued by Armour Research Foundation in collaboration with the Air Material Command of the U.S.A. This research programme involves the study of ternary and quaternary ceramic oxide systems in search of a glass composition which will fuse to a homogeneous mass at a temperature within the normal temperature range of ceramic enamels. The coating is to be applied in either of the two conventional ways, *i.e.*, by sifting the dry material on to the heated metal part, or by dipping the object in a slip or slurry of the ceramic composition.

After the unfired ceramic coating has been applied, the metal object is to be subjected to sufficient heat to cause the ceramic materials to fuse to a smooth adherent coating in the usual manner of porcelain enamels. The enamelled object will then be heat-treated or annealed, causing the glass coating to separate into two continuous, but mutually immiscible phases. One of these phases should be more soluble than the other, so that it may be leached out of the glass structure with acid, leaving the other less soluble, more refractory glass in place on the metal. A third heat treatment or perhaps service conditions should cause the vesicular glass residue to fuse to a smooth thin impervious, highly refractory protective coating.

Essentially this process is similar to that involved in the manufacture, of Vycor, a heat resistant glass made by Corning in U.S.A. In this process a borosilicate glass is melted in a tank, from which it is drawn to form beakers, flasks, crucibles and other chemical wares. After the ware has been moulded, it is annealed to cause separation of the glass into two distinct immiscible phases. Sulphuric or hydrochloric acid is used to dissolve out the more soluble glass, leaving a porous structure composed largely of a thickly silicious glass in the original form of the object. Reheating causes the silica glass to soften slightly well below its melting point, converting the cellular structure to a non-porous, vitreous condition.

The gas turbine is the latest form into which the internal combustion engine has developed. It operates on the same basic thermodynamic cycle as the Diesel engine. Although only Diesel fuel is being used at present for most of the gas turbines, heavier fuels and even pulverised coal will soon be used in them. Even now experiments are conducted in the U.S.A. for the use of pulverised fuel in locomotives fitted with gas turbines. When problems connected with the use of coal for running a gas turbine are solved, it will be in a position to extend its challenge to practically the whole gamut of heat engines within its range of powers which, at the moment, extends from about 1500 to 20,000 H.P. In following up this challenge the gas turbine has the advantage that it may be built in many forms, so that quite

apart from questions of cost or efficiency it is mechanically capable of satisfying the most varied requirements from those of the power units for fighter air-crafts to those of huge turbo-alternators of base load electricity generating stations. Unless some means is found for direct conversion of fission energy, the closed cycle gas turbine\* with helium as the working fluid is likely to find extensive use as the most favoured method of power generation from atomic piles. Intermediate and more immediate application of promise include the powering of locomotives and ships.

The future of gas turbine, jet turbines and even perhaps the efficient utilisation of atomic energy rest upon the ability to construct working parts and housings that will function at higher and higher operating temperatures, up to and beyond  $1400^{\circ}\text{C}$ . And at those temperatures the materials must have strength, resistance to creep, resistance to impact and heat shock, corrosion resistance and sufficient hardness to resist the abrasions and erosions of extremely high speed gas streams.

To combine such properties is quite a task which the mechanical engineer, the power engineer and the atomic engineer are anxiously waiting for the metallurgist to fulfil. And fulfil he shall.

JAMSHEDPUR ENGINEERING AND MACHINE  
MANUFACTURING, CO. LTD., TATANAGAR.

\* Gas turbines where the fuel is burnt directly in the working air are known as "open cycle" machines. If, however, it is desired to use some medium other than atmospheric air for the working fluid then this can be done by using a "closed cycle arrangement", where the exhaust gas from the turbine is passed through a cooler and then returned to the compressor inlet, the same gas being used continuously over and over again.

Various gases have been proposed for use as the working fluid in closed cycle machines, but the most popular at present is compressed air. The advantage of using compressed air instead of atmospheric air is that because of its greater density compressed air has better heat conduction and convection characteristics and thus enables heat exchanges and inter-coolers to be made both smaller and more efficient. As a result of large scale atomic fission, helium is expected to be both cheap and plentiful. In that event it will be the gas to be used in closed cycle gas turbines.

The closed arrangement does, therefore, lend itself to the relatively economic production of the more complicated cycles with several stages of intercooling, several stages of reheating, extensive heat exchange etc. Its advantages show up best on large machines of say 30,000 K.W. and above.

The disadvantage is that without these complicated refinements the closed cycle is less efficient than the open cycle and it is, therefore, not altogether suitable for marine or locomotive use where space is at a premium, nor is it attractive for peak load or stand-by plants in which simplicity and low first cost are more important than a slight saving in fuel.

#### REFERENCES

- ASTM, 1946, Symposium on materials for gas turbines, June.  
Research Memo, 1947, No 5-47, Navships 250-330-12 of U. S. Navy Bureau of ships, Sept.



## ON THE RAMAN SPECTRUM OF DIPHENYLMETHANE

BY S. K. MUKERJI AND BANARSI LAL

*(Received for publication, Nov. 2, 1950)*

Plate I

**ABSTRACT.** The Raman spectrum of diphenylmethane has been studied by using  $\lambda$  4358 as the exciting line, the substance has yielded 18 Raman lines, some of them being not recorded before. These lines are at 3057(6), 2914(3), 2789(4), 1610(6), 1590(4), 1425(2), 1280(2), 1180(2)bd, 1026(6), 1004(10), 813(4)diff., 740(4), 612(4), 550(2), 461(1), 280(2), 231(4) and 194(4)  $\text{cm}^{-1}$  respectively. The observed frequencies have been compared with those of diphenyl observed by previous authors, and it has been found that all the frequencies of diphenyl are also present in diphenylmethane.

## INTRODUCTION

Elizabeth and Grigler (1932) were the first investigators who made an attempt to obtain the Raman spectra of diphenylmethane. They have reported that the lines in the Raman spectrum of diphenylmethane are characteristic of both aromatic and aliphatic linkages. Later, Donzelot and Chaix (1935) investigated the Raman spectrum of this substance but their results do not agree with those of the previous workers. The present investigation on diphenylmethane was undertaken after the Raman spectrum of diphenyl was thoroughly studied in this laboratory by one of us (Mukerji and S. Abdul Aziz, 1938). It was, therefore, considered worth while investigating how far the lines observed in diphenylmethane agreed with those of diphenyl as investigated by them. Our investigation not only verifies the frequencies present in diphenyl but clearly demonstrates that all the important vibrations of diphenyl remain intact in diphenylmethane. In addition, in this substance we have obtained the very important characteristic frequency of the methyl group at 2914  $\text{cm}^{-1}$ . The remarkable coincidence between the frequencies of diphenyl and of those of diphenylmethane can be seen in the accompanying Table I. The substance, which was liquid at ordinary temperature, was highly fluorescent but by using suitable filters the continuous spectrum was very greatly suppressed, and the back-ground was more or less free from fluorescence. With an exposure period of about 40 hours as many as eighteen lines were recorded.

## EXPERIMENTAL

Diphenylmethane obtained from the Research Laboratory of Eastman Kodak Company was further purified by slow distillation in vacuum. The distillate was directly taken into the U-tube. It was then exposed to the light of a 1000-watt high pressure mercury arc lamp, consuming a

current of about three and a half amperes. Exposures of the order of 40 hours were given and Ilford Selochrome plates were used for photographing the spectra. The spectrograms were obtained with a fairly rapid glass spectrograph, having a dispersion of about 21 A.U. per mm in the region  $\lambda 4358\text{\AA}$ . The plates were measured with an accurate Zeiss Ikon Comparator and the wavelengths were calculated by the usual method.

TABLE I

Raman shifts in wavenumbers for Diphenylmethane along with those of Diphenyl and Methane.

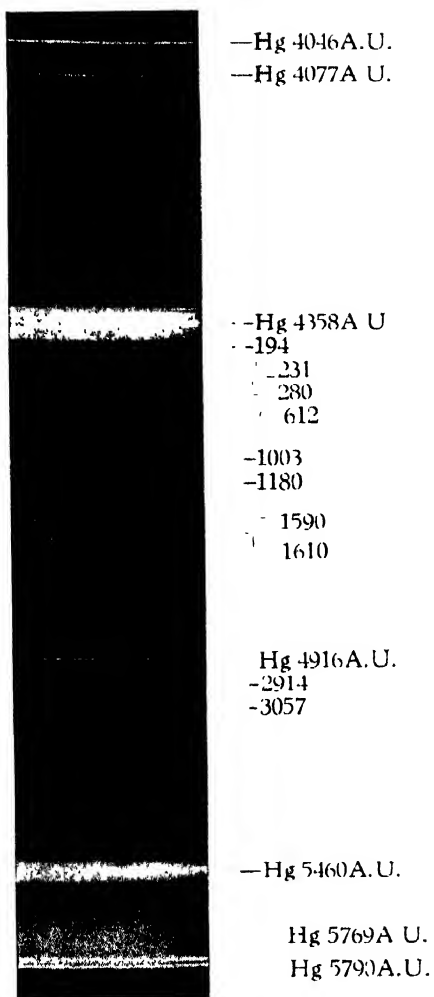
No.	Diphenylmethane.	Diphenyl (Mukerji & Aziz)	Methane
1	194 (4)	193 (0)	
2	231 (4)		
3	280 (2)	267 (4) bd	
4	461 (1)	449 (0)	
5	550 (2)	548 (1)	
6	612 (4) diff	614 (4)	
7	740 (4)	740 (5)	
		779 (4)	
8	813 (4) diff		
		838 (4) bd	
9	1003 (10)	1003 (10)	
10	1026 (6)	1032 (5)	
11	1180 (4) bd	1189 (3)	
12	1280 (2)	1283 (10)	
13	1425 (2)		
14	1590 (4)	1590 (8)	
15	1610 (6)	1610 (10)	
16	2789 (4)		
17	2914 (3)		2914 (10)
			3022 (2)
18	3057 (6) db	3062 (5)	3071 (1)

bd=broad and diffused

d=diffused.

## RESULT AND DISCUSSION

Diphenylmethane which was obtained by replacing two of the hydrogen atoms of methane by phenyl groups, was expected to give the fundamental frequencies of benzene which were also found to be present in diphenyl, (Mukerji and Aziz, 1938). As the table given here will show all the seven Raman active modes of vibration of benzene which are considered to be fundamental modes of vibration, have been observed to be present in diphenylmethane. The characteristic frequency of methane at  $2914\text{ cm}^{-1}$  is, as the above table will show, was also observed in diphenylmethane. Amongst the other most important frequencies of diphenyl, viz., frequencies at  $1610$ ,  $1590$  and  $1003\text{ cm}^{-1}$  respectively observed in diphenyl, have also been found to exist fairly strongly in diphenylmethane. The line at  $1178$



Raman spectrum of diphenylmethane



$\text{cm}^{-1}$  of benzene is also given by this substance on Plate I as a broad and diffused band at  $1180 \text{ cm}^{-1}$ . But the most intense line of diphenyl at  $1283 \text{ cm}^{-1}$ , which is not present in benzene, and which appears equally strong in all the compounds of diphenylbenzene family, appears only feebly in diphenylmethane. This shows that the line at  $1283 \text{ cm}^{-1}$  observed in diphenylmethane has a different origin from that of  $1283 \text{ cm}^{-1}$  observed in diphenyl and other compounds of the diphenylbenzene family. (Mukerji and L. Singh, 1942, 1945).

Three very low frequency lines, have also been observed in diphenylmethane at 280, 231 and  $194 \text{ cm}^{-1}$  respectively. The frequency at  $231 \text{ cm}^{-1}$  which is found to be fairly strong, does not appear in diphenyl. But the very low frequency at  $194 \text{ cm}^{-1}$  which appears fairly strongly in this substance, appears only as a very feeble line in diphenyl. These low frequency lines are evidently due to lattice oscillations which appear only feebly in diphenyl but are remarkably prominent in diphenylmethane.

DEPARTMENT OF PHYSICS,  
AGRA COLLEGE, AGRA.

#### REFERENCES

- Donzelot and Chaix 1935, *Compt. Rend.*, 201, 301,  
Elizabeth A. Grigler 1932, *Ann. Chem. Soc. J.*, 54, 4199,  
Mukerji and Aziz 1938, *Ind. J. Phys*, 12, Part IV.



## ON WAVE NATURE OF MATTER\*

By BRAHMANANDA MISHRA

*(Received for publication, July, 19, 1950)*

## Plates II A and B

**ABSTRACT.** The molecular beams obtained by vaporising sulphur and paraffin have been allowed to pass through a slit and condense on an ice-cooled glass plate. It is observed that the deposited pattern consists of parallel lines with their lengths parallel to the length of the slit. A tentative explanation is offered that the fringe system is produced by diffraction of a type of waves associated with the molecules at the slit. On this assumption the corresponding wavelengths have been calculated and have been found to be of the order of .027 mm in both the cases. Such a wavelength is different from De Broglie waves and is of the order of those corresponding to vibrations of the single molecules.

## INTRODUCTION

In 1947, while working under the guidance of Professor Massey of London University, the author observed that vapours of paraffin and sulphur, after passing through a circular aperture, deposit in the form of concentric rings on an ice-cooled plate but could not ascertain the phenomenon to be the diffraction of a type of radiation associated with the molecular beam. On reaching India, the author pursued the investigation to study the actual nature of the phenomenon.

## PRINCIPLE OF THE EXPERIMENT

The actual experimental arrangement is illustrated in Fig. 1 and the parts are given below :

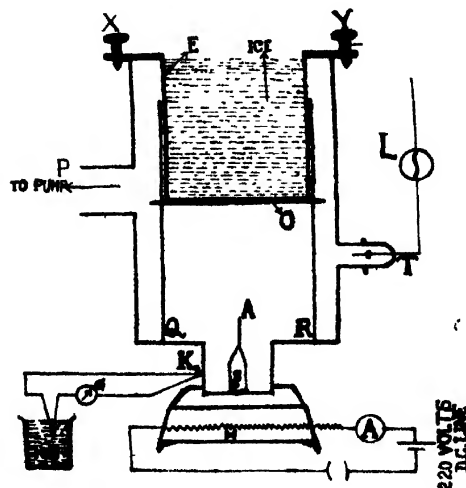


FIG. 1

\* Communicated by Prof. S. N. Bose.

*K*—Calibrated thermo-junction for recording temperature.

*H*—An electric heater.

*L*—An induction coil for passing a discharge through a tungsten electrode, I.

*P*—Pump. The pumping system consisted of an Apiezon oil pump backed by an oil diffusion pump. Pressure was judged from the no-discharge state and blue luminescences on the glass walls.

A thin film *S* of the substance was slowly evaporated at pressures of  $10^{-4}$  cms. of mercury and at temperatures near the melting point of the substance ; and the vapours, after passing through the slit *A*, were deposited on the collecting plate *O*. The fringe-width was measured with a comparator and the wavelength of the corresponding radiation was measured by assuming that the fringe system is produced by diffraction at the slit. The radiations gave a system of overlapping fringes, as indicated in Fig. 4 of Plate II B, from which the different fringe systems were sorted out and the wavelength was calculated from the equation  $\lambda = aW/d$ , where *a*=slit width, *W*=fringe width and *d*=distance between the collecting plate and the slit. Only three of the patterns are reproduced in figures 2, 3 and 4, of Plates II A, B.

## RESULTS

The results are given in Table I for sulphur and paraffin vapours at two different temperatures.

## DISCUSSION

In Table I, column 5, we calculate the average wavelength to be associated with a molecule to produce the kinetic energy given by the kinetic theory of gases with the help of the formula  $\frac{1}{2}mv^2 = h\nu$ , where  $v^2 = 3RT/M$ . This gives us the average wavelength  $\lambda_{av} = 2hcN/3RT$ . From the table it appears that the calculated wavelength is in the range of the observed wavelengths.

From columns 4 and 6, it can be seen that in the case of paraffin three distinct fringe systems give us three different wavelengths, wave numbers corresponding to which are 33.8, 166.3 and 1240.1  $\text{cm}^{-1}$  respectively at 74°C, which increase to 57, 248 and 2756  $\text{cm}^{-1}$  at 110°C. Similarly in the case of sulphur there are four different wavenumbers ranging from 71 upto 2481  $\text{cm}^{-1}$ . Of these only the first two increase at 120°C, the other two remain unaffected by the rise of temperature. These wavenumbers thus correspond to the vapours of the single molecule in the case of paraffin, the smallest wave number, however, is much too small to be accounted for in this way. In the case of sulphur, the frequencies 71 and 213  $\text{cm}^{-1}$  are in



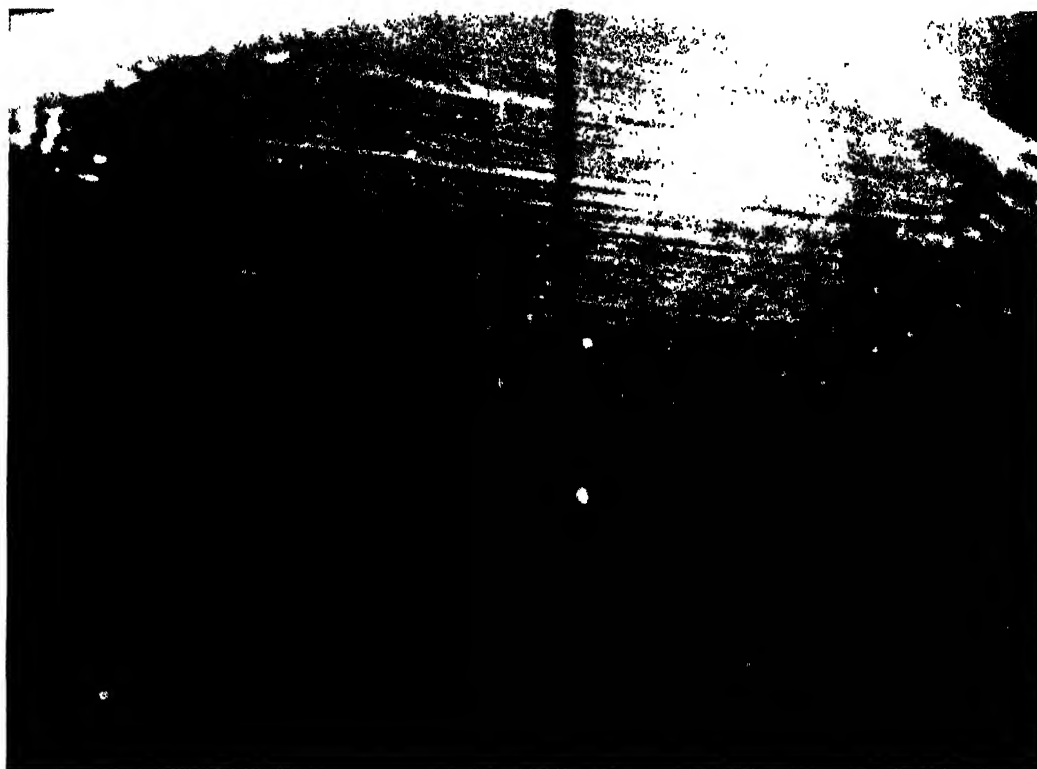


Fig 2

Single slit— $6.2 \times 0.17$  cms. Temperature =  $110^{\circ}\text{C}$ . Substance paraffin.

More than two systems of overlapping fringes are distinctly seen. The finest fringe system is due to C—H stretching vibrations.

$\lambda = 0.0036$  mms., Wave number =  $2756 \text{ cm.}^{-1}$

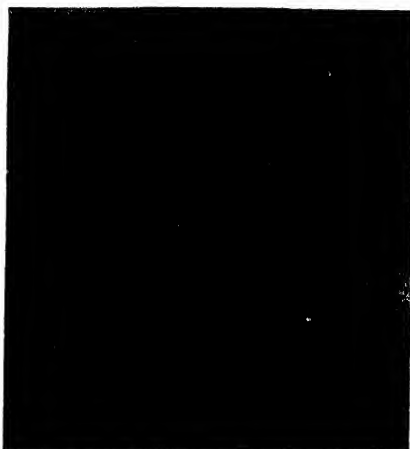


Fig. 3

Single slit  $-6.2 \times 0.17$  cms. Temperature  $-74^{\circ}\text{C}$ . Substance - sulphur

$\lambda = 0.01411$  mms. Wave number  $= 71 \text{ cm}^{-1}$

Since the fringe width of the fringe system increases with the rise of temperature, no definite conclusion regarding the interpretation of the associated radiation has yet been arrived at.

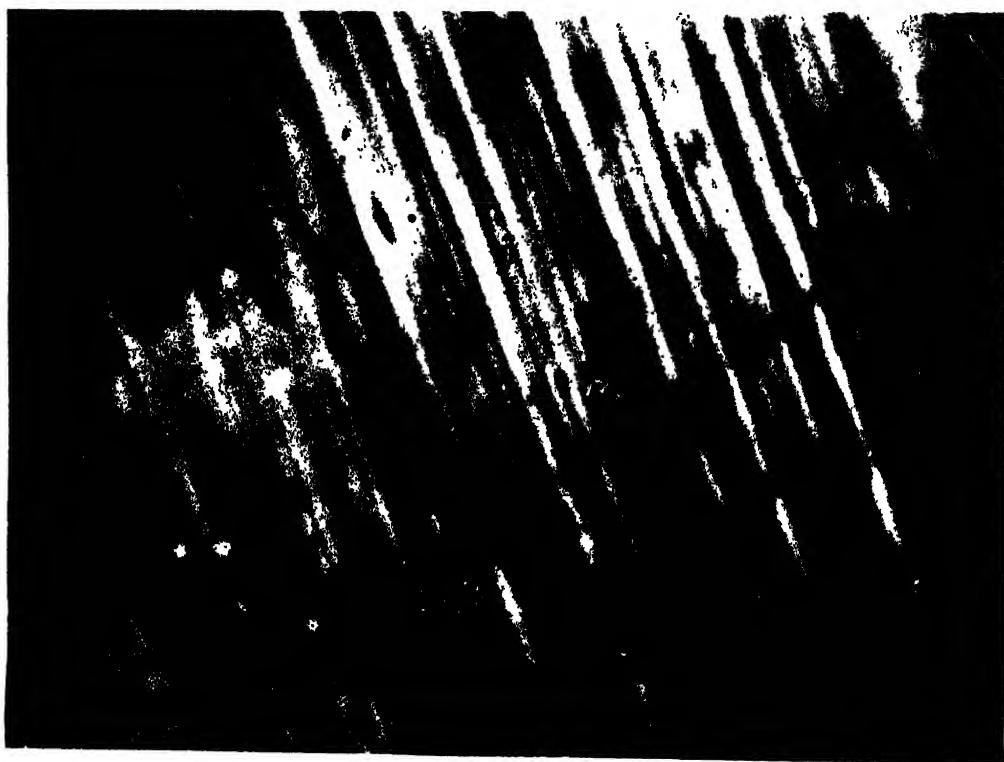


Fig. 4.

Single slit  $-6.2 \times 0.17$  cms. Temperature  $= 120^{\circ}\text{C}$  Substance - sulphur.

From the picture it is distinct that the fringe system at places is crossed by still finer fringe systems. They are due to the overtones of the fundamental vibration of the  $\text{S}_2$  molecule.

$\lambda_1 = 0.0081$  mms.  $\lambda_2 = 0.004$  mms.  $\lambda_3 = 0.0022$  mms. denote the wavelengths of the associated radiations due to the vibrations of the  $\text{S}_2$  molecule.

TABLE I

Substance	Slit-width	Temperature in degree centigrade	$\lambda$ from single slit eqn.	Theoretical average wavelength from eqn. $\lambda_{av} = \frac{2hcN}{3RT}$	Wave number in $\text{cm}^{-1}$	Raman's wave number in $\text{cm}^{-1}$	Interpretation
Paraffin	1.7 mms	74°C	0.2957 mm 0.0941 mm 0.0081 mm	0.0275 mm	$\left. \begin{matrix} 33.8 \\ 166.3 \\ 1240.1 \end{matrix} \right\}$	900 (Herzberg, 1945)	Rotational oscillation of a part of the molecule about the other part. —C—C—vibration.
Paraffin	Do	110°C	0.1747 mm 0.0403 mm 0.0037 mm	0.0254 mm	$\left. \begin{matrix} 57 \\ 248 \\ 2756 \end{matrix} \right\}$	3019 (Herzberg, 1945)	Rotational oscillation of a part of the molecule about the other fundamental C—H stretching vibration.
Sulphur	Do	74°C	0.1411 mm 0.047 mm 0.0081 mm 0.004 mm	0.0275 mm	$\left. \begin{matrix} 71 \\ 213 \\ 1240 \\ 2481 \end{matrix} \right\}$	$\left. \begin{matrix} 38 \\ 216 \end{matrix} \right\}$ (Venkateswaran, 1937)	Vibrational wave numbers of $S_2$ molecule
Sulphur	Do	120°C	0.109 mm 0.0202 mm 0.0081 mm 0.004 mm 0.0022 mm	0.0244 mm	$\left. \begin{matrix} 92.6 \\ 496 \\ 1240 \\ 2481 \\ 4651 \end{matrix} \right\}$	$\left. \begin{matrix} 85 \\ 479 \end{matrix} \right\}$ (Venkateswaran, 1937, 1935)	Vibrational wave numbers of $S_2$ molecule (fundamental and overtones).

the neighbourhood of those Raman lines observed in the case of crystals of sulphur. It is difficult at this stage to visualise how these vibrations give us the diffraction fringe system, as observed in the present case; the investigation with different slitwidths and other substances at different temperatures are in progress in order to verify that this is actually case of diffraction.

RAVENSHAW COLLEGE,  
CUTTACK.

#### REFERENCES

Herzberg, 1945, *Infra-red and Raman Spectra*, pp. 195, 316 and 462.

Venkateswaran, C. S. 1935, *Proc Ind. Acad. Sci* 1, 120

„ „ 1937, „ „ 4, 345.

# A NOTE ON THE RAMAN SPECTRA OF $\text{CH}_2\text{Cl}_2$ AND $\text{CHCl}_3$ IN THE VAPOUR STATE\*

By M. V. RAO

(Received for publication, January 16, 1951)

## Plate II

**ABSTRACT.** The Raman spectra of methylene chloride in the liquid state at  $55^\circ\text{C}$  and in vapour state at  $60^\circ\text{C}$  as well as those of chloroform in the liquid state at  $90^\circ\text{C}$  and in vapour state at  $95^\circ\text{C}$  have been investigated. It is observed that in both the cases some of the prominent lines undergo changes in the intensity and position with the changes from liquid to vapour state. In the case of chloroform the line  $3014\text{ cm}^{-1}$  seems to be weakened very much with the vaporization of the liquid. It is also suggested that the probability of inelastic scattering may be increased by action of intermolecular field in the state of aggregation.

## INTRODUCTION

The Raman spectra of a large number of substances in that vapour state were studied by Nielsen and Ward (1942) who observed that some changes in intensity, position and width of some of the lines take place with the change from liquid to vapour state. It was observed by those authors that it was difficult to record satisfactorily the Raman spectra of the vapours owing to appearance of continuous background at the high temperatures and also owing to photochemical decomposition in some cases. A programme for the study of the Raman spectra of a few organic compounds in the vapour state was, however, undertaken in this laboratory in order to find out whether the intensities of Raman lines due to the molecule in the vapour state are of the same order of magnitude as those observed in the case of the liquid state and also to find out in some particular cases whether any large change takes place in the structure of the molecule in passing from the liquid to the vapour state. The technique used was first tested with some simple molecules and the results obtained in the case of  $\text{CH}_2\text{Cl}_2$  and  $\text{CHCl}_3$  are discussed in the present paper.

## EXPERIMENTAL

The experimental arrangement was similar to that used by Nielsen and Ward (1942) excepting the fact that solution used for filtering out particular lines of the mercury arc was not used in the present case. Six mercury arcs in Pyrex glass each 15" long, made in the laboratory, were used for illuminating the vertical tube containing the vapour at a temperature much above the boiling point of the liquid. Hot air was circulated through the double-

\* Communicated by Prof. S. C. Sirkar.

walled tube in which the tube containing a calculated small quantity of the liquid was placed in order to get the vapour at a high pressure. An Adam Hilger two-prism spectrograph with a dispersion of about  $27 \text{ \AA/mm}$  in the  $4358 \text{ \AA}$  region was used in the present investigation. The exposure needed just to record the Raman spectra was about 72 to 90 hours in spite of the high light-gathering power of the spectrograph and the large intensity of illumination.

### RESULTS

The spectrograms obtained in the case of methylene chloride and chloroform in the liquid and vapour states are reproduced in Plate III. The lines for the vapour are very weak in the original spectrogram and therefore they are not reproduced satisfactorily. They were, however, intense enough to allow the correct measurement of their frequencies and the rough estimation of their relative intensities. The faint lines could not be recorded, because on increasing the exposure, the continuous background of the spectrum of light from mercury arc seemed to mask them. The results are given in Tables I and II. The data published by Nielsen and Ward (1942) have also been included in the table for comparison.

TABLE I  
Methylene chloride

Nielsen and Ward (1942)		Present author	
Liquid $\Delta\nu$ in $\text{cm}^{-1}$	Vapour $\Delta\nu$ in $\text{cm}^{-1}$	Liquid at $55^\circ\text{C}$ $\Delta\nu$ in $\text{cm}^{-1}$	Vapour at $60^\circ\text{C}$ $\Delta\nu$ in $\text{cm}^{-1}$
284 (5) 700 (10) 2990 (7)	281 (5) 712 (10) 3002 (15)	281 (5) <i>c, k</i> 700 (8) <i>c, k</i> 1418 (6) <i>c, k</i> 2986 (6) <i>c, k</i> 3044 (6) <i>c, k</i>	276 (6) <i>c, k</i> 708 (2) <i>c, k</i> 2988 (2) <i>c, k</i>

TABLE II  
Chloroform

Nielsen and Ward (1942)		Present author		
Liquid $\Delta\nu$ in $\text{cm}^{-1}$	Vapour $\Delta\nu$ in $\text{cm}^{-1}$	Liquid at $32^\circ\text{C}$ $\Delta\nu$ in $\text{cm}^{-1}$	Liquid at $90^\circ\text{C}$ $\Delta\nu$ in $\text{cm}^{-1}$	Vapour at $95^\circ\text{C}$ $\Delta\nu$ in $\text{cm}^{-1}$
261 (10) 366 (10) 668 (10) 760 (6d) 1217 (2) 3019 (6)	261 (2d) 363 (3) 672 (4) 760 (1 vd) 1217 (1) 3030 (1)	260 (10) $\pm c, \pm k$ 365 (8) $\pm c, \pm k$ 671 (8) $c, \pm k$ 760 (5d), <i>c, k</i> 1219 (1) <i>c, k</i> 3014 (5) <i>c, k</i>	260 (10) $\pm c, \pm k$ 365 (8) $\pm c, \pm k$ 671 (8) $c, \pm k$ 760 (5dd), <i>c, k</i> 1219 (1) <i>c, k</i> 3014 (5) <i>c, k</i>	246 (2) <i>c, k</i> 363 (3) <i>c, k</i> 675 (4) <i>c, k</i> 765 (2) <i>c, k</i>

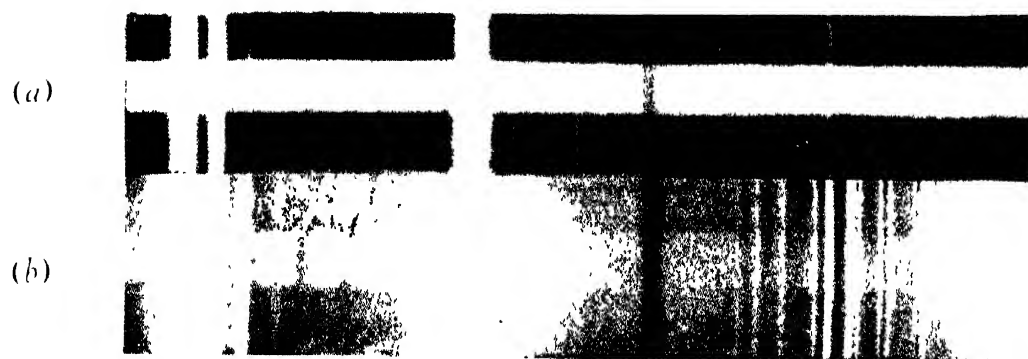


Fig. 1

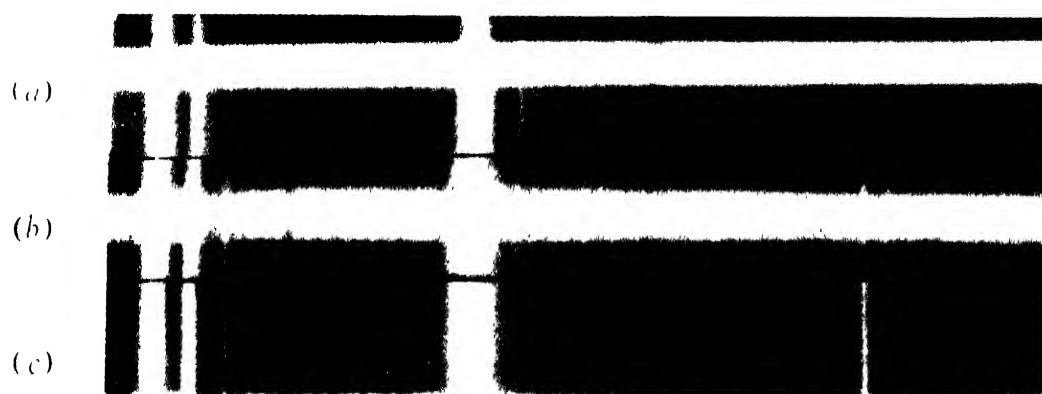


Fig. 2

### Raman Spectra

Fig 1. (a) Methylene chloride, liquid at 55°C.

(b) „ „ vapour at 60°C

Fig. 2. (a) Chloroform, liquid at 30°C.

(b) „ „ 90°C.

(c) „ vapour at 95°C.





## DISCUSSION

It can be seen from Table I that in the case of methylene chloride the three prominent lines  $281$ ,  $700$  and  $2986\text{ cm}^{-1}$  change respectively to  $276$ ,  $708$  and  $2988\text{ cm}^{-1}$  when methylene chloride at  $60^\circ\text{C}$  changes from liquid to vapour state. The magnitudes of the shifts are slightly different from those reported by Nielsen and Ward (1942), but this may be due to the fact that the temperature of the vapour in the present investigation is a little lower than that in the investigation of the previous authors. The relative intensities of the three lines observed in the case of the vapour in the present investigation indicate a diminution of the intensity of the line  $276\text{ cm}^{-1}$  with the change from liquid to vapour phase. This may be due to broadening of the line in the vapour phase.

In the case of chloroform the lines  $260\text{ cm}^{-1}$  and  $760\text{ cm}^{-1}$  shift respectively to  $246\text{ cm}^{-1}$  and  $765\text{ cm}^{-1}$  with the change from liquid to vapour phase. No such shifts were observed by Nielsen and Ward (1942). The line  $3014\text{ cm}^{-1}$  due to C-H valence oscillation is totally absent in the spectrogram due to the vapour, although the other lines of slightly higher intensities are recorded distinctly. It is doubtful whether this may be due to insufficient exposure and the effect of inertia of the photographic plates, because the line  $760\text{ cm}^{-1}$  which is of the same intensity as this line in the liquid state has been clearly recorded in the spectrogram due to the vapour. It seems, therefore, that either the line  $3014\text{ cm}^{-1}$  becomes very diffuse or its integrated intensity actually diminishes appreciably with the change from liquid to vapour state. This observation is not in agreement with that of Nielsen and Ward (1942) who did not observe any change in intensity of the line, but actually recorded a line at  $3030\text{ cm}^{-1}$  in the vapour state. Also the shift of the line  $760\text{ cm}^{-1}$  to  $765\text{ cm}^{-1}$  was not observed by them.

The preliminary results obtained in the present investigation also indicate that the absolute intensity of the Raman lines due to all the different modes of vibration of the molecule diminishes with the change from the liquid to the vapour state. This conclusion is drawn from the fact that the intensity of the lines due to a particular mass of vapour recorded with very long exposures seems to be much lower than that of the lines due to the same quantity of the liquid. This may partly be due to the extra loss of intensity of the incident light caused by total reflection at the inner surface of the wall of the Pyrex tube containing the vapour and absence of such reflection in the case of the liquid, but the observed low intensity of the Raman lines in the case of the vapour cannot be wholly accounted for in this way. It seems to be likely that the probability of inelastic scattering is increased by intermolecular field in the liquid and solid states of the molecules. No definite conclusion can, however, be drawn without making quantitative estimation of the intensities in the case of liquid and vapour states.

## ACKNOWLEDGMENT

The author's thanks are due to Prof. S. C. Sirkar of his kind interest in the work.

OPTICS DEPARTMENT,  
INDIAN ASSOCIATION FOR THE CULTIVATION OF SCIENCE,  
JADAVPUR, CALCUTTA, 32.

## REFERENCES

Nielsen and Ward, 1942, *Jour. Chem. Phys.*, **82**, 10, 82.

## THE ABSORPTION SPECTRUM OF BISMUTH SULPHIDE BiS

By P. K. SUR

*(Received for publication, August 24, 1950)*

**ABSTRACT.** Two band systems of the BiS molecule have been obtained in absorption in the near and farther ultraviolet regions ( $\lambda\lambda 3056-2351$ ) and ( $\lambda\lambda 2312-2133$ ). Most of the bands in the two system have been classified, and their vibrational levels assigned. A number of bands, however, remains unclassified of which a list is given in Table II. The band heads seem to fit in the following formulae within experimental error which, in a few cases of weak and diffuse bands, amount to more than  $1 \text{ \AA}$ , i.e., about 25 wave numbers in the farther ultraviolet region.

$$\text{System I } \gamma = 37217.35 + 378.4 u' - 5.7 u'^2 - 386 u'' + 3.5 u''^2$$

$$\text{System II } \gamma = 45530 + 775 u' - 6.0 u'^2 - 386 u'' + 3.5 u''^2$$

where  $u = (v + \frac{1}{2})$ .

## INTRODUCTION

Sharma (1948) had observed in absorption two prominent band system of the BiSe molecule in the ultra violet regions ( $\lambda\lambda 2900-2700$ ) and ( $\lambda\lambda 2350-2200$ ) respectively at temperatures from  $950^\circ\text{C}$  to  $1150^\circ\text{C}$  using an absorbing column of vapour of the mixture of bismuth and selenium metals in proportional parts, heated within a graphite tube furnace. It was thought that a similar molecule like BiS of the same group might also give rise to absorption bands near about the same region. Further, there was chemical evidence of the independent and stable existence of BiS molecule with a definite melting point  $685^\circ\text{C}$ , which was quite suitable for obtaining an absorbing column of vapour inside the available graphite tube furnace. These considerations led to the present investigation. Two band systems, one very extended and the other much shorter, were obtained in absorption as expected of the molecule in the regions ( $\lambda\lambda 3056-2351$ ) and ( $\lambda\lambda 2312-2133$ ) which were degraded to the red and to the violet end respectively. The heads of nearly all the bands of the extended system seem to fit in the formula,

$$\text{I } \gamma = 37217.35 + 378.4 u' - 5.7 u'^2 - 386 u'' + 3.5 u''^2$$

and those fewer band heads of the shorter system fit in the formula

$$\text{II } \gamma = 45530 + 775 u' - 6.0 u'^2 - 386 u'' + 3.5 u''^2$$

The agreement between the observed and calculated values of the band heads of the first system, particularly for higher values of  $v'$ , is not satisfactory in view of the fact that proper assignment of  $v'$  values for a case like this is not possible, as discussed later. The constants for the system II are not quite

certain on account of very insufficient number of bands. The formula proposed is, however, the best approach possible to explain the position of the band heads observed.

#### EXPERIMENTAL

A pure specimen of the  $\text{Bi}_2\text{S}_3$  molecule could not be obtained, and hence a sample of the salt was prepared by passing  $\text{H}_2\text{S}$  in a  $\text{BiCl}_3$  solution. The precipitate was washed several times repeatedly until it was definitely established by chemical tests that it became free from hydrochloric acid. The precipitate was left for several days inside a desiccator. The salt so prepared was introduced into a vitreosil tube, about 5 mm bore and 20 cms long, which was inserted into the Acheson graphite tube of a vacuum furnace. The furnace was originally designed and used by Saha, Sur and Mazumdar (1926) for their work on thermal ionisation and later on modified and used in this laboratory by many workers for experiments on absorption spectra. The graphite tube was held in a horizontal position by means of carbon blocks fixed to the electrodes with nuts and bolts. The electrodes, as well as the walls of the furnace, were kept cool by a water circulating arrangement. The projecting ends of the furnace in the lengthwise direction were closed by quartz windows which were cemented by sealing wax. The line joining the centres of the windows was adjusted to coincide with the axis of the hollow graphite tube. The furnace was provided with side windows to make observation inside the furnace. The electrodes were heated electrically by a heavy current of several amperes derived from the secondary of a step down 10 k.w. transformer operated by 110 volts-A.C. The graphite tube could be heated to a temperature of about  $2000^\circ\text{C}$  by inductive control in the primary circuit of the transformer.

The source of continuum was a water cooled hydrogen discharge tube fitted with a quartz window. The discharge was run by a 3-k.w., H.T. transformer operated by 110 volts-A.C. The spectrum was photographed with a copper comparison spectrum on B.20 Kodak plates with a medium sized quartz spectrograph. An optical pyrometer was used for measuring the temperature of the furnace. An exposure ranging from 45 minutes to 1 hour 20 minutes was necessary to bring out the bands on the plates.

Both the systems of absorption bands develop within  $850^\circ\text{C}$ – $1000^\circ\text{C}$  which seems to be the optimum range for observing these bands. Three different exposures are taken at temperatures  $(850-875)^\circ\text{C}$ ,  $(925-950)^\circ\text{C}$  and  $(950-1025)^\circ\text{C}$ . A progressive development of bands was observed. In the first plate was recorded only 25 bands. In the second, additional bands  $\lambda_{2980.5}$ ,  $\lambda_{2732.7}$ ,  $\lambda_{2569.7}$ ,  $\lambda_{2554.8}$ ,  $\lambda_{2516.7}$ ,  $\lambda_{2498.8}$ ,  $\lambda_{2481.2}$ ,  $\lambda_{2435.7}$ ,  $\lambda_{2418.8}$ ,  $\lambda_{2406.7}$  and  $\lambda_{2392.3}$  were recorded, and in the third a number of additional bands were developed, though very weak, towards the  $\nu'$  progression, as analysis has revealed. The following additional bands were observed on the third spectrogram :  $\lambda_{3055.8}$ ,  $\lambda_{2560.9}$ ,  $\lambda_{2477.2}$ ,  $\lambda_{2470}$ ,  $\lambda_{2464.5}$ ,  $\lambda_{2453.9}$  ;  $\lambda_{2451.3}$ ,  $\lambda_{2447.3}$ ,  $\lambda_{2433.3}$ ,  $\lambda_{2392.3}$ ,  $\lambda_{2377.3}$ ,  $\lambda_{2357.8}$ ,  $\lambda_{2351.6}$ .

## SYSTEM I

TABLE I

$\lambda$ in Å	Int. in absorption	$\gamma$ obs. in $\text{cm}^{-1}$	$\gamma$ cal $\text{cm}^{-1}$	Analysis $\nu'$ , $\nu''$
3055.8	3	32715	32713	2, 16
3044.8	1	32833	32832	0, 13
3024.6	3	33053	33057	3, 16
3017.9	2	33126	33127	0, 12
2999.2	3	33333	33331	3, 15
2990.5	3	33430	33429	0, 11
2980.5	2	33542	33556	2, 13
2954.0	3	33843	33851	1, 12
2961.2 ?	5	33760	33758	0, 10
2927.4	6	34150	34152	2, 11
2921.4	3	34220	34232	4, 13
2888.3	4	34612	34607	8, 16
*2861.5	5	34937	.....	
2825.9	6	35377	35388	0, 5
2800.4 ?	0	35698	35674	11, 15
2797.2	10	35740	35739	0, 4
2769.5	10	36097	36097	0, 3
2741.8	7	36462	36462	0, 2
2713.9	6	36836	36834	0, 1
2687.1	9	37204	37201	1, 1
2663.3	10	37536	37529	3, 2
2638.0	9	37896	37901	3, 1
2615.1	9	38230	38234	4, 1
2593.1	8	38553	38555	5, 1
2554.1 ?	0	39143	39164	7, 1
2517.2	2	39247	39244	6, 0
2528.2	4	39542	39543	7, 0
2516.7	1	39723	39727	9, 1
2509.3	1	39810	39830	8, 0
2507.2	3	39873	39872	11, 2

Some of the bands which came out on the 2nd plate were found missing on the 3rd plate taken at a higher temperature. These are  $\lambda 2857.0$  and  $\lambda 2569.7$  which fall in the list of unclassified bands as appended in Table II.

### RESULTS

In making out the final list of band heads of the BiS molecule, the best possible mean of the measurements from the different plates are taken wherever the bands are observed on more than one plate. Table I gives the wave lengths in  $\text{\AA}$  in air, visual estimates of their intensities on the scale of 10, wave numbers observed in  $\text{cm}^{-1}$  in vacuum and those calculated from the formula. The last column gives the vibrational analysis.

Table V gives the Deslandre's scheme for system I, Fig 1 gives the intensity plots of the band heads and the Frank Condon parabola, Table III and Table IV give the corresponding arrangements for system II.

Table II gives the list of unclassified bands which are all of very poor intensity. The position of their heads are mostly uncertain, and they are observed in any one plate.

General features of transitions in absorption for system I, as depicted in Table V, can be explained by the upper and lower states *A* & *B*, as shown in Fig. 2 in which  $r_e' > r_e''$ ,  $\omega' < \omega''$  and  $D_0'$  slightly less than  $D_0''$ . Table V shows that bands  $v'', 0$  and  $v', 0$  to 5 are not observed, which is explained by the above figure. The thin continuous lines, shown vertically from  $v''$  to  $v'$  levels of the electronic states *B* and *A* respectively, serve to explain the

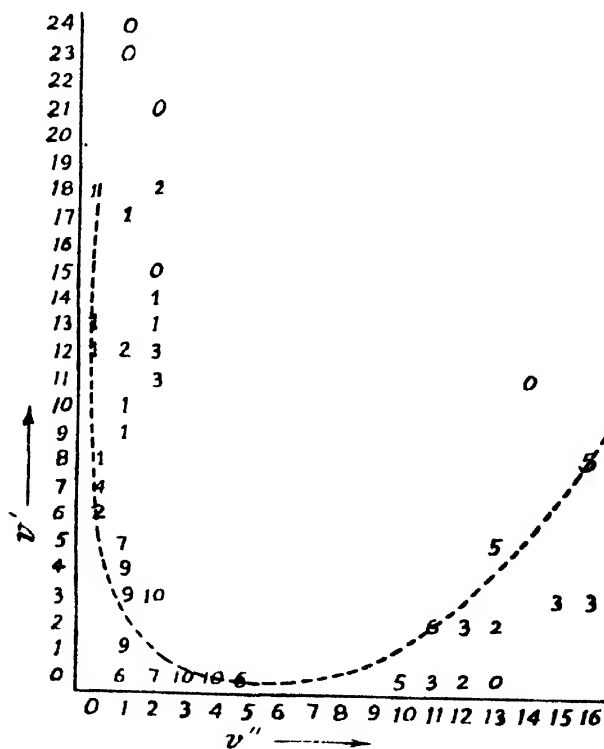


FIG. 1

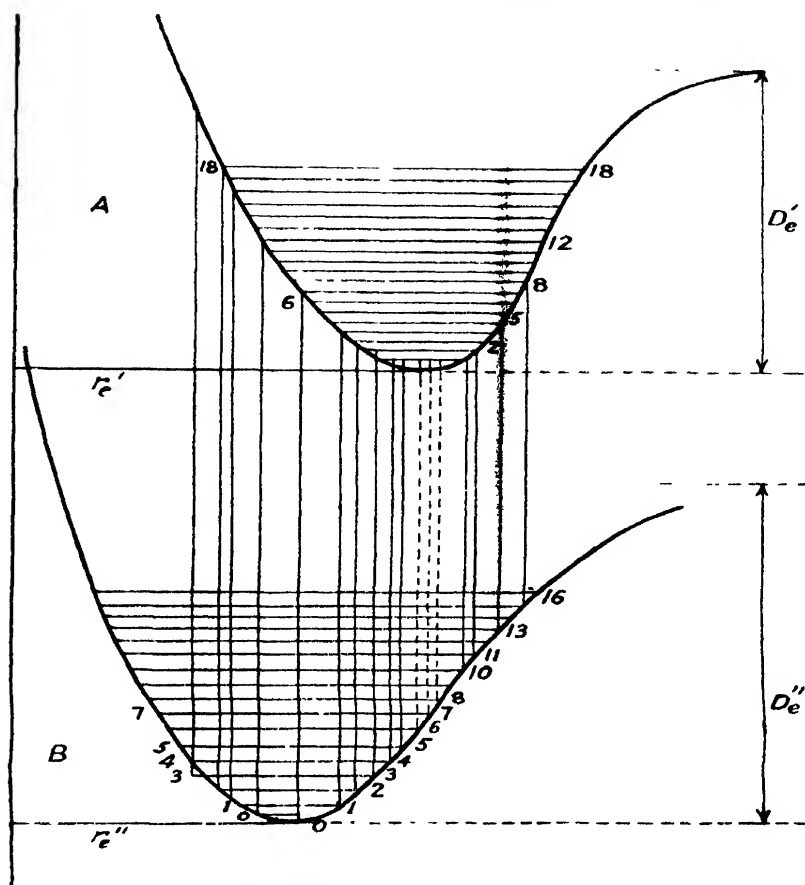


FIG. 2

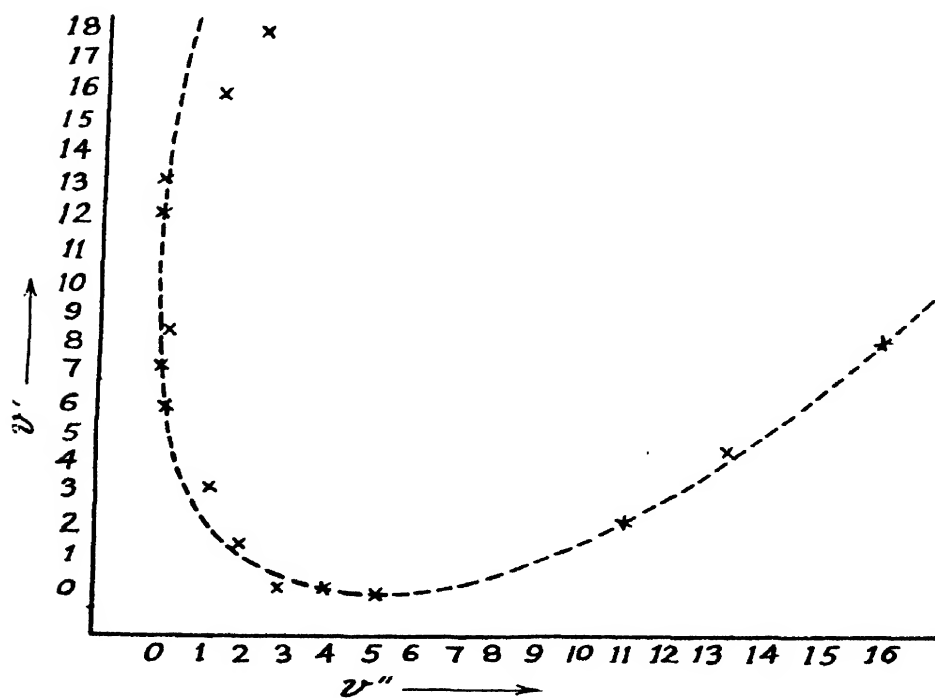


FIG. 3

observed bands of strong and moderately strong intensities according to Frank and Condon principle. The figure explains that transitions from the  $r_{\min}$  side of  $v''$  levels 3, 4 and 5 are not possible so that bands with  $v''$  equal to 3, 4 and 5 to  $v', 0$  are only possible from  $r_{\max}$  side of these  $v''$  levels as are actually observed, and shown in Table V.

Transition indicated by thin dotted lines are either inadmissible or else have poor intensities, as they end on about the middle of the 0-0 level of the upper state  $A$  where the kinetic energy of oscillation of the level is greatest. This possibly explains why in Table V no bands are observed for  $v', 0$  and  $v'', 6$  to 9.

For a typical case as this where  $r_e' > r_e''$ ,  $\omega' < \omega''$  and  $D_0'$  slightly less than  $D_0''$ ,  $u_r$  curves are asymmetrical about  $r_e$ , i.e., equilibrium positions and molecules spend an extended period of stay at the  $r_{\max}$  positions, so that transitions from  $r_{\max}$  positions of the  $\mu_r$  curves are more probable.\*

Intensities, as expected in absorption from the ground state  $B$  to the upper state  $A$  according to Frank and Condon principle, are shown in figure 3. The expected Frank Condon parabola shows the asymmetrical branches along the  $v'$  and  $v''$  progression with the intensities along  $v''$  more pronounced. All these facts are in agreement with the observed intensity plots of the bands and the Frank Condon parabola as shown in Fig. 1. (Only strong transitions according to Frank-Condon principle are considered in obtaining this curve from the two states  $A$  and  $B$  of Fig. 2.

\* Type IV discussed on page 39 in Introduction to Molecular Spectra by R. C. Johnson (Methuen).

#### ACKNOWLEDGMENT

The author is grateful to Dr. K. Mazumdar, D.Sc. for his interest and guidance in this investigation.

#### REFERENCES

- Sharma, C. B. 1950, for the *Curr. Sci.*, **90**, 648.  
Saha, Sur and Mazumdar, 1926, *Zeit fur Physik*, **40**, 648.



## ULTRASONIC VELOCITY IN ORGANIC SOLUTIONS II

By K. C. LAL

*(Received for publication, July 15, 1950)*

**ABSTRACT.** In this paper is reported the ultrasonic velocities and adiabatic compressibilities of solutions of benzoic acid in absolute alcohol, iso-butyl alcohol and carbon tetrachloride at various temperatures.

The results are in agreement with those reported in the previous paper.

## INTRODUCTION

In a paper recently communicated the author (Lal, 1950) gave experimental determinations of ultrasonic velocities in solutions with a solid solute. It was observed that the presence of a solid, however small it may be, always lowers the velocity. The present paper forms a continuation of the series, the investigations being on the following solutions.

1. Benzoic acid in ethyl alcohol.
2. Benzoic acid in iso-butyl alcohol.
3. Benzoic acid in carbon tetrachloride.

The experimental arrangement is the one followed in earlier investigations and it has been described in full in the first paper.

The liquids were of the purest stock and used after distillation; the solid benzoic acid was recrystallised.

The frequencies and the temperatures at which the determinations were made, are noted against each solution.

## RESULTS

The following tables contain the results of determination of ultrasonic velocities in the solutions at different temperatures and concentrations.

TABLE I. Benzoic acid and ethyl alcohol solutions.

(a) *Variation of velocity and adiabatic compressibility with concentration.*

No.	Concentration	Temperature °C	Density gms./c.c.	Frequency Mc/sec.	Velocity Metres/sec.	Adiabatic- compressibility $\times 10^6$
1.	M/5	28	0.7990	4.275	1102	115.10
2.	M/10	28.5	0.7961	4.380	1107	114.90
3.	M/15	28.5	0.7937	4.325	1113	114.71
4.	M/20	29.5	0.7923	4.425	1122	113.98
5.	Pure Alcohol	29.5	0.7905	4.425	1158	110.70

TABLE I (contd.).

No.	Concentration	Temperature °C	Frequency Mc/sec	Velocity. Metres/sec.
1.	M/5	18	4.275	1110
2.	M/10	18	4.380	1116
3.	M/15	18	4.275	1145
4.	M/20	18	4.275	1158
5.	Pure ethyl alcohol	18	4.275	1172

No.	Concentration	Temperature °C	Frequency Mc/sec.	Velocity. metres/sec
1.	M/5	2.8	4.425	1132
2.	M/10	2.8	4.380	1179
3.	M/15	3	4.275	1215
4.	M/20	2.8	4.275	1220
5.	Pure ethyl alcohol	2.8	4.275	1252

## (b) Variation of velocity with temperature.

No.	Concentration	Temperature °C	Velocity metres/sec
1.	M/5	28	1102
		18	1110
		10	1122
		2.8	1132
2.	M/10	28.5	1107
		18	1116
		10	1143
		2.8	1179
3.	M/15	28.5	1113
		18	1145
		7	1197
		2.8	1215
4.	M/20	29.5	1122
		18	1158
		2.8	1220
5.	Pure ethyl alcohol	29.5	1158
		18	1172
		9	1201
		2.8	1252

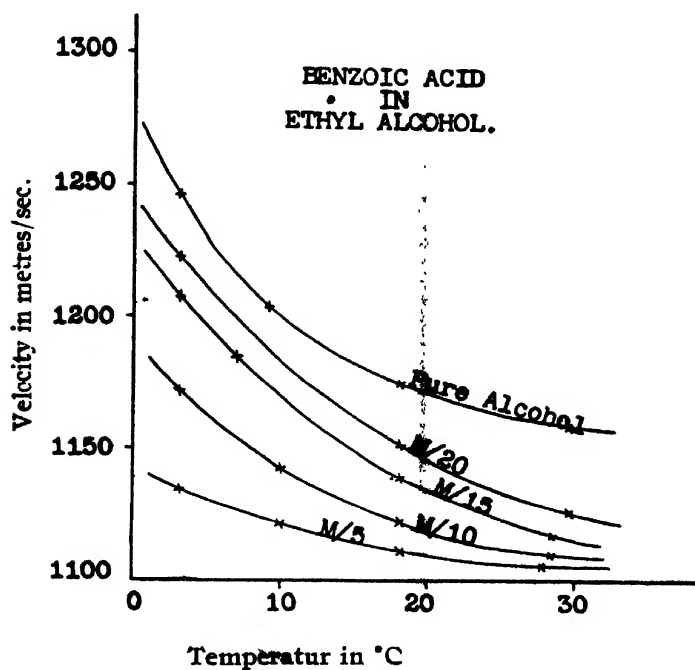


FIG. 1

TABLE II. Benzoic acid in iso-butyl alcohol.

(a) Variation of velocity and adiabatic compressibility with concentration.

No.	Concentration	Temperature °C	Density gms/c.c.	Frequency Mc./sec.	Velocity Metres/sec.	Adiabatic-compressibility $\times 10^6$
1.	M/5	28.5	0.8036	4.655	1197	88.01
2.	M/10	29	0.7996	4.65	1204	87.42
3.	Pure iso-butyl alcohol	29	0.7951	4.45	1212	86.36

No.	Concentration	Temperature °C	Frequency Mc./sec.	Velocity metres/sec.
1.	M/5	20	4.655	1234
	M/10	20	4.65	1246
	Pure iso-butyl alcohol	20	4.75	1252
2.	M/5	10	4.655	1276
	M/10	10	4.65	1284
	Pure iso-butyl alcohol	10	4.75	1289
3.	M/5	4.5	4.655	1298
	M/10	4.5	4.65	1305
	Pure iso-butyl alcohol	4.6	4.75	1312

(b) Variation of velocity with temperature.

No.	Concentration	Temperature °C	Velocity metres/sec
1.	M/5	28.5 20 10 4.5	1197 1234 1276 1298
2.	M/10	29 20 10 4.5	1204 1246 1284 1305
3.	Pure iso-butyl alcohol	29 20 10 4.6	1212 1252 1289 1312

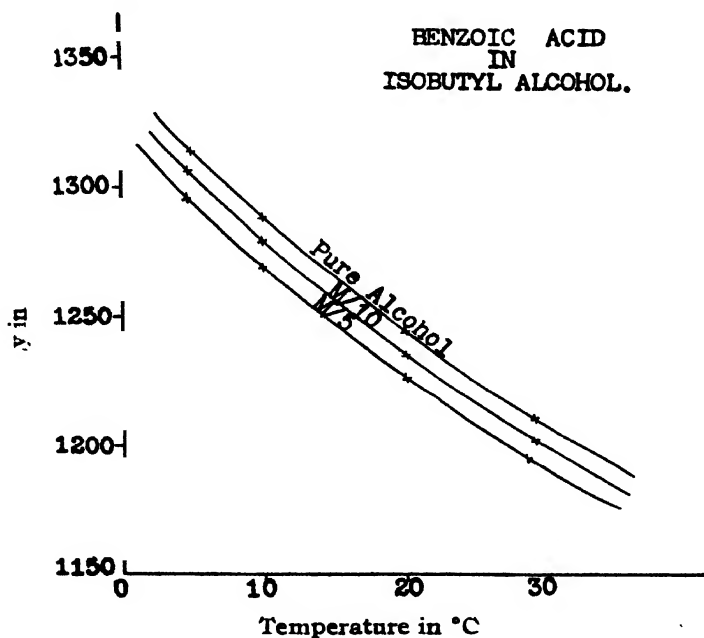


TABLE III. Benzoic acid and carbon tetrachloride solution.

(a) Variation of velocity and adiabatic compressibility with concentration.

No.	Concentration	Temperature °C	Density gms/c.c.	Frequency Mc/sec.	Velocity metres/sec.	Adiabatic compressibility $\times 10^6$
1.	M/5	31	1.556	4.13	819	79.5
2.	M/10	31	1.560	4.13	823	78.9
3.	M/15	31	1.562	4.13	825	78.6

No.	Concentration	Temperature. °C	Frequency Mc/sec	Velocity metres/sec.
1.	M/5	20	4.13	833
	M/10	20	4.13	840
	M/15	20	4.13	845
2.	M/5	10	4.13	852
	M/10	10	4.13	869
	M/15	10	4.13	880
3.	M/5	2.6	4.13	884
	M/10	2.6	4.13	901

(b) Variation of velocity with temperature.

No.	Concentration	Temperature °C	Velocity metres/sec.
1.	M/5	31	819
		20	833
		10	852
		2.6	884
2.	M/10	31	823
		20	840
		10	869
		2.6	901
3.	M/15	31	825
		20	845
		10	880

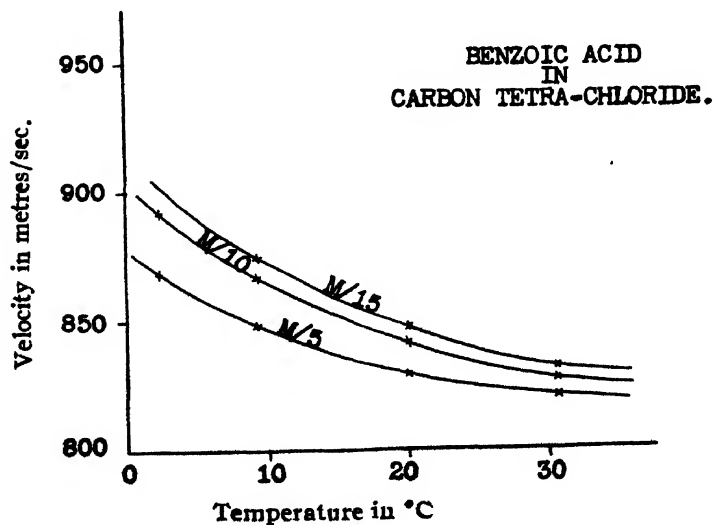


FIG. 3

## I N F E R E N C E S

The results are in agreement with those reported in the first paper. They are:

1. The velocity in a pure solvent is always greater than that in the solution.
2. The presence of a solid constituent, however small, always lowers the velocity.
3. The velocity in a solution increases with dilution.
4. The adiabatic compressibility in a solution increases with concentration.
5. The ultrasonic velocity in a solution decreases with the rise in temperature.

Discussion on the above results will be given in subsequent papers.

## A C K N O W L E D G M E N T S

In conclusion the author expresses his very grateful thanks to Dr. D. B. Deodhar for his guidance and kind interest and his deep indebtedness to Dr. P. N. Sharma for encouragement and helpful discussions.

PHYSICS DEPARTMENT,  
LUCKNOW UNIVERSITY.

## R E F E R E N C E S

- Lal, K. C., 1950, *Ind. Jour. Phy.*, **24**, 461.

# LOW-FREQUENCY RAMAN LINES IN PARA-DICHLORO-BENZENE

By HARI NARAIN AND BISHAMBHAR DAYAL SAKSENA

(Received for publication, October 3, 1950)

Plates IV A, B.

**ABSTRACT.** The low frequency lines of para-dichlorobenzene have been studied in different orientations of the crystal which was in the form of a cylinder with the symmetry axis along the length of the cylinder. Raman spectra of the liquid and of a different specimen of solid para-dichlorobenzene have also been studied. The Raman spectrum shows six polarised frequencies 330, 747, 1071-1084, 1106, 1169, 3072 and seven depolarised frequencies 299, 628, 675, 1248, 1376, 1485, 1573. In the directional excitation of the solid in the form of a single crystal it is found that if the crystal be illuminated with its symmetry axis along the direction of observation and the electric vector be along the direction of, observation or perpendicular to it along OZ, it is noticed that the frequencies 747, 1071, 1106, 3072 are very much increased in intensity in the latter case than in the former while 308, 630, 1376 remain nearly of the same intensity in the two cases and 330, and 1576 are reduced in intensity. Similarly the low frequency line 94 is much weaker than 27 when the electric vector is along OY and stronger when the electric vector is along OZ. The frequency 54 remains strong in all the cases. The tensors have been derived for these frequencies, which indicate that each frequency represents a symmetric and an asymmetric oscillation. The tensor for 94 also indicates that the asymmetric component is much weaker than the component of symmetric oscillation. This frequency, therefore, behaves like the frequencies 747, 1106, etc.

The frequencies 299 and 330 also show variations in intensity. The frequency 299 in liquid is increased to 308 in solid. In the liquid 299 is weaker than 330 but in the solid 308 is comparable to and even greater than 330.

In the solid pictures we find two different low frequency spectra. In our picture we get the frequencies 27, 54 and 94 while in the other we get 45, 57 and 84 although the liquid spectrum is the same in the two cases. As 27 does not vanish in any orientation, it follows that the disappearance of frequency 27 in the second case is not an orientation effect. The latter frequencies were obtained by Venkateswaran by rapid cooling from the melt and it is likely that the second solid was obtained in that way. It is suggested that the results reveal a change of structure of para-dichlorobenzene in the way the crystal is grown.

## INTRODUCTION

The low frequency Raman spectrum of para-dichlorobenzene has been investigated by Vuks (1936, 1937), Sirkar and Gupta (1936, 1937), Sirkar and Bishui (1937) and Venkateswaran (1938). Vuks found that the low frequency spectrum changes with temperature and from this he concludes that there are two modifications of the substance—the  $\alpha$ -modification being stable below 32°C and the  $\beta$ -modification is stable above 32°C. The transformation according to Vuks does not involve any change of volume. Vuks has called these low frequencies as lattice oscillations. Sirkar and Gupta and also Sirkar and Bishui find that there is no change in the Raman spectra at 32°C and 45°C.

They, however, report a change when the mass is cooled in ice and brought to the room temperature. The former authors also report that there is no change in Laue patterns with the hot and the cold crystal. Venkateswaran is also unable to confirm the change in the spectra of para-dichlorobenzene at less than  $25^{\circ}\text{C}$  and greater than  $33^{\circ}\text{C}$  as reported by Vuks attributing it to a change of crystal form, although the substance was kept for well over a week at ice-cold temperature. Sirkar and his co-workers aver that these oscillations are not of the lattice but arise from intermolecular oscillations of polymerised groups in the solid. The results of these authors are given in the Table I.

It may be seen from Table I that the frequency 27 has been obtained only by Vuks and that he has distinguished between the  $\alpha$ - and  $\beta$ -modifications by the appearance or disappearance of this frequency. It is now well known that the intensity of Raman lines in a crystal varies with directional excitation. It is therefore important to study whether its disappearance is an orientation effect or due to crystal modification as suggested by Vuks. It may be stated that the pictures reproduced by Sirkar and co-workers and also by Venkateswaran are not good enough to clearly bring out the frequency 27. Both these authors have not worked with single crystals with the result that the Rayleigh line has become much over-exposed due to extraneous light. By working with single crystals we have been able to get very good pictures and the low frequency lines have come out very distinctly without being masked by the halation due to Rayleigh line.

#### CRYSTAL STRUCTURE

According to Hendricks (1933) para-dichlorobenzene belongs to the mono-

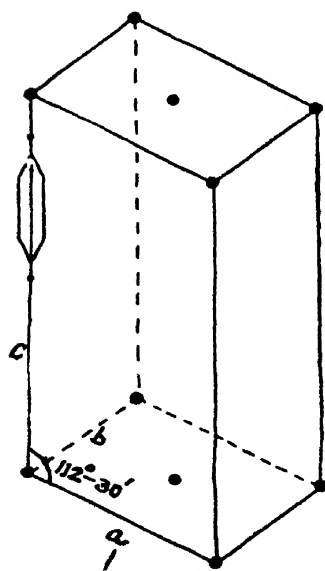


FIG. 1

clinic prismatic class having the point group  $C_{2h}$ , and the unit cell contains two molecules. The dimensions of the unit cell are  $a=5.88\text{\AA}$ ,  $b=4.1\text{\AA}$  and  $c=14.88\text{\AA}$ ,  $\angle \theta=112^{\circ} 30'$ . The unit cell is shown in figure 1. The centre of inversion is located at the centre of each molecule and the orientation of other molecules can be obtained by the glide plane of reflection in (010) planes, the gliding being parallel to the  $a$ -axis. The elements of symmetry are

- $C_2$  Screw axis (1, 2)
- $i$  Centre of symmetry (1) (2)
- $\sigma_h$  Glide plane (1, 2)

The  $b$ -axis in the crystal is the axis of two fold symmetry while the  $c$ -axis is easily identified as the crystal is elongated along this axis. The crystal



TABLE I

Liquid	Vnks Solid		Sirkar and Gupta Solid			Sirkar and Bishui		Venkateswaran Solid
	<25°C	>32°C	45°C	32°C	32°C	31°C	31°C	
	$\alpha$ -mod.	$\beta$ -mod.	(melted and cooled)	mass once cooled in ice			after cooling in ice	
	27.5							
	46.5	43.3	40(11)	46(2)	55(2)	40(25)		43(6)
	54	54.5	50(2)	50(2)	60(2)	50(25)	48(2)	55(5)
	93	82	82(2)	93(2)	105(2)	82(2)	93(2)	88(5)
299.7 (5)	307.6 (5)	304.1 (5)				309(2)	308(1)	
329.5(10)	328 (10)	329.5(10)				330(3)	327(1)	
748.1(10)	745 (10)	745.2(10)				745(4)	745(3)	
1108.4(10)	1104.5(10)	1103.9(10)				1106(5)	1102(4)	
3071.3(10)	3071.3(10)	3072.2(10)				3072(5)	3070(4)	
							3070(3)	

being monoclinic, one of the optic axes  $\beta$  coincides with the symmetry axis  $b$  of the crystal, the other two optic axes namely  $\alpha$  and  $\gamma$  lie in the plane (010). Their exact orientation is not known but as  $\angle \theta = 112^\circ 30'$  they will be making small angles with the  $a$ - and  $c$ -axes. Bragg (1939) has shown that for aromatic crystal of the naphthalene class the length of the molecule lies along the elongated axis. In the case of para-dichlorobenzene, since  $c$  is very large in the unit cell, the length of the molecule should be nearly parallel to the  $c$ -axis along which the optical polarisation should be maximum. According to Hendricks, the molecules are almost parallel to the  $c$ -axis in the projection of the unit cell on the  $ac$  plane. We may therefore consider the molecules as roughly lying in the  $bc$  plane, the breadth of the molecule being along the  $b$ -axis and the length along the  $c$ -axis. We may therefore roughly regard  $b$ -axis as the axis of intermediate polarisability and the  $a$ -axis as the axis of minimum polarisability. We have assumed for the sake of simplicity that  $\gamma$ -axis of polarisability lies along the  $c$ -axis and the  $\alpha$ -axis along the  $a$ -axis although these will in general be slightly inclined to these directions.

#### LATTICE OSCILLATIONS IN PARA-DICHLOROBENZENE

It is now well known that all crystals give low frequencies. Placzek (1934) has shown that the modes of vibration of a crystal lattice may be analysed by considering the unit cell as the basis. Bhagavantam (1939) has in this way considered the modes of vibration of a number of crystals such as calcite,  $\text{NaNO}_3$ , gypsum and Saksena of quartz. Experimental work on the directional excitation in crystals by Bhagavantam (1940) in calcite, Nedungadi (1939) in  $\text{NaNO}_3$  and Saksena (1940) in quartz agree completely with the theoretical predictions which shows that all frequencies shown by a crystal are lattice frequencies. In a molecular crystal the low frequency region appears well separated from the regions of high frequencies which represent the molecular frequencies, but this is not so in the case of a linked crystal like quartz where such a distinction cannot be made. The low frequencies in a crystal are particularly sensitive to temperature.

In para-dichlorobenzene the low frequency spectrum is well separated from the high frequency region which represents molecular frequencies. The molecule  $\text{C}_6\text{H}_4\text{Cl}_2$  has a symmetry  $D_{2h}$  and possesses a centre of symmetry. The thirty internal modes are therefore equally divided in the Raman active and infra-red active classes, the Raman active modes being infrared inactive. Out of the 15 Raman active modes 6 are polarised and 9 depolarised.

The crystal of para-dichlorobenzene has a symmetry  $C_{2h}$  and has a centre of symmetry at each molecule. The Raman active modes will therefore be infra-red inactive. As there are two molecules in the unit cell, there are now 24 atoms and 72 degrees of freedom. For the two molecules we will

have 60 internal and 12 external degrees of freedom. The 30 internal modes and the six degrees of translation and rotation of each molecule, can be coupled in the same or opposite phase to give 60 internal modes and 12 external modes. As regards the internal modes, we may not expect any appreciable change of frequency of molecular vibrations by coupling them because the bindings in a molecule are very much stronger than those between the two molecules. Each of the 30 internal modes will therefore be merely doubly degenerate without showing any appreciable change of frequency.

The external modes will be of two types namely translational and rotational produced by coupling of translations and rotations of the two molecules. As the centre of symmetry is preserved in rotation, the rotational modes will be Raman active and translational modes Raman inactive. Mathematically these results may be expressed in the following Table II.

TABLE II

$C_{2h}$	$E$	$C_2$	$\sigma_h$	$i$	$n_t$	$T$	External modes $T'$ $R'$		$n_i'$	Selection rules $R$ $IR$		Surviving tensor components
$A_g$	1	1	1	1	18	0	0	3	15	$p$	$f$	$\epsilon_{\alpha\alpha}, \epsilon_{\beta\beta}, \epsilon_{\gamma\gamma}, \epsilon_{\alpha\gamma}$
$A_u$	1	1	-1	-1	18	$T_z$	2	0	15	$f$	$a$	
$B_u$	1	-1	1	-1	18	$T_x, T_y$	1	0	15	$f$	$a$	
$B_g$	1	-1	-1	1	18	...	0	3	15	$p$	$f$	$\epsilon_{\alpha\beta}, \epsilon_{\beta\gamma}$
$U_R$	24	0	0	0								
$\epsilon_R$	72	0	0	0								

$n_t$  is the total number of modes,  $n_i'$  the number of internal modes,  $T'$ ,  $R'$  the modes of translational and rotational type and  $T$  pure translations. The Raman active modes in the crystal may be divided into two classes, namely, totally symmetric  $A_g$  and assymmetric  $B_g$ . As the centre of symmetry lies at each molecule in the crystal, each of the Raman active modes of the molecule will be Raman active in the crystal and will belong to both the symmetric and anti-symmetric class. Similarly the three rotations of the molecule will give rise to three totally symmetric and three anti-symmetric Raman active rotational modes in the crystal.

The three symmetric modes are those in which the rotations are in the opposite sense in the two molecules. As the lattice modes involve intramolecular forces, we may not expect the same frequency for the two modes, but as these frequencies are small it may not be possible to resolve the differences and the lines will therefore appear as broad bands. According to Bhagavantam (1941) oscillations coming under the translatory type have

small frequencies and the Raman lines are weak while those coming under the rotatory type will be characterised by relatively large frequencies and will give rise to strong lines if the rotating group has large anisotropy.

The tensor components of the Raman active modes in the crystal can be determined by their behaviour in directional excitation. If  $OX$  be the direction of illumination,  $OY$  the direction of observation and  $OZ$  at right angles to both, then the depolarisation ratio  $\rho$ , for the electric vector along

$OY$  is  $\rho_{oy} = \frac{e_{\alpha\alpha}^2}{e_{\beta\beta}^2}$  and for the electric vector along  $OZ$ ,  $\rho_z = \frac{e_{\alpha\alpha}^2}{e_{\beta\beta}^2}$ . If  $\alpha, \beta, \gamma$

be the directions of the optic axes of the crystal then since  $\beta$  axis is the axis of symmetry a totally symmetric vibration has four surviving tensor components  $e_{\alpha\alpha}, e_{\beta\beta}, e_{\gamma\gamma}, e_{\gamma\gamma}$  and an anti symmetric vibration only two components  $e_{\alpha\beta}, e_{\beta\gamma}$ . The method of deriving the behaviour of these vibrations for directional excitation has been discussed by Saksena (1940). These are given in Table III.

TABLE III

Symmetry axis	$OZ$			$OY$			$OX$		
Electric vector	$OZ$	$OY$	un-pol	$OZ$	$OY$	un-pol	$OZ$	$OY$	un pol
Symmetric $e_{\alpha\alpha}=a, e_{\beta\beta}=b, e_{\gamma\gamma}=c,$ $e_{\alpha\gamma}=d, e_{\alpha\beta}=0, e_{\beta\gamma}=0.$	$\frac{0}{b^2}$	$\frac{d^2}{0}$	$\frac{d^2}{b^2}$	$\frac{d^2}{c^2}$	$\frac{0}{0}$	$\frac{d^2}{c^2}$	$\frac{0}{a^2}$	$\frac{0}{d^2}$	$\frac{0}{a^2+d^2}$
Antisymmetric $e_{\alpha\alpha}=e_{\beta\beta}=e_{\gamma\gamma}=e_{\alpha\gamma}=0.$ $e_{\alpha\beta}=e, e_{\beta\gamma}=f.$	$\frac{f^2}{0}$	$\frac{0}{c^2}$	$\frac{f^2}{c^2}$	$\frac{0}{0}$	$\frac{c^2}{f^2}$	$\frac{c^2}{f^2}$	$\frac{e^2}{0}$	$\frac{f^2}{0}$	$\frac{e^2+f^2}{0}$
Both type symmetric and antisymmetric	$\frac{f^2}{b^2}$	$\frac{d^2}{c^2}$	$\frac{d^2+f^2}{b^2+c^2}$	$\frac{d^2}{c^2}$	$\frac{c^2}{f^2}$	$\frac{d^2+c^2}{c^2+f^2}$	$\frac{e^2}{a^2}$	$\frac{f^2}{d^2}$	$\frac{e^2+f^2}{a^2+d^2}$

We thus see that with the symmetry axis along the direction of observation, the symmetric vibrations will be absent when the electric vector is along the direction of observation while the anti-symmetric vibrations will be absent when the electric vector is along the perpendicular direction  $OZ$ . If a vibration is both symmetric and anti-symmetric the depolarisation ratios are as shown in the third row.

Bhagavantam has considered the lattice modes of para-dichloro-benzene but he has omitted the frequency 27 observed by Vuks. According to him only three oscillations are observed and each is a symmetric and anti-symmetric mode.

#### EXPERIMENTAL

The crystal was supplied to us by late Shrimati S. Bai. It was grown from melt by the process of slow cooling and was free from impurities as it was grown after several crystallizations. The crystal was in the form of

a cylinder with its symmetry axis along the length of the cylinder. As the crystal evaporates rapidly and internal cracks develop easily, it was not cut in the form of a cube whose axes are along the axes of polarisability ellipsoid, but was worked as such. The crystal was quite clear in a fairly large region and free from internal strains. The light from a horizontal arc was focused on the crystal contained in a glass tube and was polarised with the help of a polaroid with an efficiency of 90% in the 4358 Å region. A double image prism of calcite was used to split the scattered light into horizontal and vertical components. The pictures were taken on a Hilger two prism glass spectrograph and measured on a Hilger comparator. These results are shown in Tables V and VI. One picture (Fig. c, Plate IV A) of the liquid spectrum and one picture (Fig. c and Fig d) of the solid taken on a Fuess glass spectrograph were also given to us by late Shrimati S. Bai and their results are also included here.

The low-frequency spectrum of the solid picture (Fig. b) taken by Shrimati S. Bai differs materially from that of our crystal although the molecular frequencies are identically the same. This crystal must have grown under different conditions. The results of measurements of the low frequency lines on the solid pictures taken by S. Bai support the results of Sirkar and co-workers and of Venkateswaran while the results of measurements of the spectra taken by us with the other crystal support the results of Vuks. The results of measurements on the two solid pictures and the liquid picture are given in Table IV and the results of directional excitation in Table V.

TABLE IV

Low frequencies				Molecular frequencies								Spectrograms	
Solid I	27 (15)	54 (30)	94 (8)	308 (10)	330 (10)	630 (8)	747 (10)	1071 (2)	1106 (10)	1169 (0)	(a) & (f)		
Solid II	45 (12)	57 (8)	84 (5)	308 (8)	330 (8)	630 (6)	747 (6)	1071 (0)	1106 (6)		(b) & (c)		
Solid II	45 (8)	57 (6)	84 (6)	308 (2)	330 (8)	630 (5)	747 (8)	1071 (2)	1106 (8)	1169 (1)	d.		
Liquid Polarisation				299 (5) D	330 (8) P	628 (4) D	675 (0)	747 (8) P	1071 (3) P	1084 (3) P	1106 (8) P	1169 (2) P	(e)
Solid I						1376 (1)	1485 (1)	1573 (8)	3072 (15)				(a) & (f)
Solid II						1376 (1)	1485 (1)	1573 (4)	3072 (10)				(b) & (c)
Solid II						1376 (1)	1485 (1)	1573 (6)	3072 (12)				(d)
Liquid Polarisation				1248? (0)	1376 (1) D	1485 (1)	1573 (6) D	3072 (10) P					(e)

The liquid spectrum has been reported earlier by Kohlrausch and co-workers who report 11 frequencies (for reference vide Hibben, 1939). The liquid picture (c) reported here is a very overexposed one and it shows the presence of weak frequencies 675, 1248, 1485. The  $f$ -excitation of strong frequencies 747 and 1573 should fall at 690 and 1516 which are far removed from the observed values. The frequency 1485 also occurs in several solid pictures. The polarisation picture shows that there are 7 well polarised lines in the liquid while there should be only 6 according to theory. The frequencies 1071 and 1084 form a close doublet both being polarised. It is interesting to note that the sum of two strong frequencies 331 and 747 is 1078 which lies in between the observed frequencies 1072 and 1084. It is possible therefore that the frequency at 1078 has split as a result of Fermi resonance. A comparison of the solid and liquid picture shows a definite frequency shift for the frequency 299 in the liquid to 308 in the solid [Figs. (c) and (d)]. A comparison of the pictures of the two solids (I) and (II) shows remarkable differences. The frequency 27 of solid (I), Fig. (a) is absent in solid (II), Fig. (b) where a new frequency at 45 is present. There is also a shift in the frequency 94 reported for solid (I). Also in solid (I) 54 is the strongest frequency while in solid (II) it is 45. The spectrum of solid (I) is the same as that of Vuks and the spectrum of solid (II) the same as that of Sirkar and Venkateswaran. By a comparison of the two spectra (c) and (d) for solid (II) we find that while the spectrum (d) is stronger, the lattice lines and frequency 308 in (d) are weaker than in (c) and the remaining molecular frequencies, excepting 308, are stronger. The frequency 308 shows a much larger diminution of intensity than the lattice frequencies.

The low frequency Raman lines are very strong compared to molecular frequencies. The visual intensities recorded for them are of the anti-Stokes lines in 4046 excitation while the intensity recorded for the molecular frequencies are of the Stokes lines in the 4358 excitation.

The following points may be noted :

(1) A comparison of the spectrograms (f) and (g) (Plate IV B) of total intensity taken with symmetry axis along  $OY$  but with the electric vectors along  $OY$  in one and  $OZ$  in the other shows that the frequencies 747, 1071, 1106, 3072—particularly the first three, are very much increased in intensity in the latter case when the electric vector is along  $OZ$ , while the frequencies 308, 630, 1376 remain nearly of the same intensity in the two cases and the frequencies 330, 1573 are reduced in intensity in the latter case. The frequencies 747, 1071, 1106 and 3072 are almost of the same intensity as 630 and 1573 when excited by the electric vector along  $OY$ .

(2) Among the low frequencies 54 remains the strongest in all the spectrograms. With the symmetry axis along  $OY$ , the frequency 27 is stronger than 94 when the electric vector is along  $OY$  in (f), while it is much weaker than 94 when the electric vector is along  $OZ$  in (g). The frequency

TABLE V

*Directional excitation of Raman lines*

Illumination along OX						Observation along OY											Spectrogram.
Symm. axis along	Electric vector along	Scattered component.	Low frequencies.			Molecular frequencies											
			27	54	94	308	330	630	747	1072	1106	1376	1485	1573	3072		
OY	OY	$S_x$	6	20	4	6	5	4	5	2	6	1	$\frac{1}{2}$	1	10	(i) $\longleftrightarrow$ $\odot$	
OY	OY	$S_z$	8	12	6	5	8	5	8	3	8	2	$\frac{1}{2}$	6	12		
OY	OY	$S_x, S_z$	15s	30	6br	10	10	6	6	2	5	1	1	5	12	(f) $\longleftrightarrow$	
OY	OZ	$S_z$	4	6	5	1	0	0	1	1	1				2	(k) $\odot$ $\longleftrightarrow$	
OY	OZ	$S_x$	3	5	3	1	1	1	2	1	2				4		
OY	OZ	$S_x, S_z$	15	30	25	10	6	6	12	6	12	2		2	15	(g) $\longleftrightarrow$	
OZ	OY	$S_x$	1	2	3											(j) $\longleftrightarrow$ $\odot$	
OZ	OY	$S_z$	1	8	0												
OZ	OY, OZ	$S_z$	5	12	3	2	2		2	0	2			$\frac{1}{2}$	3	(l) $\longleftrightarrow$ $\odot$	
OZ	OY, OZ	$S_x$	5	12	1	1	3		2	$\frac{1}{2}$	2			1	3		
OX	OY, OZ	$S_z$	5	8	1	0	2		1		1			$\frac{1}{2}$	2	(h) $\longleftrightarrow$ $\odot$	
OX	OY, OZ	$S_x$	6	6	2	0	2		1		1			$\frac{1}{2}$	2		

94 also appears weakest when the symmetry axis is along OX in (h). The behaviour of 94 is thus similar to the behaviour of frequencies 747, 1071, 1106, 3072, which get stronger when the electric vector is along OZ and symmetry axis along OY.

(3) The frequency 27 does not disappear in any picture.

#### DISCUSSION OF SPECTRA OF SOLID II.

(a) Molecular frequencies :

We shall first consider the liquid spectrum. According to theory we should get 15 Raman lines of which 6 should be polarised and 9 depolarised. The six polarised frequencies are 330, 747, 1071-1084, 1106, 1169, 3072 and seven depolarised lines are 299, 628, 675, 1248, 1376, 1485, 1573. The six polarised frequencies naturally represent the planar vibrations of the molecule; of these 330 is a C-Cl oscillation, 3072 is a C-H oscillation and the others are C-C oscillations. Among the depolarised oscillations 299 and 630 represent vibrations perpendicular to the plane of the benzene ring.

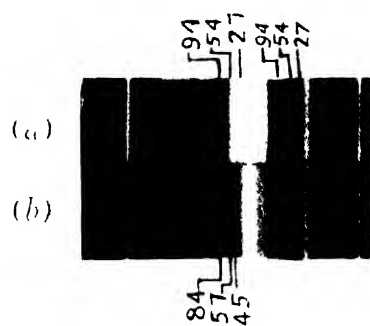
All the lines in the liquid spectrum<sup>7</sup> appear in the solid with the same frequency. Each of these lines is both a symmetric and anti-symmetric

oscillation with respect to the crystal and the behaviour of these lines in directional excitation is dependent upon the fact as to which of the two is stronger. From Table III we see that if the symmetry axis of the crystal is along the direction of observation, the symmetric oscillations are absent and the anti-symmetric oscillations appear with great intensity if the electric vector is along the direction of observation but the reverse happens if the electric vector is along the perpendicular direction  $OZ$ . Now since the molecular frequencies appear in both the cases they are both symmetric and anti-symmetric. The total intensity of a symmetric oscillation when the electric vector as well as the symmetry axis are both in the direction of observation is 0, while that of an anti-symmetric oscillation is  $e^2 + f^2$ . If a vibration is both symmetric and anti-symmetric its intensity will be  $e^2 + f^2$  where  $e$  and  $f$  are component tensors of the anti-symmetric type. If, however, the electric vector is along  $OZ$  the intensity of both together will be  $d^2 + c^2$  where  $d$  and  $c$  are component tensors of the symmetric type of oscillation. If, therefore, greater intensity occurs for a particular oscillation in the second case, the symmetric tensor components must be greater than the anti-symmetric ones. In this way it has been possible to write the tensor components and analyse the vibrations.

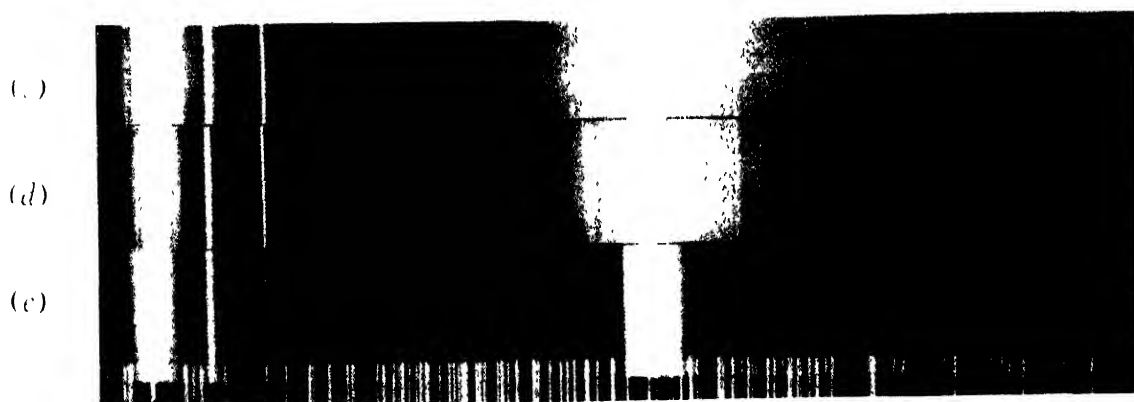
It has been stated in the previous section that when the symmetry axis is along  $OY$  and the exciting electric vector along  $OZ$  or  $OY$ . [spectrograms (g) and (f)], the frequencies 747, 1071, 1106, 3072 are stronger in the former case than in the latter while 330 and 1576 are stronger in the latter case than in the former and the frequencies 308, 630, 1376 remain nearly of the same intensity in the two cases. It follows from what has been stated above that the sum of the tensor components  $d^2 + c^2$  of symmetric oscillation of the frequencies 747, 1071, 1106, 3072 is much greater than the sum of tensor components  $e^2 + f^2$  of the anti-symmetric oscillation of these frequencies, while for 330 and 1573 the sum  $d^2 + c^2$  is smaller than  $e^2 + f^2$  and for frequencies 308, 630, 1376 the two are almost the same.

The frequencies 747, 1071, 1106, 3072 are the polarised frequencies in the liquid spectrum, and therefore represent the totally symmetric planar vibrations of the molecule. It has been shown by Nedungadi (1941, 42) in naphthalene that when the electric vector is in the plane of the molecule, the planar vibrations are excited more strongly than when it is perpendicular to the molecular plane. In the case of a para-dichlorobenzene the molecule lies roughly in the  $bc$  plane where  $b$  is the symmetry axis and  $c$  the length of the molecule. If the symmetry axis  $b$  is along the direction of observation  $OY$ , and the  $c$ -axis vertical along  $OZ$  then whether the electric vector is along  $OZ$  or  $OY$  it remains in the plane of the molecule. But the electric vector will excite more strongly in the direction  $OZ$  because this direction is along the length of the molecule which is the direction of maximum optical polarisation (*vide* Plate IVB, Fig. g). If the electric vector is along  $OY$  the





Low frequency lines of solid (I) and (II).



Raman spectra of solid (II) and liquid.

308  
330  
630  
747  
1071  
1106  
1169  
13072  
1376  
1485  
1573



Two different Raman Spectra of solid(I).



Polarisation of Raman lines of solid (I) in different orientations.

direction of observation, it lies along the breadth of the molecule, and these frequencies will be weaker for two reasons, firstly because the breadth of the molecule is in a direction of intermediate polarisation and secondly because the totally symmetric vibrations will scatter weakly when the electric vector is along the direction of observation. From Fig. (k) Plate IV B we see that the molecular frequencies have come out very weak when the electric vector is along  $OZ$  and the symmetry axis along  $OY$ . This is easily explained if we imagine the  $c$ -axis to lie along the direction of illumination  $OX$  so that the electric vector  $OZ$  is now perpendicular to the plane  $bc$  of the molecule. In this case the electric vector  $OZ$  shall excite very weakly.

The behaviour of the frequency 330 appears to be different from those of the other lines 747, 1071, 1106, 3072 in the liquid. The former decreases in intensity when the electric vector is along  $OZ$  and symmetry axis along  $OY$  while the latter increases in intensity. As all these frequencies represent the totally symmetric vibrations of the molecule, they should be expected to behave alike. It is possible that the difference in behaviour may be related to the nature of the vibration.

The frequency 299 also shows large variation in intensity and frequency in passing from solid to liquid. In the liquid the frequency 299 is weaker than 330 but in the solid it becomes comparable in intensity to 330 and even stronger and its frequency also increases to 308, [Plate IVA, Figs. (e), (d) and (c)]. This frequency, like 628, is an anti-symmetric oscillation perpendicular to the plane of the ring, and so the anti-symmetric tensor components would be larger than the components of the symmetric tensor. It is possible that 308 represents the anti-symmetric oscillation and 300 the symmetric one but the latter may be too weak to appear. No such variation of frequency has been noticed in other lines. But the frequency 330 in the solid behaves differently from other polarised vibrations like 747, 1106, etc. and more like the depolarised frequency 1573. This may be explained by supposing that it is also an anti-symmetric oscillation, in the crystal.

#### (b) Lattice frequencies :

The behaviour of the low frequency Raman lines in the crystal in directional excitation can be explained if we represent the frequencies by the three tensors :

27			51			94		
6	5	3	12	12	5	4	2	4
6	5	6	12	5	8	2	2	3
3	6	4	5	8	9	7	8	7

The figures which are only relative and give the squares of tensor components, have been arrived at by a careful study of all the spectrograms taken with crystal and in different orientations with the help of Table III by following the method described in the preceding paragraphs. It may be

seen that each frequency consists of a symmetric and an anti-symmetric part but in the frequency 94 we find that the components  $e$  and  $f$  representing the anti-symmetric oscillation are smaller than the remaining tensor components  $a, b, c, d$  which represent a symmetric oscillation. Thus 94 behaves in the same way as the polarised molecular frequencies 747, 1106 etc. When the symmetry axis is along  $OY$  and electric vector along  $OZ$ , the intensities of the three frequencies 27, 54, 94 being given by the value of  $d^2 + c^2$  are as 7 : 14 : 11 while if the electric vector be along  $OY$  they will be given by the value of  $e^2 + f^2$  and are as 11 : 20 : 5. Thus in the first case 94 is stronger than 27 and in the second case weaker while 54 is always the strongest. Using these tensors the polarisation of the lattice frequencies have also been written down and compared with the observed values :

Symmetry axis Electric Vector	OZ      OZ      OY      OY      OX				
	OY	OY & OZ	OZ	OY	OY & OZ
27 Calculated	3/5	9/10	3/4	3/6	11/15
Observed	1/1	5/5	3/4	6/8	5/6
54 Calculated	5/12	13/17	5/9	12/8	20/17
Observed	2/8	12/12	5/6	20/12	8/6
94 Calculated	4/2	7/4	4/7	2/3	5/8
Observed	3/10	3/1	3/6	4/6	1/2

It has been stated earlier that the low frequency Raman lines represent rotational oscillations. The frequency of a rotational oscillation will depend upon the moment of inertia involved in a given oscillation while its intensity will depend upon the molecular anisotropy produced in a given vibration. The frequency 94 may therefore be regarded as due to oscillations about the length of the molecule or the  $c$ -axis as the moment of inertia about this axis is minimum, while the frequency 27 will represent an oscillation about an axis perpendicular to the plane of the molecule or roughly the  $a$ -axis as the moment of inertia involved in this case will be the largest. The moment of inertia will have an intermediate value about the breadth of the molecule and the intermediate frequency 54 may reasonably be assigned to oscillations about this axis. As the intensity depends upon the optical anisotropy coming into play during a vibration, we may expect the frequency 54 to be the strongest as the oscillations about the breadth of the molecule will involve the largest anisotropy.

It is to be remarked that the lattice frequencies are very much more intense than the molecular frequencies. If we take three soft crystals—gypsum, naphthalene and para-dichlorobenzene, we find that the lattice lines are much weaker than the molecular Raman lines in gypsum, of comparable intensity in naphthalene and of large intensity in para-dichlorobenzene. As

the lattice Raman lines are rotational oscillations, it is likely that this difference is due to the anisotropy of the rotating group. In gypsum the rotating group  $\text{SO}_4$  is tetrahedral and has the smallest anisotropy and so the lattice lines will be weak. In para-dichlorobenzene, however, the anisotropy of the rotating group is the largest, firstly, because the molecule is plane and secondly because it is very much elongated along one of the axes, and so the lattice lines may be expected to be very intense.

*Comparison of the spectra of the solids (I) and (II).*

Several spectrograms of solid (I) reveal clearly the three low frequency lines 27, 54 and  $94 \text{ cm}^{-1}$  both in the 4046 and 4358 excitations, but the two pictures (c) and (d) taken with Buess glass spectrograph by S. Bai reveal three different frequencies 45, 57 and 84 although the liquid spectrum is the same in the two cases. The frequency 27 does not appear in that picture. The spectrograms taken with crystal in different orientations also reveal the fact that the frequency 27 does not vanish in any orientation. Hence its disappearance in one picture is not due to an orientation effect.

The difference in behaviour between solids (I) and (II) is also indicated by the behaviour of the molecular frequencies 308 and 330. In the two pictures (c) and (d) of solid (II) we find that in one picture (d) which is stronger of the two, the molecular frequencies have come out stronger than in the other but all the lattice frequencies and the frequency 308 are weaker. This is different from the behaviour of solid (I) in which the lattice frequency 94 behaves differently from other lattice frequencies and more like the symmetrical oscillations. Further, when the symmetrical vibrations are stronger, the frequency 330 is weaker than 308 in solid (I) (Fig. g) but 308 is weaker than 330 in solid (II) (Fig. d). Also 54 is the strongest frequency in solid (I) and 45 in solid (II).

Venkateswaran, while working with para-dichlorobenzene cooled from melt also gets the same frequencies as those of solid (II) namely 45, 57, 84. In this case the substance cooled was not a single crystal, while in our case it is a single crystal since it was grown from melt by slow cooling. It is possible that a change of structure may occur in rapid cooling and in fact Sirkar and Bishui and also Vuks report change of frequencies by sudden cooling in ice. We therefore feel inclined to think that a change of structure does occur in sudden cooling.

Bech (1906) and Vuks have discussed the transformations of para-dichlorobenzene. Bech points out that when this liquid is cooled below  $39^\circ\text{C}$  a sudden contraction of volume takes place, and this is considered as a modification of the lattice. Vuks has discussed a transformation in which the molecules rotate in their position so that the projection on the  $ac$  plane is now inclined to the  $c$ -axis. This transformation would require no change of volume as the lattice is unaltered and it takes place at  $32^\circ\text{C}$ . But according to Sirkar and Gupta this transformation would involve a change of X-ray

intensities in Laue spots which has not been noticed by them. Venkateswaran and also Sirkar and co-workers fail to report any change of spectra by change of temperature. It however, appears definite to us that some change of structure does take place in the way the crystal is grown and the point requires further investigation.

#### ACKNOWLEDGMENT

We have to acknowledge our grateful thanks to Sir C. V. Raman for kindly placing the Hilger two-prism glass spectrograph at the disposal of one of us, and to late Shrimati S. Bai for giving us the crystal and the two plates for our use.

DEPARTMENT OF PHYSICS,  
UNIVERSITY OF ALLAHABAD

#### REFERENCES

- Bech and Ebbinghaus, 1906, *Ber.* **29**, 3870.  
 Bhagavantam, 1941, *Ind. Acad. Sc.* **13**, 513  
     1939, *ibid* **9**, 221  
     1940, *ibid* **11**, 62.  
 Bragg, 1939, *Crystalline State* (G. Bell & Sons), 161 pp  
 Hendricks, 1933, *Z. S. Krys*, **84**, 85.  
 Hibben, 1939, *Raman & Infrar-red spectra*, pp 225.  
 Nedungadi, 1942, *Ind. Acad. Sc.*, **15**, 376.  
     1941, *ibid* **13**, 161  
     1939, *ibid* **10**, 197.  
 Placzek, *Hand Buch der Radiology*, Bd. VI, Vol 2.  
 Saksena, 1940, *Proc. Ind. Acad. Sc.*, **11**, 229.  
     1940, *ibid* **12**, 93.  
 Sirkar and Bishui, 1937, *Ind. Jour. Phy.*, **11**, 418  
 Sirkar and Gupta, 1936, *Ind. Jour. Phy.* **10**, 473  
 Sirkar and Gupta, 1937, *Ind. Jour. Phy.*, **11**, 287  
 Venkateswaran, 1938, *Ind. Acad. Sc.*, **8**, 448.  
 Vuks, 1936, *Com. Ren*, **1**, 73  
 Vuks, 1937, *Acta. Phy. Chem.*, **6**, 11

## ALUMINIUM IN STEEL

By K. C. MAZUMDER

*(Received for publication, September 25, 1950)*

**ABSTRACT** Inspite of its favourable size-factor the primary solid solution of Al in the  $\gamma$ -iron is very small; this is due to its strong electro-chemical factor. When the steel exists in the  $\gamma$ -form, the excess of Al is driven to the grain boundary and inhibits the grain growth. The electro-chemical factor makes it form readily the compound FeAl which has a body centred cubic structure. It has been further shown that the grain of FeAl has a pronounced solubility in the  $\alpha$ -iron; this is why only a single-phase is observed up to 50% Al added to the  $\alpha$ -iron.

Aluminium was used in the beginning for deoxidizing steel; but traces of it left after deoxidation or added intentionally have been found to inhibit the anstenitic grain growth and thus acts as a grain refiner. The classical metallurgy tried to explain this property of aluminium in various ways, the latest suggestion being that aluminium dissolved in the ferritic grains or otherwise locate itself at the anstenitic grain boundaries and does the refining work, (Nijhawan, 1948). An attempt will be made in the present paper to explain the situation in the light of the modern atomic theory.

A look at the phase-diagram of the Fe-Al system shows that Al dissolves in the  $\gamma$ -iron only to the extent of 1 to 1.2% and that too between the temperatures, 900°C to 1400°C, whereas, it has an extended solid solutions in the  $\alpha$ -iron. This in itself is a peculiar thing, so far as the steel metallurgy is concerned. The elements, particularly the metals which alloy with iron to large extents, can be in a broad way divided into two groups. One group when alloyed with iron widens the  $\gamma$ -range at the expense of the  $\alpha$ -range, the second group does the reverse. The elements Co, Ni, Cu, Au, Pt have the face centred cubic structure; they belong to the first group and widen the  $\gamma$ -range the  $\gamma$ -iron also having the face centred cubic structure. Cr, V, Mo, and W have the body centred cubic structure like the  $\alpha$ -iron and widen the  $\alpha$ -range. They thus belong to the 2nd group. Aluminium has the face centred cubic structure but is found to alloy extensively with the body centred  $\alpha$ -iron. Aluminium has a favourable size-factor with respect to iron and it has the same structure as the  $\gamma$ -iron. Under the circumstances it can reasonably be expected that there will be a wide solid solution of Al in the  $\gamma$ -iron. The fact being to the contrary, there must be some other factor coming into play and restricting the solution. It is suggested here that the electro-chemical factor of Al, with respect to iron, is responsible for this anomaly and on this basis it will also be possible to understand the real nature of the apparently wide solution of aluminium in the  $\alpha$ -iron.

Besides size-factors and the valences, the electro-chemical factor also, to a considerable extent, determines the extent and the nature of the solution. The magnitude of the influence of the electro-chemical factor will be appreciated if one examines the phase diagrams of a few alloy systems of magnesium with some metals and metalloids, specially the elements belonging to the groups IV, V and VI of the periodic table. Most of these alloy systems have greatly restricted primary solid solutions at either end of the diagrams; but  $\alpha + \beta$ ,  $\beta$  and  $\beta + \gamma$  regions are widely extended. The solidus and the liquidus curves at a certain composition in the  $\beta$ -range (or some time in the  $\gamma$ -range) rise to a maximum and almost touch each other. This shows that the alloys of these compositions have attained higher stability (higher melting points) than the alloys of other compositions belonging to the same phase and generally to the neighbouring phases also. The compositions corresponding to these maxima can be expressed by definite chemical formula satisfying ordinary valence relations also. Some of these are:  $\text{Mg}_2\text{Si}$ ,  $\text{Mg}_2\text{Ge}$ ,  $\text{Mg}_2\text{Sn}$ ,  $\text{Mg}_2\text{Pb}$ ,  $\text{Mg}_3\text{P}_2$ ,  $\text{Mg}_3\text{As}_2$ ,  $\text{Mg}_3\text{Sb}_2$ ,  $\text{Mg}_3\text{Bi}_2$ ,  $\text{MgS}$ ,  $\text{MgSe}$ ,  $\text{MgTe}$ . These are called normal valency intermetallic compounds. They have also ordered or super structures like ordinary chemical compounds, *e.g.*,  $\text{NaCl}$ ,  $\text{CaF}_2$ . A few other metals also form such compounds as  $\text{Zn}_3\text{Sb}_2$ ,  $\text{CdS}$ ,  $\text{AlAs}$ ,  $\text{AlSb}$ . "These compounds have a metallic lustre and a slight electrical conductivity. The formation of these compounds is a continuation of the typical ionic compounds into the region of weakly electro-negative elements. Compounds of this kind are often formed when one element is highly electro-positive compared with the other and they may be regarded as the result of the electro-chemical factor." Zn and Cd, which occupy similar positions as Mg in the periodic table, form a few compound of this nature; but they are not as extensive as those of Mg. This is due to the fact that Mg is much more electro-positive than the other.

The Ag-Mg alloy system is one of the most suitable one for the study of the effect produced by the electro-chemical factor. The system is exactly equivalent to the Cu-Zn system both as regards the configuration of the valence electrons and the crystal structures of the corresponding elements. But a comparison of the phase diagrams of the two systems shows that the Ag-Mg system is much simpler, its primary solid solution—the  $\alpha$ -phase, is much restricted, the atomic per cent dissolved being a little over 20 instead of 40 as roughly is the case for the Cu-Zn system and others satisfying the Hume-Rothery electron atom ratio for the phase. The  $\beta$ -phase ( $\equiv \beta'$ ) has an ordered structure at all temperatures and it is like that of  $\text{CsCl}$ . The solidus and the liquidus rise to a maximum at the equi-atomic composition  $\text{AgMg}$  and almost touch one another. "It is, therefore, clear that increasing electro-chemical factor has made the  $\beta$ -silver-magnesium phase acquire some of the characteristic (maximum freezing point and ordered structure) usually associated with definite chemical compounds."



Even in cases where definite compounds do not exist, the electro-chemical factor may exert an important influence on the type of alloy structures formed. The strengths of the electro-chemical factor and the effects produced by it are of different degrees. The tendency for the formation of superstructure is the first indication; the ultimate effect is the formation of definite chemical compounds if the electro-chemical factor is sufficiently powerful.

There are instances when the irregularities found in some binary alloys of aluminium have been explained by its electro-chemical factor. Andrews and Hume-Rothery (1941), have shown by plotting the electron concentrations against the volume per valence electron for  $\alpha$  and  $\beta$  phases of Cu-Zn, Cu-Ga, Cu-In, Cu-Sn and Cu-Al systems that "there is a linear relation between the electron concentration and the mean volume per electron of the points lying midway between the  $\alpha/\alpha+\beta$  and  $\alpha+\beta/\beta$  boundaries in the equilibrium diagrams." The only exception is the Cu-Al system and this has been attributed to the pronounced electro-positiveness of aluminium.

In many alloys of Al it is found that the apparent size of the Al-atom in the alloy is smaller than that indicated by the inter-atomic distances in the crystal of the element. A part at least of this contraction has been ascribed to the large electro-chemical factor of aluminium. The position of aluminium in the electromotive force series of elements is found to be very high with respect to many elements and its electro-positiveness is just next to magnesium. The restricted primary solid solution when size-factor is favourable is due to the electro-chemical factor, as has been shown in the case of the Ag-Mg system; there are other instances also for similar effects produced by the above factor. As mentioned previously, Al forms a few normal valence inter-metallic compounds with weakly electro-negative elements. Sb and As are two such elements and Al is fairly strongly electro-positive with respect to them. The compounds thus formed may be regarded as the result of the electro-chemical factor. From the phase diagram of Al-Sb system, for instance, it is quite evident that the primary solid solution of either of them into the other is extremely small. The  $\alpha+\beta$  region is extended. The solidus rises to a maximum at the equi-atomic point. The superstructure is like that of ZnS. If we now consider the alloys of Al with Ni and Co—the neighbouring elements of Fe belonging to the same transition period—the electro-positiveness of Al will be quite evident. The phase diagram of the Co-Al system shows that the solid solubility of Al in the hexagonal cobalt is practically nothing; the face-centred cubic Co—having the same structure and a favourable size factor as Al, takes into solution only a limited amount of Al. It is only 7% at 1300°C and comes down to 2% at 500°C. The  $\xi+\epsilon$  ranges are extended, the solidus rising to a pronounced maximum at the equi-atomic composition, CoAl. The corresponding melting point is 1630°C which is higher than that of Co and Al both. All the three characteristics—namely the restricted primary solid

solution, higher stability of some of the intermediate phases and the ordered structure like that of chemical (ionic) compounds—of high electro-chemical factor, are present to a pronounced degree in the Co-Al alloys. The same is also true to a correspondingly high degree in the Ni-Al alloys. Here also one can see in a restricted primary solid solution, an ordered structure, a higher stability, the melting point of the equi-atomic composition, NiAl, being  $1640^{\circ}\text{C}$  which is higher than that of both aluminium and nickel. The alloys of both Co-Al and Ni-Al systems have been influenced to a considerable degree by the high electro-positiveness of Al with respect to the elements Co and Ni. The strength of the relative electro-positiveness of Al with respect Co and Ni can be seen from the values of the electromotive force found for these elements. They are  $+1.70$  for  $\frac{1}{2}\text{Al}^{+++}$ ,  $+0.278$  for  $\frac{1}{2}\text{Co}^{++}$  and  $.231$  for  $\frac{1}{2}\text{Ni}^{++}$ . For  $\frac{1}{2}\text{Fe}^{+++}$  it is much less than those of Co and Ni; therefore the relative electro-positiveness of Al with respect to  $\text{Fe}^{+++}$  is much stronger; but for  $\text{Fe}^{++}$  the value is less, still it is sufficient to make its existence felt. This is, therefore, the explanation which is being offered here for the restricted solid solution of Al in the  $\gamma$ -iron.

Beyond the small  $\gamma$ -loop ( $900^{\circ}\text{C}$ – $1400^{\circ}\text{C}$  and  $0$ – $1.2\%$  Al) for various temperatures and  $0$ – $50$  atomic percents of Al one gets only body centred ferrite grains in which have been embedded Al atoms with great tendency for superlattice formation. This tendency is so great that is cited as a typical example for such structure. In this range no intermediate phase boundary has been found to exist and it has been accepted as a single phase region by several authors. But just at  $50$  atomic percent of Al a boundary exists and the alloy at this point can be expressed by the formula,  $\text{FeAl}$  like  $\text{CoAl}$ ,  $\text{NiAl}$  and a large number of others belonging to Cu-Zn and various other systems. Above all the composition,  $\text{FeAl}$  gives the electron-atom ratio,  $3/2$ , the well known Hume-Rothery ratio established for the  $\beta$ -phase. It has also the body centred cubic structure like many other  $\beta$ -phase alloys. Thus the existence of the  $\beta$ -phase is definitely established. If then it is a single phase region it must be a widely extended  $\beta$ -phase. This is rather peculiar. It should be noted that this complication arises from the fact that both the iron and the  $\text{FeAl}$  grains have the body centred cubic structure. There are other instances also of two neighbouring phases having the same structure but by proper heat treatment at some point two grains can generally be obtained which, though of the same structure, have different compositions and this proves the existence of two distinct phases. No such observation has been made in the case of the Fe-Al system. In this system two superstructures have been obtained at different points having the compositions  $\text{Fe}_3\text{Al}$  and  $\text{FeAl}$ . It should, however, be noted that these two ordered structures are not of two distinct types, the structures of  $\text{Fe}_3\text{Al}$  being only a step towards the formation of the final structure of  $\text{FeAl}$ . In the Fe-Al system, therefore, the region of the primary solid solution ( $\alpha$ -phase) or that of the  $\alpha + \beta$  have not been distinguished from that of the

$\beta$ -phase. On account of the electro-chemical factor the primary solid solution is so very restricted that its range becomes too small for observation, but this does not explain the non-existence of the  $\alpha + \beta$  range. From this, as well as from the fact that the  $\beta$ -range is very extended, one can conclude that on account of strong electro-chemical factor even for a small quantity of Al added to the  $\alpha$ -iron, a proportionate amount of the FeAl grains is formed and this latter having a wide solubility into the former goes at once into solution. From 0 to 50 atomic percent of Al added we get a solid solution of FeAl grains into the  $\alpha$ -iron. This is thus a single phase region of Fe-FeAl having body centred cubic structure culminating at equi-atomic point into a full-fledged ordered  $\beta$ -structure of Hume-Rothery.

We then find that two effects of strong electro-chemical factor have fully been developed in the Fe-Al system; one is the restricted primary solid solution, the other is the quick formation of FeAl grains from the very beginning of alloying and the ordered structure of the  $\beta$ -phase. There is no maximum at the corresponding point like CoAl and NiAl but a tendency of the solidus to rise is quite evident just after the equi-atomic point culminating in a definite, though small, maximum at the mid point of the  $\theta$ -phase with the composition FeAl<sub>3</sub>.

In the light of the foregoing remarks it is now possible to discuss the situation occurring actually in the steel making industry. When the  $\gamma$ -range is extended beyond the  $\gamma$ -loop for aluminium by the alloying elements added to iron, the excess of aluminium left after the complete de-oxidation, will not be retained in the  $\gamma$ -grains on account of the restricted solid solubility. It will either be thrown completely out of the metal or held up in the grain boundaries. On account of the ease with which aluminium forms FeAl grains with iron it is likely to remain in the boundaries in the forms of the above grains. The location of these grains in the boundaries will hinder the grain growth. This then is the explanation for the grain refinement of steel by aluminium. When, however, the steel is heated and the temperature range, 900°C-1400°C is reached the  $\gamma$ -grains will now be in the position to absorb the Al-atoms locked up as the FeAl grains and the grains of steel will then grow. The above temperature range may be modified to different degrees in the presence of the different alloying elements present in the steel. The reverse process will take place if the sample is again cooled.

THE NEW CONTROL AND RESEARCH LABORATORY,  
TATA IRON & STEEL CO. LTD., JAMSHEDPUR.

#### REFERENCES

- Andrews, K. W. and Hume Rothery, W., 1941, *Proc. Roy. Soc., [A]*, **178**, 464.  
Nijhawan, B. R., 1948, *J. of Sc. and Ind. Res.*, **7**, 447.

# REVIEW

(1)

**A Text Book of General Physics**—By G. R. Noakes. Pp. 415. Macmillan and Co. Ltd., St. Martin's Street, London, 1950. Price 10 s. 6 d.

This book deals with general properties of matter, the standard adopted being equivalent to that of the B. Sc. (Pass) course of Indian Universities. In the first few chapters some elementary problems, such as units and dimensions, vectors, laws of motion, conditions of equilibrium, impact of solid bodies and friction have been discussed. Chapters 7—12 deal with some important topics on general properties of matter, e.g., pressure in a fluid, elastic deformation of solids, viscosity, surface tension and gravitation. Topics on simple harmonic motion and wave motion have also been included in two of these chapters. Some of the problems have been solved with the help of dimensional equations and a few others geometrically. There are numerous illustrations which are helpful for understanding the topics. The diagrams have, however, not been marked serially. The book will be useful to students for preparing for the B.Sc. (Pass) course of Indian Universities.

S. C. S.

## ANALYSIS OF TRIGGER CIRCUITS\*

By RAIS AHMED

(Received for publication, November 10, 1950)

**ABSTRACT.** At the present time the basic properties of the trigger circuit are generally understood in terms of the voltages existing on different electrodes during states of equilibrium in between the triggering signals. In the present paper the properties of the circuit have been studied in relation to the nature of the driving pulses. Experimental results are presented to confirm the theoretical conclusions.

In recent years the use of trigger circuits has become very common in various special-purpose electronic devices. The basic properties of this circuit are generally understood in terms of the voltages existing on the different electrodes during states of equilibrium in between the triggering signals. However, in order to be able to design a trigger circuit for operation at high repetition rates it is necessary to analyse the actual switching operation that takes place upon the application of proper driving signals. It is possible to extend the transient analysis of switching made in connection with multivibrators (Ahmed 1948, 1950; Williams *et al*, 1950) to considerably systematize the knowledge about the pulse signals required to actuate trigger circuits.

At the present time there are certain mathematical difficulties in carrying out a complete theoretical study of the switching phenomenon in trigger circuits. Since the nature of the switching action depends on the applied signal, it would be necessary, for the purpose of a mathematical analysis, to know the exact expression for the applied signal as a function of time. It is, therefore, convenient to idealize the applied signals and later to obtain the results for actual signals by the method of analogy. The use of experimental data is then doubly desirable to check the assumptions made in such a theoretical analysis.

The well known Eccles-Jordan trigger circuit, shown in Fig. 1, may be

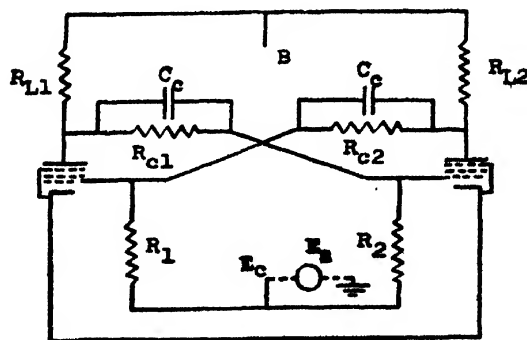


FIG. 1

The Eccles Jordan trigger circuit

\* A part of this work was done as contract research for Princeton University, U. S. A.

taken for the purpose of the present discussion. An equivalent circuit will have a general admittance network as shown in Fig. 2, and if it is assumed

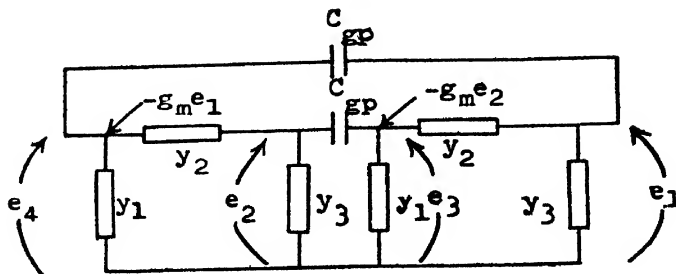


FIG. 2

The equivalent admittance net work for the Eccles-Jordan trigger circuit

that pentode tubes are used (with grid to plate capacitance nearly zero) then the determinant characterising the circuit will be :

$$\Delta = (y_1 y_2)^2 + (y_2 y_3)^2 + (y_3 y_1)^2 + 2 y_1 y_2 y_3 (y_1 + y_2 + y_3) - g_m^2 y_2^2 \quad \dots \quad (1)$$

If proper values for the admittances  $y$  are substituted, and then  $\Delta$  is equated to zero, it is possible to get a set of exponential functions representing the free response of the circuit. In practice, however, the d-c bias  $-E_c$  is so adjusted as to prevent a tube from coming on once it has been cut off. The exponential solutions inherent in the determinant will come into existence only when the circuit is once driven into the region where two-tube conduction is possible. The nature of the switching is, therefore, different from that in the case of the multivibrator, and it depends on the nature of the applied driving signal and its manner of application.

#### CONVENTIONAL ANALYSIS

To start from the conventional analysis, the following values may be given to the various components shown in Fig. 1 :

$R_{L1} = R_{L2} = 170 \text{ k}\Omega$ ,  $R_1 = R_2 = 1/G = 100 \text{ k}\Omega$ ,  $R_{c1} = R_{c2} = 1/G_3 = 500 \text{ k}\Omega$ ,  $C_c$  very small and neglected,  $C = 10^{-10}$  farads. If the plate supply voltage is taken to be 180 volts, the proper value of the biasing voltage  $E_c$  may be found from the equivalent circuits of Fig. 3. These circuits represent the conditions when one of the tubes is on and the other is off. It is desired to make  $E_c$  so large negatively that the voltage produced between the points  $a$  and  $b$  will be larger than the cut-off voltage of the tubes, and from the circuit of Fig. 3 it appears that this value should be at least  $-14$  volts if the cut-off voltage is  $-10$  volts. In practice,  $E_c$  may be made  $-16$  volts and in this case the voltage produced at the grid of the second tube (point  $c$ ) will be more than a tenth of a volt positive. Having thus ensured that the voltage at one of the grids will be negative beyond cut-off, and that at the other will be just slightly positive, it is possible to discuss the switching operation.

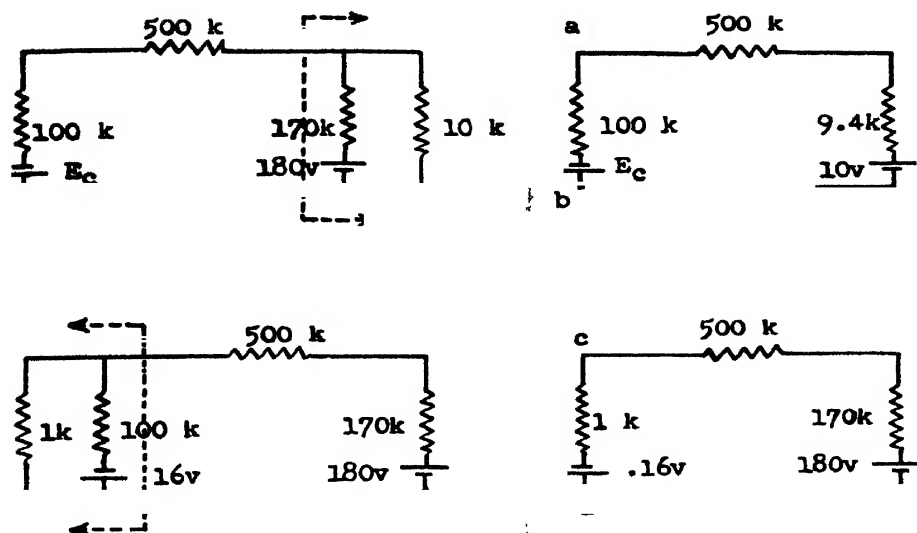


**FIG. 3**  
**Equivalent circuits for determining the biasing voltage**

Ordinarily it is said that a positive pulse at the negative grid, or a negative pulse at the positive grid will drive the circuit into a state of two-tube conduction which is unstable because of the positive feed-back arrangement in the circuit. The tube that was previously conducting will now go off, and the other that was off will now start to conduct current. Although this description of the operation of the circuit is quite true, it is not quite complete. For instance, the following questions may be raised regarding the possibility of conducting current switching from one tube to the other: (1) What will be the maximum and minimum amplitude of the pulse required? (2) What will be the maximum and minimum pulse width necessary? (3) How quickly can one pulse follow another for triggering action? (4) How are the above three properties inter-related?

The first of these questions can be answered, approximately, on the basis of a semi-static circuit consideration. Fig. 4 represents conditions when the

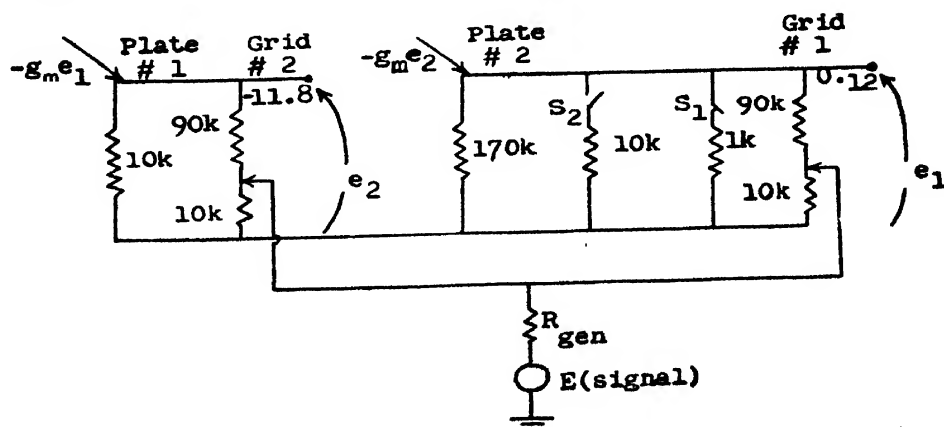


**FIG. 4**  
**Equivalent circuit for roughly determining the actual voltage**

d.c. voltages shown in Fig. 3 have been applied and tube 1 is conducting while tube 2 is off. It is here assumed that the shunting capacitances are negligible and that the coupling condenser is such that negligible delay is produced in transmitting a signal round the circuit.

For a positive step voltage applied at grid 2, the amplitude should first be large enough to make the potential of this grid  $-10$  volts. If the signal feeding arrangement is as shown in Fig. 4, then the voltage necessary will be  $1.8 \times 10 = 18$  volts and it will raise the potential of grid 1 also by  $18 \times 1/91 = 0.2$  volt. Now the voltage at grid 2 should be further raised into the conducting region so that the voltage at grid 1 may be depressed to zero by opening switch  $S_1$  and causing full amplification through tube 2. The positive step voltage would thus have to be greater than 18 volts.

In a similar manner a negative step voltage applied at grid 1 should first be large enough to overcome the positive potential of this grid. Due to voltage division this will be found to be  $-0.12 \times 91 = -10.9$  volts. A further negative increase in this voltage will open the switch  $S_1$  allowing full amplification to take place.

The above discussion shows that with this type of signal feeding the circuit is more sensitive to negative pulses than it is to positive pulses. It also indicates that this sensitivity can be changed by altering the resistance ratios in the circuit or by applying the signal at some other point. It may be noticed, for example, that the minimum signal required for the positive pulse depends on (1) how far below the cut-off voltage the tube was permanently biased, and (2) the grid resistance of the conducting tube when the grid voltage is slightly positive. Sensitivity to negative pulses on the other hand, is determined primarily by the voltage division between external grid resistance  $R_g$  and the conducting resistance of the tube.

The above discussion was based on a step signal, although in practice the applied signal will have a definite initial slope and duration. The exact minimum found in this manner may not be very accurate but the comparative sensitivity is quite reliable.

It is further to be seen that if the voltage  $-E_c$  and the resistances are so arranged as to produce a voltage 0 and  $-E_{c0}$  at the two grids, then the positive and negative sensitivity both become increased, and theoretically any small signal will trigger the circuit. For a further study of the previously mentioned questions regarding the actuating signals, it is necessary to analyse the switching operation during the time that both tubes are conducting. It may be re-emphasized that the present analysis has not been carried so far as to answer all the questions for all types of applied pulses. In what follows, first a pulse of rectangular shape is applied from a source in series with the external grid resistance of the tubes, and the proper amplitude and duration necessary for such a signal have been studied. Next, operation of the circuit by a pulse of the form  $kt - mt^2$  has been indicated.



This is followed by experimental results which confirm the general mathematical conclusions.

### THE RECTANGULAR PULSE

The rectangular pulse generator may be assumed to have zero internal resistance and it may be connected as shown by dotted lines in Fig. 1. It is also assumed that the coupling capacitance is very large. The equivalent circuit can be represented by Fig. 5. The circuit equations will be as follows :

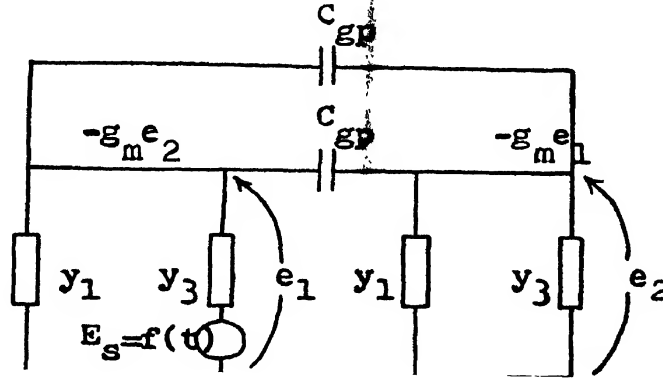


FIG. 5  
The simplified equivalent circuit

$$(g_m - 2pC_{gp})e_1 + (y_1 + y_3 + 2pC_{gp})e_2 = 0 \quad \dots (2)$$

$$(y_1 + y_3 + 2pC_{gp})e_1 + (g_m - 2pC_{gp})e_2 = -G_3 f(t) \quad \dots (3)$$

where  $G_3$  is the conductive part of  $y_3$ ,  $f(t)$  represents the form of the generated signal, and  $p$  stands for  $d/dt$ . The voltage  $e_1(t)$  will be given by  $\Delta_1/\Delta$  where :

$$\Delta = \begin{vmatrix} g_m - 2pC_{gp} & (y_1 + y_3 + 2pC_{gp}) \\ (y_1 + y_3 + 2pC_{gp}) & g_m - 2pC_{gp} \end{vmatrix} \quad (4)$$

and

$$\Delta_1 = \begin{vmatrix} 0 & (y_1 + y_3 + 2pC_{gp}) \\ -G_3 f(t) & (g_m - 2pC_{gp}) \end{vmatrix} \quad (5)$$

If  $y_1 = G_1 + pC_1$  and  $y_3 = G_3 + pC_3$ , then the further expansions of the above determinants are :

$$\Delta = p^2(C_1 + C_3)(C_1 + C_3 + 4C_{gp}) + 2p[(G_1 + G_3)(C_1 + C_3 + 2C_{gp}) + 2g_m C_{gp}] + [(G_1 + G_3)^2 - g_m^2] \quad \dots (6)$$

and

$$\Delta_1 = G_3 f(t)[p(C_1 + C_3 + 2C_{gp}) + G_1 + G_3] \quad \dots (7)$$

The expression for  $\Delta$  may be written in terms of its factors  $(p - \alpha_1)(p - \alpha_2)$  where :

$$\alpha_1 = \frac{[g_m - (G_1 + G_3)]}{C_1 + C_3 + 4C_{gp}} ; \quad \alpha_2 = \frac{-[g_m + (G_1 + G_3)]}{C_1 + C_3}$$

The Laplace transform of  $\Delta$  is then : (Churchill, 1944)

$$L(\Delta) = (s - \alpha_1)(s - \alpha_2) \quad (8)$$

The Laplace transform of  $\Delta_1$  is :

$$L(\Delta_1) = G_3 [s(C_1 + C_3 + 2C_{gp}) + G_1 + G_3] Lf(t) \quad (9)$$

To take the Laplace transform  $Lf(t)$  for a rectangular pulse in general (shown in Fig. 6) it is necessary to consider the rectangle as composed of two step functions,  $T$  units of time apart. Thus,

$$Lf(t) = \frac{E_a}{s} - \frac{E_b}{s} e^{-t/T} \quad \dots \quad (10)$$

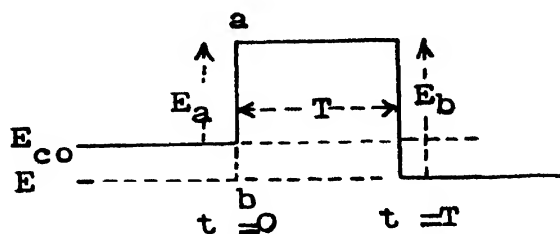


FIG. 6

The rectangular pulse

If this transform is plotted for the various values of  $t$ , it will be necessary to omit the terms with the exponential until  $t=T$ . In the present case the significance of the unequal pulse amplitudes is that the leading edge  $ab$  of the pulse does not operate on the equivalent circuit till the voltage  $-E_{co}$  is reached by the grid. When this happens the amplitude of the pulse still to go is only  $E_a$ . It is true that in actual application the rectangular shape will not be maintained by the pulse, and instead, due to shunting capacitance  $C_3$ , the grid voltage will rise with a definite slope. The second edge of the pulse is effective with its entire amplitude since it will be superimposed on a rising grid voltage. Thus, using the above Laplace transform of the driving voltage  $f(t)$ , the Laplace transform of the grid voltage  $e_1$  is :

$$Le_1(t) = \frac{G_3 E_a [1 - (E_b/E_a)e^{-t/T}] [s(C_1 + C_3 + 2C_{gp}) + (G_1 + G_3)]}{s(s - \alpha_1)(s - \alpha_2)} \quad (11)$$

This may be broken into partial fractions and its inverse transform may be taken to give the following result : (Campbell and Foster, 1942)

$$e_1(t) = -1 \left( 1 - \frac{E_b}{E_a} (G_1 + G_3) \right) \frac{1}{2} \left( 1 - \frac{E_b}{E_a} e^{-|\alpha_1|T} \right) (g_m + G_1 + G_3) e^{+\alpha_1 t} \\ - \frac{1}{2} \left( 1 - \frac{E_b}{E_a} e^{-|\alpha_2|T} \right) (g_m - G_1 - G_3) e^{-|\alpha_2| t} \left\{ \frac{G_3 E_a}{[g_m^2 - (G_1 + G_3)^2]} \dots \right. \quad (12)$$

It may be stated again that at  $t=0$ , the terms with  $E_b$  are to be completely omitted since they affect the value of  $e_1(t)$  only when  $t \geq T$ . It is quite

evident from an examination of the coefficient accompanying the positive exponential  $e^{+\alpha_1 t}$  that if a certain relation holds between  $T$  and  $E_b/E_a$  and  $\alpha_1$ , this coefficient will become negative and will come into play (at  $t=T$ ) in such a way that the rising grid voltage will be made to fall instead. The condition for this improper or reverse switching to take place is :

$$1 - \frac{E_b}{E_a} e^{-\alpha_1 T} \leq 0$$

$$\text{or} \quad T < \frac{C_s + C_1 + 4C_g}{g_m - (G_1 + G_3)} \log_e \frac{E_b}{E_a} \quad (13)$$

It may be seen that if  $E_a$  becomes very large then  $E_b/E_a \rightarrow 1$  and  $\log_e (E_b/E_a) \rightarrow 0$ , resulting in the critical width of the rectangular pulse  $T_c \rightarrow 0$ . On the other hand, if  $E_a$  is very small then a definite minimum width of the pulse is necessary in order that a complete switch (interchange) in the tube currents may take place. Furthermore, if the steady-state voltage on the grid of the tube which remains off is exactly  $-E_c$  and that at grid of the other tube is exactly zero, then  $E_a = E_b$  and again any pulse of a theoretically infinitesimal duration will be able to trigger the circuit. (Obviously, the d-c adjustment for such a condition is very critical, as also indicated in the quasi-static consideration mentioned already. It may also be noticed that for any given  $E_a$  and  $E_b$ , the minimum pulse required will be narrower, if the shunting and grid-plate capacitances are small and if  $g_m$  is large.

#### THE PARABOLIC PULSE

An equivalent circuit for the Eccles-Jordan trigger has been drawn in Fig. 7. In this case the coupling condenser  $C_c$  may be neglected in order

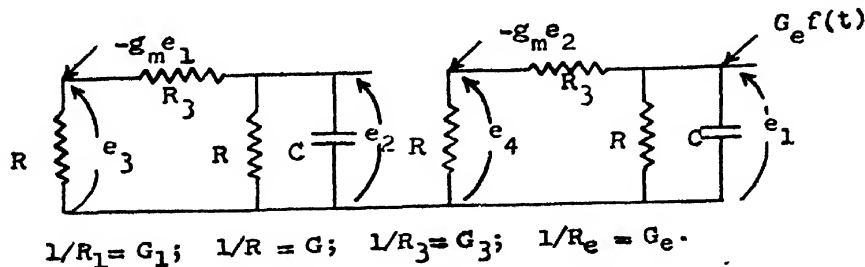


FIG. 7

Equivalent resistance net work for the trigger circuit

to simplify the differential equations, and the smallness of its size justifies such an assumption. The shunting capacitance has been lumped between the grid and the cathode since the amplification involved in the circuit makes the grid-cathode capacitance effectively more important than the others. The driving signal is again represented by the symbol  $f(t)$  and is shown as a current entering one of the grids from a high impedance source. The impedance of

this external source is taken to be  $R_e = 1/G_e$ , and the differential equations are as follows :

$$g_m e_1 + \left( G + G_1 + \frac{G G_1}{G_3} + pC + \frac{G_1}{G_3} pC \right) e_2 = 0 \quad \dots (14)$$

$$\left( G + G_1 + \frac{G G_1}{G_3} + pC + \frac{G_1}{G_3} pC \right) e_1 + g_m e_2 = G_e \left( 1 + \frac{G_1}{G_3} \right) f(t) \quad \dots (15)$$

A simultaneous solution of the above two equations gives the following differential equation for the voltage  $e_1$  :

$$\left[ \left( G_1 + G + \frac{G G_1}{G_3} + pC + \frac{G_1}{G_3} pC \right)^2 - g_m^2 \right] e_1 = \left( G_1 + G + \frac{G G_1}{G_3} + pC + \frac{G_1}{G_3} pC \right) \left( 1 + \frac{G_1}{G_3} \right) G_e f(t) \quad \dots (16)$$

The exponents of the transient part of the solution may first be obtained by putting the right-hand side of (16) equal to zero. Further, if the driving function  $f(t) = kt - mt^2$ , it is possible to assume a particular or steady-state solution of the form :

$$e_1 = A_1 + A_2 t + A_3 t^2$$

When this expression is differentiated and substituted in (16), the constants  $A_1$ ,  $A_2$ , and  $A_3$  can be found in terms of the circuit constants and  $k$  and  $m$ . When the transient and steady-state solutions are written as a sum, the constants accompanying the transient part of the solution can be evaluated by applying the boundary conditions, which are similar to the ones used in connection with the multivibrator (Ahmed, 1950). The conditions are that at  $t=0$ , the grid voltage must be equal to  $-E_{co}$ , and the rate of rise of the grid voltage must be the same as the rate of rise of the applied signal, i.e.  $=k$  in this case. It will be found upon examination of the final equation that when  $m$  becomes larger than a certain amount, the coefficient accompanying the positive exponential becomes zero. Actually minimum value for the ratio  $k/m$  is found, and that is a specification regarding the minimum width of the applied signal. It will also be found that a higher value of  $g_m$  makes the minimum duration of the signal required smaller. A reduction in the shunting condenser  $C$  leads to an almost proportional reduction in the minimum value of  $k/m$ .

Apart from an idea of the minimum duration and amplitude of the operating signal, an analysis of this type also indicates that for any given width of the pulse there will be a certain maximum of the applied signal, beyond which the signal will again fail to produce a proper switching operation. In the above-mentioned case, given a certain pair of values of the signal constants  $k$  and  $m$ , the time taken by the grid voltage to reach zero volt can be found, and this time may also be the time required by the voltage on the other grid to reach  $-E_{co}$ . Obviously, when such a switching has taken place the positive

exponential does not exist any more. If the applied pulse were still decreasing this would tend to reverse the switch, making such a choice of  $k/m$  also undesirable.

Since similar considerations apply to the rectangular pulse, it may be concluded that although the particular limits may be different for different kinds of actuating pulses, a maximum and a minimum amplitude will generally exist for all types of pulses. It may also be concluded that the minimum amplitude for sharper pulses of given initial slope will be greater than that required for comparatively wider pulses. On the other hand, the maximum amplitude is likely to become smaller as the pulse width increases. As the pulse becomes wider than the time of rise, the maximum amplitude of the positive pulse for a proper triggering action will approach the minimum amplitude of the negative pulse required to trigger the circuit in the opposite direction.

### EXPERIMENTAL RESULTS

Experiments were carried out on a trigger circuit for investigating the relation of maximum and minimum operating pulses with the width of the pulses. The results for exponential pulses obtained from a differentiated square wave source are given in Tables I, II, and III and have been plotted in Fig. 8.  $C_p$  is the value of the peaking condenser used in conjunction with a resistance of 10 k $\Omega$ , and represents the effective width of the pulses. Other circuit constants are shown in the figure.

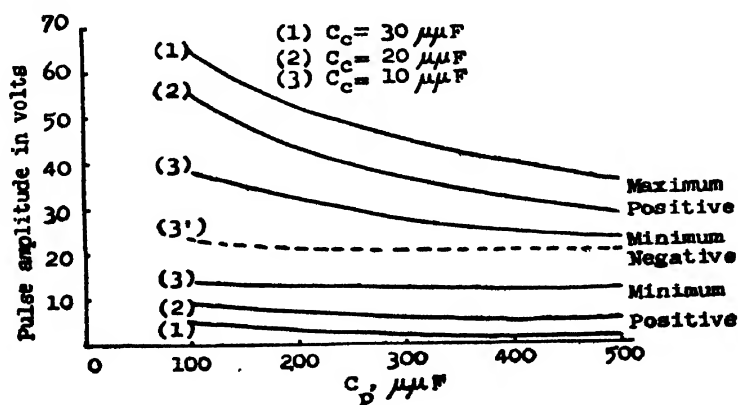


FIG. 8

Exponential pulse amplitude required Vs. pulse sharpness

The results for rectangular pulses are given in Table IV, and have been plotted in Fig. 9.

These tables and the accompanying figures generally support the conclusions that (a) the minimum amplitude for sharper pulses is greater than that for wider pulses; (b) increased pulse-width decreases the maximum amplitude required; (c) for very wide pulses the maximum amplitude for positive pulses approaches the minimum amplitude for negative pulses.

TABLE I

External shunting capacitance between grid and cathode  $C_{gk} = 0$ , and the coupling condenser  $C_c = 10\mu F$ .

$C_p$	Minimum positive pulse amplitude	Minimum negative pulse amplitude	Maximum amplitude for both pulses
100 $\mu F$	13.0 v	22.0 v	38.0 v
200 „	13.0	22.0	33.0
300 „	13.0	21.5	27.5
400 „	12.5	20.5	25.0
500 „	12.0	20.0	23.0

TABLE II

$C_{gk} = 0$ ,  $C_c = 20\mu F$ .

$C_p$	Minimum positive pulse amplitude	Minimum negative pulse amplitude	Maximum amplitude for both pulses
100 $\mu F$	7.5 v	17.0 v	55.0 v
200 „	7.0	16.0	43.0
300 „	6.5	15.0	37.0
400 „	5.5	14.5	32.0
500 „	5.5	14.0	28.0

TABLE III

$C_{gk} = 0$ ,  $C_c = 30\mu F$ .

$C_p$	Minimum positive pulse amplitude	Minimum negative pulse amplitude	Maximum amplitude for both pulses
100 $\mu F$	4.0 v	10.0 v	65.0 v
200 „	3.5	9.0	50.0
300 „	2.5	9.0	44.0
400 „	2.0	8.0	40.0
500 „	1.5	8.0	36.0

It is further shown by these results that a greater value of  $C_c$  increases the pulse size range ; and it is also strongly indicated (Fig. 10) that a certain

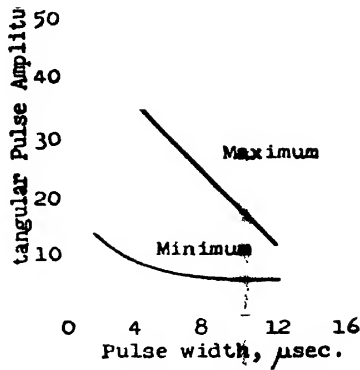


FIG. 9

Rectangular pulse amplitude Vs. pulse width

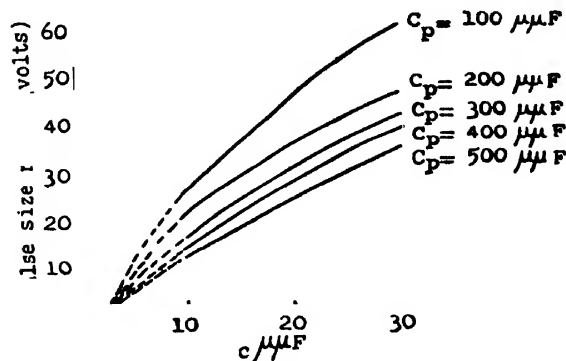


FIG. 10

Pulse size range Vs. coupling capacitance

TABLE IV

$C_{gk} = 0, C_c = 20\mu\mu F.$

Pulse width in $\mu$ sec.	Minimum amplitude in volts	Maximum amplitude in volts
1.8	12.3	35.0
2.9	10.0	35.0
3.5	8.5	35.0
4.1	7.5	35.0
4.5	7.0	34.0
4.8	7.0	33.0
5.5	6.5	31.5
6.4	6.0	27.5
7.0	6.0	26.0
8.0	6.0	23.5
9.5	5.5	20.0
12.0	5.5	12.2

minimum value of  $C_c$  is necessary for proper switching. From the point of view of design it might appear that there is a definite advantage in having an appreciable value of coupling capacitance present in the circuit. However, there is a disadvantage in increasing the value of  $C_c$  and it will be clear from

Table V, where for given pulse heights the minimum possible separation between successive pulses has been studied.

TABLE V

$$C_{gt} = 50\mu F \approx C_c$$

Pulse height in volts	Minimum separation in $\mu$ sec.
6.5	14.0
5.4	16.0
4.2	19.5
3.0	24.1

It is clear that because of the discharging of the large  $C_c$ , the grid voltage waveform is similar to that in the case of the multivibrators, and hence a small positive pulse, coming soon after the condenser  $C_c$ , has started to discharge, is incapable of driving the grid to the cut in voltage region. The larger the amplitude of the pulses the closer they are for producing proper switching. It was found that a reduction in  $C_c$  made successive switching possible with smaller interval between the pulses. It is obvious, therefore, that when the pulse repetition rate is high,  $C_c$  cannot be increased beyond a certain limit. This, in conjunction with the amplitude range consideration mentioned earlier, will determine the proper size of the coupling condenser.

In conclusion, it may be said that the linear analysis of switching operation does lead to a systematic understanding of the operation of trigger circuits. The design considerations indicated here also serve to clarify some properties of the trigger circuit.

#### ACKNOWLEDGMENTS

The help and advice of Professor W. H. Surber of Princeton University, Princeton, N.J., are gratefully acknowledged. The author also wishes to thank Professor P. S. Gill, Dean of the Faculty of Science, Aligarh University, for his advice and permission for continuation of the work.

ALIGARH UNIVERSITY,  
ALIGARH.

#### REFERENCES

- Ahmed, R., 1948, Master's Thesis, Princeton University, U. S. A.
- Ahmed, R., 1950, *Ind. J. Phys.*, **24**, 281.
- Williams, E. M., 1950, *Proc. I. R. E.*, **38**, 1, 65.
- Churchill, R. V., 1944, *Modern Operational Mathematics in Engineering*, McGraw Hill Book Company, Inc.
- Campbell, G. A., and Foster R. M., 1942, *Fourier Integrals for Practical Applications*, Bell Telephone System, Technical Publications, *Mathematical Physics Monograph B-584*.



# ELECTRICAL PROPERTIES OF INDIAN MICA

## IV. ELECTRIC STRENGTH\*

By S. S. MANDAL

(Received for publication, December 14, 1950)

**ABSTRACT.** The paper reports the results of measurements of electric strength of red and green varieties of muscovite micas of different qualities available in the mica mines of Bihar, Madras and Rajputana. The effect of thickness and pre-conditioning of specimens upon their electric strength has been studied. Their intrinsic electric strength is found to be independent of thickness as predicted in Fröhlich's theory of electronic breakdown in polar crystals.

### INTRODUCTION

It is well known that in order to assess the usefulness of a solid dielectric for different service requirements in electrical industry, a knowledge of its dielectric loss, electric strength, volume and surface resistivities, in addition to its physical and chemical properties, is essential. The dielectric loss is generally estimated from the permittivity and power factor values of a dielectric while its electric strength and resistivities are directly measured. In previous communications (Datta, SenGupta and Mahanti, 1943 ; Mahanti, Mukherjee and Roy, 1945 ; Mahanti and Mandal, 1948) were reported the results of measurements of permittivity, power factor and dielectric loss of different types of Indian micas of different origins and of the effect of humidity and preheating temperatures upon these quantities.

The present investigation was undertaken mainly to make a comparative study of the electric strength of the more abundant red and green varieties of Indian muscovite micas of different qualities and origins and of its variation with thickness and pre-conditioning. For this purpose it was considered more advantageous to measure the electric strength of micas in transformer oil than in air, as this would enable us to use a voltage source not higher than 50 k. v. and test pieces of comparatively smaller area without any occurrence of flash over. Moreover, the use of transformer oil as the immersion medium would avoid the source of uncertainty due to varying atmospheric conditions, which influence the electric strength measurements in air. The electric strength in air was, however, determined for the clear red and green varieties. This was done with a view to ascertaining how far the value of their electric strength in transformer oil deviates from that in air. An attempt was also made to determine their intrinsic electric strength.

\* Communicated by Prof. P. C. Mahanti.

The following muscovite micas were investigated. They were obtained in the form of booklets from the Geological Survey of India.

1. Bihar Red (Bengal Ruby), clear.
2. Bihar Red, stained.
3. Bihar Red, stained and slightly spotted.
4. Madras Green, clear.
5. Madras Green, stained.
6. Madras Green, stained and slightly spotted.
7. Rajputana Red, clear.
8. Rajputana Red, stained and slightly spotted.
9. Rajputana Green, slightly stained.

It may be noted here that the mica mines of Bihar, Madras and Rajputana are the chief sources of Indian muscovite micas.

#### PREPARATION OF TEST-PIECES

Mica samples of each variety and quality were visually examined as regards their transparency, colour, spots, loose layers and pits. From the samples thus chosen were cut or split out test pieces of different thicknesses and having an area of six inch square for tests in air and of one inch square for tests in transformer oil. They were then thoroughly cleansed with rectified spirit and stored at room temperature in desiccators until required.

#### PRE-HEATING OF TEST-PIECES

In a previous communication (Mahanti and Mandal, 1948) it was reported that the muscovite micas of nominal thickness of 2 mils show a minimum power factor when pre-heated at a temperature of about 200°C for a period not less than half-an-hour. Hence in the present work the range of pre-heating temperature was limited up to 300°C only. At each pre-heating temperature, groups of test-pieces of nominally different thicknesses were heated for a period of five hours to ensure their uniform conditioning. An electrically heated muffle-furnace was used for the purpose and its temperature was regulated to the desired value by controlling the heating current. A calibrated platinum—platinum-rhodium thermocouple was employed to record the temperature of the furnace. It was only when the temperature of the furnace was found steady at the desired value that the test-pieces were introduced into it and left therein for five hours. At the end of this period, they were transferred to desiccators containing anhydrous  $\text{CaCl}_2$  to cool down to the room-temperature, at which electric strength measurements were made.

#### MEASUREMENT TECHNIQUE

In order to apply uniform electric stress to the test-pieces, two stainless steel spherical electrodes, each of half-inch diameter, were mounted co-axially

on ebonite stands fixed to a circular ebonite base. One of the electrodes was fixed in position while the other was movable in a horizontal plane with the help of an accurate micrometer screw-gauge. The ebonite base has a circular groove cut near its periphery so as to fit exactly at the mouth of a cylindrical glass cell of about  $\frac{1}{2}$  gallon capacity.

The A. C. test voltage, which was of good wave-form at power frequency of 50 c/s, was supplied by high-voltage transformers. Three such transformers of different ratings up to 50 k. v. were used for convenience in manipulating the rate of raising the test-voltage across the test-pieces. As an induction regulator was not available, the voltage was regulated in each case with the help of an auto-transformer having steps of 10 volts, each step being further adjusted by a rheostat as necessary. The input voltages of the high voltage transformer were measured on a precision A. C. voltmeter. The high voltage electrode was connected through a 4.5 megohm safety resistance. The A. C. peak voltages were measured on a calibrated electrostatic voltmeter of range 0-25/50/100 k. v. and also checked from the product of the input voltage of the high voltage transformer in operation with its turn ratio.

For each sample, a preliminary observation was made on a test piece of a particular thickness to get an approximate idea of its breakdown voltage. This being known, breakdown test on a fresh test piece of the same nominal thickness was made by raising the voltage from zero smoothly and uniformly at such a rate that breakdown occurred within 30 to 60 seconds. In this way similar observations were made on test-pieces of the same or of different nominal thicknesses of the same sample. The duration of impulse was kept constant in each case.

For breakdown tests in transformer oil, the glass-cell was filled with the oil (Grade A) to  $\frac{2}{3}$ rd of its height, so that the electrodes lay well under the surface of the oil.

A few observations were also made, using D. C. voltage supplied from the same set of transformers in conjunction with a 150-k. v. Kenotron rectifying valve and was measured on the same electrostatic voltmeter.

Intrinsic electric strength measurements, using both A. C. and D. C. voltages, were made only in the case of clear Bihar Red and Madras Green micas. It has been shown by Hackett and Thomas (1949) that in intrinsic electric strength measurements on plane specimens of mica it is essential to prevent premature breakdown of the ambient medium. When using spherical electrodes, this can be done by selecting a liquid medium of relatively high conductivity, such that

$$\epsilon_m \sigma_m \geq \epsilon_s \sigma_s \text{ for D. C.}$$

$$\text{and } \epsilon_m \sigma_m = \epsilon_s \sigma_s k. f., \text{ for A. C.}$$

where  $\epsilon$ =field strength, in volts per cm ;  $\sigma$ =effective conductivity, in mhos per cm ;  $k$ =permittivity ;  $f$ =frequency and the subscripts  $m$  and  $s$  refer

to the medium and to the specimen respectively. A mixture of castor oil (medicinal) and nitrobenzene was used as the immersion medium. After many trials, it was found that when the mixture was made with 27 % of castor oil and 73% of nitrobenzene by volume, the puncture in Madras Green mica took place exactly at electrode-vertices. But in the case of Bihar Red mica, using the same mixture, the puncture spot was found to lie slightly away from the vertices and may probably be responsible for the difference between the observed D. C. and A. C. values of the intrinsic breakdown voltage.

The thickness of test-pieces before tests was measured with a dial micrometer to an accuracy of  $\pm 0.01$  mil. This was further checked from the reading of the micrometer screw gauge when during the breakdown tests the movable electrode was pressed lightly on the surface of the test-pieces to hold them in position. The reading of the screw gauge was in no case found higher than that of the dial micrometer.

### RESULTS

The experimental data for different varieties and qualities of Indian muscovite micas of various localities are given in Tables I—VI. In each case the mean electric strength has been obtained firstly by dividing the actual breakdown voltage by thickness for each test-piece and then taking the mean of all such values for all test-pieces of all the same nominal thickness. In no case less than five test-pieces were used.

The data of electric strength in air of clear Bihar Red and Madras Green micas of different thicknesses are given in Table I.

TABLE I

Electric strength of micas in air at 30°C (Relative humidity :—56%)  
and Effect of thickness.

Nominal thickness (mils)	Mean Electric strength in volts/mil (peak)	
	Bihar Red (clear)	Madras Green (clear)
0.5	15000	13680
1.0	12500	11400
2.0	8550	6840
3.0	6600	5320
4.0		4560
5.0	4050	3520
7.5	2650	2360
10.0	1920	1680
12.5	1780	1480
15.0	1580	1400
20.0	1480	
25.0	1380	
30.0	1320	

Table II contains the data of their electric strength in transformer oil for a nominal thickness of 5 mils, from which their relative strength to withstand A. C. voltage can be judged.

TABLE II

Comparative tests of electric strength of micas for a nominal thickness of 5 mils in transformer oil at 30°C.

Muscovite mica		Number of test-pieces	Mean electric strength, volts/mil	
Variety	Quality		peak	% dispersion
Bihar Red	Clear	10	2015	±5.0
	Stained	12	1853	±4.1
	Stained & slightly spotted	11	1905	±4.5
Madras Green	Clear	9	1840	±4.3
	Stained	15	1700	±5.0
	Stained & slightly spotted	20	1683	±5.3
Rajputana Red	Clear	8	2150	±5.2
	Stained & slightly spotted	6	1920	±5.1
	slightly stained	8	1720	±4.4

TABLE III

Effect of thickness on electric strength of micas in transformer oil at 30°C.

Nominal thickness (mils)	Mean electric strength, volts/mil (Peak)					
	Bihar Red mica			Madras Green mica		
	Clear	Stained	Stained & slightly spotted	Clear	Stained	Stained & slightly spotted
2	3485	3040	3250	2650	2147	2250
4	2375	2115	2235	2043	1854	1800
6	1725	1528	1650	1700	1688	1600
8	1353	1335	1455	1452	1502	1445
10	1200	1230	1385	1355	1382	1406
12	1100	1185	1335	1286	1290	1290
14	1040	1140	1300	1245	1137	1276

Table III includes data showing the effect of thickness on their electric strength in transformer oil while in Table IV are given data to show the effect of the application of D. C. voltages. The data showing the effect of pre-conditioning the micas at different temperatures on their electric strength are included in Table V. The data on the intrinsic electric strength of clear Bihar Red and Madras Green micas are contained in Table VI.

TABLE IV

D. C. electric strength of micas in transformer oil at 30°C  
and Effect of Thickness.

Nominal thickness (mils)	Mean D. C electric strength, volts/mil	
	Bihar Rred clear	Madras Green clear
1	13,025	12,030
2	11,030	10,135
4	7,875	7,530
6	5,592	5,234
8	4,278	4,035
10	4,025	3,780

TABLE V

Effect of conditioning for five hours at different temperatures on electric strength of micas of different thicknesses in transformer oil at 30°C.

Nominal thickness (mils)	Mean electric strength ; volts/mil (Peak)							
	Before conditioning		100°C		200°C		300°C	
	Bihar Red (clear)	Madras Green (clear)	Bihar Red (clear)	Madras Green (clear)	Bihar Red (clear)	Madras Green (clear)	Bihar Red (clear)	Madras Green (clear)
2	3485	2650	3560	3285	3632	3410	3092	2750
4	2375	2043	2935	2831	3168	2850	2473	2400
6	1725	1700	2250	2345	2680	2450	2285	2100
8	1363	1452	2000	2150	2435	2225	2190	1800
10	1200	1355	1743	2021	2175	2115	2100	1625

TABLE VI

Intrinsic electric strength data :

Immersion mixture : 27% medicinal castor oil to 73% nitrobenzene by volume.

Thickness (mils)	Type of voltage	Madras Green		Bihar Red	
		B. D. V. (kv)	Mean electric strength (Peak) (kv/mil)	B. D. V. (kv)	Mean electric strength (Peak) (kv/mil)
1	A.C.	17.5	17.5	22.0	22.0
	D.C.	18.0	18.0	25.0	25.0
1.5	A.C.	26.0	17.4	32.5	21.66
	D.C.	26.0	17.4	37.0	24.6
2	A.C.	35.0	17.5	43.0	21.5
	D.C.	35.0	17.5	48.0	24.0

### CONCLUSIONS

It will be seen from the data in Tables I and II that the electric strength of red muscovite mica is greater than of green muscovite mica of the same quality. It is further found from Table II that the electric strength of a particular variety and quality of mica is quite independent of the locality from where it is obtained.

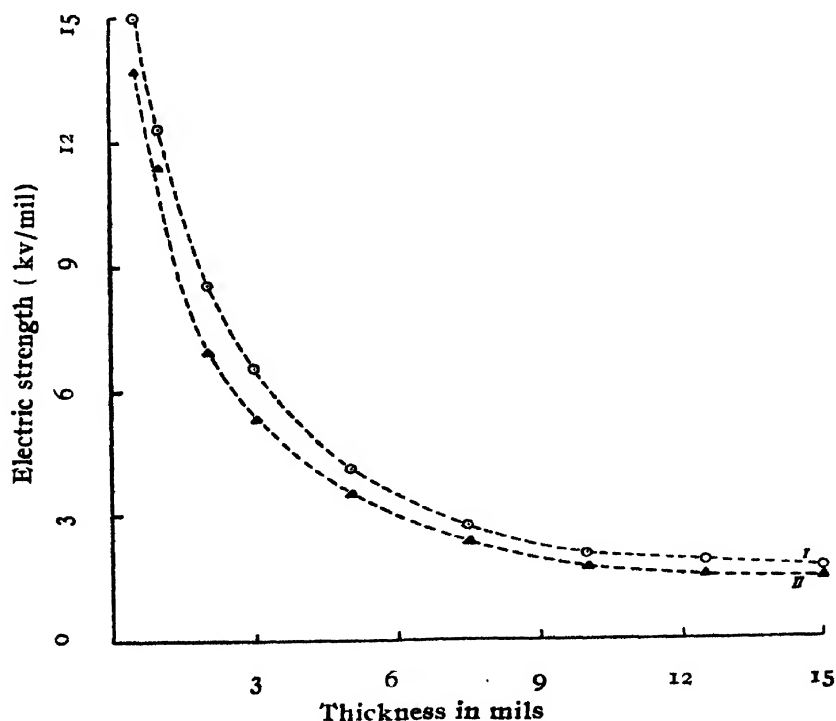


FIG. I

Effect of thickness on electric strength in air

I—Bihar Red, clear

II—Madras Green, clear

Figs. 1-4 show the variations of electric strength with thickness for different varieties and qualities of Indian muscovite micas at a temperature of 30°C. It is easily seen that the electric strength in each case decreases with increasing thickness and the nature of variation is as one would expect. It may be noted here that from theoretical considerations, Joffe (1926) concluded that in the case of thin films the electric strength (expressed as volts/mil) should vary inversely as the thickness of the specimen and confirmed this by experiments on thin glass films. Moon and Norcross (1930) reached the same conclusion as a result of measurements on thin mica films of thickness below 2 mils. Lewis, Hall and Caldwell (1931), however, found that over the range of thickness from 0.1 mil to 17 mils the electric strength (expressed in k.v./mil) of mica falls off more rapidly than  $1/t$ , where  $t$  is the thickness of the specimen in mils and seems to be more adequately expressed by the equation

$$kv/mil = \frac{A}{\sqrt{t}} + B$$

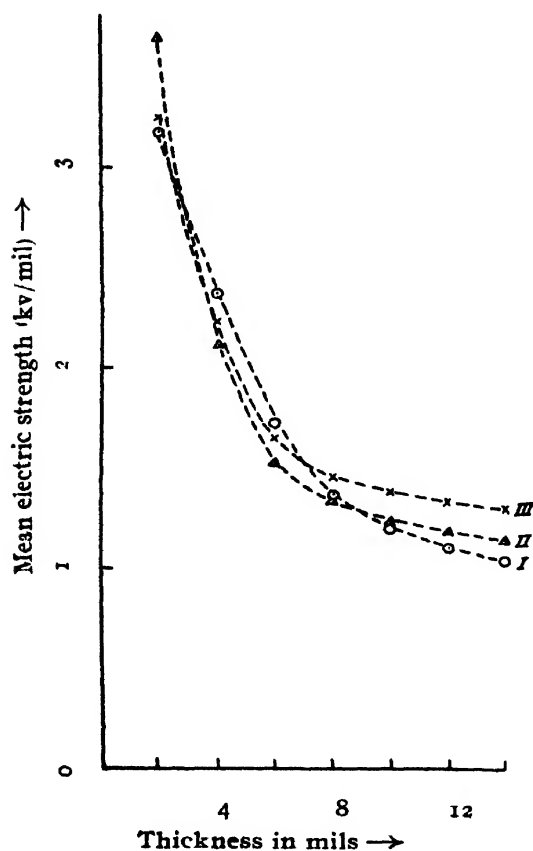


FIG. 2

Effect of thickness on electric strength in transformer oil

- I—Bihar Red, clear  
 II— „ „ , stained  
 III— „ „ , slightly spotted

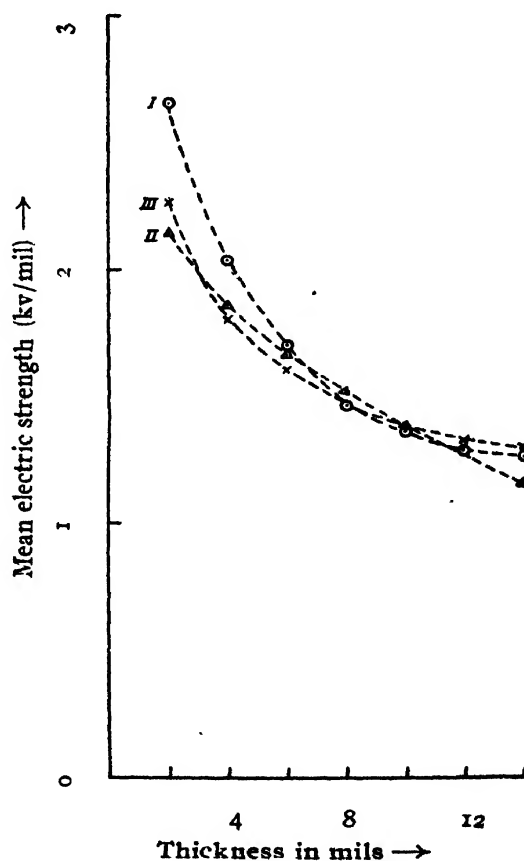


FIG. 3

Effect of thickness on electric strength in transformer oil

- I—Madras Green, clear  
 II— „ „ , stained  
 III— „ „ , stained and slightly spotted



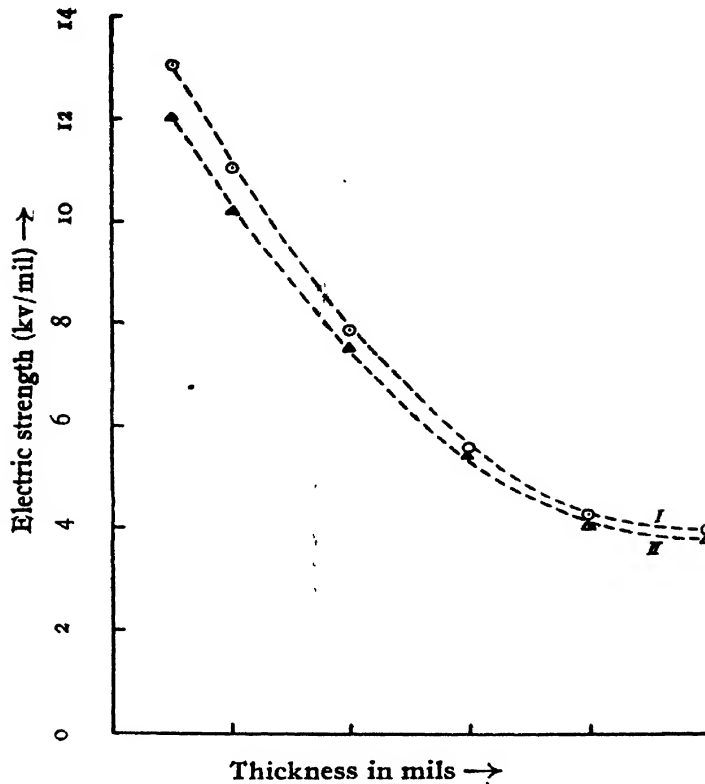


FIG. 4

Effect of thickness on D. C. electric strength in transformer oil

I—Bihar Red, clear

II—Madras Green, clear

where  $A$  and  $B$  are constants, although below about 3 mils, the two laws are practically identical within the limits of dispersion of their data. The present data are in conformity with this view.

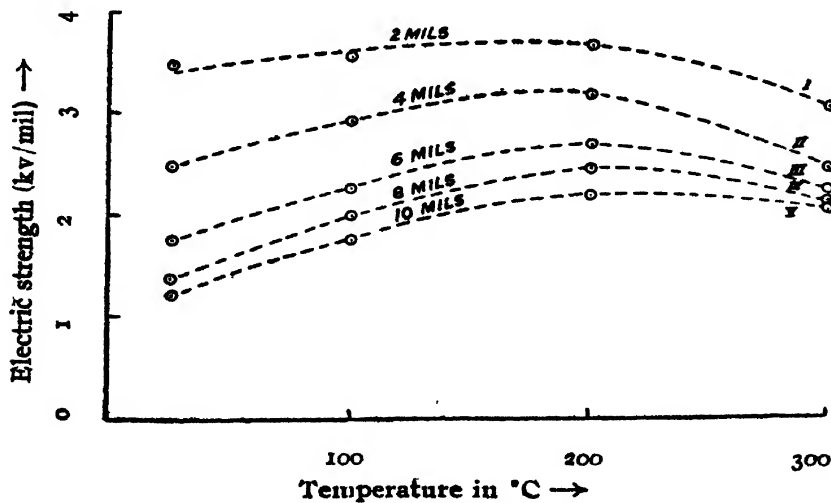


FIG. 5

Effect of conditioning on electric strength of Bihar Red mica, clear

It is further found that although the ability of mica to withstand A. C. voltage is much lower in transformer oil than in air, there is practically no difference when D. C. voltage is applied. This is probably due to the different types of discharges which occur in gaseous and liquid media depending on the nature of the applied voltage.

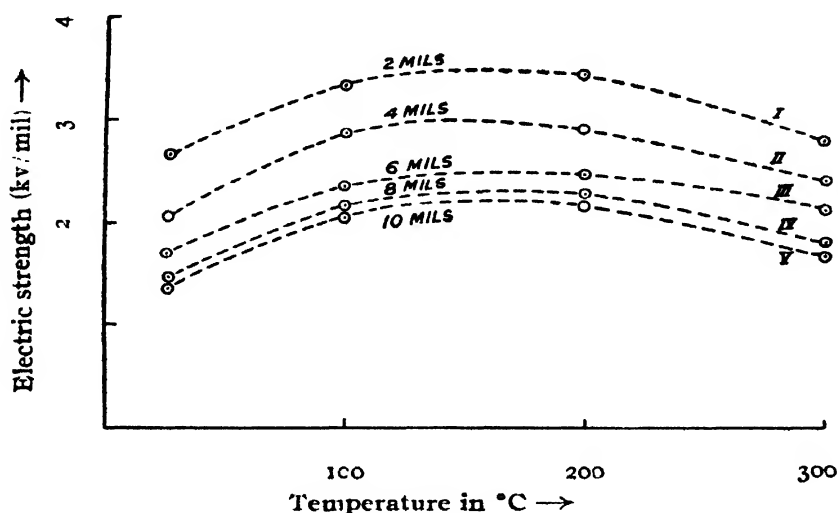


FIG. 6

Effect of conditioning on electric strength of Madras Green mica, clear

Figs. 5 and 6 show the variation of electric strength of red and green muscovite micas with their conditioning temperatures. It is found that the electric strength in each case increases from the value obtained before conditioning the specimen and reaches a maximum at a conditioning temperature of 200°C and then decreases. This observation, together with the data presented in a previous paper (*loc. cit.*) on the effect of pre-heating on power factor, leads one to conclude that when muscovite micas are conditioned at a temperature lying between 150°C to 200°C, their electrical properties show very marked improvement.

Fig. 7 shows the variation of intrinsic breakdown voltage with thickness for clear Bihar Red (Bengal Ruby) and Madras Green micas. It will be easily seen that their intrinsic electric strength is independent of thickness in conformity with a prediction of Fröhlich's (1937) theory of electronic breakdown in polar crystals. It will be further seen that the intrinsic electric strength of Bihar Red mica is also greater than that of Madras Green mica. It may be noted, however, that in practical applications of micas for electrical design work, an electric strength approaching the intrinsic value

is hardly attained due to various causes which are often unavoidable. Hence their electric strength in air forms a better guide for the purpose.

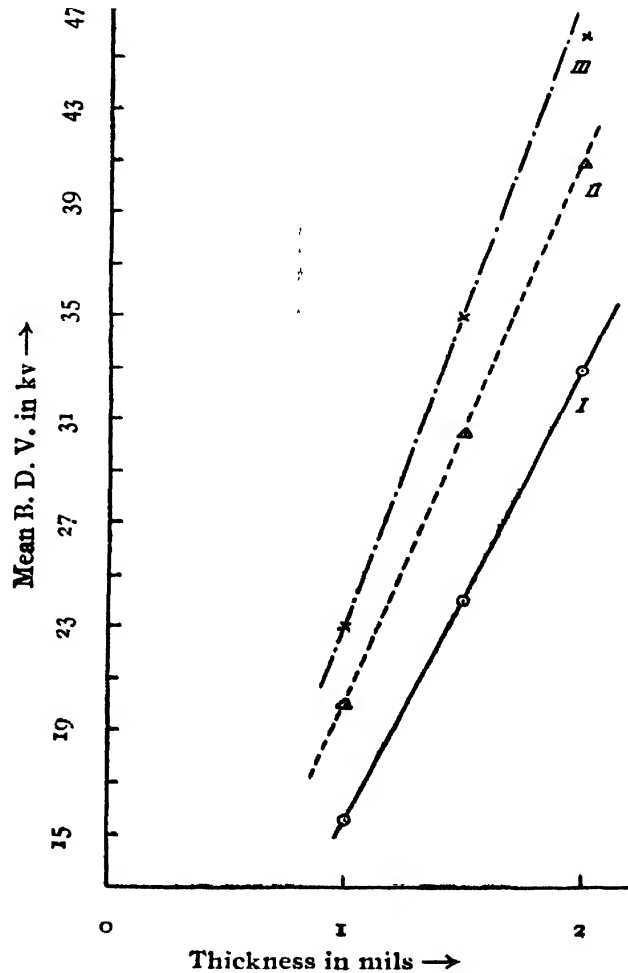


FIG. 7

Effect of thickness on intrinsic breakdown voltage.

- I—B. D. V. (A. C. and D. C.) for Madras Green, clear
- II—B. D. V. (A. C.), Bihar Red, clear
- III—B. D. V. (D. C.), Bihar Red, clear

#### ACKNOWLEDGMENTS

The author acknowledges with great pleasure his indebtedness to Prof. P. C. Mahanti for his guidance and encouragement during the work.

DIELECTRIC RESEARCH LABORATORY,  
DEPARTMENT OF APPLIED PHYSICS,  
UNIVERSITY OF CALCUTTA.

## REFERENCES

- Datta, S., Sen Gupta, J., and Mahanti, P. C., 1943 ; *Ind. J. Phys.*, **17**, 79.  
Fröhlich, H., 1937, *Proc. Roy. Soc. (A)*, **160**, 230.  
Hackett, W., and Thomas, A. M., 1941, *J. I. E. E.*, **88**, Part I, 295.  
Joffe, A., 1926, *J. Math and Physics*, M. I. T., **6**, 133.  
Mahanti, P. C., Mukherjee, M. K., and Roy, P. B., 1945, *Ind. J. Phys.*, **19**, 33.  
Mahanti, P. C., Mandal, S. S., 1948, *Ind. J. Phys.* **22**, 8.  
Moon, P. H. and Norcross, A. S., 1930, *J. Am. I. E. E.*, **49**, 125

# ABSORPTION SPECTRUM OF PHENETOLE

By K. SREERAMAMURTY

(Received for publication, November 22, 1950)

## Plate V

**ABSTRACT.** About 90 bands were measured in the near ultra-violet absorption spectrum of phenetole vapour in the region  $\lambda 2785$  to  $\lambda 2385$ . The bands were broader than those of its lower homologue, anisole. An analysis is suggested on the basis of upper state frequencies, 159, 344, 354, 704, 907, 952, 1263, and  $1542\text{ cm}^{-1}$ . These are compared with the Raman frequencies.  $\nu$ - $\nu$  transitions giving difference frequencies 23 and  $35\text{ cm}^{-1}$  have been established.

## INTRODUCTION

Substituted benzenes have spectra in the near ultra-violet region which are more intense than the spectrum of benzene. One type of substituents previously investigated are  $\text{NH}_2$ ,  $\text{OH}$ ,  $\text{F}$  and  $\text{Cl}$  all of which possess an unshared pair of electrons in suitably oriented  $p$  orbitals. Such electrons give rise to a migration of charge between ring and substituent and produce, as Sklar (1939) has shown, an intensification of the spectrum relative to that of benzene, the intensity being a function of the extent of migration. Another type of substitution is the  $\text{CH}_3$  and other alkyl radicals which do not possess an unshared pair of electrons or a structure conjugate to the ring giving rise to a resonance effect of the kind existing in the first type of substitution. Still as Mulliken, Rieke and Brown (1941) have shown, the alkyl substituents can resonate with the ring due to what is called by them as "hyper-conjugation." The methyl group has approximately the same effect on intensity as has the  $\text{Cl}$  atom. The calculated intensity of absorption (Sklar, 1939) is in agreement with experiment. Ginsburg, Robertson and Matsen (1946) have also shown that the substitution of the  $\text{CH}_3$  group affects the spectrum of the nucleus in much the same way as the other substituents  $\text{Cl}$ ,  $\text{F}$ ,  $\text{NH}_2$  and  $\text{OH}$ , with the difference that the transitions in toluene, involving the higher vibrational quantum numbers, are not so well developed. Another set of substitution which, in the light of the above discussion, is considered worthwhile studying is the  $\text{OCH}_3$  and its homologues. The spectrum of anisole ( $\text{OCH}_3$ ), the first of such a set of molecules was described in a previous paper by the author (1950). Its interpretation was discussed in terms of electronic states and vibration frequencies of the molecule. The absorption spectrum of phenetole ( $\text{O.CH}_2.\text{CH}_3$ ) form the subject of this paper.

## EXPERIMENTAL

As in anisole (Sreeramamurty, 1950), the spectrum of phenetole was photographed on Hilger medium and large Littrow spectrographs. A pure specimen of phenetole supplied by B.D.H., was redistilled into the absorption tube in vacuum. Absorption cells of different lengths were used varying between 2.5 cms to 100 cms. The longer column was used specially in an attempt to extend the absorption spectrum as far to the region of longer wavelengths as possible. The amount of phenetole vapour introduced into the tubes and its pressure was adjusted by varying the temperature of the reservoir containing the liquid. The range of temperatures at which the spectrum was photographed was  $-15^{\circ}\text{C}$  to  $60^{\circ}\text{C}$ . While working with higher temperatures, the absorbing tube was heated to the same temperature or maintained at a slightly higher temperature than that of the reservoir. No photo-decomposition was found either for anisole or phenetole. Even long exposures extending over four hours could be maintained without appreciable diminution in intensity from deposit on the windows. Absorption picture taken at the end through the windows did not reveal any selective absorption.

A Hilger hydrogen lamp, run on the secondary of a transformer giving 2000 volts and current of about 300 ma, was employed as a source of continuous radiation. For preliminary experiments, in order to save the life of standard hydrogen lamp, the continuum provided by an oscillator discharge through iodine vapour developed in our laboratory was also used. The exposure times with the Littrow instrument extended to about four hours. Final measurements were adopted from the Littrow plates.

## DESCRIPTION

The spectrum extended from  $\lambda_{2785}$  to about  $\lambda_{2388}$ . About 90 bands could be measured in all. The development of the long wavelength end of the spectrum could not be extended further than  $\lambda_{2785}$  even with the longest absorbing column of one metre and a maximum temperature of  $80^{\circ}\text{C}$  attained in the experiments. The boiling point of phenetole is  $172^{\circ}\text{C}$  and spectra at about this temperature might perhaps reveal an extension of the spectrum. These experiments are in progress. Plate V is a reproduction of the band system at different temperatures and absorbing lengths.

Two distinct types of band structure are observed. (1) Bands with sharp heads on the violet edge and degraded towards the red. (2) Diffuse bands with no sharp edges but generally having maximum intensity at the centre. While measuring the second type of bands, the crosswire of the micrometer was necessarily set against the intensity peak, while in the first set the edges were measured. (3) A third type of bands was also observed showing a doublet structure. These doublets are not sharp as in phenol or exactly like those observed in toluene. They consist of one intense component with a

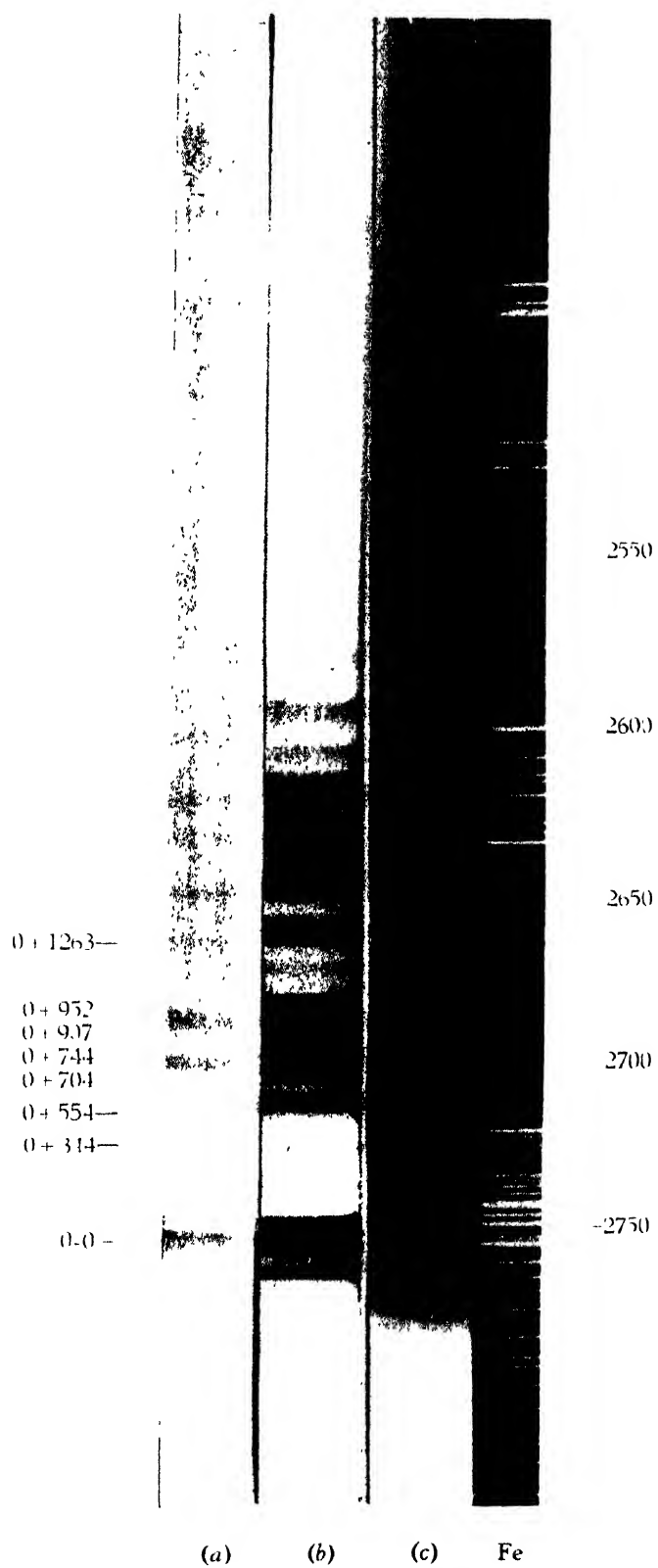
TABLE I

Wavelength	Wavenumber	Int.	Diff. from o,o	Assignment
2785.02	35896	vvw	466	
75.47	36019	w	343	o-343
75.12	024	m	338	
74.20	036	m	326	
71.79	067	w	295	
67.58	122	m	240	
66.65	134	mst	228	o-228
65.68	147	m	215	
62.37	190	w	172	
60.52	214	vvw	148	
58.19	245	m	117	
54.03	300	vst	62	o-62
53.32	309	vvw	53	o-744+796, } o-704+755, }
51.99	327	st	35	o-35
51.08	339	mst	23	o-23
49.32	362	vvst		o,o
47.30	389	st	27	o+27 (o+1263-1235)
46.02	406	nw	47	
37.39	521	mst	159	o+159
36.84	528	m	166	o+344
23.57	706	m	344	
22.34	722	mw	360	
14.45	829	m	467	o+467
11.94	863	w	501	o+344+159
11.28	872	m	510	o+554-2x23
09.58	895	mst	533	
08.05	916	mst	554	o+554
04.17	969	w	607	o+554+2x27
03.17	983	vvw	621	
01.06	37012	w	650	
2699.47	033	mst	671	o-228+907

TABLE I (contd.)

Wavelength	Wavenumber	Int	Diff. from o.o	Assignment
2697.07	37066	st	704	0+704
95.95	082	mst	720	0-228+952
95.42	089	st	730	704+27
94.15	106	vst	744	0+744
92.38	130	mst	768	0+744+27
91.22	147	mw	785	
88.31	187	vvw	825	
84.35	239	mw	877	0+907-35, 0+952-2×35
82.93	262	m	900	0+554+344
82.40	<u>269</u>	vst	907	0+907
81.97	275	m	913	0+952-35
79.27	314	mst	952	0+952
78.80	320	m	958	
77.18	342	m	980	0+952+26
76.20	355	m	993	
73.81	389	mw	1027	0+3×344
70.92	429	w	1067	0+907+159
67.70	474	mw	1112	0+952+159 ; 0+2×554
61.74	558	mw	1196	0+1263-2×35
59.22	594	m	1232	0+1263-35
58.14	609	w	1247	0+907+344
57.05	625	vst	1263	0+1263
56.45	633	mw	1271	
52.24	693	m	1331	
46.75	771	vvw	1409	0+2×704
46.02	781	m	1419	0+467+952, 0+1263+159
43.74	814	m	1452	0+744+554 +159
41.52	846	w	1484	0+2×744, 0+554+2×467 0+554+952-23





Absorption spectrum of phenetole vapour

(a) 2.5cm., -15°C, (b) 15cm., 0°C, (c) 50cm., 30°C



TABLE I (contd.)

Wavelength	Wavenumber	Int	Diff. from 0,0	Assignment
2639.72	37872	m	1510	0+534+952
37.47	904	m	1542	0+1542
28.45	38034	w	1672	0+159+554+952
24.93	085	m	1723	0+1263+467
16.93	201	vw	1839	0+952+907-23
16.36	210	w	1848	0+2×554+744 0+344+554+952
15.55	222	w	1860	0+952+907
13.61	250	vw	1888	0+952+2×467, 0+1263+467+159, 0+1542+344
12.44	267	vw	1908	0+2×952
10.16	300	vw	1938	0+2×952+27
03.91	392	w	2030	0+952+704+344 +27
03.26	402	vw	2040	0+952+744+344
01.58	575	w	2213	0+1263+952
2590.59	38590	w	2228	0+3×744
78.94	764	vw	2402	
78.26	774	w	2412	0+554+907+952
76.14	806	vvw	2444	0+907+1542
61.13	39034	w	2672	0+467+554+744 +907
51.91	175	w	2813	0+907+2×952
18.43	695	vvw	3333	
2487.43	40190	vvw	3828	
69.04	489	vvw	4127	
12.21	41443	vvw	5081	
2388.22	859	vvw	5497	

sharp edge accompanied by a fainter component towards the violet. The doublet width is about  $7\text{ cm}^{-1}$ . The stronger component is much broader than the other component. In general, the bands are very broad even at the lowest temperature— $15^{\circ}\text{C}$  at which they were photographed. Table I records the wavelength, wavenumber and intensity data of all the bands. The intensities are, following the usual practice, expressed as vst, st, and mat

indicating very strong, strong and medium strong and respectively similarly vw, mw and w. The fourth column gives the difference from o, o band and the last one the assignment of the bands in terms of the characteristic frequencies.

#### DISCUSSION AND ANALYSIS

For the purpose of interpreting the absorption spectrum of phenetole, the molecule may be regarded as a mono-substituted benzene, the effect of the  $\text{OC}_2\text{H}_5$  group on the benzene ring being analogous to that of the halogens or the  $\text{OH}$ ,  $\text{CH}_3$  or  $\text{O.CH}_3$  groups. The symmetry of the benzene molecule is modified to that of  $C_{2v}$ , the allowed electronic transition  $A_1 - B_1$  giving rise to the spectrum. The vibrational states involved are of symmetry class  $A_1$ . In addition, vibrations of symmetry class  $B_1$  and  $A_2$  may also appear but should be weak. The  $B_2$  vibrations should be absent. If the perturbation of the benzene ring by the substituent  $\text{O.C}_2\text{H}_5$  is not very great the forbidden transition made allowed in the benzene spectrum by the  $\epsilon_g^+$  vibration might also be expected in the spectrum of phenetole.

The strong band at  $\nu_{36362}$  is classified as the  $o \rightarrow o$  transition. This does not present a doublet appearance but is broad with a sharp violet edge. The  $o - 1 \times \nu$  transitions corresponding to the Raman frequencies have not been obtained beyond  $\nu_{343}$  as the spectrum did not extend further than  $\nu_{35896}$  ( $o - 466$ ). (Only two frequencies 228 and  $343 \text{ cm}^{-1}$  are observed which agree with 236 and  $347 \text{ cm}^{-1}$ , as reported by Kahovec and Reitz (1936). The Raman frequency  $424 \text{ cm}^{-1}$  is not found in the ultra-violet spectrum although it is recorded to have intensity (4) in the Raman spectrum. The two frequencies  $613$  and  $510 \text{ cm}^{-1}$  of the ground state are the two components resulting from the removal of degeneracy of the  $\epsilon_g^+$  vibration by the substituent. The corresponding frequencies in the excited state are probably 554 and  $467 \text{ cm}^{-1}$ . The 544 frequency is non-totally symmetric and is found to combine with all the other totally symmetric vibrations. The band at  $\nu_{37474} \text{ cm}^{-1}$  giving a difference 1112 is assigned either as  $o + 2 \times 554$  or  $o + 952 + 159$ . Perhaps the latter assignment is more probable since the transition involving the doubly excited non-totally symmetric vibration is expected to be very faint on the basis of the Franck-Condon principle. Other upper state frequencies established in this work, as can be seen in the last column of Table I, are 159, 344, 744, 907, 952, 1263 and  $1542 \text{ cm}^{-1}$ . They are adopted on the basis of their correlation with Raman frequencies, intensity of the transition  $o + 1 \times \nu$  and the combinations that they present. The frequencies are correlated with the corresponding Raman data and are shown in Table II. In general, it may be assumed that due to electronic excitation of a molecule the vibration frequency of the excited state would be smaller than that in the ground state. On this basis, the associations of all the strong totally symmetric frequencies in the ground and excited states, shown in the Table II, appear to be satisfactory except the upper state frequency 1263, which is

higher than 1235 in the ground state. Perhaps the strong band  $o + 27$  at  $\nu_{36389}$  representing  $o + 1263 - 1235$  supports this correlation. An association for a similar nature was observed also in phenol (1273 upper state, 1263 ground state). Another striking feature is the absence of the frequency corresponding to  $1166 \text{ cm}^{-1}$  in the ground state which yields a fairly strong Raman line.

First column in Table II contains the symmetry classification of the vibration suggested from the intensity of the corresponding band heads. In toluene two frequencies 216 and 730, ascribed to symmetry  $B_2$ , have been observed in the ground state from Raman data. The corresponding excited state frequencies were not observed since such vibrations should not appear. In phenetole since the frequencies 159 and  $704 \text{ cm}^{-1}$  are intense, these, as well as the ground state frequencies 236 and  $755 \text{ cm}^{-1}$  with which they are correlated, may probably be of the symmetry class  $A_1$ .

Table II

Probable symmetry characterization	Ground State		Excited State Present work
	Raman Kahovec and Reitz	U.V. Present Author	
Symmetry $A_1$	510 (1)		457 m
"	796 (3)		744 vst
"	995 (7)		907 vst
"	1023 (4)		952 mst
"	1166 (3)		
"	1235 (3b)		1263 mst
Symmetry $B_1$	347 (3)	343 w	
"	613 (3)		554 m
Symmetry $A_2$	424 (4)		344 m
*	236 (3b)	228 mst	159 mst
*	755 (2)		704 st

From a scrutiny of last column of Table I it will be seen that many of the transitions of the type  $o + 1 \times \nu'_i + 1 \times \nu'_j$  are present as also  $o + 2 \times \nu'_i$ . The three quantum number transitions of the type  $o + 3 \times \nu'_i$  are absent with the exception of  $o + 3 \times 344$  and  $o + 3 \times 744$  while a larger number of the type  $o + 1 \times \nu'_i + 1 \times \nu'_j + 1 \times \nu'_k$  are observed. In general, as in toluene, the phenetole spectrum is not well developed for transitions involving the higher vibration as quantum numbers. In this respect it differs from the spectra of other substituents such as F, Cl,  $\text{NH}_2$  and OH.

Close to the  $o, o$  band on the red side three strong bands appear giving the differences 23, 35 and  $62 \text{ cm}^{-1}$ . These are too small for assignment as the Raman frequencies and probably represent the difference frequencies corresponding to  $1 \rightarrow 1$  transitions detected in most of these substituted benzene spectra. Of these 23 and 35 alone could be established as such, since they occur in combination with other frequencies resulting in the ultra-

violet bands although their correlation with any of the assigned fundamental frequencies is not possible. The  $62\text{ cm}^{-1}$  frequency could not at all be established on any basis.

Following Ginsburg (*et al*); an interesting comparison might be made of the frequency change: (1) in benzene and substituted benzenes, (2) in the ground and excited states in the same substituted molecule. Table III shows these differences with respect to benzene and phenetole for certain vibrations. The first column represents the Wilson notation for the frequency. Two points might be considered in this comparison: (1) Since the  $(\text{O})\text{C}_2\text{H}_5$  group replaces a hydrogen atom in benzene, a large change in frequency may be expected for the predominantly hydrogen than for the carbon vibrations. This is seen for the vibrations 7a and 12. (2) The electronic excitation affects the electrons in the C-C bond so that the C-C frequencies will undergo a large change in the process of excitation. This is evident in vibrations 1 and 18a. The 6a vibration cannot be concluded on this basis alone as a carbon or a hydrogen vibration. A discussion of this point in comparison with several other substituted molecules will be given elsewhere.

Table III

Frequency	Frequency Differences		Vibration
	Benzene Raman- Phenetole Raman	Phenetole Raman- Phenetole excited	
1	-3	88	C-C
6a	96	43	
7a	1812	-28	C-H
9a	12	...	
12	215	52	C-H
18a	14	71	C-C
8a	-1	55	C-C

## ACKNOWLEDGMENT

The author is highly grateful to Prof. K. R. Rao for his kind guidance and interest in the work.

DEPARTMENT OF PHYSICS

ANDHRA UNIVERSITY, WALTAIR.

## REFERENCES

- Ginsburg, Robertson and Matsen, 1946, *J. Chem. Phys.*, **14**, 511  
 Kahovec and Reitz, 1936, *Monatsh. f. Chemie*, **69**, 372.  
 Mulliken, Rieke and Brown, 1941, *J. Am. Chem. Soc.*, **63**, 41.  
 Sklar : 1939 *T. Chem. Phys.*, **7**, 984.  
 Sreeramamurthy, K., 1950, *Ind. J. Phys.*, **24**, 421.

# RAMAN SPECTRA OF ORGANIC CRYSTALS AT DIFFERENT LOW TEMPERATURES. II. ETHYL BENZENE AND BENZYL CHLORIDE.\*

By A. K. RAY.

(Received for publication, March 12, 1951)

## Plate VI

**ABSTRACT.** The Raman spectra of crystals of ethyl benzene at  $-100^{\circ}\text{C}$  and  $-180^{\circ}\text{C}$  and of benzyl chloride at  $-50^{\circ}\text{C}$  and  $-180^{\circ}\text{C}$  have been investigated. Each of these substances in the solid state at a temperature a few degrees below the melting point yields four new Raman lines in the low-frequency region and this number increases to five when the solid is further cooled down to  $-180^{\circ}\text{C}$ . The intensity of some of the lines also increases with the lowering of temperature. It is pointed out that these results cannot be explained on the hypothesis that the lines are due to angular oscillation of the molecules pivoted in the lattice and that they can be explained by assuming that groups of associated molecules are formed in the solid state as pointed out earlier by Sirkar (1936).

The prominent Raman lines of the liquids are observed to become sharper with solidification of the liquid and some of the lines undergo slight changes in position. It is pointed out that these changes are also compatible with the formation of groups of associated molecules in the solid state.

## INTRODUCTION.

To explain the origin of the low frequency Raman spectra observed in the case of different substances like benzene, naphthalene, diphenylether, para-dichlorobenzene, etc., in the solid state, Kastler and Rousset (1941), Bhagavantam (1941) and Rousset (1948) postulated that these lines are due to oscillations of the molecules pivoted in the crystal lattice. This hypothesis can be tested by studying the temperature-dependence of intensities and frequencies of the new lines as pointed out earlier by the author in the case of chlorobenzene and toluene (Ray 1950), benzene (Sirkar and Ray, 1950) and naphthalene (Ray, 1950). The results led to the conclusion that the low-frequency lines might be due to oscillations of the groups formed by association of the molecules and that the results could not be explained satisfactorily by the hypothesis put forward by Kastler and Rousset (1941) and Bhagvantam (1941). As the angular oscillations of the benzene ring pivoted in the lattice are expected to be greatly affected by the presence of substitution groups in the molecule, the results obtained in the case of a large number of substituted benzene compounds may be helpful in understanding the nature of oscilla-

\*Communicated by Prof. S. C. Sirkar.

tions which give rise to these new lines in the case of the organic crystals. It is therefore intended to study the Raman spectra of a few substituted benzene compounds in the solid state at different temperatures and the results obtained in the case of ethyl benzene and benzyl chloride are discussed in the present paper.

## EXPERIMENTAL

The liquids ethyl benzene and benzyl chloride used for the present investigation were obtained from U. S. A. and were of chemically pure quality. The purity of the liquids was tested by comparing the Raman spectra of the liquids with those observed by the previous workers. In order to study the Raman spectra of the substances in the solid state at different low temperatures, the liquids distilled in vacuum were taken in cylindrical pyrex glass containers, each about one inch in diameter, provided with a long narrow neck with its mouth sealed. The container was suspended in a transparent Dewar vessel and the substance was kept at different temperatures by adjusting the position of the level of liquid oxygen in the transparent Dewar vessel. The temperature was measured with a pentane thermometer. Other experimental details were the same as those described by the author in a previous paper (Ray, 1950). Care was taken to solidify the liquid slowly in order to obtain a homogeneous mass so that the proportion of the extraneous light due to diffuse reflection from the volume of the crystal was small. The aperture of the collimator lens was effectively cut down in order to reduce the coma in the region of  $4358 \text{ \AA}$ . In the case of ethyl benzene two spectrograms with the solid at about  $-100^{\circ}\text{C}$  and  $-180^{\circ}\text{C}$  were obtained and in the case of benzyl chloride the corresponding temperatures of the solid were about  $-50^{\circ}\text{C}$  and  $-180^{\circ}\text{C}$  respectively. Iron-arc spectrum was used as comparison in each case.

## RESULTS

The spectrograms obtained for the two substances in the liquid state and in the solid state at different temperatures are reproduced in figures 1 and 2 in the Plate VI. The low-frequency region enlarged about six times is reproduced in figures 3 and 4. The frequency-shifts are given in Tables I and II in which those for the liquids reported by previous authors (Magat, 1934 and Petrikaln & Hochberg, 1929) are also included. No attempts were made to record the faint lines in the case of the liquids, as these lines were masked by the continuous background due to stray light in the case of the solid.

## DISCUSSION OF RESULTS

### (a) *New lines in the low-frequency region*

It can be seen from Tables I and II that in the case of both the compounds some new lines appear in the low-frequency region when the liquids



are solidified. The number of new lines in the case of solid ethyl benzene at  $-100^{\circ}\text{C}$  (melting point  $-92.8^{\circ}\text{C}$ ) is four, the frequency-shifts being 45, 68, 95,  $128\text{ cm}^{-1}$  respectively. When the temperature is lowered to  $-180^{\circ}\text{C}$  the line at  $68\text{ cm}^{-1}$  splits up into two lines at 63 and  $81\text{ cm}^{-1}$  respectively. All the other three lines also shift a little away from the Rayleigh line with the lowering of temperature from  $-100^{\circ}\text{C}$  to  $-180^{\circ}\text{C}$ . In the case of benzyl chloride at  $-50^{\circ}\text{C}$  (melting point  $-39^{\circ}\text{C}$ ) also four new lines appear in the low-frequency region at 46, 60, 86,  $116\text{ cm}^{-1}$  respectively and of

TABLE I

Ethyl Benzene ( $\text{C}_6\text{H}_5\text{C}_2\text{H}_5$ )

Magat (1934) Liquid $\Delta\nu$ in $\text{cm}^{-1}$	Present author		
	liquid at $30^{\circ}\text{C}$ $\Delta\nu$ in $\text{cm}^{-1}$	Solid at about $-100^{\circ}\text{C}$ $\Delta\nu$ in $\text{cm}^{-1}$	Solid at about $-180^{\circ}\text{C}$ $\Delta\nu$ in $\text{cm}^{-1}$
	Continuous wing extending upto $100\text{ cm}^{-1}$	45 (ob); e, k 68 (1b); e, k 95 (1); e, k 128 (o); e, k 148 (2); e, k	48 (o); e, k 63 (2); e, k 81 (2); e, k 100 (2); e, k 130 (1); e, k 152 (2); e, k
457 (o)	145 (2b); e, k		
490 (1)	493 (1b); e, k	493 (1s); e, k?	493 (1s); e, k
538 (o)	556 (1b); e		
620 (2)	623 (2); e, k	623 (2); e, k	620 (2); e, k
724 (o)	745 (1); e, k	745 (1); e, k	745 (1); e, k
773 (o)	772 (4); e, k	768 (2); e, k	768 (2); e, k
	848 (1); e, k		
962	962 (2); e, k	962 (2); e, k	957 (1); e, k
1000 (4)	1000 (5); e, k	997 (4); e, k	994 (4); e, k
1032 (2)	1032 (3); e, k	1030 (2); e, k	1027 (2); e, k
1057 (o)	1055 (1); e, k	1052 (o); e, k	1050 (o); e, k
1106 (o)			
1156 (1)	1156 (2); e, k	1157 (1); e, k	1158 (1); e, k
1176 (1)	1175 (o); e, k	1170 (1); e, k	1170 (1); e, k
1204 (3)	1205 (3); e, k	1205 (2); e, k	1205 (2); e, k
1260 (1)	1262 (ob); e, k	1261 (1); e, k	1259 (1); e, k
	1325 (1b); k		
1381 (o)			
1448 (1dd)	1448 (1d); e, k	1448 (1); e, k	1450 (1); e, k
1465 (1dd)			
1587 (1)	1588 (1); e, k	1586 (1); e, k	1586 (1); e, k
1608 (3)	1608 (4); e, k	1608 (2); e, k	1604 (2); e, k
	2880 (1b); e, k	2878 (1b); e, k	2860 (1b); e, k
	2912 (1); e, k	2912 (ob); e, k	
2936 (2d)	2936 (2); e, k	2930 (2); e, k	2925 (o); k 2942 (2); k 2957 (1); k
	3036 (1); e, k	3040 (1); k	3036 (2); k
3053 (2)		3050 (4); k	3050 (4); k
3066 (2)	3064 (5b); e, k	3068 (1); k	3060 (o); k

these the line at  $86\text{ cm}^{-1}$  splits up into two lines at  $82$  and  $88\text{ cm}^{-1}$  respectively at  $-180^{\circ}\text{C}$ . The centre of gravity of these two lines is at  $85\text{ cm}^{-1}$  and therefore, the line does not shift appreciably with the lowering of temperature of the solid. Of the remaining three lines the line at  $46\text{ cm}^{-1}$  remains in the same position and the lines  $86$  and  $116\text{ cm}^{-1}$  shift respectively to  $88$  and  $119\text{ cm}^{-1}$  when the crystal is cooled from  $-50^{\circ}\text{C}$  to  $-180^{\circ}\text{C}$ . Thus it can be concluded that these changes in position of the lines in the low-frequency region in this case are smaller than and quite different from those observed in the case of ethyl benzene.

An attempt may now be made to explain these results on the different hypotheses put forward by previous workers to explain the origin of these new lines in the low-frequency region. According to the theory put forward by Kastler and Rousset (1941) and also by Bhagavantam (1941) the lines are due to angular oscillations of the rigid molecule pivoted in the lattice, and the frequencies of such oscillations depend on the moments of inertia of the molecule about three axes. The line with minimum frequency-shift is due to the oscillation of the pivoted molecule about an axis perpendicular to the plane of the molecule, according to the theory mentioned above. The

TABLE II  
Benzyl Chloride  $\text{C}_6\text{H}_5\text{CH}_2\text{Cl}$

Petrikain & Hochberg (1929) liquid $\Delta\nu$ in $\text{cm}^{-1}$	Present author		
	Liquid at $25^{\circ}\text{C}$ $\Delta\nu$ in $\text{cm}^{-1}$	Solid at about $-50^{\circ}\text{C}$ $\Delta\nu$ in $\text{cm}^{-1}$	Solid at about $-180^{\circ}\text{C}$ $\Delta\nu$ in $\text{cm}^{-1}$
	Continuous wing extending upto $100\text{ cm}^{-1}$	46 (1) ; e, k 60 (1) ; e, k 86 (2) ; e, k 116 (2) ; e, k 136 (5) ; e, k	46 (2) ; e, k 62 (2) ; e, k 82 (3) ; e, k 88 (3) ; e, k 119 (3) ; e, k 142 (5s) ; e, k
138	134 (4b) ; e, k		
275	274 (ob) ; e, k		
338			
476	478 (1b) ; e	478 (1b) ; e	478 <sup>31</sup> (2) ; e, k
622	625 (2) ; e, k	625 (2) ; e, k	625 (3) ; e, k
682	681 (3b) ; e, k	673 (4b) ; e, k	670 (5s) ; e, k 674 (1a) ; e
772	767 (2) ; e, k	767 (2) ; e, k	767 (3s) ; e, k
816	820 (1) ; e, k		
1001	997 (10) ; e, k	997 (11) ; e, k	997 (12) ; e, k
1038	1025 (1) ; e, k	1025 (1) ; e, k	1025 (1) ; e, k
1156	1162 (1) ; e, k	1162 (1) ; e, k	1163 (2) ; e, k
1212	1210 (2) ; e, k	1222 (2) ; e, k	1210 (2) ; e, k
1267	1263 (1b) ; e, k	1265 (4) ; e, k	1265 (4s) ; e, k
1608	1608 (5) ; e, k	1608 (5) ; e, k	1608 (5) ; e, k
2967	2967 (2b) ; k	2975 (1) ; k	2975 (2) ; k
3064	3063 (3) ; k	3065 (3) ; k	3065 (3) ; k

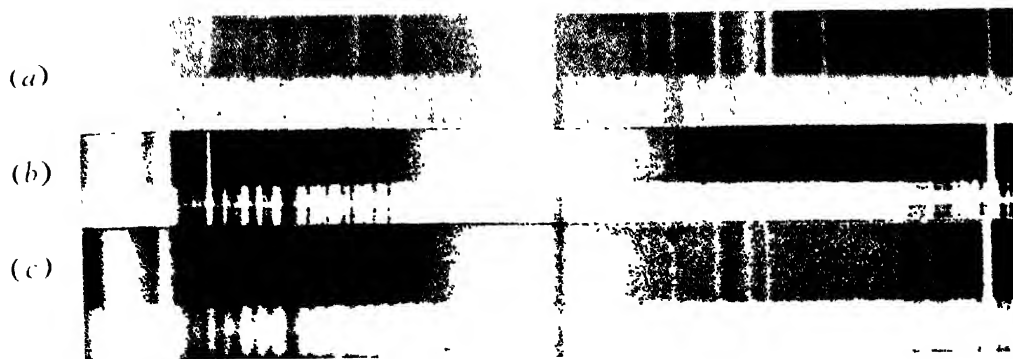


Fig. 1



Fig. 2

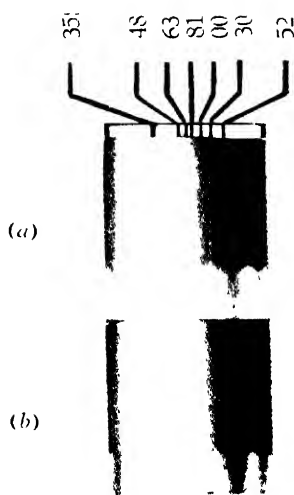


Fig. 3.

- (a)  $C_6H_5C_2H_5$  - Liquid at  $30^\circ C$   
 (b) " - Solid at about  $-100^\circ C$   
 (c) " - Solid at about  $-180^\circ C$   
 (a)  $C_6H_5C_2H_5$  - Solid at about  $-180^\circ C$   
 (b) " - Solid at about  $-100^\circ C$

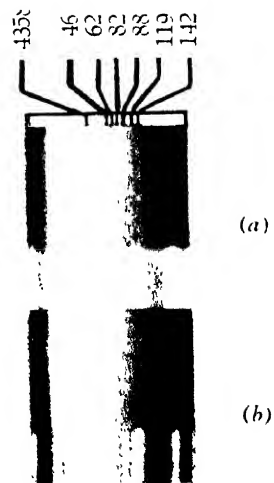


Fig. 4.

- Fig. 2 (a)  $C_6H_5CH_2Cl$  - Liquid at  $25^\circ C$   
 (b) " - Solid at about  $-50^\circ C$   
 (c) " - Solid at about  $-180^\circ C$   
 Fig. 4. (a)  $C_6H_5CH_2Cl$  - Solid at about  $-180^\circ C$   
 (b) " - Solid at about  $-50^\circ C$



examination of the data compiled in Table III, however, shows that molecules having widely different moments of inertia yield a line having the same minimum frequency-shift. For instance, the line at about  $47\text{ cm}^{-1}$  is present in the Raman spectra of benzene, chlorobenzene, toluene, benzyl chloride and ethyl benzene at  $-180^{\circ}\text{C}$ .

TABLE III

Substance in the solid state	temperature	$\Delta\nu$ in $\text{cm}^{-1}$
Benzene	$-180^{\circ}\text{C}$	47, 53, 78, 95, 134
chloro benzene	$-180^{\circ}\text{C}$	46, 63, 83, 102, 135
Toluene	$-180^{\circ}\text{C}$	47, 66, 86, 108, 127
Benzyl Chloride	$-180^{\circ}\text{C}$	46, 62, 82, 88, 119
Ethyl benzene	$-180^{\circ}\text{C}$	48, 63, 81, 100, 130

Careful examination of the direct mercury arc spectrum photographed with the same spectrograph has shown that there is no trace of any line in this position and therefore this line is not a spurious one. The presence of this line in all these cases thus clearly shows that the frequency of the line is not at all determined by the moment of inertia of the molecule, because the moment of inertia of the benzene molecule about an axis perpendicular to its plane is much smaller than that of any of the other four compounds mentioned in Table III. Such a conclusion is further supported by the fact that corresponding to a line at  $134\text{ cm}^{-1}$  in the case of benzene, chlorobenzene yields a line at  $135\text{ cm}^{-1}$ , although the corresponding moment of inertia of chlorobenzene is much larger. Thus these results do not support the hypotheses that the lines are due to angular oscillations of the molecules pivoted in the lattice. The increase in intensity of some of the lines with the lowering of temperature also cannot be explained on such a hypothesis.

The results can, however, be explained on the hypothesis put forward by Sirkar (1936) that these lines are due to inter-molecular oscillations in groups of associated molecules. It is well known that a particular atomic group, present in different molecules, yields Raman lines of almost identical frequencies in all the cases, and therefore, it could be expected that the benzene ring present in the different molecules mentioned in Table III would yield almost the same set of lines due to intermolecular oscillations in associated groups of molecules. The results given in Table III corroborate such a statement, because each of these substances, having widely different molecules, yields five lines.

The frequency of the line at  $53\text{ cm}^{-1}$  increases to about  $63\text{ cm}^{-1}$  on substituting one of the hydrogen atoms by a chlorine atom, a  $\text{CH}_2\text{Cl}$  group

or a  $\text{CH}_3$  group. This increase may be due to the fact that the strength of the virtual bond between two associated molecules is larger in the case of the substituted molecules which are polar than that in the case of the benzene molecule. On the other hand, frequency of this line would diminish considerably with the substitution of the hydrogen atom in the benzene molecule had the line been due to the angular oscillation of the molecule about an axis in the plane of the molecule.

(b) *Molecular frequencies*

As regards the frequency-shifts of the lines due to intramolecular oscillations the changes, observed with the solidification and with further lowering of the temperature of the solid up to about  $-180^\circ\text{C}$ , are larger in the case of ethylbenzene than those observed in the case of benzyl chloride. Thus in the former case the frequency-shifts of the lines 145, 772, 1000, 1032, 1055, 1175, 2936 and  $3036\text{ cm}^{-1}$  change respectively to 148, 768, 997, 1030, 1052, 1170, 2930 and  $3040\text{ cm}^{-1}$  and the line  $3064\text{ cm}^{-1}$  splits up into two lines at 3050 and  $3068\text{ cm}^{-1}$  when the liquid is solidified, while in the latter case only the lines 134, 681 and  $2967\text{ cm}^{-1}$  undergo changes in position with the solidification of the liquid. On further cooling the solid to a temperature of  $-180^\circ\text{C}$ , the lines 148, 623, 962, 997, 1030, 1052, 2878, 3040 and  $3068\text{ cm}^{-1}$  of solid ethyl benzene shift to 152, 620, 957, 994, 1027, 1050, 2860, 3036 and  $3060\text{ cm}^{-1}$  respectively and the line  $2930\text{ cm}^{-1}$  splits up into three lines at 2925, 2942 and  $2957\text{ cm}^{-1}$  respectively. As the line  $2878\text{ cm}^{-1}$  is due to the C-H oscillation in the  $\text{C}_2\text{H}_5$  group, it is evident that strength of the C-H bond changes considerably with the lowering of temperature of the solid. In the case of benzyl chloride, on the other hand, very little change takes place in the positions of lines with the lowering of temperature of the solid except in the case of the lines 136, 673 and  $3065\text{ cm}^{-1}$  which shift respectively to 142, 670 and  $3060\text{ cm}^{-1}$ . Further, the line  $670\text{ cm}^{-1}$  is accompanied by a weak satellite at  $674\text{ cm}^{-1}$  at  $-180^\circ\text{C}$ .

These data thus show that the changes taking place in the strength of the bonds are different for the two molecules and that the modes of oscillations, the frequencies of which are affected by the change of temperature, are not identical in the two cases. This may be due to the fact that the modes of oscillations which are affected by association of the molecules depend on the actual location of the point at which the molecule is associated with its neighbour.

Examinations of the spectrograms reproduced in Plate VI shows that the prominent Raman lines due to single molecules observed in the case of each of the two liquids become much sharper when the liquid is solidified. As pointed out in previous papers (Ray, 1950 ; Sirkar & Ray, 1950), these results are contradictory to the hypothesis put forward by Bhagavantam (1941) that it is the change of polarisability of the unit cell containing more than one molecule which determines the intensity of the Raman line. If such

hypothesis would be correct each of the prominent Raman lines would be split up into two components, one polarised and another totally depolarised in each case. Since no such doubling is observed even at  $-180^{\circ}\text{C}$  this probability of the occurrence of coincidence or opposition of phases of oscillation of the molecules in the unit cell is negligible in comparison with that for the random oscillation of the single molecules, and the Raman lines are due to changes of polarisability in the single molecule in the crystal.

#### ACKNOWLEDGMENT

The author is indebted to Prof. S. C. Sirkar for his kind interest and helpful guidance during the progress of the work.

OPTICS DEPARTMENT  
INDIAN ASSOCIATION FOR THE CULTIVATION  
OF SCIENCE  
JADAVPUR, CALCUTTA

#### REFERENCES

- Bhagavantam, S. 1941, *Proc. Ind. Acad. Sc.*, **13A**, 543.  
Kastler, A and Rousset A., 1941, *Comptes Rendus*, **212**, 645.  
Magat, M., 1934, *Annual Tables, Paris*, **26**, 73.  
Petrikaln, A., and Hochberg, J., 1929, *Zeit. f. Phys. Chem.*, **4**, 299.  
Rousset, A., 1948, *Jour de. Phys.*, **9**, 101.  
Ray, A. K., 1950, *Ind. Jour. Phys.*, **24**, 111.  
Ray, A. K., 1950, *Ibid.*, **24**, 539.  
Sirkar, S. C., 1936, *Ibid.*, **10**, 109, 189.  
Sirkar, S. C., and Ray, A. K., 1950, *Ibid.*, **24**, 189.

# A NOTE ON THE EFFECT OF THE PHOTO-ELECTRIC EMISSION FROM THE ELECTRODES ON THE RECTIFYING ACTION OF A DISCHARGE

By V. T. CHIPLONKAR

(Received for publication, December 11, 1950)

**ABSTRACT.** The effect of the photoelectric emission from one of the electrodes on the rectifying effect of a discharge has been quantitatively investigated by using an improved dynamic method. The rectification is found to be affected to some extent by the onset of the emission, but the effect is found to be non-selective, it increases the current during one half of the cycle, leaving the current in the other half unaffected.

The effect of some of the parameters of the discharge, like the nature of the gas in the discharge tube, its pressure, the relative areas of the electrodes etc., on the rectifying action of a discharge have been reported in some detail by the author (Chiplonkar 1939, 1941). The method used was to connect a D.C. and an A.C., milliammeter in the earth circuit, the former indicating the D.C. component and the latter the total current. It is the object of the present paper to report some observations, with an improved and more accurate method on the possible role of an important process in the discharge tube, *viz.*, the photo-electric emission from the electrodes, in determining its rectifying action. The existence of an asymmetric process occurring at only one of the electrodes leads, as we know, to rectification in the plate and point rectifier. It was thought, therefore, worthwhile to investigate if the presence of the photo-electric emission from one of the electrodes would result in a selective action on the part of the discharge, the discharge passing with greater ease in one direction than in the other.

The observations were made with a gas-filled photo-cell (R.C.A. 868) The conditions obtaining in this type of cell would not be far different from those in ordinary discharge tubes. One electrode consists of a concave metal plate, the other is a thin wire placed in front of it. A variable A.C. voltage (0-90 volts) was applied across the cell; the anode being connected to the A.C. source, as shown in Fig. 1. The earth current

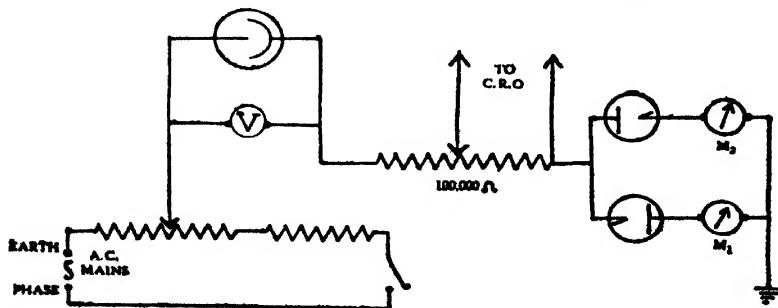


FIG. 1



through the cathode was analysed with the help of two diodes and two galvanometers (microammeters). The current pattern was also observed on a cathode ray oscillograph, by putting the potential drop across part of the high resistance, placed in series with the cell, on the vertical plates of the C.R.O. When the rectification is absent the currents indicated by  $M_1$  and  $M_2$  are equal and the pattern on the C.R.O. is symmetrical. The presence of rectification is shown by unequal readings in  $M_1$  and  $M_2$  and by an asymmetry in the C.R.O. pattern. The method is sensitive and enables one to evaluate the impedance of the tube in the two directions and thus helps to determine dynamically in an accurate manner the rectification produced.

The observations taken are shown in Table I. Readings have been taken when the cell is in the dark and next when exposed to light from a lamp kept at a fixed distance from it. On incidence of light the P.D. across the cell falls; for the sake of comparison the readings obtained in dark and in light are shown side by side. The rectification ratio  $\rho$  now gives the value of  $\frac{M_2 - M_1}{M_2 + M_1}$ . Complete rectification is obtained for  $\rho = 1$ .

TABLE I

In dark				Under light			
P. D. across cell, volts	$M_1$ divs	$M_2$ divs	$\rho$	P. D. volts	$M_1$ divs	$M_2$ divs	$\rho$
2.0	0.00	1.50	1.00	1.0	0.00	1.50	1.00
4.0	0.25	1.75	0.75	3.0	0.25	2.00	0.77
6.0	0.50	2.00	0.60	5.0	0.50	2.50	0.66
10.0	0.50	3.00	0.71	9.0	0.50	3.25	0.73
20.0	1.00	4.50	0.63	17.0	1.00	5.50	0.67
30.0	1.75	6.50	0.57	27.0	1.75	7.50	0.61
40.0	2.75	8.67	0.51	35.0	2.75	9.50	0.55
50.0	4.25	10.00	0.40	46.0	4.25	11.50	0.45
60.0	5.50	11.75	0.36	53.0	5.75	13.50	0.40
70.0	7.00	13.50	0.31	61.0	7.00	15.00	0.36
80.0	9.00	15.00	0.25	69.0	9.00	16.50	0.29
90.0	11.00	16.50	0.20	79.0	11.00	18.00	0.24

The effect of the photo-electric emission seems to be merely to increase the current during the half of the cycle when the potential on the cathode is negative, the current in the positive half of the cycle remains unaffected. In the observations given above, the rectification, which is

initially present, increases in value when the photo-electric emission takes place. For the voltages used, the cell does not function as a rectifier except at very low voltages of the order of 0.5 volts. This result has been found to be characteristic not only of the photo-cell used above, but is shown by a photronic cell, and an ordinary discharge tube when they are used in place of the cell. The magnitude of the rectification is found to diminish with increasing voltage. There does not appear to be present a selective action of a marked magnitude. The observations with the C.R.O. confirm the general results discussed above. There is assymetry not only in the positions of the peaks but also in the wave-form in the two half cycles; the curve during the positive cycle shows a sharper maximum than that obtained during the negative half of the cycle. The double diode arrangement is found to be more sensitive than the C.R.O. as far as the quantitative results are concerned. Incidentally, these results indicate that the measurement of an A.C. current, in circuits where partial rectification effects are obtained by means of a rectifier or any other similar type of instrument may not give sufficiently detailed information about the current.

M. N. COLLEGE, VISNAGAR.

#### REFERENCES

- Chiplonkar, V. T., 1939, *Proc. Ind. Acad. Sc.* **10**, 381.  
,, ,, 1941, *ibid* , **13**, 323.

# ON A METHOD OF STUDYING SMALL-ANGLE SCATTERING OF MONOCHROMATIC X-RAYS.

By K. BANERJEE AND J. C. MAITRA.

*(Received for publication, March 2, 1951)*

Plates VIIA, B

**ABSTRACT.** A method of studying small-angle scattering of monochromatic X-rays has been developed. The blurring effect of the direct beam is eliminated by reflecting the direct beam as well as the scattered one by a crystal oriented at a small deviation from the Bragg angle for the characteristic radiation. Out of the scattered beam the ray that is incident at the Bragg angle for the characteristic wavelength is reflected to an intensity comparable with that of the reflected direct beam. By rotating the crystal, variation of intensity of the scattered monochromatic radiation with angle of scattering may be studied.

In recent years the study of very small-angle scattering has come to great importance particularly for the study of sizes of crystallites and colloidal particles and structures of macro-molecules. In this communication, preliminary results are presented of a simple method of studying extremely low angle scattering of monochromatic X-rays.

The method consists in the utilisation of the Bragg principle of X-ray reflection to eliminate the incident beam which is the principal disturbing factor in the studies of low angle scattering. In Fig. 1,  $AS$  represents a

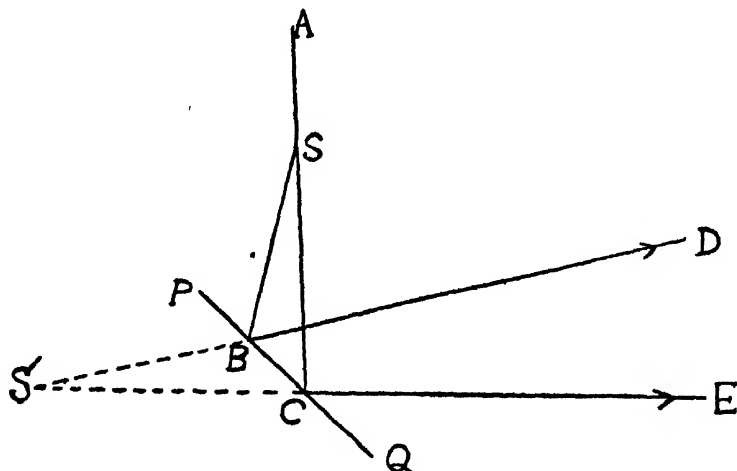


FIG. 1

narrow X-ray pencil incident on the scatterer  $S$ . The direct and the scattered beams, represented by  $SC$  and  $SB$  respectively, are incident on a crystal face  $PQ$  the latter, which is very close to the former, being incident on the crystal at the Bragg angle of reflection for a characteristic radiation from

the anticathode. Two reflected rays,  $BD$  and  $CE$ , will proceed from the crystal,  $BD$  being due to the characteristic radiation scattered from  $S$  and reflected from the crystal, and while  $CE$  being the Laue reflection of a non-characteristic component of X-ray from the crystal. Since the scattered radiation is much weaker than the direct, while on the other hand the characteristic radiation is for suitable voltage of the X-ray tube much stronger than any other component of the white radiation, these two reflected rays will generally be of comparable intensities. If  $S'$  be the optical image of  $S$  by reflection at a plane mirror in place of the crystal face, the angle  $DS'E$  is equal to the angle of scattering  $BSC$ . The angle  $DS'E$  can be easily measured from the distance  $ED$ , the inclination of  $ED$  to the rays  $BD$  or  $CE$  and the sum of the distances  $SB$  and  $BD$ . If the slit is moderately fine, the Laue reflection is quite sharp and, therefore, does not swamp the monochromatic scattered ray arriving at  $E$  even when they are so close as to be just short of overlapping. By rotating the crystal through small angles it can be set for studying the scattered radiations at different angles and a survey of the region of small angle of scattering may be made. The method of eliminating the strong direct ray by reflecting the scattered ray under observation by crystal underlines also the double crystal spectrometer method used by Fankuchen and Jellinek (1945) for the purpose. The intensity in his method necessarily becomes feeble due to two reflections, and the operations are much more complex. In the above method the same advantage of getting rid of the direct beam as well as monochromatisation are attained by one reflection only.

For the study of low-angle scattering by this method the photographic method is the least suited since we can obtain only one angle of scattering in one photograph for a characteristic ray. Even taking into account the  $K\alpha$  and  $K\beta$  emissions from the X-ray tube we obtain two discrete directions of scattering for one exposure. The natural method for such studies would, therefore, be the ionisation or the counter method. But in this communication are presented the results of a preliminary study in which the practicability of the method has been investigated by the photographic method. A method based on the uses of a photo-multiplier tube to measure the intensity of excited fluorescence is being developed for determining X-ray intensity. A continuous record of low-angle scattering intensity may thereby be obtained.

The X-ray tube used is a Hadding tube in which the voltage can be adjusted up to a maximum of 60 PKV. The adjustment is necessary in order to control the relative intensities of the monochromatic radiation to that of the background white radiation. Thus the orders of intensities of the Laue reflection and the monochromatised scattered radiation may be made comparable. The slit system  $S$  is obtained in either of the two ways: (1) by two steel rods of semi-circular cross-section with their polished plane faces set against each other but separated by thin distance pieces, the end of the slit away from the X-ray tube is widened in order to eliminate diffraction effects

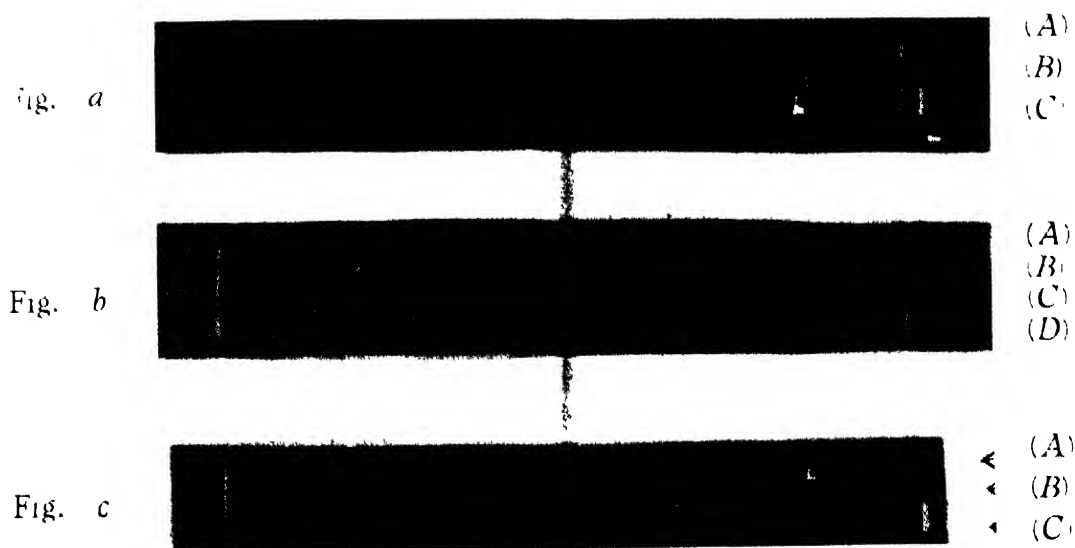
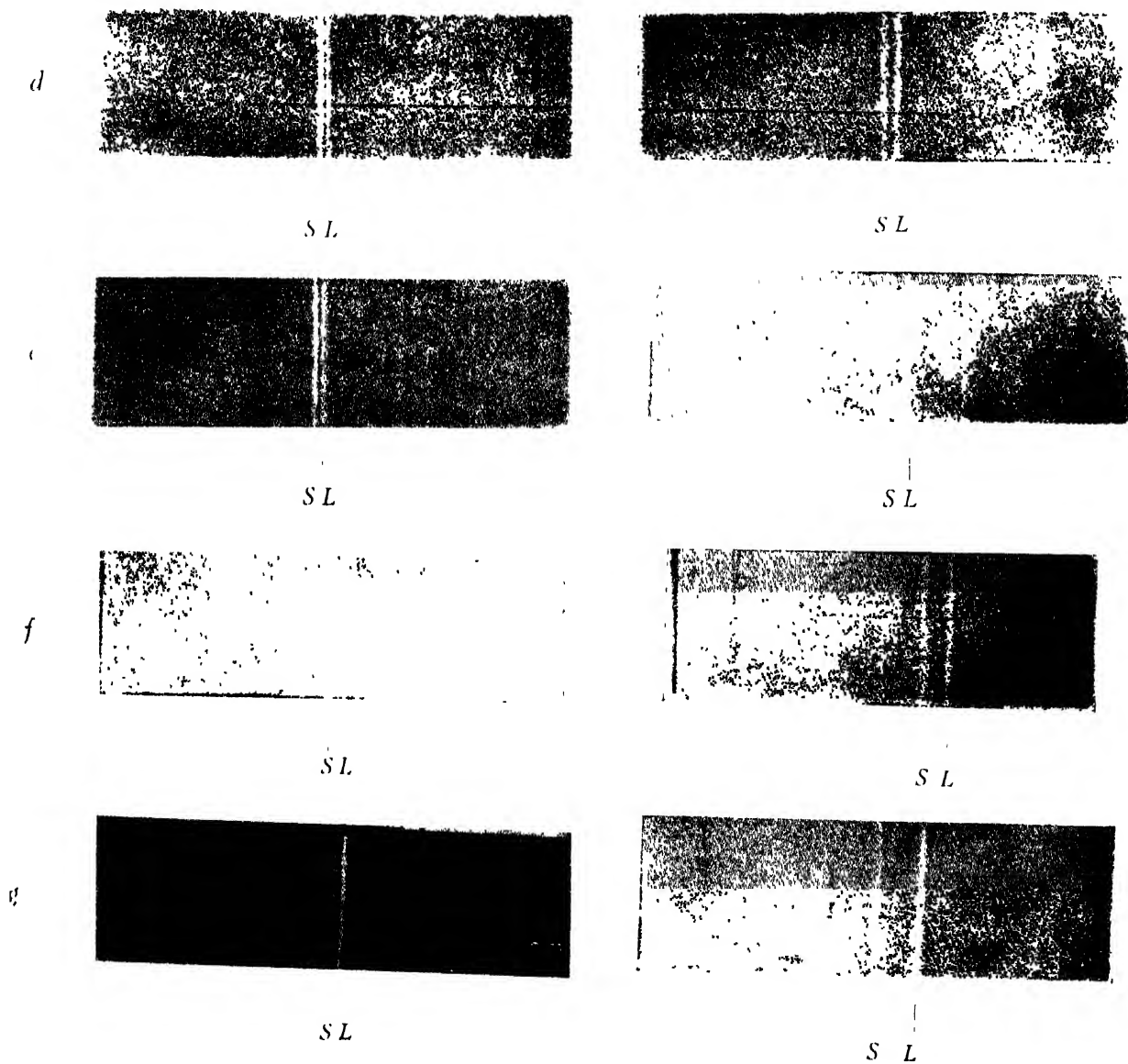


Fig. a.—(A) Oscillation photograph  
 (B) Laue photograph,  $\theta_i < \theta_B$  for Cu  $K\beta$   
 (C) „ „ „  $\theta_i > \theta_B$  for Cu  $K\alpha$

Fig. b. (A) Oscillation photograph  
 (B) Laue photograph,  $\theta_i > \theta_B$  for Cu  $K\alpha$   
 (C) Oscillation photograph  
 (D) Laue photograph,  $\theta_i < \theta_B$  for Cu  $K\alpha$

Fig. c.—(A) Oscillation photograph  
 (B) Laue photograph,  $\theta_i < \theta$  for Cu  $K\beta$   
 (C) „ „ „ ,  $\theta_i \approx \theta_B$  for Cu  $K\alpha$



*S* -- Scattered beam

*L* -- Laue line

Fig. *d.*  $\alpha = 6'$

" *e.*  $\alpha = 9'$

" *f.*  $\alpha = 12'$

" *g.*  $\alpha = 15'$

Fig. *h.*  $\alpha = 18'$

" *i.*  $\alpha = 36'$

" *j.*  $\alpha = 40'$

" *k.*  $\alpha = 1^{\circ}13'$

of the slit, (2) by using three slits made of double knife-edges of which the first two collimate the X-ray beam and the third eliminates the rays diffracted from the second slit. The rays from the slit falls on the scatterer *S* and then on the calcite crystal *PQ* set very close to the Bragg angle. In the following experiments a slit system of the second type was used without the third slit so that the rays diffracted by the second slit were actually studied. The photographic film to receive the reflected rays is mounted on a lever that can rotate round an axis that passes along the surface of the crystal and through the point of incidence of the incident ray on the crystal. The film holder is set at right angles to the lever so that the reflected rays are received on the film normally.

The distance of the film from the crystal is made much larger than the distance of the crystal from the slit. This is done in order to avoid the effect of crystal imperfection or thermal diffusion to overlap on the scattered radiation that is to be measured. This can easily be seen from Fig. 2. where the notations have the same significance as in Fig. 1,  $L$  being on the

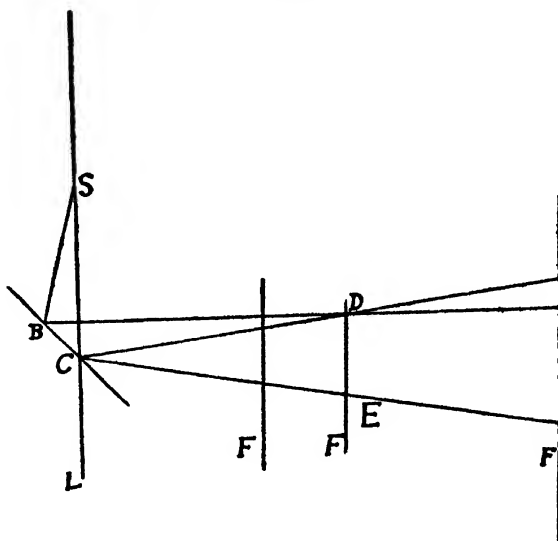


FIG. 2

extension of SC. The scattering angle  $CD$  for the diffuse maximum or the reflection due to crystal imperfection is very close to  $2\theta_B$  where  $\theta_B$  is the Bragg angle. If  $SC = CD$ , the Bragg focussing condition is satisfied and the scattered ray after reflection at the crystal will pass through  $D$ . Consequently, there will be overlapping of the two effects. If the photographic film  $F$  be placed between  $C$  and  $D$ , the reflection due to crystal imperfection will be between the Laue reflection and the reflection of the scattered radiation and the separation will not be very clear. When the film lies beyond  $D$ , the disturbing radiations will lie beyond and will not affect the lines.

For determining the angle of scattering, the distance between the Laue line and the characteristic line can be accurately measured as both of them are

sharp lines on the photographic plates as shown in Plate VIIA, Figs *a*, *b*, and *c*. For Plate VIIA, though the calcite crystal that was used was a very fine crystal, it had polished surfaces and so the extra lines due to crystal imperfection appear prominently as shown in the plates. The other two crystals that were tried had cleaved faces. These do not show those extra lines. But in any case it is always best to avoid Bragg focussing position.

The photographs for the different orientations are shown in Plate VIIB. The angle of scattering as determined from the distance between the Laue line and the scattered line are mentioned below the photographs. Though  $6'$  is the lowest angle that has been measured, it is not difficult to push the limit further upto about a minute.

In trying this photographic method for studying the low-angle scattering the appearance of the  $K\alpha$  and  $K\beta$  lines in the same photograph is an advantage as it puts checks on the intensities of the incident beam for photographs with different orientations of the crystal. A thin uniform layer of aluminium powder dusted on the crystal surface gives a better check as a line of standard intensity is present on all the photographs. But in any case there is always the possibility of missing important maxima as photographs can be taken only in discrete positions. Consequently an ionisation method or the photomultiplier method is preferable to the photographic method.

INDIAN ASSOCIATION FOR THE CULTIVATION OF SCIENCE,  
JADAVPUR, CALCUTTA

#### REFERENCE

Fankuchen, I, and Jellinek, M. H., 1945, *Phy. Rev.*, **67**, 201.



# THE METHOD OF SHADOW-CASTING IN PHOTOMICROGRAPHY

By D. L. BHATTACHARYA\*

(Received for publication, January 9, 1951)

## Plate VIII

**ABSTRACT.** A discussion of the shadow-casting method in increasing contrast of unstained biological objects for use in optical microscope is presented. A calculated quantity of silver is deposited on the specimen at an angle in this technique and estimates are made for the thickness that can be profitably deposited to provide proper opacity and contrast. Optical micrographs of the protozoa *L. Donovanii* when shadow-cast with different thickness of silver are reproduced.

## INTRODUCTION

The observation of unstained bacteria or protozoa with the usual optical microscope requires the closing down of the substage illuminator to a very narrow aperture in case of bright field illumination with widely convergent light or recourse has to be taken to dark ground illumination. This narrowing down of condenser aperture decreases the obliquity of the illuminating beam and hence increases the contrast of the image against the background brightness. The extent to which the condenser iris has to be stopped down depends on the opacity and refractive properties of the object imaged. For micro-organisms, the iris diaphragm may have to be closed down to such an extent that diffraction fringes become prominent around the contours which tend to spoil the image quality. In any case, the gain in contrast achieved by this process of constricting the illumination is at the expense of resolution of the instrument together with a possible increase in visual discomfort arising out of a large decrease in brightness of the microscope field. The usual procedure to obviate this difficulty is by the use of stains which enhance absorption contrast of the image. However, staining methods do not give any idea of the surface structure of the organisms, for which purpose other methods have to be employed. One of these methods, which has found extensive use in electron microscopy, is the shadow-casting technique of Williams and Wyckoff (1946). This method is not restricted to electron microscopy alone but can be employed to yield useful information in the case of optical microscopy of surfaces (Scott and Wyckoff, 1949). The present paper indicates how surface characteristics of unstained protozoa can be obtained by the

\* I. C. M. R. Research Fellow.

employment of shadow-casting technique for enhancing contrast as well as revealing surface details without imposing too much restriction on the aperture of illumination.

Briefly, the method of shadow-casting consists of depositing a thin film of metal on the specimen at an angle and then observing it in the microscope. The specimen is placed in an evacuated chamber and the metal is evaporated from a hot tungsten coil situated at a suitable distance from the specimen. With a sufficiently good vacuum, the metal atoms proceed in straight lines and condense on the specimen from an angle. A deposit of heavy metal thus builds up on the exposed side of the specimen and radiation shadows free from metal are produced in the background behind high details. Due to the obliquity of the beam, the condensed metal film is of varying thickness over the surface according to the heights of the surface irregularities and these become prominent in the micrograph which presents a three dimensional appearance together with an increase in the contrast of the image. Further, from the length of the shadows and the geometry of the experimental arrangement, the average height of the specimen and also differences in surface elevation can be estimated. In the present paper, the conditions for an optimum deposit of metal have been discussed with particular reference to the parasite *Leishmania Donovanii* (flagellate state) and photo-micrographs of the organism shadow-cast with silver have been obtained.

#### THICKNESS OF SHADOWED FILM OF METAL AND CONSIDERATIONS OF CONTRAST

The technique of shadow-casting is essentially similar for optical as well as electron microscopy. The difference lies only in the nature and amount of metal used. The nature of metal selected for shadowing in electron microscopy is primarily determined by the absence of structure in the shadow-cast film and considerations of electron scattering power. Very thin films, with thickness of the order of 10 Å. U. are usually required (Drummond, 1949) for electron microscopy. As light has greater penetrating power than electrons, the metal coating can be made thicker for optical microscopy and since the structure present in the shadowed-film is not of primary importance here, metals like silver, which are easily evaporated, can be used. The amount of silver that can be deposited without appreciable restriction of the available illumination can be estimated as follows.

The theory of passage of plane electro-magnetic wave through a homogeneous, isotropic absorbing medium shows that if  $I_0$  is the intensity of the incident radiation, the intensity  $I$  after travelling a distance  $t$  through the medium is given by

$$I = I_0 e^{-4\pi k t / \lambda} \quad \dots (1)$$

where  $\lambda$  is the wavelength of incident light in vacuum and  $k$  is the extinction coefficient determining absorption in the metal. For silver,  $k = 3.638$

for the *D*-line of sodium ( $\lambda 5893 \text{ \AA}$ .) as determined by Minor (1903). Assuming this value of  $k$ , the variation of transparency of silver films, i.e the ratio  $I/I_0$  with thickness  $t$ , has been calculated from equation (1) and plotted in Fig. 1. This curve is strictly applicable only for the *D*-line of sodium and

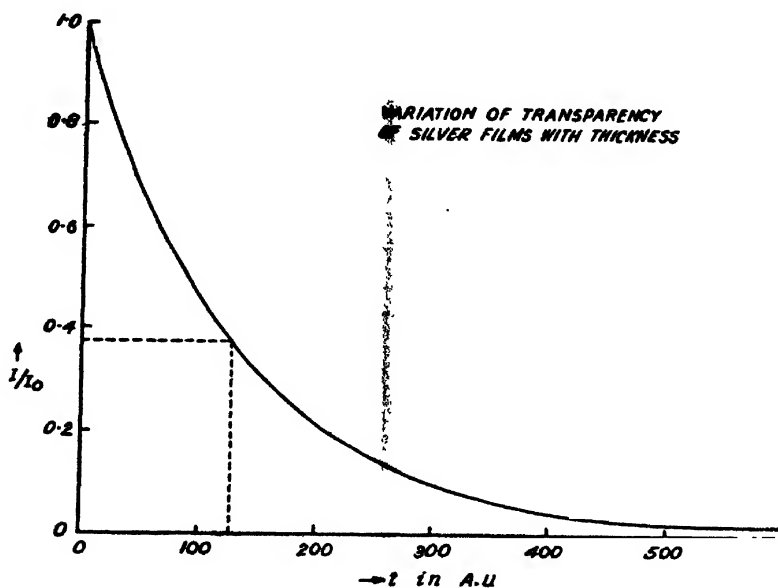


FIG. 1

for silver films, as  $k$  in equation (1) varies with wavelength and nature of the metal. However, the variation of  $k$  with  $\lambda$  for silver in the visible region is not very great and the conclusions that follow are applicable approximately to the whole of visible spectrum.

To deduce the maximum limit for the thickness of silver that can be deposited, we define a 'depth of penetration'. This is the thickness  $t_m$  which reduces light intensity by the factor  $e^{-4\pi}$ , that is, the amplitude is reduced by a factor  $e^{-2\pi}$ . From (1), we immediately get  $t_m = \frac{\lambda}{k} \approx 1600 \text{ A.U.}$  This is the thickness of silver that will reduce incident intensity by about  $3.5 \times 10^{-6}$  and will thus screen off all transmission in the visible region.

Another definition which is useful is the 'penetration thickness'  $\delta$  in which the light intensity drops to  $\frac{1}{e}$  th of its initial value. From equation (1) we get

$$\delta = \lambda / 4\pi k = 129 \text{ A.U.} \quad \dots (2)$$

Let us now suppose that a specimen of height  $h$  and width  $b$  mounted on a slide is shadowed obliquely by evaporation of metal placed at  $M$ , the shadowing beam striking the slide at an angle  $\alpha$  (Fig. 2) For consideration of metal deposit we may consider three regions : (a) specimen surface of area  $h.b$

facing the beam. (b) regions of shadow cast by the specimen and (c) open portions of the slide exposed to the beam and away from all obstructions.

Let  $r$  cm be the distance of the source from the slide.  $r$  may be considered approximately constant over the slide, provided it is located at a sufficient distance away.

The solid angle subtended by the exposed side of the specimen at the source is then  $h \cdot b \cdot \cos \alpha / r^2$  and since  $M/4\pi$  is the mass of metal (in grams) evaporated per unit solid angle, the amount deposited on the specimen is

$\frac{M}{4\pi} \cdot \frac{h \cdot b \cdot \cos \alpha}{r^2}$ . The thickness  $t_B$  in A. U. that is built up on the exposed side of the specimen is then given by

$$t_B = \frac{M \cos \alpha}{4\pi r^2 \rho} \times 10^8 \quad \dots (3)$$

where  $\rho$  is density of metal in gms/cm<sup>3</sup>.

It is usual to include a factor of  $3/4$  from considerations of efficiency of evaporation, so that in actual case (3) becomes

$$t_B = \frac{3}{4} \cdot \frac{M \cos \alpha}{4\pi r^2 \rho} \times 10^8 \text{ A.U.} \quad \dots (4)$$

For the region (c), which constitutes the background, we get from similar considerations the thickness  $t_B$  of metal as

$$t_B = \frac{3}{4} \cdot \frac{M \sin \alpha}{4\pi r^2 \rho} \times 10^8 \text{ A.U.} \quad \dots (5)$$

If the specimen is of length  $l$ , then the top of the specimen of area  $l \cdot b$  will be covered with the thickness  $t_B$  of metal.

The region (b) behind high details will be the shadow region completely free from metal. The length of shadow  $l'$  is then given by the relation.

$$l' = h \cot \alpha \quad \dots (6)$$

and is measured perpendicularly to the surface in consideration.

Let us now make the following assumptions: (a) The specimen contains details which can be resolved by the optical microscope. Thus the minimum height of a surface irregularity can be taken to be  $0.2\mu$ , which is the resolving power of the microscope for visible radiation  $\lambda 5550 \text{ \AA}$ . and (b) the specimen has got no appreciable absorption for light rays; which implies that the unshadowed object has got negligible contrast. Contrast of the object is only brought about by absorption in the shadowed silver film.

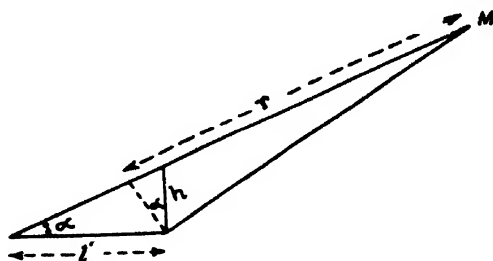
Now, the contrast  $g$  of an object against its surroundings is defined by the relation

$$g = \frac{B_s - B}{B_0} \quad \dots (7)$$

where  $B_0$  is the brightness of the background and  $B$  is the brightness of the object. This holds for visual observation only. In case of photographic image, the  $B$ 's are replaced by transmission of the different parts of the negative, the transparency ratio in a photographic, negative corresponding to a brightness ratio in the subject being given by the relation

$$\frac{T}{T_0} = \left( \frac{B_0}{B} \right)^\gamma \quad \dots (8)$$

where  $\gamma$  is obtained from the straight portion of the  $H$  and  $D$  characteristic of the negative material where the densities are assumed to lie.  $T$  and  $T_0$  are respectively the transparencies of the light and dense portions of the negative. Expression (8) immediately shows that a detail invisible to the eye can show up in the negative, the gamma-value of a process panchromatic plate can be as great as 3.0. In microscopy, the field brightness is usually about 1000 candles/cm<sup>2</sup>. At this level of illumination, the contrast sensitivity of the average human eye is approximately 10 per cent which means that two contiguous areas with brightness difference of 10 per cent can just be perceptible. Accordingly, we assume the minimum perceptible contrast to be 10 per cent and from Fig. 2 we find that if the film thickness



Shadowing at an oblique angle

FIG. 2

is reduced below about 13 A. U., the contrast between a shadow and the contiguous area will be less than 10 per cent and the shadows will be indistinguishable from the background. Assuming a usual gamma-value of unity, this then will be the minimum value of film thickness for visual as well as photographic records.

We thus see that enhancement of contrast of objects can be brought about by silver shadowing over wide limits. For example, for a thickness  $t=130$  A. U. the contrast is found to be 63.2 per cent, which increases still further as  $t$  is increased.

Again, the contrast between a specimen detail of height  $h$  facing the beam and its immediately contiguous background is given by the relation

$$gs = \frac{I_B - I_S}{I_B} = 1 - e^{-h/s} \quad \dots (9)$$

where  $I_B$  is the intensity transmitted by the background which has a thickness  $t_B$  and  $I_S$  is the intensity transmitted through a thin film of metal of thickness  $h$  deposited at a thickness  $t$ , on the specimen, given by  $I_S = I_0 e^{-(A \sin \alpha) t}$

where  $A = \frac{3}{4} \cdot \frac{M}{4\pi r^2 \rho}$  Since  $\delta$  for silver is only 130 A. U., and the specimen

is assumed to be not less than  $0.2 \mu$  or 2000 A. U. high, we get  $g_t = 1 - e^{-15}$ , which shows that the object has nearly cent per cent contrast against the background. Thus there appears to be no difficulty arising from image contrast in silver shadowed objects and the substage iris can always be adjusted to the optimum value for critical microscopy. Since silver shadowing and the resulting deposit of silver on the side of the object facing the beam will produce a modification of dimension on one side, which for a given film thickness  $t$  is  $t_s = A \cos \alpha$ , the film thickness has to be adjusted to as small a value as is compatible with adequate shadow contrast. The contrast of the image against its shadow is given by  $g_s = 1 - e^{-A \sin \alpha / \delta}$  and as we found earlier, for  $g_s = 0.1$ ,  $A \sin \alpha$  should not be less than 13 A. U. The contrast increases as  $A \sin \alpha$ , which can be seen from the attached micrographs of L. Donovan (Plate VIII). A limit to the increase in  $A \sin \alpha$  can be put by adopting a minimum for the thickness of the shadowing layer  $t_s$ . If we define this thickness to be of such magnitude that it must not alter the actual dimension by more than 10 per cent, we at once find that a  $0.2 \mu$  specimen is not to have a coating more than 200 A. U. thick on its exposed side. Changing  $\alpha$  from  $\tan^{-1} \frac{1}{2}$  to  $\tan^{-1} \frac{1}{3}$ , we find that the background depth  $t_B$  ranges from 100 A. U. to

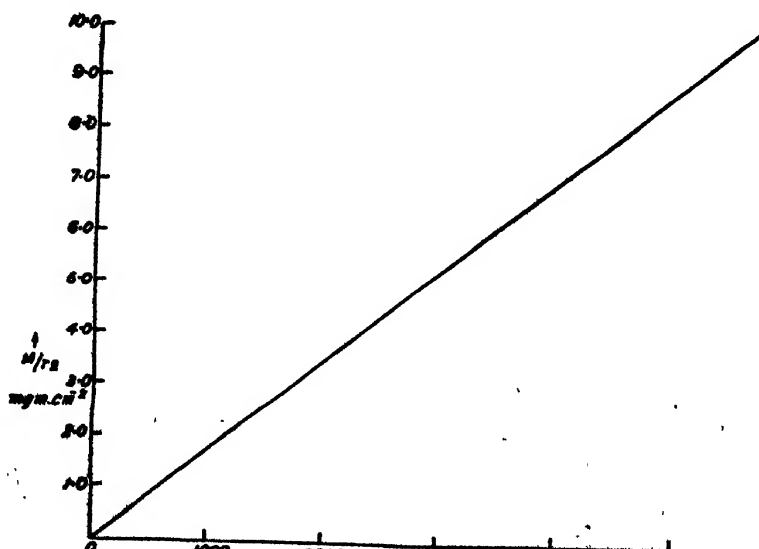
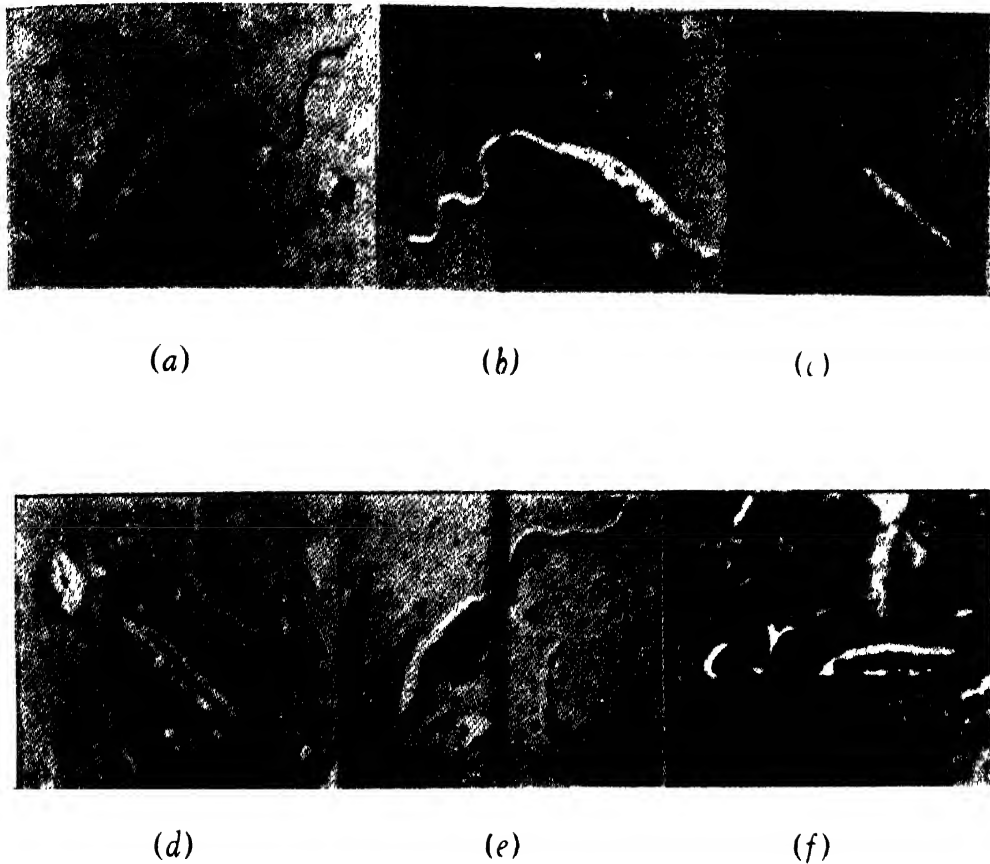


FIG. 3

40 A. U. respectively and the shadow contrast then ranges from 35 to a little more than 25 per cent. Shadowing considerations for deciding



All the photomicrographs of *L. Donovanii* were taken with Leitz Panphot camera microscope using their  $\frac{1}{2}$ " objective with numerical aperture 1.30. The magnification of all figures is 1830 X. All the specimens except that of Fig. *a* were fixed in osmic acid and subsequently washed with water prior to shadow-casting.

Fig. *a*. *L. D.* flagellate stained with Leishman's stain ; unshadowed.

Fig. *b*. *L. D.* flagellate shadow-cast with silver. Computed thickness 50 A. U. at an angle of  $\tan^{-1} \frac{1}{5}$ .

Fig. *c*. Do. Computed thickness 112 A.U. at  $\tan^{-1} \frac{1}{5}$

Fig. *d*. Do. Computed thickness 200 A.U. at  $\tan^{-1} \frac{1}{4}$ .

Fig. *e*. Do. Computed thickness 250 A.U. at  $\tan^{-1} \frac{1}{3}$ .

Fig. *f*. Do. Computed thickness 330 A.U. at  $\tan^{-1} \frac{1}{3}$ .





A  $\sin \alpha$  for optical microscopy should be made within these limits. For angles  $\alpha$  not greater than  $15^\circ$ ,  $\sin \alpha$  can be replaced by  $\tan \alpha$  and a curve like Fig. 3 plotted from equation (5) will be helpful in obtaining any of the four quantities when the other three are fixed.

The above discussion indicates a thickness of 50-100 A.U. of silver at angles  $\alpha$  from  $\tan^{-1} \frac{1}{4}$  to  $\tan^{-1} \frac{1}{2}$  as useful for routine shadowing of specimens which are suspected to possess surface irregularities. For the visualisation of low details, long shadows are useful but since any given specimen for optical microscopy will, in general, contain details with variable heights, the possibility of overlapping of these shadows must be borne in mind when shadowing at very oblique angles.

For quantitative work, the source should subtend as small a solid angle at the specimen as possible so that the condition of a point source assumed in the calculation of thickness is approximated. This implies that the source of metal has to be made as small as possible and the distance of the specimen from the source as large as possible. Further, devices for measuring the angle  $\alpha$  with reasonable accuracy have to be provided.

## ACKNOWLEDGMENTS

The author wishes to express his gratitude to Prof. M. N. Saha for laboratory facilities and to Dr. N. Das Gupta for kind help and encouragement during the progress of these studies. Thanks are also due to Dr. P. C. Sen Gupta of the School of Tropical Medicine, Calcutta, for the L. D. cultures, to the Ministry of Education, Government of India for a grant for the purchase of equipments and to the Indian Council of Medical Research for a Fellowship.

INSTITUTE OF NUCLEAR PHYSICS,  
UNIVERSITY OF CALCUTTA

## REFERENCES

- Drummond D G, 1950, *J. Roy. Mic. Soc.* 70 102  
Minor R S, 1953, *Ann der Physik.* 10 581  
Scott D G and Wyckoff R W G, 1949, *Am. J. Clin Path.* 10, 63.  
Williams R. C. and Wyckoff R. W. G. 1946, *J Appl Phys.* 17 23.



# DYNAMICS OF THE VIBRATION OF A BAR EXCITED BY THE LONGITUDINAL IMPACT OF AN ELASTIC LOAD

By M. GHOSH AND S. K. GHOSH

(Received for publication, October 10, 1950)

**ABSTRACT.** Dynamics of the vibration of a bar excited by longitudinal impact by an elastic load has been worked out, following operational method. The main idea upon which the dynamics is built up is that the bar behaves like a loaded bar so long the load is in contact with it, and the elastic load is supposed to behave like a hard load backed by a weightless spring. Two distinct cases have been worked out from the general solution, namely, (i) when the load strikes the free end, and (ii) when the load strikes the fixed end of the bar. The method gives the solution for any epoch very easily, unlike the method of the variation of integration constant where solution for any particular epoch can be obtained after a long laborious calculation.

## INTRODUCTION

The theory of the extensional vibration of a bar excited by the impact of a rigid load has been worked out by a number of workers (Boussinesq, 1885). Ghosh (1935) extended the case, applying the same method, for an elastic load struck at the free end of a bar, the other end being fixed. Later Ghosh and Dhar (1930) worked out the case for a bar struck at the fixed end by an elastic load, the other end remaining free. But the method appears to be a lengthy one.

In this paper we solve the general problem of the extensional vibration of a bar excited by the impact of an elastic load in a simpler way using the powerful operational method in a similar way as adopted by Ghosh (1938, 1939, 1940, 1941) in solving the general problem of pianoforte string.

In solving the problem we assume that the bar behaves like a loaded one so long as the load is in contact, and the elastic load is supposed to behave like a hard load backed by weightless spring.

We consider in section I the case when the load strikes at the free end of the bar, the other end being fixed and in section II when the load strikes at the fixed end.

### *Explanation of the symbols used*

$l$  = Length of the bar.

$t$  = Variable time.

$s$  = Variable length, measured along the length of the bar, the bar being fixed at  $s=0$  and struck at  $s=l$  (in sec. I). But in sec. II, the bar is fixed at  $s=l$  and struck at  $s=0$ .

$w$  = Displacement at any section of the bar.

$w_l$  = Displacement at  $s=l$ , the struck point.

$\rho$  = Linear density of the bar.

$\alpha$  = Area of the cross-section of the bar.

$E_1$  = Young's modulus of the material of the bar.

$m$  = Mass of the load.

$E_2$  = Elastic constant of the material of the load

$c$  = Velocity of the longitudinal wave propagation along the bar.

$\theta_1 = 2l/c$  = Period of the free vibration of the bar.

$t_n = t - n\theta_1$  ;

$v_0$  = Velocity of impact.

$J = mv_0$

$u$  = Compression of the load.

$z = w_l + u$  = Displacement of the load.

$P$  = Pressure exerted by the load.

$D$  = Operator  $d/dt$ .

The differential equation of the extensional vibration is

$$\frac{d^2 w}{dt^2} = c^2 \frac{d^2 w}{ds^2} \quad (1)$$

which is equivalent to

$$\frac{d^2 w}{ds^2} - \frac{d^2}{c^2} w \quad (1.1)$$

where  $c^2 = E_1 \alpha / \rho$  and  $s$  is measured from the fixed end of the bar,  $w$ , the longitudinal displacement.

The elastic hammer strikes at  $s=l$ , and let  $w_l$  be the displacement at the struck point.

The solution of eqn. (1) is, in general, of the form,

$$w = A \sinh \frac{Ds}{c} + B \cosh \frac{Ds}{c} \quad (2)$$

The pressure  $P$  exerted by the load is given by

$$P = m \frac{d^2 Z}{dt^2} = -E_1 \alpha \left( \frac{dw}{ds} \right)_{s=l} = -E_2 u \quad (3)$$

where

$$z = w_l + u \quad (4)$$

### Section I

The terminal conditions are :  $w=0$  at  $s=0$  and  $w=w_l$  at  $s=l$ . This reduces equation (2) to

$$w = w_l \frac{\sinh \frac{Ds}{c}}{\sinh \frac{Dl}{c}} \quad (5)$$

Now with the help of eqns. (4) and (5), eqns. (3) and (4) can be written in the form,

$$\left[ mD^2 + \frac{E_1\alpha}{c} D \coth \frac{Dl}{c} \right] w_1 + mD^2 u = JD \quad (6)$$

and  $mD^2 w_1 + (mD^2 + E_2)u = JD. \quad (7)$

Now replacing  $JD$  by  $mv_0$  and solving the simultaneous equations (6) and (7) for  $w_1$  and  $u$ ,

we get  $w_1 = \frac{1}{F(D)} v_0 \quad (8)$

and  $u = \frac{D}{F(D)} \frac{E_1\alpha}{E_2c} \coth \frac{Dl}{c} v_0 \quad (9)$

$$\text{where } F(D) = D + \left( \frac{E_1\alpha}{E_2c} D^2 + \frac{E_1\alpha}{mc} \right) \coth \frac{Dl}{c} \quad (8.1)$$

Also combining (8) and (9)

$$u = \frac{E_1\alpha}{E_2c} \coth \frac{Dl}{c} D w_1 \quad (9.1)$$

$$= \frac{E_1\alpha}{E_2c} \coth \frac{Dl}{c} w'_1 \quad (9.2)$$

In our case the load strikes at the free end at  $s=1$  so that,

$$F(D) = D + \left( \frac{E_1\alpha}{E_2c} D^2 + \frac{E_1\alpha}{mc} \right) \coth \frac{Dl}{c} = \frac{D_1 D_2}{(q+p)(1-e^{-D\theta_1})} \left[ 1 - \left\{ \frac{2(q+p)D}{D_1 D_2} - 1 \right\} e^{-D\theta_1} \right] \quad (10)$$

Therefore from eq. (8)

$$w_1 = \frac{(q+p)(1-e^{-D\theta_1})}{D_1 D_2} \left[ 1 - \left\{ \frac{2(q+p)D}{D_1 D_2} - 1 \right\} e^{-D\theta_1} \right]^{-1} v_0 \quad (11)$$

where  $D_1 D_2 = (D+q)(D+p) \equiv D^2 + \frac{E_2c}{E_1\alpha} D + \frac{E_2}{m};$

and  $-q$  and  $-p$  are the roots of the eq.  $D_1 D_2 = 0$  and are given by

$$[q, p] = \frac{E_2c}{2E_1\alpha} \mp \frac{1}{2} \sqrt{\left( \frac{E_2c}{E_1\alpha} \right)^2 - \frac{4E_2}{m}} \quad (11.1)$$

From eq. (11)

$$\begin{aligned} w_1 = & \frac{(q+p)}{D_1 D_2} \left[ 1 + \left\{ \frac{2(q+p)D}{D_1 D_2} - 1 \right\} e^{-D\theta_1} \right. \\ & \cdot \left\{ \left( \frac{2(q+p)D}{D_1 D_2} - 1 \right)^2 - \left( \frac{2(q+p)D}{D_1 D_2} - 1 \right) \right\} e^{-2D\theta_1} \\ & \cdot \dots + \left\{ \left( \frac{2(q+p)D}{D_1 D_2} - 1 \right)^n - \left( \frac{2(q+p)D}{D_1 D_2} - 1 \right)^{n-1} \right\} e^{-nD\theta_1} \left. \right] v_0 \end{aligned} \quad (12.1)$$

$$\begin{aligned}
&= \left[ \frac{(q+p)}{D_1 D_2} + \left\{ \frac{2(q+p)^2 D}{D_1^2 D_2^2} - \frac{2(q+p)}{D_1 D_2} \right\} e^{-D\theta}, \right. \\
&\quad + \left\{ \frac{4(q+p)^3 D^2}{D_1^3 D_2^3} - \frac{6(q+p)^2 D}{D_1^2 D_2^2} + \frac{2(q+p)}{D_1 D_2} \right\} e^{-D\theta}, \\
&\quad + \left\{ \frac{8(q+p)^4 D^3}{D_1^4 D_2^4} - \frac{16(q+p)^3 D^2}{D_1^3 D_2^3} + \frac{10(q+p)^2 D}{D_1^2 D_2^2} - \frac{2(q+p)}{D_1 D_2} \right\} e^{-3D\theta}, \\
&\quad + + + \dots + \left\{ \frac{2^n (q+p)^{n+1} D^n}{D_1^{n+1} D_2^{n+1}} - \frac{2(n+1)(q+p)^n D^{n-1}}{D_1^n D_2^n} + - + - + \dots \right. \\
&\quad + (-1)^r ({}^n C_r + {}^{n-1} C_{r-1}) \frac{2^{n-r} (q+p)^{n-r+1} D^{n-r}}{D_1^{n-r+1} D_2^{n-r+1}} + - + - + \dots - \\
&\quad \left. + (-1)^n \frac{2(q+p)}{D_1 D_2} \right\} e^{-nD\theta} \Big] v_0 \quad (12.1)
\end{aligned}$$

$$\begin{aligned}
&= f_1(t) + 2f_2(t_1) - 2f_1(t_1) + 4f_3(t_2) - 6f_2(t_2) + 2f_1(t_2) + 8f_4(t_3) - 16f_3(t_3) + 10f_2(t_3) \\
&\quad - 2f_1(t_3) + \dots + 2^n f_{n+1}(t_n) - 2^{n-1}(n+1)f_n(t_n) \dots + (-1)^r ({}^n C_r \\
&\quad + {}^{n-1} C_{r-1}) 2^{n-r} f_{n-r+1}(t_n) + \dots + (-1)^n 2f_1(t_n) \quad \dots (12.3)
\end{aligned}$$

The values of these functions are (Ghosh, 1938.)

Case I

$$\text{When } \left( \frac{E_2 c}{E_1 \alpha} \right)^2 > \frac{4E_2}{m};$$

$$f_1(t) = \frac{(q+p)}{D_1 D_2} \cdot v_0 = v_0 A \left[ \frac{1}{q} (1 - e^{-qt}) - \frac{1}{p} (1 - e^{-pt}) \right] \quad \dots (12a.1)$$

$$f_2(t) = \frac{(q+p)^2 D}{D_1^2 D_2^2} e^{-D\theta_1} v_0 = v_0 A^2 \left[ \frac{e^{-qt_1}}{q} (1 - A + qt_1) + \frac{e^{-pt_1}}{p} (1 + A + pt_1) \right] \quad (12a.2)$$

$$\begin{aligned}
f_3(t_2) &= \frac{(q+p)^3 D^2}{D_1^3 D_2^3} e^{-D\theta_1} v_0 = v_0 A^3 \left[ \frac{e^{-qt_2}}{q} \left\{ \frac{3}{2} (A-A)^2 + \frac{1}{2} (3A-1) qt_2 - \frac{q^2 t_2^2}{2!} \right\} \right. \\
&\quad \left. + \frac{e^{-pt_2}}{p} \left\{ \frac{3}{2} (A+A)^2 + \frac{1}{2} (3A+1) + \frac{p^2 t_2^2}{2!} \right\} \right], \quad \dots (12a.3)
\end{aligned}$$

...

...

...

...

$$f_n(t) = \frac{(q+p)^n D^{n-1}}{D_1^n D_2^n} v_0$$

$$\begin{aligned}
&= A^n v_0 \left[ \sum_{r=1}^n (-1)^{r-1} \frac{|(n+r-1)|}{|(n)|(r)} \beta^{r-1} e^{-qt} (D-q)^{n-1} \frac{t^{n-r}}{(n-r)!} \right. \\
&\quad \left. + (-1)^n \sum_{r=1}^n \frac{|(n-r+1)|}{|n|(r)} \beta^{r-1} e^{-pt} (D-p)^{n-1} \frac{t^{n-r}}{(n-r)!} \right] \quad (12a.n)
\end{aligned}$$

and so on :

where

$$A = \frac{q+p}{p-q}, \quad \text{and} \quad \beta = \frac{1}{p-q}.$$

Case II

$$\text{When} \quad \left( \frac{E_2 c}{E_1 \alpha} \right)^2 = \frac{4E_2}{m}; \quad \text{i.e.} \quad \frac{4\rho}{m} = \frac{E_2}{E_1 \alpha}$$

and

$$D_1 = D_2 = D + q.$$

$$f_1(t) = \frac{2q}{(D+q)^2} v_0 = \frac{2v_0}{q} \left[ 1 - e^{-qt} (1 + qt) \right] \quad \dots \quad (12b.1)$$

$$f_2(t_1) = \frac{4q^2 D}{(D+q)^4} v_0 e^{-D\theta_1} = 4v_0 \frac{e^{-qt_1}}{q} \cdot \frac{(qt_1)^3}{3!}; \quad \dots \quad (12b.2)$$

$$f_3(t_2) = \frac{8q^3 D^2}{(D+q)^6} e^{-2D\theta_1} v_0 = \frac{8v_0}{q} e^{-qt_1} \left[ \frac{(qt_2)^4}{4!} - \frac{(qt_2)^5}{5!} \right] \quad \dots \quad (12b.3)$$

etc., etc. . . . .

$$\begin{aligned} f_n(t_{n-1}) &= \frac{(2q)^n D^{n-1}}{(D+q)^{2n}} e^{-(n-1)D\theta_1} v_0 = \frac{2^n v_0}{q} e^{-qt_{n-1}} \left[ \frac{(qt_{n-1})^{n+1}}{(n+1)!} - {}^{n-2}C_1 \frac{(qt_{n-1})^{n+2}}{(n+2)!} \right. \\ &\quad + - + - + (-1)^{r-1} {}^{n-2}C_{r-1} \frac{(qt_{n-1})^{n+r}}{(n+r)!} + - + - \dots \\ &\quad \left. + (-1)^{n-2} \frac{(qt_{n-1})^{2n-2}}{(2n-2)!} \right] \quad \dots \quad (12b.n) \end{aligned}$$

Case III

$$\text{When} \quad \left( \frac{E_2 c}{E_1 \alpha} \right)^2 < \frac{4E_2}{m} \quad \text{both } p \text{ and } q \text{ are complex quantities, from}$$

$$\text{eqn. (11.1)} \quad [q, p] = \mu \mp iv$$

where,

$$\mu = \frac{1}{2} \frac{E_2 c}{E_1 \alpha} \quad \text{and} \quad v = \frac{1}{2} \sqrt{\frac{4E_2}{m} - \left( \frac{E_2 c}{E_1 \alpha} \right)^2}$$

Now putting these values of  $q$  and  $p$  in eqns. 12a.1 ; 12a.2, etc.

we have,

$$f_1(t) = \frac{2\mu}{v} v_0 \left[ \frac{v}{\mu^2 + v^2} - \frac{1}{\sqrt{\mu^2 + v^2}} e^{-\mu t} \sin \left( vt + \tan^{-1} \frac{v}{\mu} \right) \right] \quad (12c.1)$$

$$f_2(t_1) = \frac{2\mu^2}{v^3} v_0 e^{-\mu t_1} [\sin vt_1 - vt_1 \cos vt_1] \quad \dots \quad (12c.2)$$

$$\begin{aligned} f_3(t_2) &= \frac{\mu^3}{v^5} v_0 e^{-\mu t_2} \left[ \sqrt{\mu^2 + v^2} \left\{ v^2 t_2^2 \sin \left( vt_2 - \tan^{-1} \frac{v}{\mu} \right) + vt_2 \cos \left( vt_2 - \tan^{-1} \frac{v}{\mu} \right) \right\} \right. \\ &\quad \left. + \mu \left\{ 2vt_2 \cos vt_2 - 3 \sin vt_2 \right\} \right] \quad (12c.3) \end{aligned}$$

and so on. These are similar to those obtained by Ghosh.

## Case IV

$E_2 = \infty$ , here  $u = 0$ , hence,  $p = \infty$ ,  $q = +\frac{c}{m_1 l}$  and  $A = 1$ ,  $\beta = 0$ .

where,

$$m_1 = \frac{m}{\rho l}.$$

$$f_1(t) = \frac{v_0}{q} (1 - e^{-qt}) \quad \dots \quad (12d.1)$$

$$f_2(t_1) = \frac{v_0}{q} e^{-qt_1} q t_1 \quad \dots \quad (12d.2)$$

$$f_3(t_2) = \frac{v_0}{q} e^{-qt_2} \left\{ q t_2 - \frac{q^2 t_2^2}{2!} \right\} \quad \dots \quad (12d.3)$$

and so on :

The displacement at the struck point during contact in different intervals can be obtained easily from eqn. (12.3).

Thus, during

$$0 < t < \theta_1;$$

$$w_1 = f_1(t),$$

during

$$\theta_1 < t < 2\theta_1$$

$$w_1 = f_1(t) + 2f_2(t_1) - 2f_1(t_1),$$

during

$$2\theta_1 < t < 3\theta_1$$

$$w_1 = f_1(t) + 2f_2(t_1) - 2f_1(t_1) + 4f_3(t_2) - 6f_2(t_2) + 2f_1(t_2)$$

and so on.

The pressure exerted by the load is numerically equal to  $E_2 u$  which, by the help of eqn. (9.2), is given by

$$P = \frac{E_1 \alpha}{c} \text{Coth } \frac{Dl}{c} \cdot w_1'.$$

$$= \frac{E_1 \alpha}{c} \left\{ 1 + 2e^{-D\theta_1} + 2e^{-2D\theta_1} + 2e^{-3D\theta_1} + \dots + \dots \right\} w_1' \quad \dots \quad (13)$$

The eqn. (13) by the help of (12.3) can be written as,

$$P = \frac{E_1 \alpha}{c} \left[ f_1'(t) + 2f_2'(t_1) + 4f_3'(t_2) - 2f_2'(t_2) + 8f_4'(t_3) - 8f_3'(t_3) \right. \\ \left. + 2f_2'(t_3) + \dots + \dots \right] \quad \dots \quad (14)$$

So, neglecting the sign for the time being (as  $P = E_2 u$ ), we get, the expression for pressures at different intervals.

$$P_1 = \frac{E_1 \alpha}{c} f_1'(t) \quad \dots \quad (14.1)$$



$$P_2 = P_1 + \frac{2E_1\alpha}{c} f_2'(t_1) \quad \dots \quad (14.2)$$

$$P_3 = P_2 + \frac{2E_1\alpha}{c} [2f_3'(t_2) - f_2'(t_2)] \quad \dots \quad (14.3)$$

$$P_4 = P_3 + \frac{2E_1\alpha}{c} [4f_4'(t_3) - 4f_3'(t_3) + f_2'(t_3)] \quad \dots \quad (14.4)$$

and so on :

These pressures may be calculated in the different cases mentioned above.

### Case I

Combining (14.1) with the first differential of (12a.1) we get,

$$P_1 = \rho v_0 A (e^{-qt} - e^{-pt}) \quad \dots \quad (15.1)$$

In a like manner,

$$P_2 = P_1 + 2\rho v_0 c A^2 [e^{-qt_1}(A - qt_1) - e^{-pt_1}(A + pt_1)] \quad \dots \quad (15.2)$$

$$P_3 = P_2 + 2\rho v_0 c A^2 [e^{-qt_1}\{Aq^2t_2^2 - qt_2(3A^2 + A - 1) - 3A^3\} - e^{-pt_1}\{Ap^2t_2^2 - pt_2(2A + 1) + 3A^2(A + 2)\}] \quad \dots \quad (15.3)$$

and so on :

### Case II

Similarly, combining (14.1) with the first differential of (12b.1) we get,

$$P_1 = 2\rho v_0 c e^{-qt} \cdot qt ; \quad \dots \quad (15.4)$$

In a like manner,

$$P_2 = P_1 + 8\rho v_0 c e^{-qt_1} \left\{ \frac{(qt_1)^2}{2!} - \frac{(qt_1)^3}{3!} \right\} \quad \dots \quad (15.5)$$

$$P_3 = P_2 + 8\rho v_0 c e^{-qt_1} \left[ \frac{(pt_2)^2}{2!} - 5 \cdot \frac{(qt_2)^3}{3!} + 8 \cdot \frac{(qt_2)^4}{4!} - 4 \cdot \frac{(qt_2)^5}{5!} \right] \quad \dots \quad (15.6)$$

$$P_4 = P_3 + 8\rho v_0 c e^{-pt_1} \left[ \frac{(qt_3)^2}{2!} - 9 \cdot \frac{(qt_3)^3}{3!} + 32 \cdot \frac{(qt_3)^4}{4!} - 56 \cdot \frac{(qt_3)^5}{5!} + 48 \cdot \frac{(qt_3)^6}{6!} - 16 \cdot \frac{(qt_3)^7}{7!} \right] \quad \dots \quad (15.7)$$

and so on :

### Case III

When 
$$\left( \frac{E_2 c}{E_1 \alpha} \right)^2 < \frac{4E_2}{m}$$

We get, before, combining eqn. (14.1) with the first differential of (12c.1)

$$P_1 = 2\rho v_0 c \mu e^{-\mu t} \sin \nu t \quad \dots \quad (15.8)$$

In a like manner,

$$P_2 = P_1 + 4\rho v_0 c \frac{\mu^2}{v^3} e^{-\mu t_1} \left[ \sqrt{\mu^2 + v^2} \cdot v t_1 \cos \left( v t_1 - \tan^{-1} \frac{v}{\mu} \right) - \mu \sin v t_1 \right] \dots \quad (15.9)$$

$$P_3 = P_2 + 4\rho v_0 c \frac{\mu^3}{v^5} e^{-\mu t_1} \left[ \left( 3\mu^2 - \frac{v^4 t_2}{\mu} - 2\mu v^2 t_2 + v^2 \right) \sin v t_2 \right. \\ \left. - 2(2v\mu^2 t_2 + \mu v + v^3 t_1) \cos v t_2 + \sqrt{\mu^2 + v^2} \{v^2 t_2 (1 - \mu t_2) \sin (v t_2 - \tan^{-1} \frac{v}{\mu}) \right. \\ \left. + v(v^2 t_2^2 - \mu t_2 + 1) \cos (v t_2 - \tan^{-1} \frac{v}{\mu}) \} \right] \dots \quad (16)$$

and so on.

Case IV

$E_2 = \infty$ , i.e., in the case of hard load, combining (14.1) with the first differential co-efficient of (d.1),

$$\text{we get,} \quad P_1 = \rho v_0 c e^{-q t} \dots \quad (16.1)$$

In a like manner,

$$P_2 = P_1 + 2\rho v_0 c e^{-q t_1} (1 - q t_1) \dots \quad (16.2)$$

$$P_3 = P_2 + 2\rho v_0 c e^{-q t_1} (q^2 t_2^2 - 2q t_2 - 3) \dots \quad (16.3)$$

and so on :

## SECTION II

Here the terminal condition at  $s=0$  is  $\frac{dw}{ds} = 0$  for all values of  $t$ , and at  $s=l$ , the terminal condition is the equation of motion of the striking body.

With help of the above terminal conditions eqn. (2) becomes

$$w = w_1 \frac{\cosh \frac{Ds}{c}}{\cosh \frac{Dl}{c}} \dots \quad (17)$$

with the help of eqns. (4) and (17) eqns. (3) and (4) can be written in the

$$\text{form} \quad \left[ mD^2 + \frac{E_1 \alpha}{c} D \tanh \frac{Dl}{c} \right] w_1 + mD^2 u = JD \dots \quad (18)$$

and

$$mD^2 w_1 + (mD^2 + E_2) u = JD \dots \quad (19)$$

Now replacing  $JD$  by  $mv_0$  and solving the simultaneous equations (18) and (19) for  $w_1$  and  $u$ , we get,

$$w_1 = \frac{1}{F(D)} v_0 \dots \quad (20)$$

and

$$u = \frac{D}{F(D)} \cdot \frac{E_1 \alpha}{E_2 c} \tanh \frac{Dl}{c} v_0 \dots \quad (21)$$

where 
$$F(D) = D + \left( \frac{E_1 \alpha}{E_2 c} D^2 + \frac{E_1 \alpha}{m c} \right) \tanh \frac{Dl}{c} \quad \dots (22)$$

Also combining (20) and (21)

$$u = \frac{E_1 \alpha}{E_2 c} \tanh \frac{Dl}{c} Dw_1 \quad \dots (22.1)$$

$$= \frac{E_1 \alpha}{E_2 c} \tanh \frac{Dl}{c} w_1' \quad \dots (22.2)$$

From eqn. (22)

$$F(D) = \frac{D_1 D_2}{(q+p)(1+e^{-D\theta_1})} \left[ 1 - \left( 1 - \frac{2D(q+p)}{D_1 D_2} \right) e^{-D\theta_1} \right] \quad \dots (23)$$

Therefore, from eqn. (20)

$$w_1 = \frac{(q+p)(1+e^{-D\theta_1})}{D_1 D_2} \left[ 1 - \left( 1 - \frac{2D(q+p)}{D_1 D_2} \right) e^{-D\theta_1} \right]^{-1} v_0 \quad \dots (24)$$

where, 
$$D_1 D_2 = (D+q)(D+p) \equiv D^2 + \frac{E_2 c}{E_1 \alpha} D + \frac{E_2}{m}$$

and  $-q, -p$  are the roots of the eqn.  $D_1 D_2 = 0$

and are given by 
$$[q, p] = \frac{E_2 c}{2E_1 \alpha} \mp \frac{1}{2} \left[ \left( \frac{E_2 c}{E_1 \alpha} \right)^2 - \frac{4E_2}{m} \right]^{\frac{1}{2}}$$

From eqn. (24)

$$w_1 = \frac{(q+p)}{D_1 D_2} \left[ 1 + \left\{ 2 - \frac{2D(q+p)}{D_1 D_2} \right\} e^{-D\theta_1} + \left\{ \frac{4(q+p)^2 D^2}{D_1^2 D_2^2} - \frac{6D(q+p)}{D_1 D_2} + 2 \right\} e^{-2D\theta_1} - \left\{ \frac{8(q+p)^3 D^3}{D_1^3 D_2^3} - \frac{16D^2(q+p)^2}{D_1^2 D_2^2} + \frac{10D(q+p)}{D_1 D_2} - 2 \right\} e^{-3D\theta_1} + \dots \right] v_0 \quad \dots (25)$$

$$= f_1(t) - 2f_2(t_1) + 2f_1(t_1) + 4f_3(t_2) - 6f_2(t_2) + 2f_1(t_2) - 8f_4(t_3) + 16f_3(t_3) - 10f_2(t_3) + 2f_1(t_3) + \dots \quad \dots (26)$$

The values of these functions, however, are the same as those derived in section I.

Further, the displacement equation shows, that the wave train does not return after reflection, as shown by the second term of eqn. (27) below.

The pressure exerted by the load is numerically equal to  $E_2 u$  and given by eqn. (21.2) as,

$$P = \frac{E_1 \alpha}{c} \tanh \frac{Dl}{c} w_1' = \frac{E_1 \alpha}{c} \left\{ 1 - 2e^{-D\theta_1} + 2e^{-2D\theta_1} - 2e^{-3D\theta_1} + \dots \right\} w_1' \quad \dots (27)$$

Eqn. (27) with the help of eqn. (26) can be written as

$$P = \frac{E_1 z}{c} \left[ f_1'(t) - 2f_2'(t_1) + 4f_3'(t_2) - 2f_2'(t_2) + \dots \right] \quad \dots (28)$$

The pressure equation shows that it terminates during the first interval only and can be evaluated for all the three cases with the help of the values of  $q$  and  $p$ . Thus pressure during the interval,

$$0 < t < \theta_1$$

$$P_1 = \rho c v_0 A (e^{-qt} - e^{-pt}), \quad \text{where} \quad A = \frac{q+p}{p-q}$$

By studying the pressure functions from eqns. (14) and (15) it can be easily shown that when  $E_2 = \infty$ , pressure increases by sudden jump in magnitude  $E_1 \alpha v_0 / c$  at  $t=0$ , whence it falls down slowly to a minimum value till at  $t=2l/c$  the pressure again rises suddenly in magnitude  $E_1 \alpha v_0 / c$ . This process continues with the sudden rise of pressure in magnitudes  $E_1 \alpha v_0 / c$  at  $t=0, 2l/c, 4l/c$ , etc. till the impact terminates.

But in the case when  $E_2 \neq 0$ , we find that this discontinuous periodic rise of pressure as obtained when  $E_2 = \infty$ , gradually lose their sharp angularities and well-rounded humps appear instead. As the value of  $E_2$  is diminished, the humps become less and less pronounced and we find that the duration of contact gradually increases as the hardness of the striking hammer gradually decreases.

In the second case when the load strikes at the fixed end, the pressure for  $E_2 = \infty$  suddenly rises by the same magnitude  $E_1 \alpha v_0 / c$  at  $t=0$  and terminates at  $t=2l/c$ . But when  $E_2 \neq 0$ , pressure continuously increases, attains a maximum value and then gradually falls to zero. The duration of contact in this case is found to be greater than  $2l/c$ ; but in case of small value of  $E_2$  i.e., for light and soft load, duration of contact is found to be less than  $2l/c$ . The experimental study of the problem is in progress and will be published in due course.

PHYSICAL LABORATORY  
CITY COLLEGE,  
CALCUTTA.

## REFERENCES

- Boussinesq, 1885, *Application des potential*.  
Love, *The Mathematical theory of Elasticity*, 4th Ed., p. 431  
Ghosh, M., 1935, *Bull. Cal. Math. Soc.*, **27**, 1  
" " 1938, *Ind. Jour. Phys.*, **12**, 317, 437  
" " 1939, " " " **13**, 277  
" " 1940, " " " **14**, 475, 489  
" " 1941, " " " **15**, 13, 15  
Ghosh, M. and Dhar, S. C., 1930, *Bull. Cal. Math. Soc.*, **27**, 171

# DIELECTRIC PROPERTIES OF SALT SOLUTIONS AT ULTRA-HIGH FREQUENCIES

By RAMU SATYANARAYANA AND S. R. KHAISTGIR

*(Received for publication, November 13, 1950)*

**ABSTRACT** The dielectric properties of (1) sodium chloride (2) magnesium chloride (3) potassium chloride and (4) copper sulphate solutions over a range of ultra-high frequencies (60–110 Mc/s) were studied by employing a Lecher-wire system terminating at the input end by a condenser filled with each of the solutions. The length of the Lecher-wire was adjusted for maximum voltage across the experimental condenser with the help of a valve-detector unit.

The dielectric constant of the solutions was found to increase, attaining a saturation value at a particular concentration (0.4–0.6%), except in the case of copper sulphate solution.

The ultra-high frequency absorption in each of the four salt solutions was studied by drawing the space-resonance curves with different concentrations of the salt solution. Absorption curves were then drawn by plotting the values of the width of resonance against concentration for several frequencies in the case of sodium chloride solution and for one frequency in the case of the other solutions. From these absorption curves, the frequencies of the maximum absorption for certain concentrations in the case of sodium chloride solution were found. From the observed values of the frequencies of maximum absorption the relaxation times were determined for these concentrations by applying Debye's formula. Relaxation time for a particular concentration of each of the other three solutions was also similarly obtained. The values of the product of the wavelength corresponding to the maximum absorption and the normality of the solution, expressed in gram-equivalents per litre, have been found to be constant which agree well with the values obtained by other workers. With the values of relaxation time obtained from the absorption data, Debye's dispersion, absorption and loss-tangent curves have been drawn for each of the four solutions. The values of relaxation time were also computed from Debye-Falkenhagen formula for comparison. In the case of copper sulphate, there was discrepancy.

The values of the high-frequency electrical conductivity of sodium chloride have also been calculated for different concentrations for three different frequencies within the experimental range.

## INTRODUCTION

As a large part of wireless communication is conducted over the seas, the study of dielectric properties of seawater is of considerable importance for radio communications. From theoretical aspects also, the subject is worthy of systematic investigations. Experiments were therefore, undertaken by various workers for finding the dielectric properties of sea-water.

As early as 1907 the electrical conductivity of different samples of sea-water was measured by Hill (1907) in the audio-frequency range and later by Van der Pol (1918), in the range of low and medium frequencies. Drysdale (1920), studied the dielectric behaviour of sea-water up to a

frequency of 1 Mc/s and Smith-Rose (1933-34) carried out similar measurements up to 10 Mc/s

Sea-water mostly contains sodium chloride solutions in water and the salt-content varies from about 0.2 to about 3%. It also contains other salts in smaller quantities, viz., potassium chloride, magnesium chloride etc. (Dors, 1940). The dielectric behaviour of these salt solutions was also studied experimentally by different workers. Drake, Pierce and Dow (1930) measured the dielectric properties of potassium chloride solution at lower frequencies. Cooper (1946) measured the dielectric properties of sodium chloride solution over a frequency of 0.95–13 Mc/s and 690–4320 Mc/s. Some accurate measurements of the absorption coefficients of common salt in solution were made by Saxton and Lane (1947) for very high radio frequencies. The absorption and other associated properties of some salt solutions that compose average sea water were also studied recently by Chatterjee and Sreekantan (1948) in India over a frequency range of 300–500 Mc/s. An optical method was adopted in their work and the percentage of absorption of ultra-high frequency waves in these solutions as found for different concentrations over the experimental range of frequencies. Attenuation coefficients and hence absorption indices were calculated for different frequencies for certain fixed dilutions. Several other associated properties, e. g., relaxation time, dielectric constant, loss-tangent value, dipole-conductivity, etc. were also calculated from the absorption data for these solutions.

In the present work, the dielectric properties of sodium chloride, potassium chloride, magnesium chloride and copper sulphate solutions were investigated for a range of concentrations from 0 to 3% with ultra-high frequency fields ranging from about 90 Mc/s to 110 Mc/s. Regarding the effective dielectric constants of the solutions, no attempt was made to find their absolute values. Only a qualitative study of the variation of the dielectric constant of the different solutions with concentration was made for different frequencies within the experimental range. Within the same frequency range, measurements were made of H.F. absorption in water and in the different solutions. These absorption measurements were carried out for varying concentrations by keeping frequency constant and the results have been theoretically examined. The relaxation times have been computed from these absorption data, and with these computed values, the dielectric constant and the absorption coefficient have been obtained from the dispersion and absorption formulæ of Debye.

An expression for the H.F. electrical conductivity has been obtained in terms of absorption and its values have been obtained in the case of sodium chloride for different concentrations and for some fixed frequencies.

#### EXPERIMENTAL PROCEDURE

The Lecher-wire method was employed in studying the dielectric properties of the different salt solutions, viz. sodium chloride, magnesium chlo-

ride, potassium chloride, and copper sulphate for a range of ultra-high frequencies. The experimental arrangement consisted of a pair of Lecher wires terminating at the generator end by a parallel-plate condenser inside a glass receptacle for containing water or any solution as dielectric between

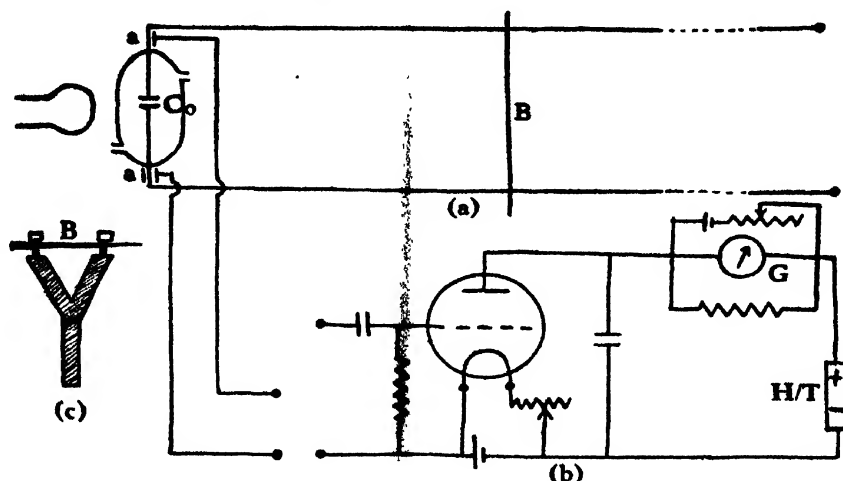


FIG. I

- (a) Lecher-wire arrangement
- (b) Detector unit
- (c) Short-circuiting bridge.

the plates. When ultra-high frequency voltage was applied to the input end of the Lecher-wire system and standing waves were produced, the position of a potential node was obtained by sliding a short-circuiting bridge to-and-fro along the wires till the voltage across the terminal condenser as indicated by a suitable valve-detector unit was maximum\*

#### DIELECTRIC CONSTANT VARIATIONS WITH CONCENTRATION

The length  $l$  of the Lecher wire (as measured from the generator end) was first adjusted for resonance with air in the experimental condenser. When water or any solution was introduced in the experimental condenser, the length  $l'$ , when adjusted for resonance, was found to be shorter than the previous length  $l$ . The shortening indicated an increase of dielectric constant of the medium inside the condenser. The shift of resonance point was noted for different concentrations (0–3%) for each of the four salt solutions under examination. In the case of sodium chloride solution, five different frequencies from 62 Mc/s to 110 Mc/s were tried, while for other solutions, the

\* It should be noted that the condition, for maximum voltage across the terminal condenser was the same as that for current-resonance. The voltage-resonance adjustment was not only found convenient but also extremely useful, as it was possible to eliminate any conductivity effect across the experimental condenser. It is well known that the L-C value necessary for maximum voltage across the condenser should be independent of the conductivity or leakage across the same.

variation of the shift of resonance with concentration was studied for only one frequency within the experimental range.

#### H.F. ABSORPTION MEASUREMENTS

The study of the H.F. absorption in water and in the different solutions was done by drawing the space-resonance curves with pure water and with different amounts of salts dissolved in it. The "sharpness" or "flatness" of resonance obtained with water or any solution was then measured by noting the distance between two points on either side of the resonance point on the Lecher wire, giving currents  $1/\sqrt{2}$  times the current at resonance.

Keeping the frequency of oscillation fixed, the width of resonance, as a measure of H.F. absorption, was measured from each of the space-resonance curves obtained with the solutions of different concentrations from 0 to 3%. With sodium chloride solution, fresh sets of observations were made for different frequencies within the range under investigation. Measurements were made with one frequency only for the other solutions.

The values of H/F electrical conductivity were determined from the absorption data in the case of sodium chloride solution for different concentrations (0-3%) for three fixed frequencies in the manner described in the next section.

#### THEORY OF THE METHOD OF MEASURING THE H.F. ELECTRICAL CONDUCTIVITY OF WATER AND THE SALT SOLUTIONS

The measurement of the H.F. electrical conductivity of the liquid between the plates inside the cell is possible by determining the attenuation constants of a Lecher wire system (1) when there is between the plates of the terminal condenser and (2) when the liquid (water or any solution) is there as the dielectric. The attenuation constant  $\alpha_0$  in the first case is easily obtained from

$$\alpha_0 = \frac{R}{2Z_0} \quad \dots (1)$$

where  $R$  is the H.F. resistance per unit length and  $Z_0$  the surge-impedance of the Lecher system. The resistance  $R$  per unit length can be determined from

$$R = \sqrt{\frac{R_0 \omega}{1 - (d/a)^2}} \quad \dots (2)$$

where  $R_0$  denotes the direct-current resistance per unit length of the parallel wires,  $d$  the diameter of the wires and  $a$  the spacing. The units in (2) are in c.m.c.g.s. units. The surge-impedance is obtained from

$$Z_0 \text{ (ohms)} = 276 \log_{10} \frac{2a}{d} \quad \dots (3)$$



The attenuation constant  $\alpha$ , in the second case when water or any solution is inside the terminal condenser of the Lecher-wire system, can be determined in the following manner.

With the liquid inside the experimental condenser there will be a leakage of resistance  $\rho$  across the same. This leakage resistance is in parallel with the liquid condenser and can be replaced by a series resistance  $r.l'$ , where  $r$  = resistance per unit length distributed uniformly over the entire resonance length  $l'$ . The attenuation constant under this condition is given by

$$\alpha = \frac{R + r}{2Z_0} \quad \dots (4)$$

Thus from (1) and (4)

$$r = 2Z_0(\alpha - \alpha_0)$$

or  $r.l' = 2Z_0(\alpha - \alpha_0)l' \quad \dots (5)$

Now the leakage resistance is given by

$$\rho = \frac{1}{\omega^2 \epsilon^2 C_0^2 (r.l')} \quad \dots (6)$$

The capacity  $C_0$  of the terminal condenser can be eliminated from the resonance condition, when there is just air between the plates of the terminal condenser of the Lecher system, viz.,

$$Z_0 \tan \frac{2\pi l}{\lambda} = \frac{1}{\omega C_0}$$

or 
$$C_0 = \frac{1}{\omega Z_0 \tan \frac{2\pi l}{\lambda}}$$

Substituting this value of  $C_0$ , we obtain from (5) and (6)

$$\rho = \frac{Z_0 \tan^2 \frac{2\pi l}{\lambda}}{2(\alpha - \alpha_0) \epsilon^2 l'} \quad \dots (7)$$

Remembering that

$$\rho = \frac{1}{4\pi\sigma C_0}$$

and substituting the value of  $C_0$ , we get

$$\rho = \frac{\omega Z_0 \tan^2 \frac{2\pi l}{\lambda}}{4\pi\sigma} \quad \dots (8)$$

From (6) and (7)

$$\sigma = \frac{\omega(\alpha - \alpha_0)l' \epsilon^2}{2\pi \tan \frac{2\pi l}{\lambda}} = \frac{c(\alpha - \alpha_0)l' \epsilon^2}{\lambda \tan \frac{2\pi l}{\lambda}} \quad \dots (9)$$

where  $c$  is the velocity of light and  $\lambda$ , the wavelength corresponding to  $\omega$ .

Since the attenuation constant  $\alpha$ , as seen from (1), is negligible, the electrical conductivity  $\sigma$  is given by

$$\left[ \frac{\epsilon^2 l' C}{\lambda \tan \frac{2\pi l}{\lambda}} \right] \alpha = k_1 \alpha \quad \dots (10)$$

where

$$k_1 = \epsilon^2 l' C / \lambda \tan \frac{2\pi l}{\lambda}$$

The attenuation constant  $\alpha$  is obtained from the theoretical relation between  $\alpha$  and the 'width' of the resonance curve. In the case of 'half-width', the attenuation coefficient is given by

$$\alpha = \frac{2}{m} \left( \frac{\pi e}{\lambda^2} \right) \quad (11)$$

where  $e$  is the half-width,  $m$  is the order of the potential node on the Lecher wire and  $\lambda$  the wave-length of the oscillation induced into the Lecher-wire system. In the case of the  $(1/\sqrt{2})$  width as in the present work, we have

$$\alpha = \frac{\sqrt{2}}{m} \left( \frac{\pi \cdot e}{\lambda^2} \right) \quad \dots (12)$$

where  $e$  is the  $(1/\sqrt{2})$  width.

In view of (10) and (12), the H.F. conductivity will be given by the relation :

$$\begin{aligned} \sigma &= k_1 \left( \frac{\sqrt{2}}{m} \frac{\pi}{\lambda^2} \right) e \\ &= \left[ \frac{\epsilon^2 l' C}{\tan \frac{2\pi l}{\lambda}} \cdot \frac{\pi \sqrt{2}}{m \lambda^3} \right] e \quad \dots (13) \end{aligned}$$

#### EXPERIMENTAL ARRANGEMENTS

A Philco H.F. signal generator (Type 7070) was used as source of ultra-high frequency oscillations. The output of the signal generator, when set for requisite ultra-high frequency, was applied across the parallel-plate condenser which served as the terminal condenser of a parallel-wire Lecher system at the generator end.

The pair of parallel Lecher-wires (S.W.G. No. 12 copper wire, diameter 0.259 cms.) were set up horizontally about 4 feet from the floor. The distance between the pair of parallel wires was 6.29 cms. As already mentioned above, the terminal condenser of the Lecher-wire system was a parallel-plate condenser enclosed in a glass receptacle with lead-in wires from the two plates. The glass receptacle could be filled with water or any other solution which also could be made to run out through an outlet tube fitted with a glass stop-cock. With ultra-high frequency oscillations on, the resonance length adjustments were made by sliding a short-circuiting bridge  $B$  across the Lecher-wires.

The short-circuiting bridge was made of thick copper wire and was mounted on a long ebonite handle. The under-side of the short circuiting bridge was filed and shaped in the form of a sharp edge and a pointer was attached to the bridge. A scale was kept horizontally fixed alongside the Lecher-wires and the pointer on the sliding bridge indicated its position on the horizontal scale. The resonance was indicated by means of a valve-detector with a balanced mirror galvanometer  $G$  in the anode circuit. The detector unit was coupled to the Lecher-wire system at the input end by means of two small condensers  $a, a$  consisting of short brass tubes insulated from the Lecher-wires by glass sleeves. The diagram of the entire experimental arrangement is shown in Fig. 1. The circuit diagram of the detector unit is shown separately in the same figure.

EXPERIMENTAL RESULTS SHOWING SHIFTS OF  
RESONANCE POINTS FOR DIFFERENT CON-  
CENTRATIONS OF THE SOLUTIONS DUE TO  
DIELECTRIC CONSTANT VARIATIONS.

The shifts of resonance point on the Lecher-wires towards the generator end indicated smaller resonance lengths and hence increasing dielectric constant values. It was observed that the resonance length decreased gradually with the increased concentration, attaining a constant value after a certain concentration.

The shifts of resonance point for sodium chloride for increasing concentration from 0 to 3% (normality from 0 to 0.5129 N) for five different ultra-high frequencies are shown in Fig. 2. The shifts of resonance points

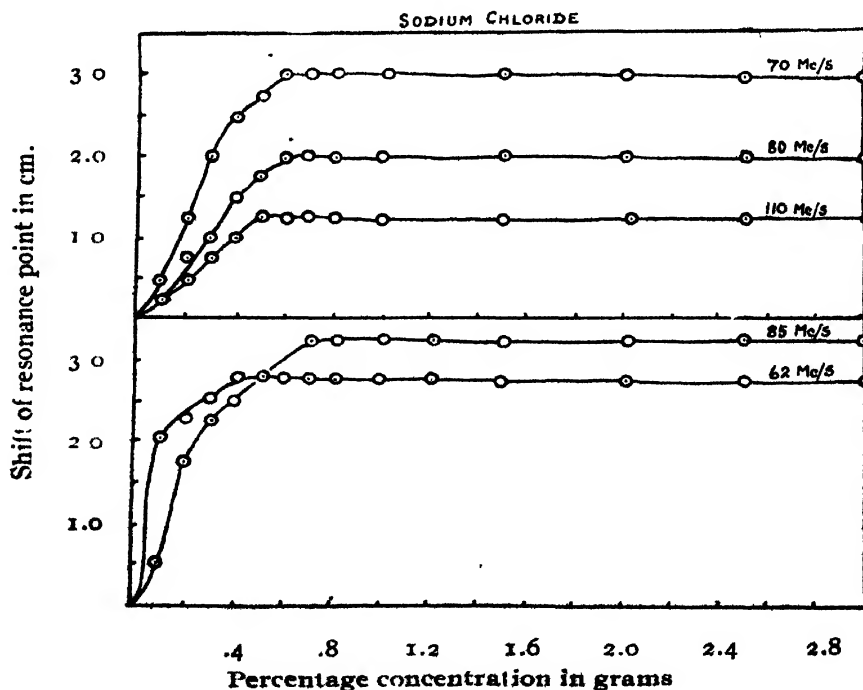


FIG. 2

for magnesium chloride, potassium chloride, and copper sulphate solutions with increasing concentration from 0 to 3% are illustrated in Fig. 3 for only one frequency.

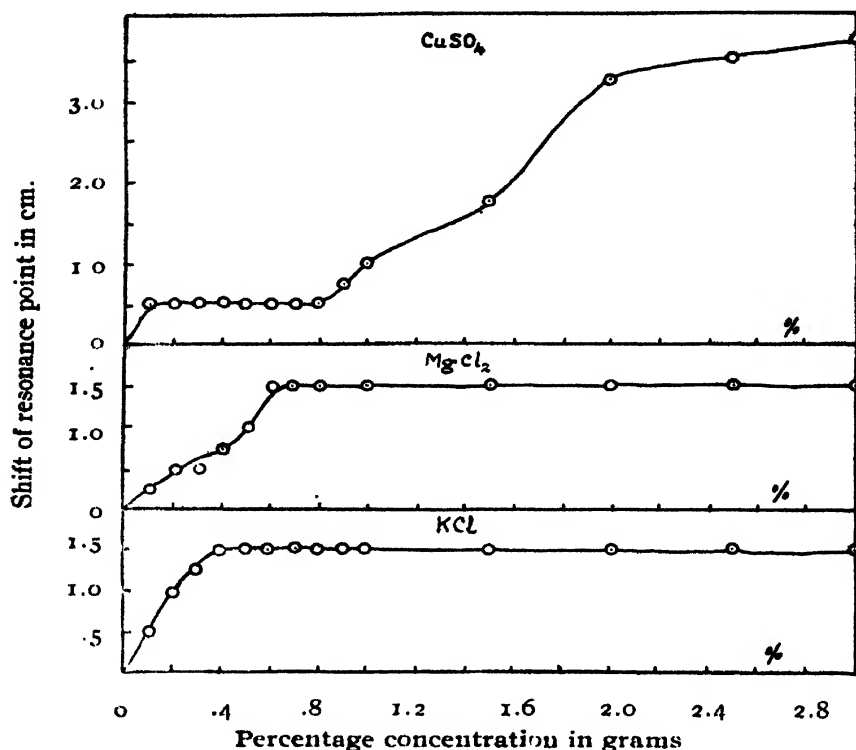


FIG. 3

It will be noticed that in all solutions, except copper sulphate solution, the shift increases gradually (*i.e.*, the resonance length  $l'$  decreases slowly) till it attains a steady value at a particular concentration. The maximum shift observed was indeed small, indicating only a small increase of dielectric constant of the solution. The dielectric constant attained a saturation value at 0.5 to 0.6% concentration. In the case of copper sulphate solution the dielectric constant was, however, found to remain constant from 0 to 0.8% concentration. For concentration values from 0.8 to 3%, it was found to increase considerably.

#### ABSORPTION MEASUREMENTS AND DETERMINATIONS OF H.F. ELECTRICAL CONDUCTIVITY OF THE SALT SOLUTIONS.

##### (a) Absorption-concentration curves for fixed frequencies

For each frequency, resonance curves showing deflections in the galvanometer of the valve-detector unit against the scale divisions representing the wire-lengths were experimentally obtained with water and with solutions of different concentration used as dielectric between the plates of the experi-

mental condenser. From the resonance curves for each concentration, the  $(1/\sqrt{2})$  width was measured carefully. The values of the width of resonance when plotted against the corresponding values of concentration gave the absorption-concentration curve for a particular frequency. Such absorption curves were obtained for different frequencies

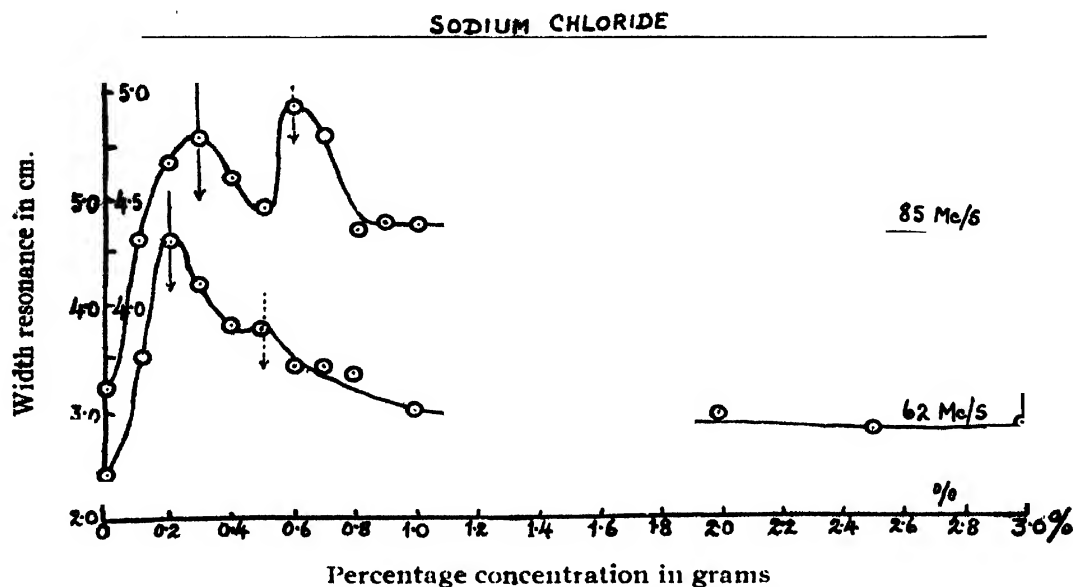


FIG. 4

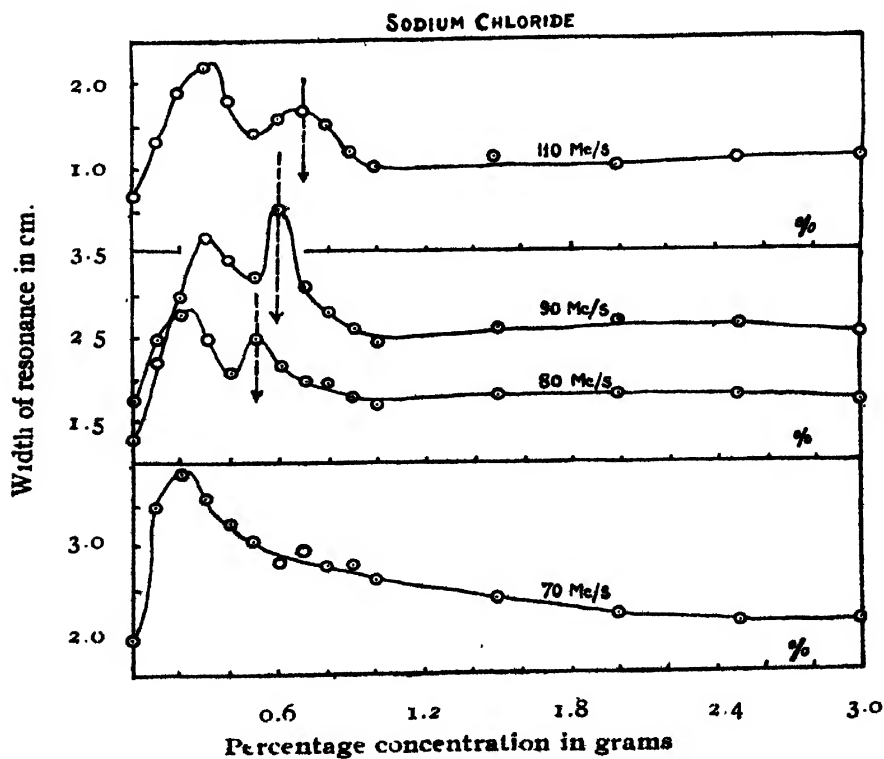


FIG. 5

in the case of sodium chloride solution; and for one frequency for other solutions. In almost all the curves there was distinct evidence of *two maxima* at particular values of the concentration, the positions of the maxima depending upon the frequency of the field. For sodium chloride solution two sets of absorption curves showing width of resonance against concentration are shown in Fig. 4 for 62 Mc/s and 85 Mc/s. In Fig. 5 are shown four other sets of similar absorption curves for sodium chloride for 70 Mc/s, 80 Mc/s, 90 Mc/s and 110 Mc/s. The figures illustrate a definite shift of the maximum towards the higher concentration side for the higher frequencies. We have reasons to believe that the two maxima generally observed are associated with the fundamental and the first harmonic frequencies. It can be seen that the position of the first maximum (which is associated with the fundamental) lies between 0.2 and 0.3% conc. whereas, the position of the second maximum (which is associated with the first harmonic) lies within 0.5 and 0.7% conc. within the frequency range from 72 to 110 Mc/s. The shift of the second maximum with frequency is indicated in the absorption curves. The absorption-concentration curves for magnesium chloride, potassium chloride and copper sulphate solutions for one particular frequency are illustrated in Fig. 6.

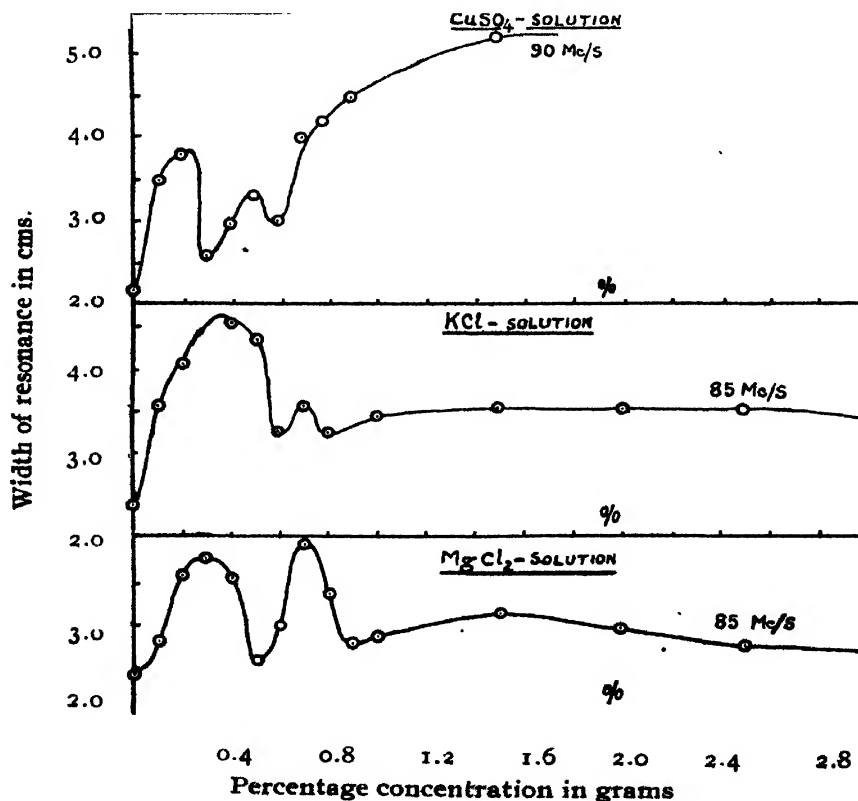


FIG. 6

In obtaining the values of the high-frequency electrical conductivity of the sodium chloride solution, which are given in Table I., calculations were

made according to (13). In computing the values, the dielectric constant of the aqueous solutions, which are all dilute, is taken as 80. The constant resonance-length  $l$  with air in the terminal condenser of the Lecher wire system and the resonance length  $l'$  with the solution inside the condenser after it attained a constant value were taken for the calculation.

TABLE I  
(Sodium chloride solution)

% Concentration (grms.)	Normality (gms./litre)	H.F. elec. conductivity (e.s.u.)		
		70 Mc/s	80 Mc/s	90 Mc/s
0	0.0	0.07295	0.2303	0.4567
0.1	0.01709 N	0.10580	0.3036	0.7731
0.2	0.03419 N	0.15010	0.3350	1.0540
0.3	0.05129 N	0.13820	0.3036	1.3000
0.4	0.06834 N	0.12670	0.2617	1.1950
0.5	0.08547 N	0.11910	0.3036	1.1240
0.6	0.10260 N	0.10750	0.2722	1.4060
0.7	0.11960 N	0.11520	0.2513	1.0890
0.8	0.13680 N	0.10750	0.2513	0.9840
0.9	0.15380 N	0.10750	0.2303	0.9137
1.0	0.17090 N	0.09982	0.2199	0.8433
1.5	0.25640 N	0.09212	0.2303	0.9137
2.0	0.34130 N	0.84450	0.2303	0.9488
2.5	0.42740 N	0.08061	0.2303	0.9137
3.0	0.51290 N	0.08061	0.2303	0.8784

(b) Frequency of Maximum Absorption and its Relation with Concentration

From each absorption-concentration curve for a particular frequency, the concentration value for maximum absorption (*i.e.*, maximum width of resonance) was noted and the particular frequency was then regarded as the frequency for maximum absorption for that concentration. As already mentioned, there were two maxima in one absorption-concentration curve. The concentration values corresponding to the two maxima in the absorption curves were associated with the particular frequencies which were regarded as frequencies of maximum absorption for these concentrations. In Table II are given the different concentration values corresponding to frequencies

of maximum absorption for the two maxima. The values of the product of the wavelength in cms corresponding to the frequency of maximum absorption and the concentration expressed in gram-equivalent per litre are also entered in Table II.

TABLE II  
(Sodium chloride solutions)

## Set I

First maximum					Second maximum				
% conc. (gms)	$\gamma$ gm. equiv. per litre	$f$ Mc/s	$\lambda_{cm}$	$(\gamma \cdot \lambda_{cm})$	% conc. (gms.)	$\gamma$ gm. equiv. /litre	$f$ Mc/s	$\lambda_{cm}$	$(\gamma \cdot \lambda_{cm})$
0.20	0.0342 N	62	483.7	16.54	...	...	...	...	...
0.275	0.0470 N	85	352.9	16.59	0.6	0.1026	170	176.5	18.1
			mean	16.57					

## Set II.

0.225	0.03846 N	70	428.6	16.48	...	...	..	...	...
0.250	0.04274 N	80	375.0	16.03	0.5	0.08547	160	177.5	16.03
0.300	0.05129 N	90	335.3	17.09	0.6	0.10260	180	167.7	17.09
0.325	0.05556 N	110	272.7	15.15	0.7	0.11960	220	136.4	15.15
				.....					.. ...
				mean value, 16.19					mean value, 16.48

It is to be observed that the product  $(\gamma \cdot \lambda_{cm})$  comes out to be a constant, being equal to 16.19 for the first maximum. Accepting the first harmonic wavelength values for the second maximum, the product  $(\gamma \cdot \lambda_{cm})$  is found to have practically the same constant value. This equality of the values of  $(\gamma \cdot \lambda_{cm})$  for the two maxima can be regarded as a good justification for believing that the first harmonic is responsible for the second maximum.

The experimental value of  $(\gamma \cdot \lambda_{cm})$  for sodium chloride agrees well with the value 16.45 given by Forman and Crisp (1946) and also with that obtained by Chatterjee and Sreekantan (1948).

Similar experimental results with magnesium chloride, potassium chloride and copper sulphate solutions gave the frequencies of maximum absorption. The values of these frequencies and the corresponding concentrations together with the values of product of the wavelength corresponding to the frequency of maximum absorption and concentration in gram-equivalents per litre are given in the Table III.



TABLE III

		% Conc. (grms)	$\gamma$ gm. equiv. per litre.	$f$ Mc/s.	$\lambda_{cm.}$	$(\gamma. \lambda_{cm.})$
Potassium chloride.	1st max.	0.35	0.04693 N	85	352.9	16.56
	2nd max.	0.70	0.09386 N	170	176.5	16.56
						mean value 16.56
Magnesium chloride.	1st max.	0.30	0.02950 N	85	352.9	10.41
	2nd max.	0.70	0.06885 N	170	176.5	12.15
						mean-value : 11.28
Copper sulphate.	1st max.	0.275	0.02205 N	90	333.3	7.35
	2nd max.	0.50	0.04004 N	180	166.7	6.68
						mean value : 7.02

In Table IV the values of  $(\gamma. \lambda_{cm.})$  obtained by different experimenters are given for comparison.

TABLE IV

Salt solution	Satyanarayana & Khastgir	Forman & Crisp	Chatterjee & Sreekantan
Sodium chloride	16.34	16.45	16.64
Potassium chloride	16.56	..	15.96
Magnesium chloride	11.28	...	11.96
Copper sulphate	7.02	...	8.65

## DISPERSION AND ABSORPTION FORMULÆ

The well-known Lorentz expression for the local field at a molecule is given by

$$E_{local} = E + 4\pi P \quad \dots (14)$$

where  $P$  is the electric polarisation.

On the basis of this expression, Debye (1929) derived the expressions for the real and imaginary dielectric constants :

$$\left. \begin{aligned} \epsilon' &= \epsilon_{\infty} + \frac{\epsilon_0 - \epsilon_{\infty}}{1 + y^2} \\ \epsilon'' &= \frac{\epsilon_0 - \epsilon_{\infty}}{1 + y^2} \cdot y \end{aligned} \right\} \quad \dots \quad (15)$$

where  $y = \left( \frac{\epsilon_0 + 2}{\epsilon_{\infty} + 2} \right) \omega \tau$ .

$\epsilon_0$  = static dielectric constant,

$\epsilon_{\infty}$  = dielectric constant for extremely high frequencies,

and  $\tau$  = relaxation time.

The Lorentz expression was considered inadequate for representing the local field, and the hypothesis of 'hindered rotation' was introduced later by Debye (1935, 1937) and Fowler (1935). Reconsideration of the problem by Onsager (1936) led to a 'reaction field' which is due to the polarization of the dielectric in the electric field of the molecule itself. Considering the reaction field with certain simplifying assumptions and introducing the effect of an alternating field, Onsager derived

$$\left. \begin{aligned} \epsilon' &= \epsilon_{\infty} + \frac{\epsilon_0 - \epsilon_{\infty}}{1 + x^2} \\ \epsilon'' &= \frac{\epsilon_0 - \epsilon_{\infty}}{1 + x^2} \cdot x \end{aligned} \right\} \quad \dots \quad (16)$$

where  $x = \omega \tau_0$  and  $\tau_0$  is another relaxation time.

Onsager's expressions were similar to Debye's except for the interchange of parameters  $x$  and  $y$ . This interchange of parameters gives a larger value for the relaxation time according to Onsager than that on Debye's theory.

Van Vleck (1937) suggested an assemblage of discrete particles rather than a continuous medium. On this view Cole (1937) also obtained expressions similar to Debye's formulæ. The relaxation time was, however, different and there was an empirical factor.

#### EXPERIMENTAL DETERMINATION OF RELAXATION TIME FROM THE ABSORPTION MEASUREMENTS

Let us take Debye's expression for  $\epsilon''$  :

$$\epsilon'' = \frac{\epsilon_0 - \epsilon_{\infty}}{1 + y^2} \cdot y,$$

where

$$y = \omega \tau \cdot \left( \frac{\epsilon_0 + 2}{\epsilon_{\infty} + 2} \right)$$

When concentration is varied, both relaxation time and dielectric constant change, so that

$$\frac{\partial \epsilon''}{\partial y} = (\epsilon_0 - \epsilon_\infty) \frac{\partial}{\partial y} \left( \frac{y}{1 + y^2} \right) + \frac{y}{1 + y^2} \cdot \frac{\partial}{\partial y} (\epsilon_0 - \epsilon_\infty)$$

If now the dielectric constant is assumed to remain constant the second term becomes zero and  $\epsilon''$  becomes maximum, when  $y=1$ . The constancy of the dielectric constant has been assumed for determining the frequency of maximum absorption. Thus according to Debye

$$\omega_{\max} = 2\pi f_{\max} = \left( \frac{\epsilon_\infty + 2}{\epsilon_0 + 2} \right) \frac{1}{\tau} \quad (y=1).$$

or

$$\tau = \frac{1}{2\pi f_{\max}} \left( \frac{\epsilon_\infty + 2}{\epsilon_0 + 2} \right) \quad \dots (17)$$

According to Onsager

$$\tau_0 = \frac{1}{2\pi f_{\max}}$$

In the range of ultra-high frequencies the difference between the two relaxation times is extremely small.

The calculation of  $\tau$  from (17) has been primarily based on the observed value of the frequency of maximum absorption.  $\epsilon_\infty$  may be assumed to be equal to the dielectric constant of water at ultra-high frequencies which is 80 and  $\epsilon_0$  at the audio frequencies can be obtained from Falkenhagen's

$$\text{relation :} \quad \epsilon_0 - \epsilon_s = \frac{1.97 \times 10^6}{2\epsilon_s} \frac{Z_1 Z_2}{T^{\frac{1}{2}} (1 + 1/\sqrt{q})^2} \left\{ \left| \frac{Z_1}{1} \right| + \left| \frac{Z_2}{1} \right| \right\}^{\frac{1}{2}} \cdot (q \cdot \gamma) \quad (19)$$

where  $Z_1$  = valency of Na-ion = 1

$Z_2$  = valency of Cl-ion = 1

$T = 300^\circ \text{K}$

$\epsilon_s$  = dielectric constant of water at u.h.f. = 80 c.s.u.

$q = 0.5$  for NaCl

$\gamma$  = concentration in gram-equivalents per litre.

Thus  $\epsilon_0 - \epsilon_s = 3.536 \sqrt{\gamma}$  for NaCl-solution.

Similarly the following can be worked out.

$$\epsilon_0 - \epsilon_s = 9.281 \sqrt{\gamma} \text{ for } \text{MgCl}_2 \text{ at } 23^\circ \text{C.}$$

$$\epsilon_0 - \epsilon_s = 3.51 \sqrt{\gamma} \text{ for } \text{KCl at } 23^\circ \text{C.}$$

$$\epsilon_0 - \epsilon_s = 28.95 \sqrt{\gamma} \text{ for } \text{CuSO}_4 \text{ at } 23^\circ \text{C}$$

The relaxation time according to Debye-Falkenhagen theory (Falkenhagen, 1935) for a salt solution is given by :—

$$\tau = \frac{8.85 \times 10^{-11} \times D_0}{\Delta \epsilon \cdot \gamma} \quad (20)$$

where  $D_0$  = dielectric constant of water

$\gamma$  = concentration expressed in gram equivalents per litre,

$\Delta_\infty$  = equivalent conductivity of solution at infinite dilution,

= 108.99 for sodium chloride

= 110.88 for magnesium chloride

= 133.10 for potassium chloride

= 113.85 for copper sulphate

The values of  $\epsilon_0$ , as calculated from (19), and of  $\tau$ , as calculated from (17) are given in Table V in the case of NaCl for three different concentrations. The values of  $\tau$ , as computed from Debye-Falkenhagen formula, are also entered in the same table for comparison.

TABLE V

Sodium chloride solution.

 $\epsilon_s = 80$ 

% conc. (gms.).	$\gamma$ normality (gms./litre)	$\epsilon_0$	$f_{\max}$ Mc/s.	Relaxation time $\tau$	
				Obs. in secs. $\times 10^{10}$ (Debye)	Cal. in secs. $\times 10^{10}$ (Debye-Falkenhagen)
0.7	0.11960 N	81.223	110	14.25	11.69
0.6	0.10260 N	81.132	90	17.44	12.67
0.5	0.58547 N	81.034	80	19.63	15.20

The values of  $\epsilon_0$  and  $\tau$  for KCl,  $MgCl_2$ , and  $CuSO_4$  for one concentration are given in Table VI.

TABLE VI

Salt	% conc. (gms.)	$\gamma$ normality (gms./litre)	$\epsilon_0$	$f_{\max}$ Mc/s.	Relaxation time $\tau$	
					Obs in secs. $\times 10^{10}$ (Debye)	Cal. in secs $\times 10^{10}$ (Debye-Falkenhagen)
KCl	0.35	0.04693 N	80.761	85	19.01	11.60
$MgCl_2$	0.70	0.06885 N	82.435	85	18.18	21.79
$CuSO_4$	0.50	0.04064 N	85.794	90	16.84	28.19

It is to be observed that Debye-Falkenhagen expression for  $\tau$  gives somewhat smaller values than our observed values for NaCl and KCl. In the case of  $MgCl_2$ , the observed value is slightly higher. The discrepancy between the observed value and the value computed from Debye Falkenhagen expression is indeed large for  $CuSO_4$  solution.

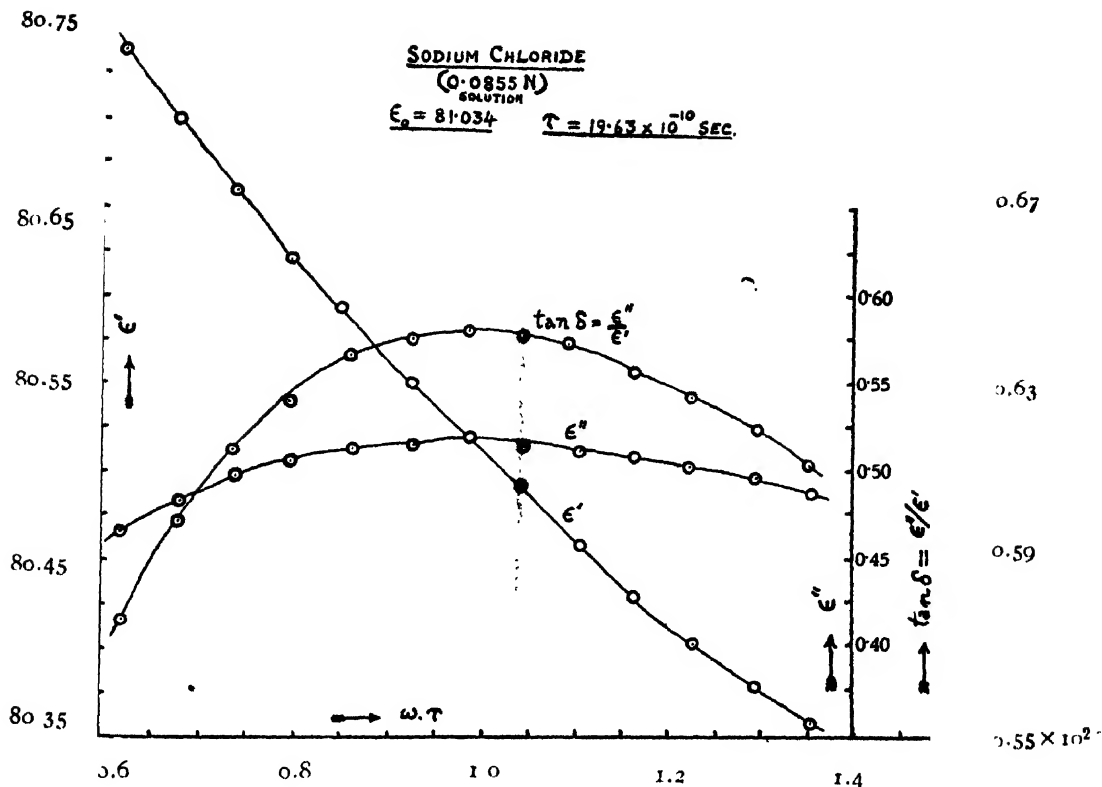


FIG. 7

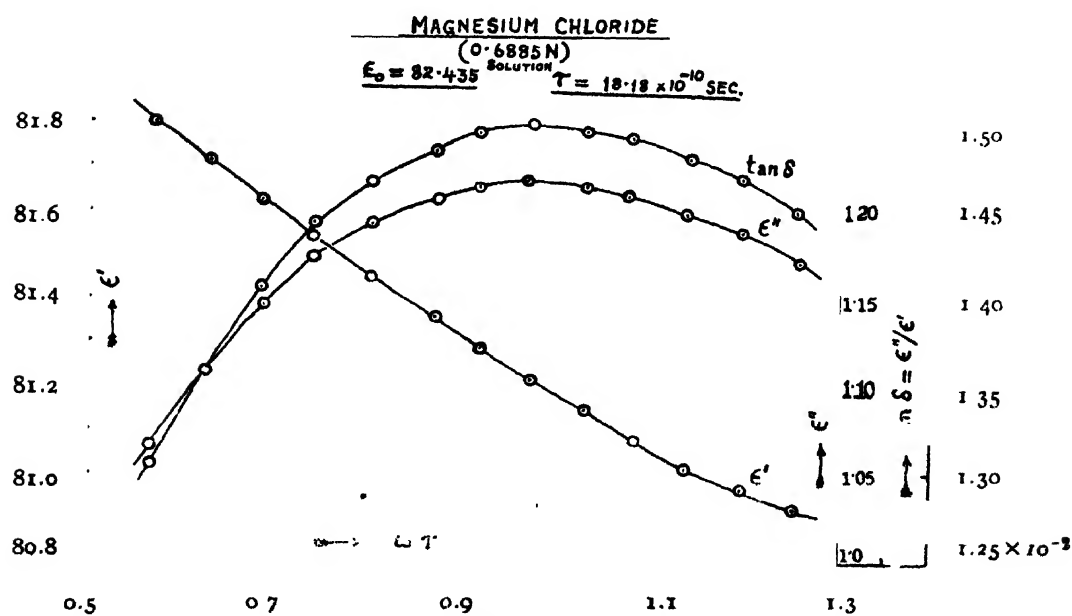


FIG. 8

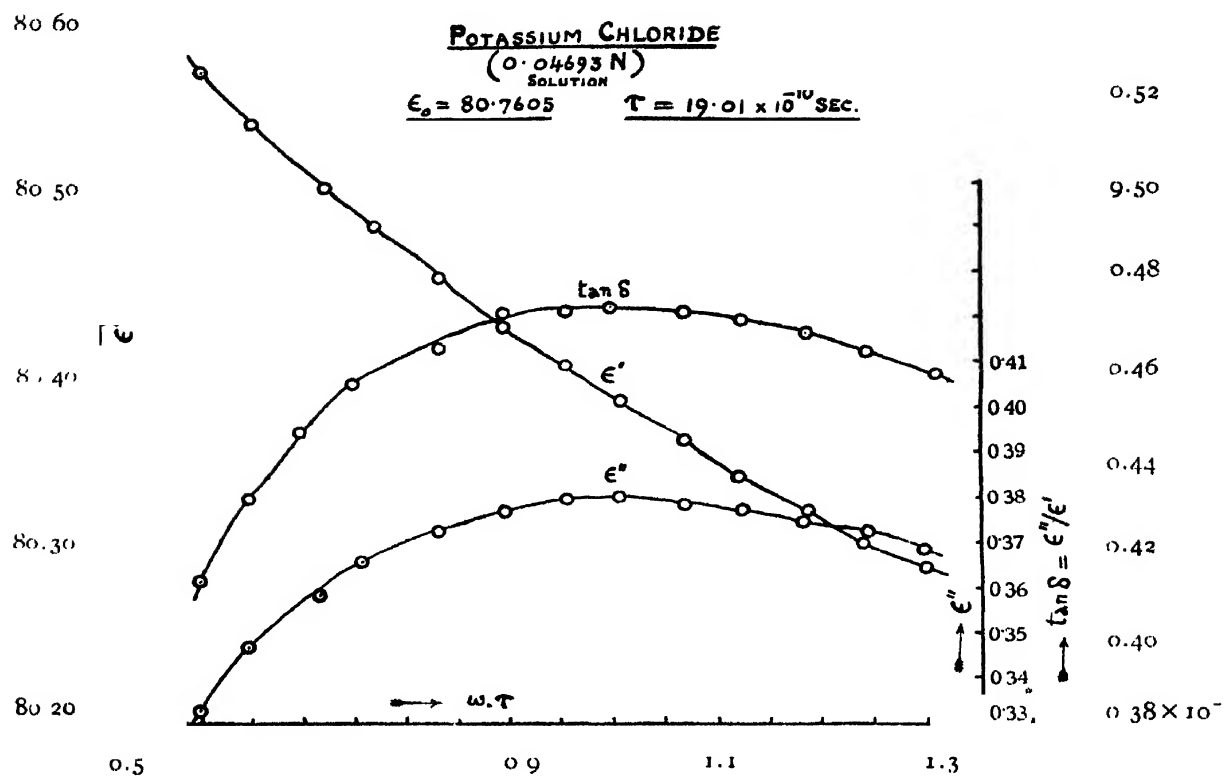


FIG. 9

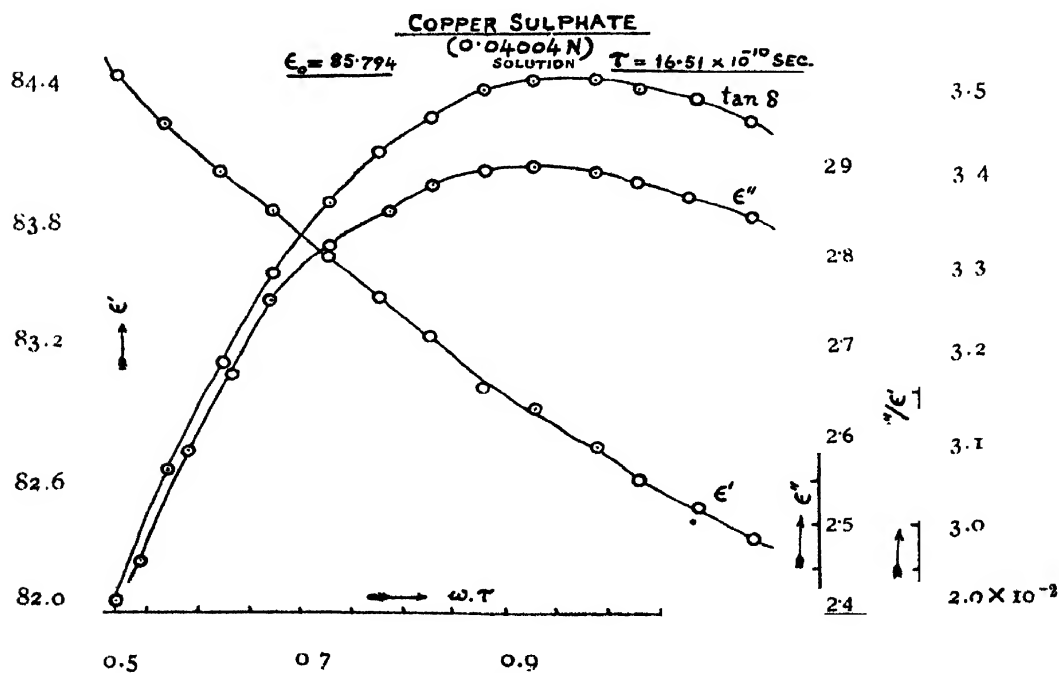


FIG. 10

CALCULATED VALUES OF  $\epsilon'$ ,  $\epsilon''$  AND THE LOSS-TANGENT

Accepting Debye's formulæ for  $\epsilon'$  and  $\epsilon''$ , we have substituted our observed values of the relaxation time and have calculated  $\epsilon'$  and  $\epsilon''$  for different ultra-high frequencies within the experimental range for one concentration value for each of the four salt solutions. The loss-tangent  $\tan \delta = \frac{\epsilon''}{\epsilon'}$  has also been calculated. The variations of  $\epsilon'$ ,  $\epsilon''$  and  $\tan \delta$  with frequency are illustrated in figures 7-10. It will be seen that the maximum for either  $\epsilon''$  or  $\tan \delta$  appears at the frequency of maximum absorption. It should be remembered that the values of  $\epsilon''$  and  $\tan \delta$  were calculated by taking the relaxation time value corresponding to the frequency of maximum absorption.

WIRELESS LABORATORY  
PHYSICS DEPARTMENT  
BANARAS HINDU UNIVERSITY

REFERENCES

- Chatterjee, S. K. and Sreekantan, B. V., 1948, *Ind. Jour. Phys*, **22**, 5 329  
 Cole, 1937, *Jour. Chem. Physics*, **5**, 385  
 Cooper, R., 1946, *J. I. E. E.*, **93**, 69.  
 Debye, P., 1929, Polar molecules.  
 „ 1935, *Phys. Zeits*, **36**, 193.  
 „ 1937, *Ann. Phys.*, **28**, 28.  
 Dorsey, N. E., 1940, Properties of ordinary water substance p. 641 (Reynold Publishing Corp. N. Y.)  
 Drake, Pierce, and Dow., 1930, *Phys. Rev.*, **35**, 613,  
 Drysdale, C. V., 1920, *J. I. E. E.*, **58**, 572.  
 Falkenhagen, H., 1934, *Electrolysis*. pp 100, 106. 176  
 Forman, and Crisp., 1946. *Trans. Far. Soc.*, **42**, A, 187.  
 Fowler, R. H., 1937, *Proc. Roy. Soc. A*, **149**, 1.  
 Hill, E. G., 1907, *Proc. Roy. Soc., Edin*, **72**, 233.  
 Onsager, L., 1936, *Jour Amer. Chem. Soc.*, **58**, 1486.  
 Saxton, and Lane, 1947, Meteorological factors in radio wave propagation (published by Phys. Soc Lond.)  
 Smith-Rose, R. L., 1933-34, *Proc. Roy. Soc. A.*, **143**, 135.  
 Vander Pol, B., 1918, *Phil. Mag.* **36**, 88.  
 Van Vleck 1937, *Jour, Phys. Chem.*, **5**, 320.  
 „ „ *Ibid.*, **5**, 556.

## AN EXTERNALLY COATED PYREX G-M COUNTER

By M. YASIN, R. AHMED AND P. S. GILL

*(Received for publication, January 13, 1951)*

**ABSTRACT.** A Geiger-Muller counter, using an externally coated pyrex envelope, is reported as possessing a plateau of more than 1600 volts. Some other properties of this counter are also described, together with a tentative explanation of its characteristics.

## INTRODUCTION

The Geiger-Muller counter, being one of the most sensitive detectors of radiation, is needed in many branches of scientific research. In view of this, various attempts have been made in the past to improve the technique of production, so that a large number of reliable counters can be easily and cheaply made available to scientific workers.

Rochester and Janossy (1943) reported preparation of counters which had not been chemically treated and which were quite efficient for coincidence work. In order to obtain a better geometry, all-metal counters have been widely reported (Korff, 1943; Neher, 1946; Regener, 1947) but they involve many technical problems. Internal coating of glass tubes by copper evaporation method has been practised in some laboratories (De Vos and Du Toit, 1945) and since it obviates the necessity of surface oxidation, it can be considered a definite step forward in the development of Geiger counter production techniques. However, an internal coating of some conducting paint, such as commercial aquadag, is just as efficient as an evaporated layer of copper, and for this reason aquadag-coated counters are at present widely employed. In fact, in order to make the construction still simpler, Maze (1946) reported the use of soft glass with an external coating of conducting material. These counters were found to have a plateau of as much as 400 volts and a slope which was less than that of internal cathode counters.

In this laboratory, since we were faced with the problem of manufacturing a large number of rugged but reliable counters under the circumstances that metal tubing itself is hard to obtain, work was undertaken to further improve the techniques of counter production. At first, soft glass tubes were coated by commercial aquadag and the G-M counters so produced were found to be highly photo-active. This defect was removed by painting the entire counter with a non-conducting black paint. Further, in order to study the effect of the material of the counter envelope, some pyrex tubes were similarly prepared and they exhibited the properties mentioned below.



### *Plateau and Slope*

Conventional G-M counters are considered to be very satisfactory if they have a plateau of about 300 volts, and a slope of 1 to 2% per 100 volts. In the case of externally coated pyrex G-M counters, the threshold potential was found to be slightly higher than that of comparable internal cathode counters, but the plateau was found to be nearly five times longer. In some carefully prepared tubes, the plateau turned out to be even 2000 volts, and it had a slope of less than 0.4% per 100 volts. The characteristics of conventional and new type of counters are shown in Fig. 1 and it is obvious that the plateau and slope of the latter are superior to those of the former.

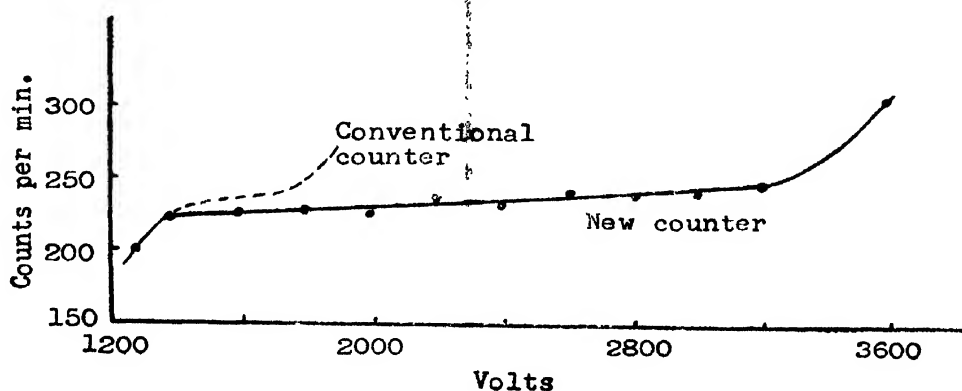


FIG. 1

The plateau characteristic of an externally coated pyrex counter: argon and alcohol 9 and 1 cm of mercury respectively, internal diameter 23 mm, external diameter 36 mm, 7 mil central tungsten wire, observed plateau 1800 volts, slope better than 0.4% per 100 volts.

### *Threshold voltage and pulse size*

As stated above, under normal operating conditions, due to the presence of glass between the anode and cathode, the threshold potentials of these counters are generally higher than those of conventional counters of similar dimensions and gas pressure. The threshold voltage appears to increase if the number of counts that have to be recorded increases. This apparent change of threshold voltage is due to the fact that there is a decrease in pulse size if the rate of counting is high. This does not, however, affect the length and the slope of the plateau, which under these conditions, extend to higher voltages. It is obvious that when the size of the pulses diminish beyond the minimum amplitude necessary for operating the scaler, the number of counts recorded by the system goes down, and in order to restore counting, the applied voltage has to be increased. Fig. 2 shows the variation of pulse size and threshold voltage with the number of counts that have to be recorded. This figure shows that even when the rate of counting

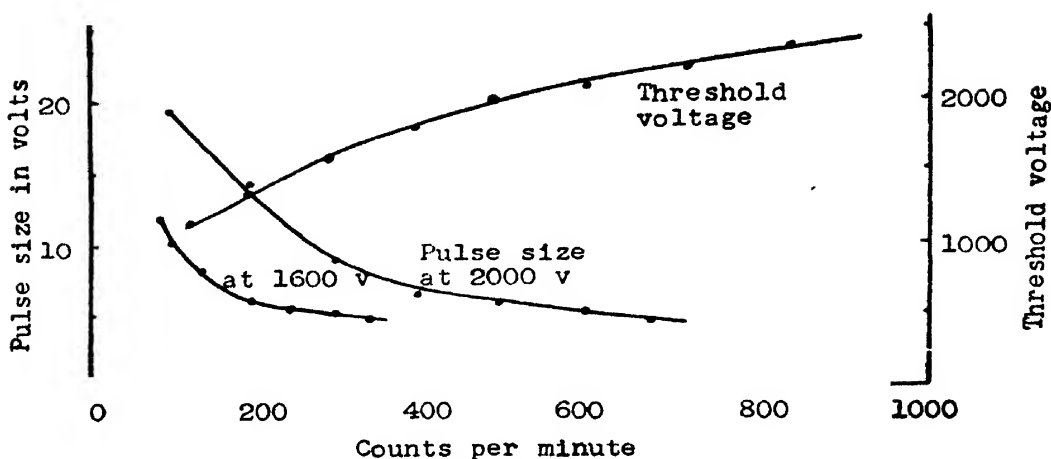


FIG. 2

The reduction in pulse size and the increment in threshold voltage observed with a scaler of 5 volts sensitivity. Same counter as used for plateau characteristic shown in Fig. 1.

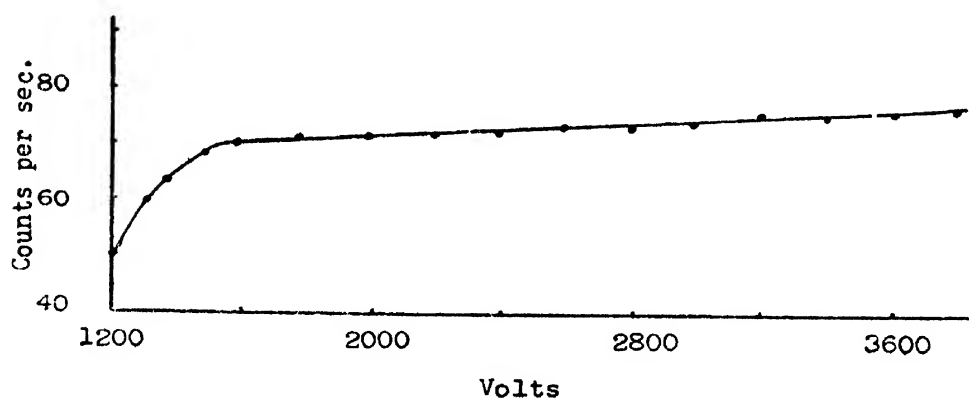


FIG. 3

The plateau characteristic of an externally coated pyrex counter with higher rate of counting. The counts were obtained from a beta ray source, and a single tube pre-amplifier was used at the input of the scaler whose sensitivity was 5 volts. This counter was different from the one used for Fig. 1 but its dimensions were the same.

becomes quite high, the pulse size, instead of continuing to diminish, becomes more or less stabilized. As can be expected, the use of a pre-amplifier to increase the sensitivity of the scaler brings the threshold voltage almost to its original value. The counter is thus capable of efficiently recording radiations producing up to several thousand impulses per minute. Fig. 3 gives a curve of the tube's performance when the rate of counting is high.

*Dead time*

The dead time of the counter, measured by the trigger method suggested by Stever (1942), was found to be about  $3 \times 10^{-4}$  sec. This does not compare too unfavourably with dead times of the order of  $2 \times 10^{-4}$  sec generally reported for internal cathode counters, and indicates that there is no reason to consider the new counter to be inherently much slower than the conventional ones.

## TENTATIVE THEORY OF OPERATION

The difference in the mode of operation of the externally coated counters and those which have internal cathodes can be explained by putting three questions, namely, (1) Why does pulse size decrease with greater strength of incident radiation? (2) Why is the slope so small? (3) Why is the plateau so long? In order to answer these questions it is appropriate to mention briefly the discharge mechanism and the action of the quenching gas in conventional counters.

When an ionizing particle passes through the counter it leaves some ion pairs, and from these pairs electrons start moving towards the central wire. As they proceed into the region of intense electric field, the energy of the electrons rapidly increases and they produce further ionisation by collision. This avalanche spreads along the length of the wire by photon action and leaves positive ions in the form of a sheath all round the central wire. Due to the presence of this sheath between the anode and the cathode, the field in the anode region is reduced beyond the threshold value so that no further ionising event can produce another avalanche before the sheath has had a chance to move out towards the cathode by a certain critical distance. The photons which are formed by recombination of a certain number of ions are absorbed by the quenching polyatomic gas and spurious counts are avoided.

The quenching gas chosen is such that its ionising potential is lower than that of the noble gas used in filling the counter. On account of this fact the positive ions of the noble gas pass their ionization on to the molecules of the polyatomic gas. Again, photons released in this process are absorbed by the quenching gas, and finally it is the positive ions of the polyatomic gas that reach the cathode. When this ion sheath reaches within about  $10^{-7}$  cm of the cathode, electrons are taken out from the latter for neutralizing the ions. Photons are not emitted in this process because energised polyatomic molecules dissociate within about  $10^{-13}$  sec. (for alcohol), that is, before they can emit photons which require about  $10^{-8}$  sec. This is the most important function of the quenching gas and is responsible for the plateaus in conventional counters.

In the case of external cathode counters the ion sheath is not able to approach within  $10^{-7}$  cm of the cathode and therefore, instead of being neutralized, a good part of it stays on the surface of hard glass. Very soon,

at a particular counting rate, a balance is reached between the rate of accumulation and the rate of neutralization, resulting in the stabilization of the surface sheet of charge. This results in the reduction of the effective voltage on the counter and is responsible for the extraordinarily long plateau. When the average rate of counting increases, the sheath becomes even more positive and thus reduces the size of the pulses that are transmitted to the counting system. It has already been explained in a previous section how this can be overcome either by increasing the applied voltage or by using a pre-amplifier at the input of the scaler.

In conventional counters the plateau comes to an end when spurious counts increase enormously and discharge becomes self-maintained. These spurious counts are produced by unquenched photons formed either during recombination or during the process of neutralization of the ion sheath. In the external cathode counters photons have to pass through a region of ionized polyatomic gas molecules before they can reach the glass surface. This increases the probability of absorption of the photons and makes the slope of the plateau so small.

The idea of the formation of a surface layer is supported by other observations such as :

(1) the plateau is shorter in a freshly filled counter than in one which has been used for some time,

(2) when voltage is suddenly brought down from a high value to the threshold voltage, counts are only observed a few seconds after this change has taken place.

Further investigation is being carried out on this counter but it now appears certain that this type of counter has considerable advantages over the conventional one, since it is rugged and cheap and can be operated with inexpensive unregulated high voltage supplies.

MUSLIM UNIVERSITY,  
ALIGARH, U. P.

#### REFERENCES

- Beers, Y. 1942, *Rev. Sci. Inst.*, **13**, 72.  
 De Vos, P. J. G. and Du Toit, S. T., 1945, *Rev. Sci. Inst.*, **16**, 270.  
 De Vos, P. J. G. and Gurgun, K., 1946, *Rev. Sci. Inst.*, **17**, 516.  
 Korff, S. A., 1946, *Electron and Nuclear Counters*, D. Van Nostrand and Co.  
 Korff, S. A. and Present, D., 1944, *Phys. Rev.*, **65**, 274.  
 Maze, R., 1946, *Jour. de Phy.*, **6**, 164.  
 Montgomery, D. D., and Montgomery, C. G., 1945, *Phys. Rev.*, **67**, 1030.  
 Neher, H. V., 1946, *Modern Physical Laboratory Practice*. Blackie and Son Ltd.  
 Regener, V. H., 1947, *Rev. Sci. Inst.*, **18**, 267.  
 Rochester, G. D. and Janossy, L., 1943, *Phys. Rev.*, **63**, 52.  
 Stever, H. G., 1942, *Phys. Rev.*, **61**, 38.

# ON THE ABSORPTION OF U. H. F. RADIO WAVES IN SOME ALIPHATIC KETONES DISSOLVED IN NON-POLAR SOLVENTS.\*

By S. N. SEN.

*(Received for publication, March 28, 1951)*

**ABSTRACT.** The absorption of ultra-high frequency radio waves in solutions of different concentrations of aliphatic ketones in benzene and also in solutions of a particular concentration in different solvents has been studied in the frequency range 250-510 Mc/sec. It has been observed that the heights of the absorption peaks decrease greatly in all cases when the pure liquid is dissolved in the solvent to make even a 80% solution and the curves become flatter and flatter as the dilution is increased, except in the case of ethyl isobutyl ketone in which case the height of the peak tends to attain a constant value with increase of dilution.

It is further observed that the maximum in the absorption curve shifts towards higher frequencies both with dissolution and increase in dilution of the solution. It is suggested that the diminution in the height of the absorption peak is due to breaking of associated groups of molecules and the shift is due to change in the internal viscous forces acting on the polar molecules caused by the surrounding non-polar molecules of the solvent.

## INTRODUCTION

It was observed in some previous investigations (Sirkar and Sen, 1949; Sen, 1949, 1950, 1951) that, except in a few cases, the height of absorption peak observed in the region 250 Mc/sec—510 Mc/sec in the case of some liquids having polar molecules increases and also the peak becomes sharper when the temperature of the liquid is lowered. It was suggested from these results that probably the arrangement of molecules is more regular at lower temperatures than at higher temperatures and therefore the field due to surrounding molecules has a well-defined value in the former case while variation from point to point in the arrangement of molecules at higher temperatures creates an inter-molecular field having values lying within a definite range at a definite temperature. It was also suggested that the intermolecular field might have influence on the value of the permanent electric moment of the molecule and in the case of highly anisotropic molecules large energies might be absorbed due to fluctuation of the permanent moment of the molecule occurring during the oscillation of the molecules in unison with the impressed oscillating electric field. The intermolecular field, however, is expected to be changed considerably if the polar molecules are

\* Communicated by Prof. S. C. Sirkar.

dissolved in solvents having non-polar molecules. The results might throw light on the question whether it is the macroscopic viscosity or something else which determines the relaxation time of the molecules. It was, therefore, thought worthwhile to study the absorption of U. H. F. radio waves in solutions in the cases of some liquids which in the pure state exhibit such an absorption in the region 250-510 Mc/sec. As it is already known (Whiffen and Thompson, 1946) that in the case of very dilute solutions of toluene the maximum absorption is observed only in the microwave region, only concentrated solutions of different strengths have been used in the present investigation and such absorption has been studied in solutions of some aliphatic ketones of different concentrations in benzene and also in solutions of a particular concentration of acetone and methyl ethyl ketone in benzene, heptane, carbon tetrachloride and cyclohexane.

#### EXPERIMENTAL

The experimental arrangement used to measure the absorption of ultra-high frequency radio waves has been described in detail in the previous papers (Sen, 1949, 1950 and 1951). All the liquids were chemically pure and were distilled three times before being used for taking observation. In the case of acetone and methyl ethyl ketone, solutions of strengths 80% and 60% by volume were prepared and in the case of diethyl ketone, dipropyl ketone and ethyl isobutyl ketone solutions in benzene of strengths 80%, 60% and 40% by volume were prepared. The absorption of U. H. F. radio waves in the region 250-510 Mc/sec were studied in the pure liquids as well as in these solutions.

In order to study the influence of solvents on the position of absorption maximum, 80% solutions of acetone and methyl ethyl ketone in benzene, heptane, carbon tetrachloride and cyclohexane were used. Graphs were plotted with attenuation coefficients as ordinate and corresponding frequencies as abscissa. From these graphs the value of the frequency for maximum absorption was obtained. The same process was repeated for all the liquids studied. In calculating the attenuation coefficient, the thickness of the liquid proportional to the concentration of the liquid was taken into consideration.

#### RESULTS AND DISCUSSION

The results for the solutions of different strengths in benzene have been shown graphically in figures 1, 2, 3, 4 and 5, and those for solutions of acetone and methyl ethyl ketone in different solvents are given in Tables I and II respectively. These latter results are also shown graphically in figures 6 and 7.

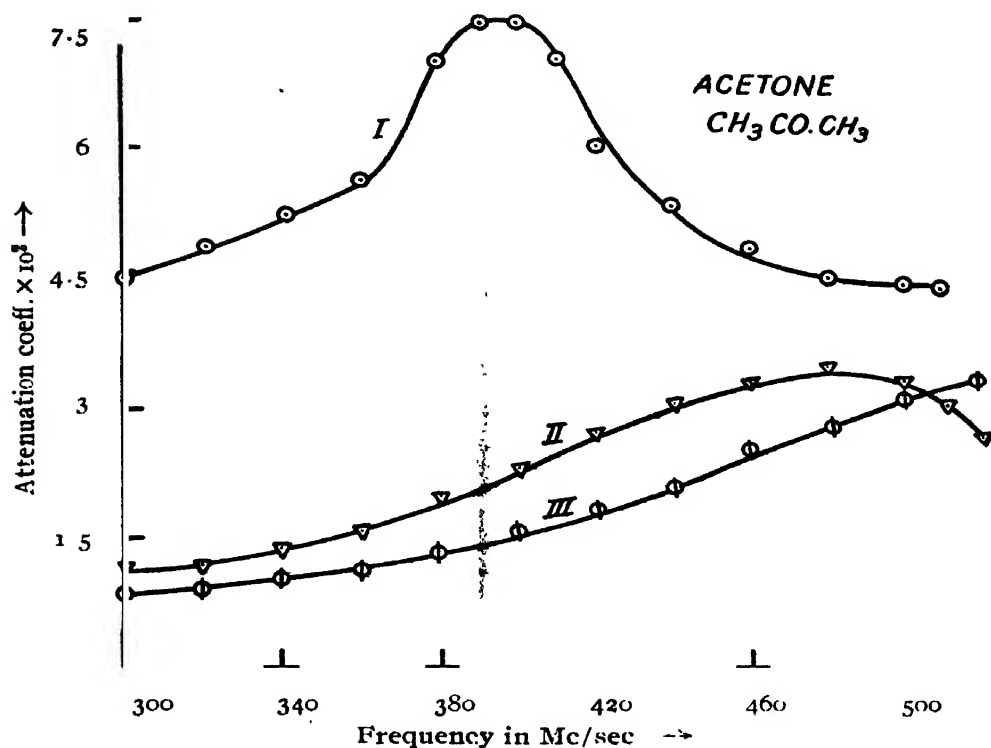


FIG. 1

I. Pure liquid, II. 80% solution in  $\text{C}_6\text{H}_6$ , III. 60% solution in  $\text{C}_6\text{H}_6$ .

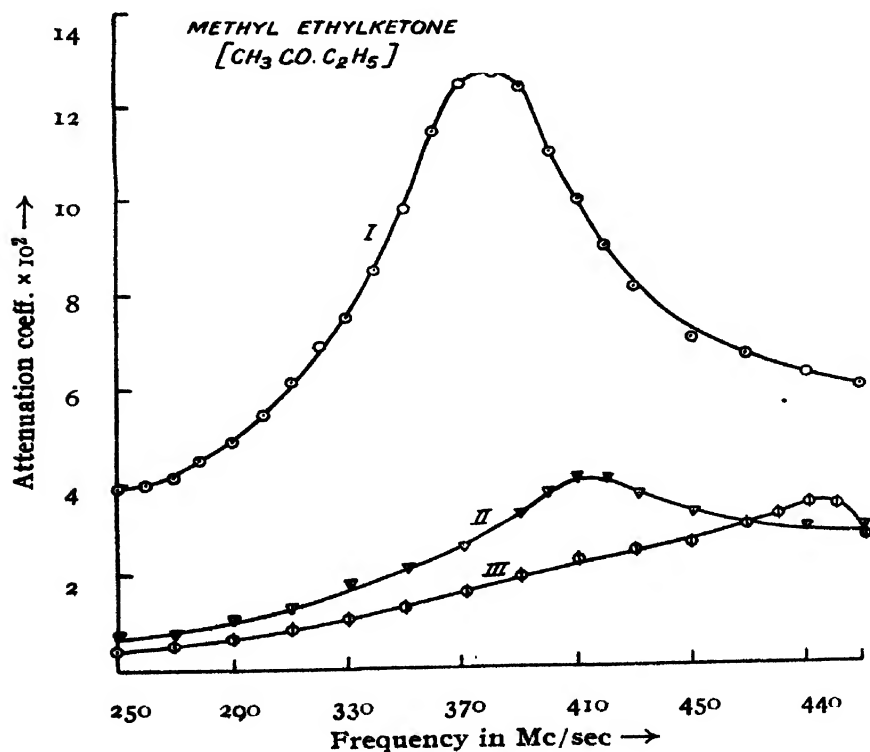


FIG. 2

I. Pure liquid, II. 80% solution in  $\text{C}_6\text{H}_6$ , III. 60% solution in  $\text{C}_6\text{H}_6$ .

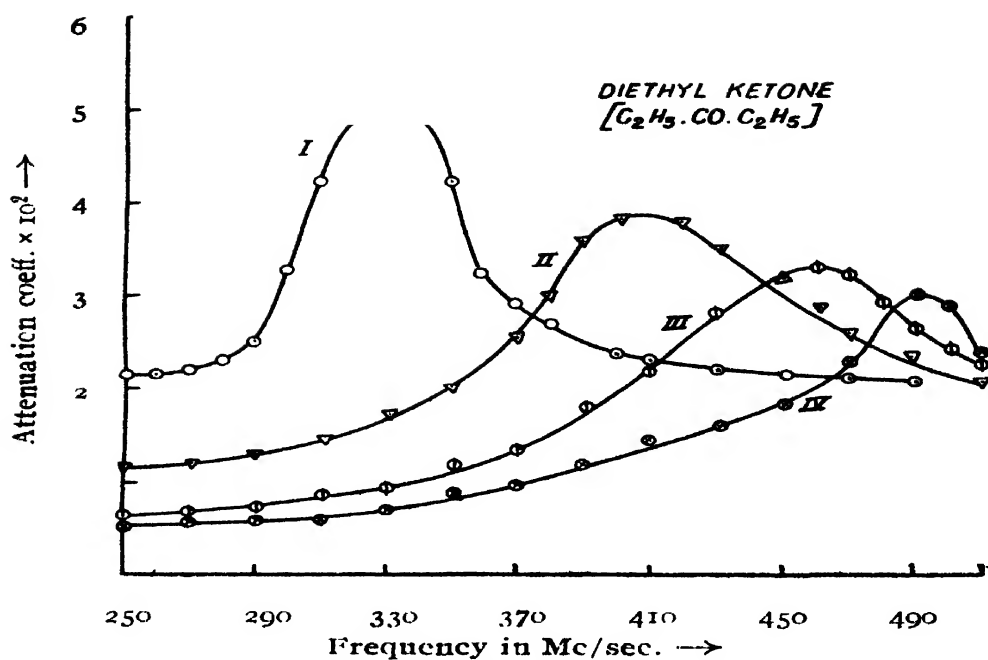


FIG. 3

- I. Pure liquid  
 II. 80% solution in  $C_6H_6$   
 III. 60% " " "  
 IV. 40% " " "

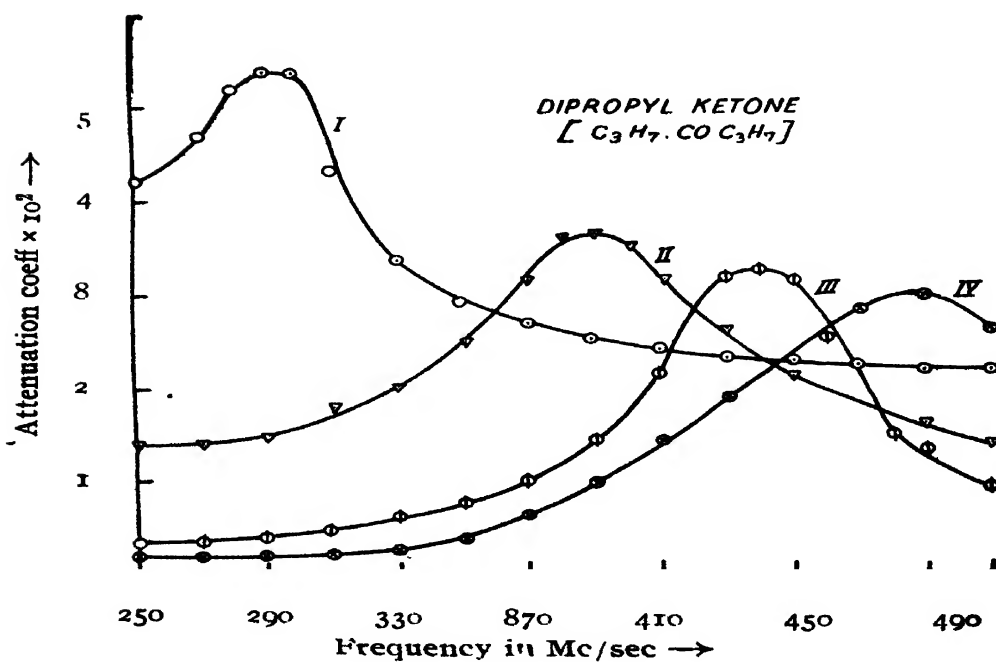


FIG. 4

- I. Pure liquid  
 II. 80% solution in  $C_6H_6$   
 III. 60% " " "  
 IV. 40% " " "



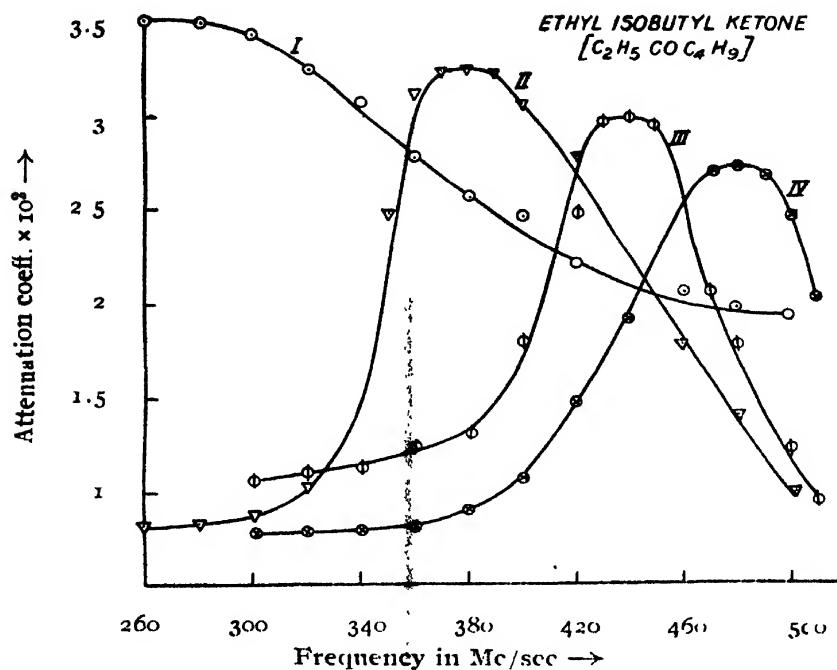


FIG. 5

I. Pure liquid, II. 80% solution in C<sub>6</sub>H<sub>6</sub>  
 III. 60% soln., IV. 40% " "

TABLE J

Attenuation co-efficient of acetone in different solvents.

Solvents.				
Frequency in Mc/sec.	Benzene	Heptane	CCl <sub>4</sub>	Cyclohexane
300	.0105	.0128	.0081	.0044
320	.0112	.0149	.0102	.0058
340	.0118	.0165	.0120	.0098
360	.0144	.0189	.0147	.0151
380	.0162	.0214	.0187	.0250
400	.0218	.0254	.0220	.0324
420	.0249	.0293	.0288	.0396
440	.0284	.0329	.0357	.0455
460	.0315	.0378	.0431	.0462
480	.0333	.0438	.0499	.0434
500	.0336	.0509	.0511	.0389
510	.0322	.0562	.0494	.0366

TABLE II

Attenuation co-efficient of methyl ethyl ketone in different solvents.

Solvents	Benzene	Heptane	Carbon tetra- chloride	Cyclohexane
Frequency in Mc/sec.				
250	.0070	.0070	.0035	.0058
270	.0073	.0091	.0046	.0088
290	.0114	.0109	.0063	.0108
310	.0126	.0145	.0086	.0151
330	.0182	.0175	.0116	.0173
350	.0277	.0203	.0144	.0202
370	.0252	.0256	.0189	.0254
390	.0324	.0270	.0235	.0316
410	.0392	.0301	.0284	.0355
430	.0358	.0336	.0311	.0352
450	.0322	.0382	.0340	.0327
470	.0308	.0429	.0352	.0296
490	.0291	.0473	.0338	.0280
510	.0280	.0529	.0284	.0252

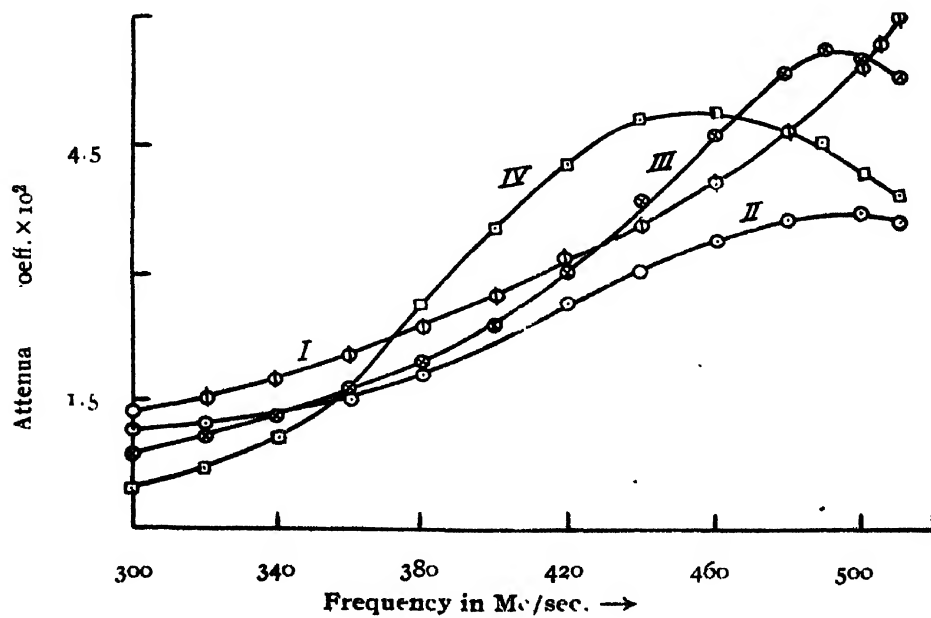


FIG. 6

I. Acetone—Heptane, II. Acetone—Benzene, III. Acetone—CCl<sub>4</sub>, IV. Acetone—Cyclohexane.

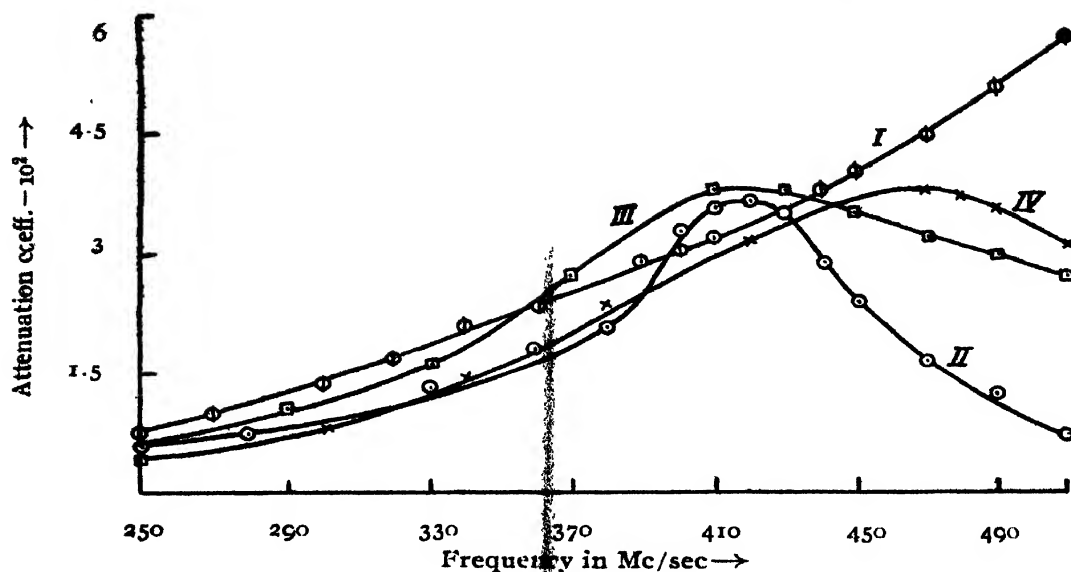


FIG. 7

- I. Methyl ethyl ketone—Hepthane  
 II. " " " —Benzene  
 III. " " " —Cyclohexane  
 IV. " " " —GCl<sub>4</sub>

## DISCUSSION

From the series of curves reproduced in figures 1–5, it is evident that the integrated intensity in the peak becomes smaller in all the cases when the liquids are dissolved in benzene and, except in the case of ethyl isobutyl ketone, the peaks become flatter with increase in dilution. In the case of ethyl isobutyl ketone, it is found that the peak becomes narrower as the liquid is dissolved in benzene and the width of the peak still decreases as the concentration is gradually decreased. The integrated absorption in the pure liquid, however, is much larger than that in the solution. This particular liquid shows an anomaly when absorption is studied in the liquid at different temperatures. Unlike other ketones, it shows a much broader absorption peak at the room temperature than at higher temperatures (Sen, 1951). In the case of the other ketones, on the other hand, the absorption peak becomes wider with rise of temperature of the liquids. It can thus be concluded from these results that in the case of these ketones the dissolution of the liquids in solvents has an influence on the absorption similar to that observed with increase in temperature of the pure liquid. The decrease in the height of the peak observed in the case of acetone and methyl ethyl ketone with dissolution in benzene is, however, much larger than that observed with increase of temperature of the liquid.

Since the effective thickness of the liquid in the solution has been taken in calculating the attenuation coefficient, it is evident that the diminution in integrated absorption indicates a diminution in the number of polar molecules set in

oscillation by the impressed oscillating field. In the case of acetone and methyl ethyl ketone, the number of such molecules diminishes to about  $1/10$ th of its original value even in solution of strength 80%. If the molecules of the solvent would only diminish the internal viscosity  $\eta$ , the peak would only shift towards regions of higher frequencies without having its height diminished appreciably. The molecules of the solvent thus seem to have a kind of influence different from this. Probably the actual unit responsible for absorption in the pure liquid is a group of associated molecules and probably most of these groups are broken up in the solution so that the single molecules show absorption at much higher frequencies beyond the range used in the present investigation and only a few of the groups persist in the solution. The influence of the molecules of the solvent on the internal viscosity being different at different points in the solution, the peak, which persists in the solution, is broader than that due to pure liquid. It may be mentioned in this connection that the radius of the rotor calculated from Debye's theory was found to be too high in the case of acetone (Sen, 1951). It is also interesting that frequencies of some of the Raman lines of acetone alter a little when the liquid is dissolved in carbon disulphide (Whiting and Martin, 1931).

If such a hypothesis be applied to the other three cases, it is seen that the breaking up of associated groups with increase in dilution of the solution takes place less rapidly, the rate being gradually slower for higher dilutions. For instance, in the case of 40% solution of dipropyl ketone the integrated intensity of the peak is about the same as that observed in the case of the 90% solution. Thus it appears that besides changing the internal viscosity, the solvent also breaks up groups of associated molecules.

This question can be more thoroughly investigated by studying the absorption in solution of a particular strength in different solvents because in that case the influence on internal viscosity would be different for different solvents. The data for solutions of acetone and methyl ethyl ketone in different solvents, given in Tables I and II and plotted in figures 6 and 7, show that the shift of the maxima in the absorption curve is different for different solutions. The curves, however, reveal the fact that the diminution in the integrated absorption is largest in the case of solution in benzene and smallest in the case of solution in  $\text{CCl}_4$ . Hence it can be concluded that anisotropy of the molecules of the solvent plays an important role in the absorption of U.H.F. radio waves by the solutions. Probably the anisotropic molecules offer a greater hindrance to the orientation of the polar molecules during oscillation of the molecules in unison with the impressed oscillating electric field than isotropic molecules.

An attempt may now be made to find out whether the frequency corresponding to the maximum in the absorption curve is determined by the

macroscopic viscosity or not. In the case of mixtures of two liquids the coefficient of viscosity  $\eta$  is given by the expression (Hatschek, 1930)

$$\eta^{\frac{1}{2}} = x\eta_1^{\frac{1}{2}} + (1-x)\eta_2^{\frac{1}{2}} \quad (1)$$

where  $\eta_1$  and  $\eta_2$  are the coefficient of viscosity of the two constituent liquids and  $x$  the volume fraction of one of the liquids. It is possible to calculate  $\nu_m$ , the frequency at the maximum in the absorption curve with the help of the data for the pure liquid by assuming that  $\nu_m$  is inversely proportional to  $\tau$  and using the values of  $\eta$  obtained from (1). This has been done and the results obtained are given in column 3 of Table III. The observed values are given in column 4. The values of  $\eta$  for the solutions given in column 2 of Table III are calculated from (1). The data given in columns 3 and 4

TABLE III

Comparative study of the absorption of U. H. F. electrical oscillations in solutions of ketones in different solvents.

Liquid	Viscosity in centipoise.	Frequency at maximum absorption Mc/sec	
		calculated	observed.
1. (a) Acetone (pure).	.3085		400
(b) 80% soln. in benzene.	.3340	363	503
(c) 60% soln. in benzene.	.3715	324	beyond 510
(d) 80% soln. in heptane.	.3019	405	beyond 510
(e) Do in $\text{CCl}_4$ .	.3798	323.5	497
(f) Do in cyclo hexane.	.3739	324.7	450
2. Methyl ethyl ketone (pure).	.3861		378
80% soln. in benzene	.3781	390	415
60% soln. in benzene	.3959	370	500
Do in heptane	.3817	382	510 beyond
Do in $\text{CCl}_4$	.4624	313.4	475
Do in cyclo hexane.	.4583	316.2	430
3. Diethyl ketone (pure)	.4228		330
80% soln. in $\text{C}_6\text{H}_6$	.4015	347.7	412
60% soln. „	.4474	312.2	460
40% soln. „	.4632	301	490
4. Dipropyl ketone (pure)	.5653		295
80% soln. in $\text{C}_6\text{H}_6$	.5098	327	390
60% soln. in $\text{C}_6\text{H}_6$	.5248	317	440
40% soln. in $\text{C}_6\text{H}_6$	.5349	300	490
5. Ethyl isobutyl ketone (pure)	data not available		250 (approx)
80% soln. in $\text{C}_6\text{H}_6$			378
60% „ „ „			440
40% „ „ „			480

show that the agreement between calculated and observed values is not quite good. The observed values of  $\nu_m$  are always higher than the calculated values. This indicates that if Debye's theory be assumed to be correct, the frictional forces acting on the polar molecules in the solution are smaller than those due to macroscopic viscosity.

## ACKNOWLEDGMENT

The author is indebted to Prof. S.C. Sirkar, D. Sc., F.N.I. for his kind interest and guidance during the progress of the work.

OPTICS DEPARTMENT,  
INDIAN ASSOCIATION FOR THE CULTIVATION OF SCIENCE,  
CALCUTTA.

## REFERENCES

- Hatschek, 1930, *Viscosity of liquids*.  
Sen, S. N., 1949, *Ind. J. Phys.*, **23**, 495.  
Sen, S. N., 1950, *Ind. J. Phys.*, **24**, 163.  
Sen, S. N., 1951, *Ind. J. Phys.*, **25**, 25.  
Sirkar, S. C. and Sen S. N. 1949, *Science & Culture*, **15**, 155.  
Whiffen, D. H. and Thompson H. W., 1946, *Trans. Farad. Soc.*, **42**, 122.  
Whiting, R. E. and Martin, 1931, *Trans. Roy. Soc. Canada*, **15**, 87.

# ON THE POISONING OF OXIDE-COATED CATHODE DUE TO ADSORPTION OF PARTICLES LIBERATED FROM THE ANODE

B. S. DEB

(Received for publication, January 29, 1951)

**ABSTRACT.**—The paper presents a theoretical treatment of the rate of decay of current due to adsorption of particles liberated from the anode of a valve using oxide-coated cathode. The cases of mobile and immobile adsorption are separately considered and graphical solutions for different conditions of the cathode surface and for different values of partial pressures of the poisoning agent are given. An approximate analytical solution of the problem is also given and this is found to predict a time constant of decay of current of about  $10^{-3}$  sec. under suitable conditions. It is shown that if one wants to ascribe the recently discovered phenomenon of pulsed emission decay in oxide-coated cathodes to adsorption of gases liberated from the anode, one must assume that the adsorption is mobile with low energy of activation the adsorbed particles in all probability being oxygen. On the basis of these assumptions attempt is made to explain the principal characteristics of the phenomenon. A number of experimental tests for the hypothesis is also suggested.

## INTRODUCTION

Early in the history of the development of oxide-coated cathodes, it was observed that their emission is adversely affected when exposed to gases like  $O_2$ , CO etc. Appreciable work on the subject was done by Becker and others (Becker, 1929) and their results showed that elimination of these gases from a radio valve by maintaining the highest possible vacuum is very necessary in order to preserve good thermionic efficiency for a long time. Improved vacuum techniques and powerful getters were therefore developed and with their help large emission and long life could be obtained simultaneously.

Nevertheless, it was known that these cathodes almost invariably showed a current decay immediately on application of the anode voltage. The decay continued in some cases even for a few minutes. On switching off the voltage a time of the same order was required for the cathode to regain its initial emission. This phenomenon could not be satisfactorily explained although the possibility that it might be due to gases liberated from the anode was not overruled. In recent years it has been discovered that with pulse voltage of micro-second's duration on the anode, a current larger than 10 times the current obtainable with d.c. voltage could be obtained from the same cathode. This phenomenon is also ascribed to another very sharp and recoverable decay of current which follows the application of anode voltage.

The time constant of this decay is  $10^{-4}$ — $10^{-2}$  seconds. Quite a number of papers have already been published on the subject and attempt has been made to trace the origin of this decay. Assuming that Fowler-Wilson theory of semi-conductor is applicable to thermionic emission from an oxide cathode, Coomes (1946) had tried to explain this on the argument that electrons from the impurity atoms in the oxide, which are thermally excited to the conduction band before the application of the anode voltage, are trapped so as to act as a reservoir for unusually high emission when the anode voltage is applied. A decay of current results as this reservoir becomes exhausted with the drawing of current. Sproull (1945) ascribed this decay to the electrolytic conduction of barium ions from the surface towards the interior of the cathode under the influence of anode voltage. This is countered by a process of diffusion of Ba atoms outwards and a steady condition is ultimately reached when the two rates of flow become equal. The theory gives a time of decay which agrees with experimental value but is unable to explain many other aspects of the phenomenon. Later, Wagerer (1949) modified Sproull's theory by assuming that the decay is due to electrolytic flow of negative oxygen ions outwards under the influence of the anode voltage. Very recent experiments, however, seem to indicate that nothing very fundamental is responsible for this short-time decay. Wright (1949) and Feaster (1949) have both shown that decay occurs only when the anode surface is contaminated with a poisoning agent. Wright has further shown that decay occurs only when the usual operating anode and the anode used in activating the filament are one and the same. This shows that the anode is probably contaminated with poisonous substances during the activation process and when current is drawn, these get ejected from the anode and travel on to the cathode surface to destroy its activities, in part, temporarily. The exact nature of these particles remains yet to be determined. It may also be mentioned that occurrence of a permanent decay due to gases released from the anode under electron bombardment was also suggested by the results of some earlier experiments (Jacobs 1946, Hamaker, Bruining and Aten, 1947). But time constant of this type of decay is much larger. In the present paper an attempt has been made to develop a mathematical expression for the rate at which the current decays as the surface becomes covered due to adsorption of poisonous particles liberated from the anode, and this has been used to examine how far such adsorption can be a factor in causing the short-time decay as described above. Interest is restricted only to the simplest types of adsorption phenomena.

#### FORMULATION OF THE MATHEMATICAL EQUATION

We will assume that electrons striking the anode surface liberate a large number of particles which travel on to the cathode surface and get adsorbed. As soon as a few particles have settled down an opposite phenomenon



of evaporation (or better we call it desorption) sets in. This process increases as the fraction of the available surface area covered up by adsorption increases. If  $N$  denotes the number of particles actually remaining on unit area of the surface, then

$dN/dt$  = rate of adsorption—rate of desorption.

Case (a).

*Mobile adsorption*—If we assume that the particles adsorbed are mobile on the surface then theory of absolute reaction rate gives us (*vide* Glasstone *et al* 1941)

$$\text{rate of adsorption} = N_g \frac{kT}{h} \frac{f_o}{f_g} e^{-E/kT} \quad \dots (1)$$

where

$N_g$  = Concentration of gaseous particles in front of the surface ;

$E$  = Energy of activation for adsorption ;

$f_o$  = Complete partition function of particles in the activated state ;

$f_g$  = Complete partition function of particles in the gaseous state ;

$k$  = Boltzmann's constant ;

$h$  = Planck's constant ;

$T$  = Absolute temperature.

$N_g$  is related to the current  $i$ . We assume that  $N_g = \alpha' i$ , where  $\alpha'$  is a constant dependant on anode voltage, the anode material and the nature of the particles and  $i$  is in amperes. We assume that the emission of an electron from the surface and the arrival of a poisoning particle liberated by it in front of the cathode are almost simultaneous. This is not correct. But for simplicity we can assume this, remembering that it will give us a somewhat flatter rate of adsorption particularly during the initial stages, *i.e.*, theoretical time of decay will be on the higher side on account of this assumption.

Rate of desorption will be proportional to the number of particles already adsorbed ; the theory of absolute reaction rate gives us,

$$\text{rate of desorption} = kT\beta N e^{-E'/kT} \quad \dots (2)$$

where  $\beta$  is a constant involving partition functions and  $E'$  is the energy of activation for desorption. We thus obtain

$$\frac{dN}{dt} = \alpha' i \frac{kT}{h} \frac{f_o}{f_g} e^{-E/kT} - kT\beta N e^{-E'/kT} \quad (2.1)$$

In order to express this equation in terms of the fraction  $\theta$  of area covered up by the adsorbed particles we note that

$$N = L\theta \quad \dots (2.2)$$

where  $L$  = number of particles required to completely cover up unit area of cathode surface. For a fully bare surface, this is  $10^{14} - 10^{15}$ . We note, however, that the area available for adsorption may be a fraction of the total cathode area. In such a case the value of  $L$  would be

Substituting in (2.1)

$$L \frac{d\theta}{dt} = \alpha i \frac{kT}{h} \cdot \frac{f_0}{f_a} e^{-E/kT} - LkT\beta\theta e^{-E'/kT} \quad \dots (2.3)$$

$$= \alpha i - AL\theta \quad \dots (2.4)$$

where

$$\alpha = \alpha' \frac{kT}{h} \cdot \frac{f_0}{f_a} e^{-E/kT} \quad \dots (2.5)$$

and

$$A = kT\beta e^{-E'/kT} \quad \dots (2.6)$$

It remains to express (2.4) in terms of current. To do this we follow the procedure adopted by Sproull and Wagner. From experiments carried out by Becker (1929) with oxygen it is found that

$$\log i/i_0 = b(\theta_0 - \theta) \quad \dots (2.7)$$

where

$i_0$  = the limiting value of the current for large values of  $t$ ,

$\theta_0$  = value of  $\theta$  corresponding to  $i_0$ ,

$b$  = a slowly varying function of  $\theta$  and for changes in current of the order of 1 : 10 ; this may be taken as constant.

Differentiating (2.7)

$$\frac{1}{i} \frac{di}{dt} = -b \frac{d\theta}{dt} \quad \dots (2.8)$$

For (2.4), (2.7) and (2.8) we obtain

$$\begin{aligned} \frac{1}{i} \frac{di}{dt} &= -A \log \frac{i}{i_0} - \frac{b\alpha i}{L} + Ab\theta_0 \\ &= -A \log i/i_0 - Bi + C \end{aligned} \quad \dots (2.9)$$

where

$$\left. \begin{aligned} B &= \frac{b\alpha}{L} \\ C &= Ab\theta_0 \end{aligned} \right\} \quad \dots (2.10)$$

Equation (2.9) is difficult to be solved mathematically. It is easier to find a solution by graphical method. Separating the variables and integrating we obtain,

$$t = \int \frac{di}{i \left[ -A \log \frac{i}{i_0} - Bi + C \right]} \quad \dots (2.11)$$

In order to compute the value of this integral numerically, we have to estimate the values of the constants  $A$ ,  $B$  and  $C$ .

*Immobile Adsorption.* When the adsorbed particles are immobile we have from the theory of absolute reaction rate

$$\text{rate of adsorption} = N_a N_s \frac{kT}{h} \cdot \frac{f_0}{f_a f_s} e^{-E/kT}$$

$$= \alpha' i N_s \frac{kT}{h} \cdot \frac{f_0}{f_a f_s} e^{-E/kT}$$

where  $N_s$  = Number of vacant places available for adsorption/cm<sup>2</sup>

$f_s$  = Complete partition function of particle in the adsorbed state.

and  $f_0$ ,  $f_g$ ,  $h$ ,  $T$ ,  $E$ , and  $i$  have the same meanings as in mobile adsorption.

Rate of desorption =  $kT\beta N e^{-E'/kT}$ ,  $\beta$  and  $E'$  having the same meaning as in the case of mobile adsorption. We can write

$$\frac{dN}{dt} = \alpha' i N_s - \frac{kT}{h} \cdot \frac{f_0}{f_g f_s} e^{-E/kT} - kT\beta N e^{-E'/kT} = \alpha i N_s - A N \quad \dots (2.12)$$

where

$$\left. \begin{aligned} \alpha &= \alpha' \frac{kT}{h} \cdot \frac{f_0}{f_g f_s} e^{-E/kT} \\ A &= kT\beta e^{-E'/kT} \end{aligned} \right\} \quad \dots (2.13)$$

We assume that

$$N = L\theta \text{ and } N_s = L(1 - \theta)$$

Expressing (2.12) in terms of  $\theta$

$$\frac{d\theta}{dt} = \alpha i (1 - \theta) - A\theta = \alpha i - \theta(A + \alpha i) \quad \dots (2.14)$$

Eliminating  $\theta$  in terms of  $i$  with the help of equation (2.7),

$$-\frac{1}{bi} \frac{di}{dt} = \alpha i + \frac{\log \frac{i}{i_0} - b\theta_0}{b} (\alpha i + A) \quad \dots (2.15)$$

This can be rearranged and rewritten as

$$\begin{aligned} \frac{1}{i} \frac{di}{dt} &= \alpha(b\theta - b + \log i_0) i - \alpha i \log i - A \log i + A(\theta_0 b + \log i_0) \\ &= Bi - \log i(\alpha i + A) + C \end{aligned} \quad \dots (2.16)$$

where

$$\left. \begin{aligned} B &= \alpha(b\theta_0 - b + \log i_0) \\ C &= A(b\theta_0 + \log i_0) \end{aligned} \right\} \quad \dots (2.17)$$

Integrating (2.16),

$$t = \int \frac{di}{i[Bi - \log i(\alpha i + A) + C]} \quad \dots (2.18)$$

To evaluate the integral numerically, we must estimate values of  $\alpha$ ,  $A$ ,  $B$  and  $C$ .

#### DETERMINATION OF CONSTANTS AND NUMERICAL COMPUTATION

(a) *Mobile adsorption.* We note that there is no time variation of current when the value  $i_0$  has been attained, i. e., for  $i = i_0$ ,  $\frac{di}{dt} = 0$

Substituting this boundary condition in (2.9), we obtain

$$C = Bi_0 \quad \dots (3.1)$$

Integral (2.11) can therefore be rewritten as

$$t = \int \frac{di}{i[+A \log \frac{i_0}{i} + B(i_0 - i)]} = \int \frac{di}{i(-A \log i - Bi + C')} \quad \dots (3.2)$$

where

$$C' = Bi_0 + A \log i_0 \quad \dots (3.3)$$

We now proceed to estimate the values of  $A$ ,  $B$  and  $C$ , for particular cases of decay.

We note that values of  $A$  and  $C'$  can be calculated in terms of  $B$  by means of (2.11), (3.1) and (3.3). Let us, therefore, estimate the value of  $B$  first.

For mobile adsorption the gaseous and activated particles will have almost identical degrees of rotational and vibrational freedom. For evaluation of the ratio  $f_0/f_a$  we are thus left with the consideration of the contribution due to translation alone. Since there are three degrees of translation in the gaseous state and two degrees in the activated state. (*Vide* Glasstone *et al*, 1941).

$$\frac{f_0}{f_a} \simeq \sqrt{\frac{h}{2\pi m k T}}$$

with

$$T = 1000^\circ \text{K} \text{ and } m \simeq 10 - 100 \text{ atomic units}$$

$$\frac{f_0}{f_a} \simeq 10^{-9}$$

also  $\frac{kT}{h} \simeq 2 \times 10^{13}$ . It remains only to find a probable value of  $b$  and  $\alpha$ .

At  $t=0$ ,  $\theta=0$  and  $i=i_m$  (say)

From (2.7)

$$\frac{i_m}{i_0} = e^{b\theta}.$$

Let us assume that the decay is such that  $\frac{i_m}{i_0} = 10$  and 100. It may be noted

that the usual value of the ratio between the pulsed and d. c. current obtainable from an oxide cathode is roughly of this order. We thus get

$$\text{for } \frac{i_m}{i_0} \simeq 100, b\theta_0 \simeq 4.6$$

$$\text{and for } \frac{i_m}{i_0} \simeq 10, b\theta_0 \simeq 2.3$$

We have no information about  $\theta_0$ . It may be noted that value of  $B$  is determined mainly by  $\alpha$  and  $L$ . It does not change appreciably even if  $\theta_0$  is varied over a range .1 to 1. So let us put  $\theta = .5$  so that

$$\text{for } \frac{i_m}{i_0} = 100, b = 9.2$$

$$\text{and for } \frac{i_m}{i_0} = 10, b = 4.6$$

To determine  $\alpha'$  we must have some idea about the partial pressure of the adsorbed gas. Ordinarily, the pressure inside a valve is of the order of  $10^{-6}$  mm of Hg. It is difficult to estimate the partial pressure of the poisoning agent unless we know something about its nature. Without entering into any discussion about the precise nature of the poisoning agent, let us assume that the initial partial pressure of the poisoning agent inside the valve is of the order of  $10^{-8}$  mm of Hg. On application of the anode voltage, the pressure suddenly increases to a high value  $p_1$ . It then decreases as the current decays and attains a final equilibrium value  $p_2$  such that

$$\frac{p_1}{p_2} \approx \frac{i_m}{i_0}$$

and  $10^{-6}$  mm  $> p_2 > 10^{-8}$  mm. Let us assume that  $p_2$  is greater than the initial partial pressure by about an order. On this assumption we obtain

$$\alpha \approx 2 \times 10^9 / \text{amp.}$$

For a fully bare surface  $L$  is  $10^{14} - 10^{15}$ . We, however, note that the cathode surface may be already covered by Ba and oxygen to a large extent. In that case the full surface will not be available for adsorption. If 1/10th of the surface is only available  $L$  will have a value of  $10^{14} - 10^{13}$ . If 1/100th of the surface is available then  $L$  will be between  $10^{13}$  and  $10^{12}$ . We will try to obtain solutions for all these three values of  $L$ . For a rapid process and also for the case when the adsorbed particles are atomic, the energy of activation is very small. These conditions probably exist for the short-time decay that is observed. Such decay, however, shows a slowing down with lowering of temperature. This suggests that energy of activation should be appreciable. Blewett (1939), who ascribed the decay to diffusion inside the body of the oxide, found that the activation energy of diffusion is about .7 volt. Rate of diffusion and adsorption are expressible in the same form., viz.,  $Re^{-E/kT}$  and if it is ascribed to adsorption, the activation energy should come out to be of the same order. Blewett, however, confined his calculations to decay which lasted for several minutes and as such his results may be taken as the upper limit of the usual values. For decays which occur within a few micro- or milli-seconds, a value of .2 to .3 volt might be a more balanced estimate. In the absence of any precise data on the relative rates of decay at various temperatures a more correct estimate is not possible. That the energy of activation for short-time decay is not large compared with the thermal energy

of the particles is also shown by the fact that activity of the cathode is quickly restored when the plate voltage is switched off, a pulse recurrence frequency of even 300 with several tens of micro-seconds duration being unable to affect any change in the pulsed current. We thus conclude that while for long period decay  $E$  may be large, for short time-decay its value will be within the range of 0–.2 volt. Attempt will be made to obtain the solutions for the two cases when  $E=0$  and  $E=.2$  volt.

Values of  $A$ ,  $B$  and  $C'$ , calculated for various values of  $L$  and  $E$ , have been shown in Table I.

Solution of equation (3.2) obtained with the various sets of values of the constants have been shown graphically in figures 1–4.

It may be noted from Table I that the value of  $A$  is always less than that of  $B$  by more than an order. If, therefore, as a first approximation we neglect the term  $A \log i/i_0$  in the denominator of the r. h. s. of equation (3.2), we obtain

$$t = \int \frac{\alpha i}{Bi(i_0 - i)} di$$

This is readily integrable and it can be easily shown that the final solution is

$$i = \frac{i_0}{1 - De^{-Bt}} \quad (3.4)$$

where

$$D = \frac{i_m - i_0}{i_m} \quad \dots (3.5)$$

and

$$\text{at } t=0, i=i_m$$

Time required for the current to fall to  $\frac{1}{e}$ th of its initial value is given by

$$\tau = - \frac{1}{Bi_0} \log \frac{i_m - ei_0}{i_m - i_0} \quad \dots (3.6)$$

and this may be defined as the 'time constant' of the decay. As an example, we may take the case of the set No. 3. in Table I, i.e., the case of adsorption with zero activation energy on a surface whose 1/10th part is available for adsorption and which leads to a decay of current from 10 to .1 amp.

For this case,

$$\tau \approx 10^{-3} \text{ sec}$$

This agrees well with the value observed for the pulsed decay of current.

(b) *Immobile adsorption* :—

If we assume  $\frac{di}{dt} = 0$  for  $t=0$  we obtain from (2.14)

$$A = \frac{\alpha}{a} (1 - \theta_0) i_0$$

so that

... (3.7)

$$C = \frac{\alpha i_0}{a} (1 - \theta_0) (b \theta_0 + \log i_0)$$

When the adsorbed particles are immobile, and presumably also are the activated complexes,  $f_0$  and  $f_s$  will not have any contribution due to translation. Rotation can also be neglected.  $f_0$  will have contributions due to three degrees of translatory motion. If the particles are atomic there will not be any contribution to it due to rotation and vibration and we can therefore write

$$\frac{f_0}{f_0 f_s} = \frac{h^3 b_0}{(2\pi m k T)^{3/2} b_s}$$

where  $b_0$  and  $b_s$  are the contribution to  $f_0$  and  $f_s$  respectively due to vibration. Taking the ratio  $b_0/b_s$  as sensibly equal to unity

$$\frac{f_0}{f_0 f_s} = 10^{-}$$

value of  $\alpha'$  will be the same as in the case of mobile adsorption if the same values of current and pressures are assumed. For the same ratio of  $i_m$  to  $i_0$  the values of  $b$  and  $\theta_0$  will also be the same as before. The constants  $A$ ,  $B$  and  $C$  can therefore be calculated. These are given in Table II. The rate of adsorption comes out as independent of  $L$ . It shows that the rate of activation must either be independent of the amount of vacant space available or that the theory developed is applicable only to a fully bare surface. If the former conclusion is correct, then the results obtained should be taken at their face values. If, however, the latter conclusion is correct, then a modified theory for a partially covered surface should be developed. It is likely that the modified theory would give a lower rate of decay compared to that given by the present theory. As will be seen presently, the present theory gives too low a rate of decay compared to the experimentally observed values. Results obtained from the modified theory are, therefore, likely to be in worse agreement with experimental facts.

## RESULTS AND THEIR DISCUSSIONS

Results obtained with different sets of values of  $A$ ,  $B$ ,  $C$  etc., in Tables I and II are shown graphically in Figs. 1, 2, 3 and 4. Curve 1 in Fig. 1 is for the following set of values :

$$i_m = 10, \quad i_0 = 1 \text{ and } E = 0;$$

TABLE I

	$i_a$ (amps)	$i_c$ (amps)	$L$	$E$ (volts)	$A$	$B$	$C$	$C'$
1	10	.1	$10^{12}$	0	+8	$3.68 \times 10^2$	$+3.68 \times 10^1$	$1.84 \times 10$
2	"	"	"	.2	$+8 \times 10^{-1}$	$3.66 \times 10^1$	+3.68	1.84
3	"	"	$10^{13}$	0	$+8 \times 10^{-1}$	$3.68 \times 10^1$	+3.68	1.84
4	"	"	"	.2	$+8 \times 10^{-2}$	$3.68^2$	$+3.68 \times 10^{-1}$	$1.84 \times 10^{-1}$
5	"	"	$10^{14}$	0	$+8 \times 10^{-2}$	$3.68^{-1}$	$+3.68 \times 10^{-1}$	$1.84 \times 10^{-1}$
6	"	"	"	.2	$+8 \times 10^{-3}$	$3.68 \times 10^{-1}$	$+3.68 \times 10^{-2}$	$1.84 \times 10^{-2}$
7	10	1	$10^{12}$	0	$+8 \times 10^1$	$1.84 \times 10^2$	$+1.84 \times 10^2$	$1.84 \times 10^2$
8	"	"	"	.2	+8	$1.84 \times 10^1$	$+1.84 \times 10^1$	$1.84 \times 10^1$
9	"	"	$10^{13}$	0	+8	$1.84 \times 10^1$	$+1.84 \times 10^1$	$1.84 \times 10^1$
10	"	"	"	.2	$+8 \times 10^{-1}$	1.84	+1.84	1.84
11	"	"	$10^{14}$	0	$+8 \times 10^{-1}$	1.84	+1.84	1.84
12	"	"	$10^{14}$	.2	$+8 \times 10^{-2}$	$1.84 \times 10^{-1}$	$+1.84 \times 10^{-1}$	$1.84 \times 10^{-1}$
13	1	.1	$10^{12}$	0	+8	$1.84 \times 10^2$	$+1.84 \times 10^1$	0
14	"	"	"	.2	$+8 \times 10^{-1}$	$1.84 \times 10^1$	+1.84	0
15	"	"	$10^{13}$	0	$+8 \times 10^{-1}$	$1.84 \times 10^1$	+1.84	0
16	"	"	"	.2	$+8 \times 10^{-2}$	1.84	$+1.84 \times 10^{-1}$	0
17	"	"	$10^{14}$	0	$+8 \times 10^{-2}$	1.84	$+1.84 \times 10^{-1}$	0
18	"	"	"	.2	$+8 \times 10^{-3}$	1.84	$+1.84 \times 10^{-2}$	0

TABLE II

	$i_a$ (amps)	$i_c$ (amps)	$E$ (volts)	$a$	$A$	$B$	$C$
1	10	.1	0	$4 \times 10^{-5}$	$4 \times 10^{-6}$	$-2.76 \times 10^{-4}$	$9.2 \times 10^{-8}$
2	"	"	.2	$4 \times 10^{-6}$	$4 \times 10^{-7}$	$-2.76 \times 10^{-5}$	$9.2 \times 10^{-7}$
3	10	.1	0	$4 \times 10^{-5}$	$4 \times 10^{-5}$	$-9.2 \times 10^{-5}$	$9.2 \times 10^{-5}$
4	"	"	.2	$4 \times 10^{-6}$	$4 \times 10^{-6}$	$-9.2 \times 10^{-6}$	$9.2 \times 10^{-6}$
5	1	.1	0	$4 \times 10^{-5}$	$4 \times 10^{-6}$	$-1.84 \times 10^{-4}$	0
6	"	"	.2	$4 \times 10^{-6}$	$4 \times 10^{-7}$	$-1.84 \times 10^{-5}$	0



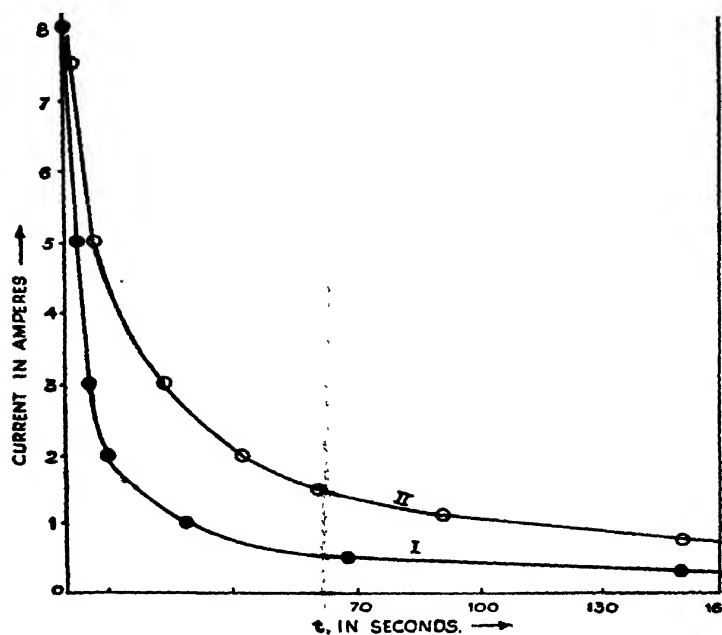


FIG. 1

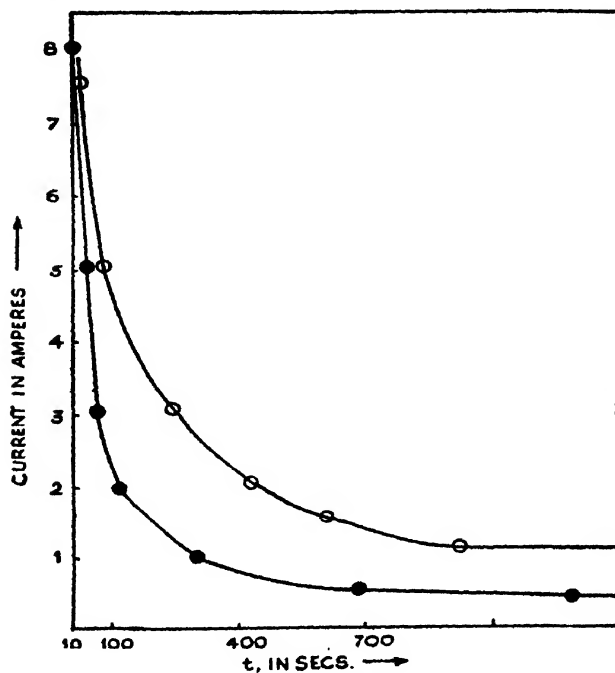
Decay curve for mobile adsorption;  $E=0$ ,(1)  $i_m=10$  amps,  $i_0=1$  amp; (2)  $i_m=10$  amps,  $i_0=1$  amp.The time scales are (i)  $t \times 10^4$  sec. (ii)  $t \times 10^3$  sec. (iii)  $t \times 10^3$  sec.

FIG. 2

Decay curve for mobile adsorption,  $E=.2$  volt(1)  $i_m=10$  amps,  $i_0=1$  amp; (2)  $i_m=10$  amps,  $i_0=1$  amp.The time scales are (i)  $t \times 10^4$  sec. (ii)  $t \times 10^3$  sec. (iii)  $t \times 10^3$  sec.

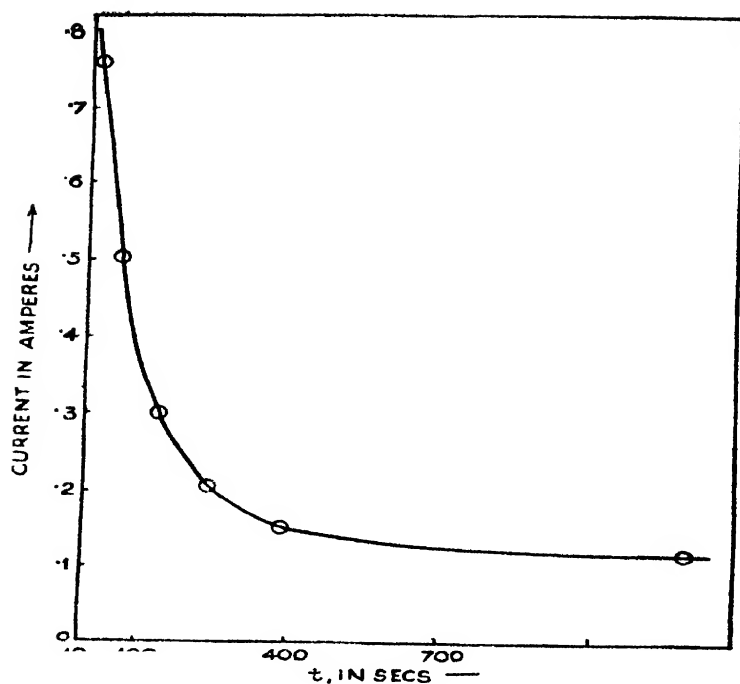


FIG. 3

Decay curve for immobile adsorption,  $E=0$ ,

$$i_m = 1, \quad i_0 = .1$$

The time scales are (i)  $t \times 10^4$  sec. (ii)  $t \times 10^3$  sec. (iii)  $t \times 10^2$  sec

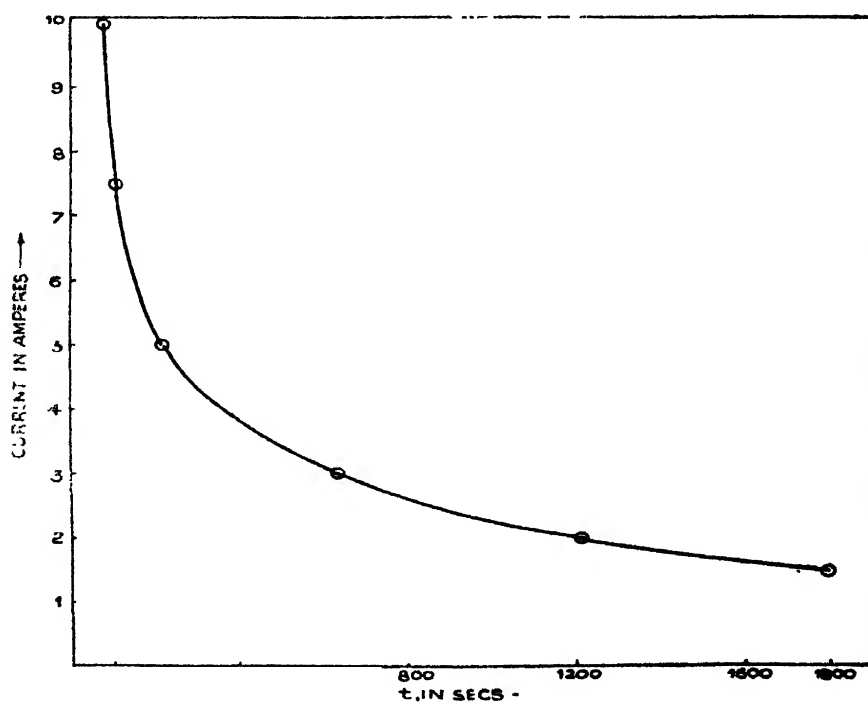


FIG. 4

Decay curve for immobile adsorption,  $E=0$ .

$$i_m = 10 \text{ amps.} \quad i_0 = 1 \text{ amps.}$$

and curve 2, for

$$i_m = 10, \quad i_0 = 1 \text{ and } E = 0.$$

The topmost time scale is for the case when  $L = 10^{12}$ , the middle scale for  $L = 10^{13}$  and the lowest scale for  $L = 10^{14}$ . Fig. 2. is for the same sets of values with  $E = .2$  volts. Fig. 3 is for the case

$$i_m = 1, \quad i_0 = .1 \text{ and } E = 0.$$

Here again the topmost time scale is for  $L = 10^{12}$ , the middle scale for  $L = 10^{13}$  and the lowest scale for  $L = 10^{14}$ . Fig. 4 is for the case of immobile adsorption with the following values:

$$i_m = 10, \quad i_0 = .1 \text{ and } E = 0.$$

This last curve shows that for a 100:1 decay of current to be observed with immobile adsorption a time of the order of a few minutes is required even if the energy of activation is taken as zero. With a value of .2 volt for the latter the decay will be a matter of about an hour. Although such time interval is often observed when the poisoning agent destroys the activity permanently, it is unknown to the recoverable type of decay. It might therefore, be concluded that immobile adsorption can cause only permanent decay and that during a time period of the order of  $10^{-4} - 10^{-2}$  second such a process cannot proceed to any material extent.

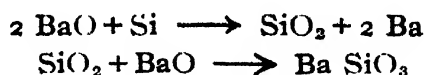
Let us now examine the curves for mobile adsorption. The common feature of all the curves under this category is that the bulk of the decay takes place within a very short time interval of the order of  $10^{-4} - 10^{-2}$  second. This is followed by a much slower rate of decay which lasts for .1 to a few seconds. An initial rapid decay of about  $10^{-4}$  second is found to occur for the following cases.

$$L = 10^{12} \text{ and } E = 0; \quad L = 10^{13} \text{ and } E = .2$$

i.e., either for a surface whose 1/100th part is available for adsorption and energy of activation is zero or, for one whose 1/10th part is available for adsorption and energy of activation is of the order of .2 volts. The nature of the adsorbed poison in both the cases should be such that during the process of decay its partial pressure should vary from  $10^{-6} - 10^{-7}$  or  $10^{-8}$  mm. of mercury.

Let us now examine what kind of poisonous particles liberated from the anode can affect change in emission current to a remarkable extent for a variation of partial pressure through this range. Whatever be the nature of these particles, it is certain that they find their way on to the anode during the period of activation of the cathode, as is also indicated by the experimental results of Wright (1949). Substances which are generally liberated from an oxide coated cathode during activation are CO, Ba, BaO and oxygen. CO is liberated through the reducing action of carbon contained as an impurity in the core of the cathode. Pulsed decay has, however, been observed in cathodes whose cores are free from carbon impurity. It

is therefore likely that CO does not cause the decay. Sproull obtained appreciable decay with a core which contained a very small amount of silicon as impurity. Silicon is an efficient reducing agent which liberates free Ba by the reactions



Equilibrium pressures of Ba for these reactions at  $1000^\circ \text{K}$  is pretty high, about  $10^{-6}$  cm (White, 1949). As the pressure necessary for causing the short time decay is also of the same order it is unlikely that Ba can cause the decay. For a decrease of pressure through 1 order near about the equilibrium value will require a large time interval and as such, short period decay is unlikely to be linked with Ba. Further, most generally accepted theories of thermionic emission from oxide cathode tell us that Ba is the active element responsible for emission. De Boer, in fact, assumes that isolated Ba atoms on the oxide-vacuum interface are the seats of emission. A decay in emission due to adsorption of Ba on the surface is therefore, unconceivable. BaO is liberated by evaporation from the surface. At  $1275^\circ \text{K}$ , the vapour pressure of BaO is about  $10^{-8}$  cm. of mercury which decreases to about  $10^{-13}$  cm. at  $1000^\circ \text{K}$ . (White, 1949; Blewett 1939). A process involving change of partial pressure from  $10^{-6}$  to  $10^{-7}$  or  $10^{-8}$  cm. at  $1000^\circ \text{K}$ . will occur well before the equilibrium state and hence a marked change accompanied by a 10:1 or 100:1 variation in current might become possible. Evaporation from the surface is, however, present all the while and is not particularly enhanced during activation. Further, even if appreciable deposit of BaO on the anode occurs, it is very likely that it will breakdown under the impact of oncoming electrons giving rise to free Ba and oxygen.

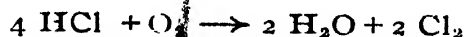
In the absence of any extreme reducing agent, oxygen is liberated by the dissociation of BaO according to the reaction



Equilibrium pressure of oxygen at  $1275^\circ \text{K}$  is of the order of  $10^{-16}$  cm at  $1000^\circ \text{K}$ ,  $10^{-12}$  cm of mercury (White, 1949). It would thus appear that at any given temperature evaporation of BaO would be a more pronounced effect than dissociation. The latter process, however, takes place both from the surface and in the volume of the oxide. During activation, oxygen liberated within the body of the oxide is urged towards the surface electrolytically and under this external stimulus the rate of loss of oxygen from the surface is enormously increased, which increases the pressure inside the valve, an increase of pressure to  $10^{-8}$  cm of Hg or so being quite general. Contamination of the anode by oxygen during activation is therefore likely to be heavy, and attainment of a pressure near about  $10^{-6}$  mm. due to the subsequent release of the particles under electron bombardment is also possible. Since this pressure lies far away from the equilibrium pressure for

dissociation, changes involving variations of 10 : 1 or 100 : 1 in emission within a very short time is also possible. This conclusion is further strengthened by the fact that oxygen is known to have a very adverse effect on thermionic activity of an oxide-coated cathode.

Another poisoning agent, likely to be released during activation is chlorine. This happens when the glass envelope and the electrode assembly are contaminated with HCl. The reaction is



Water is carried away by the pump and chlorine might remain adsorbed or as chloride in combination with any other metallic ions on the anode. It may also be noted that decay was observed by Feaster (1949) with an anode contaminated with NaCl and NaF. Ordinarily, however, the probability of contamination with oxygen is much higher than that of chlorine.

It therefore, appears that the short-time decay effect, in all probability, is connected with oxygen and to a lesser extent with chlorine and BaO. In further discussion it may be assumed that it is oxygen which is responsible for the decay. X-ray study shows that (Fineman and Eisenstein, 1946, Wagener, 1948) the surface of the oxide-cathode is composed of well-defined lattice of BaO when fully activated. A layer of SrO appears gradually as the cathode becomes more aged. The BaO lattices are not, however, perfect. There are many places which are deficient either in Ba or in oxygen giving rise to lattice defects. Regions with oxygen deficiency are, however, very large compared with the regions with barium deficiency (Wagener, 1948). It is not unlikely, particularly in view of the rapid rate of loss of oxygen atoms during activation, that region of oxygen deficiency would constitute roughly from .1 to .01th part of the total cathode area. Now, when adsorption occurs, it is likely that it will be mostly confined to these regions. Deduction that the observed time of decay also agrees with theoretical calculations when  $L$  is taken less than  $10^{14}$ , therefore, receives a very simple explanation.

Let us now examine if this picture of mobile adsorption of oxygen, mainly on the oxygen vacancies on the cathode surface, can explain the outstanding properties of the pulsed emission. These properties are the facts that :

- (i) Rate of decay is accelerated with increasing anode voltage and increasing anode current.
- (ii) Rate of decay is slower at lower temperature.
- (iii) Pulsed work function is equal to or higher than d.c. work function.
- (iv) Deviation from theory of Scottckey-effect is larger for pulsed emission.
- (v) The short-period decay is observed best in aged cathodes.

- (vi) Good pulsed emitters are also good d.c. emitters but the reverse is not always true.
- (vii) Rate of decay is independent of thickness of the coating and
- (viii) Pulsed decay of emission current is also accompanied by an almost similar decay of coating conductance.

An explanation for (i) may be suggested by assuming that  $\alpha'$  in (2.1.) increases with increase in anode voltage. In previous calculations value of  $\alpha'$  have been determined from an assumed value of pressure. In actual physical process, it happens the other way round, i.e., the value of  $\alpha'$  determines the pressure. The greater the anode voltage, greater will be the energies of the electrons bombarding the anode and hence the larger will be the value of  $N_0$  and hence of  $\alpha'$ . It is easy to see from equation (2.10) that this will increase the value of  $B$  and hence diminish the value of  $dt/di$ . In other words, this will increase the rate of decay. It is also evident from (2.9) that  $dt/di$  would decrease with increasing value of  $i$ , which might account for the higher rate of decay for larger currents. This is also evident from a comparison of curves 1, in figures 1 and 3. Assuming that a small but finite energy of activation exists for the process of adsorption, an explanation of (ii) is readily obtained. It should be noted that the non-exponential factor of (2.5) also varies directly as the square root of temperature. Thus with the decrease in temperature, value of  $B$  would decrease and that of  $dt/di$  increase. Thus due to this factor as well, rate of decay would be slowed down at lower temperature. However, this slowing down is likely to be almost of no consequence, compared with that caused by the exponential factor in the presence of a finite value of activation energy. A tentative explanation of (iii) can be suggested if we assume that the region on the oxide surface where oxygen is in deficit are also regions of higher work functions. Since these are the regions where adsorption is mainly confined, at the end of the process surface of higher work function almost cease emitting and we are left with emitting surface of lower work functions only. Under d.c. conditions we measure only this work function. Under pulsed condition, on the other hand, we measure the effective work function due to both the higher and lower values. D.C. work functions thus appear slightly lower than pulsed work function. This explanation is merely a suggestive one and there remains room for further development.

Accepting the explanation for work function, one can also readily explain (iv). Removal of surfaces of higher work function by adsorption renders the emitting surface more homogeneous so far as thermionic activity is concerned. At the end of the process therefore, the surface exhibits a lesser deviation from Schottky's theory.

Explanation of (v) is very easily suggested. Good d.c. emission may be obtained from a surface which has been affected to some extent by immobile adsorption. For these, there will not be any spectacular difference between the pulsed and the d.c. emission. A good pulsed emitter would be one with no initial effect due to immobile adsorption and with a very small fraction of

its area having a higher work function, (*i.e.* area having oxygen deficit). Such a cathode will have little space for mobile oxygen adsorption and hence d.c. emission will also be very high. For such cathode, probably work functions for pulsed and d.c. emission will not be very much different and a small but extremely rapid decay will be observed. This may be tested experimentally.

The theory requires that the rate of decay should not have anything to do with the thickness of oxide coating which agrees with (vi)

Diminution of coating conductivity with emission decay, *i.e.* (vii), may be due to increased insulation of the portion of the coating, bounded by the region of surface over which adsorption occurs.

That the short-period decay is more prevalent in aged cathode, *i.e.* (viii) can be explained on the assumption that with aging the regions having oxygen deficit are affected by long-period immobile adsorption. Thus the values of  $I$  must diminish with time. This will increase the value of  $B$  and hence diminish the value of  $dt/di$  more so during the initial stage when the current is high. Very short time effect therefore appears as the cathode gets aged. However, a simultaneous decrease in the ratio of pulsed to d.c. current should also be observed. Experimental works published so far do not mention this effect. The point should therefore be experimentally tested.

The picture of surface adsorption as the cause of emission decay does not appear to accord well with the Wilson-Fowler semi-conductor model of emission, but seems to agree more favourably with emission mechanism suggested by de Boer, according to which emission takes place from isolated Ba atoms on the surface of the oxide.

According to the mechanism suggested, the current should remain steady for some time till the arrival of the poisoning agent from the anode. The current pulses should, therefore, have a square-topped appearance at the initial stage for a time period of the order of micro-second. This is perhaps the reason why steady current pulses are always obtained with voltages of micro-second duration.

A point which is open to criticism is the assumed values of partial pressures of the adsorbed poison at the beginning and at the end of the decay process. In particular, the values of  $10^{-6}$  mm of Hg assumed at the initial stage for some of the cases might appear to be rather high. A lower value, on the other hand, would give a time of decay of the order of  $10^{-2}$  sec. or higher still if the value of  $E$  is appreciable. Such value does occur for some cathodes but a lower value is also obtained for many. It may, however, be noted that the values of partition functions have been calculated approximately. Rigorous consideration of contributions due to vibration and rotation is likely to give concordant results with lower values of partial pressures. Further, the relation between  $\theta$  and  $i$  is based on Becker's results which in all probability were for immobile adsorption. Mobility of adsorbed

particles is likely to affect the average emission current more adversely. A better  $\theta-i$  relationship might also give results consistent with experimental facts for lower values of partial pressures.

Mobility of adsorbed particles and low energy of activation which seem to be essential conditions for agreement between theory and experiment indicates that the adsorption is more of physical type. As the temperature is sufficiently high, activation with high energies is also likely to occur. This might, however, be an immobile process involving a very long time adsorption. The possibility of existence of such adsorption has been pointed out already.

#### CONCLUDING REMARKS

We are therefore, in a position to conclude that if pulsed decay of current is due to adsorption of gases liberated from the anode, it is likely to be due to oxygen which remains mobile after being adsorbed on the cathode surface.

It is to be admitted that numerical values of some of the constants used in calculation involves uncertainties. Because of this agreement obtained between theoretical and experimental results would appear to be more on the qualitative side. For quantitative results one must await the the availability of more precise experimental data. It is, however, likely, as is evident from some of the results already obtained, that the phenomenon does not involve any fundamental change in the structure of the cathode and that this will not necessitate the formulation of a new theory of emission from oxide-coated cathode. (Deb 1949; Feaster 1948.) Some of the earlier workers on the subject obtained results which did not support this idea. But these results have not been confirmed by other and a systematic investigation of the pulsed and d. c. emission properties of the same cathode in all their aspects should be made to test their contention. Other experimental tests might include

- (i) measurements of pulsed and d. c. work function of efficient pulsed emitters.
- (ii) measurement of variation of the ratio of pulsed to d. c. emission of a cathode as it gets aged.

#### ACKNOWLEDGMENTS

It is a pleasure to thank Prof. S. K. Mitra, Ghosh Professor of Physics, Calcutta University, who first interested the author in the subject and to Prof. M. N. Saha, Palit Professor of Physics, Calcutta University, for permission to to carry out the work and going through the manuscript. Thanks are also due to Dr. H. Rakshit, Associate Professor of Bengal Engineering College, Howrah, for kindly going through the manuscript and to Messrs U. C. Guha



and B. K. Banerjee of the Institute of Nuclear Physics, Calcutta University, for helpful discussion.

UNIVERSITY COLLEGE OF SCIENCE AND TECHNOLOGY,  
DEPARTMENT OF RADIO PHYSICS AND ELECTRONICS.  
CALCUTTA

REFERENCES

- Recker, J. A., 1929, *Phys. Rev.*, **34**, 1323.  
Blewett, J. P., 1939 (a), *Phys. Rev.*, **55**, 713.  
1939 (b), *Jour. App. Phys.*, **10**, 668 and 831.  
Deb, S., 1949, *Jour. Sci. & Ind. Res.*, **8**, 214.  
de Boer, J. H. 1935. *Electron Emission and Absorption Phenomena*, Cambridge University Press.  
Feaster, G. R., 1949, *Jour. App. Phys.*, **20**, 415.  
Fineman, A. and Eisenstein, A., 1946, *Jour. App. Phys.*, **16**, 663.  
Friedenstein, H., Martin, S. L. and Munday, G. L. 1946 47, *Rep. Prog. Phys.*, **11**, 298.  
Glasstone, S., Laidler, K. J., and Eyring, H., 1941. - *The theory of Rate Processes*, (McGraw Hills)  
Hamaker, H. C., Bruining, H. and Aten, A. H. W., (Jr.), 1947, *Phil. Res. Rep.*, **2**, 171.  
Jacobs, H., 1946, *Jour. App. Phys.*, **17**, 1595.  
Sproull, R. L., 1945, *Phys. Rev.*, **67**, 166.  
Wagener, S., 1948, *Proc. Phys. Soc.*, **61**, 521  
White, A. H., 1949, *Jour. App. Phys.*, **20**, 856.  
Wright, D. A. 1949, *Proc. Phys. Soc.*, **62**, 398.



# STUDIES IN FADING OF MEDIUM-WAVE RADIO SIGNALS

BY B. A. P. TANTRY AND S. R. KHASTGIR.

(Received for publication, December 9, 1950)

**ABSTRACT.** In the present investigation, intensity variations of the down-coming waves of medium radio frequencies from Delhi, Dacca, Lahore and Vijayawada Broadcasting stations as received at Banaras were studied in the evening and early night hours, there being no ground waves from these distant stations at the receiving point. Medium-wave signals from Lucknow, Patna and Allahabad Radio Stations were also received at Banaras and their intensity variations investigated.

The observations were made with a straight receiver having a suitable galvanometer in the balanced anode circuit of the detector valve. In most cases visual observations of the galvanometer deflections due to the varying intensities of the signals were made. In a few cases only the galvanometer deflections were recorded photographically on a rotating drum system.

The following types of fading patterns were observed :

- (i) Periodic or *quasi*-periodic fading of slow and quick periods.
- (ii) Random fading.

Regarding the observed periodic or *quasi*-periodic fading, there were two distinct orders of periodicity. The 'slow' periodicity has been attributed to the interference of the ordinary and extraordinary components of the wave in the ionosphere as described by Appleton and Beynon (1947). The comparatively 'quick' periodicity, which was also frequently observed, has been considered as due to the vertical movement of the ionospheric layer which usually takes place in the early morning or in the evening or early night hours. The Döppler-beat interpretation of this type of periodic fading is outlined and the expressions for the periodicity given.

The vertical velocity of the ionospheric layer, as computed from the Döppler-beat consideration of the so-called 'quick' periodicity, was found to be of the order of 3.5 metres/sec. during the evening or early night hours.

With regard to random fading observed with signals from distant stations, the analysis showed that the actual distribution curve did not agree with the Rayleigh's formula for random scattering. Rayleigh's formula is applicable to one downcoming wave only. With longer distances the existence of a number of waves following slightly different paths in the ionosphere may partly explain the discrepancy between the observed results and those computed from Rayleigh's formula. For more distant stations, more than one peak in the observed intensity distribution curve were observed. This must be due to the simultaneous single and double reflections from the E-layer.

## INTRODUCTION

It is generally known that with medium-wave radio signals from distant stations, the intensity-variation is of a random nature. With short-wave signals, however, periodic or quasi-periodic types of intensity variation are often observed, besides the random type of fading. The object of the present

investigation was to find whether any periodic variation prevailed in the reception of medium-wave signals from distant stations and to obtain a detailed knowledge regarding the nature and origin of such periodic fading, if and when it was observed. The object was also to analyse the random type of intensity variation observed with medium-wave signals. Signals from some of the broadcasting stations of medium wavelengths in India and Pakistan were therefore received at Banaras in the evening hours after sunset. The names, wavelengths, powers of these stations and their distances from Banaras are tabulated below.

TABLE I

No.	Broadcasting station.	Power in kw	Wavelength in metres.	Distance from Banaras in km.
1	Delhi	10.0	338.6	680
2	Dacca	5.0	257.1	775
3	Vijayawada	1.0	357.1	1050
4	Lahore	5.0	276.0	1145
5	Allahabad	1.0	389.6	120
6	Patna	5.0	265.3	224
7	Lucknow	5.0	293.5	268

In the case of the first four stations, the ground waves do not usually reach Banaras even in the night time. For the last three stations, ground waves are present along with the sky waves at the receiving station.

The usual modulated waves, when the programme was on, were studied. Measurements were made on a specially constructed straight receiver with a mirror galvanometer in the anode circuit of the detector valve, the steady anode current of which was balanced out. The galvanometer deflections  $\delta$  were noted at regular intervals of 10 seconds continuously for a long interval of time. An attempt was also made to record photographically the galvanometer deflections for varying intensities of the signals on a rotating drum-system.

In the present paper, the fading of signals, as indicated by the galvanometer deflections noted at intervals of 10 seconds, has only been considered. The observed periodic patterns have been classified and the origin of the fading pattern has been fully discussed.

#### EXPERIMENTAL ARRANGEMENTS

##### (a) Receiver with galvanometer at the detector output :

The circuit diagram of the receiving set used in the investigation is shown in figure 1. An outdoor aerial was used with the receiving set. For

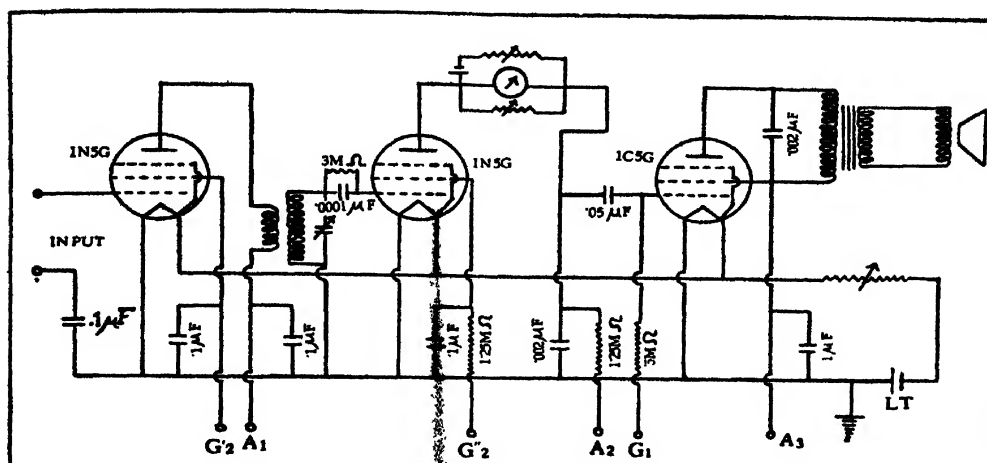


FIG. 1

absolute determinations of the field-strength, a loop aerial was also at times employed. The first valve (1N5-G) of the receiver was an H.F. amplifier followed by a transformer-coupled detector valve (1N5-G). A suitable current-sensitive mirror galvanometer was inserted in the anode circuit of the detector valve. The galvanometer was shunted by some suitable resistance and there was the conventional arrangement for balancing the no-signal anode current by sending a current from a storage cell through a variable resistance to the galvanometer in the opposite direction. The detector valve was followed by an R-C coupled L.F. amplifier (1C5-G). The loudspeaker, which was connected through an output L.F. transformer to the anode circuit of the L.F. amplifying valve, was used for the aural response of the signal and was found extremely useful for tuning purposes.

(b) *Calibration of the receiver and calculation of the field-strength in some cases.*

The receiver was calibrated in the usual way and the calibration graphs were drawn showing galvanometer deflections for different input voltages for the various frequencies corresponding to the broadcasting stations which were received for the study of signal variations. It is to be noted that for each frequency, the curve is almost linear, except for very small and large input voltages.

The relevant characteristic curve was used to find the induced voltages due to different signal intensities in any set of experiments. For the purpose of determining the field-strength a tuned loop aerial was worked with the receiver and the field-strength was calculated with the help of the standard formula.

### EXPERIMENTAL RESULTS

With signals of medium wavelengths from distant broadcasting stations (Delhi, Dacca, Lahore and Vijayawada) from where ground-waves could not

reach the receiving station, the fading patterns observed in the early night hours were of the following types :

- (i) *Periodic or quasi-periodic fading.*
  - (a) With a slow period.
  - (b) With a comparatively quick period.
  - (c) With a combination of slow and quick periods.
- (ii) *Random fading.*

With signals from Lucknow and Patna, which are not too distant to transmit ground waves to a certain extent during the night hours, the above types of fading were also observed. With signals from Allahabad, which is only at a distance of 120 km. from Banaras, random fading was most frequently observed. Only in a few cases there was evidence of a quasi-periodic variation of somewhat rapid period.

(i) *Periodic or quasi-periodic fading :*

It is to be noted that there were two distinct orders of periodicities in the fading patterns: one a very slow periodic variation, the periodicity ranging from about 3 to 8 minutes (the quasi-frequency range being 0.12-0.31 cycles per minute) and the other, a comparatively quick variation, the periodicity of which ranged from about 25 to 110 seconds (the quasi-frequency ranging from about .55-2.5 cycles/minute). Both types of periodic fading were observed with the signals from the distant stations, *viz*, Delhi, Dacca, Vijayawada, Lahore and Lucknow. With the signals from Patna and Allahabad which are near Banaras, only the quick periodic type was observed.

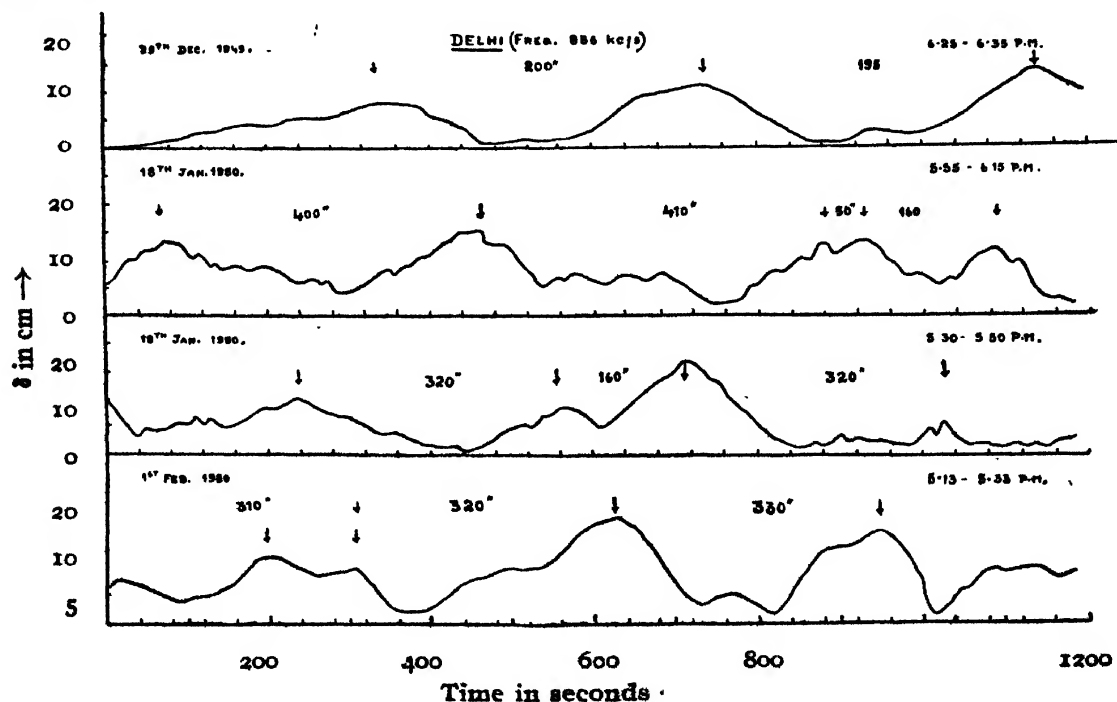


FIG. 2

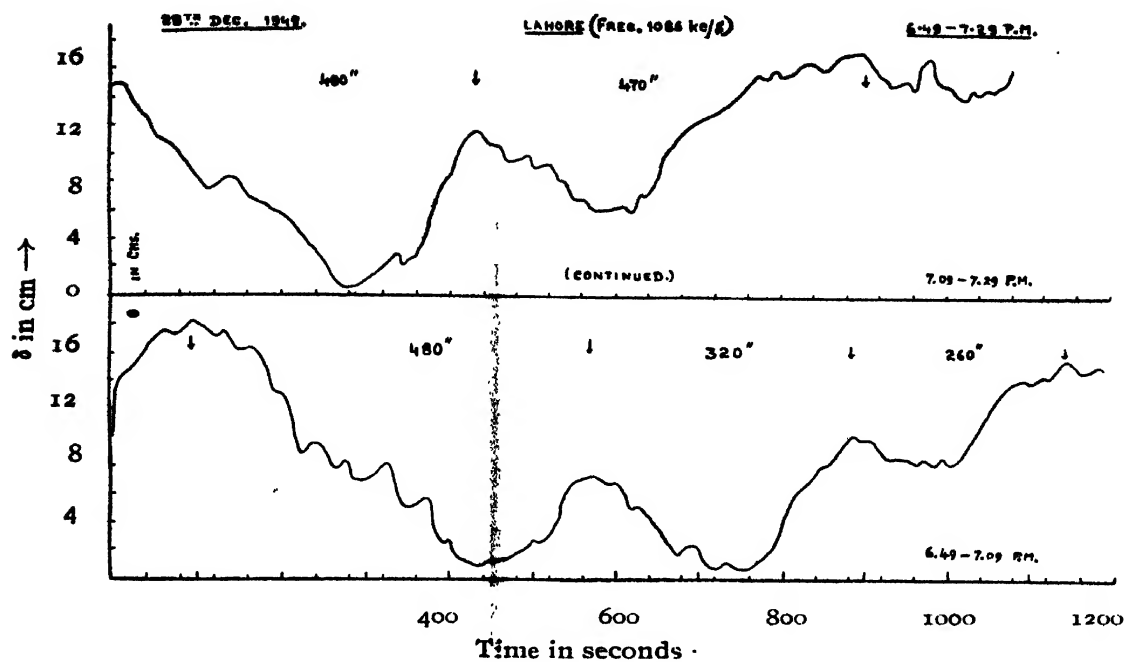


FIG. 3

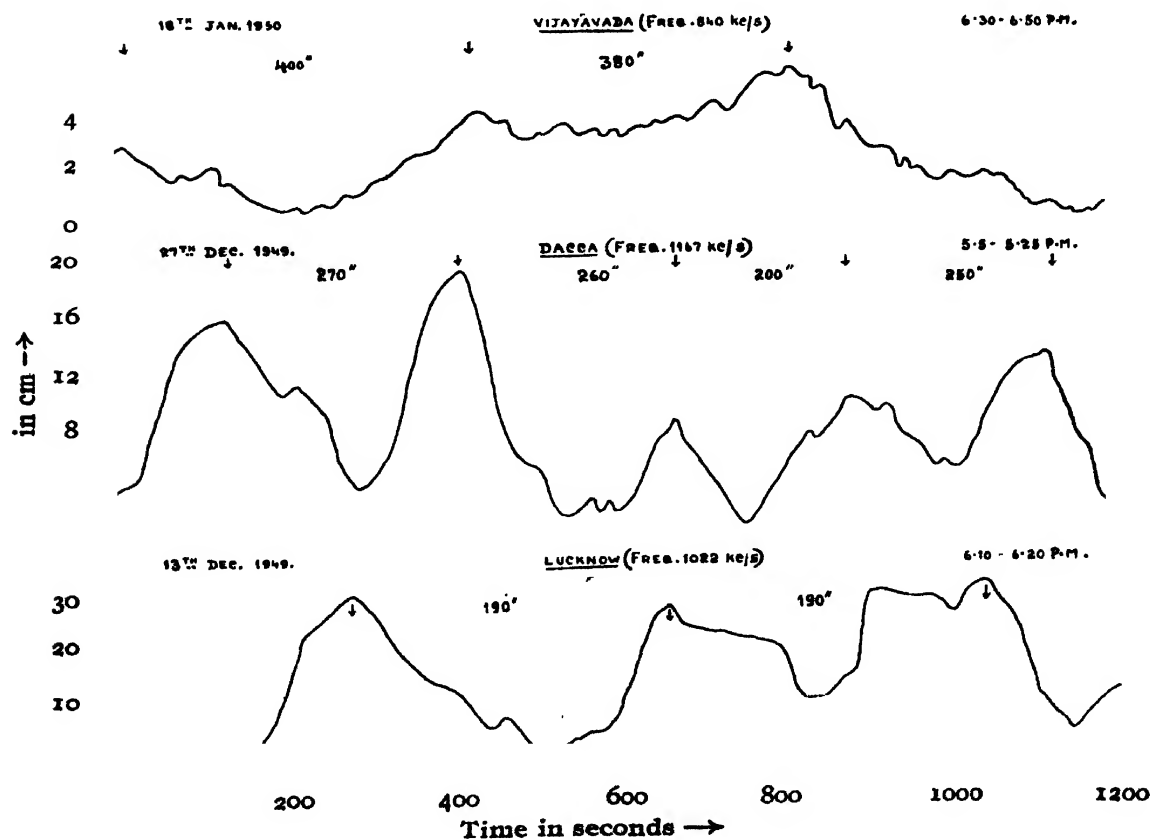


FIG. 4

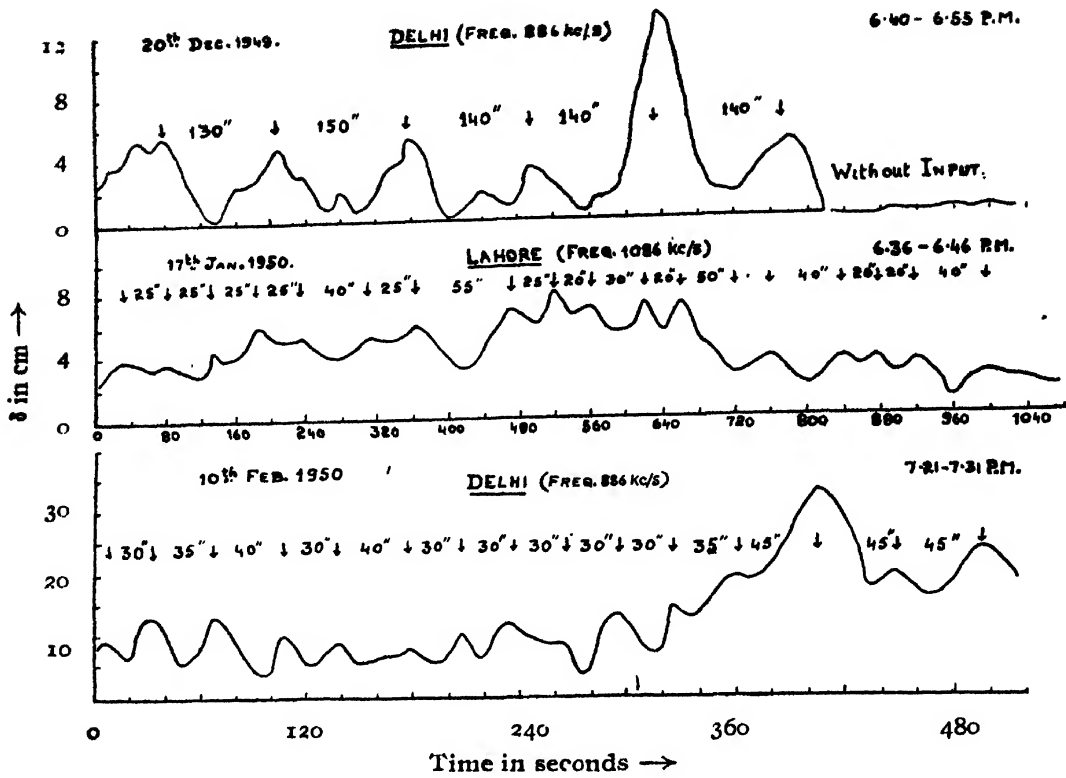


FIG. 5

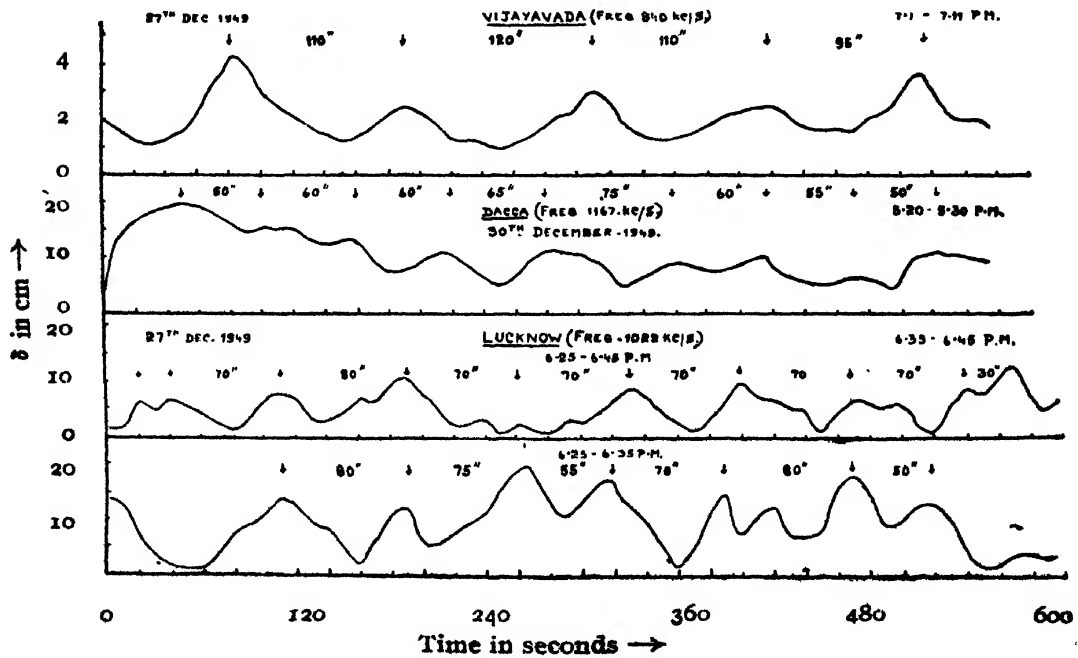


FIG. 6



Representative slow and quick periodic patterns, observed with the signals from the distant stations, are shown in figures 2-6. Figure 7 illustrates some observations showing the slow periodic type with quicker periodicity superposed on the slow one. The quick periodic patterns observed with Patna and Allahabad signals are shown in figure 8.

Actual field-strength variations, as determined from the calibration curves and the field-strength formula for two typical sets of observations, are illustrated in figure 9.

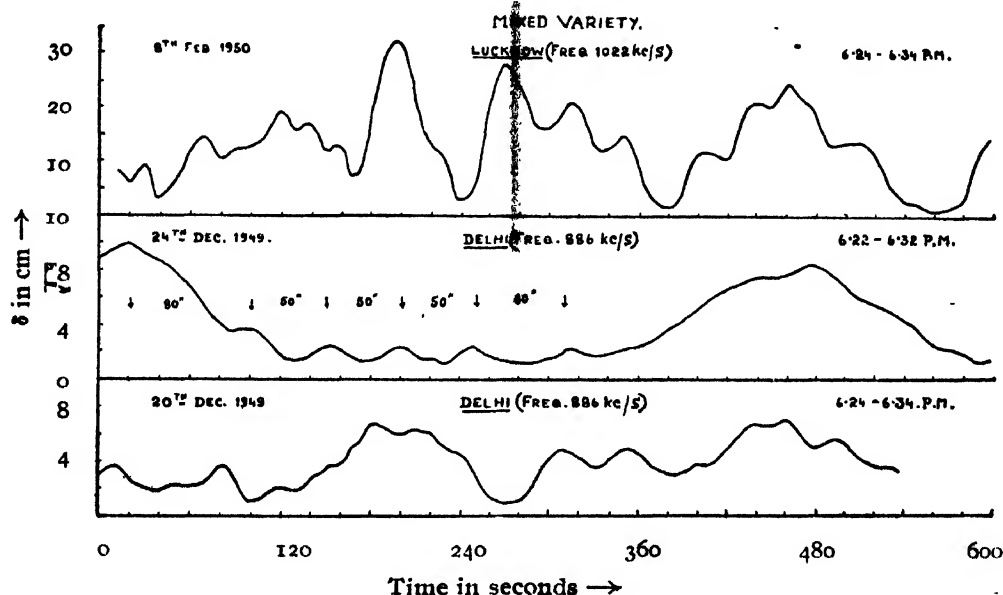


FIG. 7

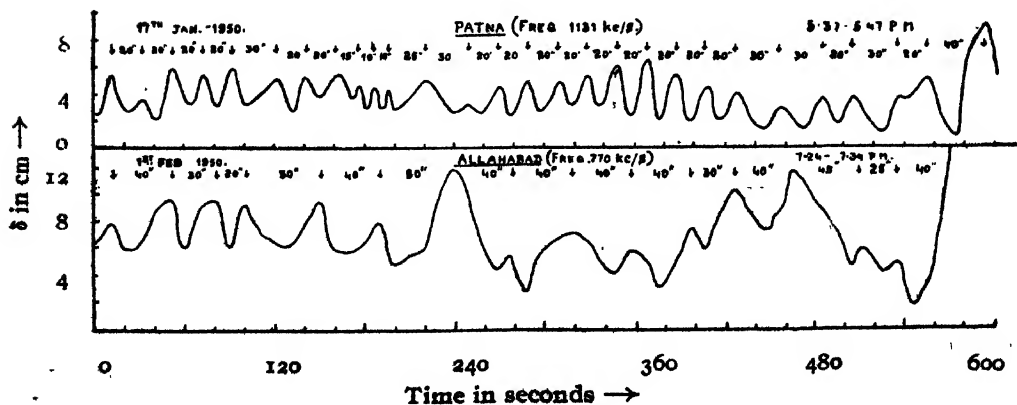


FIG. 8

The quasi-frequency and other details of the observed periodic patterns are given in Table II.

TABLE II

Date	Time P.M. I.S.T.	Periodicity in secs.		Frequency in cycs./minute.		Remarks.
		Slow	Quick	Slow	Quick	
DELHI						
20-12-49	6.40—6.55		140		.43	$\lambda = 338.6$ metres. Banaras-Delhi distance = 680 km.
24-12-49	6.25—6.30		50-60		1.10	
29-12-49	6.25—6.35	200-195		.30		
1-2-50	5.13—5.33	320		.19		
18-1-50	5.30—5.50	320		.19		
18-1-50	5.55—6.15	400-410		.15		
10-2-50	7.21—7.30		30-45		1.58	
10-2-50	7.33—7.43		107		.56	
DACCA						
27-12-49	3.5 —5.25	260		.23		$\lambda = 257.1$ metres Banaras-Dacca distance = 775 km.
30-12-49	5.20—5.30		50-75		.97	
VIJAYAWADA						
27-12-49	7.1 —7.11		109		.55	$\lambda = 357.1$ metres. Banaras-Vijayawada distance = 1050 km.
18-1-50	6.30—6.50	380-400		.15		
LAHORE						
28-12-49	6.49—7.29	260.480		.23-.12		$\lambda = 276$ metres. Banaras-Lahore distance = 1145 km.
17-1-50	6.38—6.46		25-65		1.5	
LUCKNOW						
13-12-49	6.10—6.20	190		.32		$\lambda = 293.5$ metres Banaras-Lucknow distance = 268 km.
24-12-49	7.00—7.5		55-70		.96	
25-12-49	7.20—7.25		40-70		1.09	
27-12-49	6.25—6.35		50-80		.93	
27-12-49	6.35—6.45		70		.86	
PATNA						
29-12-49	5.20—5.30		55-60		1.04	$\lambda = 265.3$ metres. Banaras-Patna distance = 224 km.
29-12-49	5.30—5.40		60		1.00	
29-12-49	5.40—5.50		50-70		1.00	
29-12-49	5.50—6.00		40-50		1.33	
17-1-50	5.37—5.47		20-30		2.39	
10-2-50	6.38—6.48		40-80		1.00	
10-2-50	6.51—7.01		50-60		1.09	
ALLAHABAD						
1-2-50	7.24—7.32		40		1.5	$\lambda = 389.6$ metres. Banaras-Allahabad distance = 120 km.

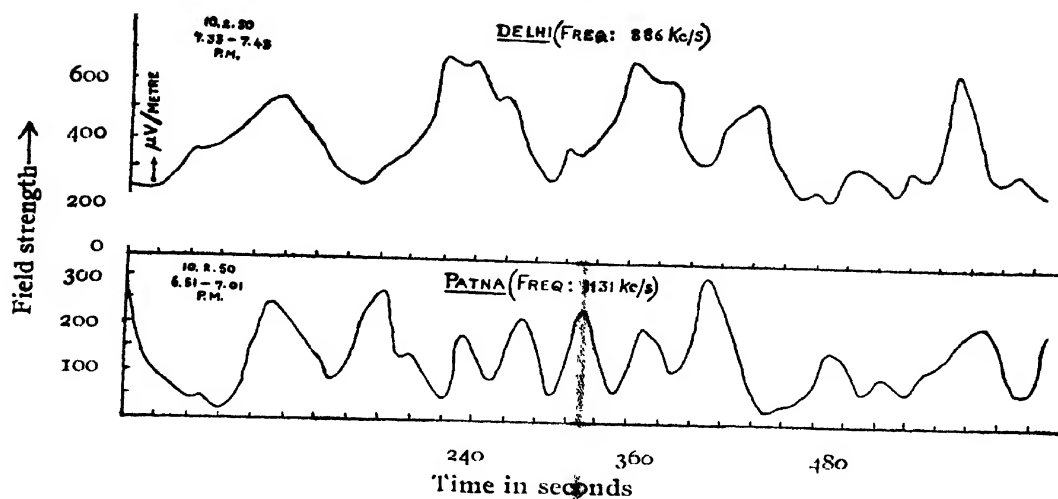


FIG. 9

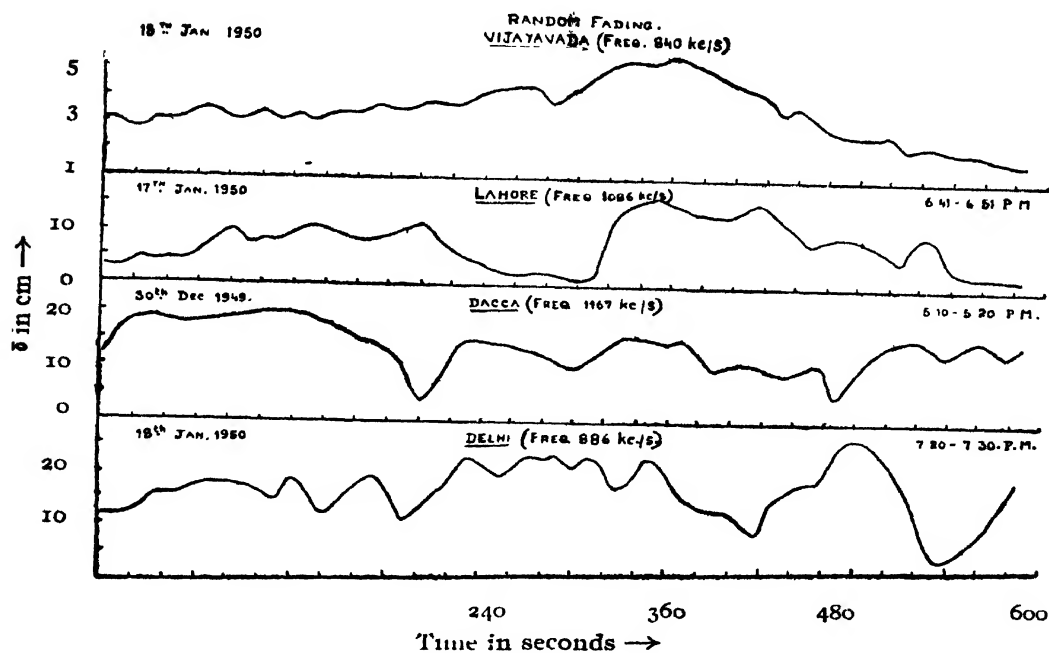


FIG. 10

## (ii) Random fading of medium-wave signals

The random fading curves for some of the distant stations from which the ground waves cannot reach the receiving point are shown in the figure 10.

## ORIGIN OF PERIODIC FADING

With regard to the periodic or quasi-periodic type of fading observed usually with short waves, it is now known that there are two distinct conditions under which the periodic type of fading can be observed. Appleton and Beynon (1947) have shown that the interference of ordinary and extraordinary components of the wave caused by magneto-ionic splitting gives

rise to a periodic fading at a time, usually during the evening or early morning hours when there is a continuous decrease or increase of electron density of the ionospheric layer. The slow periodic fading is usually associated with the interference between the lower-trajectory ordinary and extraordinary waves. The rapid periodicity arises only when the upper trajectory ordinary wave (which is often termed the Pedersen ray) is received along with the lower trajectory ordinary and extraordinary waves. For this interference of magneto-ionic components, the electron density of the ionosphere should be just enough for a single reflection between the transmitting and receiving stations. This means that the frequency of the transmitter should be in the neighbourhood of the maximum usable frequency (M.U.F.) for the particular reflecting layer and over the particular transmission distance. Under such condition, we may say that the Appleton-Beynon type of periodic fading is expected. The possibility of a periodic fading of a different origin under relatively high ionospheric ionisation, when the Appleton-Beynon type of periodic fading is too slow to be discernible in the fading records, was reported by Banerjee and Mukherjee (1949) and by Banerjee and Singh (1949) and later by Khastgir and Das (1950). Under conditions of high electron density, periodic patterns were observed and the periodicity was attributed by Banerjee and his colleagues to the interference between the two waves singly and doubly reflected from the same ionospheric layer or between the singly reflected waves from the two different layers, when one or both possessed a vertical movement producing a continuous change in the path-difference of the two interfering waves and yielding thereby intensity maxima and minima with a periodicity depending on the vertical velocity of the ionospheric layer or layers. Such periodic type of fading was usually observed in the evening or early night hours when the ionospheric layer tended to move upwards.

An equivalent representation of the same phenomenon was put forward by Khastgir (1949) and this view-point was outlined as follows:

With a vertical movement of the ionospheric layers in the evening (or early morning), when the ionospheric ionization is sufficient for the simultaneous single and double reflections from the same layer, it is evident that they will suffer different amounts of Doppler change of frequency as they proceed towards the receiving point from distinctly different directions. Thus there will be a difference in the frequencies of the singly and doubly reflected waves from the same moving layer. A similar difference in frequency is also expected in the case of simultaneous single reflections from the E and F-layers when both have vertical movement. In either case the two interfering waves of slightly different frequencies would give a resultant beat-note with a progressively increasing amplitude followed by a corresponding decrease in amplitude in a periodic manner. When the beat-note is received by the receiver, the output after rectification in the detector stage would constitute the envelope of such resultant beat-note with one side wiped out. This would be similar in

appearance to a slow rhythmic fading, the periodicity of which would correspond to the difference in the frequencies of the down-coming waves as determined by the Doppler effect formula. It has been shown by Khastgir and Das (1950) that the Doppler-beat interpretation of the observed periodic fading is essentially the same as the path-retardation theory of Banerjee and his colleagues.

With regard to the periodic fading of magneto-ionic origin, it is extremely difficult to calculate the periodicity. In the case of periodic fading due to vertical movement of the ionosphere, when there are simultaneous single and double reflections from the same moving layer or when there are simultaneous single reflections from both the moving layers, it has been found possible to obtain expressions for the periodicity from Doppler effect considerations.

Considering the case when the singly and doubly reflected waves from the same layer proceed towards the receiving point, the quasi-frequency of the fading pattern is given by

$$n = \frac{2v}{\lambda} (2 \cos \theta_2 - \cos \theta_1) \quad \dots (1)$$

where  $\theta_1$  and  $\theta_2$  are the angles of incidence for the singly and doubly reflected waves from the same layer moving with a velocity,  $v$  in the vertical direction and  $\lambda$ , the wavelength of the up-going waves. In the case of singly reflected waves from the two layers moving with the same vertical velocity  $v$  the quasi-frequency of periodic fading is given by

$$n = \frac{2v}{\lambda} (\cos \phi_1 - \cos \theta_1) \quad \dots (2)$$

where  $\theta_1$  and  $\phi_1$  are the angles of incidence at the E- and F-layers respectively for simultaneous single reflections.

#### OBSERVED PERIODIC FADING WITH MEDIUM WAVE SIGNALS

##### *(a). Periodic fading of magneto-ionic origin*

In the present investigation the wavelengths of the medium waves ranged from 257.1 to 357.1 metres and the distance of the transmitting stations from Banaras ranged from 120 to 1145 km. In most cases, there was reflection only from the E-layer. The M. U. F. value for the E-layer for the average transmission distance would be in the neighbourhood of 3.4 Mc/s in the evening and early night hours. The frequencies of the signals were therefore very much less than the M. U. F. value. It is therefore expected that the interference between the ordinary and extra-ordinary components would give rise to an extremely slow periodic pattern, if that is at all discernible. The slow periodic patterns (.12 to .31 cycles/minute) observed in the investigation have been attributed to this cause.

(b) *Periodic fading due to vertical movement of the ionospheric layer or layers*

The relatively quick periodic fading (.55 to 2.5 cycles/min) has been considered to be due to the vertical movement of the ionospheric layers during the evening hours. With medium waves it is possible to have both single and double reflections from the E-layer. In rare cases we may expect single reflection from the F-layer, when the E-layer is 'patchy' enough to allow penetration of the medium waves through it. The angles of incidence  $\theta_1$  and  $\theta_2$  for the singly and doubly reflected waves from the same E-layer and also the angle  $\phi_1$  for the singly reflected wave from the F-layer are determined by taking the E-layer to be at a height of 90 km. and the F<sub>2</sub> region at a height of 360 km. above the earth's surface.

Taking the values of  $\theta_1$ ,  $\theta_2$  and  $\phi_1$  for different transmission distances between the transmitting station and the receiving station the factors,  $(2 \cos \theta_2 - \cos \theta_1)$  and  $(\cos \phi_1 - \cos \theta_1)$ , in the formulæ (1) and (2) are calculated and shown in the Table III.

TABLE III

To Banaras	$(2 \cos \theta_2 - \cos \theta_1)$	$(\cos \phi_1 - \cos \theta_1)$
Delhi	.68	.47
Dacca	.62	.46
Vijayawada	.48	.40
Lahore	.45	.38
Lucknow	1.048	.38
Patna	1.060	.33
Allahabad	1.066	.155

Using formulæ (1) and (2) with the relevant multiplying factors given in Table III, the vertical velocity of the ionospheric layer can be calculated from the observed frequency of the periodic fading patterns. The observed quick periodicity ranging from about 25 seconds to about 110 second (the corresponding quasi-frequency being .55 to 2.5 cycles/minute) is considered as due to the vertical movement of the ionosphere when the singly and the doubly reflected waves from the E-layer (or when the singly reflected waves from both E- and F-layers) interfere.

The calculated values of the vertical velocity for the various observed quick periodicities are given in Table IV.

The vertical velocity computed from the observed quick periodicities according to the formula (1) ranges from 1.8 to 7.7 metres per second, the mean value being 3.6 metres per second. As this agrees fairly with the

TABLE IV

Date	Time P. M. I S.T.	Transmitting station	Observed quick fading in cycles/ min. (mean value)	Ionospheric vertical velocity	
				From (1) m/sec.	From (2) m/sec
20-12-49	6.40-6.55	Delhi	.43	1.79	2.58
24-12-49	6.25-6.30	Delhi	1.09	4.52	8.02
10- 2-50	7.21-7.30	Delhi	1.58	6.50	9.47
10-2 -50	7.33-7.43	Delhi	.56	2.33	3.37
30-12-49	5.20-5.30	Dacca	.97	3.34	4.51
27-12-49	7.01 7.11	Vijavawala	.55	3.41	4.10
17- 1-50	6.38-6.46	Lahore	1.50	7.66	9.08
24-12-49	7.00-7.5	Lucknow	.96	2.26	6.22
25-12-49	7.20-7.25	Lucknow	1.09	2.00	7.07
27-12-49	6.25-6.35	Lucknow	.93	2.16	5.94
27-12-49	6.35-6.45	Lucknow	.86	2.01	5.52
29-12-49	5.20-5.30	Patna	1.04	2.17	6.97
29-12-49	5.30-5.40	Patna	1.00	2.09	6.70
29-12-49	5.40-5.50	Patna	1.09	2.28	7.31
29-12-49	5.50-6.00	Patna	1.30	2.81	8.93
17- 1-50	5.37-5.47	Patna	2.39	4.98	16.00
10- 2-50	6.38-6.41	Patna	1.00	2.09	6.7
10- 2-50	6.51-7.01	Patna	1.09	2.28	7.31
1- 2-50	7.24-7.34	Allahabad	1.50	4.60	

approximate estimate from the ionospheric data, we are inclined to the view that the quick periodic fading was more often due to the interference of the singly and doubly reflected waves from the E-layer.

#### RANDOM FADING OBSERVATIONS WITH DOWNCOMING WAVES ONLY AND COMPARISON WITH RAYLEIGH'S FORMULA FOR RANDOM SCATTERING

Random fading, which was frequently observed with downcoming waves of medium wavelengths, was explained by Ratcliffe and Pawsey (1933) as due to the random scattering of the waves from a large number of diffracting centres in the ionosphere. Late Lord Rayleigh deduced an expression for the probability of occurrence of any resultant amplitude on the assumption

of a large number of components of random phases. The probability is given by

$$P' = \frac{2r}{R^2} e^{-r^2/R^2} \quad (8)$$

where  $R^2$  = sum of the squares of the components and  $P'dr$ , the probability of a resultant amplitude between  $r$  and  $(r+dr)$ .

The actual distribution curves showing the number of observations for different amplitudes of the downcoming wave were drawn for the several random fading patterns obtained with medium wave signals from the various transmitting stations. The procedure was as follows: Taking amplitudes of the downcoming wave at regular short intervals of time (10 seconds), the whole range of observed amplitudes for a continuous set of observations was divided into a number of equal parts ( $dr$ ) and the number of times the observed amplitude lies between  $r$  and  $(r+dr)$  was counted. A distribution curve was thus drawn showing the number of amplitudes lying between  $r$  and  $(r+dr)$  against the mean value of  $r$  and  $r+dr$ .

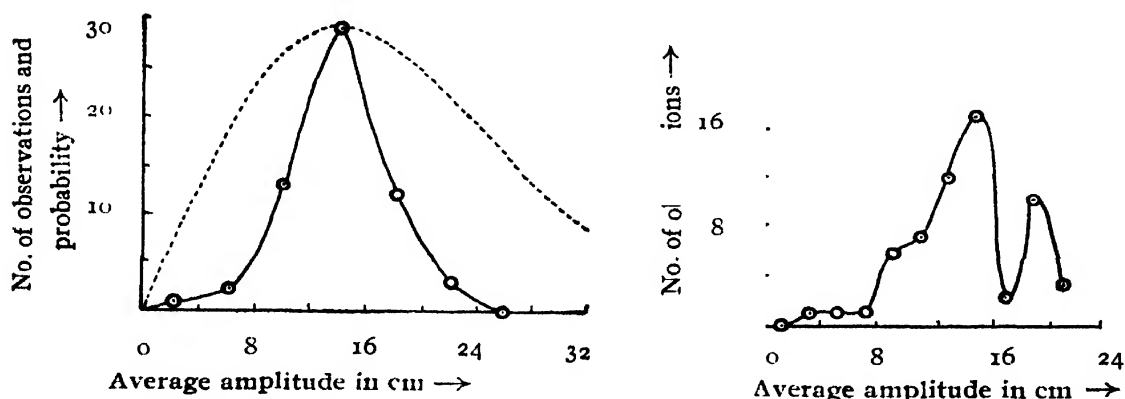


FIG. 11 a (Dacca)

— — — Rayleigh  
—○—○— Experiment

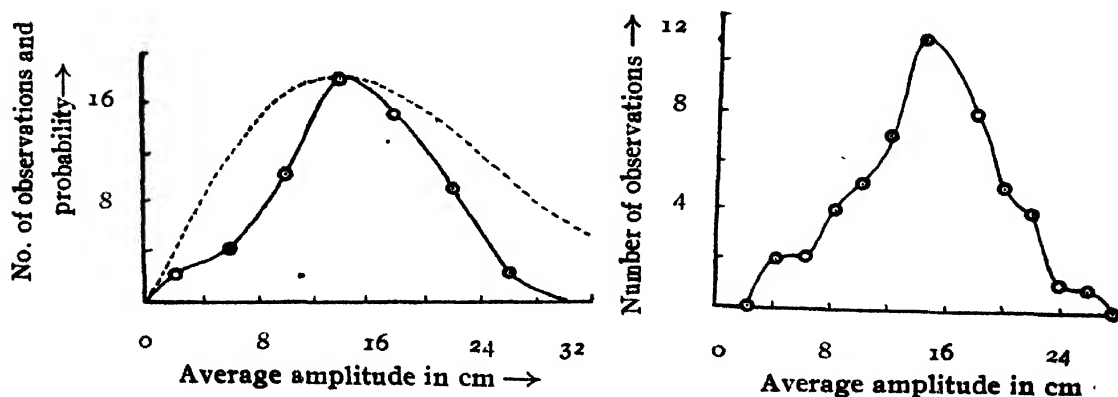


FIG. 11 b (Delhi)

— — — Rayleigh  
—○—○— Experiment



The Rayleigh distribution curves were drawn in the manner already described by Khastgir and Ray (1940) and Khastgir and Das (1950). Each of the theoretical distribution curves is shown along with the actual distribution curve in the figures 11 and 12

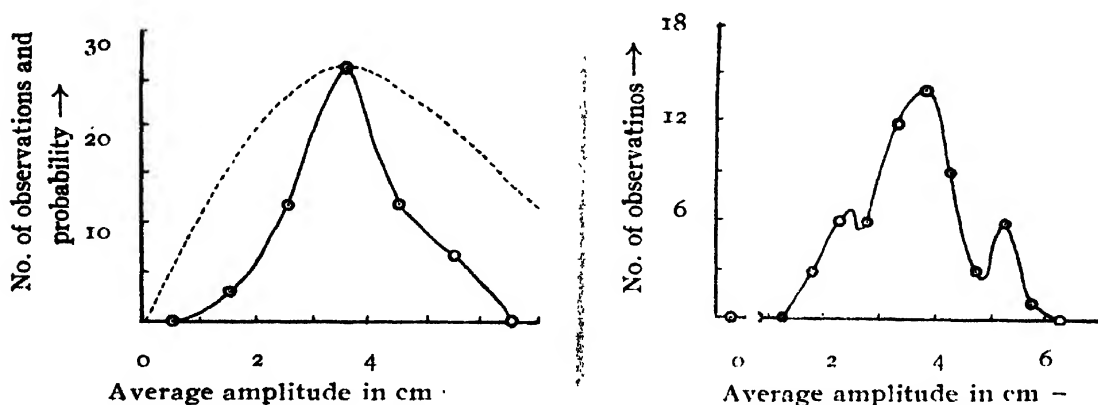


FIG. 12 a (Vijayawada)

— — — — Rayleigh  
—o—o— Experiment

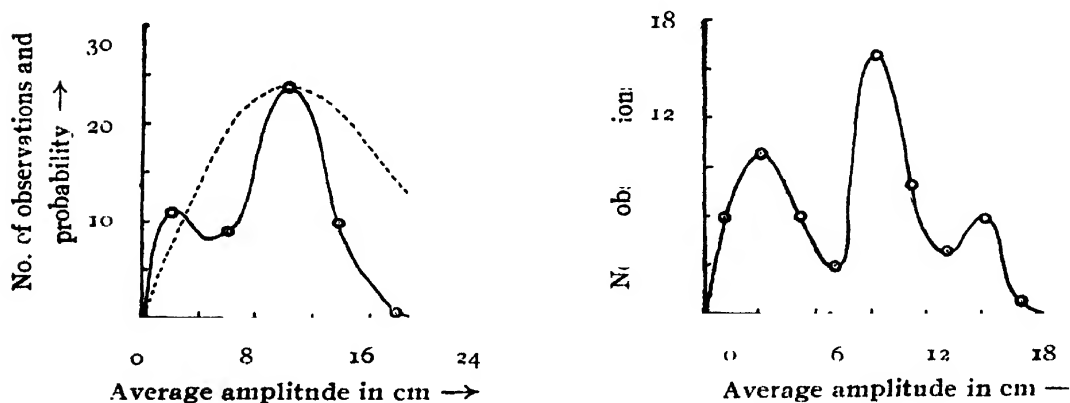


FIG. 12 b (Lahore)

— — — — Rayleigh  
—o—o— Experiment

It will be observed that there is no agreement between the observed distribution of intensity and the theoretical distribution according to Rayleigh's formula. In the case of Delhi, Dacca, and Lahore signals, when the intensity values are divided into four centimetres groups, there appeared one pronounced peak for Delhi and Dacca and two for Lahore. When the dispersion was doubled, there appeared one peak for Delhi, two for Dacca and three for Lahore signals. For Vijayawada signals, there appeared one pronounced peak when the intensity was taken to lie within 1 cm and three peaks when the dispersion was doubled.

For distant stations like Lahore (1145 km) and Vijayawada (1050 km) it was likely to have singly and doubly reflected waves from the E-layer.

It is to be noted that Rayleigh's formula for random scattering is valid for only one downcoming wave. Even for a single reflection, if the distance between the transmitting and receiving station is large, we may have a number of waves following slightly different paths in the ionosphere. The existence of a number of waves following slightly different paths will partly explain the cause of the discrepancy between the observation and Rayleigh's formula.

WIRELESS LABORATORY  
PHYSICS DEPT.  
BANARAS HINDU UNIVERSITY.

## REFERENCES

- Appleton, E. V. and Beynon, W. J. G., 1947, *Proc. Phys. Soc.*, (Lond.), **58**, 59.  
 Banerjee, S. S. and Mukerjee, G. C., 1946, *Science and Culture*, **11**, 571.  
 1948, *Phil. Mag.*, **39**, 697  
 Banerjee, S. S. and Singh, R. N., 1948, *Ind. J. Phys.*, **22**, 413.  
 1949; *Science and Culture*, **14**, 293  
 Khastgir, S. R., 1949, *Science and Culture*, **55**, No. 3.  
 Khastgir, S. R. and Das, P. M., 1950, *Science and Culture*, **15**, 445.  
 1950, *Ind. J. Phys.*, **24**, 277.  
 1950, *Proc. Phys. Soc.* (Lond ),  
 Khastgir, S. R. and Ray, A. K., 1940, *Ind. J. Phys.*, **14**, 283.  
 Pawsey, J. L., 1933, *Proc. Camb. Phil. Soc.*, **33**, 125.  
 Ratcliffe, J. A. and Pawsey, J. L., 1933, *Proc. Camb. Phil. Soc.*, **29**, 301

# ON THE ULTRAVIOLET ABSORPTION SPECTRA OF ANISOLE IN THE LIQUID AND SOLID STATES\*

By A. R. DEB

(Received for publication, April 20, 1951)

## Plate IX

**ABSTRACT.** The absorption spectra of anisole ( $C_6H_5.O.CH_3$ ) have been studied in the liquid and solid states in the ultraviolet region. In the liquid state three bands have been observed in the region 2650–2800 Å. Absorption again begins at about 2370 Å and total absorption occurs below 2330 Å. In the solid state at about  $-170^\circ C$ , these three bands split up into six bands, with the first band at long wavelength side slightly shifted towards the shorter wavelength side from its position in the liquid state. It is pointed out that in the solid state at low temperatures the electronic energy levels are perturbed by the intermolecular field.

## INTRODUCTION

It is well known that many organic substances in the vapour state exhibit bands with distinct structures in the ultraviolet absorption spectra and that in the liquid state the structure is modified owing to the influence of the intermolecular field. In the case of benzene, for instance, Kronenberg and Pringsheim (1926) observed that the absorption spectrum in the vapour state consists of a large number of bands, each consisting of a large number of narrower bands, and in the liquid state the absorption spectrum consists of only broad bands, the structure being hardly visible. In the solid state at  $-170^\circ C$  again, the width of the individual bands diminishes considerably and fine structure is replaced by a few fainter absorption lines in the intervening regions.

The question whether the bands generally behave in the same way on lowering of temperature and on solidification in the case of aromatic organic compounds, having both polar and non-polar molecules, has not been fully investigated. Also it is only the comparison of the absorption spectra in the liquid and solid states that can show whether any profound change in the electronic energy levels of the molecules takes place with the change of state. Such an information would be helpful in understanding also the changes which take place in the Raman spectra of these substances with the change of state.

In a programme of work undertaken for this purpose, the absorption spectra of anisole in the liquid and solid states have been studied in the ultraviolet region in order to compare these with the absorption spectrum recorded by Sreeramamurty (1950) in the case of vapour, and to find out

\* Communicated by Prof. S. C. Sirkar.

whether in the case of these polar molecules any striking change occurs with solidification of the liquid. The results have been discussed in the present paper.

#### EXPERIMENTAL

The source of ultraviolet continuum was a hydrogen discharge tube, made of pyrex glass, provided with quartz window and aluminium electrodes prepared in the laboratory. The tube was run at about 3 K.V. Pure anisole supplied by B.D.H., was redistilled in vacuum three times before use. The liquid cell consisted of a pair of plane parallel quartz plates with a thin film of the liquid between them and held in a suitable brass frame. It was found that even the small thickness of the film was too large and produced total absorption in the region of the bands. The plates were then pressed together and very carefully slid along each other so as to reduce the thickness of the film. In this way it was possible to obtain a particular small thickness of the film which produced bands in the absorption spectrum.

For studying the absorption spectrum of the substance in the solid state, a Dewar vessel of fused silica was used to contain liquid oxygen, and the brass frame containing the cell with the liquid was introduced into the Dewar vessel, so that the lower part of the frame was dipped in liquid oxygen. No ice was found to be deposited on the surfaces of the cell, as the moisture

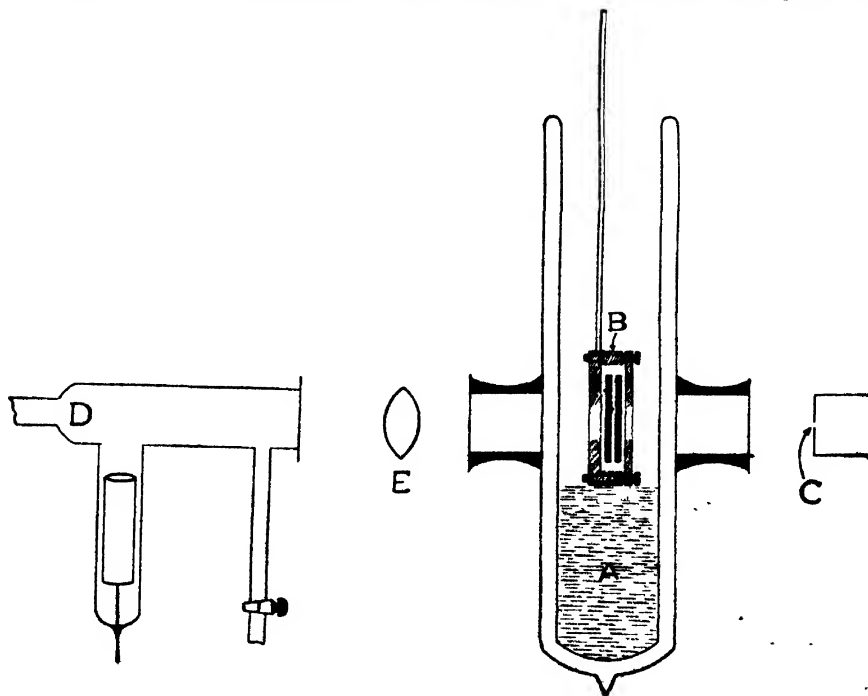
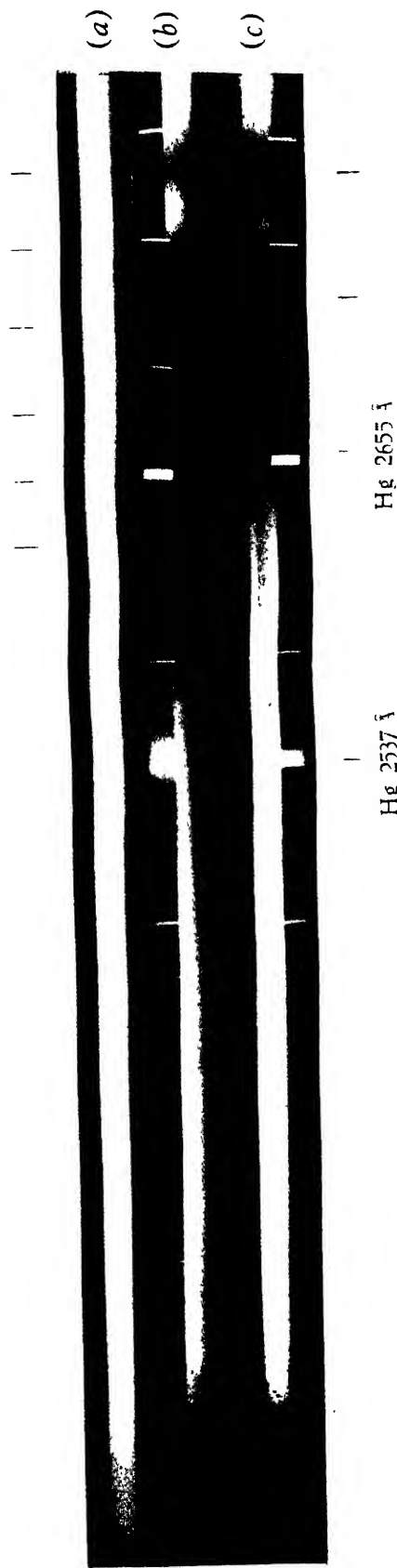


FIG. 1

- A—Liquid oxygen
- B—Brass frame containing the cell.
- C—Spectrograph slit
- D—Discharge tube
- E—Quartz lens,



Absorption spectra of anisole.

- (a) Hydrogen continuum
- (b) Anisole—solid at about  $-170^{\circ}\text{C}$
- (c) .. liquid ..  $30^{\circ}\text{C}$



in the air was condensed at the mouth of the vessel. Entrance of moisture into the vessel was also prevented by the upward drift of air due to rapid evaporation of the liquid air. Two pieces of pyrex glass tube, each about one inch in length, were sealed on the opposite sides of the Dewar vessel with sealing wax and the ends closed by quartz plates in order to prevent deposit of moisture in the path of the light beam (Fig. 1.). To maintain a fairly steady temperature inside the cell, the level of the liquid oxygen was always kept just below the cell after allowing the lower portion of the brass frame to dip in the liquid oxygen.

An Adam Hilger E<sub>r</sub> quartz spectrograph, giving a dispersion of about 3 A.U. per mm. in the region of 2600 Å was used in the present investigation. In the case of the liquid, an exposure of 6 minutes on Ilford H.P.3 films was sufficient, whereas, in the case of the solid an exposure of one and a half hours was necessary. This was due to the fact that the uneven walls of the Dewar vessel used in the latter case scattered away a large portion of the radiation.

# RESULTS AND DISCUSSION

The absorption spectra for the substance in the liquid state at 30°C and in the solid state at about -170°C are reproduced in Plate IX. The wave numbers of the bands are given in Table I, along with those reported for the solution of anisole in ether by Kato and Someno (1938).

The sharp bands, large in number observed in the case of vapour (Sreeramamurty, 1950), are replaced by three broad bands in the liquid state. The spectrogram resembles that observed in the case of solution of anisole

TABLE I

Soln. in ether (Kato & Someno)			Pure liquid at 30°C (Present author)				Solid at -170°C (Present author)			
Band	Wave no. cm <sup>-1</sup>	Diff.	Band	Wave no. cm <sup>-1</sup>	Diff.	Assignment	Band	Wave no. cm <sup>-1</sup>	Diff.	Assignment
1	35900		1 (s)	35845		0-0	1 (s)	35870		0-0
2	36800	900	2 (vs)	36760	915	0+915	2 (s)	36340	470	0+470
3	37700	900	3 (w)	37668	908	0+2 × 911	3 (vs)	36807	467	0+2 × 468
		900							468	0+937
4	38600		4	...			4 (vs)	37275	421	0+3 × 468
							5 (w)	37696	460	0+2 × 913
										0+4 × 456
							6 (w)	38156		0+5 × 457

(s) - strong, (vs) - very strong, (w) - weak

in ether by Kato and Someno (1938). They observed four bands, the frequency-difference between successive bands being  $900\text{ cm}^{-1}$ , whereas, in the present investigation only three bands are observed. The centres of these broad bands at  $35845$ ,  $36760$  and  $37668\text{ cm}^{-1}$  respectively, may correspond to the first three bands observed in the case of the solution. In the vapour state the o-o band observed by Sreeramamurty (1950) is at  $36359\text{ cm}^{-1}$ . This shows that the bands have shifted towards the longer wavelength side with change from vapour to liquid phase. When the liquid is solidified, three bands, corresponding to those observed in the case of the liquid, are observed in positions slightly shifted towards shorter wavelengths and each of these three bands is further followed by another band shifted from the former by about  $460\text{ cm}^{-1}$  towards shorter wavelengths.

This phenomenon cannot be considered as sharpening and splitting up of the broad bands in the solid state, because in the position of the three new bands there are no absorption minima in the case of the liquid. Also the new frequency-shift  $460\text{ cm}^{-1}$  between the first and the second band observed in the case of the solid is not observed in the case of the liquid. From these facts it can be concluded that the electronic configuration in the molecule undergoes changes with solidification of the substance. From a comparison of the absorption spectrum of the vapour reproduced by Sreeramamurty (1950) with that for the liquid observed in the present investigation, it is found that the structure of the bands observed by the former author is absent in the case of the liquid. This again is due to the influence of the intermolecular field in the liquid state. It has to be pointed out in this connection that the bands on the longer wavelength side of o-o band observed by Sreeramamurty are not observed in the case of the liquid in the present investigation. Further, theoretically the intensity of the o-1301 or o-1412 band ought to be too feeble to be recorded in the spectrogram.

#### ACKNOWLEDGMENTS

The author wishes to express his indebtedness to Prof. S. C. Sirkar, D.Sc., F.N.I. for his kind permission to carry out the investigation in the laboratory of the Optics Department and for his guidance during the progress of the work. Thanks are also due to Sri B. M. Bishui for his encouragement in the work.

OPTICS DEPARTMENT  
INDIAN ASSOCIATION FOR THE  
CULTIVATION OF SCIENCE  
CALCUTTA

#### REFERENCES

- Kato, S. and Someno, F., 1938, *Sci. Pap. Inst. Phys. Chem. Res. Tokyo*, **31**, 905 and 912.  
Kronenberg, A. and Pringsheim, P. 1926, *Z.f. Phys.*, **40**, 75  
Sreeramamurty, K., 1950, *Ind. J. Phys.*, **24**, 421.



# ON THE ABSORPTION OF U. H. F. RADIO WAVES IN FATTY ACIDS\*

BY S. N. SEN

(Received for publication, April 14, 1951)

**ABSTRACT.** The absorption of ultra-high frequency radio waves in lower fatty acids, namely formic acid, acetic acid, propionic acid and *n*-butyric acid has been studied in the frequency-range 250-510 Mc/sec. at different temperatures by the optical method. An absorption maxima has been observed in the latter three cases and it has been found that, in general, the integrated absorption diminishes and the absorption maxima shifts towards higher frequencies with the rise of temperature. The radius of the rotating unit actually responsible for absorption of these ultra-high frequency radio waves, has been calculated on Debye's theory and it is concluded that probably the molecules of these acids exist as dimers in the liquids.

The absorption indices calculated from Debye's theory agree approximately with those observed in case of propionic acid and *n*-butyric acid but wide divergence is found in the case of formic acid and acetic acid.

## INTRODUCTION

It was observed previously (Sen, 1951) that in the case of aliphatic ketones, although the height of the absorption peak in the ultra-high frequency region increases with lowering of temperature, some exceptions are observed in the case of methyl-ethyl ketone and ethyl iso-butyl ketone. It was suggested from these results that these deviations might be due to the asymmetric form of the molecule which is responsible for the occurrence of abrupt association of the molecules at certain temperature or some other change in the relative orientations of the molecules in the liquid. No definite conclusion could, however, be drawn from the data observed only in these isolated cases and it was therefore thought worthwhile to study the phenomenon in the case of a large number of liquids having polar molecules. Lower fatty acids are some of the liquids suitable for such investigation and therefore the investigations have been extended to formic acid, acetic acid, propionic acid and *n*-butyric acid.

## EXPERIMENTAL

The experimental technique has been described completely in previous papers (Sen, 1949, 1950, 1951). All the liquids were chemically pure and each was distilled three or four times before taking observation. Formic acid was found invariably mixed up with water. As the boiling points of water and formic acid are almost the same, *viz.*, 100°C and 108°C, water could not be

\* Communicated by Prof. S. C. Sirkar.

removed by vacuum-distillation. Hence the given sample of formic acid was first treated with anhydrous sodium sulphate which partly removed the water present as impurity. The liquid was then purified by solidification. As the melting point of water is lower than that of formic acid, the first fraction which melted was rejected; thereby the portion left became richer in formic acid. The process was repeated several times and the liquid was finally made free from water. The experimental arrangement used to study the absorption of U .H. F. radio waves by the liquids at different temperatures was the same as that described in detail in previous papers (Sen, 1949, 1951). The same absorption cell was used in the present investigation also. The values of attenuation co-efficient were calculated as before. Then graphs were plotted for different temperatures with attenuation co-efficient as ordinate and the corresponding frequency as abscissa. From these graphs the values of maximum frequency of absorption for the different liquids were calculated. The same process was repeated for all the three liquids.

## RESULTS

The values of  $\mu$ , the attenuation co-efficient have been calculated from the relation

$$\mu = \frac{2.34}{x} \log_{10} (I_0/I),$$

$x$  being the thickness of the liquid in the cell. The results are given in Tables I, II, III and IV and these results have been plotted graphically against frequency in figures 1-4.

## DISCUSSION

It can be seen from figure 1 that in the case of formic acid, although the maximum absorption appears to take place at a frequency higher than 510 Mc/sec. both at 10°C and 34°C, the integrated intensity seems to increase and the position of the absorption peak seems to shift towards lower frequencies with the lowering of temperature. In the case of acetic acid, on the other hand, the height of the peak increases when the liquid is cooled down from 67.5°C to 35°C, but the integrated intensity seems to be the same at both the temperatures as can be seen from figure 2. In the case of propionic acid, the curves represented in figure 3 show that the integrated intensity diminishes when the temperature of the liquid is raised from 65°C to 85°C, but on further heating the liquid up to 110°C, no further diminution in integrated intensity takes place. In the case of *n*-butyric acid, the integrated intensity diminishes gradually with rise of temperature up to 120°C as is evident from figure 4. This diminution in the height of the absorption peak and in total integrated absorption may be due either to breaking up of associated molecules with rise of temperature or to fluctuation in the value of the permanent electric moment within wide limits due to variation in the intermolecular field at different points. To ascertain which of these two effects is predominant, the molecular radius of the unit actually

responsible for such absorption has been calculated from the relation given by Debye (1929)—

$$\omega\tau = \frac{\epsilon_0 + 2}{\epsilon_1 + 2} \sqrt{\frac{\epsilon_1}{\epsilon_0}}$$

TABLE I

Attenuation co-efficient of formic acid (H.COOH)

Temp °C	34°C	10°C
Frequency Mc/sec.		
300	.1050	.2530
310	.1178	.2530
320	.1302	.2553
330	.1427	.2582
340	.1575	.2626
350	.1703	.2703
360	.1825	.2782
370	.1978	.2878
380	.2104	.3002
390	.2252	.3124
400	.2358	.3253
410	.2473	.3403
420	.2625	.3506
430	.2758	.3702
440	.2878	.3873
450	.3003	.4002
460	.3108	.4153
470	.3305	.4375
480	.3407	.4573
490	.3625	.4759
500	.3875	.4923
505	.4030	.5073
510	.4060	.5128

TABLE II

Attenuation co-efficient of acetic acid (CH<sub>3</sub>COOH)

Temp °C	35°C	67°.5C
Frequency Mc/sec.		
300	.0452	.0303
310	.0473	.0312
320	.0523	.0343
330	.0564	.0342
340	.0623	.0343
350	.0720	.0356
360	.0849	.0402
370	.1043	.0413
380	.1152	.0452
390	.1153	.0532
400	.1062	.0582
410	.0869	.0632
420	.0682	.0685
430	.0559	.0702
440	.0473	.0723
450	.0412	.0725
460	.0362	.0720
470	.0308	.0703
480	.0286	.0684
490	.0262	.0623
500	.0243	.0576
505	.0202	.0536
510	.0202	.0528

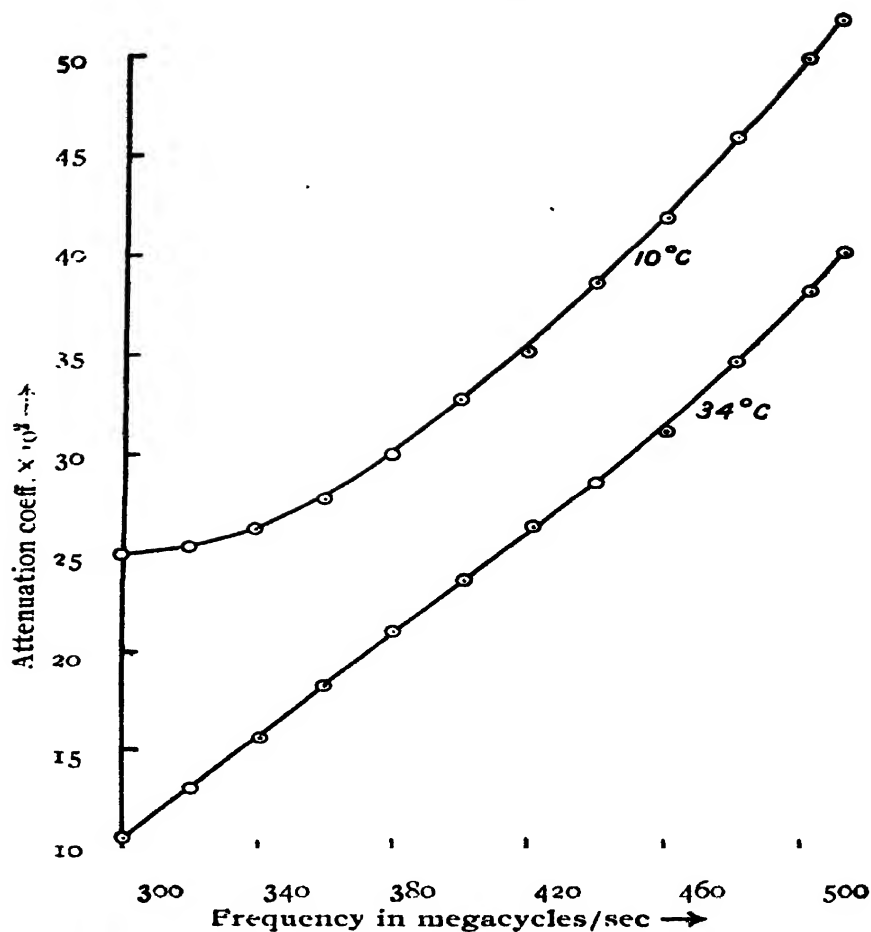


FIG. 1 Formic acid (HCOOH)

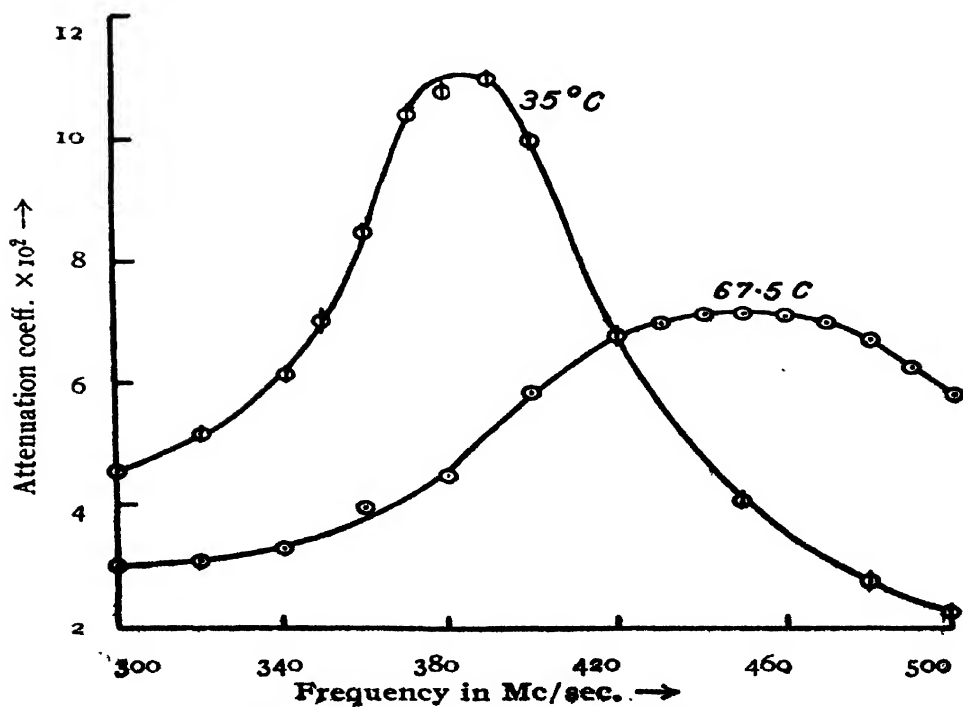
FIG. 2 Acetic acid (CH<sub>3</sub>COOH)

TABLE III

Attenuation co-efficients of  
propionic acid

Temp. °C Frequency in Mc/sec.	65°C	85°C	110°C
260	.0250	.0152	.0063
270	.0275	.0162	.0063
280	.0302	.0162	.0063
290	.0305	.0167	.0064
300	.0300	.0174	.0066
310	.0285	.0187	.0068
320	.0275	.0213	.0068
330	.0257	.0225	.0068
340	.0246	.0230	.0068
350	.0230	.0230	.0068
360	.0210	.0225	.0072
370	.0201	.0213	.0080
380	.0186	.0200	.0080
390	.0175	.01826	.0082
400	.0160	.0171	.0118
410	.0151	.0162	.0138
420	.0140	.0157	.0170
430	.0135	.0152	.0176
440	.0128	.0150	.0204
450	.0120		.0210
460	.0113		.0212
470	.0107		.0210
480	.0105		.0201
490	.0103		.0182
500	.0100		.0180
505			.0170
510			.0163

TABLE IV

Attenuation co-efficient of  
*n*-butyric acid

Temp. in °C Frequency in Mc/sec	67°.5°C	92°C	120°C
250	.0350	.0203	
260	.0326	.0210	
270	.0288	.0212	
280	.0263	.0246	
290	.0236	.0276	
300	.0213	.0320	.0050
310	.0196	.0345	.0055
320	.0173	.0352	.0057
330	.0163	.0353	.0062
340	.0150	.0338	.0065
350	.0136	.0323	.0070
360	.0123	.0283	.0087
370	.0113	.0253	.0098
380	.0100	.0212	.0100
390	.0088	.0193	.0105
400	.0087	.0176	.0115
410	.0078	.0163	.0128
420	.0070	.0152	.0158
430	.0063	.0138	.0175
440	.0058	.0130	.0213
450	.0050	.0126	.0242
460		.0113	.0248
470		.0105	.0256
480			.0255
490			.0250
500			.0226
505			.0203
510			.0178

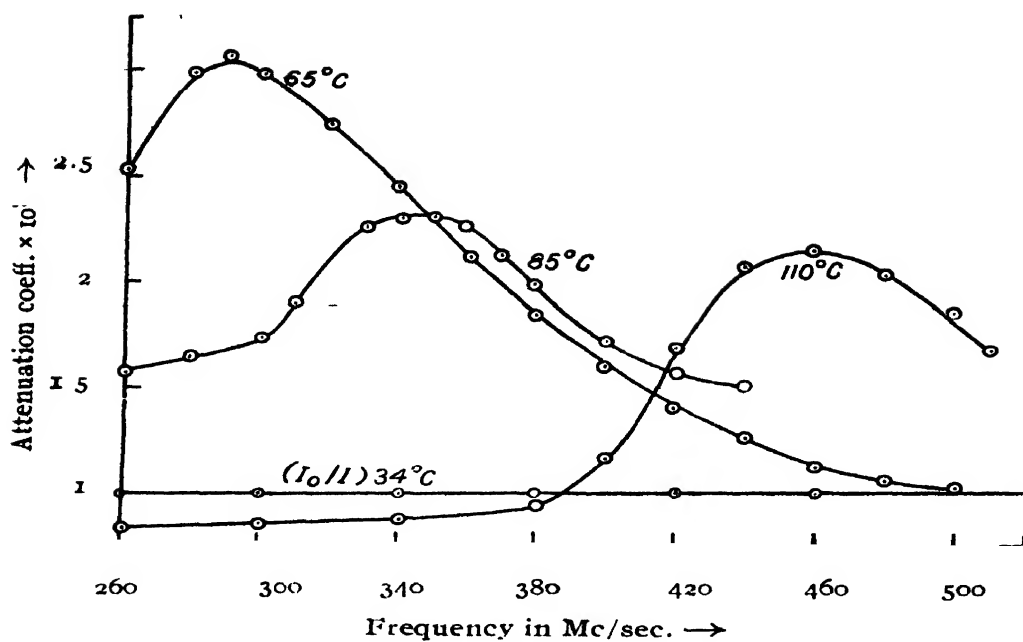


FIG 3  
Propionic acid ( $C_2H_5COOH$ )

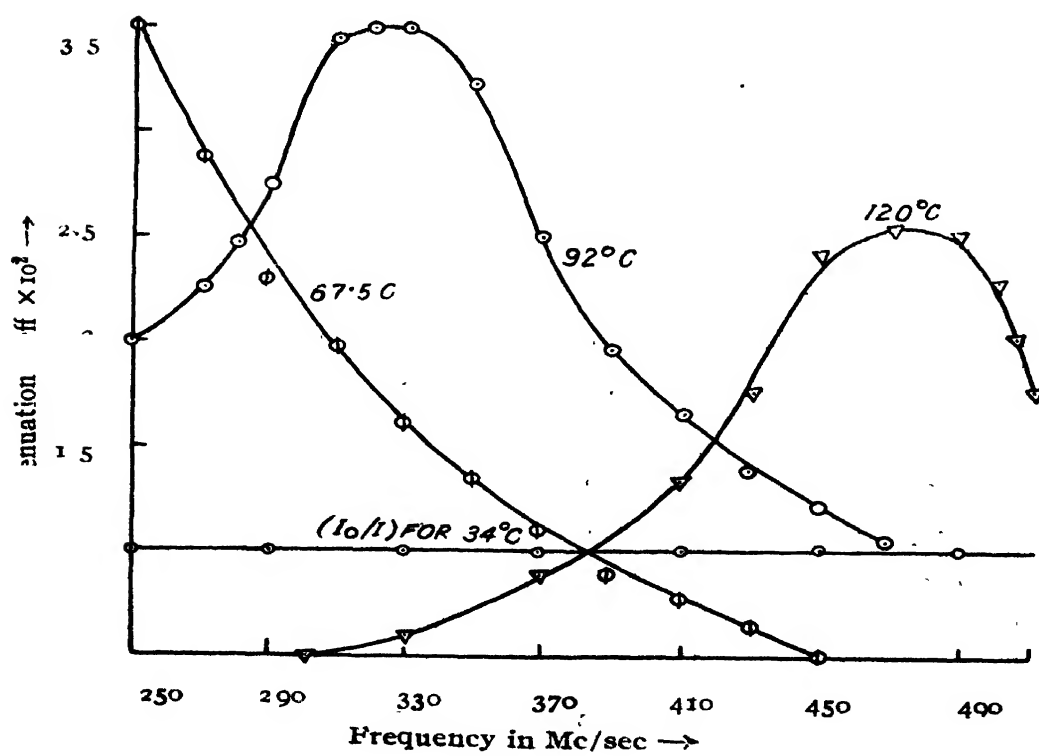


FIG 4  
 $n$ -Butyric acid ( $C_3H_7COOH$ )

where,  $\tau$  = time of relaxation,

$\omega$  = angular frequency at the centre of the absorption peak,

$\epsilon_0$  = square of the refractive index,

$\epsilon_1$  = dielectric constant for static field.

The molecular radius  $a$  has been calculated from the relation

$$a^3 = \frac{\tau k T}{4\pi\eta}.$$

where,  $k$  = Boltzman constant,

$T$  = absolute temperature,

$\eta$  = coefficient of viscosity.

The values thus obtained have been listed in columns 5 and 6 of Table V.

TABLE V

Comparative study of the absorption of U.H.F. radio waves in fatty acids.

Liquid	Temp. °C	Frequency for max. absorption in megacycles/sec.	Viscosity in centipoise	$\tau \times 10^{10}$	$a \times 10^8$
1. Formic acid ... (H.COOH)	34°C 10°C	beyond 510 beyond 510	1.379	1.042	< 2.8
2. Acetic acid ... (CH <sub>3</sub> COOH)	35°C 67.5°C	385 450	1.025	3.002	4.2
3. Propionic acid ... (C <sub>2</sub> H <sub>5</sub> COOH)	65°C 85°C 110°C	290 348 460	.642	4.52	6.6
4. n-butyric acid ... (C <sub>3</sub> H <sub>7</sub> COOH)	93°C 120°C	330 480	.580	4.807	7.26

The expected radius of the single molecule in each case is about half of the calculated value given in the last column. This discrepancy can be explained satisfactorily if it is assumed that the internal viscosity is the same as the macroscopic viscosity and that the molecules exist as dimers in all these acids. In the case of formic acid the diminution in the intensity of integrated absorption with rise of temperature may be partly due to breaking up of some of the dimers into monomers which may show absorption at much higher frequency and partly to the diminution in the intermolecular field. In the case of acetic acid, the number of dimers is the same both at 35°C and 67.5°C, because the integrated absorption is the same. The internal viscosity seems to have different values at different points in the liquid,

because the peak becomes wider at the higher temperature. This may be due to want of regularity in the arrangement of the molecules in the liquid at the higher temperature. In the remaining two cases, the integrated intensity first diminishes rapidly and then slowly. This shows that probably the number of dimers does not diminish appreciably with rise of temperature but the energy absorbed by the dimers diminishes at higher temperatures owing to diminution in the intermolecular field acting on them.

The value of the maximum coefficient of absorption for these fatty acids has been calculated from the following relation given by Debye (1929) :

$$K_m = \frac{\sqrt{\epsilon_1} - \sqrt{\epsilon_0}}{\sqrt{\epsilon_1} + \sqrt{\epsilon_0}}.$$

In calculating the value of  $K_m$  from that of  $\mu$ , the expression  $\mu = \frac{2\pi}{\lambda} \cdot \tau \cdot K_m$  has been used, where  $\tau$  has been calculated from the relation

$$\tau^2 = \frac{1}{2} \cdot \frac{\sqrt{\epsilon_1 \epsilon_0}}{\epsilon_1 + \epsilon_0} (\sqrt{\epsilon_1} + \sqrt{\epsilon_0})^2.$$

TABLE VI

Values of absorption index for fatty acids.

Liquid	Temp. °C.	Attenuation coeff.	$K_{\max}$ . Calculated.	$K_{\max}$ . Observed.
1. Formic acid ... (H.COOH)	34°C	.4002	.6682	1.127
	10°C	.5150		
2. Acetic acid ... (CH <sub>3</sub> COOH)	35°C	.1152	.4032	.6284
	67.5°C	.0725		
3. Propionic acid ... (C <sub>2</sub> H <sub>5</sub> COOH)	65°C	.0325	.2885	.3453
	85°C	.0225		
	110°C	.0215		
4. n-butyric acid ... (C <sub>3</sub> H <sub>7</sub> COOH)	93°C	.0352	.2680	.2804
	120°C	.0252		

The theoretical and experimental values are listed in columns 3 and 4 respectively of Table VI. On comparison the values are found to be almost in agreement with theoretical values in the case of propionic acid and n-butyric acid, but the observed values depart largely from theoretical value in the case of formic acid and acetic acid, the observed values being too high in these cases.



ACKNOWLEDGMENT

The author is indebted to Prof. S. C. Sirkar, D.Sc., F.N.I. for his kind interest and guidance throughout the progress of the work.

OPTICS LABORATORY  
INDIAN ASSOCIATION FOR THE CULTIVATION OF SCIENCE  
CALCUTTA

REFERENCES

- Debye, P., 1929, Polar molecules.  
Sen, S. N., 1949, *Ind. J. Phys* , **23**, 495  
Sen, S. N., 1950, *Ind. J. Phys.* **24**, 163.  
Sen, S. N., 1951, *Ind. J. Phys.*, **25**, 25.

# SCATTERING OF NEUTRONS BY PROTONS AT HIGH ENERGIES

By D. BASU

(Received for publication, April 20, 1951)

**ABSTRACT.** It has been shown here that the recent experimental results on the neutron-proton scattering at 260 Mev energy favours the Möller-Rosenfeld interaction and rules out the pseudoscalar theory. Contrary to the general expectation that the Born approximation is valid before the influence of the radiation reactions needs to be taken into account, it is found that the Born approximation, which is reasonably valid for 260 Mev energy, gives the theoretical value twice as large as the experimental one but the inclusion of the radiation damping term brings the theoretical value in good agreement with the experimental result.

## INTRODUCTION

In the theoretical investigation of the scattering of neutrons by protons, one is faced with the following difficulties: The exact nature of the meson field giving rise to the nuclear interaction is not definitely known. All the four representatives of the meson field so far proposed give rise to nuclear interactions containing inadmissible singularity at  $r \rightarrow 0$ , the presence of which prevents us from having proper solution of the Schrödinger equation. However, without knowing the proper solution, it is possible to calculate the neutron-proton scattering cross-section in the Born approximation which can be applied only in the high energy region. On the other hand, for such relativistic energies, the influence of the field reactions, namely the radiation damping, cannot be neglected, the integral equation describing the influence of the radiation damping is mathematically very complicated.

In the earlier paper the present author investigated the cross section of neutron-proton (in short n-p.) scattering at high energy region in the Born approximation, the Möller-Rosenfeld (in short M.-R.) version of the meson field was chosen for the interaction between the neutron and the proton, the effect of the retardation is accounted for by the mechanism of exchange of charged and neutral mesons of vector and pseudoscalar type. Using the ordinary Born approximation, the cross section for the n-p scattering is found to increase indefinitely with increasing energy of the incident neutron in the relativistic region, no matter whether the vector or the pseudoscalar or the M.-R. mixed meson field is used. In a subsequent paper (Basu, 1950) it was shown that the influence of radiation damping on n-p scattering cross-section is sufficient to prevent the indefinite increase of the cross-section, it was found that the inclusion of radiation damping makes the cross-section decrease as  $1/E'$  for high values of  $E'$ , where  $E'$  is the energy of the neutron

in the rest system. At that time the experimental data on n-p scattering at high energy region was not available to make comparison possible with our theoretical findings.

It is our object in the present paper to compare the theoretical findings of our previous two papers with the recent experimental results of n-p scattering at 260 Mev energy which have appeared in three papers by Kelly, Leith, Segre and Wiegand (1950); Fox, Leith, Wouters and Mackenzie (1950) and Dejuren (1950). Such a comparison would give us an indication as to what will be our choice of the meson field. We shall see here that the M.-R. version of the meson field gives a good fit of the theoretical findings with the experimental values of the total cross section of the n-p scattering at 260 Mev energy.

The M.-R. interaction in the non-relativistic limit contains three constants, one is related to the mass of the meson and the other two represent the strength of the charge and spin coupling. The latter two can be fixed from a comparison of the calculated and the experimental values of the binding energies of the triplet and singlet states of deuteron. The mass of the meson, which determines the first constant, is known from measurements of cosmic ray and artificially produced mesons. It is the  $\pi$ -meson which is responsible for the nuclear force and its mass is 286 electron masses ( $m_e$ ) (Bishop, 1949). In the M.-R. theory, the meson mass corresponding to the pseudoscalar part of the field is assumed to have the same value as the vector counterpart, the pseudoscalar mesons would be spinless particles; there is no experimental evidence yet of spinless mesons of the same mass as  $286 m_e$  which enter into the M.-R. combination. The  $\mu$ -meson, whose mass and spin are 215 (Ratallack and Brode, 1949) and  $\frac{1}{2}$  respectively, has very little influence on the nuclear forces; on the other hand, the contribution to the nuclear force of the  $\tau$ -mesons of mass 800-1000  $m_e$  has not been incorporated in the theory. The three constants of the M.-R. interaction having been thus fixed from the experimental values of the deuteron, binding energies in the singlet and triplet states and direct mass measurements of the observed mesons, a check on the correctness of the M.-R. interaction can then be made by comparing the theoretical value of the n-p scattering cross section so calculated with the recently published experimental values on the same. It is shown here that the value of the total cross section of n-p scattering at 260 Mev energy favours the M.-R. interaction and further, under certain approximations, the influence of radiation damping at this energy is to reduce the cross-section by about one half.

The M.-R. interaction is preferable to other meson field forces because of two other evidences coming out of the experimental results on n-p scattering at different energies. The value of the differential cross-section of n-p scattering at 40, 90 and 260 Mev energies (Kelly and others, 1950) shows a minimum at  $90^\circ$  angle and an increase for forward and backward angles. The results for backward scattering are subject to considerable

errors and the values for angles smaller than  $40^\circ$  are not available yet. In view of the fact that complete and very reliable results of the differential cross-section of n-p scattering are not available yet, it is not possible to make any definite conclusion regarding the charge symmetry of the M.-R. theory.\* If we draw curves through the experimental points of Kelly and others, we can find at 40, 90 and 260 Mev energies the anisotropy of scattering which is expressed as the ratio  $T = d\sigma(\pi)/d\sigma(\pi/2)$ . Moreover, the areas under the curves would give us relative measures of the total cross-sections for the three energy values. We shall see that  $T$  increases and  $Q$  decreases with increasing energy values of the scattered neutrons. Hulthén (1944) has investigated the anisotropy ratio for different meson fields in the non-relativistic limit and he finds that in the M.-R. theory the ratio tends towards infinity for increasing energy values which is borne out by the experimental finding. According to Hulthén, the anisotropy ratio for the symmetrical pseudoscalar theory decreases with increasing energy and tends to the limit 1 for very high energies, the same ratio for the symmetrical vector meson theory tends to the limit  $3 + 2g_1^4/g_2^4$  ( $\approx 3.1$ ) for every high energies, whereas, the experimental value for 260 Mev neutron energy is 9. The value of the total cross-section for 260 Mev neutron energy is nearly one half the value for 90 Mev. We shall presently see that this decrease of the total cross-section with increasing energy values can be satisfactorily explained in the M.-R. theory but not in the pseudoscalar theory.

There is, however, one difficulty with the M.-R. theory in which the tensor force is eliminated in the non-relativistic limit, as such the M.-R. theory fails to explain the presence of the quadrupole moment of the deuteron. The tensor force, which contains the inadmissible singularity at  $r \rightarrow 0$  of the type  $1/r^3$  but explains the presence of the quadrupole moment, appears in both the vector and pseudoscalar theory. However, the quadrupole moment, as calculated from the pseudoscalar theory, agrees in sign but not in magnitude with the experimental value. In the non-relativistic limit the tensor force term of the pseudoscalar theory has the same form but with the opposite sign as that of the vector theory; that is why the mixed M.-R. field eliminates the tensor force in the static interaction if the constants are given the same value for both the fields. The subsequent generalization of Schwinger (1942) does not give the correct value of the quadrupole moment of the deuteron as has been shown by Jauch and Hu (1944) and Ramsey (1948). It may be mentioned in this connection that the elimination of the tensor force in the M.-R. theory is effected only in the

\* From the angular distribution of the scattered neutrons it was tentatively suggested by Serber (quoted by Yukawa, 1949) that a mixture of the exchange and non-exchange forces in the ratio 1:1 gives a good fitting with the experimental findings. Prof. Rosenfeld thinks (in course of a conversation) that the experimental results that are in progress may not bear out Serber's suggestion.

static potential, the tensor force reappears, as has been shown by Hu (1945), in the relativistic region.

The Born approximation, which we have applied in our calculations, is valid when the energy of the colliding particles is large compared with their interaction energy. From calculations regarding the criterion of the validity of the Born approximation, it appears that it is valid for energies above 50–100 Mev (measured in the centre of mass system). While on the high energy side, when the Born approximation becomes valid, the question arises as to the necessity of including the influence of radiation damping. Heitler (1948) and Janossy and McConnell (1950) have probed into the problem of finding the energy region within which the Born approximation is sufficiently good and yet the influence of the radiation damping is not pronounced. According to Heitler (1948), the Born approximation becomes valid before the effects of the field reactions have to be taken into account; however, we shall see that a closer examination makes this view untenable. The Born approximation is reasonably valid for 63.0 Mev energy (this value in CM corresponds to 260 Mev energy in the rest system), and for this energy we find that the theoretical value of the cross-section without the inclusion of radiation damping is twice the experimental value; further if the influence of the radiation damping is included, there is reasonable agreement between the theoretical and the experimental values. It means that when the Born approximation is applicable, it becomes also necessary to include the influence of the radiation reactions.

#### THE MÖLLER-ROSENFELD INTERACTION

The M.-R. interaction between two nucleons in the non-relativistic limit takes the simple form given by

$$W^{12} = (\tau^1 \tau^2) \left\{ g_1^2 + g_2^2 (\sigma^1 \sigma^2) \right\} \left\{ \frac{e^{-\lambda r}}{r} \right. \quad \dots \quad (1)$$

where  $\tau^1, \tau^2$ ;  $\sigma^1, \sigma^2$  denote the isotopic spin-vectors and spin operators of the two particles numbered 1 and 2 and  $r$  is the distance between the two nucleons. The constant  $\lambda = \mu/\hbar c$ ,  $\mu$  being the mass of the meson in energy units and  $\hbar, c$  have their usual meanings. The constants  $g_1$  and  $g_2$ , which have the dimension of electric charge, denote the strengths of the two types of coupling.

The Schrödinger equation of the deuteron with the above potential can be solved numerically, then the values of the binding energies in the triplet and singlet states make it possible to determine  $g_1$  and  $g_2$ . The recent calculation of Fröhlich, Huang and Sneddon (1947) gives their values as

$$\frac{g_1^2}{\hbar c} = 0.0246, \quad \frac{g_2^2}{\hbar c} = 0.000306 \frac{m_p}{m_e} + 0.0085 \quad (2)$$

The experimental value for the ratio of the meson mass to that of the electron ( $m_u/m_e$ ) is 286, in which case the constants become

$$\frac{g_1^2}{\hbar c} = 0.024, \quad \frac{g_2^2}{\hbar c} = 0.096 \quad \dots (3)$$

The constant  $g_1^2$  is smaller than  $g_2^2$  by a factor 4, the scattering cross-sections are proportional to the fourth power of  $g_1$  and  $g_2$ . We shall see in the next section that the scattering at high energy due to the  $g_1$  part of the interaction can be neglected because of two reasons: (1)  $g_1^4$  is much smaller than  $g_2^4$  and (2) the scattering cross section due to the  $g_1$  interaction falls quite sharply with increasing energy of the incident particle.

#### N-P SCATTERING CROSS SECTION

The exact relativistic expression for neutron-proton interaction according to the M.-R. version of the meson field is given in equations (5) and (6) of the earlier paper (Basu, 1949). This interaction includes in it such terms as would make it free, in the non-relativistic limit, from contact potentials of the form of  $\delta$ -function. Such an elimination of the  $\delta$ -functions has an important bearing on the  $g_1$ -scattering of neutrons by protons, the cross section of which decreases with increasing energy and tends to a constant in the extreme relativistic region. This decrease of cross section with increasing energy is reversed if the  $\delta$ -functions are not eliminated in the above mentioned way.

The calculation of the scattering cross-section with the M.-R. interaction is very laborious, the part played by the  $g_1$ -interaction will be shown to be small enough to be neglected, as such, we have avoided some labour by calculating the relative contributions of the vector and the pseudoscalar meson fields separately, we shall see that so far as  $g_1$ -scattering is concerned the contribution of the pseudoscalar field is exceedingly small compared with that of the vector field. Representing the nucleon by the Dirac spinor, the total cross section of the n-p scattering due to the  $g_1$ -interaction of the vector (charged or neutral) meson field is given by

$$Q_0 = \frac{2\pi}{\lambda^2} \frac{g_1^4}{\hbar^2 c^2} \frac{a^2}{1+x^2} \left[ \frac{2}{a^4} \left\{ 1 + \frac{1}{1+4a^2x^2} (2a^2x^2 + 16a^4x^4) \right. \right. \\ \left. \left. - \left( 1 + \frac{1}{4a^2x^2} \right) \log (1+4a^2x^2) \right\} + \frac{8}{a^2} \left\{ 1 - \frac{1}{4a^2x^2} \log (1+4a^2x^2) \right\} + \frac{8}{1+4a^2x^2} \right] \\ \dots (4)$$

where  $a$  is the ratio of the nucleon mass to the meson mass and is 6.42 for the meson mass being equal to 286  $m_e$ ,  $x$  is the ratio  $p_0/M$ ,  $p_0$  and  $M$  both expressed in energy units are the momentum in the centre of mass system and the rest mass of the incident neutron or proton. The reciprocal of  $\lambda$  has the dimension of length and its value for the meson mass 286  $m_e$

is  $1.35 \times 10^{-13}$  cm. The numerical value of the above expression is  $Q_0^v(g_1) = 0.11 \times 10^{-26}$  cm<sup>2</sup> for 260 Mev neutron energy.

The similar cross-section due to the  $g_1$ -interaction of the pseudoscalar (charged or neutral) meson field has the form

$$Q_0^{ps} = \frac{2\pi}{\chi^2} \frac{g_1^4}{\hbar^2 c^2} \frac{a^2}{1+x^2} \left[ \frac{1}{a^4} \right]^{\frac{1}{2}} + \frac{1}{2(1+4a^2x^2)} - \frac{1}{4a^2x^2} \log(1+4a^2x^2) \quad (5)$$

$Q_0^{ps}(g_1) = 0.00005 \times 10^{-26}$  cm<sup>2</sup> for 260 Mev neutron energy.

It is evident that in a mixture of the vector and pseudoscalar fields, the contribution to the  $g_1$ -scattering at 260 Mev energy, of the pseudoscalar part of the field is smaller than the vector part by a factor  $5 \times 10^{-4}$ ; as such in the  $g_1$ -scattering only the addition of the pseudoscalar field to the vector field does not give anything different from what would be obtained from the pure vector field. However, if we combine the charged and the neutral field in a way to ensure charge symmetry, the value of the cross section would be roughly multiplied by a factor 2. Hence the value of the total cross-section due to the  $g_1$ -interaction of the M.-R. theory will be approximately

$$Q_0^{MR}(g_1) \approx 0.22 \times 10^{-26} \text{ cm}^2 \text{ for 260 Mev neutron energy.}$$

We shall see in the next paragraph that the total scattering cross-section due to the  $g_2$  interaction alone of the M.-R. theory has the value  $7.02 \times 10^{-26}$  cm<sup>2</sup> (for 260 Mev neutron energy) which is roughly 30 times the value of the above cross section due to the  $g_1$ -interaction at the same energy value. Since the evaluation of the general expression for the cross section of the n-p scattering is exceedingly complicated when both  $g_1$  and  $g_2$  of the relativistic M.-R. interaction are different from zero; we shall simplify our calculations by putting  $g_1=0$  it would mean that the value of the cross section so obtained would be less than that of the exact expression which includes both  $g_1$  and  $g_2$  by 5 to 10 per cent.

If we neglect the contribution of the  $g_1$ -scattering for reasons stated above, the total cross-section of n-p scattering with the M.-R. version as the interaction between the neutron and proton is given by

$$\begin{aligned} Q_0^{MR} = & \frac{2\pi}{\chi^2} \frac{g_2^4}{\hbar^2 c^2} \frac{a^2}{1+x^2} \left[ x^4 \left\{ \frac{32}{3} + \frac{6}{a^2x^2} + \frac{25}{24a^4x^4} + \frac{5}{8a^4x^4(1+4a^2x^2)} \right. \right. \\ & - \left. \left( \frac{13}{3a^2x^2} + \frac{41}{24a^4x^4} + \frac{5}{12a^6x^6} + \frac{5}{4a^2x^2(1+2a^2x^2)} \right) \log(1+4a^2x^2) \right\} \\ & + 4x^2 \left\{ \frac{1}{a^2x^2} + \left( \frac{19}{12a^2x^2} - \frac{1}{4a^4x^4} - \frac{5}{4a^2x^2(1+2a^2x^2)} \right) \log(1+4a^2x^2) \right\} \\ & + 3 \left\{ \frac{10}{1+4a^2x^2} - \frac{1}{a^2x^2(1+2a^2x^2)} \log(1+4a^2x^2) \right\} \Bigg] \quad \dots \quad (6) \end{aligned}$$

The above expression (6) for  $Q$  decreases with increasing  $x$  in the low energy region from  $x=0$  to about  $x=0.5$  (the latter value would correspond to a kinetic energy of the value 110 Mev in the centre of mass system or 470 Mev in the system in which the proton is at rest) after which it increases in the relativistic region indefinitely with increasing values of  $x$ . The value of  $Q$  is sensitive to the value of the meson mass. The numerical values of the cross sections as calculated from the above expression are as follows :

$$Q_0^{MR} = \begin{cases} 7.02 \times 10^{-26} \text{ cm}^2 & \text{for 260 Mev neutron energy} \\ 12.73 \times 10^{-26} \text{ cm}^2 & \text{,, 90 Mev ,, ,, } \end{cases}$$

It must be borne in mind that the relativistic Born approximation which we have employed in our calculations is not quite good for 90 Mev neutron energy which would correspond to 21.6 Mev energy in the centre of mass system.

To compare the relative contributions of the vector and the pseudoscalar fields in the mixed field of the M.-R. theory, we consider the  $g_2$ -scattering due to the pseudoscalar interaction alone. Contrary to what we have seen for the  $g_1$ -scattering, we notice that the  $g_2$ -scattering due to the pseudoscalar interaction is larger than the same due to the M.-R. interaction. Bearing in mind that every interaction between two nucleons, in the non-relativistic limit, should be free from  $\delta$ -functions, the total cross section for n-p scattering due to the pseudoscalar (charged or neutral) field is given by

$$Q_0^{ps} = \frac{2\pi}{\chi^2} \frac{g_2^4}{\hbar^2 c^2} \frac{a^2}{1+x^2} \frac{32}{9} \left[ \frac{8}{3}x^4 + x^2 + \frac{8}{3} + \frac{9}{4(1+4a^2x^2)} - \frac{8}{3} \frac{1}{2a^2x^2} \log(1+4a^2x^2) \right] \dots (7)$$

The cross-section  $Q_0^{ps}$  (7) increases indefinitely with increasing  $x$  right from  $x=0$ . The numerical values as calculated from the above expression are as follows :

$$Q_0^{ps}(g_2) = \begin{cases} 18.02 \times 10^{-26} \text{ cm}^2 & \text{for 260 Mev neutron energy,} \\ 14.42 \times 10^{-26} \text{ cm}^2 & \text{,, 90 Mev ,, ,, } \end{cases}$$

We notice that the  $g_2$ -scattering cross section, when calculated with the pseudoscalar interaction, is very much larger than the similar expression calculated with the M.-R. interaction.

If we denote the matrix elements of the process of scattering by  $H_A$  the square of which is proportional to the cross section, it is clear from a comparison of the numerical values of the cross-section, as calculated with the M.-R. interaction, and the interaction due to the pseudoscalar field that the absolute value of the matrix elements for the M.-R. interaction is less than the same for the pseudoscalar interaction round about 260 Mev energy.



It follows from the method of Hsüeh and Ma (1945) that the scattering cross section is influenced by the radiation damping in the following way :

$$Q = \frac{Q_o}{1 + b^2/a^2} \quad \dots \quad (8)$$

where  $Q_o$  denotes the ordinary cross section in which radiation damping has been neglected.  $b$  and  $a$  are given by

$$a = \sum_i \sum_f \int H_{if} H_{fi} \rho_f d\Omega_f, \quad (9a)$$

$$b = \pi \sum_i \sum_f \sum_{f'} \int \int H_{if} H_{ff'} H_{f'i} \rho_f \rho_{f'} d\Omega_f d\Omega_{f'}. \quad (9b)$$

The suffices  $f$  and  $i$  stand for the final and initial states,  $\rho_{f'}$  denotes the density of energy levels corresponding to the state  $f'$ . The evaluation of  $a$  and  $b$  with the  $H_{fi}^{M.-R.}$  for the M.-R. interaction is the proper procedure, but such a procedure is exceedingly involved to calculate. To simplify labour  $a$  and  $b$  have been calculated in a previous paper (Basu, 1950) with the matrix elements  $H_{fi}^{ps}$  for the pseudoscalar field. As  $|H_{fi}^{M.-R.}|$  is smaller than  $|H_{fi}^{ps}|$ , therefore the exact value of  $|b/a|$ , as evaluated with the matrix elements  $H_{fi}^{M.-R.}$  for the M.-R. interaction, would be somewhat smaller than what is calculated here with the pseudoscalar interaction. We give below the expression for the ratio  $b/a$

$$\frac{b}{a} = \frac{g_2^2}{4} \frac{a^2 x}{(1+x^2)^{\frac{1}{2}}} \frac{F_b(x)}{F_a(x)} \quad \dots \quad (10)$$

where  $F_a(x)$  and  $F_b(x)$  are functions of the variable  $x$  and their forms are quoted for convenience in the Appendix. The numerical values are as follows :

$$1 + \frac{b^2}{a^2} = \begin{cases} 2.19 & \text{for 260 Mev neutron energy,} \\ 1.23 & \text{,, 90 Mev ,, ,, } \end{cases}$$

It shows that the influence of radiation damping at 260 Mev energy is to reduce the ordinary cross section by about one half, which is by no means negligible. We regard the influence of damping as a correction factor to the ordinary expression for the scattering cross section, the procedure of calculating the damping term with the pseudoscalar interaction is justified on the ground that it gives the order of the correction. However, it must be remembered that the exact numerical values for the M.-R. interaction would be somewhat smaller than the above figures.

We now give below in a tabular form the numerical values so far derived from the theoretical expressions :

$E'_{\text{kin}} \text{ (RS)}$	$E_{\text{kin}} \text{ (CM)}$	$\alpha$	$Q_{\text{MR}} \times 10^{26} \text{ cm}^2$	$Q_{\text{MR}} \times 10^{26} \text{ cm}^2$ (with damping)	$Q_{\text{Ps}} \times 10^{26} \text{ cm}^2$	$Q_{\text{Ps}} \times 10^{26} \text{ cm}^2$ (with damping)
90 Mev	21.6 Mev	0.219	12.7 <sup>*</sup>	10.3 <sup>*</sup>	14.4 <sup>*</sup>	11.7 <sup>*</sup>
260 Mev	63.0 Mev	0.372	7.0	3.2	18.0	8.2

$E'_{\text{kin}}$  denotes the kinetic energy in the system in which the proton is at rest whereas,  $E_{\text{kin}}$  is the corresponding kinetic energy in the centre of mass-at-rest-system.

We then compare the above with the experimental findings of different workers. The curves drawn through the experimental points of Kelly and others give us the following results.

*Experimental Results of Kelly and Others.*

$E'_{\text{kin}} \text{ (RS)}$	$T = \frac{dQ(\pi)}{dQ(\pi/2)}$	$Q \text{ (in arbitrary units)}$
40 Mev	1.6	25.1
90 Mev	3.7	13.4
260 Mev	9.2	7.0

The value of the total n-p scattering cross section has been measured by Fox, Leith, Wouters and MacKenzie (1950) who have used a double coincidence anthracene scintillation counter telescope as the neutron detector. The same measurement has been done by DeJuren (1950) using bismuth fission ionization chamber as the neutron detector.

$E'_{\text{kin}} \text{ (RS)}$	Total cross section $Q \times 10^{26} \text{ cm}^2$	
	Fox and others	DeJuren
85 Mev	$8.3 \pm 0.4$	
95 "		7.3
270 "		$3.8 \pm 0.2$
280 "	$3.3 \pm 0.3$	

$$\frac{Q(260 \text{ Mev})}{Q(90 \text{ Mev})} = 0.52 \quad (\text{from Kelly and others})$$

\* We have marked the values of the cross section for 21.6 Mev energy (CM) with asterisks to indicate that the Born approximation is not good for such an energy.

$$\frac{Q(280 \text{ Mev})}{Q(85 \text{ Mev})} = 0.40 \quad (\text{Fox and others})$$

$$\frac{Q(270 \text{ Mev})}{Q(95 \text{ Mev})} = 0.52 \pm 0.03 \quad (\text{DeJuren})$$

The theoretical value of the total scattering cross section after being corrected for radiation damping is  $3.2 \times 10^{-26} \text{ cm}^2$  and the two experimental values are  $3.3 \pm 0.2 \times 10^{-26} \text{ cm}^2$  and  $3.8 \pm 0.2 \times 10^{-26} \text{ cm}^2$ . The agreement appears to be very good, the fact that our theoretical value is on the side of being slightly less than the experimental one is expected because the calculations can be improved in two ways each of which would increase the value slightly and as such the two together would make the agreement much better. The two improvements consist of taking both  $g_1$ - and  $g_2$ -interactions and the evaluation of the radiation correction with the M.-R. theory. The M.-R. theory allows us to fix the two constants from the deuteron problem, the determination of the third constant from the observed mass of the  $\pi$ -meson leaves no arbitrariness about the n-p scattering cross-section, as such the agreement of the theoretical and the experimental values of the scattering cross section shows that the deuteron and n-p scattering problem can be consistently framed in one picture with the help of the M.-R. theory.

It is quite evident, as was expected to be so, that the Born approximation is not good for 21.6 Mev energy (corresponding to 90 Mev in RS), for such low energies the Born approximation gives too large values for the cross section compared with what they should be. The pseudoscalar field alone fails to explain the n-p scattering results.

#### ACKNOWLEDGMENTS

The author's sincerest thanks are due to Prof. M. N. Saha who initiated a discussion on n-p scattering by requesting him to deliver a course of seminar lectures in the Institute of Nuclear Physics, Calcutta University. The discussion formed the starting point of the present paper.

## APPENDIX

$$F_a(x) = \frac{8}{9} \left\{ \frac{2}{3} x^4 + x^2 + \frac{3}{2} + \frac{9}{4} \frac{1}{1+4a^2x^2} - \frac{3}{4a^2x^2} \log(1+4a^2x^2) \right\}$$

$$F_b(x) = \frac{32}{9} \left\{ \frac{16}{27} x^6 + \frac{4}{3} x^4 + 2x^2 + 1 \right\} + \frac{1}{8} (x^2 + 1) \left\{ x^4 + 4x^2 + 8 \right\} A \\ - \frac{2}{3} (x^2 + 1) \left\{ x^4 + 4x^2 + 7 \right\} B - \frac{x^4}{18} (x^2 + 1) C + \frac{x^2}{32} \left\{ 2x^4 + 2x^2 + 7 \right\} C^2$$

where (putting  $x = \frac{1}{2a^2} + 1$ )

$$A = 16\alpha - 6x^2 + (8 + 2x - 16\alpha^2 + 6x^3) \log \frac{\alpha + 1}{\alpha - 1} \\ + \left( \frac{5}{2} - 4\alpha - x^2 + 4x^3 - \frac{3}{2} x^4 \right) \left( \log \frac{\alpha + 1}{\alpha - 1} \right)^2$$

$$B = 2 - (\alpha - 1) \log \frac{\alpha + 1}{\alpha - 1}$$

$$C = 2x - (x^2 - 1) \log \frac{\alpha + 1}{\alpha - 1}$$

## REFERENCES

- Basu., 1949, *Proc. Roy. Ir. Acad.*, **52**, 127.  
 1950, *ibid* **53**, 31.  
 Bishop, 1949, *Phys. Rev.*, **15**, 1468.  
 DeJuren, 1950, *Phys. Rev.*, **80**, 27.  
 Fox, Leith, Wouters and MacKenzie, 1950, *Phys. Rev.*, **80**, 23.  
 Fröhlich, Huang and Sneddon., 1947, *Proc. Roy. Soc.*, **191A** 61.  
 Heitler, 1948, *Proc. Roy. Ir. Acad.*, **52**, 95,  
*Cf. Acta Phys. Austriaca Bd. 1*, 110.  
 Hsüeh and Ma., 1945, *Phys. Rev.*, **67**, 303.  
 Hu, 1945, *Phys. Rev.*, **67**, 339.  
 Hulthén, 1944, *Arkiv. Mat. Astr. Fys.* **31A**, No. 15.  
 Janossy and McConnell, 1950, *Proc. Roy. Ir. Acad.*, **53**.  
 Jäuch and Hu, 1944, *Phys. Rev.*, **65**, 289.  
 Kelly, Leith, Segre, and Wiegand, 1950, *Phys. Rev.*, **79**, 96.  
 Ramsey, 1948, *Proc. Phys. Soc.*, **61**, 297.  
 Ratallack and Brode, 1949, *Phys. Rev.*, **75**, 1716.  
 Schwinger, 1942, *Phys. Rev.*, **61**, 287A.  
 Yukawa, 1949, *Rev. Mod. Phys.*, **21**, 474.

# PARTICULAR SOLUTIONS OF EINSTEIN'S RECENT UNIFIED THEORIES\*

By G. BANDYOPADHYAY

(Received for publication, February 15, 1951)

**ABSTRACT** Different field equations, one proposed by Einstein and Straus in 1946 and the other by Einstein in 1950, have been solved for the particular case analogous to an infinite charged plane.

## INTRODUCTION

Einstein has developed a new generalized theory (Einstein and Straus, 1946) in which the field variables are the sixteen components of a non-symmetric tensor  $g_{\mu\nu}$  ( $\mu, \nu = 1, 2, 3, 4$ ). It has been suggested by Einstein that the antisymmetric part of this tensor corresponds to the electromagnetic field.

In order to obtain the field equations one has first to obtain the non-symmetric  $\Gamma$ 's from the sixty-four equations

$$g_{ik,a} - g_{sk}\Gamma_{ia}^s - g_{is}\Gamma_{ik}^s = 0 \quad \dots (1)$$

and then obtain  $P$ 's defined by

$$P_{ik} = \Gamma_{ik,a}^a - \frac{1}{2}(\Gamma_{ia,k}^a + \Gamma_{ak,i}^a) - \Gamma_{ib}^a \Gamma_{ak}^b + \frac{1}{2}\Gamma_{ik}^a (\Gamma_{ab}^b + \Gamma_{ba}^b) \quad \dots (2)$$

and finally write down the equations

$$\frac{1}{2}(\Gamma_{ia}^a - \Gamma_{ai}^a) = 0 \quad \dots (3a)$$

$$\frac{1}{2}(P_{ik} + P_{ki}) = 0 \quad \dots (3b)$$

$$\frac{1}{2}(P_{ik,i} - P_{ki,i}) + \frac{1}{2}(P_{ki,i} - P_{ik,i}) + \frac{1}{2}(P_{il,i} - P_{il,i}) = 0 \quad \dots (3c)$$

(in terms of  $g$ 's) which comprise the field equations propounded in 1946. It may be mentioned in passing that there exists no simple method of solving equation (1). Straus (1949), however, has recently developed a method which reduces the labour of calculations to some extent.

Einstein (1950), however, has very recently modified the field equations. The new equations are equivalent to equations (3a), (3b) and the equation

$$\frac{1}{2}(P_{ik} - P_{ki}) = 0 \quad \dots (3d)$$

instead of (3c). We shall designate the field equations given by (3a), (3b), (3c) as I and those given by (3a), (3b), (3d) as II.

It may be noted that II is stronger than I. This paper discusses a particular solution of the above field equations.

\* The contents of this paper was published in the Abstracts of the 38th session (January, 1951) of the Indian Science Congress (Mathematics Section). The result, however, has since been slightly modified.

## CALCULATIONS

We take

$$g_{11}=1, \quad g_{22}=g_{33}=G(x_1), \quad g_{44}=H(x_1), \quad g_{14}=-g_{41}=I(x_1)$$

The sixty-four equations (1) now break up into a number of partial sets and we obtain the following non-vanishing  $\Gamma$ 's :

$$\Gamma^1_{14} = -\frac{1}{2} \frac{dH}{dx} - 2I \frac{HI' - \frac{1}{2}IH'}{I^2 + H}$$

$$\Gamma^1_{14} = -\Gamma^1_{41} = \frac{HI' - \frac{1}{2}IH'}{I^2 + H}$$

$$\Gamma^1_{14} = \Gamma^4_{41} = \frac{II' + \frac{1}{2}H'}{I^2 + H}$$

$$\Gamma^2_{12} = \Gamma^2_{21} = \Gamma^3_{13} = \Gamma^3_{31} = \frac{1}{2G} \cdot \frac{dG}{dx}$$

$$\Gamma^1_{22} = \Gamma^1_{33} = -\frac{1}{2} \frac{dG}{dx}$$

$$\Gamma^2_{42} = -\Gamma^2_{24} = \Gamma^3_{43} = -\Gamma^3_{34} = -\frac{I}{2G} \cdot \frac{dG}{dx},$$

dash denoting differentiation with respect  $x(x=x_1)$ .

The expressions for  $P$ 's are now calculated by formula (2) as follows :

$$P_{11} = -\frac{d}{dx} \left( \frac{G'}{G} + \frac{II' + \frac{1}{2}H'}{I^2 + H} \right) - 2 \left( \frac{G'}{2G} \right)^2 - \left( \frac{II' + \frac{1}{2}H'}{I^2 + H} \right)^2$$

$$P_{14} = \frac{1}{2} \frac{d}{dx} \left( \frac{HI' - \frac{1}{2}IH'}{I^2 + H} \right) - \frac{d}{dx} \left( \frac{IG'}{2G} \right) - 2 \cdot \frac{G'}{2G} \cdot \frac{IG'}{2G} + 2 \cdot \frac{G'}{2G} \left( \frac{HI' - \frac{1}{2}IH'}{I^2 + H} \right)$$

$$P_{22} = P_{33} = -\frac{d}{dx} \left( -\frac{1}{2}G' \right) - \frac{1}{2}G' \cdot \frac{II' + \frac{1}{2}H'}{I^2 + H}$$

$$P_{44} = \frac{d}{dx} \left[ -\frac{1}{2} \frac{dH}{dx} - 2I \frac{HI' - \frac{1}{2}IH'}{I^2 + H} \right] + \left( \frac{HI' - \frac{1}{2}IH'}{I^2 + H} \right)^2 - 2 \left( \frac{IG'}{2G} \right)^2 \\ + \left( -\frac{1}{2} \frac{dH}{dx} - 2I \frac{HI' - \frac{1}{2}IH'}{I^2 + H} \right) \left( 2 \frac{G'}{2G} - \frac{II' + \frac{1}{2}H'}{I^2 + H} \right)$$

other  $P$ 's vanish.

We now proceed to form field equations I. Of the four equations (3a) three are satisfied identically and we are left with only one equation; viz.,

$$\frac{HI' - \frac{1}{2}IH'}{I^2 + H} + \frac{IG'}{G} = 0 \quad \dots (4a)$$

Of the ten equations (3b) five are identically satisfied due to vanishing of

corresponding  $P$ 's, one is identically satisfied due to antisymmetry of  $P_{14}$ , and of the rest two become identical. So we get the three equations

$$\frac{d}{dx} \left( \frac{G'}{G} + \frac{II' + \frac{1}{2}H'}{I^2 + H} \right) + \frac{1}{2} \left( \frac{G'}{G} \right)^2 + \left( \frac{II' + \frac{1}{2}H'}{I^2 + H} \right)^2 = 0 \quad \dots (4b)$$

$$G'' + G'' \cdot \frac{II' + \frac{1}{2}H'}{I^2 + H} = 0 \quad \dots (4c)$$

$$\begin{aligned} \frac{d}{dx} \left( \frac{1}{2}H' + \frac{HI' - \frac{1}{2}IH'}{I^2 + H} \right) - \left( \frac{HI' - \frac{1}{2}IH'}{I^2 + H} \right)^2 - \frac{1}{2} \left( \frac{IG'}{G} \right)^2 \\ + \left( \frac{1}{2}H' + \frac{HI' - \frac{1}{2}IH'}{I^2 + H} \right) \left( \frac{G'}{G} - \frac{II' + \frac{1}{2}H'}{I^2 + H} \right) = 0 \quad \dots (4d) \end{aligned}$$

Equation (3c) is identically satisfied because  $P_{14}$  is antisymmetric and other non-diagonal  $P$ 's vanish.

It may be noted that the field equations I are not affected by the expression for  $P_{14}$ .

In field equations II, the contributions of (3a), (3b) are the same, but (3d) give an additional equation corresponding to

$$\frac{1}{2}(P_{14} - P_{41}) = 0$$

which leads to the additional equation

$$\frac{1}{2} \frac{d}{dx} \left( \frac{HI' - \frac{1}{2}IH'}{I^2 + H} \right) - \frac{d}{dx} \left( \frac{IG'}{2G} \right) - \frac{IG'^2}{2G^2} + \frac{G'}{G} \left( \frac{HI' - \frac{1}{2}IH'}{I^2 + H} \right) = 0 \quad \dots (4e)$$

#### SOLUTION OF FIELD EQUATIONS I

We are to solve for the three quantities,  $G$ ,  $H$ ,  $I$ , from the four equations (4a), (4b), (4c), (4d).

From (4c) we get

$$I^2 + H = \frac{a}{G^{1/2}}, \quad (a, \text{ constant}) \quad \dots (5a)$$

Substituting from (4c) in (4b) we have

$$\frac{d}{dx} \left( \frac{G'}{G} - \frac{G''}{G'} \right) + \frac{1}{2} \left( \frac{G'}{G} \right)^2 + \left( \frac{G''}{G'} \right)^2 = 0$$

From this we get, after some manipulation

$$G'^2 = b \cdot G^{\frac{1}{2}} e^{cG^2}, \quad (b, c, \text{ constants}), \quad \dots (5b)$$

(4a) can be written as

$$\frac{(H + I^2)I' - I(II' + \frac{1}{2}H')}{H + I^2} + \frac{IG'}{G} = 0,$$

which leads to the solution

$$\frac{IG}{\sqrt{I^2 + H}} = \text{const.}$$

which again, on using (5a), reduces to

$$I = \frac{d}{GG'}, \quad (d, \text{constant}) \quad \dots \quad (5c)$$

(5a), (5b), (5c), obtained without using (4d), determine  $G, H, I$  completely; because  $G$  being known by (5b),  $I$  can be determined from (5c) and can then be used to determine  $H$  from (5a). We proceed to obtain an expression using (4d) in order to test the consistency of (5a), (5b), (5c) with (4d).

Using (4a) and (5c), (4d) can be written as

$$\frac{d\lambda}{dx} + \frac{d}{dx} (\log GG') \cdot \lambda = \frac{3}{2} \frac{d^2}{G^4}$$

where

$$\lambda = \frac{1}{2}H' + 2I \frac{HI' - \frac{1}{2}IH'}{I^2 + H}$$

the solution of which, on using (4a) again, can be written as

$$H' = \frac{1}{GG'} \left( \frac{5}{2} \cdot \frac{d^2}{G^2} + e \right), \quad (e, \text{constant})$$

We shall test the consistency of this with (5a), (5b) and (5c). (5a) and (5c) give

$$H = \frac{1}{G'^2} \left( a - \frac{d^2}{G^2} \right)$$

Differentiating and using

$$\frac{2G''}{G'^2} = \frac{1}{2G} + 2G$$

which can easily be derived from (5b), we have

$$H' = \frac{1}{GG'} \left( \frac{5}{2} \cdot \frac{d^2}{G^2} + 2acG^2 + 2cd^2 - \frac{1}{2}a \right) \quad \dots \quad (5e)$$

Consistency of (5d) and (5e) requires

$$c = 0, \quad e = -\frac{1}{2}a$$

The full solutions of  $g$ 's with these restrictions on the constant lead to

$$g_{11} = 1, \quad g_{22} = g_{33} = \left( k + \frac{3}{4} \sqrt{bx} \right)^{4/8}, \quad g_{44} = \frac{16}{9(k + \frac{3}{4} \sqrt{bx})^{2/8}} \left( a - \frac{d^2}{(k + \frac{3}{4} \sqrt{bx})^{8/8}} \right)$$

$$g_{14} = -g_{41} = \frac{4d}{3\sqrt{b}(k + \frac{3}{4} \sqrt{bx})^{5/8}}$$

If  $g_{14}$ , and therefore  $I$ , be interpreted as the electric field then  $d$  may be taken to be related to charge per unit area and the case may be taken as the analogue of an infinite charged plane.



SOLUTION OF FIELD EQUATIONS II

In this case the additional equation (4e), can be solved on using (4a) and the solution gives

$$IG'G^{1/2}=f, (f, \text{constant}) \quad \dots (5f)$$

This is inconsistent with (5c) unless both the constants  $f$  and  $d$  vanish. This leads to either  $I=0$ , or  $G'=0$ .  $I=0$  makes the field purely gravitational.  $G'=0$  leads to (as can easily be seen from field equations)

$$G=\text{const}, H=\text{const}, I=\text{const}.$$

Thus the only solution in which electromagnetic field exists is one in which the symmetric elements are those corresponding to a flat space. This solution is also included in I as II is a stronger set.

CONCLUSION

If the symmetric parts of  $g$ 's are interpreted as the metric and  $g_{44}$ , as electric field then for an infinite charged plane massless charge as well as charged mass are possible according to the older field equations (1946) but in the new field equations (1950) massless charge is the only possibility if charge is to exist.

GOVT. COLLEGE  
DARJEELING, WEST BENGAL.

REFERENCES

- Einstein, A., and Straus, E. G., 1946., *Ann. Math.*, **47**, 731.  
Einstein, A., 1950, *The Meaning of Relativity*, Methuen & Co., 4th Ed., Appendix 11.  
Starus, E. G., 1949, *Rev. Mod. Phys.*, **20**, 414.

# ON THE ABSORPTION SPECTRA OF TOLUENE IN THE LIQUID AND SOLID STATES\*

By H. N. SWAMY

(Received for publication, April 20, 1951)

## Plate X

**ABSTRACT.** The absorption spectra of toluene in the ultraviolet region have been investigated in the liquid state at 30°C and in the solid state at -180°C. An examination of the photographs reveals that lowering of temperature, contrary to the results reported by some previous workers, causes the bands to become wider; so that only one band is observed in the solid state, the others merging into one another. It is pointed out that the intermolecular field in the solid state has great influence on the electronic energy levels of the molecule.

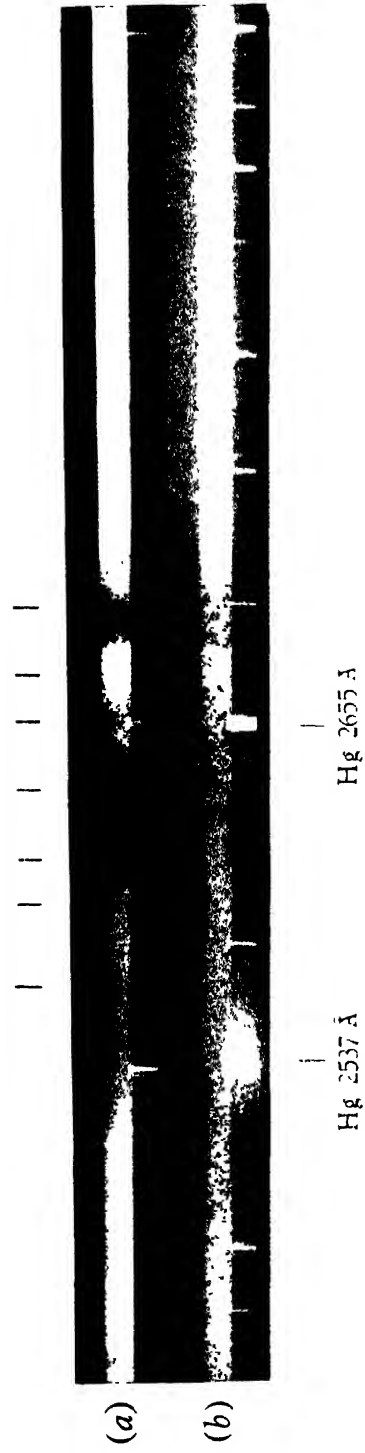
## INTRODUCTION

The ultraviolet absorption spectrum of toluene in the vapour state was studied by several previous authors viz., Savard (1929), Sponer (1942), Ginsberg (1946), and others. Recently Padhye (1949) has reported some new bands in the ultraviolet absorption spectrum of toluene in the vapour state. The absorption spectra of toluene in the liquid and solid states, however, were not studied very exhaustively by the previous workers. Very recently, Kanda and Tsu Ji Kawa (1950) have reported some results in the case of toluene in the liquid and solid states at different temperatures and data have been given in the form of microphotometric records. The results observed by them indicate that there is change in intensity and width of bands with the solidification and lowering of temperature of solid. Slight changes also have been observed in the structure and position of the bands. In the programme of work undertaken to study the influence of temperature and change of state on the electronic energy levels of organic molecules in this laboratory, toluene was chosen as one of the substances and it was observed that the results obtained did not agree thoroughly with those reported by Kanda and Tsu Ji Kawa (1950). It was, therefore, thought worth while to report the results obtained in the present investigation.

## EXPERIMENTAL

The source of continuous spectrum used is a hydrogen discharge tube fitted with a quartz window. The tube is constantly evacuated and pressure of hydrogen is adjusted by operating stop cocks. About 3 K. V. is applied to run the discharge tube. A Hilger quartz H $\gamma$  spectrograph with a dispersion

\* Communicated by Prof. S. C. Sirkar



Absorption spectra of toluene.

(a) Liquid at about 30°C.

(b) Solid " " -180°C.



of 3 A.U. per mm. in the region of 2600 Å was used for photographing the absorption spectra. Dust free toluene, distilled four times was used for the study.

It was found that a layer of liquid having a thickness of about 0.1 mm. produced absorption bands in the spectrum. Such a layer was obtained by introducing a drop of liquid between two quartz plates held together in a brass frame by screws. An exposure of about 20 minutes was necessary in the case of the liquid.

For studying the absorption at low temperatures, the frame containing the cell with the liquid was suspended in a Dewar vessel of fused silica containing some liquid oxygen. The annular region between the walls of the vessel was constantly evacuated. The lower portion of the brass frame was dipped in the liquid oxygen to solidify the substance. Liquid oxygen was replenished from time to time to keep it at a proper level in the vessel. The upward drift of cold air prevented the condensation of water vapour on the surfaces of the quartz plates. The beam of light coming from the hydrogen tube was made parallel with a quartz lens and the cell was placed in the path of the parallel beam. An exposure of about one and a half hours was necessary to record the absorption spectrum of the solid.

# RESULTS

Two spectrograms, one for the liquid state and another for the solid state are reproduced in Plate X. The wave numbers of the bands observed are given in Table I in which the data reported by Kanda and Tsu Ji Kawa (1950) are also included for comparison. The absorption spectrum of the liquid was investigated at 30°C.

TABLE I  
Absorption bands of toluene  
 $\nu$  in  $\text{cm}^{-1}$

Kanda and Tsu Ji Kawa (1950)				Present Author				
Band No	Liquid at -88°C	Band No	Solid at -173°C	Band No	Liquid at 30°C	Remarks	Solid at -180°C	Remarks
1	37372	1	37330	1	37122	Broad, extends from 2704 to 2688 A.U.	37161	Broad, extends from 2705 to 2684 A.U.
2	37792	2	37768	2	37428			
3	38180	3	38152	3	37649			
4	39112	4	38392	4	38039			
5	39400	5	39069	5	38142			
		6	39310	6	38376			
		7	40312	7	39066			

## DISCUSSION

The results given in Table I show that while in the liquid state toluene gives seven bands, in the solid state, it shows only one broad band and in the place of the other bands there is continuous feeble absorption. Probably the latter bands become broader and merge into one another in the solid state. These results are contradictory to those reported by Kanda and Tsu Ji Kawa (1950) who reported that there are only five bands in the liquid state and that the bands become sharper and more intense in the solid state. As regards the position of the band which persists in the solid state it is observed in the present investigation that there is a small shift towards shorter wavelength side with the solidification. The previous authors also mentioned in the abstract of their paper that the bands shift towards the shorter wavelength side, but the microphotometric records reproduced by them show that the shift is towards the longer wavelength side. It is difficult to understand these discrepancies. The fact that the general absorption in the region between 2537 and 2654 A.U. increases at  $-180^{\circ}\text{C}$  indicates that the bands in this region become broader and produce continuous absorption.

The results show that solidification and lowering of temperature has considerable influence on the electronic energy levels of the molecule. It has been observed by Ray (1950) that in the Raman spectrum of toluene in the solid state, a few sharp lines appear in the low-frequency region. These lines were attributed by him to the oscillations in groups of associated molecules. Probably the change in absorption spectra, which is observed to take place with the change of state of the substance and lowering of temperature, indicates that such association has influence on the electronic state of molecules in the solid state at low temperatures. The investigations are being continued with other substances.

## ACKNOWLEDGMENTS

The author is indebted to Prof. S. C. Sirkar for his kind interest and guidance throughout the progress of the work and to the Government of India, Ministry of Scientific Research for the award of a scholarship.

OPTICS DEPARTMENT,  
INDIAN ASSOCIATION FOR THE  
CULTIVATION OF SCIENCE,  
CALCUTTA—32.

## REFERENCES

- Ginsberg, Matsen and Robertson. 1946, *J. Chem. Phys.*, **14**, 511.  
Kanda and Tsu Ji Kawa. 1950, *Science Reports Tohoku University*, **5**.  
Padhye, M. R. 1949, *Ind. J. Phys.*, **23**, 339  
Ray, A. K. 1950, *Ind. J. Phys.*, **24**, 111.  
Savard, 1929, *Ann. de. Chimie.*, **11**, 287.  
Spöner, 1942, *J. Chem. Phys.*, **10**, 672.

# REVIEWS

( 2 )

**Fundamental of Optics**—By F. A. Jenkins and H. E. White Pp. 647. McGraw-Hill Book Company, Inc. New York, Toronto, London, 1950. Price \$ 7.00.

The present volume is the second edition of a similar volume published in 1937. The first ten chapters dealing with geometrical optics and the last chapter on photons are new additions in this edition. As mentioned in the preface to the first edition, the book was intended for use in an advanced undergraduate course in optics. The discourses on geometrical optics are also of the same standard, excepting those on lens aberrations given in Chapter 9. Quantitative expressions for various types of aberrations used in this chapter has raised the standard a little.

Chapters 11 and 12 dealing with wave motion includes detailed discussions on Doppler effect, superposition of waves and group velocity. Chapters 13 and 14 deal with interference of two beams of light and interference involving multiple reflection respectively. As usual, principles of different types of refractometers, *e.g.*, Michelson's, Jamin's and Rayleigh's refractometers have been explained in the former chapter and discussions on interferometers have been included in the latter chapter. Numerous illustrations have been included to explain the use of the interferometers. The phenomenon of diffraction of light has been discussed elaborately in chapters 15-18. These chapters will be useful even to the students preparing for the B.Sc. Honours course of any Indian University. The principle of phase contrast microscope has been explained briefly at the end of Chapter 15. The treatment of diffraction by a grating is quite exhaustive. Also, Fresnel's diffraction has been discussed in great detail and a table of Fresnel's integrals has been included in Chapter 18.

Chapter 19 deals with velocity of light. Principle of Relativity has also been briefly mentioned at the end of this chapter. In the next chapter a brief exposition of electromagnetic theory of light has been included. Different sources of light and their spectra have been described in Chapter 21 and the next chapter deals with absorption, scattering and dispersion of light. Polarization of light, optical properties of transparent crystals and double refraction have been discussed exhaustively with the help of illustrations in chapters 24-26. The phenomenon of optical activity of liquids and crystals has been explained in the next chapter. Chapter 28 dealing with reflection is of a little higher standard as the phenomenon of reflection including metallic reflection has been explained on the electro-magnetic theory of light. The treatment of the problems on magneto-optics and electro-optics given

in the next chapter does not include such theoretical deductions. The last chapter on photons deals briefly with the dual character of light.

The book is beautifully got up, and is printed on real art paper. The quality of illustrations leaves nothing to be desired and the number of such beautiful illustrations is quite large. Chapters on interference and diffraction deserve special mention in this respect. The book will certainly prove useful not only to undergraduate students who are preparing for the B.Sc. Pass course but also to those who have taken up B.Sc. Honours course in any Indian University.

S. C. S.

( 3 )

**Heat and Temperature Measurement.**—By Robert L. Weber, Pp. 422 + x. Prentice Hall Inc., New York, 1950. Price \$ 6.65.

The book is divided into two parts. The first part deals with well known principles of heat, but the order in which these topics have been arranged is a little different from that found in conventional text books. After chapters on temperature scales and different forms of thermometers, theory of conduction of heat has been discussed. This has been followed by two chapters dealing with thermo-electricity and thermo-electric measurements. Laws of radiation and theory of optical and radiation pyrometers have been given in the next two chapters. This has been followed by two chapters dealing with resistance thermometers and temperature recording. Chapter 10 deals with calorimetry in a rather elementary way and phase diagram and phase rule have been discussed in the next chapter. This has been followed by chapters on laws of thermodynamics, production and measurement of extreme temperatures and some special methods of temperature measurement. In the last chapter of part I international temperature scale has been discussed.

Part II of the book deals with 29 laboratory experiments on heat. These experiments include, besides those on different methods of measuring temperatures, a few on calorimetry, relative humidity and viscosity of fluids. The theory of the experiment has been given in each case and in some cases photographs of the actual apparatus have been included.

The book is copiously illustrated and printed on art paper. The book may be useful to under-graduate science students of Indian Universities preparing for their practical course and also to those who are engaged in any work in which accurate temperature measurement is involved.

S. C. S.



# ON AN INTERPRETATION OF THE LIMITS OF PRE-DISSOCIATION IN THE SPECTRUM OF CARBON MONOXIDE AND THE LATENT HEAT OF SUBLIMATION OF GRAPHITE \*

By PRABHAT K. SEN GUPTA

(Received for publication, April 12, 1951)

**ABSTRACT.** From a survey of the available data on predissociation phenomena in carbon monoxide, the energy of dissociation into C ( $^3P$ ) and O ( $^3P$ ) atoms has been found to be 8.87 volts. This assignment gives the latent heat of sublimation of graphite into C ( $^3P$ ) atoms as 118.74 kcal. These figures give a satisfactory account of the known experimental results. It has also been shown that the average energy of the C-H bond in methane, calculated with the results for graphite, is of the right order.

## I

The spectrum of the carbon monoxide molecule is well known but the convergence limit of the ground state  $X\ ^1\Sigma^+$  (figure 1), which specifies the energy of dissociation of the molecule into C ( $^3P$ ) and O ( $^3P$ ) atoms has not been located yet with certainty. Data for the vibrational levels of the  $X\ ^1\Sigma^+$  state are available only up to  $v=25$  corresponding to an energy level of 5.6 volts, which is nowhere near the dissociation continuum. The Birge-Sponer extrapolation method leads usually to an upper limit, and therefore the value 11.34 volts obtained for this state by extrapolation over a long range with the few known vibrational levels has been discarded by other workers as being 20 to 40 % high. (Herzberg, 1942).

In the spectrum of a molecule, the predissociation and dissociation limits are known to give an idea of the products of dissociation of the states involved, and the different combinations of the atomic states in which they occur. Consequently, a scrutiny of the energy differences of the various limits enables us to identify the one which represents the energy of dissociation of the ground state. An estimate made with reference to a predissociation limit is considered fairly accurate, provided predissociation is established without any ambiguity. A mere weakening of the intensity of a few bands unless backed by other evidence may be misleading.

## II

### *Available data on Predissociation.*

From a study of the predissociation phenomena in the spectrum of CO, many workers in the field (Schmid and Gerö, 1937, 1938; Herzberg 1937; Gaydon and Penney, 1944; Hagstrum, 1947; Valatin, 1948; Springall,

\* Communicated by Prof. M N, Saha.

1950) have assigned different values to  $D(\text{CO})$ , with the support of evidence available from electron impact experiments, photo-dissociation of CO, thermochemical data and direct experimental measurements on the sublimation of graphite. The various limits of predissociation established by different investigators are reproduced in Table I.

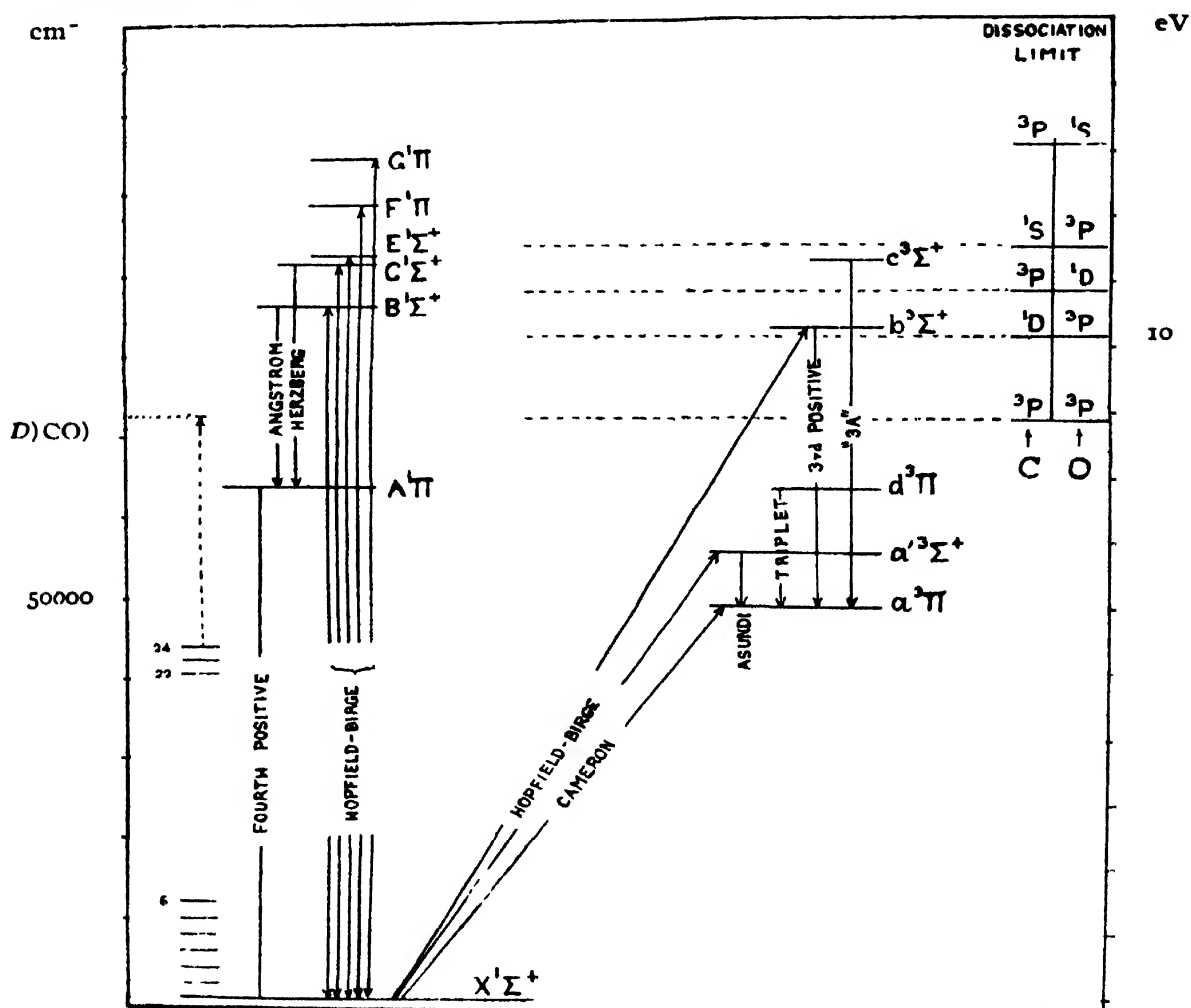


FIG. 1  
Energy levels of CO

There is good deal of controversy as regards the interpretation and assignment of the levels of the various predissociation effects; in fact, some of these are not considered true predissociations at all (Hagstrum, 1947; Herzberg, 1937; Gaydon and Penney, 1944). For instance, Gaydon and Penney (1944) have observed that as the "3A" bands are superposed on the fourth positive system, anomalous intensities in the lines of the latter are not unlikely, and may have the appearance of predissociation. According to Hagstrum (1947), the predissociation in  $B^1\Sigma^+$  and  $b^3\Sigma^+$ , observed at 11.11 volts, is maximum for the potential curve of the  $a^3\Sigma^+$  state (which predissociates the former two), the true dissociation limit being estimated

TABLE I

Predissociation limits in CO spectrum

Limits in volts above $X^1\Sigma^+$	Band System	Nature of Effect
6.89 (Schmid & Gerö)	Cameron [ $a^3\Pi \rightarrow X^1\Sigma^+$ ]	Intensity break off in vibrational structure of $a^3\Pi$ state.
8.19 (Schmid & Gerö)	Asundi [ $a'^3\Sigma^+ \rightarrow a^3\Pi$ ]	Intensity break off in vibrational structure of $a'^3\Sigma^+$ state.
8.87 (Schmid & Gerö)	Triplet [ $d^3\Pi \rightarrow a^3\Pi$ ]	Intensity break off in vibrational structure of $d^3\Pi$ state
8.87 (Schmid & Gerö)	Angstrom [ $B^1\Sigma^+ \rightarrow A^1\Pi$ ]	Predissociation in $A^1\Pi$ state
9.6 (Schmid & Gerö)	Fourth Positive [ $A^1\Pi \rightarrow X^1\Sigma^+$ ]	Predissociation in $A^1\Pi$ state, probably accidental predissociation or only perturbation.
9.14 (Herzberg)		
10.13 (Schmid & Gerö)	Fourth Positive.	Predissociation in $A^1\Pi$ state.
10.87 (Hagstrum)	Angstrom [ $B^1\Sigma^+ \rightarrow A^1\Pi$ ] Third Positive, [ $b'^3\Sigma^+ \rightarrow a^3\Pi$ ]	Predissociation in $B^1\Sigma^+$ and $b'^3\Sigma^+$ states, by $a'^3\Sigma^+$ state. The potential maximum of $a'^3\Sigma^+$ state lies at 11.11 volts, the true limit being situated at 10.87 volts (Hagstrum, 1947).
11.55 (Schmid & Gerö)	Herzberg [ $C^1\Sigma^+ \rightarrow A^1\Pi$ ] "3A" [ $c^3\Sigma^+ \rightarrow a^3\Pi$ ] Hopfield-Birge [ $E^1\Sigma^+ \rightarrow X^1\Sigma^+$ ]	Predissociation in $C^1\Sigma^+$ , $c^3\Sigma^+$ , $E^1\Sigma^+$ states respectively.
12.9 $\pm$ 0.3 (Howell)	Hopfield-Birge [ $F^1\Pi \rightarrow X^1\Sigma^+$ ]	Extrapolated term convergence in $F^1\Pi$ state, with a possible error of 0.3 volt (Howell, 1949)

to be 10.87 volts. The effect at 9.6 volts is probably doubtful, as Herzberg (1937) has observed that the nature of weakening of a few vibrational lines may indicate accidental predissociation or only perturbation instead of real predissociation.

In view of the above, it is proposed to consider the effects at 8.87, 10.13, 10.87, 11.55 and 12.9 volts, as the rest appear to be doubtful.

### III

#### Value Proposed for $D(\text{CO})$

It is known from the experiments of Faltings, Groth and Harteck (1938) that light of  $\lambda$  1470 Å is not able to dissociate CO. This means that the value of  $D(\text{CO})$  is higher than 8.44 volts corresponding to  $\lambda$  1470 Å, and supports the view that the effects listed below 8.44 volts in Table I are not real predissociations. The same absorption experiments also show that light of  $\lambda$  1295 Å (corresponding to 9.57 volts) is able to dissociate CO, thereby providing us with a range 8.44–9.57 within which the value of  $D(\text{CO})$  must lie. As will be seen from Table I that within this range there is only one value, viz., 8.87 volts, which obviously is the figure for  $D(\text{CO})$ .

This deduction apparently does not agree with the results of Kenty, Aicher, Noel, Paritsky and Paolino (1946), who found that metastable xenon atoms with an excitation energy of 9.4 volts failed to dissociate CO. Valatin

(1948), however, feels that this value does not give a lower limit for  $D(\text{CO})$ , as dissociation by collision is a function of transition probability.

With the assignment of  $D(\text{CO}) = 8.87$  volts, the various levels corresponding to dissociation of CO into products with different combinations of atomic states may now be calculated with the known atomic term values of carbon and oxygen (Bacher and Goudsmidt; Shenstone, 1947) given in Table II.

TABLE II

Atomic term differences of carbon and oxygen

Carbon $1s^2 2s^2 2p^2$	Oxygen $1s^2 2s^2 2p^4$
$s^2 p^2 \ ^3P - s^2 p^2 \ ^1D = 1.26$ volts	$s^2 p^4 \ ^3P - s^2 p^4 \ ^1D = 1.96$ volts
$s^2 p^2 \ ^3P - s^2 p^2 \ ^1S = 2.67$ „	$s^2 p^4 \ ^3P - s^2 p^4 \ ^1S = 4.17$ „
$s^2 p^2 \ ^3P - s p^3 \ ^5S = 4.16$ „	

The results have been given in Table III, in the last column of which the observed limits from Table I have been reproduced for comparison.

TABLE III

Calculated limits on the basis  $D(\text{CO}) = 8.87$  volts

Dissociation scheme	Calculated limits above $X \ ^1\Sigma^+$ in volts	Observed limits in volts.
$\text{C}(^3P) + \text{O}(^3P)$	—	8.87
$\text{C}(^1D) + \text{O}(^3P)$	10.13	10.13
$\text{C}(^3P) + \text{O}(^1D)$	10.83	10.87
$\text{C}(^1S) + \text{O}(^3P)$	11.54	11.55
$\text{C}(^3P) + \text{O}(^1S)$	13.04	12.9

It is obvious that the dissociation scheme proposed by the author with  $D(\text{CO}) = 8.87$  volts explains the observed results satisfactorily.

## IV

Value of  $L(\text{C})$

Taking  $D(\text{CO}) = 8.87$  volts the value of  $L(\text{C})$ , latent heat of sublimation of graphite into  $\text{C}(^3P)$  atoms is obtained from the following thermochemical equations.

$$\begin{array}{ll}
 \text{From heat of formation} & \text{CO} + 27.2 \text{ kcal} = [\text{C}] + \frac{1}{2}\text{O}_2 \\
 \text{From heat of dissociation} & \\
 \text{of O}_2 \text{ (Spectroscopic value)} & \frac{1}{2}\text{O}_2 + 58.6 \text{ kcal} = \text{O}(^3P) \\
 \text{By definition} & [\text{C}] + L(\text{C}) = \text{C}(^3P) \\
 & \text{CO} + D(\text{CO}) = \text{C}(^3P) + \text{O}(^3P) \\
 \\ 
 \text{Adding} & L(\text{C}) = D(\text{CO}) - 85.80 \text{ kcal.} \\
 & = 204.54 - 85.80 \text{ ,,} \\
 & = 118.74 \text{ ,,}
 \end{array}$$

It is worthwhile comparing this result with the figures available from the experiments on the sublimation of graphite. The experimentally determined values of  $L(\text{C})$  cover a wide range, (Springall, 1950). There is a set of low values near 120-125 kcal, and at the highest limit values up to 170-210 kcal (Goldfinger and Jeunehomme, 1936; Marshall and Norton, 1937; Vaughan and Kistiakowsky, 1932) have been claimed. Some of the investigators have supported the higher values at about 170 kcal (Long and Norrish, 1946; Valatin, 1948) on the assumption that graphite requires this amount of energy to vaporize into  $\text{C}(s^2p^3^5S)$  atoms. The presence of the  $^5S$  state of carbon in equilibrium vapour pressure measurements has, however, been questioned (Shenstone, 1947; Hagstrum, 1947; Springall, 1950) on the ground that this state is not a metastable state. In the opinion of the majority of the investigators  $L(\text{C})$  is less than 140 kcal, but the adoption of a single value for the sublimation of carbon does not fully account for the higher figures obtained by direct measurements.

If it is postulated that the lowest figures ( $\sim 120$  kcal.) available from the experiments on the sublimation of graphite correspond to its vaporization into  $\text{C}(^3P)$  atoms, the higher figures can be explained by assuming that under different experimental conditions the products of sublimation of graphite are  $\text{C}(s^2p^2^1D)$  and  $\text{C}(s^2p^2^1S)$  atoms as given in Table IV.

TABLE IV

Latent heat of sublimation of graphite, taking  $D(\text{CO})=8.87$  volts.

State of C atom	$1s^2 2s^2 2p^2$			$1s^2 2s 2p^3$ $^5S$
	$^3P$	$^1D$	$^1S$	
$L \text{ kcal} \rightarrow$	118.74	147.80	180.31	215.14 kcal

For comparison, calculations for the  $^5S$  state of carbon are given the last column, which disagree with the experimental results. It appears that the  $^5S$  state of carbon does not take part in these measurements.

*Average energy of C-H bond in methane.*

In  $\text{CH}_4$  the 4 C-H bonds require different amounts of energy to get ruptured in succession. From direct measurements of the photobromination

of  $\text{CH}_4$  (Anderson, Kistiakowsky and Van Artsdalen, 1942; Kistiakowsky, and Van Artsdalen, 1944) and electron impact experiments (Stevenson, 1942), the energy required to rupture the first C-H bond, denoted as  $D(\text{CH}_3\text{-H})$ , has been found to be  $101 \pm 1$  kcal. The energy required to rupture the successive C-H bonds is lower than this figure (Voge, 1936, 1948). For the last C-H bond, we get from predissociation in  $\text{CH}$ ,  $D(\text{C-H})$  equal to 80 kcal, (Shidei, 1936). Thus on the basis of direct measurements only, the average energy of the C-H bond in  $\text{CH}_4$  lies somewhere between the limits 102 and 80 kcal.

Calculation with the aid of thermochemical equations are expected to give only the average value of the energy of C-H bond in  $\text{CH}_4$ . In the thermochemical cycles it is, however, necessary to make a fundamental assumption as to whether in  $\text{CH}_4$ , tetravalent C is in the  $s^2p^2-^3P$ ,  $^1D$ ,  $^1S$  states or  $sp^3-^3S$  state. As an example, the calculations on the basis that C is in the  $s^2p^2-^3P$  state are given below.

Let  $D(\text{CH}_4)$  represent the total energy required to dissociate  $\text{CH}_4$  into  $\text{C}(^3P)$  atom and 4  $\text{H}(^2S)$  atoms.

$$\begin{aligned} \text{Then } \text{CH}_4 + D(\text{CH}_4) &= \text{C}(^3P) + 4\text{H} \\ \text{C}(^3P) &= [\text{C}] + L(\text{C}) \end{aligned}$$

$$\begin{aligned} 4\text{H} &= 2\text{H}_2 + 210 \text{ kcal. (spectroscopic value)} \\ [\text{C}] + 2\text{H}_2 &= \text{CH}_4 + 17.87 \text{ ,, (from heat of formation)} \end{aligned}$$

$$\begin{aligned} \text{Adding } D(\text{CH}_4) &= L(\text{C}) + 227.87 \text{ kcal.} \\ &= 118.74 + 227.87 \text{ ,,} \\ &= 346.61 \text{ ,,} \end{aligned}$$

$$\begin{aligned} \text{Therefore average energy of} \\ \text{C-H bond} &= 86.65 \text{ ,,} \end{aligned}$$

Other values calculated on the basis of the C atom being in the  $^1D$ ,  $^1S$ ,  $^3S$  states are given in Table V.

TABLE V

State of carbon atom in $\text{CH}_4$	$1s^2 2s^2 2p^2$			$1s^2 2s^2 2p^3$ $^3S$
	$^3P$	$^1D$	$^1S$	
Average energy of C-H bond in kcal.	86.65	93.92	102.04	110.75

As the average value of the energy of C-H bond in methane cannot be higher than 102 kcal., it appears that the assumption made in the last column is not valid. It would be more justified if we assume that in  $\text{CH}_4$  the tetravalent C atom is in the  $^3P$ ,  $^1D$  or  $^1S$  state of the configuration  $1s^2 2s^2 2p^2$ .

Voge's (1936, 1948) calculations for  $\text{CH}_4$  also show that the " $^5\text{S}$  level does not properly measure the energy of the carbon atom in the quadrivalent state"

# ACKNOWLEDGMENTS

The author's thanks are due to the authorities of the Indian Association for the Cultivation of Science, Calcutta, and to Professor D. M. Bose, Director, Bose Research Institute, Calcutta for giving him library facilities for this investigation.

METEOROLOGICAL OFFICE,  
CALCUTTA AIRPORT, DUMDUM.

# REFERENCES

- Anderson, H. G., Kistiakowsky, G. B., Van Artsdalen, R. R., 1942, *J. Chem. Phys.*, **10**, 305.
- Bacher and Goudsmidt, Atomic Energy States
- Fallings, K. Groth W. and Harteck, P. 1938, *Z. f. Phys. Chem.*, **B41**, 15
- Gaydon, A. O., Penney W. G., 1945, *Proc. Roy. Soc. Lond.*, **183A**, 374.
- Gerö L., 1948, *J. Chem. Phys.*, **16**, 1011.
- Goldfinger, P. and Jeunehomme W., 1936, *Trans. Far. Soc.*, **32**, 1591.
- Hagstrum, H. D., 1947, *Phys. Rev.* **72**, 736.
- "    "    1947, *Phys. Rev.*, **72**, 947.
- Herzberg, G., 1937, *Chem. Rev.*, **20**, 145.
- "    "    1942, *J. Chem. Phys.*, **10**, 306
- Howell, H. G., 1949, *Nature.*, **163**, 773.
- Kenty, C., Aicher J. O., Noel E. B., Paritsky A., and Paolino V., 1946, *Phys. Rev.*, **69**, 36.
- Kistiakowsky, G. B. and Van Artsdalen, R. R., 1944, *J. Chem. Phys.*, **12**, 469
- Long, L. H. and Norris, R. G. W., 1946, *Proc. Roy. Soc. Lond.*, **187A**, 337
- Marshall, A. L. and Norton, F. J. 1937, *J. Amer. Chem. Soc.*, **59**, 337.
- Schmid, R. and Gerö, L., 1937, *Z. f. Phys. Chem.*, **B36**, 105.
- "    "    1937, *Z. f. Phys.*, **106**, 205
- "    "    1938, *Phys. Zeit.*, **39**, 460.
- Shenstone, A. G., 1947, *Phys. Rev.*, **72**, 411.
- Shidei, T., 1935, *Jap. J. Phys.*, **11**, 23.
- Springall, H. D., 1930, *Research Lond.*, **3**, 260.
- Stevenson, D. P., 1942, *J. Chem. Phys.*, **10**, 291.
- Valatin, J. G., 1948, *Phys. Rev.*, **74**, 340.
- "    "    1948, *J. Chem. Phys.*, **16**, 1018.
- Vaughan and Kistiakowsky, G. B., 1932, *Phys. Rev.*, **40**, 457.
- Voge, H. H., 1936, *J. Chem. Phys.*, **4**, 581.
- "    "    1948, *J. Chem. Phys.*, **16**, 984.

# JOSHI-EFFECT AND THE H. F. COMPONENTS

By G. V. BAKORE

(Received for publication, February 26, 1951)

**ABSTRACT.** The theory of Joshi-effect, as proposed by Deb and Ghosh is shown to be inadequate. It is pointed out that the occurrence of both the positive and the negative Joshi-effect is possible on Joshi's theory consistent with the findings of Klemenc, Hinterberger and Hoffer.

Results of Warburg and Leithauser (1903) indicated the presence in the discharge current of frequencies much higher than that of the exciting field. Klemenc, Hinterberger and Hoffer (1937) have shown that the h. f. components of the discharge current originate from the neutralisation of surface charges when the exciting potential is passing through its zero value. Since the surface charges are deposited on the dielectric surface (*e.g.* the glass walls) the neutralisation takes place in a number of sparks between small isolated elements of the surface charges. Joshi (1944) has observed that decrease in the discharge current under irradiation is associated with the suppression of these high frequency components. Deb and Ghosh (1946-47, 1948) have offered an explanation for the suppression of the h. f. components under light. According to these authors (1946-47) "The effect of light is to restrict the formation of the surface charges on the glass walls. This is because the electron-affinity of the glass surface is small and even the red light has sufficient energy to detach the electrons from it." In a later paper these authors (1948) remarked "The surface charges are deposited not directly on the surface of the glass walls but rather on the adsorbed mono-molecular layer of the contained gas which is formed on the dielectric surface. The surface charges will therefore be quickly and more completely formed if the electron-affinity of the gas molecules is high. Hence the greater the electron-affinity of the gas used, the greater will be the proportion of the h. f. components (produced by the discharging of the surface charges) in the total current and the greater the percentage reduction".

If the surface charges are deposited on the adsorbed layer of a gas of high electron-affinity, the detachment of electrons by ordinary light will be difficult and the effect will therefore be least in case of a gas of high electron-affinity. The effect, on this theory, should therefore be least and not greatest, as has been argued in case of chlorine. In addition, the statements of the authors are in themselves contradictory.

Other drawbacks of the Deb-Ghosh's theory are that the occurrence of the positive Joshi-effect and that of the irreversible negative Joshi-effect



recently observed by Marathe and Bommannver (1950) cannot be anticipated from the theory.

Earlier, Joshi (1946) advanced a theory to explain the phenomenon. According to him: (1) under the electric discharge, an activated layer is formed on the electrodes and it is in dynamic equilibrium with the excited gas phase; (2) as a primary step, photo-electrons are emitted from the active layer and (3) the photo-electrons are converted into slow moving negative ions due to the electron-affinity of the excited gas molecules; these negative ions account for the effect.

The theory is not inconsistent with the findings of Klemenc *et al* (1937). The liberation of the photo-electrons from the active layer reduce the surface charges, thus reducing the intensity of the discharge pulses. The conversion of these photo-electrons into slow moving negative ions increases the sparking potential of the surface charges. The increase in the sparking potential suppresses the discharging of the reduced surface charges when the exciting potential is passing through its zero value. It is obvious that the magnitude of the increase in the sparking potential will depend on the negative ions formed and therefore on the electron-affinity of the excited gas. The suppression of the h.f. components will therefore be more complete with increasing electron-affinity of the excited gas. This accounts for the maximum %  $\Delta i$  in chlorine.

The conversion of the electrons into negative ions will be permanent at low electron energies and therefore should be favoured at low  $x/p$  or/and with light of low frequency. It is therefore expected that the irreversible negative Joshi-effect should occur at low exciting potentials and with light of low frequency. This is actually observed.

If, however, the liberated electrons are not converted into slow moving negative ions of low mobility, they will reduce the sparking potential of the surface charges by ionisation by collision and thus facilitate the discharging of the surface charges with a consequent increase in the current. This is the positive Joshi-effect. The probability of electron-attachment decreases at large electron energies and also with the decrease in the electron-affinity of the excited gas. It is therefore only to be expected that the positive Joshi-effect will occur with a gas of low electron-affinity as also at large  $x/p$  or/and with light of high frequency as observed.

On this basis it is clear that the net effect  $\Delta i$  will be the algebraic sum of  $-\Delta i$  due to negative ion formation and  $+\Delta i$  due to ionisation by collision caused by the liberated photo-electrons.

Joshi's theory (1946) thus gives a more detailed picture of the mechanism of the light-effect consistent with the findings of Klemenc, Hinterberger and Hoffer (1937).

#### ACKNOWLEDGMENTS

The author's grateful thanks are due to Prof. S. S. Joshi, Principal, College of Science, Hindu University, Banaras; to Prof. M. F. Soonawala,

Head of the Department of Physics, Maharaja's College, Jaipur, and to Prof. W. V. Bhagwat, Head of the Department of Chemistry, Holkar College, Indore for their interest and kind encouragement.

DEPARTMENT OF CHEMISTRY,  
MAHARAJA'S COLLEGE, JAIPUR

#### REFERENCES

- Deb and Ghosh, 1946-47, *Sci. and Cult.*, **12**, 17.  
,, 1948, *J. Ind. Chem. Soc.*, **25**, 462.  
Joshi, 1944, *Nature*, **154**, 147.  
,, 1946, *Proc. Ind. Sci. Congress*, Part III, Phys. Sec. Abst. No. 26.  
Klemenc, Hinterberger and Hoffer, 1937, *Z. Electrochem.* **43**, 708.  
Marathe and Bommannaver, 1950, *Nature*, **165**, 890.  
Warburg and Leithanser, 1903, *Ann. Phys.*, **28**, 1.

# PATTERN OBSERVED IN ELECTROLYSIS

By BRAHMANANDA MISHRA

(Received for publication, February 28, 1951)

## Plate XI

**ABSTRACT.** Very dilute solutions of  $\text{HCl}$ ,  $\text{H}_2\text{SO}_4$ ,  $\text{CuSO}_4$  and  $\text{NaCl}$  were electrolysed in a rectangular trough. Regular linear patterns were produced by the chemical action of chlorine and sulphate ions on the anode plate and by the deposit of sodium and copper ions on the cathode plate. Evolution of hydrogen ions in the form of linear vertical patterns was also noticed on the cathode plate. From the observations it is suggested that the motion of ions takes place in discrete layers under the action of electric field.

## INTRODUCTION

While performing an experiment on electrolysis with a very dilute solution of  $\text{CuSO}_4$ , it was observed that chemical action took place over the anode in the form of linear vertical lines separated by distinct regions of no chemical action. The experiment was repeated with various dilute solutions and identical effect was noticed in all cases.

## EXPERIMENTAL ARRANGEMENT

In figure 1,  $DF$  is a rectangular trough containing a vertical anode plate  $B$  and a vertical cathode plate  $C$ , each having an area of nearly 200 sq. cms. The concentration of the solute was roughly 1 grm. per litre. A current of 0.2 amp was passed for about 3 hours. On the anode side, the pattern was produced by the chemical action of chlorine or sulphate ions on the anode plate. The pattern came on all plates but the best contrast was produced when aluminium was used as anode. On the cathode side, the pattern was produced by the deposit of sodium or copper ions on the cathode plate. Evolution of hydrogen ions also produced the pattern on the cathode plate. The anode and the cathode plates were cut at random from one big sheet so that the orientation of the edges of the different plates were different with respect to the edges of the original big sheet.

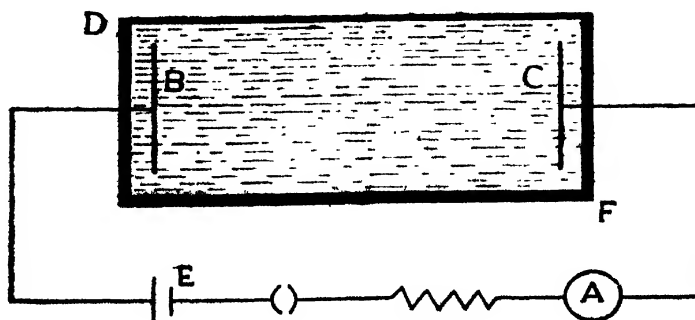


FIG. 1

## EXPERIMENTAL RESULTS

The experimental result is indicated in Plate XI. By illuminating the electrode plates from one side, the pattern can be demonstrated to a large audience while electrolysis is going on. About 70 exposures were given and each time a pattern was observed. The result is also reproduced when the solutes are changed. Attempts with  $\text{HCl}$ ,  $\text{H}_2\text{SO}_4$ ,  $\text{NaCl}$  and  $\text{CuSO}_4$  solutions have been successful. On the cathode side brass and aluminium plates were used and the fringe system due to hydrogen ion was photographed. With the change of cathode plate, the hydrogen ion pattern is reproducible with almost identical spacings.

The spacing of the fringe system depends on the current and diminishes when the current is increased. The distance of separation between two consecutive lines of the pattern were measured with a comparator and the values were found to lie between 0.24 mm. and 0.74 mm.

## DISCUSSION

The observation recorded in the paper does not appear to have been noticed by previous experimenters. This may be due to the fact that for the successful production of the pattern reported by the author, it is very much necessary to use very dilute solution, to keep the current density low, and to pass the current for a long interval of time. With comparatively strong solutions or larger current densities, the spacings between successive lines get reduced and escape observation.

In all the observations, vertical linear patterns are simultaneously produced on the cathode and anode plates. The distances of separation between the lines on both the plates are of the same order. With the change of plate on the cathode side, the hydrogen ion lines are produced with almost identical spacings. If this phenomenon were due to surface action, the patterns observed could not have been vertical on all the plates. In some plates these would have been obviously oblique, because the edges of these plates were inclined to the edges of the original sheet. So the possibility of the phenomenon being produced by surface conditions of the electrodes is ruled out. It is suggested that under the action of the electric field the solutes arrange themselves in discrete layers inside the solution. Further experiment is being done to study the actual nature of the phenomenon.

## ACKNOWLEDGMENT

The author is indebted to Dr. G. B. Banerjee, Principal, Ravenshaw College, for valuable discussions and help during the progress of the experiment.

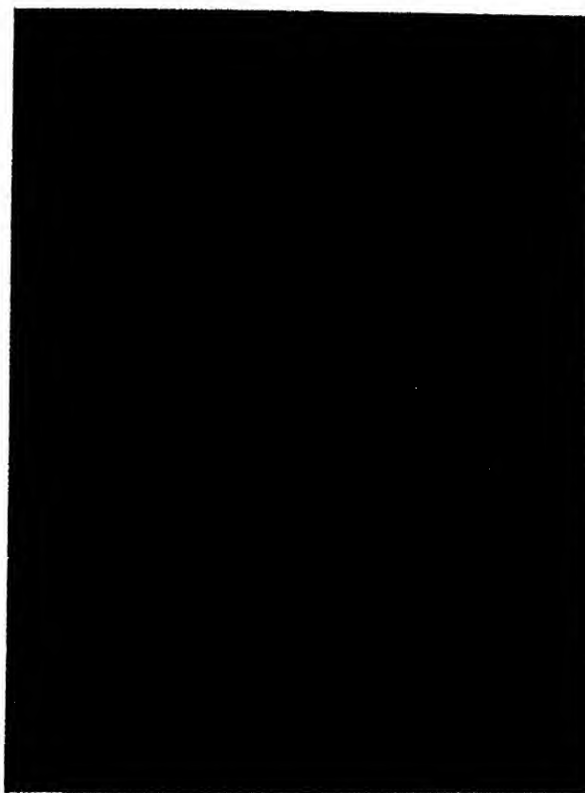


Fig 2

Pattern observed on the aluminium anode plate.



# STANDARDIZATION OF WIND PRESSURE AND TEMPERATURE VARIATIONS AS REGARDS THE DESIGN OF OVERHEAD LINES WITH PARTICULAR REFERENCE TO CONDITIONS IN WEST BENGAL\*

By M. DATTA

(Received for publication, March 15, 1951)

**ABSTRACT.** In the present paper a modified formula for calculating the tension of overhead transmission lines has been developed after critically examining the climatic conditions prevailing in the state of West Bengal. It is found that we are increasing unnecessarily the cost of construction of such overhead lines by using the existing formula which is based on climatic conditions not prevailing in this state.

## INTRODUCTION

Overhead line design is generally governed by official regulations which lay down factors of safety, loading conditions, minimum ground clearances, and provisions relating to road crossings, telephone interference, etc. The object of the present paper is to discuss the adequacy or otherwise of the existing regulations for meeting the climatic conditions prevailing in West Bengal.

## EXISTING REGULATIONS

The design conditions specified for the state of West Bengal are briefly as follows :

- (1) Ice loading is to be ignored.
- (2) The minimum and maximum temperatures specified are  $50^{\circ}\text{F}$  and  $130^{\circ}\text{F}$  respectively.
- (3) The wind is assumed to blow horizontally on the line conductors and to exert a pressure equivalent to 20 lb. sq. ft. calculated on  $\frac{1}{3}$ rd of the projected area of the conductors.
- (4) Factors of safety.
  - (i) 2, for conductors (under conditions of maximum loading and minimum temperature).
  - (ii) 2.5, for metal supports (wind assumed to exert a pressure equivalent to 20 lb./sq. ft. on  $1\frac{1}{2}$  times the area of one face of the support.)
  - (iii) 3, for guard wires or bearer wires.

\* Communicated by Prof. P. C. Mahanti.

- (5) The minimum height of conductors is to be not less than 20 ft. from the ground at any point of the span at a temperature of  $130^{\circ}\text{F}$ .

The loading conditions in Bengal are not only less severe than in the U.K. but there is less difference between the loaded and unloaded conditions. The same minimum figures for safety factors as El.C.53 in the U.K. are, however, specified : this would appear to be unreasonable.

#### PROPOSED ALTERATION OF REGULATIONS

The loading conditions adopted by the different Indian Provincial Governments have been criticised as irrational, and further consideration has been recommended with a view to reduction in line costs (Coventry, 1949).

In Britain also, as the result of extensive experience of high-voltage overhead lines, suggested modifications of the present code of Overhead Line Regulations El.C.53 (1947 Revised) have been published (Grimmitt, 1949) to elicit criticism before the preparation of a final draft.

The object of the proposed amended regulations is to reduce the capital cost of overhead lines, to simplify construction, to reduce ground clearance and to improve appearance without affecting public safety.

Many of these suggestions will, no doubt, be suitable to Indian conditions, and if implemented will materially reduce the cost of line construction. As examples the following may be cited :

(a) *Minimum Conductor Ground Clearance.*

This is 17 ft. for 11 kV lines, and 20 ft. upto 66 kV lines, except at road crossings where the clearance is 19 ft. for 11 kV and 20 ft. for the higher-voltage lines.

(b) *Earthing and Bonding.*

The new regulations permit non-earthed metal work on wood pole supports.

(c) *Road Crossings.*

It will not be necessary to provide duplicate insulators, earth bars or arching horns at road crossings. The construction will be similar to that for normal spans, subject to the use of insulators of the next higher rating to that recommended in Table 2 of B.S. 137, 1941 for the appropriate line voltage.

(d) *Factors of Safety.*

There is a suggestion for dropping of the term "Factor of Safety" in the case of overhead lines. An empirical formula has been proposed for tensioning line conductors. Such tension is not to exceed 75% of the breaking load at  $22^{\circ}\text{F}$  instead of 50% as hitherto.

It is noteworthy that the Central Electricity Commission in India has directed its attention to the question of standardization of wind pressure and temperature variations to be adopted for simplification of overhead line design and construction.



## SPECIAL FEATURE PERTAINING TO WEST BENGAL

In planning a regional scheme for electrification, it is necessary to consider the special local climatic and geographical conditions prevailing.

(1) *Temperature.*

To estimate the normal variations of temperatures to be expected in the area, Table I has been compiled from records of the Meteorological Dept., Alipore (Calcutta) (Lat.  $22^{\circ}32'$  N; Long.  $88^{\circ}20'$  E; height 20 ft.)

TABLE I

Maximum and minimum shade temperatures, °F

Months	1941		1942		1943		1944		1945		1946		1947	
	Max	Min	Max	Min	Max	Min	Max	Min	Max	Min	Max	Min	Max	Min
Jan. ...	84	49	84	51	88	52	89	50	86	47	87	47	83	50
Feb. ...	93	54	94	50	88	49	90	54	92	49	93	55	92	52
Mar. ...	106	63	101	64	101	60	97	63	100	57	102	62	100	63
Apr. ...	107	73	103	69	101	67	101	66	101	68	96	68	108	74
May ...	102	72	108	74	100	73	105	72	100	72	101	69	103	73
June ...	100	74	106	76	97	74	109	75	104	76	98	74	99	75
July ...	95	75	95	77	95	76	95	76	94	78	93	76	95	78
Aug. ...	95	75	93	75	93	76	97	75	96	76	...	...	95	75
Sept. ..	96	77	93	76	95	77	95	75	94	76	95	75	96	76
Oct. ...	95	67	94	71	95	68	94	67	94	70	93	69	95	66
Nov. ...	90	57	89	61	92	59	92	55	89	57	88	59	92	59
Dec. ...	86	53	86	50	85	55	86	51	84	47	86	54	86	51

Approximate additions to above for sun temperatures in °F are as follows :

Jan. 55 ; Feb. 64 ; March, 63 ; April, 62 ; May, 66 ; June, 71 ; July, 71 ; Aug. 67 ; Sept. 66 ; Oct. 67 ; Nov. 62 ; Dec. 65.

The figures in Table I indicate that the normal range of shade temperature variation is  $47^{\circ} - 109^{\circ}\text{F}$ , no temperature higher than  $109^{\circ}$  having been recorded during the last 10 years. The corresponding sun temperatures are  $47^{\circ} + 55^{\circ} = 102^{\circ}\text{F}$  in January and  $109^{\circ} + 71^{\circ} = 180^{\circ}\text{F}$  in June. Thermal ratings of transformers and feeder equipments have to be reduced considerably in view of these high ambient temperatures.

(2) *Wind Velocities.*

Table II gives the maximum wind velocities recorded at the Alipore Observatory for the years 1939-47.

TABLE II  
Maximum wind velocities in m.p.h.

	1939	1940	1941	1942	1943	1944	1945	1946	1947
Jan. ...	28	21	45	20	22	27	18	24	30
Feb. ..	38	43	37	44	39	37	26	32	27
Mar. ...	33	53	34	36	46	51	29	38	35
Apr. ...	40	35	52	46	46	42	39	62	38
May ...	74	60	48	50	44	46	36	80	48
June ...	64	67	46	50	39	50	...	52	49
July ...	35	69	43	50	40	34	...	44	40
Aug. ...	57	33	47	34	30	27	...	34	48
Sept. ...	39	41	37	30	38	25	...	36	32
Oct. ...	29	31	33	67	39	30	...	50	40
Nov. ...	28	20	22	34	20	20	28	22	22
Dec. ...	20	23	20	22	20	16	28	26	26

..... No record.

The table indicates that the maximum wind velocities were recorded in summer months for each of the nine years of record examined. Meteorological records also show that over the same period only on three days did the maximum velocity exceed 70 m.p.h. and that only for a few minutes. The normal wind velocity seldom exceeded 30 m.p.h.

The effective wind pressure on a plane surface may be obtained from  $p = 0.0032 V^2$ , where  $p$  is the pressure in lb./sq. ft. exerted by a wind of velocity  $V$  m.p.h. In calculating pressure, only the projected area of the surface need be taken into account. For circular conductors the streamlining of the air flow permits two-third of the projected area to be used. For the maximum recorded velocity of 80 m.p.h., wind pressure is 20.5 lb./sq. ft. For a velocity of 30 m.p.h., the corresponding pressure is only 2.88 lb./sq. ft. It is to be noted that the worst wind loading condition does not occur at the time of minimum temperature, when the stress in the conductor is high, but is to be expected in the summer, when sudden squalls of short duration may occur. During the low-temperature period the wind loading is relatively light.

As tower costs are affected by sag, it is a matter for careful consideration whether conductors should be strung at maximum temperature to a definite tension limit or to a higher sag. This is discussed more fully later.

Further, the British proposal to drop "factor of safety" in favour of an empirical formula for tensioning line conductors presents the question whether this method could be satisfactorily applied in West Bengal. Here maximum working stress in the conductor does not occur at the minimum temperature where no wind loading is likely to be encountered, unlike the usual limiting consideration of the existing regulation, *i.e.*, maximum working tension at minimum temperature with maximum loading. The maximum sag of conductors also would occur at maximum temperature with maximum loading and this condition determines the height of the supporting structure.

#### MODIFIED FORMULA FOR CALCULATION OF SAG

The line must be erected so that at the conditions then prevailing, usually a lower temperature and no wind, the above conditions are complied with.

Let  $w$  — the weight in lb. per foot of conductor.

$W$  — the resultant pressure in lb./foot of line when subjected to wind.

$Z_q$  — ( $\frac{1}{2}$ ) length of the line in ft. under worst condition at maximum temperature and maximum wind pressure.

$T_q$  — the line tension in lb. being half the breaking load.

$t^\circ$  — the erection temperature in defect of  $130^\circ\text{F}$ .

$Z_t$  — the line length in feet during erection, *i.e.*,  $(130^\circ - t^\circ)$ , assuming still air.

$T_t$  — the tension at erection.

$E$  — the modulus of elasticity in lbs./sq. inch

$a$  — Cross-sectional area of the line in sq. inch.

$\lambda$  —  $E \times a$  (modulus of the wire of area  $a$ ).

$\alpha$  — co-efficient of linear expansion of the material of the conductor.

The line will contract due to thermal effect for a temperature fall of  $t^\circ\text{F}$  by an amount  $= Z_q \alpha t$ .

The line will also contract elastically when wind load is removed by an amount  $\beta$ .

Calculation of  $\beta$ .

We know,  $\frac{\text{change of stress}}{\text{change of strain}} = E$ .

change of tension  $= T_q - T_t$

change of stress  $= \frac{T_q - T_t}{a}$

change in strain  $= \frac{\beta}{Z_q}$

$$\therefore \frac{T_g - T_t}{a} \cdot \frac{Z_g}{\beta} = E$$

$$\text{or} \quad \beta = Z_g \frac{T_g - T_t}{\lambda}$$

Hence the total contraction  $(Z_g - Z_t)$

$$= Z_g \alpha t + Z_g \frac{T_g - T_t}{\lambda}$$

Hence the line length at erection is given by

$$\begin{aligned} Z_t &= Z_g \left( 1 - \alpha t - \frac{T_g - T_t}{\lambda} \right) \\ &= l \left( 1 + \frac{l^2 W^2}{6 T_g^2} \right) \left\{ 1 - \alpha t - \frac{T_g - T_t}{\lambda} \right\} \\ &\quad \left( 1 + \frac{w^2 l^2}{6 T_t^2} \right) \end{aligned}$$

Neglecting product of small quantities the above equation may be reduced to the form

$$T_t^3 + T_t^2 \left\{ \frac{W^2 l^2 \lambda}{6 T_g^2} - \lambda \alpha t - T_g \right\} = \frac{w^2 l^2 \lambda}{6} \quad \dots (1)$$

which is of the form

$$T_t^3 + T_t^2 A - B = 0$$

This is a cubic equation in  $T_t$  and may be solved by a graph or by Newton's approximation or by slide rule.

It may be remarked here that the existing formula is

$$T_t^3 + T_t^2 \left\{ \frac{W^2 l^2 \lambda}{6 T_g^2} + \lambda \alpha t - T_g \right\} = \frac{w^2 l^2 \lambda}{6} \quad \dots (2)$$

which is being wrongly used on the assumption that worst loading condition occurs at the time of minimum temperature during winter months, while the statistical data mentioned earlier clearly indicate otherwise.

The positive sign before  $\lambda \alpha t$  indicates that the erection temperature is higher than the temperature when worst loading condition will occur. But in equation (1),  $\lambda \alpha t$  is negative because the erection temperature is below the temperature of worst loading condition.

For a comparative study an example is given below.

#### OVERHEAD LINE DESIGN AND CALCULATION OF TENSION

**Basis**

Span - 400'

Size of conductor - 3/.147 or .05 sq. inch copper equivalent.

Temperature - min - 50°F

max - 130°F

Wind pressure = 20 lbs./ sq. foot

Wt/ft. run of conductor = .200 lb.

Windage =  $\frac{.317}{12} \times 20 = .528$  lb.

Resultant wt/ft. of conductor including windage

$$= \sqrt{.528^2 + .2^2} = \sqrt{.04 + .279} = \sqrt{.319} = .565 \text{ lb.}$$

Breaking load = 2920 lb.

Safe working load =  $\frac{2920}{2} = 1460$  lb. (assuming factor of safety 2)

$$E = 18 \times 10^6 \text{ lbs./sq. in.}$$

$$\alpha = 9.22 \times 10^{-6} \text{ }^\circ\text{F}$$

$$\lambda = Ea$$

$$\lambda \alpha t = 18 \times 10^6 \times 9.22 \times 10^{-6} \times .05 \times t$$

$$\frac{W^2 l^2 \lambda}{6 T_s^2} = \frac{.565^2 \times 200^2 \times 18 \times 10^6 \times .05}{6 \times 1460^2} \quad 900$$

$$\frac{w^2 l^2 \lambda}{6} = \frac{.2^2 \times 200^2 \times 18 \times 10^6 \times .05}{6} = 240 \times 10^6$$

TABLE III

Tension at different erection temperatures (without wind load)

Temperature °F	Existing formula		Modified formula	
	Equation	Solution. Tension in lbs.	Equation	Solution. Tension in lbs.
130	$T^3 + 104 T^2$ $= 240 \times 10^6$	588	$T^3 - 560 T^2$ $= 240 \times 10^6$	874
120	$T^3 + 21 T^2$ $= 240 \times 10^6$	615	$T^3 - 643 T^2$ $= 240 \times 10^6$	924
110	$T^3 - 62 T^2$ $= 240 \times 10^6$	643	$T^3 - 726 T^2$ $= 240 \times 10^6$	977
100	$T^3 - 145 T^2$ $= 240 \times 10^6$	674	$T^3 - 809 T^2$ $= 240 \times 10^6$	1034
90	$T^3 - 228 T^2$ $= 240 \times 10^6$	708	$T^3 - 892 T^2$ $= 240 \times 10^6$	1093
80	$T^3 - 311 T^2$ $= 240 \times 10^6$	745	$T^3 - 975 T^2$ $= 240 \times 10^6$	1155
70	$T^3 - 394 T^2$ $= 240 \times 10^6$	785	$T^3 - 1058 T^2$ $= 240 \times 10^6$	1219
60	$T^3 - 477 T^2$ $= 240 \times 10^6$	828	$T^3 - 1141 T^2$ $= 240 \times 10^6$	1286
50	$T^3 - 560 T^2$ $= 240 \times 10^6$	874	$T^3 - 1224 T^2$ $= 240 \times 10^6$	1355

TABLE IV.  
Tension for different span lengths at 130°F (without wind load)

Span in ft.	$\lambda at$		$\frac{w^2 l^2 AE}{6T_q^2}$		$\frac{w^2 l^2 AE}{6}$		Equation		Tension (lbs)	
	for existing formula.	for modified formula.	for existing formula.	for modified formula.	for existing formula.	for modified formula.	by existing method	by modified method.	by existing method	by modified method.
375	664	0	789	789	$211 \times 10^6$	$211 \times 10^6$	$T^3 - 7T^2 = 211 \times 10^6$	$T^3 - 671T^2 = 211 \times 10^6$	598	920
400	664	0	900	900	$240 \times 10^6$	$240 \times 10^6$	$T^3 + 104T^2 = 240 \times 10^6$	$T^3 - 560T^2 = 240 \times 10^6$	588	874
500	664	0	1405	1405	$375 \times 10^6$	$375 \times 10^6$	$T^3 + 609T^2 = 375 \times 10^6$	$T^3 - 55T^2 = 375 \times 10^6$	565	740
550	664	0	1700	1700	$453 \times 10^6$	$453 \times 10^6$	$T^3 + 904T^2 = 453 \times 10^6$	$T^3 + 240T^2 = 453 \times 10^6$	557	696
600	664	0	2025	2025	$540 \times 10^6$	$540 \times 10^6$	$T^3 + 1229T^2 = 540 \times 10^6$	$T^3 + 555T^2 = 540 \times 10^6$	550	663

Erection temperature = 130°F i.e. rise of temp.  $t = 80^\circ\text{F}$  (for existing method). Defect of temp.  $t = 0^\circ\text{F}$  (for modified method).

It is assumed that at the time of erection there will be no wind load.

#### CONCLUSIONS

Tables III and IV show the increased tension of the order allowed by the modified formula. It will be clearly seen that the lines may be stressed to considerably reduced sag to obtain much larger spans with the same height of pole and same clearance.

The condition stipulated by the modified formula exists on the warmer and central side of West Bengal where at the temperature of 50°F (assumed minimum temperature), a wind loading which produces a horizontal pressure of 20 lbs. per sq. ft. upon the "projected area" is never obtained. It is thus evident that by using equation (2), which is based on the prevailing British climatic conditions, one increases unnecessarily the cost of overhead line construction.

#### ACKNOWLEDGMENT

The author's best thanks are due to Prof. P. C. Mahanti, Head of the Department of Applied Physics for his helpful discussions in the subject.

DEPARTMENT OF APPLIED PHYSICS,  
UNIVERSITY COLLEGE OF SCIENCE & TECHNOLOGY,  
CALCUTTA.

#### REFERENCES

- Coventry, 1949, *Proc. I.E.E.*, **96** (II), 521.  
Grimmitt, 1949, *Proc. I.E.E.*, **96** (II), 673.

# ANOMALOUS VARIATIONS IN THE ANGLE OF DOWN-COMING RADIO WAVES AND THEIR BEARING ON THE FADING OF SHORT WAVE SIGNALS

By J. P. SRIVASTAVA AND V. D. RAJAN

*(Received for publication, January 2, 1951)*

**ABSTRACT.** It has been found that there are often anomalous variations in the angles of arrival of the down-coming radio waves from the ionosphere. A detailed study of the variations of intensity of short wave signals in the range between 16 m and 41 m bands, along with the simultaneous measurement of the angles of arrival of the down-coming waves, has therefore been made. The circumstances under which such anomalous variations resulting in abnormal values for the angle of arrival may be obtained, are discussed. It has been shown that when singly or doubly reflected waves are present, normal values of angles are obtained, which agree with the theoretically computed results. The anomalous variations and abnormal values of the angles have been explained to be due to the presence of ordinary and extraordinary rays arising from magneto-ionic splitting. This is borne out by the normal and fairly constant values of angle obtained when the extraordinary wave alone is present after disappearance of the ordinary wave component. A few examples of such observations have been given.

## INTRODUCTION

During our observations on the variation of intensity of short wave signals it was found useful to measure simultaneously the angles of arrival of the down-coming waves in order to obtain information about the exact region of the ionosphere which was responsible for the reflection of these waves. The results of such observations have been briefly stated in some of the earlier publications from this laboratory (Banerjee and Mukherjee, 1946, 1948; and Banerjee and Singh, 1948). A detailed study of such observations, however, reveals that there are very often anomalous variations in the angles of arrival of the down-coming waves which are associated with abnormal values of these angles. It is the purpose of this paper to discuss the various circumstances under which such anomalous results are obtained, and also when normal values of the angles are observed. The correlation between the variations in the angles of arrival and the intensity of the received signals has been shown and its importance in finding out the conditions of the ionosphere for the suitability of the frequency which may be employed for transmission at oblique incidence has been indicated.

## THEORETICAL CONSIDERATIONS AND EXPERIMENTAL ARRANGEMENTS

The method adopted for the measurement of the angle of arrival of the down-coming waves is similar to that used earlier in this laboratory by

Banerjee and Mukherjee (1948). For clarification, however, a brief summary of the principles of the method and the experimental arrangement is given below.

In this method, the mutually perpendicular electric and magnetic fields associated with the down-coming wave are received separately by a vertical and a frame aerial (Appleton and Barnett, 1925) connected to two superhet receivers as shown in block diagrams in figures 1 and 2. Taking into

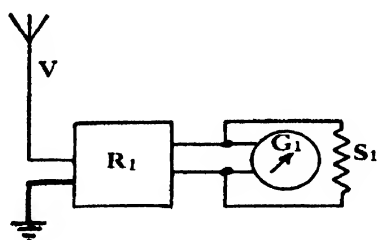


FIG. 1

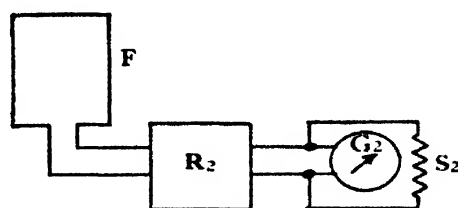


FIG. 2

account the absence of ground wave at the present working range of distance, a simple formula connecting signal currents due to the two aerials and the angle of arrival can be derived as shown below.

If  $I$  be the mean total current in the detector circuit connected to any of the aerials, and  $A$  and  $K$  be the constants of the aerial and the detector respectively, it can be shown that,

$$I_v = 2A_v K_v E \cos \phi \quad \dots (1)$$

$$\text{and,} \quad I_f = 2A_f K_f H \quad \dots (2)$$

where the suffixes  $v$  and  $f$  relate to the vertical and the frame aerials.  $E$  and  $H$  are the electric and magnetic vectors associated with the down-coming wave whose front makes an angle  $\phi$  with the ground.

Let  $G_1$  and  $G_2$  be the resistances of the galvanometers and  $S_1$  and  $S_2$  those of the shunts across them as shown in figures 1 and 2. If we denote the currents in the galvanometers by  $i_1$  and  $i_2$ , then,

$$i_1 = I_v \cdot \frac{S_1}{S_1 + G_1} = 2A_v K_v E \cos \phi \cdot \frac{S_1}{S_1 + G_1} = K' \cdot d_1 \quad \dots (3)$$

$$i_2 = I_f \cdot \frac{S_2}{S_2 + G_2} = 2A_f K_f H \cdot \frac{S_2}{S_2 + G_2} = K'' \cdot d_2 \quad \dots (4)$$

where  $d_1$  and  $d_2$  are the deflections in the galvanometers produced by the rectified currents, and  $K'$  and  $K''$  are the current constants of the galvanometers. Dividing equation (3) by (4) we get,

$$\frac{K'}{K''} \cdot \frac{d_1}{d_2} = \frac{2A_v K_v E \cos \phi}{2A_f K_f H} \cdot \frac{S_1}{S_1 + G_1} \cdot \frac{S_2 + G_2}{S_2}$$

$$\text{or } \frac{d_1}{d_2} = \frac{K''}{K'} \cdot \frac{A_v}{A_f} \cdot \frac{K_v}{K_f} \cdot \frac{S_1(S_2 + G_2)}{S_2(S_1 + G_1)} \cdot \frac{E}{H} \cdot \cos \phi \quad \dots (5)$$



Now, since  $E \equiv H$  in proper units, and all other terms within the brackets are constant so long as the shunts are the same, we have,

$$\frac{d_1}{d_2} = K \cos \phi \quad \dots (6)$$

It may, however, be noted that the above deductions have been made on the assumption of linear characteristics of the two detecting circuits as used in the present receiving sets. In actual measurements, however,  $K$  is made equal to unity by adjusting the shunts so that the overall sensitivities of the two receiving systems may be equal.

In the present investigations two similar superheterodyne receivers without automatic volume control systems were used as the detectors. Suspended coil mirror galvanometers were connected in the second detector stages of the two receivers and the deflections were measured by lamp and scale arrangements. For making adjustments for the sensitivity, as mentioned above, a valve oscillator was placed at the same height as the two receivers at a sufficient distance away from them. The output of the oscillator was fed to a vertical aerial of suitable height. The direct pick-up of the signal, particularly by the frame aerial, was thus considerably minimised. The values of the shunts were then adjusted till the deflections in the two scales were equal after allowing for the deflections due to the noise levels in the sets. As the ground wave alone is present in the above experiment, the angle of arrival of the waves at the receivers is zero and thus  $\cos \phi = 1$ . Now, when  $d_1$  is made equal to  $d_2$ , the value of  $K$  in equation (6) becomes equal to unity, and we get,

$$\frac{d_1}{d_2} = \cos \phi \quad \dots (7)$$

The adjustment of the shunts for the above conditions was verified by elevating the oscillator with its aerial system to a measured height. The deflection in the galvanometer with vertical aerial decreased, and the angle of elevation obtained from the deflections  $d_1$  and  $d_2$  by equation (7) was verified by the actual angle obtained from the distance and height of the oscillator.

As the sensitivities of the two receivers did not remain the same for all the frequency bands, the above adjustments were made for various wave bands used in the present investigations.

#### OBSERVATIONS

Observations were taken at various hours of the day and night and on various wave lengths in the range of 16m to 41m bands, especially for the transmissions from Delhi. The variations of the angles of arrival and the corresponding variations of intensity have been divided into four different types depending on the number of reflections from the ionosphere. It has

been observed that the angle of arrival is fairly constant and the variations of the angle are also normal as long as there is only single reflection from the ionosphere. The variation of the angle of arrival increases with the occurrence of more than one reflection and anomalous results are obtained when there are two components of the wave due to magneto-ionic splitting. Based on the above considerations the four different types of observations mentioned above are under the conditions shown below.

1. *Single reflection at conditions remote from the maximum usable frequency (m. u. f.)* Figure 3 gives the observations for transmission from Karachi in morning hours (0749 I. S. T. on 13.10.50.). The variations of intensity in the vertical and frame aerial systems are marked V and F respectively. The angle of arrival obtained was about  $20^\circ$ .

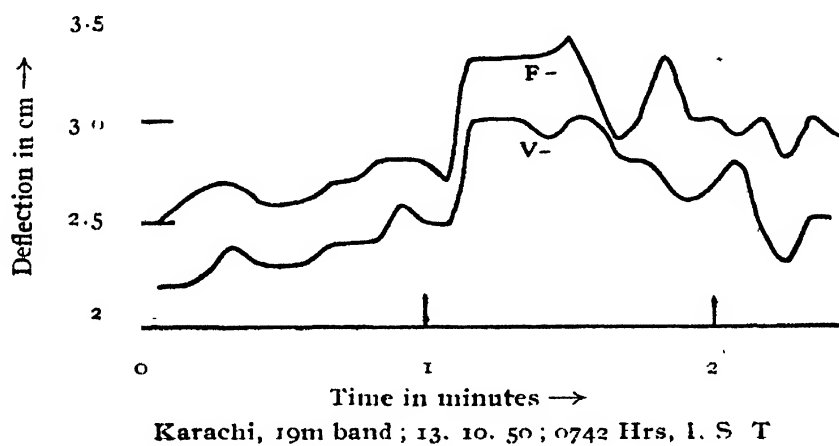


FIG. 3

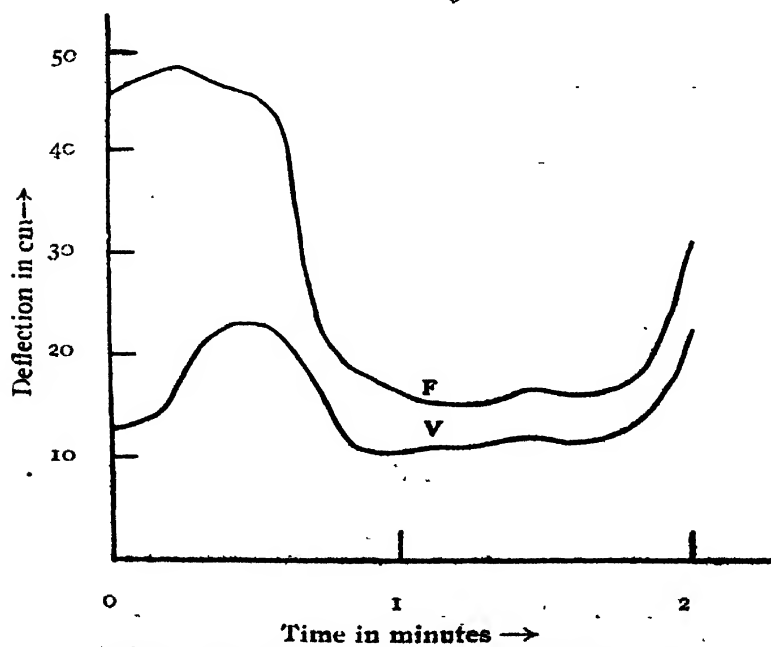


FIG. 4

2. *Single reflection due to extraordinary ray only at conditions very near m. u. f.* Figures 4 to 7 show similar observations as above for transmissions from Delhi. The various types of fading patterns under this condition have been discussed in detail in the subsequent section.

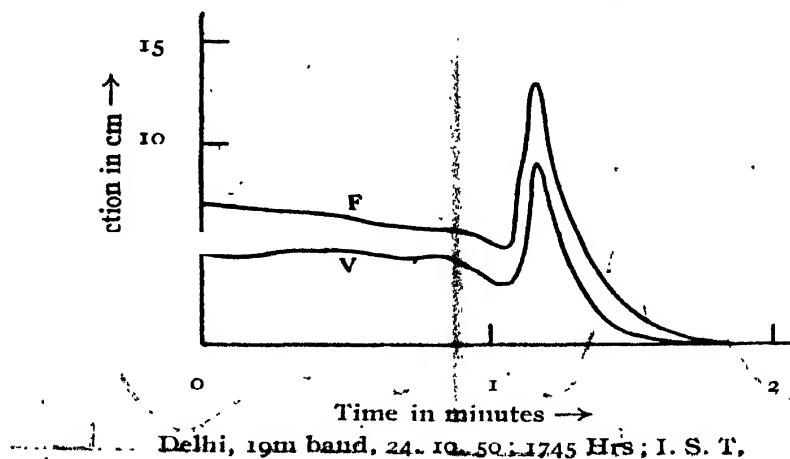


FIG. 5

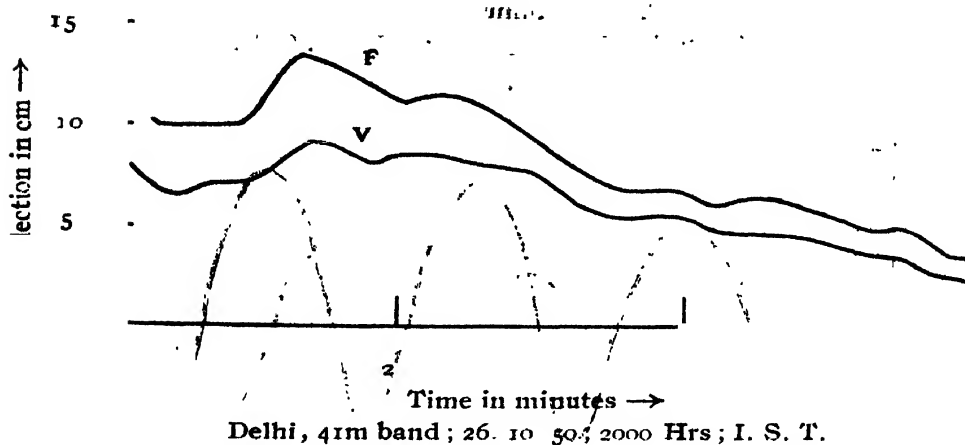


FIG. 6

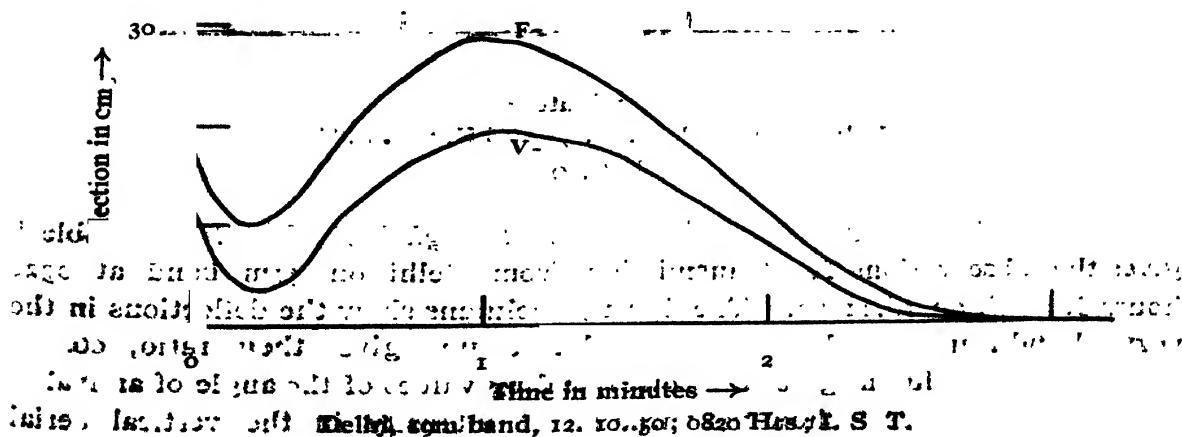


FIG. 7

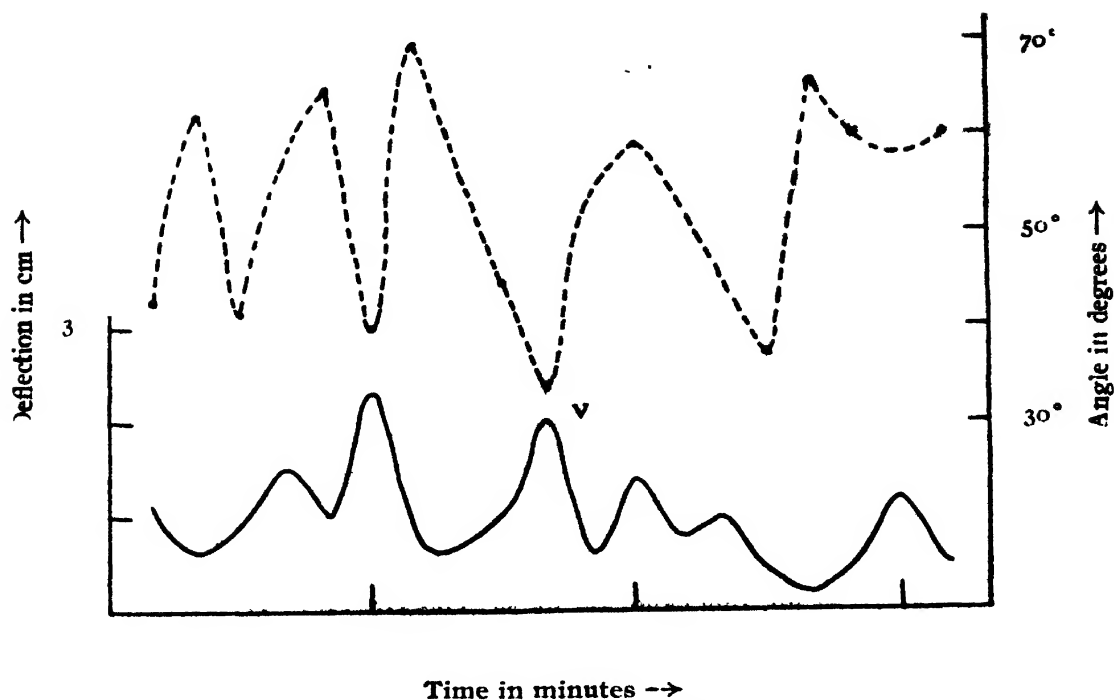


FIG. 8

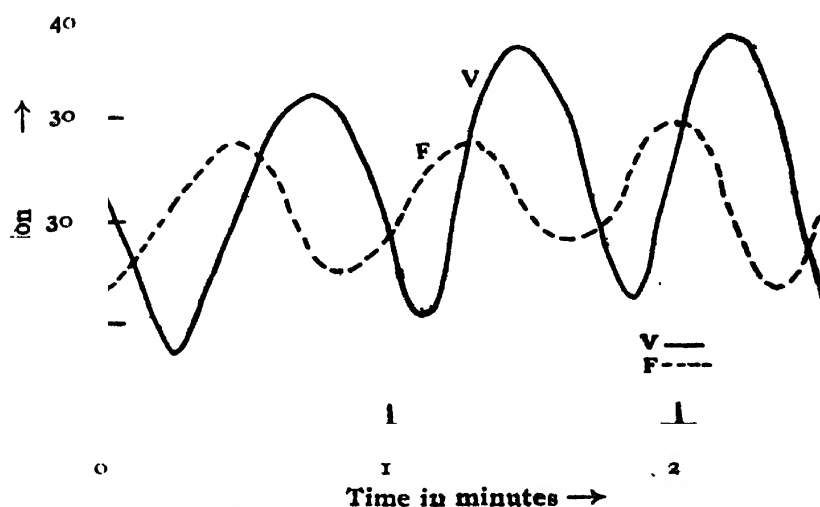


FIG. 9

3. *Single and double reflections due to high ionic densities.* Table I gives the observations for transmission from Delhi on 41m band at 0928 hours I. S. T. on 16.11.50. The first two columns show the deflections in the vertical and frame aerial systems; the third column gives their ratio,  $\cos \phi$ , and the last column gives the corresponding values of the angle of arrival  $\phi$ . The curves in figure 8 show the variation of intensity in the vertical aerial system and the variation of the angle of arrival.

TABLE I

Time Interval : 5 seconds.

$d_1$ (cm.)	$d_2$ (cm.)	$\cos \phi$	$\phi$ (degrees)
8	13	0.62	52
11	18	0.61	52.5
15	24	0.63	51
14	23	0.61	52.5
11	15	0.73	43
9	16	0.56	56
12	14	0.86	...
11	17	0.65	49.5
18	37	0.5	60
22	29	0.75	42.5
12	18	0.67	48
14	26	0.54	57
18	26	0.7	45
14	18	0.78	40
14	21	0.67	48
11	13	0.85	...
13	20	0.65	49.5
10	14	0.71	45
12	21	0.57	55
12	29	0.41	65.5
14	21	0.67	48
14	27	0.52	59
16	22	0.73	43
16	24	0.67	48
14	23	0.61	52.5
13	28	0.47	62
14	24	0.58	54
9	15	0.60	53
11	22	0.50	60

4. *Anomalous variations in the angle of arrival due to magneto-ionic splitting.* A typical set of observations of the above type are shown by the curves  $V$  and  $F$  in figure 9. The dotted curve  $F$  shows the intensity variation in the frame and the full line curve  $V$  shows the variation in the vertical aerial.

The observations in all the above sets have been taken at intervals of 5 seconds (except in the case of those relating to figure 8 where the interval was 10 seconds), simultaneously in the vertical and frame systems. The correlation between the variation of intensity and the angle of arrival has been discussed in the following section.

#### DISCUSSION OF RESULTS

The following discussions are based on the above four types of observations.

1. When the operating frequency is far away from the m.u.f., towards the lower side, only one reflected wave is present and the variations of signal intensity in both frame and vertical aeriels are small and in phase, giving a sensibly constant value of angle that agrees with the calculated angle for waves from the transmitting station reflected from layers whose heights are known from ionospheric data. The intensity patterns for both vertical and frame aeriels in figure 3 show a slow rate of variation. The value of the angle obtained ( $20^\circ$ ) is consistent, and this corresponds to a height of 350 Km. It may be mentioned that as the layer is fairly thin in the morning the magneto-ionic components are not pronounced.

2. When the ionic density is so low that the working frequency is very near the m.u.f. for that density, there is no possibility of double reflection. Hence when the ionization is falling, the condition is reached when the ordinary ray can no longer be reflected. After the disappearance of the ordinary ray, only the extraordinary ray arrives and gives rise to single wave reception. Under this condition, a constant value of angle is obtained. The extraordinary ray, however, may also disappear subsequently, as shown in figures 5 and 7.

It will be seen in figure 4 that just before 1846 hrs IST a hump appeared in both  $V$  and  $F$ , a peak of intensity, which was more pronounced in  $F$ . This signifies the disappearance of the ordinary ray. Thereafter the variations of intensity became smooth, in phase, and a consistent value of the angle ( $44^\circ$ ) was obtained, showing the presence of the extraordinary ray only. Had the station continued this might also have disappeared with its final peak of intensity due to 'focussing effect', as indicated by the rising trends of the two curves. But the station was tuned off the air at 1847 hours. This later stage of disappearance of the extraordinary ray was noticed in Delhi 19 m-band at 1746 hours IST on 24th October, 1950, shown in figure 5. Here the  $V$  and  $F$  deflections were almost steady for 3 minutes. Their ratio led to an angle of  $45^\circ$  during all this interval and also at the peak of intensity in both, after which the signal disappeared. Figure 6 shows a very slow and gradual rate of

fading of the extraordinary ray Delhi 41 m. signal on 26th October, 1950, beginning at 2000 hours IST. The graphs have been drawn on a contracted time scale, to bring out the slow rate of fading over a large period of time. All along, a value of  $45^\circ$  was obtained for the angle. Actually the intensity fell down and continued at a low level for more than an hour.

Figure 7 is an interesting pattern of fading. In the morning time the disappearance may be attributed to the over-balancing of the growth of ions by thermal expansion of the layer (Banerjee and Singh, 1949). This may be seen in the slow and long-drawn out pattern of the final hump before disappearance of the extraordinary ray and during which period a constant angle of  $45^\circ$  was observed.

It may be noted that these disappearance phenomena were observed to occur more frequently in the lower wavelength bands (16 and 19 m) and shorter distance stations, that is, of signals from Delhi but not from Karachi or Ceylon.

3. If the electronic density in the ionospheric layer is sufficiently high, rays from the transmitter can reach the receiver by single and double reflections both. It may be seen that many of the values of angle, given in column 4 of Table I, centre round the value  $47^\circ$ ; this corresponds to single reflection. A smaller number of values comes out around  $6^\circ$ , which corresponds to double reflection. The remaining values fall between these two limits. It may be seen that there are no abnormal values of  $\cos \phi$  whose occurrence is a marked feature of magneto-ionic variations of intensity as mentioned previously. In Fig. 8, the general coincidence of a lower intensity of signal when the angle corresponds to double reflection and higher intensity when the angle corresponds to single reflection may be noticed. Also, the observations indicate which reflection is predominating and what are the modes of variation of intensity of singly and doubly reflected waves. Thus, it will be seen in figure 8 that at the beginning of the observations, second reflection was of higher intensity than the first but towards the end the intensity of doubly reflected waves was generally weak. It may be mentioned that such double reflections have been observed during pulse transmissions from Delhi. The exact nature of the contribution of the doubly reflected wave to the angle is, however, discussed below.

It can be shown theoretically how much the measured angle will be nearer to the value corresponding to the more predominant reflection, assuming the path difference between the rays arriving by single and by double reflection to be constant, and that there is no appreciable vertical movement of the layer to affect the angle of incidence. Let the electric and magnetic vectors associated with the singly and doubly reflected waves be  $E_1, H_1$  and  $E_2, H_2$  respectively, and the angles of arrival of these waves be  $\phi_1$  and  $\phi_2$ . As the field strength at the receiver will be the vector sum of those due to the individual waves, the total fields causing deflections in the vertical and frame aerial systems are respectively,  $E_1 \cos \phi_1 + E_2 \cos \phi_2$  and

4. *Anomalous variations in the angle of arrival due to magneto-ionic splitting.* A typical set of observations of the above type are shown by the curves  $V$  and  $F$  in figure 9. The dotted curve  $F$  shows the intensity variation in the frame and the full line curve  $V$  shows the variation in the vertical aerial.

The observations in all the above sets have been taken at intervals of 5 seconds (except in the case of those relating to figure 8 where the interval was 10 seconds), simultaneously in the vertical and frame systems. The correlation between the variation of intensity and the angle of arrival has been discussed in the following section.

#### DISCUSSION OF RESULTS

The following discussions are based on the above four types of observations.

1. When the operating frequency is far away from the m.u.f., towards the lower side, only one reflected wave is present and the variations of signal intensity in both frame and vertical aeriels are small and in phase, giving a sensibly constant value of angle that agrees with the calculated angle for waves from the transmitting station reflected from layers whose heights are known from ionospheric data. The intensity patterns for both vertical and frame aeriels in figure 3 show a slow rate of variation. The value of the angle obtained ( $20^\circ$ ) is consistent, and this corresponds to a height of 350 Km. It may be mentioned that as the layer is fairly thin in the morning the magneto-ionic components are not pronounced.

2. When the ionic density is so low that the working frequency is very near the m.u.f. for that density, there is no possibility of double reflection. Hence when the ionization is falling, the condition is reached when the ordinary ray can no longer be reflected. After the disappearance of the ordinary ray, only the extraordinary ray arrives and gives rise to single wave reception. Under this condition, a constant value of angle is obtained. The extraordinary ray, however, may also disappear subsequently, as shown in figures 5 and 7.

It will be seen in figure 4 that just before 1846 hrs IST a hump appeared in both  $V$  and  $F$ , a peak of intensity, which was more pronounced in  $F$ . This signifies the disappearance of the ordinary ray. Thereafter the variations of intensity became smooth, in phase, and a consistent value of the angle ( $44^\circ$ ) was obtained, showing the presence of the extraordinary ray only. Had the station continued this might also have disappeared with its final peak of intensity due to 'focussing effect', as indicated by the rising trends of the two curves. But the station was tuned off the air at 1847 hours. This later stage of disappearance of the extraordinary ray was noticed in Delhi 19 m-band at 1746 hours IST on 24th October, 1950, shown in figure 5. Here the  $V$  and  $F$  deflections were almost steady for 3 minutes. Their ratio led to an angle of  $45^\circ$  during all this interval and also at the peak of intensity in both, after which the signal disappeared. Figure 6 shows a very slow and gradual rate of



fading of the extraordinary ray Delhi 41 m. signal on 26th October, 1950, beginning at 2000 hours IST. The graphs have been drawn on a contracted time scale, to bring out the slow rate of fading over a large period of time. All along, a value of  $45^\circ$  was obtained for the angle. Actually the intensity fell down and continued at a low level for more than an hour.

Figure 7 is an interesting pattern of fading. In the morning time the disappearance may be attributed to the over-balancing of the growth of ions by thermal expansion of the layer (Banerjee and Singh, 1949). This may be seen in the slow and long-drawn out pattern of the final hump before disappearance of the extraordinary ray and during which period a constant angle of  $45^\circ$  was observed.

It may be noted that these disappearance phenomena were observed to occur more frequently in the lower wavelength bands (16 and 19 m) and shorter distance stations, that is, of signals from Delhi but not from Karachi or Ceylon.

3. If the electronic density in the ionospheric layer is sufficiently high, rays from the transmitter can reach the receiver by single and double reflections both. It may be seen that many of the values of angle, given in column 4 of Table I, centre round the value  $47^\circ$ ; this corresponds to single reflection. A smaller number of values comes out around  $6^\circ$ , which corresponds to double reflection. The remaining values fall between these two limits. It may be seen that there are no abnormal values of  $\cos \phi$  whose occurrence is a marked feature of magneto-ionic variations of intensity as mentioned previously. In Fig. 8, the general coincidence of a lower intensity of signal when the angle corresponds to double reflection and higher intensity when the angle corresponds to single reflection may be noticed. Also, the observations indicate which reflection is predominating and what are the modes of variation of intensity of singly and doubly reflected waves. Thus, it will be seen in figure 8 that at the beginning of the observations, second reflection was of higher intensity than the first but towards the end the intensity of doubly reflected waves was generally weak. It may be mentioned that such double reflections have been observed during pulse transmissions from Delhi. The exact nature of the contribution of the doubly reflected wave to the angle is, however, discussed below.

It can be shown theoretically how much the measured angle will be nearer to the value corresponding to the more predominant reflection, assuming the path difference between the rays arriving by single and by double reflection to be constant, and that there is no appreciable vertical movement of the layer to affect the angle of incidence. Let the electric and magnetic vectors associated with the singly and doubly reflected waves be  $E_1, H_1$  and  $E_2, H_2$  respectively, and the angles of arrival of these waves be  $\phi_1$  and  $\phi_2$ . As the field strength at the receiver will be the vector sum of those due to the individual waves, the total fields causing deflections in the vertical and frame aerial systems are respectively,  $E_1 \cos \phi_1 + E_2 \cos \phi_2$  and

$H_1 + H_2$ . We may assume that the ratio between the two vectors  $E_2/E_1 = k$  which may vary. As all other conditions are the same, we can write equation (7) as.

$$\frac{d_1}{d_2} = \frac{E_1 \cos \phi_1 + E_2 \cos \phi_2}{H_1 + H_2} = \frac{E_1 (\cos \phi_1 + k \cos \phi_2)}{H_1 (1 + k)} = \frac{\cos \phi_1 + k \cos \phi_2}{1 + k} \quad (8)$$

According to the ratio of deflections we will get an angle  $\phi_3$  say, such that

$$\cos \phi_3 = \frac{d_1}{d_2} = \frac{\cos \phi_1 + k \cos \phi_2}{1 + k}$$

Thus the measured angle will depend on the value of  $k$ .

For illustration, let  $\cos \phi_1 = 0.7$  and  $\cos \phi_2 = 0.5$ , corresponding to the angles  $45^\circ$  and  $60^\circ$  respectively. Then,

$$\cos \phi_3 = \frac{0.7 + 0.5k}{1 + k}$$

For different values of  $k$ , we get different angles as shown in Table II below :

TABLE II

$k$	0	$\frac{1}{2}$	$\frac{1}{3}$	1	2	5	10	$\infty$
$\cos \phi_3$	0.7	0.66	0.63	0.60	0.57	0.53	0.52	0.5
$\phi_3$ (degrees)	45	48.5	51	53	55	58	59	60

A fractional value of  $k$  means that the doubly reflected wave is weaker. A value of 0.6 for  $\cos \phi_3$  means that the two are of equal intensity. Thus, if either the first or the second is more strong, the angle will change correspondingly. Since in general the chances are more for the intensity of a singly reflected wave to be greater than that of one arriving by double reflection, the occurrences of angle corresponding to double reflection should be fewer than for single reflection and this is found to be so.

4. Due to the effect of the earth's magnetic field, the incident wave in the ionosphere is split into ordinary and extraordinary waves, and the difference in the reflected intensities and phases of these two rays is more pronounced when the ionic density is low. The variations of intensity due to interference between the two rays give rise to an interference pattern as shown in figure 9. Such a type of fading is accompanied by wider and more rapid fluctuations in the vertical than in the frame system of aerials. There also appears a large difference in phase in the variations of the two intensities as will be observed in the figure. Further, abnormal values of the angle of arrival are obtained when the intensity in the vertical aerial is too high or too low compared to the intensity in the frame aerial.

## SUMMARY

Simultaneous observations have been recorded for the angles of arrival of the down-coming waves and the variations and abnormal values of the angles of arrival have often been observed which have been explained to be due to the presence of magneto-ionic split components of the waves in the ionosphere. It has been further shown that normal values of angles of arrival are obtained when the waves mainly undergo single or double reflections from the ionized layer. The above conclusions have been verified for single reflection when the extraordinary wave alone is present.

## ACKNOWLEDGMENTS

In conclusion, we have to record our grateful thanks to the Government of Uttar Pradesh for providing grants for carrying out the above investigations. Our thanks are due to Dr. S. S. Banerjee for suggesting the problem and guidance during the course of the investigations. Thanks are also due to Principal M. Sengupta for his helpful interest in the work.

ENGINEERING COLLEGE,  
BANARAS HINDU UNIVERSITY,  
BANARAS.

## REFERENCES

- Appleton E. V. and Barnett, M. A. F. 1925, *Proc. Roy. Soc.* **A109**, 630.  
Banerjee, S. S. and Mukherjee, G. C. 1948, *Phil. Mag.*, **39**, 697.  
Banerjee, S. S. and Mukherjee, G. C. 1946, *Nature*, **158**, 413.  
Banerjee, S. S. and Singh R. N. 1948, *Ind. J. Phys.*, **22**, 413.  
Banerjee, S. S. and Singh R. N. 1949, *Nature*, **164**, 925.

# ULTRASONIC ABSORPTION IN NORMAL AIR AT 456 Kc/s FOR DIFFERENT HUMIDITIES

By GOPALJI

(Received for publication, December 4, 1950)

## Plate XII

**ABSTRACT.** A simpler treatment of the ultrasonic absorption formula

$$\mu = \frac{2.303 [\log_{10} \Delta \theta_A - \log_{10} \Delta \theta_B]}{n_B - n_A}$$

is presented here. A stable and sensitive Pierce interferometer has been used to measure ultrasonic absorption in normal air at 455.8 Kc/s for different humidities. The special features of the work are the use of a proper crystal mounting and the use of a large volume humidity cabinet in which the interferometer was placed. It is found that the absorption curve shows a peak at about 48% humidity for the frequency used in the work.

## INTRODUCTION

It is now well established that absorption of ultrasonic energy in fluids is not only the result of viscous and conductivity losses but some sort of relaxation phenomenon is responsible for it. Three types of relaxation effects have been suggested: firstly the lag in sharing of energy by vibrational states, secondly the lag in chemical or quasi-chemical changes and lastly configurational relaxation. In the case of gases, in which we are concerned here, vibrational relaxation has been found widely evident. The absorption due to this effect is explained qualitatively as follows: As pressure waves pass through a gas, there occurs a sinusoidal variation in temperature along its path. The molecules get energised and transfer a part of their translational and rotational energy to inner vibrational states during compression and take it back while rarefaction occurs, or say a number of molecules are excited to higher vibrational energy levels and then brought back to normal state. But the inner states do not follow readily in taking the energy or giving it back and consequently there is always a phase lag between ultrasonic pressures and corresponding volume changes. Such a lag leads to a closed  $PV$  curve implying thermodynamically that fluid has done some work, absorbing energy from the ultrasonic waves. The amplitude of the lag can be varied either by changing the acoustical period or the relaxation period. The relaxation period depends upon the collision rate and the efficiency of collision to bring about transition. The efficiency function varies with the nature of the colliding molecules which is a fact of importance in the case of mixture of gases.

Our present case is a mixture of nitrogen, oxygen and carbon dioxide in normal air proportions with varying water content.

# INTERFEROMETER THEORY:

The determination of absorption of the ultrasonic energy in fluids is done by the method of ultrasonic interferometry. The method was put in use as early as 1925 by Pierce (1925) which has been later improved by several workers to an extent that its accuracy is quite at par with its optical analogue. It is a standing wave method where the source of ultrasonic waves is an oscillating piezo-electric plate set into vibrations by usual vacuum tube oscillators, and the reflector is either of metal or glass. The ultrasonic waves after multiple reflections react cumulatively on the crystal source which also acts as the detector of the standing waves. Due to reaction pressure electrical constants of the crystal change, which gives rise to variations in crystal voltage and the current in its circuit. The reaction will be a function of the density of the fluid, velocity of the waves and the attenuation of the energy in the medium. Hence knowing the variations in the circuit current or voltage and the relevant relation, attenuation can be calculated. Calculations have been made by Hubbard, (1931) Herzfeld (1938) and Alleman (1939). A simpler treatment is given below :

Assuming plane waves we write down the particle velocity  $\dot{\xi}$  of attenuated waves as

$$\dot{\xi}_t = A \exp \left[ (j\omega - k) \left( t - \frac{x}{v} \right) \right] \quad (1)$$

where  $\omega$ ,  $k$  and  $v$  are angular frequency, attenuation constant and velocity of sound waves respectively in the fluid. The origin of  $x$ -axis is the surface of the quartz crystal.

The particle velocity of the reflected waves will be given by the expression

$$\dot{\xi}_r = B \exp \left[ (j\omega - k) \left( t + \frac{x}{v} \right) \right] \quad \dots (2)$$

where  $A$  and  $B$  are complex velocity amplitudes of the waves. The resulting particle velocity at any point  $x$  will be

$$\dot{\xi} = \exp(j\omega - k) t [A e^{-(j\omega - k) x/v} + B e^{-(j\omega - k) x/v}] \quad \dots (3)$$

Since the particle velocity on the surface of the reflector is zero, we find that at  $x=l$ , where  $l$  is the distance of the reflector from the source,

$$A e^{-(j\omega - k) l/v} = -B e^{-(j\omega - k) l/v} = \frac{C}{2} \text{ (say)} \quad \dots (4)$$

Substituting for  $A$  and  $B$  from (4) in (3), we get

$$\dot{\xi} = C \exp(j\omega - k) t \sinh (j\omega - k) \left( \frac{l-x}{v} \right) \quad \dots (5)$$

Since the pressure is given by

$$p = - \frac{v^2 \rho}{(j\omega - k)} \frac{d\xi}{dx} \quad \dots (6)$$

we find at  $x=0$

$$\frac{p}{\dot{\xi}_0} = v \rho \coth(j\omega - k) \frac{l}{v} \quad \dots (7)$$

where  $\dot{\xi}_0$  represents the particle velocity at the crystal surface. Equation (7) can be expanded in the form

$$p = v \rho \dot{\xi}_0 \frac{\sinh \frac{2kl}{v} + i \sin \frac{2\omega l}{v}}{\cosh \frac{2kl}{v} - \cos \frac{2\omega l}{v}} \quad \dots (7a)$$

Equation (7a) shows that as the length  $l$  is altered, the pressure will pass through maximum and minimum values. When  $l = r\lambda/2$  the pressure will be

$$p_{\max} = v \rho \dot{\xi}_0 \frac{\sinh 2kl/v}{\cosh 2kl/v - 1} \quad \dots (8)$$

and when

$$l = \left(r + \frac{1}{2}\right) \frac{\lambda}{2} = l' \text{ (say)}$$

$$p_{\min} = v \rho \dot{\xi}_0 \frac{\sinh 2kl'/v}{\cosh 2kl'/v + 1} \quad \dots (9)$$

Since  $l' \approx l$ ;  $[\lambda/4 \text{ too small as compared to } l]$

$$p_{\min} = v \rho \dot{\xi}_0 \frac{\sinh 2kl/v}{\cosh 2kl/v + 1} \quad \dots (9')$$

Thus pressure difference

$$(p_{\max} - p_{\min}) = \Delta p = \frac{2v\rho\dot{\xi}_0}{\sinh 2kl/v} \quad \dots (10)$$

At any position  $A$  of the reflector at a distance  $l_A$  from the source the pressure difference is

$$\Delta p_A = \frac{2v\rho\dot{\xi}_0}{\sinh 2kl_A/v} \quad \dots [11]$$

Similarly for the position  $B$

$$\Delta p_B = \frac{2v\rho\dot{\xi}_0}{\sinh 2kl_B/v} \quad \dots [12]$$

Taking  $\dot{\xi}_0 \approx \dot{\xi}_0$ , we get

$$\frac{\Delta p_A}{\Delta p_B} = \frac{\sinh 2kl_B/v}{\sinh 2kl_A/v} \quad [13]$$

It can be shown for the Pierce oscillator, treating on similar lines as that followed by Hardy, (1943) that

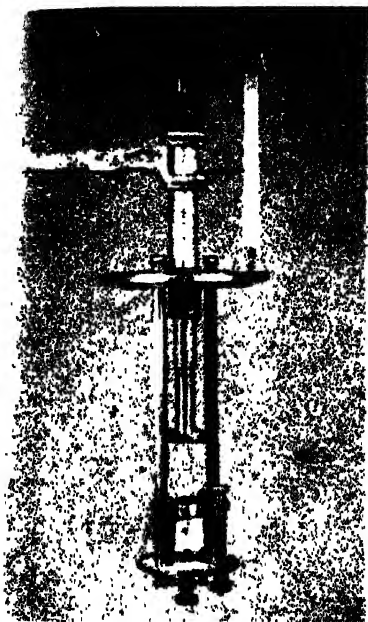


Fig. 1.  
The interferometer



Fig. 2  
The crystal holder

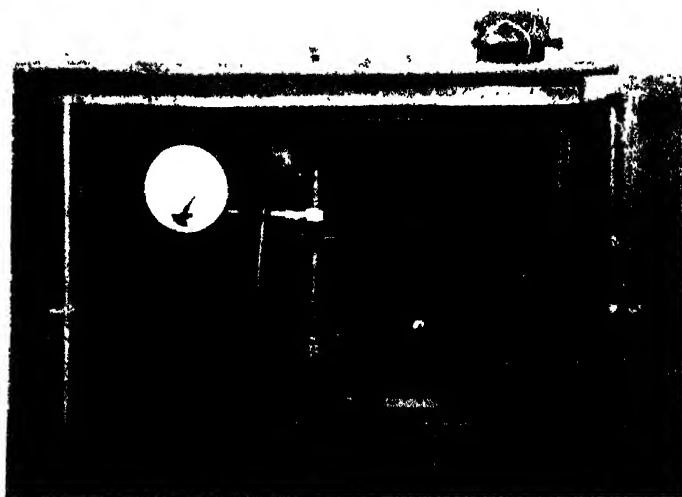


Fig. 3  
The humidity chamber





$$\frac{\Delta p_A}{\Delta p_B} = \frac{\Delta E_A}{\Delta E} = \frac{\Delta I_A}{\Delta I_B} = \frac{\sinh 2kl_B/v}{\sinh 2kl_A/v} \quad \dots [14]$$

where  $\Delta E_A$  and  $\Delta E_B$  are crystal voltages corresponding to  $\Delta p_A$  and  $\Delta p_B$  and  $\Delta I_A$ ,  $\Delta I_B$  are corresponding changes in the plate current. Putting  $k/v = \alpha$  and assuming either  $\alpha$  or  $l$  to be large we get,

$$\frac{\Delta I_A}{\Delta I_B} = \frac{\Delta \theta_A}{\Delta \theta_B} = e^{2\alpha(l_B - l_A)} = e^{\mu(n_B - n_A)}$$

( $\Delta \theta_A$  and  $\Delta \theta_B$  are the deflections observed in a sensitive galvanometer placed in the plate circuit).

$$= \frac{2.303[\log_{10} \Delta \theta_A - \log_{10} \Delta \theta_B]}{(n_B - n_A)} \quad \dots [15]$$

where  $\mu$  is the 'coefficient of energy absorption per wavelength' and  $(n_B - n_A)$  is the number of full wavelengths between the two positions of the reflector *A* and *B*.

#### EQUIPMENT

Our interferometer (figure 1) is of the usual type having a quartz plate as a source of ultrasonic waves and well-polished brass reflector moved by a precision micrometer screw. The arrangement for the movement of the reflector is so managed that there is no rotation of the reflector plane when it is moved along its axis and if it is once carefully made parallel it remains so throughout its movement.

The crystal mounting is of great importance in the interferometric work as a faulty setting will create distortion in crystal oscillations and the changes in the plate current will be unreliable. Distortion in wave form occurs if the crystal is placed on a plate electrode because it knocks against it while oscillating. Thus a rigid mounting, yet free in longitudinal direction, is required. The crystal in our interferometer has been fixed in its median nodal plane by four screws and electrical contacts have been made by light springs (figure 2) after silvering the crystal surfaces thinly. Although our crystal was not a  $71^\circ$  cut, yet it is hoped that this kind of mounting gives more or less a piston like motion of the crystal thus producing plane waves.

The interferometer was placed in a humidity chamber (figure 3). The reflector is moved by a knob attached to a graduated disc kept outside the chamber. The rod connecting the knob and the reflector is passed through a well-greased air-tight hole in the chamber roof. The double doors of the chamber have thick paddings on their sides to make them air-tight. The whole chamber is covered inside by thick copper sheets and outside by asbestos sheets to avoid temperature variation inside the chamber. Electrical heaters, with automatic electric temperature control, are provided to dry the chamber. To increase humidity a water tank and a pipe surrounded by a heater coil with regulator for its controlled evaporation are fitted. A fan for the suction of water vapour inside the chamber is also provided. To

obtain uniform humidity throughout the chamber, it is allowed to stabilise itself by leaving the chamber to stand for a few hours with a particular water content. Humidity is measured by a calibrated hair hygrometer.

As regards the excitation of the quartz plate Pierce oscillator, using a low power triode (Philips A 410), has been employed for stable vibrations. Dry batteries have been used for high tension to avoid spurious fluctuations due to power supply.

Frequency of the oscillations has been measured by a standard Signal Corps frequency meter (Type No. BC 221 AH) which comes out to be 455.8 Kc/s.

#### OBSERVATIONS

Observations have been taken at room temperature ( $32^{\circ}\text{C}$ ) at a frequency of 455.8 Kc/s at five different humidities ranging from 30% to 70% in normal air. A representative set of variations of plate current with respect to reflector positions is shown in figure 4. The plate current undergoes quite

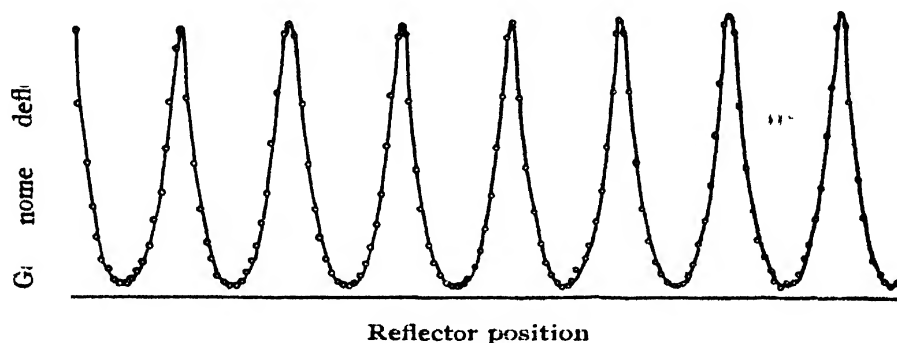


FIG. 4

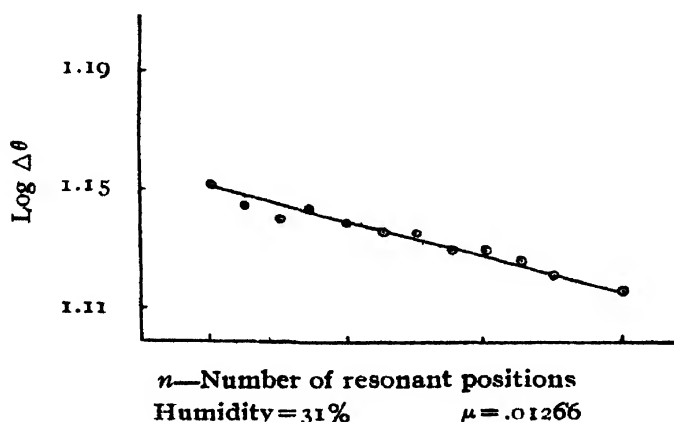


FIG. 5

smooth and regular changes which shows that source is giving out fairly plane waves and the reflector remains parallel to the source. Figures 5 and 6 are two representative graphs of  $\log \Delta\theta$  against number of resonant positions. The mean straight curve is drawn through the points and  $\mu$  is calculated from the slope of the straight line.

## RESULTS

Absorption values have been calculated from the slope of the curves given above. Table I shown underneath gives the absorption values at different humidities :

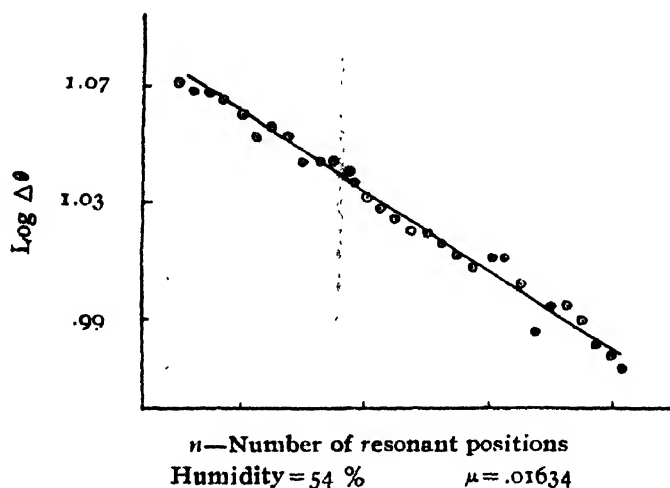


FIG. 6

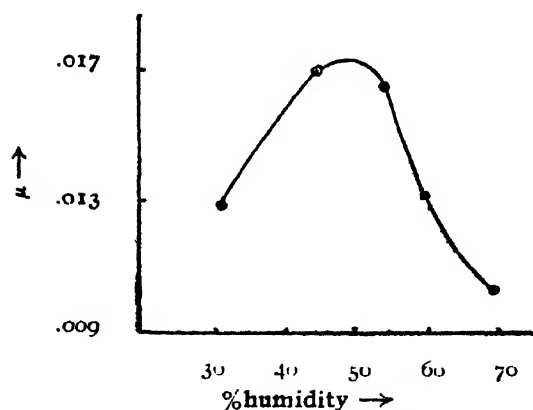


FIG. 7

Table I

Relative humidity ...	31%	44.5%	54%	59.5%	70%
Absorption ( $\mu$ ) ...	.01266	.01675	.01634	.01289	.00998

Coefficient of absorption per wave length,  $\mu$ , is plotted against percentage humidity shown in figure 7. The curve is similar to that for carbon-dioxide (Pielmier, *et al*, 1940) and shows a peak near 48% of humidity.

## ACKNOWLEDGMENTS

In conclusion, the author wishes to express his respectful thanks to Dr. R. N. Ghosh, Head of the Physics Department, under whose guidance the work has been conducted.

DEPARTMENT OF PHYSICS  
ALLAHABAD UNIVERSITY.

## REFERENCES

- Alleman, R. S., 1939, *Phys. Rev.*, **55**, 87.  
Hardy, H. C., 1943, *J. A. S. A.*, **15**, 91.  
Herzfeld, K. F., 1938, *Phys. Rev.*, **53**, 899.  
Hubbard, 1931, *J. C. Phys. Rev.*, **38**, 1011.  
Pielmier, Saxtan and Telfair, 1940, *J. Chem. Phys.*, **8**, 106.  
Pierce, G. W., 1925, *Proc. Am. Acad. of Arts and Sci.*, **60**, 271.

# A NOTE ON MASS MOTION OF A GAS

By DULEH SINGH KOTHARI AND LAXMAN SINGH KOTHARI

(Received for publication, January 29, 1951)

**ABSTRACT.** In the present note we have applied the method of collisions to Fermi-Dirac and Bose-Einstein statistics to establish that the total kinetic energy of a gas is compounded of two independent terms, one being the energy of mass motion and the other that of molecular motion.

The theorem that the total kinetic energy of a Maxwell-Boltzmann gas is composed of two independent terms one of which is related to molecular motion and the other to mass motion is a fundamental one in the kinetic theory of gases. The purpose of the present note is to show that the usual proof is easily extended to include Fermi-Dirac and Bose-Einstein distributions.

It is advisable to start with the deduction of the general distribution law

$$f = \frac{1}{(1/A)e^{hmc^2} + \beta} \quad \dots (1)$$

where  $m$  is the mass of the molecule,  $c$  is its velocity,  $A$  and  $h$  are two constants to be determined, and  $\beta$  takes up the values  $+1$  or  $-1$  according as the gas obeys Fermi-Dirac or Bose-Einstein statistics. The treatment adopted is based on the method of collisions as given in Jeans' Dynamical Theory of Gases (Chapter II).

A molecule having its velocity components lying between  $u$  and  $u + du$ ,  $v$  and  $v + dv$ ,  $w$  and  $w + dw$  will be referred to as belonging to class  $A$  and a molecule of class  $B$  will have its velocity components ranging between  $u'$  and  $u' + du'$ ,  $v'$  and  $v' + dv'$ ,  $w'$  and  $w' + dw'$ . Denoting by  $n$  the number of molecules per unit volume, the density of molecules of class  $A$  becomes

$$nf(u, v, w) du dv dw \quad \dots (2)$$

The probability of collision, in time  $dt$ , between two molecules, one of which belongs to class  $A$  and the other to class  $B$  is

$$n^2 f_K (1 - \beta f_{K'}) f_e (1 - \beta f_{e'}) V \sigma^2 \cos \theta du dv dw du' dv' dw' dt d\Omega \quad \dots (3)$$

where  $f_K$  and  $f_e$  denote the initial and  $f_{K'}$  and  $f_{e'}$  the final values of the distribution functions of the two molecules of class  $A$  and  $B$  respectively,  $V$  is the relative velocity,  $\sigma$  the collision radius (i.e., the diameter of the molecules),  $\theta$  the angle between the velocity vector and the line joining the centres of the two molecules and  $d\Omega$  is the solid angle within which the line joining the centres of the two molecules lies at the moment of impact.

The factors  $(1 - \beta f_{K'})$  and  $(1 - \beta f_{e'})$  take account of the 'already occupiedness' of the cells in the phase space.

Let us now consider collisions between molecules which after impact pass over into states  $A$  and  $B$ . If quantities with bars are taken to represent the state of the molecule before impact, the probability of collision in the case under consideration would be

$$n^2 \bar{f}_K (1 - \beta f_K) \bar{f}_e (1 - \beta f_e) V \sigma^2 \cos \theta d\bar{u} d\bar{v} d\bar{w} d\bar{u}' d\bar{v}' d\bar{w}' dl d\Omega \quad \dots (4)$$

On account of the reversibility of motion, we have

$$du dv dw du' dv' dw' = d\bar{u} d\bar{v} d\bar{w} d\bar{u}' d\bar{v}' d\bar{w}' \quad \dots (5a)$$

$$\text{and} \quad f_{K'} = \bar{f}_K; \quad f_{e'} = \bar{f}_e. \quad \dots (5b)$$

From (3), (4) and (5) we find that the change in the value of  $f$  due to collisions is

$$\frac{\delta f}{\delta t} = n \iiint \{ f_{K'} (1 - \beta f_K) f_{e'} (1 - \beta f_e) - f_K (1 - \beta f_{K'}) f_e (1 - \beta f_{e'}) \} V \sigma^2 \cos \theta du' dv' dw' d\Omega$$

For equilibrium, making use of generalised H-Theorem, we have

$$f_{K'} (1 - \beta f_K) f_{e'} (1 - \beta f_e) - f_K (1 - \beta f_{K'}) f_e (1 - \beta f_{e'}) = 0$$

or

$$\frac{f_{K'} f_{e'}}{(1 - \beta f_{K'}) (1 - \beta f_{e'})} = \frac{f_K f_e}{(1 - \beta f_K) (1 - \beta f_e)}$$

$$\text{or} \quad \log \frac{f_{K'}}{1 - \beta f_{K'}} + \log \frac{f_{e'}}{1 - \beta f_{e'}} = \log \frac{f_K}{1 - \beta f_K} + \log \frac{f_e}{1 - \beta f_e}, \quad \dots (6)$$

The general solution of this equation is

$$\log \frac{f}{1 - \beta f} = \alpha_1 \chi_1 + \alpha_2 \chi_2 + \alpha_3 \chi_3 + \dots (7)$$

where  $\alpha$ 's are arbitrary constants and  $\chi$ 's are functions of velocity. From relation (6), it is obvious that when two molecules collide the sum of the  $\chi$ 's before and after impact remains unaltered. Thus  $\chi$  can be interpreted as energy or as one of the three components of linear momentum or as a constant. The equation (7) may, therefore be expressed as

$$\begin{aligned} \log \frac{f}{1 - \beta f} &= \alpha_1 m(u^2 + u'^2 + w^2) + \alpha_2 mu + \alpha_3 mv + \alpha_4 mw + \alpha_5 \\ &= \alpha_1 m\{(u - u_0)^2 + (v - v_0)^2 + (w - w_0)^2\} + \alpha_6 \end{aligned}$$

where  $u_0, v_0, w_0, \alpha_6$  are new constants.

On further changing the constants the above relation takes up the form

$$\frac{f}{1 - \beta f} = A e^{hm[(u - u_0)^2 + (v - v_0)^2 + (w - w_0)^2]}$$

$$\text{or} \quad f = 1 / \left\{ \frac{1}{A} e^{hm[(u - u_0)^2 + (v - v_0)^2 + (w - w_0)^2]} + \beta \right\}$$

Substituting

$$\begin{aligned}u - u_0 &= U \\v - v_0 &= V \\w - w_0 &= W\end{aligned}$$

we have 
$$f = 1 / \left\{ \frac{1}{A} e^{hm(U^2 + V^2 + W^2)} + \beta \right\}$$

To evaluate the arbitrary constants involved in (8) we must determine the total energy and momentum of the gas.

The value of any function  $\psi$  averaged over all molecules contained in unit volume, is

$$\frac{1}{n} \sum \psi = \iiint \frac{\psi dU dV dW}{\frac{1}{A} e^{hm(U^2 + V^2 + W^2)} + \beta} \quad \dots (9)$$

If  $c$  is the velocity vector (i.e.,  $U^2 + V^2 + W^2 = c^2$ ) we have  $4\pi c^2 dc = dU dV dW$ . Putting  $\psi = 1$  we find  $\sum \psi = n$ , and equation (9) yields

$$1 = 4\pi \int_0^\infty \frac{c^2 dc}{\frac{1}{A} e^{hmc^2} + \beta}$$

From the above relation  $A$  can be evaluated.

Taking  $\psi = U$

$$\sum U = n \int_{-\infty}^{+\infty} \int \int \frac{U dU dV dW}{\frac{1}{A} e^{hm(U^2 + V^2 + W^2)} + \beta}$$

Since the integrand on the right hand side is an odd function of  $U$ , the integral, between the limits  $-\infty$  to  $+\infty$  vanishes and so we have

$$\sum U = 0$$

We, therefore obtain

$$\sum u = \sum u_0 = nu_0$$

This leads to the conclusion that  $u_0$  represents the  $x$ -component of the average velocity of the molecules. Evidently  $u_0$  may also be interpreted as the  $x$ -component of the velocity of mass motion of the gas. A similar significance may also be attributed to  $v_0$  and  $w_0$ .

Finally putting  $\psi = U^2 + V^2 + W^2 = c^2$ , we get

$$\sum (U^2 + V^2 + W^2) = 4\pi n \int_0^\infty \frac{c^4 dc}{\frac{1}{A} e^{hmc^2} + \beta} \quad \dots (10)$$

The total kinetic energy of the system per unit volume is

$$E = \frac{1}{2} m \sum (u^2 + v^2 + w^2) = \frac{1}{2} m \sum \{ (U + u_0)^2 + (V + v_0)^2 + (W + w_0)^2 \}$$

or,

$$E = \frac{m}{2} \sum \{ (U^2 + V^2 + W^2) + (u_0^2 + v_0^2 + w_0^2) \}$$

From (10) it is obvious that

$$E = \frac{m}{2} 4\pi n \int_0^\infty \frac{c^4 dc}{\frac{1}{A} e^{hmc^2} + \beta} + n \frac{m}{2} (u_0^2 + v_0^2 + w_0^2)$$

Hence we observe that the total energy of a gas is obtained by adding together the energy due to molecular motion and that due to mass motion. It may be noted that the energy contributions arising out of these two types of motions are quite independent.

For a gas at rest ( $v_0 = v_0 = w_0 = 0$ ) we find that

$$E = E_0 = 4\pi n \cdot \frac{m}{2} \int_0^\infty \frac{c^4 dc}{\frac{1}{A} e^{hmc^2} + \beta}$$

PHYSICS DEPARTMENT  
M. B. COLLEGE, UDAIPUR



# ON THE RAMAN SPECTRUM OF THIANTHRENE IN THE SOLID STATE

By S. K. MUKERJI AND BANARSI LAL

(Received for publication, December 28, 1950)

## Plate XIII

**ABSTRACT.** The Raman spectrum of thianthrene in the solid state has been studied for the first time. The substance is highly fluorescent; but by using special technique the continuous fluorescent background has been considerably suppressed and the substance in the solid state has yielded 11 Raman lines not recorded before. These lines are at 3044(6), 2912(2), 2462(2), 1571(4), 1275(4), 1125(10), 1033(10), 650(4), 561(4), 319(4), 241(4), 159(4), 85(2) and 62(2)  $\text{cm}^{-1}$  respectively. An anti-stokes line at 159(2)  $\text{cm}^{-1}$  has also been observed.

The strongest characteristic shifts are at 1125 and 1033  $\text{cm}^{-1}$  respectively. The frequency due to the C-S linkage is found at 650  $\text{cm}^{-1}$ .

## INTRODUCTION

It appears that the Raman spectra of linear tricyclic compounds have not been studied in any detail. This is perhaps due to the fact that these compounds are highly fluorescent under the radiation of the mercury arc, and require a laborious process of purification for obtaining the Raman spectra. The only reference to the Raman spectra of such compounds appears in the works of Ansaldi (1936, 37). Anthracene is the simplest compound of this series and its structural formula is as follows :

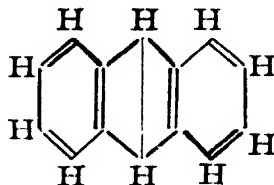


Fig. 1a

If the two CH groups in the para positions in the central ring of anthracene be substituted by S atoms, thianthrene is formed. Its structural formula is as follows :

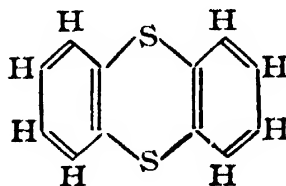


Fig. 1b

The substitution of the two CH groups by S atoms produces a reorientation of the valency bonds inside the benzene ring. It would, therefore, be an interesting study to examine the effect of this substitution. The structures of anthracene and thianthrene then become entirely different from one

another, and we should, therefore, not expect any similarity between the Raman spectra of the two compounds.

# EXPERIMENTAL

Thianthrene, obtained from the Research Laboratory of Eastman Kodak Co., was purified by repeated crystallization with extra pure benzene till perfectly transparent crystals were obtained. These crystals scattered sufficient light to produce the Raman spectrum on the plate but the fluorescence on the plate was very intense and no Raman lines could be observed until the crystals were melted in the Raman tube and allowed to solidify slowly. The solidified mass, on exposure to the light of the mercury arc filtered through a concentrated solution of sodium nitrite, yielded 14 new Raman lines, not recorded before.

TABLE I

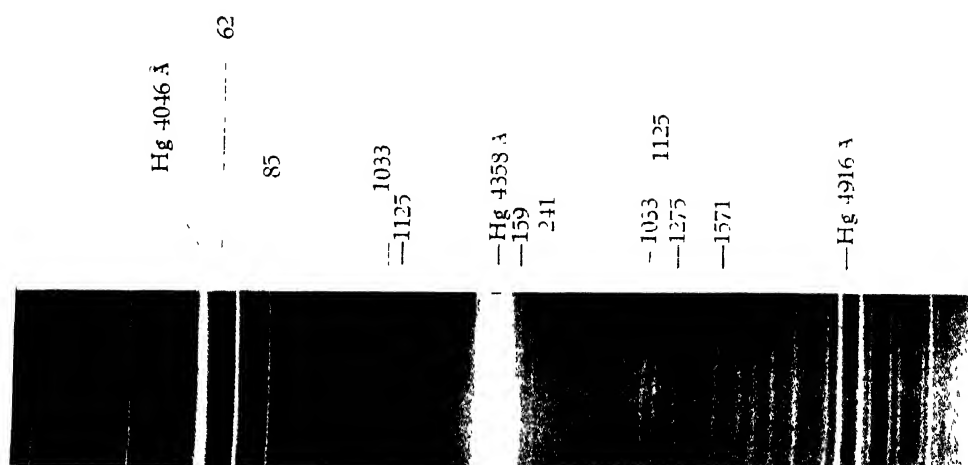
Raman shifts in wave numbers for thianthrene in the solid state

Raman shifts in $\text{cm}^{-1}$	Intensity	Assignment
85	4	A
159	4	A $\pm$
241	4	A
319	4	A
565	5	A
650	4	A
1033	10	A
1125	10	A
1275	4	A
1571	4	A
2462	2	A
2912	2	A
3044	6	A
62	2	B
85	2	B
561	4	B
1033	4 <i>bd</i>	B
1125	4	B

*bd* means broad and diffused

A =  $\lambda$  4358 excitation

B =  $\lambda$  4046 excitation



Raman spectrum of thianthrene in the solid state



The spectra were taken with a Fuess glass spectrograph having a dispersion of about 21 A.U. per mm in the  $\lambda_{4358}$  region. Ilford Selochrome plates were used and the exposures lasted for about 40 hours. The measurements were made with an accurate Zeiss Ikon Comparator and the wavelengths were calculated in the usual manner.

#### OBSERVATIONS AND DISCUSSIONS

It has been shown by Hendricks (1930) by X-ray measurements, that the simplest linear tricyclic hydrocarbon, anthracene, has all the 14 carbon atoms lying in the same plane, and that the two carbon atoms in para-positions in the central ring are also connected with each other as shown in the structural formula. From the mode of formation of anthracene, chemical evidence also verifies the same structural formula.

Thianthrene, which is the object of this investigation, differs from anthracene in this respect that the two CH groups of anthracene in the para-positions have been replaced by divalent atoms of sulphur. This substitution produces a reorientation of the valency bonds inside the molecule and gives quite different Raman frequencies from those of anthracene.

The central ring of thianthrene is not a benzene ring, but the other two rings are benzenoid in structure. Hence according to the Fixer rule, which states that the most stable form of a polynuclear hydrocarbon is that in which the maximum number of rings have the normal benzenoid arrangement of three double bonds, the compound should be only fairly stable. This is the reason why thianthrene begins to decompose when kept above its melting point for a few hours. The structural formula of thianthrene with all atoms lying in the same plane, gives the molecule a high degree of symmetry. Its two end rings have the same bond arrangement as the benzene molecule, so its Raman spectrum should have some frequencies due to the benzene rings, and a few others due to C-S linking.

As given in Table I, 14 Raman lines have been observed with thianthrene in the solid state, and four of these frequencies, *viz.*, 3044, 2462, 1571 and 1275  $\text{cm}^{-1}$  respectively agree fairly well with the Raman frequencies of benzene. The frequencies, at 3044  $\text{cm}^{-1}$  and at 2912  $\text{cm}^{-1}$  may be taken to represent C-H vibrations, as no other type of vibration is expected to give the frequencies of this order. The frequency at 1571  $\text{cm}^{-1}$  appears to be due to the C=C link of the benzenoid rings. A similar frequency at 1573  $\text{cm}^{-1}$  occurs in naphthalene, which is slightly lower than C=C linkage in benzene occurring at 1596  $\text{cm}^{-1}$ .

From the observations of the Raman shifts of thio-ethers, thio-acids and polysulphides, it is found that C-S shift falls near 645  $\text{cm}^{-1}$ . Venkateswaran (1930) has shown that C-S shift in methyl mercaptan is 704  $\text{cm}^{-1}$  which decreases to 659  $\text{cm}^{-1}$  in ethyl mercaptan and to approximately 652  $\text{cm}^{-1}$  in higher homologues. In thianthrene the carbon atoms connected

to the S atoms form part of a heavy ring, so the shift observed at  $650\text{ cm}^{-1}$  may be due to C-S link. By comparing these Raman spectra with those of substituted benzene compounds it can be concluded that the frequencies at  $1045\text{ cm}^{-1}$  and  $1150\text{ cm}^{-1}$  relate to C-C link.

The frequencies observed at  $319\text{ cm}^{-1}$ ,  $241\text{ cm}^{-1}$  and  $159\text{ cm}^{-1}$  respectively in thianthrene containing condensed benzene rings, may be attributed to the deformational vibrations of the benzene rings against one another. Such low frequency lines are not generally observed in compounds possessing a single ring like benzene and its derivatives. The very low frequencies observed at  $85\text{ cm}^{-1}$  and  $62\text{ cm}^{-1}$  respectively may be attributed to the oscillations of the lattice. The substance has also been examined by us in the molten state (still unpublished) and it is found that the frequencies at  $85$  and  $62\text{ cm}^{-1}$  completely disappear as the substance passed from the solid to the molten state. Hence, evidently, these two frequencies are due to the oscillations of the lattice.

DEPARTMENT OF PHYSICS,  
AGRA COLLEGE.

#### R E F E R E N C E S

- Ansidei Manzoni, 1936, *Atti. Accad. Lincei.*, **24**, 368  
" " , 1936, *Ricerca Sci*, **7**(1), 314.  
" " , 1937 *Gazz. Chem. ital* , **67**, 790  
Hendricks, Sterling B., *Chem. Rev.*, **4**, p. 470, Dec. (1930)  
Venkateswaran, 1930, *Ind. J. Phys.*, **5**, 219.

## ENERGY OF DISSOCIATION OF CYANOGEN\*

BY PRABHAT K. SEN GUPTA

(Received for publication, April 20, 1951)

**ABSTRACT.** The energy of dissociation of CN into C(<sup>3</sup>P) and N(<sup>4</sup>S) atoms has been estimated to be 6.02 volts with the aid of known thermochemical and spectroscopic data.

## I

*Spectrum of CN*

The spectrum of cyanogen has not been of much help in the determination of the energy of dissociation of this molecule in view of the scanty experimental data available. Only a few electronic states have been discovered and predissociation phenomena, which are known to give fairly reliable estimates of the limits, have not been established without ambiguity so far. The vibrational levels of the ground state,  $X^2\Sigma^+$  as well as those of the upper state,  $A^2\Pi$ , of the red system  $A^2\Pi \rightarrow X^2\Sigma^+$  have been followed up to an energy level of about 3.4 volts above the ground level. The convergence limit, reached by a rather long Birge-Sponer extrapolation is not reliable. The appearance of perturbations in the violet system  $B^2\Sigma^+ \rightarrow X^2\Sigma^+$ , however, has been made use of by Schmid, Gerö and Zemlen (1938) to reach up to  $v=30$  of the  $A^2\Pi$  state corresponding to  $51000\text{ cm}^{-1}$  (6.32 volts) and then locate the convergence limit of this state at  $60500 \pm 1000\text{ cm}^{-1}$  ( $7.50 \pm .12$  volts) by only a short extrapolation. Schmid *et al* found evidence to conclude that the ground state,  $X^2\Sigma^+$ , converges to the same limit as  $A^2\Pi$  state. The extrapolated convergence limit of the next upper state,  $B^2\Sigma^+$ , is found to be  $65500 \pm 1000\text{ cm}^{-1}$  ( $8.12 \pm .12$  volts). In Table I the limits located by Schmid, Gerö and Zemlen (1938) are given.

TABLE I

Limits above $X^2\Sigma^+$ in volts	Nature of effect according to Schmid, Gerö and Zemlen
7.38-7.62	Convergence of $A^2\Pi$ and $X^2\Sigma^+$ states
8.00-8.24	Convergence of $B^2\Sigma^+$ state
6.62	Perturbation in $v=15$ of $B^2\Sigma^+$ state, probably in the vicinity of a predissociation limit
6.32	Perturbation in $v=14$ of $B^2\Sigma^+$ state
3.93	Drop in intensity in $v=3$ of $B^2\Sigma^+$ state, probably due to predissociation.

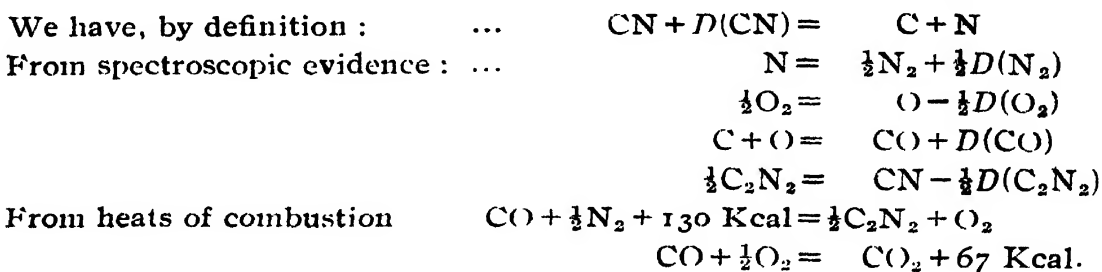
\* Communicated by Prof. M. N. Saha, F.R.S.

In this table, the effects at 6.62, 6.32 and 3.93 volts require further confirmation, particularly the exact locations of the limits. The exact positions of even the two convergence limits at  $7.50 \pm .12$  and  $8.12 \pm .12$  volts are not known with certainty. Therefore it is not surprising that the attempts to propose a dissociation scheme which will satisfactorily interpret the limits have not been successful.

## II

*Value of  $D(\text{CN})$* 

A better estimate of the energy of dissociation can be formed in the case of CN by combining reliable spectroscopic and thermochemical data as given in the following calculations. The terms have their usual meanings and the atoms and molecules occur in the lowest spectroscopic states.



By addition we get,

$$D(\text{CN}) = \frac{1}{2}D(\text{N}_2) + D(\text{CO}) - \frac{1}{2}D(\text{O}_2) - \frac{1}{2}D(\text{C}_2\text{N}_2) - 63 \text{ Kcal} \quad \dots (1)$$

In this expression the following figures are being adopted :

- (i)  $D(\text{O}_2) = 5.08$  volts. This is the generally accepted value for the heat of dissociation of oxygen.
- (ii)  $D(\text{CO}) = 8.87$  volts. This value of the energy of dissociation of carbon monoxide has been recently proposed by the author, (Sen Gupta, 1951) and found to give a satisfactory explanation of known predissociation phenomena in CO and the results of the experiments on the sublimation of graphite.
- (iii)  $D(\text{N}_2) = 9.76$  volts. Although this is the generally accepted figure for the heat of dissociation of nitrogen (Gaydon, 1947), other investigators (Glockler, 1948; Long, 1949; Springall, 1950) have made use of an earlier figure, 7.38 volts, for comparison in their discussions. Datta's (1932) experiments on the photodissociation of  $\text{N}_2\text{O}$  and the author's (Sen Gupta, 1934) experiments on the fluorescent radiation from  $\text{N}_2\text{O}$ , both confirm that the value is nearer 9.76 than 7.38 volts.
- (iv)  $D(\text{C}_2\text{N}_2) = 4.93$  volts, being the energy of dissociation of  $\text{C}_2\text{N}_2$  into two CN radicals. Long (1949) arrived at this figure from a study of the absorption spectra of  $\text{CH}_3\text{CN}$ ,  $\text{ICN}$  and  $\text{HCN}$ , and found it to be comparable with Glockler's (1948) values, viz., 117.6 and 119.6 Kcal for NaCN and KCN respectively, calculated with



the aid Born-Haber cycles. The value given by Hogness and Lui-Sheng (1932) as well as Robertson and Pease (1942), that is, 5.52 volts is also worth consideration. Some of the investigators have made use of 6.34 volts evaluated by White (1940).

In view of the above it is proposed to consider the three values, 4.93, 5.52 and 6.34 volts for  $D(C_2N_2)$  in the expression (1). The deduced value of  $D(CN)$  corresponding to each of the figures for  $D(C_2N_2)$  are given in Table II.

TABLE II

$D(C_2N_2)$ in volts	4.93	5.52	6.34
$D(CN)$ in volts	6.02	5.72	5.31

Herzberg (1942) has pointed out that as the  $C \equiv N$  bond in CN is much stronger than the C—C bond in  $C_2N_2$ , the value of  $D(CN)$  should be much higher than  $D(C_2N_2)$ . Rejecting the figures given in the last two columns of the above table by this test, we get  $D(CN)=6.02$  volts, which indirectly confirms Long's estimate of the value of  $D(C_2N_2)$ .

On the basis of  $D(CN)=6.02$  volts, a probable dissociation scheme for the spectrum of CN may now be drawn up as follows (Table III).

TABLE III

Products of dissociation	Calculated limits above $X^{2\Sigma^+}$ in volts
$C(^3P)+N(^4S)$	6.02
$C(^1D)+N(^4S)$	7.28
$C(^3P)+N(^2D)$	8.39

It will be seen from Table I that there are some observed limits in the vicinity of the above calculated positions, but for reasons already mentioned, no attempt at a correlation is being made in this paper, pending further work on the spectrum of CN.

#### ACKNOWLEDGMENT

The author's thanks are due to the authorities of the Indian Association for the Cultivation of Science, Calcutta, for giving him facilities of their library for the investigation.

## REFERENCES

- Datta, A. K., 1932, *Proc. Roy. Soc.*, A136, 84.  
Gaydon, A. G., 1947, *Dissoiation Energies and Spectra of Diatomic Molecules*.  
Gaydon, A. G., and Penney, W. G., 1945, *Proc. Roy. Soc.*, 183 , 374.  
Glockler G., 1948, *J. Chem. Phys.*, 16, 630.  
Herzberg, G., 1942, *J. Chem. Phys.*, 10, 306.  
Hogness, T. R., and Lui-Sheng, 1932, *J. Ame. Chem. Soc.*, 54, 123.  
Long, L. H., 1949, *Proc. Roy. Soc.*, 198 , 62.  
Robertson, N. R. and Pease, R. N., 1942, *J. Chem. Phys.*, 10, 490.  
Schmid, R., Gerö, L., and Zemplén, J., 1938, *Proc. Phys. Soc. Lond.*, 50, 290.  
Sen Gupta, P. K., 1934, *Proc. Roy. Soc.*, 146, 824.  
Sen Gupta, P. K., 1951, *Ind. Jor. Phys.*, 25, 234.  
Springall, H. D , 1950, *Research, London*, 3, 260.  
White, E. U., 1940, *J. Chem. Phys.*, 8, 459.

# THERMODYNAMIC BEHAVIOUR OF A GASEOUS ASSEMBLY OF POINT-MOLECULES ASSUMING ASSOCIATION\*

By M. DUTTA

(Received for publication, April 19, 1951)

**ABSTRACT.** In nature, for many gases, *viz.*, sulphur vapour, water vapour, etc., there is decisive evidence of associations of molecules, yielding higher polymers. Here, on starting from some well-known results previously obtained by Darwin-Fowler method, various properties of the assembly, *viz.*, isothermal and adiabatic compressibilities, coefficient of expansion, etc., have been investigated and have been expressed in terms of degree of associations such that an estimation can also be made from measurements of these quantities. Many of those properties have remarkable deviations from those of ideal gases in a direction, opposite to that of usual real gases. These peculiarities have also been justified qualitatively from Le Chatelier and Braun's principle.

## INTRODUCTION

In usual investigations of properties of ideal gases, either by thermodynamic or by statistical methods, no consideration is taken for associations of molecules, *i.e.*, constituent particles are assumed to exist in the simplest form. But, in nature, for many gases, *viz.*, sulphur vapour,  $\text{NO}_2$ , water vapour (near about the boiling-point), iodine vapour, oxygen in presence of ozone, etc., in some suitable temperature-range, it has been found conclusively that there exists varying degree of association. Now Darwin-Fowler method is very suitable for discussion of behaviour of assemblies in which constituent particles are associating and dissociating. Starting from some well-known results obtained by this method, the isothermal compressibility for an assembly of point molecules, assuming associations, has been obtained and proved to be greater than that for ideal gases composed of molecules of permanent type. This conclusion has also been shown to be plausible in a qualitative manner from a discussion based on Le Chatelier and Braun's principle. The expression for isothermal compressibility has been written in a form, appearing to be suitable for determining degree of dissociation (or better association) from measurements on isothermal compressibility. After this, expression for coefficient of volume-expansions,  $C_p$ ,  $C_v$ ,  $\gamma$  etc., have been calculated for assembly of this type. Finally, the expression for velocity of propagation of sound through gases of this type has been obtained, and this, after putting in suitable form, appears to be useful for determining degree of association by measuring velocity of propagation of sound in gases of this type under consideration.

\* Communicated by Prof. S. N. Bose.

## DESCRIPTION OF THE ASSEMBLY

For simplicity, it has been assumed that the assembly is composed of molecules, essentially of the same type, existing in the simplest form, or in form of simply associated polymers. Thus, if  $X$  represents the molecule in the simplest form, then the assembly consists of  $(X)_1, (X)_2, \dots (X)_r, \dots (X)_n$ , where the suffix ' $r$ ' represents the number of molecules, associated in forming polymers of  $r$ -order. Let  $N_1, N_2, \dots N_n$  be the average number of  $(X)_1, (X)_2, \dots (X)_n$  polymers in the assembly, and so

$$\sum_r r N_r = A \quad \dots (1)$$

where  $A$  is the total number of  $X$  molecules present in the assembly. Again, if  $N$  represents total number of molecules existing in free state in the volume, then

$$\sum_r N_r = A \quad \dots (2)$$

## SOME IMPORTANT WELL-KNOWN RESULTS

Now, the thermodynamic probability in the Darwin-Fowler sense is

$$C = \frac{1}{(2\pi i)^2} \int_{\Gamma} \int_{\Gamma} \frac{dz}{z^{E+1}} \frac{dt}{t^{A+1}} \exp\{P_1(z_1)t + P_2(z_1)t^2 + \dots + P_n(z_1)t^n\} \quad \dots (3)$$

where

$P_r(z)$  = partition function of polymer  $(X)_r$

$$\log \left( \frac{1}{z} \right) \left( \frac{2\pi m_r}{h} \right)^{\frac{3}{2}} V z^{\chi_r + r b}$$

$$= P(z) \cdot \left( \frac{2\pi m_r}{h} \right)^{\frac{3}{2}} z^{\chi_r + r b}, \quad \dots (4)$$

on writing

$$P(z) = \left( \frac{2\pi m}{\log(1/z_1)} \right)^{\frac{3}{2}} \cdot \frac{V}{h^3} \quad \dots (5)$$

In the above expressions,  $V$  is the volume of the assembly  $m_r$  is mass of  $(X)_r$ , and  $m$  is mass of  $(X)$ , ' $b$ ' the rest energy,  $\chi_r$  the binding energy of  $r$  molecules in polymers of  $r$ th type, and, here, it is taken as

$$m_r = r m$$

So, the above can be written as

$$C = \frac{1}{(2\pi i)^2} \int_{\Gamma} \int_{\Gamma} \frac{dz_1}{z_1^{E+1}} \frac{dt}{t^{A+1}} \exp\{P(z)Q(t, z)\} \quad \dots (6)$$

where

$$Q(t, z) = t z^b + z^{\frac{3}{2}} \cdot t^2 z^{2b + \chi_2} + z^{\frac{3}{2}} \cdot t^3 z^{3b + \chi_3} + \dots + n^{\frac{3}{2}} t^n z^{nb + \chi_n} \quad \dots (7)$$

Now, by the method of steepest descent, the approximating value of  $C$  is given by

$$C = \frac{\exp\{P(z_0)Q(t_0, z_0)\}}{t_0^A z_0^B} \quad \dots (8)$$

where  $t_0, z_0$  are determined from the equations,

$$E = Q(t_0, z_0)z_0 \frac{\delta P}{\delta z_0} + P(z_0)z_0 \frac{\delta Q(t_0, z_0)}{\delta z_0} \quad \dots (9)$$

and

$$\begin{aligned} A &= P(z_0)t_0 \frac{\delta Q(t_0, z_0)}{\delta t_0} \\ &= P(z_0)Q_1(t_0, z_0) \end{aligned} \quad \dots (10)$$

where

$$Q_1(t_0, z_0) = t_0 z_0^b + 2^{5/2} t_0^2 z_0^{2b+\chi_1} + \dots + n^{5/2} t_0^n z_0^{nb+\chi_n} \quad \dots (11)$$

Now, as shown by Darwin and Fowler, we have

$$\left. \begin{aligned} z_0 &= e^{-1/kT} \\ t_0 &= e^{\psi/kT} \\ N_r &= t^r P_r(z_0) \end{aligned} \right\} \quad \dots (12)$$

$$\text{and } p = \frac{kT}{V} (\sum N_r) = \frac{kT}{V} \left\{ \sum t^r P_r(z_0) \right\} = \frac{kT}{V} P(z_0)Q(t_0, z_0) \quad \dots (13)$$

where  $p$  is the pressure,  $T$  the temperature of the assembly,  $\psi$  is the partial thermodynamic potential and  $k$  the Boltzmann constant. The equation of state is same as that for mixture of ideal gases.

#### ISOTHERMAL COMPRESSIBILITY

Now, if  $p$  and  $T$  are taken as independent thermodynamic variables of the system, then, from the above, we see that  $V, t_0$ , etc., are functions of  $p, T$  both, and,  $z_0$  and so,  $P(z_0)/V$  of  $T$  alone. Then, on differentiating the equation (11) partially with respect to  $p$ , it becomes

$$\begin{aligned} \frac{1}{p} &= \frac{1}{Q(t_0, z_0)} \cdot \frac{\delta Q(t_0, z_0)}{\delta t_0} \left( \frac{\delta t_0}{\delta p} \right) \\ \text{or } \frac{1}{t_0} \left( \frac{\delta t_0}{\delta p} \right)_T &= \frac{Q(t_0, z_0)}{Q_1(t_0, z_0)} \cdot \frac{1}{p} \end{aligned} \quad \dots (14)$$

$$\begin{aligned} &\dots \\ &A k T \end{aligned} \quad \dots (15)$$

On differentiating partially and logarithmically the equation (10), it becomes

$$\begin{aligned} -\frac{1}{V} \left( \frac{\delta V}{\delta p} \right)_T &= \frac{1}{Q_1(t_0, z_0)} \left\{ \frac{\delta}{\delta t_0} Q_1(t_0, z_0) \right\} \left( \frac{\delta t_0}{\delta p} \right)_T \\ &= \frac{1}{p} \frac{Q(t_0, z_0) Q_2(t_0, z_0)}{\{Q_1(t_0, z_0)\}^2} \quad \dots (16) \end{aligned}$$

after substituting the value of  $\frac{1}{t_0} \left( \frac{\delta t_0}{\delta p} \right)_T$  from the equation (11) where

$$Q_2(t_0, z_0) = t_0 \frac{\delta}{\delta t_0} Q_1(t_0, z_0)$$

From the equation (12), they become

$$\begin{aligned} P(z_0)Q(t_0, z_0) &= \sum N_r \\ P(z_0)Q_1(t_0, z_0) &= \sum r N_r = A \\ P(z_0)Q_2(t_0, z_0) &= \sum r^2 N_r \\ \therefore -\frac{1}{V} \left( \frac{\delta V}{\delta p} \right)_T &= \frac{1}{p} \frac{(\sum N_r)(\sum r^2 N_r)}{\{\sum r N_r\}^2} \\ &= \frac{1}{p} \left[ 1 + \frac{(\sum N_r)(\sum r^2 N_r) - (\sum r N_r)^2}{(\sum r N_r)^2} \right] \\ &= \frac{1}{p} \left[ 1 + \frac{\sum_r \sum_m (r-m)^2 N_r N_m}{(\sum r N_r)^2} \right] \leq \frac{1}{p} \quad \dots (18) \end{aligned}$$

Now, for an ideal gas at the same temperature and pressure, the compressibility is equal to  $1/p$ . Thus, the system is more compressible than an ideal gas at the same temperature and pressure, though both of them satisfy the equation of state of the same form.

Now, the equation (17) can be put in a very useful form as follows

$$-\frac{1}{V} \left( \frac{\delta V}{\delta p} \right)_T = \frac{1}{p} \left[ 1 + \sum_r \sum_m \frac{(r-m)^2}{rm} \xi_r \xi_m \right] \quad \dots (19)$$

where

$$\xi_r = \frac{r N_r}{A} = \frac{\text{number of constituent molecules (X) associated to form polymer (X)}}{\text{total number of constituent molecules (X) present in assembly}}$$

In the simplest case, where polymers of the type  $(X)_2$  only exists, as in the assemblies of  $\text{NO}_2$  and  $\text{N}_2\text{O}_4$ , or of  $\text{I}$  and  $\text{I}_2$ , the equation (18) reduces to the following form

$$-\frac{1}{V} \left( \frac{\delta V}{\delta p} \right) = \frac{1}{p} \left[ 1 + \frac{1}{2} \xi_1 \xi_2 \right] \quad \dots (20)$$

where

$$\xi_1 = \frac{N_1}{A} = \xi, \quad \xi_2 = \frac{2N_2}{A} = 1 - \xi \quad \dots (21)$$

and  $\xi$  may be called as degree of association.

Then,

$$-\frac{1}{V} \left( \frac{\partial V}{\partial p} \right)_T = \frac{1}{p} \left[ 1 + \frac{1}{2} \xi (1 - \xi) \right] \quad \dots (22)$$

For the range of temperature and pressure when  $\xi=0$  or  $\xi=1$ , the compressibility, as expected, (since the assembly reduces to that of ideal gases), is equal to  $1/p$ .

The maximum deviation occurs when  $\xi=\frac{1}{2}$  and is equal to  $12\frac{1}{2}\%$ .

#### SOME REMARKS BASED ON LE CHATELIER AND BRAUN'S PRINCIPLE

Now, the principle of Le Chatelier and Braun asserts that the increase of a generalised force  $Y_i$  (*i.e.*, intensity) produces a displacement of equilibrium attended by a process (transformation or chemical reaction) in which the change of the conjugate variables  $\Delta X_i$  is positive (Epestein, 1947).

So, when the pressure is increased, chemical reaction will take place in such a way that the conjugate variable ( $-\Delta V$ ) is positive, *i.e.* volume decreases. Evidently more association of molecules cause a decrease in volume. So, with increase of pressure, there will be more association in the system. This will yield some positive contribution to the compressibility over and above the usual compressibility expected for ordinary ideal gas. Thus, the gas of the type considered here is more compressible than the ordinary ideal gas at some temperature and pressure.

#### ISOTROPIC COEFFICIENT OF EXPANSION

Now, on differentiating the equation (11) with respect to  $T$  after keeping  $p$  constant, the following is obtained :

$$0 = \frac{1}{T} + \left\{ \frac{3}{2} kT + \frac{QZ'(t_0, z_0)}{Q(t_0, z_0)} \left\{ z_0 \frac{\delta z_0}{\delta T} + \frac{Q_1(t_0, z_0)}{Q(t_0, z_0)} \frac{1}{t_0} \left( \frac{\delta t_0}{\delta T} \right) \right\} \right\}_p$$

where

$$QZ'(t_0, z_0) = z_0 \frac{\delta Q(t_0, z_0)}{\delta z_0} \quad \dots (24)$$

$$\frac{1}{t_0} \left( \frac{\delta t_0}{\delta T} \right)_p = -\frac{3}{2} \frac{Q(t_0, z_0)}{Q_1(t_0, z_0)} \frac{1}{T} - \frac{QZ'(t_0, z_0)}{Q_2(t_0, z_0)} \cdot \frac{1}{kT^2} \quad \dots (25)$$

On taking  $p$ ,  $T$  as variables and on differentiating the equation (10) logarithmically and partially with respect to  $T$ , the following is obtained :

$$-\frac{1}{V} \left( \frac{\delta V}{\delta T} \right)_p = \left[ \frac{z_0 \frac{\delta}{\delta z_0} \left\{ \frac{P(z_0)}{V} \right\}}{P(z_0, t_0)} + \frac{Q_1 Z'(t_0, z_0)}{Q_1(t_0, z_0)} \right] \frac{1}{z_0} \frac{\delta z_0}{\delta T} + \frac{Q_2(t_0, z_0)}{Q_1(t_0, z_0)} \cdot \frac{1}{t_0} \left( \frac{\delta t_0}{\delta T} \right)_p$$

where

$$Q_1 Z'(t_0, z_0) = z_0 \frac{\delta Q_1(t_0, z_0)}{\delta z_0} \quad \dots (26)$$

On the substitution of the value of  $\frac{1}{t_0} \left( \frac{\delta t_0}{\delta T} \right)_p$  from (25) the above becomes

$$\begin{aligned} \frac{1}{V} \left( \frac{\delta V}{\delta T} \right)_p &= \frac{5}{2} \frac{Q_2 Q}{Q_1^2} \cdot \frac{1}{T} + \frac{Q_2 Q Z'}{Q_1^2} \cdot \frac{1}{k T^2} - \frac{3}{2} \frac{1}{T} - \frac{Q_1 Z'}{Q_1} \cdot \frac{1}{k T^2} \\ &= \frac{1}{T} \left[ 1 + \frac{5}{2} \sum \sum \frac{(r-m)^2 N_r N_m}{A^2} \right. \\ &\quad \left. + \frac{1}{k T} \left\{ \sum r^2 N_r \right\} \left\{ \sum N_r (\lambda_r + r b) \right\} - \frac{\left\{ \sum N_r r (\lambda_r + b) \right\} \left\{ \sum r N_r \right\}}{A^2} \right] \\ &= \frac{1}{T} \left[ 1 + \frac{5}{2} \sum \sum \frac{(r-m)^2}{r m} \xi_r \xi_m + \sum \sum \frac{(1-m)}{r m} \xi_r \xi_m \left( \frac{r \lambda_m}{k T} - \frac{m \lambda_r}{k T} \right) \right] \end{aligned} \quad \dots (27)$$

In the simple case, where polymers of the type (X)<sub>2</sub> only exist, the expression becomes

$$\frac{1}{V} \left( \frac{\delta V}{\delta T} \right)_p = \frac{1}{T} \left[ 1 + \frac{1}{2} \xi (1 - \xi) \left( \frac{5}{2} - \frac{\chi}{k T} \right) \right] \leq \frac{1}{T} \quad \dots (28)$$

if

$$\frac{\chi}{k T} < \frac{5}{2}.$$

#### SPECIFIC HEAT AT CONSTANT PRESSURE

Now, according to the equation (9) the total energy is

$$\begin{aligned} E &= \frac{3}{2} k T P(z_0) Q(t_0, z_0) + P(z_0) Q Z'(t_0, z_0) \\ &= \frac{3}{2} k T [\sum N_r] + \sum N_r (\lambda_r + r b) \end{aligned}$$

On differentiating this partially with respect to  $T$ , this becomes

$$\begin{aligned} \left( \frac{\delta E}{\delta T} \right)_p &= \frac{3}{2} k P(z_0) Q(t_0, z_0) + \left[ z_0 \frac{\delta}{\delta z_0} \left\{ \frac{P(z_0)}{V} \right\} \left\{ \frac{3}{2} k T Q(t_0, z_0) + Q Z'(t_0, z_0) \right\} V \right. \\ &\quad \left. + \frac{3}{2} k T P(z_0) Q Z'(t_0, z_0) + P(z_0) Q Z' Z'(t_0, z_0) \right] \frac{1}{z_0} \frac{\delta z_0}{\delta T} \end{aligned}$$



$$\begin{aligned}
 & + \left[ \frac{3}{2} kTP(z_0)Q(t_0, z_0) + P(z_0)QZ'(t_0, z_0) \right] \frac{1}{V} \left( \frac{\delta V}{\delta T} \right)_p \\
 & + \left[ \frac{3}{2} kTP(z_0)Q_1(t_0, z_0) + P(z_0)Q_1Z'(t_0, z_0) \right] \frac{1}{t_0} \left( \frac{\delta t_0}{\delta T} \right)_p \\
 & = \frac{3}{2} kP(z_0)Q(t_0, z_0) + \left[ \frac{3}{4} kTP(z_0)Q(t_0, z_0) + 3P(z_0)QZ'(t_0, z_0) \right. \\
 & \quad \left. + P(z_0)QZ'Z'(t_0, z_0) \right] \frac{1}{T} \\
 & + \left[ \frac{3}{2} kTP(z_0)Q(t_0, z_0) + P(z_0)QZ'(t_0, z_0) \right] \left[ \frac{1}{2} \frac{Q_2(t_0, z_0)Q(t_0, z_0)}{[Q_1(t_0, z_0)]^2} - \frac{3}{2} \frac{1}{T} \right. \\
 & \quad \left. + \frac{Q_2QZ' - Q_1Z'Q_1}{kT^2Q_1^2} \right] \\
 & - \left[ \frac{3}{2} kTP(z_0)Q_1(t_0, z_0) + P(z_0)Q_1Z'(t_0, z_0) \right] \left[ \frac{1}{2} \frac{1}{T} \frac{Q(t_0, z_0)}{Q_2(t_0, z_0)} \right. \\
 & \quad \left. + \frac{QZ'(t_0, z_0)}{Q_1(t_0, z_0)} \frac{1}{kT^2} \right]
 \end{aligned}$$

after substituting the values of  $\frac{1}{t_0} \left( \frac{\delta t_0}{\delta T} \right)_p$ ,  $\frac{1}{V} \left( \frac{\delta V}{\delta T} \right)_p$ , from (25) and (27).

Then

$$\begin{aligned}
 C_p & = \left( \frac{\delta E}{\delta T} \right)_p + p \left( \frac{\delta V}{\delta T} \right)_p \\
 & = -\frac{15}{4} kP(z_0)Q(t_0, z_0) - \frac{5P(z_0)Q(t_0, z_0)}{T} \cdot \frac{Q_1Z'(t_0, z_0)}{Q_1(t_0, z_0)} \\
 & \quad - \frac{2}{kT^2} \frac{P(z_0)Q_1Z'(t_0, z_0)Q(Z't_0, z_0)}{Q_1(t_0, z_0)} + \frac{P(z_0)QZ'Z'(t_0, z_0)}{kT^2} \\
 & \quad + \frac{1}{T} \left[ \frac{3}{2} kTPQ + p(z_0)QZ'(t_0, z_0) \right] \left[ \frac{Q_2(t_0, z_0) \left\{ \frac{3}{2} Q(t_0, z_0) + \frac{QZ'(t_0, z_0)}{kT} \right\}}{\{Q_1(t_0, z_0)\}^2} \right] \\
 & = Ak \left[ -\frac{15}{4} \left( \sum_r \xi_r \right) - 5 \left( \sum_r \xi_r \right) \left( \sum_r \xi_r \frac{\chi_r + rb}{kT} \right) - 2 \left( \sum_r \xi_r \frac{\chi_r + rb}{kT} \right) \left( \sum_r \xi_r \frac{\chi_r + rb}{kT} \right) \right. \\
 & \quad + \sum_r \xi_r \left( \frac{\chi_r + rb}{kT} \right)^2 + \left( \frac{3}{2} \sum_r \xi_r + \sum_r \xi_r \frac{\chi_r + rb}{kT} \right) \left\{ \left( \sum_r \xi_r \right) \left( \frac{3}{2} \sum_r \xi_r \right. \right. \\
 & \quad \left. \left. + \sum_r \xi_r \frac{\chi_r + rb}{kT} \right) \right\} \dots \quad (29)
 \end{aligned}$$

Now, in the simplest case, referred to above, [where polymers of the type  $(X)_2$  only exist], this reduces to

$$\begin{aligned}
 C_p = & Ak \left[ -\frac{15}{4} \frac{(1+\xi)}{2} - \frac{5}{2} \frac{1+\xi}{2} \right] \left\{ \frac{\xi b}{kT} + \frac{1-\xi}{2} \frac{\chi+2b}{kT} \right\} \\
 & - 2 \left\{ \frac{\xi b}{kT} + \frac{1-\xi}{2} \frac{\chi+2b}{kT} \right\} \left\{ \frac{\xi b}{kT} + (1-\xi) \frac{\chi+2b}{kT} \right\} \\
 & + \left\{ \frac{5}{2} \frac{1+\xi}{2} + \xi \frac{b}{kT} + \frac{1-\xi}{2} \frac{\chi+2b}{kT} \right\} \left\{ (2-\xi) \left( \frac{1+\xi}{2} \cdot \frac{5}{2} + \frac{\xi b}{kT} + \frac{1-\xi}{2} \frac{\chi+2b}{kT} \right) \right\} \\
 & + \left\{ \frac{\xi b^2}{(kT)^2} + \frac{(1-\xi)}{2} \left( \frac{\chi+2b}{kT} \right)^2 \right\} \quad \dots \quad (29a)
 \end{aligned}$$

#### ISOTHERMAL ELASTICITY

To calculate the isothermal elasticity and the specific heat at constant volume,  $V$  and  $T$  are to be taken as independent variables.

On differentiating the equation (10) partially with respect to  $V$ , the following relation is obtained :

$$\begin{aligned}
 -\frac{A}{V^2} &= \frac{P(z_0)}{V} Q_2(t_0, z_0) \cdot \frac{1}{t_0} \left( \frac{\delta t_0}{\delta V} \right)_T \\
 \text{or} \quad -\frac{1}{t_0} \left( \frac{\delta t_0}{\delta V} \right)_T &= \frac{A}{V} \frac{1}{P(z_0) Q_2(t_0, z_0)} \quad \dots \quad (30)
 \end{aligned}$$

Now, on differentiating (13) with respect to  $V$  and keeping  $T$  constant, the expression for isothermal elasticity is obtained as :

$$\begin{aligned}
 -V \left( \frac{\delta p}{\delta V} \right)_T &= -kTP(z_0)Q_1(t_0, z_0) \frac{1}{t_0} \left( \frac{\delta t_0}{\delta V} \right)_T \\
 &= \frac{A^2 kT}{V} \frac{1}{P(z_0) Q_2(t_0, z_0)} \\
 &= kT \frac{P(z_0)}{V} Q(t_0, z_0) / \frac{Q(t_0, z_0) Q_1(t_0, z_0)}{Q_1(t_0, z_0)} \\
 &= p / \{1 + \sum \sum \frac{(r-m)^2}{rm} \xi_r \xi_m\} \leq p \quad \dots \quad (31)
 \end{aligned}$$

In this connection, it is to be remembered that for ideal gas, this is equal to  $p$ .

# SPECIFIC HEAT AT CONSTANT VOLUME

On differentiating the equation (10) partially with respect to  $T$ , keeping  $V$  constant, the following relation is obtained :

$$0 = \frac{3}{2}kTP(z_0)Q_1(t_0, z_0) \frac{1}{kT^2} + P(z_0)Q_1Z'(t_0, z) \frac{1}{kT^2} + P(z_0)Q_2(t_0, z_0) \frac{1}{t_0} \left( \frac{\delta t_0}{\delta T} \right)_v$$

$$\text{or} \quad \frac{1}{t_0} \left( \frac{\delta t_0}{\delta T} \right)_v = - \frac{1}{T} \left\{ \frac{3}{2} \frac{Q_1(t_0, z_0)}{Q_2(t_0, z_0)} + \frac{1}{kT} \frac{Q_1Z'(t_0, z_0)}{Q_2(t_0, z_0)} \right\} \quad \dots (32)$$

Then, on differentiating the equation (9) partially with respect to  $T$  and, on substituting the value of  $\frac{1}{t_0} \left( \frac{\delta t_0}{\delta T} \right)_v$  the expression for the specific heat at constant volume is obtained as

$$\begin{aligned} C_v = & \frac{3}{2}kP(z_0)Q(t_0, z_0) + \frac{1}{T} \left[ \frac{9}{4}kTP(z_0)Q(t_0, z_0) + 3P(z_0)QZ'(t_0, z_0) \right. \\ & \left. + \frac{P(z_0)QZ'Z'(t_0, z_0)}{kT} \right. \\ & \left. - \frac{1}{T} \left[ \frac{3}{2}kTP(z_0)Q_1(t_0, z_0) + P(z_0)Q_1Z'(t_0, z_0) \right] \left[ \frac{3}{2} \frac{Q_1(t_0, z_0)}{Q_2(t_0, z_0)} \right. \right. \\ & \left. \left. + \frac{1}{kT} \frac{Q_1Z'(t_0, z_0)}{Q_2(t_0, z_0)} \right] \right] \\ = & Ak \left[ \frac{15}{4} \sum \frac{\xi_r}{r} + 3 \sum \xi_r \left( \frac{\chi_r + rb}{kT} \right) + \sum \frac{\xi_r}{r} \left( \frac{\chi_r + rb}{kT} \right) \right. \\ & \left. - \left\{ \frac{3}{2} + \sum \xi_r \frac{\chi_r + rb}{kT} \right\} \left\{ \frac{\frac{3}{2} + \sum \xi_r \left( \frac{\chi_r + rb}{kT} \right)}{\sum r \xi_r} \right\} \right] \quad \dots (33) \end{aligned}$$

In the case where polymers of the type (X)<sub>2</sub> only exist the expression reduces to the following form :

$$C_v = Ak \left[ \frac{15}{4} \frac{1+\xi}{2} + 3\xi \frac{b}{kT} + \frac{1}{2} (1-\xi) \left( \frac{\chi_r + 2b}{kT} \right) + \left( \frac{b}{kT} \right)^2 \xi + \frac{1-\xi}{2} \left( \frac{\chi_r + 2b}{kT} \right)^2 \right. \\ \left. - \left\{ \frac{3}{2} + \xi \frac{b}{kT} + (1-\xi) \left( \frac{\chi_r + 2b}{kT} \right) \right\} \left\{ \frac{\frac{3}{2} + \xi \frac{b}{kT} + (1-\xi) \frac{\chi_r + 2b}{kT}}{2-\xi} \right\} \right] \dots \quad (33a)$$

Expression for  $C_p + C_v$  and  $\gamma = \frac{C_p}{C_v}$  :

From equations (29) and (33), straightforwardly it follows that

$$C_p - C_v = Ak \left[ -\frac{15}{2} \sum_r \xi_r - 3 \sum_r \xi_r \frac{\chi_r + rb}{kT} - 5 \left( \sum_r \xi_r \right) \left( \sum_r \xi_r \frac{\chi_r + rb}{kT} \right) \right. \\ \left. - \left( \sum_r \xi_r \frac{\chi_r + rb}{kT} \right) \left( \sum_r \xi_r \frac{\chi_r + rb}{kT} \right) + \left( \sum_r \xi_r \right) \left\{ \frac{3}{2} + \sum_r \xi_r \left( \frac{\chi_r + rb}{kT} \right)^2 \right\} \right. \\ \left. + \left\{ \frac{3}{2} \left( \sum_r \xi_r \right) + \sum_r \xi_r \frac{\chi_r + rb}{kT} \right\} \left( \sum_r \xi_r \right) \left\{ \frac{3}{2} \sum_r \xi_r + \sum_r \xi_r \frac{\chi_r + rb}{kT} \right\} \right] \dots \quad (34)$$

and

$$\gamma = \left[ -\frac{15}{4} \left( \sum_r \xi_r \right) - 5 \left( \sum_r \xi_r \right) \left( \sum_r \xi_r \frac{\chi_r + rb}{kT} \right) - 2 \left( \sum_r \xi_r \frac{\chi_r + rb}{kT} \right) \left( \sum_r \xi_r \frac{\chi_r + rb}{kT} \right) \right. \\ \left. + \left\{ \sum_r \xi_r \left( \frac{\chi_r + rb}{kT} \right) + 3 \sum_r \xi_r \right\} \left\{ \sum_r \xi_r \right\} \left\{ \frac{3}{2} \sum_r \xi_r + \sum_r \xi_r \frac{\chi_r + rb}{kT} \right\} + \sum_r \xi_r \left( \frac{\chi_r + rb}{kT} \right)^2 \right] \\ \times \left[ \frac{15}{4} \left( \sum_r \xi_r \right) + 3 \sum_r \xi_r \frac{\chi_r + rb}{kT} + \sum_r \xi_r \left( \frac{\chi_r + rb}{kT} \right)^2 \right. \\ \left. - \frac{1}{\left( \sum_r \xi_r \right)} \left\{ \frac{3}{2} + \sum_r \xi_r \frac{\chi_r + rb}{kT} \right\}^2 \right]^{-1} \dots \quad (35)$$

#### VELOCITY OF PROPAGATION OF SOUND

From the well-known thermodynamic relation

$$v^2 = - \frac{\gamma V \left( \frac{\partial p}{\partial V} \right)_T}{\rho} = - \frac{\gamma V^2 \left( \frac{\partial p}{\partial V} \right)_T}{Am} \dots \quad (36)$$

(where  $v$  is velocity of sound,  $\rho$  = density), the velocity of propagation of sound in the gas, of the type considered here, is expressible in terms of  $T$ ,  $V$  and degrees of dissociations. In the case where only polymers of the type  $(X)_2$  can be formed,  $\xi$ , the degree of association can be determined from measurements of velocity of sound.

REMARKS ON THE DEDUCTION OF VELOCITY OF  
PROPAGATION OF SOUND

In deducing the equation (36) for velocity of propagation of sound, it has been tacitly assumed that all variations, considered, are reversible, *i.e.*, at every stage there is a state of thermodynamic equilibrium, and so, the variations are infinitely slow. In 1920, Einstein (1920) pointed out that during propagation of sound, variations, *i.e.*, propagations of expansions and compressions, are so rapid that the time is not sufficient for establishing thermodynamic, or better, chemical equilibria. According to him, for these processes, the gas is to be treated as a pure mixture. Thus, the equation (36), supplemented with equations (30) and (33), is expected to be valid to those cases, if any, where the velocity of chemical reactions are much greater than that of propagation of sound. Objection, as put forward by Einstein, can be raised for all sorts of thermodynamic variations (not only chemical reactions). In all thermodynamic methods for deduction of velocity of propagation of sound, the formula is deduced on considering reversible variations (which are infinitely slow processes) after using different laws, *viz.*, the equation of state, laws of thermodynamics, which are really valid for reversible variations, but the results obtained thereby are found to be in agreement with the experiments. So, the same agreement of the formula, obtained here, with experimental results is expected in wider range than that mentioned above.

CONCLUSION

According to Fowler (1936), the usual results of real gases can be obtained very easily by treating the assembly of real gases as an assembly of point-molecules participating in associations. But, as shown here, the behaviours of isothermal compressibility, the coefficient of cubical expansion, etc. suggest that the thermodynamic behaviours of the assembly of associating molecules have a deviation from that of ideal gases, and the deviation is in the direction opposite to that of real gases.

The results, obtained in this present paper, give the relations of the compressibilities, coefficients of expansion, etc. with degree of associations. So, these are expected to be helpful for determinations of degree of associations in gas of the type considered in this paper from measurements of compressibilities, cubical expansions, etc., Now, from Vant-Hoff's (or Guldberg's) equations for mass-actions, degree of associations can be obtained as functions of temperature and pressure, so, ultimately all these compressibilities (isothermal or adiabatic), coefficient of cubical expansions etc., can be expressed (at least theoretically) in terms of temperature and pressure or temperature and volume as required.

## ACKNOWLEDGMENTS

In conclusion, the author wants to express his hearty thanks and deep gratitude to Dr. S. C. Kar, Prof. S. N. Bose and Prof. N. R. Sen for their interest shown in the work and for their helpful discussions.

KHAIRA LABORATORY OF PHYSICS,  
UNIVERSITY COLLEGE OF SCIENCE & TECHNOLOGY,  
92, UPPER CIRCULAR ROAD, CALCUTTA.

## REFERENCES

- Einstein, A., 1920, *Sitz. u. ber. Berlin*, pp. 380-85.  
Fowler, R. N., 1930, *Statistical Mechanics*, pp. 157-61 and 214-89.  
Epstein, P. S., 1947, *Text-book of Thermodynamics*, p. 379.

# A STUDY OF THE SWITCHING ACTION IN A MULTIVIBRATOR CIRCUIT. PART II.

By B. M. BANERJEE

(Received for publication, June 5, 1951)

Plate XIV A D

**ABSTRACT.** An experimental study of the switching action of a plate-coupled multivibrator is presented. It is a continuation of a previous publication on the same subject. This part concentrates on the study of the phenomenon at the initial - regenerative part of the switching process—in the microsecond time interval when current flows in both the multivibrator tubes, as it transfers from one tube to the other.

The results of the study has been condensed into a table that lists the characteristics of thirty-two representative cases. A summary of results, oscillograms of switching waveforms and a general discussion on all aspects of the switching process and generation of fast waveforms, follow.

## INTRODUCTION

In the previous publication (Banerjee, 1950) of this series, we have discussed the switching action of a multivibrator. In that discussion, it was found that the phenomenon may be conveniently divided into two parts, *viz.*, the first one or two microseconds, during which current transfers from one tube to the other, and the next few microseconds after this current transfer, during which the electrode voltages go on changing till they ultimately attain the new equilibrium values. In the previous publication, we have indicated that the electrode potentials, in the first part of this phenomenon, change with time following an exponential with positive index. In the terminating part of the phenomenon, the electrode potentials change following roughly an exponential with negative index—or a combination of exponentials with negative indices. The experimental studies made in the first phase of these investigations, obtained mainly oscillograms of the terminating part. The potential changes during the first part are usually small, about five to fifteen volts, so that they occupy relatively small parts in an oscillogram. The terminating part usually occupy the major part of these oscillograms. The total change of electrode potentials due to switching, which the oscillograms delineate, is the greater fraction of the H T. supply voltage, normally well over a hundred volts in amplitude.

## ALTERATIONS IN THE EXPERIMENTAL ARRANGEMENT

In order to be able to study the characteristics of the first part of the switching process, it was necessary to somehow increase the voltage changes

The insertion of resistors of small values between the cathode and chassis of the multivibrator tubes  $T_1$  and  $T_2$ , (Figure 1) together with returning the grid leaks to a positive supply, allowed a further extension of this voltage span. The conducting tube cathode and grid would then be positive (about 10 to 40 volts) at the start of the process, and the first or the regenerative part would end when this tube is cut off. The voltage span is, therefore, increased by as much as the cathode and grid remains positive, *i.e.*, by the

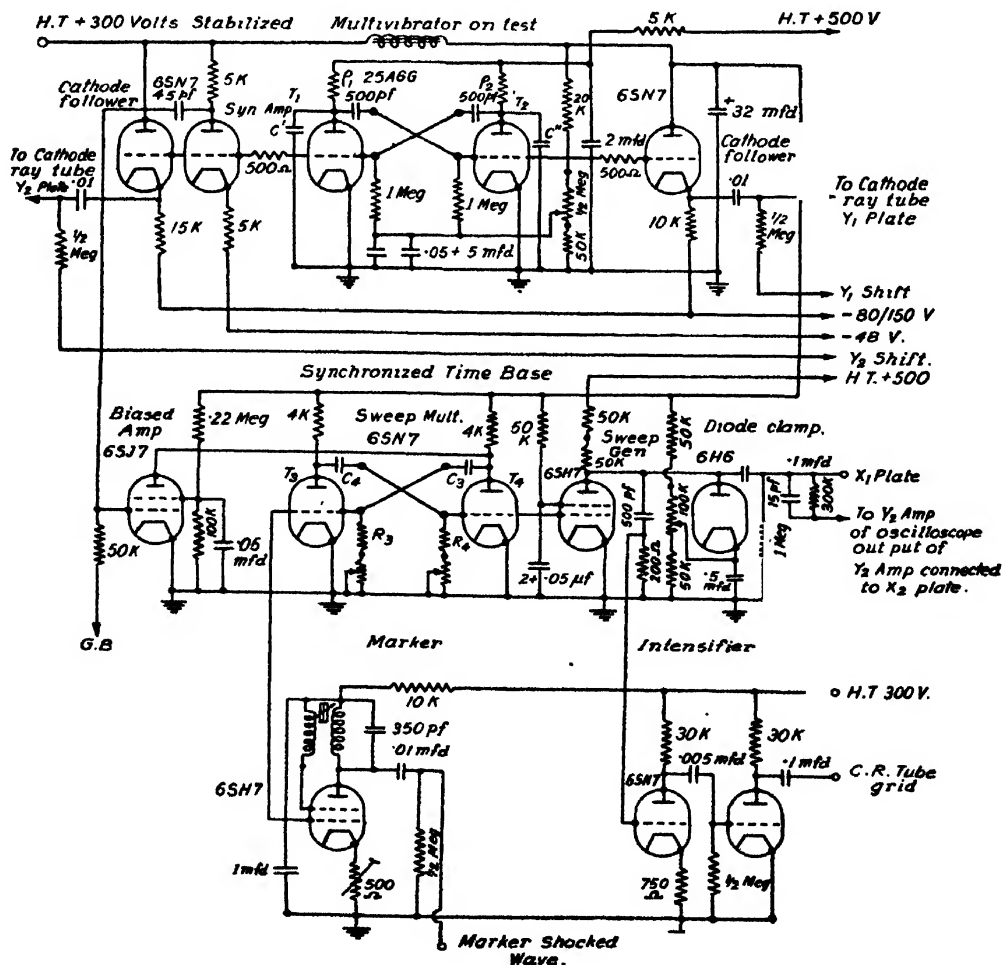


FIG. 1

\* See discussion—different periods in the switching process.



amount of the voltage drop across the cathode resistor. The other effect of this cathode resistor is to restrict the variation of the transconductance (see discussion).

The other alterations in the experimental arrangement (see Figure 1) were chiefly of a minor nature, although they improved the accuracy and reliability of measurements very greatly. On the sweep circuit, they were the alterations of the sweep circuit constants and incorporation of an unity gain sweep-amplifier operating on the  $X_2$  plate, to increase sweep speed and linearity. The altered marker circuit utilized a higher  $Q$  ( $Q=250$ ) coil, with regeneration, to produce virtually undamped oscillations of 720 Kc/s as marker signals. Provision was made for two cathode followers, so that simultaneous oscillograms of the grid voltages of the two tubes could be taken. The synchronizing amplifier circuit and circuit constants were also altered, and this improved synchronization.

The symmetrical  $X$  deflection keeps the cathode ray spots in perfect focus practically at all positions of the flat face of the 89D cathode ray tube. The clamping diode at the grid of the C. R. tube in the Cossor model 1035 oscilloscope utilized in these measurements, permits of an easy adjustment and holds constant the intensity level of the spots. This materially assists in retaining the good focus. The remarkably good definition of the spots produced by an 89D tube backed up by these circuit refinements greatly increased the accuracy of the measurements.

To ensure stability of pattern positions—i.e., freedom from “jitter”—so necessary to obtain good oscillograms, the entire A. C. supply, including that of the oscilloscope, was derived from a stabilizing transformer. Besides, the 300-volt supply was further stabilized by an electronic regulator (Banerjee, 1942).

#### EXPERIMENTAL PROCEDURE

Simultaneous changes of the grid voltages of the two 25A6G multivibrator tubes, obtained at the output of the two cathode followers, were applied to the two beams,  $Y_1$  and  $Y_2$  of a double-beam oscilloscope—a Cossor 89D tube inside a 1035 model oscilloscope. The symmetrical sweep voltages were applied to the horizontal deflection,  $X_1$  and  $X_2$  plates. Oscillograms were taken utilizing a plate camera at fixed magnification. Each plate recording the simultaneous oscillogram, was exposed thrice, first with the oscilloscope beams connected to the cathode followers giving the multivibrator switching waveforms, next with  $Y_1$  connected to the time marker signal of 720 Kc/s, and  $Y_2$  to a fixed voltage of -22 volts given by a battery, and finally to both  $Y_1$  and  $Y_2$  connected to a fixed battery voltage of -58 volts. The plates, therefore, contain both time and voltage calibrating marks.

Besides oscillograms, many cyclograms were taken. In these, the grid voltage fall was applied to  $X_1$  plate. The grid voltage rise was applied to  $Y_1$  plate. The  $Y_1$  beam, therefore, drew out the cyclogram— $T_1$  grid voltage

rise vs  $T_2$  grid voltage fall. The sweep was applied to the  $Y_2$  beam so that the  $Y_2$  beam depicted the grid voltage fall with time. This was necessary to make sure that the cyclogram taken did correspond to the switching process. The marker of 720 Kc/s shocked oscillation was next connected to  $X_1$ , while  $Y_2$  remained connected to the sweep, and  $Y_1$  to a large fixed voltage so as to deflect it off the marker pattern, for the next exposure that marked out time. In the third exposure, all the  $X_1$ ,  $Y_1$  and  $Y_2$  plates were connected to a rapidly changing voltage such as the grid voltage fall or the sweep, which drew out a cross. This cross gave reference co-ordinates, representing lines when  $X$  and  $Y$  change equally with time.

The oscillograms were reduced to the same scale with the help of a photographic enlarger. The plates were put inside the enlarger and the enlarged image obtained on squared paper. The base lines of constant battery voltage were made to coincide with one set of parallel lines of the squared paper. By adjustment of the enlargement ratio, the difference between the 22-volt line and the 58-volt line was made equal to nine divisions. Each division, therefore, corresponds to four volts. The switching waveforms were then traced out, following the image on the squared paper produced by the enlarger. The crest and troughs of the timing sinusoids marked out on squared paper, gave 0.7 microsecond intervals [see figure 3].

For comparison of oscillograms, the photographic enlarger was again exploited. One of the two plates that were to be compared was placed inside the enlarger and the properly enlarged\* image compared against the pencil curve on squared paper of the other. With this method, very accurate and critical comparison was possible. As the oscillograms were taken with the switching waveforms at about the same position with respect to the start of the sweep, the residual non-linearity of the time-base does not interfere with the accuracy of comparison.

The switching waveforms, traced out on squared paper with the help of the enlarger, were then analysed. As the theoretical analysis (Williams *et al* 1949 : Ahmed, 1950) indicate that the first part would be an exponential with positive index, the points in these curves were plotted on semi-log paper. The first step in this plotting must be the selection of the zero time. The most distinct criterion of the start of the switching process is the progressively rapid fall of the otherwise constant grid voltage of the conducting tube. But as the changes at the start of the switching process are very small, it is difficult to fix the point precisely and there may be uncertainties in time of as much as a microsecond. This uncertainty leads to an alteration in the shape of the semi-log plot at the starting point, besides errors in the constants of the exponential curve, that is a near fit to the experimental curve. This will be seen in Figure 4(a), where two such plots of the same experimental curve with starting points altered in time by 1.4 microseconds

\* As described in the previous paragraph.

are given. It is apparent that the curvature of the starting part of the semi-log plot changes from concave inwards to concave outwards as the starting point is advanced in time. With a suitable choice of the starting point, the initial part of the curve may be made to roughly follow the straight line of the main curve. While this may be used as an additional confirmation of the proper selection of the zero time in some cases, it must be used with caution as in others, the start of the correct semi-log plots are not actually straight lines (see discussion).

#### RESULTS OF EXPERIMENTS

The semi-log plots of the switching waveforms were found to follow approximately a straight line over a voltage span of 30-60 volts in most cases. In these, straight lines were drawn through the ten volt and thirty volt points and their slope gave the indices characteristic of an exponential that is a near fit to the experimental waveforms. Besides the exponential indices and co-efficients, other data, such as the maximum rates of the voltage rise and fall, the time shift between the rise and fall at ten volts change etc., for thirtytwo representative cases are given in Table I. Eighteen oscillograms and six cyclograms are shown in the plates XIV A-D. Semilog plots of several representative cases are also shown in Figures 4(a) and 4(b).

#### SUMMARY OF RESULTS

The findings of these experiments may be summarised as below :

(1) The switching wave forms approximately follow an exponential with positive index over a voltage span of 30-60 volts—a voltage span less than that corresponding to the regenerative period.\*

(2) The fall of voltage is generally faster than the rise of voltage. The exponential index and the maximum rate of the waveform of the fall of voltage is greater than the 'rise'.

(3) The initial rate of rise of voltage is almost always greater than the 'fall'—and the change of voltage of 'rise' waveform remains greater than the 'fall' waveform up to a considerable time from the start of the switching. The change of voltage of rise waveform exceeds the fall up to 50-60 volts—up to about the end of the regenerative period.

The same change of voltage at the early part of the regenerative period is obtained in the fall waveform sometime later than the rise waveform. This is referred to as the time lag between rise and fall in the table.

(4) Increase of the shunt capacities and the anode resistances generally reduces the 'fastness' of these waveforms without much change in their character. Decrease of tube transconductances have a similar effect.

\* See discussion—different periods in the switching process.

TABLE I

No.	Circuit parameters	Index and co-efficient of exponential curve $A.e^{mt}$		Rise exceeds fall	Time lag for 10 volts change	Maximum rate of change of voltage	
		Rise	Fall			Rise	Fall
1	$R_1 = R_2 = 7.5 \text{ K}$ $C' = C'' = \text{none}$ $R_1$ cathode resistance $380 \Omega$	$m = 1.8$ $A = 0.2$ volts Good fit up to 70 volts Both slightly faster than exponential	$m = 2.87$ $A = 0.01$ Good fit up to 70 volts. Both slightly faster than exponential.	Upto 70 volts	0.33 micro-conds.	180 volts/micro-seconds.	180 volts/micro-second.
2	$R_1 = R_2 = 7.5 \text{ K}$ $C' = C'' = 35$ of $R_1 = 380 \Omega$	$m = 1.43$ $A = 0.5$ volts Good fit up to 60 volts	$m = 1.9$ $A = 0.1$ Fair fit; faster than exponential	Upto 80 volts.	0.45 $\mu$ sec.	100 volts/ $\mu$ sec.	140 volts/ $\mu$ sec
3	Same as above except $C' = 100$ pf. $C'' = 100$ pf.	$m = 1.05$ $A = 1.8$ volts Fair fit up to 50 volts; Faster than exponential.	$m = 1.35$ $A = 1.1$ Fair fit up to 50 volts. Faster than exponential.	Upto 70 volts.	0.5 $\mu$ sec.	70 volts/ $\mu$ sec.	120 volts/ $\mu$ sec.
4	Same as above except $C' = \text{none}$ $C'' = 100$ pf.	$m = 1.05$ $A = 0.35$ volts. Bad fit; faster than exponential up to 50 volts.	$A = 1.64$ $A = 0.05$ Fair fit up to 50 volts. Faster than exponential.	Upto 60 volts.	0.6 $\mu$ sec.	80 volts/ $\mu$ sec.	180 volts/ $\mu$ sec.
5	Same as above except $C' = 100$ pf. $C'' = \text{none}$	$m = 1.18$ $A = 0.38$ volts Good fit upto 50 volts. Faster than exponential.	$m = 1.70$ $A = 0.02$ Good fit upto 50 volts. Faster than exponential.	Upto 120 volts; almost the end of the voltage rise.	0.65 $\mu$ sec.	110 volts/ $\mu$ sec.	130 volts/ $\mu$ sec.
6	Same as No. 5 except $C' = \text{none}$ $C'' = 500$ pf.	$m = 0.56$ $A = 1.6$ volts Fair fit upto 50 volts.	$m = 0.73$ $A = 0.5$ Good fit upto 50 volts.	Upto 55 volts.	0.75 $\mu$ sec.	27 volts/ $\mu$ sec.	45 volts/ $\mu$ sec.

7	Same as above except $C = 500$ pf. $C'' = \text{none}$	$m = 0.65$ $A = 1.7$ volts. Good fit upto 50 volts.	$m = 0.83$ $A = 0.4$ Good fit upto 50 volts.	till end— 120 volts ; after rise is completed fall exceeds.	1.15 $\mu\text{sec.}$	70 volts/ $\mu\text{sec.}$	85 volts/ $\mu\text{sec.}$
8	Same as above except $C = C'' = 500$ pf.	$m = 0.35$ $A = 2.9$ volts, Good fit upto 50 volts,	$m = 0.45$ $A = 0.96$ Very good fit upto 70 volts.	Upto 80 volts.	1.70 $\mu\text{sec.}$	23 volts/ $\mu\text{sec.}$	40 volts/ $\mu\text{sec.}$
9	$R_1 = R_2 = 7.5$ K $C = C'' = 100$ pf. $R_1$ of $T_1$ 380 ohm $R_2$ of $T_2$ zero	$m = 1.35$ $A = 0.7$ volts. Very good fit upto 50 volts. Slightly faster than exponential.	$m = 2.0$ $A = 0.09$ Very good fit upto 50 volts. Slightly faster than exponential.	till end— 100 volts	0.55 $\mu\text{sec.}$	70 volts/ $\mu\text{sec.}$	110 volts/ $\mu\text{sec.}$
10	$R_1 = R_2 = 7.5$ K $C = C'' = 100$ pf. $R_1$ of $T_1$ zero $R_2$ of $T_2$ 380 ohm	$m = 0.94$ $A = 0.8$ volts Good fit upto 50 volts; Faster than exponen- tial till end	$m = 1.35$ $A = 0.11$ Good fit upto 40 volts; much faster than exponential till end	Upto 50 volts.	0.58 $\mu\text{sec.}$	100 volts/ $\mu\text{sec.}$	140 volts/ $\mu\text{sec.}$
11	$R_1 = R_2 = 7.5$ K $C = C'' = 100$ pf. $R_1 = \text{zero}$	$m = 1.21$ $A = 0.13$ volts. Fair fit upto 50 volts Faster than exponen- tial.	$m = 2.1$ $A = 0.01$ Bad fit; faster than exponential.	Upto 60 volts.	0.6 $\mu\text{sec.}$	120 volts/ $\mu\text{sec.}$	150 volts/ $\mu\text{sec.}$
12	$R_1 = R_2 = 7.5$ K $C = C'' = 500$ pf. $R_1 = \text{zero}$	$m = 0.59$ $A = 1.6$ volts Fair fit upto 50 volts.	$m = 0.8$ $A = 0.26$ Fair fit upto 50 volts.	Upto 70 volts.	1.5 $\mu\text{sec.}$	30 volts/ $\mu\text{sec.}$	70 volts/ $\mu\text{sec.}$
13	$R_1 = 8$ K, $R_2 = 6.7$ K $C = C'' = 500$ pf. $R_1 = 1000$ ohms.	$m = 0.25$ $A = 5.8$ volts. Bad fit; less fast compared to exponential.	$m = 0.26$ $A = 5.0$ Bad fit; less fast compared to exponential.	Upto 70 volts.	0.55 $\mu\text{sec.}$	13 volts/ $\mu\text{sec.}$	20 volts/ $\mu\text{sec.}$
14	$R_1 = 8$ K, $R_2 = 6.7$ K $C = 500$ pf $C'' = \text{zero}$ $R_1 = 1000$ ohms.	$m = 0.38$ $A = 3.5$ volts. Fair fit; less fast than exponential.	$m = 0.36$ $A = 2.5$ Good fit upto 50 volt; little less than expo- nential.	till end— 120 volts.	0.9 $\mu\text{sec.}$	28 volts/ $\mu\text{sec.}$	38 volts/ $\mu\text{sec.}$

TABLE (contd.)

No.	Circuit parameters	Index and co-efficient of exponential curve $A.e^{st}$		Rise exceeds fall	Time lag for 10 volts change	Maximum rate of change of voltage	
		Rise	Fall			Rise	Fall
15	$R_1=8K, R_2=6.7K$ $C''=none$ $C'=500$ pf. $R_3=1000$ ohms.	$m=0.37$ $A=4.0$ volts. Good fit upto 40 volts. Less fast compared to exponential.	$m=0.43$ $A=2.7$ Good fit upto 50 volts. Less fast compared to exponential.	Upto 50 volts.	1.4 $\mu$ sec.	17 volts/ $\mu$ sec.	28 volts/ $\mu$ sec.
16	$R_1=8K, R_2=6.7K$ $C'=C''=100$ pf, $R_3=1000$ ohms.	$m=0.44$ $A=5.0$ volts. Very good fit upto 80 volts.	$m=0.54$ $A=1.5$ Very good fit upto 100 volts.	Upto 90 volts.	1.0 $\mu$ sec.	35 volts/ $\mu$ sec.	55 volts/ $\mu$ sec.
17	$R_1=8K, R_2=6.7K$ $C'=100$ pf. $C''=none$ $R_3=1000$ ohms	$m=0.47; 0.56$ $A=1.1; 2.3$ volts. Good fit upto 80 volts. Faster than exponential.	$m=0.56; 0.59$ $A=0.90; 0.52$ Good fit upto 50 volts. Faster than exponential.	Upto 100 volts	1.15 $\mu$ sec.	50 volts/ $\mu$ sec.	58 volts/ $\mu$ sec.
18	$R_1=8K, R_2=6.7K$ $C'=none$ $C''=100$ pf. $R_3=1000$ ohms	$m=0.54$ $A=2.0$ volts Good fit upto 90 volts.	$m=0.73$ $A=0.62$ Very good fit upto 90 volts.	Upto 80 volts.	0.9 $\mu$ sec.	42 volts/ $\mu$ sec.	60 volts/ $\mu$ sec.
19	$R_1=8K, R_2=6.7K$ $C'=C''=none$ $R_3=1000$ ohms	$m=0.66$ $A=1.6$ volts. Good fit upto 30 volts. Faster than exponential.	$m=0.92$ $A=0.38$ Good fit upto 30 volts. Faster than exponential.	Upto 80 volts	0.82 $\mu$ sec.	75 volts/ $\mu$ sec.	140 volts/ $\mu$ sec.
20	$R_1=50K, R_2=6.7K$ $C'=C''=200$ pf. $R_3=1000$ ohms.	$m=0.39$ $A=2.5$ volts Good fit upto 30 volts; greater than exponential.	$m=0.46$ $A=0.5$ Very good fit upto 60 volts.	Upto 70 volts	1.7 $\mu$ sec.	47 volts/ $\mu$ sec.	70 volts/ $\mu$ sec.

21	$\rho_1 = 7.5K, \rho_2 = 50K$ $C = C'' = 100 \text{ pf.}$ $R_4 = 1000 \text{ ohms.}$	$m = 0.62$ $A = 3.2 \text{ volts.}$ Good fit upto 30 volts; much less than exponential; bad fit afterwards.	$m = 0.66$ $A = 1.9$ Better fit upto 50 volts; less fast compared to exponential.	Upto 70 volts.	0.75 $\mu\text{sec.}$	24 volts/ $\mu\text{sec.}$	32 volts/ $\mu\text{sec.}$
22	$\rho_1 = 8K, \rho_2 = 6.7K$ $C = C'' = 1000 \text{ pf.}$ $R_4 = \text{zero}$	$m = 0.42$ $A = 2.8 \text{ volts.}$ Good fit upto 50 volts; less fast compared to exponential	$m = 0.61$ $A = 0.58$ Good fit upto 50 volts; Less fast compared to exponential.	Upto 70 volts.	1.65 $\mu\text{sec.}$	16 volts/ $\mu\text{sec.}$	36 volts/ $\mu\text{sec.}$
23	$\rho_1 = 8K, \rho_2 = 6.7K$ $C' = 1000 \text{ pf.}$ $C'' = \text{none}$ $R_4 = \text{zero}$	$m = 0.7$ $A = 1.0 \text{ volt}$ Very bad fit; faster than exponential.	$m = 1.6$ $A = 0.01$ Bad fit; faster than exponential.	Till end - 100 volts; fall exceeds after rise is com- pleted.	1.55 $\mu\text{sec.}$	100 volts/ $\mu\text{sec}$	100 volts/ $\mu\text{sec.}$
24	$\rho_1 = 8K, \rho_2 = 6.7K$ $C' = \text{none}$ $C'' = 1000 \text{ pf.}$ $R_4 = \text{zero}$	$m = 0.58$ $A = 1.5 \text{ volts}$ Fair fit upto 50 volts; less fast compared to exponential.	$m = 0.88$ $A = 0.025$ Good fit upto 50 volts; less fast compared to exponential	Upto 48 volts.	1.05 $\mu\text{sec}$	20 volts/ $\mu\text{sec.}$	48 volts/ $\mu\text{sec.}$
25	$\rho_1 = 8K, \rho_2 = 6.7K$ $C = C'' = 200 \text{ pf.}$ $R_4 = \text{zero.}$	$m = 1.24$ $A = 1.8 \text{ volts}$ Fair fit upto 80 volts.	$m = 2.1$ $A = 0.13$ Good fit upto 70 volts.	Upto 60 volts.	0.6 $\mu\text{sec.}$	80 volts/ $\mu\text{sec.}$	130 volts/ $\mu\text{sec.}$
26	$\rho_1 = 50K, \rho_2 = 6.7K$ $C = C'' = 200 \text{ pf.}$ $R_4 = \text{zero.}$	$m = 1.12$ $A = 1.3 \text{ volts.}$ Very good fit upto 50 volts; faster than exponential after- wards.	$m = 1.6$ $A = 0.17$ Very good fit upto 30 volts; decidedly faster than exponen- tial afterwards.	Upto 60 volts.	0.65 $\mu\text{sec}$	80 volts/ $\mu\text{sec.}$	130 volts/ $\mu\text{sec.}$
27	$\rho_1 = \rho_2 = 50K$ $C = C'' = 200 \text{ pf.}$ $R_4 = \text{zero.}$	$m = 0.77$ $A = 2.6 \text{ volts.}$ Bad fit; less fast com- pared to exponen- tial.	$m = 0.95$ $A = 0.8$ Very good fit upto 40 volts; afterwards bad.	Upto 58 volts	0.8 $\mu\text{sec.}$	19 volts/ $\mu\text{sec.}$	38 volts/ $\mu\text{sec.}$
28	$\rho_1 = \rho_2 = 50K$ $C = 200 \text{ pf.}$ $C'' = \text{none}$ $R_4 = \text{zero.}$	$m = 1.0$ $A = 1.8 \text{ volts.}$ Very good fit upto 40 volts; faster than exponential upto 62 volts	$m = 1.6$ $A = 0.13$ Very good fit upto 60 volts.	Upto 70 volts.	0.9 $\mu\text{sec}$	55 volts/ $\mu\text{sec}$	100 volts/ $\mu\text{sec.}$

TABLE I (contd.)

No.	Circuit parameters	Index and co-efficient of exponential curve $A.e^{-t}$		Rise exceeds fall	Time lag for 10 volts change	Maximum rate of change of voltage	
		Rise	Fall			Rise	Fall
29	$R_1 = R_2 = 50K$ $C' = \text{none}$ $C'' = 200 \text{ pf}$ $R_4 = \text{zero}$	$m = 0.89$ $A = 2.9 \text{ volts}$ Fair fit upto 30 volts; bends down progressively afterwards; less fast.	$m = 1.15$ $A = 1.2$ Fair fit upto 30 volts; bends down progressively afterwards; faster than rise throughout.	Upto 50 volts.	0.5 $\mu\text{sec}$ .	22 volts/ $\mu\text{sec}$ .	28 volts/ $\mu\text{sec}$ .
30	$R_1 = R_2 = 50K$ $C' = C'' = \text{none}$ $R_4 = \text{zero}$	$m = 2.55$ $A = 0.14 \text{ volts}$ Very good fit upto 30 volts; afterwards less fast and bends down progressively.	$m = 2.0$ $A = 0.7$ Very good fit upto 50 volts; afterwards bends progressively.	Rise later than fall from the beginning.	-0.35 $\mu\text{sec}$ .	70 volts/ $\mu\text{sec}$	100 volts/ $\mu\text{sec}$ .
31	$R_1 = 8K, R_2 = 6.7K$ $C' = C'' = 200 \text{ pf}$ $R_4 = 1000 \text{ ohms}$	$m = 0.32$ $A = 4.2$ Good fit upto 80 volts	$m = 0.39$ $A = 1.8 \text{ volts}$ Good fit upto 80 volts.	Upto 90 volts.	1.45 $\mu\text{sec}$ .	21 volts/ $\mu\text{sec}$ .	35 volts/ $\mu\text{sec}$ .
32	$R_1 = 8K, R_2 = 6.7K$ $C' = C'' = 33 \text{ pf}$ $R_4 = 1000 \text{ ohms}$	$m = 0.56$ $A = 1.6 \text{ volts}$ Good fit upto 80 volts.	$m = 0.74$ $A = 0.45$ Good fit upto 80 volts.	Upto 100 volts.	1.0 $\mu\text{sec}$ .	60 volts/ $\mu\text{sec}$ .	70 volts/ $\mu\text{sec}$ .

The switching waveforms, whose semi-log plots lie on a straight line over the entire regenerative period obey an exponential law. "Faster than exponential" are those whose semi-log plots have a slope increasing with time and "Slower than exponential" are those that have a slope decreasing with time.

The values of the index " $m$ " given in the Table are correct when the time unit is a micro-second. When time is expressed in seconds these values must be multiplied by  $10^6$ .



(5) Addition of capacity between anode and cathode of the non-conducting tube whose grid is rising, produce a smaller reduction in the fastness—the exponential indices and also the maximum rates of change of voltage. The important change noticeable with such unsymmetrical capacity loading, is the delaying of the 'fall' waveform with respect to the 'rise'. This is clearly discernible in the oscillograms and also manifest itself as an increase in the time lag for ten volts change. As a consequence, the span of the regenerative period of switching gets increased and the waveforms follow an exponential over a greater region.

The delaying of the 'fall' waveform make 'rise' voltage changes exceed the 'fall' for a longer period and a greater voltage span—so much so that the grid voltage rise may even be completed before the grid voltage fall has cut off the current in the corresponding tube.

Increase of anode resistance ( $\rho_1$ ) of the tube whose grid is rising, actually increases the 'fastness' by a small amount. If the circuit is symmetrical as to capacities, the waveforms are similar to that of the case of equally small resistances—only the corresponding 'fall' waveform is somewhat faster.

Addition of capacity to the anode of the tube whose grid is falling has a greater effect in reducing the 'fastness'. Unsymmetrical capacity loading of this type restricts the regenerative period and the exponential part of the switching waveform. It increases the intermediate period—a period in which current is shut off in the tube whose grid is falling while the grid voltage of the tube that is rising has not yet reached the cathode voltage. In the intermediate period, the fall of voltages are approximately linear, while the rise is an exponential with negative index. With unsymmetrical capacity loading of this type, the delay between the rise and fall is reduced to a minimum.

Increase of anode resistance of the tube whose grid is falling produces effects similar to the increase of anode cathode capacity.

(6) The chief effect of the cathode resistors in the multivibrator tubes is to restrict the effective transconductance and thereby reduce its variation. They also increase the voltage span of the regenerative period. It is, therefore, natural to expect that the rise and fall waveforms should follow more accurately the predictions of the simple theory (Williams *et al* 1950; Ahmed, 1950) that assumes constant transconductances,—that of exponentials with the same positive index. This is actually observed. The reduction in the effective transconductance also reduces the 'fastness' of the switching waveforms.

The cathode resistors also increase the effective plate resistance of the tubes and limit the maximum anode current. This reduces the maximum rate of fall of voltage so that it cannot become much greater than the maximum rate of rise.

The cathode resistor in the tube whose grid is rising has the greater effect in reducing the fastness of switching.

(7) As the fastness of switching gets reduced due to increase of shunt capacity or decrease of tube transconductance—a considerable loss of feed back voltage takes place across the coupling condensers, if the time constant of the coupling network is also small. This reduces the fastness in a greater proportion compared to what may be expected in terms of the increase of shunt capacities and cathode resistors. Besides, as the shunt capacities and the cathode resistors are increased, the nature of the waveforms change from 'faster than exponential' to 'slower than exponential.'

## DISCUSSION

### (a) *Concerning Experimental Oscillograms*

The experiments were conducted with two 25A6G tubes connected as triodes. Connected as triode, these tubes have an unusually low amplification factor,\* a property which has been taken advantage of in increasing the voltage span of the regenerative period of switching. The electrode geometry which gives this low amplification factor also produces what is known as an extended 'tail' of the grid voltage anode current characteristic. This characteristic of low  $\mu$  tubes of usual electrode construction is a continuously curved one\*—so that the transconductance progressively increases from zero to a high value as the anode current increases. While the variation of transconductance with anode current occurs in all practical tubes, those having higher amplification factors ( $\mu=20-30$ ) as are commonly used for multivibrators, are of a different nature. The transconductance *vs.* grid voltage curve of the usual tubes (amplification factor 20-30) follows more or less a straight line at the start, bending to reduced slopes later. Thus there is a rapid increase of transconductance as the anode current increases from zero and later, the transconductance-increase gets progressively reduced. With low  $\mu$  tubes of usual construction such as that of 25A6G tubes, the transconductance rise rate increases progressively in the low anode current region and a large rate is maintained to the region of very large anode current—almost up to zero grid bias. The resistors between the cathode and ground restrict the variation of effective transconductance as it approaches high values. So that the characteristics of the low  $\mu$  25A6G tube approached those of conventional tubes when the 380 ohm cathode resistor was employed. With 1000 ohm cathode resistors, the variation of the effective transconductance was less than that of conventional tubes. The oscillograms obtained with 1000 ohm cathode resistors, therefore, represented a case almost approaching the idealized one of constant transconductance.

\* See figure 2.

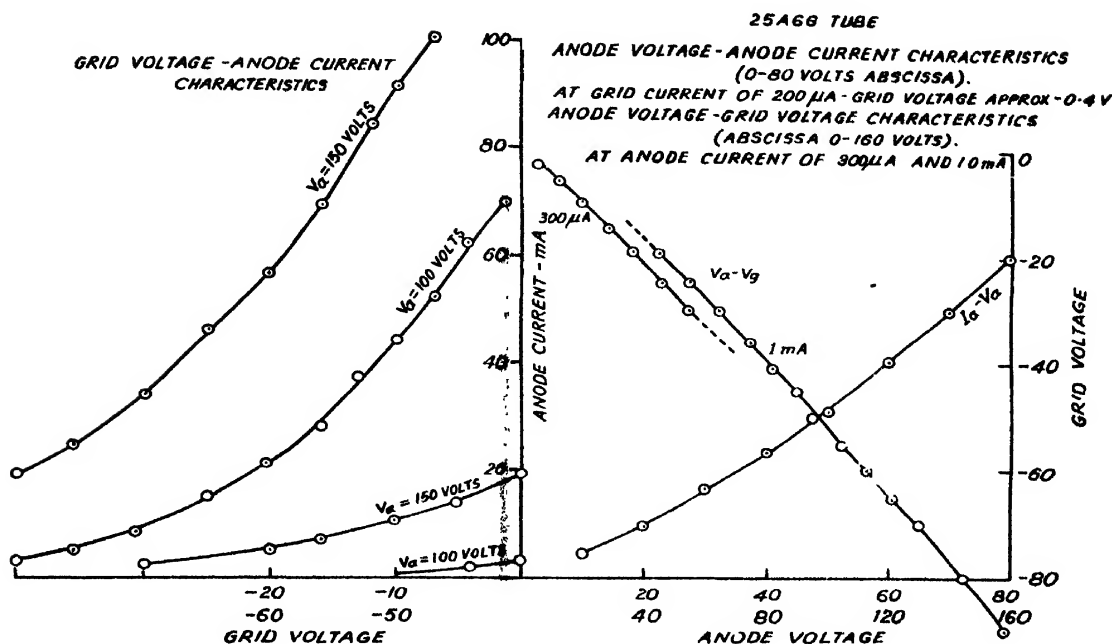


FIG. 2

## (b) Nature of Switching Phenomenon

Switching in multivibrators using practical tubes, where the tube transconductances always vary over a great range, is a complicated phenomenon. While it is quite possible to guess and even estimate as to the nature of the phenomenon, accurate prediction is very difficult. There are various aspects and their inter-relation is complicated. In what follows we shall discuss them one after another.

The switching phenomenon can be adequately described only with the help of the complete set of switching waveforms as are obtained in a simultaneous oscillogram. One set of oscillograms may differ from another in a variety of ways. In Table I that attempts to describe the thirty-two representative cases, the values of certain criteria that may describe and differentiate the different oscillograms, are listed. These criteria are not necessarily complete or unique, in that even though they are the same, the actual switching waveforms may, conceivably, be different. Individually, they cannot specify the process at all, the complete set must be compared with another, if conclusions are to be drawn. The summary of results presents the conclusions of the author drawn after a study of the table and what is more important—a critical comparison of the actual oscillograms.

## (c) Different Periods in the Switching Process : [Figures 3(a), (b), (c)]

This experimental study has given a clearer insight into the nature of the switching process. In the previous publication, we have divided the switching phenomenon into two parts. In the first part, currents in the

two tubes change—increasing to the maximum limit in one tube and decreasing to zero in the other. This may be called the driven or regenerative period. The second part begins just after this current transfer in the tubes. As a result of this current transfer, the electrode voltages, which have changed to some extent in the first regenerative period, would take up new and widely different equilibrium values. Because the tube electrodes have shunt capacities unavoidably associated with them, they take some time to reach the new equilibrium values. The period after the current transfer during which the electrode voltages go on changing to ultimately attain the final equilibrium values may be called the “terminal” period. Williams *et al* (1950) have envisaged the existence of an intermediate period—a period starting with the current cut off in the tube whose grid is going negative and ending with the other tube grid reaching the cathode voltage. An intermediate period of this definition was found in many of the observed cases [see figure 3]. This has been rightly considered as a separate period inasmuch, a separate mechanism takes place in this period. The current cut off in the negative going tube severs the feedback connection so that it is a non-regenerative period. The anode voltage of this tube goes on increasing—following an exponential of negative index—to reach the H. T. supply voltage. This voltage gets applied to the other tube grid through the coupling  $C$ - $R$  network. The other tube grid voltage, therefore, continues increasing. This increase may permit an increasing anode current in this

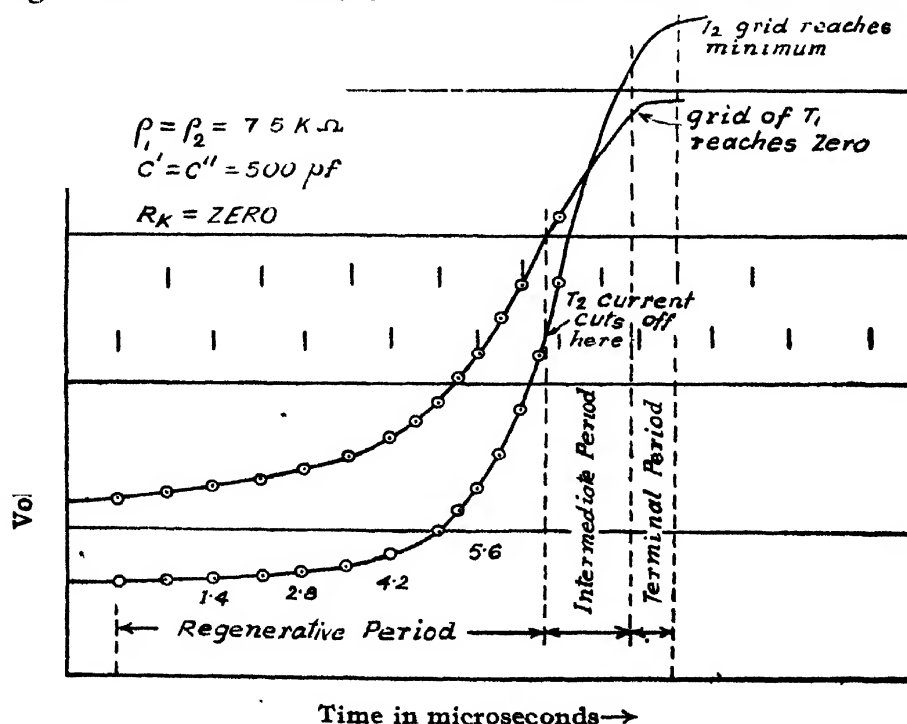


FIG. 3a

Plot of multivibrator switching waveforms illustrating the different periods of the switching process.

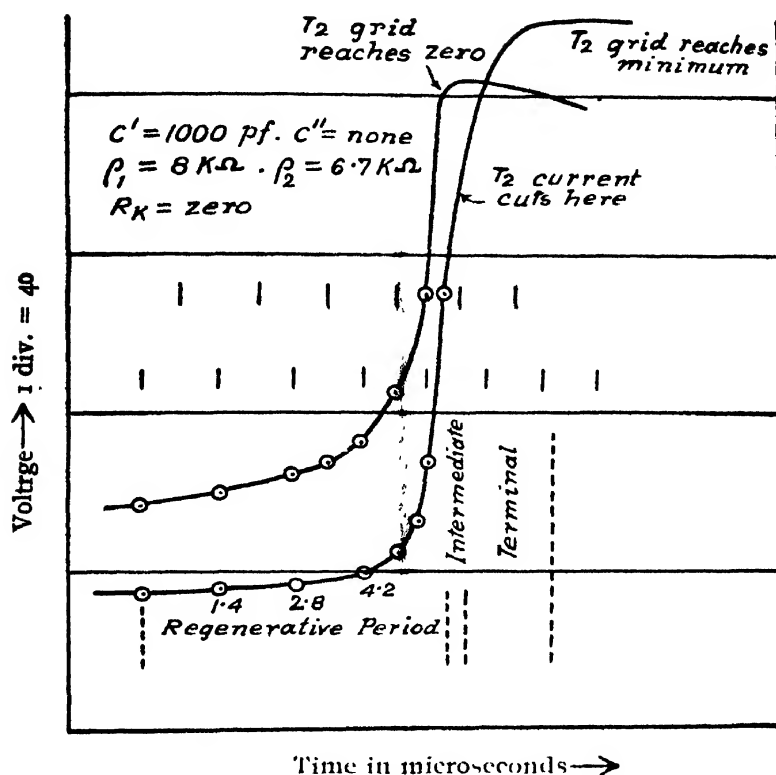


FIG. 3b

Plot of multivibrator switching waveforms illustrating the different periods of the switching process.  $T_1$  grid reaches zero just before  $T_2$  current cuts off. The intermediate period is of the less common type and is very short.

last mentioned tube. The anode voltage, therefore, falls faster as time progresses. It usually falls faster than linear in this period.

The reverse phenomenon may also take place. In certain cases, the grid voltage rise is completed, *i.e.*, grid has reached cathode voltage, before the grid voltage fall has cut off the anode current in the other tube. Such cases are encountered when the fall waveform is delayed too much behind the rise waveform [*e.g.*, unsymmetrical cases with large capacity loading on the anode of the tube whose grid is rising, see figure 3(b)] as also in cases where the negative going tube requires a large voltages to cut off.

In some cases, the grid voltage reaches cathode voltage in the positive going tube and cut off in the negative going tube almost simultaneously [figure 3(b)]. The intermediate period vanishes in those cases.

The voltage span and duration of the intermediate period is large in the case of low  $\mu$  tubes used with high anode resistances. Increase of the anode capacity of "falling grid" tube enhances it still further [see figure 3]. Increase of anode capacity of "rising grid" tube reduces it. In a symmetrical case, with medium  $\mu$  triodes and pentodes the duration and voltage span of the intermediate period is quite small.

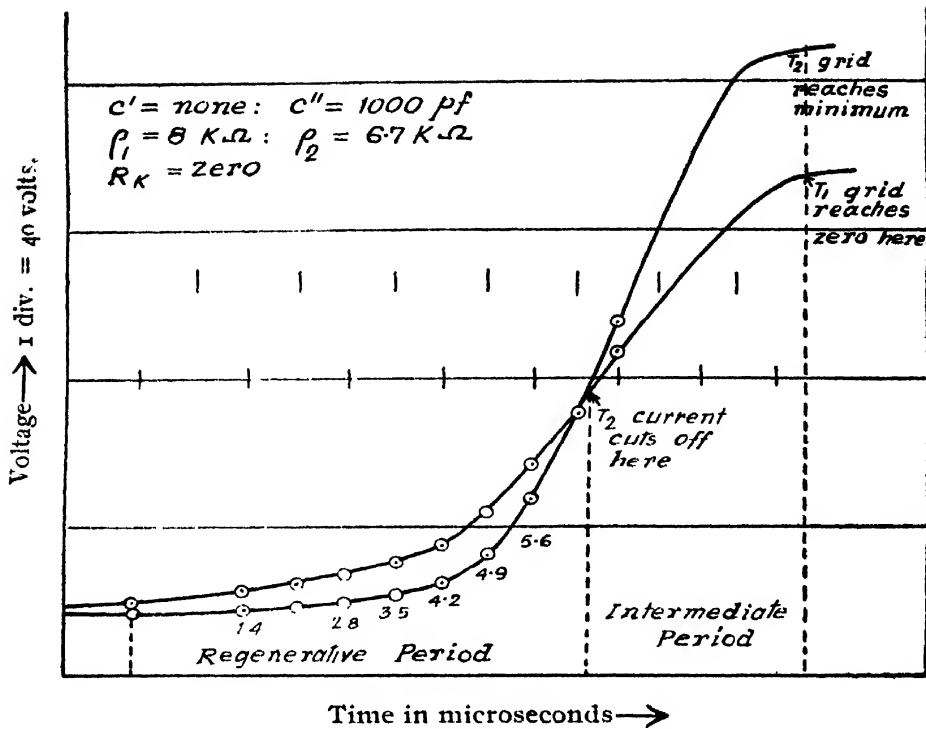


FIG. 3c

Plot of multivibrator switching waveforms illustrating the different periods of the switching process. No terminal period.

In the observed cases, because of the employment of low  $\mu$  triodes as the experimental tubes, the anode current of the conducting tube in the intermediate period was found almost constant, as the negative going voltage changed almost linearly with time. This resulted because the increase of grid voltage in this period was more or less compensated by the more rapid fall of anode voltage, so that the anode current could not sensibly increase. With medium  $\mu$  triodes and pentodes, the anode current would increase till the anode voltage drops down very low so that the fall waveform would continue faster than linear till the end of the intermediate period, or almost the end of the fall waveform if it is so rapid as to get completed (and reach the new equilibrium voltage) within the intermediate period. Maximum speed of fall is attained at the end of the intermediate period or within it, if the fall is completed within the intermediate period.

The start of the switching process forms an important part of the entire phenomenon. Switching is initiated due to the arrival of anode current in the non-conducting tube. This causes a progressive fall of the anode potential which is transmitted to the grid of the conducting tube through the  $C$ - $R$  coupling network. Regenerative build-up, to start a similar progressive fall with an increasing rate, marks the initiation of the switching process. Regenerative build-up of the grid voltage begins only after the tube transconductance has exceeded a certain limit, so that the anode voltage

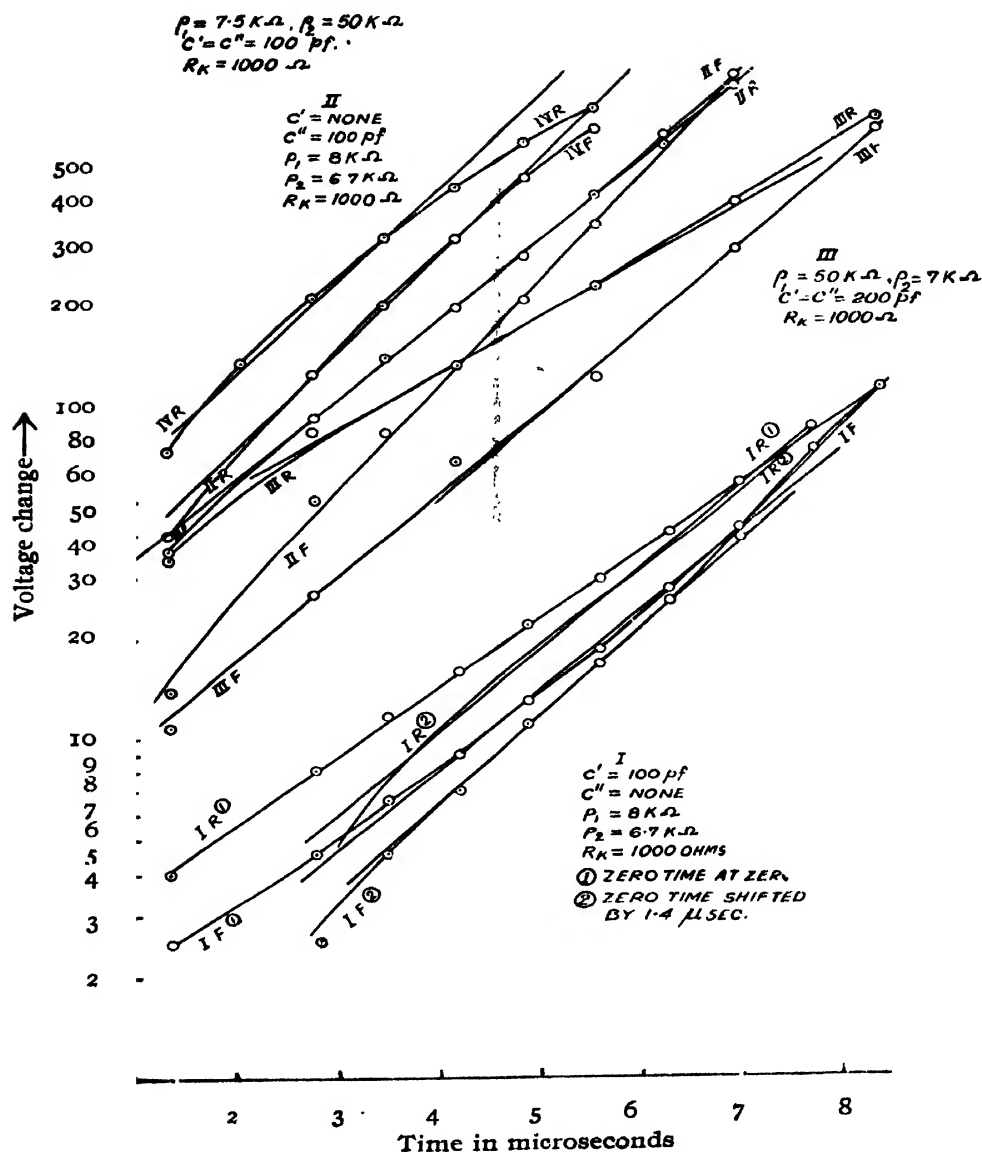


FIG. 4a

Representative semi-log plots of multivibrator switching waveforms. Note that the semi-log plots are not accurately straight lines, so that the switching waveforms cannot be expressed by simple exponentials. Note also that the plots of rise waveforms (R) have different slopes compared to the plots of fall waveforms (F).

drops sufficiently rapidly to transmit an appreciable fraction to the conducting tube grid through the coupling network. The rate of fall of anode voltage is determined roughly by the  $G/C'$  ratio. So, if the shunt capacity  $C'$  has a greater value, the start of switching is delayed to the region of greater transconductance and hence higher anode current. In extreme cases of large shunt capacities and short time constant of coupling network the switching

may not take place at all. Such cases were actually observed, *e.g.*, when the external shunt capacities  $C' = C''$  were increased to 1000 pf, in case where  $\rho_1 = 8k \Omega$ ,  $\rho_2 = 6.7 k \Omega$ ,  $R_k = 1000$  ohms.

(d) *Voltage Waveforms:*

While the simple theory (Williams *et al* 1950 ; Ahmed 1950) that assumes constant transconductances of the tubes, indicates exponentials with the same positive index for both the rise and fall waveforms as solutions, the

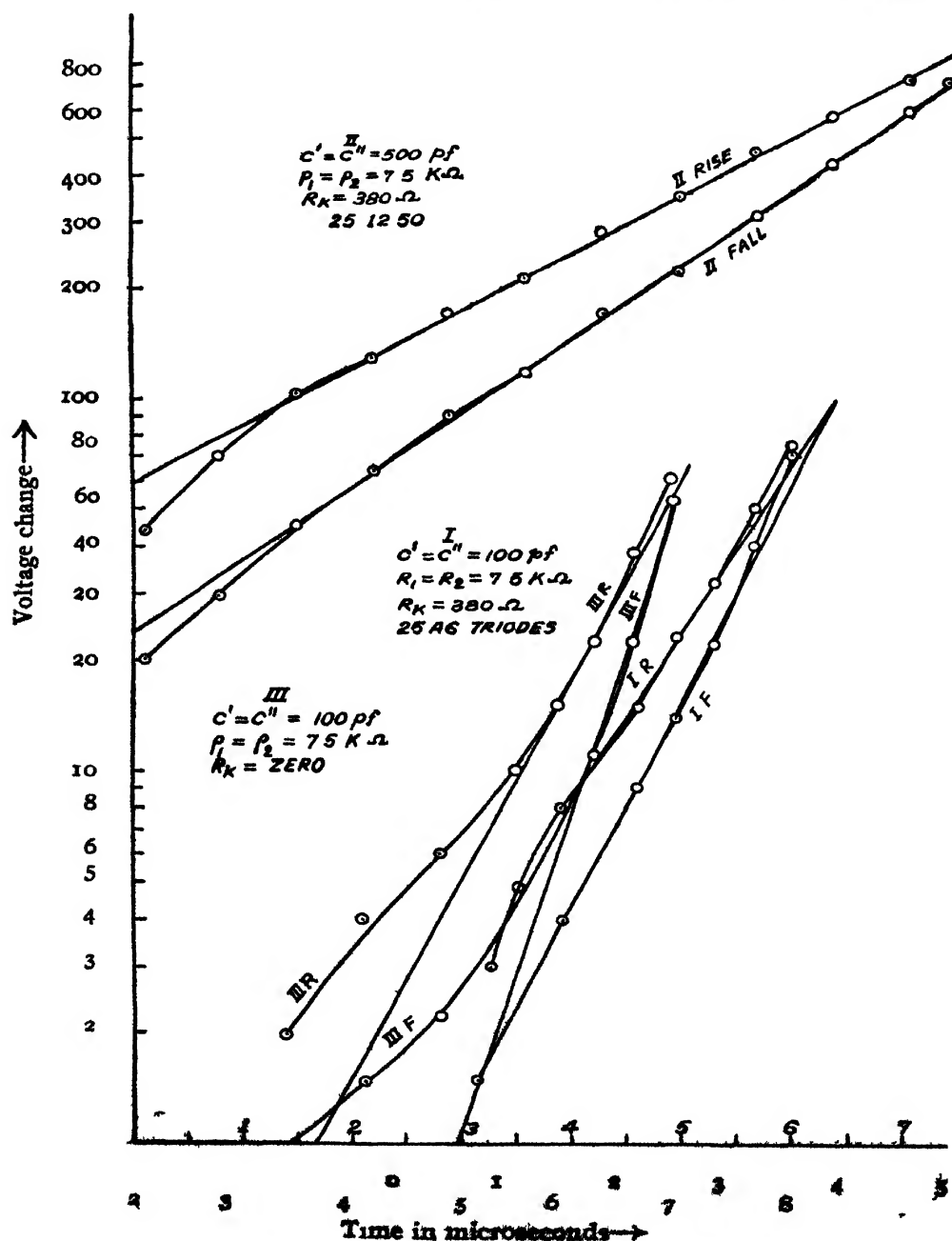
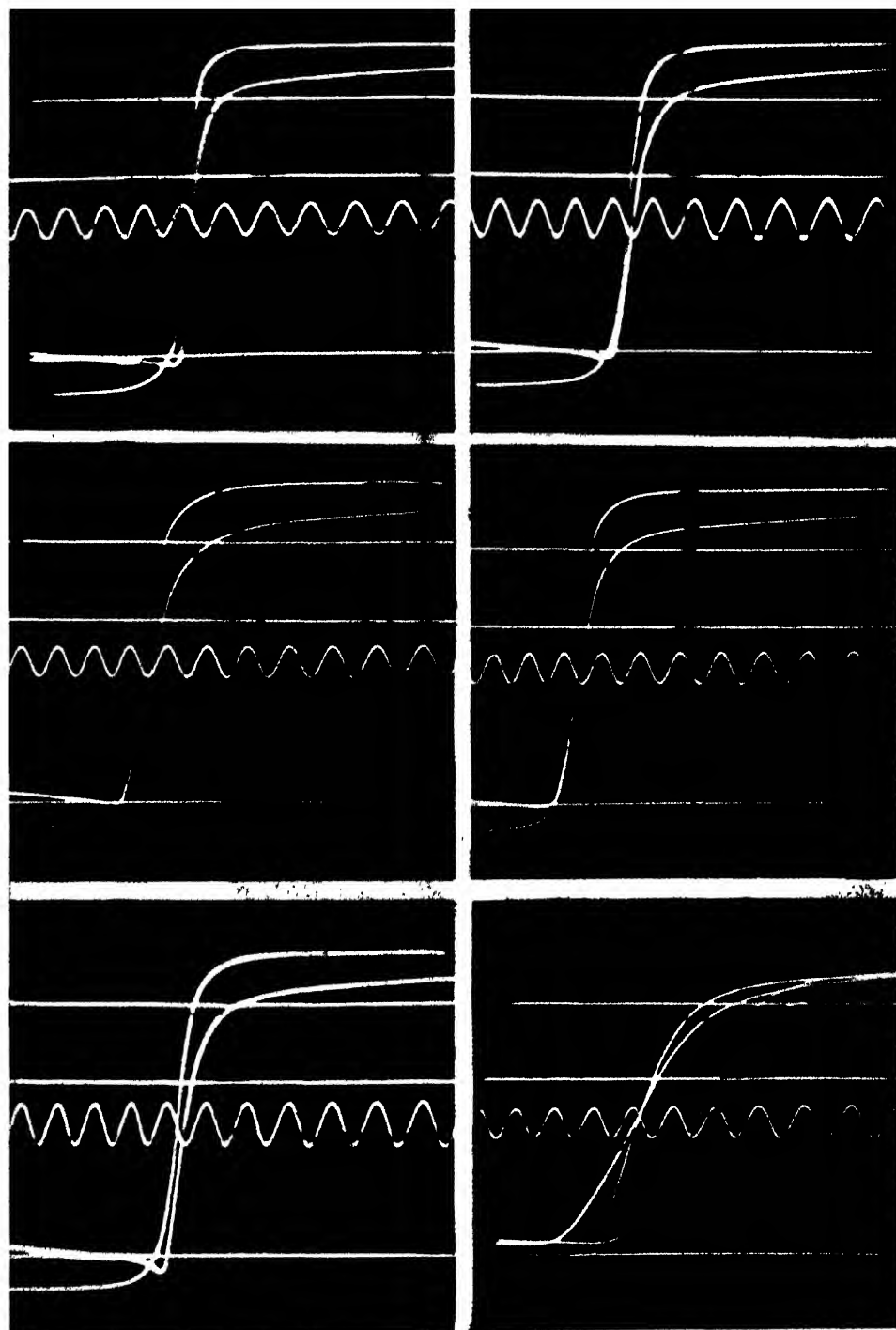


FIG. 4b

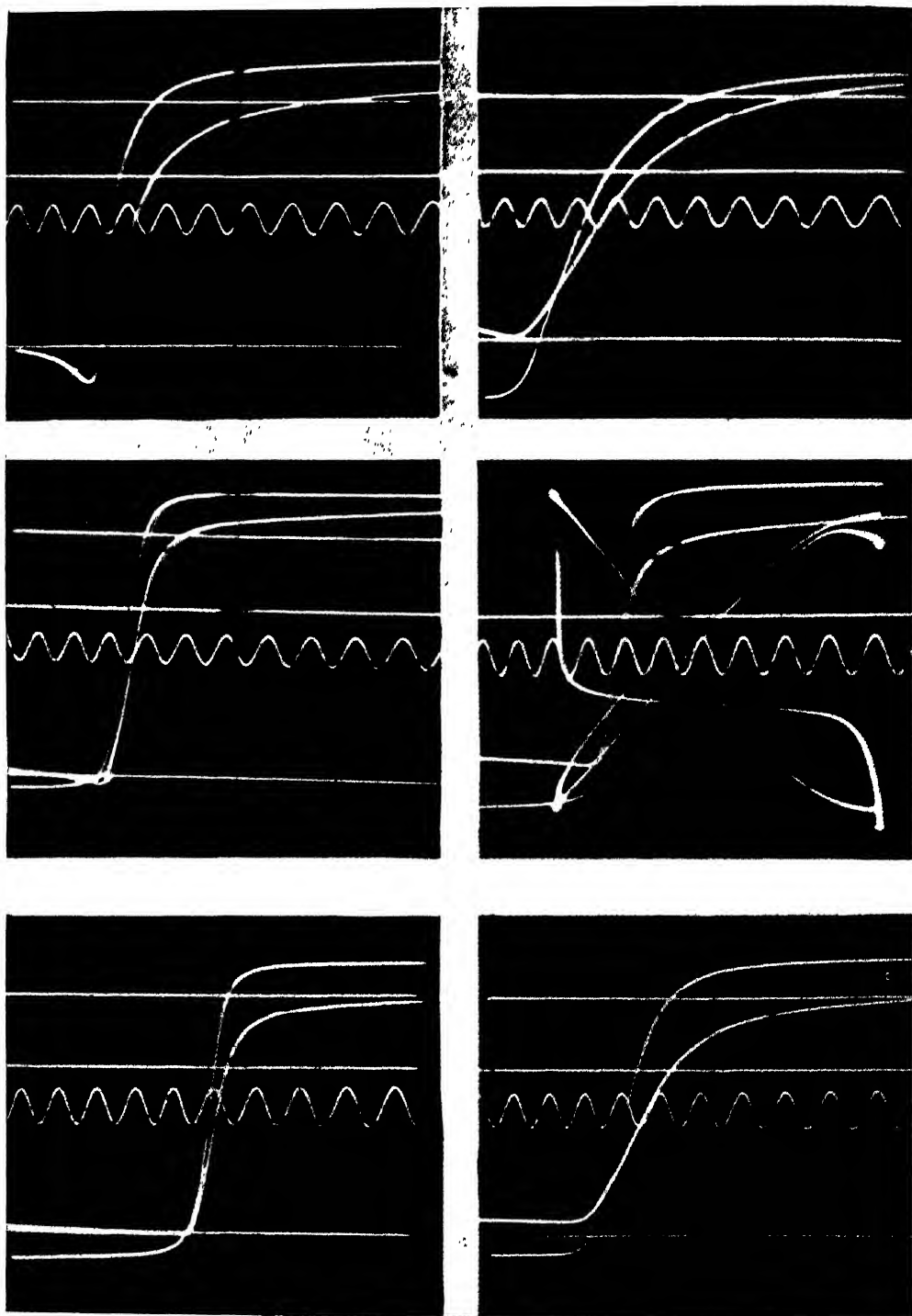
Representative semi-log plots of multivibrator waveforms.





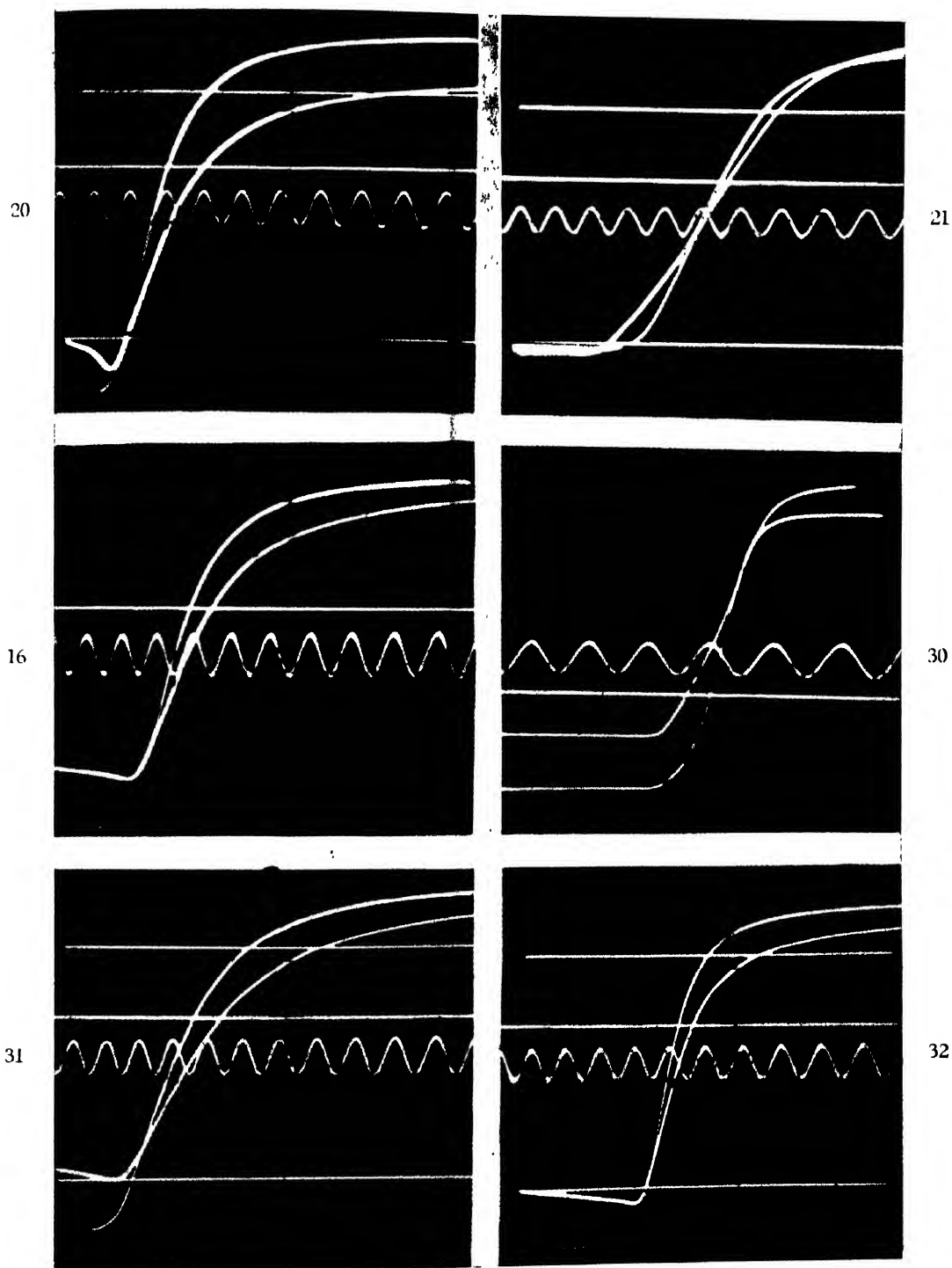
OSCILLOGRAMS

The numbers adjacent to the oscillograms are the serial numbers of Table I. The multivibrator circuit constants whose switching gave rise to these oscillograms may, therefore, be obtained by reference to the table, according to the serial numbers, and the circuit given in figure 1.



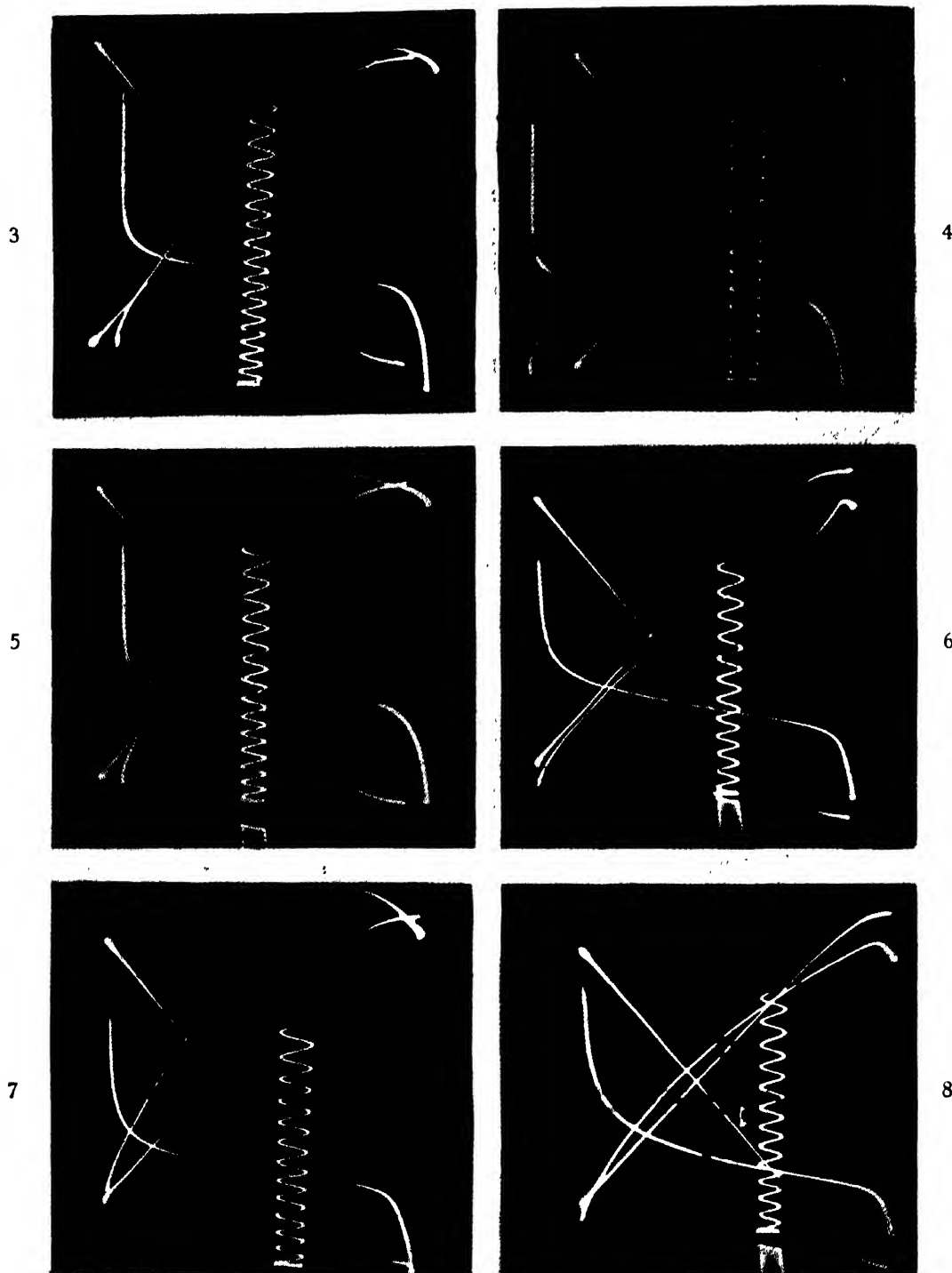
## OSCILLOGRAMS

The numbers adjacent to the oscillograms are the serial numbers of Table I. The circuit constants of the multivibrator whose switching gave rise to these oscillograms may, therefore, be obtained by reference to the table, according to the serial number and the circuit given in figure 1.



## OSCILLOGRAMS

The numbers adjacent to the oscillograms are the serial numbers of Table I. The circuit constants of the multivibrator whose switching gave rise to these oscillograms may, therefore, be obtained by reference to the table, according to the serial number, and the circuit given in figure 1.



CYCLOGRAMS

The numbers adjacent to the cyclograms are the serial numbers of Table I. The circuit constants of the multivibrator whose switching gave rise to these cyclograms may therefore be obtained by reference to the table, according to the serial number, and the circuit given in figure 1.

experimental observations have been different. The primary cause of this divergence from theory, must be the variation of the transconductance with grid voltage.

The semi-log plots of many of the experimental wave-forms lie more or less on a straight line over a voltage span of five to fifty volts, indicating that they will fit well with an exponential of appropriate index and co-efficient. However, it has been found that a shift of the point chosen as the zero time point, alters the semi-log plots, so much so, that although again another nearly straight line is obtained over a similar region, the index and co-efficient of this new exponential are different. Experimentally it is difficult to fix precisely the point of zero time on the oscillograms so that an uncertainty and error remain as to these values.

While at first sight this may appear rather strange how the same curve may fit well with two exponentials, nevertheless it is quite natural and is to be expected. It is not possible to precisely evaluate the constants of an exponential of positive index which is a near fit to an experimental curve, when the zero point of the abscissa is somewhat uncertain. This would have been possible if measurements permitted accurate evaluation of the quantity (voltage) on the log axis over a range of a hundred times or more.

As most of the experimental semi-log plots perceptibly deviate from straight lines when considered over the entire regenerative period and as the rise index indicated by the ten volt—thirty volt intercept line on the semi-log-plots are different from the fall index, it seems better not to describe these practical experimental waveforms as exponentials. They are actually different—something which cannot be described by a simple mathematical function. The root cause is the transconductance variation of the practical tube.

While the idea of an exponential variation arising out of the regenerative build-up may be helpful, one should remain conscious to the fact that the actual phenomenon is always more complicated, and that it is unwise to push forward the predictions too far—of the simple theory, to estimate unknown cases.

#### (e) *Rate of Change of Voltage :*

The rate of change of electrode voltages continue to increase throughout the regenerative period. The "rise" voltage rate becomes a maximum at the end of the regenerative period. After that, it diminishes following an exponential with negative index. The "fall" voltage rate is maintained and may continue increasing throughout the intermediate period, if the fall is not so rapid as to get completed within this period. At about the end of the "fall," the rate diminishes rapidly and when the minimum voltage is reached it reverses in sign. The switching may be considered to be terminated at this point, as relaxation of the grid that has been driven negative follows.

The maximum rate of fall is almost always greater than the maximum rate of rise. The maximum fall rate may be as much as three times greater than the maximum rise rate. Larger ratios are obtained with higher values of anode load resistances, but even when the anode resistances are made very large, a ratio of three is not exceeded. This happens because the increased speed of fall quickly brings about its termination, so that the fall rate has no opportunity to increase to very high values.

The plate and grid voltage fall terminate at the same time. The grid voltage rise is brought to a stop and reversed as the grid voltage exceeds cathode voltage. A much slower plate voltage rise continues for a further period,—following an exponential of a much smaller negative index\*—until the plate voltage almost reaches the H. T. supply voltage and relaxation of the grid condenser brings about the reverse switching.

(f) *Current Waveforms :*

The current waveforms differ from an exponential change still more compared to the voltage waveforms. The current in the tube that is cut off, decreases roughly according to the equation  $I = I_0 - A_1 G \cdot e^{k_1 t}$ , until it drops to zero. The current in the tube that is switched on increases from zero roughly according to the relation  $I = A_2 G \cdot e^{k_2 t}$ . This fast rise continues till the end of the regenerative period. Later, in the intermediate period, the fastness of increase is checked. In the case of low  $\mu$  triodes, the current becomes nearly constant. It increases at a more or less constant rate, with high  $\mu$  triodes and pentodes, till the end of the intermediate period or the end of the fall waveform, whichever is earlier. Afterwards, as the grid voltage settles down close to the cathode voltage, having gone through a maximum in the positive direction, the current decreases somewhat to attain the steady equilibrium value.

The changes of current are completed within the regenerative period (for current cut off) and the regenerative and intermediate period (for current switch on). There is little change of current in the terminal period.

(g) *Relaxation Switching and Triggered Switching :*

The experiments were performed with self-running multivibrators in which the switching was brought about by the slow relaxation of the grid condenser. This was done with a view to studying as to how the electrode voltages build up due to the regenerative action and attain the extremely fast rising and falling rates, that are characteristics of the process. A satisfactory study of the build up process is possible only if the initial rate of the voltage that starts the switching is smaller compared to the final rates, by a factor of a hundred times or more. In our experimental set up, the relaxation rate of the negative grid was about half a volt per microsecond.

\* See Part I.

Thus the starting rate was about fifty to four hundred times smaller than the final rates. While a still lower rate is no doubt desirable, it could not be utilized as the attempt to reduce the relaxation rate, increased "jitter" of the oscilloscope patterns.

In triggered switching, the voltage signal that starts the process, increases very rapidly. The final rates of the electrode voltages are usually not greater than three to ten times the starting rate brought about by the triggering signal. This reduces the triggering delay—the time that elapses between the injection of the triggering signal (and/or start of the switching process) and the attainment of the maximum rates. A theoretical analysis of the idealized case indicates that the exponentials that describe the process have the same index, whatever the triggering signal rate, but of different co-efficients. A reduction of the triggering delay is also indicated.

#### (h) *Generation of Fast Waveforms :*

In most of the applications of the multivibrators, the switch over of its states are utilized to generate waveforms that have an extremely rapid rise and fall. In many such applications, the ultimate performance of the complete unit depends critically on what is spoken loosely as the "fastness" of the rise and fall. The requirements in these cases are threefold, *viz.*, (1) the time between the application of the triggering signal and the attainment of a high speed of change over should be as small as possible; (2) this triggering time delay should be constant; (3) the maximum rate of the rise or fall voltage should be as large as possible.

The maximum rate of voltage rise is obtained just after the regenerative period. An equally great rate of voltage fall is obtained about the same time. The triggering time delay is, therefore, practically equal to the regenerative period.

If the triggering signal starts the switching over with a certain initial rate ( $dV/dt$ ) and if the final rate attained is  $n$  times this value, then the triggering time  $\tau$  is approximately given by

$$\tau = \frac{\ln (2n)}{m} \quad (1)$$

where  $m$  is the positive index of the exponential switching waveform.  $\tau$  can be reduced by increasing  $m$  and decreasing  $n$ .

So far as the triggering signal is concerned, a large rate of rise is desirable as this would diminish the triggering delay. A satisfactory amplitude is also necessary as otherwise the triggering point is not well defined so that triggering may not be ensured.

Regarding  $m$ , it is approximately given by the expression

$$m \approx (G/C - 1/RC), \quad \dots (2)$$

where  $G$  represents the transconductance,  $C$  the shunt capacities, and  $R$

the effective anode resistance of the equivalent circuit (the tube internal resistance, the anode resistance and the grid leaks in parallel).

The shunt anode capacities,  $C'$  and  $C''$  comprise the following :

- (a) anode cathode capacity of the tube concerned,
- (b) grid cathode capacity of the other tube,
- (c) approximately twice\* the sum of the two grid anode capacities.

We come to the usual discussion concerning triodes and pentodes in connection with shunt capacities. While pentodes would necessarily have increased grid cathode and anode cathode capacities, the selection is to be based as to whether the sum of these two would be greater or smaller compared with the equivalent capacity of a suitable triode. A comparison between actual tubes shows that some improvement, though small, may be secured by using pentodes.

Since pentodes have a high plate resistance, the reduction of the exponential index due to the negative term  $1/RC$  is much smaller, so that a decided improvement is secured, on this score, by using pentodes.

The maximum rates of the rise voltage is obtained just after the regenerative period. This rate is given approximately by the usual relation

$$(dV/dt) = (V_b - V_a) / \rho_2 C'' \approx I_0 / C'' \quad \dots (3)$$

where  $V_b$  is the H. T. supply voltage and  $V_a$  the plate voltage at the end of the regenerative period ;  $I_0$  is the standing current in the (conducting) tube that is cut off in the switch over. A large value of  $I_0$  may be obtained only if the corresponding anode resistor  $\rho_2$  has a small value. It is preferable

\* The grid anode capacities are connected between the rising and the falling voltages. The rise and fall voltages differ in magnitude and rate by a factor of one to three. The current through the grid anode capacities produces an effective increase of shunt capacities of magnitudes equal to about 1.5 to four times the sum of the grid anode capacities. At the start of switching and in the first half of the regenerative period, the rise rate is greater than the fall rate. As a result, in this part the equivalent increase in  $C''$  is less than twice while the equivalent increase in  $C'$  is greater than twice the sum of the grid anode capacities. In the second half of the regenerative period, the rise and fall rates get almost equalised, so that the equivalent increase in both  $C'$  and  $C''$  is twice the sum of the grid anode capacities. The action is complicated, but for a rough estimation, the equivalent shunt capacity may be considered to be increased by twice the sum of the grid anode capacities—throughout the regenerative period. In the intermediate period, the equivalent increase of  $C''$  is much greater and that of  $C'$  less than the commonly taken value of twice the sum of the grid anode capacities. This arises as a result of the increased values of the fall rate, compared to the rise rate, in this period. An increased fall rate increases  $C''$  which in turn diminishes the rise rate. The ratio of the rise and fall rates, therefore, has a tendency to get accentuated. An extreme example of such accentuation was obtained in case 30 where the current through the large grid anode capacities of the 25A6G experimental tubes, succeeded in reducing the rise rate, so as to keep it smaller than the fall rate over the entire region. No external capacities were connected to the tubes in this case, and the large anode resistances (50 K) ensured quick establishment of a more rapid fall rate compared to the slow rise rate.



to have this large anode current at a low anode voltage, as this reduces the plate dissipation and allows the use of a somewhat larger resistor value for  $\rho_2$ . The use of pentodes as the conducting tube is desirable on this consideration also.

The final rate of the fall voltage will almost always be greater than the rise rate. An equal, if not a greater rate, compared to the rise, is secured at the end of the regenerative period. The fall rate, as has been mentioned before, increases in the intermediate period. If a fast rise rate is secured, an equally fast fall rate is almost always obtained.

Equations (1), (2) and (3) above give approximate expressions of triggering delay and final rates of the change over. These two criteria are distinctly separate and they specify completely what is loosely spoken of as "fastness". The triggering delay approximately depends upon  $G/C$  which has the dimension of  $1/t$ . The final rates depend upon  $I_0/C$  which has the dimension of  $V/t$ . A reduction of the shunt capacities  $C$  improves "fastness" on both scores by reducing the triggering time and increasing the final rates. Increase of the transconductance figure  $G$ , do not increase the final rates materially, although it reduces the triggering delay in proportion. The final rates are increased by reducing  $\rho_2$  so that a larger value of  $I_0$  may be obtained. The triggering delay is, however, increased by this procedure. If larger final rates are the chief requirement, it matters little whether triodes or pentodes are used (cf. Part I, summary of experimental results) and what their transconductance figures are. A low value of  $\rho_2$  must be used and the tube  $T_2$  is to be selected so that a large  $I_0$  is obtainable.

If the circuit application would unavoidably place a large capacity on the multivibrator electrode, it is highly desirable to connect the external circuit on the anode of the non-conducting tube—the tube that is switched on in the important one of the two switchings that requires the generation of the faster wave-front. While this increases the triggering delay somewhat, the rapidity of the change over is not hampered. A negative pulse is fed on to the external circuit in such connection. The opposite connection, which would feed a positive pulse, to the external circuit would drastically reduce the final rates of change over and increase the triggering delay.

Plate-coupled multivibrators are not suitable for feeding positive pulses (with a sharp leading edge) to external circuits, that would invariably put a large capacity, when connected direct on the multivibrator electrodes. Positive pulses are conveniently obtained from the output electrode of a cathode coupled multivibrator, triggered by positive pulses. Capacity loading of the output electrode of a cathode coupled multivibrator, does not increase the triggering delay—although the final rate of rise of voltage is decreased in proportion to the increase of the capacity.

The triggering delay in a plate-coupled multivibrator is smaller than that of a cathode coupled multivibrator, because the exponential index characteristic of the switch over is greater in plate coupled multivibrator.

The final rate of rise voltage in both will be the same, if the conducting tubes pass equal currents and have the same external capacity. While the final rate of fall of voltage in a plate-coupled multivibrator is always greater than the rate of rise, that in a cathode coupled multivibrator (triggered by positive pulses) is always smaller. This is so, because while the switch on current in a plate-coupled type is always greater than the cut off current, that in a cathode coupled variety is always smaller. Thus the final rate of fall of voltage in a plate-coupled multivibrator is always greater than the cathode-coupled one using the same tubes.

Blocking oscillators attain very great final rates because the large positive drive on the grid force much larger switch on currents in a blocking oscillator. Because of the transformer, the blocking oscillators deliver into the output, positive and negative pulses with equal ease. The large final currents also enable them to handle large capacity loads satisfactorily. The relatively large self-capacity of the transformer windings, however, reduces the exponential index, characteristic of the switch over, to values smaller than that of multivibrators, so that the triggering delay is somewhat greater.

#### ACKNOWLEDGMENT

The author is indebted to Professor M. N. Saha, F.R.S., for his kind interest and encouragement.

INSTITUTE OF NUCLEAR PHYSICS,  
CALCUTTA UNIVERSITY.

#### REFERENCES

- Ahmed, Rais, 1950, *Ind. J. Phys.*, **24**, 281.  
Banerjee, B. M., 1942, *Ind. J. Phys.*, **16**, 87.  
Banerjee, B. M., 1950, *Ind. J. Phys.*, **24**, 361.  
Williams, Aldrich and Woodford, 1950, *Proc. I. R. E.*, **38**, 65.

# THE SCHOTTKY ANALOGUE IN THE PRODUCTION OF THE POSITIVE JOSHI EFFECT IN HYDROGEN

By H. J. ARNIKAR

(Received for publication, March 27, 1951)

**ABSTRACT.** A lowering of the surface work function of a thermionic emitter in proportion to the square root of the intensity of the applied field, as suggested by Schottky, leads to a linear relation between  $\log I$  and  $\sqrt{X}$  or  $\sqrt{V}$ , where  $I$  is the thermionic current under the field  $X$  due to the potential  $V$ . This Schottky relation being known to be valid for both thermionic and photoelectric emission, the present work was carried out to understand its applicability in the production of the positive Joshi effect. Results for the positive Joshi effect ( $+\Delta i$ ) in hydrogen for 5 different gas pressures show that  $\log (+\Delta i)$  varies linearly as  $\sqrt{V}$ , thus substantiating Joshi's theory of the photoelectric origin of  $\Delta i$ . Results also suggest the co-occurrence of positive and negative Joshi effects ( $+\Delta i$  and  $-\Delta i$ ) above a limiting potential  $V_l$ .

## INTRODUCTION

The Schottky effect refers to a continuous increase of the thermionic current  $I$  with the strength of the applied field  $X$  without reaching saturation. This was attributed by Schottky (1923) to a lowering of the surface work function in proportion to  $\sqrt{X}$ . On this consideration, the Richardson equation for  $I$  becomes,

$$I = A e^{-(\phi - c\sqrt{X})e/kT} \quad \dots (1)$$

where  $c$  is the constant of proportionality and  $c\sqrt{X}$  is the lowering in the work function  $\phi$ . Representing by  $I_0$  the current in the absence of external field, the above equation may be written as,

$$I = I_0 e^{cc\sqrt{X}/kT} \quad \dots (2)$$

whence it follows that  $\log I$  will be linearly related to  $\sqrt{X}$  or to  $\sqrt{V}$ , if  $V$  be the potential causing the field. The validity of this was verified experimentally by Pforte (1928) for thermionic emission for field strengths "as high as 1000 KV/cm." Later, Lawrence and Linford (1930) showed that the Schottky relation (Eqn. 2) holds for photoelectric emission as well under field strengths "up to 63 KV/cm."

In his theory of the above effect, Joshi (1946, 1947a, and 1947b), postulated: (a) the formation of an adsorption-like electrode layer consisting of ionised and excited particles and characterized by a low work function, as a primary reaction; (b) light releases electrons from (a); and (c) these lead to a reduction of the discharge current to give the negative Joshi effect as

a space-charge effect due to negative ion formation by the capture of the photoelectrons by the gas particles owing to their enhanced electron affinity under excitation. Within limits, the space charge effect is favoured by increased  $X$ . The positive Joshi effect should therefore occur at low voltages associated with the photoelectric emission as in (b). It was of interest, therefore, to investigate its production from the standpoint of the Schottky relation (2).

#### EXPERIMENTAL ARRANGEMENT

Hydrogen prepared by the electrolysis of N/15 barium hydroxide solution was freed from traces of oxygen and stored in a Töpler evacuated reservoir after drying it over phosphorus pentoxide. The gas was admitted into the annular space of a large size Siemens' ozonizer with a total electrode surface of about 1300 sq. cm., and its pressure was read by a mercury manometer. All the joints in the apparatus were of fused glass. The gas was subjected to a 50 c/s A.C. ozonizer discharge, the details of the electric circuit and current measurement being same as in earlier works on the Joshi effect, (Prasad, 1946, and Rao and Sarma, 1949). For each applied potential  $V$ , the values of the discharge current  $i_{\text{Dark}}$  and  $i_{\text{Light}}$ , were measured in the dark and under irradiation respectively, by light from a 200-watt incandescent bulb run at a constant potential. A centimetre thick column of dilute sulphuric acid solution surrounding the ozonizer served both as the L.T. electrode and as a filter to cut off the heat radiation. The results for 5 different gas pressures in the range 7—30 mm Hg and for potentials varying in the range 0.23 to 0.60 KV (r.m.s.), are entered in Table I, and the variation of  $\log (+\Delta i)$  with  $\sqrt{V}$  is plotted in figure 1, following Schottky.

#### DISCUSSION

The dark current values ( $i_0$ ) in Table I indicate the potential range for the occurrence of the positive Joshi effect is the narrow region near the beginning of the intermittent corona, the current just beginning to rise but not rapidly as at the threshold  $V_m$ . This region is highly photo-sensitive even in the visible range, as revealed by the large (several hundred per cent) positive Joshi effect. In other words, the current under irradiation ( $i_L$ ) rises precipitously over this potential range. The lowering of  $V_m$  under light, thus implied, is an expected consequence of postulates (a) and (b) of Joshi's theory of the origin of  $\Delta i$ , described earlier.

The system can thus be considered as a phototube with amplification both in the gas phase, mainly due to the Townsend ( $\alpha$ ) factor, and at the electrode surface due to the lowering of the work function as a Schottky consequence. Under conditions of the positive Joshi effect ( $+\Delta i$ ), viz., potentials near  $V_m$ , the gas amplification factor is assumed to be less important on account of low  $V$ - $i_0$  slope, and the following expression for  $+\Delta i$  is sug-

gested analogous to the Schottky relation (2) in thermionics and extended to photoelectric phenomena by Lawrence and Linford (1930) :

$$(+\Delta i) = (+\Delta i_0) B e \sqrt{V} / kT \quad (3)$$

where  $B$  is a constant, and  $+\Delta i_0$  is the hypothetical positive Joshi effect due to the primary photoelectric current with zero field, *i.e.*, in the absence of Schottky lowering of the surface work function.

The straight lines obtaining for the plots of  $\log (+\Delta i)$  versus  $\sqrt{V}$  (figure 1), for 5 different gas pressures are in accord with the above deduction. The curves in figure 1, it may be noted, are not only linear, but sensibly parallel to one another, indicating a constant slope independent of gas pressure, as expected on the Schottky equation (2). Further, a limiting potential ( $V_l$ ) can be discerned in each case where linearity abruptly ceases. It is suggested

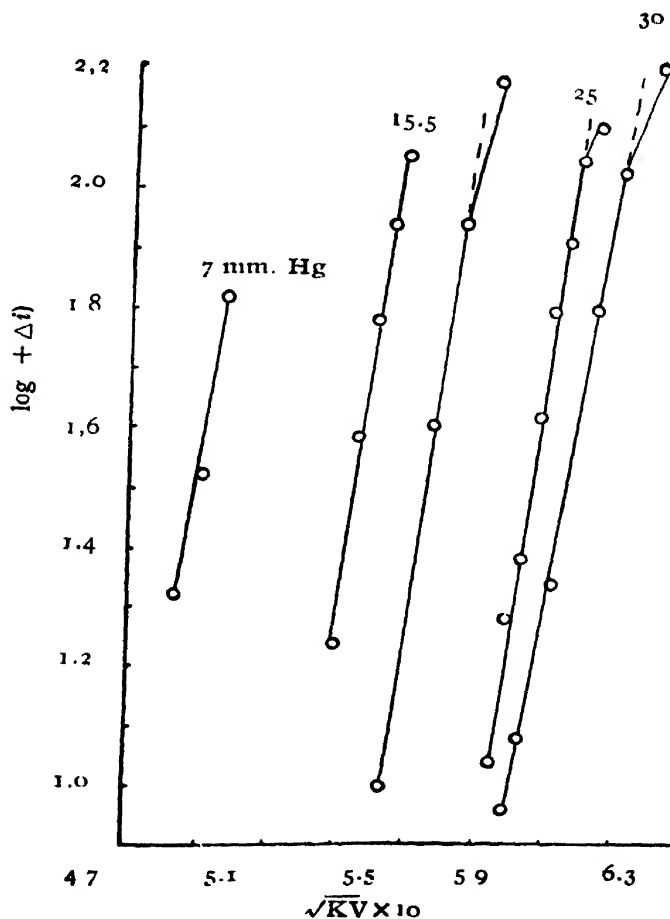


FIG. 1

Potential variation of the positive Joshi effect in hydrogen : The Schottky analogue that  $V_l$  marks the incipience of the co-occurrence of the positive and negative Joshi effects, with the positive predominating. Evidence for such a co-occurrence has been independently established in these laboratories by the oscillographic study of the phenomenon, (Jatar, 1950). As the potential is

TABLE I

Potential variation of the Joshi effect in hydrogen

EV	$\sqrt{KV}$	$t_D$	$t_L$	$\Delta t$	$\% \Delta t$	$\log (+ \Delta t)$
(i) $pH_2 = 7$ mm Hg						
0.23	0.4796	3	24	+21	+700	1.3222
0.24	0.4899	3	36	+33	+1100	1.5185
0.245	0.4950	3	69	+66	+2200	1.8195
0.255	0.5050	5	44	+39	+780	1.5910
0.27	0.5200	30	48	+18	+60	1.2550
0.30	0.5477	82	78	-4	-4	
0.34	0.5831	132	112	-20	-15	
0.38	0.6164	140	56	-84	-60	
0.40	0.6325	110	1	-109	-99	
0.49	0.7600	60	18	-42	-70	
(ii) $pH_2 = 15.5$ mm Hg						
0.28	0.5291	12	28	+16	+130	1.2041
0.285	0.5338	13	52	+39	+300	1.5911
0.29	0.5385	13	74	+61	+470	1.7853
0.295	0.5431	14	103	+89	+640	1.9494
0.30	0.5477	14	129	+115	+820	2.0607
0.305	0.5523	224	167	-57	-25	
0.33	0.5745	727	260	-467	-64	
0.375	0.6124	862	175	-687	-80	
0.40	0.6325	625	215	-410	-66	
(iii) $pH_2 = 20$ mm Hg						
0.205	0.5431	21	31	+10	-50	1.0000
0.31	0.5568	21	62	+41	+200	1.6128
0.32	0.5657	22	110	+88	+400	1.9445
0.33	0.5745	25	178	+153	+610	2.1847
0.34	0.5831	170	230	+60	+40	
0.35	0.5916	555	335	-220	-40	
0.425	0.6519	1280	645	-635	-50	
0.525	0.7426	1400	880	-520	-37	
(iv) $pH_2 = 26$ mm Hg						
0.33	0.5745	15	26	+11	+70	1.0414
0.335	0.5788	16	34	+19	+120	1.2788
0.34	0.5831	17	41	+24	+140	1.3802
0.345	0.5873	18	60	+42	+230	1.6232
0.35	0.5916	18	81	+63	+350	1.7993
0.355	0.5958	20	102	+82	+410	1.9138
0.36	0.6000	23	136	+113	+490	2.0531
0.365	0.6041	26	156	+130	+500	2.1139
0.375	0.6124	410	235	-185	-45	
0.425	0.6519	1170	585	-585	-50	
0.575	0.7583	1620	1020	-600	-37	
(v) $pH_2 = 30$ mm Hg						
0.335	0.5788	17	26	+9	+50	0.9542
0.34	0.5831	18	30	+12	+60	1.0792
0.35	0.5916	20	42	+22	+110	1.3424
0.365	0.6041	21	84	+63	+300	1.7993
0.375	0.6124	24	131	+107	+450	2.0294
0.39	0.6245	24	186	+162	+680	2.2095
0.405	0.6364	320	260	-60	-19	
0.425	0.6519	690	440	-250	-36	
0.45	0.6708	1150	650	-500	-43	
0.505	0.7106	1560	930	-630	-40	
0.605	0.7778	1680	1280	-400	-24	

further raised beyond  $V_1$ , the negative Joshi effect, anticipated on postulate (c) of Joshi's theory, increases rapidly in magnitude finally reverses the sign of net  $\Delta i$  observable.

#### ACKNOWLEDGMENTS

The author's grateful thanks are due to Professor S. S. Joshi, for his valuable advice and kind encouragement. Thanks are also due to Mr. V. V. Agashe, for his help in the experiment.

CHEMICAL LABORATORIES,  
BANARAS HINDU UNIVERSITY.

#### REFERENCES

- Jatar, D. P., 1950, *J. Sci. Ind. Research*, **9B**, 283.  
Joshi, S. S., 1946, *Proc. Ind. Sci. Congress, Part III, Phys. Sect., Abs. No. 26*.  
Joshi, S. S., 1947a, *Proc. Ind. Sci. Congress, Part III, Phys. Sect., Abs. No. 25*.  
Joshi, S. S., 1947b, *Curr. Sci.*, **16**, 19.  
Lawrence, E. O., and Linford, L. B., 1930, *Phys. Rev.* **36**, 482.  
Pförte, W. S., 1928, *Z. f. Phys.*, **49**, 46.  
Prasad, B. N., 1946, *Ind. J. Phys.*, **20**, 187.  
Rao, D.V R. and Sarma, B. K., 1949, *J. Phys. and Colloidal Chem.*, **53**, 753.  
Schottky, W., 1923, *Z. f. Phys.*, **14**, 63.





## STUDIES ON THE SPORADIC E-LAYER\*

By R. B. BANERJI

*(Received for publication, May 1, 1951)*

**ABSTRACT.** Attempt has been made to investigate the structure and properties of the sporadic  $E_s$  region of the ionosphere from a study of the fading of the echoes from this region. Statistical analysis shows that the echo consists of two components, one superposed on the other. One of the components is due to random scattering and the other to a steady reflection. This shows that the  $E_s$  region consists of a regularly reflecting region and a region of ion-clouds. A method for estimating the average number density of electrons in the clouds has been developed. It is found that the average number density is below that required for totally reflecting the exploring waves. Expressions for the variation of reflection coefficient with the variation of exploring frequency has been developed for a thin and for a semi-infinite layer (The electron distribution at the boundary is assumed to have a linear profile). The expression shows that it is possible from the observation of reflection-characteristics to distinguish between the two cases. Hence with the help of this expression one can investigate the structure of that part of the  $E_s$  region which gives rise to the steady echo.

## 1. INTRODUCTION

The irregularly occurring region of ionisation, known as the sporadic E-layer ( $E_s$ ), presents many perplexing problems regarding its origin and structure. As is well-known, the  $E_s$ -echoes are characterised by the facts that they are obtained on frequencies much higher than the normal E-layer critical frequency (from about the same height as that of the normal E-layer) and that the 'reflections' are only partial. These phenomena are explained by Best, Farmer and Ratcliffe (1938) on the hypothesis that sporadic E region consists of ion-clouds and that the observed echoes are due to scattering, rather than reflection from these clouds. This view has been experimentally corroborated by Eckersely and Farmer (1945). Booker (1950) has recently given a theory of scattering from such clouds. (A similar theory applied to the case of propagation of microwaves through the troposphere shows that the observed variation of signal intensity with distance agrees with that calculated from the theory.) However, Appleton, Naismith and Ingram (1939) explain the  $E_s$  echoes as due to partial reflection from extremely thin layer of ionisation embedded within the E-layer. One of the ways of investigating the  $E_s$  region, *i.e.* determining how far it consists of irregularly distributed clouds and how far it has a thin-layer structure, is to make a statistical study of the fading of the  $E_s$  echoes. This is because, as pointed

\* Communicated by Prof. S. K. Mitra.

out by McNicol (1949), the probability distribution of the amplitude of the echoes, if they are only due to scattering, will be different from that if they have a steady component (due to partial reflection from a thin layer) superposed on them. Such studies have been made by the author and the results of the analysis show that even when there are echoes only from the sporadic E region, there is a strong component which can only be ascribed to regular reflection from a layer. A quasi-periodic variation of the ionospheric fading characteristics has also been noticed. This suggests the existence of a steady drift. Attempt has also been made, by extending Booker's formula, to determine the ionic density of the E<sub>s</sub> clouds from the variation of scattered intensity with frequency. It is found that the observed ionic density of the clouds bear no relation to the normal E-layer critical frequency.

## 2. EXPERIMENTAL SET-UP AND PROCEDURE

The apparatus used was the 500-watt ionospheric sounding equipment used for routine observations installed at the University College of Science, Calcutta. The intensity of the E<sub>s</sub> echo was delineated on the C.R.O. screen and its amplitude was noted visually every five seconds to the nearest half-centimetre of length. This gave a measure of the fluctuation of the reflection coefficient on an arbitrary scale. Observations were taken continuously for five minutes (giving sixty values of the amplitude) on each of a number of sounding frequencies. Care was taken to keep the aerial current constant during the observations. As the radiation pattern of the inverted-L aerial which was used for transmission would not change much within the range of frequencies employed (0.5 to 1.0 Mc/sec.), the constancy of aerial current ensured an appreciably constant value of the radiated power. Observations extending over periods of 7 to 20 minutes were also taken to detect any variation of the scattering characteristics.

## 3. THE SCATTERED AND STEADY COMPONENTS

(a) *The probability distribution curves.*—If the returned echo consists of a steady component and a scattered component then the probability distribution of the amplitude of the echo follows the curve given by Rice (1945).

$$\psi(r) = \frac{2\tau}{R^2} I_0 \left( \frac{2\tau B}{R^2} \right) e^{-(B^2 + r^2)/R^2} \quad \dots (1)$$

where  $I_0$  is the Bessel function of zero order with imaginary argument,  $B$  is the amplitude of the steady component, and  $R$  the amplitude of the scattered component, i.e., root mean square amplitude due to a large number of waves in random phase. McNicol has pointed out that if  $B\sqrt{2}/R < 1$ , the Rice distribution approximates to the Rayleigh distribution

$$\psi(r) = \frac{2\tau}{R^2} e^{-r^2/R^2} \quad \dots (2)$$

and, if  $B\sqrt{2}/R > 3$ , it approximates to the Gaussian distribution

$$\psi(r) = \frac{1}{\sqrt{\pi R^2}} e^{-(r-r_m)^2/R^2} \quad (3)$$

where

$$r_m^2 = B^2 + \frac{R^2}{2} \quad (\text{see figure 1})$$

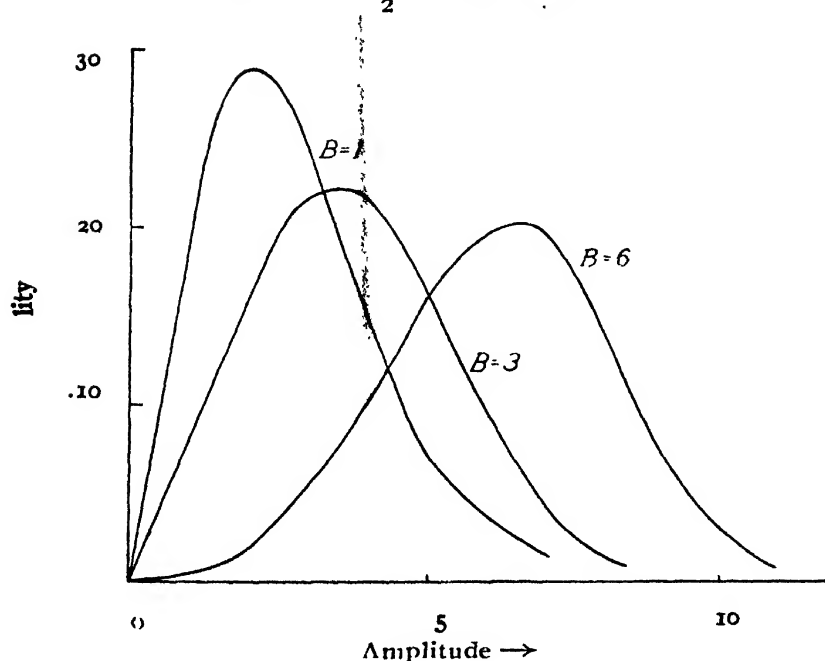


FIG. 1

Rice curves with  $R = 2\sqrt{2}$  and  $B = 1, 3$  and  $6$  as noted against each curve. Note how the form of the curve goes over to the Gaussian type from the Rayleigh type as the ratio  $B\sqrt{2}/R$  increases from below 1 to above 3.

From a study of the closeness of fit of the observed distribution curves with the one or the other of the theoretical curves (1), (2) or (3), it is possible to estimate the respective proportions of  $R$  and  $B$ , *i.e.*, of the scattered and steady components in the received  $E_s$  echoes.

McNicol (1949) has analysed a large amount of fading data, both at high and medium frequencies at both vertical and oblique incidence. He found that echoes on high frequency and on medium frequencies at oblique incidence have a large steady reflection component.

(b) *Fitting of the curves.*—To draw the probability distribution curves from the fading data the amplitudes recorded were divided into groups differing from one another by 0.5 cm. The number of amplitudes falling into each group was plotted against the corresponding amplitude to give the frequency distribution or, when normalised, the probability distribution of the echo intensity. The form of the probability distribution gave an indication of the approximate values of the parameters of the distribution curve. It was found, however, that these values did not conform to either

of the two limiting conditions (2) or (3), in which case the process of curve fitting could have been simplified by transformation to a case of straight line fitting. In this case intermediate values of  $B\sqrt{2}/R$  were most frequent. Accurate determination of  $B$  and  $R$  was, therefore, very difficult and trial-and-error method was adopted. Values of the parameters differing by finite steps were taken and the theoretical curves corresponding to these values were fitted to the experimental distribution curves. A set of typical results is shown in Table I. Figure 2 shows one such curve.

TABLE I

A typical set of observations

Date : January 1, 1951 ; Time : 12.10 hrs. to 12.30 hrs.

$f^0 E_s = 4.65$  Mc/sec ;  $f^0 E = 3.60$  Mc/sec.

Frequency of observations	Number of data	Significance of fit	$B$	$R$	$\nu_c$
4.55	61	0.60	2	$1\sqrt{2}$	4.15 Mc/sec.
4.45	61	0.85	5	$2.5\sqrt{2}$	4.33 Mc/sec.
4.30	56	0.70	2	$2\sqrt{2}$	3.50 Mc/sec.

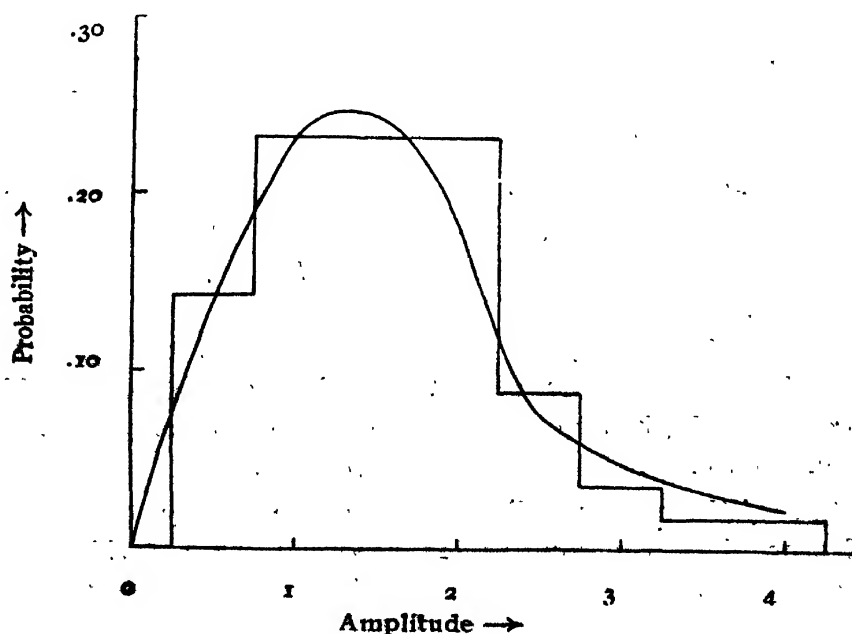


FIG. 2

Probability histogram of amplitude recorded on Jan. 1 at a frequency of 4.30 Mc/sec. The distribution curve with  $B=2$  and  $R=2\sqrt{2}$  (0.5 cm. being chosen as unit) is shown for comparison.

The significance of the closenesses of the fits could not, however, be well estimated by only a visual comparison of the theoretical and experimental histograms due to the statistical scatter of the points introduced by the smallness of the sample. Recourse was, therefore, taken to the well-known method of significance test due to Pearson. Out of 25 curves with short periods of observation (size of sample=60) 22 were found to have probabilities of fit greater than .05. This is sufficient evidence to the effect that Rice distribution is being followed. Values of  $B\sqrt{2}/R$  as found, varied generally from 1 to 3, showing that there was a distinct steady echo in addition to the scattered wavelets.

#### 4. THE SCATTERED COMPONENT—CALCULATION OF ELECTRON DENSITY IN THE CLOUDS

Booker and Gordon (1950) have given a theory of scattering of microwaves in the troposphere which Booker later applied with appropriate modifications to the  $E_s$  layer. Their formula provides a means of estimating the mean electron density of the scattering clouds. It is shown below that the variation of the mean scattering coefficient (characterised by the parameter  $R$  of the probability distribution) with the frequency of the sounding wave can be used for this calculation.

According to Booker, the scattering coefficient ( $\sigma$ ) of a bunch of clouds with a scale of fine structure  $l$ , mean dielectric constant  $\epsilon$  and mean variation thereof  $\Delta\epsilon$  is given by

$$\sigma = \frac{\left(\frac{\Delta\epsilon}{\epsilon}\right)^2 \left(\frac{2\pi l}{\lambda}\right)^2}{\lambda \left[1 + \left(\frac{4\pi l}{\lambda}\right)^2\right]^2} \quad (4)$$

for perpendicular incidence.

Replacing  $4\pi l$  by  $\lambda_0$ , the penetration wavelength, we can write,

$$\sqrt{\sigma} = \frac{1}{\sqrt{8}} \cdot \frac{\frac{\Delta\epsilon}{\epsilon} \sqrt{\lambda_0^3}}{\sqrt{\lambda} \left[1 + \left(\frac{\lambda_0}{\lambda}\right)^2\right]}$$

Now, neglecting the magnetic field of the earth, the dielectric constant of an ionic cloud is given by

$$\epsilon = 1 - \frac{4\pi N e^2}{m p^2} \quad \Delta\epsilon = \frac{-\frac{4\pi N e^2}{m p^2}}{1 - \frac{4\pi N e^2}{m p^2}} \cdot \frac{dN}{N}$$

Putting  $\frac{4\pi Ne^2}{m} = 4\pi^2 \nu_c^2$  for convenience ( $\nu_c$  having no significance except that this would be the penetration frequency of a thick layer having this ionic density)

$$\frac{\Delta\epsilon}{\epsilon} = \frac{-\frac{\nu_c^2}{\nu^2}}{1 - \frac{\nu_c^2}{\nu^2}} \frac{dN}{N}.$$

Hence

$$\sqrt{\sigma} = \frac{1}{\sqrt{8}} \cdot \frac{\nu_c^2}{\sqrt{\nu_0^3}} \cdot \frac{1}{1 + \left(\frac{\nu}{\nu_0}\right)^2} \cdot \frac{1}{1 - \frac{\nu_c^2}{\nu^2}} \cdot \frac{dN}{N} \quad \dots (5)$$

If  $\sigma$  and  $\sigma'$  be the scattering coefficients at two frequencies  $\nu$  and  $\nu'$  ( $\nu_c$  being the same under constant conditions) we have

$$\sqrt{\frac{\sigma}{\sigma'}} \cdot \frac{1 + \left(\frac{\nu}{\nu_0}\right)^2}{1 + \left(\frac{\nu'}{\nu_0}\right)^2} = \frac{1 - \frac{\nu_c^2}{\nu'^2}}{1 - \frac{\nu_c^2}{\nu^2}} \quad \dots (6)$$

Now  $\sqrt{\sigma}$  is proportional to the amplitude of the echo, as depicted on the oscillograph screen. Thus by noting the mean amplitude of the echoes at two frequencies and also the penetration frequency, we can calculate the value of  $\nu_c$ , which is a measure of the ionic density in the clouds.

In course of our observations we were able to measure  $\nu_c$  on six days. For each of three of these days, only two values of  $\sigma$  could be obtained. The values of  $\nu_c$  were found to be between 2 and 5 Mc/sec. For each of the three other days, three values of  $\sigma$  were obtained. These latter observations naturally allowed us to calculate three independent values of  $\nu_c$  and hence afforded a means of checking the theory and observations. The general values of  $\nu_c$  agreed with those given above and also among themselves within  $\pm 0.5$  Mc/sec. One such set of values is given in Table 1.

In addition to our own observations, we utilised some of the earlier data of Rawer (1949) on the variations of the reflection coefficient of the E<sub>s</sub> layer with exploring frequency. Rawer noted the frequencies at which the ratios of the amplitudes of the E<sub>s</sub> and simultaneous F-echoes were 100:1, 10:1, 1:1, 1:10 and 1:100. Some curves showing the hourly values of these frequencies were used to verify our analysis. In these calculations, the values of the frequencies for 1:100 were taken to be the penetration frequency. From the four other frequencies, six values of  $\nu_c$  were deduced; these six agreeing among themselves in each case. The frequencies were of the order of 2–4 Mc/sec.

### 5. THE STEADY COMPONENT—REFLECTIONS FROM A THIN LAYER

The presence of a steady reflected component in the echo from the  $E_s$  region (Sec. 3) indicates the presence of a stratum of ionisation of horizontal extent much greater than the length of the exploring wave. Also, the phenomenon of partial reflection associated with  $E_s$  echoes indicates that the thickness of the stratum must be comparable to the wavelength. A part of the  $E_s$  region may thus be identified with a thin layer.

It is possible in principle, by measuring the variation of reflection coefficient with change of exploring frequency and comparing results with the deductions from the theoretical formulæ for reflection coefficient under similar conditions [as given by Hartree (1929), Saha and Rai (1937) and Deb (1940)] to make an estimate of the thickness of the layer. Unfortunately, on account of experimental difficulties, reflection coefficients could not be obtained over a sufficiently large range of exploring frequencies. However, over our limited range of observations we obtained a result which indicates qualitative agreement with the variation of reflection coefficient with wave length as given by Hartree's formula. In two of our observations the parameter  $B$  of the distribution curve (which characterises the coefficient corresponding to the steady component) passed through a maximum with change of the exploring wave frequency having values higher than  $\nu_c$ . According to Hartree's formula also the reflection coefficient should pass through a number of maxima and minima as the frequency of the exploring wave is changed in the range greater than the 'penetration' frequency (by this term we mean here a frequency that would be just reflected by a thick layer of same ionic density).

It may be mentioned in this connection that Best, Farmer and Ratcliffe (1938) suggest that the  $E_s$  reflections may be due to a sharp gradient of ionisation in the lower part of the  $E$  region. It is clear from the above that observations on the variation of the parameter  $B$  over a wide range of  $\nu$  may yield sufficient data to discriminate between the two points of view (thin layer or sharp gradient).

An alternative and simpler method for determining the reflection coefficient of a sharp gradient or a thin layer, as developed by the author, is given below. The starting point of the analysis is the expression given by Rayleigh for reflection from a medium of varying refractive index. Rayleigh's expression for the reflection coefficient may be written as

$$\frac{B_1}{A_1} = - \int_0^{\mu_1} \frac{d\mu}{\mu} e^{-\frac{4\pi i}{\lambda} \int_0^{\mu} \mu dZ}.$$

It is assumed that the reflection coefficient is small at all points.

Let the reflecting medium consist of electrons distributed in a thin layer of triangular profile having semi-thickness  $Z_1$ , and maximum ionic density  $N_1$ , (corresponding to the critical frequency  $\nu_c$  of a thick layer). The number

density of the electrons at any height is then given by

$$N = \frac{N_1}{Z_1} \quad \text{for } 0 < Z < Z_1 \quad \dots (7)$$

and

$$N = \frac{N_1}{Z_1} \left( 2 - \frac{Z}{Z_1} \right) \quad \text{for } Z_1 < Z < 2Z_1 \quad \dots (8)$$

Then, since

$$\mu = \sqrt{1 - \frac{4\pi N e^2}{m \hbar^2}},$$

we can split the integral into two parts and write,

$$\begin{aligned} \frac{B_1}{A_1} = & \int_0^{Z_1} \frac{\frac{v_c^2}{v^2} \cdot \frac{1}{Z_1}}{4 \left( 1 - \frac{v_c^2}{v^2} \cdot \frac{Z}{Z_1} \right)} e^{-\frac{4\pi i}{\lambda} \int_0^Z \sqrt{1 - \frac{v_c^2}{v^2} \cdot \frac{Z}{Z_1}} dZ} dZ \\ & - \int_{Z_1}^{2Z_1} \frac{\frac{v_c^2}{v^2} \cdot \frac{1}{Z_1}}{4 \left\{ 1 - \frac{v_c^2}{v^2} \left( 2 - \frac{Z}{Z_1} \right) \right\}} e^{-\frac{4\pi i}{\lambda} \int_0^Z \sqrt{1 - \frac{v_c^2}{v^2} \left( 2 - \frac{Z}{Z_1} \right)} dZ} dZ \end{aligned}$$

In the second integral, the transformation  $2 - \frac{Z}{Z_1} = \frac{x}{Z_1}$  yields, on making the running variable uniform,

$$\frac{B_1}{A_1} = \int_0^{Z_1} \frac{\frac{v_c^2}{v^2} \cdot \frac{1}{Z_1}}{4 \left( 1 - \frac{v_c^2}{v^2} \cdot \frac{Z}{Z_1} \right)} \left[ e^{-\frac{4\pi i}{\lambda} \int_0^Z \sqrt{1 - \frac{v_c^2}{v^2} \cdot \frac{Z}{Z_1}} dZ} - e^{-\frac{4\pi i}{\lambda} \int_{Z_1}^Z \sqrt{1 - \frac{v_c^2}{v^2} \cdot \frac{Z}{Z_1}} dZ} \right] dZ,$$

which yields

$$\begin{aligned} \frac{B_1}{A_1} = & \frac{1}{4Z_1} \cdot \frac{v_c^2}{v^2} \left[ e^{-\frac{8\pi i}{\lambda} \cdot \frac{v^2}{v_c^2} Z_1} - e^{-\frac{8\pi i}{\lambda} \cdot \frac{v^2}{v_c^2} Z_1 \left( 1 - \frac{v_c^2}{v^2} \right)^{3/2}} \right] \\ & \times \int_0^{Z_1} \frac{e^{-\frac{8\pi i}{\lambda} \cdot \frac{v^2}{v_c^2} Z_1 \left( -1 - \frac{v_c^2}{v^2} \cdot \frac{Z}{Z_1} \right)^{3/2}}}{\left( 1 - \frac{v_c^2}{v^2} \cdot \frac{Z}{Z_1} \right)} dZ. \end{aligned}$$

putting  $\left( 1 - \frac{v_c^2}{v^2} \cdot \frac{Z}{Z_1} \right)^{3/2} = \eta$ , the above can be written as

$$\frac{B_1}{A_1} = -\frac{1}{8} \left[ e^{-\frac{8\pi i}{\lambda} \cdot \frac{Z_1}{v_c^2} \cdot \frac{v^2}{v^2}} - e^{-\frac{8\pi i}{\lambda} \cdot \frac{Z_1}{v_c^2} \cdot \frac{v^2}{v^2} \left( 1 - \frac{v_c^2}{v^2} \right)^{3/2}} \right] \int_1^0 \frac{e^{ix}}{x} dx \quad \dots (9)$$

$$\frac{8\pi}{\lambda} \cdot \frac{Z_1}{v_c^2} \cdot \frac{v^2}{v^2} \left( 1 - \frac{v_c^2}{v^2} \right)^{3/2}$$



This expression ceases to be valid when  $\nu$  approaches  $\nu_c$  i.e. near critical reflection, since the reflection here is very profuse and our initial assumption breaks down. Within the region of validity, the lower limit of integration is greater than 1. The modulus of the integral has no pronounced variation in this range (figure 3) and hence the maxima and minima of the reflection coefficient are determined by the first factor.

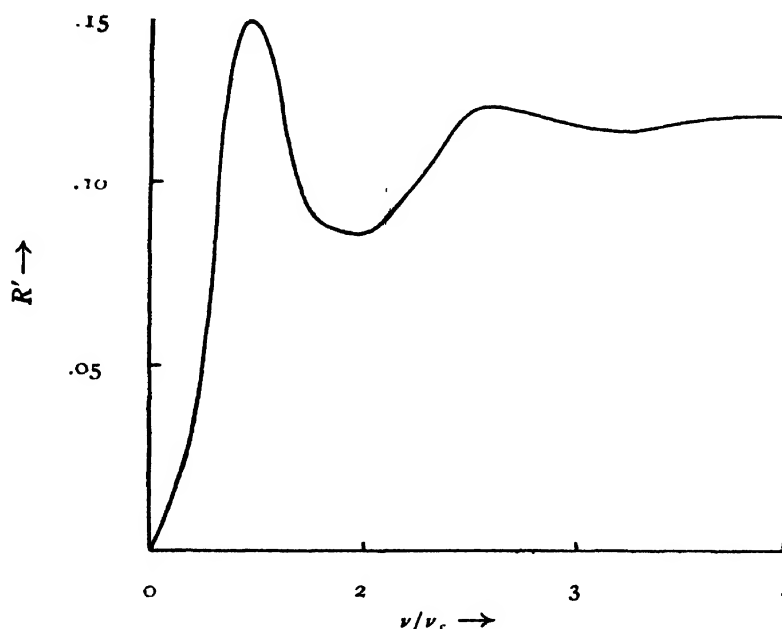


FIG. 3

Variations of the integral  $R' = \frac{1}{2} \int_1^{\infty} \frac{e^{-x}}{x} dx$  with  $\nu$  when  $\frac{\nu_1}{\nu_c} = 2.5$

$$\frac{8\pi}{3c} \cdot \frac{Z_1}{\nu_c^2} \left(1 - \frac{\nu_c^2}{\nu^2}\right)^{3/2}$$

The first factor is maximum when the arguments of the two complex quantities differ by an odd multiple of  $\pi$ , i.e. when

$$\frac{8\pi}{3c} \cdot \frac{Z_1}{\nu_c^2} \nu^3 = (2n+1)\pi + \frac{8\pi}{3c} \cdot \frac{Z_1}{\nu_c^2} \nu^3 \left(1 - \frac{\nu_c^2}{\nu^2}\right)^{3/2},$$

$$\text{i. e. } \left(1 - \frac{\nu_c^2}{\nu^2}\right)^{3/2} = 1 - \frac{(2n+1)3c}{8} \cdot \frac{\nu_c^2}{Z_1 \nu^3}$$

Or, putting  $c/Z_1 = \nu_1$ ,

$$\left(1 - \frac{\nu_c^2}{\nu^2}\right)^{3/2} = 1 - \frac{3(2n+1)}{8} \nu_c^2 \nu_1 \quad \dots \quad (10)$$

Graphical solution of this equation shows that the function  $B_1/A_1$  will go through a series of maxima and minima. The spacings between the maxima and the frequency for the first maximum are dependent on the

ratio  $\nu_1/\nu_c$ , i. e. is a function of the thickness and density of the layer. However, the frequency separation of the maxima are of the same order as  $\nu_c$ , (see figure 4).

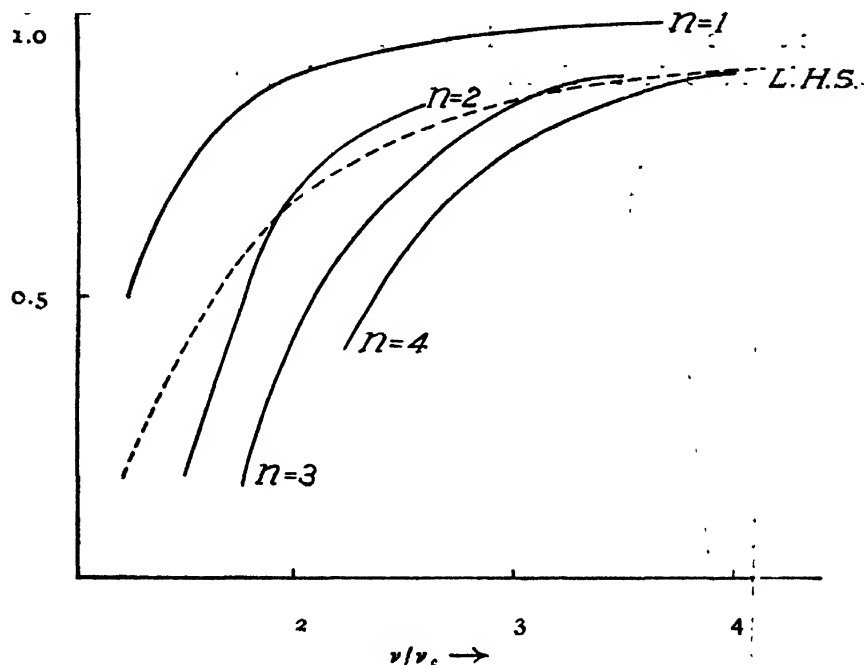


FIG. 4

Graphical solution of Eq. (10). The dotted lines represent the L. H. S. and the bold lines the R. H. S. for the various values of  $n$  noted against each. The intersections give values of  $\nu/\nu_c$  for maxima.  $\nu_1/\nu_c = 2.5$

If instead of a layer of finite thickness we have a semi-infinite layer of steep boundary (the electron distribution at the boundary being given by eqn. 7, then the condition for maximum reflection coefficient is given by

$$\frac{8\pi}{3c} \frac{\omega_1}{\nu_c^2} \nu^3 = (2n + 1)\pi;$$

i. e.,

$$\nu^3 = \frac{3(2n + 1)}{8} \nu_c^2 \quad (11)$$

It is to be noted that the spacings between the cubes of the maxima are constant. Thus a measurement of the spacings between the maxima when the exploring wave frequency is varied can provide a test for the nature of the layer, whether it is a thin layer or has a thickness large compared to the wavelength having a steep lower boundary.

## 6. A NOTE ON THE OBSERVED VARIATION OF FIT

During our observations it was noticed that the fits for smaller samples (50 to 60 data) were more significant than those for larger samples (100 to

200 data). It was suspected that the misfit was being caused by a change in the ionospheric conditions (as characterised by the distribution parameters  $B$  and  $R$ ) during the period of observation, which was perforce rather long (15 to 20 minutes) for the larger samples. Such changes would cause a variation of the closeness of the fit as the time of observation is gradually lengthened. It is evident that a functional relationship exists between the variation of fit and the variation of the distribution parameters.

To study this effect a number of long duration observations (ranging from 8 to 20 minutes) were taken. Instead of calculating the actual value of the Pearson's  $\chi^2$  function, the closeness of fit was calculated by the quantity  $\chi^2/N$ ,  $N$  being the total number of observations. This quantity is given by the equation

$$\frac{\chi^2}{N} = \sum_i \frac{(\psi_i - p_i)^2}{\psi_i}$$

where  $\psi_i$  is the theoretical probability of occurrence of the  $i$ th amplitude range and  $p_i$  the experimentally observed probability. The analysis was carried out as follows :

The total number of data was first fitted to the nearest Rice curve. The set was then considered up to the first 40 observations and the value of  $\chi^2/N$  calculated with the Rice curve deduced before. The number of data was then progressively increased and  $\chi^2/N$  recalculated till the end of the set.

The investigation of the functional relationship between variations of  $\chi^2/N$  and the characteristics is complicated by the finite size of each sample. As a first approximation we will assume that the whole deviation of the fit is due to the variation of the characteristics or, in effect, that the samples behave as infinitely large ones. A general analysis of the variation of Rayleigh fits is given below. The parallel analysis for Rice curves is made difficult by the comparatively complicated Bessel function with imaginary arguments. -

The Rayleigh distribution

$$\psi_0 = \frac{2r}{R^2} e^{-\frac{r^2}{R^2}} dr,$$

can be written as

$$\psi_0 = -\frac{d}{dr} \left[ e^{-\frac{r^2}{R^2}} \right] dr.$$

If  $1/R^2$  be a function of time, given generally by

$$\frac{1}{R^2} = \frac{1}{R_0^2} + \phi(t)$$

(ii) Case of no variation,  $\phi(t) = 0$ .

i.e.,  $G(t_0) = c \approx 1/R_d^2$

$$\frac{\chi^2}{N} : \frac{R_0^4}{4} \left( \frac{2c}{t_0} \right)^2 = \frac{1}{t_0^2} \left[ \frac{R_0}{R_d} \right]^4 \quad \dots (14)$$

Five curves were analysed. Of these, three indicated a periodic fluctuation, one a constant parameter and another a constant parameter after a small increase (figures 5 and 6).

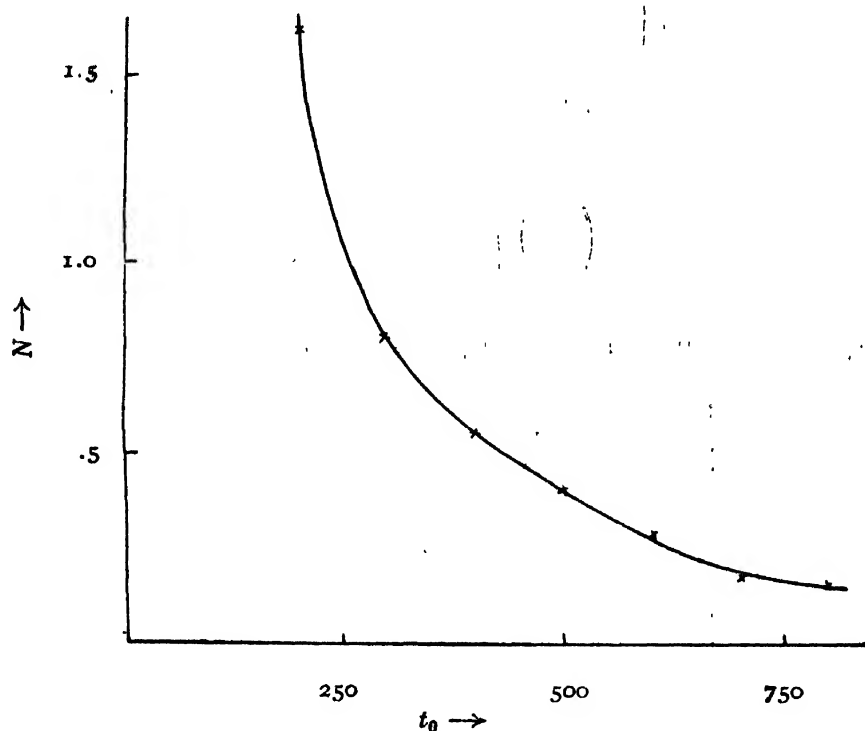


FIG. 6

Variations of closeness of fit with increasing duration of observation. The sample was observed on Sep. 22 at a frequency of 2.60 Mc/sec. The hyperbolic variation is indicative of steady value of the parameters.

## 7. CONCLUDING REMARKS

The experimental equipment does not allow a continuous observation of variation. Hence a large number of data is necessary to approximate the true probability distribution curve. This latter, in its turn, necessitates a long period of observation. Thus the assumption that the ionospheric conditions are constant during the period of observation ceases to be valid. This results in considerable dispersion of the experimental histogram and renders an accurate determination of the Rice parameters very difficult. For better

results a continuous photographic method for quick accumulation of a large amount of data in a short time is, therefore, essential. This would allow a more thorough statistical analysis of the data.

Significant divergences of the fit may be due to causes other than statistical. In the analysis it has been assumed that waves from a very large number of independent scatterers are reaching the receiver. This would necessitate a large 'angle of spread' of the scattered wave. However, the reason for fluctuation of echo intensity may not be only an effect of interference. It is possible that there is specular reflection from clouds of rather large size which pass above the point of observation. For such cases the fluctuations would obviously not follow the Rice law. The effect due to passage of large size clouds would increase as the critical frequency is approached, *i.e.*, when back-scatter decreases markedly. Thus  $\nu_c/\nu$ , the ratio of critical frequency to the frequency of observation ought to be positively correlated to  $P$  the probability of fit.

The variation of the radiated power with changing frequency and also absorption in the lower strata introduce other sources of error in the evaluation of the reflection co-efficient. Rawer (1949) has suggested that a comparison of the E<sub>s</sub> and F echo strengths would give a more correct measure of the reflection coefficient of the E<sub>s</sub> layer. Simultaneous recordings of the E<sub>s</sub> and F echoes are, therefore, necessary. A method for carrying out such observations by a pair of gated amplifiers and a narrower pulse to resolve the different echoes is being developed at present,

#### 8. ACKNOWLEDGMENTS

The author wishes to express his gratitude to Professor S. K. Mitra, D.Sc. for his constant encouragement and interest. Thanks are also due to the Ministry of Education, Government of India for having provided him with a scholarship under the Research Training Scheme, as recommended by the Scientific Manpower Committee, which has enabled him to carry out the work.

INSTITUTE OF RADIO PHYSICS AND ELECTRONIC  
UNIVERSITY COLLEGE OF SCIENCES,  
CALCUTTA.

#### REFERENCES

- Appleton, E. V., Naismith, R. and Ingram, L. J., 1939, *Proc. Phys. Soc.*, **51**, 81  
Best, J. E., Farmer, F. T. and Ratcliff, J. A., 1938, *Proc. Roy. Soc.*, **184**, 96.

- Booker, H. G., 1950, Conference on Ionospheric Research, Pennsylvania State College
- Booker, H. G., and Gordon, W. E., 1950, *Proc. I.R.E.*, **38**, 404.
- Deb, A. C., 1940, *Ind. J. Phys.*, **14**, 451.
- Eckersley, T. L. and Farmer, F.T., 1945, *Proc. Roy. Soc.*, **184**, 196.
- Hartree, D. R., 1929, *Proc. Camb. Phil. Soc.*, **25**, 47.
- McNicol, R. W. E., 1949, *Proc. I.E.E.*, **96**, 517.
- Rawer, K., 1949, *Nature*, **163**, 528.
- Rice, S. O., 1945, *Bell System Tech. Jour.*, **24**, 46
- Saha, M N and Rai, R. N., 1937, *Proc. Nat Inst. Sci.*, **3**, 359.

## SODIUM IN THE UPPER ATMOSPHERE\*

By ARUN KUMAR SAHA

*(Received for publication, July 3, 1951)*

**ABSTRACT.** The paper first surveys the available data for the sodium phenomena in the upper atmosphere, namely, intensity variations of the D-lines in the night air-glow and in the twilight flash, the height of the emitting layers, the distribution of sodium in the atmosphere and its probable source. The various excitation processes, both regarding the twilight flash and the night air-glow emission are closely examined. It is shown that the most probable mode of production of the twilight flash is resonance excitation of neutral sodium atoms in 35-65 km. region by solar radiation  $\lambda 5893$ , there being no significant effect of ozone screening. The possible excitation processes in the night air-glow are examined critically on the assumption that the height of the emitting layer is 250 km. (as obtained by Barbier and Roach) and that above 100 km. sodium exists wholly in the ionized state (as shown by Bates). Two possible excitation processes are examined: (1) Radiative recombination of  $\text{Na}^+$  ions and (2) mutual neutralization of  $\text{Na}^+$  and  $\text{O}^-$  ions. Of these two processes the latter seems more probable as the former requires impossibly high concentration of  $\text{Na}^+$  ions. But the latter process cannot maintain the observed intensity of the radiation throughout the dark hours of the night. Hence it is concluded that extra terrestrial particles must be bombarding the upper atmospheric regions, ionizing and/or exciting the neutralized  $\text{Na}^+$  ions. Alternatively, it may be assumed that sodium atoms are entering the atmosphere from interplanetary space.

## INTRODUCTION

The presence of the element sodium in the upper atmospheric regions has been proved beyond doubt by the identification of the yellow D-lines in the night air glow spectrum. A large number of workers have made observations on the intensity variation of these lines both in the night air-glow and in the twilight flash, with a view to determine the height of the emitting layer, the distribution of the sodium content with height and also the total number of sodium atoms. Unfortunately, the results obtained are not concordant. For example, while according to some observers the sodium is concentrated in a comparatively thin layer between 70 and 110 km., others estimate the height of emission of the D-lines to be 250 km., i.e., in the region of the F-layer of the ionosphere. Further, the modes of excitation of the sodium D-lines, both in the night air-glow and also during the twilight flash, are still insufficiently understood. The purpose of the present paper is, firstly, to give a connected account of our present state of knowledge of upper atmospheric sodium, and secondly, to examine and extend the theories of the excitation of the D-lines, and to deduce therefrom the probable distribution and source of sodium in the upper atmosphere.

\* Communicated by Prof. S. K. Mitra

PRESENT STATE OF KNOWLEDGE OF UPPER  
ATMOSPHERIC SODIUM

Sodium gives one of the most prominent and easily observed lines in the spectrum of the night air-glow. It was first identified by Bernard (1938) by accurate measurement of wavelength with Fabry-Perot interferometer.

*Intensity and its variations.*—The absolute intensity of the radiation has been measured by several authors (Cabannes, Dufay and Gauzit, 1938; Barbier and Roach, 1950a; Bates and Nicolet, 1950) and has been found to correspond to  $2 \times 10^8$  to  $8 \times 10^7$  transitions per sec. per  $\text{cm}^2$  column of atmosphere.

The intensity of the D-emission remains fairly constant throughout the night (Elvey and Farnsworth, 1942). During the morning and evening twilights, however, the sodium light is enhanced in the illuminated upper atmosphere to 50 to 100 times the night air-glow intensity. This enhancement is generally referred to as the *twilight flash* of sodium.

The intensity is, however, subject to considerable fluctuations from night to night. There may be nights when under the most favourable conditions the lines are absent from the twilight spectrogram (Vegard and Tönsberg, 1941). Further, the emission is not uniform from all parts of the sky.

There is also a seasonal variation in the intensity with a maximum in winter and a minimum in summer.

*Height of the emitting layer*—Many attempts have been made to determine the height of the layer emitting the D-lines in the night air-glow by the well known van Rhijn technique. The results obtained, however, are widely divergent amongst themselves as will be seen from Table I.

TABLE I

Observer	Height obtained	Remarks
Cabannes, Dufay and Gauzit (1938)	130 km.	Based on observations by Garrigue at Pic-du-Midi, France in 1936.
Dufay and Tcheng Mao-Lin (1948)	80 km.	Used only two zenith distances.
Barbier and Roach 1950a, Roach and Petit, 1951).	250 km.	Used interference type filters to transmit narrow bands, in conjunction with a photo-electric photometer

*Observations on the twilight flash.*—Bernard (1938) was the first to make systematic observations on the twilight flash. He found that the flash disappeared when the edge of the shadow cast by the earth passed at a height of about 60 km.



Vegard and Tönsberg (1940; 1941) found that the upper limit to the height of the emitting layer as deduced from observations of the twilight flash made near the horizon always gave a much larger value than those deduced from similar observations made near the zenith. This discrepancy they explained by assuming that the excitation of the D-lines was caused by ultraviolet light in a wave-length range that is absorbed by ozone. When calculating the height of the upper limit they, therefore, took into account the effective increase in the radius of the earth shadow by the ozone screening. From a large number of observations made at Oslo and Tromsø Vegard and Tönsberg determined the value of the screening height and also the upper limit of the height at which the flash disappeared. The mean value of the former (screening height) was found to be 49 km. and of the latter 110 km.

Cario and Stille (1950) made similar experiments over northern Germany in 1941. They measured the upper limit of the height of emission to be  $118 \pm 2.5$  km and the screening to be  $54 \pm 3$  km.

Barbier (1948) from twilight observations in Haute-Provence (France) estimated the base of the sodium layer at 70 km.

In addition to the ordinary twilight flash, as described above, a late twilight effect consisting of a slow steady decrease of the intensity for an hour or so after the astronomical twilight has also been observed by Barbier and Roach (1950b). Identical observations have been recorded for both evening and morning twilights. The measurements indicated the region of emission in the range 200 to 600 km. (However, in a private communication Roach states that the late twilight flash was not observed again and that he is inclined to believe that it is a sporadic phenomenon).

*Distribution of sodium in the upper atmosphere.*—Attempts have been made to determine the location and distribution of sodium in the upper atmosphere from observations on the night air-glow emission as also from those on the twilight flash. The results obtained by the different workers are as follows:

An estimate of the total number of sodium atoms in the upper atmosphere has been made by Bates and Massey (1946) from the observed intensity of the twilight emission and the flux of solar quanta (taking account of Fraunhofer absorption), and using the known probability of transitions yielding the D-lines. The estimated number of sodium atoms above 70 km. was found to be of the order  $10^9$  per  $\text{cm}^2$  column of atmosphere.

Barbier (1948) has also given a similar estimate from twilight observations, namely, that in the 70 to 100 km region the number of sodium atoms per  $\text{cm}^2$  column is  $5 \times 10^8$ . It will be seen that according to both the estimates the total sodium content is only a minute fraction ( $10^{-12}$ ) of

## A. K. Saha

the total atmospheric constituents. If it is assumed that sodium in the above proportion is distributed over the whole atmosphere then the number per  $\text{cm}^2$  column would be  $2 \times 10^{13}$ .

In view of its minute proportion, the interesting suggestion has been made by Bates (1950) that it can be increased by a significant amount by ejecting sodium vapour in, say, 70 km. region from a rocket. This would enable controlled experimental observation on sodium emissions to be carried out.

An estimate of the thickness of the sodium layer was made by Vegard and Tönsberg (1940; 1941) by observing the time at which the intensity of the twilight flash began to drop rapidly (as the sun sank more and more below the horizon) and the time at which it vanished *i.e.*, fell to the night-time value. The former gave the time at which the shadow formed by the ozone screening sphere passed the lower border and the latter the time at which it passed the upper limit of the sodium layer. The thickness of the layer was obtained from a knowledge of this time interval and the height of the ozone screening sphere (*vide supra*). The thickness was found to vary between 8.4 and 27 km (with a mean value of 16.2 km). Hence it was concluded that the sodium producing the twilight flash was situated in a comparatively thin layer between the heights 85 km. and 110 km.

Elvey and Farnsworth (1942) put a different interpretation to the phenomenon of sudden disappearance of the twilight flash. This, according to the authors, was not due to the edge of the shadow having passed above the sodium layer, but was merely an effect of the sodium content falling exponentially to a low value. According to the observations of these authors, the decrease of intensity with height followed a logarithmic law and ran parallel to the decrease of number density of atmospheric molecules with height.

Barbier and Roach (1950a; also Roach and Pettit, 1951) have estimated the height of the emitting layer (see Table 1) to be around 250 km. *i.e.*, in the F-region of the ionosphere. In view of the many precautions taken by these authors the results obtained appear to be more reliable than those obtained by previous workers. This observation together with those on the twilight flash leads one to conclude that sodium is not confined within a narrow layer (as had been supposed by some authors), but is distributed in two layers: one in the 80 or 85 to 110 km. region, and another in the region of the F-layer of the ionosphere. Or, it may be that sodium in the atmosphere extends from a level of about 80 km. upto the F-region. (See however, discussion in the next section. The base of the sodium layer is taken at 35 km. and not at 80 km.).

*Source of the upper atmospheric sodium.*—Nothing definite is known about the source of the upper atmospheric sodium. The sodium may be of terrestrial origin, but there are strong reasons to believe that at least a part of the sodium comes into the atmosphere from outer space.

In favour of the terrestrial origin it has been suggested that ascending air currents may carry sodium salt from ocean sprays. Volcanic dust containing sodium compounds have also been known to shoot up to great heights—30 km. (Bernard, 1939).

Cabannes, Dufay and Gauzit (1938) and others attribute the origin of the atmospheric sodium to meteorites. The D-lines have been detected in meteoric spectra. But, it has been argued that the lines may be due to excitation of *atmospheric* sodium atoms (Roach, 1949).

Bates (1947) favours a cosmic origin from consideration of the density gradient of atmospheric sodium obtained from twilight investigations. Vegard (1940) suggests that sodium comes into the atmosphere from the sun along with the solar corpuscular streams that produce auroral and magnetic disturbance phenomena.

It has also been suggested that the earth is sweeping through interplanetary sodium clouds and the sodium is swept into the earth's atmosphere as the latter moves through space (Barbier and Roach, 1950b). This hypothesis promises an explanation of the seasonal variation of intensity of nocturnal D-lines.

It is difficult to judge the relative merits of the different hypotheses because we do not know how and at what rate the sodium is disappearing from the regions from which it emits light.

#### EXCITATION PROCESSES

(a) *Twilight flash*.—There have been two views regarding excitation of the sodium atom in the twilight flash.

According to Vegard and Tönsberg (1940, 1941) the exciting radiation is in the ultraviolet lying between  $1900\text{\AA}$  to  $2900\text{\AA}$ . They arrive at this conclusion from the fact that according to their observations the exciting radiation has to pass above the ozone layer (*vide supra*). Also the exciting radiation cannot be less than  $1900\text{\AA}$  because such radiation will be absorbed by the overlying mass of air. The wavelength, also, cannot be longer than  $2900\text{\AA}$  as otherwise ozone screening (Hartley bands) will not have any effect.

According to Barbier and Roach (1950b), however, the twilight flash is simply a case of resonance excitation, the active wavelength being  $5893\text{\AA}$ . They take into account the effect of ozone screening, but this effect is assumed to be due to the feeble absorption in the region of Chappuis bands and not to the strong Hartley bands.

A close examination of the two hypotheses shows that neither is wholly correct. The twilight flash is due to resonance excitation as proposed by Barbier and Roach, but the exciting radiation ( $5893\text{\AA}$ ) need not pass above the ozone layer. This will be clear from the consideration of the maximum possible absorption which can be effected by ozone in the region of Chappuis bands. Barbier, Chalonge and Vigroux (1942) made observations during a

lunar eclipse when they followed spectroscopically the sunlight passing obliquely through the earth's atmosphere on the darkening moon. Using absorption in the region of Chappuis bands they determined the ozone masses for the different ray paths which passed over the earth's surface within 4 to 17 km. They found that the maximum value of the ozone mass traversed was 11 cm. and that this occurred when the distance of the ray from the earth's surface was 12 km. Since the maximum absorption coefficient in the Chappuis bands is 0.05 at  $6100\text{\AA}$ , the maximum reduction in intensity of solar radiation may be 40%. If the solar ray passes by the top of the ozone layer (40 to 50 km.) the absorption will be insignificant. It is, therefore, difficult to see how the resonance excitation process of sodium atoms by  $\lambda 5893$  can be significantly affected by the ozone absorption in the region of Chappuis bands.

One has, however, to explain the observations of Vegard and Tönsberg namely, that there was a systematic difference between the height measurements of the upper limit of the sodium flash when observed along the zenith and when observed along a direction close to the horizon (and which was interpreted as due to the exciting radiation having to pass above the ozone layer). It should, however, be remembered that the results of height determinations, as carried out by Vegard and Tönsberg, were not sufficiently accurate. The spectrographs in the experiments were exposed for 3–6 minutes at the zenith and 6–10 minutes and sometimes 20–30 minutes at the low angles. If the time of disappearance occurs within the exposure interval it cannot be noted with accuracy; and an inaccuracy of 5 minutes would lead to an error in the height measurement of about 30 km. The conclusion of Vegard and Tönsberg, therefore, that the exciting radiation has to pass above the ozone screening height, is not fully warranted. It may, therefore, be concluded that the twilight flash is caused by resonance absorption of radiation  $\lambda 5893$  and that any increase in the screening radius of the earth is only due to terrestrial absorption due to haze etc. extending up 5 km. at a liberal estimate.

A result of the above conclusion is that the height of the sodium layer as measured from observations of twilight flash by Vegard and Tönsberg, as also by Barbier will have to be reduced by about 45 km. This means that the bottom of the sodium layer, as indicated by the lower limit of the flash (corresponding to the time at which the intensity of the flash begins to drop rapidly), is at 35 to 40 km. and the top, as indicated by the upper limit, is at about 65 km. (of the same order as obtained by Bernard, who did not consider ozone screening). This result is more in conformity with the findings of Bates (1947), according to whom, due to the ionizing action of solar radiation, sodium above 80 or 90 Km. will almost wholly be in the ionized state. And, in such case, in the absence of neutral sodium atoms, no twilight enhancement is possible, though according to observations of Vegard and Tönsberg and Barbier twilight flash is observed (assuming ozone screening) even up to 110 km.

(b) *Nocturnal emission*.—To explain the nocturnal emission of the D-lines the presence of neutral sodium atoms is generally assumed. According to Chapman (1939) the energy of excitation of the sodium atom is derived from the solar energy which has been spent in dissociating the  $O_2$  molecules in the upper atmosphere. Thus we may imagine the following reactions :



In reaction (1) the presence of the compound NaO is assumed. This may be produced by the following processes :



In reaction (3) M is the third body which carries away the excess of energy and momentum.

It may also be mentioned that Penndorf has sought to explain both the night emission and the twilight flash by a process in which  $Na_2O$  is produced through the presence of  $N_2O$  in the upper atmosphere (Penndorf, 1950). The region of emission is assumed to be 90 to 105 km.

Bates and Nicolet (1950) have made a close examination of the various processes that have so far been suggested and have come to the conclusion that for any of these processes to be effective, the effective level of emission cannot be much above 70 km.

Now, as already mentioned, the mean height of the emitting layer, according to measurements of Barbier and Roach is 250 km. In view of the considerable care which these authors have taken in their measurements, the result cannot be seriously in error. It, therefore, appears that none of the reactions proposed above can be responsible for the D-line emission. Further, it has been shown by Bates (1947) that at heights above 100 km. sodium is present only in the ionized state. One is thus forced to the conclusion that it is the  $Na^+$  ions (and not neutral sodium atoms) that take part in the emission mechanism.

This conclusion raises the following problems regarding the D-line emission.

(i) What is the most likely process of neutralization of the  $Na^+$  ions by which the Na atom produced is excited to the  $2p$  level ?

(ii) What is the concentration of the  $Na^+$  ions necessary in order that the radiation may have the observed intensity, namely, that corresponding to  $8 \times 10^7$  transitions per  $cm^2$  column ? How far is this concentration compatible with the observed ionization density in the F-region ?

(iii) Is the initial concentration of  $\text{Na}^+$  sufficiently high to maintain the intensity of radiation throughout the dark hours of night with very little decrease as observed ?

Let us discuss these problems as far as possible with the available data and with the contemporary knowledge of the physical state of the upper atmosphere.

*Emission processes (with  $\text{Na}^+$  ions).*—In view of the height of emission being 250 km., the region of emission may be identified with the F-layer of the ionosphere. This region contains  $\text{N}_2$  molecules and O atoms, positive ions  $\text{N}_2^+$  and  $\text{O}^+$ , negative ion  $\text{O}^-$  and electrons. It also contains possibly N atoms.

We first consider the process of radiative electronic recombination,



The resulting sodium atom may be in the ground state or in any one of the excited states from which transitions may occur to the ground state (directly or in successive steps). Apparently, in this process lines of sodium other than  $\lambda 5893$  would also be present. The presence of these lines has not yet been established, although detection of  $\lambda 3303$  has been reported by some workers.

We next consider the mutual neutralization of  $\text{O}^-$  and  $\text{Na}^+$ ,



The process may be expected to have a high probability when the resonance condition is satisfied, i.e., when the energy released on neutralization is taken up wholly as energy of excitation of the reaction products. Since the ionization potential of sodium is 5.1 eV and the electron affinity of oxygen is 3.0 eV (Vier and Mayer, 1944), the energy released on neutralization is  $5.1 - 3.0 = 2.1$  eV. Since this is also the energy of excitation of the sodium atom to the  $2p$ -state there is energy balance. Hence the mutual neutralization of  $\text{Na}^+$  and  $\text{O}^-$  ions may be regarded as a very likely process for the emission of the D-lines.

*Calculation of  $\text{Na}^+$  ions necessary.*—We now calculate the number density of  $\text{Na}^+$  ions necessary to produce the observed intensity of radiation by the neutralization processes (5) and (6).

Let us consider first process (5). We assume that the height distribution of electrons follows a parabolic law in the region of maximum number density (as in a Chapman layer). The distribution of  $\text{Na}^+$  ions is not known with any certainty. It may decrease exponentially following the decrease of atmospheric density, or there may be region of maximum concentration as in ionospheric layer formation. However, to simplify the calculation, we

will assume a constant concentration with height for the  $\text{Na}^+$  ions. We shall presently see that so far as qualitative result is concerned, this assumption does not lead to any erroneous conclusions.

With the above assumptions the number of transitions per  $\text{cm}^2$  at height  $h$  is given by

$$\alpha n^+ n_e(h)$$

where  $\alpha$  is the coefficient of recombination and  $n^+$  and  $n_e(h)$  are the number densities of sodium ions and electrons respectively at the height concerned. Bates (1947) has given a value  $2 \times 10^{-12} \text{ cm}^3$  per second for the total recombination coefficient i.e., for electrons captured in the ground state or in any of the possible excited states. But the electrons captured in the ground state or in any of the  $p$ -states, other than the  $2p$ -states, will not contribute to the D-lines. Hence the value of the recombination coefficient for only the states that are of interest to us will be somewhat lower. We assume this value to be  $1 \times 10^{-12} \text{ cm}^3$  per second.

Since we have assumed that the variation of electron concentration with height follows a parabolic law, we may write

$$n_e(h) = n_e(0) \left\{ 1 - \frac{h^2}{4H^2} \right\}$$

where  $n_e(0)$  = number density of electrons in the region of maximum ionization =  $5 \times 10^5$  per  $\text{cm}^3$ .

$H$  = scale height in the F-region at night = 50 km.

We assume that the bulk of the electrons in the parabolic layer lies within the heights  $\pm 2H$ , above and below the level of maximum concentration. Hence, since the number of transitions per  $\text{cm}^2$  per sec. at height  $h$  is  $\alpha n^+ n_e(h)$ , we obtain by integrating over the whole layer the number of transitions per sec. per  $\text{cm}^2$  column,

$$\begin{aligned} & \alpha n^+ n_e(0) \int_{-2H}^{+2H} \left( 1 - \frac{h^2}{4H^2} \right) dh \\ &= \alpha n^+ n_e(0) \times \frac{8}{3} H. \end{aligned}$$

Since this must be equal to the observed number of transitions, namely,  $8 \times 10^7$  per sec. per  $\text{cm}^2$  column we have for the concentration of  $\text{Na}^+$  ions,

$$\begin{aligned} n^+ &= \frac{8 \times 10^7 \times 3}{\alpha \times n_e(0) \times 8H} \\ &= 1.2 \times 10^7 \text{ per cm}^3. \end{aligned}$$

But this concentration is improbably high because the electrons produced by the ionization would raise the concentration of electrons also to the same order. We know, however, from radio measurements that the maximum concentration of electrons in the F-region is of the order  $10^5$  to  $10^6$  per  $\text{cm}^3$ .

Calculations, exactly similar to the above, may also be carried out for process (6). The coefficient for the process may be assumed to be of the order  $10^{-7}$  cm<sup>3</sup> per sec. (Mitra, 1947). Since the number density of O<sup>-</sup> ions (during night time) is  $2 \times 10^{-1}$  times the electron density, the average concentration of Na<sup>+</sup> ions is  $6 \times 10^4$  per cm<sup>3</sup>. This value of the concentration of Na<sup>+</sup> ions is obviously more acceptable than the one deduced above by the process (5). The total number of ions within the layer of thickness  $4H$  is then  $1.2 \times 10^{12}$  ions per cm<sup>2</sup> column.

Thus we arrive at the conclusion that the number density of Na<sup>+</sup> ions in the F-region must be at least of the order  $6 \times 10^4$  per cm<sup>3</sup>, in order that the observed intensity of the D-lines in the night air-glow may be produced. This number constitutes about  $10^{-5}$  of the total number of atmospheric particles in the region concerned.

*Intensity variation throughout the night.*—The intensity of the D-lines has been found to remain fairly constant throughout the dark hours of the night. Hence, if there be no means of replenishing the Na<sup>+</sup> ions lost by neutralization, the initial number of ions has to be so high that the number lost during the dark hours is but a small fraction of the initial number. Now, the total number of transitions per cm<sup>2</sup> column throughout the night (say, 8 hrs.) is of the order  $2.5 \times 10^{12}$ . But, the number of Na<sup>+</sup> ions per cm<sup>2</sup> column as deduced above is only  $1.2 \times 10^{12}$ . This number is obviously quite inadequate to maintain the required constancy of the radiation intensity. One is thus forced to assume that some process of re-ionization of the neutralized Na-atoms must be operative during the dark hours of the night. Such a process may be impact of particles of some sort incident on the atmosphere from outer space.

#### CONCLUDING REMARKS

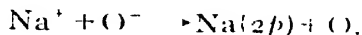
In the light of the discussions given above, we may now draw the following conclusions regarding the distribution of sodium in the upper atmosphere, and also on the possible processes of emission of the D-lines.

It appears that sodium is concentrated in two layers: one in the 35 to 65 km. region, and the other in the F-region of the ionosphere. The former consists of neutral sodium atoms and the latter of ionized atoms (ionized by solar ultra-violet radiation). Alternatively, we may imagine that sodium in the upper atmosphere spreads from a height of 35 km to the F-region of the ionosphere. At lower altitudes sodium exists in the neutral state. The percentage of ionized sodium atoms increases with height and at altitudes above 100 km. all the sodium atoms are ionized.

The twilight flash of the D-lines is due to resonance excitation of neutral Na atoms by solar radiation  $\lambda 5893$ .



The D-lines in the night air-glow are emitted in the process of neutralization of  $\text{Na}^+$  ions in the F-layer of the ionosphere. Of the two possible processes of neutralization—radiative recombination with electron and mutual neutralization with  $\text{O}^-$  ion—the latter appears to be the more likely process. Thus



The observed intensity of the nocturnal lines leads to the conclusion that the average density of  $\text{Na}^+$  ions in the F-region is of the order  $6 \times 10^4$  per  $\text{cm}^3$ , constituting about  $10^{-7}$  of the total number of atmospheric particles in the region. In the region of emission of the twilight flash the concentration is much less (by several orders). It is clear that the sodium distribution in the atmosphere does not follow the general exponential distribution law of the atmospheric particles.

The concentration of  $6 \times 10^4$   $\text{Na}^+$  ions per  $\text{cm}^3$  as given above is sufficient to produce the required rate of emission initially. But, it is totally inadequate to maintain the same (with only a small decrease in the rate) throughout the dark hours of the night. There must, therefore, be some process by which the neutral Na atoms, produced are constantly re-ionized during the night. Such night time re-ionization may be imagined to be produced by impact of extra-terrestrial particles. These particles may also contribute partly to the D-line emission by exciting the neutralized Na atoms to the  $2p$ -states.

Alternatively, one may imagine that sodium atoms are entering the upper atmospheric regions from inter-stellar space and are being excited by collision with atmospheric particles. This latter hypothesis has the advantage that it can explain the high concentration of sodium (high in relation to that expected from the exponential law) in the 250 km. region.

#### ACKNOWLEDGMENT

The author is indebted to Professor S. K. Mitra, D.Sc., F.N.I., for suggesting the work to him and for his interest and guidance throughout its progress. Thanks are also due to the Council of Scientific & Industrial Research, Government of India, for financial assistance.

INSTITUTE OF RADIO PHYSICS AND ELECTRONICS,  
UNIVERSITY COLLEGE OF SCIENCE,  
92, UPPER CIRCULAR ROAD, CALCUTTA.

#### REFERENCES

- Barbier, D., 1948, *Ann. de Geophys.*, **4**, 193.  
Barbier, D., Chalonge, D. and Vigroux, E., 1942, *Ann. de Astrophys.*, **8**, 1.  
Barbier, D. and Roach, F. E., 1950a, *Trans. Amer. Geophys. Union*, **31**, 7.  
Barbier, D. and Roach, F. E., 1950b, *Trans. Amer. Geophys. Union*, **31**, 13.  
Bates, D. R., 1947, *Terr. Mag. Atmos. Elect.*, **52**, 71.

- Bates, D. R., 1950, *J. Geophys. Res.*, **55**, 347.
- Bates, D. R. and Massey, H. S. W., 1946, *Proc. Roy. Soc. A*, **187**, 261.
- Bates, D. R. and Nicolet, M., 1950, *J. Geophys. Res.*, **55**, 235.
- Bernard, R., 1938, *Zeit. f. Phys.*, **110**, 291.
- Bernard, R., 1939, *Astrophys. Jour.*, **89**, 133.
- Cabannes, J., Dufay, J., and Gauzit, J., 1938, *Astrophys. J.*, **88**, 164.
- Cario, G. and Stille, U., 1950, *Abhandlungen der Braunschweig Wiss. Gesellschaft*, Bd. II, p. 40.
- Chapman, S., 1939, *Astrophys. J.*, **90**, 309.
- Dufay, J. and Tcheng Mao-Lin, 1948, Gassiot Committee Report on 'Emission Spectra of the Night Sky and Aurorae,' *Phys. Soc., London*, p. 62.
- Elvey, C. T. and Farnsworth, A. H., 1942, *Astrophys. J.*, **98**, 451.
- Mitra, S. K., 1947, *Upper Atmosphere*, p. 288.
- Penndorf, R., 1950, *Phys. Rev.*, **78**, 66.
- Roach, F. E., 1949, *Astrophys. J.*, **110**, 314.
- Roach, F. E. and Pettit, H., 1951, *J. Geophys. Res.* (to be published in Sept 1951).
- Vegard, L., 1940, *Nature*, **145**, 623.
- Vegard, L. and Tönsberg, E., 1940, *Geofys. publ.* **13**, No. 1.
- Vegard, L. and Tönsberg, E., 1941, *Geofys. Publ.* **13**, No. 5.
- Vier, D. T. and Mayer, E. E., 1944, *J. Chem. Phys.*, **12**, 26.

# ON A DISSOCIATION SCHEME FOR THE SPECTRUM OF $\text{CO}^+$ \*

BY PRABHAT K. SEN GUPTA

(Received for publication, May 3, 1951)

**ABSTRACT.** A dissociation scheme has been proposed for the spectrum of  $\text{CO}^+$  and correlated with the convergence limits of the known spectroscopic states. For the energy of dissociation of  $\text{CO}^+$  the values 5.58 and 7.92 volts have been considered likely according as the products of dissociation are  $\text{C}^+ (^2P) + \text{O}(^3P)$  and  $\text{C}(^3P) + \text{O}^+(^4S)$  respectively.

In a recent paper the author (Sen Gupta, 1951) has shown that the use of the value  $D(\text{CO}) = 8.87$  volts explains satisfactorily the predissociation effects in the spectrum of  $\text{CO}$  and the results of the experiments on the sublimation of graphite. As the energy of dissociation of  $\text{CO}^+$  is closely interrelated with that of  $\text{CO}$ , an attempt is made here to find out whether a dissociation scheme with the assignment of  $D(\text{CO}) = 8.87$  volts is able to account for the observed effects in the spectrum of  $\text{CO}^+$ .

For  $\text{CO}^+$ , three band systems are known, viz,

First negative :  $B \ ^2\Sigma^+ \rightarrow X \ ^2\Sigma^+$

Comet tail :  $A \ ^2\Pi \rightarrow X \ ^2\Sigma^+$

Baldet-Johnson :  $B \ ^2\Sigma^+ \rightarrow A \ ^2\Pi$

The data so far available are given in the following Table.

TABLE I

(Sponer, 1935 ; Biskamp, 1933)

State	Energy height above ground state in volts	Vibrational levels observed		Extrapolated convergence limits	
		Number	Energy height above $v=0$ in volts	above $v=0$ of state. in volts	Above ground state. in volts
$X \ ^2\Sigma^+$	0	$v=13$ ( $v=33$ )	3.21 (6.90)	9.90	9.90
$A \ ^2\Pi$	2.53	$v=14$	2.50	~4.8	~7.33
$B \ ^2\Sigma^+$	5.66	$v=10$	1.80	3.70	9.36

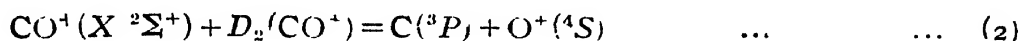
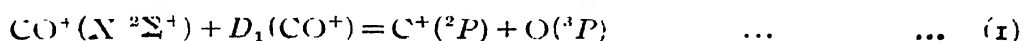
\* Communicated by Prof. M. N. Saha, D.Sc., F.R.S.

The location of the convergence limit of the ground state  $X^2\Sigma^+$ , is most important, but it will be seen that only a few vibrational levels have been observed. Biskamp's (1933) linear extrapolation, yielding 9.9 volts for this limit covers an unknown region of about two-thirds of this value and can be regarded only as an upper limit for the energy of dissociation. Other investigators (Biskamp, 1933 ; Asundi and Samuel, 1937 ; Asundi, 1943 ; Gaydon and Penney, 1945) have made use of the extrapolated value 9.9 in their discussions, but it is felt that the extrapolation is too long for this value to be reliable. For molecules of this type Gaydon (1946) has given some examples showing that the Birge-Sponer extrapolation is about 20% high when the extrapolation is long. Allowing for this error, the convergence limit of the  $X^2\Sigma^+$  state would be expected to lie at about  $9.9 - 1.98 = 7.92$  volts. Asundi (1943), by observing perturbations in  $v=7$  level of the  $B^2\Sigma^+$  state, followed the vibrational levels of the  $X^2\Sigma^+$  state up to  $v=33$  corresponding to  $55082\text{ cm}^{-1}$  (6.90 volts), which may be taken as a lower limit for the position of convergence of the  $X^2\Sigma^+$  state.

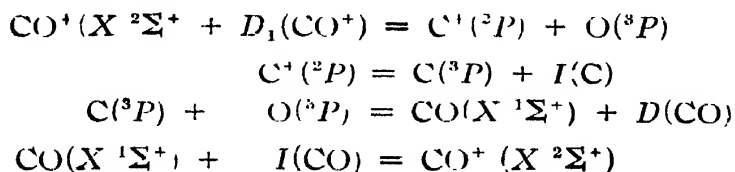
For the states  $A^2\Pi$  and  $B^2\Sigma^+$ , the ranges of extrapolation are comparatively shorter and consequently uncertainties lesser.

## II

For  $\text{CO}^+$ , two dissociation processes may be considered :



in which  $D_1$  and  $D_2$  represent the respective energies of dissociation. Let  $I(\text{C})$ ,  $I(\text{O})$  and  $I(\text{CO})$  denote the first ionization potentials C, O and CO respectively. Then the interrelations of these quantities are obtained from the following expressions :



Therefore,

$$D_1(\text{CO}^+) = I(\text{C}) + D(\text{CO}) - I(\text{CO}) \quad \dots \quad (3)$$

$$\text{Similarly, } D_2(\text{CO}^+) = I(\text{O}) + D(\text{CO}) - I(\text{CO}) \quad \dots \quad (4)$$

The known spectroscopic values of the quantities in the above expressions are :

$$\begin{aligned} I(\text{C}) &= 11.26 \text{ volts} \\ I(\text{O}) &= 13.60 \text{ volts} \\ D(\text{CO}) &= 8.87 \text{ ,, (Sen Gupta, 1951)} \\ I(\text{CO}) &= 14.55 \text{ ,, (Anand, 1942)} \end{aligned}$$

Substituting these values in (3) and (4) we get,

$$D_1(\text{CO}^+) = 5.58 \text{ volts} \quad \dots \quad (5)$$

$$D_2(\text{CO}^+) = 7.92 \text{ ,,} \quad \dots \quad (6)$$

Asundi and Samuel (1937) also considered the possibility of the processes (1) and (2) given, but they have a different dissociation scheme.

The limits arising out of the different combinations of the products of dissociation may now be calculated with the aid of (5) and (6) and the atomic term differences  $^3P \sim ^1D = 1.26$  volts for carbon and 1.96 volts for oxygen. The results are given in Table II.

TABLE II

Products of dissociation	Calculated limits, volts	Observed limits volts	State
$\text{C}^+(^2P) + \text{O}(^3P)$	5.58	—	—
$\text{C}^+(^2P) + \text{O}(^1D)$	7.54	~7.33	$A \ ^2\Pi (?)$
$\text{C}(^3P) + \text{O}^+(^4S)$	~9.0	(7.92)	$X \ ^2\Sigma^+$
$\text{C}(^1D) + \text{O}^+(^4S)$	9.18	9.36	$B \ ^2\Sigma^+$

In the last two columns the experimental results have been reproduced from Table I, but, for the  $X \ ^2\Sigma^+$  state, the estimated value 7.92 volts, has been shown instead of the extrapolated value 9.0 volts, as already discussed. The effect corresponding to 5.58 volts does not appear to have been observed so far. Thus within the limits of error in extrapolation the agreement between the calculated and the observed limits appears to be fairly satisfactory.

Gaydon and Penney (1945) have indicated the extrapolated limit of the  $A \ ^2\Pi$  state to be at 9.2 volts, that is, almost at the same height as that of the  $B \ ^2\Sigma^+$  state. If this value is accepted, it would mean that the effects expected at 5.58 and 7.54 volts are missing. Such a contingency is not unlikely, if we consider that the vibrational levels of the  $A \ ^2\Pi$  and  $B \ ^2\Sigma^+$  states have not been observed in emission beyond  $v=14$  and  $v=10$  respectively. The unobserved limits lie in the vicinity of the energy heights of these vibrational levels and suggest the possibility of the existence of repulsive states.

#### ACKNOWLEDGMENT

The author is thankful to the authorities of the Indian Association for the Cultivation of Science, Jadavpur, Calcutta, for giving facilities in their library for the investigation.

## REFERENCES

- Asundi, R. K., 1943, *Proc. Ind. Acad. Sc.* **18A**, 8.  
Asundi, R. K. and Samuel, R., 1937, *ibid.*, **5A**, 235.  
Biskamp, 1933, *Z. f. Phys.* **86**, 33.  
Gaydon, A. G., 1946, *Proc. Roy. Soc.* **58A**, 525.  
Gaydon, A. G. and Penney, W. G., 1945, *ibid.*, **183A**, 374.  
Sen Gupta, P. K., 1951, *Ind. J. Phys.*, **25**, 267.  
Spöner, H., 1935, *Molekulespektren, Tabellen.*

## ON UNIFIED THEORIES OF THERMAL AND SHOT NOISE\*

By S. DEB

*(Received for publication, June 18, 1951)*

**ABSTRACT.** The paper presents an outline of the principal characteristics of the thermal and the shot types of noise (in circuits and in valves respectively) and examines the similar features of the two phenomena. The unified theories of the two types of noises proposed recently by Campbell and Francis, and by Firth are reviewed and discussed critically. The phenomenon of space-charge reduction of noise has been explained from a new statistical standpoint. It is shown that although the two types of noises owe their origin to the same basic phenomenon, they differ in one essential respect, viz: the presence of thermal equilibrium in the one (thermal) and its absence in the other (shot). It is concluded that thermal noise can be looked upon as a special case of shot noise when thermal equilibrium exists. As such, the unified thermo-dynamical theory of Firth becomes unacceptable.

## INTRODUCTION

The possibility of existence of spontaneous fluctuations of current in a conductor was first suggested by Einstein (1906). Einstein showed that the mean-square-charge crossing any cross-section of a conductor (of resistance  $R$ ) in thermal equilibrium, over a finite time interval  $\tau$  is given by

$$\bar{Q}^2 = \frac{2kT}{R} \tau \quad (1.1)$$

Nyquist (1928) showed that the mean-square fluctuation voltage appearing at the output of a network over the entire frequency range would be

$$\bar{v}^2 = \frac{2kT}{\pi R} \int_0^\infty |Z(\omega)|^2 d\omega \quad (1.2)$$

provided classical law of equipartition holds. In (1.2),  $Z(\omega)$  is the transfer impedance of the circuit over the frequency range  $f$  to  $f+df$ . If  $Z(\omega) = R$  then over the range  $f$  to  $f+df$

$$\overline{de}^2 = 4RkTdf \quad \dots (1.3)$$

The possibility of the existence of a similar type of fluctuations of current as obtained in a valve was suggested by Schottky (1918). Schottky gave

\* Communicated by Prof. S. K. Mitra.

the following expression for the mean-square-fluctuation current over the frequency range  $f$  to  $f + df$  associated with a diode valve carrying a current  $i$ , under temperature-limited condition,

$$\overline{di^2} = 2\epsilon i, df \quad \dots (1.4)$$

where  $\epsilon$  is the electronic charge. (This relation holds for retarding fields as well. For space-charge-limited condition (1.4) has to be multiplied by a factor  $I^{1/2}$  which is much less than unity).

From the very beginning, thermal noise and shot noise have been looked upon as two distinct phenomena owing their origin to entirely different physical causes. The former was assumed to be due to the thermal agitational motion of electrons and the latter to the granular nature of electrical carriers, *viz.* the electrons. Only recently it has been recognised that the two types of noise are only two different aspects of the same basic phenomenon. This is understood if one remembers that the existence of random thermal agitation of electrons in a resistance is only possible because the electrons are granular. Also, electrons emitted by heating are the thermal electrons and not the Fermi electrons. As such, any observed fluctuation in emission is entirely due to this fact. Starting with these premises, attempts have been made in recent years to develop a unified theory which embraces both the types of noises. Campbell and Francis (1946) have given such a theory based on statistical reasonings. Fürth (1948) has given another based on thermodynamic reasonings. It is the purpose of this paper to critically review these two theories and to show that a better approach to the problem is made if thermal noise is looked upon as a special case of shot noise as encountered in a valve.

#### SIMILARITIES IN SHOT AND THERMAL NOISE

The first suggestion of a possible identity of shot and thermal noise arose out of the phenomenon of space-charge-reduction of noise. It was argued that a valve carrying space-charge-limited current differs from one carrying a temperature-limited current only in having a differential resistance  $R_a$ . The reduction effect was, therefore, sought to be explained in terms of thermal noise in  $R_a$ . But this attempt was unsuccessful. A striking correspondence was, however, established by Williams (1936) under retarding field condition. The expression for valve current under retarding field condition is given by

$$i = i_s \exp \left[ - \frac{\epsilon V}{k T_e} \right]$$



and

$$R_a = \left( \frac{dV}{di} \right)_{i_s} = \frac{ie}{kT_c}$$

Hence,

$$\begin{aligned} \overline{di}^2 &= 2iedf = 2R_a kT_c df \\ &= 4R_a k(T_c/2)df \end{aligned} \quad \dots (2.1)$$

Relation (2.1) shows that a valve, under condition of retarding field, behaves as an ordinary resistance  $R_a$  at half the cathode temperature. North (1940) has given a more general expression for valve noise. According to him the mean-square-fluctuation-current in a valve is always expressible in the form,

$$\overline{di}^2 = 4R_a kT_c \theta df \quad \dots (2.2)$$

where,  $\theta$  has a value  $\frac{1}{2}$  under retarding field condition and approximately 0.644 under space-charge-limited condition. The value of  $\theta$  changes rapidly, increasing without limit, as the condition of saturation is approached. North was also able to show that Nyquist's formula (1.2) holds for a valve in thermal equilibrium.

#### UNIFIED THEORIES: CAMPBELL AND FRANCIS

##### (a) Campbell and Francis's treatment :

The method is based upon two theorems, the 'mean' and the 'mean-square' theorems which are collectively known as Campbell's theorems'. These theorems are helpful in calculating the effect of random-fluctuation-noise in any electrical device having a linear response characteristic and may be explained as follows :

Let us observe any random process-thermionic emission, for example, and divide the time preceding the instant of observation into a large number of intervals  $\tau$ . Suppose  $a$  is the average number of particles emitted per unit time. Then  $v = a\tau$  may be looked upon as the probability of emission of a particular particle within a selected time interval. Suppose now that we observe the effect of these random events in a device whose response is linear. If the instantaneous effects observed in the device due to all the random events occurring within a time  $t$  prior to the instant of observation be  $S(t)$ , then Campbell's theorems state : *In the limit when  $\tau \rightarrow 0$  and Poisson's distribution law for the events of low probabilities holds, the mean-effect observed in the network will be given by*

$$\bar{y} = a \int_0^\infty S(t) dt \quad \dots (3.1)$$

and the mean-square-effect by

$$\overline{(y - \bar{y})^2} = a \int_0^\infty [S(t)]^2 dt = aS \text{ (say)} \quad \dots (3.2)$$

where  $S$  is the value of the integral on the left hand side.

The value of  $[S(t)]^2$  can be calculated by the method of Fourier integrals. Campbell and Francis have shewn that if the elementary events giving rise to the fluctuations are a series of current impulses of strength  $X_0\tau$ , then

$$\overline{(y - \bar{y})^2} = \frac{a}{\pi} \int_0^\infty X_0^2 \tau^2 [\phi(j\omega)]^2 d\omega \quad \dots (3.3)$$

where  $X_0$  = height of the impulses,

$\tau$  = duration of the impulses

and  $\phi(j\omega)$  = frequency response of the network in which the noise is being observed.

Eq. (3.3) can now be applied to deduce expressions for the mean-square-fluctuation-noise, of both the types—shot noise in valves (Schottky's equation) and thermal noise in resistive circuits (Nyquist's equation).

#### (b) Shot noise

For the shot noise three cases may be distinguished :

(i) When the valve carries temperature-limited current, (ii) when it carries space-charge-limited current and (iii) when the valve is under a retarding field.

Of these, Campbell and Francis have discussed fully only the first one. The second and the third cases were not fully discussed by them because their theorems are not applicable to non-linear device. We give below discussions of all the three cases. The first as developed by Campbell and Francis and second and third as developed by the author of this paper.

*Case (i). Valve carrying temperature-limited current.*—Schottky's equation for noise in temperature-limited current in a valve can be easily derived from (3.3) by the general method suggested by Campbell and Francis.

Let us consider the case when the noise is observed directly in the plate circuit of the valve. If the mean square-fluctuation in current is observed then

$$[\phi(j\omega)] = |Y(\omega)| = 1 \quad \dots (3.4)$$

where  $Y(\omega)$  = transfer admittance of the network over  $\omega$  to  $\omega + d\omega$ .

The elementary events giving rise to shot noise is the passage of a charge  $\epsilon$  over a small interval of time  $\tau$  during which a small current  $i_\tau$  flows.

Thus

$$X_0 = i_\tau \text{ and } X_0\tau = \epsilon \quad \dots (3.5)$$

and from (3.3), (3.4) and (3.5)

$$\overline{(y - \bar{y})^2} = \bar{i}^2 = \frac{a\epsilon^2}{\pi} \int_0^\infty d\omega \quad \dots (3.6)$$

If observations are restricted over a frequency range  $f$  to  $f + df$ , then because  $a\epsilon$  = average rate of flow of charge

$$\overline{di^2} = 2ae^2 df = 2\bar{i}_s e df$$

This is identical with the expression given by Schottky.

*Case (ii). Valve carrying space-charge-limited current.*—This case has not been fully discussed by Campbell and Francis as their equation holds only for linear device and the characteristic of a valve under space-charge-limited condition is not linear. However, if one takes into consideration the portion of the curve which is linear, one may arrive at an expression for shot noise as reduced by space-charge effects.

We note that fluctuation voltages are usually very small and for such small ranges of values the characteristics may be taken approximately as linear. Further, under many practical conditions of operation of diode and triode valves reasonably accurate results are obtained by assuming them to behave as linear device and in these cases too, space-charge-reduced noise equation holds. It is likely that in these cases at least individual events separated by infinitesimal time interval would add up linearly. We can therefore, treat the valve as an approximately linear device and try to get some qualitative interpretation of space-charge-reduction of noise. In figure 1, has

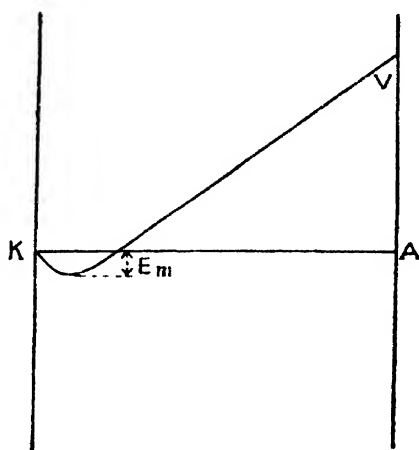


FIG. 1

been shown a voltage distribution curve for a valve carrying space-charge-limited current. Here the passage of an electron from cathode to anode can be considered under two parts :

(I) A part in which the journey is performed in a retarding field between the cathode and the negative potential dip  $E_m$ . Due to this the current in the plate circuit will be as shewn in figure. 2 (a).

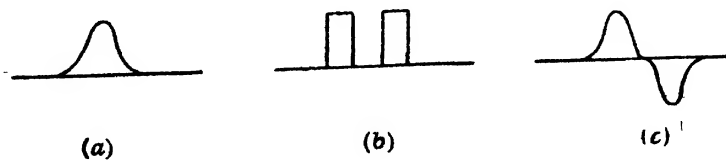


FIG. 2

(II) A part in which the journey is performed in an accelerating field between  $E_m$  and the anode. The corresponding current in the circuit will also be of the form shewn in figure. 2 (a). The combination of these two current component can be looked upon as a pair of impulses as shewn in figure. 2 (b). Since each of these pulses depicts the transit of an electron over only a part of the distance between the cathode and the anode, the strength of these impulses  $X_0\tau$  will now be less than  $\epsilon$ . If we write it as  $\Gamma\epsilon$  ( $F \ll 1$ ), then it follows from (3.3), (3.5) and (3.6) that

$$d\bar{i}^2 = 2\epsilon i \Gamma^2 df \quad (\Gamma^2 \ll 1)$$

As regards those electrons which fail to cross the potential dip and return to the cathode it may be observed that they give rise to doublet impulses of the type shown in figure, 2 (c). It may be shewn that so long as the frequencies are low enough to make the transit angle small, contribution due to these impulses will be negligible.

If the two pulses are of equal strength then  $\Gamma^2 \approx 25$  which is of the order of the value as obtained experimentally. Value of  $\Gamma$  would depend on the potential distribution, geometry of the valve and the energy distribution of the electrons.

It should be noted that a clear resolution between the two pulses, as shewn in figure 2 (b), is possible only under condition of complete space-charge-limitation. In the general case there may be overlapping of the two to some extent.

(iii) *Valve under retarding field condition.*—This case has also not been considered by Campbell and Francis on account of lack of linearity. However, the above considerations may also be applied to provide a simple explanation of the nature of noise equation for a valve under retarding field. For this case the potential decreases monotonously from cathode to anode. The passage of an electron to the anode would, therefore, be represented by an impulse of the type shewn in figure 2 (a), but having a much greater strength. Since this pulse depicts the passage of one electron from cathode to anode the strength would again be  $\epsilon$ . Thus it is obvious that Schottky's relation should hold for this region.

#### (b) *Thermal Noise.*

Nyquist's equation (eqn. 1.2) for thermal noise has also been deduced by Campbell and Francis from (3.3). The method of deduction, however, does not make it evident that the condition of thermal equilibrium is essential. The following slightly modified deduction by the author is believed to make this clear in a simple manner.

Let us imagine that the source of thermal noise is composed of a large number of constant current generators in series such that the  $k$ th generator

gives rise to a current pulse  $i_k$  lasting over a time  $\tau_k$  and that these are uncorrelated with respect to time. Thus

$$S'_k(j\omega) = i_k \tau_k \quad \dots (3.7)$$

and

$$S_k = \frac{1}{\pi} i_k^2 \tau_k^2 \int_0^\infty [\phi(j\omega)]^2 d\omega \quad \dots (3.8)$$

From (3.2)

$$(\bar{y} - \bar{y})^2 = \frac{1}{\pi} \sum_k a_k i_k^2 \tau_k^2 \int_0^\infty |\phi(j\omega)|^2 d\omega \quad \dots (3.9)$$

Suppose now that the network whose noise is being observed is a circuit whose transfer impedance is  $Z(\omega)$ , then

$$\phi(j\omega) = Z(\omega)$$

Thus the mean-square-voltage-fluctuation is given by

$$\bar{e}^2 = \frac{1}{\pi} \sum_k a_k i_k^2 \tau_k^2 \int_0^\infty [Z(\omega)]^2 d\omega \quad \dots (3.10)$$

Here a deviation will be made from Campbell and Francis treatment and the value of  $\sum a_k i_k^2 \tau_k^2$  will be calculated by applying equation (1.1) which holds only for a resistor in thermal equilibrium. This would make the calculation more simple and straightforward. We note that

$$i_k \tau_k = \text{charge conveyed in a single event in the } k\text{th generator}$$

and  $i_k^2 \tau_k^2 = e_k^2 = \text{square-charge conveyed in a single event in the } k\text{th generator}$  and  $\sum a_k i_k^2 \tau_k^2 = \text{mean-square-charge conveyed by all the generators over a time } \tau$ .

Hence

$$\sum a_k i_k^2 \tau_k^2 = \frac{\bar{Q}^2}{\tau} = \frac{2kT}{R} \text{ from (1.1)} \quad \dots (3.11)$$

Thus we get from (3.10)

$$\bar{e}^2 = \frac{1}{\pi} \frac{2kT}{R} \int_0^\infty |Z(\omega)|^2 d\omega$$

which is identical with (1.2)

#### UNIFIED THEORY: FÜRTH

Fürth has given a unified theory from thermodynamical reasonings. The main advantage of this treatment, as compared to that of Campbell and Francis, is that it deals with macroscopic quantities only and in the final expression for noise only such quantities appear. However, Fürth had anticipated several objections against the application of thermodynamic reasonings to conditions as exist in a valve and had tried to answer them.

But, as shown in the discussion, the objections have not been fully met with. To understand these discussions the arguments that have been advanced against the thermodynamical treatment and Fürth's answers to them are given below.

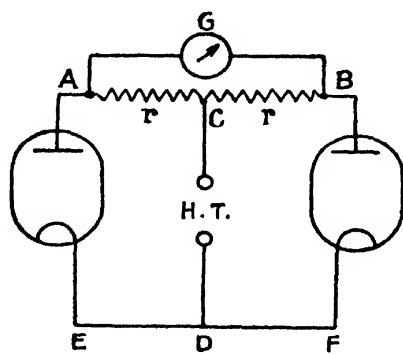
(a) Whereas, shot noise is associated with the flow of an average current  $i$ , thermal noise exists even in its absence.

(b) There is no temperature equilibrium in the case of a valve and the velocity distribution law is essentially asymmetrical.

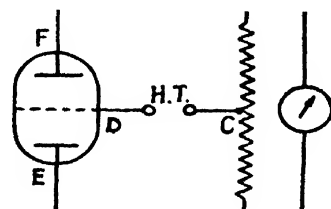
(c) The external circuit is at different temperature from that of a valve.

Fürth's answers to these objections are as follows :

(a) Thermal noise in a conductor remains unaltered even when a non-vanishing steady current is flowing. Also shot noise exists even when no mean current flows. Now, consider the circuit shown in figure 3 (a) in



(a)



(b)

FIG. 3

which the two valves are exactly similar. In this case no mean current flows through the galvanometer  $G$ . Yet this will certainly register independent shot fluctuations due to the two halves,  $ACDEA$  and  $BCDFB$ .

(b) Figures 3 (a) and 3 (b) are equivalent and Fürth contends that the two symmetrically placed emitting electrodes would render the velocity distribution law symmetrical.

(c) As long as  $2\tau T \ll \frac{dV}{di} T$ , thermal fluctuations in the external circuit would remain small enough to be negligible and in such a case the third point of objection can be waived,

Fürth then assumes that the noise currents are produced by an irregular voltage fluctuation  $\delta V_e$  originating in the inter-electrode space and another similar quantity  $\delta V_c$  originating in the surface layer of the cathode. On this basis the mean square-fluctuation current for the double-cathode valve shown in figure 3 (b) is found to be

$$\overline{\delta i^2} = 4kT \left( g_c \frac{\delta V_c}{\delta V} + g_a \frac{\delta V_a}{\delta V} \right) df$$

where

$$g_a = \left( \frac{\overline{\delta i}}{\delta V} \right)_{i_s}, \quad g_c = \left( \frac{\overline{\delta i}}{\delta i_s} \right) \frac{ei_s}{kT}$$

bar indicating the average values. Fürth then proceeds with the argument that the fluctuations observed across  $2r$  due to the double-cathode valve should be just twice that due to a single similar cathode in an asymmetric case. Thus for a single-cathode valve

$$\overline{\delta i^2} = 2kT \left( g_c \frac{\delta V_c}{\delta V} + g_a \frac{\delta V_a}{\delta V} \right) df \quad \dots (4.1)$$

This expression has been used by Fürth to obtain expression for noise of a valve carrying (i) temperature-limited current, (ii) space-charge-limited current and (iii) retarding field current.

## DISCUSSIONS

(A) *Campbell and Francis' theory.*—The success of the treatment of Campbell and Francis in explaining the different types of noise proves conclusively the basic identity between valve and circuit noise. Its treatment of both the phenomena is based on statistical reasonings and, as such, helps to bring out clearly the fact that noise is of microscopic origin. The method of mathematical treatment, though a little involved, is quite elegant. Perhaps the only drawback of the treatment is that it is not applicable to a non-linear device. But, as shown by the author this is not an insuperable difficulty. Subject to certain approximations one can extend the treatment to the case of a non-linear device, like a valve under condition of space-charge-limitation. This extension, incidentally, leads to an interpretation of the phenomenon of space-charge-reduction of noise, from a new angle, which, though qualitative, is more convincing and straightforward than the earlier theories. For example, the earlier theories sought to attribute the reduction to the increase in the magnitude of off-cathode potential dip  $E_m$  with the increase in space-current-density. But, this would mean that the chance of an electron at any instant, being thrown into the inter-electrode space and passed to the anode, depends on the space-current-density and hence on the electrons emitted at the preceding instants, that is, on some amount of correlation in the elementary events giving rise to noise. But, as is well known, this is not true for space-charge-reduced shot noise. This difficulty is not encountered in the interpretation of the author.

(B) *Fürth's theory.*—As mentioned earlier the objections that have been raised against Fürth's theory are not fully met by the arguments advanced by him. In what follows we will first discuss the several defects

in Fürth's arguments, as pointed out by McDonald (1948) and as also are apparent according to the author of this paper. It will then be shown that the ultimate ground of all these objections against Fürth's theory is the lack of thermal equilibrium in a valve.

According to McDonald, the magnitude of the fluctuation current remains unaffected by the flow of a non-vanishing steady current in a metallic conductor only so long as the drift velocity thus produced is comparatively small—a condition which is wanting in a valve. Even in a metallic conductor, substantial deviation is likely to occur when the mean-free-path becomes very large. Again, the particular circuit arrangement in figure 3(b), proposed by Fürth (to show that the flow of a mean current is not necessary for the production of valve noise) is open to criticism because, although the detecting galvanometer  $G$  does not carry any mean current, the valves, which are the primary seats of noise, do in fact, carry mean currents. McDonald also points out that thermodynamical reasoning cannot be applied to the double-cathode valve of figure 3(b), because the two electron-streams inside this valve would present a symmetrical velocity-distribution only in the absence of the intervening grid. In the presence of this grid they are simply two asymmetrical beams inside a common enclosure.

Apart from the objections of McDonald, as discussed above, a close scrutiny shows that the theory has other serious difficulties. For example, one finds it difficult to agree with the suggestion that the total noise appearing across  $2r$  in figure 3(b) would be just twice that of a single valve in the asymmetrical case. This is because an electron, which succeeds in penetrating the space-charge barrier in front of a cathode and is not captured by the grid, would introduce a partition type of noise which is absent in an ordinary diode. Further, it is not clear how the presence of the battery could be ignored in figure 3(b).

All these objections, however, are essentially inter-connected and arise out of the one and the same factor, *viz.* the presence or the absence of thermal equilibrium. To show this we will analyse the objections to Fürth's arguments discussed above.

According to McDonald, the flow of mean-current is a differentiating factor between shot and thermal noise. Now, a valve is in effect a combination of an electronic switch and a resistance  $R_a$  in series. The current  $i$ , is brought about in the process of the switching-on operation. Here the noise and the mean-current are two inevitable companions but are not inherently interdependent. It may also be noted that Schottky's expression gives the noise in a valve correctly, even if no mean current is flowing in the valve. This would remain valid even if a mean-current flows, provided thermal equilibrium is not disturbed. In a valve, however, due to the combined influence of large mean-free-path and accelerating field, the flow



of mean-current is brought about through a process which disturbs the thermal equilibrium and that is why Nyquist's treatment is not applicable to it.

Let us next examine closely the arguments that a large mean-free-path would make a difference between the two types of noises. Let us consider, for example, a valve of the type shown in figure 3(b) from which the intervening grid has been removed. As will be shewn below, Nyquist's formula, which is applicable to thermal noise, is also applicable to it under certain conditions. We assume that the conditions are such that the mean-free-path of an electron is  $l$ , the separating distance between the two electrodes. Suppose also that the system is in thermal equilibrium. Under this condition cathode  $F$  will send a current  $i_0$  (say) towards  $E$  which again would send an identical current towards  $F$ . The total noise in the valve would be twice the noise associated with these two currents and from Schottky's equation,

$$\overline{\delta i^2} = 4i_0 e df. \quad \dots (5.1)$$

If the electrons move through the same distance between two successive collisions and have all the same average thermal agitational velocity  $V$  and if the collisions are all mutually uncorrelated, then from simple application of electron theory the value of the resistance of the system is given by

$$R_a = \frac{6kTl}{nAe^2\lambda V}, \quad \dots (5.2)$$

where  $A$  is the area of the cathodes and  $n$  the electronic concentration within the inter-electrode space.

For the case under consideration  $\lambda = l$  and  $nA/3$  represents the number of electrons crossing per unit area of a surface parallel to  $F$  and  $E$  per second. Half of this constitutes the number travelling in the same direction. Thus,

$$\frac{nAeV}{6} = i_0$$

From (5.1) we obtain

$$R_a = \frac{kT}{i_0 e} \quad \dots (5.3)$$

From (5.1) and (5.3) we get

$$\overline{\delta i^2} = 4 \frac{kT}{R_a} df$$

which is identical with Nyquist's formula. It is thus obvious that shot and thermal noises would merge with one another only when thermal equilibrium exists, irrespective of the question of mean-free-path. A large drift velocity appears when large mean-free-path and an external voltage exist simultaneously and it affects the situation by rendering the velocity distribution asymmetrical i.e., by disturbing the thermal equilibrium.

It should be noted that relation (5.3) is not peculiar to the special case considered here. Meltzer (1949) has shown in a very simple manner, that it holds for any resistance in thermal equilibrium,

## CONCLUDING REMARKS

It appears that thermal and valve noises have their origin in the same basic physical phenomenon, *viz.*, the existence of discrete carriers of electricity endowed with irregular agitational motion. This motion may or may not be in thermal equilibrium. For the resistor there is thermal equilibrium in agitational motion. For the case of the valve this is not so. A resistor and a valve differ from one another from the standpoint of noise in so far as thermal equilibrium may be assumed to exist in the case of the latter but not in the former. Hence one may look upon ordinary thermal noise as shot noise for the special case when thermal equilibrium exists and a valve may be looked upon as a special type of conductor devoid of thermal equilibrium. It, therefore, appears that the unified thermodynamical theory, as postulated by Fürth for ordinary valves, is improbable. Compared to this, the theory proposed by Campbell and Francis is distinctly a better approach to the problem. It is the elementary electrons which give rise to noise and the fact that our ultimate observations are concerned with macroscopic quantities only does not, in any way, affect the position. Hence a statistical treatment of the problem is more rigorous and elegant.

## ACKNOWLEDGMENTS

Thanks are due to Prof. S. K. Mitra for his advice in course of preparation of the paper. It is also a pleasure to thank Prof. M. N. Saha for introducing the author to the subject.

INSTITUTE OF RADIO PHYSICS AND ELECTRONICS,  
UNIVERSITY OF CALCUTTA

## REFERENCES

- Campbell, N. R., and Francis, V. J., 1946, *I-E, E.*, **93**, (III), 46.  
 Einstein, A, 1906, *Ann. Phys.*, **19**, 371.  
 Fürth, R, 1948, *Proc. Roy. Soc.*, **192A**, 503.  
 Meltzer, B., 1949, *Phil. Mag.*, **40**, 1224.  
 McDonald, D. K. C., 1948, *Proc. Roy. Soc.*, **195A**, 225.  
 North, D. O., 1940, *R. C. A. Rev.*, **4**, 441.  
 Nyquist, H., 1928, *Phys. Rev.*, **32**, 110.  
 Schottky, W., 1918, *Ann. Phys.*, **57**, 541.  
 Williams, F. C., 1936, *I. E. E*, **78**, 471.

# ON THE APPROXIMATE SOLUTIONS OF MAXWELL'S EQUATIONS IN AN INFINITE MEDIUM WITH REGIONS OF FINITE CONDUCTIVITY

By K. V. KRISHNA PRASAD

*(Received for publication, March 15, 1951)*

**ABSTRACT.** The approximate solutions of Maxwell's equations lead to solutions of the normal mode type for the propagation of electromagnetic waves inside wave guides. The failure of such normal mode type solutions to describe the entire field of a given source has been discussed. The discussion is restricted to the case of propagation along a tube of circular cross-section.

## INTRODUCTION

The propagation of electromagnetic waves through a wave guide, with walls assumed to be of infinite conductivity, has been discussed in detail in recent years by Condon (1942) and Slater (1942). In a case like this, the problem is relatively simple and resolves itself to the solution of the wave equation in a finite region bounded by the walls of the wave guide. An infinite number of normal mode solutions, which are orthogonal, can be easily found and a linear combination of these solutions is the most general solution possible. Even if the conductivity of the walls is large, but not infinite, an approximate solution in fair agreement with practical results can be easily found by assuming that the above normal mode solutions are applicable and that the tangential magnetic field at the boundary is essentially unchanged. For a bounded region with discontinuities in the properties of the medium however, solutions of the normal mode type can be found but they will not be orthogonal.

In the case of semi conductors and dielectric wave guides, which have become important in the last two or three years, the conductivity is small and the wave equation has to be solved in an infinite region. For an infinite region having zero conductivity, Sommerfeld (1912) has shown in a general way that solutions of the normal mode type do not exist. Hondros and Debye (1910) have shown that for a dielectric wire embedded in another dielectric, there can be only a finite number of normal mode solutions.

The purpose of the present paper is to show that these solutions of the normal mode type are not enough to describe the complete field of a given source. As an example, the propagation of electromagnetic waves along a tube of circular cross-section will now be considered.

## THEORY

Maxwell's equations for a homogeneous isotropic medium are :

$$\left. \begin{aligned} \nabla \cdot \bar{E} &= 0 \\ \nabla \cdot \bar{H} &= 0 \\ \nabla \times \bar{E} &= -\mu \frac{\partial \bar{H}}{\partial t} \\ \nabla \times \bar{H} &= \sigma \bar{E} + \epsilon \frac{\partial \bar{E}}{\partial t} \end{aligned} \right\} \quad (1)^*$$

where  $\bar{E}$  and  $\bar{H}$  are respectively the electric and magnetic field vectors,  $\sigma$  the conductivity,  $\epsilon$ , the dielectric constant and  $\mu$ , the permeability of the medium.

Using cylindrical coordinates  $r, \theta, z$ , and confining the discussion to sinusoidal fields, the components of the electric and magnetic fields resulting from equation (1) are :

$$\left. \begin{aligned} E_r &= \frac{\partial^2 \phi^{(e)}}{\partial z \partial r} + \frac{i\mu\omega}{r} \frac{\partial}{\partial r} \phi^{(m)} \\ E_\theta &= \frac{1}{r} \frac{\partial^2 \phi^{(e)}}{\partial z \partial \theta} - i\mu\omega \frac{\partial}{\partial r} \phi^{(e)} \\ E_z &= \left( k^2 + \frac{\partial^2}{\partial z^2} \right) \phi^{(e)} \end{aligned} \right\} \quad (2)$$

and

$$\left. \begin{aligned} H_r &= \frac{\partial^2 \phi^{(m)}}{\partial z \partial r} + \frac{k^2}{i\mu\omega r} \frac{\partial}{\partial \theta} \phi^{(e)} \\ H_\theta &= \frac{1}{r} \frac{\partial^2}{\partial z \partial \theta} \phi^{(m)} - \frac{k^2}{i\mu\omega} \frac{\partial}{\partial r} \phi^{(e)} \\ H_z &= \left( k^2 + \frac{\partial^2}{\partial z^2} \right) \phi^{(m)} \end{aligned} \right\} \quad (3)$$

where the  $\phi$ s are related to the  $\bar{E}$  and  $\bar{H}$  vectors by the equations :

$$\left. \begin{aligned} \bar{E} &= \nabla \times \nabla \times (\bar{a}_z \phi^{(e)}) + i\mu\omega \nabla \times (\bar{a}_z \phi^{(m)}) \\ \bar{H} &= \frac{k^2}{i\mu\omega} \nabla \times (\bar{a}_z \phi^{(e)}) + \nabla \times \nabla \times (\bar{a}_z \phi^{(m)}) \end{aligned} \right\} \quad (4)$$

Here  $\bar{a}_z$  is a unit vector in the  $z$  direction and the angular frequency of the sinusoidal field appearing in the expression  $e^{-i\omega t}$ , which has been omitted

\* The units used are the rationalized M. K. S. system of units.

in the above equations for brevity. The scalar functions  $\phi^{(e)}$  and  $\phi^{(m)}$  must individually satisfy the wave equation

$$\nabla^2 \phi + k^2 \phi = 0 \quad \dots (5)$$

where

$$k^2 = \mu \epsilon \omega^2 + i \mu \sigma \omega \quad \dots (6)$$

$k$  being the usual propagation constant with the convention that the imaginary part of  $k$  is always positive. Fields derived from  $\phi^{(e)}$  and  $\phi^{(m)}$  are usually referred to as Transverse Magnetic (TM) and Transverse Electric (TE) waves respectively.

Let the radius of the circular tube be  $a$  and let the discussion be confined to TM waves having radial symmetry for the sake of algebraic simplicity. Then the functions  $\phi^{(e)}$  and  $\phi^{(m)}$  must be of the form :

$$\phi_1^{(e)} = \frac{A}{\lambda_1^2} \frac{J_0(\lambda_1 r) e^{ihz}}{J_0(\lambda_1 a)}; \quad \phi_1^{(m)} = 0 \quad \dots (7)$$

$$\phi_2^{(e)} = \frac{A}{\lambda_2^2} \frac{H_0^{(1)}(\lambda_2 r) e^{ihz}}{H_0^{(1)}(\lambda_2 a)}; \quad \phi_2^{(m)} = 0 \quad \dots (8)$$

where the subscripts 1 and 2 refer to the regions inside  $r < a$  and outside  $r > a$  respectively and  $h$  is the propagation factor,  $J_0$  is the Bessel function and  $H_0^{(1)}$  is the Hankel function of the first kind. To satisfy the wave equation (5) these solutions satisfy the relations :

$$\lambda_1^2 + h^2 = k_1^2 \text{ and } \lambda_2^2 + h^2 = k_2^2 \quad \dots (9)$$

and so,

$$\lambda_2^2 = \lambda_1^2 + (k_2^2 - k_1^2) \quad \dots (10)$$

The continuity of the tangential components of  $H$  at  $r=a$  requires that

$$\frac{k_1^2 J_1(u)}{\mu_1 u J_0(u)} = \frac{k_2^2 H_1^{(1)}(V)}{\mu_2 V H_0^{(1)}(V)} \quad \dots (11)$$

$$\text{where } u = \lambda_1 a \text{ and } v = \lambda_2 a$$

The pair of equations (10) and (11) are satisfied only by certain discrete values of the parameters  $u$  and  $v$ . The physically feasible solutions require that the imaginary part of the roots  $V_n$  be positive.

Certain features of equation (11) in some special cases are interesting. When the conductivities of both the media inside as well as outside the cylinder are zero, so that  $k_1$  and  $k_2$  are both real, it can be easily shown that there are no proper roots if  $k_1 < k_2$  and only a limited number of proper roots—roughly  $a \sqrt{k_1^2 - k_2^2} / \pi$ , if  $k_1 > k_2$ . This result agrees with that of Hondros and Debye (1910). But when one or both of the conductivities  $\sigma_1$  or  $\sigma_2$  are finite, the  $k$ 's are no longer real, and the problem becomes a little complicated. To consider a typical case, let the medium outside the cylinder be a metal so that  $k_2$  is very large. Then for the lower order modes it is easily seen that  $V_n$  has a positive imaginary part as required. But when  $n$  is sufficiently large, the imaginary part

of  $V_n$  may or may not be positive. To ascertain this, consider the following relations which hold good when  $n$  is large :

$$\left. \begin{aligned} |u_n| &\gg 1 \\ |u_n^2| &\gg |k_2^2 - k_1^2| \\ |u_n a| &\gg |k_2^2 \mu_1 / 8 k_1^2 \mu_2| \end{aligned} \right\} \quad (12)$$

Then  $V_n$  should be of the form :

$$V_n = -\alpha u_n - \frac{1}{2} \frac{\alpha}{u_n} (k_2^2 - k_1^2) + f(u_n^{-3}) \quad (13)$$

where

$$\alpha = \pm 1$$

Using Hankel's asymptotic expressions for the Bessel functions valid for terms of order  $\frac{1}{|u_n|} \ll 1$ , the following relations are obtained for the higher order roots of equation (11) :

$$u_n a \approx -\left(n - \frac{1}{4}\right)\pi - \tan^{-1} \left( \frac{\mu_1 k_2^2 \alpha}{i \mu_2 k_1^2} \right) + \frac{1}{8\pi n} \frac{3\mu_2 k_1^2 - \mu_1 k_2^2}{\mu_2 k_1^2 + \mu_1 k_2^2} + f(n^{-2}) \quad \dots \quad (14)$$

and,

$$\begin{aligned} V_n a \approx x\pi \left(n - \frac{1}{4}\right) + \alpha \tan^{-1} \left( \frac{\alpha \mu_1 k_2^2}{i \mu_2 k_1^2} \right) - \frac{\alpha}{8\pi m} \frac{3\mu_2 k_1^2 - \mu_1 k_2^2}{\mu_2 k_1^2 + \mu_1 k_2^2} \\ + \frac{\alpha a^2}{2n\pi} (k_1^2 - k_2^2) + f(n^{-2}) \end{aligned} \quad (15)$$

The second term on the right hand side of equation (15) determines uniquely whether the imaginary part of  $V_n$  is positive or not. Since the imaginary part of  $\tan^{-1}\theta$  has the same sign as the imaginary part of  $\theta$  and since  $\alpha^2 = 1$  it follows that

$$\left[ \frac{\mu_1 k_2^2}{i \mu_2 k_1^2} \right] = - \frac{\sigma_1 \sigma_2 + \epsilon_1 \epsilon_2 \omega^2}{\sigma_1^2 + \epsilon_1^2 \omega^2} < 0$$

Thus the imaginary part of  $V_n$  will be negative instead of positive, as required.

For the case of a perfect dielectric inside a metal  $\sigma_1$  will be zero and  $\sigma_2$  will be very large so that equation (15) becomes :

$$\begin{aligned} V_n a \approx \left(n - \frac{1}{4}\right)\pi + \left( \frac{\pi}{2} - \frac{\epsilon_1 \omega}{\sigma_2} - i \frac{\epsilon_1 \epsilon_2 \omega^2}{\sigma_2^2} \right) + \frac{1}{8\pi m} \left( 1 + \frac{4i\epsilon_1}{\sigma_2} \right. \\ \left. + \frac{a^2 \omega^2}{2m\pi} \left( \mu_2 \epsilon_2 - \mu_1 \epsilon_1 + i \frac{\mu_2 \sigma_2}{\omega} \right) \right) \end{aligned} \quad (16)$$

The imaginary part of  $V_n$  will then be positive only if

$$m < \frac{a^2 \mu_2 \sigma_2^3}{2\pi \omega \epsilon_1 \epsilon_2} \quad (17)$$

Since the conductivity occurs in the third power, the number of permissible normal mode solutions will be very large for metallic wave guides, where

as, for dielectric wave guides, the number will be very small. In fact in the limiting case of zero conductivity there will be no solutions of the normal mode type. Even in case of metallic wave guides, since there are only a finite number, though large, of normal mode solutions they cannot form a complete set or represent the complete field of a given source. The additional solutions required to form a complete solution of the problem will probably be negligible for all practical calculations on metallic wave guides but will certainly contribute an appreciable part in the case of dielectric wave guides.

Thus the usual methods of dealing with electromagnetic wave propagation in wave guides, leading to solutions just of the normal mode type are not adequate to describe the complete field of a given source. The inadequacy is particularly evident in case of dielectric wave guides. The problem is whether the transition from the case in which there are no normal mode type of solutions for zero conductivity to that in which there exists a complete set of normal mode type of solutions for infinite conductivity occurs abruptly when the conductivity changes from zero to a small but finite value, or in steps as the conductivity is gradually increased, or abruptly when the conductivity changes from a large but finite value to infinity.

This question will be dealt with in detail in another paper dealing with an exact solution of the above problem

#### ACKNOWLEDGMENT

This work was done at the National Bureau of Standards Washington, D. C., for whose facilities, the author is grateful.

NATIONAL PHYSICAL LABORATORY OF INDIA  
NEW DELHI

#### REFERENCES

- Condon, E. U., 1942, *Rev. Mod. Phys.*, **14**, 341.  
Hondros, D., and Debye, P., 1910, *Ann. der Phys.*, (4) **32**, 465.  
Slater, J. C., 1942, *Microwave Transmission*.  
Sommerfeld, A., 1912, *Jahresbericht der Deutschen Math. Vereinigung*, **21**, 309





# THE MISSING HEAVY ELEMENTS\*

BY N. K. SAHA AND JAGDISH VERMA

(Received for publication, July 3, 1951)

**ABSTRACT.** With a view to analysing the possible causes of (1) absence of natural elements having atomic number  $Z > 92$  and (2) non-occurrence of isotopes of the  $(4n+1)$  type among the natural elements, the known isotopes of 92 N and of the transuranium elements from 93 Np to 95 Cm are compiled from the recent works of Seaborg and others. A plot of the Heisenberg energy surfaces for the observed  $\alpha$ -emitting nuclei on a neutron-proton diagram reveals the probable existence of an energy-high in the region of lower isotopes of N, Np and Pu. Natural extinction of these isotopes by short-life radioactive  $\alpha$ -decay is, therefore, considered possible. The mean life of spontaneous fission of heavy isotopes is also calculated from Turner's extension of Bohr and Wheeler's theory of nuclear fission. The results show that the elements 95 Am and higher would have too short mean fission life to survive in nature. The higher isotopes of 93 Np and 94 Pu present difficulties as neither their radioactive decay period nor spontaneous fission life seems to be short enough to account for their non-existence. The processes of production of these isotopes by the observed nuclear reactions in the laboratory are compared with the natural processes of formation of heavy elements in the interior of dense stars as postulated by Weissäcker, Mayer and Teller and others. It is pointed out that, unlike in the laboratory reactions, the heavy elements are probably formed in the stellar processes in very high states of excitation favourable for spontaneous fission and subsequent neutron evaporations from the fission fragments which can lead only to lower isotopes of medium heavy elements. This seems to offer at least a qualitative explanation of the absence of heavy isotopes of Np and Pu in nature, the lower isotopes of which are, as already shown, highly unstable against radioactive decay. The same reason makes it possible that the nuclear reactions which lead to the formation of  $(4n+1)$  nuclei in the laboratory cannot take place in the stellar processes on account of serious competition from spontaneous fission processes of the highly excited heavy nuclei formed in these processes.

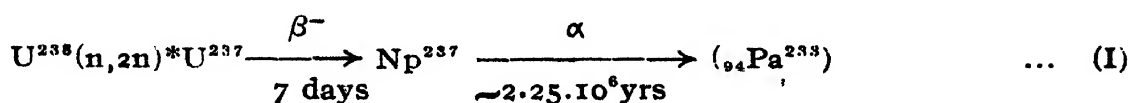
Natural radioactive elements fall under the three well-known families, U-Ra, Th and Ac-series, which all begin with a long lived heavy parent element, pass through comparatively short-lived intermediate products and ultimately terminate in a stable end product, which is an isotope of Pb. The heaviest element occurring in the series is  ${}_{92}\text{U}^{238}$ , the parent of the U-Ra-series, having an  $\alpha$ -decay mean half-life  $T \sim 4.5 \times 10^9$  years.  ${}_{91}\text{Pa}^{231}$ , the parent of the Ac-series, is geneologically connected to a rarer isotope of uranium,  $\text{U}^{235}$  ( $T \sim 7.1 \times 10^8$  years) through an  $\alpha$ - and  $\beta^-$ -disintegration. The Th-series originates from  ${}_{90}\text{Th}^{232}$  itself possessing a mean half-life  $\sim 1.39 \times 10^{10}$  years. The nuclear masses occurring in the three-series are of the  $(4n+2)$ ,  $4n$  and  $(4n+3)$  type respectively. The three series run nearly parallel courses in many respects in their decay processes and

\* Communicated by Prof R. C. Majumder.

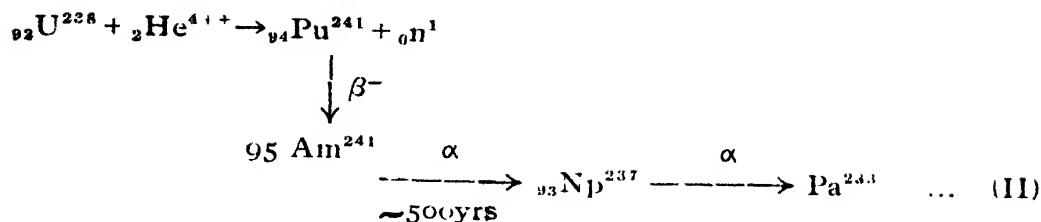
altogether 42 radioactive nuclei occur under them. There are, however, two outstanding features of these nuclei, the significance of which is not yet clearly understood, namely, (1) elements with atomic number ( $Z$ ) higher than 92 do not occur, (2) no member of a radioactive series of the type  $(4n+1)$  occurs among the natural isotopes. Attempts have been made by Turner (1945), Feather (1944-46) and others to analyse the possible cause of absence of elements higher than  $Z=92$ , as being either very high susceptibility to spontaneous fission or short-life radioactivity of the absent heavy nuclei. Sufficient data regarding radioactive decay of heavy nuclei in or near this region did not exist at that time to lead to any definite conclusion on the point; but as pointed out by Feather (*loc.cit.*), the possibility of spontaneous fission being the cause of extinction of the heavy elements beyond uranium seemed to be more or less ruled out. Regarding the non-occurrence of the  $(4n+1)$ -radioactive series, it has been argued that the elements that could be considered as natural starting points of the series are  $\text{Th}^{233}$ ,  $\text{U}^{237}$ ,  $\text{U}^{233}$  or  $\text{Np}^{237}$ , and that none of these nuclei are likely to form in nature, as the  $\alpha$ - or  $\beta^-$ -disintegrations of the corresponding nuclei which would lead to these parent nuclei do not appear to be possible (Stephens, 1948).

The position has changed somewhat since the discovery of the transuranium elements 93Np, 94 Pu, 95 Am 96 Cm in the laboratory and considerable progress in the studies of their properties. Several isotopes of these elements have now been identified by Seaborg and his associates and their radioactive properties carefully investigated. The relevant results are collected in Table I below (Seaborg, 1942 ; 1946). The purpose of this note is to review the present position of the problem in the light of these new data and to examine the possibility of any further progress in its solution.

Np 239 and Pu 239 are produced in the non-fission neutron-capture in  $\text{U}^{238}$  followed by two successive  $\beta^-$ -disintegrations (McMillan and Abelson, 1940). The non-fission capture process in  $\text{U}^{238}$  shows a resonance effect at the neutron energy  $E_n \sim 25$  eV (Meitner, Hahn and Strassmann, 1937). Pu 239 is  $\alpha$ -active having a mean half-life of  $\sim 24,000$  years. The first isotope of Np and Pu to be discovered was, however, 238, by the  $(d, 2n)$  process in  $\text{U}^{238}$  followed by a  $\beta^-$ -disintegration of  $\text{Np}^{238}$  with 2 days half-life (Seaborg, McMillan, Wahl and Kennedy, 1941). Then the lighter isotope  $\text{Np}^{237}$  was obtained by Wahl and Seaborg (1942) by the reaction :



$\text{Np}^{237}$  has a long half life of  $\alpha$ -decay and degenerates into  $\text{Pa}^{233}$ . The transplutonium element  $\text{Am}^{241}$  was produced by bombarding  $\text{U}^{238}$  with 40-44 MeV  $\text{He}^{4++}$  nuclei in the Berkeley cyclotron (Seaborg, 1945). Possible reactions involved are :



The highest element  ${}_{96}\text{Cm}^{242}$  has also been synthesised with the fast  $\text{He}^{4+}$  ions by the reaction  $(\alpha, n)$  in  $\text{Pu}^{239}$  which was already obtained by the simple capture of  ${}_0\text{n}^1$  in  $\text{U}^{238}$ .  $\text{Cm}^{242}$  has probably a short  $\alpha$ -decay life of the order of five months. A branch reaction  $(\alpha, 3n)$  in  $\text{Pu}^{239}$  also gives  $\text{Cm}^{240}$  having a still shorter  $\alpha$ -half life of  $\sim 1$  month.

TABLE I  
Transuranium and uranium isotopes

${}_{93}\text{Np}$	${}^{234}\text{K}, \gamma$ 4.4 d.	${}^{235}\text{K}$ 8 mo.	${}^{236}\beta^-$ 20 hrs	${}^{237}2\ 25\ 10^6\ \text{yrs}$ (408)	${}^{238}\beta^-$ 2 d.	${}^{239}\beta^-$ 2.3 d	${}^{231}53\ \text{min.}$ (6 2)
${}_{94}\text{Pu}$	${}^{232}22\ \text{min.}$ (6.6)	${}^{234}8\ \text{hrs.}$ (6.2)	${}^{236}2.7\ \text{yrs}$ (5.7)	${}^{238}50\ \text{yrs.}$ (5.5)	${}^{339}24,000\ \text{yrs.}$ (5.1)	${}^{240}6,000\ \text{yrs.}$ (5.1)	${}^{241}\sim 10\ \text{yrs.}$ (5.0)
${}_{95}\text{Am}$			${}^{239}\sim 12\ \text{hrs}$ (5.8)	${}^{241}500\ \text{yrs.}$ (5.5)	${}^{242}\sim 400\ \text{yrs.}$ (5.2)		
${}_{96}\text{Cm}$			${}^{238}\sim 2.5\ \text{hrs.}$ (6.5)	${}^{240}\sim 1\ \text{mo}$ (6.3)	${}^{242}5\ \text{mo.}$ (6 1)		
${}_{92}\text{U}$	${}^{228}9.3\ \text{min.}$ (6 72)	${}^{229}58\ \text{min.}$ (6.42)	${}^{230}20\ 8\ \text{d.}$ (5.85)	${}^{232}\ 234\ 70\text{--}30\ 2.3\cdot 10^6\ \text{yrs.}$ (5.3) (4.75)	${}^{235}8.9\cdot 10^8\ \text{yrs.}$ (4.52)	${}^{*237}\beta^-$ 6 8 d.	${}^{238}\ 239\ 4.5\cdot 10^9\ \beta^- 23\ \text{yrs.}$ (4 13) min.

(*Italicised data* are from Seaborg and Perlman (1948). All figures in parenthesis denote radiation energy in MeV. All nuclei are  $\alpha$ -emitters, except stated otherwise. When a nucleus decays by  $\beta^-$  or  $\gamma$ -emission or by K-electron capture, the emitted radiation is mentioned below the isotope). \*Stephens (1948).

With the new data for many artificially produced heavy radioactive isotopes thus available, we may examine afresh the possible reasons why the heavy elements beyond  $Z=92$  would be missing in nature. The limits of stability of nuclei against  $\alpha$ -emission have been examined by Heisenberg (Solvay Congress, 1933) by plotting the energy surfaces of the radioactive nuclei for  $\alpha$ -emission on a neutron-proton ratio diagram of elements. The general treatment of this type gives a reasonable account of known natural radioactive isotopes, the shortlived C'-products falling into a closed region of energy-high. The new data for  $\alpha$ -emission from heavy nuclei as far as curium (96) are, therefore, plotted on an extension of the Heisenberg diagram shown in figure 1. The energy values have been taken, wherever

available, from the experimental data published by Seaborg and others (1942, 1946) from time to time and also from the comprehensive review\* of data by Seaborg and Perlman (1948). Doubtful energy values not confirmed by more than one sources and which do not agree with an extrapolation of the Geiger-Nuttall curves have not been plotted.

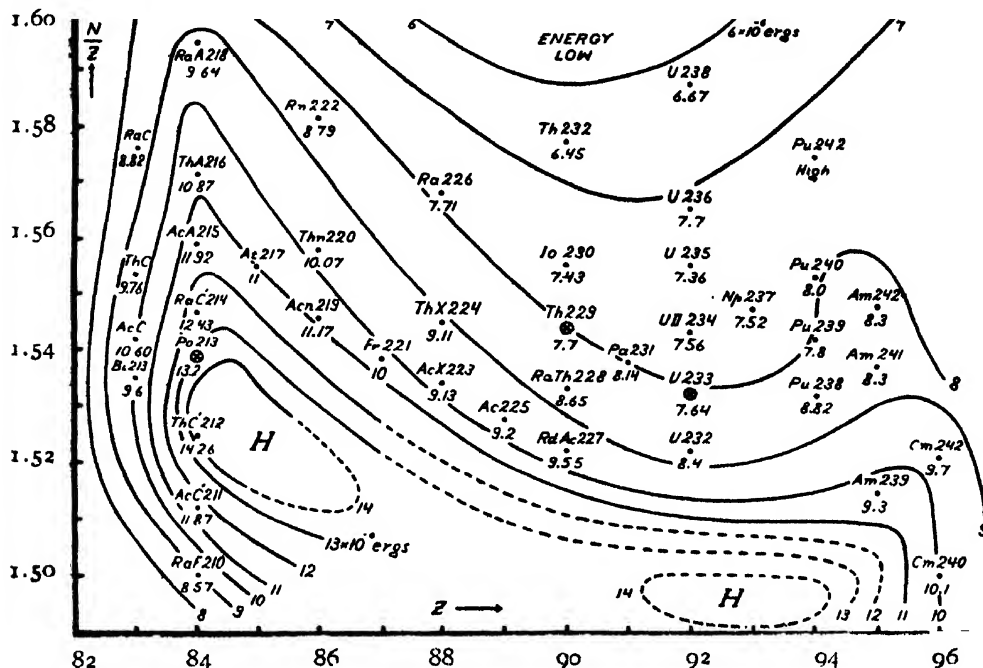


FIG. 1

TABLE II

Isotopes of the  $(4n+1)$  series. Seaborg (1941).

Nucleus	Radiation	Half-life	Energy of radiation
$^{92}\text{U}^{233}$	$\alpha$	$1.62 \times 10^5$ yrs.	4.80 MeV
$^{90}\text{Th}^{229}$	$\alpha$	$7000 \pm 2000$ yrs.	4.45
$^{89}\text{Ac}^{227}$	$\alpha$	$10.1 \pm 0.1$ day.	5.80
$^{87}\text{Fr}^{221}$	$\alpha$	$4.8 \pm 0.1$ min.	6.30
$^{85}\text{At}^{217}$	$\alpha$	$0.018 \pm 0.002$ sec.	7.00
$^{83}\text{Bi}^{213}$	$\alpha$ (4%)	$47 \pm 1$ min.	6.00
$^{81}\text{Po}^{211}$	$\alpha$	very short.	8.30

The rest of the values have been obtained by an approximate extrapolation of the Geiger-Nuttall curves. The values for  $\text{Th}^{229}$  and  $\text{Po}^{211}$ , two members of the  $(4n+1)$  series, taken from Table II (see discussion at the end)

are seen to fit well in the curves. These two new isotopes, among the well-known radioactive elements, serve well as a check on the new experimental data. The value for  $U^{233}$  from the same experimental source does not, however, agree so well. The values extrapolated from the G. N.-curve appear to be slightly higher than the experimental energy values in general wherever both the values are available for comparison. But the difference is not so serious as to affect the general run of the Heisenberg curves, which can, therefore, be taken as fairly representative. The position beyond the element 92 is obviously far from satisfactory. But the two isotopes  $Cm^{242}$  and  $Cm^{240}$  are of great significance as they help to close up the energy curves 10 upwards on the lower side of the  $N/Z$  scale. Thus the existence of a second high energy closed region between  $Z=91$  and 94 near the bottom of the  $N/Z$  scale appears to be fairly certain. We can, therefore, conclude that the lower isotopes of these elements from U to Pu would be highly unstable towards  $\alpha$ -decay, and it is no wonder that they do not exist in the earth's crust which formed a few thousand millions years ago.

The higher isotopes of these elements clearly fall on a flat plateau region on the energy diagram. Their  $\alpha$ -decay lives are, therefore, not short enough to account for their natural extinction. It is, therefore, necessary to examine the possibility of their decay by alternative mechanisms, like spontaneous fission, neutron-evaporation and  $\beta^-$ -emission. The last two alternatives do not probably play any part, as the neutron-evaporation process would lead to lower isotopes which would decay by radioactive emission, while  $\beta^-$ -emission would lead to still higher elements which would readily die out by spontaneous fission.

The relative probability of spontaneous fission of heavy isotopes have been considered by Bohr and Wheeler (1939) and by L. A. Turner (1945). While it is clear that the limit of instability of nuclei by spontaneous fission sets in at  $(Z^2/A)$  critical  $\geq 47.8$ , Turner has shown that the mean life of spontaneous fission of a heavy nucleus is approximately given by

$$\tau_f \approx \frac{1}{\lambda_f} \approx 10^{-21} \exp. [(2 M E_f)^{\frac{1}{2}} \cdot \alpha / \hbar]$$

$$\approx k. \exp. \{A^{7/6} \cdot [f(x)]^{\frac{1}{2}}\}$$

where  $f(x) = 98(1-x)^3 / 135 - 11368(1-x)^4 / 34425 + \dots$

$$x = (Z^2/A) \div (Z^2/A)_{\text{critical}}, \quad k = \text{constant},$$

$$E_f = 4\pi r_0^2 \cdot O. A^{2/3} \cdot f(x),$$

and the other symbols have their usual meanings. According to this,  $94 Pu^{239}$  should be about 7000 times more spontaneously fissionable than  $U^{235}$  which shows spontaneous fission to the extent of  $\approx 1\%$  of the radioactive  $\alpha$ -decays.  $Pu^{239}$  has, therefore, a spontaneous fission life  $\tau_f \approx 100.7 \times 10^6 / 7000$  years  $\approx 10^7$  years. The ratio of spontaneous fission life of a nucleus to that of

$\text{Pu}^{239}$ , denoted by  $R_f$ , the relative mean fission life is computed for a number of isotopes by the above formulae and collected in the Table III below.

TABLE III

Spontaneous fission life,  $R_f$ , of heavy nuclei relative to  $\text{Pu}^{239}$   
[recalculated from  $f(x)$ ].

		$R_f$			$R_f$
92 U	235	$7.6 \cdot 10^3$	94 Pu	244	$5.2 \cdot 10^4$
	233	$1.1 \cdot 10^3$		242	$5.9 \cdot 10^2$
				241	62
93 Np	237	66	96 Cm	229	1.00
				238	0.12
95 Am	243	0.51		240	$7.2 \cdot 10^{-7}$
	241	0.011		242	$7.4 \cdot 10^{-6}$

$R_f$  = Ratio of spontaneous fission life of a nucleus to that of  $\text{Pu}^{239}$ .

The above results show that only Am and Cm possess fission mean life low enough to decay completely from the earth's crust in course of geological epochs. Elements higher than Cm will have, of course, still less chance of surviving.

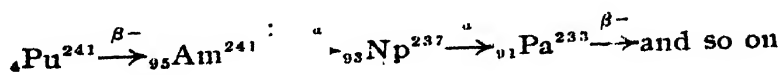
The position of heavy nuclei, therefore, appears to be this: Lower isotopes of elements from 92U to 94 Pu would be extinct through short life  $\alpha$ -emission, while the absence of still heavier elements Am and Cm would be accounted for by their high susceptibility to spontaneous fission. The higher isotopes of Np and Pu, which are produced in the laboratory, but do not exist in nature in any appreciable extent are still to be accounted for. Perhaps we can look for an explanation to the probable mechanism of evolution of heavy elements originally in the cosmology as postulated by Weizäcker (1947), Gamow (1948), Mayer and Teller (1948) and others (Haar, 1949).

In the original formation of heavy elements in the interior of very dense and hot stars there must have been heavy nuclei present, because large neutron excess is required for stability of these nuclei in view of strong coulomb interaction of protons. Nuclei with such large neutron excess will not be stable, but would break up by spontaneous fission. The fission products would be unstable and through radioactive changes decay finally into stable nuclei. Mayer and Teller have considered these processes in detail; they assume that after the fission of the neutron-rich nuclei the residual nuclei will be highly excited. The excess energy of excitation will be first relieved of through "neutron evaporation from the droplet of nuclear

fluid". If the energy of the nucleus has decreased so far that no more neutrons can evaporate, normal radioactive processes will follow, which will most frequently be  $\beta^-$ -processes ( $N \xrightarrow{\beta^-} P^+$ ). The final results will be a stable nucleus—one of the isotopes observed in nature. Starting from the concentrations of neutron-rich nuclei from the stellar interior and making reasonable assumptions as to the excitation energy of the fission products, one can calculate the abundance of the stable isotopes on these lines. Mayer and Teller have found reasonably good agreement between the observed and the calculated values of abundances obtained in this way.

The production of the transuranium elements in the laboratory is probably a process quite analogous to the above natural process, but the degree of energy excitation of the neutron-rich nuclei obtained by the neutron-capture process in  $U^{238}$  in the laboratory is much lower than that attainable in the stellar processes. Consequently the subsequent  $\beta^-$ -decay process of the compound nucleus formed by the neutron-capture has to suffer little or no competition with the fission process. It is unlikely, therefore, that the neutron-evaporation process can proceed very far, or set in at all. Quite heavy neutron-capture products are, therefore, left behind which, on account of  $\beta^-$ -instability setting in quite early, transform gradually to heavier isotopes of Np, Pu, Am and Cm. In the natural evolution process, on the contrary, the fission of very heavy nuclei, followed by neutron-evaporations and  $\beta^-$ -decays, probably cannot yield nuclei beyond Th or U.

A few speculative remarks can now be made in the light of the above discussions regarding the non-occurrence of isotopes of the  $(4n+1)$ -series among the natural radioactive elements. Turner's (1940) suggestion that the starting point of the  $(4n+1)$ -radioactive series would be  $_{92}U^{237}$  has not been wholly fulfilled in practice. Extensive experimental researches carried out in connection with the plutonium project have led to the observation of many members of this series and establishment of the sequence of disintegrations almost in complete agreement with Turner's prediction. Only the starting point of the series is found to be the long life  $\alpha$ -active  $Np^{237}$  which comes out to be genetically related to  $Pu^{241}$  and  $Am^{241}$  according to the following scheme :



The first two members enclosed separately replace  $U^{237}$  in Turner's suggestion. The  $\alpha$ -emitting nuclei which occur in this series are reproduced (Seaborg, McMillan and others, 1941) in Table II, together with their periods and energy of radiation and have been plotted in the energy diagram, figure 1.

As stated under scheme (II),  $\text{Pu}^{241}$  is produced from an  $(\alpha, n)$ -reaction in  $\text{U}^{238}$  by a non-fission capture of 40-44 MeV.  $\alpha$ -particle. An alternative process of production of  $\text{Np}^{237}$  is shown in scheme I, which consists of an  $(n, 2n)$ -reaction in  $\text{U}^{238}$  resulting in  $\text{U}^{237}$ , which is a  $\beta^-$ -active body giving rise to  $\text{Np}^{237}$ . Cross-section for this reaction, as for all  $(n, 2n)$ -reactions (Weisskopf, 1950), is extremely small. Therefore, the main reaction giving the isotope  $\text{Np}^{237}$  in the laboratory must be that under scheme II involving the non-fission capture of an  $\alpha$ -particle in  $\text{U}^{238}$ . But under natural conditions of stellar evolution the non-fission capture will have very little probability, as due to high excitation of the compound nucleus  $\text{Pu}^{242}$  formed, the fission process would be a serious competitor of the non-fission capture; indeed the spontaneous fission of  $\text{Pu}^{242}$  may be the main process in nature. This seems to offer at least a qualitative explanation of the non-occurrence of the members of the  $(4n+1)$ -series among the natural radioactive elements.

DEPARTMENT OF PHYSICS  
UNIVERSITY OF DELHI.  
DELHI

#### REFERENCES

- Alpher, Herman and Gamow, G. 1948, *Phys. Rev.* **74**, 1198 and 1737, *Nature*, **162**, 774  
 Bohr, N., and Wheeler, J. A., 1937, *Phys. Rev.*, **56**, 526.  
 Feather, N., 1944-46, *Proc. Roy. Soc. Edin.* LXII, 211.  
 Haar, D. T. 1949, *Am. J. Phys.* **17**, 282.  
 Heisenberg, 1933, Report of the Solvay Congress.  
 Mayer, M. G., and Teller, E., 1948, Solvay Congress.  
 McMillan, E. M. and Abelson, 1940, *Phys. Rev.* **57**, 1185.  
 Meitner, L., Hahn, O. and Strassmann, F., 1937, *Z. f. Phys.* **106**, 249.  
 Seaborg, G. T., 1942, *Chemical and Engineering News*, **24**, 1192;  
 „ „ 1945, *Science*, **23**, 2190  
 „ „ 1946, *Science*, **124**, 379.  
 Seaborg, G. T., McMillan E. M., Wahl, A. C., and Kennedy, J. W., 1941, *Phys. Rev.* **69**, 366.  
 Seaborg, G. T., and Perlman, I., 1948, *Rev. Mod. Phys.* **20**, 585.  
 Stephens, W. B., 1948, *Nuclear Fission and Atomic Energy* (The Science Press), p 55.  
 Turner, L. A., 1940, *Phys. Rev.*, **57**, 940.  
 Turner, L. A. 1945, *Rev. Mod. Phys.*, **17**, 292.  
 Wahl, A. C., and Seaborg, G. T., 1948, *Phys. Rev.* **73**, 940  
 Weissacker, C. F. von., 1947, *Z. f. Phys.* **24**, 181.  
 Weisskopf, V., 1950, *Helv. Phys. Acta*, **23**, 187.

\* A complete summary now appears in 'The Transuranium Elements, Part II, p 1274 Seaborg, Katz and Manning (1949), National Nuclear Energy Series, Manhattan Project, Technical Section.



# RIGOROUS SOLUTION FOR THE CASE OF ELECTROMAGNETIC WAVE PROPAGATION ALONG A CIRCULAR WAVE GUIDE OF FINITE CONDUCTIVITY

By K. V. KRISHNA PRASAD

(Received for publication, March, 15, 1951)

**ABSTRACT.** The complete solution for the propagation of electromagnetic waves along a circular wave guide has been worked out. The final solution can be grouped into two parts. One part which can easily be computed in practice has the form of the usual normal mode type solutions, but they are neither orthogonal nor a complete set. The other part represented by contour integrals cannot be so easily computed. In the case of metallic wave guides the contribution by the latter type of fields is indeed negligible, but they do have practical significance and contribute a major part in case of wave guides of small conductivity.

## INTRODUCTION

In a previous paper by the author (1951) it was shown that the usual methods of dealing with electromagnetic wave propagation in wave guides, leading to solutions just of the normal mode type are not adequate to describe the complete field of a given source. The additional solutions, though necessary to form a complete solution of the problem, may not be significant in case of metallic wave guides, but they do form a major part in the case of guide walls of finite conductivity, as for example, in the practical case of dielectric wave guides.

The clue to obtain these additional solutions or rather the complete solution of the problem is found in a paper by Sommerfeld (1912), which gives the connection between the normal mode solutions and the residues of a contour integral while discussing the eigenfunction problem for finite regions. And so a solution in the form of a contour integral of the Green's function may give the desired result. In this process, those normal mode solutions, which are permissible for the infinite region under consideration, will automatically appear as the residues of the contour integral.

## THEORY

As a general case of the source field, consider the field of an electric dipole of moment  $P_0$  located at the point  $Z=0$ ,  $r=r_0$  and  $\theta=\theta_0$ , within the cylinder of radius  $a$ . Let the axis of the dipole make an angle  $\alpha$  with the  $Z$  axis and let its projection on the  $Z=0$  plane make an angle  $\beta$  with the  $X$ -axis ( $\theta=0$ ).

Following Stratton (1941), the expressions for the electric and magnetic field intensities of the dipole in an infinite, homogeneous, isotropic medium are :

$$\begin{aligned}\bar{E} &= \nabla \times \nabla \times (\bar{P} e^{ikR/4\pi\epsilon R}) \\ \bar{H} &= -\frac{k}{i\mu\omega} \nabla \times (\bar{P} e^{ikR/4\pi\epsilon R})\end{aligned}\quad (1)$$

where  $\epsilon$  is the dielectric constant,  $\mu$  is the permeability and  $k$  is the propagation constant,  $\omega$  is the angular frequency of the radiation and  $R = \sqrt{r_1^2 + Z^2}$  where  $r_1$  is the radial distance from the dipole to the point of observation. The vector  $\bar{P}$  is given by

$$\bar{P} = P_0 (\bar{i}_\phi \sin \alpha \cos \theta_1 - \bar{i}_\theta \sin \alpha \sin \theta_1 + \bar{i}_z \cos \alpha)$$

where  $\theta_1$  is the angle between  $r_1$  and the projection of  $\bar{P}$  on the  $Z=0$  plane. The corresponding field potentials of the source are :

$$\phi_s^{(1)} = \frac{P_0}{4\pi\epsilon} \left( \cos \alpha - \frac{Z}{r_1} \sin \alpha \cos \theta_1 \right) e^{ikR/R} \quad (2)$$

and

$$\phi_s^{(2)} = -\frac{P_0}{4\pi\epsilon} \frac{k}{\mu\omega} \frac{\sin \alpha \sin \theta_1}{r_1} e^{ikR} \quad \dots \quad (3)$$

where the superscripts 1 and 2 refer to the transverse magnetic and transverse electric cases respectively.

The spherical forms in equations (2) and (3) should be converted into cylindrical ones, so as to match the fields at the cylindrical surface ( $r=a$ ) with the result :

$$\phi_s^{(1)} = \frac{P_0}{8\pi\epsilon} \int_{-\infty}^{\infty} \left\{ i \cos \alpha H_0^{(1)}(ur) + \sin \alpha \cos \theta_1 \frac{h}{u} H_1^{(1)}(u_1) \right\} e^{ihz} dh \quad \dots \quad (4)$$

and

$$\phi_s^{(2)} = \frac{P_0}{8\pi\epsilon} \frac{k_1^2}{\mu\omega} \sin \alpha \sin \theta_1 \int_{-\infty}^{\infty} H^{(1)}(ur) e^{ihz} \frac{dh}{u} \quad \dots \quad (5)$$

In these integrals the  $H^{(1)}$ s are Hankel functions of the first kind and  $u = \sqrt{k_1^2 - h^2}$  with the path of integration below the branch point at  $h = k_1$  in the first quadrant,  $h$  is the familiar propagation factor.

The total field potential which is a combination of  $\phi_s^{(1)}$  and  $\phi_s^{(2)}$  plus the non-singular fields may be written as :

$$\phi_1^{(m)} = \sum_{n=-\infty}^{\infty} e^{in\theta} \int_{-\infty}^{\infty} \left\{ \bar{F}_n^{(m)}(h) J_n(ur) - F_n^{(m)}(h) G_n^{(m)}(h) J_n(ur) \right\} e^{ihz} \times dh$$

for  $0 \leq r_0$

$$\phi_n^{(m)} = \sum_{n=-\infty}^{\infty} e^{in\theta} \int_{-\infty}^{\infty} F_n^{(m)}(h) \{ H_n^{(1)}(ur) - G_n^{(m)}(h) J_n(ur) \} e^{ihz} \times dh$$

for  $r_0 \leq a$

$$\text{and } \phi_2^{(m)} = \sum_{n=-\infty}^{\infty} e^{in\theta} \int_{l_1} F_n^{(m)}(h) \{H_n^{(1)}(ua) - G_n^{(m)}(h) J_n(ua)\} \times \frac{H_n^{(1)}(vr) e^{ihz}}{H_n^{(1)}(va)} \frac{u^2}{v^2} dh$$

for  $r \geq a$  ... (6)

In these expressions, the superscript  $(m)$  in general can be either 1 or 2 ;  $u = \sqrt{k_1^2 - h^2}$  and  $v = \sqrt{k_2^2 - h^2}$ .  $Z$  is assumed to be positive and the path of integration passes below the branch points at  $h = k_1$  and  $h = k_2$  in figure 1 both  $u$  and  $v$  having imaginary parts along the path. Further,

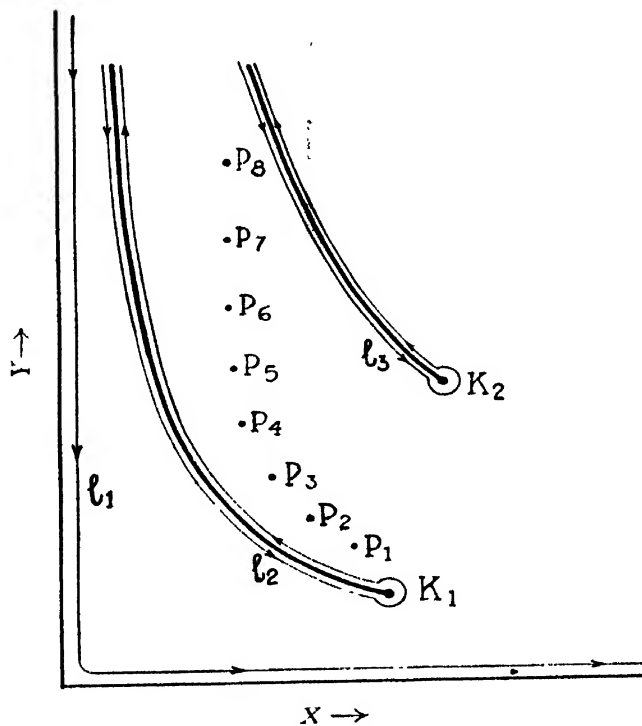


FIG. 1

Path of integration in the  $h = X + iY$  plane

$$F_n^{(1)}(h) = \frac{iP_0}{8\pi\epsilon_1} e^{-in\theta} \left[ \left\{ \cos \alpha - \left( \frac{hn}{u^2 r_0} \right) \sin \alpha \sin \beta \right\} J_n(ur) - \left( \frac{ih}{u} \right) \sin \alpha \cos \beta J_n'(ur_0) \right]$$

and

$$F_n^{(2)}(h) = \frac{iP_0}{8\pi\epsilon_1} \frac{k^2}{i\mu_1 \omega} e^{-in\theta} \left[ -\frac{in}{u^2 r_0} \sin \alpha \cos \beta J_n(ur_0) - \sin \alpha \sin \beta J_n'(ur_0)/u \right] \dots (7)^*$$

\*  $\tilde{F}_n^{(m)}(h) = F_n^{(m)}(h)$  with the Bessel functions  $J_n$  and  $J_n'$  replaced by  $H_n$  and  $H_n'$  respectively. The prime denotes differentiation with respect to the argument.

And further, the co-efficients  $G_n^{(m)}(h)$  in the set of equations (6) are given by :

$$G_n^{(1)}(h) = \frac{H_n^{(1)}(ua)}{J_n(ua)} \left\{ 1 + \frac{J_n(ua) - H_n^{(1)}(ua)}{A_n(h)} \times \left[ i\mu_1 \omega n h a^{-2} (u^{-2} - v^{-2}) \frac{F_n^{(2)}(h)}{F_n^{(1)}(h)} - f_1(\mu_1 J_n(ua) - \mu_2 H_n^{(1)}(va)) \right] \right\}$$

and

$$G_n^{(2)}(h) = \frac{H_n^{(1)}(ua)}{J_n(ua)} \left\{ 1 + \frac{[J_n(na) - H_n^{(1)}(ua)]}{A_n(h)} \left[ \frac{k_1^2 n h}{i\omega a^2 \mu_1} (u^{-2} - v^{-2}) \frac{F_n^{(2)}(h)}{F_n^{(1)}(h)} - \mu_1 \left( \frac{k_1^2}{\mu_1} J_n(ua) - \frac{k_2^2}{\mu_2} H_n^{(1)}(va) \right) \right] \right\} \quad \dots (8)$$

with

$$A_n(h) = \left\{ \frac{k_1^2}{\mu_1} J_n(ua) - \frac{k_2^2}{\mu_2} H_n^{(1)}(ua) \right\} \{ \mu_1 J_n(ua) - \mu_2 H_n^{(1)}(va) \} - n^2 h^2 a^{-4} (u^{-2} - v^{-2})^2 \quad \dots (9)$$

The functions  $J_n(x)$  and  $H_n^{(1)}(x)$  in equations (8) and (9) are defined by :

$$J_n^{(x)} \equiv \frac{J_n^{(1)}(x)}{x J_n(x)} \quad \text{and} \quad H_n^{(1)(x)} \equiv \frac{H_n^{(1)'}(x)}{x H_n^{(1)}(x)} \quad \dots (10)$$

Equations (8), (9) and (10) result from the continuity of the tangential components  $E_\theta$  and  $H_\theta$  at  $r=a$ , while the continuity of  $E_r$  and  $H_r$  at  $r=a$  is given by the last expression in equation (6). The fields derived from the first two expressions in equation (6) match at  $r=r_0$  while the first terms within the brackets in these represent the source field. For  $r > a$ , the fields represent outgoing waves only.

The integrands in the integrals of equation (6) have branch points at  $h=k_1$  and  $h=k_2$  and poles  $P_j$  at the zeros of  $A_n(h)=0$ . Figure 1 shows the location of these poles. In drawing this figure the Riemann sheet has been so chosen that the real parts of  $u$  and  $v$  are positive below and negative above the hyperbolae passing through  $k_1$  and  $k_2$  respectively. The imaginary parts of  $u$  and  $v$ , however, are positive everywhere. Along an arc at  $|h| \rightarrow \infty$  in the first quadrant the integrands vanish exponentially, and the path of integration will be deformed into the paths  $l_2$  and  $l_3$  around the branch points at  $k_1$  and  $k_2$  plus residues at the poles  $p_j$ . As the integrands of the set of equations in (6) are even functions of  $u$  the integrals along the contour  $l_2$  will vanish. But as they are not even functions of  $v$  the integral along  $l_3$  will give a finite contribution to the total field.

After evaluating the residues at the poles  $p_j$ , the rigorous solution for the complete field of an electric dipole located inside an infinite circular of radius  $a$  may be written in the abbreviated form :

$$\phi_{1,2}^{(m)} = \sum_j B_{1,2}^{(m)}(h_j) + C_{1,2}^{(m)} \quad \dots (11)$$

where the summation over  $j$  includes the sum over all  $n$  and for each  $n$  the sum over all the roots of  $A_n(h_j)=0$  for which the imaginary part of  $V_j$  is positive.

Further,

$$B_1^{(m)}(h_j) = D^{(m)}(h_j) e^{im\theta} J_n(u, r) e^{ih_j Z}$$

$$B_2^{(m)}(h_j) = D^{(m)}(h_j) \frac{u_j^2}{v_j^2} \frac{J_n(u, a)}{H_n^{(1)}(va)} e^{im\theta} H_n^{(1)}(vr) e^{ih_j Z}$$

where,

$$D^{(m)}(h_j) = \frac{-4F_n^{(m)}(h_j)E^{(m)}(h_j)}{\left\{u, aJ_0(u, a)\right\}^2 \left[\frac{d}{dh} A_n(h)\right]_{h=h_j}}$$

$$E^{(1)}(h_j) = \left[ i\mu \omega \frac{nh_j F_n^{(2)}(h_j)}{a^2 F_n^{(1)}(h_j)} (u^{-2} - v^{-2}) - \frac{k_1^2}{\mu_1} \{ \mu_1 J_n(ua) - \mu_2 H_n^{(1)}(va) \} \right]$$

and,

$$E^{(2)}(h_j) = \left[ \frac{k_1^2 nh_j F_n^{(1)}(h_j)}{iu_1 \omega a^2 F_n^{(2)}(h_j)} (u^{-2} - v^{-2}) \right. \\ \left. - \mu_1 \left\{ \frac{k_1^2}{\mu_1} J_n(ua) - \frac{k_2^2}{\mu_1} H_n^{(1)}(va) \right\} \right] \quad (12)$$

The terms  $C_1^{(m)}$  and  $C_2^{(m)}$  in equation (11) are given by the first and third expressions respectively in equation (6) with the path of integration  $l_1$  replaced by  $l_3$ .

The first term in equation (11) can be easily computed by evaluating the roots  $h_j$ , but not so, the second term represented by the  $C$ 's. For a metallic wave guide with  $\sigma_2$  large, the second term in equation (11) falls off very rapidly—as fast as  $e^{-Z\sqrt{\frac{\sigma_2\mu_2\omega}{2}}}$ —for large  $Z$ , as a first approximation. But if  $\sigma_2$  is small as is the case in a dielectric wave guide, the contribution by the  $C$ 's can be significant. As an example, if the conductivity  $\sigma_1$  of the region inside the guide is zero, and that of the guide is small the  $C$ 's in equation (11) for the case of a dipole oriented along the axis of the cylinder are given by the integral expressions:

$$C_1^{(1)} = \frac{-P_0 k_1^2 \mu_2}{4\pi\epsilon_1 k_2^2 \mu_1} \int_{k_1}^{\infty} \frac{4iJ_0(ur)e^{ihZ} dh}{\pi \{uaJ_0(ua)\}^2 H_1^{(1)}(va) H_1^{(2)}(va) X^{(1)} X^{(2)}} \\ C_2^{(1)} = \frac{-P_0 k_1^2 \mu_2}{4\pi\epsilon_1 k_2^2 \mu_1} \int_{k_1}^{\infty} \frac{e^{ihZ}}{vaJ_0(ua)} \left\{ \frac{H_0^{(1)}(vr)}{X^{(1)} H_1^{(1)}(va)} - \frac{H_0^{(1)}(vr)}{X^{(2)} H_1^{(2)}(va)} \right\} dh \\ \text{and} \quad C_1^{(2)} = C_2^{(2)} = 0 \quad \dots (13)$$

where

$$X_{m=1,2}^{(m)} = 1 - \frac{k_1^2 \mu_2 v J_1(ua) H_0^{(m)}(vr)}{k_2^2 \mu_1 u J_0(ua) H_1^{(m)}(va)}$$

and the  $H^{(2)}$ ,  $s$  refer to Hankel functions of the second kind.

For  $Z$  large, the expressions in equation (13) will simplify to the approximate forms :

$$C_1^{(1)} \approx \frac{P_0 k_1 \mu_2}{4\pi\epsilon_1 k_2^2 \mu_1} \frac{J_0(r\sqrt{k_1^2 - k_2^2})}{J_0^2(a\sqrt{k_1^2 - k_2^2})} \frac{2k_2 e^{ik_2 Z}}{iZ^2(k_1^2 - k_2^2)}$$

and,

$$C_2^{(1)} \approx \frac{P_0}{4\pi\epsilon_1} \frac{k_1^2 \mu_2}{k_2^2 \mu_1} \frac{1}{J_0(a\sqrt{k_1^2 - k_2^2})} \frac{e^{(ik_2\sqrt{Z^2 + r^2})}}{\sqrt{Z^2 + r^2}} \dots (14)$$

which have the form of dipole type fields reduced in amplitude at the discontinuity ( $r=a$ ).

Thus the complete field of an electric dipole located inside an infinite circular cylinder can be divided into two parts. The first part represented by the fields  $B_{1,2}^{(m)}$  in equation (11) has the form of the usual normal modes, though they are not orthogonal and do not form a complete set. These fields could be easily computed in any practical case under consideration. The second part represented by the fields  $C^{(m)}_{1,2}$  in equation (11), however, does not lend itself to easy computation. These latter type of fields are not significant and contribute but a negligible correction term in case of metallic wave guides, but they, however, become important and contribute a major part in case of dielectric wave guides. In the special case of a region of zero conductivity bounded by a guide of small conductivity discussed above, the fields  $C^{(m)}_{1,2}$  represent space waves. The field  $C_1^{(1)}$ , in particular, represents energy from the out-going space wave  $C_2^{(1)}$  which has re-entered the region inside the cylinder, because the propagation constant ( $k_2$ ) of the outer medium ( $r > a$ ) occurs in its exponential instead of the propagation constant ( $k_1$ ) of the inner medium, ( $r < a$ ).

#### ACKNOWLEDGMENT

This work was done at the National Bureau of Standards, Washington, D. C., for whose facilities the author is grateful.

NATIONAL PHYSICAL LABORATORY,  
NEW DELHI.

#### REFERENCES

- Krishna Prasad, K. V., 1951, *Ind. J. Phys.*, **25**, 403.  
Sommerfield, A., 1912, *Jahresbericht der Deutschen Math. Vereinigung*, **21**, 309.  
Stratton, J. A., 1941, *Electromagnetic Theory*, p. 434.

# INVESTIGATION ON THE BOWED STRING WITH AN ELECTRICALLY DRIVEN BOW. (PART I)

By K. C. KAR, N. K. DATTA, AND S. K. GHOSH

(Received for publication, May 3, 1951)

**ABSTRACT** — The paper describes the construction of a new electrically bowed violin with very sensitive arrangements for measuring bowing pressure and velocity. Experiment is carried on to study the relation between minimum bowing pressure  $P_{min}$  to elicit a steady fundamental tone with distance  $d$  of the bowed region. Keeping the distance  $d$  fixed, the relation between minimum bowing pressure  $P_{min}$  and the bowing velocity  $V$  is studied thoroughly at two different frequencies and also the effect of change of the vibrating length of the string in  $P_{min}$ - $V$  curves. A full theoretical interpretation of the curves has been given for the first time.

## INTRODUCTION

The present paper describes the construction of an improved type of electrically driven bow and experiments carried on with it. The field traversed is not new. Previously Raman (1920), Saunders (1940) and Sen (1949) carried on experiments with mechanical violin player. Saunders used a motor-operated circular elastic celluloid disk whose outer edge rubbed against the string producing a tone similar to that of a real bow and with the help of a harmonic analyser he measured the intensity of partials with violins of different makes and thereby studied the tone qualities of different violins. Raman and Sen carried on experiments much in the same line as we have, with apparatus not as sensitive as ours.

The apparatus which we have constructed departs widely from that of Raman. Its velocity recording arrangement is similar to that of Sen but its pressure recording arrangement is different and is much more sensitive. In this respect there has been a distinct improvement on the previous methods.

Raman studied the variation of minimum pressure  $P_{min}$  to excite the fundamental with distance  $d$  from the bridge. He showed that the minimum pressure exerted by the bow on the string to excite the fundamental varies inversely as the square of the distance from the bridge. He also studied the variation of  $P_{min}$  with velocity  $V$  of the bow. In both the cases the string was tuned to only one frequency. Sen obtained the  $P_{min}$ - $V$  and  $P_{min}$ - $d$  curves and showed that the minimum pressure approximately varies inversely as the distance of the bow from the bridge and not as the square of the distance as observed by Raman.

We have studied the variation of  $P_{min}$  with distance and velocity more thoroughly at different frequencies and also the effect of the change of the

vibrating length of the string in  $P_{\min}-V$  curves. Further, with the new apparatus a systematic study has been made and a theoretical interpretation of the curves has been given.

## EXPERIMENTAL ARRANGEMENT

The bow is fixed to a heavy iron shaft  $MN$  resting on two pulleys  $P_1P_2$ . It is made to move to and fro in a horizontal direction by means of an electric motor, the speed of which is reduced by means of a reducing gear  $G$  (*vide* figure 1). The speed of the bow is controlled by adjusting a

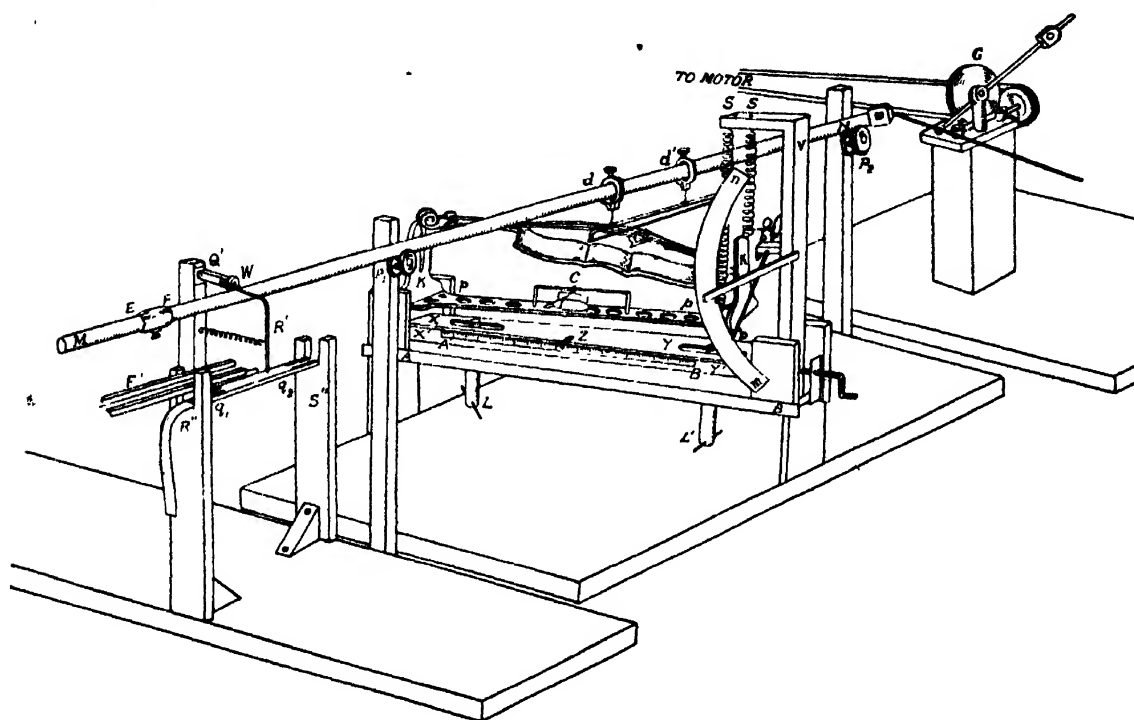


FIG. 1

rheostat put in series with the motor and also by taking pulleys of different diameters connected to the shaft of the motor. The bow can be made exactly horizontal by adjusting the screws *dd'*.

The violin is fixed on a light floating platform  $pp$ , hinged at one end and supported on two long spring systems  $SS$  connected to an upright  $V$  fixed vertically to a horizontal platform  $XY$  which is capable of horizontal movement along another grooved platform  $X'Y'$  in a direction perpendicular to the bow. Both  $XY$  and  $X'Y'$  along with the vertical stand  $V$  and the floating violin can be moved in a vertical direction with respect to another horizontal platform  $AB$  fixed to a wooden table  $T$  by means of screws  $LL'$ . The button at the end of the tail piece of the violin is made to rest in a socket in an upright  $K$  fixed at the end of the floating platform  $pp$ . The handle of the violin is clamped to a second upright  $K'$  also fixed to the other end of the



floating platform  $pp$  by means of an adjustable screw such that the violin may be moved about a horizontal axis with its face upward and be fixed rigidly at any position to enable one of the four strings to come under the bow. This adjustable screw may be moved in a vertical direction along a slot at the upright  $K'$  and can be fixed at any position to make the experimental string exactly horizontal.

A pin mark  $Z$  fixed to  $XY$  which moves horizontally along a metre scale  $A'B'$  fixed to  $X'Y'$  indicates the position of the bow with respect to the bridge.

#### *Measurement of Pressure*

The arrangement is made sensitive by taking two long light springs  $SS$ . There is a light long pointer  $ll$  capable of moving along a vertical graduated semicircular scale  $mn$ . The fulcrum about which the pointer turns and the circular scale are fixed to the upright  $V'$  attached to  $XY$ . The movement of the pointer is made frictionless as far as practicable. A pin ( $\circ$ ), fixed to one upright of the floating platform, presses from above on the shorter arm of the pointer when the longer arm moves over the scale. The magnification is sufficient to record a pressure of one milligram for a subdivision of the scale. The semicircular scale has been calibrated by placing actual weights on the scalepan  $C$  which is adjusted each time to be just vertically under the bowed point.

#### *Measurement of Velocity*

The arrangement is not very much different from that of Sen (1949). A long, narrow smoked paper  $q_1q_2$  is drawn along a grooved horizontal wooden platform  $R''S''$  placed parallel to the bow. A fine pin attached to the prong of a horizontal tuning fork  $F'$  just touches the smoked paper and traces out a wave as long as the paper is drawn. A long lever  $Q'R'$  is hinged at  $Q'$  and rests on the iron shaft carrying the bow. At the end of the lever  $Q'R'$  a fine pin is attached which ordinarily traces a straight line just by the side of the wavy curve on the smoked paper. A small color  $EF$  is fixed on the shaft at a point corresponding to the middle of the bow. With the movement of the bow the color comes under the lever  $Q'R'$  and raises it, thereby producing a gap in the straight line drawn by the pin. The pin again traces the line as soon as the lever just passes over  $EF$ . The actual number of waves corresponding to this gap is counted and the length of the gap is measured accurately by means of a travelling microscope. The velocity is thus accurately determined from the known values of the frequency of the fork, the length of the color  $EF$  and number of waves corresponding to the gap.

## EXPERIMENTAL RESULTS

*Minimum bowing pressure and bowing distance*

Experiment is carried on with the G string of the violin. The string is made of cat gut having a linear density .00845 gm. per cm., the vibrating length being 32 cm. The violin is a copy of Antinio Stradivarius. Keeping the bowing speed constant and frequency fixed the minimum bowing pressure  $P_{\min}$  required to elicit a full steady tone with pronounced fundamental is measured for different distances of the bowed region  $d$  from the bridge. The distance is always taken from the centre of the bowed region. The pressure can be somewhat increased beyond  $P_{\min}$  without greatly changing the tone characteristic up to a limit  $P_{\max}$  beyond which the string becomes loaded and the note emitted is unmusical. Below  $P_{\min}$ , the fundamental, however, falls off in intensity and the octave and the higher harmonics become prominent. The results obtained show that  $P_{\min}$  varies approximately as  $1/d$  (figure 2). This experiment is carried on for two different frequencies. The frequency is changed by altering the tension of the string alone. In each case the relation  $P_{\min} \propto 1/d$  holds good approximately. It is, however, found that  $P_{\min}$  for given distance slightly increases with increase of frequency. (figure 2).

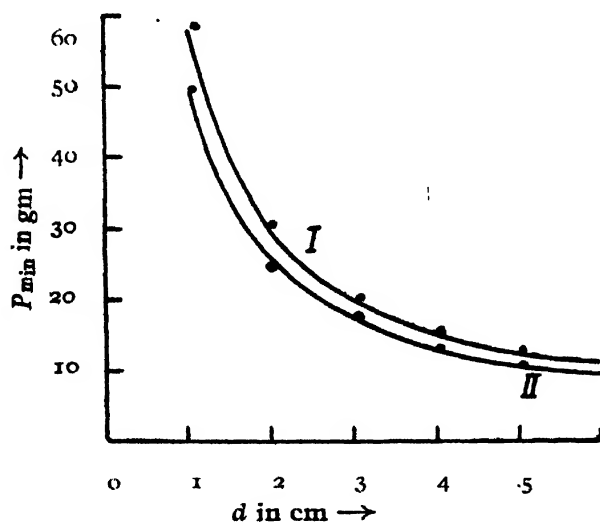


FIG. 2

I. Frequency = 341 (approx.)

II. „ = 256 ( „ )

Velocity of the bow = 15.6 cm/sec

Vibrating length = 32 cm.

*Minimum bowing pressure and bowing velocity*

Keeping the bowing distance  $d$  constant and frequency fixed, the experiment is carried on to study the relation between  $P_{\min}$  and the bowing

velocity. The  $P_{\min} - V$  curve is obtained for the two different frequencies 256 and 341. The graphs show that  $P_{\min}$  at first increases slowly with velocity and then rapidly as the velocity of the bow increases. It is interesting to note that the upper part of the  $P_{\min} - V$  curve is a straight line showing that in this region  $P_{\min}$  varies as  $V$ . The lower bend of the curve suggests that  $P_{\min}$  tends to a finite minimum value as  $V$  is decreased (figures 4 and 5). The variation of  $P_{\max}$  (as explained before) with  $V$  has been also studied for frequency 256 and the corresponding curve is given in figure 3.

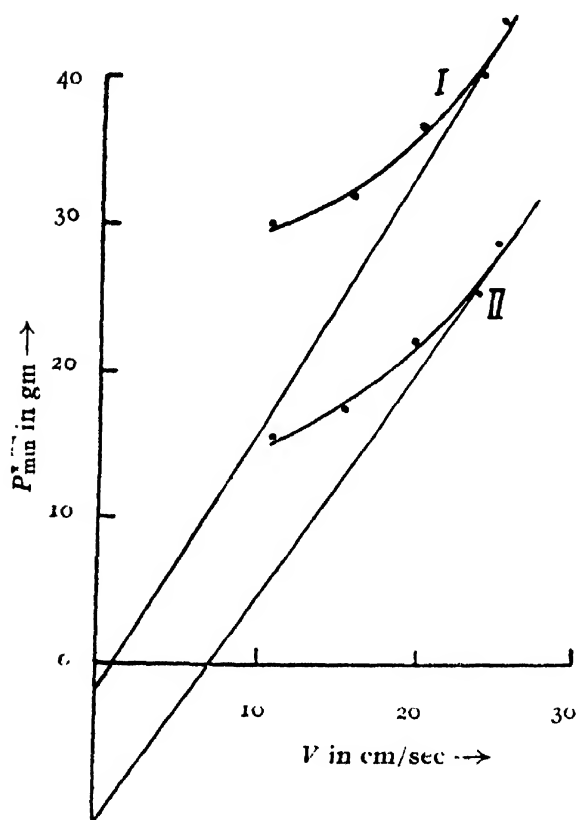


FIG. 3

I.  $P_{\max}$  curve }  $d = 3$  cm  
II.  $P_{\min}$  curve } Frequency = 256

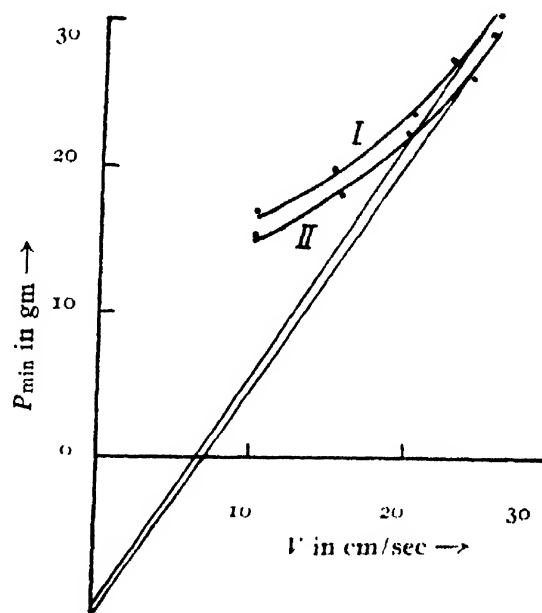


FIG. 4

I. Frequency = 341 (approx) }  $d = 3$  cm  
II. " = 256 ( " ) }  $l = 32$  cm

Keeping the bowing distance  $d$  constant, the full vibrating length  $l$  of the string is decreased to  $\frac{3}{4}l$ . This is done by making  $\frac{1}{4}l$  of the string from the ear of the violin dead over the finger board by a small piece of wood very firmly tightened by a cord so that no vibration is transmitted to the dead part. With this decreased length the above experiment is repeated and  $P_{\min} - V$  curves are obtained for frequencies 256 and 341 (figures 5 (a) and 5 (b)). The nature of the curves is same as that for full length.

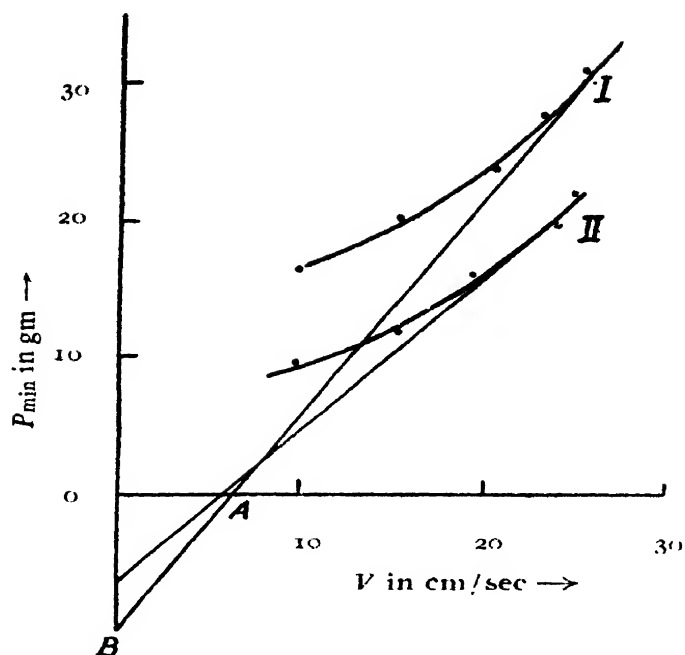


FIG. 5 (a)

- I. Full length ( $l$ ) } Frequency = 341  
 II.  $\frac{3}{4} l$  }  $d = 3$  cm  
                                $l = 32$  cm

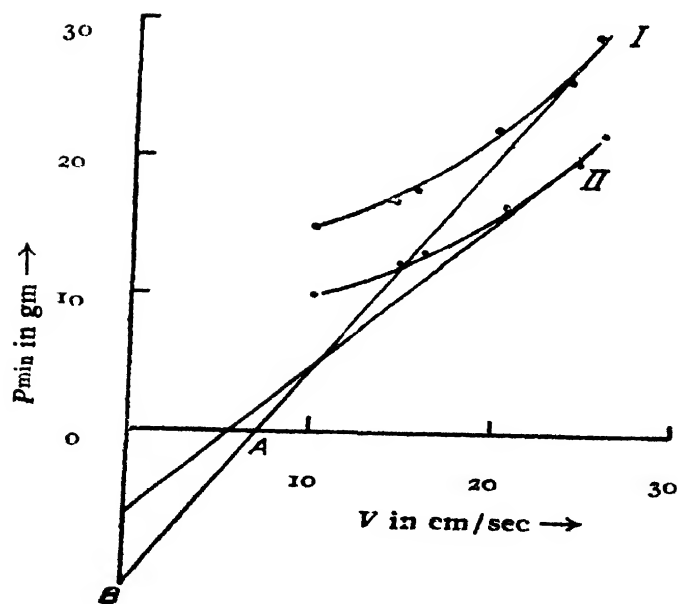


FIG. 5 (b)

- I. Full length ( $l$ ) } Frequency = 256  
 II.  $\frac{3}{4} l$  }  $d = 3$  cm  
                                $l = 32$  cm

# THEORETICAL INTERPRETATION

Before going to interpret the different results obtained from our experiment, it would be useful to make some general remarks on the nature of the variation of  $P_{\min}$  or  $P_{\max}$  with the velocity of the bow and deduce a formula connecting them.

It is evident from figure 3 that  $P_{\min} - V$  and  $P_{\max} - V$  curves are both straight at high velocity showing that the dynamical frictional force exerted by the bow at high velocity increases linearly with bowing velocity. Thus at this stage the dynamical coefficient of friction is independent of velocity and is constant. However, at lower velocity the  $P_{\min} - V$  curve is bent showing that the dynamical coefficient here is no longer constant but increases with decreasing velocity.

Now according to Helmholtz (*l.c.*) the forward velocity of the bowed point is approximately equal to the velocity of the bow. Raman (1918) however points out that as the rate of supply of energy by the bow should be continuous throughout the motion, i.e. should be same during forward and backward motion, the bowed point must move forward with exactly the velocity of the bow, as in that case, there would be a statical friction during forward motion. And, as the maximum statical friction is greater than the dynamical friction, the mean statical friction during forward motion might be equal to the dynamical friction during the backward motion and the principle of continuous supply of energy might not be violated. However, since the  $P_{\min} - V$  curve at low velocity shows that the dynamical coefficient increases as the relative velocity decreases, it is quite possible that the frictional force remains uniform throughout, even if the bowed point moves with a small velocity in the forward direction, the forward relative velocity being always less than the backward relative velocity.

There is another aspect of the problem which must also be considered here. Actually there is no bowed point, because the hairs of the bow are in contact with the string over a length of 1 cm. This difficulty was pointed out by one of writers (Kar, 1942) as far back as in 1922. It was also shown from experiment (Kar, *l.c.*) that the point on the string which moves with velocity of the bow i.e. the "zero point" generally lies on the outer limit of the "bowed region" but sometimes may be outside it. Thus, if  $V$  be the velocity of the bow or of the zero point, the forward velocity of the mid-point of the bowed region is less than  $V$ . Let it be  $(V - V_0)$ . Let  $V_1$  be its backward velocity and  $d$  its distance from the near end.

From the principle of constancy of the frictional force during forward and backward motion, we have for its value at any time during steady motion

$$P_1 = pb = \mu_a' V_0 = \mu_a (V + V_1) \quad \dots (1)$$

where  $p$  is the frictional force per unit length of contact,  $b$  the length of the bowed region,  $\mu_a'$ ,  $\mu_a$  the dynamical coefficients during forward and

backward motion respectively. As  $V_0$  is always small  $\mu_d$  has an uncertain value, so we shall use the other relation, namely,

$$P_1 = \mu_d (V + V_1) \quad \dots (1.1)$$

for calculating the bowing pressure. Because the mid-point of the bowed region is at a distance  $d$  from the near end, we have,

$$\frac{V - V_0}{V_1} = \frac{d}{l - d},$$

$l$  being the length of the string. We have then

$$V + V_1 = \frac{l}{d} (V - V_0) + V_0$$

(On substituting this value of  $V + V_1$  in (1.1) we have

$$P_1 = \mu_d \left\{ \frac{l}{d} (V - V_0) + V_0 \right\} \quad \dots (1.2)$$

where  $P_1$  denotes the total frictional force in the direction of bowing. Actually, however, we measure in the experiment the vertical force  $P$  exerted by the bow on the string. This force is obviously proportional to  $P_1$ . So we take  $P = \alpha P_1$ ,  $\alpha$  being the constant of proportion. We have then

$$P = \alpha \mu_d \left\{ \frac{l}{d} (V - V_0) + V_0 \right\} \quad \dots (1.3)$$

It should be noted that it is customary to call  $P$  the "bowing pressure" although actually it is the total bowing force. Now it follows from (1.3) that at given  $V$ ,  $d$ ,  $l$ , the bowing pressure  $P$  may vary from  $P_{\min}$  to  $P_{\max}$  only if  $V_0$  changes due to the shifting of the zero point. Accordingly we have

$$P_{\min} = \alpha \mu_d \left\{ \frac{l}{d} (V - V_0') + V_0' \right\} \quad \dots (1.4)$$

$$P_{\max} = \alpha \mu_d \left\{ \frac{l}{d} (V - V_0'') + V_0'' \right\} \quad \dots (1.5)$$

Thus the difference in the observed  $P_{\min} - V$  and  $P_{\max} - V$  curves (figure 3) which show that  $V_0'$  is greater than  $V_0''$  is explained. Equapin (1.4) shows that for a given velocity of bowing  $(P_{\min} - \alpha \mu_d V_0')d$  is constant because  $V_0'$  is small  $P_{\min} \times d$  is approximately constant as observed by us (figure 2)

It also follows from equapin (1.4) that at high velocity when  $\mu_d$  is constant,  $P_{\min} - V$  curve should be straight as observed by us (figures 4 and 5) and also previously by Raman and Sen. It is significant that the straight part of the  $P_{\min} - V$  curve when produced does not pass through the origin but cuts the axis of velocity at a point  $A$ . The length  $OA$  is easily obtained from (1.4) by putting  $P_{\min} = 0$  and we have

$$OA = V_0' \left( 1 - \frac{d}{l} \right) \quad \dots (2)$$

The straight line is produced further to cut the axis of pressure at a point B, then evidently (putting  $V=0$  in (1.4)) we have

$$OB = \alpha \mu_d \cdot V_0' \left( 1 - \frac{l}{d} \right) \quad (2.1)$$

Thus we have

$$\frac{OB}{OA} = -\alpha \mu_d \frac{l}{d} \quad \dots (2.2)$$

The ratio thus determined experimentally for frequencies 256 and 341 $\frac{1}{3}$  for full length  $l=32$  cms shows that it is approximately constant for a given bowing distance (figure 4). The length of the string is, however, reduced to  $\frac{3}{4}l$  and it is found that the value of the ratio is also reduced approximately to  $\frac{3}{4}$  of that for full length, for a given bowing distance (vide figure 5). These conclusions are fully supported by the theoretical formula derived in (2.2) for the ratio  $OB/OA$ .

We next proceed to find the position of the zero point. Let its distance from the mid-point of the bowed region be  $x$  and let the backward velocity at the zero point be  $V_2$ . We have then

$$\frac{V}{V_2} = \frac{x+d}{l-(x+d)}$$

$$\text{or,} \quad V + V_2 = \frac{l}{x+d} \cdot V. \quad \dots (3)$$

The corresponding relation for the mid-point of the bowed region gives

$$V - V_0 + V_1 = \frac{l}{d} (V - V_0) \quad \dots (3.1)$$

On comparing (3) and (3.1) and remembering the law that the sum of the forward and backward velocities is constant for all points (i.e.  $V + V_2 = V - V_0 + V_1$ ) we have at once

$$\frac{V}{x+d} = \frac{V - V_0}{d}$$

$$\text{or,} \quad x = \frac{V_0}{V - V_0} \cdot d \quad \dots (3.2)$$

giving the distance of the zero point from the mid-point of the bowed region. The above formula shows that  $x$  decreases as the bowing velocity  $V$  is increased for a given bowing distance  $d$ . In other words, it is possible to move the zero point towards the bowed region by increasing the bowing velocity  $V$ . Again at a given bowing distance  $d$  and velocity  $V$ ,  $x$  may be decreased by increasing the bowing pressure from  $P_{min}$  to  $P_{max}$  and thereby

decreasing  $V_0$  from  $V_0'$  to  $V_0''$ . From our experiment (*vide* figure 3) we find that at  $V=23.6$  cm/sec and  $d=3$  cm, the zero point moves from  $x=1.26$  cm. to  $x=.133$  cm. when the bowing pressure is increased from  $P_{\min}=26$  gms to  $P_{\max}=43.5$  gms. We are unable to verify this by actually determining the zero point by photographic method. Experiment in this direction is, however, in progress.

Lastly, it may be mentioned that we find  $P_{\min}-d$  curve (figure 2) for a higher frequency to be slightly above that for a lower frequency. This small difference may be explained in the following way. In figure 4 we find that  $OA$  for higher frequency is slightly less than  $OA$  for a lower frequency, i.e.  $V_0'(n_1)$  for higher frequency  $n_1, < V_0'(n_2)$  for lower frequency  $n_2$ . Therefore, from (1.4) we have, for a given bowing velocity  $V$  and distance  $d$ ,

$$P_{\min}(n_1) + \alpha\mu_d\left(\frac{l}{d} - 1\right)V_0'(n_1) = \alpha\mu_d\frac{l}{d}V = P_{\min}(n_2) + \alpha\mu_d\left(\frac{l}{d} - 1\right)V_0'(n_2) \dots (4)$$

It is obvious from (4) that

$$P_{\min}(n_1) > P_{\min}(n_2) \text{ if } V_0'(n_1) < V_0'(n_2) \dots (4.1)$$

This is what we find from figure 4. Thus  $P_{\min}-d$  curve for higher frequency will be above the  $P_{\min}-d$  curve for lower frequency.

#### ACKNOWLEDGMENTS

The authors wish to thank Prof. B. K. Sen for suggestions regarding the measurement of velocity. Thanks are due to Sri Kartic Ch. Das in helping us to set up the apparatus.

PHYSICAL LABORATORY  
PRESIDENCY COLLEGE, CALCUTTA.

#### REFERENCES

- Helmholtz H. L. F, 1895, *Sensations of tone*, pp. 384-387.  
Kar, K. C. 1922, *Phys. Rev.*, **20**, 181.  
Raman, C. V. 1920, *Proce. Ind Assoc. for the cult. of Sci.*  
Vol 6 part I and II and 1918, *Bulletin No 15. Ind. Assoc. for the Cult. of Sci.*,  
Saunders, F. A., 1940, *J. Franklin Inst.*, **229**, 1.  
Sen, B. K., 1949, *Ind. J Phys.*, **23**, 7.



# ON THE ULTRAVIOLET ABSORPTION SPECTRA OF METHYL BENZOATE AND ACETOPHENONE IN THE SOLID STATE AT LOW TEMPERATURES\*

By A. R. DLB

(Received for publication, September, 12, 1951)

## Plate XV

**ABSTRACT:** The absorption spectra of methyl benzoate ( $\text{C}_6\text{H}_5\text{COOCH}_3$ ) and acetophenone ( $\text{C}_6\text{H}_5\text{COCH}_3$ ) in the ultraviolet region have been studied in the liquid and solid states. In the case of methyl benzoate three broad bands have been observed in the liquid state in the region  $2650 \text{ \AA}$  to  $2900 \text{ \AA}$ . Continuous absorption begins below  $2500 \text{ \AA}$ . In the solid state these bands are found to be shifted considerably towards the longer wavelength side, while continuous absorption begins below  $2440 \text{ \AA}$ .

The absorption spectrum of acetophenone in the liquid state reveals three broad bands with centres at  $35744$ ,  $38748$ , and  $40277 \text{ cm}^{-1}$  respectively. On solidification, the first band widens considerably on both sides and splits up into three bands, while the second shifts towards the shorter wavelength side and the third disappears. The limit of continuous absorption recedes towards shorter wavelength side. It is pointed out that these changes cannot be due to mere lattice fields and may be due to association of the molecules in the solid state.

## INTRODUCTION

Absorption spectra of molecules in the gaseous state exhibit, in general, band systems having large number of bands, both sharp and diffuse. On change of state from vapour to liquid phase, the structure of the band system is expected to show considerable changes, because in the liquid state intermolecular forces are liable to be brought into play. Such changes are actually observed in the absorption spectra of benzene in the region  $2700 \text{ \AA}$  --  $3000 \text{ \AA}$  (Kronenberger and Pringsheim, 1926).

The experimental data are, however, not sufficient to indicate any general trend of changes suffered by the absorption spectra of molecules with change of state at low temperatures. The results reported earlier, for anisole (Deb, 1951) and toluene (Swamy, 1951) show that changes, much greater than those observed in the case of benzene, take place when these substances are solidified and cooled down to about  $-170^\circ\text{C}$ .

\* Communicated by Prof. S. C. Sirkar

In order to find out whether any other substituted benzene compound shows such remarkable changes in their absorption spectra with solidification, the ultraviolet absorption spectra of two more organic compounds, *viz.*, methyl benzoate and acetophenone, have been studied and the results have been compared with those for solutions of these substances in ether (Kato and Someno, 1938) and for solution of acetophenone in alcohol (Grammaticakis, 1950).

### EXPERIMENTAL

The experimental arrangement was the same as that used in the study of anisole (Deb, 1951). The liquids used were of chemically pure variety and were distilled repeatedly in vacuum before use. A very thin film of the liquid was necessary to produce bands in the absorption spectrum. This was obtained by pressing together the quartz plates of the cell between which the film was formed, and then by carefully sliding one plate over the other.

Spectrograms were taken on Ilford H.P.3 films and Q-plates using a Hilger H1 quartz spectrograph, giving a dispersion of about 3 Å.U per mm in the region of 2600 Å. Exposures ranging from 6 minutes to 10 minutes were necessary in the case of the liquid, and about an hour in the case of the solid. The width of the slit was about 0.2 mm.

### RESULTS AND DISCUSSION

The spectrograms are reproduced in Plate XV and the positions of the bands are given in Tables I and II. The data for solutions of both liquids in ether reported by Kato and Someno (1938) and those for solution of acetophenone in alcohol, reported by Grammaticakis (1950) are also included for comparison.

TABLE I  
Methyl benzoate

Soln. in ether (Kato & Someno, 1938)				Liquid (Present author)				Solid (Present author)			
λ AU	ν cm <sup>-1</sup>	Int	Diff	λ AU	ν cm <sup>-1</sup>	Int	Diff	λ AU	ν cm <sup>-1</sup>	Int	Diff
1	35700	4		1	2811.91	35552	st	1	2841.49	35182	st
			700				929				934
2	36400	5		2	2740.31	36481	st	2	2768.07	36116	st
			1180				947				923
3	37580	4		3	2671.0	37428	w	3	2699.0	37039	w
					?						

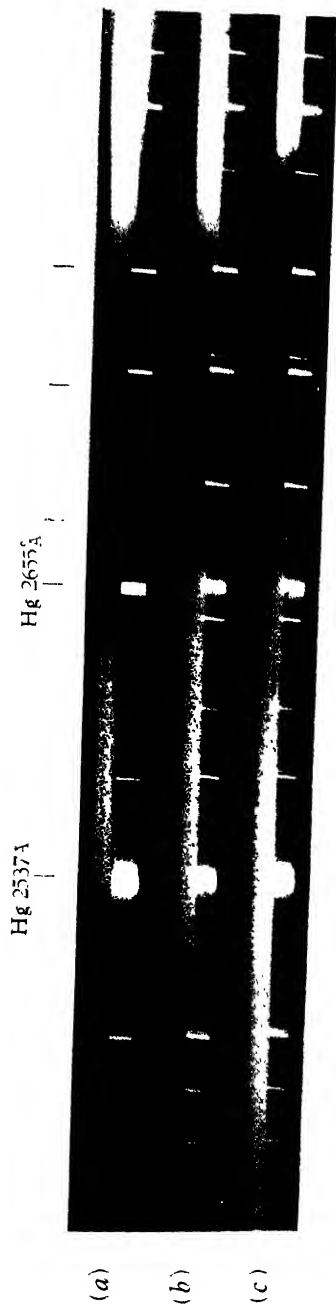


Fig 1



Fig 2

## Ultraviolet absorption spectra

Fig. 1.—Methyl benzoate

- (a) Liquid at about 30°C  
 (b) Do (Thinner film than (a))  
 (c) Solid at about -170°C

Fig 2—Acetophenone

- (d) Liquid at about 30°C  
 (e) Do (Thinner film than (a))  
 (f) Solid at about -170°C  
 (g) Do (Thinner film than (c))



TABLE II  
 Acetophenone

Soln. in ether (Kato & Someno, 1938)				Liquid (present author)				Solid (present author)					
$\lambda$ AU	$\nu$ cm <sup>-1</sup>	Int	Diff		$\lambda$ AU	$\nu$ cm <sup>-1</sup>	Int	Diff		$\lambda$ AU	$\nu$ cm <sup>-1</sup>	Int	Diff
1	34900	8	1000							1	2925.76	34170	
2	35900	9	1100	1	2706.89	35744	st			2	2836.3	35249	1079
3	37000	6						3004		3	2752.9	36315	1066
Soln in alcohol (Grammaticakis, 1950)*													
				2	2580.0	38748	w			4	2566.16	38957	
								1529					
2800	35700												
2440	40900			3	2482	40277	w						

"St" means strong and "w" means weak.

\* These results have been obtained from the frequency-log E.

#### (a) Methyl benzoate

It is seen that the absorption spectrum of methyl benzoate [figure (1) Plate XV] consists of three bands at 35552, 36481 and 37428 cm<sup>-1</sup>, the third band being weak and flat with the maximum hardly recognizable. The approximate difference between the frequencies of the successive bands are 929 and 947 cm<sup>-1</sup> respectively in the case of the liquid. The bands shift towards longer wavelength when the substance is solidified and cooled to about -170°C. The difference between the successive bands in the case of the solid are 934 and 923 cm<sup>-1</sup> respectively. This frequency seems to be that of the symmetric vibration of the benzene ring in the excited electronic state. Kato and Someno (1938), however, reported the frequencies 700 and 1180 cm<sup>-1</sup> as the difference of the successive bands in the case of the solution of methyl benzoate in ether. Neither of these frequencies have been observed in the present investigation.

#### (b) Acetophenone.

In this case the liquid gives three bands with their centres at 35744, 38748 and 40277 cm<sup>-1</sup> respectively (figure 2, Plate XV). On comparing these with the data published by Kato and Someno (1938) for solution in ether, it was found that the second band observed by these authors corresponds to the first band of the present work. A band was also observed

in this position by Grammaticakis (1950) in solution of acetophenone in alcohol. But the other two bands observed by Kato and Someno were not observed in the present work. Corresponding to the second band at  $33748\text{ cm}^{-1}$  no band was observed by those authors in solution; but the third band roughly corresponds to the second band observed by Grammaticakis in alcohol solution. The frequency-differences observed in the liquid state are  $3000$  and  $1500\text{ cm}^{-1}$ .

In the solid state at about  $-170^{\circ}\text{C}$ , in the place of the first band of liquid state, three bands are observed, two of which are on the longer wavelength side of the original one and the third band is on the shorter wavelength side. The second band observed in the liquid state shifts by about  $14\text{ \AA}$  to the shorter wavelength side in the solid state, and the third band of the liquid is not at all observed in the solid state.

These changes are too large to be explained on the assumption that the lattice field splits up the electronic levels of the molecule. Evidently these changes are due to a stronger intermolecular association in the solid state.

The investigations are being continued with other organic compounds.

#### ACKNOWLEDGMENT

The author is indebted to Prof. S. C. Sirkar, D.Sc., F.N.I., for his kind permission to carry out the investigation in the Optics Laboratory of the Indian Association for the Cultivation of Science, and for his guidance during the progress of the work.

INDIAN ASSOCIATION FOR THE  
CULTIVATION OF SCIENCE  
CALCUTTA, 32

#### REFERENCES

- Deb, A. R., 1951, *Ind J. Phys.* **25**, 233.  
Grammaticakis, M., 1950, *Compt Rend.*, **231**, 278.  
Kato, S. and Someno, F., 1938, *Sci Pap. Inst. Phys. Chem. Res. Tokyo*, **34**, 905, 912  
Kronenberger, A. and Fringsheim, P., 1926, *Z. f. Phys.*, **40**, 75.

# OVER-LAND REFRACTION OF HIGH-FREQUENCY RADIO WAVES IN INDIA

By K. R. SAHA

(Received for publication May 18, 1951)

**ABSTRACT** From a study of the vertical distribution of the mean modified refractive index of the lowest kilometre of the atmosphere over three land stations computed from routine aeroplane flight and radio-sonde reports, conclusions are drawn regarding radio propagation conditions over these stations at some selected hours of the day and in different months of the year. While combined effects of temperature inversion and humidity lapse with height explain on super-refraction at these stations most occasions, some cases of super-refraction are observed with lapse rates in both temperature and humidity. Meteorological origin of the mean M.R.I profiles is discussed.

## ATMOSPHERIC SUPER-REFRACTION AND FORMATION OF RADIO-DUCTS

The refractive index,  $\mu$  of the atmosphere for radio waves is given to a sufficient degree of accuracy, by the relation :

$$\mu = 1 + \frac{80}{T} \left( P + \frac{4800 e}{T} \right) \times 10^{-6} \quad \dots (1)$$

where

$P$  = the atmospheric pressure in millibars,

$e$  = the partial pressure of water vapour in millibars,

and  $T$  = the temperature in degrees absolute.

If  $d\mu/dh$  is the refractive index gradient at height  $h$  above the earth's surface, the curvature of a radio-ray for small angles of elevation ( $< 15^\circ$ ), at that height is

$$\frac{1}{\rho} = - \frac{1}{\mu} \frac{d\mu}{dh} \quad \dots (2)$$

where  $\rho$  is the radius of curvature of the ray. Following radio practice, we treat the earth's surface as flat and measure ray curvature with reference to a flat earth. It becomes necessary to modify the refractive index in that case and the modified refractive index (M.R.I.) is given by the following relation,

$$\mu' = (\mu - 1) + \frac{h}{R} \times 10^6 \quad \dots (3)$$

where  $R$  is the radius of the earth. It can be shown from the theory of radio-ray propagation (Appleton, 1946) that if  $\phi_h$  is the inclination of a ray to the horizontal at a height  $h$ , where the modified refractive index is  $\mu_h$ , then,

$$\frac{1}{2}(\phi_h^2 - \phi_0^2) = \mu_h' - \mu_0' = \Delta\mu' \quad (4)$$

where  $\phi_0$ ,  $\mu_0'$  are the corresponding values at the transmitter height  $h_0$ . Equation (4) gives the bending of the rays in terms of the modified refractive index variation over an interval of height  $(h - h_0)$ . If  $\Delta\mu' > 0$ ,  $\phi_h > \phi_0$ , and the ray is bent upward with reference to a flat earth. If  $\Delta\mu' = 0$ ,  $\phi_h = \phi_0$ , and the ray moves parallel to the earth's surface. But if  $\Delta\mu' < 0$ ,  $\phi_h < \phi_0$ , and the ray is bent downward to strike the earth. In the last case radio-energy is mostly confined in a narrow layer close to the earth's surface and is able to reach distances far beyond the geometrical horizon giving rise to what is known as unorthodox radio vision (Booker, 1948; Saha, 1949). The height at which upgoing radiation is reflected back downwards marks the top of a radio-duct.

The negative gradient of  $\mu'$  with height thus produces super-refraction or radio-ducts. The types of super-refracting layers commonly met with in the atmosphere are shown by the  $\mu' - h$  curves in figure 1.

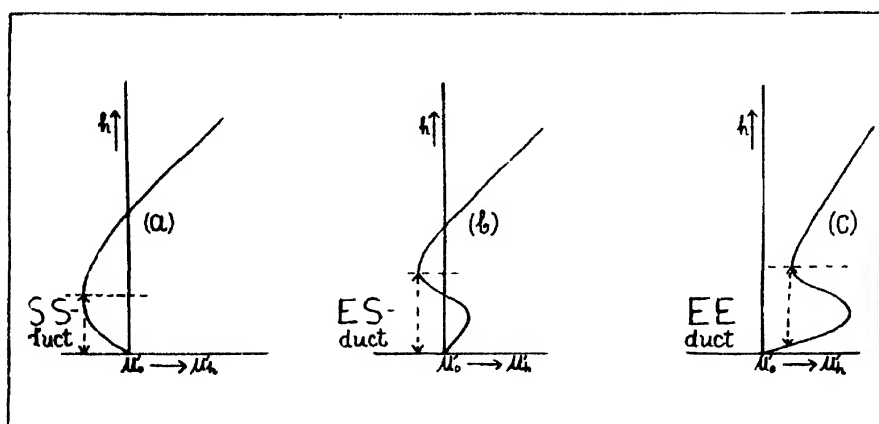


FIG. 1

Types of super-refracting layers or radio-ducts.

In the first and second curves  $\mu'$  reaches a negative value relative to the origin. In (a) the duct reaches the earth's surface and is called the SS-duct (Surface-layer and Surface-duct). In (b) the refracting layer is elevated but the radio-duct still extends from the minimum of modified refractive index (M.R.I.) to the ground level and is called the ES-duct (Elevated-layer and Surface-duct). In (c) the local minimum of the M.R.I. exceeds the value at the earth's surface giving what is known as the EE-duct (Elevated-layer and Elevated-duct). In the last case, the radio-duct only extends from the local minimum of the  $\mu'$  down to the level where this value is regained.

Considerations of the meteorological variables involved in equations (1) and (3) make it clear that while the distribution of the atmospheric pressure with height causes a slight uniform decrease of refractive index with height, temperature and humidity distributions are the main factors which determine



the vertical distribution of the M.R.I. and thus control radio propagation in the lower atmosphere. In a well-mixed atmosphere in which the lapse rate of temperature is dry, adiabatic and the specific humidity falls off slowly with height,  $\Delta\mu' > 0$  and the radio refraction is said to be normal or standard. Radio range in such an atmosphere hardly exceeds the optical range of the transmitter. But when the atmosphere is stratified, strong temperature inversion may form and there may also develop a marked negative gradient of humidity with height. In such an atmosphere  $\Delta\mu' < 0$ , and the result is the formation of a highly super-refracting layer. Sometimes the effect of temperature distribution may act in a direction opposite to that of humidity gradient but it is the resultant effect exercised through the relation (1) that becomes the determining factor.

#### RADIO REFRACTION OVER LAND

The important role played by atmospheric refraction in short wave propagation was widely demonstrated during World War II by radar operations in different parts of the world. Abnormally long ranges of communication at low levels were reported in many parts but the most impressive reports came from the tropics where the effects of high temperature and high humidity produced marked super-refraction. But the bulk of these reports related to over-water transmission. The difficulty of low-elevation wave propagation over land may have substantially restricted use of the radar in many parts of the continents.

Smith-Rose and Stickland (1946) have experimentally demonstrated that over-land radio-wave propagation between any two points on the earth's surface is affected by meteorological conditions of the medium in much the same way as over-water transmission. Variations in the refractive index gradient of the medium caused by meteorological phenomena like fog, cold front and high wind produce corresponding variations in the receiving signal strength at a distant point. Their work calls for more detailed information on the fine structure of the propagation medium. The lapse rate of the refractive index with height requires to be determined with greater accuracy than heretofore. Only then can field intensities and reception strengths be determined with any exactitude.

In the present study refractive index (modified) values have been computed for three land stations in India and their vertical profiles examined for super-refraction of radar waves. Diurnal and seasonal variations are studied and inferences drawn regarding propagation conditions at these stations at different times of the year.

#### AVAILABLE METEOROLOGICAL DATA

Theoretical works (Eckersley, 1938; Booker, 1946) have shown that efficient trapping of a radio-wave is possible only when the width of a radio-

duct is greater than a critical minimum value. The critical width, however, decreases as the frequency of the wave is increased. For high frequency radio waves, as used in radar, the critical duct-width is contained within the lowest 1,000 ft. of the atmosphere. Hence meteorological data of the lowest kilometre of the atmosphere can provide suitable basis for studying radio refraction in the atmosphere.

Low-level meteorological soundings up to a height of 1 km or so have not formed part of routine upper-air work in India. A series of clown balloon ascents were arranged by Chatterjee and Sur (1929) at Jhikergachha (Lat.  $23^{\circ} 06'$  N., Long.  $49^{\circ} 08'$  E.) in connection with a study of the Nor'-wester problem. Ramdas (1943) has recorded a series of micro-meteorological observations at Poona but these relate to the lowest 35 ft. only. Observations from high towers or low-level aeroplane flights suitable for use in radio-meteorological work are practically non-existent in this country. Perhaps, the only record of a low-level aeroplane flight specially made for radio-meteorological work is to be found in a paper by Hatcher and Sawyer (1947) on the structure of sea-breeze at Madras and the associated radio-duct.

Routine radio-sonde observations are hardly ideal for the type of work here undertaken because of the excessively high rate of ascent of recording instruments which allows only a few observations to be taken in the lowest kilometre. In the case of aeroplane flights these draw-backs may be removed if the terrain is plain but the high speed of the aircraft necessitates large corrections to the readings of the recording instruments. In spite of these sources of error, the author found it practicable to work with the routine corrected data published by the Indian Meteorological Department in daily weather reports. Volumes of these data accumulated in wartime. They are now available in suitable form for studying the refractive condition of the atmosphere. Aeroplane and balloon flight observations of temperature and humidity at Calcutta, Nagpur, and Madras during the period 1944-46 are used in the present paper. Observations of Calcutta were available at 0100, 0700 and 1300 hours G M T, for all the months and at 1700 G M.T. for the months of March, April, July, and October. Of these the observations at 0100 GMT were obtained by aeroplane flights while those at 1300 and 1700 GMT were radio-sonde observations. Observations of Nagpur and Madras were aeroplane flight observations and were available at 0100 and 0600 GMT only. Mean temperature and vapour pressure at standard and chosen pressure levels were obtained graphically for each month and these mean values were used for computing the value of the M.R.I., employing relations (1) and (3). Computed values of the M R.I. were then plotted against height in charts A1, A2, B, and C. The statistics of the data used for each curve in these charts is given in Table I and the scatter of the observations about their mean at Calcutta is given in terms of the standard deviation for four representative months in Table II.

## DIURNAL AND SEASONAL VARIATION OF REFRACTION

The vertical profiles of the modified refractive index presented in charts A1, A2, B and C show diurnal and seasonal variation which may be discussed as follows :

*Charts A1 and A2.—Calcutta.* The mean structure of the lower atmosphere over Calcutta during the night and early morning hours of the winter months of December to February is a strong temperature inversion and a normal negative gradient of humidity. Mean M.R.I. profiles for this period do not reveal the presence of any radio-duct but the vertical gradient of the modified refractive index definitely indicates marked tendency towards super-refraction. M.R.I. curves for midday hours show normal refraction. Atmospheric conditions in March become highly favourable for super-refraction. Strong temperature inversion and marked lapse of humidity with height combine to form radio-ducts during evening which continue throughout night and last as late as morning hours as evidenced by the ascent curves for the month in charts A1 and A2. These radio-ducts are of the SS-type. In April and May temperature inversion still forms but during these months the inversion layer is most often elevated above the ground. In figure 2 an early morning ascent in April at Jhikergachha, taken from the clown balloon ascent data of Chatterjee and Sur (1926), shows the presence of an elevated temperature

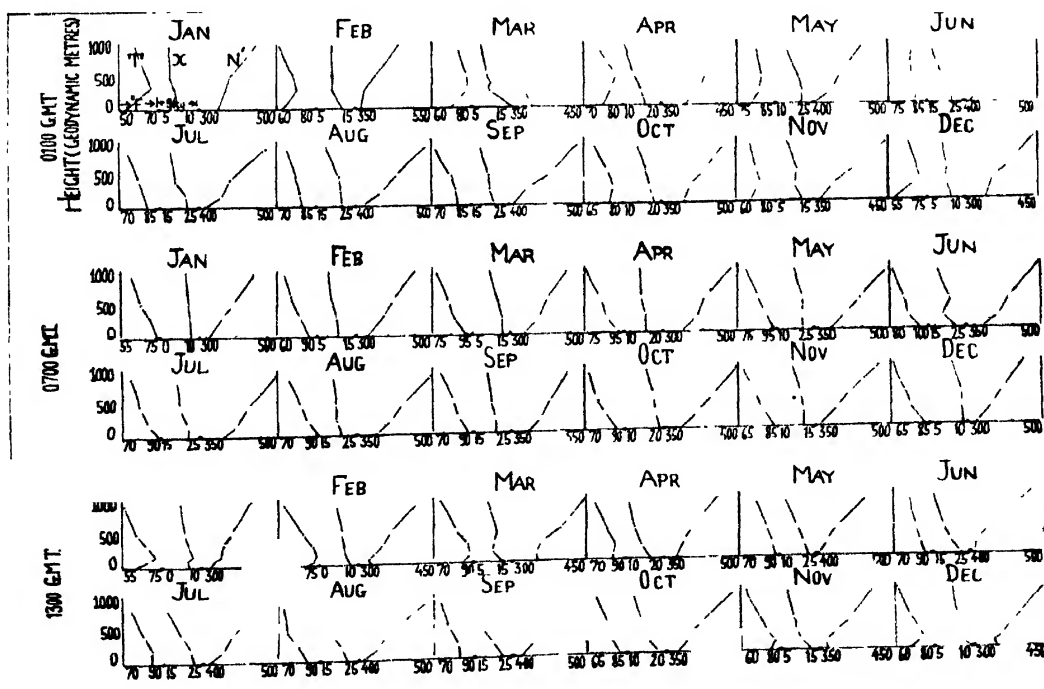


Chart A 1.

Vertical distributions of mean temperature  $T(^{\circ}F)$ , humidity mixing ratio  $x(g/Kg)$ , and modified refractive index  $\mu'$  at Calcutta in different months. Times of ascent : 0100, 0700, and 1300 GMT.

inversion and an ES-duct. Figure 3 and figure 4 show the confines of the inversion layer and the steepness of inversion over Calcutta at some hours of the day and in different months of the year. The height of the top of the inversion layer in April is probably that of the elevated inversion

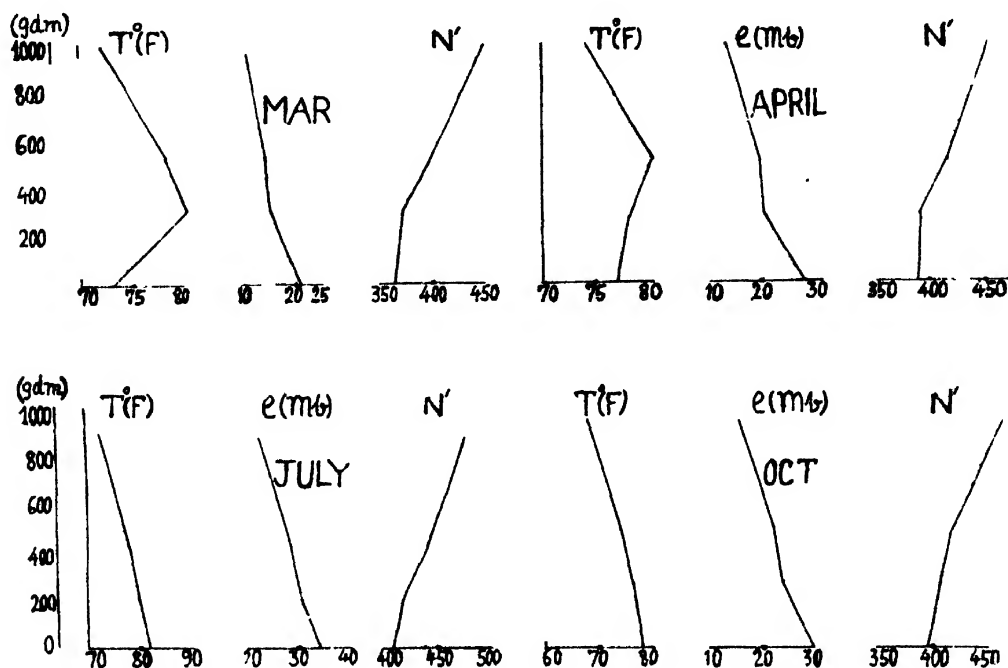


Chart A 2.

Vertical distributions of mean temperature  $T(^{\circ}\text{F})$ , vapour pressure  $e(\text{mb})$ , and *modified refractive index*  $\mu'$  at Calcutta in four months. Mean time of ascent : 1700 GMT (Mean of times of ascent between 1500 and 1800 Z)

TABLE I

Statistics of data, Number of observations used for mean M.R.I. curves.

Station.	Time of ascent	Month. J	F.	M	A	M	J	J	A	S	O	N	D
Calcutta	0100Z	22	45	45	42	21	20	40	34	12	27	12	22
	0700	19	20	17	19	18	18	38	17	12	28	02	15
	1300	50	20	09	19	22	22	20	13	10	18	10	20
	1700	—	—	07	08	—	—	12	—	—	07	—	—
Nagpur	0100	35	51	48	71	29	28	44	44	26	43	25	53
	0600	35	52	46	42	28	25	29	25	27	33	28	51
Madras	0100	24	25	24	22	27	25	29	24	23	48	27	27
	0600	25	20	22	19	07	19	28	08	—	20	18	26

layer. Temperature inversion disappears during the SW monsoon and the lapse rate of moisture is also very small then. The M.R.I. profiles show that microwave propagation must be quite orthodox from June to September. In October the inversion re-forms. It strengthens in November when the atmosphere becomes highly refracting again. It is interesting to compare the above remarks with an actual record of radar performance over the delta area of Bengal in 1943 which is reproduced in Table III below from a paper by Durst (1946). The high scatter of the observations about their mean in winter and early summer months as given by those of the representative months in Table II is probably due to the frequent changes in air masses over the area caused by the passage of western depressions during these

**TABLE II**

Scatter of temperature observations. Standard deviation values at Calcutta (°F).  
(D. B.—Dry bulb ; W. B.—Wet bulb)

Time of ascent.	Jan			April.			July			Oct		
	Ht (ft dm)	D.B.	W.B.	Ht.	D.B.	W.B.	Ht.	D.B.	W.B.	Ht.	D.B.	W.B.
0100Z	0	4.2	3.9	0	4.1	4.1	0	1.0	1.0	0	3.7	3.6
	315	4.9	3.7	274	3.0	4.4	193	1.4	1.1	276	2.0	2.8
	530	4.4	4.2	495	4.1	4.6	414	1.7	1.8	495	2.5	3.6
	980	4.2	5.1	958	4.6	3.9	876	1.7	1.5	955	2.8	4.1
0700	0	4.9	3.2	0	4.3	3.8	0	4.1	1.4	0	4.1	3.8
	323	4.6	3.6	266	4.1	3.2	187	2.7	1.3	278	3.1	3.3
	539	4.4	4.1	490	4.6	3.4	409	2.5	1.7	498	2.8	3.4
	991	4.9	4.9	955	3.5	3.8	876	1.7	1.5	960	3.1	2.7

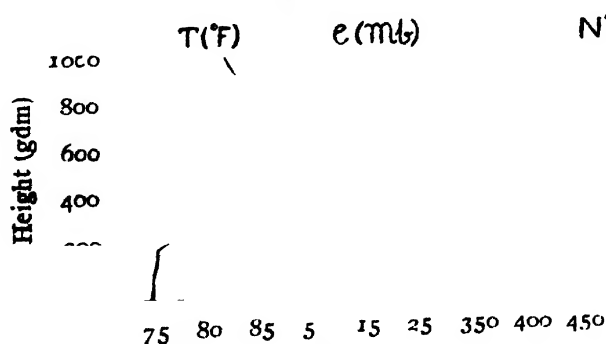


**FIG. 2**

Elevated radio-duct at Jhikergachha, Bengal. Time of ascent, 0100 GMT.  
9th April, 1949.

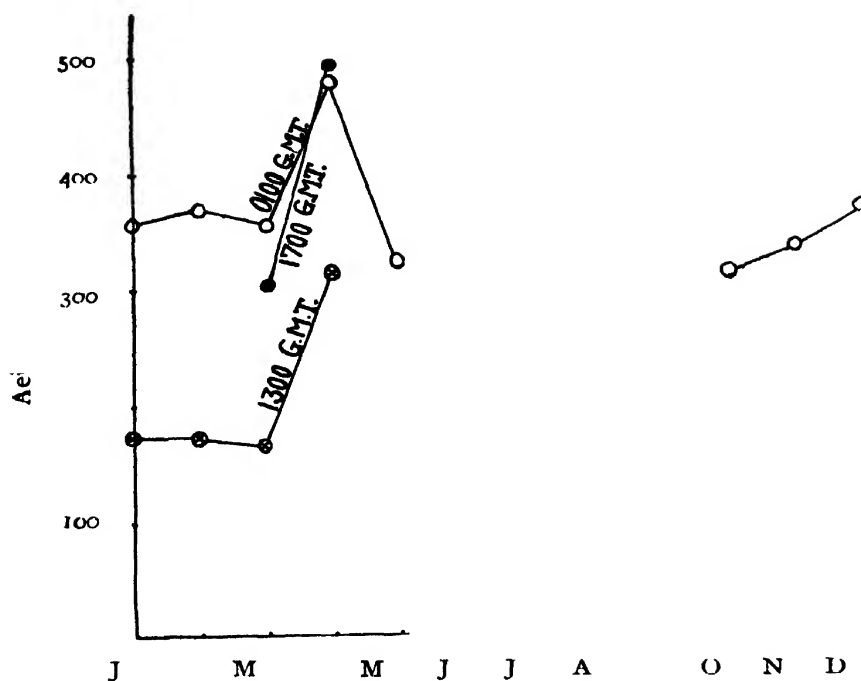


FIG. 3

Mean height of top of inversion layer at Calcutta in different months. Symbols for times of ascent are: "crossed circle" 1300, "dot" 1700, and O 0100 GMT. (1700Z is mean of ascents between 1500 and 1800Z)

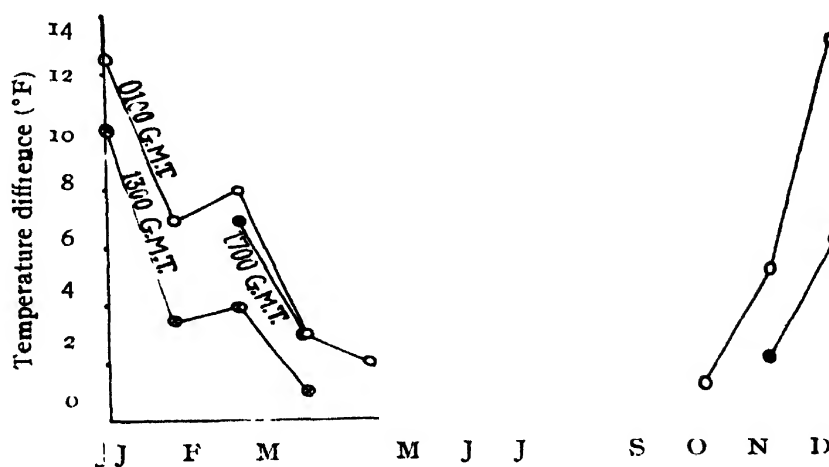


FIG. 4

Mean temperature difference between the ground and the top of the inversion layer at Calcutta in different months. Mean times of ascent in symbols are "crossed circle" 1300, "dot" 1700, and O 0100Z. (1700Z is mean of ascents between 1500 and 1800Z)

periods. Little air mass change obtains during the SW monsoon season, hence the low scatter during this period. Air mass conditions fluctuate again during the post-monsoon season when tropical cyclones from the Bay of Bengal affect the region and these fluctuations probably explain the somewhat high scatter during this period.

TABLE III

Number of nights per month on which inland super-refraction was experienced by radars in Bengal in 1943 (after Durst)

Wave length	J	F	M	M	J	A	S	O	N	D
1½ m	30	27	24	20	25	11	08	25	28	31
7 m	08	05	08	13	12	10	05	06	02	00

*Chart B—Nagpur, 0100 G M T. Curves, December—March:* In spite of strong temperature inversion small negative gradient of humidity does not permit the formation of any super-refracting layers during this period. But the trend of the M.R.I. profiles definitely indicates that during these months the lower atmosphere over Nagpur would produce radio-refraction in excess of the standard rate.

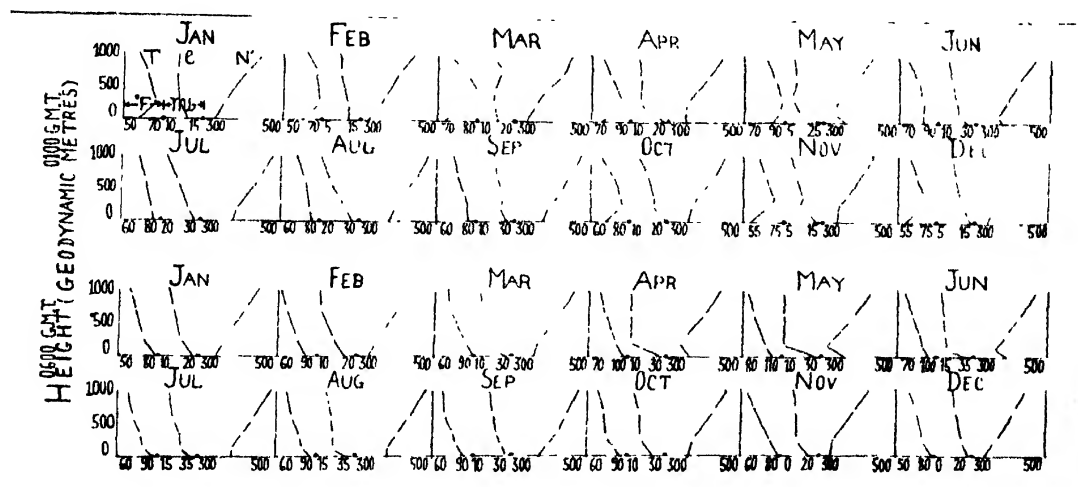


Chart B.

Vertical distributions of mean temperature  $T(^{\circ}\text{F})$ , vapour pressure  $e(\text{mb})$ , and modified refractive index  $\mu'$  at Nagpur in different months. Times of ascent : 0100 and 0600 G. M. T.

*April to mid-June and October to November.*—Strong temperature inversion or isothermal condition up to a height of 1000 feet to 1500 feet and marked vapour pressure lapse rate in the first 1000 feet of the atmosphere are favourable for pronounced super-refraction during these transition months. SS-duct forms and its width decreases from about 1000 feet in April to about 300 feet in June. The duct appears to be strongest in May.

*Mid-June to September.*—During the SW monsoon the atmosphere becomes well-mixed and homogeneous in the vertical and both temperature and humidity fall slowly with height. The resultant effect is a normal or standard lapse rate of the modified refractive index with height.

**0600 G.M.T. Curves.**—The midday temperature curves show lapse rate at all the levels. In spite of temperature lapse which by itself inhibits super-refraction of any kind, marked lapse rate of humidity in some months makes the atmosphere super-refracting even at midday. An examination of the M.R.I. profiles for midday enables us to draw the following conclusion:

*December to March.* Atmospheric refraction is normal.

*April to mid-June.*—The atmosphere is highly super-refracting. SS-duct radio-duct would appear to form, the width of which decreases from about 700 ft. in April to about 300 feet in June.

*Mid-June to November.*—M.R.I. curves for the months of July and August indicate the presence of a highly refracting layer of the SS-type within the first 400 feet of the ground. During the remaining months, the refraction is standard.

**Chart C—Madras, 0100 GMT curves. October to January.**—During these months which cover most of the period of the NE monsoon over Madras the mean temperature distribution in the lower atmosphere is either isothermal or exhibits a slight temperature inversion. But in spite of temperature condition being favourable, slow lapse rate of humidity makes refraction almost normal.

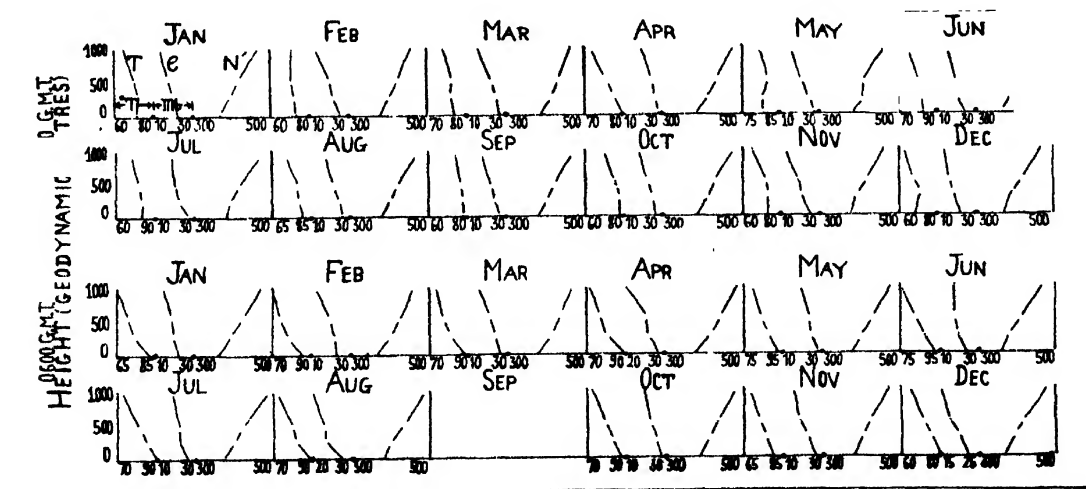


Chart C.

Vertical distributions of mean temperature  $T(^{\circ}\text{F})$ , vapour pressure  $e(\text{mb})$ , and modified refractive index  $\mu'$  at Madras in different months. Times of ascent : 0100 and 0600 G. M. T.

*February to May.*—In these summer months, except May, both temperature and humidity fall with height. But the rate of decrease of humidity being slow, the M.R.I. curves exhibit more or less normal or standard refractive condition. In May, the temperature curve shows an isothermal layer to a height of about 750 feet and an inversion layer aloft up to a height of about 1500 feet. Above 1500 feet level, there is normal temperature lapse rate. The temperature and humidity conditions as revealed by the mean



curves would give rise to an elevated duct of the ES-type, as shown in the appropriate M.R.I. curve.

*June to July.*—During these months, there is lapse of both temperature and humidity with height. The humidity lapse rate, however, is fairly high and the result is a slightly more refracting atmosphere than the normal.

*August to September.*—Temperature and humidity decrease slowly with height. M.R.I. profiles would seem to indicate normal refractive condition in these months.

*06—G.M.T. curves.* Owing to temperature lapse and slow decrease of humidity with height, refraction is normal at midday in all months except September for which no data were available.

Hatcher and Sawyer's investigation on the sea-breeze structure at Madras has shown that when strong sea-breeze prevailed during afternoon hours in summer months, radio-ducts appeared to form over the coastal strip as well as over the adjoining sea areas. ES-ducts probably form in such conditions owing to the relative orientation of the cool sea breeze underneath the warm continental air flowing out towards the sea.

#### METEOROLOGICAL ORIGIN OF THE MEAN M.R.I. PROFILES

The vertical distribution of the mean modified refractive index as shown in charts A, B and C may be explained qualitatively in terms of the mean atmospheric conditions that occur in India in different months. For this purpose, representative air-flow charts for three dominant seasons in India are presented in figures 5-7. It is well-known that temperature inversion and

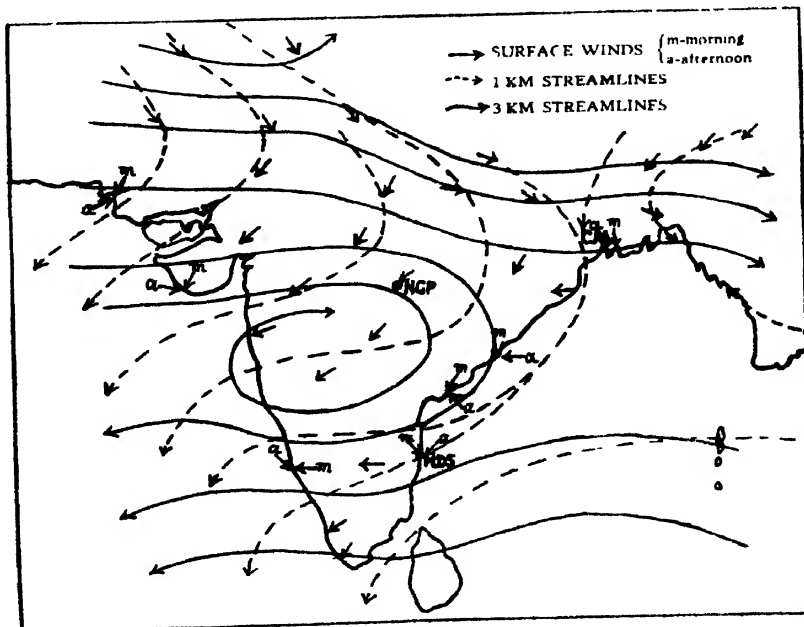


FIG. 5  
Winter air-flow chart, December

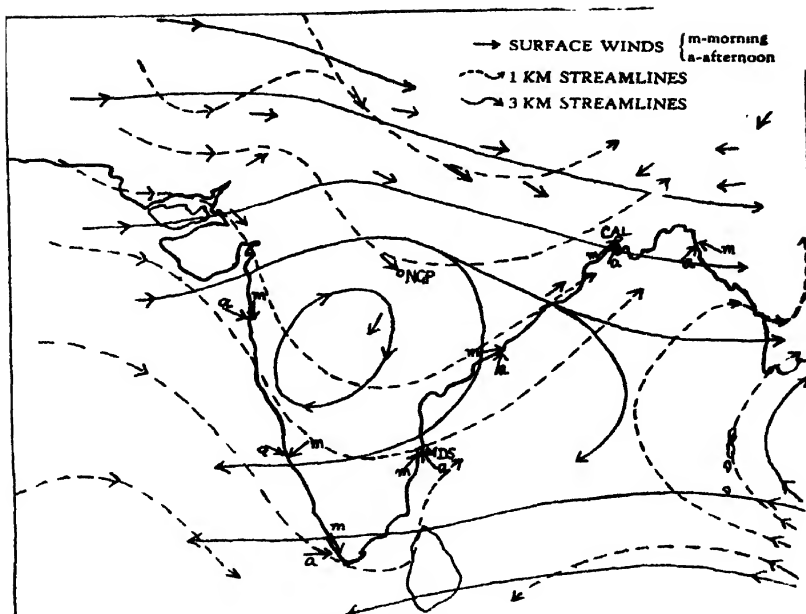


FIG. 6  
Summer air-flow chart, April

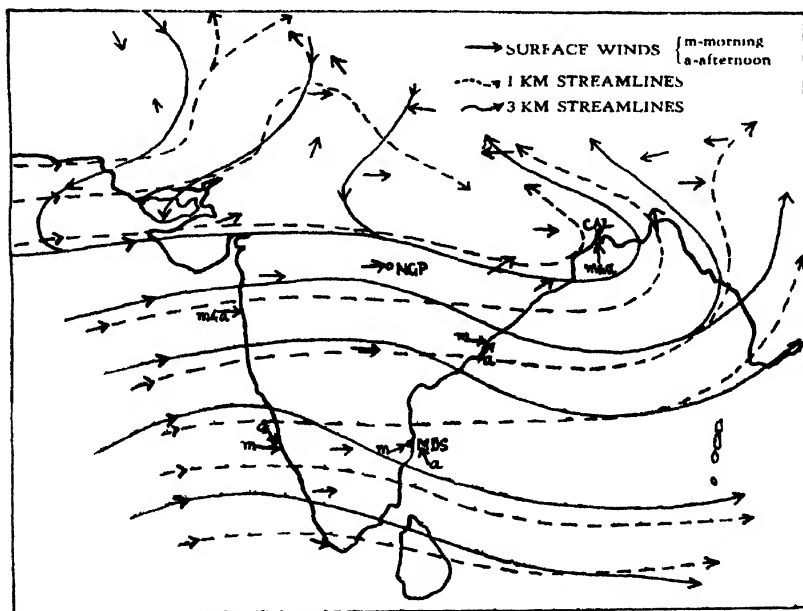


FIG. 7  
Monsoon air-flow chart, August

negative gradient of humidity with height originate in certain meteorological conditions. Some of these are: (1) rapid cooling of the ground layers by radiation at night, (2) subsidence of air from high levels, and (3) horizontal advection of dry and warm air over cool and moist air. The first two are satisfied when anticyclonic conditions prevail over the area under investigation, whereas, the third is met with mostly in coastal areas where the sea-

breeze phenomenon is common and also over some areas where the local pressure distribution brings in a thin layer of cool and moist air underneath warm continental air. An examination of figures 5-7 in the light of the foregoing observations enables the following conclusions to be drawn in regard to the mean temperature and humidity profiles. During the period October to February, which covers most of the winter season, the air circulation over India is anticyclonic from the ground to a high level. The result is large-scale subsidence of air and marked vertical stability of the lower atmosphere. Extreme dryness of the air keeps the skies cloudless and rapid nocturnal radiation builds up a steep temperature inversion which lasts till the following morning when the inversion is destroyed by insolation and replaced by a temperature lapse rate. Temperature distribution, therefore, is extremely favourable for the development of a strong radio-duct during evening and night hours but the effect of a slow lapse rate of humidity somewhat counteracts this process. Over Madras, the temperature inversion is only slight and slow lapse rate of humidity with height seldom permits the formation of a super-refracting layer in winter months. Figure 6, which depicts the mean airflow for the summer months of March to May, shows the same high level subsidence though in the very lowest levels the subsidence is being replaced by the opposite effect of convection indicated by the somewhat cyclonic bend of the streamlines. Over the land, the air still being dry, nocturnal cooling develops temperature inversion. But the inversion is less marked now than in winter months. There is also a slow decrease of humidity with height. But locally during this period there is influx of moisture in the lowest levels over deltas and coastal areas either in the form of a sea-breeze or as a steady moist current maintained by the local pressure distribution. When such incursion of moisture takes place close to the ground, an elevated temperature inversion results and the humidity falls off rapidly in going from the lower moist layer to the upper dry layer. An elevated radio-duct of the ES or EE-type forms. Examples of the formation of such elevated radio-ducts have already been cited in the case of Madras and south Bengal in the preceding pages.

During the period of the south-west monsoon from June to September the atmosphere is thoroughly mixed by marked convection indicated by the cyclonic curvature of the streamlines up to a high level and the result is a lapse rate in both temperature and humidity and a normal radio-refraction. But the propagation inferences drawn in the case of midday M. R. I. curves for Nagpur and early morning curves for Madras for this period show variations from the general rule. In spite of the normal temperature lapse rate, marked negative gradient of humidity with height makes all the difference. The rapid increase in wet-bulb temperature in unison with the rise in air temperature about midday hours close to the ground establishes a steep lapse rate of humidity with height and this more than offsets the inhibitive effect of a temperature lapse rate and favours the formation of a super-refract-

ing layer. The dependability of the observed values of the wet-bulb temperature has not been questioned in the present paper and is subject to further investigation.

#### ACKNOWLEDGMENTS

The author's grateful thanks are due to Mr. S. Basu, Deputy Director-General of Observatories (Forecasting), India, for having kindly arranged to supply the Indian daily weather reports from which the basic temperature and humidity data for the present investigation were obtained. His thanks are also due to Dr. B. N. Singh of the Defence Science Organisation, India, for having kindly gone through the paper and advanced valuable criticisms. Acknowledgment is made to Air Headquarters, India, for permission to publish the paper.

I.A.F. STATION  
PALAM, DELHI

#### REFERENCES :

- Appleton, F. 1946, Report of a conference on Meteorological factors in Radio-wave propagation, published by the Physical Society, England. pp 4-6.
- Booker, H. G. 1946, Meteorological factors in Radio-wave propagation, p. 82.
- „ „ 1948, *Weather*, **3**, 42.
- Chatterjee, G. and Sur, N. K., 1929, *Memoirs of the Ind. Met. Dep.* **26**, 171.
- Durst, C. S., 1946, Meteorological factors in Radio-wave propagation, p. 206,
- Eckeraley, T. L., and Millington, G., 1938, *Phil. Trans, Roy. Soc.*, **A. 237**, 273.
- Hatcher, R. W. and Sawyer, J. S., 1947, *Quart. J. R. Met. Soc.*, **73**, 317,
- Ramdas, L. A., 1943, *Ind. Met. Dept. Tech.*, Note No. 3.
- Saha, K. R. 1949. *Science and Culture*, **14**, 355.
- Smith-Rose, R. L. and Stickland, A. C., 1946, Meteorological factors in Radio-wave propagation, pp 18-37.

# ON THE MEASUREMENT OF THE ANGULAR CORRELATION BETWEEN TWO GAMMA RAYS OF NICKEL (60)\*

By SUDHANSU DAS AND SUNIL KUMAR SEN

(Received for publication, August 7, 1951)

**ABSTRACT.** The angular correlation between the two cascade gamma rays of  $\text{Co}^{60} \rightarrow \text{Ni}^{60}$  transitions has been measured, using Geiger Müller counters. The source was in the form of  $\text{CoCl}_2$  solution. From the correlation function  $W(\theta)$  of Hamilton, the curve  $\frac{N(\theta)}{N \pi/2}$  plotted against  $\theta$ , was explained with the assumption that the two radiations are octopole-octopole in nature. An alternative spin-parity scheme of  $\text{Co}^{60} \rightarrow \text{Ni}^{60}$  transitions has been suggested.

## INTRODUCTION

The method of determining change of angular momentum from life time of a metastable state has its natural limitations when the gamma rays have large disintegration constant, that is, half-lives shorter than  $10^{-8}$  second. In this region, the measurement of angular correlation of the successive gamma rays has been suggested, following the work of Hamilton (1940) who showed that there is correlation between the angle of emission of gamma rays and the spin change associated with the transition. The gamma rays from excited  $\text{Ni}^{60}$  following the emission of  $\beta$ -rays from 5.3 years  $\text{Co}^{60}$  have been studied. Such attempts have been made previously by Brady and Deutsch (1950) which we have repeated and extended. Dunworth (1940) first suggested that there might be some angular correlation between the directions of emission of two successive gamma rays emitted by a nucleus when this passes from an excited level  $A$  to the ground level  $C$  by way of definite intermediate level  $B$ .

On Dunworth's suggestion, the problem was theoretically investigated by Hamilton (1940) according to whom the probability of the second quantum to be emitted at an angle  $\theta$  with respect to the first per unit solid angle in cascade emission is given by the series,

$$W(\theta) = 1 + \sum_1^l a_k \cos^{2k} \theta$$

$$= 1 + a_1 \cos^2 \theta + a_2 \cos^4 \theta + a_3 \cos^6 \theta + \dots \quad (1)$$

where  $l$  is the multipole order of the gamma rays present in the transitions and the coefficient  $a_k$ 's are constants but are functions of  $J_1$ ,  $J_2$  and  $J_3$ , the respective spin values of the initial, intermediate and final states of the nucleus. For dipole-dipole transition,  $l=1$ , the equation (1) becomes

$$W(\theta) = 1 + a_1 \cos^2 \theta, \quad \dots \quad (2)$$

and for quadrupole-quadrupole transitions

$$W(\theta) = 1 + a_1 \cos^2 \theta + a_2 \cos^4 \theta, \quad \dots \quad (3)$$

\* Communicated by Prof. M. N. Saha.

and similarly for other higher poles. If, however, in the above case one of the transitions is dipole i.e. dipole-quadrupole or quadrupole-dipole, on explicit computation of  $a$ 's it has been found (Hamilton 1940) that  $a_2$  becomes zero and (3) reduces to

$$W(\theta) = 1 + a_1 \cos^2 \theta$$

In general, the number of terms in  $\cos \theta$  in equation (1) will be determined by the lowest order multipole present in the transitions.

$J_1, J_2, J_3$  take values depending on the type of radiation. For dipole-dipole transitions,  $J_1 - J_2 = J_2 - J_3 = 0$  or  $\pm 1$ , and  $a_1$  may take any value. Hamilton (1940) has calculated the values of  $a_1$  for dipole-dipole, dipole-quadrupole and those of quadrupole-quadrupole radiations for all possible values of  $J_1, J_2$  and  $J_3$ .

The values of the coefficients for octopole and of higher multipole order radiations have not yet been worked out.

From equation (1) it will be seen that at  $\theta = 90^\circ$ ,  $W(\theta) = 1$ . Thus  $W(\theta)$  in equation (1) represents also the ratio of the probability of gamma rays emitted at an angle  $\theta$  to that emitted at  $90^\circ$ .

The experimental verification is obtained by observing coincidence rates between successive gamma rays at different angles. Such experiments have been carried out during the last few years. The experiments have borne out Hamilton's idea of the existence of such correlation between successive gamma rays emitted by a nucleus and have given plausible numerical values for the spin changes in certain nuclei.

#### EXPERIMENTAL ARRANGEMENT AND DETAILS

The disintegration of  $\text{Co}^{60}$  has been thoroughly investigated by Deutsch, Elliot and Roberts (1945) and the results are shown in figure 4. We find that two gamma rays are emitted in cascade from the excited state of  $\text{Ni}^{60}$ . We have studied the angular correlation between these two gamma rays. The experimental arrangement is shown in figure 1.

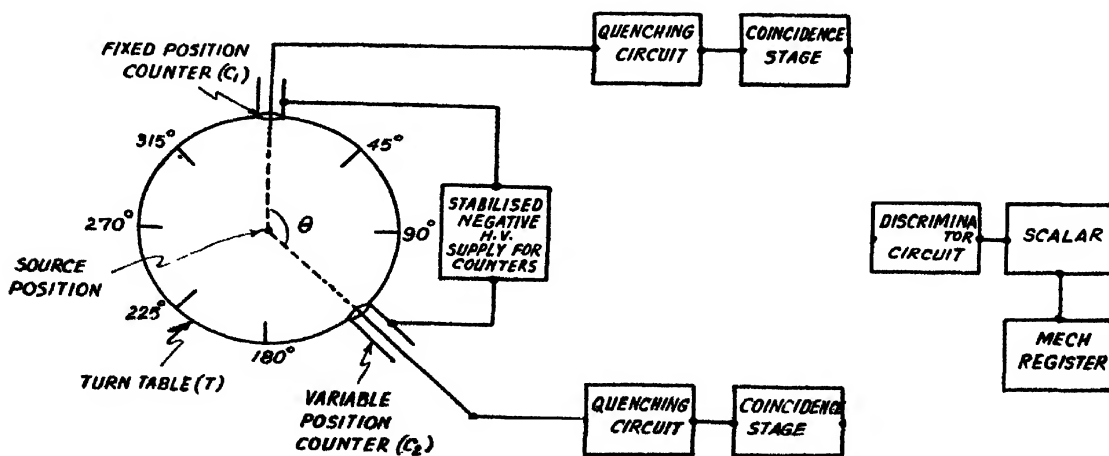


FIG. 1

Schematic diagram of the experimental arrangement

Two similar gamma counters,  $C_1, C_2$  are placed symmetrically at their end-on positions with respect to the source on a turntable  $T$ , graduated in degrees. One of the counters,  $C_1$ , is fixed in its position while the other  $C_2$ , is free such that it can be rotated about the axis of the turntable with the source as centre and then fixed at any position on it. The source, 5.3 years  $Co^{60}$ , was in the form of cobalt chloride solution contained in a cylindrical glass capsule of 0.8 centimetre diameter and its axis coincided with that of the turntable.

The effective ends of the counters were found by coincidence experiments with a radium source and taking this into account, the counters were placed in such a way that these effective ends of both the counters were just ten centimetres away from the centre of the source. The diameter of the counters was 1.8 centimetres and the angular resolution of the arrangements was  $10^\circ 18'$ .

The thickness of the glass capsule containing the source and the glass thicknesses of the counters were calculated to be sufficient to cut off all primary beta rays emitted by the disintegrating nuclei.

Since the gamma rays of  $Ni^{60}$  are fairly energetic, 1.1 and 1.3 Mev, it was apprehended that Compton scattering might give rise to stray coincidence counts. To see the effect of scattering we have observed coincidence and single counts of the counters at 180 degrees and at 90 degrees under varied conditions, namely, (a) the counters covered with lead shield of thickness  $\frac{1}{8}$  inch; (b) with a thick lead sheet of one centimetre thickness between the counters as partition; (c) with the source itself covered with thin lead sheet; (d) with the ends of the counters covered with thin aluminium sheet and (e) with no absorbers on and near about the counters. These general tests showed definitely that the presence of any material near the source or the counters increased the scattering effect. We found that except for the last case, the scattering effect had always decreased the ratio  $\frac{N(\pi)}{N(\pi/2)}$

TABLE I

Case	$\frac{N(\pi)}{N(\pi/2)}$
a	1.10
b	1.31
c	1.23
d	1.30
e	1.47

The results of these experiments are given in the Table I. We used, therefore, a minimum amount of material for mounting the counters and source-holders and avoided any material in the form of absorbers. The symmetry of the moving counter about the source was assured by observing the equality in single counts at different positions on the turntable with the source at the centre.

The output pulses from the counters (figure 2) are first applied to the grids of the two cathode follower type quenching circuits and then to Rossi type coincidence circuit using two 6SJ7 valves. The output of the coincidence circuit is fed to the input of a discriminator, which is essentially an one-shot multivibrator triggered only by pulses above a pre-determined amplitude. This removes the partials, if any, from the coincidence stage. The square top negative pulse from the discriminator operates a standard laboratory 128 scaler circuit.

Highly stabilised power supplies were used for the electronic recording circuits and the counters. The A.C. mains supply was also stabilised by a magnetic stabiliser.

The resolving time of the coincidence circuit was determined from the measurements of random coincidence counts due to two uncorrelated sources such as  $\text{Co}^{60}$  and radium. The resolving time of the circuit was found to be of the order of 0.4 microsecond.

The experiment on  $\text{Co}^{60}$  consisted of taking coincidence rates between two gamma rays at different angles between the two counters and the number of individual counts in each counter at every position, both before and after each observation. Every time the random coincidence rates due to two gamma rays from two different nuclei were subtracted from the total coincidence rates to get the genuine coincidence rates.

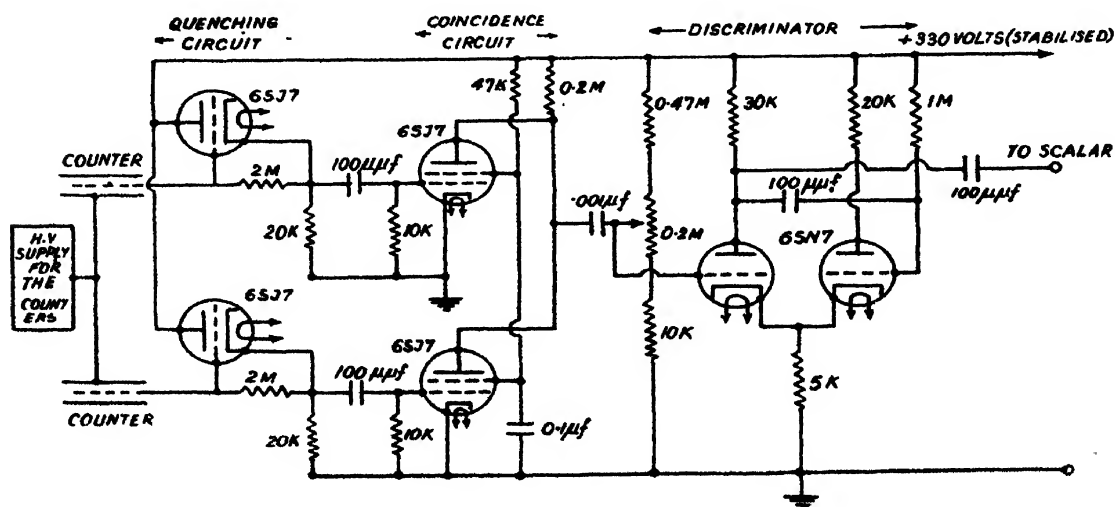


FIG. 2

Circuit diagram of the coincidence and recording unit



# EXPERIMENTAL RESULTS

The experimental results are shown in figure 3. The ordinate gives the ratio of the coincidence rates at any angle  $\theta$  to that at 90 degrees and the abscissa denotes the angle between the axis of the free counter and that of the fixed counter.

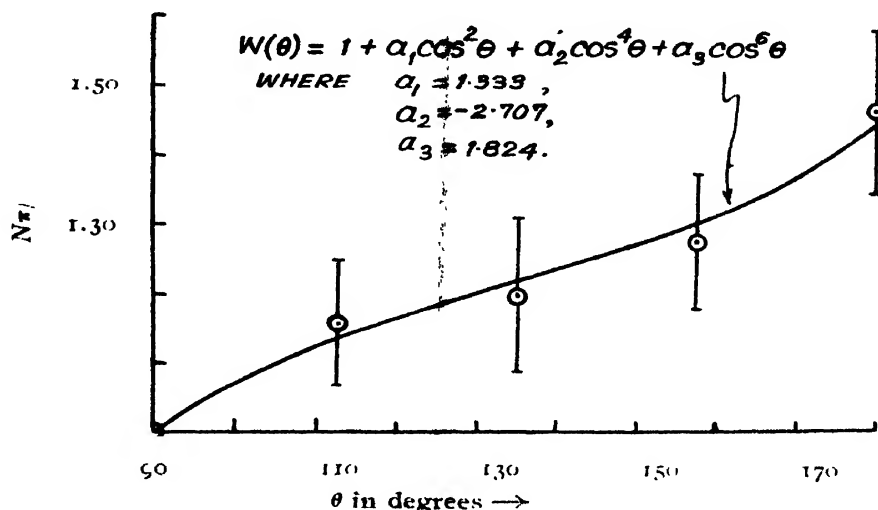


FIG. 3

Experimental curve for the angular correlation of the two gamma rays of  $\text{Ni}^{60}$

The best fit of our experimental curve, within the statistical error, is found with the equation,

$$W(\theta) = 1 + a_1 \cos^2\theta + a_2 \cos^4\theta + a_3 \cos^6\theta, \quad (4)$$

in which the values of the coefficients are given as  $a_1 = 1.333$ ,  $a_2 = -2.707$ ,  $a_3 = 1.824$ .

This shows that the lowest multipole order present in the gamma ray transitions from  $\text{Ni}^{60}$  is octopole *i.e.*  $l=3$ . Since the values of the coefficients of  $\cos \theta$  for octopole and higher multipole order radiations have not been calculated, we could not assign the definite spin values of  $\text{Ni}^{60}$ . But our experiments tend to prove that one of the radiations is octopole while the other is, at least, octopole or higher multipole order. From the above considerations we, however, assign the angular momenta of the states of  $\text{Ni}^{60}$  as 6, 3, 0, which accord with the spin assignment of the  $\beta^-$ -ray transitions from  $\text{Co}^{60}$ .

# DISCUSSION

It is interesting to note that contrary to previous results of other workers (Brady and Deutsch, 1950) whose results showed quadrupole-quadrupole transition in  $\text{Ni}^{60}$ , our experiment speaks in favour of octopole-octopole case. How far we are justified in this conclusion, can be understood mainly from two standpoints. The first is that the experimental points when plotted

against  $\theta$  yield a curve, the best fit of which can only be made out with the equation (4) and our trials with  $\cos^2\theta$  and  $\cos^4\theta$  only have produced curves of entirely different natures from the experimental mean curve. The appearance of  $\cos^6\theta$  term in equation (4) forced us to conclude that the minimum value of  $l$  should be 3.

The other feature of our result is that the ratio  $\frac{N(\pi)}{N(\pi/2)}$  is 1.45 which is rather higher than the results obtained by Brady and Deutsch whose value is 1.17.

We further lend our support of the above conclusion from the experiment of Deutsch and Siegbahn (1950) who approached the problem by an entirely different method, namely the measurement of internal conversion coefficients of the two gamma rays of  $\text{Ni}^{60}$ . In assigning the multipolarity of these gamma rays of  $\text{Ni}^{60}$ , on the evidence of their measured conversion coefficient we quote Deutsch and Siegbahn, that "both radiations are either quadrupole or possibly octopole. Thus the first excited state has probably spin 2 or possibly 3". Therefore, our results tend to agree with the findings of these authors.

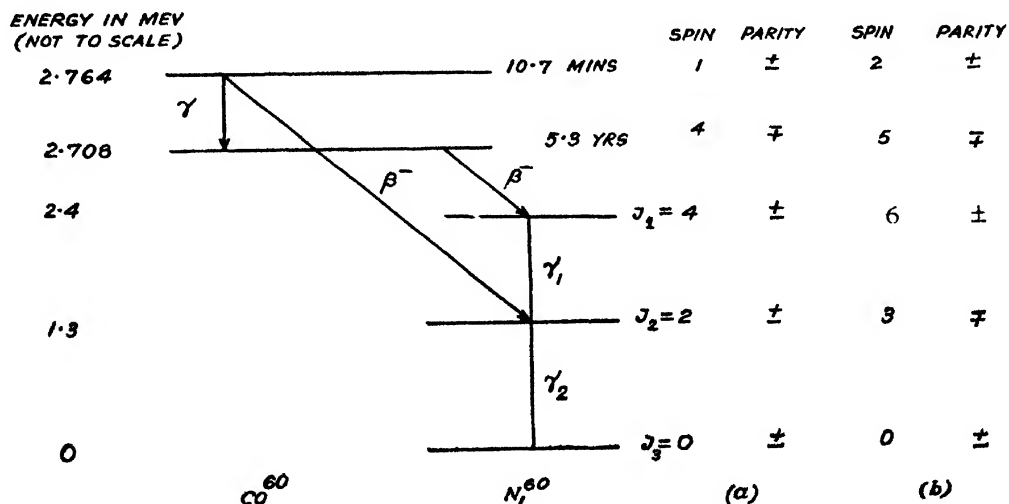


FIG. 4

Disintegration and spin-parity scheme of  $\text{Co}^{60}$

The existing spin-parity scheme of  $\text{Co}^{60} \rightarrow \text{Ni}^{60}$  transitions is reproduced in figure 4 (a) along with the one proposed by us in (b) of figure 4 for elucidation. A glance at the schemes will show that figure 4- (b) is a parallel mode of spin-parity changes of figure 4- (a).

It is also worthwhile to note that even with  $\Delta J = \pm 3$  for the excited state of  $\text{Ni}^{60}$ , have half lives less than  $10^{-9}$  seconds as calculated from Bethe's formula and explain why attempts to detect the half lives of the gamma rays by delayed coincidence method failed.

## CONCLUSION

In view of our experimental results we may say that even with octopole-octopole transitions it is possible to set up an alternative but self-consistent spin-parity scheme of the levels of  $Co^{60} \rightarrow Ni^{60}$  transitions. It is, of course, not very clear to us why our coincidence countings yielded such a high value of  $\frac{N(\pi)}{N(\pi/2)} = 1.45$  or stating otherwise, why other workers have got such a low value as 1.17. Our experience during this experiment is that the scattering phenomenon always tends to decrease the ratio. Since all these workers have used photo-electron multipliers as their detectors of gamma rays, they had to put the whole assembly in light tight metal chambers. As such, our surmise is that perhaps scattering phenomenon was far more prominent than in our case and had pulled down the ratio to such a low value.

Further work is being carried out in this laboratory using scintillation counters to study the angular correlation of two gamma rays of  $Ni^{60}$  with arrangements eliminating all possible scattering effect.

## ACKNOWLEDGMENT

Thanks are due to Prof. M. N. Saha, D.Sc., F.R.S. for his kind interest in the experiment. Authors are also thankful to Drs. B. D. Nag and A. K. Saha, for their helpful discussions during the work.

INSTITUTE OF NUCLEAR PHYSICS,  
CALCUTTA UNIVERSITY.

## REFERENCES

- Brady, E. L. and Deutsch, M., 1950, *Phys. Rev.*, **78**, 558.  
 Deutsch, M., Elliot, L. G. and Roberts, A., 1945, *Phys. Rev.*, **68**, 193  
 Deutsch, M. and Siegbahn K., 1950, *Phys. Rev.*, **77**, 680  
 Dunworth, J. V., 1940, *R.S.I.*, **11**, 167.  
 Hamilton, D. R., 1940, *Phys. Rev.*, **68**, 122



# ON THE ORIGIN OF LOW FREQUENCY RAMAN LINES IN PARA-DICHLORO BENZENE.\*

By A. K. RAY

(Received for publication, September 16, 1951)

## Plate XVI

**ABSTRACT.** The Raman spectra of the two types of the crystals of para-dichlorobenzene have been reinvestigated at different temperatures. One of the types was obtained by slowly cooling the melt (Type I) and a new line at  $17\text{ cm}^{-1}$  was observed in the spectrogram of this sample at  $45^{\circ}\text{C}$ . Another sample was prepared by suddenly cooling the melt (Type II) and at  $28^{\circ}\text{C}$  it yielded lines at 17, 40, 50 and  $84\text{ cm}^{-1}$ , but when this sample was once cooled below  $0^{\circ}\text{C}$  and brought back to  $28^{\circ}\text{C}$  the line at  $17\text{ cm}^{-1}$  was found to split up into two lines at 13 and  $27\text{ cm}^{-1}$ , and the lines at 40 and  $50\text{ cm}^{-1}$  combined to form a broad band at  $52\text{ cm}^{-1}$ . All the six lines in the low-frequency region were found to shift away from the Rayleigh line with the lowering of the temperature up to  $-18^{\circ}\text{C}$ .

It is pointed out that the different sets of lines in the low-frequency region observed in the case of the two types is due to cooling of one of the crystals once down to a few degrees above  $0^{\circ}\text{C}$  and the change is irreversible. It is further pointed out that the single crystal, which was studied by Saksena (1950), corresponds to the latter type mentioned above and the crystal in its life history might have been cooled down to a temperature a few degrees above  $0^{\circ}\text{C}$ .

The origin of these lines is discussed. The changes observed in the intensities and positions of the Raman lines due to intramolecular oscillations with solidification of the substance are also discussed.

## INTRODUCTION

The Raman spectrum of para-dichlorobenzene in the solid state was studied previously by a large number of workers. Vuks (1936) first observed that para-dichlorobenzene in the solid state (not cooled below  $35^{\circ}\text{C}$ ) yields a set of new Raman lines in the low-frequency region and at temperatures below  $35^{\circ}\text{C}$ , the number and position of these lines change. Sirkar and Gupta (1936), studied the Raman spectra of this crystal at different temperatures, going down up to  $-180^{\circ}\text{C}$ . They observed three new lines at 40, 50,  $82\text{ cm}^{-1}$  in the case of the crystals both at  $45^{\circ}\text{C}$  and  $32^{\circ}\text{C}$ . But these lines shifted to 46, 50,  $92\text{ cm}^{-1}$  respectively when the crystal was once cooled in ice and again brought to about  $32^{\circ}\text{C}$ , and this change did not take place on merely cooling the crystal to a temperature just below  $35^{\circ}\text{C}$ . At  $-180^{\circ}\text{C}$ , these lines were found to shift away from the Rayleigh line. Recently,

\* Communicated by Prof. S. C. Sirkar

Narain and Saksena (1951) have reported the results of investigation on the Raman spectra of two types of crystals of para-dichlorobenzene, one of which is assumed by them to be a single crystal and the other a poly-crystalline mass. They have concluded that as these two types yield two different sets of Raman lines in the low-frequency region, the structures of the two types are not probably the same. They have, however, overlooked the fact observed by Sirkar and Gupta (1936, 1937) that the latter authors also observed two different sets of lines for the two types of the solid, one of which had once been cooled in ice and the other had not been cooled in that way, and that the X-ray investigation showed identical structure for two types of the solid. Saksena (1950) has also suggested that in the type of the crystal which does not yield the line  $27\text{ cm}^{-1}$ , the molecule is rotating freely about an axis perpendicular to its plane, in the crystal lattice. Recently, an improved experimental arrangement was developed in this laboratory for studying the Raman spectra of organic crystals at different low temperatures (Bishui, 1948) and it was thought worthwhile to study the Raman spectra of the crystal of para-dichlorobenzene at different low temperatures to test the hypotheses put forward by previous workers regarding the origin of the lines in the low-frequency region.

#### EXPERIMENTAL

Para-dichlorobenzene, from May and Baker's original sealed bottles, was used for the present investigation. It was first crystallised out from a chemically pure benzene solution. The crystals were then melted under vacuum in a pyrex flask to which the container of pyrex glass used for the experimental observation was joined and the liquid was distilled in vacuum in the container which itself was kept at a temperature above  $53^{\circ}\text{C}$  (melting point for para-dichlorobenzene). This process was repeated a number of times. The sealed container with the final distillate was put in a heater provided with two windows at right angles to each other and the temperature inside the heater was slowly lowered to  $45^{\circ}\text{C}$ . The Raman spectra of the clear homogeneous crystal formed at this temperature, was studied with a Fuess glass spectrograph, as usual. Another sample was distilled in vacuum and condensed in a second pyrex tube, but the molten mass was solidified quickly, and cooled to about  $28^{\circ}\text{C}$ . The solid mass obtained in this way was not a single crystal and it was full of cracks. This type will be called Type II in the present paper. The Raman spectrum of this sample was first photographed at room temperature ( $28^{\circ}\text{C}$ ). The tube containing the crystal was held vertically in a transparent Dewar vessel and the Raman spectra of this sample at about  $-180^{\circ}\text{C}$  and  $-100^{\circ}\text{C}$  were next studied. The sample was again brought to a temperature of  $28^{\circ}\text{C}$  and its Raman spectrum was again photographed. The Raman spectrum of the substance in the liquid state at  $60^{\circ}\text{C}$  was also studied to test the purity of the substance. Each spectrogram contained also an iron-arc comparison.

## RESULTS AND DISCUSSION

The results are given in Table I. In Table II, the frequency-shifts of the Raman lines in the low-frequency region have been compared with those observed by previous workers. Some of the spectrograms are reproduced in Plate XVI, figures 1—3. The low-frequency region enlarged about six times is reproduced in figures 4—7.

## (a) LINES IN THE LOW-FREQUENCY REGION

From Table II it is evident that besides the three lines reported by Sirkar and Gupta (1936), a new line at  $17\text{ cm}^{-1}$  is observed in the case of the crystal at  $45^{\circ}\text{C}$ . The line is found to persist even when the crystal is cooled down to  $28^{\circ}\text{C}$ . But when the crystal is once cooled in liquid air and brought back to  $28^{\circ}\text{C}$ , an entirely different set of five lines at 13, 27, 52, 94 and  $127\text{ cm}^{-1}$  is observed in place of the lines at 17, 40, 50,  $83\text{ cm}^{-1}$  observed in the case of the crystal not cooled below  $28^{\circ}\text{C}$ . It appears that the line  $17\text{ cm}^{-1}$  splits up into two lines at 13 and  $27\text{ cm}^{-1}$  and the lines at 40 and  $50\text{ cm}^{-1}$  combine to form a broad line at  $52\text{ cm}^{-1}$ . The line  $83\text{ cm}^{-1}$  shifts to  $94\text{ cm}^{-1}$  and a new feeble line appears at  $127\text{ cm}^{-1}$ . Neither the line  $17\text{ cm}^{-1}$  observed in the case of the first type of the crystal nor the lines at 13 and  $27\text{ cm}^{-1}$  observed in the case of the crystal of 'Type II' were observed by Sirkar and Gupta (1936), probably because the quality of the spectral lines produced by the spectrograph used by them was not as good as in the present investigation. The fact, however, that on once cooling the crystal to about  $0^{\circ}\text{C}$  and again bringing it back to  $32^{\circ}\text{C}$ , a different set of lines was observed by them, is corroborated by the results obtained in the present investigation. It is also found in the present investigation that on merely cooling down the crystal of 'Type I' from  $45^{\circ}\text{C}$  and without allowing the crystal any time to come below  $28^{\circ}\text{C}$ , no change occurs in the positions of the lines in the low-frequency region. This also confirms the observation made by Sirkar and Gupta (1936).

The results obtained by Venkateswaran (1938) also seem to corroborate the fact observed previously by Sirkar and Gupta (1936) and in the present investigation that on merely cooling down the crystal from  $45^{\circ}\text{C}$  to  $25^{\circ}\text{C}$  no change in the position of the lines takes place; because at  $25^{\circ}\text{C}$  he observed a broad band at  $48\text{ cm}^{-1}$  which may be assumed to represent the two lines at 43 and  $55\text{ cm}^{-1}$  observed by him at  $45^{\circ}\text{C}$ . The frequency-shift of the other line observed by him at  $25^{\circ}\text{C}$  seems to be too high. The value ought to be  $83\text{ cm}^{-1}$  instead of  $88\text{ cm}^{-1}$ . He, however, did not investigate the Raman spectra of the crystal after cooling it down once to about  $0^{\circ}\text{C}$ .

Recently, Narain and Saksena (1951) have reported that they have observed two different sets of lines in low-frequency region for the first time in the case of two types of crystals of  $p\text{-C}_6\text{H}_4\text{Cl}_2$ . They have stated that they have observed in the case of a single crystal of  $p\text{-C}_6\text{H}_4\text{Cl}_2$  prepared by

slow cooling, three new lines at 27, 54, 94  $\text{cm}^{-1}$ , and in the case of a solid mass obtained by suddenly cooling the melt they observed these lines at 45, 57 and 84  $\text{cm}^{-1}$ . It can be seen from Table II that the latter set of lines corresponds to the three of the four lines observed in the present investigation in the case of the crystal obtained by cooling the molten mass very slowly (Type I) up to 45°C. This crystal was absolutely homogeneous and

TABLE I

Para-dichloro-benzene ( $\text{C}_6\text{H}_4\text{Cl}_2$ )

Melt at 60°C $\Delta\nu$ in $\text{cm}^{-1}$	Crystal at 45°C $\Delta\nu$ in $\text{cm}^{-1}$	Crystal at 28°C $\Delta\nu$ in $\text{cm}^{-1}$	Crystal once cooled in liquid air		
			Crystal at 28°C $\Delta\nu$ in $\text{cm}^{-1}$	Crystal at about -100°C. $\Delta\nu$ in $\text{cm}^{-1}$	Crystal at about -180°C. $\Delta\nu$ in $\text{cm}^{-1}$
			13(3)e,k	11(3),k	11(3) k
	17(3),k	17(3),k	27(4)e,k	29(4)e,k	30(4)e,k
	40(2)e,k	40(2)e,k	52(4b)e,k	53(3)e,k	55(3)e,i,k
	50(2)e,k	50(2)e,k		58(58)e,k	61(48)e,k
	83(2b)e,k	83(2b)e,k	94(2b)e,k	102(3b)e,k	106(38)e,k
			127(1)e,k	127(1)e,k	127(0)e,k
296(4)e,k,	306(4)e,k	306(4)e,k	308(4)e,k	308(4)e,k	308(4)e,k
331(6)e,k,	331(6)e,k	331(6)e,k	328(6)e,k	328(6)e,k	328(6)e,k
630(2)e,k,	630(2)e,k	630(2)e,k	631(4)e,k	632(4)e,k	633(4)e,k
675(0)e,k,					
747(5)e,k,	747(5)e,k	747(5)e,k	746(5)e,k	746(5)e,k	746(5)e,k
1062(2)k,	1056(2) k	1056(2)k	1062(2)k	1072(2)k	1072(2)k
1086(1)e,k,	1086(0),e		1086(0),e	1086(0),e	1086(0),e
1109(5)e,k,	1109(7)e,k	1109(7)e,k	1109(7)e,k	1110(7)e,k	1110(7)e,k
1170(0)k,			1170(0)e,k	1170(0),k	1170(0),k
1383(0b)e,k,	1383(0b)e,k	1383(0b)e,k	1383(0b)e,k	1383(08)e,k	1384(08)e,k
1489(0)e,k,			1489(0)e,k	1489(0)e,k	1489(08)e,k
1573(7)e,k,	1573(2)e,k	1573(2)e,k	1573(2)e,k	1573(2)e,k	1573(2)e,k
3068(10dd)k,	3072(10dd)k	3072(10dd)k	3072(4)k	3072(48)k	3072(48)k
			3076(6)k	3076(68)k	3076(68)k



Fig. 1.

Fig. 2.

Fig. 3.

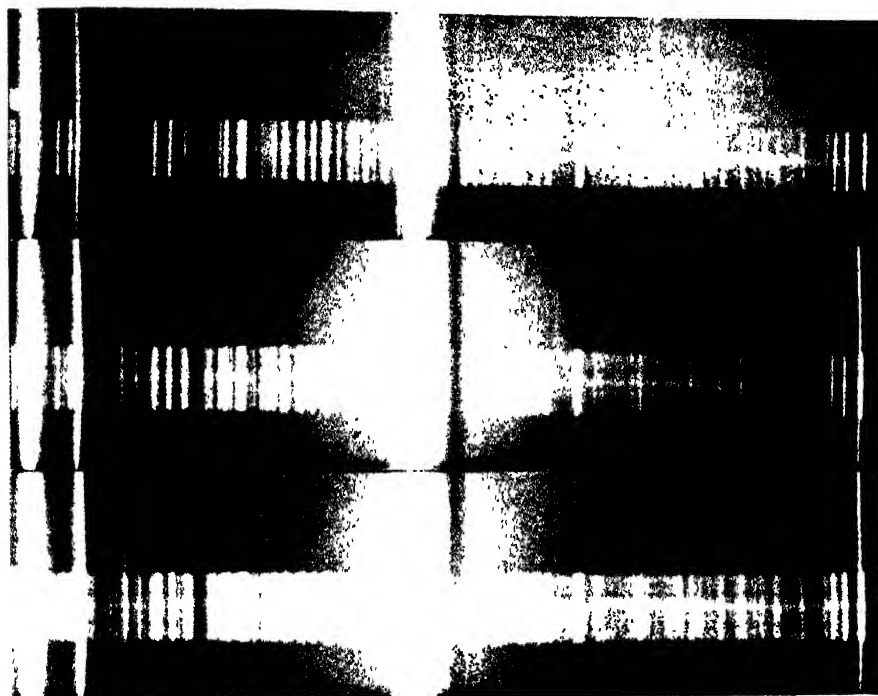


Fig. 4.

Fig. 5.



Fig. 6.

Fig. 7.



### Raman spectra of para-dichlorobenzene

- Fig. 1.  $\text{p-C}_6\text{H}_4\text{Cl}_2$  liquid at 60°C.  
 Fig. 2. - Do solid (once cooled in liqu'd oxygen) at 28°C.  
 Fig. 3. - Do solid at about -180°C.  
 Fig. 4. - Do solid (once cooled below 0°C.) at 28°C.  
 Fig. 5. - Do solid (not cooled below 45°C.) at 45°C.  
 Fig. 6. - Do solid at about -180°C.  
 Fig. 7. - Do solid at about -100°C.



TABLE II

Low-frequency Raman lines in para-dichlorobenzene.

Sirkar and Gupta (1936)				Venkateswaran (1938)		Korshunov (1950)		Narain and Saksena (1951)		Present author		
Solid at 45°C	Solid at 32°C	Solid (once cooled in ice) at 32°C	Solid at about -180°C	Solid at 25°C	Solid at 45°C $\Delta\nu$ in cm <sup>-1</sup>	$\Delta\nu$ in cm <sup>-1</sup>	$\Delta\nu$ in cm <sup>-1</sup>	Solid I $\Delta\nu$ in cm <sup>-1</sup>	Solid II $\Delta\nu$ in cm <sup>-1</sup>	Crystal at 45°C $\Delta\nu$ in cm <sup>-1</sup>	Crystal at 28°C $\Delta\nu$ in cm <sup>-1</sup>	Crystal once cooled in liquid air
$\Delta\nu$ in cm <sup>-1</sup>	$\Delta\nu$ in cm <sup>-1</sup>	$\Delta\nu$ in cm <sup>-1</sup>	$\Delta\nu$ in cm <sup>-1</sup>	$\Delta\nu$ in cm <sup>-1</sup>	$\Delta\nu$ in cm <sup>-1</sup>	$\Delta\nu$ in cm <sup>-1</sup>	$\Delta\nu$ in cm <sup>-1</sup>	$\Delta\nu$ in cm <sup>-1</sup>	$\Delta\nu$ in cm <sup>-1</sup>	$\Delta\nu$ in cm <sup>-1</sup>	$\Delta\nu$ in cm <sup>-1</sup>	
						8(2)					13(3)	11(3)
						17(2)				17(3)	17(3)	11(3)
						27.5(10)		27(15)			27(4)	29(4)
						35(2)						30(4)
40(2)	40(2)	46(2)	55(2)	48(6)	43(6)	47.5(10)			45(12)	40(2)	40(2)	55(3)
						48.7(10)					52(4b)	
50(2)	50(2)	50(2)	60(2)		55(5)	55(10)		54(3c)	57(8)	50(2)	50(2)	58(5s)
						72(1)						61(4s)
82(2bd)	82(bd)	92(2d)	105(2s)	89(5b)	88(5b)	93(6)		94(8)	84(5)	83(2b)	83(2b)	102(3b)
											127(1)	106(3s)
												127(1)

Raman lines in Para-dichlorobenzene

approached in structure a single crystal. The lines in the low-frequency region due to such a single crystal are identical with those due to a polycrystalline mass (not cooled up to  $0^{\circ}\text{C}$ ) observed by Narain and Saksena (1951). Only the line at  $17\text{ cm}^{-1}$  which is rather faint was not observed by the latter authors. On the other hand, the three lines observed by them in the case of their crystal of Type I, which was assumed to be a single crystal by them, agree with the three of the lines observed in the present investigation in the case of a polycrystalline mass which had been once cooled down to a temperature below  $0^{\circ}\text{C}$ . Hence the hypothesis put forward by Saksena (1950) that the line  $27\text{ cm}^{-1}$  is a characteristic of a single crystal and that the lines  $27$ ,  $54$ ,  $94\text{ cm}^{-1}$  are produced in such a single crystal, while the other set of the Raman lines in the region is produced by the disoriented crystal is contradicted by the results obtained in the present investigation. The change in the positions of these lines occur only when the crystal is cooled down to about  $0^{\circ}\text{C}$  and hence the specimen assumed by Saksena (1950) to be a single crystal, must have been cooled down to a few degrees above  $0^{\circ}\text{C}$  during winter, although he has not stated it in the history of the crystal given by him. It is also seen that the line at  $27\text{ cm}^{-1}$  is not exactly a new line characteristic of Type II of the present investigation, because the broad line observed at  $17\text{ cm}^{-1}$  in the case of the crystal not cooled any time to  $0^{\circ}\text{C}$  splits up into two lines at  $13$  and  $27\text{ cm}^{-1}$  on once cooling the crystal to about  $0^{\circ}\text{C}$ . As it has been shown by Sirkar and Gupta (1937) that no change takes place in the crystal structure of *p*-dichlorobenzene on cooling the single crystal once to about  $0^{\circ}\text{C}$  and bringing it back to about  $32^{\circ}\text{C}$ , the changes mentioned above cannot be due to any change in the lattice. So the suggestion made by Saksena (1950) that the structure of the single crystal used by him is different from that of the other type obtained by suddenly cooling the molten mass is not based on any experimental fact.

The new lines were attributed to association of the molecules in the lattice by Sirkar and Gupta (1936). According to the hypothesis put forward by Kastler and Rousset (1941) and Bhagavantam (1941) these lines are due to angular oscillations of the molecules pivoted in the crystal lattice. As pointed out in previous papers (Sirkar and Ray, 1950; Ray, 1950, 1951) these two hypotheses can be tested by studying the influence of temperature on the crystals on the number, position and intensities of the lines in the low-frequency region. Rousset (1948) assumed the line  $27\text{ cm}^{-1}$  to be due to asymmetric angular oscillation of the pair of molecules in the unit cell of the lattice about an axis perpendicular to the plane of the molecule and a symmetric mode of this type yields a line at  $47.5\text{ cm}^{-1}$ . The antisymmetric mode of oscillation of the pair of molecules about an axis in the plane of the molecule and perpendicular to the line joining the C—Cl line is assumed to yield a line at  $47.5\text{ cm}^{-1}$ . The symmetric mode of the latter oscillation is assumed to give a line at  $56\text{ cm}^{-1}$ . In the present investigation, however, the crystal once cooled in liquid oxygen and brought back to  $28^{\circ}\text{C}$  has

yielded five lines at 13, 27, 52, 94 and 127  $\text{cm}^{-1}$ . The line at 52  $\text{cm}^{-1}$  is a broad band which splits up into two lines at 53 and 58  $\text{cm}^{-1}$  at  $-100^{\circ}\text{C}$ . The lines at 13 and 27  $\text{cm}^{-1}$  are very sharp and they shift very slightly in opposite directions on lowering the temperature of the crystal to  $-180^{\circ}\text{C}$ . Hence Rousset's assignment cannot be assumed to be correct, because the line at 27  $\text{cm}^{-1}$  is connected intimately with the line at 13  $\text{cm}^{-1}$  as both originate from the line 17  $\text{cm}^{-1}$ . Further, if the lines were due to angular oscillations of the molecules in the Vander Waals' field in the lattice, such wide separation of the lines due to symmetric and anti-symmetric modes of oscillation would not have taken place. In fact, such a separation would indicate strong coupling between the two molecules in the unit cell. Also, the value of the frequency, especially that of the line at 94  $\text{cm}^{-1}$  would indicate a large value of the force of restitution which is hundred times larger than the Vander Waals' forces even if the oscillation is assumed to be an angular one, as pointed out by Sirkar (1951). Further, the frequencies of the four lines observed at  $28^{\circ}\text{C}$  cannot be explained by taking into account the appropriate moments of inertia of the molecule about its three axes and assuming the value of  $\nu$  to be given by the equation

$$\nu^2 = \frac{\beta}{4\pi^2 I}$$

It has previously been pointed out by the present author (Ray, 1951) that the positions of some of the new lines in the low-frequency region in some substituted benzene compounds do not depend on the moments of inertia of the molecules. The intensities of the lines in the low-frequency region do not seem to diminish appreciably when the crystal of para-dichloro-benzene is cooled down to  $-180^{\circ}\text{C}$ . Hence these results, as well as those obtained in the previous investigations do not support the theory put forward by Kastler and Rousset (1941) and by Bhagavantam (1941) that the lines are due to angular oscillations of the molecules in the Vander Waals' field in the lattice.

Recently, Korshunov (1950) has reported 9 new lines at 8, 17, 27.5, 35, 47.5, 48.7, 56, 72 and 93  $\text{cm}^{-1}$  in the case of one modification of  $p\text{-C}_6\text{H}_4\text{Cl}_2$  and he has assigned six of these lines to rotational oscillations and three (*viz.*, 8, 17 and 35  $\text{cm}^{-1}$ ) to the translational oscillation. He has stated that the non-ideality of the crystal has allowed the latter three forbidden oscillations in the Raman effect. These results are not in quite agreement with those observed in the present investigation, because the type which yields the line 27.5  $\text{cm}^{-1}$  does not yield the line 17  $\text{cm}^{-1}$ . There is, of course, a line at 13  $\text{cm}^{-1}$  which is rather sharp. As regards the lines at 8, 35 and 72  $\text{cm}^{-1}$  the spectrograms obtained in the present investigation did not record them. On the other hand, there is an extra line at 127  $\text{cm}^{-1}$ . The presence of the line at 8  $\text{cm}^{-1}$  could not be detected in the present investigation, because the spectrograph itself produces a line in this position. The postulate that non-ideality of the crystal is responsible for the appearance

of forbidden lines is rather vague, because the nature of non-ideality is not specified, and the difficulties in explaining the origin of the other six lines mentioned above are present in the explanation offered by Korshunov. The postulate given by Sirkar and Gupta (1936) that virtual bonds between neighbouring molecules alter the polarisability of the pair of molecules during oscillation against each other is more specific and all the properties of the lines in the low-frequency region can be explained on this hypothesis.

(b) *Intramolecular oscillations.* As regards the frequency-shifts of the lines due to intramolecular oscillations, the changes observed with the solidification of the melt are not remarkable, excepting that the line at  $296\text{ cm}^{-1}$  shifts to  $306\text{ cm}^{-1}$  on solidifying the melt. But when the substance is once cooled in liquid oxygen and again brought back to  $28^\circ\text{C}$  the lines at  $306\text{ cm}^{-1}$  and  $331\text{ cm}^{-1}$  shift respectively to  $308$  and  $328\text{ cm}^{-1}$ . This change is the same as that observed by Sirkar and Gupta (1936) on cooling the crystal once in ice and bringing it back to  $32^\circ\text{C}$ . The line at  $3068\text{ cm}^{-1}$  shifts to the higher wave-length side and splits up into two components at  $3072$  and  $3076\text{ cm}^{-1}$  respectively, when the melt is solidified and is further cooled down up to  $-180^\circ\text{C}$ .

The frequencies of the lines due to C-Cl and C=C valence oscillations are not found to be affected much with the lowering of temperature up to  $-180^\circ\text{C}$ . It is evident that the asymmetry in the lattice field is responsible for the splitting up of the symmetric C-H oscillation into two components at  $-180^\circ\text{C}$ .

Although the positions of the other lines due to intramolecular oscillations remain the same with the solidification of the substance, the intensities of two of these lines undergo remarkable changes. It can be seen from Table I as well as from figures 1-4, Plate XVI, that the intensity of the line  $1573\text{ cm}^{-1}$  due to the liquid is larger than that of the line  $1109\text{ cm}^{-1}$ , but in the case of the solid the line at  $1573\text{ cm}^{-1}$  is much feebler than the line at  $1109\text{ cm}^{-1}$ . Again the lines  $1109\text{ cm}^{-1}$  and  $747\text{ cm}^{-1}$  have almost the same intensity in the case of the liquid while in the case of the solid the former line becomes more intense. As the line  $1573\text{ cm}^{-1}$  can be attributed to the presence of C=C bond in the ring, it appears that the number of such bonds in the molecule in the solid state is smaller than that in the liquid state. If this assumption be true, it leads to the conclusion that probably in the case of this compound having a benzene ring in the molecule, association takes place in the solid through one of the C=C bonds. Such a hypothesis has, however, to be tested only by studying the Raman spectra of other similar molecules.

The sharpness of all the prominent Raman lines at  $28^\circ\text{C}$  and their further sharpening at lower temperatures in the present investigation indicate that the scattering is incoherent and is actually due to the oscillations in the individual molecule in the unit cell. That the probability of the simultaneous

occurrence of the same mode of oscillation for all the molecules in the unit cell is less than that for random oscillations, has been pointed out by Sirkar and Ray (1950) and the results obtained in the present investigation also corroborate such a view.

## ACKNOWLEDGMENT

The author is indebted to Prof. S. C. Sirkar for his keen interest and continued guidance during the progress of the work.

OPTICS DEPARTMENT,  
INDIAN ASSOCIATION FOR THE  
CULTIVATION OF SCIENCE,  
CALCUTTA 32

## REFERENCES

- Bhagavantam, S., 1941, *Proc. Ind. Acad. Sc.*, **13A**, 513.  
Bishui, B. M., 1948, *Ind. J. Phys.*, **22**, 167.  
Kastler, A. and Rousset, A., 1941, *Comptes. Rendus.* **212**, 645.  
Korshunov, A. V., 1950 *Doklady Acad. Nauk. S.S.S R.* **74**, 691  
Narain, H. and Saksena, B. D. 1951, *Ind. J. Phys.*, **25**, 79.  
Ray, A. K., 1950, *Ind. J. Phys.*, **24**, 111.  
Ray, A. K. 1951, *Ibid.*, **25**, 131.  
Rousset A., 1948, *Jour. de Phys.*, **9**, 101.  
Saksena, B. D., 1950, *J. Chem. Phys.*, **18**, 1653.  
Sirkar, S. C., 1951, *J. Chem. Phys.*, **19**, 255.  
Sirkar, S. C. and Gupta, J., 1936, *Ind. J. Phys.*, **10**, 473.  
Sirkar, S. C. and Gupta, J., 1937, *Ibid*, **11**, 283.  
Sirkar, S. C. and Ray A. K., 1950, *Ibid*, **24**, 189.  
Venkateswaran, C. S., 1938, *Proc. Ind. Acad. Sc.*, **8A**, 448.  
Vuks, M., 1936, *Comptes Rendus. (Doklady)*, **1**, 73.

# INFLUENCE OF THE ELECTRODE-SURFACE ON THE JOSHI-EFFECT IN CHLORINE

By P. G. DEO

(Received for publication, April 4, 1951)

**ABSTRACT.** Joshi-effect was studied in 162 mm Hg pressure chlorine contained in five ozonizers of different lengths but of identical electrode diameters in the potential range 1-8 kV. Both the net and relative Joshi-effect increased by increasing the ozonizer length which is a measure of the excited electrode area. This increase shows saturation specially at low exciting potentials. The results are in accord with Joshi's theory that an adsorption-like electrode surface layer consisting of ions and electrons derived from the discharge space is a primary seat of this phenomenon.

The spectrum of chlorine under conditions productive of a large Joshi-effect  $\Delta i$  consisted (Joshi, 1943; Deo, 1948) almost entirely of faint bands due to  $\text{Cl}_2^+$ . The absence of any emission spectrum characteristic of atomic chlorine suggested that any reaction involving the latter was confined to the container surface. The surface sensitivity of  $\Delta i$  was also illustrated by the remarkable influence on its magnitude and even sign due to increase of surface to volume ratio by introducing powdered wall material in the discharge space (Shukla, 1949). This procedure, however, alters the field strength and the nature of the discharge and irradiation. It appeared, therefore, desirable to study the surface dependance of  $\Delta i$  under comparable conditions.

## EXPERIMENTAL

Five ozonizers  $S_1, S_2, S_3, S_4$  and  $S_5$  (figure 1), of lengths 19.5, 15.8, 7.9, 3.1 and 1.9 cm respectively, were prepared from the same pair of glass tubes.

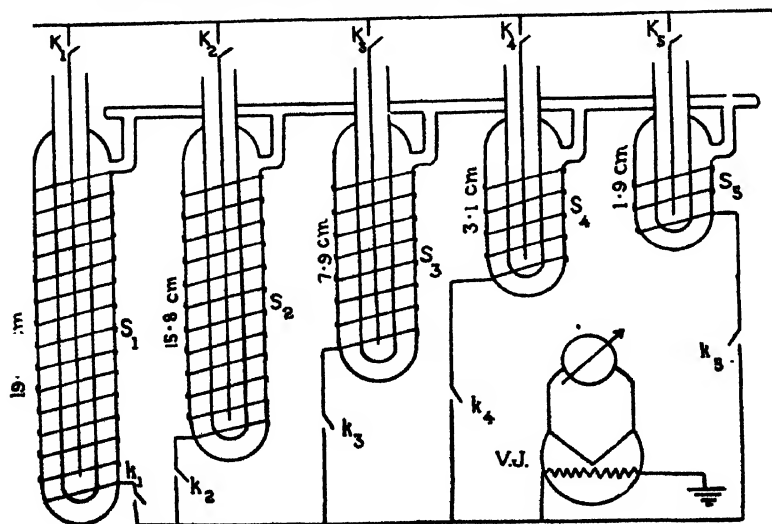


FIG. 1



They were filled carefully with purified chlorine from a given stock at the same pressure, viz. 162 mm Hg and excited by a transformer discharge. Each of the inner electrodes, formed with a saline solution, was connected to a common high tension line through a switch. The low tension electrodes formed with a solenoid-like winding of copper wire in well-spaced turns over the outer tubes were connected similarly to a common line which was earthed through a vacuo-junction feeding a mirror galvanometer. With a 180 volt, 200 watt bulb as the light source, the potential current characteristics  $V-i$  were observed in dark and under light, when (i) all the ozonizers  $S_1$ ,  $S_2$ ,  $S_3$ ,  $S_4$  and  $S_5$  connected in parallel were excited; and when each of them (ii)  $S_2$ , (iii)  $S_1$ , (iv)  $S_3$ , (v)  $S_4$ , and (vi)  $S_5$  was excited separately. The results of the observations are given in Table I (figure 2).

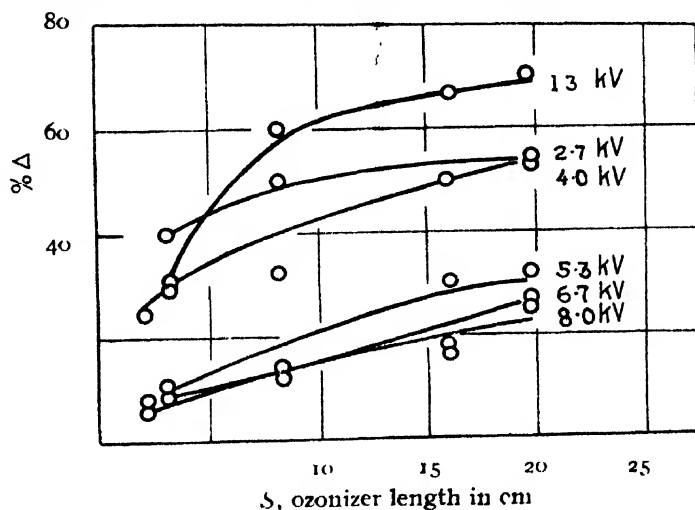


FIG. 2

TABLE I

	kV	$i_{\text{dark}}$	$\Delta i$	$\% \Delta i$		kV	$i_{\text{dark}}$	$\Delta i$	$\% \Delta i$
$S_1$	1.3	10	7	70	$S_4$	1.3	5	2	40
	2.7	16	9	56		2.7	6	2	33
	4.0	20	11	55		4.0	18	2	11
	5.3	28	9	32		5.3	21	2	9
	6.7	33	9	27		6.7	24	2	8
	8.0	38	10	26					
$S_2$	1.3	9	6	66	$S_5$	1.3	4	1	25
	2.7	12	6	50		2.7	7	1	6
	4.0	14	7	50		4.0	17	2	9
	5.3	24	6	25		5.3	21	2	8
	6.7	27	5	18		6.7	23		
	8.0	31	4	16					
$S_3$	1.3	8	5	62					
	2.7	10	5	50					
	4.0	12	4	33					
	5.3	21	3	14					
	6.7	25	3	12					
	8.0	30	4	13					

## DISCUSSION

In a discharge tube of ozonizer type the entire surface is due to the electrodes. At a given applied potential, the nature of the field at the electrodes and in the gas phase, and especially the electrode asymmetry (Deb and Ghosh, 1946) determined by the ratio of the radius of the outer to that of the inner electrode is sensibly the same, *viz.* 5.5/3.3 in all the systems  $S_1, \dots, S_5$ ; the area of the electrode surface given by the ozonizer length is the only variable so far as the study of  $\Delta i$  is concerned. It is interesting to observe (Table I) that at a given potential, kV, applied to the ozonizer, the magnitudes of  $\Delta i$  and  $\% \Delta i$  are in the order  $S_1 > S_2 > S_3 > S_4 > S_5$ . Thus, *e.g.* at 5.34 kV, the magnitudes of  $\% \Delta i$  in  $S_1, S_2, S_3, S_4$  and  $S_5$  are respectively 32, 25, 14, 11 and 6, *i.e. ceteris paribus* the Joshi-effect increases by increasing the *net* excited surface. In each case the magnitude of  $\Delta i$  increases with kV, whereas, that of  $\% \Delta i$  decreases, which is in accord with the generality of the results about this phenomenon (Deo, 1944; Prasad 1948).

Curves in figure 2 relate with the ozonizer length (which is a measure of the excited electrode area) the relative Joshi-effect  $\% \Delta i = 100 \Delta i / i$  dark. Essentially similar curves (not shown) are obtained by plotting  $\Delta i$ . Both  $\Delta i$  and  $\% \Delta i$  increase by increasing the electrode surface. This increase is practically linear at large kV and slows off at smaller ones, indicative of a saturation effect. This is also brought out by considering the values of  $\Delta i$  and  $\% \Delta i$  when all the ozonizers were connected in parallel. This is equivalent to a first approximation to a single ozonizer of area corresponding to  $19.5 + 15.8 + 7.9 + 3.1 + 1.9 = 48.2$  cm. The observed  $\Delta i$  and  $\% \Delta i$  at each of the series of applied kV for the combined system, are less than those to be anticipated by an extrapolation of the  $\Delta i$  and  $\% \Delta i$  versus electrode length curves in figure 2, due to a saturation.

It is known (McBain, 1932) that the glass surfaces take up variable quantities of gases, and that this process may be favoured by the application of an electric field. This is illustrated by the well known clean up phenomenon, *e.g.* the hardening of the X-ray tubes. Its simplest view is that the charged ions penetrate into the wall. According to Campbell (1920, 1921, 1922, 1924) neutral atoms or excited molecules produced under the discharge also take part in the process. Since rare gases also 'clean up,' it is suggested that the reaction may be of the physical type. With reactive substances, chemo-sorption is, however, possible. Langmuir (1912, 1913, 1915, 1916, 1919) regards the 'clean up' of practically all except the inert gases as purely chemical in nature. Rodebush and Klingelhofer (1933), working with chlorine subjected to an electrodeless high frequency discharge in a glass bulb, observed a white wall deposit attributed by them to chemo-sorption.

It is important to note that in all the above type of reactions the gas pressures are much lower than those now employed. An adsorption like

electrode layer would appear to be a determinant in the production of  $\Delta i$ . Rao (1945, 1948) observed that  $\Delta i$  in chlorine-air mixtures (ratio 1:1) decreased but little, when the system was evacuated completely with a topler (but not degassed), and the mixture was replaced by air alone at the original pressure. That the completion of this layer is a time reaction was suggested (Deo, 1945), since no sensible 'aging' effect obtained in the ozonizer after use for about one and a half years; and that when freshly prepared,  $\Delta i$  was found to vary appreciably with the time of exposure to the discharge. This was attributed to an interaction between the 'electrode' wall material and activated gas under the discharge. Ramanamurti (1948) observed that in a freshly prepared chlorine-filled ozonizer, the time-development of  $\Delta i$  follows equation for 'first order' reaction. It is suggested that the boundary layer formed during discharge is due to chemo-sorption involving electron transference (Ramanamurti, 1948).

According to Rebbeck and Furguson (1924) the electrical conductivity of glass is not affected sensibly by sorbed gases. They, in some cases, however, influence remarkably the conductivity of solids for high frequency currents, due to a change in the electrical capacity by sorption. This last might affect the accommodation coefficient, i.e. the degree to which reflected (Gregg, 1933) particle adjusts its energy to the reflecting surface. It is difficult to envisage how these processes would cause a large change in the *relative* Joshi-effect by variation of the electrode area  $S_1 \dots S_n$ . Formation of an adsorption layer under discharge appears to be fairly certain as the first stage in the production of  $\Delta i$ . The subsequent stages according to Joshi (1946, 1947), are the emission of electrons under irradiation from this layer; and their subsequent capture by chlorine atoms resulting in the slow negative ions, causing  $\Delta i$  as a space charge effect.

#### ACKNOWLEDGMENTS

Grateful thanks of the author are due to Prof. P. N. Sharma, D.Sc., Head of the Physics Department, Lucknow University for encouragement and to Prof. S. S. Joshi, Principal, College of Science, Banaras, for valuable suggestions.

DEPARTMENT OF PHYSICS,  
UNIVERSITY OF LUCKNOW, LUCKNOW.

#### REFERENCES

- Campbell, and co-workers, 1920, *Phil. Mag.* **40**, 585  
 " " 1921, *ibid.* **42**, 227  
 " " 1922, *ibid.* **43**, 914  
 " " 1924, *ibid.* **48**, 553  
 Deb and Ghosh, 1946, *Sci. and Cult.*, **12**, 17.  
 Deo, P. G., 1948, *Phil. Mag.*, **39**, 978.

- Deo, P. G., 1944, *Proc. Ind. Acad. Sci.*, **19**, 117.
- Deo, P. G. 1945, *Proc. Ind. Acad. Sci.*, **21**, 76.
- Glocker and Lind, 1939, *Electro-chemistry of Gases and other Dielectrics*, John Willy and Sons, Inc., New York, pp. 426-42.
- Gregg, 1933, *The adsorption of Gases by Solids*, Methuen and Co, Ltd. London, pp. 88-89.
- Joshi, S.S., 1943, *Proc. Indian Sci. Cong.*, pp. 51-77.
- Joshi, 1946, *Proc. Ind. Sci. Congr., Phys. Sec. Abstr.* 26,
- „ 1947, *Curr. Sci.* **18**, 19.
- Langmuir, 1922, *J. Am. Chem Soc.*, **34**, 1310.
- „ 1913, *ibid*, **35**, 105
- „ 1915, *ibid*, **37**, 1157
- „ 1916, *ibid*, **38**, 2279
- „ 1919, *ibid*, **41**, 167
- McBain, 1932, *Sorption of Gases and Vapours by Solids*, George Routledge and Sons Ltd, London (1932).
- Prasad, B.N., 1948, *Curr. Sci.*, **17**, 235.
- Ramanamurti, *J. Ind. Chem. Soc.*, **25**, 255.
- Rao, 1945, *Proc. Ind. Sci. Congr., Chem. Sec. Absi.* 23;
- „ 1948, *Proc. Ind. Acad. Sci.*, **A27**, 72.
- Rebbeck and Ferguson, 1924, *J. Am. Chem Soc.*, **46**, 2000.
- Rodebush and Klingelhofer, 1933, *J. Am. Chem. Soc.*, **55**, 030.
- Shukla, 1949, *J. Phy. & Coll. Chem* , **53**, 1239.

# PERFORMANCE OF SESSILE DROP IN SURFACE TENSION MEASUREMENTS

BY N. R. TAWDE AND K. G. PARVATIKAR

(Received for publication, November 11, 1950)

**ABSTRACT:** In an attempt to improve the method of sessile drop for accurate surface tension measurements, Taylor and Alexander have fitted up an empirical relation by which the values of  $h/r$  are related to  $a^2/r^2$  in a tabular form. In this paper a similar table has been drawn up, but from fundamental considerations, using Bashforth and Adams's tables. A comparative fresh experimental study of both is also presented.

The method of sessile drop for measurement of surface tension was placed on better foundations for exact work as a result of the critical study of it by Taylor and Alexander (1944). These authors have fitted up an empirical equation of the form similar to Porter's (1933), but of more accurate type to connect  $h/r$  with  $a^2/r^2$ .

In the sessile drop, the quantities to be measured are  $h$ , the height of it above the equatorial plane, and  $r$  the radius of it in that plane. The ratio  $h/r$  is then related to  $a^2/r^2$  where  $a^2$  is the capillary constant which connects the surface tension  $\gamma$  by the relation.

$$a^2 = \frac{2\gamma}{g\sigma} \quad \dots (1)$$

$\sigma$  being the density of the liquid, or more precisely  $\sigma = d_1 - d_2$ , where  $d_1$  = density of the liquid and  $d_2$  that of the saturated air. Thus the final derivation of surface tension from measured quantities involves the use of tabular functions connecting  $h/r$  with  $a^2/r^2$ . It is shown here that such a tabular function is obtainable by modifying the standard tables of Bashforth and Adams (1883).

As shown by Adam (1941), the capillary equation for sessile drop can be put in the form

$$\frac{1}{\rho/b} + \frac{\sin \phi}{x/b} = 2 + \beta \frac{z}{b} \quad \dots (2)$$

where  $\beta = 2b^2/a^2$  (involving the capillary constant  $a^2$ , defined already),  $x$  is the horizontal co-ordinate with respect to origin taken at the uppermost point of the drop,  $b$  is the radius of curvature at the origin,  $\phi$  is the inclination of the surface at any point to the horizontal, and  $\rho$  is the radius of curvature in the vertical section at that point.

Bashforth and Adams, giving numerical solution of this equation, have drawn up a table of  $x/b$  and  $z/b$  for many values of  $\phi$  and  $\beta$ . These tables are yet known to be the standard work on the phenomena of capillary action. Obviously, for the purposes of present problem of sessile drop, the relevant values of  $\beta$  range from 25 to 100 for  $\phi=90^\circ$  (this being the inclination of the surface to the horizontal).

$$\text{Now,} \quad \frac{h}{r} = \frac{Z_e}{X_e} = \frac{Z_e/b}{X_e/b} \quad \dots (3)$$

$$\text{and} \quad a^2 = \frac{2b^2}{\beta} \quad (\text{since } \beta = \frac{2b^2}{a^2}) \quad \dots (4)$$

$$\text{therefore,} \quad \frac{a^2}{r^2} = \frac{a^2}{X_e^2} = \frac{2b^2}{\beta X_e^2} = \frac{2}{\beta(X_e/b)^2} \quad \dots (5)$$

Knowing  $Z_e/b$  and  $X_e/b$  from Bashforth and Adams' tables we could calculate  $h/r$  from Eq. (3) and  $a^2/r^2$  from Eq. (5). These computed values are given in Table I.

This table thus drawn up is parallel to Taylor and Alexander's table. Table I allows for direct interpolation of intermediate values of  $h/r$ . A more detailed table can also be derived by using any intermediate values of  $\beta$ . Close scrutiny has shown that  $a^2/r^2$  values of Table I agree with those of Taylor and Alexander closely at the ratio  $h/r=0.48153$ . In the region above it, they are smaller, while below it, they are greater than Taylor and Alexander's values.

It is possible to compare the usefulness of these tabular values with Taylor and Alexander's empirical derivations. This is done here by making use of the available experimental measurements of Taylor and Alexander (1944) on sessile drop and referring them to this table for the purposes of the derivation of surface tension. Table II has been drawn up to show the two sets of results side by side. In the main columns two and four of the table are reproduced the observed values of  $h/r$  and  $r$  by Taylor and Alexander. Column three gives side by side  $a^2/r^2$  derived from Taylor and Alexander's empirical relation and from Table I above respectively. The last column shows the computed values of  $\gamma$ , the surface tension, corresponding to each of the two readings of  $a^2/r^2$ .

The comparison shows that  $a^2/r^2$  values of the new table differ more or less systematically from the values of Taylor and Alexander by a small margin, but not beyond the limits of error stated by Taylor and Alexander, viz., 0.3 in 1000. But there are unsystematic large fluctuations in the resulting values of surface tension of the successive observations. They might be a consequence of imperfections and want of precision in experi-

TABLE I

$\beta$	$h/r$	$a^2/r^2$	$\beta$	$h/r$	$a^2/r^2$
25.0	0.56006	0.34509	52.0	0.50262	0.25409
26.0	0.55679	0.33910	54.0	0.49988	0.25040
27.0	0.55366	0.33348	56.0	0.49726	0.24691
28.0	0.55067	0.32819	58.0	0.49475	0.24361
29.0	0.54781	0.32320	60.0	0.49231	0.24048
30.0	0.54504	0.31848	62.0	0.49000	0.22751
31.0	0.54239	0.31401	64.0	0.48776	0.23468
32.0	0.53984	0.30978	66.0	0.48561	0.23198
33.0	0.53737	0.30575	68.0	0.48353	0.22942
34.0	0.53500	0.30191	70.0	0.48153	0.22696
35.0	0.53270	0.29825	72.0	0.47958	0.22462
36.0	0.53049	0.29475	74.0	0.47771	0.22237
37.0	0.52837	0.29141	76.0	0.47588	0.22021
38.0	0.52629	0.28821	78.0	0.47414	0.21813
39.0	0.52426	0.28514	80.0	0.47243	0.21614
40.0	0.52231	0.28219	82.0	0.47079	0.21423
41.0	0.52042	0.27935	84.0	0.46917	0.21238
42.0	0.51859	0.27663	86.0	0.46761	0.21060
43.0	0.51680	0.27402	88.0	0.46609	0.20888
44.0	0.51506	0.27151	90.0	0.46459	0.20722
45.0	0.51337	0.26905	92.0	0.46317	0.20562
46.0	0.51171	0.26670	94.0	0.46176	0.20407
47.0	0.51009	0.26442	96.0	0.46041	0.20257
48.0	0.50852	0.26222	98.0	0.45908	0.20111
49.0	0.50699	0.26009	100.0	0.45778	0.19970
50.0	0.50549	0.25802			

mental technique. It was, therefore, thought desirable to undertake an independent experimental study of the sessile drop method of surface tension, to see if better precision could be attained in measurable quantities. This would also allow a fair comparative test of the performance of the two sets of tabular functions. Water has been chosen as the liquid for the study.

TABLE II

Surface tension of water at 27.7°C

Obs. No.	$h/r$ T & A readings.	$a^2/r^2$		$r$ in mm T & A	$\gamma$ in dynes/cm at 27.7°C.	
		T & A's Emp. relation	Present authors' Tables I.		T & A	Present authors.
1	0.46997	0.21321	0.21329	8.3097	71.68	71.70
2	0.47283	0.21655	0.21660	8.2344	71.49	71.50
3	0.48462	0.23077	0.23076	7.9860	71.66	71.65
4	0.47846	0.22324	0.22327	8.1062	71.42	71.43
5	0.47146	0.21493	0.21501	8.2759	71.68	71.70
6	0.46505	0.20760	0.20772	8.4071	71.44	71.48

## EXPERIMENTAL

The arrangement for the formation of sessile drops was perfected after many trials. It essentially consists of a U-tube  $ABC$  ( $C'$ ) (figure 1). The short arm  $A$  has a bore of about a millimetre and external diameter of about 1.2 cm. The other tubes have a bore of 6 mm. This U-tube is mounted on a sliding arrangement  $S$  which is fitted on a vertical block  $R$  with a heavy base provided with levelling screws. The drop is formed at the flat circular tip  $A$  of brass tube made accurately plane. The outer diameter of the tube was  $12.094 \pm 0.003$  mm; and this was one of the quantities in the estimation of magnification ratio. The plane of the tip  $A$  is adjusted horizontal by levelling screws.

The drop-forming system described above was housed in a thermostat provided with two glass windows on the opposite sides, one for admitting light and the other for receiving it via the drop. The thermostat consists of air chamber heated electrically and provided with an electronic temperature control gear. It was capable of giving a temperature regulation to within  $\pm 0.1^\circ\text{C}$  and worked smoothly over long periods.

As the method involved measurements on photographic images of drops, it needed optical parts free from chromatic and spherical aberrations. For this purpose a monochromatic radiation of sodium lamp and Raman effect camera were employed. A uniform illumination for the drop was obtained by a collimating lens fixed to the back glass window of the thermostat. The whole assembly of the apparatus is shown in figure 2.



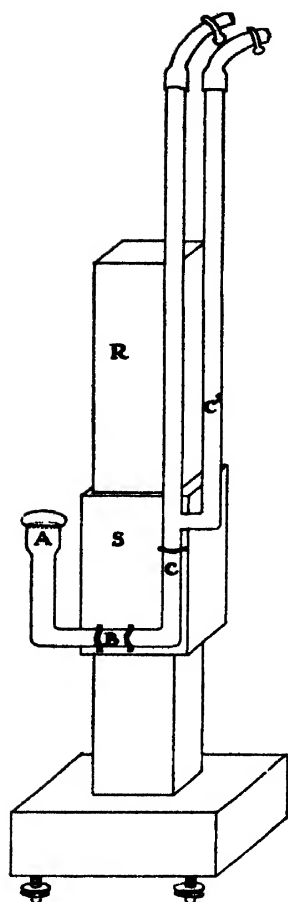


FIG. 1

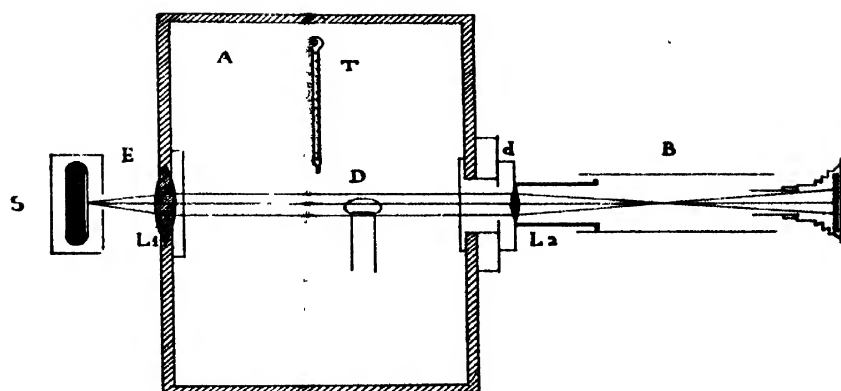


FIG. 2

- |                         |                      |
|-------------------------|----------------------|
| S—sodium lamp           | $L_2$ —focussing     |
| E—envelope of lamp      | d—variable diaphragm |
| $L_1$ —collimating lens | B—brass pipe         |
| A—thermostat chamber    | cc'—camera bellows   |
| T—thermometer           | P—plate carrier      |
| D—sessile drop          |                      |

A stable drop of double distilled water was formed on the flat end *A* by operating the pinch-cocks *C* and *C'*. A sharp picture of the outline of the sessile drop was projected on the camera plate ( $3\frac{1}{2}'' \times 2\frac{1}{2}''$ ). The size of the picture was such that four pictures of it could be taken on a single plate. Of this set, three were reserved for independent fresh drops, formed one after another and the last exposure for the tip *A* without the drop to allow for measurement of linear quantities to compute the magnification ratio. A sample set of pictures taken on a single plate is reproduced in figure 3. The exposure time was six seconds. The temperature was maintained constant at  $30^\circ\text{C}$  within the limits of variations stated already. Final negatives obtained under these conditions were subjected to measurements.

Measurements of *H* and *R* on the pictures of the drop profile were made by a comparator capable of reading to 0.001 mm. Readings were repeated a number of times to obtain confirmation of the ratio *H/R*. By measuring width of the actual circular metal base *A* and its picture on the negative the magnification *M* was obtained. Knowing *R* and *M*, the radius *r* of the actual sessile drop was computed.

Twenty independent drops were measured in this way and the readings are recorded in Table III. With the help of our values (Table I) and also

TABLE III  
Surface tension of water at 30°C

Obs. No.	Mag M	H in mm	R in mm	H/R = h/r	r=R/M in mm	a <sup>2</sup> /r <sup>2</sup> (Tabular)	a <sup>2</sup> in sq. mm	γ in dynes/cm
1	1.2859	4.789	8.950	0.5350	6.960	0.30191 (0.30208)	14.624 (14.633)	71.15 (71.19)
2	"	4.812	9.105	0.5285	7.080	0.29161 (0.29183)	14.611 (14.628)	71.12 (71.17)
3	1.2875	4.747	8.667	0.5477	6.731	0.32302 (0.32312)	14.634 (14.639)	71.20 (71.22)
4	"	4.773	8.828	0.5406	6.856	0.31104 (0.31118)	14.620 (14.626)	71.13 (71.15)
5	"	4.833	9.211	0.5246	7.154	0.28574 (0.28583)	14.624 (14.628)	71.15 (71.17)
6	"	4.772	8.817	0.5412	6.848	0.31206 (0.31218)	14.634 (14.639)	71.20 (71.22)
7	"	4.803	9.010	0.5330	6.998	0.29877 (0.29889)	14.628 (14.637)	71.17 (71.21)
8	1.2860	4.805	9.046	0.5311	7.034	0.29572 (0.29589)	14.631 (14.637)	71.18 (71.22)
9	"	4.770	8.827	0.5403	6.863	0.31054 (0.31069)	14.626 (14.633)	71.16 (71.19)
10	"	4.715	8.511	0.5539	6.618	0.33391 (0.33390)	14.624 (14.624)	71.15 (71.15)
11	"	4.747	8.695	0.5459	6.761	0.31995 (0.32005)	14.625 (14.629)	71.15 (71.19)
12	1.3126	4.849	8.893	0.5452	6.775	0.31875 (0.31887)	14.630 (14.636)	71.18 (71.21)
13	"	4.841	8.853	0.5462	6.744	0.32148 (0.32158)	14.621 (14.625)	71.13 (71.15)
14	"	4.833	8.809	0.5486	6.711	0.32458 (0.32466)	14.618 (14.621)	71.13 (71.13)
15	"	4.829	8.787	0.5495	6.694	0.32615 (0.32621)	14.614 (14.617)	71.10 (71.12)
16	1.2816	4.774	8.928	0.5347	6.966	0.30144 (0.30160)	14.627 (14.635)	71.16 (71.20)
17	"	4.805	9.132	0.5261	7.125	0.28792 (0.28812)	14.616 (14.626)	71.11 (71.16)
18	"	4.798	9.075	0.5287	7.080	0.29193 (0.29214)	14.633 (14.643)	71.19 (71.24)
19	1.2678	4.689	8.629	0.5434	6.806	0.31571 (0.31585)	14.624 (14.630)	71.15 (71.18)
20	"	4.774	9.175	0.5203	7.125	0.27917 (0.27937)	14.617 (14.627)	71.12 (71.16)

Mean γ =

71.15  
(71.18)

of Taylor and Alexander,  $a^2/r^2$  have been found for measured ratio  $H/R$  ( $=h/r$ ). The latter are entered in brackets along with our values, and  $\gamma$  determined from the equation (1).

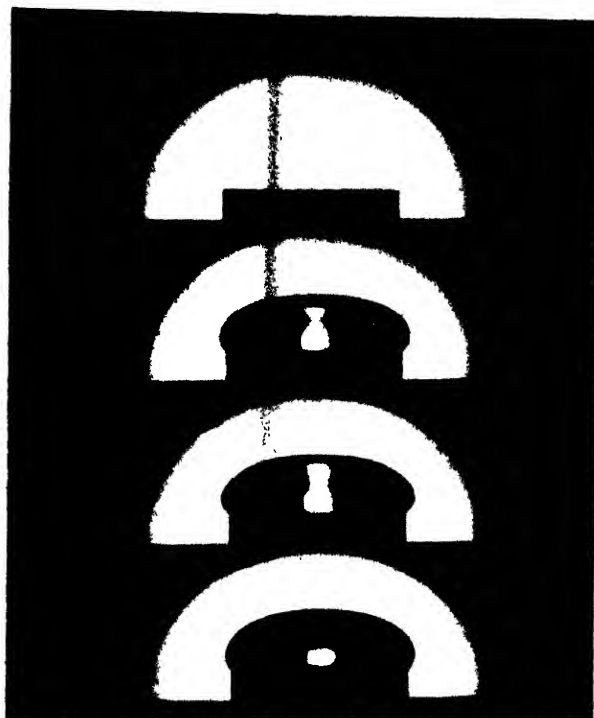


FIG. 3

## CONCLUSIONS

The mean value of surface tension obtained from these experiments by the use of functions drawn up in Table I is  $71.15 \pm 0.05$  dynes/cm at  $30^\circ\text{C}$ . When reduced to  $20^\circ\text{C}$  for comparison with standard constants, it becomes  $72.62 \pm 0.05$  dynes/cm, while the value so obtained by employing Taylor and Alexander's tables is  $72.65 \pm 0.05$  dynes/cm. Both the results compare favourably with the adopted mean  $72.75 \pm 0.05$  dynes/cm of the I.C.T. and are well within the limits of uncertainty of some of the modern results on this constant.

The small divergence between the two means is to be attributed to the differences in the two sets of tabular values. It was noted earlier that  $a^2/r^2$  values obtained by using Bashforth and Adams's tables are systematically greater than similar values of Taylor and Alexander by a small margin, but within the limits of errors stated by them. This may account for the small difference in the two values of surface tension derived above. Therefore, as far as the two tables are concerned both appear to be of comparable precision. This investigation, therefore, shows that there is an alternative way of

drawing up the tables to that of Taylor and Alexander and it is equally dependable for applicability to experimental measurements.

As regards the relative merits of the technique used in these experiments, one is guided by the nature of consistency in the several independent readings. Unfortunately, for comparison, we have only six independent observations of Taylor and Alexander, as against twenty of this investigation. With this limitation of Taylor and Alexander's results, the calculated dispersion of the mean result of surface tension from Taylor and Alexander's experiments is  $\pm 0.043$  units, as against  $\pm 0.005$  of the present experiments. The latter error which is about 1/10th of the probable error of Taylor and Alexander is a combined effect of relatively larger number of observations and the precision of technique. Choosing an equal number of readings *viz.*, six at random from our experimental observations (Table III), we obtain the probable error of  $\pm 0.027$  in the mean value of surface tension which is still smaller than the probable error  $\pm 0.043$  of Taylor and Alexander's measurements. This reduction in probable error may be taken as an evidence of a fair measure of improvement in the experimental technique adopted in this work. It may be attributed to comparatively better control of temperature and better precision in linear measurements.

#### ACKNOWLEDGMENTS

We have great pleasure in conveying our grateful thanks to Professor H. J. Taylor of Wilson College, for favour of making his personal copy of the very rare tables of Bashforth and Adams, available to us for constant use.

PHYSICS DEPARTMENT,  
THE INSTITUTE OF SCIENCE,  
BOMBAY.

#### REFERENCES

- Adam, 1941, *The Physics and Chemistry of Surfaces* Oxford U. Press, p. 366.  
Bashforth and Adams, 1883, "An Attempt to Test the Theories of Capillary Action".  
Cambridge University Press.  
Porter, 1933, *Phil. Mag.*, **15**, 163.  
Richards, Speyers and Carver, 1924, *J. Am. Chem. Soc.*, **46**, 1196.  
Taylor and Alexander, 1944, *Proc. Ind. Acad. Sc.*, **19**, A 149.

# ON AN AUTOMATIC WILSON CLOUD CHAMBER IN A MAGNETIC FIELD AND SOME ASSOCIATED TECHNIQUES\*

By RANJIT KUMAR DAS

(Received for publication, September 22, 1951)

## Plate XVII

**ABSTRACT.** An one ton electromagnet for use in cosmic ray research with a shallow cloud chamber, has been installed in the Institute of Nuclear Physics. For convenience in photography, one of the pole pieces has been bored. The field strength attainable with a current of 7 amperes is about 3630 gauss over the effective region in the pole gap. A shallow cloud chamber, 2.5 cm deep and 15 cm in internal diameter, has been used. A complete description of the automatic sequence control mechanisms has been given. In automatic test runs, the performance of the apparatus has proved quite satisfactory.

## INTRODUCTION

The importance of a properly calibrated magnetic field for some specific cosmic ray experiments cannot be over-estimated. For instance, in experiments on the determination of mass of cosmic ray particles from momentum loss in a metal plate of suitable thickness placed inside the cloud chamber, in finding out the energy spectrum of charged particles from measurement of curvatures, in distinguishing positive particles from negative ones and also, to fix the ratio of their numbers, a suitable magnetic field is a prerequisite. Most of the modern cloud chambers are fitted with very powerful magnetic field producing devices. The electromagnets used by Kunze (1933), Anderson (1933), Blackett (1936), Hughes and Jones (1940) and others are very big and massive; they are capable of producing high fields at a comparatively high power consumption. For the quantitative studies of cosmic ray particles in the high energy region of the energy spectrum, high fields are absolutely necessary. For the study of particles in the low energy region, however, smaller fields can be conveniently produced with not too massive electromagnets, at a reasonable power consumption. Besides reducing the cost, the use of lesser amount of iron and copper for the electromagnet has the additional advantage of reducing undesirable scattering effect.

With the above ends in view, and especially for experiments with a shallow cloud chamber, we have installed an electro-magnet with other accessory mechanisms. A shallow cloud chamber, 2.5 cm deep and 15 cm in internal diameter, has been used. The very light diaphragm of the chamber has necessitated the development of an automatic electro-mechanical

\*Communicated by Prof. M. N. Saha, F. R. S.

device to keep the compressing pressure stabilized within a narrow range on either side of the optimum working value. The illumination for photographing tracks is provided with an arc discharge flash lamp (F.T. 126, Int. G.E.C). A simple and reliable triggering circuit has been developed for firing the flash lamp. An objectionable feature of employing flash lamps in cloud chamber photography has been noticed and a simple electronic device has been made to counteract this.

The details of the different parts of the entire unit are given under their respective headings.

(a) *The Electromagnet.*—The electromagnet is horse-shoe shaped. The core proper weighs nearly 18 mds. (1440 lbs), each magnetising coil  $2\frac{1}{2}$  mds. (200 lbs) and the pole-pieces  $1\frac{1}{2}$  mds (120 lbs) each. The magnetising coil consists of 20 layers (each 108 turns) of 11 S.W.G. (about .345 cm) copper wire. The wire is silk covered, having a surface layer of lacquer to insure sufficient insulation. The total resistance of the magnetising coils is 3.5 Ohms. The dimensions of the magnet and coils are given in figure 1. The magnet has been seated on three massive stone chip pillars 94 cm high. To increase structural strength, the pillars have been interconnected by means of a reinforced transverse block  $17\frac{1}{2}$  cm high. Liberal spacing has been kept between front pillars seating the pole-pieces so that, if occasion demands, about 70 cm of lead absorbers can be used underneath the cloud chamber. The magnet current is supplied from the laboratory 220 D.C. mains, using variable resistances to alter the magnetising current. Considering the statistical errors involved in the types of experiments that can be done with the apparatus, we have not felt it necessary to introduce any current-stabilizing device at present. With the magnet running for 24 hours at a 6 amperes rating, the increase in the temperature of the core is just a little over  $\frac{1}{2}^{\circ}\text{C}$ . This has been measured by means of thermometer dipped in mercury in a narrow hole drilled in the pole piece carrying the cloud chamber. It is expected that with an air blast arrangement sufficient cooling can be produced to push down the rise in temperature to  $\frac{1}{2}^{\circ}\text{C}$ , which will not greatly disturb the performance of the chamber.

The pole-piece facing the cloud chamber has a cylindrical hole of  $4\frac{1}{2}$  inch diameter and 9 inch axial length, so that photographs can be taken directly. The hole has, of course, introduced a certain degree of non-uniformity and also a considerable amount of reduction in the effective field strength. For this reason, the calibration of the magnetic field has been done rather elaborately. A simple and specially designed search coil device has been used for the three dimensional mapping of the magnetic field. For this purpose, the entire pole gap has been divided into 10 vertical planes parallel to the pole faces, with a spacing of 1 cm between successive planes. Each of these planes, again, has been divided by 12 vertical and 10 horizontal lines and field strengths at the points of intersections measured. In this way the entire field space has been investigated. The results of the field

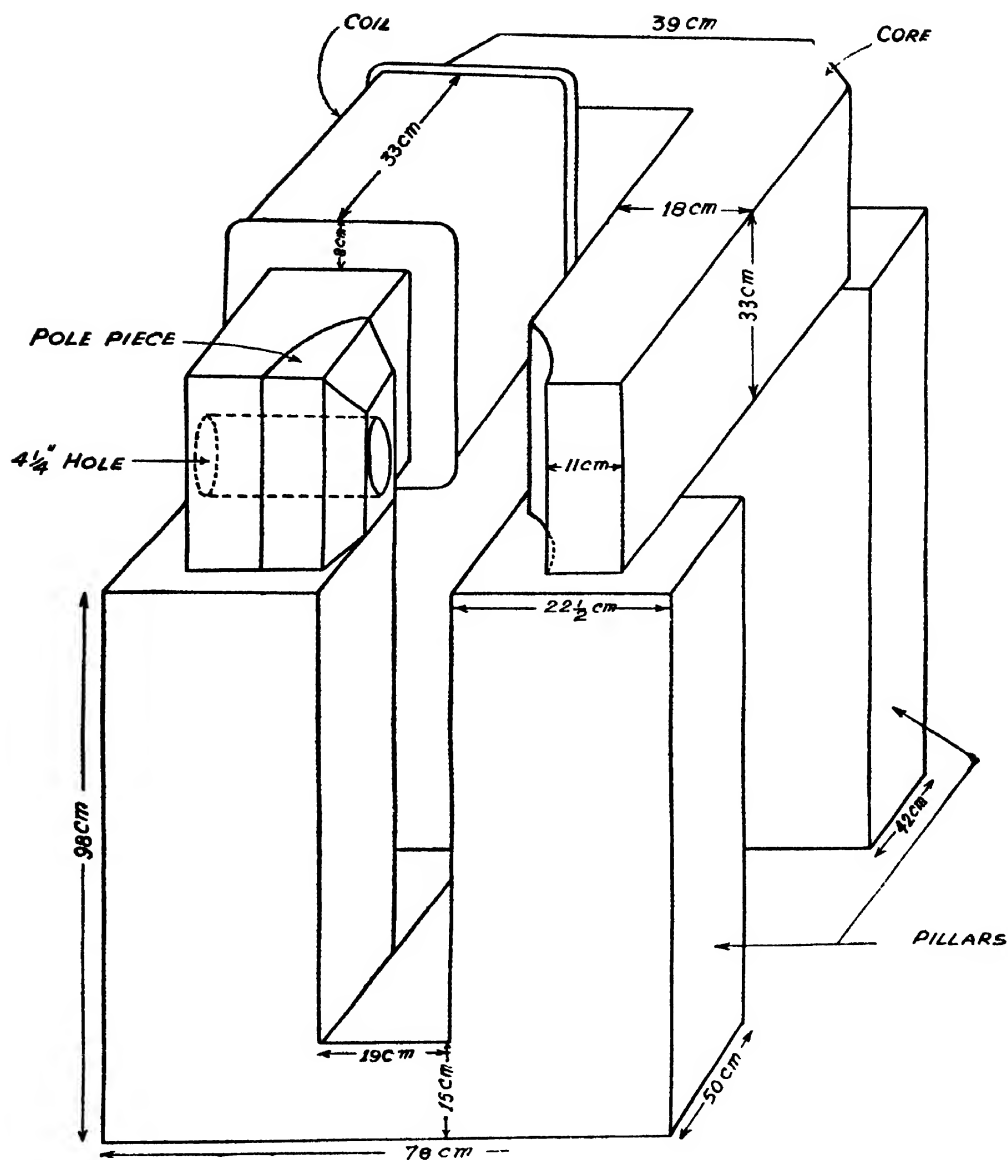


FIG. 1

Perspective view of the magnet and supporting pillars (for clarity, right hand coil and pole-piece not shown)

investigation have been graphically represented (figure 2). It has been found that for a given plane parallel to the pole faces, the deviation of the field strength near a peripheral region of about 2 cm is about 15% of the more or less uniform value in the central region of that plane. It is seen from the plot that upto a distance of about 3 cm from the pole-piece supporting the cloud chamber, the fall in the field strength in the effective region is almost linear; the field strength for the remaining region upto the drilled pole piece is sensibly constant. With the cloud chamber we have designed, the glass ring occupies the region of constant field strength. Thus, for all practical

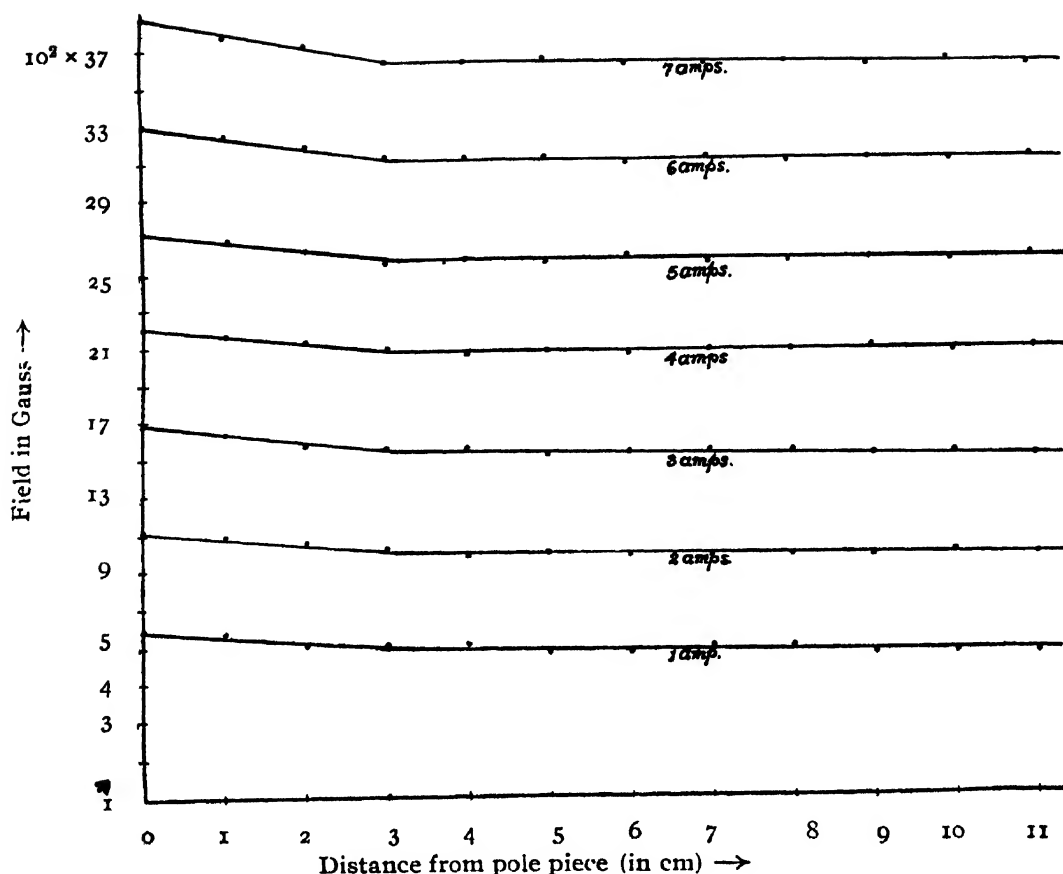


FIG. 2

Variation of field in the effective region

purposes, the same calibration curve will serve for chambers of different depths.

(b) *The magnet circuit breaking device.*—It is well known that when a coil of large self inductance carrying a sufficiently heavy current is opened, a large back E.M.F. is developed at the points of opening and thus, the breaking switch is gradually damaged due to sparking. To obviate this, a very simple device has been used (figure 5). Two 150 watts, 110 volts lamps have been arranged in parallel with the magnet coils. Normally, when the magnet is on, the lamps are off. Just prior to breaking the magnet current, the lamps are switched on, so that they glow due to the current from the mains. Now, when the mains are cut off, the magnet coils and the lamp filaments fall in series, so that the surge current due to the back E.M.F. finds a closed path of considerable resistance. Consequently, the damage due to the heavy sparking in the open circuit is avoided.

*The cloud chamber.*—A sectional diagram of the cloud chamber is given in figure 8. The bottom of the chamber has been specially designed to fit closely the protruding disc on the pole-piece on which it is secured by means of two radial screws.



The diaphragm of the cloud chamber has been made of two 5 inch circular aluminium discs  $1/16$  inch thick, with a larger diameter rubber-cloth sand-wiched between them by means of a large number of peripheral rivets. Thus constructed, the diaphragm is very light and hence, fast in action. The requisite expansion ratio is controlled by means of three lateral conical plugs carrying wedge-pieces at their ends. The conical plugs have been very carefully ground to reduce the air leakage from the back compartment as far as possible. The forward position of the diaphragm is limited by the brass ring on which the glass ring of the cloud chamber has been mounted; the backward position (that is, when the actual expansion of the chamber has taken place) is determined by the position of a baffle plate, attached to the bottom of the cloud chamber by means of three short springs. The position of the baffle plate and hence, the expansion ratio of the chamber, is controlled by moving the wedge-pieces either inwards or outward. This will be clear from the sectional diagram of the chamber. There is a pressure gauge to record the initial and final pressures in the chamber.

*The supply of compressing air.*—Although the compressing air is supplied by means of an automatic air compressor, the reducer valve itself is not sufficient to give a pressure-stabilized supply of air. As the diaphragm is rather delicate, any excess compressing pressure has a tendency to buckle it, so that, the optimum conditions for recording tracks of particles passing through the chamber are disturbed. For this reason, a subsidiary electro-mechanical device has been developed by the author (Das, 1950), which, in conjunction with a stabilizer tank, maintains the pressure of the compressing air stabilized within a narrow range. A detailed description of the construction and working of this pressure stabilizing device has been published earlier.

*The expansion valve*—The design and performance of the expansion valve is a very important consideration in any cloud chamber work. We have used a valve of the Fussell type, being the simplest and most convenient. Use of this type of valve has a few advantages over the older types.

Unlike in older procedures (Das Gupta and Ghosh, 1946), in this case the valve is directly connected to the primary control rod passing through the axis of the soft iron core of the solenoid magnet and thus, it is absolutely free from any uncertainty as regards its final action, viz., closing the expansion hole. With the older type of valve one cannot be too sure of its final action; one has to pay almost a periodical attention to it. Besides eliminating a potent source of trouble, the adoption of the Fussell type of valve has greatly simplified the accessory mechanisms controlling the automatic setting of the valve. A sectional diagram of the valve is given in figure. 3.

*The illuminating system*—As the effectively accessible region in the immediate vicinity of the sensitive volume of the cloud chamber to be photographed is rather limited, the normal procedure of using 110 volts (and usually 150 watts) lamps at a momentary over-loading of 220 volts

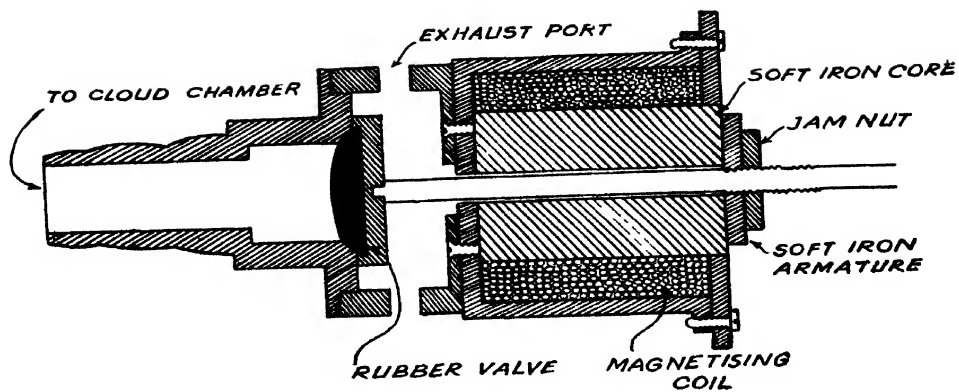


FIG. 3  
Sectional diagram of the valve system

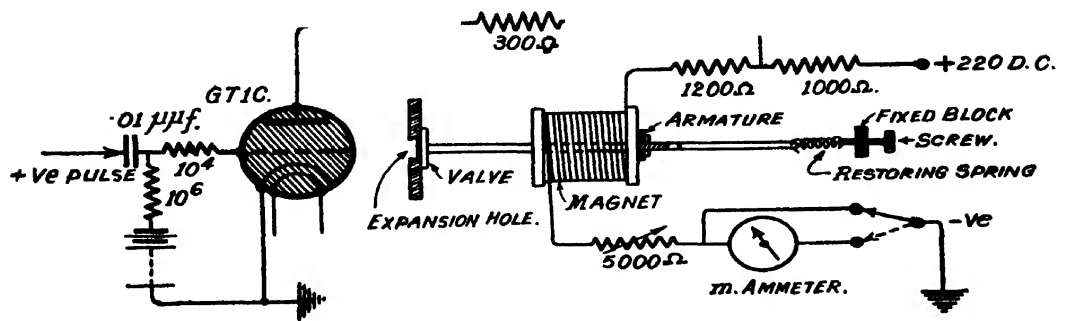


FIG. 4  
Thyatron, shunting the valve-magnet (valve-resetting mechanism not shown)

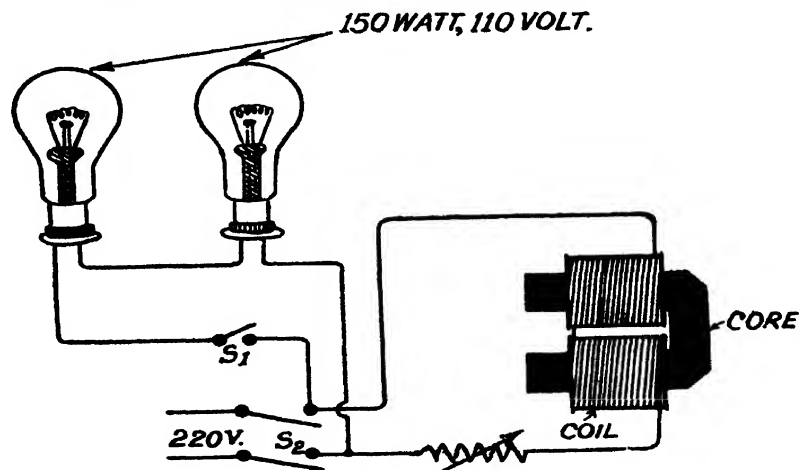


FIG. 5  
Electromagnet circuit breaker

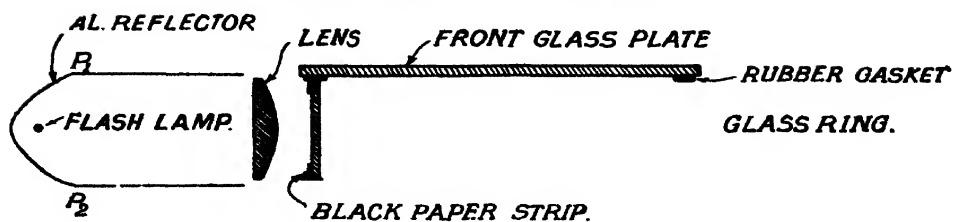


FIG. 6  
Illuminating system

would not do. The geometrical configuration in the present case would compel us to use one such bulb above and the other below the chamber; consequently, the expansion initiating G.M. counters can not be used for distances less than 16 inches. The focusing of the beam through the effective volume of the chamber also becomes very imperfect with this arrangement. Besides, the presence of the material of the bulbs in the path of the incoming cosmic rays is not desirable from more than one stand-points. We have solved this difficulty by using modern arc discharge lamps.

A single tube (capillary length 6 inches) has been used from the front edge of the chamber. The capillary of the flash tube has been backed by a 5/6 inch high parabolic cylindrical reflector, made of 1/16 inch aluminium sheet (figure 6). The part  $P_1 P_2$  of the reflector is shaped accurately parabolic, the focal axis coinciding with the capillary. The focus of the parabola is also at the focus of the plano-cylindrical condensing lens (2 inch focal length, 6 inch long, 1 inch aperture), so that we get a highly intense and almost parallel beam of light. To increase the reflecting power, an 1 mil. thick aluminium foil has been fixed, without any kink, on the reflector.

To fire the flash tube, a simple and efficient triggering device has been developed in our laboratory. A detailed description of the design and operation of the triggering device has been published earlier (Das, 1950). One objectionable feature of these flash tubes is that they sometimes flash over erratically, that is, give light flashes without any correlation with any recordable event, which, in the present case, is the passage of a charged particle through the cloud chamber. It seems that flash tubes controlled by means of external triggering electrodes invariably suffer from this defect (Bourne, 1948). To counteract the effect of this erratic behaviour on cloud chamber photography, a simple electronic device has been developed by the author (Das, 1950).

*The automatic sequence control mechanism*—The control sequences can be described under the following headings:

(1) Firing the thyatron shunting the electro-magnet of the expansion valve, by a voltage pulse from a desired event.

(2) Release of the armature carrying the valve (expansion of the chamber).

(3) Triggering the flash tube within .01 second of the expansion.

(4) Setting the driving motor in motion.

(5) Resetting the valve.

(6) Winding up the exposed portion of the film.

(7) Breaking the motor circuit at the end of the cycle.

The positive pulse due to the occurrence of a recordable event fires the thyatron which is in parallel with the magnetising coil of the valve magnet (figure 7). Now, during the conducting stage, the total resistance of the thyatron circuit (that is, internal resistance of the thyatron plus the external

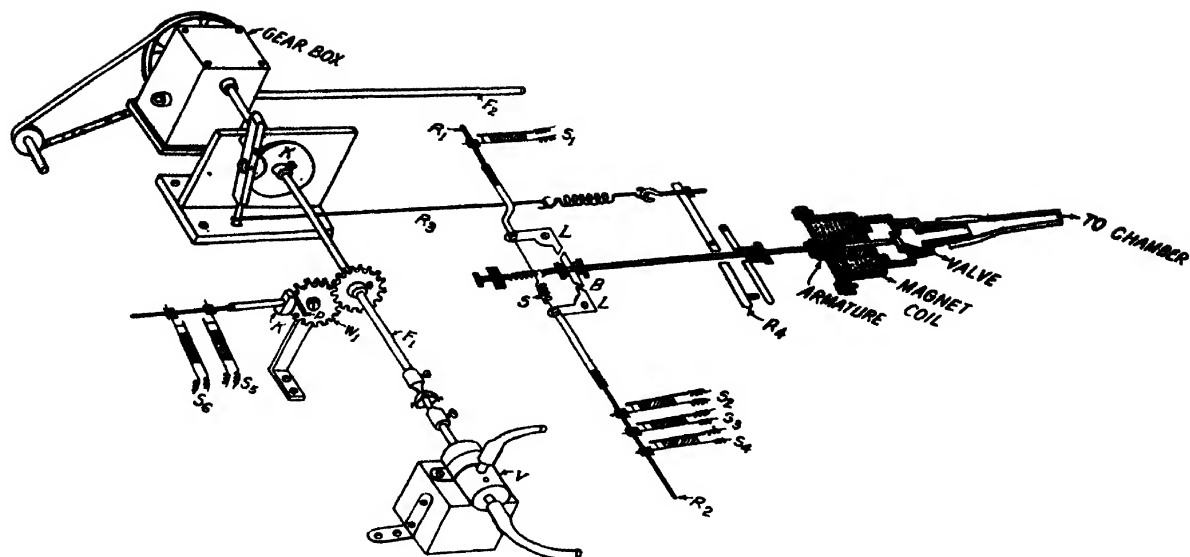


FIG. 7

Automatic sequence control mechanism (For clarity, some parts have been drawn sectionally)

current limiting resistance  $R$ ) is much smaller than the resistance of the magnetising coil, so much so, that the thyatron acts as a shunt to the magnetising circuit. As the magnetising current is kept just at the optimum level (in this case 30 milli-amps) the armature flies off; consequently, expansion of the chamber takes place (figure 4).

After the release of the valve, the bevelled aluminium block (figure 7)  $B$  occupies a position, displaced considerably in the forward direction; consequently, the  $L$ -pieces are moved laterally. This lateral movement is communicated through the long levers  $R_1$  and  $R_2$  to the various switches  $S_1$ ,  $S_2$ ,  $S_3$  and  $S_4$ . Each of the electric switches is made of a thin and a thick phosphor-bronze strip with lengths so adjusted as to give sufficient restoring force. The actual contact points are of platinum so that corrosion due to sparking is greatly reduced. The switch  $S_2$  breaks the plate of the thyatron, thus extinguishing it. The switch  $S_3$  removes the pre-expansion ion-sweeping field just after the expansion of the chamber.

The switch  $S_1$  sets the driving motor in motion. Now, the position of the cam  $K$  has been so adjusted initially, that just after the motor starts it begins to pull the lever rod  $R_3$ . This motion is transmitted through the lever arm  $R_4$  to the magnet armature which is gradually pushed toward the magnet core until it is kept attracted to it. Under the joint restoring action of the phosphor-bronze strips and the steel spring  $S$ , the switches  $S_1$ ,  $S_2$ ,  $S_3$ , and  $S_4$  are restored to their initial positions within 10 seconds of the starting of the motor. Now, the pin  $P$  fixed to the pinion wheel  $W$  is moved past the contact knob  $K_1$  so that the motor circuit is now closed through the switch  $S_6$ , until it is again broken by the separation of the



Secondary electron tracks, produced  
by  $\gamma$ -ray



contact points at the end of the cycle by the pin *P*. The switch *S*<sub>5</sub> is such that it finally closes the thyatron plate circuit. As the complete cycle of automatic sequences lasts for nearly 1½ minutes, it is clear that without the switch *S*<sub>5</sub>, which closes the thyatron plate circuit at the end of the cycle, there is always a risk of the chamber being tripped within a cycle; that is, before it has been reset completely.

The cone of the cup-cone air inlet valve *V* is rigidly pinned to the shaft *F*<sub>1</sub>. During the time the motor is in motion, the cone completes the rotation and establishes communication of the back compartment of the cloud chamber with the air pressure stabilizer. The second shaft *F*<sub>2</sub> in conjunction with two arms joined by means of universal gimbals, winds up the exposed portion of the film, so that a fresh portion of the film comes up for recording the next event. In this way, the entire sequence of automatic control is completed.

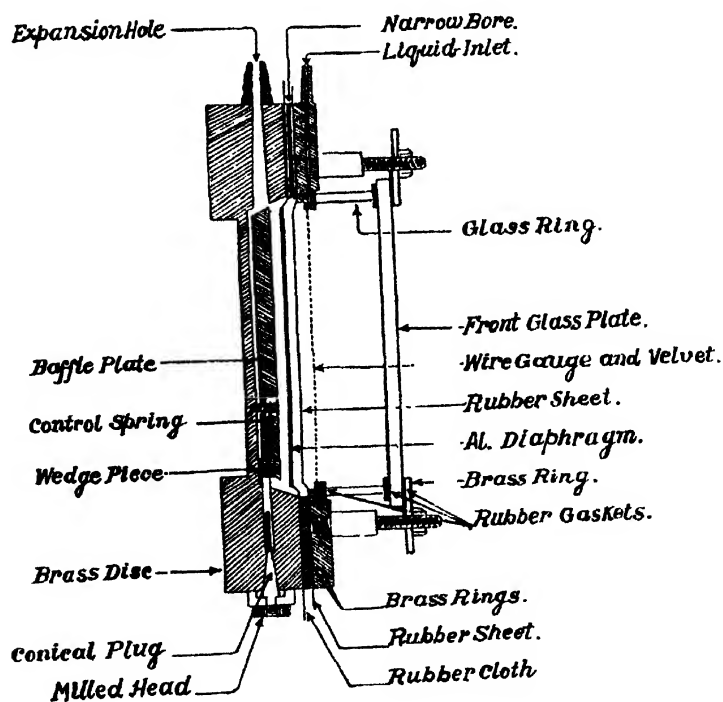


FIG. 8

Transverse view of the cloud chamber

*The Photographic Arrangement:*—At present we are using a single lens arrangement for photography. This is justified in view of the fact that the chamber is a shallow one. However, there is ample provision for diverting to a stereo arrangement, if need arises. The lens used is Sonnar 1:2/*f*=4 cm. The film plane is at an effective distance of 16 inches from the front glass plate and the pictures obtained have a diameter of 1.7 cm, that is, the reduction in size is nearly in the ratio of 8.3 : 1.

## THE PERFORMANCE OF THE APPARATUS

A few automatic test runs of the complete apparatus were made by means of three Geiger Muller counters in coincidence. The cloud chamber was filled with a mixture of air and oxygen up to a total pressure of 84 cm of mercury. The liquid mixture used was 40% water and 60% absolute alcohol. A Ra-source was placed at a distance of 8 ft. and a collimated beam of gamma rays allowed to enter the cloud chamber. This step was taken, because, when the chamber expands due to accidental coincidence of G. M. counter pulses, there will be, in general, no track formation inside the cloud chamber and, this is specially true for a shallow cloud chamber. An ionising agent, such as a weak gamma source, properly shielded from the counters, would always send a few  $\gamma$ -rays into the chamber, producing secondary electrons. Thus, the condition of the cloud chamber as regards formation of tracks can be checked at any stage of the operation of the chamber. In a test picture supplied, plate XVII, the secondary electron tracks are quite clearly seen. The picture also shows a long track presumably due to a charged cosmic ray particle. We hope to put the apparatus to the study of some suitable cosmic ray problem involving the use of a magnetic field of the order of 3, 500 gauss.

## ACKNOWLEDGMENTS

It is a pleasure to record thanks to Prof. M. N. Saha, F. R. S., for his kind interest in the work. Thanks are also due to Drs. P. C. Bhattacharya and N. N. Das Gupta for discussion and encouragements.

INSTITUTE OF NUCLEAR PHYSICS,  
CALCUTTA UNIVERSITY.

## REFERENCES

- Anderson, C. D., 1933, *Phys. Rev.*, **44**, 406.  
 Blackett, P. M. S., 1934, *Proc. Roy. Soc.*, **146**, 281.  
 „ „ 1936, *Proc. Roy. Soc.*, **154**, 573.  
 Bourne, H. K., 1948, *Discharge Lamps for Photography and Projection*, (Chapman and Hall) p. 330.  
 Das Gupta, N. N., and Ghosh, S. K., 1946, *Rev. Mod. Phys.*, **18**, 243.  
 Das, R. K., 1950, *Science and Culture*, **16**, 167.  
 „ „ 1950, *Ind. J. Phys.*, **24**, 446.  
 „ „ 1950, *Ind. J. Phys.*, **24**, 497.  
 Jones, H. and Hughes, D. J., 1940, *Rev. Sci. Inst.*, **11**, 79.  
 Kuntze, 1933, P., *Z. f. Phys.*, **80**, 559.



# ULTRASONIC ATTENUATION IN GELS

By ARVIND MOHAN SRIVASTAVA

(Received for publication, March 3, 1951)

**ABSTRACT.** In this paper the ultrasonic propagation in gels is studied from the viewpoint of attenuation of the incident waves. In a theoretical discussion the propagation in a medium having spherical particles suspended in a liquid medium has been evaluated. The paper shows that the attenuation per unit volume of such a medium is given by,

$$\alpha = 2\pi n a^3 (\rho_0/\rho') q \cdot k.$$

if the effect of scattering is to be considered too. The theory points out the different cases showing the relative importance of these terms. Considering the Lamb and Sewell theory in details, a starting point for the present author's results is also indicated

From the theoretical considerations given in this paper, the attenuation is calculated for a few gels also showing its dependence upon temperature. Furthermore, the results are satisfactorily explained by the theory outlined in the paper.

Using an ultrasonic pulse technique, the attenuation for a few gels has been practically determined and its variation with temperature and frequency studied. The diminution of the kinematic viscosity at higher temperatures and the increase in the scattering account for the values of attenuation showing a maximum near about 55°C.

## INTRODUCTION

The propagation of sound waves in a medium containing suspended particles was first studied by Lord Rayleigh (1896). Lamb (1884) took up the same problem in a more general way, considering the various modes of vibration of a sphere that scattered the incident wave. Herzfeld (1930) developed a theory for sound propagation in suspensions by extending the Rayleigh boundary conditions. Sewell (1911) studied the problem as applicable to such natural suspensions as fog and smoke particles in air. He calculated the loss of energy in case of spherical particles.

Sound propagation in aerosols has recently been studied by Brandt (1937), Heidmann, Freund and Brandt (1937). Further, the acoustic impedance of such a foggy atmosphere was investigated by Ghosh (1936) who tabulated a large amount of significant data based upon his theoretical results for particles of radius ten microns and lesser. Richardson (1938) and Epstein (1942); Hartmann and Focke (1940) developed an ultrasonic technique using a piezo-electric oscillator to study the absorption of sound in artificial fogs and smoke. Richardson's results were the first step towards the practical verification of the Lamb and Sewell's theory. Following this, Urlick (1948) applied an ultrasonic pulse technique to obtain the attenuation of sound

waves in artificial smokes and also in sand and kaolin particles suspended in water. These results also supported the Lamb and Sewell theory.

It is evident, therefore, that no significant data exists regarding the factors affecting the propagation of sound waves in a gelatinous medium. The composite nature of these gels must necessarily affect the attenuation in such a medium, where a solid phase enmeshes and entrains an overwhelmingly larger proportion of the fluid which is usually water.

#### THEORETICAL CONSIDERATIONS

Transmission of sound in fog and smoke has been studied by Lamb and Sewell. Owing to its great inertia in comparison with that of an equal amount of air, a globule of water in suspension, if not too small, may remain practically at rest as the air waves beat upon it. If, however, the radius be diminished, the inertia diminishes as  $a^3$ , and the surface on which viscosity acts diminishes as  $a^2$  and it is expected that a stage will be reached when the globule will simply drift to and fro with the vibrating air, and so causes little or no loss of energy.

#### *Scattering of Sound in Suspensions*

The scattering of waves in suspensions can be divided into two classes :

- (a) The Rayleigh scattering and,
- (b) the Lamb and Sewell scattering.

In the former case it is well established that scattering increases with the decrease of wavelength or the particle size. For larger wavelengths  $ka \ll 1$ , and the amplitude of the particles in vibration is given by,

$$1 - \frac{\rho_1 - \rho_0}{\rho_1 + \frac{1}{2}\rho_0}$$

where  $\rho_1, \rho_0$  are the densities of the solid and the fluid respectively,  $a$  is the radius of the particles and  $k$  is the propagation constant ( $2\pi/\lambda$ ), in which  $\lambda$  is the wavelength.

In the second case, the viscosity is taken into consideration, when it is seen that the scattering gives rise to additional terms in the velocity potential of the scattered waves ; the particles are dragged to and fro with the waves and the resulting amplitude is given by,

$$1 + \frac{\sigma \xi}{k} = \frac{\rho_1 - \rho_0}{\rho_1 - \rho_0 + 3\rho_0 a_1} \quad \dots (2)$$

$$\text{where,} \quad a_1 = \frac{1}{2} \left( 1 + \frac{3}{2} \frac{1}{a\beta} \right) - \frac{3}{2} \frac{j}{a\beta} \left( 1 + \frac{1}{a\beta} \right) \text{ for } a\beta < 1 \quad \dots (2)$$

and,  $\beta = \sqrt{\frac{\sigma}{2\nu}}$ ;  $\sigma$  is the angular frequency given by  $2\pi f$ , and  $\nu$  is the kinematic

viscosity. The behaviour of the particles depends upon  $\beta$ , i.e., on value of the viscosity. For the particles of larger diameter, the amplitude is the same as that of the oscillating fluid at larger wavelengths. This contention can be upheld considering the following tables which show the values of the amplitude of the particles at different wavelengths for two particle sizes.

**TABLE I**  
Radius  $a = 10^{-3}$  cm.

$\lambda$	$L$	$\lambda$	$L$
5	.019	100	.347
20	.074	400	.833
40	.147	800	.955
60	.217	Inf.	1.000
80	.284		

**TABLE II**  
Radius  $a = 10^{-4}$  cm.

$\lambda$	5	10	25	30	100	Inf
$L$	.855	.961	.990	.996	.9996	1.0000

For particles of smaller radii, it follows from the foregoing that the amplitude of the free particles will be practically zero at these smaller wavelengths (corresponding to megacycle frequencies). Table III presents the calculated values of the amplitudes which show that the value is practically zero.

**TABLE III**  
The amplitude of the particles at different values of the radius for frequency of 10 megacycles per second.

$a$	$\frac{1}{2} \left( 1 + \frac{3}{2a\beta} \right)$	$\frac{1}{2} \frac{1}{a\beta} \left( 1 + \frac{1}{a\beta} \right)$	$a_1$	$\frac{\sigma \xi}{k} + 1$	$\xi \text{ real}$
$10^{-4}$	.45	.7155	.45-.72j	1.45-.72j	$34 \times 10^{-6}$
$10^{-5}$	4.91	30.27	4.91-30.27j	5.91-30.27j	$.60 \times 10^{-5}$
$10^{-6}$	44.60	2646.0	44.6-2646.0j	45.6-2646.0j	$.6 \times 10^{-7}$

The case of the suspended fog and smoke particles in a gaseous medium known as aerosols has been investigated by Richardson (1934). Particular cases of smokes of stearic acid, magnesium oxide and lycopodium dust are included in his work. Lamb's scattering formula is used to determine the sound absorption coefficients. Remarkable agreement between the theoretical and practical values is obtained. In a particular case,

Particle size,  $a = 2.5 \cdot 10^{-4}$

Viscosity,  $\nu = .15 \text{ cm/sec.}$

Number of particles per c.c.,  $n = 1.5 \cdot 10^6$

Velocity of the waves  $= 3.4 \times 10^4 \text{ cm/sec.}$

Frequency  $= 42 \text{ Kc./sec.}$

Attenuation per unit volume  $= .0301$  (theoretical)  
 $= .029$  (practical)

In recent years Urick (*loc. cit*) studied the absorption of sound waves in sand and kaolin particles soaked in water at the megacycle frequencies. His result also shows an agreement with the above theoretical evaluations. Table IV is based on his work.

TABLE IV

The absorption values for kaolin and sand particles.

Frequency Mc/sec.	Kaolin one per cent .9 $\mu$		Fine sand one per cent 2.2 $\mu$	
	Observed	Calculated	Observed	Calculated
1.0	0.024	0.038	0.028	0.032
3.0	0.087	0.018	0.093	0.095
8.9	0.256	0.324	0.232	0.234
15.0	0.450	0.500	0.385	0.347

#### SOUND PROPAGATION IN GELS THE COMPOSITE MEDIUM

According to the present day conceptions, a gel consists of a number of particles *viz.* barium sulphate, iron silicate, thorium phosphate, etc., embedded in a fluid medium. These particles are surrounded by a layer of the fluid which acts in binding one particle with another and provides a structural bond. Thus the contiguous particles form a composite medium with the intervening liquid that is unattached to the particles. In fact, it is this absorbed layer that prevents the formation of coarser aggregation from particles of colloidal and molecular dimensions. Bradford points out that the formation of gel by cooling a sol is a case of crystallisation. Moeller (1921).

is in general agreement with the above views. Weimarn (1908, 1909) concludes from his investigations that a gel consists of highly crystallized granules soaked in the dispersive medium from a supersaturated solution. The process of a sol-gel transformation is a continuous process and there is no evidence on record to show that the aggregation of the particles changes suddenly during the transformation.

Thus Walpole (1913) showed that the refractive index changes slowly but continuously during the gelation of a sol. Ghosh (1930) supports this view and shows, from the measurements of extinction coefficients by the Nutting spectrophotometer in the region of  $6000^{\circ}\text{A}$ , that the changes are continuous and gradual. In a series of papers the elastic constants of certain gels have also been evaluated (Srivastava, 1950). These changes in the values of the Young's modulus and other moduli show a continuous variation and confirm the above views (Srivastava, 1951).

From this experimental support it becomes evident that the gel structure maintains its form during the sol-gel transformation. This gives more reason to the belief of the existence of a double layer as postulated above.

Furthermore, the X-ray work on gels carried on by Debye and Hukel (1924) confirms the above view-points. It is therefore evidently clear that there is a considerable difference between a medium of this type on the one hand and another of the type of sand and kaolin particles in water which has particles entirely independent of one another. In order, therefore, to account for the wave propagation in such a medium we have to take into consideration the density and the bulk modulus of the composite medium. The density of the composite medium will be given by,

$$\rho' = \beta\rho_1 + (1 - \beta)\rho_0 \quad \dots (3)$$

where,

$$\beta = \frac{4\pi}{3}na^3. \quad \dots (4)$$

$n$  being the number of particles per c.c.,  $\rho_1$  and  $\rho_0$  are the densities of the solid and the liquid phases respectively. The bulk modulus of the medium will be obtained as follows: For an applied pressure  $P$ , the change in volume of the gel will be say  $dV$  in an initial volume  $V$ . Then neglecting all interaction between the solid and the liquid phases, this total change  $dV$  will be made up of the sum of the changes in the volume of the solid and the liquid phases. Thus,  $dV = dV_0 + dV_1$ . Also from the definition of the bulk modulus we have,

$$P = K_0 \frac{dV_0}{V(1 - \beta)} = K_1 \frac{dV_1}{V\beta} \quad \dots (5)$$

where  $K_1$  and  $K_0$  are the bulk modulus of the solid and the liquid phases. The composite bulk modulus is given by,

$$K' = \frac{K_1 K_0}{K_1(1-\beta) + K_0\beta} \quad (6)$$

It is of interest to note here that in case the porosity  $\beta=0$ , the liquid phase only exists and the value of the composite bulk modulus  $K'=K_0$  only. This result shows that the formula derived for  $K'$  is adequate for the extreme case when  $\beta=0$ . Similarly, when  $\beta=1$ , the formula yields  $K'=K_1$ , showing that the bulk modulus is that due to the solid phase alone. This is also clear from the porosity expression because the value  $\beta=1$ , implies that the entire volume of the composite medium is made up of the solid phase. The formula, therefore, is valid for all values of  $\beta$  lying between unity and zero. In practice, however, it will be seen later on that the values of  $\beta$  with which we are concerned in the case of these gelatinous substances lies between 2% to about 10%.

As shown elsewhere (Srivastava, 1949), the formula for the composite bulk modulus, as shown above, gives results of the bulk modulus on assuming the values of  $K_0$  and  $K_1$ , and  $\beta$ , which are in fair agreement with the practically determined values. These results confirm the validity of the above theoretical results and give ground enough to treat the above gel structure established.

#### SOUND PROPAGATION IN GELS WITH SCATTERING

In the treatment so far no mention has been made of the scattering of the waves by the solid particles in a gelatinous medium. The treatment given below includes the scattering effects due to the sphere. We now proceed to evaluate the total effect of all the secondary vibrations that issue forth from the composite medium of thickness  $\Delta x$  which is large compared to the wavelength. In figure 1, the secondary vibrations at a

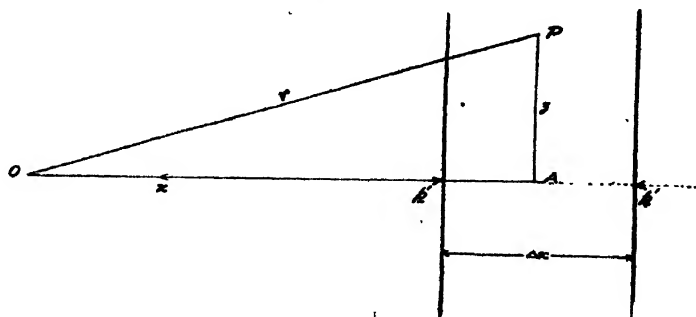


FIG. 1

The forces acting upon the composite element  $\Delta x$

distant point  $O$  due to a particle placed at  $P$  are denoted by the velocity potential

$$\phi' = A_0 f_0(kr) + (H + jK) f_1(kr) \cdot kr \cdot \cos \theta + \dots \quad (14)$$

where  $OP = r$ . If  $AP = z$ , then consider the element of thickness  $\Delta x$  having a volume  $2\pi z dz \Delta x$  which contains  $2\pi z dz \Delta x \cdot n$  particles.

$$\text{Also,} \quad r^2 = x^2 + z^2, \text{ and, } z dz = r dr; \cos \theta \simeq 1 \quad \dots (15)$$

For distant values of  $r$  the resultant of all the secondary vibrations issuing forth from the stratum will be given by,

$$\phi' = 2\pi n \Delta x \int_{-x}^{\infty} \left[ A_0 \frac{e^{-jkr}}{kr} - (H + jK) j \frac{e^{-jkr}}{kr} \right] r dr \quad \dots (16)$$

or,

$$\phi' = 2\pi n \Delta x [A_0 j + H + jK] e^{jkr} \quad \dots (17)$$

The coefficients  $A_0$  and  $(H + jK)$  have been calculated by Lamb. They are,

$$A_0 = -\frac{1}{3} k^3 a^3 \left[ 1 - \frac{k^2 a^2}{2} + j \frac{k^3 a^3}{3} \right] \quad \dots (18)$$

$$H + jK = ja_1(P + jQ) k^3 a^3 \quad \dots (19)$$

where,

$$a_1 = \frac{1}{2} \left( 1 + \frac{3}{2a\beta} \right) - \frac{3}{4} \frac{j}{a\beta} \left( 1 + \frac{1}{a\beta} \right) \left. \vphantom{\frac{1}{2} \left( 1 + \frac{3}{2a\beta} \right)} \right\} \text{For } a\beta \ll 1 \quad \dots (20)$$

$$P + jQ = (\rho_1 - \rho_0) / (\rho_1 + 3a_1\rho_0 - \rho_0) \quad \dots (21)$$

and

$$a_1 = \frac{1}{2} - j \frac{k^3 a^3}{12} \left. \vphantom{\frac{1}{2} - j \frac{k^3 a^3}{12}} \right\} \text{For } a\beta \gg 1 \quad \dots (22)$$

$$P + jQ = (\rho_1 - \rho_0) / (\rho_1 + \frac{1}{2}\rho_0) \quad \dots (23)$$

The pressure due to the resultant vibration at any point situated at a distance  $x$  from the origin of disturbance is,

$$p' = 2\pi n \Delta x k a^3 [A_0 + a_1(P + jQ)] j\omega \rho_0 \phi_0 e^{jkr} \quad \dots (24)$$

where  $\phi_0$  is the potential due to the incident waves given by,

$$\phi_0 = e^{jkr} \quad \dots (25)$$

Hence in terms of the particle velocity of the incident waves the pressure will be given by,

$$p' = 2\pi n \Delta x k a^3 [A_0 + a_1(P + jQ)] j\omega \rho_0 u e^{jkr} \quad \dots (26)$$

where,  $u$  represents the particle velocity due to the incident waves

$$u = -jk\phi_0 \text{ or, } \phi_0 = -u/jk \quad \dots (27)$$

By putting  $x=0$  we obtain the pressure  $p'_-$  at the negative side of the stratum,

$$p'_- = 2\pi n \Delta x a^3 j\omega \rho_0 [A_0 + a_1(P + jQ)] u \quad \dots (28)$$

Since the particles in the stratum scatter sound waves in the positive

direction as well a similar expression for  $p_+''$  is obtained,

$$p_+' = 2\pi n \Delta x a^3 j \omega \rho_0 [A_0 - a_1(P + jQ)]u. \quad \dots (29)$$

The net force per unit area of the composite medium at the ends of the stratum  $\Delta x$  acting in the negative direction will be  $(p_+' - p_-)$  i.e.,

$$p_+' - p_- = -4\pi n a^3 j \omega \rho_0 a_1 (P + jQ) \Delta x u. \quad \dots (30)$$

### Equation of Motion

We have assumed that the particles in a gel are bound together, the exact nature of the binding forces being not known definitely. The particles give rise to scattering and the extra pressure is developed on account of this. The equation of motion is modified to,

$$\rho' \frac{du}{dt} = \frac{K'}{j\omega} \frac{d^2 u}{dx^2} - 4\pi n a^3 j \omega \rho_0 a_1 (P + jQ)u \quad \dots (31)$$

or since,  $u \propto e^{j\omega t}$ , we have,

$$\frac{d^2 u}{dx^2} = \frac{(j\omega)^2}{(K'/\rho')} \left[ 1 + 4\pi n a^3 \frac{\rho_0}{\rho_1} a_1 (P + jQ) \right] u \quad \dots (32)$$

putting,  $C^2 = K'/\rho'$ ,  $k = \omega/c$ , the solution of the above equation is,

$$u = e^{jk'x} \quad \dots (33)$$

where,

$$k'^2 = k^2 \left[ 1 + 4\pi n a^3 \frac{\rho_0}{\rho_1} a_1 (P + jQ) \right] \quad \dots (34)$$

or approximately, [if  $a_1(P + jQ) = p - jq$ ]

$$k' = k \left[ 1 + 2\pi n a^3 \frac{\rho_0}{\rho_1} (p - jq) \right] \quad \dots (35)$$

Hence,

$$u = e^{jk_0 x} \cdot e^{\alpha x} \quad \dots (36)$$

$$k_0 = k \left[ 1 + 2\pi n a^3 \frac{\rho_0}{\rho_1} p \right] \quad \dots (37)$$

and the attenuation constant  $\alpha$  is,

$$\alpha = 2\pi n a^3 \frac{\rho_0}{\rho_1} q \cdot k. \quad \dots (38)$$

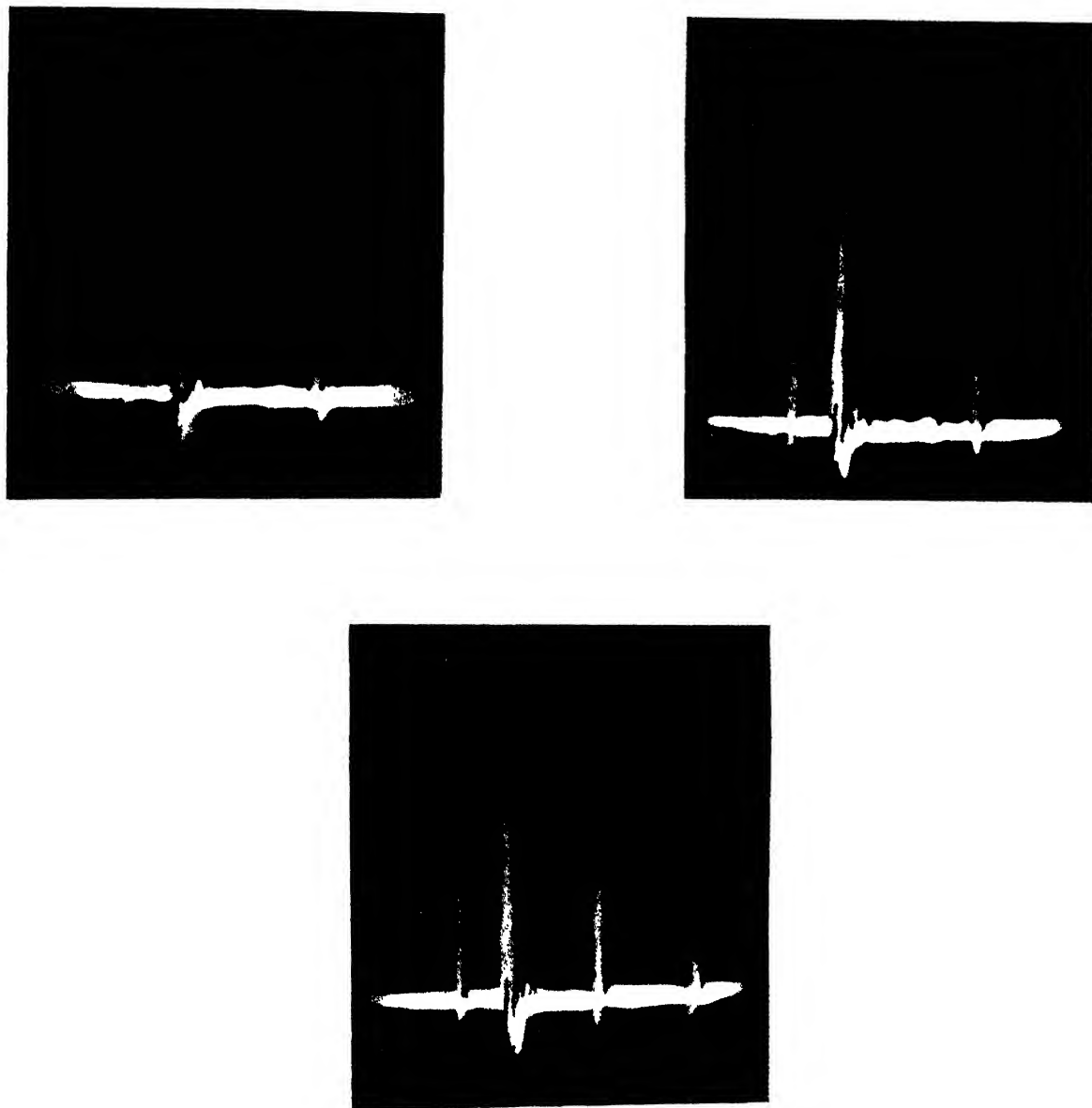
Thus from a knowledge of the quantities involved in the above equation the attenuation constant can be determined theoretically. Such values are given in Tables VI, VIII and IX.

### EXPERIMENTAL DETERMINATION OF ATTENUATION

The experimental method is based upon the successive reflection of the pulses of ultrasonic energy and an observation of the diminution in its



amplitude on an oscillograph (figure 2). The ultrasonic generator is described in detail in a previous communication (Srivastava, 1949). If



c  
FIG. 2

The oscillograms for three different values of attenuation with barium carbonate gel

$-x_1$  and  $-x_2$  are two points on the primary waves then the amplitude of the particle velocities at  $-x_1$  and  $-x_2$ , will be given by,

$$\left. \begin{aligned} u_1 &= be^{-ax_1} \\ u_2 &= be^{-ax_2} \end{aligned} \right\} \quad \dots (39)$$

and, 
$$\alpha = \frac{\pi \cdot \omega \cdot v}{x_1 - x_2} \log_{10} (u_1/u_2) \quad \dots (40)$$

The ratio of these yields the attenuation, since  $x_1 < x_2$ , the amplitude at  $-x_1 >$  that at  $-x_2$ . The amplitude of the particle velocity therefore decreases as the wave travels towards the negative direction of the  $x$ -axis.

The transmitter and receiver quartz are brought in contact with the two faces of the gel held in its holder. The waves are twice reflected

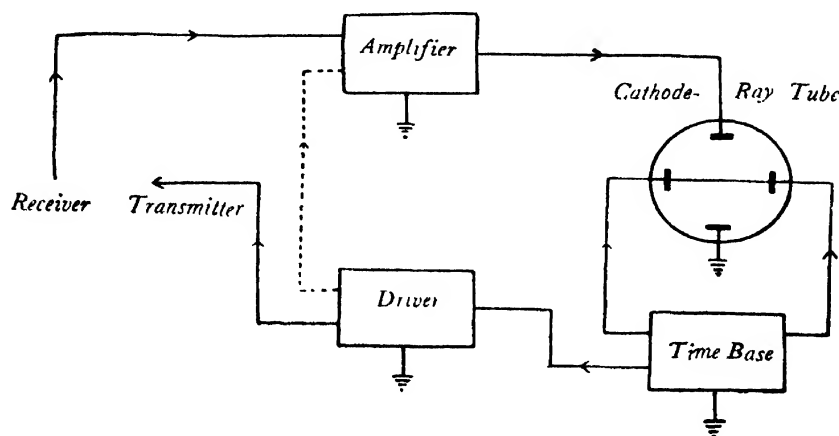


FIG. 3

The block diagram of the ultrasonic pulse generator

giving a path difference of twice the thickness of the sample, and produce two maxima on the cathode ray screen. Since reflection takes place at the surface of separation of gel and the crystal housing, a correction is applied for the loss of energy at reflection.

### Preparation of Gel

The gel used in this case is barium carbonate and is prepared as follows. Fairly concentrated solutions of barium acetate and potassium carbonate are added in almost equal volumes and the mixture is allowed to stand for about 30 minutes after a vigorous shake for a minute or two. The strengths of the two solutions are determined in the usual manner, as described elsewhere (Srivastava, 1949a). In a particular case,

Strength of barium acetate, = 4.40 N.

Strength of potassium carbonate, = 4.32 N.

Density of the resulting gel obtained by mixing 5.0 c.c. each of the above, = 1.20 gm./cm<sup>3</sup>

An opaque stiff gel is obtained which keeps for about 3 hours. For a stiffer gel the volume of barium acetate may be greater by up to 20 per cent that of the carbonate.

RESULTS

Table VI shows a set of values of attenuation for three gels that were studied in the course of these investigations. The agreement between the theoretical and the corrected practical values is satisfactory. In Table VII the variation of attenuation due to the changes in viscosity at higher temperatures is shown. The effect of viscosity is to decrease the values of attenuation. Thus by compounding the values of Tables VI and VII it is possible to obtain the effect of both viscosity and scattering. These values are shown in Table IX. In Table VIII, only the scattering effects at higher temperatures are seen.

A detailed perusal of values in Table IX shows that the observed values are adequately explained by theoretical values. Only the results for one particular gel are given here.

TABLE VI

The values of attenuation for three gels

GEL	$\rho'$	$\beta$	$na^3$	$n$	$\alpha$ (Theory)	$\alpha$ (Corrected)	$\alpha$ (Observed)
Strontium carbonate	1.16	.052	.013	2.10	.357	.340	.418
Barium carbonate	1.20	.064	.016	2.51	.257	.306	.362
Iron silicate	1.22	.080	.020	3.10	2.48	.290	.341

TABLE VII

Changes in attenuation due to a change in viscosity at higher temperatures (eq.38).

$\nu$	$\beta$ $\times 10^5$	$1/a\beta$	$q$	$\alpha$
.010	.174	.84	1.16	.696
.008	.139	.71	.92	.552
.006	.157	.63	.78	.468
.004	.190	.52	.59	.354
.002	.240	.41	.43	.258

TABLE VIII

Changes in attenuation due to a temperature variation. Values of velocity,  $c$  have been practically determined.

Temp. °C	$\rho'$	$c$ $\times 10^5$ cms/sec	$k$	Attenuation $\alpha$		
				Practical	Corrected	Theoretical
						°C
22	1.199	2.95	25.0	.275	.306	.362 20
30	1.197	2.86	26.2	.288	.313	.370 30
43	1.192	2.73	27.5	.293	.323	.395 40
55	1.187	2.65	28.3	.311	.331	.411 50
70	1.170	2.63	28.9	.315	.300	.368 60

TABLE IX

The values of attenuation.

Temperature °C	$\rho'$	$c$ $\times 10^5$	$\beta$	Attenuation $\alpha$	
				Calculated	Observed
22	1.199	2.95	.01	.275	.306
30	1.197	2.86	.09	.288	.313
43	1.192	2.73	.008	.293	.323
55	1.187	2.65	.006	.311	.331
70	1.170	2.63	.005	.354	.300

## CONCLUSIONS

In this paper the author has tried to give a theoretical expression for the attenuation of sound waves in gelatinous substances. The structure of these substances is different from that of certain suspensions in water which have been considered by the previous workers. Upon the agreed structure of gels, which is evidenced by his work and is sufficiently supported by other distinguished sources, the author built up in this paper, considering the scattering of waves by these solid spheres, a theory that stands the test of practical experimentation. The values of attenuation are determined by an ultrasonic pulse method which has not been used elsewhere to this purpose.

Also the maxima observed in the values of attenuation have been explained as the composition of two distinct effects. The first is due to scattering which increases the value of attenuation with a rise of temperature. In the absence of any other effect this will produce a gradual increase in the attenuation. But the increase in temperature results in a decrease of kinematic viscosity, which again produces a decrease in the attenuation. Upon considering both of these, it is observed that the maximum in attenuation with temperature is suitably explained.

#### ACKNOWLEDGEMENT

The author's sincerest thanks are due to Prof. R. N. Ghosh, D. Sc., F. N. I., F. A. S. (America), for his very valuable help in the preparation of this paper.

PHYSICS DEPARTMENT  
ALLAHABAD UNIVERSITY, ALLAHABAD

#### REFERENCES

- Brandt, O., 1937, *Koll. Zett.* **81**, 2.  
 Debye and Hukel, 1924, *Phy. Zett.*, **24**, 49.  
 Epstein, 1942, *C. I. T. Karman Vol*, 162.  
 Ghosh, R. N., 1944, *Ind. J. Phys.*, **18**, 341.  
 Ghosh, S. 1930, *Zeit. anorg. Chem.*, **194**, 306.  
 Hartmann and Focke. 1940, *Phys. Rev.*, **57**, 221.  
 Heidmann, Freund and Brandt, O., 1937, *Zett. Phys.*, **104**, 511.  
 Herzfeld, K. F., 1930, *Phil Mag.*, **9**, 741, 752.  
 Lamb, H., 1884, "Hydrodynamics", 6th Ed. 296, 354.  
 Moeller, 1921, *Koll. Zett.*, **28**, 281.  
 Rayleigh, 1896, *Theory of Sound*, London, p.242.  
 Richardson, E. G., 1938, *J. Acoust. Soc.*, **9**, 217.  
 " " 1935, *Proc. Phys. Soc.*, **47**, 533.  
 Richardson, E. G., 1934, *Proc. Roy. Soc.*, **146A**, 64.  
 Sewell, C. J. T., 1911, *Phil. Trans.*, **A**, 210, 239.  
 Srivastava, A. M., 1950, *Koll. Zett.*, **119**, 146.  
 " " 1951, *J. Amer. Chem. Soc.*, **73**, 489.  
 " " 1950, *Compt. Rend.*, **231**, 1225.  
 Srivastava, A. M., 1949, *Proc. Nat. Acad. Sc.*, **18A**, 51.  
 " " 1949a, D. Phil. Thesis, Allahabad University.  
 Srivastava, A. M., 1951, *Proc. Nat. Acad. Sc.*, **20A**, 156.  
 " " 1951, *J. Acoust. Soc.*, **23**, 553.  
 Walpole, 1913, *Koll. Zett.* **13**, 241.  
 Weimaren, 1908, *Koll. Zeit.* **2**, 199, 230, 275, 301, 326, Suppl. 2, L11;

# HARMONIC DISTORTION IN FREQUENCY MODULATION RECEPTION. PART I

By K. V. KRISHNA PRASAD

*(Received for publication, July 2, 1951)*

**ABSTRACT.** The two signal distortion theory of frequency modulation reception has been developed by a new method and a brief treatment of this theory together with its extension to the more complicated case of  $n$ -signals is given.

## INTRODUCTION

Transmission is possible by more than one path with the frequencies used in frequency modulation. So, two or more signals, having nearly the same amplitude, if induced in the antenna, will give rise to considerable distortion.

Large objects, such as hills or high buildings, reflect and absorb the waves and cause interference. This difficulty is encountered also in television reception. In fact, higher frequencies employed here tend to enhance this difficulty in as much as the phase changes encountered are great. This interference causes light and dark bands in the picture resulting in synchronization difficulties when frequency modulation is used on video signals. So, a theoretical and experimental study of multipath distortion would be very interesting in determining the factors which contribute to this type of distortion. The present paper is restricted only to a treatment of the theoretical aspects of the harmonic distortion in frequency modulation reception while a treatment of its experimental aspects is reserved for a latter one to follow.

The existing theories, such as those of Corrington (1945) and Meyers (1946) for the case of two signals, are complicated and they involve approximations from tables and charts in arriving at the final expression for the distortion term. In addition to these difficulties the results derived from them do not lend themselves to an easy experimental verification. The present development of the theory, treated here, involves the methods of contour-integration, leading to a rigorous mathematical treatment, which lends itself to physical interpretation. The general principles of the method are too well known to need any further elucidation. In recent years this method has been widely used in treating similar problems in the fields of electric transients and computer-electronics.

## THEORY

1. *Case of two signals* :—Now to begin with, let a sinusoidal carrier frequency modulated by a single sinusoidal modulating frequency

be assumed for the transmitted wave. Consider an ideal limiter which is independent of the frequency of the input signal. Assume also a zero order characteristic to insure limiting at low amplitudes\*. Noise is the controlling factor in any practical consideration where multipath interference reduces the strength of the signal at the receiver below it. This noise may, however, be neglected as an approximation. To develop the theory of two signal distortion, let the two signals be represented by :

$$c_1 = E_0 \sin y_1, \text{ the desired one}$$

and

$$c_2 = E_1 \sin y_2, \text{ the undesired one}$$

with

$$y_1 = \omega_c t + h \frac{\omega_d}{\omega_p} \sin \omega_p t$$

and

$$y_2 = \omega_c t + \beta + h \frac{\omega_d}{\omega_p} \sin (\omega_p t + \alpha) \quad \dots (1)$$

where,  $\omega_c = 2\pi \times$  carrier frequency

$\omega_p = 2\pi \times$  modulating frequency

$\omega_d = 2\pi \times$  maximum deviation frequency

$\alpha = \omega_p t_0$  and  $\beta = \omega_c t_0$  with  $t_0 =$  time delay in seconds

and,  $h =$  factor proportional to the amplitude of signal input at the transmitter.

Then the resultant  $E_R$  of the two signals may be written as :

$$E_R = E \sin [(y_1 + y_2)/2 + \phi(t)] \quad \dots (2)$$

where,

$$E = \sqrt{E_0^2 + E_1^2 + 2E_0E_1 \cos (y_1 - y_2)}$$

and

$$\tan \phi = \frac{E_0 - E_1}{E_0 + E_1} \tan (y_1 - y_2)/2$$

Assuming the signal above limiter level and  $E_0, E_1$  constant with respect to time, the discriminator output  $E$  is given by

$$E = \frac{d}{dt} \left[ \frac{y_1 + y_2}{2} + \phi(t) \right] \quad \dots (3)$$

$$= \omega_c h \frac{\omega_d}{2} \cos \omega_p t + h \frac{\omega_d}{2} \cos (\omega_p t + \alpha) + d\phi/dt \quad \dots (4)$$

The last term in equation (4) viz.

$$\frac{d\phi}{dt} = \frac{E_0^2 - E_1^2}{2E_0E_1} \cdot \frac{d\xi/dt}{\frac{E_0^2 + E_1^2}{2E_0E_1} + \cos 2\xi} \quad \dots (5)$$

$$\text{where,} \quad \xi = \frac{1}{2} [h(\omega_d/\omega_p) \sin \omega_p t - h(\omega_d/\omega_p) \sin (\omega_p t + \alpha) - \beta] \quad \dots (6)$$

\* This fact has been borne out in the experimental tests by operating above the limiter level.

Now  $f(\xi) = 1/(\sigma + \cos 2\xi)$  being a symmetrical function may be expanded into the series :

$$f(\xi) = a_0/2 + \sum_{v=1}^{\infty} (a_v \cos v\xi + b_v \sin v\xi) \quad \dots (7)$$

where the Fourier coefficients,

$$a_v = 0 \text{ for odd values of } v$$

and

$$b_v = 0 \text{ for all values of } v$$

Hence,

$$a_{2N} = \frac{1}{\pi} \int_{-\pi}^{\pi} \cos 2N\xi / (\sigma + \cos 2\xi) d\xi \quad \dots (8)$$

which by contour integration and substitution of  $Z = e^{2i\xi}$  becomes :

$$a_{2N} = \frac{1}{2\pi i} \int \frac{Z^N + Z^{-N}}{1 + 2\sigma Z + Z^2} dZ \quad \dots (9)$$

The path of integration is the unit circle  $|Z| = 1$  and the poles are  $Z_0 = 0$ ,  $Z_1 = -E_1/E_0$  and  $Z_2 = -E_0/E_1$

Since  $E_0 > E_1$ , consider only the poles  $Z_0 = 0$  and  $Z_1 = -E_1/E_0$ , their respective residues being  $(Z_1^N - Z_2^N)/(Z_1 - Z_2)$  and  $(Z_1^N + Z_2^N)/(Z_1 - Z_2)$ , so that :

$$a_{2N} = 4E_1E_0/(E_0^2 - E_1^2) (-r)^N, \text{ where } r = E_1/E_0 \quad \dots (10)$$

and hence

$$\frac{d\phi}{dt} = [h\omega_d \cos \omega_p t - h\omega_d \cos (\omega_p t + \alpha)] \cdot \left[ \frac{1}{2} + \sum_{N=1}^{\infty} (-r)^N \cos 2N\xi \right] \quad \dots (11)$$

Substituting the value of  $d\phi/dt$  given in expression (11) in equation (4), the expression for the discriminator output  $E$  becomes :

$$E = \omega_c + h\omega_d \cos \omega_p t - [2h\omega_d \sin \alpha/2 \sin (\omega_p t + \alpha/2)] \times \left[ \sum_{N=1}^{\infty} (-r)^N \cos 2N\xi \right] \quad \dots (12)$$

from which the instantaneous frequency  $f_i$  may be computed as

$$f_i = E/2\pi = f_c + hf_d \cos \omega_p t - [2hf_d \sin \alpha/2 \sin (\omega_p t + \alpha/2)] \times \sum_{N=1}^{\infty} (-r)^N \cos 2N\xi \quad \dots (13)$$

The distortion  $D$  represented by the last term of equation (13) is given by

$$D = lf_p \sin (\omega_p t + \alpha/2) \sum_{N=1}^{\infty} (-r)^N \cos (2N\xi)$$

or in the expanded form,

$$D = lf_p \sin (\omega_p t + \alpha/2) \sum_{N=1}^{\infty} (-r)^N \cos [Nl \cos (\omega_p t + \alpha/2) + N\beta] \quad \dots (14)$$

where  $l = 2hf_d/f_p \sin \alpha/2$ .



Equation (14) obviously can be expanded into a series of Bessel functions and hence can be written in the form :

$$D = 2f_p \left\{ \sum_{n=1}^{\infty} \left( \frac{-r}{N} \right)^N \sin N\beta \sum_{m=1}^{\infty} (-1)^m (2m) J_{2m}(Nl) \sin 2m\theta \right. \\ \left. + \sum_{n=1}^{\infty} \left( \frac{-r}{N} \right)^N \cos N\beta \sum_{m=0}^{\infty} (-1)^m (2m+1) J_{1+2m}(Nl) \sin (2m+1)\theta \right\} \dots \quad (15)$$

where  $\theta = \omega_p t + \alpha/2$ .

For purposes of experimental verification, this expression can be further simplified and put into a more convenient form by the substitution

$$J_m(l) = \sum_{p=0}^{\infty} \frac{(-1)^p (l/2)^{m+2p}}{p!(m+p)!}$$

whence :

$$D = f_p \left[ \sum_{p=0}^{\infty} \sum_{m=0}^{\infty} 2m/p!(m+p)! (\sin m\theta) (l/2)^{m+2p-1} \frac{\partial^{m+2p-1} R}{\partial \beta^{m+2p-1}} \right] \dots \quad (15a)$$

where  $R = \sum_{n=1}^{\infty} (-r)^N (\cos N\beta) l/2$  for the sake of brevity.

The parameters which are significant in equation (15) or (15a) are  $r$ , the ratio of the undesired to the desired signal,  $l$ , the product of  $h$ , the input signal strength and  $f_d$ , the deviation frequency,  $f_p$ , the modulating frequency,  $m$ , the order of the harmonic and finally  $\alpha$  and  $\beta$ , the factors involving the time delay  $t_0$ . From the stand point of high distortion, the case of interest is when  $r$  is very near unity but not exactly unity. The distortion in this case is rigorously represented by equation (15) or (15a). The distortion is zero when  $l$  is large; that is, for a system having high input signal and high deviation frequency. Further, the distortion is zero when  $\alpha = 2\pi N$  and the even order modulations vanish for  $\beta = N\pi$ . Lastly, the distortion increases with the modulating frequency  $f_p$ . So from the point of view of high distortion, the case of low signal amplitudes is interesting when  $h$  and hence  $l = 2hf_d/f_p \sin \alpha/2$  is small. Then only the first term of the Bessel series expansion in equation (15) is important. So by putting  $p=0$  in equation (15a) the resulting simplified expression for the distortion is :

$$D = f_p \left[ \sum_{m=1}^{\infty} \frac{2 \sin m\theta}{(m-1)!} (l/2)^{m-1} \frac{\partial^{m-1} R}{\partial \beta^{m-1}} \right] \quad (16)$$

From the expression it is easy to compare the amount of various harmonics by letting  $m$  have the run of values  $m=1, 2, 3, \dots$  and the results are summarized in Table I below. In these expressions  $u = (r^2 + r \cos \beta)^{1/2} (1 + 2r \cos \beta + r^2)$ .

The results given in Table I will be dealt with in detail in part II but suffice it to say that the  $n$ th-harmonic distortion is directly proportional to the  $(n-1)$ th power of the deviation frequency  $f_d$ ,  $(n-1)$ th power of the input amplitude  $h$ , and the modulating frequency  $f_p$  for small values  $\alpha = 2\pi f_p t_0$

TABLE I

Order of the harmonic $m$	Simplified expressions for the distortion ( $D$ )
Fundamental $m=1$	$D_1 = hf_d \cos \omega_p t - lf_p \sin (\omega_p t + \alpha/2) u$
Second $m=2$	$D_2 = -2hf_d/f_p \partial u / \partial \beta \sin^2 \alpha/2 / \sqrt{1+4u^2 \sin^2 \alpha/2}$
Third $m=3$	$D_3 = h^2(f_d/f_p)^2 \partial^2 u / \partial \beta^2 \sin^3 \alpha/2 / \sqrt{1+4u^2 \sin^2 \alpha/2}$
Fourth $m=4$	$D_4 = h^3 \cdot 3(f_d/f_p)^3 \partial^3 u / \partial \beta^3 \sin^4 \alpha/2 / \sqrt{1+4u^2 \sin^2 \alpha/2}$
$n$ th $m=n$	$D_n = 2h^{n-1} / (n-1)! \partial^{n-1} u / \partial \beta^{n-1} (f_d/f_p)^{n-1} \sin^n \alpha/2 / \sqrt{1+4u^2 \sin^2 \alpha/2}$

where  $t_0$  is the time delay ; and so in any practical consideration it is advisable to operate at high deviation frequency and high modulating frequency if any appreciable distortion is desired.

2. *Case of  $n$ -signals*:—A preliminary experimental survey has shown that most of the distortion is caused by the combination of two signals, the desired and undesired ones of very nearly of the same amplitude. Nevertheless, it will be interesting to study the arrival of more than two signals at the receiver by multiple reflections. So a brief treatment of the general case of  $n$ -signals is worth considering from the theoretical point view.

Let the desired signal and the  $n$ -interfering signals be represented by

$$\begin{aligned} e_1 &= E_0 \sin [\omega_c t + hf_d/f_p \sin \omega_p t] \\ e_2 &= E_1 \sin [\omega_c t + \beta_1 + hf_d/f_p \sin (\omega_p t + \xi_1)] \end{aligned} \quad (17)$$

$$e_n = E_n \sin [\omega_c t + \beta_n + hf_d/f_p \sin (\omega_p t + \xi_n)]$$

where  $\beta_n = \omega_p t_n$  and  $\xi_n = \omega_c t_n$  with  $n=1, 2, 3, \dots, n$

The resultant  $E_R$  of these signals is given by :

$$E_R = \sum_{j=0}^n E_j \sin (\omega_c t + \zeta_j)$$

where  $\zeta_j = \beta_j + hf_d/f_p \sin (\omega_p t + \xi_j)$

(On expanding,

$$E_R = [\sum E_j \cos \zeta_j] \sin \omega_c t + [\sum E_j \sin \zeta_j] \cos \omega_c t$$

$$= \sqrt{[\sum E_j \cos \zeta_j]^2 + [\sum E_j \sin \zeta_j]^2} \sin (\omega_c t + \tau)$$

where  $\tau = \arctan \frac{\sum_{j=0}^n E_j \sin \zeta_j}{\sum_{j=0}^n E_j \cos \zeta_j}$

By putting  $\zeta_1 = \zeta_0 + \epsilon_1$

$$\zeta_2 = \zeta_0 + \epsilon_2$$

where

$$\zeta_0 = hf_d/f_p \sin (\omega_p t)$$

the expression for  $\tau$  could be simplified to :

$$\tau = \zeta_0 + \tan^{-1} \frac{\sum_{j=1}^n E_j \sin \epsilon_j}{E_0 + \sum_{j=1}^n E_j \cos \epsilon_j} \quad (18)$$

$$= \zeta_0 + \psi$$

where

$$\psi = \tan^{-1} \frac{\sum_{j=1}^n E_j \sin \epsilon_j}{E_0 + \sum_{j=1}^n E_j \cos \epsilon_j}$$

Whence,

$$E_R = \sqrt{[\sum E_j \cos \zeta_j]^2 + [\sum E_j \sin \zeta_j]^2} \sin (\omega_c t + hf_d/f_p \sin \omega_p t + \psi) \quad (19)$$

Hence the distortion is given by :

$$D = \frac{d}{dt} \tan^{-1} \frac{\sum_{j=1}^n E_j / E_0 \sin \epsilon_j}{1 + \sum_{j=1}^n E_j / E_0 \cos \epsilon_j}$$

which on analogy with the two signal theory\* can be represented by :

$$D = - \sum_{j=1}^{\infty} [f(\epsilon_j)]^j \sin \sum_{p=1}^n (E_j / E_0)^p \sin (p\epsilon_j + \eta_p) \quad (20)$$

where  $f(\epsilon_j)$ , containing the amplitudes of the harmonics is a complicated function of  $\epsilon_j$ . The problem becomes then that of expanding a sine of a Fourier series into a suitable form, let alone the other complicated parameters involved. The method of approach is as follows :

The rather well known result in the theory of Bessel functions viz,

$$e^{ic_p \sin (p\theta + \delta_p)} \sin (p\theta + \delta_p) = \sum_{q=-\infty}^{\infty} e^{iq(p\theta + \delta_p)} \xi_q(cp)$$

is generalized by replacing  $c_p \sin (p\theta + \delta_p)$  on the left hand side by the

expression  $\phi_n = \sum_{p=1}^n c_p \sin (p\theta + \delta_p)$  whence

$$\begin{aligned} e^{i\phi_n} &= \frac{1}{\pi} \sum_{p=1}^n e^{ic_p \sin (p\theta + \delta_p)} \\ &= \frac{1}{\pi} \sum_{p=1}^n \left\{ \sum_{q_p=-\infty}^{\infty} e^{iq_p \delta_p} \xi_{q_p}(c_p) e^{iq_p p\theta} \right\} \\ &= \sum_{q_n=-\infty}^{\infty} \sum_{q_{n-1}=-\infty}^{\infty} \dots \sum_{q_1=-\infty}^{\infty} e^{i \sum_{p=1}^n q_p \delta_p} \left\{ \frac{1}{\pi} \sum_{p=1}^n \xi_{q_p}(c_p) \right\} e^{i \sum_{p=1}^n p q_p \theta} \\ &= \sum_{m=-\infty}^{\infty} \Gamma_m e^{im\theta} \end{aligned}$$

where the  $\Gamma_m$ s are complex, and they may be evaluated by restricting the summation over the  $q$ 's such that  $\sum_{p=1}^n p q_p = m$ .

\*c.f., equation (14)

Hence,

$$\Gamma_m = \sum_{(q_p)} \left[ e^{i \sum_p q_p \delta_p \left\{ \frac{\pi}{n} J_{q_p}(e_p) \right\}} \right]$$

which can be re-written so as to conform to the notation used in equation (20) as :

$$\Gamma_m = \sum_{(q_p)} \left[ e^{i \sum_p q_p \eta_p \left\{ \frac{\pi}{n} J_{q_p}(E_p/E_0)_p \right\}} \right] \quad (21)$$

The  $m$ th coefficient of the sine of the Fourier series is easily evaluated by taking the imaginary part of  $\Gamma_m e^{im\epsilon} + \Gamma_{-m} e^{im\epsilon}$ . Tables are given by Strachey and Wallis (1946) for evaluating some of these parameters.

Thus, while in the previous papers of Corrington (1945) and Meyers (1946), the final expressions for distortion for the case of two signals are presented in a complicated form involving too many parameters without any attempt being made to simplify the results, the present paper gives the final result in a useful series form enabling easy computation of the various harmonic contents for a particular case under test and this will be explained in detail together with experimental results, in part II.

The case of  $n$ -signals\* (Krishna Prasad, 1951) presents a rather unique and complex situation of resolving the sine of a Fourier series and a method of approach is suggested: The results, however, cannot be put into a useful practical form on account of the highly complicated nature of  $f(z_j)$  in equation (20).

#### ACKNOWLEDGMENT

This work forms part of the the thesis submitted by the author to the California Institute of Technology, Pasadena, U. S. A. for the Degree of Electrical Engineer under the title, 'Distortion in Frequency Modulation Reception'.

NATIONAL PHYSICAL LABORATORY OF INDIA,  
NEW DELHI.

#### REFERENCES

- Corrington, M. S., 1945, *Proc. Inst. Rad. Engrs*, **33**, 878  
 Krishna Prasad, K. V., 1951, *Science & Culture*, **17**, in Press.  
 Meyers, S. T., 1946, *Proc. Inst. Rad. Engrs.*, **34**, 256.  
 Strachey, C., and Walis, P. J., 1946, *Phil. Mag.*, **2**, 84

# REVIEW

(4)

**Static and Dynamic Electricity**—By William R. Smythe. Pp xxi+616. McGraw-Hill Book Company, New York, Toronto, London, 1950. Price \$ 8.5.

This is the second edition of the book, the first edition of which was published in 1939. As pointed out in the preface to the first edition, special stress has been laid on solution of problems in electricity and magnetism which are generally encountered in research. A basic knowledge in vector analysis has been assumed to be possessed by the student in treating the problems, but the use of contour integration has been avoided.

In electrostatics, method of images, Legendre polynomials and Bessel's, functions have been applied to problems on potential. In electrodynamics, besides chapters on Flow of current in networks and two and three dimensional conductors, Eddy currents, Magnetism, Electromagnetic waves, etc., there are important chapters on Electromagnetic radiation and Wave guides and Cavity resonators. There is also a chapter on special relativity and the motion of charged particles. The mks (metre-kilogram second) system of units has been used throughout, but in an Appendix the factors of conversion to cgs units have been given in different tables.

The book will be found useful to students studying for the B. Sc. (Hons.) and M. Sc. degrees of Indian Universities. It is also a good reference book which can be used profitably by research workers.

The paper used and quality of printing leave nothing to be desired.

S. C. S.

# STATISTICAL MECHANICS

## Parts I and II

By **K. C. KAR, D.Sc.,**

*Senior Professor of Physics, Presidency College, Calcutta and,  
Lecture in Physics, Calcutta University.*

It is a comprehensive and clear treatment of the subject. The different statistical methods are for the first time classified under five heads. The first part deals with the principles of classical, quantum and wave-statistics, while the second part the applications of classical and quantum statistics to problems in physics and chemistry illustrated by eighty tables and curves.

	Part I—pp. 155	Price	
1952	Part II—pp. 370	Part, I and II	Rs. 30/-

**DAS GUPTA & Co. Ltd.**

54-3 COLLEGE STREET, CALCUTTA—12

# HARMONIC DISTORTION IN FREQUENCY-MODULATION RECEPTION. PART II\*

By K. V. KRISHNA PRASAD

(Received for publication, July 10, 1951)

**ABSTRACT.** A thorough survey of field measurements on distortion in frequency-modulation reception has been made, particular stress being laid on multi-path distortion. The carrier frequency of the F. M. transmitter used in the experimental tests was 88 Mc. and the actual tests were conducted along a deep canyon near Los Angeles where path differences of about a mile can be easily obtained.

A detailed comparison with the theoretical deductions based on the two-signal theory has been effected. The results agree fairly well for small values of phase delay of the modulation frequency and estimated path differences of about a mile and half a mile.

## INTRODUCTION

The harmonic distortion in frequency modulation reception has been treated in a general way by several authors, notably by Corrington (1945) and Mayers (1946), without any real attempt being made to simplify the results to a convenient practical form for purposes of easy experimental verification. So, it is the purpose of this paper to simplify the results a great deal and present them in such a way that the distortion depends on a few and simple parameters. This will permit a direct experimental verification of the two-signal distortion theory.

## THEORY

The expression for the percentage  $n$ th. harmonic distortion according to the two-signal theory developed by the author<sup>†</sup> (1951) is :

$$D_n \% = \frac{200h^{n-1}}{(n-1)!} \frac{\partial^{n-1} u}{\partial \beta^{n-1}} (f_d/f_p)^{n-1} \sin^n \frac{\alpha}{2} \sqrt{1 + 4 \sin^2 \alpha / 2u^2}$$

With the carrier frequency,  $f_c$  at 88 Mc., and the maximum value of the modulating frequency  $f_p$  at 15 Kc., which is the limit of the audio range, it is easily seen that both  $\alpha$  and  $l = 2hf_d/f_p \sin \alpha/2$  are small for a path difference of about a mile which is customary in the experimental tests. As  $\alpha$  is small, the curves of Meyers (1946) and of Corrington (1945) are not of much use in the present discussion and a new method of approach as

\* This work forms part of the thesis submitted by the author to the California Institute of Technology, Pasadena, U. S. A., for the Degree of Electrical Engineer under the title "Distortion in Frequency modulation Reception".

† Cf. Table I in Part I.

outlined below seems necessary. Hence, using the above approximations the expression for the percentage distortion becomes :

$$D_n \% = 200f_p / (n-1)! (f_d)^{n-1} \pi^n t_0^n \partial^{n-1} u / \partial \beta^{n-1} \quad \dots (1)$$

where  $t_0$ , as before, is the time delay in seconds. So at a particular position chosen as the origin of co-ordinates and with the help of the following data, viz :

- 1- Distortion as a function of the polar angle of the receiving antenna ;
2. Radiation pattern of the receiving antenna ;
3. Distortion as a function of the deviation frequency  $f_d$  and the modulating frequency  $f_p$  for a particular orientation of the antenna.

it should be possible to determine the parameters  $\alpha$ ,  $\beta$ ,  $r$  and the direction of arrival of the desired and the undesired signals. From these data it is possible to predict from theory the distortion at neighbouring

$$U = \frac{r^2 + r \cos \beta}{1 + 2r \cos \beta + r^2}$$

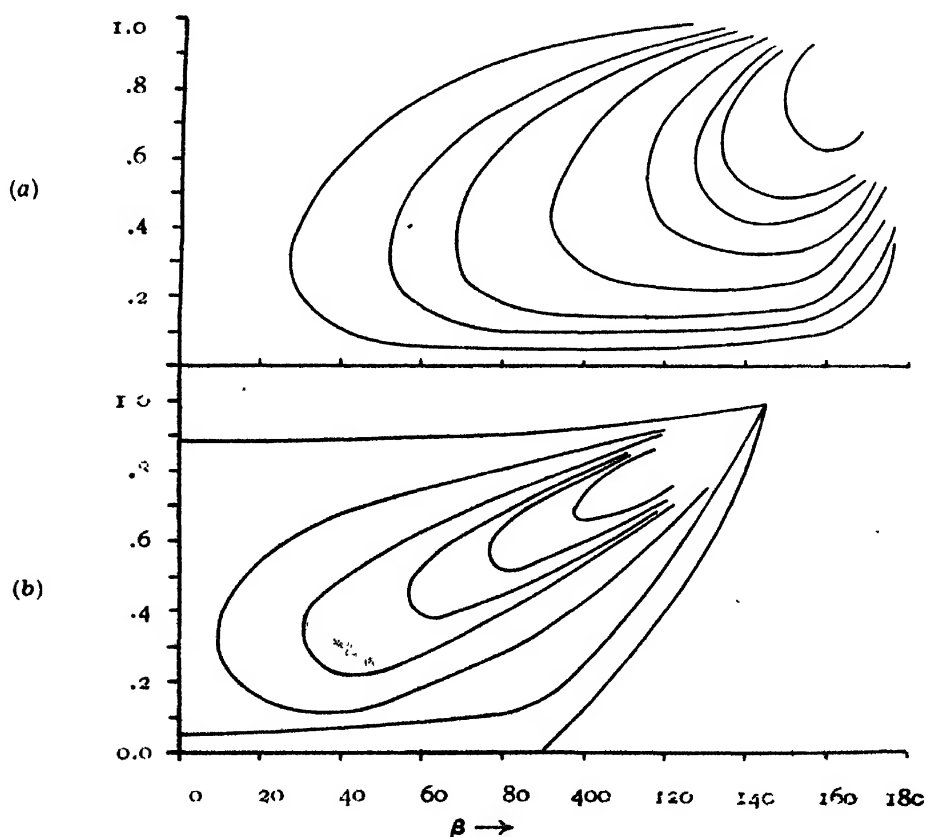


FIG. 1

Curves of  $r$  Vs.  $\beta$

- (a) With  $\partial u / \partial \beta$  as parameter Curves from top 1—0.05, 2—0.1, 3—0.15, 4—0.25  
5—0.5, 6—0.75, 7—1.0, 8—2.5
- (b) „  $\partial^2 u / \partial \beta^2$  „ „ Curves from top 1—0.1, 2—0.25, 3—0.5, 4—0.75  
5—1.0, 6—2.5, 7—0.1, 8—0.



positions separated in distance by a few wave lengths. This theoretical prediction could, in turn, be verified by experimental tests. This procedure thus will provide a direct verification of the two-signal distortion theory. The determination of the parameters  $\alpha$ ,  $\beta$  and  $r$ , however, requires the use of the graphs of  $r$  vs.  $\beta$  with  $\partial u / \partial \beta$  and  $\partial^2 u / \partial \beta^2$  as parameters. Figures 1 (a) and (b) drawn after laborious work show these two graphs, respectively. The other details of the calculations are given in the Appendix.

#### EXPERIMENTAL ASPECTS

An exhaustive treatment of the experimental aspects requires some consideration of the receiver and its associated paraphernalia. The requirements of a good receiver used in the investigation of multipath distortion are many and they will be enumerated briefly in the following :

A sensitivity of at least 10 to 20 microvolts is required of the receiver\* and for that signal strength all amplitude variations in the signal even at the ends of the swing should be absent. The selectivity of the receiver should be about 6 db. down at  $\pm 75$  Kc., and about 20 db., down at  $\pm 100$  Kc., from the centre frequency to avoid adjacent channel interference. Each coupling stage in the receiver should be separately shielded to avoid regeneration due to feedback and the consequent non-linear distortion. To avoid inherent amplitude distortion, all interstage couplings including the one between the last *i. f.* stage, the limiter and the input network of the discriminator should have transfer characteristics that are linear with respect to phase shifts. The time constants in the limiter circuits should not exceed  $3\mu$  seconds as currents due to signal frequencies up to 15 Kc., are to be transmitted. It was found advisable to use two stages of amplitude limitation and with an 1852 tube, the point where the limiter action ceases was brought down to as low as  $8\mu v$ . The discriminator circuit had a linear response upto a band width of 400 Kc. so that all the side currents could be included well within the linear portion and this was achieved by shunting the two plates of the diode in the discriminator circuit by a  $10,000\Omega$  resistance. The *i. f.*, stages should also have a band width of 0.5 Mc. to allow for the many side current pairs.

A half wave dipole with reflectors permitting a fair amount of directivity was used as the receiving antenna. The antenna was capable of rotation about a vertical axis and parallel feeders with the load impedance equal to the surge impedance were used to avoid unnecessary reflection at the input to the receiver.

#### EXPERIMENTAL RESULTS

The experimental results could be conveniently classified into (1) line of sight measurements and (2) non-line of sight measurements bearing in mind, of course, that only the non-line of sight measurements give rise to

\* The receiver used by the author had a sensitivity of  $15 \mu V/m$ .

harmonic distortion which has been discussed in great detail in Part I. The carrier frequency of the F. M. transmitter used in the tests was 88 Mc. and the non-line of sight measurements were carried out in a deep canyon near Los Angeles where a path difference of about a mile could easily be obtained.

1. *Line of sight measurements*<sup>1</sup>: Under line of sight measurements could be grouped the following :

- (i) Car ignition tests.
- (ii) Field strength as a function of the height of the receiving aerial.
- (iii) Distortion with the possibility of reception of the direct signal as well as reflected signals.

The ignition system of cars is an important source of external noise at high frequencies and the results are shown in Table I below.

TABLE I  
Car ignition tests

Field strength using a half-wave dipole 15 ft. above ground ( $\mu V/m$ ).	Noise extinction distance of a motor car from the receiver in feet (horizontal polarization F. M.)
50	600
75	500
100	420
150	300
200	250
250	200
300	150

The first column in the above table shows the field strength of the desired signal and the other column shows the distance at which a motor car should be for substantially complete elimination of interference under conditions of low ambient acoustic noise.

The height of the receiving aerial is important and the tests showed that the field strength is approximately proportional to its height.

Lastly, the distortion measurements at some locations of the receiver wherein the reception of the direct signal as well as the reflected signals could be possible due to a range of hills only on one side did not indicate any significant results and very little distortion resulted.

2. *Non-line of sight measurements*: The measurements under this type could be grouped under :

- \*(i) Distortion as a function of the modulating frequency with the deviation frequency as parameter.
- \*(ii) Distortion as a function of the deviation frequency with the modulating frequency as parameter.

\* Both these sets of measurements were made at a fixed position of the receiver and at a fixed orientation of the directional antenna, viz., near the broadside position.

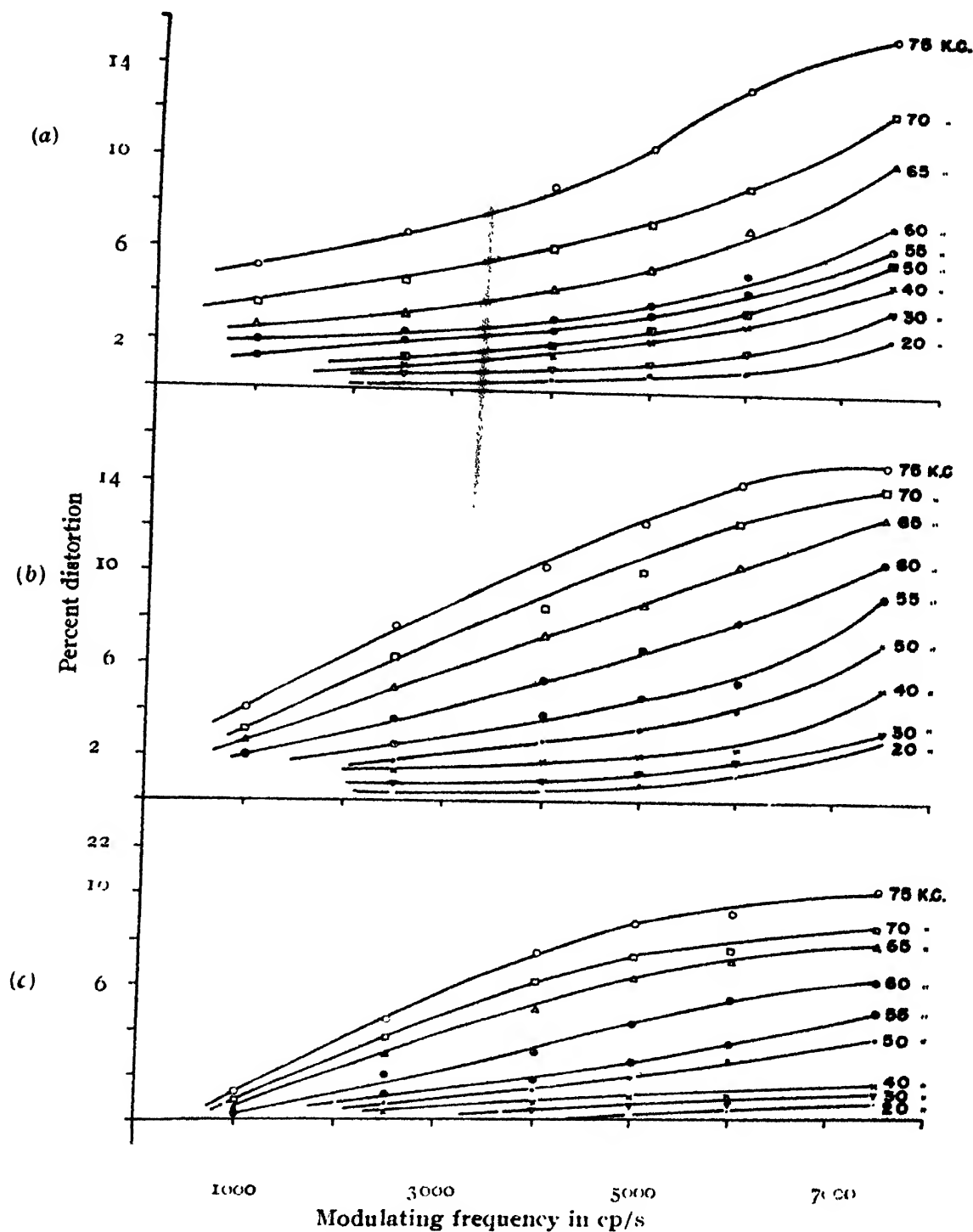


FIG. 2

(a). 2nd. harmonic      (b). 3rd. harmonic      (c). 4th. harmonic

Graphs of distortion Vs. modulating frequency with the deviation frequency as parameter.

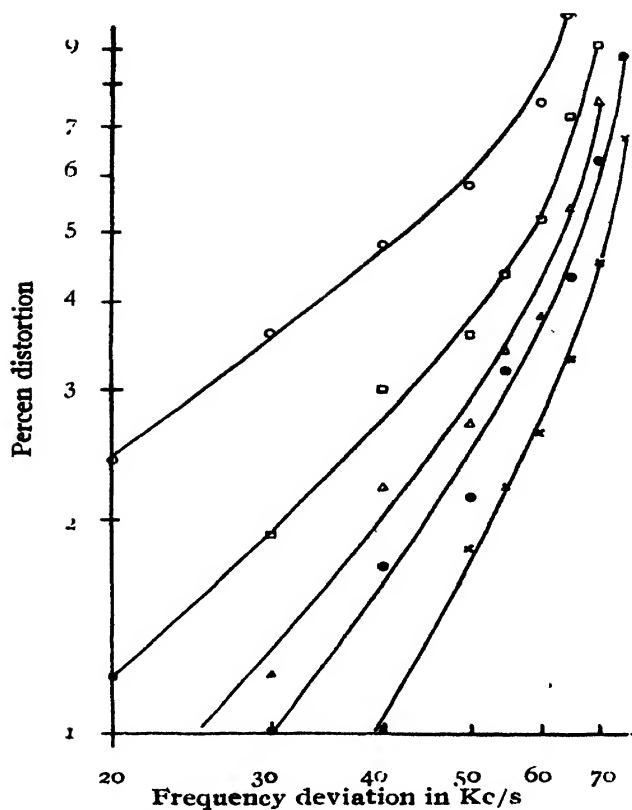


FIG. 3(a) : 2nd harmonic

Graphs of distortion Vs. deviation frequency with the modulating frequency as parameter

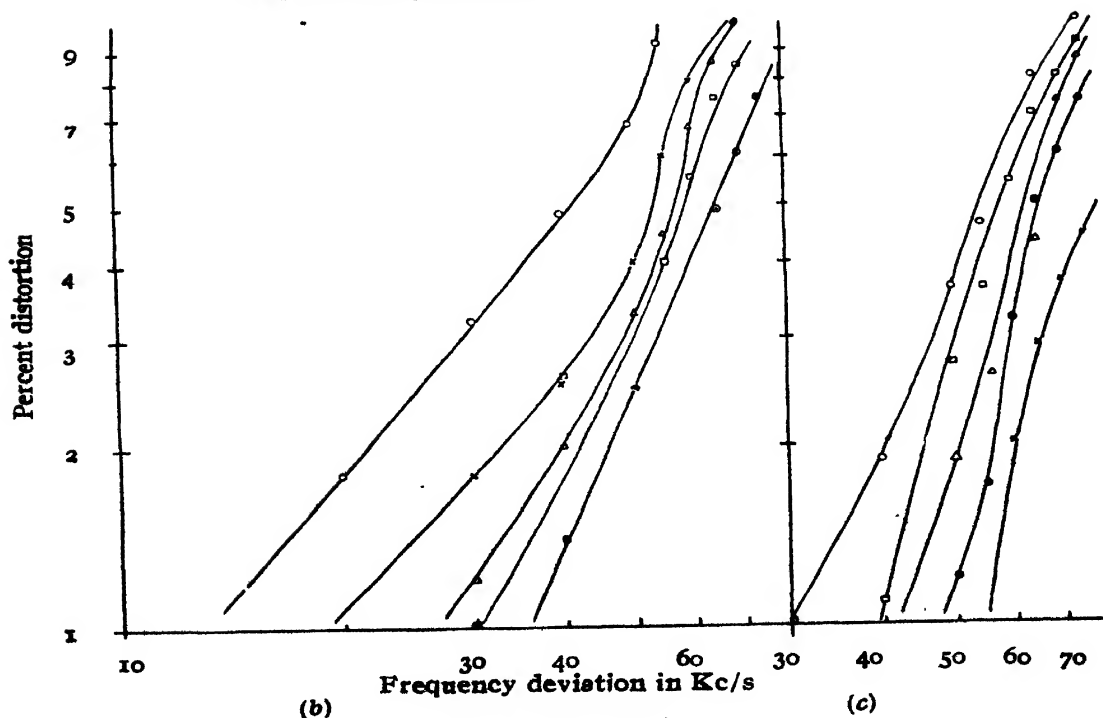


FIG. 3 (b and c)

Graphs of distortion Vs. deviation frequency with the modulating frequency as parameter  
(b), 3rd. harmonic, (c). 4th. harmonic

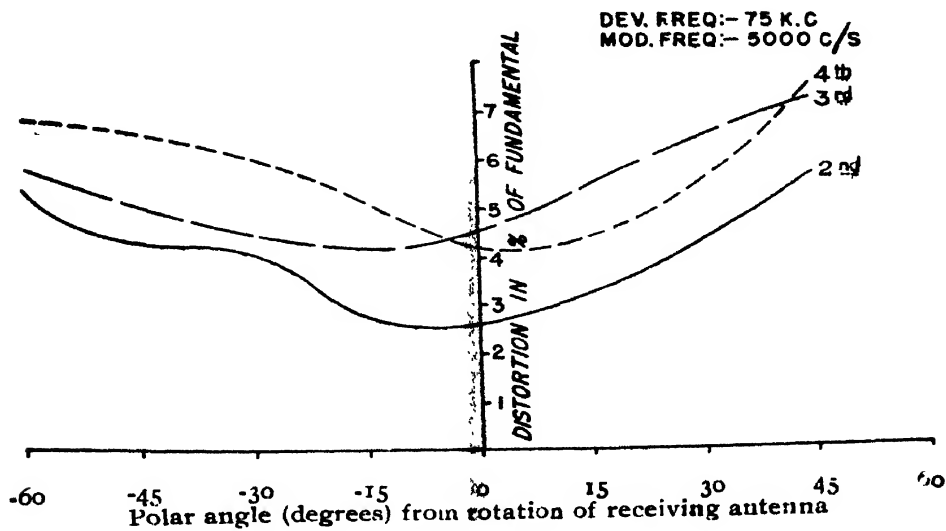


FIG. 4

Graph of percent distortion Vs. polar angle of receiving antenna at 75 Kc/s deviation frequency and 5000 c/s modulating frequency.

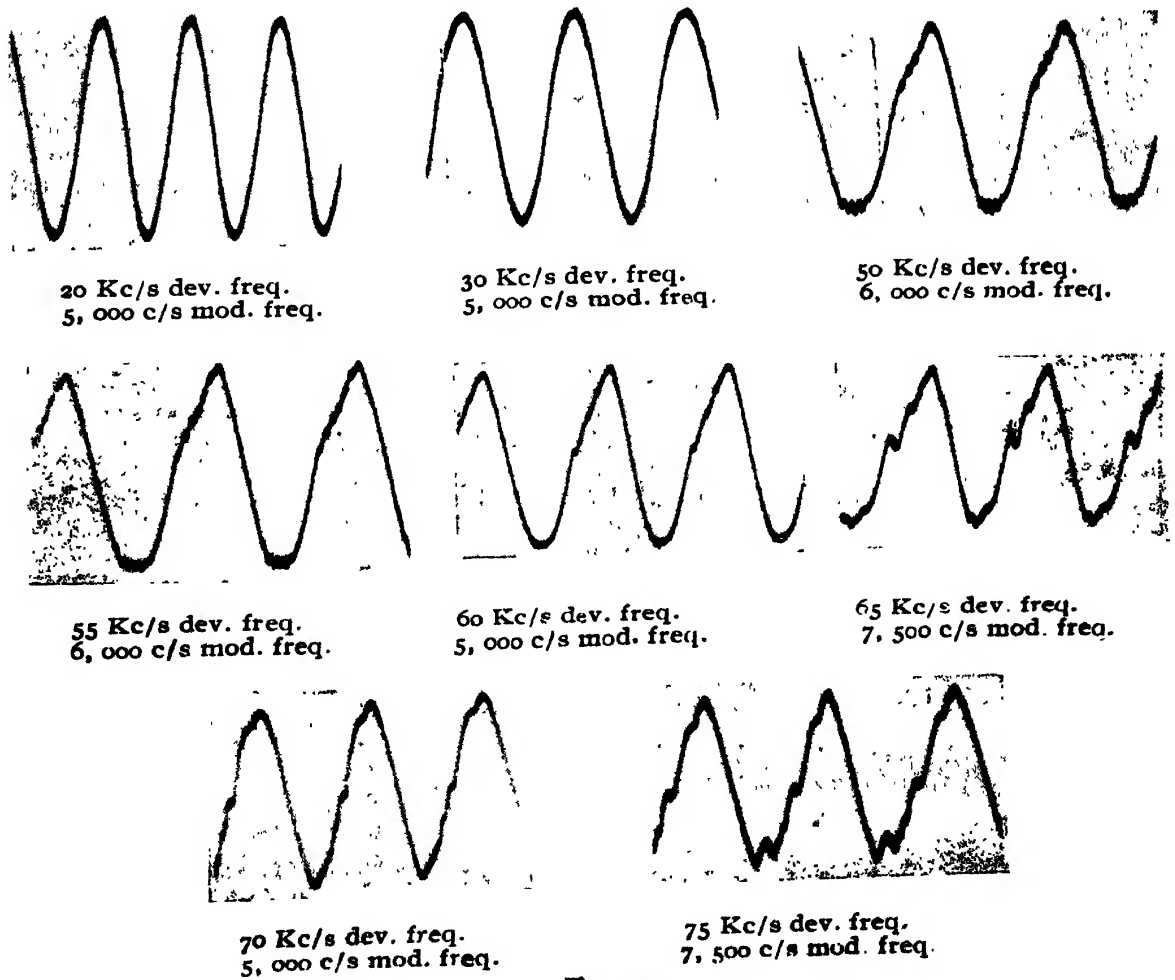


FIG. 5

Photographs of F-M distortion patterns in a few typical cases

- (iii) Distortion as a function of the orientation of the receiving antenna for a fixed modulating frequency and a fixed deviation frequency.
- (iv) Distortion at different locations of the receiving antenna within a radius of 20 metres, for a fixed orientation of the antenna.
- (v) Seasonal effects.
- (vi) Preliminary tests on the effect of tropospheric refraction.

The results of the first three measurements are included in figures 2-4. Figure 5 shows some actual photographs of the distortion patterns.

The distortion measurements at different locations of the receiving antenna within a radius of 20 metres were made with the sole purpose of verifying the two signal theory directly. The results of calculation and experiment are given in Table II below for a modulating frequency of 5000 c/s. and a deviation frequency of 75 Kc. The details of the calculation are given in the Appendix

TABLE II

Results of the second and third harmonics at the displaced positions.

Position of the antenna	CALCULATED VALUES		EXPERIMENTAL VALUES	
	% second harmonic distortion	% third harmonic distortion	% second harmonic distortion	% third harmonic distortion
Displaced position I	12.1	12.0	10.6	9.6
Displaced position II	11.8	11.9	10.4	11.4
Displaced position III	12.0	12.1	9.8	10.4

The seasonal effects on distortion are of interest and the results seem to indicate better reception in cloudy and drizzling weather than in hot and dry weather.

The tests on the effect of tropospheric refraction resulting in transmission beyond the curvature of the earth (horizon) would be of interest in investigating whether the case of diffraction was due to a single path transmission or multipath transmission. The results, however, were not significant as the signal at the receiver fell below the limiter level even though the receiver had a sensitivity of  $15\mu V/m$ .

#### DISCUSSION OF RESULTS

Equation (1), which is a simplified expression for the percentage  $n$ th harmonic distortion, shows that the distortion is a function of the following parameters, viz.,  $f_p$ , the modulating frequency,  $f_d$ , the deviation frequency,  $t$ , the time delay and lastly,  $\partial^{n-1}u/\partial\beta^{n-1}$ , which is a function of  $r$ , the ratio

of the two interfering signals and  $\beta$ , the carrier phase shift. For a fixed carrier frequency and for a particular orientation of the receiving antenna both  $\partial u / \partial \beta$  and  $t_0$  are constants so that the distortion can be conveniently studied as functions of  $f_d$ ,  $f_p$  and  $n$ , the order of the harmonics. Figures 2 and 3 show these cases. According to equation (1) for a particular harmonic  $n$  the distortion should bear a linear relationship to the modulating frequency with the deviation frequency  $f_d$  as the running parameter. Likewise, a plot of the distortion *vs.* the deviation frequency on logarithmic paper should also be a set of straight lines for a particular harmonic with the modulating frequency as the running parameter. And besides, in this case the straight lines should have increasing integral slopes with increasing order of the harmonic. These facts are borne out to a fair degree of approximation in the graphs of figures 2 and 4. A close examination of these graphs, however, reveals the following results.

Up to a deviation frequency of 50 Kc., the graphs of distortion *vs.* modulating frequency in figure 2 show a marked linear characteristic and this is particularly evident for the fourth harmonic in figure 2(c). The curves depart from the straight line behaviour at the higher modulating frequency and this is quite reasonable to expect. The graphs from 60 Kc., to 75 Kc. deviation frequency, however, do not reveal a marked linear behaviour and this fact may be interpreted to mean that distortion at these higher frequencies is not correctly given by the two-signal theory. The curves at 75 Kc., 70 Kc., and 65 Kc., in these figures, however, have the same general behaviour and this fact may be significant. The graphs of distortion *vs.* deviation frequency in figure 3 are in good agreement with the two-signal theory at modulating frequencies of 2500 c/s. and 400 c/s., and depart from the straight line behaviour at modulating frequencies of 5000 c/s., 6000 c/s., and 7500 c/s. The slopes of these curves confining only to the linear portion are nearly the same, whereas, the two signal theory demands increasing integral slopes and this fact may well be attributed to the inadequacy of the two-signal theory.

From the theoretical point of view, measurements on distortion as a function of the polar angle of the directive antenna of the receiver means that both the ratio  $r$  of the amplitudes of the desired and the undesired signal and  $t_0$ , the time delay are changed. As  $\partial^{n-1} u / \partial \beta^{n-1}$  is a fairly complicated expression, the graphs in this case cannot be expected to show any simple behaviour and this is evident in figure 4, which refers to the case of a deviation frequency of 75 Kc., and a modulating frequency of 5000 c/s. The curves show minimum distortion near the broadside position of the antenna and this fact may be significant. The lack of close agreement between the calculated and experimental values in Table II, for antenna positions separated by a few wavelengths means that the two-signal theory can predict only the order but not the actual magnitudes of the distortion at neighbouring points.

## CONCLUSIONS

The experimental investigations on multipath distortion in frequency modulation reception show fair agreement with the theoretical deductions based on the two-signal theory, viz., (1) higher distortion at higher modulating and deviation frequencies (2) fairly linear variation of distortion with modulating frequency at a particular deviation frequency for a particular harmonic and (3) more or less linear variation for a plot of logarithm of distortion *vs.* logarithm of deviation frequency at a particular modulating frequency for a particular harmonic. There is very little distortion upto a deviation frequency of 40 Kc. even at modulating frequencies of 7500 c/s. The more or less constant slopes of the curves of distortion *vs.*, deviation frequency on logarithmic paper, as contrasted with theoretically increasing integral slopes with increasing order of the harmonic, may well be attributed to the inadequacies of the two-signal theory. At least, the correct order of magnitude of distortion at neighbouring points is predicted by the two-signal theory.

The line of sight measurements indicate that (1) the reception is affected to a certain extent by car ignition systems, (2) the higher the receiving antenna the better is the reception and (3) very little distortion results when the ratio of amplitudes of the indirect signal to the direct signal is very small.

Lastly, there is better reception in cloudy and drizzling weather than in hot and dry weather, a significant point compared to amplitude modulation reception,

## APPENDIX

Method of predicting distortion at neighbouring points, separated from the original position of the receiving antenna by a few wave lengths :

Referring to figure 6, knowing the distortion at the point  $O$  as a result of the two signals reaching from  $P_1$  and  $P_2$  it should be possible to calculate the distortion at a neighbouring point  $O'$  separated by a distance  $s$  of the order of a few metres.

The path difference  $d'$  at the point  $O'$  in terms of the parameters at  $O$  can be easily calculated by methods familiar in interference-optics and is given by :

$$d' = d + 2s \cos(\psi_4 + \epsilon/2) \sin \alpha/2$$

where

$$\psi_1 + \psi_2 = \alpha, \quad \psi_2 - \psi_1 = \epsilon$$

and  $d$  is the path difference at the point  $O$ .  $s$  is small so that  $r$ , the ratio of the amplitudes of the two interfering signals can be assumed the same in moving from  $O$  to  $O'$ . But this condition also makes the difference between  $d$  and  $d'$  small so that both  $s$  and  $\psi_4$  has to be measured accurately, perhaps to a fraction of a metre.

The expressions for the percentage second and third harmonic distortions are (cf. eqn.1),

$$D_2\% = 200 f_p f_d \pi^2 t_o^2 \partial u / \partial \beta$$

and

$$D_3\% = 100 f_p f_d^2 \pi^3 t_o^3 \partial^2 u / \partial \beta^2$$



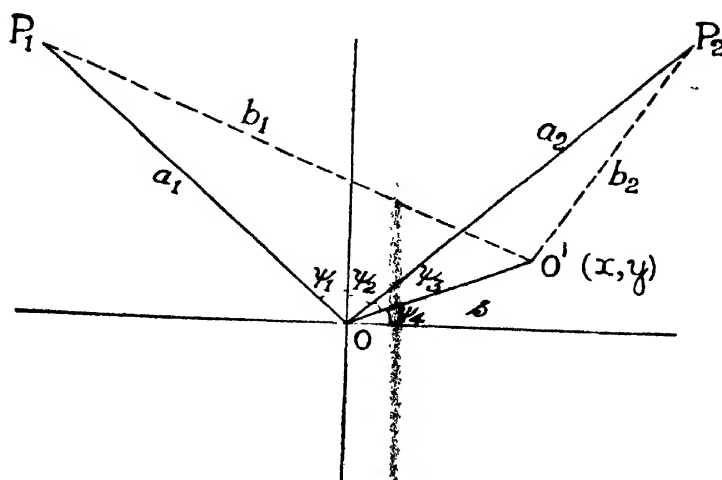


FIG. 6

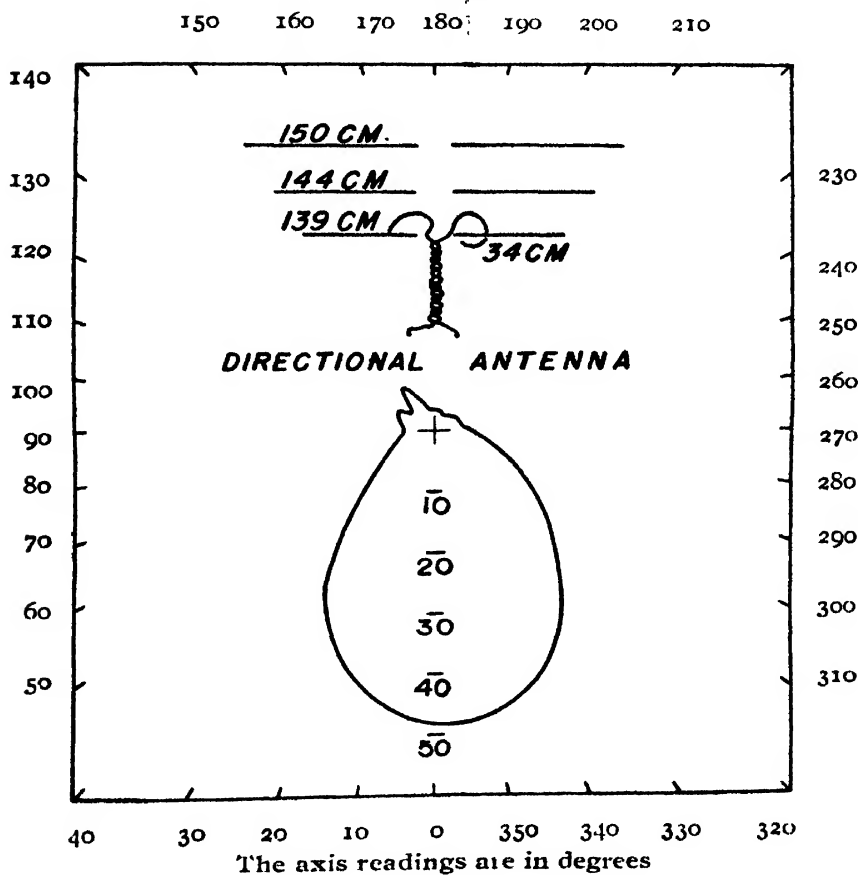


FIG. 7

Unidirectional antenna pattern of the receiving antenna without any appreciable back lobe.

Assume a set of experimental data for  $D_2\%$  and  $D_3\%$  at the point  $O$ , for a particular deviation frequency and different modulating frequencies. Then from the average values of  $D_2\%/f_p$  and  $D_3\%/f_p$ , both  $t_0^2 \partial u / \partial \beta$  and  $t_0^3 \partial^2 u / \partial \beta^2$

could be computed. From practical considerations the path difference can be estimated to be in the neighbourhood of a mile. So, by trying different values of  $d$  in the neighbourhood of a mile with a view to matching up the two theoretical plots of  $r$  vs.  $\beta$  in figures 1(a) and (b),  $r$ , the ratio of the two signals could be determined uniquely. Two values for  $r$  are usually obtained and the one near unity is chosen, as the distortion is greatest when  $r$  is near unity. In a particular case the following values were obtained :

$$t_0 = 4.65 \times 10^{-6} \text{ sec} ; d = 4.65 \times 3 \times 10^2 \text{ metres} ; \partial u / \partial \beta = 0.75 ;$$

$$\partial^2 u / \partial \beta^2 = 1.31 ; r = 0.86 ; s = 22 \text{ metres and } \psi_1 = 50^\circ.$$

From the radiation pattern of the receiving antenna (figure 7) the value of  $r = 0.86$  corresponds to  $\psi_1 = 10^\circ$  and  $\psi_2 = 23^\circ$  so that  $d' = 1401.9$  metres or  $t_0' = 4.673 \times 10^{-6}$  sec.

Hence the % second and third harmonic distortions at the displaced positions are\*

$$D\% = 12.1 \text{ and } D_s\% = 12.0$$

NATIONAL PHYSICAL LABORATORY OF INDIA,  
NEW DELHI.

\* c. f., Table II

#### REFERENCES

- Corrington, M. S., 1945, *Proc. Inst. Rad. Engrs.*, **33**, 878.  
Krishna Prasad, K. V., 1951, *Ind. J. Phys.* **25**, 504.  
Meyers, S. T., 1946, *Proc. Inst. Rad. Eng.*, **34**, 256.

# ELECTRON MICROSCOPIC DETERMINATION OF SIZE AND SHAPE OF A NEW PLANT VIRUS (SANN HEMP MOSAIC)

BY M. L. DE

(Received for publication, September, 27, 1951)

Plates A, B, XVIII

**ABSTRACT.** The size and shape of a new plant virus, *viz.*, sann hemp mosaic, has been determined with the electron microscope. The sample was obtained from a crystalline preparation of the material and was shadowed with gold for electron microscopy. The virus has been found to consist of spherical particles with a mean diameter of  $37.4 \pm 6. m\mu$ .

## INTRODUCTION

The electron microscope has found one of its most important applications in the study of viruses. These bodies, responsible for many diseases of men, animals, plants and bacteria, range in size from about 300  $m\mu$  to 10  $m\mu$ . Since the limit of resolution of microscopes using visible radiation is about 175-220  $m\mu$  and that of the ultra-violet microscope about 100  $m\mu$ , only a few of the larger viruses could be directly photographed with these microscopes. Size determination for the smaller viruses was, therefore, based on such indirect measurements as filterability, sedimentation and diffusion rate, viscosity, X-ray study, etc. Most of these estimates were based on assumptions, the validity of which was far from certain.

Thus, the method based on filterability depended on the assumption that the filter membranes had uniform pore size and that the particles were all spherical. The method, therefore, could give only approximate sizes.

The sedimentation and diffusion rate measurements provide accurate results only if the preparations are homogeneous as regards particle size and weight and moreover, if certain assumptions are made, *viz.*, that Stoke's law holds for the sedimentation of the virus particles, that these particles are smooth, unhydrated spheres, and that the solution is structureless and has no anomalous physical properties. To what extent these assumptions are valid, is very uncertain and is itself a matter for further experimental investigation.

Size determination from viscosity measurements has been made by several investigators who have, however, given divergent values for the same specimen. With regard to these measurements we can do no better than quote Bawden (1949) who observes, "there is no reason to believe that any

of these measurements were made on homogeneous preparations; all preparations contained aggregated particles and the kindest interpretation that can be put on different estimates is to assume that preparations of different states of aggregation were being studied".

X-ray analysis, while it provides accurate size estimation, is unfortunately applicable only to those viruses that form crystals, or liquid crystals, for it depends on the refraction of X-rays by regularly arranged layers of particles.

Other methods of indirect determination of size, *viz.*, stream double refraction, fluorescence microscopy, radio sensitivity, etc., give such widely varying values for any particular virus that one is at a loss to decide about the correct size. Thus, in the case of tobacco mosaic virus, the most studied of all the viruses, the length measurements based on different methods range from 1400  $m\mu$  (from bi-refringence) to 270  $m\mu$  (light scattering) (Bawden, 1950).

The electron microscope, with its present limit of resolution of the order of 1  $m\mu$ , provides a direct method of studying the shape and size of most of the viruses. Covering the entire range of sizes occupied by these bodies, the instrument has already proved, and will doubtless continue to prove, of the greatest value in such investigations.

The present paper gives an account of the electron microscopic determination of the size and shape of a new plant virus causing the mosaic disease of sann hemp plant. The virus was isolated and crystallised following the method due to Markham and Smith (1946) at the Indian Agricultural Research Institute, at Delhi (Raychaudhury, 1947). The present work was carried out with the help of the electron microscope installed at the Institute of Nuclear Physics, a detailed description of which has already been published (Dasgupta, and others 1948).

#### EXPERIMENTAL METHOD

For electron microscopy, the crystalline preparation of the sample was diluted in distilled water and a drop of the liquid was deposited on a thin collodion film supported by a 200-mesh wire screen. After allowing sufficient time for the suspended particles to settle down and adhere on to the collodion film, the excess water was drained off.

The sample thus prepared, when examined under the electron microscope gave very poor image contrast in the electron micrographs due to the low electron scattering power of the virus particles. To enhance the contrast of the micrographs, recourse was taken to metallic shadow-casting of the preparation (Wyckoff, 1949).

As usual, the specimen on collodion film was shadowed with an oblique beam of gold atoms in high vacuum. The angle of deposition of metal vapour was varied from  $\tan^{-1} 1/10$  to  $\tan^{-1} 1/12$ . Such shadowed specimens were then micrographed. Three of the electron micrographs are reproduced



Fig. 1.

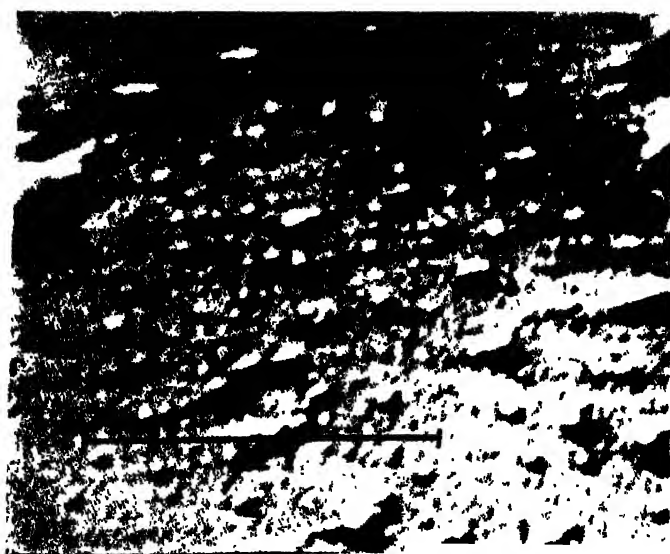


Fig. 2.

Electron micrographs of gold-shadowed sann hemp mosaic virus.

Fig. 1. { Shadowing angle :  $\tan^{-1} \frac{1}{12}$   
 Thickness of gold : 6.3 A.U.  
 Magnification : 38,300 X

Fig. 2. { Shadowing angle :  $\tan^{-1} \frac{1}{10}$   
 Thickness of gold : 12.3 A.U.  
 Magnification : 45,000 X



Fig. 3

Electron micrograph of gold-shadowed sann hemp mosaic virus.

Shadowing angle :  $\tan^{-1} \frac{1}{10}$  ;

Thickness of gold : 6.3 A.U.

Magnification : 40,800 X

in figures 1 and 2 of Plate XVIII A and figure 3 of Plate XVIII B. They show a greatly increased contrast due to enhanced scattering of electrons from the layer of metallic vapour deposited on the virus particles and the corresponding absence of the metal from the shadow regions. In addition to increasing contrast and thereby increasing the accuracy with which measurements can be made, shadowing further creates the impression that one is seeing the specimen in three dimension which greatly helps one to make an estimate of the shape of the particles.

#### *Calibration of magnification.*

In order to assess the size correctly from the micrographs, it was decided to calibrate the magnification of the instrument with the help of a collodion replica of a grating of known constant. This was done by keeping the projector current at the settings at which the virus micrographs had been taken and a grating replica was micrographed by mounting the replica sample at different distances from the objective pole piece. The corresponding objective lens focusing currents were recorded for the different mounting positions. From measurement of the line separations in the grating micrographs and knowing the grating constant, the total magnification at different objective currents were calculated and these magnifications were plotted against objective currents. From this curve of magnification *vs.*, objective current, the magnification of the virus micrographs at any specified objective current could be found out.

#### RESULTS

An inspection of the micrographs reveals that the predominating unit is essentially spherical in shape. The diameter of these units were carefully

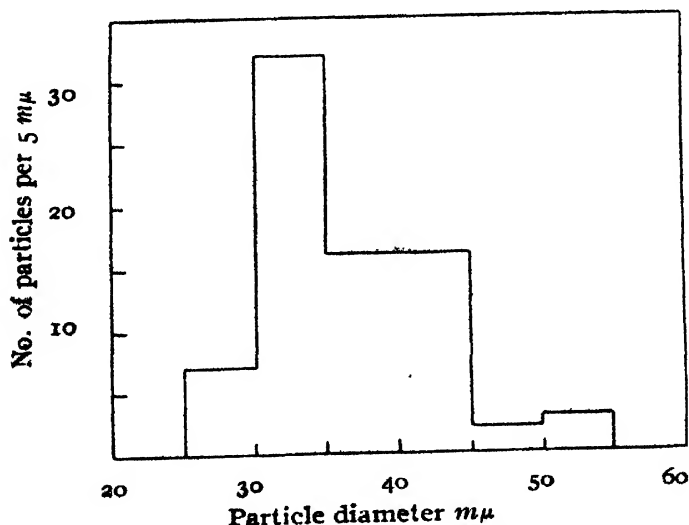


FIG. 4

Histogram illustrating the distribution of particle size in the micrographs of figures 1, 2 and 3.

measured and their actual sizes then deduced from the previously determined magnification factors. The spread of the measured particle diameters is illustrated by the histogram shown in figure 4. The mean diameter obtained is  $37.4\text{ m}\mu$  with a standard deviation of  $\pm 6.1\text{ m}\mu$ .

The micrographs show the presence of a few bodies larger than the average size particles. These are, presumably, clusters of the elementary particles, which, however, due to insufficient resolution, could not be seen as distinctly separate bodies.

For the purpose of comparison with the other plant viruses studied with the electron microscope, the following table has been prepared showing the size and shape of all the plant viruses including the one studied in the present investigation :

TABLE I

Name of virus.	Shape	Size
1. Tobacco mosaic	Rod like	280 $\text{m}\mu$ long 15 $\text{m}\mu$ wide
2. Potato virus X	Rod like	500-600 $\text{m}\mu$ long 16 $\text{m}\mu$ wide
3. Southern bean mosaic	Spherical •	26 $\text{m}\mu$ diam.
4. Tomato bushy stunt	Spherical	26 $\text{m}\mu$ diam.
5. Cucumber mosaic	Rod like	13 $\text{m}\mu$ wide.
6. Squash mosaic	Spherical	30 $\text{m}\mu$ diam.
7. Potato yellow dwarf	Rod like	270 $\text{m}\mu$ long 50 $\text{m}\mu$ wide
8. Tobacco necrosis	Spherical	20 $\text{m}\mu$ diam.
9. Turnip yellow mosaic	Spherical	22 $\text{m}\mu$ diam.
10. Sann hemp mosaic	Spherical	37 $\text{m}\mu$ diam.

## ACKNOWLEDGMENTS

The author is obliged to Prof. M. N. Saha, F.R.S., Palit Professor of Physics, Calcutta University for his kind interest in the present work. The author acknowledges with grateful thanks his indebtedness to Dr. N. N. Dasgupta, Reader in Biophysics, Calcutta University for his invaluable help and guidance. The author is also thankful to his colleagues Sri A. K. Chaudhury, and Sri D. L. Bhattacharjee, for their assistance and to the Ministry of Education, Government of India, for financial aid.



REFERENCES

- Bawden, F. C. 1950, *Plant Viruses and Virus Diseases*, 3rd Ed., p. 234. Chronica Botanica Co, U. S. A.
- Markham, R., and Smith, K. M., 1946. *Nature*. **157**, 3co.
- Raychandhury, S. P., 1947. *Current Science*, **16**, 26.
- Dasgupta, N. N., and others, 1948. *Ind. Jour. Phys.*, **22**, 497.
- Wyckoff, R. W. G., 1949. *Electron Microscopy Technique and Application*, p. 79 Interscience Publishers, N. Y.

# INFLUENCE OF JOSHI EFFECT ON THE EMISSION SPECTRUM OF CHLORINE

By P. G. DEO

(Received for publication, April 27, 1951)

Plates XIX A & B

**ABSTRACT.** When irradiated by 4750-4000 Å the relative Joshi effect,  $\% \Delta i$ , ( $100 \Delta i / i_{\text{dark}}$ ) in 100 mm chlorine was a maximum viz 86, at the threshold potential 6.9 KV: the corresponding glow intensity was extremely low. Increase of potential increased the intensity but diminished  $\% \Delta i$ . With 120 hours exposure, the spectrum was recorded (i) with the tube excited at 11.3 KV; (ii) with the tube excited and also irradiated by 4750-4000 Å, the  $\% \Delta i$  being 70 and (iii) with the tube unexcited but irradiated. The intensity distribution in the spectrum was recorded with a microphotometer in each of twelve sets of results for (i), (ii) and (iii). The spectral intensity was found to diminish by irradiation outside its wavelength limits. This is attributed to a decrease in the population of excited particles in the ionized and pre-ionized states.

Arising out of earlier work, (Joshi, 1943; Joshi and Deo, 1942) was the question, now examined for the first time in this line of work, whether the observed suppression on irradiation of the discharge current  $i$ , constituting Joshi effect, is associated with a change in the corresponding spectrum.

The experimental arrangement was similar to that used previously (Joshi, 1943): It consisted essentially of a Siemen's type ozonizer enclosed in an opaque box and fitted with a shutter; and was excited by a 50 cycle transformer discharge. It was found that the intensity of the glow under discharge was too low for a spectrographic record even with an exposure of about 300 hours near the threshold potential  $V_m$ , where the relative Joshi-effect  $\% \Delta i$  is maximum (Deo, 1948). A large increase in the applied potential is not an advantage, since while it increases the glow intensity, the corresponding  $\% \Delta i$  is reduced greatly. This is shown by one typical series of data in Table I. From the results of series of trial experiments a potential of 11.3 KV of 50 cycle frequency was found to be optimum. With minimum loss of the glow intensity, it produced about 70 % of Joshi-effect, when the tube was exposed to light from a 180 volt, 200 watt incandescent bulb and with a bulb filter (4750-4000 Å) between it and the ozonizer. Hilger's constant deviation medium spectrograph was used. The linear dispersion of the instrument was 15 Å/mm at 410 mμ and 60 Å/mm at 590 mμ. The 'end on' position of the discharge tube was adopted which provides about 50 cm depth of the glowing column under discharge. The spectrum was photographed on the same plate with identical conditions.

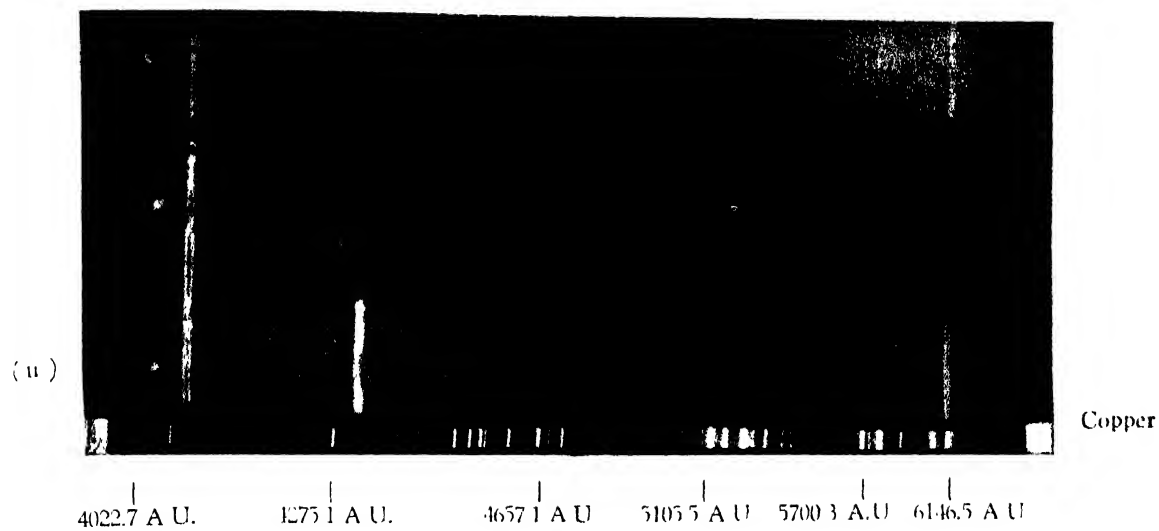


Fig 1.

Comparative emission spectra of chlorine under Joshi effect.

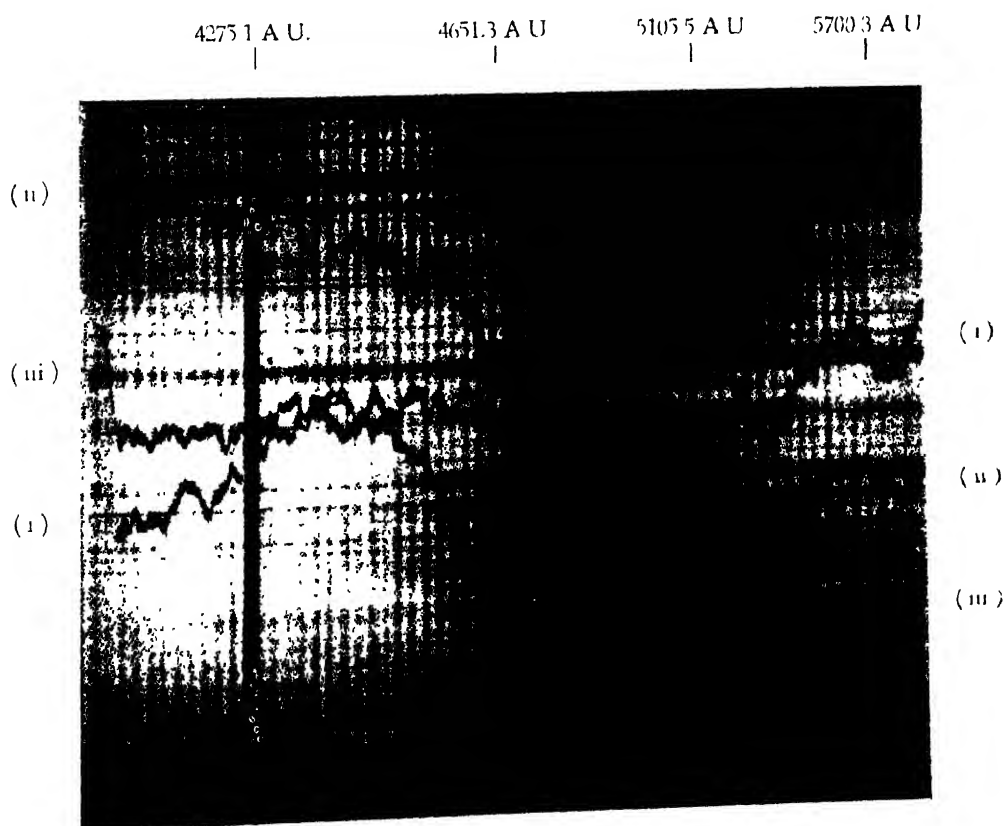


Fig 2

Microphotometer records



Copy  
arc

4022.7 Å.U.      4275.1 Å.U.      4651.3 Å.U.      5105.3 Å.U.      5700.3 Å.U.      6146.5 Å.U.

Fig. 3.

Comparative emission spectra of chlorine under Joshi effect.

4275.1 Å.U.      4651.3 Å.U.      5105.5 Å.U.      5700.3 Å.U.

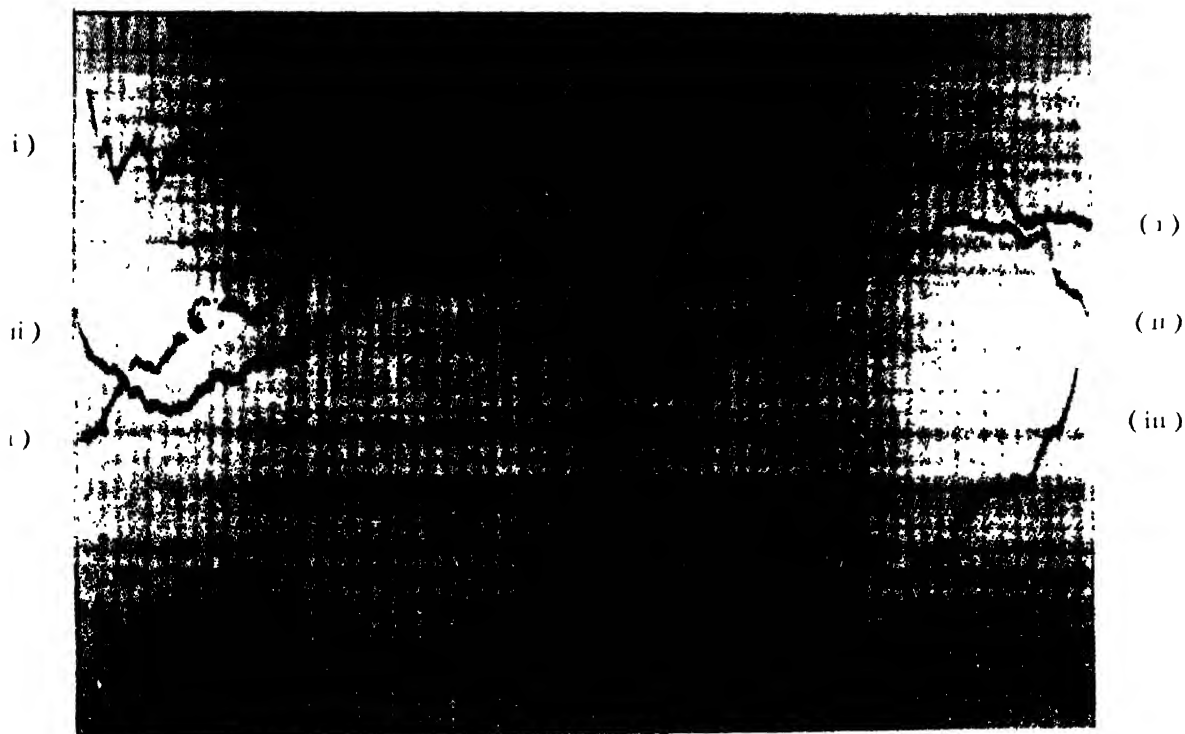


Fig. 4.

Microphotometer record.

## Influence of Joshi-effect on Emission Spectrum of Chlorine 531

of exposure as follows: (i) the tube was excited at 11.3 KV, but screened from external light; (ii) the tube excited as in (i) was exposed transversely to the above filtered light and (iii) the unexcited tube was exposed only to radiation as in (ii). The distribution of intensity in the spectrum corresponding to (i), (ii) and (iii) were recorded with a Mohlar microphotometer. With the available glow intensity and slit width of 1 mm, an exposure of 120 hours was found necessary to obtain a reasonable impression of

TABLE I

Exc. kV	Dark	Light	Net Joshi effect	Relative Joshi effect %
6.94	15	2	13	86.0
7.21	24	4	20	83.0
7.48	34	6	28	82.3
7.74	40	9	32	80.0
8.01	48	10	38	79.1
8.28	53	12	41	77.3
8.54	60	14	46	76.6

the chlorine spectrum on fast Kodak superpanchromatic TRI-X cut films. Very considerable difficulties were experienced in the maintenance of identical operative conditions during each set of observations of (i), (ii) and (iii) requiring 360 hours and necessitated the exclusion of non-winter months. Two sets of spectra and the microphotometric curves shown in Plates XIX A and B are typical of a series of 12 sets of observations made during about two years.

It is seen from curves (i) and (ii) corresponding to the discharge tube being in dark and exposed to light respectively, that within the region of irradiation represented by (iii) the intensity distribution in (ii) is greater than that in (i) as is to be expected. It is remarkable, however, that the intensity curve (ii) for the irradiated discharge tube lies sensibly below the curve (i) characteristic of the system in dark, *but outside the spectral limits of irradiation*. This latter feature brings out the Joshi effect spectrographically.

The constituents of a gas under electrical discharge are excited to different quantum states and are in a dynamic equilibrium characterised by the activation and de-activation processes. This gives rise to the production of the distinctive band or/and line spectra. The intensity of any spectral line depends *inter alia* upon the population of the particles in the corresponding quantum states, the latter being determined by the

excitation and de-excitation probabilities under the conditions of the discharge. A change in the intensity distribution under constant conditions of discharge would, therefore, suggest a change in the number of particles in the corresponding excited states. The above results indicate, therefore, that not only the ionization but also the pre-ionization states are affected.

It is known that the energy  $E$  gained by an electron in traversing a free path  $\lambda$  under an applied field  $X$  is given by  $E=Xe\lambda$ , and that during an impact a part or whole of this energy may be imparted to the gas molecule. According to Joshi, the observed decrease by light in discharge current is due to the negative space charge formed by the capture by gas (particles, chiefly atoms) of electrons, emitted under light from the electrode layer (formed in part from an absorption of ions and excited molecules). This space charge would reduce the effective field across the gas phase and therefore, cause a decrease in the number of excited molecules and the intensity distribution of the spectrum as observed.

#### ACKNOWLEDGMENTS

Grateful thanks of the author are due to Prof. P. N. Sharma, D. Sc., Head of Physics Department, University of Lucknow, for encouragement, and to Prof. S. S. Joshi, D. Sc., F. N. I., Principal, College of Science, Benares, for his kind interest.

DEPARTMENT OF PHYSICS,  
UNIVERSITY OF LUCKNOW

#### REFERENCES

- Joshi, 1943, *Proc. Ind. Sci. Cong*, Presidential Address Chem Sec.  
Joshi and Deo, 1942, *ibid*, Physics Sec.  
Deo, 1948, *Phil. Mag.*, **39**, 978.

## ELECTRON DIFFRACTION IN SOME CUBICAL CRYSTALS\*

By SUBODH KUMAR MAJUMDAR

*(Received for publication, September 19, 1951)*

## Plate XX

**ABSTRACT.** The spacings of a number of cubical crystals, obtained by metal shadowing in high vacuum, have been determined in the electron microscope from the diffraction photographs. Except for AgBr, the values tally with those obtained from X-ray diffraction measurements. The diffraction photographs obtained are very much sharper than similar pictures obtained with metal foils by previous workers.

De Broglie's theory concerning the wave nature of beams of electrons rendered it possible for a stream of accelerated electrons to be used for determining the spacings of crystals. The experiments of Davisson and Germer (1927) first demonstrated the practical possibility of using electron beams for producing diffraction patterns of crystals. Thomson (1929) and others used thin metallic foils for producing diffraction effects with high speed electrons (15KV-60KV).

Although the main use of the electron microscope has been until now the production of electron micrographs, a number of workers have in recent years utilised the interference phenomenon of electrons for measuring the spacings of different crystals. As a matter of fact, the best way to carry out these experiments would be to make parallel observations with X-rays and electron beams under similar conditions. Beischer (1943) has compared such results with fine crystalline and colloidal substances. In such comparisons, the wave-length of the electron beam was not calculated from theory, but with the help of aluminium oxide foil as the calibrating substance. Measurement of some other physical properties, such as conductivity, simultaneously with electron diffraction have been attempted by Hass (1946) with silver and aluminium shadowed samples. Other workers such as Mahl (1942), Molière (1940) and Möllenstedt (1944) have improved the technique of the measurements.

## EXPERIMENTAL

The experiments were performed at the Virusforschungsinstitut, Heidelberg, with the kind permission of Prof. G. A. Kausche. The electron microscope was of the Borres-Ruska double magnification type made by

\* This work forms a part of the investigation carried out by the author at Virusforschungsinstitut, Heidelberg/a Necker, Germany in 1950-51.

Siemens, Berlin. High voltages of 55KV and 70KV were used for accelerating the electrons in different cases. The objective aperture piece was made of platinum-gold with a diameter of 0.3 mm. For diffraction experiments, the projective magnet piece was taken out and the diffracted beams photographed.

Thin deposits of metals like gold, silver and copper were made on saponin membrane placed on the aperture piece by shadowing in high vacuum. Pieces of the metal were placed inside a tungsten spiral held in position above the aperture piece within a bell jar evacuated to high vacuum and the thickness of the deposits was controlled by the time of flow, current strength and the angle of shadowing. For silver chloride and silver bromide, the shadowing was done with silver in presence of chlorine and bromine vapour respectively within the bell jar at equally low pressure.

The distance between the objective and the plate was 57.5 cm. The plates were developed and the distances between the circles were measured under a travelling microscope.

Table I gives particulars about the high voltage used and the current strength in the different cases and Plate XX illustretes the diffraction patterns obtained.

TABLE I

Substance	High voltage KV	Current in milliamp
Gold	55	0.05
Copper	55	0.05
Silver	55	0.05
Silver chloride (Ag volatilised in $\text{Cl}_2$ )	70	0.05
Silver bromide (Ag volatilised in $\text{Br}_2$ )	70	0.05

The spacings were calculated in the following manner. If the incident beam after reflection from a particular plane ( $h, k, l$ ) makes a cone of half angle  $\theta/2$  (figure 1), then  $r/h = \tan \theta/2$ , where  $h$  is the distance of the objective from the plate and  $r$ , the radius of the particular circle.

Then  $\theta/2 = \tan^{-1}(r/h)$  and hence  $\sin \theta/2$  can be calculated for different values of  $r$ . By the method of trial and error, the constant value of  $\frac{\sin \theta/2}{n}$ , using different values of  $n (= \sqrt{h^2 + k^2 + l^2})$  are obtained, correspond-



ing to each circle. If this constant value is  $k$ , then spacing  $a_0$  is given by

$$a_0 = \frac{\lambda}{2 \frac{\sin \theta/2}{\sqrt{h^2 + k^2 + l^2}}} = \frac{\lambda}{2K}$$

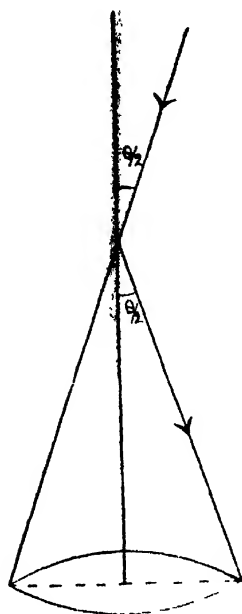


FIG. 1

The value of  $\lambda$  is calculated from the equation

$$\lambda = \frac{h}{\sqrt{2m_0 \cdot e \cdot U \left(1 + \frac{e \cdot U}{2m_0 c^2}\right)}}$$

where  $h$  = Planck's constant =  $6.626 \times 10^{-27}$  erg/sec ;  
 $m_0$  = rest mass of the electron =  $9.108 \times 10^{-28}$  gm.,  
 $e$  = charge of the electron =  $4.803 \times 10^{-10}$  C. G. S. units ;  
 $c$  = velocity of light =  $3.00 \times 10^{10}$  cm/sec ;  
 $U$  = applied E. M. F. (C. G. S. units).

The values of  $\lambda$  for 70 KV and 55 KV, the two accelerating voltages, are found to be

Voltage	$\lambda$
70 KV	0.04485 Å
55	0.05095

Tables II-VI give the values of  $x$ , the diameters of the rings in cm,  $\theta/2$ ,  $\sin \theta/2$  and  $K$ , the constant for the particular plane of reflection.

TABLE II

Gold (1034/43)

Voltage used = 55 KV  $\pm$  215 volts. $\lambda = .05095 \text{ \AA}$ .

Nature	S	W	W	W
$x(\text{cm.}) \dots$	2.595	3.015	4.320	5.110
$\theta/2 \dots$	$1^\circ 17'$	$1^\circ 30'$	$2^\circ 9'$	$2^\circ 32'$
$\sin \theta/2 \dots$	.0112	.0231	.0187	.0221
$K \dots$	.00646	.00650	.00661	.00663

Mean value of  $K = .00655$ .

Hence

$$a_0 = \frac{.05095}{2 \times .00655} \text{ \AA} = 3.90 \text{ \AA}.$$

Standard value for Au = 4.07  $\text{\AA}$ .

TABLE III

Copper (1042/46)

Voltage used = 55 KV  $\pm$  215 volts. $\lambda = .05095 \text{ \AA}$ .

Nature	W	W	S	S	W
$x(\text{cm.}) \dots$	4.795	4.050	2.880	2.490	1.940
$\theta/2 \dots$	$2^\circ 23'$	$2^\circ 1'$	$1^\circ 26'$	$1^\circ 14'$	$0^\circ 56'$
$\sin \theta/2 \dots$	.0416	.0352	.0250	.0215	.0168
$K \dots$	.006930	.006902	.006923	.006797	.006860

Mean value of  $K = .00686$ .

Hence

$$a_0 = \frac{.005095}{2 \times .00686} \text{ \AA} = 3.71 \text{ \AA}.$$

Standard value for Cu = 3.60  $\text{\AA}$ .

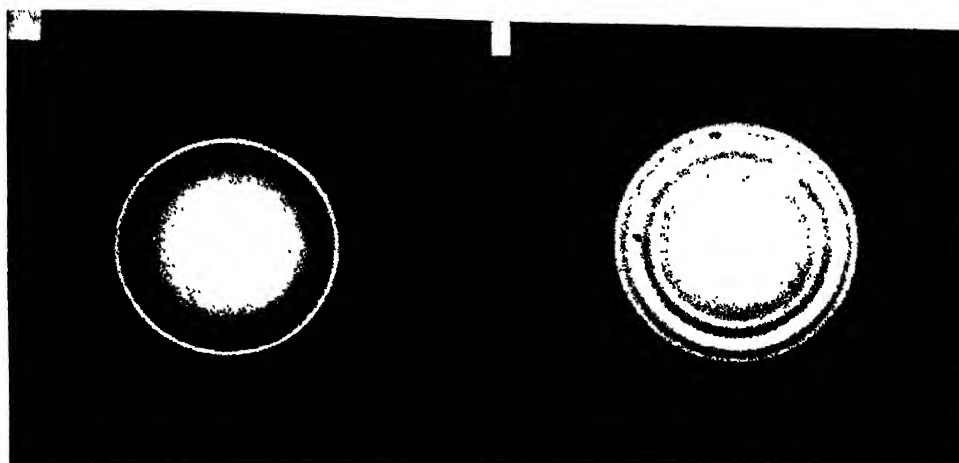
TABLE IV

Silver chloride (silver volatilised in chlorine). (1470/46).

Voltage used = 70 KV  $\pm$  215 volts. $\lambda = .0448$ 

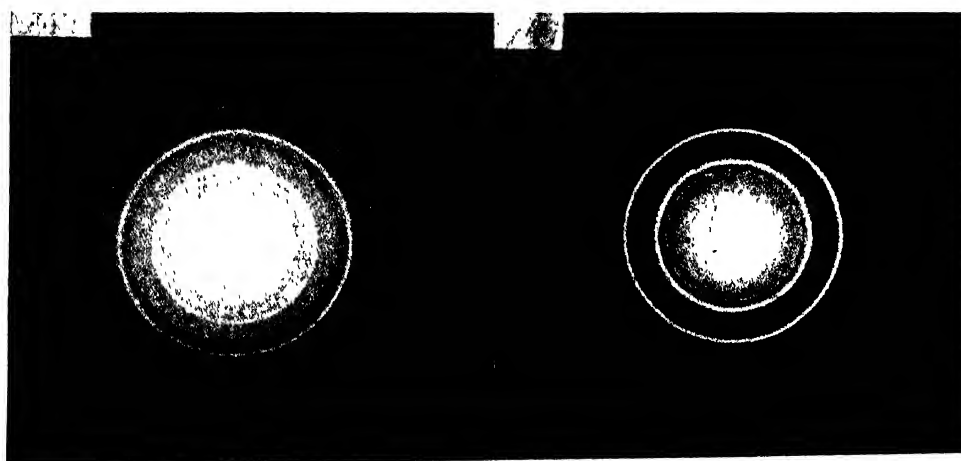
Nature	V.W	W	W	V.W	V.S	V.S	S
$x(\text{cm.}) \dots$	4.945	4.3785	3.392	3.244	2.768	1.959	1.695
$\theta/2 \dots$	$2^\circ 28'$	$2^\circ 11'$	$1^\circ 41'$	$1^\circ 37'$	$1^\circ 23'$	$0^\circ 50'$	$0^\circ 58'$
$\sin \theta/2 \dots$	.0430	.0381	.0294	.0282	.0241	.0169	.0146
$K \dots$	.004101	.00413	.00415	.00416	.00416	.00410	.004037

Mean value of  $K = .00412$ .



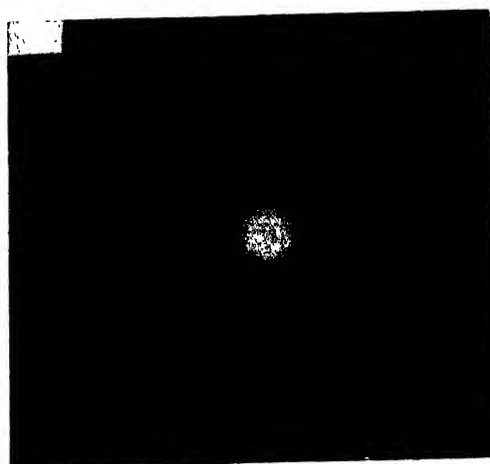
(a)

(b)



(c)

(d)



(e)

Electron diffraction patterns

Fig. (a) Gold  
(b) Copper

Fig. (c) Silver chloride  
(d) Silver bromide

Fig. (e) Silver



Hence

$$a_0 = \frac{.00448}{2 \times .00412} \text{ \AA} = 5.44 \text{ \AA}$$

Standard value for AgCl = 5.54 \AA.

TABLE V

Silver bromide (silver volatilised in bromine<sup>1</sup>). (1474/47).  
Voltage used = 70 KV  $\pm$  215 volts.  $\lambda = .0448 \text{ \AA}$

Nature	W	S	V S	S	W	W
$x(\text{cm}) \dots$	1.597	1.860	2.6545	3.251	4.215	4.627
$\theta/2 \dots$	0°47'	0°55'	1°10'	1°37'	2°16'	2°18'
$\sin \theta/2 \dots$	.01388	.0161	.0232	.0282	.0366	.0401
$K \dots$	.00462	.00467	.00468	.00470	.00463	.00466

Mean value of  $K = .00466$ 

Hence

$$a_0 = \frac{.0448}{2 \times .00466} \text{ \AA} = 4.82 \text{ \AA}.$$

Standard value of AgBr = 5.75 \AA.

TABLE VI

Silver (1046/46)  
Voltage used = 55 KV  $\pm$  215 volts.  $\lambda = .05095 \text{ \AA}$ .

Nature ...	W	W	W	S
$x(\text{cm}). \dots$	4.984	4.292	3.015	2.610
$\theta/2 \dots$	2°28'	2°8'	1°30'	1°18'
$\sin \theta/2 \dots$	.0430	.0378	.0262	.0227
$K \dots$	.00614	.00620	.00617	.00610

Mean value of  $K = .00615$ .

Hence

$$a_0 = \frac{.05095}{2 \times .00615} \text{ \AA} = 4.14 \text{ \AA}.$$

Standard value for Ag = 4.08 \AA.

It would thus appear that except for AgBr, the values obtained from electron diffraction experiments agree fairly well with those from X-ray diffraction experiments, bearing in mind the error involved in maintaining a constant primary current and in the calculation of wavelengths of electron

beams. The photographs of the diffraction rings are also much sharper than those previously obtained by other workers.

The discrepancy found in the case of AgBr may be attributed to either of the causes referred to above or to ineffective bromination in the shadowing apparatus. The value obtained ( $4.812 \text{ \AA}$ ) is too small for AgBr and too large for silver ( $4.08 \text{ \AA}$ ). It is also not due to accidental falling off of tungsten particles ( $3.15 \text{ \AA}$ ) from the electron gun, as sometimes happens.

Interesting results have been found with NaCl and KCl solutions, evaporated in high vacuum within the microscope. In these cases, in addition to the usual circles, number of spots have been noticed. These will form the subject of a later communication.

#### ACKNOWLEDGMENTS

The author's best thanks are due to the Government of West Bengal, for award of study leave, which made his stay in Germany possible, to Prof. G. A. Kasusche for kindly allowing him to work in his institute and to Dr. Haardick and Frau Amy Engel for taking the diffraction photographs.

DARJEELING GOVERNMENT COLLEGE,  
DARJEELING (WEST BENGAL)

#### REFERENCES

- Davisson and Germer, 1927, *Phys. Rev.*, **30**, 705.  
Thomson, G. P., 1929, *Proc. Roy. Soc.*, **A**, **117**, 600 ; **A**, **125**, 352.  
Beischer, 1943, *Zeit. f. Elektrochem.*, **49**, 463.  
Mollenstedt, 1946, *Optik* Part II.  
Hass, 1946, *Optik*, Part I.  
Mahl, 1942, *Naturwiss.*, **30**, 208.  
Moliere, 1940, *Zeit. f. Elektrochem.*, **46**, 514.  
Mollenstept, 1944, *Ber. Phys. Inst. Danzig*.

# ON THE EXISTENCE OF ROSSI SECOND AND THIRD MAXIMA OF COSMIC-RAYS

By P. K. SEN CHAUDHURY\*

(Received for publication, September 18, 1951)

**ABSTRACT.** The controversial existence of Rossi second and third maxima of cosmic-rays were investigated in lead with a triple coincidence arrangements of counters under different geometrical conditions and definite evidences have been obtained about the existence of a second maximum at about 18 cm of lead and a third maximum at about 23 cm of lead. Except for a drop of coincidence frequency at about 20 cm, both these maxima might be considered as a single flat maximum starting from 16 cm and upto 24 cm similar to the results reported by Schopper and others. From a careful analysis of all the investigations made by other workers, it seems to the author that the failure of some eminent workers to confirm the existence of these higher maxima may be due to (a) firstly, overlapping by oblique showers when all the counters are placed very near the absorber and (b) much greater percentage of side showers of external and internal origin when all the three counters without appreciable vertical separation are placed too far below the absorber for narrow angle showers. An ideal arrangement, as follows from this investigation, is that one of the counters should be placed immediately below the absorber and the two others as far below the absorber as possible. Incidentally, it follows that a similar arrangement should be used in a counter controlled Wilson chamber for investigating penetrating showers.

For the interpretation of the origin of these higher maxima, from their correspondence with anomalies in RaC gamma-rays absorption in lead reported by the author, it seems that either there are some residual photons in RaC gamma-rays and in cosmic-rays which do not obey the current theories of photon interaction and behave like an unstable neutrino or that some such radiations are produced by photon in lead. Further, from the fact that RaC gamma-rays are of maximum energy of only 2.4 Mev the author suggested that the new type of penetrating radiation may simply be a positron-electron dipole behaving as a neutral electro-meson before annihilation or being dissociated back to a positron and electron by Philips-Oppenheimer process. From energy consideration and the position of third maximum, it follows that such a dipole may have a maximum life of the order of  $10^{-9}$  sec only.

## INTRODUCTION

After the discovery by Rossi (1934) of the first maximum under about 2 cm of lead, a second maximum between 16 to 20 cm of lead was reported by certain workers, viz. Hummel (1934), Drigo (1934), Ackemann (1935), Clay, Gemert and Wiersma (1936) and others. Schmeiser and Bothe (1938) made an elaborate study of the second maximum and found that this maximum is prominent for narrow angle showers, being most prominent when an angle of  $4^\circ$  is subtended by the edge of the two lower counters

\* Formerly I.C.I. Research Fellow, Bose Research Institute, Calcutta.

at the centre of the absorbers and it is hardly noticeable for a divergence of more than  $15^\circ$ . By conducting the experiment in a cellar and under the open sky they concluded that the second maximum is due to the penetrating component of the cosmic rays, *e.g.*, meson. After the publication of this report by Schmeiser and Bothe, there has been a considerable controversy over the existence of this maximum. Morgan, and Nielsen (1939), although they got the Rossi second maximum using an arrangement similar to that of Bothe, failed to get it using four-fold coincidence of four counters in two vertical pairs. Dasgupta (1940) at Calcutta confirmed the result of Schmeiser and Bothe and obtained the second maximum under about 18.5 cm of lead. Altmann, Walker and Hess (1949) very carefully searched for these higher maxima using elaborate precaution. They at first, with a triple coincident arrangement, obtained some indication of two humps in the transition curve, one under about 13 cm and the other under 25 cm of lead absorber. The arrangement was such that one of the counter was immediately below the lead absorber and the two others at a distance of about 25 cm below the latter, the lower two counters subtending an angle of about  $9.6^\circ$  with the first one. But they did not get any hump in the transition curve when only coincidences between the two lower counters were recorded. All their experiments were carried out in a basement where the temperature varied between 20 to  $27^\circ\text{C}$ . Later, they repeated the experiment with an arrangement apparently identical with that of Schmeiser and Bothe but were puzzled at not getting any evidence on the presence of the second maximum. Similarly George, Janossy and McCaig (1942) using an arrangement similar to that of Hess and others failed to detect the Rossi second and higher maxima. These authors give a good summary of results and references of all the earlier investigations. Pribsch (1936) observed both second and a third maximum as early as 1936\*.

Later, certain other workers, *viz.* Trumpy and Bergens (1939-40), Ozorai (1944) and M. Delta Corte (1946) reported the existence of Rossi second maximum under certain experimental conditions. The original journals not being available in India, only their summaries in Science Abstracts could be consulted. Trumpy and Bergens observed that when the counters were surrounded by lead, there was no second maximum but the latter appears when the counter system is surrounded by wood, etc. They conclude that this maximum is due to neutron in cosmic-rays. Ozorai, although he obtained Rossi second maximum for wide angle showers, showed that it disappears for narrow angle showers. Contrary to the findings of Schmeiser and Bothe, M. Delta Corte observed Rossi second maximum for two particle showers but not for 3 or more particles. In a Wilson chamber analysis Breussard and Graver (1941) obtained evidence in favour of second maximum

\* The author is thankful to Professor W. Bothe for kindly pointing out this in a letter to the author.



of two particle shower. Similarly, Sinha (1943) with a counter controlled Wilson chamber obtained some evidence on the existence of Rossi second maximum. Mohr and Stafford (1944) using an ionisation chamber obtained a hump under about 20 cm of lead.

Recently, Clay (1949) claimed to have definitely established the existence of second maximum under about 16 cm of lead and a third maximum between 20 to 24 cm of lead. He further confirmed his results by repeating the experiment using gold and mercury absorbers under the assumption that the second maximum is produced by knock-on electron by meson. Fenyves and Haiman (1950) measuring only the vertical component, obtained evidence of a feeble maximum under 18 cm of lead and a third maximum under 26 cm of lead. The geometry of their experimental arrangement is not mentioned. Heyland and Duncanson (1951) have very recently contradicted the results of the above workers. But in their arrangements they have placed two counter trays in coincidence above the lead absorber and consequently such a system cannot detect any increase in coincidence rate due to the production of secondary showers in lead which is indicated by the absence of even the first maximum in their transition curve. Hence from this experiment, which simply measure the incident vertical component, one cannot say if the second or third maxima exists or not. Bothe and Thurn (1950) have again claimed to have definitely established the second and third maxima using very ingenious crossed counters arrangement over a large effective area and thus with a large coincidence frequency at the same time well-defined solid angle. They have selected by coincidence and anti-coincidence the showers produced by ionising or non-ionising radiation incident on the top of the absorber and from there conclude that the incident radiation producing second maximum is a single charged particle, whereas, the third maximum is produced by a long-lived neutral particle. The position of the third maximum, as found by these authors and also by Fenyves and Haiman (loc cit), is dependent on the barometric pressure. Mathov (1950) has also recently reported the existence of a second maximum at about 13 cm of lead which when corrected for the concrete roof amounts to about 18 cm of lead. Schopper, Höcker and Kulm (1951) using photographic emulsion have obtained definite evidence about the existence of a second maximum in lead starting from 15 cm and up to about 24 cm of lead.

The question arises why eminent experimental physicists like Hess and his collaborator, Janossy and his associates, could not detect these second and third maxima. The present writer, therefore, made a careful analysis of the different experimental arrangements used by these investigators and an attempt is made here to find out what may be the probable causes of their failure. It appears that (a) if such higher maxima exist at definite vertical thickness of the absorber, then unless the oblique showers generated in lead are eliminated, the maxima will be flat, if at all detectable, (b) if the three counters, in a triangular arrangements, are placed very close together and

very near the bottom of the lead absorber, such a system will be equally sensitive to oblique showers as well to showers coming from the vertical direction. This is most probably the reason why Hess, Janossy and their co-workers could not detect these higher maxima in some of their experimental arrangements. Moreover, Janossy and his co-workers in most of their experiments, used successive thickness of lead absorber in big steps. As for example, table 3 of their paper shows that after 10 cm of lead they next used 17 cm of lead absorber, to find out whether the second maximum exists assuming that after the first Rossi maximum, the minimum is reached at 10 cm of lead. But this is not true, at least under certain experimental condition as is indicated in table 4 of their paper, recording their subsequent experiments. The results obtained by us also show that the minimum is not always reached at 10 cm of lead. To eliminate the effect of oblique showers, the counter system should be at a fair distance vertically below the absorber. But again if the counter system is shifted too far below, then it becomes more and more exposed to air showers and other side showers generated in the roof, etc., reaching the counter system other than through the lead absorber. But if one of the three counters is sufficiently separated vertically from the two others then it becomes sensitive only to vertical showers coming from the top absorber. These conditions are to some extent fulfilled in the arrangement used by Clay and very nicely fulfilled in the arrangement by Bothe and Thurn in their recent experiments except when they use anti-coincidence of the top counters for neutral radiations only. This is the reason why, as stated above, Hess and his co-workers using an arrangement similar to that of Clay obtained some evidence of two humps at 13 and 25 cm of lead for triple coincidence arrangement, but not for double coincidence when the top counter was excluded. In the arrangements of Schmeiser and Bothe, as indicated by the scale of their diagram, the system of four counters in triple coincidence was placed at a distance about 30 to 40 cm below the absorber such that the two lower counters subtend an angle about  $4^\circ$  at centre of the bottom of the absorber. The two upper counters connected in parallel were shifted up by about 10 cm from the two lower counters. They used lead absorbers of two different dimensions, the first set of absorbers being of dimension  $40 \times 40 \text{ cm}^2$  and the top absorber being of dimension  $61 \times 61 \text{ cm}^2$ . Janossy attributes the second maximum obtained by Schmeiser and Bothe to be due to first maximum at the edge of the protruding top absorber as he himself, by an apparently similar arrangement, could get a second maximum at about 14 cm of lead. But both Hess and Janossy placed the counter system at a much greater distance below the absorber in order that the edge of the lower counter subtend an angle of  $4^\circ$  at the centre of the bottom of the absorber, similar to that of Bothe and Schmeiser. This is probably due to the greater horizontal separation between the two lower counters. As indicated by the scale of their diagram, Hess placed the counter system at a distance about 100 cm and Janossy at a distance about 60 cm below the bottom of the absorber

whereas, Schmeiser and Bothe placed the counter system only at a distance of about 30 to 40 cm. Moreover, in both Hess's and Janossy's arrangements the vertical separations of the top counters from the two lower counters was very small, particularly in that of Hess. As such, their arrangement of counters is more favourable for the detection of side showers of external origin and showers generated from the protruding position, if any, of the top absorber; both Hess and Janossy performed their experiments in basements with probably several stories above and as indicated by Janossy's data (loc. cit. Table 5) the number of background showers, due to air showers and the showers generated in the roof, etc., is more than the number of showers generated in lead absorber after about 10 cm of lead. Moreover, the result of present investigations by the author indicate that as the distance between the absorber and the lower counters is increased by keeping the upper counters in parallel immediately below the absorber, then the intensity of showers generated in lead and recorded falls off rapidly, following nearly an inverse square law from the bottom of the absorber. On the other hand, as the counter systems, closely placed together, are shifted more and more below the absorber, more and more background showers pass through the counter system other than through the absorber, as the shielding effect of the top absorber becomes smaller and smaller; consequently at a large distance the percentage of shower, generated in lead will be small in comparison with the background shower; so even if there is appreciable variation in the number of showers generated in lead, it will be hardly detectable in the total number of showers recorded. As stated above, Das Gupta in Calcutta obtained the Rossi second maximum, though he also placed the counter system at a distance about 80 cm below the absorber. This is due to the fact that in his arrangement, the two top counters in parallel at the top of the triangular arrangement were vertically separated from the two bottom counters by a large distance of about 20 cm. This gave a strong bias for recording only showers coming from the vertical direction. Incidentally, from this analysis as well as from the results of this investigation, it may be pointed out that to eliminate side and oblique showers, while investigating penetrating showers with a counter controlled Wilson chamber, the lower counters should be placed as far below the absorber and the Wilson chamber as is possible and another counter above the chamber and immediately below the absorber.

In the light of the above analysis, to obtain further confirmation, we did our experiment more carefully and obtained definite evidence about the existence of two higher maxima.

Five counters of length about 20 cm and diameter about 3 cm were used in a triangular arrangement of three fold coincidence, three top counters in parallel were placed immediately below the top absorber and the two lower counters were placed at three different distances 10 cm, 25 cm and 66 cm vertically below the bottom of the absorber such that the angle subtended by the centres of the two lower counters

at the centre of the bottom of the absorber were  $22.5^\circ$ ,  $9.1^\circ$  and  $3.4^\circ$  respectively from these three distances. A lead sheet, one cm thick, was placed between the two lower counters in order to eliminate coincidences due to electrons knocked out from the counter wall. A vertical section of the experimental arrangement is shown in figure 1. The experiments were conducted in open air with a bamboo-mat shed constructed in the Bose Institute garden. The circuit diagram is shown in figure 2. The absorbers used were commercial lead sheets of dimension  $12''$  by  $12''$  and of two different thickness  $1/8''$  and  $1/12''$ . Again, in order to detect

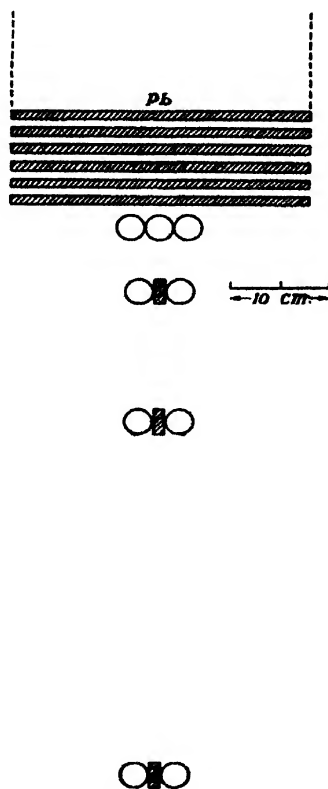


FIG. 1

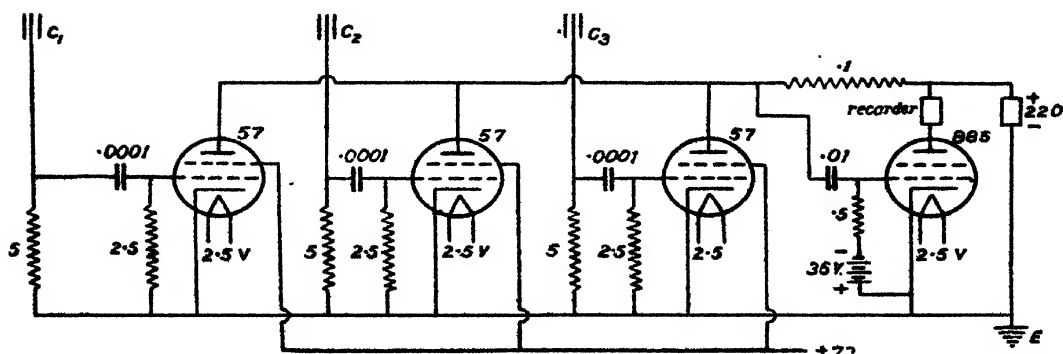


FIG. 2

(Resistances in  $M \Omega$  and capacity in  $mF$ . The grid-leak resistances are each  $25 M \Omega$ , and not  $2.5 M \Omega$  as shown in the diagram)

any variation due to comparatively narrow angle showers at the same vertical distance 10 cm below the absorber, a second arrangement of the counters was used in which the two lower counters were brought together without any gap and the lead sheet in between them was removed. The angle subtended by the centres of the two counters at the centre of the bottom of the absorber is then  $17^\circ$ . The detecting arrangement used is a simple Rossi coincidence circuit, using one stage amplification with type 57 valve. Details of the circuit is similar to that given by Strong and others (1939). The resolving time was such that the accidental coincidence rate was less than the statistical error in all the experimental values obtained. In order to eliminate the effect of statistical fluctuations and other corrections due to temperature variation etc., the experiment under each geometry was repeated at different periods under nearly constant temperature and weather condition. Every day the data of this experiment were compared with those of a continuously recording pressure ionisation chamber set up in the Bose Research Institute, and any major variations in cosmic ray intensity, due to magnetic storm, Sunspot activity etc., when detected by both the experiments, were omitted when calculating the average frequency of coincidences. As a matter of fact, such occasional variation in cosmic ray intensity itself forms a very interesting field and the author with Chakraverty (Chaudhury

TABLE I

Thickness of Pb. absorber in cm	Expt. No. 1. (March, 1950)		Expt. No. 2. (April, 1950)		Expt. No. 3. (May, 1950)		Average results of three Experiments	
	Hours of observations	Average coincidences per hour	Hours of observations	Average coincidences per hour	Hours of observations	Average coincidences per hour	Total hours of observations	Mean average coincidences per hour
nil	6	15.1					6	$15.1 \pm 1.6$
1.91	7	64.5					7	$64.5 \pm 3.0$
8.25			6	19.5	4	18.0	10	$18.75 \pm 1.37$
10.16	11	16.27	13	19.15	13	19.75	37	$18.4 \pm .71$
12.1	12	17.3	12	20.75	12	21.5	36	$19.85 \pm .75$
14.29	11	18.63	13	18.3	11	18.63	35	$18.52 \pm .73$
16.2	12	17.17	13	16.84	14	18.07	39	$17.36 \pm .67$
18.1	12	21.9	16	19.4	11	22.09	39	$21.13 \pm .74$
20.0	12	19.08	13	19.0	12	18.66	37	$18.91 \pm .71$
21.9	12	18.41	12	18.5	10	18.2	34	$18.37 \pm .74$
23.8	19	19.9	11	20.2	14	18.07	44	$19.39 \pm .66$
26.34	14	17.5	13	18.61			27	$18.05 \pm .82$

TABLE II

Thickness of Pb absorber in cm	Expt. No. 1. July—August, 1950		Expt. No. 2. Aug.—Sept. 1950		Average results of two experiments	
	Hours of observation	Average coincidence per hour	Hours of observation	Average coincidence per hour	Total hours of observations	Mean average coincidence per hour
nil	7	45.4			7	45.4 $\pm$ 2.5
1.91	9	105.6			9	105.6 $\pm$ 3.4
8.25	12	36.1			10	36.1 $\pm$ 1.9
10.16	10	35.6			10	35.6 $\pm$ 1.9
12.1	6	32.16	5	30.4	11	31.4 $\pm$ 1.7
14.29	11	33.5	6	30.0	18	31.75 $\pm$ 1.33
16.2	10	36.0	13	32.2	23	34.1 $\pm$ 1.22
18.1	15	33.0	10	32.5	25	32.75 $\pm$ 1.15
20.0	11	31.7	10	31.5	21	31.6 $\pm$ 1.23
21.9	15	32.7	11	31.36	26	32.13 $\pm$ 1.11
23.8	11	31.5	16	30.	27	30.75 $\pm$ 1.07
25.07	13	34.1	23	34.1	36	34.1 $\pm$ 0.97
26.34	18	31.8	25	29.84	43	30.82 $\pm$ 0.85

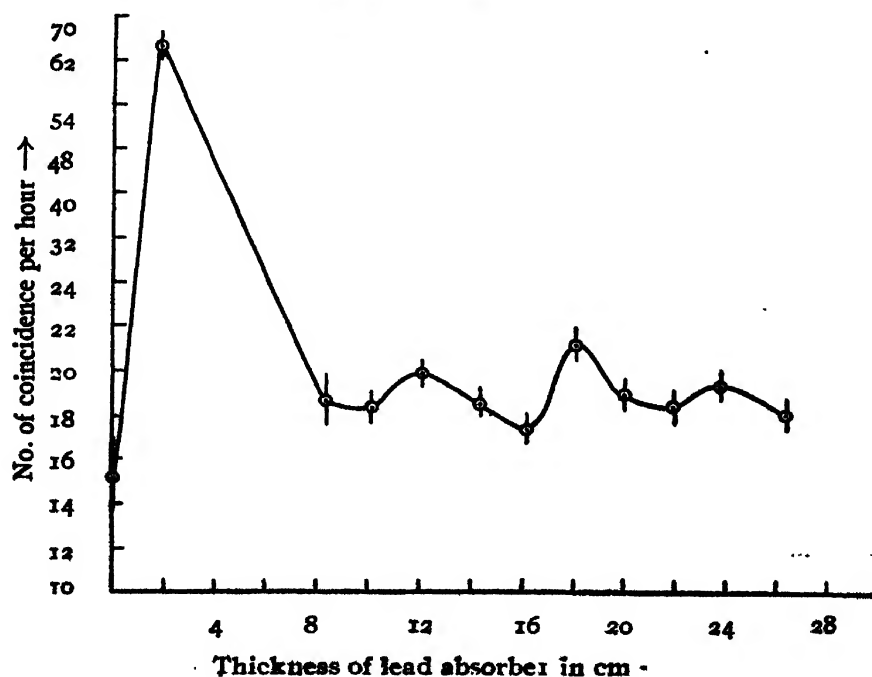


FIG. 3

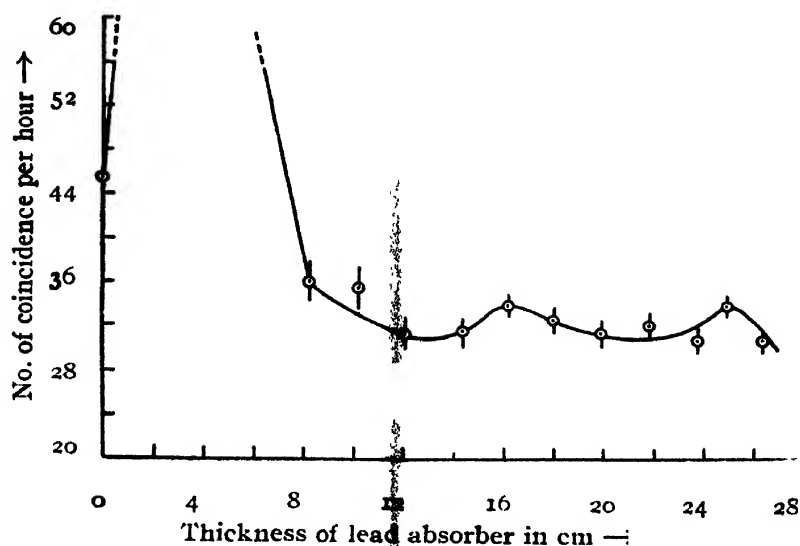


FIG. 4

TABLE III

Thickness of Pb absorber in cm	Expt. No. 1 Jan—Feb., 1951		Expt. No. 2 March—May, 1951		Total hours of observations	Average frequency per hour
	Hours of observation	Frequency per hour	Hours of observation	Frequency per hour		
7.91	8	23.4			8	23.4 $\pm$ 1.7
8.25	14	7.9			14	7.9 $\pm$ .75
10.1	17	7.7	8	5.12	25	6.87 $\pm$ .52
12.1	16	6.0	11	3.81	27	5.11 $\pm$ .44
14.29	16	4.1	16	4.38	32	4.24 $\pm$ .36
16.2	19	5.3	10	5.5	29	5.57 $\pm$ .43
18.1	16	5.4	19	5.94	35	5.69 $\pm$ .40
20.54	15	5.3	20	4.75	35	4.97 $\pm$ .38
23.03	13	5.5	14	5.14	27	5.32 $\pm$ .44
25.62	8	4.75	13	4.54	21	4.62 $\pm$ .47
29.0	33	4.61			33	4.61 $\pm$ .37

and Chakraverty, 1950) published a note on one of such variation when the intensity increased by about cent per cent. The experimental data under two different geometry are represented in Table I and Table II and the average shower frequency plotted against absorber thicknesses are shown in figure 3, and figure 4. Since the coincidence rate without the 1 cm lead between the two lower counters became nearly double that of the lead

TABLE IV

(June, 1951)

Thickness of Pb absorber	Hours of observations	Average frequency per hour
1.91 cm	16	$5.88 \pm .61$
10.10 "	16	$0.50 \pm .18$
14.29 "	16	$1.0 \pm .25$
16.2 "	16	$1.13 \pm .27$
18.0 "	20	$1.8 \pm .30$
20.22 "	14	$.57 \pm .20$
23.03 "	16	$1.13 \pm .27$
25.62 "	14	$.14 \pm .10$
27.30 "	8	$.25 \pm .18$

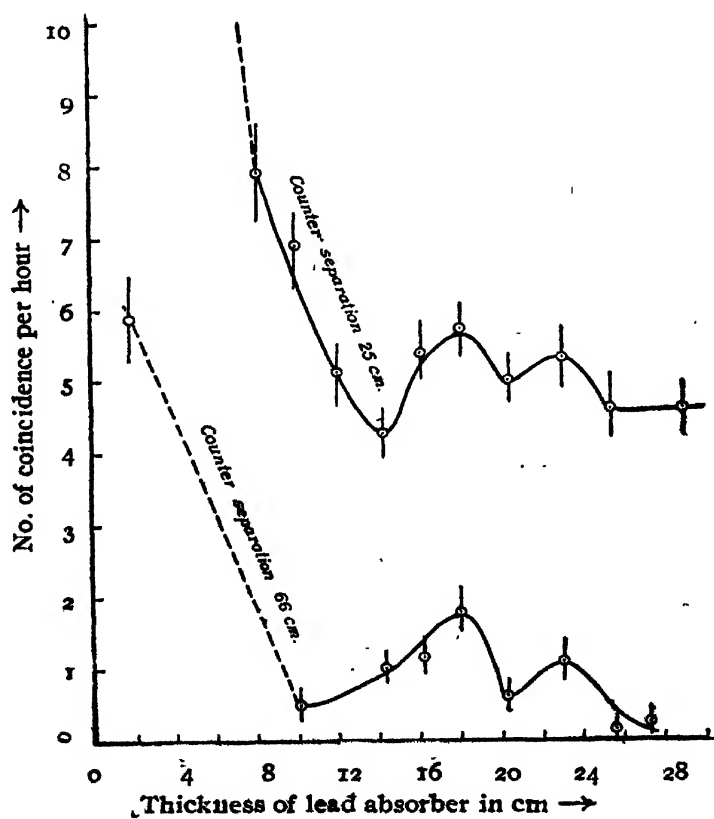


FIG. 5



sheet as shown in Table II, therefore it was suspected that so much difference might be partly due to spurious coincidences due to a single particle which simply knocks out an electron from the counter wall which passes through and excites the other counter. So the two subsequent experiments with the two lower counters at 25 cm and 66 cm below the absorber, were done only with the lead sheet between the counters so that no knock-on electron can pass through it. The experimental results are shown in Table III and Table IV and in the average shower frequency are plotted in figure 5.

#### RESULTS AND DISCUSSIONS

Table I and the curve plotted in figure 3 show that after the prominent first maximum there is definitely a second maximum at about 18 cm of lead supported by each of the three separate experiments. But in addition, there are some evidences of two less prominent maxima at about 24 and 12 cm of lead. The shape of the transition curve is rather complex in this position. When the two lower counters were brought very near and the 1 cm thick lead sheet between them eliminated, then, as stated above, there is an appreciable increase in the frequency of shower which may be partly due to such an arrangement being more sensitive to recording oblique showers and knock-on showers. Such an arrangement is also more sensitive to slightly narrow angle showers. The results in Table II and the curve plotted in figure 4 show that the second maximum has shifted to about 16 cm of lead but there is a definite third maximum at about 25 cm of lead. The slight shifting of the second maximum in this case might be due to greater predominance of oblique showers travelling a greater oblique distance than the vertical.

Tables III and IV and the corresponding transition curves plotted in figure 5 also shows that after the first maximum, there is definitely a second maximum at about 18 cm and a third maximum at about 23 cm of lead. Except for one point under 20 cm of lead, we might consider the second and third maxima to be a single rather flat maximum between 16 and 26 cm of lead exactly similar to the shape of the transition curve obtained by Schopper and other (*loc. cit.*). But in both the experiments we found the coincidence rate under 20 cm to be much less than that under 18 and 23 cm of Pb absorber. Further, as shown in the last curve (two lower counters at a distance 66 cm below), the second and third maxima are very prominent when the counters subtend an angle  $3.4^\circ$  at the centre of the bottom of the absorber. This is in agreement with Bothe and Thurn (*loc. cit.*). But this may be either due to the pair of particle responsible for these maximum are initially emitted with a very narrow angle or it may also be at least partly due to complete elimination of oblique and side showers. In our curves both the second and third maxima are much sharper than those of Bothe and Thurn who have obtained a flat-second maximum. But this

may be due to large effective area of the crossed counters used by them so that the pair of particles may come from appreciably oblique direction. Another interesting fact of our investigation is that after the third maximum at about 23 cm of lead there is an abrupt drop of coincidence frequency. A similar sudden drop in meson absorption has been reported by Aiya (1944) and Gill (1950).

From these experiments it can be definitely concluded that there is a second maximum of cosmic rays between 16 and 18 cm and a third maximum between 23 and 25 cm of lead. It should, however, be mentioned that since the old commercial lead sheets were used as absorber and since all the lead sheets are not exactly of uniform thickness, therefore, there may be an uncertainty of about 1 cm in the exact position of these maxima.

Now for the interpretation and origin of these higher maxima, various conclusions have been made by different workers. Schmeiser and Bothe from the experiments in open air and in a underground cellar, concluded that the second maximum must be due to a meson. But even in underground cellar there will always be present equilibrium amount of decay and knock-on electron associated with meson. Bothe and Thurn further confirm their previous conclusion by their recent experiments. The *C*-curve of their results showing only the second maximum is due to showers produced by a single charged particle. But in this curve both the first and the third maximum are absent. It is not clear why there should not be the first maximum in the *C*-curve. The *d*-curve of their results showing only the third maximum is due to a non-ionising radiation incident on the top. From a comparison of *C*-and *d*-curves they conclude that the second maximum is only produced by a single charged particle, probably a  $\pi$ -meson dissociating into a  $\mu$ -meson pair according to the process recently suggested by Wentzel (1950). The third maximum they believe to be produced by a long lived neutretto. But it is not clear how can a hard  $\mu$ -meson pair produced by Wentzel's process get so easily absorbed within a few cm of lead after producing the second maximum. If the  $\mu$ -meson pair are very soft then these will suffer so much multiple scattering while passing through the lead absorber that there will hardly be any chance of recording them in a narrow angle. Moreover, since both the first maximum and the third maximum are absent in the *C*-curves, therefore from their experiments one may not conclude that the third maximum cannot be produced by a single charged and energetic electron or positron which also produce the first maximum. In fact, there may be some genetic connection between the first and the third maximum. The non-ionising radiation producing the third maximum may also be an energetic photon. Schopper and others state that the stars responsible for these maxima resemble the stars produced by photon cascades. Clay believes that the second maximum is due to knock-on electron shower produced by a meson. His data shows that the second maximum is more prominent for showers of low intensity and not

necessarily a shower of two particles with narrow angular divergence. If the secondary radiation producing the higher maxima consists of photons of low energy, then of course the probability of recording threefold coincidence is decreased by a factor of the order  $10^{-2}$  to that of two-fold coincidences and in that case some of the cloud chamber and other evidence of the second maximum to be due to two particle showers, may be simply due to Compton electron instead of a meson pair. Trumphy and Bergens, who obtained the second maximum only when the counters were surrounded by wood, etc. and not when surrounded by lead, concluded that the second maximum is due to neutron. Similarly to interpret the results of Nielsen and Morgan, who obtained second maximum using a triple coincidence arrangement similar to Bothe and Schneider but failed to detect it using four-fold coincidence in two vertical pairs, it must be assumed that secondaries are soft radiation of low intensity. But we understand that Bothe and Thurn placed lead absorber a little above the crossed counters to study the nature of secondary radiation responsible for the second maximum and they found some residual effect even after 10 cm of the absorber. But there may be some difficulty in this conclusion due to the formation of third maximum and also if the secondary radiations are produced by a neutral particle with a life such that it decays or is annihilated at a distance just above the crossed counters then the absorber will have no effect on it.

From all these it appears that the origin of these higher maxima and the nature of the secondary radiations are not yet clearly explained. But we were led to these investigations due to the correspondence of these higher maxima with anomalies in RaC gamma ray absorption in lead reported by the author (Sen Choudhury 1948, 1950 and 1951). Particularly the abnormally low value of the absorption co-efficient of RaC gamma-rays in lead, as shown in figure 6 between 22 and 25 cm of lead is almost in exact coincidence with the third maximum obtained under these investigations and by Bothe and Thurn in their *d*-curve. The experimental value of the absorption co-

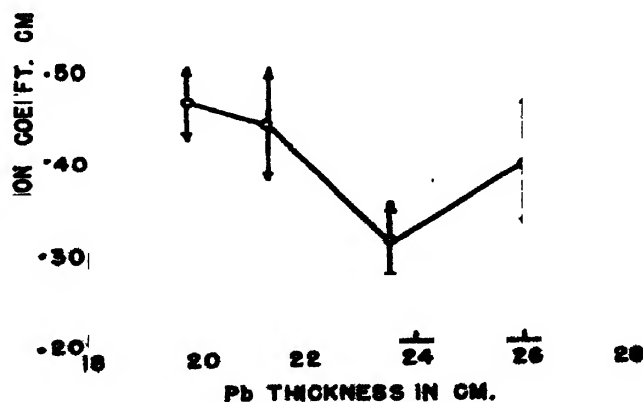


FIG. 6

efficient in this region is far behind the theoretical minimum value about  $.47 \text{ cm}^{-1}$  for photons of all energy as calculated by Heitler (1944). The experimental values of absorption co-efficient at about 20 cm of lead is in agreement with the theoretical value. Some peculiarities in absorption were also observed at about 16 cm of lead. Soddy and Russell (1910), about 40 years back, actually obtained a hump in the log intensity curve exactly in the region where Rossi second maximum is obtained. They interpreted this to be due to some, peculiar secondary radiation generated in lead and manifesting itself in this locality. They could eliminate it by bringing the electroscope very near the Radon source. Now, unless these correspondences are purely accidental, it is very likely that the higher maxima, particularly the third maximum in Rossi curve and the anomalies in RaC gamma-ray absorption have the same origin. In this case we must conclude that either there are some residual photons in RaC gamma-rays and in cosmic-rays which do not obey the current theory of photon-interaction with matter and resemble neutrino-type of radiation which is unstable or some such radiation is generated by photon in lead. Again in order to explain the dependence of the position of Rossi higher maxima on the absorber, we must assume that, however small, these radiations must have some continuous interaction with the material of the absorber before being transformed into a counter-detectable radiation. From this as well as from the fact that RaC gamma-rays are of maximum energy only 2.4 Mev, the author suggested that this radiations may be purely due to a positron-electron dipole behaving as a neutral electro-meson before annihilation. Such a dipole may again dissociate back to a positron and an electron by Phillip-Oppenheimer process in the strong nuclear field of lead. According to Wheeler (1946), such a system can only form hydrogen-like atom with parallel spin and a life of about  $10^{-8}$  sec against annihilation. The probability of their direct formation is one in million. Deutsch (1951) obtained experimental evidence of the formation of such system called positronium in abundance. But as a hydrogen-like atom of dimension about  $10^{-8}$  cm such a system has very little penetrating power as a neutral particle unless the positron and electron are much closer together like a dipole. According to Heitler (1944), again the probability of a positron capturing an electron is maximum when its kinetic energy is .5 Mev. So a positron-electron dipole with very slight interaction in lead and with this much energy requires a maximum life of about  $10^{-9}$  sec to produce the anomalies the dependence on spin may be responsible for the two groups of slightly different life.

Further, in this connection a reference may be made to certain experiments performed by some Chicago physicists. Gerhart Groetzinger, Kruger and Lloyd Smith (1945) obtained some excess of counting near a cyclotron with counters arranged in coincidence and shielded by more than 19 cm of lead absorber. They interpreted these to be due to artificial production of meson of low mass intermediate to that of a meson and an electron. The

## *Existence of Rossi Second and Third Maxima of Cosmic-rays 553*

production cross-sections are similar to that for bremsstrahlung. But they (*loc.cit.* 1947) could not confirm their hypothesis by their subsequent cloud chamber analysis. Broadbent and Janossy (1949) concluded that the particles responsible for some penetrating showers are not mesons but some other particles produced according to a  $Z^2$  law. It is not unlikely that these phenomena, the anomalous absorption of photon and the two higher cosmic-ray maxima have the same origin. All these may be satisfactorily explained by the above hypothesis of a positron electron dipole behaving as a neutral electro-meson before annihilation and with very small interaction with matter. Recently, Steinberg, Panofsky and Steller (1950) with Berkely cyclotron have definitely established the production of neutral meson along with charged meson by photon. But since the life of such a meson is found to be only about  $10^{-13}$  sec, therefore, such a neutral meson either produced by photon or knocked out from a nucleus by proton cannot explain the two Rossi higher maxima. It may, therefore, be possible that by similar mechanism neutral electro-meson, with properties described above and with longer life, can be directly or indirectly produced by less energetic photon along with positron and electron. For further elucidation we may try to repeat this investigation with a counter-controlled Wilson chamber.

### ACKNOWLEDGMENTS

In conclusion the author expresses his grateful thanks to Dr. D. M. Bose, Director, Bose Research Institute for his constant encouragement and the facilities provided for this investigation. The author is thankful to the authorities of Imperial Chemical Industries for the grant of a fellowship through the Council of National Institute of Sciences, India.

PHYSICS DEPARTMENT,  
PRESIDENCY COLLEGE,  
CALCUTTA

### REFERENCES

- Ackemann, 1934, *Naturwissenschaften*, 22, 169.  
Aiyé, Chandrasekher, 1944, *Nature*, 153, 375.  
Altmann, Walker and Hess, 1940, *Phys. Rev.*, 58, 1011.  
Bothe and Thurn, 1950, *Phys. Rev.*, 79, 544.  
Broadbent and Janossy, 1948, *Proc. Roy. Soc.*, 192A, 364.  
Broussard and Graver, 1941, *Phys. Rev.*, 60, 413.  
Clay, Ven Gemmert and Wiersma, 1936, *Physica*, 3, 627.  
Clay, 1949, *Rev. Mod. Phys.*, 21, 82, also Clay and Scheen, 1948, *Physica*, 14, 489.  
Das Gupta, 1940, *Proc. Nat. Institute. Scs. India*, 6, 65.  
Deutsch, M, 1951, *Phys. Rev.*, 82, 55.  
Drigo, 1934, *Ric. Scient.*, 5, 88; also, 1935, *Ric. Scient.*, 6, 529.  
Fenyves and Haimann, 1950, *Nature*, 165, 244.  
George, Janossy and McCaig, 1942, *Proc. Roy. Soc.*, 180A, 219.  
Gerhart Grotzinger, P. gerald Kruger. Lloyd Smith, 1945, *Phys. Rev.*, 67, 52;  
also 68, 104; 1947, 72, 357, 360.

- Gill, P.S., 1950, *Nature*, **166**, 318.
- Heyland, G. R. and Duncanson, W. E., 1951, *Nature*, **167**, 895.
- Hummel, 1934, *Naturwissenschaften*, **22**, 170.
- Methov, E. M. De, 1951, *Nature*, **167**, 192.
- M. Delta Corte, 1946, *Atti. Accad. Nza. Lincei* (R. C. cl. Sc. Fis. Mat, Nat.), **1**, 974-82.
- " " " " 1950, *Sci. Abs.*, **53**, Ret. No 537, 59.
- Morgan, Morgan and Nielsen, 1939, *Phys. Rev.*, **55**, 995.
- Mohr and Stafford, 1944, *Proc. Roy. Soc.*, **A 183**, 54.
- Ozorai, 1944, *Z. Phys.*, **122**, (No. 5-8) 413.
- Pribsch, 1936, *Sitzungsberichte d. Wiener Akademies*.
- Rossi, B., 1934, *Int. Conf. Phys.*, **1**, 233.
- Schopper. E., Hocker, K.H. and Kuhn, G., 1951, *Phys. Rev.*, **82**, 444.
- Schmeiser and Bothe, 1938, *Ann. Phys.*, pp. 32, 161.
- Sen Chaudhury, 1948, *Ind. J. Phys.*, **22**, 106 and 341.
- Sen Chaudhury, 1949, *Science and Culture*, **15**, 38.
- Sen Chaudhury, 1951, *Phys. Rev.*, **81**, 274.
- Sen Chaudhury, and Chakravorty, I. L., 1950, *Science and Culture*, **15**, 490.
- Sinha, M.S, 1942-43, *Trans. Bose Res. Inst.*, **15**, 191.
- Soddy and Russell, 1910, *Phil. Mag.*, **19**, 725.
- Steinberg, Panofsky and Steller, 1950, *Phys. Rev.*, **78**, 802.
- Strong, 1939, *Procedures in Experimental Physics*, Prentice Hall. Inc. New York.
- Trumpy and Bergens, 1939-40, *Museum Arb. No.* **8**, 20
- Wentzel, G, 1950, *Phys. Rev.*, **79**, 710.
- Wheeler, J. A., 1946, *Ann. New York. Acad. Sci.*, **48**, 219.

# SOFT X-RAY L-SPECTRA OF Fe, Co, Ni, Cu AND THEIR OXIDES\*

BY K. DAS GUPTA AND S. B. BHATTACHERJEE

(Received for publication, November 9, 1951)

**ABSTRACT.**  $L_{2,3}$  band spectra of Fe-Cu and their oxides have been investigated in the region 13-18 Å. U. with bent mica and gypsum crystal in a Siegbahn's vacuum grating spectrograph.  $L_3$  bands of Fe-Ni have more or less the same energy width of 13-16 eV. In these elements a weak extended structure on the short wavelength side of the main  $L_\alpha$  band has been observed. The main  $L_\alpha$  band having a width of 5eV approximately, along with its extended structure on the shorter wavelength side has been considered to be the valence bands of these elements.

## INTRODUCTION

The valence bands of the elements iron, cobalt, nickel and copper consist of overlapped  $3d$ ;  $4s$ ,  $p$  bands.  $L_{2,3}$  valence band spectra of these elements reflect the energy spectra of  $3d$ ,  $4s$  electrons. The wavelength range of  $L_{2,3}$  radiations lie between 13-18 Å. and is too short compared to their M spectral region. Thus there will be some broadening of the edges due to the radiation damping in the case of the  $L_{2,3}$  valence band spectra; while in the case of M spectra, due presumably to the Auger broadening of the X-ray levels, the valence band will have some broadening effect. Moreover,  $M_2$  and  $M_3$  bands might overlap quite considerably creating complications in the point of analysis, while in the  $L_{2,3}$  region of these elements, the  $L_2$  and  $L_3$  bands are distinctly separated from each other.

The L bands of metals Fe-Ge were investigated by Gwinner (1938) using a bent crystal spectrometer.

The present investigation was undertaken to obtain,  $L_{2,3}$  bands of Fe-Cu in pure elements and in their oxides. In the case of copper oxide, special attention was given to investigate the difference in the band pattern of cuprous oxide from that of cupric oxide. Special care was taken to keep the metal surface of the target of the X-ray tube free from oxidation when studying the pure elements.

## EXPERIMENTAL RESULTS

$L_{2,3}$  bands of Fe, Co, Ni and their oxides have been investigated with a bent mica crystal in a Siegbahn's vacuum grating spectrograph. For the investigation of  $L_{2,3}$  bands of copper and its oxides, a bent gypsum crystal was used. Fine platinum wire coated with suitable oxides was used as a

\* Communicated by Prof. S. N. Bose.

rated from the  $L_a$  band. The peak position of the  $L_a$  band is at 15,930 X.U. There is a sign of a distinct short wavelength structure at 15,906 X.U. This structure appears prominently in Co-Cu alloys.

*Nickel.*—The width of the  $L_a$ -band of nickel is 15.8 eV. The peak at 14,530 X.U., lies towards the low energy side of the band. The extension on the shorter wavelength side of the main peak is quite prominent. In the case of nickel oxide, the total band width of  $L_a$  band is nearly of the same width as that in pure Nickel. The prominent structure at 14,423 X.U. in the case of nickel oxide is clearly noticeable unlike the oxides of iron and cobalt.

*Copper.*— $L_a$  or  $L_s$  band of electrolytic copper is a broad band having a width of about 19.0 eV with three distinct structures in the  $L_s$  band at 13,325, 13,267 and 13,205 X.U. In  $\text{CuO}$ , the band pattern changes considerably, as shown in the microphotometer records. In  $\text{Cu}_2\text{O}$ , there is a prominent long wavelength tailing not to be found in  $\text{CuO}$  or Cu.

### CONCLUSION

The investigation of  $L_a$  bands of Fe-Cu and their oxides clearly points out the following facts:

- (1) The valence bands, viz.:  $3d$ ;  $4s$ ,  $p$  bands, of all these elements consist of a broad band with structure.
- (2) The widths of  $L_s$  band of these elements are fairly of the same order (Table I).

TABLE I

Widths of  $L_s$  of band in eV

Fe	$\text{Fe}_3\text{O}_4$	Co	$\text{CoO}$	Ni	$\text{NiO}$	Cu	$\text{Cu}_2\text{O}$	$\text{CuO}$
13.2	13.0	13.7	...	15.8	17.0	19.0	24.0	19.0

(3) The change in the band pattern of  $L_s$  band in the case of oxides points out a change in the distribution of electron density in the valence band. The cross-transition effect will also be responsible for the difference in  $L_s$  band pattern. Electrons behaving as oxygen  $2p$  can easily fill up the  $L_s$  vacancy of the metal ion, in which case, the selection principle is not disobeyed.

(4) The most prominent structure of  $L_s$  band of these elements on the low energy side, usually referred to as  $L_a$ , possibly represents  $3d$  electrons, which shifts towards the shorter wavelength side in the case of oxides. In the case of Mg, Al, Si oxides, the shift of the valence band of the metal ion is towards the longer wavelength side.



# ***Soft X-ray L-Spectra of Fe, Co, Ni, Cu and their Oxides 559***

## **A C K N O W L E D G M E N T**

The authors are thankful to Prof . S . N . Bose , Khaira Professor of Physics, for his keen interest and helpful discussion during the progress of the work.

**KHAIRA LABORATORY OF PHYSICS,  
UNIVERSITY COLLEGE OF SCIENCE, CALCUTTA**

## **R E F E R E N C E S**

- Das Gupta. K., 1950, D Sc.Dissertation(CU)  
Gwinner, 1938, *Z. f. Phys.*, **108**, 523.  
Skinner, H.W.B., 1940, *Phil. Trans.*, **2**



# ON THE EAST WEST ASYMMETRY OF THE HARD COMPONENT OF COSMIC RAYS

BY B. BHOWMIK AND G. S. BAJWA

(Received for publication, September, 26, 1951)

**ABSTRACT.** The paper deals with the asymmetry of cosmic rays at Delhi ( $\lambda = 19^\circ$ , height 700 feet).

East west asymmetry of the hard component of cosmic rays has been measured with two telescopes of angular resolution  $10^\circ$  in the vertical plane and  $38^\circ$  in the complementary plane. The soft component was filtered out by using 10 cm of lead. Errors due to fluctuation, and relative inefficiency of the counting system were minimised by frequently exchanging the position of the telescopes with a special arrangement. The asymmetry rises to a maximum of 13% at zenith angle  $40^\circ$  and falls off at higher angles.

## INTRODUCTION

The theory of the motion of charged particles in the earth's magnetic field has been developed by Stormer (1931) and later in detail by Lemaitre and Vallarta (1933). According to their theory, at a given latitude and in a given direction, all particles having energy below a critical energy are prevented to break through the earth's magnetic field and reach the earth's surface. For a particular energy the envelope of all the allowed trajectories forms a cone; a right circular cone in case of Stormer theory and a complicated one in case of Lemaitre Vallarta theory. These cones, which separate the allowed trajectories from the forbidden ones, start opening from the western sky for positively charged particles. For the negatively charged particles they open from the eastern sky, the actual cones being the mirror image of the positively charged particles about the north-south magnetic meridian. If there is preponderance of particles of one charge over those of opposite charge, there must exist the east west asymmetry. Rossi (1930) first tried to verify experimentally the idea with a twofold coincidence telescope but failed to establish it. The first experimental evidence, however, was obtained by Johnson and Street (1933) when they found that the intensity of the cosmic rays from the western sky was greater than that from the eastern sky. The following results have been more or less established by subsequent workers. The asymmetry at sea level and at equator is about 15% and it falls off at higher latitudes to about 2% at  $\lambda = 50^\circ$ . For a given latitude, asymmetry increases with altitude. The soft component of the cosmic radiation does not show any asymmetry as was shown by Johnson (1938) from the measurement of asymmetry of the shower producing cosmic rays. There is, however, lack of accurate and systematic data specially near the equator. In the present investigation the asymmetry of only the hard component of cosmic radiation has been measured,

## APPARATUS

The two triple coincidence counter telescopes used in the present investigation subtended an angle of  $10^\circ$  in the plane of resolution and  $38^\circ$  in

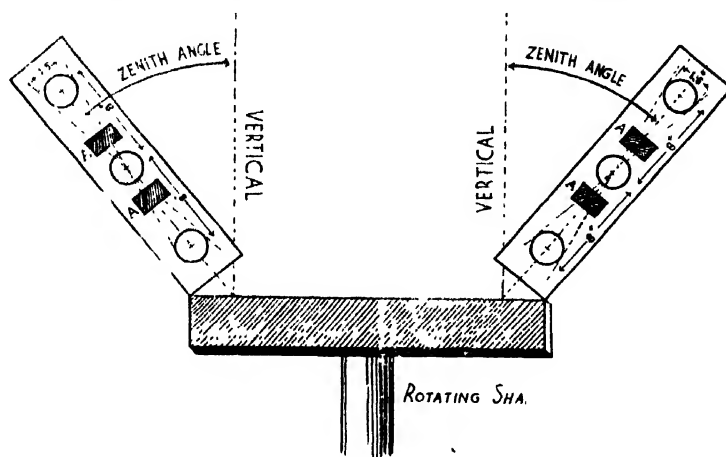


FIG. 1

Counter telescopes mounted on the rotating platform ( $\Delta = 5$  cm of lead)

the plane at right angles to that. The sensitive area was 50 sq. cm. Three argon-alcohol filled G. M. counters (conventional copper in pyrex type), having a starting potential of 1100 volts with a plateau of 250 volts, were mounted on a wooden frame to form the telescope. The central counter was completely shielded by 5 cm of lead on the top as well as bottom, so that any particle passing through all the three counters must have passed through at least 10 cm of lead. Electronically stabilised high voltage was used. The pulse from the counter was fed to a coincident circuit of Rossi type followed by a multivibrator trigger coupled to the power stage. The counts were recorded on four telephone recorders, a pair for each telescope counting east and west. The two triple coincidence telescopes were mounted along geomagnetic meridian on a rectangular wooden platform. The wooden frame of the telescopes could be tilted about two hinges to adjust the zenith angle. The platform in its turn was mounted on a rotating shaft of motor gear mechanism. The position of the telescopes were interchanged every 35 minutes with the help of a synchronous clock which starts the motor gear mechanism at the end of each interval. Each telescope, therefore, rests half the time in the east and half the time in the west for a complete cycle of 72 minutes. During the two minutes of two change over intervals in each complete cycle the mechanical recorders were automatically disconnected from the recording circuit.\* After every change over the recording circuit was also interchanged automatically so as to replace the recorder by the one relevant to the new azimuthal position of the telescope. The above method, which is called method of cycles, has several advantages, for it avoids

\* The authors are indebted to Dr. P. S. Gill for the automatic mechanism of the apparatus which was kindly loaned by him.

- (a) any instrumental selectivity
- (b) any short period change of cosmic ray intensity
- (c) any change of cosmic ray intensity due to sudden barometric change, magnetic disturbance or any other cause.

The whole assembly was mounted in a specially constructed room covered with cement asbestos sheet on the roof of the Physics Laboratory.

### RESULTS AND DISCUSSIONS

Table I shows the asymmetry of the hard component against zenith angle

TABLE I

Zenith angle	Azimuth	Intensity $I = \text{counts per minute}$	Asymmetry = $\frac{2(I_w - I_e)}{I_w + I_e}$
0°		.5204 ± .0093	
14°	West	.4807 ± .0089	.0729 ± .0273
	East	.4169 ± .0086	
23.5°	West	.4555 ± .0087	.1162 ± .0277
	East	.4052 ± .0082	
35°	West	.3108 ± .0061	.1274 ± .0262
	East	.3000 ± .0058	
47°	West	.2175 ± .0055	.1304 ± .0260
	East	.2175 ± .0043	
62°	West	.1050 ± .0030	.0695 ± .0413
	East	.0988 ± .0029	

From the graph in figure 2, it is evident that asymmetry first rises to a maximum of 13% at a zenith angle of about 40° and then falls off at higher zenith angles. Purely from the theoretical considerations it should increase continuously with the zenith angle. That will be true only for the primary particles. The field sensitive particles are absorbed by the thickness of air that they have to traverse before they reach surface of the earth. The same explanation is offered for higher values of asymmetry at high altitudes where more of field sensitive particles can reach due to lesser absorption. Comparing with the data obtained by Bhattacharya (1942) and Gill (1941) we find that there is general agreement. But there is some amount of discrepancy with the data obtained by Sharma and Sarna (1948) for the unabsorbed radiation at Lahore which is situated very nearly on the same geomagnetic latitude as Delhi. Further work is in progress.

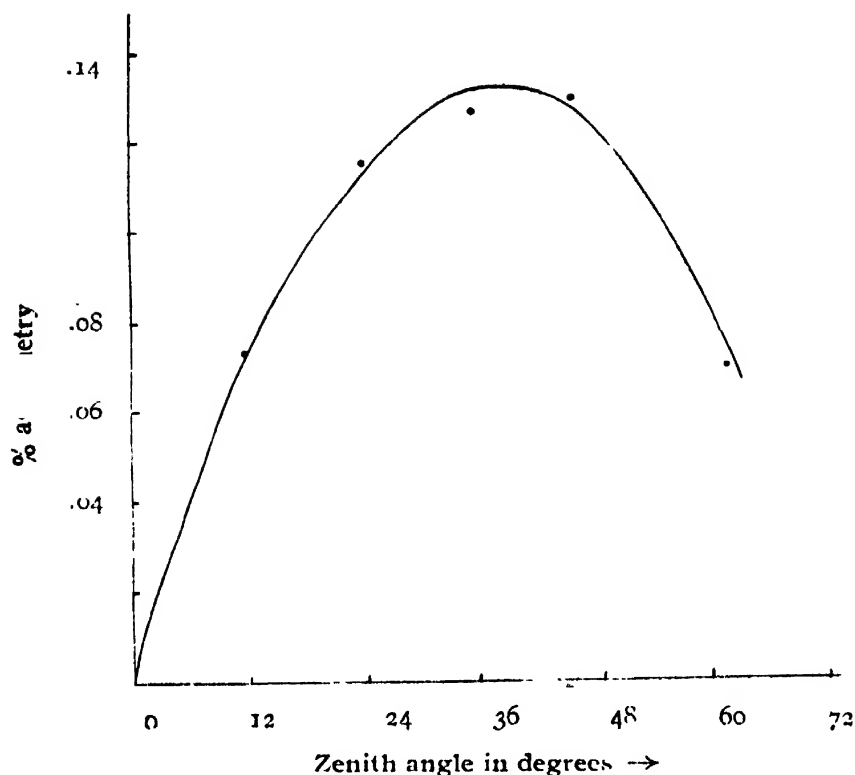


FIG. 2

Graph showing asymmetry at various zenith angles

#### ACKNOWLEDGMENTS

The authors are grateful to Prof. R. C. Majumdar, Head of the Department of Physics, University of Delhi, for his guidance and encouragement, and to Prof. P. S. Gill for useful discussions on the subject. One of us (G. S. B.) is indebted to A. E. C. for the research fellowship granted to him.

DEPARTMENT OF PHYSICS,  
UNIVERSITY OF DELHI.

#### REFERENCES

- Bhattacharya, P. C., 1942, *Proc. Nat. Inst. Sc. Ind.*, **8**, 263.  
 Gill, P. S., 1941, *Proc. Nat. Acad. Sciences Ind.*, **2**, 26.  
 Johnson, and Street, 1933, *Phys. Rev.*, **43**, 381.  
 Johnson, T. H., 1938, *Rev. Mod. Phys.*, **10**, 228.  
 Rossi, B., 1930, *Phys. Rev.*, **36**, 606.  
 Sharma, O. P. and Sarna, H. R., 1948, *Ind Jour. Phys.*, **22**, 19.  
 Stormer, C., 1931, *Ergebnisse der Kosmischen Physik*, **1**, P. I.  
 Vallarta, M. S., 1933, *Phys. Rev.*, **41**, 1.

# SINGLE-PHASE OPERATION OF THREE-PHASE MOTORS\*

BY P. VENKATA RAO AND CHANDRA SEKHAR GHOSH

(Received for publication, November 10, 1951)

**ABSTRACT.** Single-phase operation of three-phase motors has been a subject of interest to both design and operating engineers. A large amount of literature exists, in most of which the method of symmetrical components analysis has been used, for the analysis of performance of three-phase motors with unbalanced voltages. In this paper the method of Dyadic circuit analysis developed by Sah is applied to the problem of operation of three-phase motors from single-phase supply and the necessary relationships have been developed of the complete performance characteristics from standstill to synchronous speed with auxiliary impedances in circuit.

A considerable amount of work has been done on the subject of single-phase induction motors which use split-phase starting. The existing literature on these machines deals with the auxiliary impedances required and the torque developed. The use of auxiliary impedances in the single-phase operation of polyphase motors is also well known.

When a polyphase motor is operated from a single-phase supply, and auxiliary impedances are used to shift the phase currents and the motor terminal voltages so that the currents and voltages of the motor are properly balanced both as to phase and magnitude, the motor will operate as though it were supplied from its normal polyphase line. The two common methods in use are the series impedance method and the shunt impedance method. By a judicious choice of the resistance and reactance values of the auxiliary impedances it is possible to have reasonably good balancing, both as regards phase and magnitude of the currents and voltages. It happens quite often that the external impedances are used only for starting purposes, the motor being kept running with two of its terminals connected direct to the single-phase line, the third terminal being left open.

Due to the fact that the motor current and power factor both change as the speed changes, the auxiliary impedances required also must change with the motor speed. Of interest, therefore, is the determination of the performance characteristics of a three-phase motor on single-phase supply over the complete speed range from standstill to synchronous speed with the auxiliary impedance in circuit.

Lumin (1936) in his paper, outlines a method that is quite general but the utility of his method is limited by the tedious algebra involved. Reed and Koopman (1936) have presented an analysis which is neither so tedious nor highly involved. They use the exact equivalent circuit and the analytical

\* Communicated by Prof. P. C. Mahanti.

determination of the characteristics which are familiar to all designers of induction motors. In their paper they have also applied the analysis to the performance of some motors under various conditions of starting and operating with auxiliary capacitance.

Tracy and Wyss (1935) have analysed the problem of split-phase starting of three-phase motors and have arrived at some very useful conclusions. They determined the best values of resistance and reactance for series and shunt methods of split-phase starting. In the first method, the starting current is not restricted to any particular value as in the second to obtain the maximum starting torque. In the analysis, a direct solution is visualised whereby the optimum values of resistance, reactance or capacitance can be arrived at for maximum starting torque with an arbitrarily fixed starting current in the line. Thacker and Gopalakrishna (1948), in their paper have extended the work of Tracy and Wyss using the same method of symmetrical components. In their paper, methods of calculations are presented for the determination of the complete performance characteristics from standstill to synchronous speed of a three-phase motor on a single-phase supply with the auxiliary impedances in circuit. They have set up equations taking into account generalized impedances so that the equations may be applicable to any combination of resistances, reactances and capacitances. However, the final relations for the line currents, voltages and torque are expressed in terms of the sequence impedances. The vector diagrams drawn for the equivalent circuit of the motor with the auxiliary impedances are also incomplete. Further, the steps required in arriving at the final relationships are also long and involved.

The Dyadic circuit analysis method developed by Sah (1939) offers an extremely simple and short method of calculating the performance of three phase motors under unbalanced voltages. In this paper, simple calculations are given by the method of Dyadic algebra for the exact determination of the complete performance characteristics from standstill to synchronous speed of a three-phase motor run from single-phase supply with auxiliary impedances in circuit. The correct vector diagrams for the currents and voltages for conditions with series impedance and shunt impedance in circuit are given. Expressions for the starting torque and starting current have been obtained in terms of phase impedances. This is an advantage compared to the other formula developed previously in which the relationships have been obtained in terms of the sequence impedances. By simple substitution of the sequence impedance values in the final formula for the current, the relationships developed here are shown to agree with those developed by other authors.

Finally, as a matter of interest, the method has been applied to the most commonly employed system in which a capacitance is placed in shunt across two of the phases, while no other impedance is used in the other branch. Expressions for the line current, sequence currents and torque are developed for this arrangement.



## SERIES IMPEDANCE METHOD OF OPERATION

Figure 1(a) gives the equivalent circuit with series impedances and the vector diagram for the currents and voltages with this arrangement is given in figure 1(b).

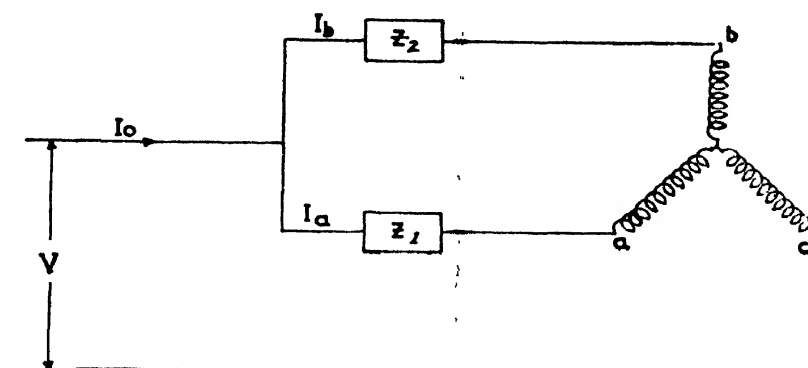


FIG. 1(a)

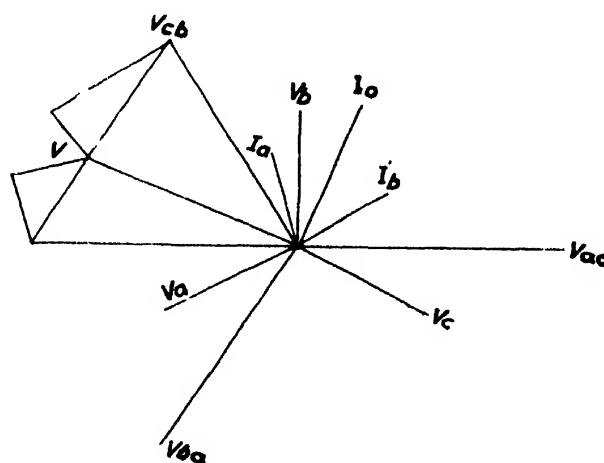


FIG. 1(b)

Vector diagram of series impedance circuit

The fundamental voltage equations are

$$\left. \begin{aligned} V_a &= AI_a + CI_b + BI_c \\ V_b &= BI_a + AI_b + CI_c \\ V_c &= CI_a + BI_b + AI_c \end{aligned} \right\} \quad \dots (1)$$

where  $V_a$ ,  $V_b$ , and  $V_c$  are the voltages to the neutral in the respective phases.

Referring to figure 1 (a) and by use of Kirchhoff's laws,

$$\left. \begin{aligned} I_o &= I_a + I_b \\ I_c &= -I_o \end{aligned} \right\} \quad \dots (2)$$

$$V = I_a Z_1 - V_{ac} = I_b Z_2 - V_{bc} \quad \dots (3)$$

Since power input is  $VA$ ,

$$\text{Efficiency} = \frac{T(1-s) - (F + W)}{VA}$$

#### SHUNT IMPEDANCE METHOD OF OPERATION

The schematic circuit arrangement is shown in figure 2(a). Figure 2(b) gives the vector diagram for the currents and voltages in the circuit of figure 2(a).

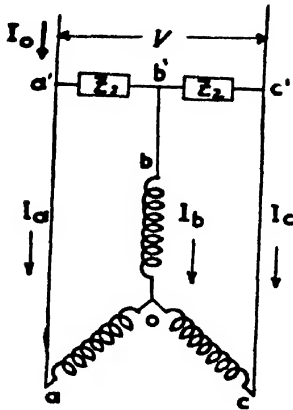


FIG 2(a)

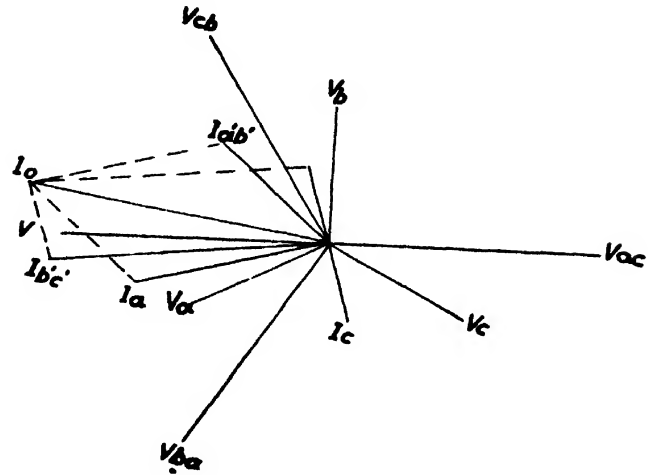


FIG 2(b)

Vector diagram of shunt impedance circuit

By use of Kirchoff's law,

$$I_b = -(I_a + I_c)$$

$$I_o = I_a + \frac{V_{ba}}{Z_1} = \frac{V_{cb}}{Z_2} - I_c \quad \dots (17)$$

and

$$V = V_{ca} \quad \dots (18)$$

Hence, by using the fundamental voltage equations (1)

$$\left. \begin{aligned} V_a &= I_a(A - C) + I_c(B - C) \\ V_b &= I_a(B - A) + I_c(C - A) \\ V_c &= I_a(C - B) + I_c(A - B) \end{aligned} \right\} \quad \dots (19)$$

Using the same notations  $K$ ,  $M$  and  $N$  as before, from equations (18) and (19), it follows

$$\left. \begin{aligned} V' = V_{ca} &= I_a(-N) + I_c M \\ V_{ba} &= I_a K + I_c(-N) \\ V_{cb} &= I_a M + I_c(-K) \end{aligned} \right\} \quad \dots (18a)$$

From equation (17) therefore

$$Z_1 I_o = Z_1 I_a + V_{ba} = Z_1 I_a + I_a K + I_c(-N) = I_a(K + Z_1) - I_c N \quad \dots (20)$$

Similarly,

$$Z_2 I_o = I_a M - I_c(K + Z_2) \quad \dots (21)$$

Solving for  $I_a$  and  $I_c$

$$\left. \begin{aligned} I_a &= \frac{I_o \{Z_1(K + Z_2) - NZ_2\}}{(K + Z_1)(K + Z_2) - MN} \\ I_c &= \frac{I_o \{MZ_1 - Z_2(K + Z_1)\}}{\{(K + Z_1)(K + Z_2) - MN\}} \end{aligned} \right\} \dots (22)$$

Substituting these values of  $I_a$  and  $I_c$  in (18a)

$$V = I_o \left[ \frac{-N\{Z_1(K + Z_2) - NZ_2\}}{\{(K + Z_1)(K + Z_2) - MN\}} + \frac{M\{MZ_1 - Z_2(K + Z_1)\}}{\{(K + Z_1)(K + Z_2) - MN\}} \right]$$

Hence

$$I_o = \frac{V\{(K + Z_1)(K + Z_2) - MN\}}{[N^2Z_2 - NZ_1(K + Z_2) + \{M^2Z_1 - MZ_2(K + Z_1)\}]} \dots (23)$$

It is thus possible to predetermine the value of the line current from the known values of the auxiliary impedances and the phase impedance. Since  $K, M, N$  can be easily determined for any value of slip, it is possible to determine the current  $I_o$  at any slip.

The conditions at standstill are,

$$Z_+ + Z_- = Z ; B = C$$

$$M = N = B - A = -Z$$

$$K = 2Z$$

Hence, by substitution in (23)

$$I_o = \frac{V\{(K + Z_1)(K + Z_2) - M^2\}}{[N^2Z_2 - NZ_1(K + Z_2) + M^2Z_1^2 - MZ_2(K + Z_1)]} \dots (24)$$

In terms of symmetrical components

$$MN = (o^2Z_+ + aZ_-)(aZ_+ + a^2Z_-) = Z_+^2 + Z_-^2 - Z_+Z_-$$

$$M^2 = aZ_+^2 + a^2Z_-^2 + 2Z_+Z_-$$

$$N^2 = a^2Z_+^2 + aZ_-^2 + 2Z_+Z_-$$

$$K^2 = Z_+^2 + Z_-^2 + 2Z_+Z_-$$

∴ From (23)

$$I_o = \frac{V[Z_1Z_2 + (Z_1 + Z_2)(Z_+ + Z_-) + 3Z_+Z_-]}{[(Z_+ + Z_-)Z_1Z_2 + 3Z_+Z_-(Z_1 + Z_2)]} \dots (23a)$$

and from (24)

$$I_o = \frac{V[Z_1Z_2 + 2Z(2Z_1 + Z_2) + 3Z^2]}{[2ZZ_1Z_2 + 3Z^2(Z_1 + Z_2)]} \dots (24a)$$

also

$$I_a = I_o \frac{Z_1(Z_2 + 2Z) + ZZ_2}{(Z_1 + 2Z)(2Z + Z_2) - Z^2}$$

$$I_c = I_o \frac{-2Z_1 - Z_2(Z_1 + 2Z)}{(Z_1 + 2Z)(Z_2 + 2Z) - Z^2}$$

and the positive and negative sequence currents are

$$\left. \begin{aligned} I_+ &= \frac{I_a(1-a) + I_c(a^2-a)}{\sqrt{3}} \\ I_- &= \frac{I_a(1-a^2) + I_c(a-a^2)}{\sqrt{3}} \end{aligned} \right\} \quad \dots (25)$$

as before, torque  $T = 3 \left[ \frac{r'}{s} \left| I_+ \right|^2 - \frac{r''}{(2-s)} \left| I_- \right|^2 \right] \quad \dots (26)$

#### A particular case

The special case in which a capacitance is connected across two of the phases while there is no impedance connected across the other side is shown diagrammatically in figure 3(a) and the corresponding vector diagram for currents and voltages is given in figure 3(b).

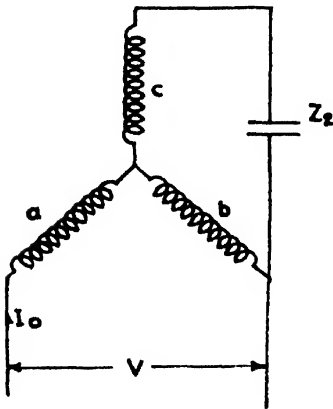


FIG. 3(a)

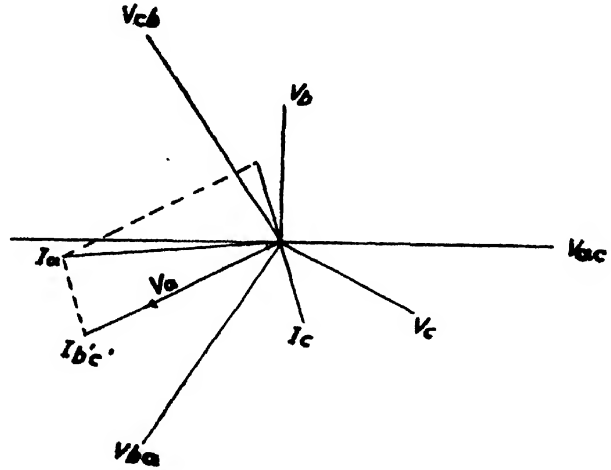


FIG. 3(b)

Vector diagram of capacitor in shunt circuit

As shown in figure 3(a), the conditions in this case are

$$Z_1 = \infty \text{ and } Z_2 = -jX$$

Hence from equation (24a), after dividing the numerator and denominator by \$Z\_1\$

$$I_{+1} = V \left[ \frac{Z_2 + 2Z + (Z/Z_1)(3Z + 2Z_2)}{2ZZ_2 + 3Z^2 + 3Z^2Z_2/Z_1} \right]$$

Now, substituting the values of \$Z\_1\$ and \$Z\_2\$ in this case,

$$I_{+1} = \frac{V(2Z - jX)}{Z(3Z - 2jX)} \quad \dots (27)$$

In the same way, substituting the values for \$Z\_1\$ and \$Z\_2\$ in eqn. (23a) after proper transformation, the current during running condition is

$$I_o = \frac{V(Z_+ + Z_- - jX)}{[3Z_+ Z_- - jX(Z_+ + Z_-)]} \quad \dots (28)$$

The values of  $I_+$  and  $I_-$  are the same as given in equation (25). The currents in the other branches at standstill condition are also determined as below.

Since  $I_a = I_o$ , and  $Z_2 = -jX$ , in this case, and remembering that  $M = -Z$  and  $K = 2Z$  at standstill, from equation (21)

$$I_c = I_o \frac{(M - Z_2)}{(K + Z_2)} = I_o \left\{ \frac{-(Z + Z_2)}{(2Z + Z_2)} \right\} = I_o \left\{ \frac{-(Z - jX)}{(2Z - jX)} \right\}$$

After substituting for  $I_o$ , the expression obtained in (27)

$$I_c = I_o \left\{ \frac{-(Z + jX)}{Z(3Z - 2jX)} \right\} \quad \dots (29)$$

Substituting for  $I_a$  and  $I_c$  in equations (25)

$$\begin{aligned} \sqrt{3}I_+ &= V \left\{ \frac{(2Z - jX)(1 - a)}{Z(3Z - jX)} + \frac{(Z + jX)(a^2 - a)}{Z(3Z - 2jX)} \right\} \\ &= V \left\{ \frac{3Z + jX(a^2 - 1)}{Z(3Z - 2jX)} \right\} \quad \dots (30a) \end{aligned}$$

$$\text{Similarly} \quad \sqrt{3}I_- = V \left\{ \frac{3Z + jX(a - 1)}{Z(3Z - 2jX)} \right\} \quad \dots (30b)$$

$$\text{torque} \quad T = 3 \left[ \frac{r'}{s} |I_+|^2 - \frac{r''}{(2-s)} |I_+|^2 \right]$$

*Symbols used in the paper*

$V_a, V_b, V_c$  - Voltages of the three respective phases to neutral

$Z_1, Z_2$  - External auxiliary impedances

$T$  - Torque developed in synchronous watts

$P$  - Power converted to mechanical form

$F + W$  - Friction and windage loss in watts

$Z$  - Machine phase impedance

$Z_+, Z_-$  - Positive and negative sequence impedances

$A, B, C$  - Respective phase impedance parameters of the machine

$I_o$  - Single-phase line current

$I_+, I_-$  - Sequence components of current

$V$  - Applied single-phase voltage.

The steady state values for the machine constants are :

$$A = r_a + jX_a + \frac{3X_m^2}{4} \left\{ \frac{s}{(r_x + jsX_x)} + \frac{2-s}{\{r_x + j(2-s)X_x\}} \right\}$$

$$B = -jX_{ab} + \frac{3X_m^2}{4} \left\{ \frac{a^2 s}{(r_x + jsX_x)} + \frac{a(2-s)}{\{r_x + j(2-s)X_x\}} \right\}$$

$$C = -jX_{ab} + \frac{3X_m^2}{4} \left\{ \frac{as}{(r_x + jsX_x)} + \frac{a^2(2-s)}{\{r_x + j(2-s)X_x\}} \right\}$$

DEPARTMENT OF POWER ENGINEERING  
INDIAN INSTITUTE OF SCIENCE, BANGALORE.

#### REFERENCES

- Lumm, E. O., 1936, *Trans. A. I. E. E.*, **55**, 387.  
 Reed, H. R. and Kyopman, R. J. W., 1936 *Trans. A. I. E. E.*, **55**, 1206.  
 Tracy, G. F., and Wyss, W. E., 1935, *Trans. A. I. E. E.* **54**, 1068.  
 Thacker, M. S., and Gopalakrishna, H. V., 1948, *Electrotechnics*, **20**, 82.  
 Sah, A. Pen-Tung, 1939, "Dyadic Circuit Analysis" International Text Book Co.,  
 Scranton, Pa.

# ON THE FLUORESCENCE IN DIAMOND EXCITED BY X-RAYS\*

By B. M. BISHUI.

(Received for publication, November 30, 1951)

Plate XXI

**ABSTRACT.** The fluorescence of four specimens of diamond of Type I (common) and of one specimen of diamond of Type II (rare) has been excited by X-rays and the spectra have been photographed with a spectrograph of high light-gathering power and moderate dispersion. The spectra have been compared with those excited by ultraviolet light. It has been observed that all the four specimens of Type I show continuous fluorescence extending from  $5650 \text{ \AA}$  upto about  $3700 \text{ \AA}$ . In the case of two specimens showing strong absorption band at  $4156 \text{ \AA}$ , the fluorescence spectrum excited by X-rays shows an absorption band at this position accompanied by a few other similar bands on the shorter wave-length side. The diamond of Type II does not show any fluorescence in the visible region when irradiated by X-rays. These results are contradictory to those published by Ramachandran (1946) who claimed to have observed bands in the spectrum of fluorescence excited by X-rays in diamond of Type I, and weak fluorescence in diamond of Type II.

It is shown that these results can be explained only on the hypothesis that the fluorescence is due to presence of chemical impurities in the lattice of diamond of Type I and that diamond of Type II contains no such impurity.

## INTRODUCTION

It was shown in a paper published earlier (Bishui, 1950) that the fluorescence of diamond is due to presence of some impurity in the lattice, the latter acting as a phosphor in presence of the impurity, and that the absence of fluorescence in diamond of Type II, which is transparent to ultraviolet light beyond  $3000 \text{ \AA}$ , is due to the absence of such impurity. The fluorescence spectrum of diamond excited by X-rays was compared previously by Ramachandran (1946) with the spectrum of fluorescence excited by ultraviolet light in the case of a particular specimen of diamond and it was observed that the  $4156 \text{ \AA}$  band appeared as an absorption band in the spectrum excited by X-rays, although its companions on the longer wavelength side were present as emission bands. In the spectrum excited by ultraviolet light in the same specimen, the  $4156 \text{ \AA}$  band was the strongest of all the bands in the visible region. It is difficult to understand, however, how the same specimen which does not absorb completely the band at  $4156 \text{ \AA}$  excited by ultraviolet rays, can absorb completely the same band excited by X-rays. It was, therefore, thought worthwhile to study the fluorescence spectra of

\* Communicated by Prof. S. C. Sirkar.

a few specimens of diamond of Type I and Type II excited by X-rays in order to understand the mechanism of excitation of the fluorescence in the crystal by these rays. The present paper deals with the results obtained with D I, D II, D V and D VI of Type I and D IV of Type II described in an earlier paper (Bishui, 1950).

#### EXPERIMENTAL TECHNIQUE

A commercial medical unit manufactured by Picker X-ray Corporation was used for the irradiation of the crystals with X-rays. The tube is a sealed one and it is provided with a filament cathode and an arrangement for cooling the target with circulating oil. The tube was operated at 4 MA. and 45 KV. A lead disc, about 1 cm. thick and provided with a small hole was placed on the window to get a narrow beam of X-rays, and to stop any light that may come from the inside of the X-ray tube the aperture in the lead disc was closed with black paper. The specimen of diamond was placed on a stand and it was completely covered by a light-tight box provided with two windows through one of which X-rays were passing through the crystal and through the other the light emitted by the crystal came out and was focused on the slit of the spectrograph. As preliminary investigations showed that the fluorescence excited under the conditions mentioned above was weaker than that excited by a mercury arc in quartz tube. An Adam Hilger two-prism glass spectrograph of high light-gathering power was used to photograph the spectrum. Special care was taken to ensure that no day light could in any way enter into the slit of the spectrograph or into the box containing the specimen of diamond. On observing visually through the spectrograph, it was found that the spectrum of the light emitted by any diamond of Type I was a continuous one and it disappeared as soon as the X ray tube was switched off. In the case of D IV, which is of Type II, no fluorescence could be detected on visual observation. The spectra were next photographed, using in each case an exposure of about 15 hours. The width of the slit of the spectrograph had to be increased to about 0.5 mm in order to diminish the time of exposure to a reasonable value. The spectrum of fluorescence excited by ultraviolet light was photographed with the same slit-width in a particular case for comparison. Gevaert 'superchrome' plates were used.

#### RESULTS AND DISCUSSION

The spectrograms obtained in the case of the five specimens excited by X-rays are reproduced in figures 1-5 in Plate XXI and figure 6 shows the spectrogram obtained in the case of D VI excited by light from a mercury arc in silica tube. It can be seen that all the four specimens DI, DII, DV and DVI show continuous fluorescence extending from about 5650 Å upto about 3700 Å, and in the case of DII and DVI the spectrum shows the



absorption band at  $4156 \text{ \AA}$  together with a few other such bands on the shorter wave-length side. These absorption bands are not present in the spectra due to DI and DV, because, as pointed out earlier (Bishui, 1950), these specimens do not show absorption band at  $4156 \text{ \AA}$  at room temperature, although the band appears at  $-180^\circ\text{C}$ . The spectrogram due to DIV is a blank one, showing that there is no fluorescence in any part of the visible region.

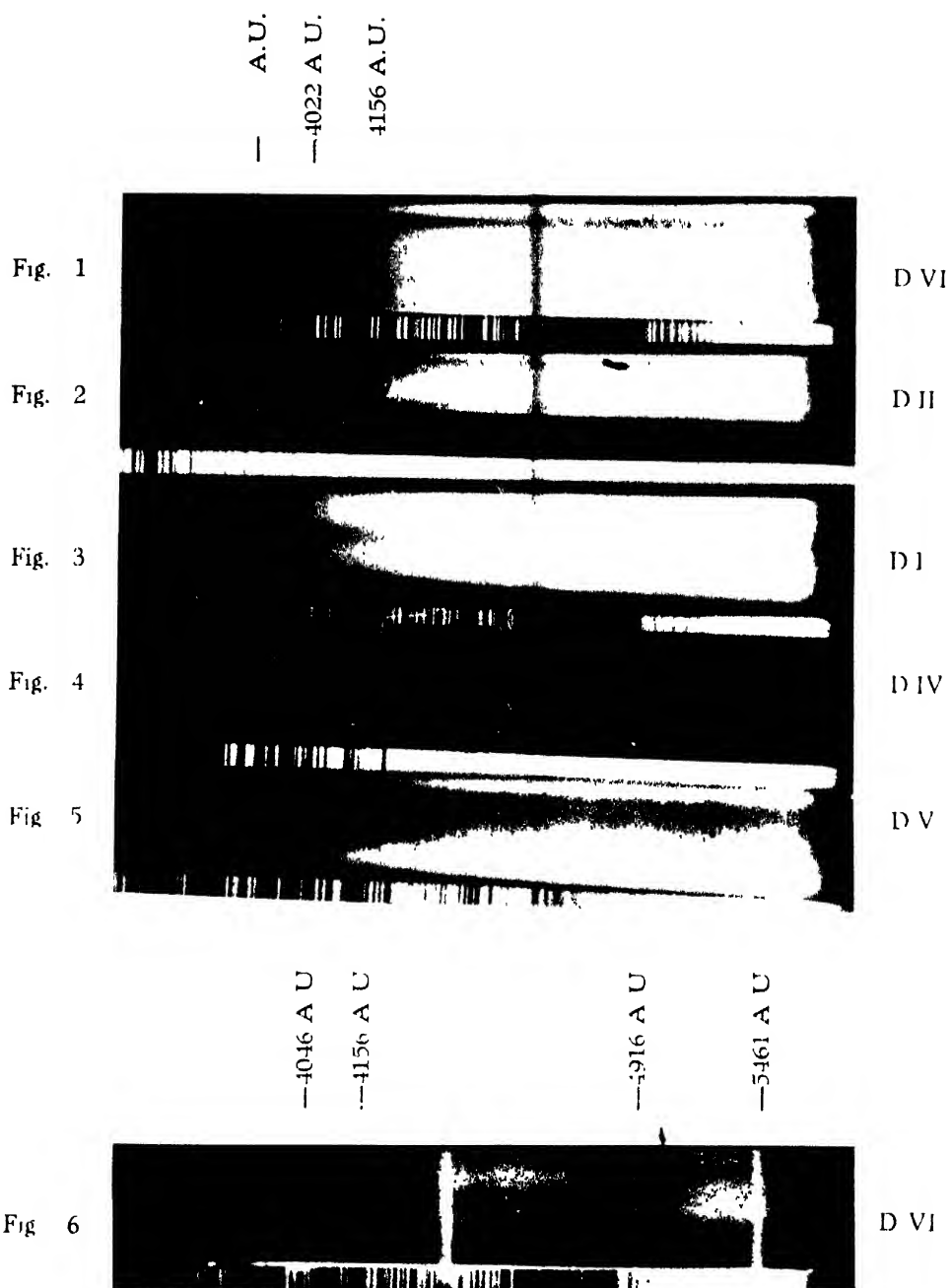
The results mentioned above do not agree with those reported by Ramachandran (1946) who claimed to have observed emission bands in the fluorescence spectrum of diamond excited by X-rays. The spectrum is a continuous one with large intensities in the region between  $4200 \text{ \AA}$  and  $5600 \text{ \AA}$ . Figure 6, however, shows that bands are observed, using the same slit-width of the spectrograph, in the case of excitation by mercury lines. The absence of any fluorescence in the case of DIV irradiated by X-rays is also contradictory to the conclusion arrived at by Ramachandran (1946) that diamond of Type II fluoresces feebly on being irradiated by X-rays. The conclusion arrived at by Bull and Garlick (1950) that all specimens of diamond of fluorescent and non-fluorescent types fluoresce when irradiated by X-rays is not generally true, because DIV, which is transparent in the region of  $2250 \text{ \AA}$ , does not show any fluorescence in the visible region under X-ray excitation.

It is evident from the above facts that for the appearance of bands in the fluorescence spectrum of diamond the exciting energy should be of such a magnitude that it should raise the electron to the excited state corresponding to the absorption band at  $4156 \text{ \AA}$  or to the sub-levels lying above it. If the excitation energy is much higher than this the electron is raised to the conduction level and it produces a continuous spectrum in the fluorescence. This statement is supported by the fact observed earlier (Bishui 1950) that when the Hg line  $4046 \text{ \AA}$  is used for excitation only sharp bands appear in the fluorescence spectrum in the case of diamond of Type I, but when the whole ultra-violet light emitted by the mercury arc in silica tube is used for excitation, the fluorescence spectrum consists of bands superposed on a continuous background. In the case of X-ray excitation the electrons are raised only to conduction levels. The fact that the absorption band at  $4156 \text{ \AA}$  with its companions on the shorter wave-length side appear in the continuous fluorescence excited by X-radiation in diamond of Type I shows that the ground and excited levels of these bands are not affected by the presence of photo-electrons in the lattice. The absence of the emission bands, however, shows that the photo-electrons do not return to the upper metastable states from which they can jump back to the ground level to produce the bands. If the electrons would return from conduction level to the ground level including its sub-levels a continuous spectrum with its long wavelength limit somewhere at  $4200 \text{ \AA}$  would be produced. Since a continuous spectrum extending from about  $3700 \text{ \AA}$  upto about  $5650 \text{ \AA}$  is emitted by diamond of

Type I irradiated by X-rays, we have to postulate a different type of transition to explain the origin of the portion of the continuous spectrum having wavelengths longer than  $4200 \text{ \AA}$ . It is essentially necessary to assume the presence of chemical impurities to account for this portion of the continuous fluorescence spectrum. Probably the conduction electrons find atoms of impurity around them and are captured by these atoms more easily than by the carbon atoms and the corresponding radiations produce the continuous spectrum extending from  $4200 \text{ \AA}$  upto about  $5650 \text{ \AA}$ . Radiation of wavelengths shorter than  $4156 \text{ \AA}$  is also present in the spectrum of fluorescence and this may be due to transitions of the conduction electron to the ground level of the diamond lattice corresponding to the absorption band at  $4156 \text{ \AA}$ . Had the fluorescence been due to pure diamond lattice without any impurity, the fluorescence spectrum would be the same for both ultraviolet and X-ray excitation, because Roth (1949) has come to this conclusion in the case of pure anthracene crystal.

The occurrence of transport of energy through solids has been demonstrated by the results reported by Bowen *et al* (1949). It has also been shown by several authors (Kallman and Furst, 1950, Ageno, Chiozotto and Querzoli, 1949) that some liquids containing small quantities of impurities fluoresce appreciably on being irradiated by X-rays or  $\gamma$ -rays. The phenomenon has been explained on the assumption that the pure liquid itself does not fluoresce owing to self extinction, but the energy absorbed by the molecules of the solvent is transferred to the impurity molecules in which the energy is trapped and is thus radiated by the latter molecules as fluorescence. In the case of diamond excited by X-rays probably similar transfer of energy takes place. The band at  $4156 \text{ \AA}$  and its companions may be due to the carbon atoms of diamond lattice linked in some way to impurity molecules. The impurity atoms or molecules may have independent fluorescence radiation which is ordinarily weak but brightens up when the energy absorbed by most carbon atoms is transferred to those impurity atoms or molecules. Such a process may give rise to the continuous fluorescence which is observed in the region from  $4200 \text{ \AA}$  to  $5650 \text{ \AA}$ .

Ramachandran and Chandrasekharan (1946) and later Bull and Garlick (1950) have concluded that as the fluorescence band at  $4156 \text{ \AA}$  is a doublet, it may be due to transitions  $^1S_0 - ^3P_1$  and  $^1S_0 - ^3P_2$  in the carbon atom, these forbidden transitions being allowed in the lattice owing to influence of lattice-defect. It was pointed out, in an earlier paper (Bishui 1950) however, that the fluorescence band at  $4156 \text{ \AA}$  is not a doublet, but it is a single one and its appearance as a doublet in thick crystals is due to self-reversal. Their hypothesis that only lattice-defect without the presence of any chemical impurity is the cause of fluorescence can not explain the facts observed in the present investigation. First, the portion of the continuous spectrum of wavelength longer than band  $4156 \text{ \AA}$  cannot be due to transitions



Fluorescence of diamond

Figs. 1—5. Fluorescence excited by X-rays

Fig. 6. " " " Ultraviolet light



from conduction levels to any sub-level of the ground level of the absorption band at  $4156 \text{ \AA}$ . Secondly, the total absence of the fluorescence in D IV under X-ray excitation cannot be due to want of lattice-defect in the crystal, as the crystal is highly birefringent and is full of local flaws. The fact observed by Blackwell and Sutherland (1949) that a particular specimen of diamond, which does not show fluorescence and absorption bands at  $4156 \text{ \AA}$  and yet exhibits yellow fluorescence, cannot be explained by assuming the fluorescence to be due to lattice-defect in pure diamond lattice, because such lattice-defect would produce, according to the hypothesis of Bull and Garlick (1950), only blue fluorescence. Probably, impurities of different types are responsible for the fluorescence in the blue and yellow regions and when both the impurities are present in the same specimen it exhibits fluorescence in both the regions, as observed in the case of D I and D VI earlier (Bishui, 1950). The absence of the bands in the spectrum of fluorescence excited by X-ray in diamond of Type I and the presence of strong continuous spectrum on the longer wavelength side of  $4200 \text{ \AA}$  thus show that chemical impurities are responsible for such emissions.

Another feature of the fluorescence of some specimens of diamond observed by Sir C. V. Raman (1951) can be explained on the hypothesis mentioned above. It was observed by him that in some specimens showing banded green luminescence there was correlation between birefringence and luminescence observed at different parts of the crystal for its different orientations. As pointed out earlier (Bishui, 1950), the birefringence may be due to frozen-in ultrasonic waves and any trace of impurity present in the melt is likely to collect at the nodes of these stationary ultrasonic waves. In such a crystal the planes containing the impurities are likely to be highly birefringent and regions in the neighbourhood of these planes will also fluoresce strongly according to the hypothesis given above. The fluorescent portions of such a crystal will, therefore, appear to have a banded structure.

The hypothesis of presence of chemical impurity in diamond of Type I and its absence in diamond of Type II can also explain the nature of photo-conductivity of these two types. Photo-electrons ejected in the lattice fall into traps created by the impurities and are recaptured in the atoms in diamond of Type I, while in diamond of Type II, the number of the photo-electron is not diminished in this way and, therefore, Ohm's law is obeyed, as shown by Robertson Fox, and Martin (1934).

#### ACKNOWLEDGMENTS

The author is indebted to Prof. S. C. Sirkar for his kind interest and helpful suggestions during the progress of the work and to Prof. M. N. Saha, F.R.S. for kindly lending the Hilger two-prism spectrograph.

## REFERENCES

- Ageno, Chiozzotto and Querzoli, 1949, *Acc. dei Lincei*, **6**, 626.  
Bishui B. M., 1950, *Ind. J. Phys.*, **24**, 441.  
Blackwell, E. D. and Sutherland, G.B.B.M., 1949, *Jour. de Chimie Physique*, **46**, 9.  
Bowen, E. J., Mikiewicz, E. and Smith, F W , 1949, *Proc. Phys. Soc. A*, (London) **62**, 26.  
Bull, C. and Garlick, G.F.J., *Proc. Phys. Soc. A* (London), **63**, 1283.  
Kallman, H. and Furst, M, 1950, *Phys. Rev.*, **79**, 857.  
Ramachandran, G. N., 1946, *Proc. Ind Acad. Sc.*, **24A**, 81.  
Ramachandran, G. N. and Chandrasekharan, V., 1946, *Proc Ind. Acad. Sc* , **24A**, 176.  
Raman, Sir C. V., 1951, *Current Science*, **20**, 55.  
Robertson, R., Fox J. J. and Martin, A. E., 1934, *Phil. Trans. Roy. Soc. A*, **232**, 463.  
Roth, L., 1949, *Phys. Rev.*, **75**, 983.

# STUDIES ON THE SHARP EXTRA REFLECTIONS FROM PHLOROGLUCINE DIHYDRATE CRYSTAL

Part I. Effect of Orientation of the Crystal with respect to  
the X-ray Beam.

By M. N. DATTA

(Received for publication, December 1, 1951)

Plate XXII A-D

**ABSTRACT.** The sharp extra reflections from phloroglucine dihydrate have been studied for various orientations of the crystal with respect to the incident X-ray beam. It has been found that the variations of the intensities of the spots are extremely slow and continuous as the crystal rotates from one Bragg position to another with the same values of  $h$  and  $k$  indices. The intensities are maxima at the Bragg positions and pass through minimum values at intermediate positions. The extra spots with indices  $h=0$  or  $k=0$  are not absent when the incident beam is inclined to the  $c$ -axis.

Extra reflections in Laue photographs have been studied very extensively during the last decade in various laboratories. The phenomena observed are usually described as diffuse spots and are explained as originating from thermal elastic waves. It was, however, pointed out by Raman and Nilakantan (1940) that there are extra spots due to the (111) planes of diamond which are very sharp. This was later corroborated by Lonsdale (1942). A very interesting series of extremely sharp extra spots have been described by Banerjee and Bose (1944) and Bose (1944). Banerjee (1948) has accordingly divided extra reflections into three groups. The first group consists of the diffuse spots that are ordinarily produced by crystals and are of thermal origin. Their reciprocal lattice representations have extensions in three dimensions but the intensities fall off very rapidly from reciprocal lattice points. The sharp extra reflections are of two types namely sharp streaks, e.g. in the case of benzil (Lonsdale and Smith, 1941; Banerjee, Sen and Khan, 1945) and sharp spots observed in the cases of diamond and phloroglucine dihydrate as mentioned above. In the reciprocal lattice representations the extensions are two-dimensional and linear respectively and they cannot be explained as due to thermal oscillations.

The following special features have been observed by Banerjee and Bose in the case of the sharp extra spots in phloroglucine dihydrate:

- (1) The spots are extremely sharp.

- (2) The positions of the spots correspond to the Laue equations with the index  $l$ , assuming fractional values though  $h$  and  $k$  are accurately integral.
- (3) Spots for which  $h=0$ , or  $k=0$  are absent.
- (4) The central parts of the spots are blank, although the Laue reflections do not show any difference between the central and the peripheral parts.

In view of the difficulties of explaining the above phenomena by the existing theories, we have set ourselves to study X-ray diffraction by phloroglucine dihydrate in greater details.

Single crystals of phloroglucine dihydrate were obtained by the process of slow evaporation of alcohol made aldehyde free by treatment with caustic potash and distillation. Very clear crystals, which did not show any sign of deformation, were chosen. The crystal was mounted on the axis of a cylindrical camera with the  $b$ -axis vertical and X-ray beam normal to the  $c$ -face with the help of a theodolite goniometer. The advantages of a cylindrical camera for the study of extra spots in a Laue photograph and the methods of indexing the spots in such a camera have been described by Ganguly (1942).

The angular coordinates of the direction of scattering for any of the spots were determined from the position of the spot on the photographic film. From the known orientation of the crystal with reference to the incident beam and the known wave-length of the X-ray beam, the spots could be indexed by the help of the section of the sphere of reflection on the reciprocal net. On indexing these spots one finds that the indices  $h$  and  $k$  are integers while  $l$  takes up, in general, fractional values. We started with the position where the X-ray beam is along the  $c$ -axis. The crystal was rotated gradually about the  $b$ -axis and Laue photographs at successive orientations over the whole range were taken. The angle of rotation for each photograph was measured accurately from the displacements of known Laue spots. The results were projected on the reciprocal lattice according to the usual method (Banerjee, 1948). It was found that the Fourier transform of the extra reflections consisted of straight lines passing through the reciprocal lattice points parallel to the  $c$ -axis. These lines run continuously. There are small variations of the intensities along the lines, the regions in the neighbourhood of the reciprocal lattice points being more intense than midway between such points.

In Plates XXII A-D are shown the diffraction photographs for some out of the various orientations of the crystal with respect to the incident beam, the  $b$ -axis being vertical for all the orientations. The special features of the spots, namely their sharpness, central gap, and distribution conforming to a two-dimensional grating, are apparent from the figures. The persistence of the points even for large changes of orientations show the continuity of



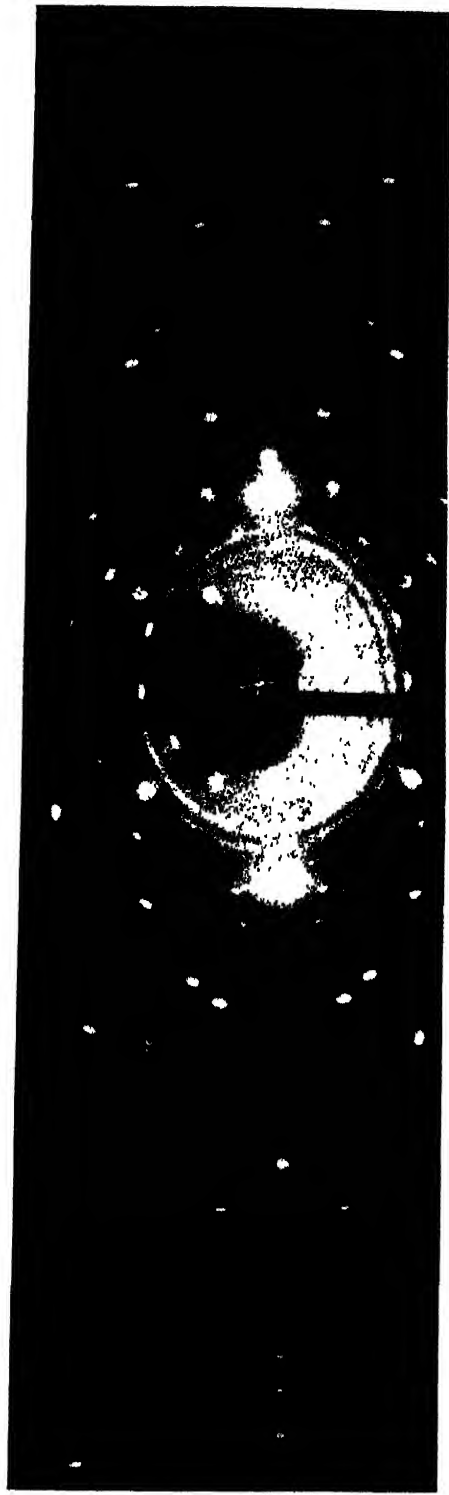


Fig. (a)  
X-ray at 230 to C



Fig. (b)  
X-ray at 10 to C

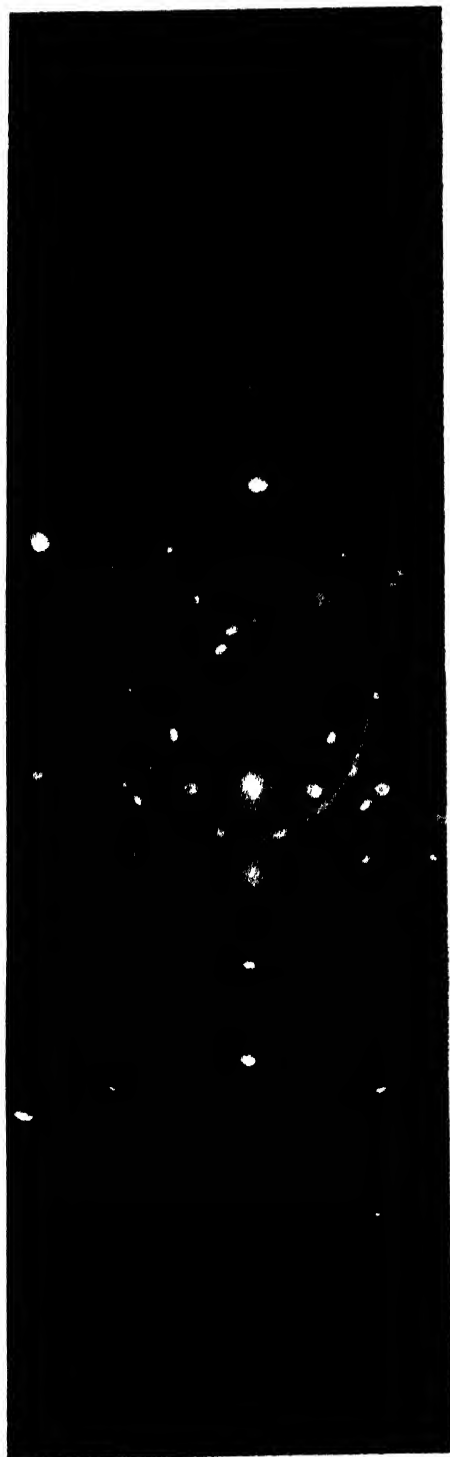


Fig  
X 20 o C



Fig. (d)

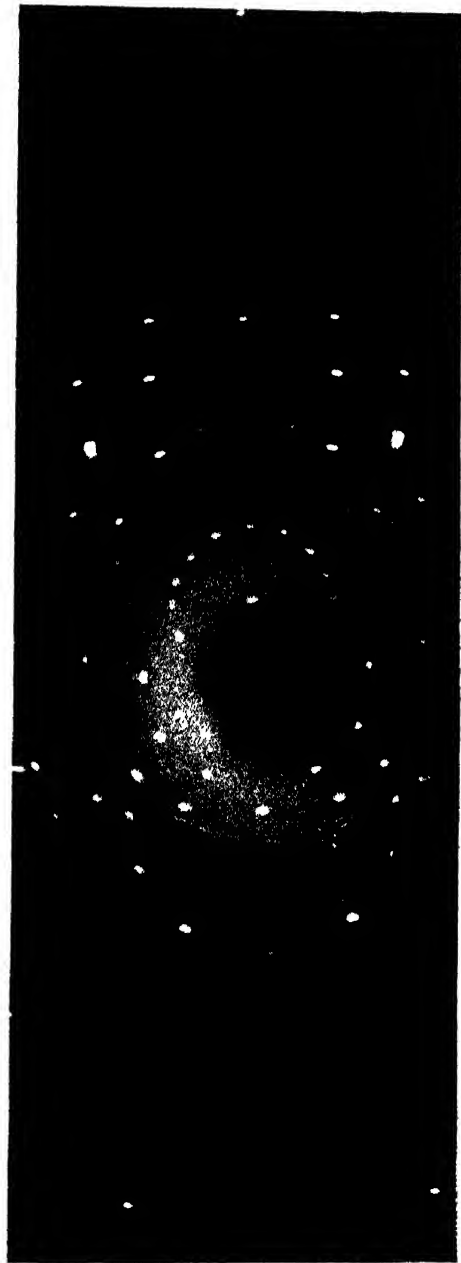


Fig. (e)

X-ray at 45 to C

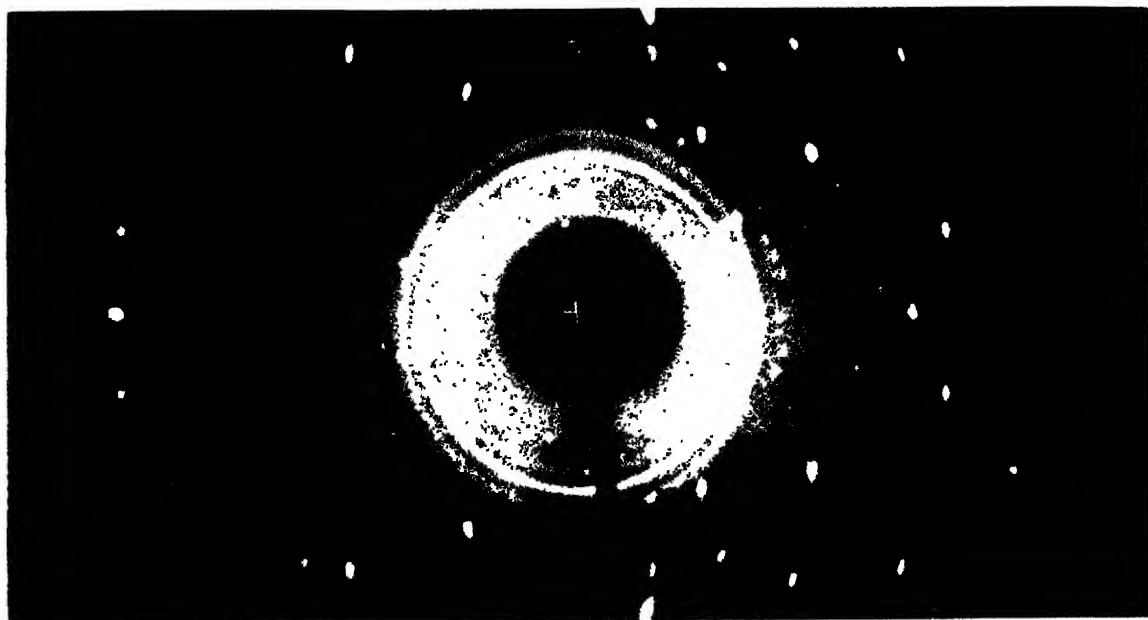


Fig. (f)  
X-ray at  $60^\circ$  to  $C$

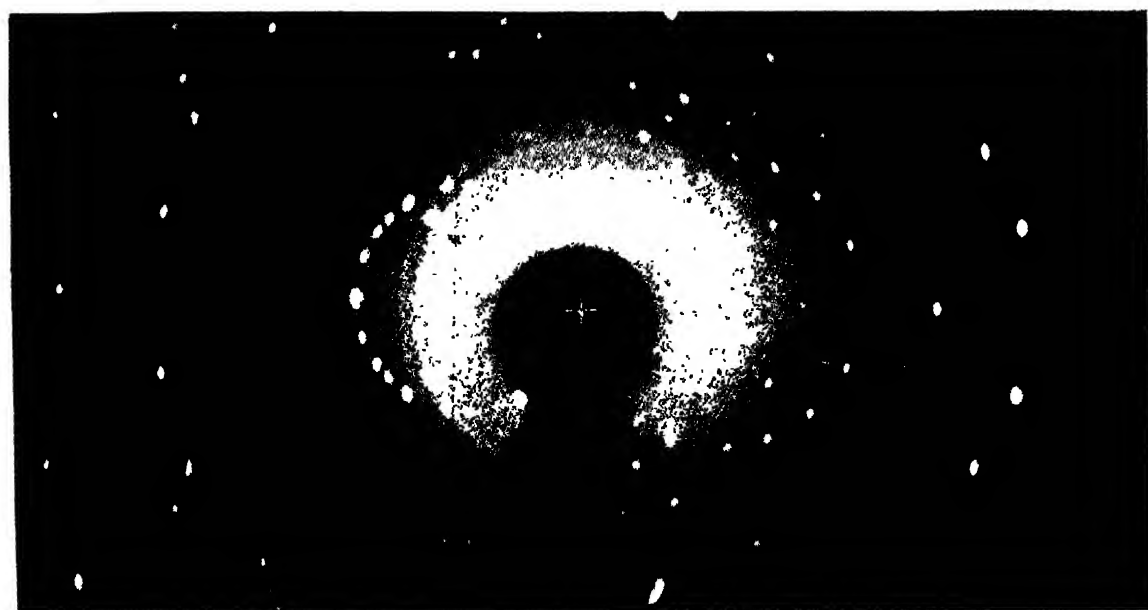


Fig. (g)  
X-ray at  $75^\circ$  to  $C$

the liner extensions in the reciprocal lattice. Figures 1 (a), (b) and (c) show the variation of estimated intensity with  $l$ .

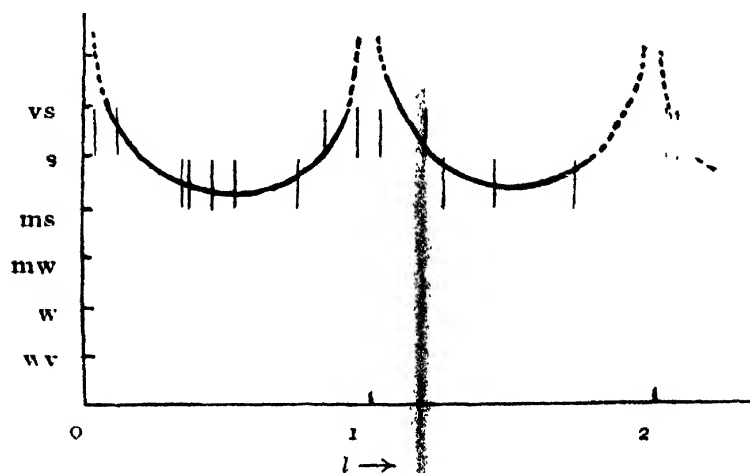


FIG. 1(a)

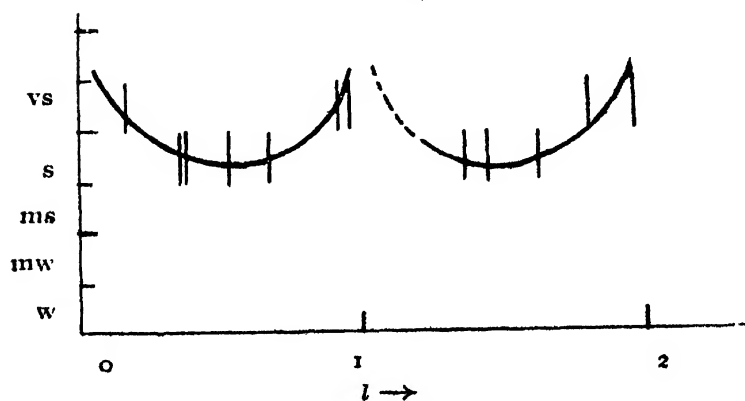


FIG. 1(b)

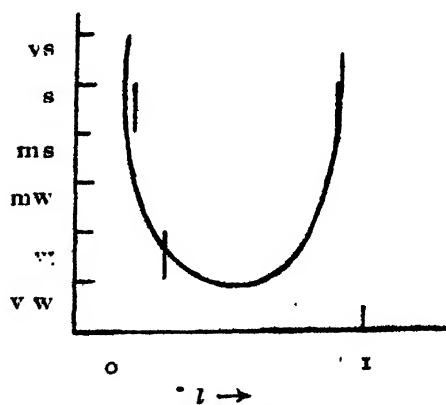


FIG. 1(c)

The most striking result that we have found from these studies is that variation of the intensities of the spots from the Bragg position are very slow so much so that  $l$  varies continuously from the neighbourhood of an

integral value to the next, passing through minimum values in the neighbourhoods of half integral values of  $l$ , while in the neighbourhood of the integral values the intensities are maxima.

Another result of importance is that absence of the extra spots with  $h=0$ , or  $k=0$  that was observed by the earlier workers has exceptions. The spot of index (20) appeared in many of the photographs and (40) appeared in two of the photographs. But they did not appear in any photograph for which the X-ray beam makes an angle smaller than  $10^\circ$ . The conditions under which these spots occur or not has, therefore, to be more critically studied. Similar absence of the sharp extra spots in the case of diamond, as pointed out by Lonsdale and Smith, also require, closer scrutiny.

#### ACKNOWLEDGMENTS

The author wishes to express his grateful thanks to Prof. K. Banerjee for suggesting the problem and advice and to Sri R. K. Sen for guidance in carrying out the experiments and to the authorities of the Indian Association for the Cultivation of Science for a scholarship and facilities to carry out the work at the laboratory of the association.

INDIAN ASSOCIATION FOR THE CULTIVATION OF SCIENCE  
JADAVPUR, CALCUTTA

#### REFERENCES

- Banerjee, K., 1947, *Proc 34th Indian Science Congress*, Part II, Presidential Address of the Physics Section.  
 Banerjee, K. and Bose, C. R., 1944, *Nature*, **153**, 23.  
 Banerjee, K., Sen, R. K., and Khan, F. M., 1945, *Proc. Nat. Inst. Sci.*, **11**, 4.  
 Bose, C. R., 1944, *Proc. Nat. Inst. Sci.*, **10**, 291.  
 Ganguly, M., 1942, *Proc. Nat. Inst. Sci.*, **8**, 389.  
 Lonsdale, K., 1942, *Proc. Roy. Soc. A*, **179**, 315.  
 Lonsdale, K. and Smith, H., 1942, *Proc. Roy. Soc. A*, **179**, 8.  
 Raman, C. V. and Nilakantan, P., 1940, *Nature*, **448**, 667.

## POINCARÉ'S THEOREM AND ITS USES

BY R. P. SINGH

*(Received for publication, February 16, 1951)*

**ABSTRACT.** The paper contains a general statement of the Virial Theorem which has been applied to find the periods of fundamental mode of oscillation of the electronic cloud of an atom and also of an atomic nucleus. The method adopted is the same as used by Ledoux (1945) and Pekeris (1941) for calculating the period of oscillation of a variable star. The method seems to give values of correct order for the above quantities.

## INTRODUCTION

The present paper consists of the generalisation of well known Poincaré's theorem  $2T + \Omega = 0$  for the steady state of a system of detached mass points or cloud of particles. The equation has been extended by Eddington (1926)

to the form  $\frac{1}{2} \frac{d^2 I}{dt^2} = 2T + \Omega$ . In the above equations  $T$  is the kinetic energy of

the particles,  $\Omega$  their potential energy and  $I$  is the moment of inertia about some common origin. In his derivation of the above equation, Poincaré assumes a potential between two particles of the form

$V_{ik} = -\frac{Gm_i m_k}{r_{ik}}$  where  $V_{ik}$  is the interaction between two particles and  $r_{ik}$

is the mutual distance between them. The subscripts  $i$  and  $k$  denote the numbers of the particles. We shall now derive the same equation for a more general case.

1. *Derivation of Poincaré's Theorem* for the case when the potential function is of the form  $V_{ik} = f(r_{ik}^{-n})$ , where  $n$  is an integer greater than one :

Consider the general motion of a cloud of particles and let the position of each particle be described by  $N$  generalised positional coordinates  $q_1, q_2, q_3, \dots, q_r, \dots, q_N$ , and let the corresponding force components acting on any particle be denoted by  $X_1, X_2, \dots, X_r, \dots, X_N$ . Then according to Newton's laws of motion we have

$$m_k \frac{d^2 q_r^k}{dt^2} = X_r^k,$$

where  $m_k$  is the mass of  $k$ th particle and  $q_r^k$  is  $r$ th positional coordinate of the particle whose equation of motion we have written and  $X_r^k$  is the  $r$ th component of the force acting on this particle. We have now for  $k$ th particle

$$\begin{aligned}
 \frac{1}{2} \frac{d^2}{dt^2} (m_k q_r^{k^2}) &= \frac{d}{dt} (m_k q_r^k \dot{q}_r^k) \\
 &= m_k q_r^{k^2} + m_k q_r^k \dot{q}_r^k \\
 &= m_k \dot{q}_r^{k^2} + q_r^k X_r^k. \quad \dots (1)
 \end{aligned}$$

If we now consider all the particles we have

$$\begin{aligned}
 \frac{1}{2} \frac{d^2}{dt^2} \left( \sum_k \sum_{r=1}^N m_k q_r^{k^2} \right) &= \sum_k \sum_{r=1}^N m_k \dot{q}_r^{k^2} + \sum_k \sum_{r=1}^N q_r^k X_r^k \\
 \text{or } \frac{1}{2} \frac{d^2 I}{dt^2} &= 2T + \sum_k \sum_{r=1}^N q_r^k X_r^k \quad \dots (2)
 \end{aligned}$$

where  $I$  is again the moment of inertia of the system about the origin defined by  $I = \sum_k \sum_{r=1}^N m_k q_r^{k^2}$  and  $T$  is the kinetic energy of the motion of particles forming the cloud. The second term on the right of equation (2) is the well known Virial of Clausius.

To evaluate the virial we consider two specific particles of masses  $m_i$  and  $m_k$  and at  $(q_1^i, q_2^i, \dots, q_r^i, \dots, q_N^i)$  and  $(q_1^k, q_2^k, \dots, q_N^k)$ . Let the force exerted on the particle  $i$  due to the particle  $k$  have components  $A_1, A_2, \dots, A_N$ , then the force acting on the particle  $k$  due to particle  $i$  will have components  $-A_1, -A_2, \dots, -A_N$ . Hence the contribution by these to the virial is

$$A_1(q_1^i - q_1^k) + A_2(q_2^i - q_2^k) + \dots + A_N(q_N^i - q_N^k), \quad \dots (3)$$

and if we consider all pairs of particles we have the total contribution by the whole cloud as

$$\begin{aligned}
 \frac{1}{2} \sum_i \sum_{k \neq i} \left[ A_1(q_1^i - q_1^k) + \dots + A_N(q_N^i - q_N^k) \right] \\
 = \frac{1}{2} \sum_i \sum_{k \neq i} \left[ \sum_r A_r(q_r^i - q_r^k) \right] \quad \dots (4)
 \end{aligned}$$

If  $W_{ik} = f[r_{ik}^{-(n+1)}]$  is the force exerted between two particles we have various components of this force  $A_1, A_2, \dots, A_N$  etc. as

$$A_1 = f(r_{ik}^{-(n+1)}) \times \frac{q_1^i - q_1^k}{r_{ik}}$$

and

$$A_r = f(r_{ik}^{-(n+1)}) \times \frac{q_r^i - q_r^k}{r_{ik}}$$



and hence the virial is

$$\begin{aligned}
 \frac{1}{2} \sum_i \sum_{k \neq i} \left[ \sum_r f(r_{ik}^{-(n+1)}) \times \frac{q_r^i - q_r^k}{r_{ik}} (q_r^i - q_r^k) \right] \\
 = \frac{1}{2} \sum_i \sum_{k \neq i} \left[ \sum_r f(r_{ik}^{-(n+1)}) \frac{(q_r^i - q_r^k)^2}{r_{ik}} \right] \\
 = \frac{1}{2} \sum_i \sum_{k \neq i} \left( - \frac{\partial V_{ik}}{\partial r_{ik}} r_{ik} \right) \\
 = \frac{1}{2} n \sum_i \sum_{k \neq i} V_{ik} \\
 = n\Omega. \quad \dots (5)
 \end{aligned}$$

Hence the equation (2) takes the form

$$\frac{1}{2} \frac{d^2 I}{dt^2} = 2T + n\Omega. \quad \dots (6)$$

2. If we take the potential function as well known Yukawa potential  $v = \frac{A}{r} e^{-r/\lambda}$  so that we have  $V_{ik} = \frac{A}{r_{ik}} e^{-r_{ik}/\lambda}$ . In this case the virial would be

$$\begin{aligned}
 \frac{1}{2} \sum_i \sum_{k \neq i} - \frac{\partial V_{ik}}{\partial r_{ik}} r_{ik} \\
 = \frac{1}{2} \sum_i \sum_{k \neq i} V_{ik} + \frac{1}{2} \times \frac{1}{\lambda} \sum_i \sum_{k \neq i} A e^{-r_{ik}/\lambda} \\
 = \Omega + \frac{1}{\lambda} \frac{\delta \Omega}{\delta (1/\lambda)} \\
 = \Omega + \frac{1}{\lambda} \frac{\delta \Omega}{\delta \lambda} \cdot \frac{1}{\delta (1/\lambda)} \\
 = \Omega - \lambda \frac{\delta \Omega}{\delta \lambda}. \quad \dots (7)
 \end{aligned}$$

Therefore in this case Poincare's equation is

$$\frac{1}{2} \frac{d^2 I}{dt^2} = 2T + \Omega - \lambda \frac{\delta \Omega}{\delta \lambda}. \quad \dots (8)$$

3. *Application of Poincare's Theorem* for finding out the period of radial pulsation of Thomas-Fermi atom. For a cloud of electrical charge, various elements of which have an electrostatic interaction, we have the equation

$$\frac{1}{2} \frac{d^2 I}{dt^2} = 2T + \Omega,$$

where  $I$  is as before the moment of inertia with respect to the origin,  $T$  the

kinetic energy and  $\Omega$  is the electrostatic potential energy of the electron cloud of the atom. For a spherically symmetrical distribution of the charge, we have

$$I = \int_0^m r^2 dm(r)$$

where  $m(r)$  denotes the mass interior to  $r$  and  $m$  is the total mass of the charge cloud. We shall consider the application of the above equation to the steady radial pulsation of a Thomas-Fermi cloud and in studying the problem we shall adopt Lagrangian mode of description, in which we follow each particle (or element of mass) during its motion. Let the distance  $r$  from the centre of symmetry be used as such a Lagrangian coordinate. Let  $\delta r$  denote the displacement from the equilibrium position  $r_0$ . The conservation of mass requires that

$$m(r_0 + \delta r) = m(r_0). \quad \dots (9)$$

If  $\delta I$ ,  $\delta\Omega$  and  $\delta T$  denote the corresponding changes from the equilibrium values in respective quantities at time  $t$ , we have

$$\frac{1}{2} \frac{d^2}{dt^2} (\delta I) = 2\delta T + \delta\Omega. \quad \dots (10)$$

Now to a first order in  $\delta r$  we have

$$\begin{aligned} \delta I &= 2 \int_0^m r \delta r dm(r) \simeq 2 \int_0^m \frac{\delta r}{r_0} r_0^2 dm(r) \\ &\simeq 2 \int_0^m \frac{\delta r}{r_0} dI_0 \text{ where } I_0 = m r_0^2 = r_0^2 \int_0^m dm(r) \end{aligned} \quad \dots (11)$$

The potential energy  $\Omega$  of the charged cloud distributed uniformly in a sphere of radius  $r_0$  surrounding a nucleus of charge  $Z$  is given by

$$\Omega_0 = -\frac{9}{10} \frac{Z^2 e^2}{r_0} \quad \dots (12)$$

So if the charged sphere assumes a radius  $r$ , the potential energy becomes

$$\Omega = -\frac{9}{10} \frac{Z^2 e^2}{r} \quad \dots (13)$$

and hence

$$\begin{aligned} \delta\Omega &= +\frac{9}{10} \frac{Z^2 e^2}{r^2} \delta r \\ &= -\frac{|\delta r|}{r_0} \times \frac{Z^2 e^2}{r_0} \times \frac{9}{10} \\ &= +\Omega_0 \frac{\delta r}{r_0}. \end{aligned} \quad \dots (14)$$

Since the charge cloud of the electron behaves as a degenerate electron gas and, therefore, the kinetic energy is given by

$$T = \frac{3}{5} \times \frac{h^2}{2m} \left( \frac{3n}{8\pi} \right)^{\frac{2}{3}} \times Z \quad \dots (15)$$

where  $Z$  is the number of electrons in the atom and  $n$  is the density of the electron. The electron density  $n$  is

$$\frac{Z}{\frac{4\pi}{3}r_0^3}$$

and so we have

$$T_0 = \frac{3}{5} \times \frac{h^2 Z}{2m r_0^2} \left( \frac{9Z}{32\pi^2} \right)^{\frac{2}{3}} \quad \dots \quad (16)$$

and in the displaced position  $r$  we have

$$T = \frac{3}{5} \times \frac{h^2 Z}{2m r^2} \left( \frac{9Z}{32\pi^2} \right)^{\frac{2}{3}} \quad \dots \quad (17)$$

so

$$\begin{aligned} \delta T &= -\frac{3}{5} \times \frac{h^2 Z}{m r^3} \left( \frac{9Z}{32\pi^2} \right)^{\frac{2}{3}} \delta r \\ &= -\frac{2T_0}{r_0} \delta r. \end{aligned} \quad \dots \quad (18)$$

Substituting these values of  $\delta I$ ,  $\delta \Omega$ ,  $\delta T$  in (10) we get

$$\frac{1}{2} \frac{d^2}{dt^2} \left( 2 \int_0^m \frac{\delta I}{r_0} \delta I_0 \right) = -\frac{4T_0}{r_0} \delta r + \Omega_0 \frac{\delta r}{r_0} \quad \dots \quad (19)$$

Now for small periodic oscillations we can write

$$\frac{\delta r}{r_0} = \xi = \xi e^{i\sigma t}$$

In the evaluation of  $\delta T$  we may observe that  $T$  consists of two parts ; (1) the kinetic energy due to thermal motions and kinetic energy due to vibrations. It is evident that the latter is of second order in  $\xi$  and therefore can be ignored in a first order theory. Thus we have equation (19) as

$$\frac{d^2}{dt^2} \int_0^m \xi_0 e^{i\sigma t} dI_0 = -4T_0 \xi_0 e^{i\sigma t} + \Omega_0 \xi_0 e^{i\sigma t}$$

$$\text{or} \quad -\sigma^2 e^{i\sigma t} \int \xi_0 dI_0 = -4T_0 \xi_0 e^{i\sigma t} + \Omega_0 \xi_0 e^{i\sigma t}$$

$$\text{or} \quad \sigma^2 = \frac{4T_0 \xi_0 - \Omega_0 \xi_0}{\int \xi_0 dI_0} \quad \dots \quad (20)$$

If we consider  $\xi_0$  as constant we get

$$\sigma^2 = \frac{4T_0 - \Omega_0}{I_0}$$

$$\text{For } Z=1, \text{ we have } \sigma^2 = \frac{6}{5} \left( \frac{h^2}{m r_0^2} \right) \left( \frac{9}{32\pi^2} \right)^{\frac{2}{3}} + \frac{9}{10} \frac{e^2}{r_0}$$

$$= \frac{3 \times (6.62)^2 \times 9^{2/3} \times 10^{33}}{(9.105)^2 \times (.528)^4 \times (4 \times 3.14 \times 3.14)^{2/3}} + \frac{9 \times (4.80)^2 \times 10^8}{9.105 \times (.528)^2}$$

$$= 91.73 \times 10^{32}$$

or  $\sigma = 9.58 \times 10^{16}$ .

From this we get the period of oscillation

$$\tau = \frac{2\pi}{\sigma} = \frac{2\pi}{9.58 \times 10^{16}}$$

$$= .104 \times 10^{-16} \text{ seconds}$$

#### 4. Oscillation period of a nucleus.

Inside a nucleus composed of  $Z$  protons and  $N$  neutrons there are various types of interactions existing. We have at first the Yukawa potential of the form  $A/r e^{-r/\lambda}$ , then there is the Coulombian interaction between the protons. The Yukawa potential gives the neutron-proton interaction. In addition to these there are minute neutron-neutron interaction and exchange interactions. We shall here consider only first two which are important in the case of potential energy of the nucleus. We can write down the Poincare's equation for the nucleus as

$$\frac{1}{2} \frac{d^2 I}{dt^2} = 2T + \Omega - \lambda \frac{\delta \Omega}{\delta \lambda} + W ; \quad \dots (22)$$

where  $\Omega$  is the potential energy due to Yukawa interaction and  $W$  is the Coulomb interaction potential energy. Confining ourselves to the assumption that both the interactions are effective in the whole nucleus we get

$$W = \frac{3}{5} \times \frac{Ze^2}{R} \quad \dots (23)$$

as before. The potential energy  $\Omega$  due to the interaction of the form

$\frac{A}{r} e^{-\frac{r}{\lambda}}$  can be found in a simple way.

Let  $P$  be a point outside the shell at a distance  $c$  from the centre  $O$  of a spherical shell. Consider a narrow zone of the shell  $QQ'$  at a distance  $r$

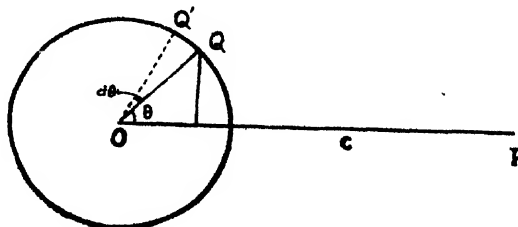


FIG. 1

from  $P$ . If  $a$  is the radius of the shell and  $\theta$  denotes the angle  $QOP$ , the

area of the zone is  $2\pi a^2 \sin \theta d\theta$  so that if  $m$  is the mass per unit area of the zone, the potential at  $P$  due to this zone is

$$2\pi m a^2 \frac{A}{r} e^{-\frac{r}{\lambda}} \sin \theta d\theta \quad \dots (24)$$

and so potential due to whole shell is

$$\begin{aligned} V &= \int_0^\pi 2\pi a^2 m \sin \theta \frac{A}{r} e^{-\frac{r}{\lambda}} d\theta \\ &= \frac{2\pi m a^2 A}{ac} \int_{c-a}^{c+a} e^{-\frac{r}{\lambda}} dr = \frac{4\pi m A \lambda}{c} e^{-\frac{c}{\lambda}} \sinh \frac{a}{\lambda} \text{ for } c > a \quad \dots (25) \end{aligned}$$

and 
$$V = \frac{2\pi m A a}{c} \int_{a-c}^{a+c} e^{-\frac{r}{\lambda}} dr$$

$$= \frac{4\pi m A a}{c} \lambda e^{-\frac{a}{\lambda}} \sinh \frac{c}{\lambda} \text{ for } c < a \quad \dots (26)$$

Using (25) and (26) we find the potential due to a solid sphere at a point whose distance is  $c$  from the centre of the sphere. If the point  $P$  is outside the sphere we have

$$\begin{aligned} V &= \int_0^R 4\pi r^2 \times \frac{M}{\frac{4\pi R^3}{3}} \times \frac{A\lambda}{cr} e^{-\frac{r}{\lambda}} \sinh \frac{r}{\lambda} dr \\ &= \frac{3MA\lambda e^{-\frac{c}{\lambda}}}{R^3 c} \left[ R\lambda \cosh \frac{R}{\lambda} - \lambda^2 \sinh \frac{R}{\lambda} \right], \quad \dots (27) \end{aligned}$$

and if the point  $P$  is inside the sphere we have

$$\begin{aligned} V &= \frac{4\pi}{c} \times \frac{3MA\lambda}{4\pi R^3} \left[ \int_0^c r \sinh \frac{r}{\lambda} e^{-\frac{c}{\lambda}} dr + \int_c^R r e^{-\frac{r}{\lambda}} \sinh \frac{c}{\lambda} dr \right] \quad \dots (28) \\ &= \frac{3MA\lambda}{R^3 c} \left[ \lambda c - (\lambda R + \lambda^2) e^{-\frac{R}{\lambda}} \sinh \frac{c}{\lambda} \right] \quad \dots (29) \end{aligned}$$

Using the equation (29) we can find  $\Omega$ . It is given by

$$\begin{aligned} \Omega &= \frac{1}{2} \int V dm \\ &= \frac{1}{2} \int_0^R \frac{3MA\lambda}{R^3} \times \frac{1}{r} \left\{ \lambda r - (\lambda R + \lambda^2) e^{-\frac{R}{\lambda}} \sinh \frac{r}{\lambda} \right\} \times 4\pi r^2 dr \times \frac{3M}{4\pi R^3} \\ &= \frac{9M^2 A \lambda}{2R^3} \left[ \lambda R^3 - (\lambda R + \lambda^2) e^{-\frac{R}{\lambda}} \left( R \cosh \frac{R}{\lambda} - \lambda^2 \sinh \frac{R}{\lambda} \right) \right] \quad \dots (30) \end{aligned}$$

Now from equation (22) we have

$$\frac{1}{2} \frac{d^2}{dt^2} (\delta I) = 2\delta T + \delta \Omega - \lambda \frac{\delta}{\delta \lambda} (\delta \Omega) + \delta W \quad \dots (31)$$

and again

$$\delta I = 2 \int R \delta R dM(R) = 2 \int \frac{\delta R}{R} dI_0; \quad \dots (32)$$

$$\delta T = 2T \frac{\delta R}{R}; \quad \delta W = -W \frac{\delta R}{R} \quad \dots (33)$$

while

$$\begin{aligned} \delta \Omega = \frac{9M^2 A}{4} \left[ \left\{ \frac{\lambda^2}{R} + \frac{3\lambda^3}{R^2} + \frac{4\lambda^4}{R^2} + \frac{\lambda^3}{R} + \frac{3\lambda^5}{R^3} \right\} + e^{-\frac{2R}{\lambda}} \left\{ 2\lambda + \frac{3\lambda^2}{R} \right. \right. \\ \left. \left. + \frac{\lambda^3}{R^2} - \frac{2\lambda^4}{R^2} - \frac{\lambda^4}{R} - \frac{3\lambda^5}{R^3} \right\} \right] \frac{\delta R}{R} \quad \dots (34) \end{aligned}$$

and

$$\begin{aligned} \lambda \frac{\delta \Omega}{\delta \lambda} = \frac{9M^2 A}{4} \left[ 2\lambda + \frac{27\lambda^3}{R^2} + \frac{64\lambda^4}{R^2} + \frac{9\lambda^3}{R} + \frac{75\lambda^3}{R^3} \right] e^{-\frac{2R}{\lambda}} \frac{\delta R}{R} \\ + \frac{9M^2 A}{4} \left[ \frac{2\lambda^2}{R} + \frac{9\lambda^3}{R^2} + \frac{16\lambda^4}{R^2} + \frac{3\lambda^3}{R} + \frac{15\lambda^5}{R^3} \right] \frac{\delta R}{R} \\ - \frac{9M^2 A}{2} \left[ 2 + \frac{3\lambda}{R} + \frac{\lambda^2}{R^2} - \frac{2\lambda^3}{R^2} + \frac{\lambda^2}{R} - \frac{3\lambda^4}{R^3} \right] e^{-\frac{2R}{\lambda}} \frac{\delta R}{R} \quad \dots (35) \end{aligned}$$

Putting  $\frac{\delta R}{R} = \xi = \xi_0 e^{i\sigma t}$  and substituting these in (31) we get as before

$$\begin{aligned} \sigma^2 = \frac{4T+W}{MR^2} - \frac{9M^2 A}{4R^2} \left[ \frac{3\lambda^2}{R} + \frac{12\lambda^3}{R^2} + \frac{20\lambda^4}{R^2} + \frac{4\lambda^3}{R} + \frac{18\lambda^5}{R^3} \right] \\ - \frac{9MA^2}{4R^2} e^{-\frac{2R}{\lambda}} \left[ 4\lambda + \frac{9\lambda^3}{R} + \frac{4\lambda^2}{R^2} - \frac{10\lambda^4}{R^2} + 4\lambda^3 - \frac{18\lambda^5}{R^4} \right] \\ + \frac{9M^2 A}{2R^2} e^{-\frac{2R}{\lambda}} \left[ 2 + \frac{3\lambda}{R} + \frac{\lambda^2}{R^2} - \frac{2\lambda^3}{R^2} + \frac{\lambda^2}{R} - \frac{3\lambda^4}{R^3} \right] \quad \dots (36) \end{aligned}$$

Now for a nucleus with  $Z$  protons and  $N$  neutrons the kinetic energy of the nuclear particles is

$$\begin{aligned} T = \frac{3}{5} \times \frac{h^2}{4\pi^2 M_p^3} \left( \frac{9\pi}{4} \right)^{2/3} \frac{N^{5/3} + Z^{5/3}}{R^2} \\ = 2980 \text{ M. e. volts for a nucleus with } Z=80 \text{ and } N=120 \text{ i.e. Hg}^{200}. \end{aligned}$$

For the same  $\lambda = 2.37 \times 10^{-13}$  cm and  $R = 8 \times 10^{-13}$  cm. The mass of the nucleus is 200 A. M. units. Substituting these we obtain

$$T_{\text{nucleus}} \approx 10^{-21} \text{ seconds.}$$

#### ACKNOWLEDGMENT

The author's thanks are due to Prof. D. S. Kothari for his interest in the progress of this work.

DEPARTMENT OF PHYSICS,  
UNIVERSITY OF ALLAHABAD, ALLAHABAD.

#### REFERENCES

- Eddington, A. S., 1926, *Internal Constitution of Stars*, 260, Cambr. Univ. Press.  
Ledoux, P., 1945, *Astr. Phy. J.*, **102**, 143.  
Ledoux, P., and Pekeris, C. L., 1941, *Astr. Phy. J.*, **94**, 124.

# ELECTRON DIFFRACTION IN SODIUM AND POTASSIUM CHLORIDE CRYSTALS\*

By SUBODH KUMAR MAJUMDAR

(Received for publication, September 27, 1951)

Plates XXIII A and B

**ABSTRACT.** The electron diffraction patterns of NaCl and KCl crystals have been investigated with an electron microscope. The mean values, as calculated from the observed rings, come out to be 5.529 Å for NaCl and 6.22 Å for KCl, the standard values being 5.63 Å and 6.28 Å respectively.

## INTRODUCTION

In a previous paper, the electron diffraction patterns of different metals, as well as of AgCl and AgBr have been communicated (Majumdar, 1951). In all these experiments, the metals were vaporised in high vacuum on saponin membrane over the objective piece. In the case of halides, silver was vaporised in presence of halogen vapours. It has been found that the spacings as measured from the electron diffraction photographs, agree fairly well with those obtained from X-ray diffraction methods.

In the present investigation diffraction patterns of sodium and potassium chloride crystals have been investigated with electron microscope.

## EXPERIMENTAL

The electron microscope was of the Borres-Ruska type (Siemens) and the experiments were carried out at the Virusforschungsinstitut, Heidelberg, Germany. As usual, the projective magnet piece was taken out for diffraction experiments. The objective piece, which was made of platinum-iridium, had an aperture of 0.5 mm. It was placed in water saturated with amyl acetate so that the solution just covered the aperture. A drop of a solution of saponin in amyl acetate was placed on the aqueous solution just over the aperture, when the drop spread itself and covered the aperture. The solution was then drained off and the deposit dried in air. In this way a very thin membrane was obtained on the objective piece. A drop of sodium or potassium chloride solution of different concentrations was next placed on the membrane, and the objective piece replaced within the electron microscope. The vacuum was then turned on. In this way crystals were precipitated on the membrane. A large number of experiments

\* This work forms a part of the investigation carried out by the author at Virusforschungsinstitut, Heidelberg, Neckar, Germany in 1950-51.



were done with different concentrations of the salts and also by exposing the crystals to the action of electron beams for different periods of time before taking the photographs. A primary voltage of 160 volts and a secondary voltage of 73 KV in a 9-stage transformer were used in most experiments. For comparison, a few photographs were taken with 70 KV and 56 KV. The photographs of the pictures are given in figures 1-13 of Plates XXIII A and B. The distance between the objective piece and the plate was 57.5 cm.

## RESULTS

Table I gives the description of the treatment of the various samples.

TABLE I.

Fig. No.	Substance & conc.	Treatment.	Voltage used.
1	NaCl, dil. sol.	Taken after 3 min.	73 KV $\pm$ 125 V.
2	"	after 6 min.	"
3	NaCl, 1 mol. sol.	after 3 min.	"
4	NaCl, 1 mol. sol.	after 6 min.	"
5	NaCl, 1 mol. sol.	Immediate exposure.	70 KV $\pm$ 115 V.
6	KCl, dil. sol.	Taken after 3 min.	73 KV $\pm$ 215 V.
7	KCl, dil. sol.	after 6 min.	"
8	KCl, satd. sol. dil. 1 : 1	Immediately taken	70 KV $\pm$ 215 V.
9	"	After longer exposure,	73 KV $\pm$ 215 V.
10	"	Immediately taken.	70 KV $\pm$ 215 V.
11	"	Taken after longer exposure.	56 KV $\pm$ 215 V.
12	"	"	"
13	"	Taken immediately.	"

All the diffraction patterns of the same salt with the same high voltage are similar. Certain peculiarities, however, appear with the change of concentration, voltage and the time of exposure to the electron beams before photographing.

The spacings of the crystals were determined by the usual method of trial and error. The distance between the objective piece and plate was 59.5 cm. If  $\theta/2$  is the half angle of any particular cone of reflected beams from any particular plane ( $h, k, l$ ) of the crystal and if  $x$  cm is the radius of the particular circle, which represents the section of the cone on the photographic

plate, then  $\tan \theta/2 = \frac{x/2}{59.5}$ , from which  $\theta/2$  and  $\sin \theta/2$  can be calculated.

For each value of  $x$ , the values of  $\sin \frac{\theta/2}{\sqrt{1}}$ ,  $\sin \frac{\theta/2}{\sqrt{2}}$ ,  $\sin \frac{\theta/2}{\sqrt{3}}$ ,  $\sin \frac{\theta/2}{\sqrt{4}}$ , etc. are

calculated and tabulated. The value of constant  $K$  in the equation

$$a_0 = \frac{\lambda}{\frac{2 \cdot \sin \theta/2}{\sqrt{h^2 + k^2 + l^2}}} = \frac{\lambda}{2K}$$

is next determined for a particular value of  $x$ , and the mean value of  $K$  is taken.  $\lambda$  is then determined from the equation.

$$\lambda = \frac{h}{\sqrt{2m_0 \cdot e \cdot U \left( 1 + \frac{e \cdot U}{2m_0 c^2} \right)}}$$

where  $h$  = Planck const. =  $6.626 \times 10^{-27}$  erg/sec. ;

$m_0$  = rest mass of the electron =  $9.108 \times 10^{-28}$  gm.,

$e$  = charge of the electron =  $4.803 \times 10^{-10}$  C. G. S.,

$c$  = velocity of light =  $3.00 \times 10^{10}$  cm/sec.,

$U$  = applied E. M. F. (C. G. S.).

The values of  $\lambda$  for 73 KV and 56 KV are found to be .04386 Å and .0504 Å respectively.

Tables II-IV give the analysis of two typical photographs of NaCl and KCl with 73 KV and one photograph of KCl with 56 KV.

TABLE II

## NaCl

Voltage = 73KV  $\pm$  215 volts $\lambda = .04386$  Å

Nature	S	S	W	W
$x$ (cm)	1.845	2.615	3.200	4.060
$\theta/2$	1°55'	1°18'	1°36'	2°0'
$\sin \theta/2$	.0160	.0227	.0279	.0349
$K$	.00400	.003950	.00398	.00398

Mean value of  $K = .00397$ . Hence  $a_0 = \frac{.04386}{2 \times .00397}$  Å = 5.529 Å.

Standard value of NaCl is 5.63 Å.

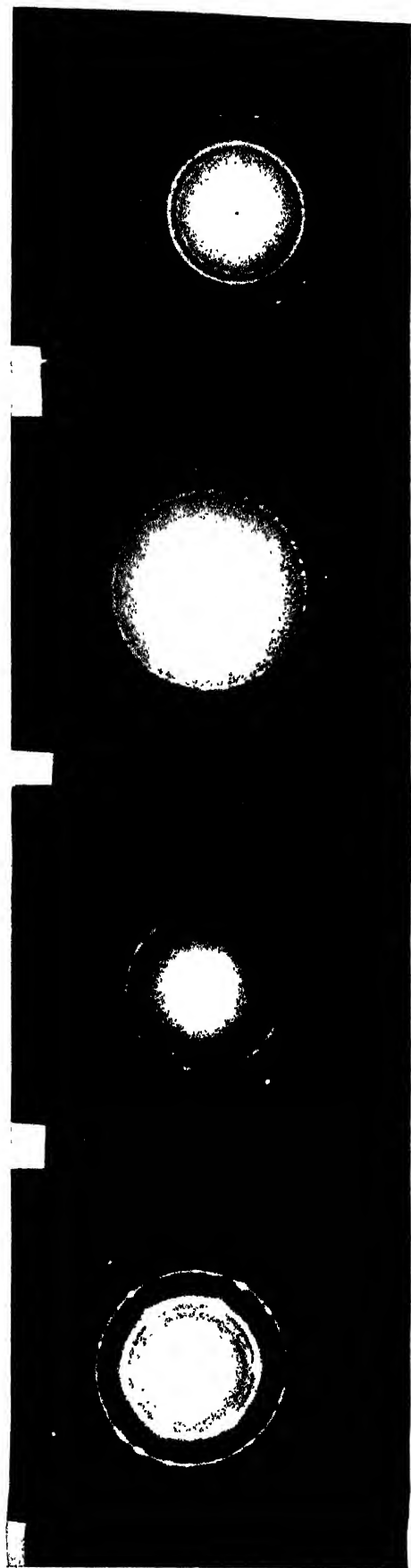


Fig. 1

Fig. 2

Fig. 3

Fig. 4

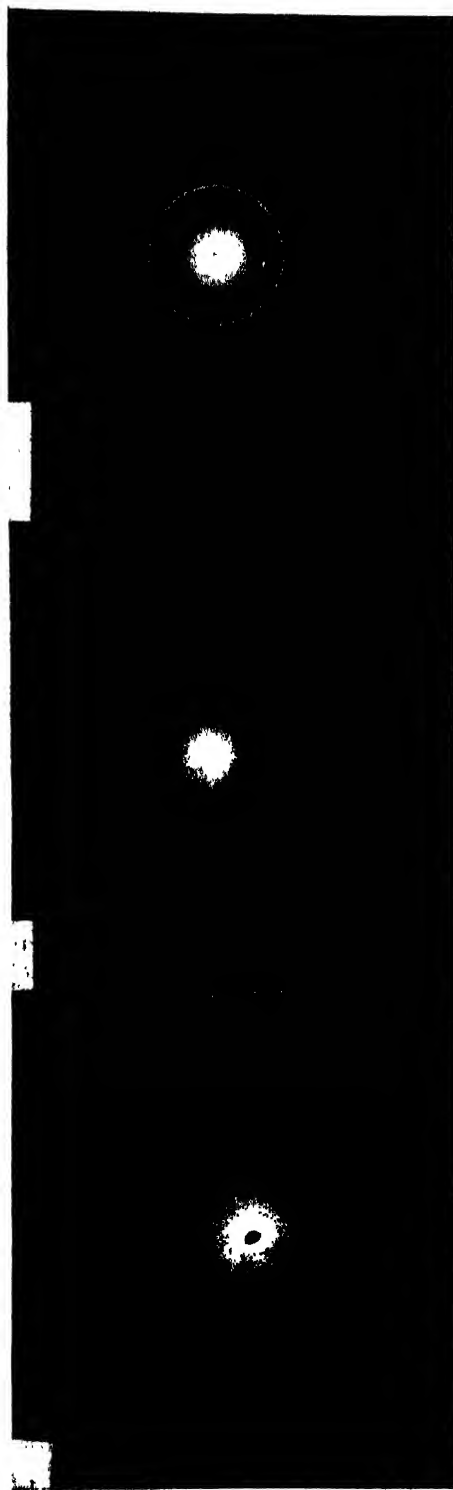


Fig. 5

Fig. 6

Fig. 7

Fig. 8

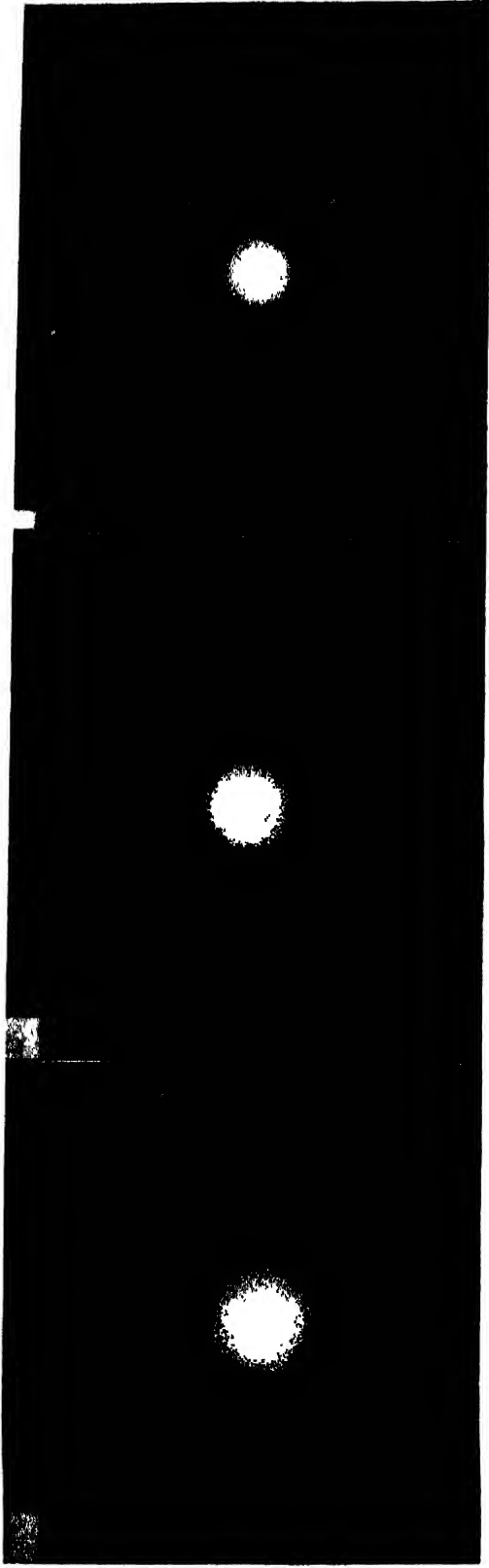


Fig 8

Fig. 9

Fig. 10

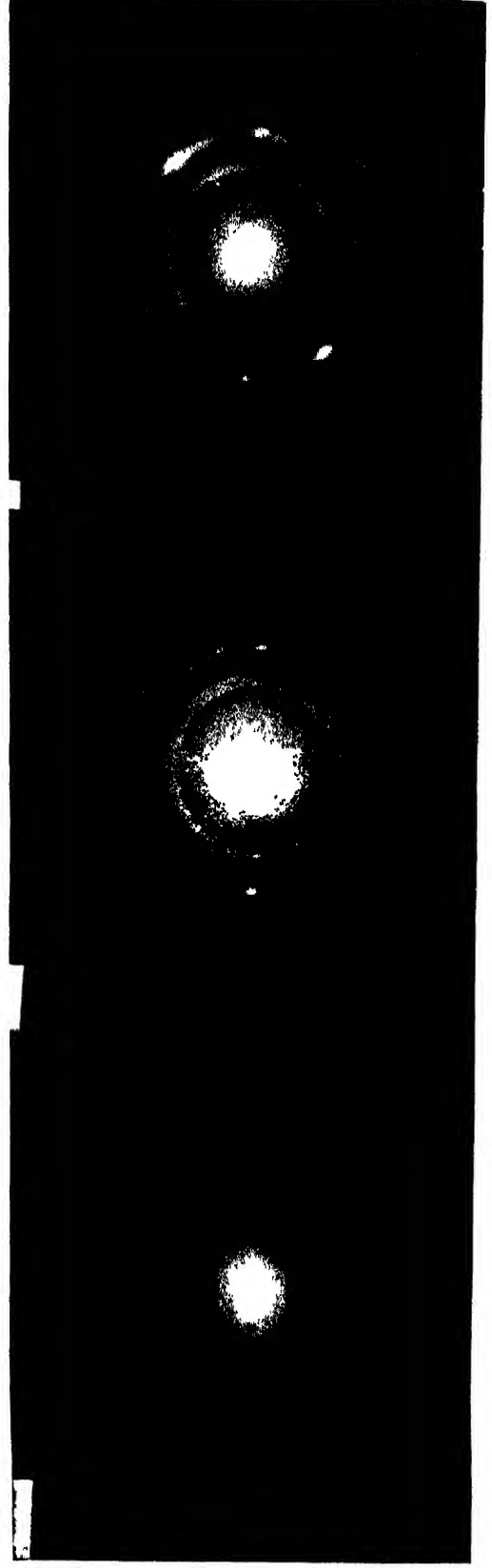


Fig 11

Fig 12

Fig 13

TABLE III

KCl.

Voltage = 73 KV  $\pm$  215 $\lambda = .04386 \text{ \AA}$ 

Nature	S	S	W	VW	W	VW
$x(\text{cm})$	1.602	2.360	2.885	3.450	3.750	4.00
$\theta/2$	$1^\circ 49'$	$1^\circ 11'$	$1^\circ 26'$	$1^\circ 43'$	$1^\circ 52'$	$1^\circ 59'$
$\sin \theta/2$	.0144	.0206	.0250	.0300	.0326	.0348
$K$	.00360	.00363	.00368	.00361	.00360	.00360

Mean value of  $K = .00360$  Hence  $a_0 = \frac{.04386}{2 \times .00360} \text{ \AA} = 6.09 \text{ \AA}$ .

Standard value for KCl = 6.28  $\text{\AA}$

TABLE IV

KCl.

Voltage 56 KV  $\pm$  215 Volts. $\lambda = .0504 \text{ \AA}$ 

Nature	S	S	W	V. W.	V. W.
$x(\text{cm})$	1.60	2.75	3.25	4.25	4.75
$\theta/2$	$0^\circ 48'$	$1^\circ 22'$	$1^\circ 37'$	$2^\circ 7'$	$2^\circ 22'$
$\sin \theta/2$	.0139	.0240	.0282	.0368	.0413
$K$	.00401	.00400	.00402	.00409	.00413

Mean value of  $K = .00405 \text{ \AA}$ .

Hence  $a_0 = \frac{.0504}{2 \times .00405} \text{ \AA} = 6.22 \text{ \AA}$ .

Standard value for KCl = 6.28  $\text{\AA}$ .

The values of the spacings of NaCl and KCl thus found agree fairly well with those obtained from X-ray diffraction experiments. An interesting point, however, is the occurrence of spots in some of the pictures. It will be noticed that spots invariably occur with NaCl solutions, whether dilute or strong and also after short or long exposure, whereas, with KCl there are practically no spots with dilute solutions. These points, which are apparently of Laue pattern, do not always indicate cubical symmetry.

Two reasons may be ascribed to the occurrence of these spots. It is possible that some bigger single crystals, in addition to finer ones, are separated on the membrane while the solution evaporates in the vacuum. While the smaller crystals, haphazardly oriented give typical Debye-Scherrer patterns, the bigger ones, which partially cover the objective aperture, give Laue spots.

below.  $\beta$  is positive to the right of the  $y$ -axis and negative to the left.  $\beta=0$  on the  $y$ -axis except between the limiting points, where  $\beta=\pm\pi$ . At infinity  $z=0$ ,  $\beta=0$ .

we have,

$$x = \frac{a \sin \beta}{\cosh \alpha - \cos \beta}, \quad y = \frac{a \sinh \alpha}{\cosh \alpha - \cos \beta}$$

and

$$h = \frac{d(z + i\beta)}{d(x + iy)} = \frac{\cosh \alpha - \cos \beta}{a}$$

In terms of the stress function  $\chi$ , the stresses are given by, (Jeffery, 1921)

$$\begin{aligned} \widehat{xz} &= \left\{ (\cosh \alpha - \cos \beta) \frac{\partial^2}{\partial \beta^2} - \sinh \alpha \frac{\partial}{\partial \alpha} - \sin \beta \frac{\partial}{\partial \beta} + \cosh \alpha \right\} (h\chi) \\ a\widehat{\beta\beta} &= \left\{ (\cosh \alpha - \cos \beta) \frac{\partial^2}{\partial \alpha^2} - \sinh \alpha \frac{\partial}{\partial \alpha} - \sin \beta \frac{\partial}{\partial \beta} + \cos \beta \right\} (h\chi) \quad (2) \\ a\widehat{\alpha\beta} &= -(\cosh \alpha - \cos \beta) \frac{\partial^2}{\partial \alpha \partial \beta} (h\chi) \end{aligned}$$

The general solution for  $\nabla^4 \chi = 0$  is obtained in the form, (Jeffery, 1921)

$$\begin{aligned} h\chi &= \{B_0 z + K \log(\cosh \alpha - \cos \beta)\} (\cosh z - \cos \beta) \\ &+ \sum_{n=1}^{\infty} \left\{ \phi_n(z) \cos n\beta + \psi_n(z) \sin n\beta \right\} \quad \dots \quad (3) \end{aligned}$$

where,

$$\begin{aligned} \phi_n(z) &= A_n \cosh(n+1)\alpha + B_n \cosh(n-1)\alpha \\ &+ C_n \sinh(n+1)\alpha + D_n \sinh(n-1)\alpha \\ \psi_n(\alpha) &= A_n' \cosh(n+1)\alpha + B_n' \cosh(n-1)\alpha \\ &+ C_n' \sinh(n+1)\alpha + D_n' \sinh(n-1)\alpha \end{aligned} \quad (4)$$

if  $n \geq 2$ , and

$$\left. \begin{aligned} \phi_1(z) &= A_1 \cosh 2\alpha + B_1 + C_1 \sinh 2\alpha \\ \psi_1(\alpha) &= A_1' \cosh 2\alpha + C_1' \sinh 2\alpha \end{aligned} \right\} \quad (5)$$

In this solution the term in  $K$  may be omitted when the region considered lies entirely on one side of the  $x$ -axis.

The necessary and sufficient condition for a boundary to be free from stress are, (Jeffery, 1921)

$$\frac{\partial}{\partial \alpha} (h\chi) = \text{constant} = \rho \quad (\text{say}) \quad \dots \quad (6)$$

and

$$h\chi = \rho \tanh \alpha + \sigma (\cosh \alpha - \cos \beta - 1) + \tau \sin \beta \quad \dots \quad (7)$$

where  $\rho$ ,  $\sigma$  and  $\tau$  are Mitchells' constants for the boundary.

A SEMI-INFINITE PLATE CONTAINING AN UNSTRESSED CIRCULAR HOLE UNDER A UNIFORM TENSION PERPENDICULAR TO THE STRAIGHT EDGE

Let the hole be defined by  $z = z_1 > 0$ , and the straight edge by  $z = 0$ . If  $T$  be the tension perpendicular to the straight edge, we get at a great distance from the hole,

$$\chi_0 = \frac{1}{2} T z^2$$

Therefore, when  $z > 0$

$$\begin{aligned} h\chi_0 &= \frac{1}{2} a T \frac{\sin^2 \beta}{\cosh \alpha \cos \beta} \\ &= \frac{1}{2} a T \left[ e^{-\alpha} + e^{-2\alpha} \cos \beta + \sum_{n=2}^{\infty} \left\{ e^{-(n+1)\alpha} - e^{-(n-1)\alpha} \right\} \cos n\beta \right] \end{aligned}$$

We have to add to  $\chi_0$  a stress function  $\chi_1$ , which gives no stress at infinity and no stress over the straight boundary, and is such that the complete stress function  $\chi_0 + \chi_1$  gives no stress over the boundary  $z = z_1$ .

In the solution (3), we omit the term in  $K$  as the region considered is entirely on one side of the  $x$ -axis and we also omit the terms in  $\psi_n z$  as the required stress function is clearly even in  $\beta$ .

For condition of no stress on  $\alpha = 0$  and at infinity ( $\alpha = 0$ ,  $\beta = 0$ ),  $\phi_n(0) = 0$  for  $n \geq 1$ ,  $B_0 = \phi_1'(0)$  and  $\phi_n'(0) = 0$  for  $n \geq 2$ . Therefore, we get,  $A_n + B_n = 0$  for  $n \geq 1$ ,  $B_0 = 2C_1$  and  $(n+1)C_n + (n-1)D_n = 0$  for  $n \geq 2$ .

Hence we can write,

$$\begin{aligned} h\chi_1 &= aT \left[ 2C_1 \alpha (\cosh \alpha - \cos \beta) + A_1 (\cosh 2\alpha - 1) \cos \beta + C_1 \sinh 2\alpha \cos \beta \right. \\ &\quad \left. + \sum_{n=2}^{\infty} \left\{ A_n [\cosh (n+1)\alpha - \cosh (n-1)\alpha] \right. \right. \\ &\quad \left. \left. + E_n [(n-1) \sinh (n+1)\alpha - (n+1) \sinh (n-1)\alpha] \right\} \cos n\beta \right] \quad (8) \end{aligned}$$

The constant coefficients are calculated as in (9), by imposing the boundary conditions (6) and (7) on the complete stress function  $h\chi_0 + h\chi_1$  for the condition of no stress on the boundary  $z = z_1$ ,

$$A_1 = -\frac{1 + e^{-2\alpha_1}}{2(\cosh 2\alpha_1 - 1)}, \quad C_1 = \frac{1 - e^{-2\alpha_1} + \sinh 2\alpha_1}{2 \cosh 2\alpha_1 - 1}$$

$$A_n = -\frac{1}{2} + \frac{\sinh 2n\alpha_1 - n \sinh 2\alpha_1}{4(\sinh^2 n\alpha_1 - n^2 \sinh^2 \alpha_1)}$$

$$E_n = -\frac{n \sinh^2 \alpha_1}{2(\sinh^2 n\alpha_1 - n^2 \sinh^2 \alpha_1)}$$

Calculating the stress  $\widehat{\beta\beta}_1$  on the circular boundary from  $(\chi_0 + \chi_1)$ , we get,

$$\widehat{\beta\beta}_1 = 2T(\cosh\alpha_1 - \cos\beta) \times \left[ \frac{2\cosh\alpha_1 - \sinh\alpha_1}{2\sinh^2\alpha_1} + \frac{\cos\beta}{\sinh^2\alpha_1} - \sum_{n=2}^{\infty} M_n \cos n\beta \right] \quad \dots (10)$$

where,

$$M_n = \frac{n(n-1)\sinh(n+1)\alpha_1 - n(n+1)\sinh(n-1)\alpha_1}{2(\sinh^2 n\alpha_1 - n^2 \sinh^2 \alpha_1)} \quad \dots (11)$$

The series in (10) is slowly convergent, so for convenience of numerical calculations the more slowly converging part is separated out by putting

$$M_n = 2n(n\sinh\alpha_1 - \cosh\alpha_1)e^{-n\alpha_1} + N_n \quad \dots (11a)$$

we obtain,

$$\begin{aligned} & 2(\cosh\alpha_1 - \cos\beta) \sum_{n=1}^{\infty} n(n\sinh\alpha_1 - \cosh\alpha_1)e^{-n\alpha_1} \cos n\beta \\ &= 1 - \frac{2\sinh^2\alpha_1 \sin^2\beta}{(\cosh\alpha_1 - \cos\beta)^2} \end{aligned}$$

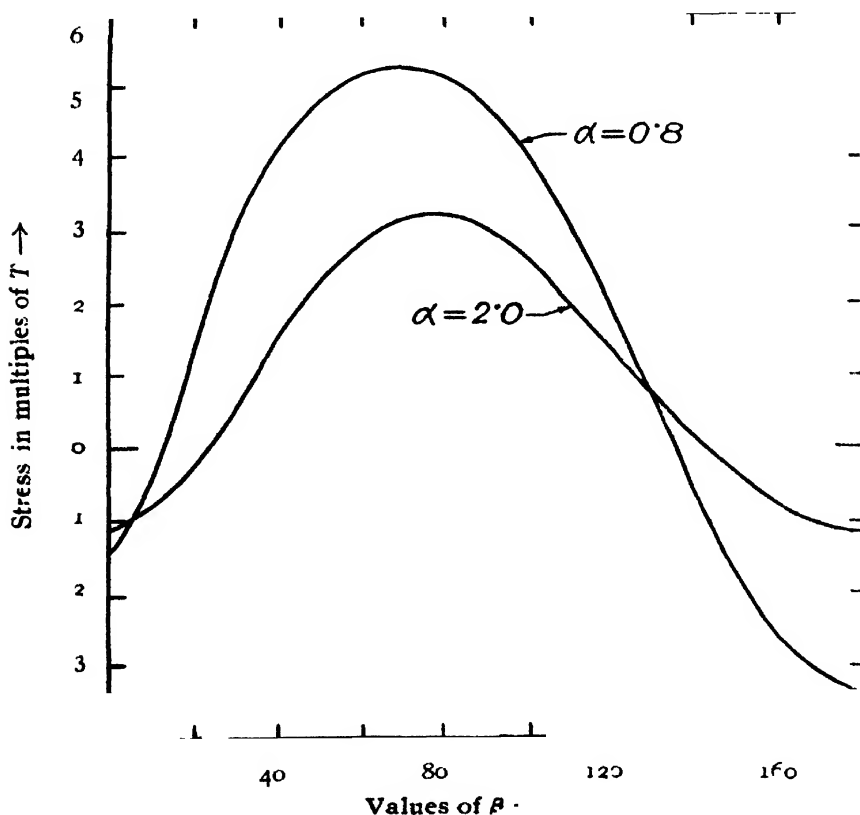


FIG 1



Substituting in (10) we get

$$\begin{aligned} \widehat{\beta\beta} = & 2T(\cosh\alpha_1 - \cos\beta) \\ & \times \left[ \frac{2\cosh\alpha_1 - \sinh\alpha_1}{2\sinh^2\alpha_1} + \frac{\cos\beta}{\sinh^2\alpha_1} - 2e^{-2\alpha_1} \cos\beta - \sum_{n=2}^{\infty} N_n \cos n\beta \right] \\ & - 2T \left[ 1 - \frac{2\sinh^2\alpha_1 \sin^2\beta}{(\cosh\alpha_1 - \cos\beta)^2} \right] \quad \dots (12) \end{aligned}$$

The values of the stress  $\widehat{\beta\beta}_1$ , in multiples of  $T$ , is shown in figure 1 against different values of  $\beta$  for  $\alpha=0.8$  and for  $\alpha=2.0$ .

The maximum stresses are found to be  $5.22T$  at  $\beta=68.5^\circ$  for  $\alpha=0.8$ , and  $3.23T$  at  $\beta=76.0^\circ$  for  $\alpha=2.0$ . The ratios of the distance of centre of the hole from the edge to the radius of the hole are 1.337 for  $\alpha=0.8$  and 3.762 for  $\alpha=2.0$ . The point of maximum stress shifts towards the point nearest to the straight edge and the amount of the maximum stress increases as the value of  $\alpha$  decreases. It is known that when the hole is at a great distance from the edge, the maximum stress is  $3T$  at the two ends of the diameter perpendicular to the direction of the applied tension. The result obtained here for  $\alpha=2.0$  where the point of the hole nearest to the edge is at a distance of about 2.76 times the radius of the hole, fairly compares with that known result.

#### A SEMI-INFINITE PLATE CONTAINING AN UNSTRESSED CIRCULAR HOLE UNDER UNIFORM SHEAR.

At a great distance from the circular hole the given stress condition may be obtained if we choose a solution

$$\chi_0 = -Sxy$$

where  $S$  is the given shear.

Therefore, for  $\alpha > 0$

$$\begin{aligned} h\chi_0 = & -aS \frac{\sinh\alpha \cdot \sin\beta}{\cosh\alpha - \cos\beta} \\ = & -2aS \sinh\alpha \sum_{n=1}^{\infty} e^{-n\alpha} \sin n\beta \quad \dots (13) \end{aligned}$$

To obtain the complete stress function we have to add to  $\chi_0$  another stress function  $\chi_1$ , which gives no stress at infinity ( $\alpha=0, \beta=0$ ) and no stress over the boundary  $\alpha=0$ .  $\chi_1$  must be such that the complete stress function ( $\chi_0 + \chi_1$ ) gives no stress over the circular boundary.

To choose a solution of the general form (3), we need only take the terms in  $\psi_n(\alpha)$  as the required stress function must be odd in  $\beta$ .

For the condition of no stress on  $\alpha=0$ ,  $\psi_n(0)=0$  for  $n \geq 2$  and  $\psi_n'(0)=0$  for  $n \geq 1$ . Hence we can write

$$h\chi_1 = aS \left[ A_1' \cosh 2\alpha \sin \beta + \sum_{n=2}^{\infty} \left\{ A_n' [\cosh(n+1)\alpha - \cosh(n-1)\alpha] + E_n' [(n-1)\sinh(n+1)\alpha - (n+1)\sinh(n-1)\alpha] \right\} \sin n\beta \right]$$

Calculating the constant co-efficients from the boundary conditions (6) and (7) for no stress due to the complete stress function  $(\chi_0 + \chi_1)$ , over the boundary  $\alpha=\alpha_1$ , we get,

$$\begin{aligned} A_1' &= \frac{e^{-2\alpha_1}}{\sinh 2\alpha_1} \\ A_n' &= -1 + \frac{\sinh 2n\alpha_1 - n \sinh 2\alpha_1}{2(\sinh^2 n\alpha_1 - n^2 \sinh^2 \alpha_1)} \\ E_n' &= -\frac{n \sinh^2 \alpha_1}{\sinh^2 n\alpha_1 - n^2 \sinh^2 \alpha_1} \end{aligned} \quad (14)$$

Hence when  $\alpha > 0$ , we get

$$\begin{aligned} h\chi &= aS \left[ \frac{\cosh 2(\alpha - \alpha_1) - \sinh 2\alpha_1}{\sinh 2\alpha_1} \sin \beta - 2 \sum_{n=2}^{\infty} \frac{1}{\sinh^2 n\alpha_1 - n^2 \sinh^2 \alpha_1} \right. \\ &\quad \times \left. \begin{aligned} &\left\{ n \sinh \alpha_1 \sinh n\alpha \sinh(\alpha - \alpha_1) \right. \\ &\left. - \sinh \alpha \sinh n\alpha_1 \sinh n(\alpha - \alpha_1) \right\} \sin n\beta \end{aligned} \right] \quad \dots \quad (15) \end{aligned}$$

The stress  $\beta\beta_1$  over the circular boundary, calculated by equations (2), is obtained as

$$\beta\beta_1 = 4S(\cosh \alpha_1 - \cos \beta) \left[ \frac{\sin \beta}{\sinh 2\alpha_1} - \sum_{n=2}^{\infty} M_n \sin n\beta \right] \quad \dots \quad (16)$$

where  $M_n$  has the same value as in (11). Separating out the more slowly converging part in the series in (16) by the same substitution for  $M_n$  as in (13a), we obtain,

$$\begin{aligned} \beta\beta_1 &= 4S(\cosh \alpha_1 - \cos \beta) \times \left[ \frac{\sin \beta}{\sinh 2\alpha_1} - 2e^{-2\alpha_1} \sin \beta - \sum_{n=2}^{\infty} N_n \sin n\beta \right] \\ &\quad - 4S \frac{2 \sinh \alpha_1 \sin \beta}{(\cosh \alpha_1 - \cos \beta)} (\cosh \alpha_1 \cos \beta - 1) \quad \dots \quad (17) \end{aligned}$$

In figure 2 the intensity of stress over the circular boundary at varying values of  $\beta$  is shown in multiples of  $S_1$  for  $\gamma = 0.8$  and  $\gamma = 2.0$ .

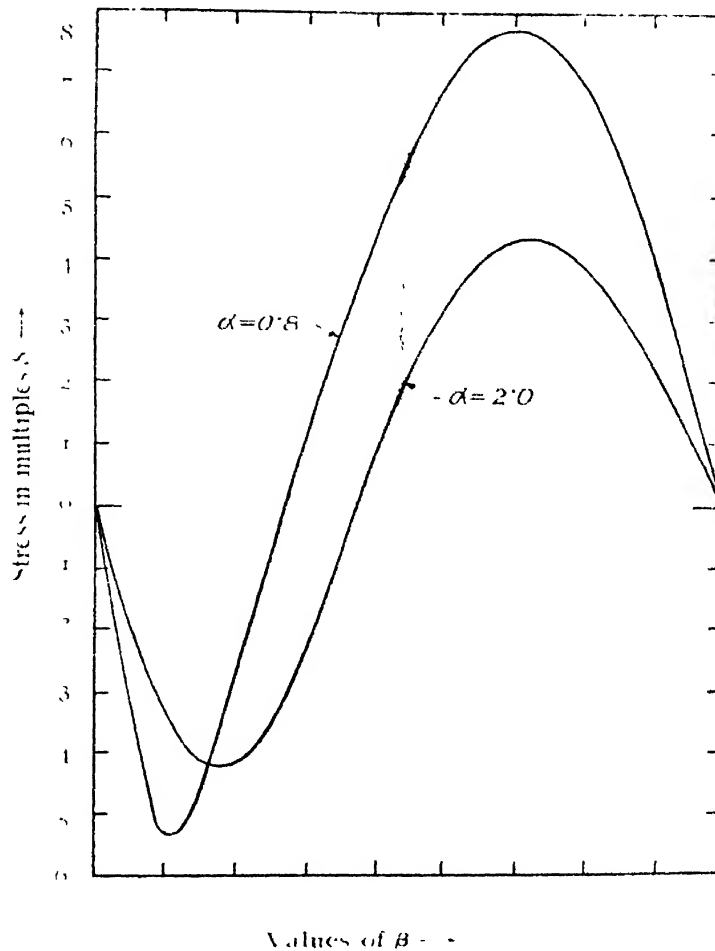


FIG. 2

The maximum stresses are found to be  $7.74S_1$  at  $\beta = 124^\circ$  for  $\alpha = 0.8$ , and  $4.39S_1$  at  $\beta = 126^\circ$  for  $\alpha = 2.0$ . In this case also the point of maximum stress shifts towards the point on the hole nearest to the straight edge with lesser values of  $\alpha$ . With higher values of  $\gamma$  the point of maximum stress on the hole tends to coincide with the point of maximum stress in the case of a hole in an infinite plate.

#### ACKNOWLEDGMENTS

In conclusion, the author wishes to express his respectful thanks to Dr. S. Ghosh of the Department of Applied Mathematics for suggesting the problems and for his kind guidance during the preparation of this paper.

DEPARTMENT OF APPLIED PHYSICS,  
UNIVERSITY COLLEGE OF SCIENCE AND TECHNOLOGY CALCUTTA

## REFERENCES

- Jeffery, G. B , 1921, *Phil. Trans Roy. Soc* , **A221**, 265.  
Mindlin, R D , 1939, *Proc. Am. Soc. Civ. Eng.*, **65**, 619.  
,, ,, 1948, *Proc. Soc. Exp. Sts. An.*, **8**, 56

**PROCEEDINGS  
OF THE  
INDIAN ASSOCIATION FOR THE  
CULTIVATION OF SCIENCE**



# LAPINONE, A NEW ANTIMALARIAL\*

By LOUIS F. FIESER

*Sheldon Emery Professor of Organic Chemistry, Harvard University*

Lapinone is an antimalarial of novel chemical type and unusual physiological properties. It is a hydroxyalkylnaphthoquinone composed of only carbon, hydrogen, and oxygen, and hence it is of simpler composition than all other known antimalarials and, indeed, than any other chemotherapeutic agent.

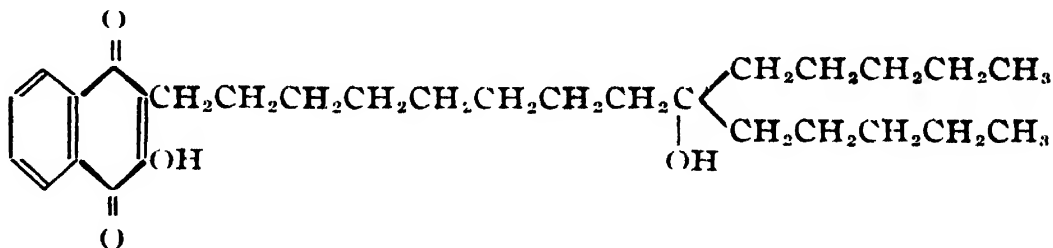


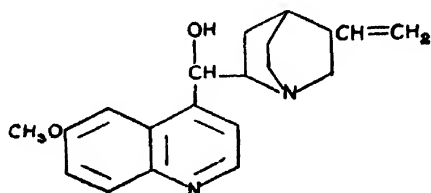
FIG. 1

Quinine is a 6-methoxyquinoline derivative with a nitrogen-containing side chain at position 4. Atabrine, the synthetic substitute suppressive introduced by the I. G. Farbenindustrie (1930), is an acridine derivative, but it is related to quinine in that the first two rings constitute a 6-methoxyquinoline unit with a nitrogen side chain at the 4-position. The other I. G. Farbenindustrie drug plasmochin (1926), now often called pamaquine in the United States, has the atabrine side chain moved to the 8-position of 6-methoxyquinoline ; it is an 8-aminoquinoline derivative. The new American drugs pentaquine (Drake and co-workers, 1946) and primaquine (Elderfield and co-workers, 1946) are related 8-aminoquinolines with small variations from plasmochin in the structure of the side chain ; thus primaquine is simply plasmochin minus the two N-ethyl groups. These 8-aminoquinolines have little suppressive action, but when administered in conjunction with quinine they effect a high percentage of cures of relapsing vivax malaria. Plasmochin is too highly toxic for safe use ; the status of the newer substances in this respect is still uncertain. Among a large number of other compounds synthesized, the Germans prepared the 4-aminoquinolines santochin and the substance now known as chloroquine, but their pharmacologists did not rate the compounds very highly. American research showed that chloroquine is a very effective suppressive and led to

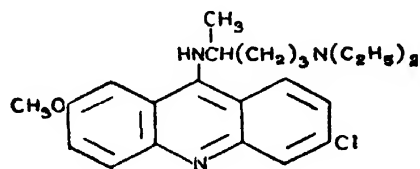
\* Cooch-Bihar Professorship Lecture delivered in the Indian Association for the Cultivation of Science, Calcutta, on the 12th, 13th and 16th January, 1951

**L. F. Fieser**

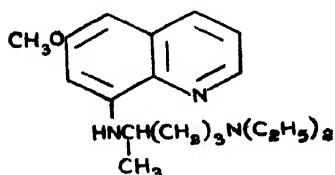
the introduction of the related camoquine (Burckhalter, *et al.*, 1948). The 4-aminoquinolines are suppressive only and lack curative properties. The same is true of the biguanide derivative paludrine (Curd, Davey and Rose, 1945), developed in England by I. C. I. workers.



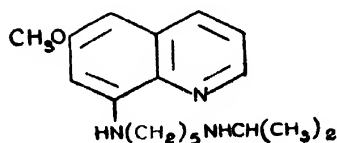
Quinine



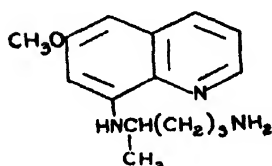
Atabrine



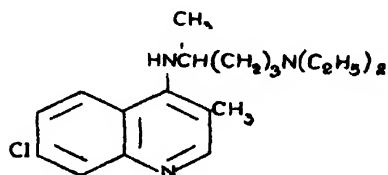
Plasmoquin  
(Pamaquine)



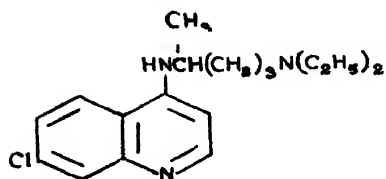
Pentaquine



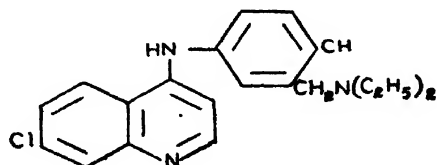
Primaquine



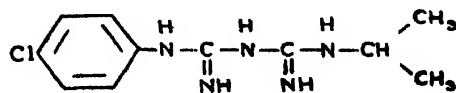
Santochin



Chloroquine



Camoquine



Paludrine

FIG. 2

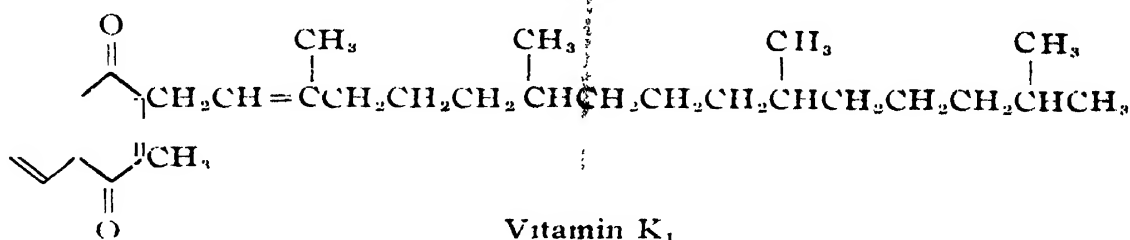
All of these antimalarials, natural and synthetic, contain nitrogen, and some contain chlorine as well; lapinone contains neither nitrogen nor



chlorine. The sulfa drugs and penicillin are also of elaborate composition, since they contain carbon, hydrogen, oxygen, nitrogen, and sulfur.

Lapinone functions by a mechanism evidently different from that of any other antimalarial. It destroys malarial parasites by inhibiting a respiratory enzyme of parasitized cells. The naphthoquinone seems of particular interest because of indications that it has high potency as both a suppressive and curative drug.

Lapinone resembles vitamin K<sub>1</sub> in elementary composition, structure, and physical properties. Both substances are 1,4-naphthoquinones, and both



Vitamin K<sub>1</sub>

FIG. 3

are lipid-soluble, water-insoluble, viscous yellow oils. The antimalarial has at the 2-position a hydroxyl group and at the 3-position a 19-carbon side chain containing a hydroxyl group; the vitamin has a 2-methyl group and the substituent at position 3 is a 20-carbon side chain containing a double bond.

The development of the new antimalarial resulted from systematic exploitation of a fortuitous clue uncovered in the extensive program of antimalarial research sponsored by the United States government during World War II and organized by the Committee on Medical Research of the Office of Scientific Research and Development. In this program of the C. M. R., some thirty-nine chemical research groups operated under government contract in coordination with pharmacological and clinical research groups. One line of investigation was the synthesis and biological documentation of all conceivable isomers, derivatives, and analogs of the known antimalarials of the quinoline and acridine series; such work led to the development of camoquine, pentaquine, and primaquine and to recognition of the value of chloroquine. The second line of attack consisted in the biological screening of organic chemicals of a wide variety of types in the search for antimalarials of a new kind. In one such screening program, chemists of the Abbott Laboratories in North Chicago visited some of the larger universities to collect and code miscellaneous research samples and send them to the pharmacological group of Dr. Arthur P. Richardson at the University of Tennessee Medical School at Memphis for screening assays against *Plasmodium lophurae* in ducks. Of several hundred compounds assayed, all but three proved to be completely inactive. The three active compounds, which possessed definite if weak antimalarial activity, were related naphthoquinones that had come from my laboratory at Harvard and that I had taken from

## L. F. Fieser

a collection of lapachol samples bequeathed to me by Samuel C. Hooker on his death in 1935. The most interesting of the three compounds was hydro-lapachol, the dihydro derivative of lapachol.

Samuel C. Hooker (1889-1896; 1915-1935)

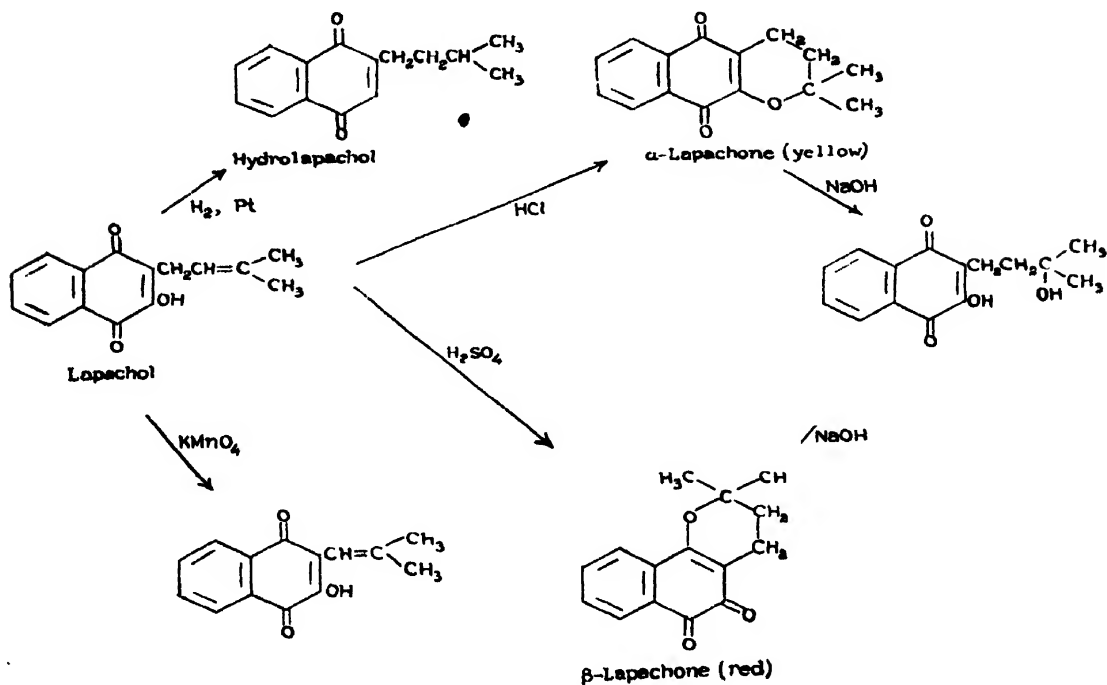


FIG. 4

Lapachol, a yellow pigment that occurs in the grain of certain tropical woods, had been the subject of a remarkable series of researches by the English-born chemist Hooker, a masterful experimentalist whose lot was cast in the field of American sugar technology, in which he achieved brilliant success. A romance with an American girl student at Munich had led Hooker to come to the United States, where, finding no suitable academic posts open, he had accepted employment in a sugar refinery in Philadelphia. Hearing of the presence in the city of a young German-trained chemist, a Philadelphian manufacturer of fine fishing rods and bows and arrows from the rare Bethabarra wood, imported at considerable expense from South America, consulted Hooker about the possible utilization of the yellow pigment of the wood, and provided the young chemist with quantities of Bethabarra sawdust and waste cuttings. Hooker found the chemistry of lapachol a fascinating subject for spare-time research, and in the period 1889-1896 he published a series of brilliant papers reporting the complete elucidation of the structure of lapachol and a description of an amazing array of novel reactions of the interesting substance [Greene and Hooker (1889); Hooker and Greene (1889); Hooker (1892, 1893, 1894, 1896); Hooker and Gray (1893); Hooker and Carnall (1894); Hooker and Walsh (1894); Hooker and Wilson (1894)]. In 1896, although he had not completed the research and had stated in his last paper

that "I shall hope to return to the consideration of this problem in the future" he felt obliged to abandon this side-activity and devote his whole energies to the professional field of sugar technology. His efforts in this direction were eminently successful; he introduced the beet sugar industry into American practice and achieved so many other successes that he eventually rose to the post of executive vice-president of his company. But he had not forgotten lapachol, and he was ever conscious of the promise of further work stated in his last paper. So, as soon as he had acquired an adequate competency, Hooker retired from the sugar business in 1915, built a private laboratory in the former stable in back of his elegant residence in Brooklyn, and shortly resumed the lapachol research exactly where he had left off in 1896.

It was my good fortune to meet Dr. Hooker in 1926 and to be in close association with his scientific work until the time of his death. I had applied techniques of oxidation-reduction potential measurements learned in my work for the Doctorate under Professor James B. Conant [Conant, Kahn, Fieser and Kurtz (1922); Conant and Fieser (1922, 1923, 1924)] to studies of heterocyclic quinones [Fieser (1926); Fieser and Ames (1927); Fieser and Peters (1931); Fieser and Hartwell (1935); Fieser and Kennelly (1935); Fieser and Martin (1935)] and polynuclear quinones, [Fieser (1929); Fieser and Dietz (1931)] and to an investigation of the tautomerism of hydroxyquinones [Fieser (1928, 1929); Fieser and Fieser (1934); Fieser and Thompson (1939)]. Through Dr. Hooker's generosity in supplying me with samples, I was able to include 16 quinones of the lapachol series in my potentiometric study of tautomerism.

I was fascinated by my contacts with this elderly gentleman who appeared to me to be an extraordinarily gifted experimentalist and a rare personality. Having lost contact with the academic chemists of his own age, Hooker was glad to have a young friend enthusiastically interested in his beloved lapachol chemistry. On his death in 1935, I edited a series of eleven posthumous papers reporting his researches of 1915 to 1935, [Hooker (1936); Hooker and Steyermark (1936); Hooker and Fieser (1936)] and I was bequeathed his extensive collection of beautiful samples of compounds derived from or related to lapachol.

When Richardson's assays revealed antimalarial activity in the relatively simple naphthoquinone hydrolapachol, I was in a particularly favorable position to investigate this new clue. In conducting the potentiometric investigations cited above I had acquired experience with practically all the known methods for the preparation of naphthoquinones and had introduced a few new procedures. Inspired by my association with Dr. Hooker, I had achieved the first synthesis of lapachol. (Fieser, 1927) My student Jesse T. Dunn had synthesized plumbagin in 1936 (Fieser and Dunn, 1936) and I had synthesized vitamin K<sub>1</sub> in 1939 (Fieser, 1939, 1940). My associates and I had developed other syntheses in the naphthoquinone [Fieser, Campbell,

Fry and Gates (1939); Fieser and Weighard (1940); Tishler, Fieser and Wendler (1940); Fieser, Gates and Kilmer (1940); Fieser and Gates (1941); Fieser and Jones (1942); Fieser, Turner (1942); Fieser and Turner (1947)], phenanthrenequinone (Fieser, 1929), anthraquinone (Fieser and Fieser, 1935) and 1,2-benzanthraquinone (Fieser and Dietz, 1929) series, and we had investigated a number of interesting reactions of quinones. [Fieser and Peters (1931, 1935); Fieser (1931); Fieser and Seligman (1934); Fieser and Hartwell (1935); Fieser and Dunn (1936, 1937); Fieser, Hartwell and Seligman (1936); Fieser and Bradsher (1939); Fieser and Fieser (1939, 1941)]. Of particular importance to the problem at hand was the timely discovery with F. C. Chang and A. E. Oxford of the method of peroxide alkylation (Fieser and Chang, 1942; Fieser and Oxford, 1942), whereby hydroxynaphthoquinone is converted into a 2-hydroxy-3-alkyl-1,4-naphthoquinone by reaction in acetic acid solution with the peroxide of an acid. This convenient one-step process provided a quick method for the synthesis of a large number

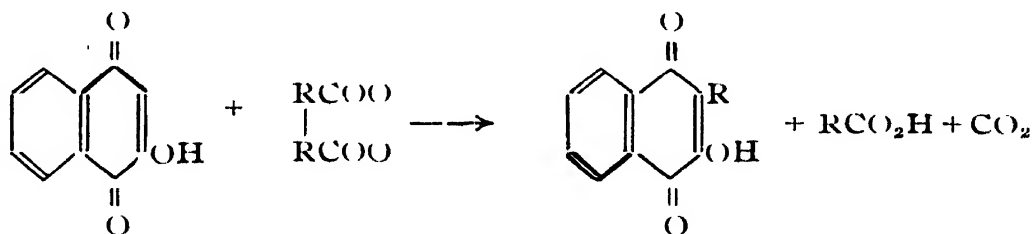


FIG. 5

of substances of the hydrolapachol type having hydrocarbon chains (R) of varying length and including straight chain structures, chains with branches at various points, and chains containing aromatic and alicyclic rings.

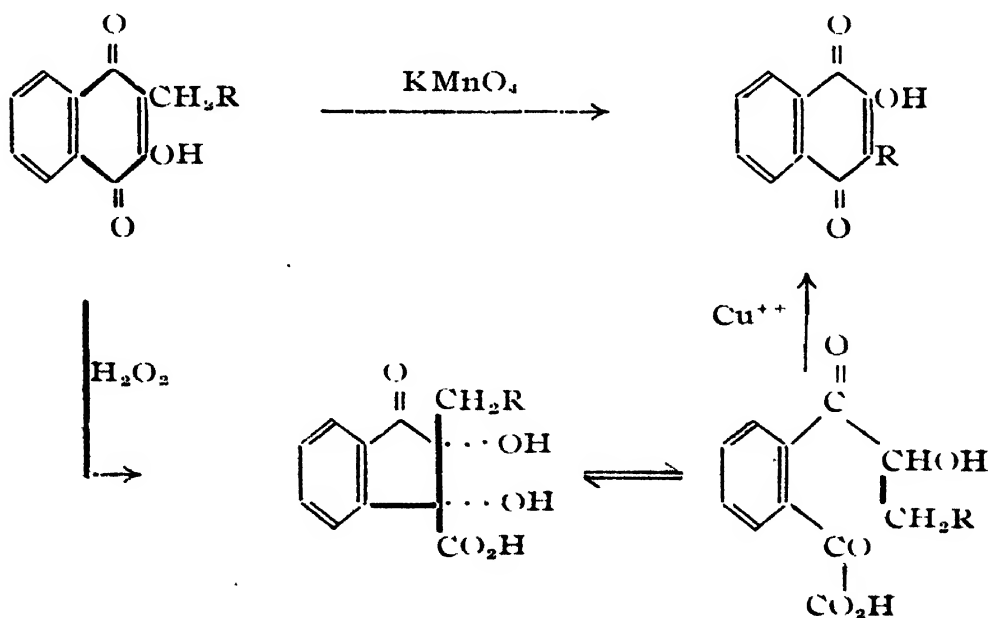


FIG. 6

A second general method that proved of great use to us was a remarkable oxidation discovered by Dr. Hooker, the Hooker oxidation (Hooker, 1936). Hooker had discovered that a hydroxyalkylnaphthoquinone can be converted into the next lower homolog by oxidation with alkaline permanganate in the cold, and he had found that the mysterious disappearance of the methylene group occurs even in the case of lapachol without disturbance of the double bond. He had synthesized the derivative with a seven-carbon side chain and degraded it by seven Hooker oxidations to every one of the lower homologs. The reaction was of great service in our synthetic program; for example, the readily available even-carbon acids afforded, by peroxide alkylation, the series of quinones with  $C_9$ ,  $C_{11}$ ,  $C_{13}$ , etc. side chains, and Hooker oxidation of the products then yielded the otherwise inaccessible homologs with  $C_8$ ,  $C_{10}$ ,  $C_{12}$ , etc. side chains. Hartwell, Seligman and I (Fieser, Hartwell and Seligman, 1936) had made a preliminary study of the mechanism of the Hooker oxidation, and in 1940 Mary Fieser and I discovered an intermediate in the reaction and she had subsequently established its structure. When, later, the reaction became of importance to our synthetic program, I worked on the experimental procedure and was able to develop a high-yield two-step process that is applicable to large as well as small quantities and represents a distinct improvement over the original one (Fieser and Fieser, 1948).

My research group, which eventually was expanded to a total of thirteen chemists, plunged into the work of exploring variations in the naphthoquinone structure and synthesized a total of some 250 new quinones. The Abbott Laboratories joined us in the initial synthetic program, and a group of five of their chemists under the direction of Dr. Marlin T. Leffler synthesized an additional 75 quinones for bioassay. The total effort reported in a series of eight joint papers (Fieser *et al*, 1948) included also the preparation of 46 quinone derivatives and of a considerable number of new intermediates. One of my co-workers, Dr. W. G. Dauben, completed some of the synthetic work at the University of California in Berkeley. Another, Dr. Ernst Berliner, spent his summers in Cambridge and continued the synthetic work during term time at Bryn Mawr, with the collaboration of his student Frances Bondhus, now Mrs. Berliner. My Ph. D. students Armin G. Wilson and Evelyn Hodes were married in the course of the work. Finding some periods of respite from my wartime activities in the development of new incendiary munitions, I had the pleasure of personal participation in various phases of the experimental program and worked out procedures for the preparation of several of the key naphthoquinones and intermediates on a practical scale by a diene synthesis (Fieser, 1948).

Interest in the naphthoquinones as antimalarials was greatly enhanced when cooperating workers of the Rockefeller Foundation found that the substances not only suppress malarial infections in chickens but are effective prophylactic agents [Clarke and Theiler, (1948); Whitman, (1948)]. In 1944

these investigations established that the naphthoquinone drugs effectively destroy both the trophozoites of the red blood cells and the exoerythrocytic forms of malaria parasites found in the reticulo-endothelial cells of chickens infected with *Plasmodium gallinaceum*. Quinine and atabrine suppress the trophozoites, but exert no control whatever over the exoerythrocytic forms. These observations strongly suggested that the naphthoquinones would exhibit curative as well as suppressive action, and such an effect was subsequently established in three different avian infections. Walker and Richardson (1948) and Walker, Slanber and Richardson (1948) later observed a very interesting synergistic or potentiating effect of a naphthoquinone and the 8-aminoquinoline derivative plasmochin (pamaquine); a combination of one/tenth the curative dose of each drug resulted in 100% cures.

The program of synthesis by our chemical groups, coupled with prompt and able bioassays by Dr. Richardson's group in Memphis, soon outlined rough relationships between chemical constitution and biological potency (Fieser and Richardson, 1948). We were eventually able to produce compounds possessing no less than one hundred times the potency of hydro-lapachol, the compound that had given the principal clue to the new development. The assays for suppressive activity against *Plasmodium lophurae* in ducks were expressed in terms of the effective dose, in mg. of drug per kg. of body weight, required to effect 95% reduction of parasitemia, represented by the symbol  $ED_{95}$ . For hydrolapachol,  $ED_{95} = 68$  mg./kg., and hence the substance is only about one-seventh as active as quinine (base),  $ED_{95} = 10.25$  mg./kg. The most active naphthoquinone encountered had the high potency  $ED_{95} = 0.67$  mg./kg., but the compound was available only by a very difficult synthesis.

In 1943 an initial clinical trial was conducted at the Goldwater Memorial Hospital in New York on syphilitic patients undergoing malaria therapy (Wiselogle, 1946). Each cooperating laboratory supplied for the trial the

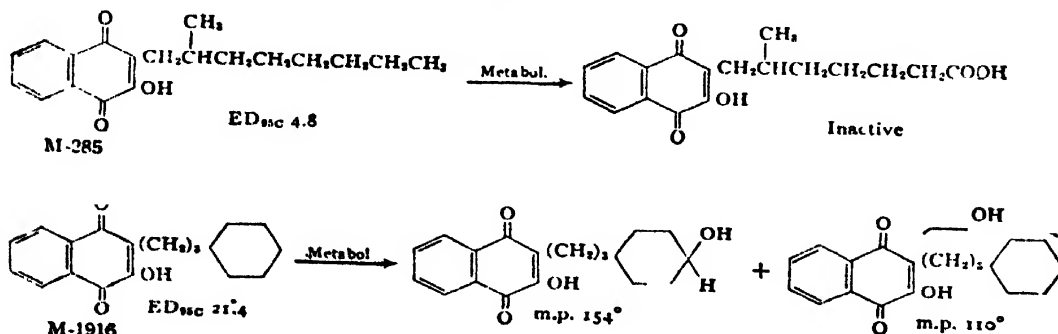


FIG. 7

most promising naphthoquinone that could be produced in a hurry in adequate quantity (250 g.); these were the substances coded as M-285 (Abbott) and M-1916 (Harvard), whose structures and activities are shown in the chart. Although M-285 is four times as potent in the duck assay as M-1916, it proved to be completely inactive in five patients (blood-induced *P. vivax* and

## Lapinone, A New Antimalarial

*P. falciparum*), whereas M-1916 produced a temporary suppression of fever extending for an average of 9.5 days in eight cases. The effect was not satisfactory, but enough to show that M-1916 has definite antimalarial activity in man.

The results were very disappointing. The medical authorities of the CMR felt that the naphthoquinones had been given a fair trial and had failed, and they discouraged us from continuing the study; they pointed to other instances where results in animals fail to carry over to man. The Abbott Laboratories group merely finished off such synthetic work as they had in hand. But my group was not satisfied. We did not like to rest the case without trying to find out why compounds so active in ducks and chickens proved inactive, or only weakly active, in man. We were particularly intrigued with the curious reversal in activity: why is M-285, so potent in ducks, completely inactive in man, whereas M-1916, the weak sister in the duck assays, exerts a mild therapeutic effect in man?

So some of the chemists of my group, particularly Dr. Hans Heymann and Dr. Frederic C. Chang, became biochemists and plunged into the problem of investigating the metabolic fate of naphthoquinones administered to nonmalarial human subjects (Fieser and others, 1948). We soon despaired of the idea of obtaining supplies of urine from the subjects of the clinical trial or of surmounting the governmental red tape involved in obtaining conscientious objectors as subjects, and initiated the study by eating the compounds ourselves. I participated in this phase of the work by consuming a total of 33 g. of various naphthoquinones and working up all the urines and several plasma samples; it was a thrilling experience to have blood drawn from my arm and spun down, and to look at the raspberry red plasma containing metabolites and know that my own liver had accomplished the metabolic oxidations concerned. Later, after returning on VE-day from participation in the Alsos Mission of scientific intelligence that accompanied our armies of conquest in Germany, I enjoyed a period of freedom from both war work and teaching and was able to carry out in the test tube some of the oxidative changes that had occurred in my liver (Fieser, 1948).

After an initial start in which we chemists served as our own guinea pigs, Dr. Arnold M. Seligman came to our aid and provided subjects for study of drug metabolism from the Beth Israel Hospital. He instituted the ingenious practice of administering some of the compounds to polycythemic patients prior to the drawing of the necessarily large volumes of blood in order to provide us with amounts of plasma adequate for isolation of metabolites from this source; in several instances the metabolites extracted from plasma were found to be identical with those excreted in the urine. The required pharmacology was ably done at the Harvard Medical School by Professor Otto Krayer, Dr. E. B. Astwood, and Dr. A. M. Seligman.

In studies that, after expiration of our war-time contract, were continued under a grant from the Rockefeller Foundation, we found that metabolism

of the naphthoquinones in man consists in oxidative attack of the hydrocarbon side chain. Thus the side chain of hydrolapachol,  $-\text{CH}_2\text{CH}_2\text{CH}(\text{CH}_3)_2$ , is metabolized to  $-\text{CH}_2\text{CH}_2\text{C}(\text{OH})(\text{CH}_3)_2$ ; the product was identified by comparison with a sample of hydroxyhydrolapachol taken from the Hooker collection. Hooker's samples were of the greatest service in development of colorimetric methods for separating and identifying various alcoholic and unsaturated derivatives of the naphthoquinones (Fieser, 1948).

In all, some eight crystalline products of metabolism were isolated and their structures established. We found that M-285 is metabolized to a carboxylic acid and that M-1916 is metabolized to two hydroxy derivatives, as shown in the formulation above, but the substances were isolable only on a micro scale and not in quantity sufficient for bioassays. We had submitted a few synthetic compounds with oxygenated side chains and they had all been found devoid of activity. "What substance," we kept asking ourselves, "was responsible for the weak therapeutic effect resulting from administration of M-1916?" Dr. W. B. Wendell (1946) at Memphis had discovered that the naphthoquinones are very powerful inhibitors of respiratory enzymes and are effective at dilutions in the order of  $1 \times 10^{-6}\text{M}$ . The antirespiratory activity of a given member of the series, relative to that of a reference standard, can be measured on a micro scale in a Warburg apparatus by determining the concentration required to half-inhibit the respiration of a suspension of parasitized red blood cells drawn from a duck infected with *P. lophurae*. By the spring of 1945 Wendell's results so strongly suggested that the convenient *in vitro* determination of antirespiratory activity affords a reliable guide to *in vivo* antimalarial activity that we decided to install the *in vitro* test in our own laboratory for the more precise study of drug metabolism. This meant establishment and maintenance of a colony of malarial infected ducks, housed under some protest in the biological laboratory, and installation and operation of a Warburg apparatus in our own laboratory. The senior chemist of my group, Dr. Hans Heymann, rose to the occasion of mastering the many biological and biochemical techniques involved and ably conducted an extended series of antirespiratory studies, [Heymann and Fieser (1948); Fieser and Heymann (1948)]. Determinations of the relative antirespiratory activities of 76 naphthoquinones in Memphis and of 82 in Cambridge showed conclusively that the *in vitro* test is a safe measure of *in vivo* activity.

The micro test permitted study of the course of metabolic drug deactivation in the following manner. A given compound was administered to a patient by Dr. Seligman, usually intravenously, and small blood samples were drawn from time to time, spun down, and the plasmas sent over to Dr. Heymann in Cambridge. Since oxygenation of the side chain does not alter the chromophoric properties of the naphthoquinone nucleus, colorimetric determination of the pigment extracted from a plasma gave the value of total naphthoquinone, degraded and (or) undegraded. A small sample of pigment



was then put into the Warburg machine and a determination made of the antirespiratory activity per colorimetric equivalent of pigment as compared to that of the drug administered. Naphthoquinones of all of the types initially available proved to be metabolized completely within 3-4 hours. In most cases the initial activity, however high, was completely lost in the process. This was true of M-285, and an *in vitro* test of the carboxylic acid metabolite that we had isolated showed to be completely inactive. The case of M-1916 was different. Here, metabolic change was as rapid as ever but the activity dropped, in four hours, to a level one-tenth that of M-1916 and then persisted at the same level for some twenty hours. The two hydroxylated metabolites that we had isolated were then found, in repeated trials, to possess antirespiratory activity just one-tenth that of M-1916. We thus reached the conclusion that the weak antimalarial action of M-1916 in the clinical trials must have been due to the weakly active but persistent hydroxylated metabolites. A hydroxyl group in the side chain provides protection against metabolic attack but, at least in the case of M-1916 and the few other compounds that we had then investigated, the introduction of a hydroxyl group into the side chain detracts very materially from the potency of the parent compound.

However, our program of systematically investigating all types of side chains eventually afforded results suggesting that the deactivating influence of oxygen substitution can be offset by an increase in the carbon content of the side chain. We were later able to rationalize this empirical finding by a physico-chemical study of distribution characteristics. Richardson's assays had shown that in any homologous series, for example hydroxynaphthoquinones with *n*-alkyl-, isoalkyl-,  $\omega$ -phenylalkyl-, or  $\omega$ -cyclohexylalkyl-side chains, biological activity increases with increasing molecular weight for a time, passes through a maximum, and then falls off. However, the optimum molecular weight varied considerably from one series to another; in the *n*-alkyl series a  $C_9$ -side chain afforded optimum activity, whereas in the  $\omega$ -cycloalkyl and  $\omega$ -phenylalkyl series highest potency was reached with  $C_{10-11}$  and  $C_{15}$ -side chains, respectively. These relationships became clear from a study of the distribution of the naphthoquinones between ether, in which the free acid dissolves with a yellow colour, and aqueous buffers, which extract a certain amount of the red anion (Fieser, Littlinger and Fawaz, 1943). By colorimetry, it is a simple matter to make an accurate determination of the constant  $pK$ , which characterizes the balance of hydrophilic-lipophilic properties of a given member of the series. This constant is defined (see equation) as the  $pH$  of an aqueous buffer

$$pK = \log \frac{[\text{Quinone in ether layer}]}{[\text{Quinone in water layer}]} + pH - 2$$

capable of extracting just 1/101-part of pigment from an equal volume of ether. In each series  $pK$  increases with increasing molecular weight, and the

curves for the different series are parallel. The effect of the introduction of cyclohexyl and phenyl groups into the side chain is to produce progressive shifts in the direction of increased hydrophilic character. These shifts follow closely the displacements in the peaks of antimalarial activity from series to series, and the compounds of highest activity in the different series all have  $pK$  values in the range 10-12. Thus a naphthoquinone, to possess high biological potency, must have a balance between hydrophilic and lipophilic properties corresponding to a  $pK$  of this favourable range.

A hydroxyl group in the side chain, desired for protection against metabolic attack, very greatly enhances the hydrophilic character of the molecule; the effect amounts to a displacement in  $pK$  of about 4 units. M-1916 is close to being the peak compound in its series, but the hydroxyl group in the metabolites reduces  $pK$  to an unfavorably low level. However, an appropriate increase in the molecular weight should compensate for the hydrophilic shift caused by the hydroxyl group. We therefore decided to try to synthesize a naphthoquinone with a hydroxyl group substituted in a very large hydrocarbon side chain. At the time this project was taking shape we had the pleasure of the addition to our group of Dr. George Fawaz, on leave of absence in 1945-1946 from the Department of Chemistry of the American University of Beirut, Labanon, and now Professor of Pharmacology at Beirut. Dr. Fawaz, who with the able assistance of his wife Eva, participated in the distribution study cited, undertook the synthesis of a compound of the type specified and, by application of a method developed by Dr. Heymann for the synthesis of a similar model compound, synthesized the compound coded as M-2350, now designated lapinone. He synthesized three related homologs, but they proved less promising. Later, three Ph.D. students synthesized a large number of analogous quinones with hydroxylated side chains, and with side chains containing ketonic, oxide, sulfide, and nitrogen functions [Cram (1949); Paulshock and Moser (1950); Moser and Paulshock (1950)] but most of these compounds proved to be much less potent than lapinone and none seem more promising. The first guess was thus a lucky one.

M-2350, lapinone, was initially assayed by Dr. Richardson by the usual route of oral administration and found to be only moderately active. I thought this might be due to poor absorption from the gut of this compound of high molecular weight and asked for a reassay. Surely enough, intramuscularly administered material proved to possess the high antimalarial potency that we had predicted. We then, hopefully, investigated the resistance of the substance to metabolic deactivation in the human body. Dr. Seligman administered the compound intravenously to patients of the Beth Israel Hospital and Dr. Heymann determined the residual activity of extracted plasma pigments (Fieser, Heymann and Seligman, 1948). The results were very encouraging. Unlike M-1916, M-285, and all the other naphthoquinones with hydrocarbon side chains, lapinone retained a large measure of its original

activity for periods of 20-40 hrs, after administration. The results were substantiated by experiments with animals of seven species. Mice metabolize M-1916 more nearly like humans than do any of the six other test animals studied, and lapinone administered to mice shows good retention of antirespiratory activity.

By the criteria of the laboratory tests, it appeared that the goal of developing a naphthoquinone of high potency and of adequate resistance to metabolic deactivation in man had been achieved. We thus awaited with great interest the outcome of an initial, small scale clinical trial conducted by Dr. Fawaz on his return to the American University at Beirut. Nine patients infected with primary vivax malaria were given 2 g. of lapinone per day for four days by intravenous injection in gelatine solution. All patients were relieved very promptly of fever and the blood was freed of parasites. Thus, unlike M-285 and M-1916, lapinone exerts a fully satisfactory suppressive action in man just as it does in ducks and chickens. The result showed that the defect in the early compounds had been corrected and it justified our sustained effort to solve a problem in chemotherapy through a program of rational research aimed at understanding the fundamental phenomena involved. The Lebanese clinical trial was planned merely as a test for suppressive action in man, and the period of administration was not at all comparable to the 14-day regime employed in the standard test for curative action. Nevertheless, six of the patients treated had gone without relapses when last checked after periods of from thirteen to fifteen months after termination of treatment. The result tentatively suggests a carry-over to man of the curative action of other naphthoquinones observed in birds.

More recently, Dr. Alexander M. Moore of Parke, Davis and Co. has reported results of a reliable new test for suppressive and curative action against *P. lophurae* in white leghorn chicks that he had previously applied to all the standard antimalarials and to several of the newer compounds. In a letter of January 3, 1951, Dr. Moore states that: "As a suppressive, lapinone was about three times as active as quinine, i. e.  $ED_{50}$  ca. 5 mg./kg. daily for 4 days, when administered intramuscularly. As a curative agent, lapinone was highly effective when administered intramuscularly at the maximum tolerated dose. Of all the types of antimalarial drugs tested, only the 8-aminoquinolines and the 2-hydroxy-3-alkyl-1, 4-naphthoquinones have cured young chicks infected with *lophurae* malaria. Although the 8-aminoquinolines cured only a fraction of the infected birds, lapinone was much more effective. Indeed, you will observe from the attached reports that lapinone cured every one of the infected birds. No other substance tested in this laboratory to date has proved so effective in the curative test."

Lapinone thus appears promising enough to warrant further pharmacological study and clinical evaluation. A practical synthesis from  $\beta$ -naphthol and sebacic acid was reported in 1950 (Fawaz and Fieser, 1950). Endo Products Inc. of New York has initiated manufacture of lapinone, at least

on a scale adequate for pharmacological and clinical evaluation. Since the substance is a water-insoluble oil, in our laboratory tests and in the Lebanese trial it was administered by intravenous or intramuscular\* injection in order to by-pass the question of efficiency of absorption from the intestines. However, Dr. Nathan Weiner of Endo Products has recently developed a promising formulation for oral administration and is investigating its efficacy.

I hope that some of the many able medical scientists of India will apply their knowledge, experience, and vast test material to the study of this new compound. It would be very gratifying if our own prolonged research, as well as the early fundamental investigations of Dr. Hooker, should turn out to be of some service to the people of this great country, where malaria is still a major problem.

\**Solution for intravenous injection* (developed by Dr. A. M. Seligman): dissolve 2 g. of lapinone in 50 cc. of alcohol and add all at once with agitation a solution prepared from 1500 cc. of physiological saline, 200 cc. of 6% Knox pyrogen-free gelatin solution (pH 7.4), and 1.2 g. of sodium carbonate monohydrate; the solution should not be prepared more than a few hours before required for injection.

*Solution for intramuscular injection* (developed by Dr. George Fawaz): dissolve 5 g. of lapinone in 13 cc. of sterile peanut oil and to the solution add a solution of 0.2 g. of Butescin  $H_2NC_6H_4CO_2C_4H_9-p$  in 2 cc. of ether.

#### REFERENCES

- Burckhalter, H. J. and others, 1948, *J. Am. Chem. Soc.*, **70**, 1363.  
 Clarke, D. H. and Theiler, M., 1948, *J. Infectious Diseases*, **82**, 138.  
 Conant, J. B. and Fieser, L. F., 1922, *J. Am. Chem. Soc.*, **44**, 2480.  
 " " 1923, *ibid.*, **45**, 2194.  
 " " 1924, *ibid.*, **46**, 1858, 2633.  
 Conant, J. B., Khan, H. M., Fieser, L. F., and Kurtz, S. S. Jr., 1922, *J. Am. Chem. Soc.*, **44**, 1382.  
 Cram, D. J., 1949, *J. Am. Chem. Soc.*, **71**, 3950, 3953.  
 Curd, F. H. S., Davey, D. C., and Rose, F. L., 1945, *Ann. Trop. Med.*, **39**, 220.  
 Drake, N. L. et al, 1946, *J. Am. Chem. Soc.*, **68**, 1529.  
 Elderfield, R. E. et al, 1946, *ibid.*, **68**, 1524.  
 Fawaz, G. and Fieser, L. F., 1950, *J. Am. Chem. Soc.*, **72**, 996.  
 Fieser, L. F., 1926, *J. Am. Chem. Soc.*, **48**, 1077.  
 " " 1927, *J. Am. Chem. Soc.*, **49**, 857.  
 " " 1928, *ibid.*, **50**, 439.  
 " " 1929, *ibid.*, **51**, 3101.  
 " " 1929, *ibid.*, **51**, 940, 1806, 1935.  
 " " 1931, *Ber.*, **64**, 701.  
 " " 1931, *J. Am. Chem. Soc.*, **53**, 2327.  
 " " 1939, *ibid.*, **61**, 2559, 2567, 3467.

- Fieser, L. F., 1940, *J. Biol. Chem.*, **133**, 391.  
 " " 1948, *J. Am. Chem. Soc.*, **70**, 3165.  
 " " 1948, " " 3237.  
 " " 1948, " " 3232.  
 " " and Ames, M. A., 1927, *J. Am. Chem. Soc.*, **49**, 2604.  
 " " and Bradsher, C. K., 1939, *ibid.*, **61**, 417.  
 " " and Campbell, W. P., Fry, R. M., Gates, M. D., Jr., 1939, *J. Am. Chem. Soc.*, **61**, 3216.  
 " " and Chang, F. C., 1942, *ibid.*, **64**, 2045.  
 " " " " Dauben, W. C., Heidelberger, C., Heymann, H. and Seligman, A. M., 1948, *J. Pharm. Exp. Therap.*, **94**, 85.  
 " " and Deitz, R. M., 1931 *J. Am. Chem. Soc.*, **53**, 1128.  
 " " " " " 1929, *ibid.*, **51**, 3141.  
 " " and Dunn, J. T., 1936, *ibid.*, **58**, 1054.  
 " " " " " 1936, *ibid.*, **58**, 572.  
 " " " " " 1937, *ibid.*, **57**, 1016, 1021, 1024.  
 " " Ettlinger, M. G., and Fawaz, C., 1948, *ibid.*, **70**, 3228.  
 " " and Fieser, M., 1934, *ibid.*, **56**, 1565.  
 " " " " 1935, *ibid.*, **57**, 1679.  
 " " " " 1939, *ibid.*, **61**, 595.  
 " " " " 1941, *ibid.*, **63**, 1572.  
 " " " " 1948, *ibid.*, **70**, 3215.  
 " " and Gates, M. D., Jr., 1941, **68**, 2948.  
 " " " " and Kilmer, G. W., 1940, *ibid.*, **62**, 2966.  
 " " and Hartwell, J. L., 1935, *ibid.*, **57**, 1479.  
 " " " " 1935, *ibid.*, **57**, 1479, 1482, 1484.  
 " " Hartwell, J. L., and Seligman, A. M., 1936, *ibid.*, **58**, 1223.  
 " " and Heymann, H., 1948, *J. Biol. Chem.*, **176**, 1363.  
 " " Heymann, H., and Seligman, A. M., 1948, *J. Pharm. Exp. Therap.*, **94**, 112.  
 " " and Jones, R. N., 1942, *J. Am. Pharm. Assoc.*, **31**, 315.  
 " " and Kennelly, R. G., 1935, *J. Am. Chem. Soc.*, **57**, 1611.  
 " " Leffeler, M. T., and co-workers, 1948, *ibid.*, **70**, 3174, 3181, 3185, 3195.  
 " " 3197, 3203, 3206, 3212.  
 " " and Martin, E. L., 1935, *ibid.*, **57**, 1835, 1840, 1844.  
 " " and Oxford, A. F., 1942, *ibid.*, **64**, 2060.  
 " " and Peters, M. A., 1931, *J. Am. Chem. Soc.*, **53**, 4030, 793.  
 " " 1935, *ibid.*, **57**, 491.  
 " " and Richardson, A. P., 1948, *ibid.*, **70**, 3156.  
 " " and Seligman, A. M., 1934, *ibid.*, **56**, 2690.  
 " " and Thompson, H. T., 1939, *ibid.*, **61**, 376.  
 " " Tishler, M. and Wendler, N. L., 1940, *ibid.*, **62**, 2861.  
 " " and Turner, R. B., 1947, *ibid.*, **69**, 2335, 2338.  
 " " and Weighard, C. W., 1940, *ibid.*, **62**, 153.  
 Greene, W. H., and Hooker, S. C., 1889, *Am. Chem. J.*, **11**, 267.  
 Heymann, H. and Fieser, L. F., 1948, *J. Pharm. Exp. Therap.*, **94**, 97.  
 " " " " " 1948, *J. Biol. Chem.*, **176**, 1359.  
 " " and Seligman, A. M., 1948, *J. Pharm. Exp. Therap.*, **94**, 85.  
 Hooker, S. C., 1892, *J. Chem. Soc.*, **61**, 611.  
 " " 1893, " " **63**, 1376.  
 " " 1894, " " **65**, 15.

- Hooker, S. C., 1896, *J. Chem. Soc.*, **69**, 1355, 1381.
- „ „ 1936, *J. Am. Chem. Soc.*, **58**, 1163, 1168, 1174, 1181, 1190, 1212, 1179.
- „ „ and Carnell, W. C., 1894, *J. Chem. Soc.*, **65**, 76.
- „ „ and Fieser, L. F. 1936, *J. Am. Chem. Soc.*, **58**, 1216.
- „ „ and Grey, A. D., 1893, *J. Chem. Soc.*, **63**, 424.
- „ „ and Greene, W. H., 1889, *Am. Chem. J.*, **11**, 393.
- „ „ „ „ 1889, *idem.*, *Ber.*, **22**, 1723.
- „ „ and Steyermark, A. R., 1936, *J. Am. Chem. Soc.*, **58**, 1179, 1198, 1202, 1207.
- „ „ and Walsh, J. G., Jr., 1894, *J. Chem. Soc.*, **65**, 321.
- „ „ and Wilson, R., 1894, *ibid.*, **65**, 717.
- Moser, C. M., and Paulshock, M., 1950, *J. Am. Chem. Soc.*, **72**, 5419.
- Paulshock, M., and Moser, C. M. 1950, *J. Am. Chem. Soc.*, **72**, 5073.
- Tishler, M., Fieser, L. F. and Wendler, N. L., 1940, *ibid.*, **62**, 1982, 2856.
- Walker, H. A., and Richardson, A. P., 1948, *J. Nat. Med. Soc.*, **7**, 4.
- Walker, H. A., Stauber, L. A. and Richardson, A. P., 1948, *J. Infectious diseases.*, **82**, 187.
- Wendell, W. B., 1946, *Federation Proc.*, **5**, 406.
- Whitman, L., 1948, *J. Infectious Diseases*, **82**, 251.
- Wiselogle, R. Y., 1946, *Survey of Antimalarial Drugs.*